



N6315976

**NTIS**<sup>®</sup>  
Information is our business.

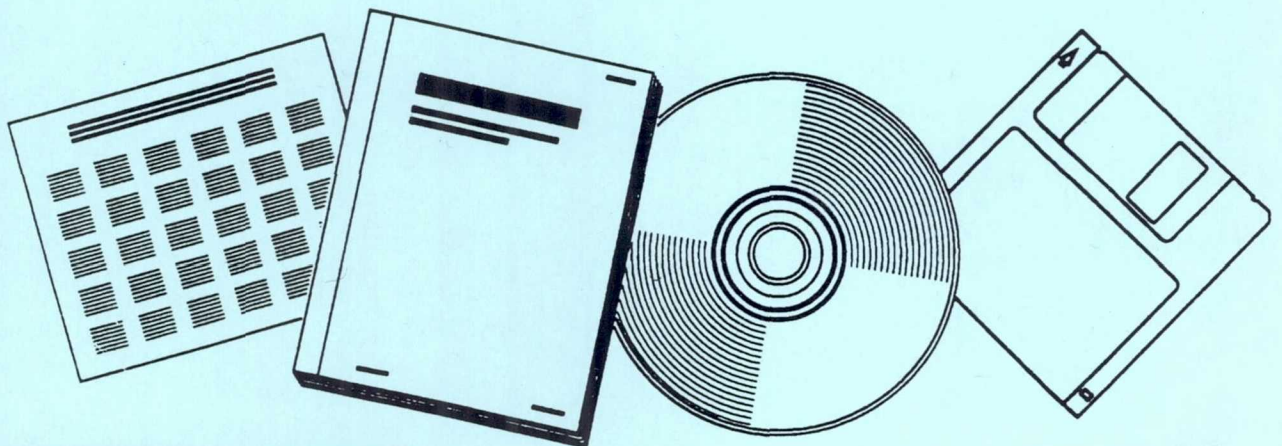
---

---

## FROM PEENEMUNDE TO OUTER SPACE

GEORGE C. MARSHALL SPACE FLIGHT CENTER  
HUNTSVILLE, AL

MAR 62



U.S. DEPARTMENT OF COMMERCE  
National Technical Information Service

---

---

N63-15976 - N63-16015

**From  
PEENEMÜNDE  
to  
OUTER SPACE**

Commemorating  
the Fiftieth Birthday of  
Wernher von Braun  
March 23, 1962

Edited by Ernst Stuhlinger  
Frederick I. Ordway, III  
Jerry C. McCall  
George C. Bucher

REPRODUCED BY  
**NATIONAL TECHNICAL  
INFORMATION SERVICE**  
U. S. DEPARTMENT OF COMMERCE  
SPRINGFIELD, VA. 22161

GEORGE C. MARSHALL SPACE FLIGHT CENTER  
National Aeronautics and Space Administration  
Huntsville, Alabama

*"From Peenemünde to Outer Space"*  
Presented to  
Wernher von Braun on his Fiftieth Birthday

Written by  
former and present associates  
in Peenemünde, Fort Bliss, Huntsville  
and on the launching pad

LIST OF CONTRIBUTORS

- |                                     |                                                 |
|-------------------------------------|-------------------------------------------------|
| Wilhelm Angele, Chap. 27            | Billy P. Jones, Chaps. 10 and 16                |
| J. Boehm, Chaps. 9 and 20           | J. W. Keller, Chap. 11                          |
| Charles O. Brooks, Chap. 5          | J. C. King, Chap. 16                            |
| Rudolf Bruns, Chap. 23              | H. H. Koelle, Chap. 7                           |
| George C. Bucher, Chap. 15          | Joachim P. Kuettner, Chap. 28                   |
| T. A. Buchhold, Chap. 21            | H. F. Kurtz, Chap. 26                           |
| M. O. Burrell, Chap. 11             | Oswald H. Lange, Chap. 1                        |
| Keith B. Chandler, Chap. 13         | Wei Ching Lin, Chap. 33                         |
| Kurt H. Debus, Chap. 3              | Robert G. Lindberg, Chap. 36                    |
| Walter R. Dornberger, Epilogue      | Charles F. Lombard, Chap. 36                    |
| J. A. Downey, III, Chap. 11         | Charles A. Lundquist, Chap. 34                  |
| Daniel H. Driscoll, Chap. 24        | A. A. McCool, Chap. 13                          |
| J. S. Farrior, Chap. 18             | William L. Mitchell, Chap. 5                    |
| H. J. Fichtner, Chaps. 9 and 29     | F. B. Moore, Chap. 19                           |
| G. G. Gassaway, Chap. 19            | Robert J. Naumann, Chap. 10                     |
| W. Haeussermann, Chap. 19           | Hermann Oberth, Chap. 17                        |
| Gerhard B. Heller, Chaps. 10 and 15 | Frederick I. Ordway, III, Chap. 4               |
| Ray V. Hembree, Chap. 34            | William H. Pickering, Chap. 8                   |
| Rudolf Hermann, Chap. 12            | Richard W. Porter, International<br>Cooperation |
| Otto A. Hoberg, Chaps. 9 and 22     | James E. Rorex, Chap. 22                        |
| H. H. Hosenthien, Chap. 20          | Ludwig Roth, Chap. 36                           |
| Dieter K. Huzel, Chap. 32           | Harry O. Ruppe, Chap. 6                         |
| W. G. Johnson, Chap. 16             | Eugen Sanger, Chap. 14                         |

H. Schlitt, Chap. 25	F. A. Speer, Chap. 26
Hellmut Schmid, Chap. 35	E. A. Steinhoff, Chap. 38
Albert E. Schuler, Chap. 24	Ernst Stuhlinger, Chap. 15
R. J. Schwinghamer, Chap. 31	Arthur W. Thompson, Chap. 34
Robert N. Seitz, Chap. 15	James A. Van Allen, Chap. 33
Karl Sandler, Chap. 23	James E. Webb, Prologue
R. D. Shelton, Chaps. 11 and 16	James R. White, Chap. 23
Robert L. Smith, Jr., Chap. 2	Richard S. Young, Chap. 37
William C. Snoddy, Chap. 10	Helmut Zoike, Chap. 30

## Preface

Whenever Wernher von Braun is asked the secret of his amazing success, he invariably answers, "It's not my success; it's the success of our team!"

Ever since Wernher von Braun joined a group of young rocket enthusiasts on the "Raketenflugplatz Reinickendorf" more than 30 years ago, he has been the center of a team. Obsessed by a passionate drive to make space flight come true, he easily conveyed the same passion to those who gathered around him. There has often been, to Dr. von Braun's delight, a good deal of honest arguing and disputing within the team about the best technical approach; however, the many individual thrust vectors were always aligned toward the same common goal: the continuous evolution of space flight. Predecessors and contemporaries of Dr. von Braun may have had a visionary genius equal or superior to his, but none of them had his gift of awakening in others such strong enthusiasm, faith and devotion, those indispensable ingredients of a successful project team. In the Peenemünde days, there were about 10,000 men and women in industry, universities, and the government who belonged to the team and made their contributions to the development of the V-2 although they had never seen the little island of Peenemünde in the Baltic Sea. When Dr. von Braun speaks of "the team" today, he does not identify it by his own name, but by the project on which the team is working; and he includes everyone in government, universities, and industry who ever gave a helping hand to the Redstone, the Explorer satellites, the Pioneer lunar probes, the Jupiter, the Pershing, and the Saturn.

What are Dr. von Braun's most remarkable talents? Those who have met him only once may believe that he is most talented in the role in which they saw him. Perhaps he was, at the time, describing a project to a congressional committee in a presentation which was outstanding for technical competence, acuteness of expression, and power of persuasion. Or, perhaps, he was addressing an audience of legislators or educators with a brilliant speech on the need for a better educational system in our country. He may have been discussing, among his close associates, the team's role in future space exploration projects or debating the merits of his point of view with an adversary, which often converted the adversary into an ally and admirer. Visitors to the George C. Marshall Space Flight Center in Huntsville often express the belief that his most striking accomplishment was the building up of a team and endowing it with a phenomenal stability that has carried it through almost 20 years of turbulent and hectic work. Others may think that he is at his best when it comes to the initiation of a bold new project, when he takes the right step exactly at the right time and in the right place.

However, those who have worked with him for years point to another gift that may be more responsible for his unparalleled successes than any other of his many brilliant talents. It is his innate capability, as a great engineer, to make the transition from an idea, a dream, a daring thought to a sound engineering plan and to carry this plan most forcefully through to its final accomplishment. His teammates, intimately involved in this process, have seen it happen many times; the V-2, the Redstone, the Jupiter, the Explorer satellites, the Moon probes, and now the big Saturn project, all went through this transition.

The reins are loose during the first phase: many ideas are considered and pursued--the best ones coming frequently from Dr. von Braun himself; a large number of studies are made; different designs are investigated; schedules are established and modified. Ideas of others are analyzed and compared, and opinions are requested from many outside sources. Every possible facet of the new project is discussed in technical meetings where Dr. von Braun always provides guidance with the most inquisitive questions, with the sharpest mind, with the most convincing arguments, and with the most tireless quest for further analyses. By the time the project is ready for its engineering phase, Dr. von Braun is by far the best informed man. There is no part of the project scope which he does not fully understand, no major step which he cannot justify. This is the time when the analytical phase of the project makes the transition into the project synthesis. Some of the team members reduce or terminate their contributions to the project at this point, while the efforts of others become more vigorous.

Dr. von Braun stays in the project with full authority, but re-orientes his effort: objectives are now delineated; designs are frozen; project engineers are named; responsibilities are assigned; a systems management is organized; and a development and test schedule is established which, from then on, is the holy gospel of the project. The process is like well-defined crystals precipitating from a super-saturated solution: each part of the project is clearly defined, every seamline becomes visible from beginning to end. Dr. von Braun, the unchallenged master of each phase of the project, holds the many strings of the system in his hands--those leading to his own group and those leading to the many companies contributing to the project. As work progresses, cross contacts between all the members of the project team provide an ample and continuous flow of information. Normally, decisions need be made during this phase only when unforeseen difficulties arise. These difficulties are invariably brought before Dr. von Braun not because he orders it but simply because everyone knows that he finds better and faster solutions than anyone else. And, what is even more important, everybody accepts his decisions with satisfaction.

This very careful and conscientious organization of the engineering phase of a rocket or spacecraft project makes it relatively easy to establish and maintain prime schedules. It may not be too surprising therefore that the completion dates of Dr. von Braun's projects generally coincide well with the promised dates. Or, to put it differently, the schedules are established so that they can be promised with a clear conscience.

This system of scheduling does not lead, however, to the customary spectacular and glamorous promises of anticipated accomplishment. It prompted a noteworthy remark from the late Dr. Donald Quarles, Assistant Secretary of Defense, who some years ago headed an investigating committee for missile projects and who obviously knew the rules of salesmanship inside and out. After touring the other missile development centers of the country, he visited the Redstone Arsenal at Huntsville, Alabama. When Dr. von Braun's presentation was over, Dr. Quarles said: "What you have shown me here gives me an excellent impression of sound engineering; but, fellows, when I compare you with other centers, I must tell you one thing: you are very poor promisers!"

Dr. von Braun has successfully solved one of the most acute problems facing the manager of a team effort: he delegates many of the management responsibilities to his deputy directors, concentrating his own efforts primarily on program planning and on project engineering. This delegation enables him to concern himself with detailed technical and scientific questions and to maintain a uniform, well-balanced program structure throughout each of his projects. Leading a bold idea from its conception to its accomplishment--this is where Dr. von Braun puts his mind, and his heart.

"I am an evolutionary, but not a revolutionary," Dr. von Braun often says. In fact, the history of his last 30 years has some resemblance to the steady evolution of a live organism. Every achievement during that time was accomplished by the energetic but quiet and patient fulfillment of directives given him. It is no secret, though, that these directives did not come (and perhaps would never have come) without some persuasive influence on his part: the first flight of an inertially guided, liquid propellant rocket (A-5) in 1937; the first flight of a radio-guided, liquid propellant rocket with substantial payload (V-2) in 1942; the first large guided rocket (Redstone) in this country in 1953; the first high-precision inertial guidance system (Redstone) in 1954; the first intermediate range ballistic missile (Jupiter) in 1957; the first ablation reentry nose cone in 1957; the first U.S. satellite (Explorer I) in 1958; the first monkeys into and back from space (Able and Baker) in 1959; the first U.S. space probe near the Moon (Pioneer IV) in 1959; the first U.S. astronaut in space (Shepard) in 1961; the first big space carrier (Saturn C-1) in 1961.



In all these projects, Dr. von Braun adhered painstakingly to the letter and the spirit of his orders. Those who know Dr. von Braun best agree that the strongest guiding force in his life is his desire to be absolutely loyal to his superiors.

Wernher von Braun was 50 years old on March 23, 1962. When this day began to approach, many of his former and present associates desired to show their affection by a birthday gift worthy of the event.

It is customary in the scientific community to honor a respected master on his fiftieth birthday with a volume of papers written by those who have been privileged to work with him. What could be more appropriate for Wernher von Braun than a volume of technical and scientific papers on the subject which, for more than 30 years, has been so close to his heart? The only problem was in keeping the number of enthusiastic contributors small enough to hold the volume within manageable size.

Here is our book, Dr. von Braun: please accept it as a sign of our deepest admiration. You will find-- although you would never admit it--that many of the thoughts expressed in the following pages are fruits from seeds you have planted.

Your first 50 years have been filled with magnificent accomplishments, yet they are only a prelude to what the future may bring: the fulfillment of your boldest dream, a trip to the planet Mars, for you-- and for the rest of us, your safe return to Earth.

Ernst Stuhlinger  
Frederick I. Ordway, III  
Jerry C. McCall  
George C. Bucher

## CONTENTS

	Page
List of Contributors . . . . .	v
Preface . . . . .	vii
Prologue <i>James E. Webb</i> . . . . .	1

### SYSTEMS AND OPERATIONS

1. Development of the Saturn Space Vehicle	<i>Oswald H. Lange</i>	5
2. Prelaunch Readiness of Space Vehicles	<i>Robert L. Smith, Jr.</i>	25
3. The Evolution of Launch Concepts and Space Flight Operations	<i>Kurt H. Debus</i>	43
4. Space Carrier Vehicle Firing Histories	<i>Frederick I. Ordway, III</i>	63
5. Automation in Orbital and Space Missions	<i>William L. Mitchell and Charles O. Brooks</i>	95
6. On the Theory of Optimization of Step Rockets	<i>Harry O. Ruppe</i>	107
7. Evolution of Earth-Lunar Transportation Systems	<i>H. H. Koelle</i>	121

### SPACECRAFT DESIGN AND ENGINEERING

8. History of the Cluster System	<i>William H. Pickering</i>	141
9. Explorer Satellites Launched by Juno 1 and Juno 2 Vehicles	<i>J. Boehm, H. J. Fichtner, and Otto A. Hoberg</i>	163
10. Correlation of the Thermal Behavior of Satellites and the Rotational Momentum Vector	<i>Gerhard B. Heller, Billy P. Jones, Robert J. Naumann, and William C. Snoddy</i>	203
11. Problems in Radiation Shielding for Space Vehicles	<i>J. W. Keller, M. O. Burrell, R. D. Shelton, and J. A. Downey, III</i>	241
12. Evaporative Film Cooling for Hypersonic Reentry Vehicles	<i>Rudolf Hermann</i>	261

### PROPULSION

13. Development Trends of Liquid Propellant Rocket Engines	<i>A. A. McCool and Keith B. Chandler</i>	289
14. Über Ballistische und Aeronautische Raumfahrt	<i>Eugen Sänger</i>	309

	Page
15. <i>N63-15991</i> Electric Propulsion - A New Technology <i>Ernst Stublinger,</i> <i>Gerhard B. Heller, Robert N. Seitz, and George C. Bucher</i> . . . . .	319
16. <i>N63-15992</i> A Performance Analysis of Electrical Propulsion Systems <i>R. D. Shelton, W. G. Johnson, Billy P. Jones, and J. C. King</i> . . . . .	349
17. <i>N63-15993</i> A Proposed Electric Spaceship Engine <i>Hermann Oberth</i> . . . . .	377
<b>GUIDANCE AND CONTROL</b>	
18. <i>N63-15994</i> Inertial Guidance, its Evolution and Future Potential <i>J. S. Farrior</i> . . . . .	399
19. <i>N63-15995</i> Guidance and Control Systems for Space Carrier Vehicles <i>W. Haussermann, G. G. Gassaway, and F. B. Moore</i> . . . . .	413
20. <i>N63-15996</i> Flight Simulation of Rockets and Spacecraft <i>H. H. Hosenthien and J. Boehm</i> . . . . .	437
21. <i>N63-15997</i> A Comparison of Two Superconductive Bearing Principles <i>T. A. Buchhold</i> . . . . .	471
<b>INSTRUMENTATION AND TRACKING</b>	
22. <i>N63-15998</i> Telemetry Development for Large Guided Missiles and Space Carrier Vehicles <i>Otto A. Hoberg and James E. Rorex</i> . . . . .	487
23. <i>N63-15999</i> Application of the Doppler Principle to Rocketry <i>Karl Sendler, James R. White, and Rudolf Bruns</i> . . . . .	517
24. <i>N63-16000</i> Space Vehicle Tests and Measurements <i>Daniel H. Driscoll</i> <i>and Albert E. Schuler</i> . . . . .	535
25. <i>N63-16001</i> Torque Modulation and Modulation Error Detection Concepts in Modern Guidance Instruments <i>H. Schlitt</i> . . . . .	561
26. <i>N63-16002</i> Ground Versus On-Board Tracking for Space Navigation <i>F. A. Speer and H. F. Kurtz</i> . . . . .	573
27. <i>N63-16003</i> Pilot Manufacturing for Spacecraft <i>Wilhelm Angele</i> . . . . .	601

## ENGINEERING AND COMPONENTS

28. Manrating Space Carrier Vehicles *Joachim P. Kuettner* . . . . . *N63-16004* 629
29. Electrical Systems in Missiles and Space Vehicles *H. J. Fichtner* . . . . . *N63-16005* 641
30. The Propellant Management Field *Helmut Zoike* . . . . . *N63-16006* 653
31. Stored Energy and Magnetic Fields in Space Applications *R. J. Schwinghamer* . . . . . *N63-16007* 685
32. The Interval Transformer Tank Level and Flow Gage *Dieter K. Huzel* . . . . . *N63-16009* 711

## PHYSICS AND BIOLOGY

33. Observation of Galactic and Solar Cosmic Rays with Explorer 7 *Wei Ching Lin and James A. Van Allen* . . . . . *N63-16009* 725
34. Scientific Results from Juno Launched Spacecraft *Charles A. Lundquist, Arthur W. Thompson, and Ray V. Hembree* . . . . . *N63-16010* 749
35. The Relationship between Geodesy and Rocketry *Hellmut Schmid* . . . . . *N63-16011* 769
36. The Influence of Man on the Design of Spacecraft *Robert G. Lindberg, Charles F. Lombard, and Ludwig Roth* . . . . . *N63-16012* 775
37. Experimental Biology in Space *Richard S. Young* . . . . . *N63-16013* 791
38. A Possible Approach to Scientific Exploration of the Planet Mars *E. A. Steinboff* . . . . . *N63-16014* 803
- International Cooperation in Space *Richard W. Porter* *N63-16015* . . . . . 837
- Epilogue *Walter R. Dornberger* . . . . . 851

#### ACKNOWLEDGMENTS

The editors express their appreciation for the excellent cooperation of the many authors who contributed to "From Peenemünde to Outer Space." Special thanks are due Ira Remer, Mitchell R. Sharpe and William J. Ziak of the George C. Marshall Space Flight Center for their continuous assistance in the production of this volume.

## Prologue

James E. Webb

Administrator  
National Aeronautics and Space Administration  
Washington, D. C.

I am delighted that present and former colleagues of Dr. Wernher von Braun are carrying forward in this country a fine European custom in honoring an outstanding individual with a collection of technical papers on his fiftieth birthday.

Dr. von Braun, as Director of NASA's Marshall Space Flight Center-- which has charge of facilities in Huntsville, Alabama; Cape Canaveral, Florida; Southwest Mississippi; and New Orleans, Louisiana--is responsible for the development of the large launch vehicles required to carry out many projects involved in the national space program. A heavy burden of responsibility rests on his shoulders because it is in the area of large launch vehicles that the United States has lagged in the past. We are confident that Dr. von Braun and his team of scientists and engineers will fulfill that responsibility well.

It was the von Braun team, working in collaboration with another outstanding group of scientists at the Jet Propulsion Laboratory of the California Institute of Technology, which produced the Jupiter C (Juno 1) that launched Explorer 1, the first United States satellite. The same combination produced the Juno 2 vehicle that launched Pioneer 4, the first United States spacecraft to be propelled free of the Earth. The von Braun team produced the Redstone, a modification of which became the launch vehicle for the first two American astronauts on suborbital space flights in Project Mercury. Finally, this team developed the Saturn that was launched October 27, 1961--the heaviest object that we, or to our knowledge anyone else, have launched into space.

Still more challenging tasks lie ahead for the National Aeronautics and Space Administration. But with scientists of the caliber of Wernher von Braun in our ranks, I am sure that we will accomplish them.

## DEVELOPMENT OF THE SATURN SPACE VEHICLE

Oswald H. Lange

Saturn Systems Office  
George C. Marshall Space Flight Center  
National Aeronautics and Space Administration  
Huntsville, Alabama

The Saturn launch vehicle program has become a major element in our national space effort within little more than 3 years. At the beginning of the program, in 1958, various Saturn configurations were planned to lift instrumented payloads of 20,000 to 40,000 lb into Earth orbit. As research and development progressed, it became apparent that the vehicle design approach had far more potential than anticipated - that it was, in fact, a breakthrough into a new class of heavy launch vehicles.

Thus, within the space of a few years, it was possible to consider even more advanced missions. In addition to placing multiton payloads in orbit, we can seriously conceive sending over 90,000 lb of instruments on escape missions, using advanced Saturn-class vehicles. With these vehicles, we plan to accomplish lunar reconnaissance and manned lunar landings scheduled for the latter part of this decade. Likewise, these vehicles will permit flight tests of advanced nuclear power plants and stages.

The increased performance of these advanced launch vehicles is a direct result of the first (C-1) Saturn development program. The advanced vehicles are to be considerably larger than the present Saturn while not requiring designs or concepts greatly beyond the present state of the art. Basically, they are extensions of the present program, the summation of research and development activities, and long range planning making up the C-1 program.

To understand present trends in vehicle development, we must turn to the C-1 development program. In this paper we will review some of the major decisions and activities made during the C-1 development. These link together, step by step, from the concept of a multistage carrier vehicle to vehicles that will support advanced missions in space.

**Preceding page blank**

During 1957, the Department of Defense considered certain advanced missions using space devices for communication. Clear need was also seen for other scientific payloads, including weather satellites and heavily instrumented space probes. The weight of these satellites, however, virtually precluded the use of available military missiles. To orbit 20,000 to 40,000 lb of payload or to escape with 6000 to 12,000 lb required a booster stage generating about 1,500,000 lb of thrust.

A heavy payload capability was urgently needed. In consequence, development of a high-thrust booster with associated equipment had to be accomplished within an exceedingly short time. Moreover, the development had to be performed within strict budgetary limitations.

In terms of design simplicity, a booster stage using a single engine was preferable. In 1957, no such engine existed, although feasibility studies of a rocket engine producing about 1,000,000 lb of thrust were being performed under an Air Force program. Full-scale tests of this engine were still 2 years away, a delay too long for the accelerated booster program.

For this reason, our designers considered several clustered booster concepts, securing the required thrust by grouping a number of engines and off-the-shelf tankage into a single stage. One of these early concepts proposed clustering four Rocketdyne E-1 engines, each providing 360,000 lb of thrust. The E-1 was still early in development; however much time and cost were required to make it operational. The proposal was dropped for these reasons, and preliminary design work continued on other concepts.

What would become the Saturn program was formally initiated on August 15, 1958. On that date, the Advanced Research Projects Agency (ARPA) of the Department of Defense authorized development of a 1,500,000 lb thrust booster using a cluster of available rocket engines. The design of the Thor/Jupiter S-3D engine was selected for this application. Besides being flight tested and of proven reliability, the design was straightforward and adaptable to the booster at relatively low cost.

On September 11, 1958, Rocketdyne was selected to modify the S-3D engine design. Engine packaging was improved and the lubrication system was simplified. Engine starting was simplified to use a solid propellant drive turbine spinner and hypergolic ignition. The turbopump, mounted on the swivel-suspended combustion chamber, was deflected along with the chamber, so that the flex lines carried only the low-intake pressure of the pumps. Using LOX and RP-1 propellants, the engine would initially produce 165,000 lb of thrust; additional development would give up to 188,000 lb of thrust. Eight of these H-1 engines were clustered to produce the total thrust needed.



Engine redesign had just begun when, in October 1958, the ARPA program objectives were expanded. The booster to be developed would serve as the first stage of a multistage carrier vehicle, capable of performing advanced space missions. Four flight vehicles were authorized. A static firing test to demonstrate the feasibility of the clustering concept was scheduled by the end of 1959, with the first flight test planned for late in 1960.

The final two flight vehicles would use unsophisticated upper stages to provide a payload capability as rapidly as possible. While design of the booster continued, parallel studies were carried out to define the upper stages and identify staging problems. Concurrently with this activity, work began in December 1958 to determine design requirements of the launch facility and the required static test facilities.

A series of studies indicated that already proven IRBM and ICBM components could be adapted for use as upper stages of the new vehicle. These off-the-shelf components would permit rapid development with a minimum expenditure of funds. As a result of these studies, in May 1959 a modified Titan missile with a 120-in. diameter was selected as the second stage.

The Centaur vehicle, under development by Convair, was selected as the third stage. This selection was guided by the necessity to choose components capable of satisfying current needs and of being easily adapted to future requirements.

The choice of Centaur had far-reaching effects on the Saturn development program. At this time, Pratt & Whitney, in association with Convair, was developing a new rocket engine. A major breakthrough, this engine burned liquid hydrogen and liquid oxygen, providing approximately 50 per cent more specific impulse than conventional hydrocarbon fuels. To take full advantage of this development, it was decided that the new engine would become the propulsion unit for the third Saturn stage. By the time second-stage testing was complete, the engine would be sufficiently developed for use with the third stage.

While speeding development of the immediate vehicle, use of the Titan-type second stage did not provide the desired performance. On July 29, 1959, ARPA ordered that effort be redirected from the Titan to development of larger-diameter upper stages to support certain spacecraft projects. Authorization was given to consider components other than those available from ICBM programs.

A series of studies began of upper stage configurations for the Saturn vehicle. Late in October, four upper-stage combinations were proposed. The most feasible of these was identified as the Saturn B-1. Offering the best growth potential and mission flexibility, plus the

best cost to payload-weight ratio, the B-1 included a second and third stage 220 in. in diameter, both using liquid hydrogen engines. The principal disadvantage was that the B-1 required either a high initial cost in the first two years of development or a longer development schedule, with corresponding delays in operational availability.

As a result, a further series of studies was performed, culminating in December 1959, with a recommendation by a NASA appointed team, headed by Dr. A. Silverstein, that the present C-1 vehicle configuration be adopted.

The Silverstein Report marked a major milestone in the Saturn program. A long-range vehicle development program was recommended, beginning with the C-1 Saturn. Advanced configurations, the C-2 and C-3, would evolve by adding advanced, high-thrust stages to the initial configuration.

The C-1, based on a first stage clustered booster, would use liquid hydrogen as fuel for the upper stages. Ten R&D vehicle flights were planned. In addition, a high-thrust liquid hydrogen engine, generating 200,000 lb, would be developed for use on advanced vehicle configurations, beginning with the C-2.

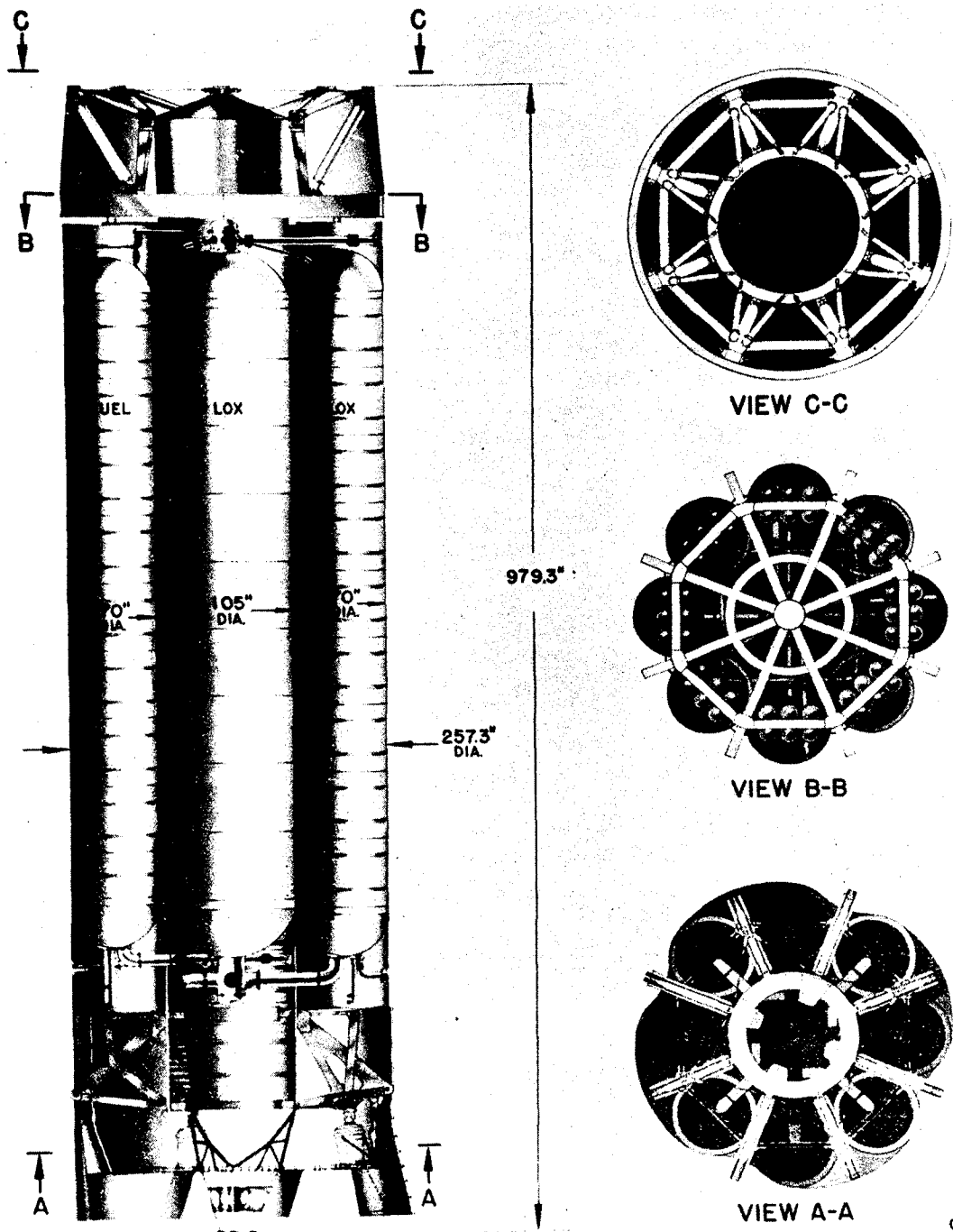
The three-stage C-1 configuration evolving from these plans offered distinct advantages in terms of payload capability at an early date in addition to a final configuration that would fully exploit the performance of the booster stages. The vehicle itself would be about 185 ft high and weigh over 1,000,000 lb when fully fueled. About 750,000 lb of this weight would be propellants.

The booster, or S-I stage, used in the first portion of the present R&D flight test program, is substantially the same as that first proposed (Fig. 1.1). The stage is 82 ft long and 21.5 ft in diameter. It is powered by eight H-1 engines, each producing 165,000 lb of thrust; later in the R&D program, these engines will be rated at their full 188,000 lb of thrust.

The engines are attached to a thrust frame on the aft end of the stage. The four inboard engines are rigidly fixed at a 3 deg cant to the vehicle centerline. The four outboard engines, canted at 6 deg and mounted to alternate outriggers, are mounted on gimbals that permit them to be turned  $\pm 10$  deg. This permits vehicle roll and attitude control during the first phase of flight, which lasts about 120 sec.

The general booster structure consists of nine tanks, an upper-stage adapter, tail section, and shrouding. The tail section, composed largely of 7075-T6 aluminum, includes a corrugated central barrel, eight outriggers, firewall, heat shield, shrouding, and associated members. The tail section also provides support and holddown points.

# **SYSTEMS AND OPERATIONS**



GE 79-59  
2 JULY 59

Fig. 1.1 Saturn booster structure.

Preceding page blank

Eight 70-in. propellant containers, four fuel and four oxidizer, are clustered alternately around a central 105-in. oxidizer tank. All tanks are of semimonocoque construction, built up from 5456-343 aluminum skin segments. The oxidizer tanks carry the entire axial loading from the upper stages. Four other containers contribute only to lateral stiffness, since they must have a slip joint on their upper end to compensate for the 2.5 in. shrinkage of the oxidizer tanks after filling.

Each of the container systems is interconnected to permit equalizing the liquid level during propellant loading and flight. The total capacity of the containers is 750,000 lb. Sloshing is suppressed by fixed baffles running accordion-like down the interior of the tanks.

The oxidizer tanks are pressurized by gaseous oxygen, obtained by passing a small portion of the liquid oxygen flow through heat exchangers and channeling the gas through a manifold system at the top of the booster. In this way, equal pressure is furnished for all oxidizer tanks. The fuel containers are pressurized by gaseous nitrogen, carried in 48 Fiberglas spheres at the top of the booster.

The upper-stage adapter and spider beam assembly consists of an I-beam and tube truss combination, which holds the upper ends of the clustered tanks and provides support for the upper stage. For this latter purpose, a 220-in. diameter mounting ring is located 90 in. above the spider beam. Eight 7075-T6 aluminum extruded I-beams compose the spider. The beams attach to each outboard oxidizer tank. Lateral restraint is provided for the fuel containers.

The upper shroud provides a transition between the 257-in. diameter S-I and the 220-in. diameter second stage S-IV. The stainless steel shroud supports the telemetry antennas and a power supply umbilical connection point. The tail shroud, designed to minimize the effects of inflight air flow and high-altitude jet ballooning, is attached to the tank section and extends to a point somewhat below the level of the heat shield. The shroud is composed of aluminum alloy skin for the upper panels, with stainless steel used for the lower panels because of the higher temperatures encountered.

Protection against heat radiation is provided by a heat shield located at the levels of the throats of the engines. A separate flame shield to prevent backflow is mounted in the diamond-shaped area between the nozzles of the four inboard engines. A fire wall, located immediately above the engine compartment, protects the fuel and oxidizer tanks in case of engine compartment fires.

The on-board electrical network system integrates all vehicle electrical, electro-mechanical, and electronic equipment in a single functional system. A major design parameter of this system was the provision for checkout and countdown procedures. The vehicle network

consists of about 500 electrical cables, interconnecting a group of distributor boxes, which, in turn, combine junction and relay patch boards in single units.

For the initial boosters, four instrument canisters are located in the upper-stage adapter. These canisters contain the telemetry and tracking transmitters, power distribution functions, guidance and control units, and related instrumentation. On later vehicles, this equipment will be contained in an instrument unit, located between the payload and last stage.

The S-I stage control system uses thrust vectoring to achieve the control torques required to stabilize the vehicle. Control forces are obtained by engine gimbaling in response to signals from the flight control computer, activating the two hydraulic actuators for each engine. Certain Jupiter system components have been adapted for use in this system. Rate gyros are used as sensing elements, an application dictated by structural bending of the large and relatively flexible vehicle. A shaping network separates structural bending from the synthetic control mode.

In carrying out the general development philosophy at MSFC, it was decided that the guidance system would be standardized as far as possible (Fig. 1.2). This assures maximum use of proven components, eliminates considerable development expense, and allows the vehicle to support readily a variety of missions. This concept is termed the adaptive guidance mode and is sufficiently comprehensive to include all foreseeable guidance schemes. The fundamental principle of the adaptive guidance mode is that any specific guidance scheme derived from the general mathematical structure will cause the vehicle to fly an optimum trajectory. The assigned mission dictates the features for optimum development.

The guidance system includes an inertial reference subsystem comprising a stabilized platform and accelerometers, platform electronics, and associated ground support equipment. The guidance computer subsystem consists of a guidance computer, guidance signal processor, and a body-fixed accelerometer. A number of Jupiter and Juno 2 components (including the ST-90 stabilized platform) have been selected for the very early flights, since they have the accuracy, size, and weight suitable for the Saturn.

The second stage of the Saturn launch vehicle (S-IV) is under development by the Douglas Aircraft Corporation (DAC). The S-IV stage represents the second application of liquid hydrogen technology to a space vehicle (Centaur was the first); as a result, the stage includes many design innovations. Formal procurement of the S-IV began in July 1960 when DAC was requested to design, develop, and test a four-engine stage. Later, in March 1961, the number of engines was increased to six, providing better inflight control and increased payload capability.

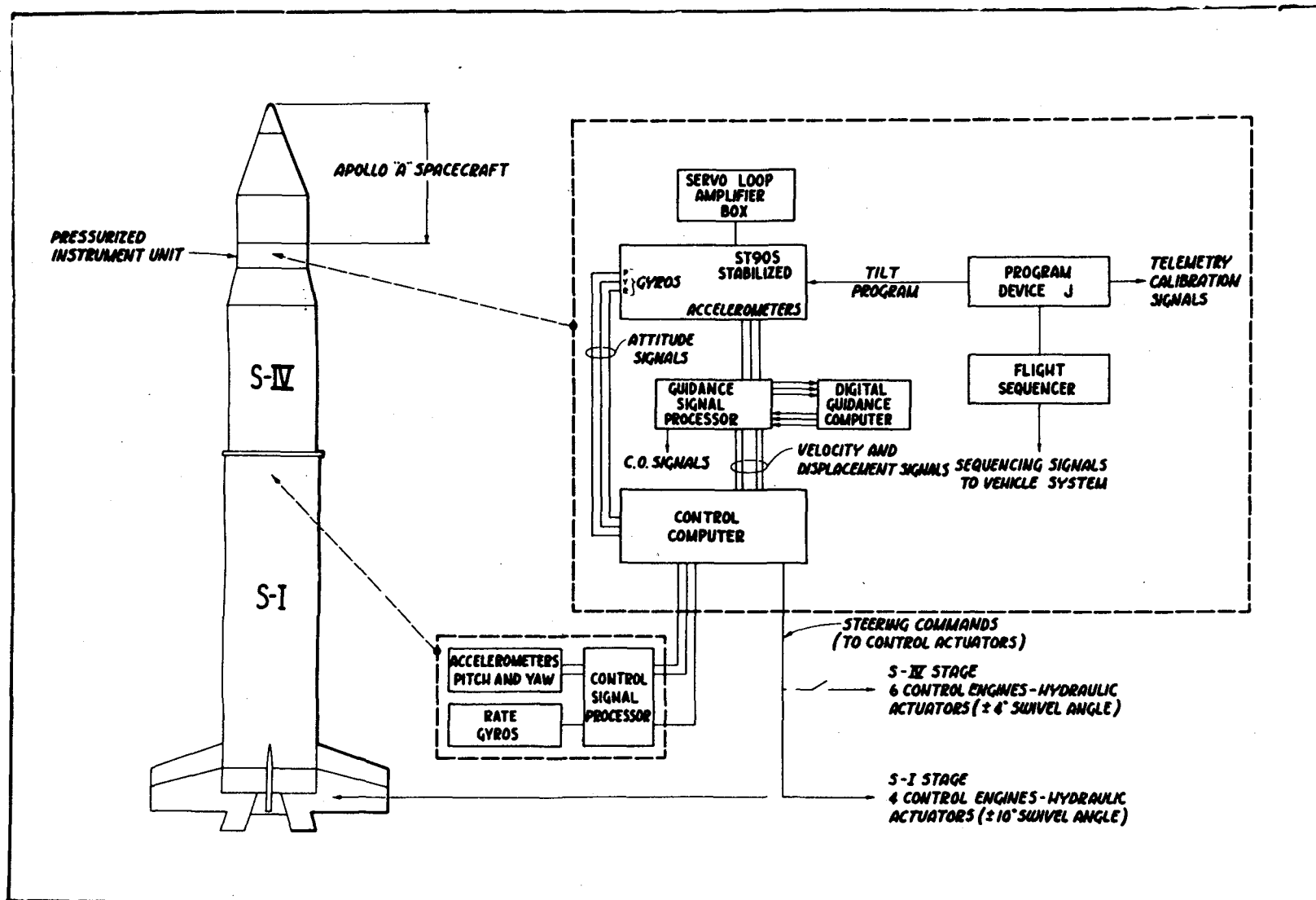


Fig. 1.2 Guidance and control system, C-1 Saturn (block II).

The present S-IV stage is about 41 ft in length, with a diameter of 220 in. (Fig. 1.3). The stage is powered by six liquid hydrogen RL10A-3 engines (also used on the Centaur vehicle) being developed by Pratt & Whitney. Each engine will provide 15,000 lb of thrust for a total stage thrust of 90,000 lb.

The stage is a self-supporting structure containing two propellant tanks fabricated of 2014-T6 aluminum alloy. The liquid oxygen tank, located aft, is separated from the liquid hydrogen tank by a common insulated bulkhead made of a Fiberglas, honeycomb core between aluminum faces. The bulkhead is designed to withstand reverse pressures that may result from maximum pressure in the liquid hydrogen tank and ambient pressure in the oxidizer tank while the vehicle is on the launch pedestal.

The cylindrical portion of the tank consists of three segments of machine-milled waffle skin, longitudinally welded. End bulkheads, fabricated from six segments, are welded to form a hemisphere. All welds are made in sections thickened to keep stresses well below the yield point in the "as welded" condition.

The entire inner surface of the hydrogen tank, excepting only the common bulkhead, is insulated. Slosh baffles are included in both tanks.

The engine thrust structure, a truncated cone of conventional skin and stringer construction, is bolted to the aft bulkhead. A base heat shield is installed behind the gimbal plane; the shield, constructed of an insulated honeycomb sandwich, is supported from the thrust structure. Additional thermal protection is afforded the structure and components located forward of the base heat shield.

The forward interstage structure and aft skirt are constructed of aluminum honeycomb core between aluminum faces. The aft end of the skirt forms the forward face of the S-I and S-IV inflight separation plane.

The S-IV vehicle is steered by gimbaling the six engines in response to signals contained in the vehicle instrument unit, located forward of the stage. The S-IV mounted control hardware is capable of providing engine deflection rates proportional to the pitch, yaw, and roll control signals, furnished by the MSFC guidance and control computer. The engines, mounted with an outboard cant of 6 deg, can be gimbaled  $\pm 4$  deg. The engines are attached to the conical aluminum thrust structure joined to the aft bulkhead. Propellants are supplied to the engines through individual, low-pressure ducting from pressurized propellant tanks.

Separation of the S-I and S-IV stages takes place at the time when an electrical signal triggers explosive bolts installed at the aft separation plane. Separation is accomplished by retrorockets on the S-I stage and



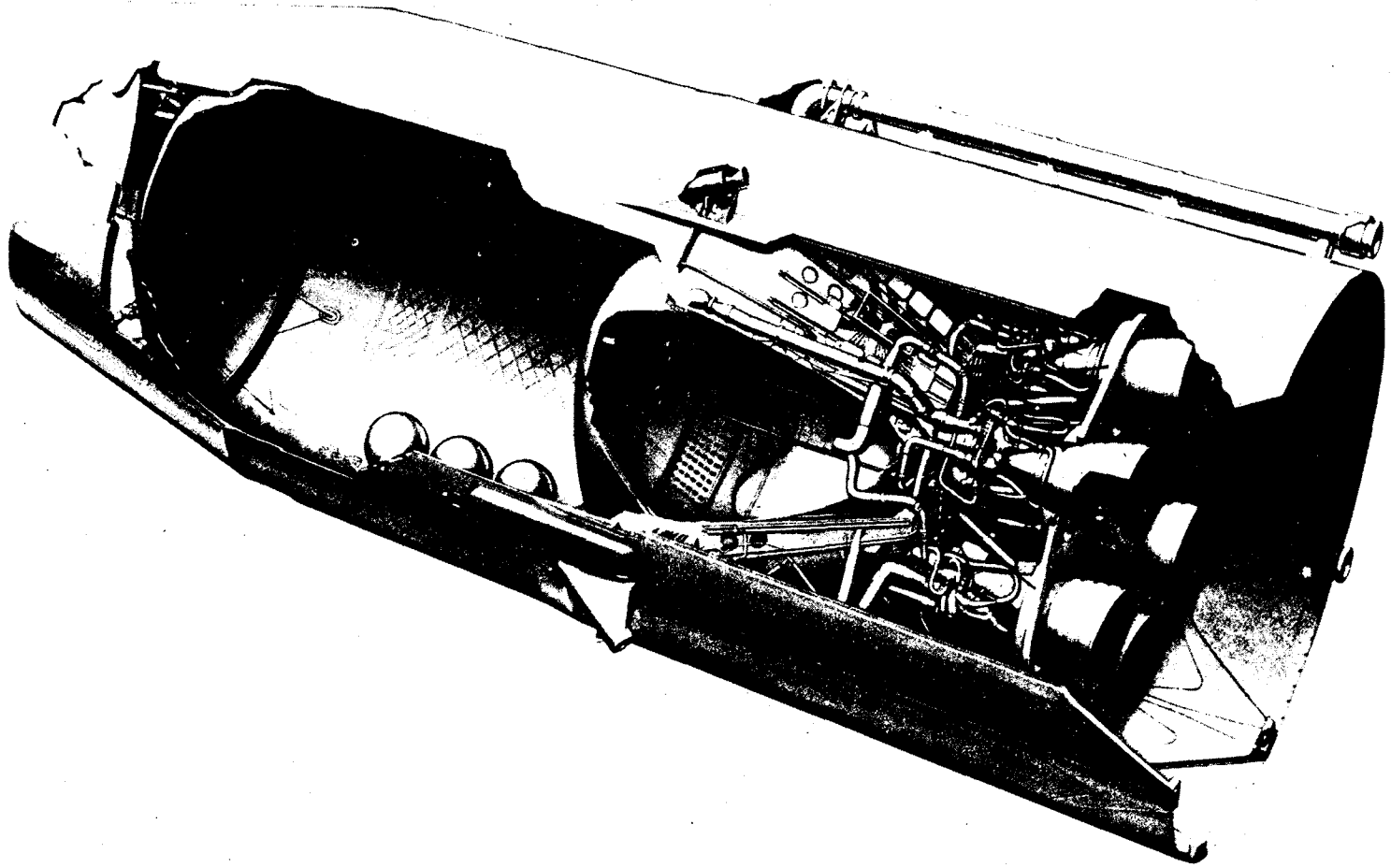


Fig. 1.3 Saturn S-IV stage.

ullage rockets on the S-IV vehicles. The ullage rockets give sufficient forward movement to the S-IV to position the propellants before engine ignition. A short period of uncontrolled coast occurs between separation and stage ignition to make sure that the stages are a sufficient distance apart.

Inflight control of the succession of events in the S-IV stage is provided by the S-IV sequencer, a separate unipackaged subsystem that receives signals from the S-I stage, the guidance and control package, and other S-IV subsystems. The sequencer provides sequential commands to initiate S-IV functions and stage separation, and is mounted, with other operational components, in the engine compartment.

NASA policy is to base programs on the use of a few multipurpose vehicles, thus achieving high reliability through many flights. In keeping this policy, the third stage of the C-1 configuration (the S-V stage) was to be the Centaur vehicle, the upper stage of the Atlas-Centaur launch vehicle. Powered by two liquid hydrogen engines, the Centaur vehicle would be slightly modified by increasing the skin thickness to accommodate the heavier Saturn payloads. The vehicle was intended to perform escape and deep space missions.

All of these stages would be used on the proposed C-2 vehicle configuration, differing from the C-1 only in having a new high-energy stage inserted immediately above the booster (Fig. 1.4). Later to be identified as the S-II, this stage was first conceived as using two advanced liquid hydrogen engines, generating a total thrust of 400,000 lb. Being the third application of liquid hydrogen technology to a space vehicle, the stage development program would benefit from the experience gained in the Centaur and S-IV programs.

By the early part of 1960, the Saturn program had taken great strides toward developing an operational launch vehicle. The first eight prototype engines were initially tested on a single engine test stand. Then, on March 28, two engines were fired together; on April 6, four engines were fired; and, finally, on April 29, all 8 engines of the booster were fired in demonstration of the clustered booster concept. On May 26, 1960, assembly of the S-I stage began for the first flight vehicle. In the same month, Rocketdyne was awarded a contract for the development of an advanced high-thrust liquid hydrogen engine, the J-2, the type defined by the Silverstein Committee in December, 1959.

These varied development programs of stages and engines were paralleled by the F-1 development program, formally initiated as a NASA project in January 1959. The F-1, an engine of simplified conventional design, incorporates proven concepts of liquid propellant technology. Liquid oxygen and RP-1 are burned to generate 1,500,000 lb of thrust. Basic components of the engine are a tubular wall, regeneratively cooled thrust chamber assembly, and direct drive turbopumps, and gas generator.

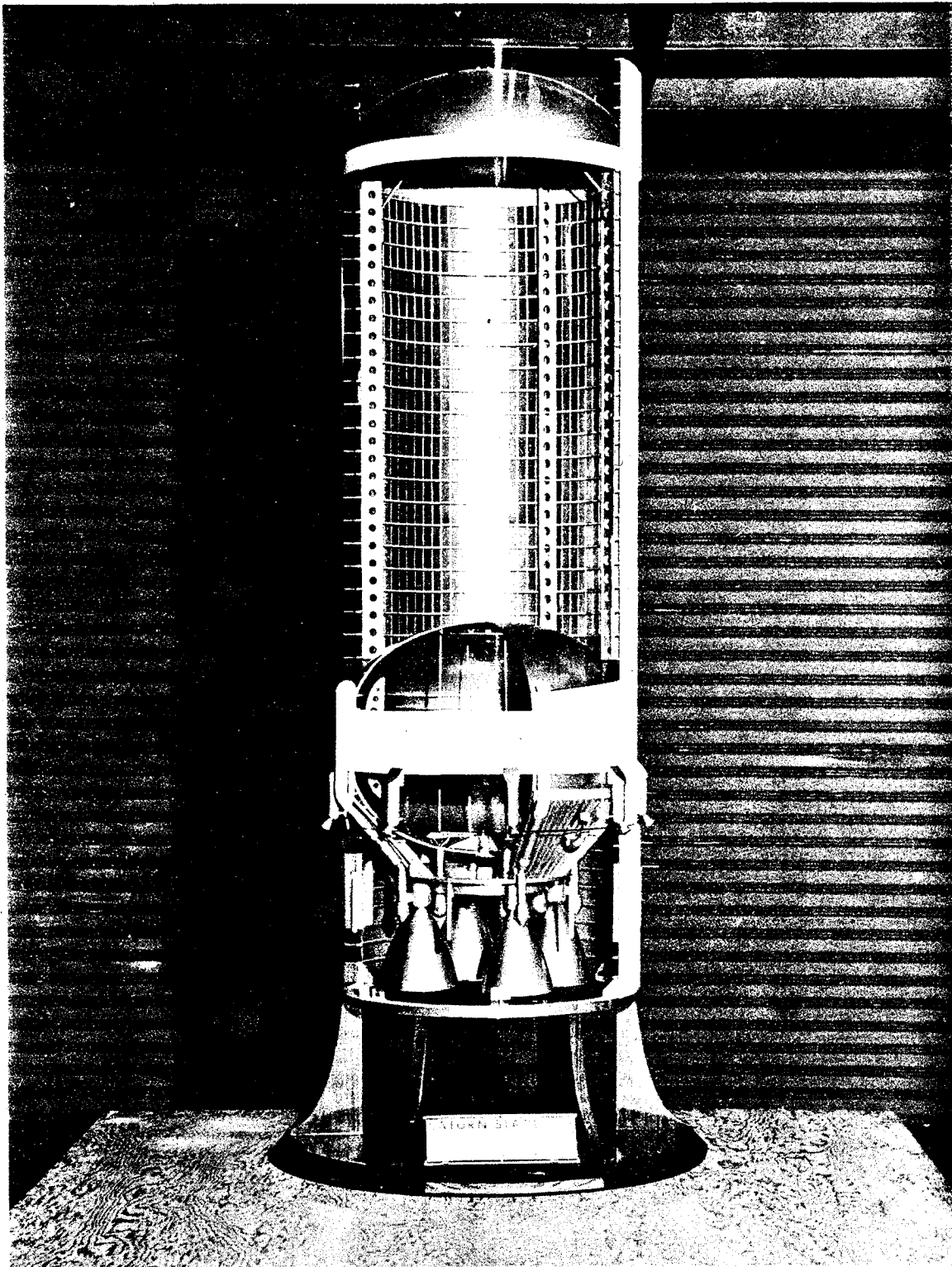


Fig. 1.4 Saturn S-II stage.

To summarize the status of the program at the end of 1960, the S-I and S-IV stage development programs were underway, preliminary design studies of the S-V (modified Centaur) stage had begun; and detailed performance studies of the C-1 configuration were continuing. Static firing of the test booster, modified to the configuration of the SA-1 flight booster, had been completed. Assembly of the first flight booster was almost complete, and assembly of the SA-2 booster was about to begin.

Four individual engine development programs were underway: two liquid hydrogen engines for the Centaur vehicle and the advanced S-II stage, respectively, and the H-1 and the F-1 engines. Studies were also being completed on the C-2 configuration of the Saturn launch vehicle. Concurrently with this activity, construction continued of the launch facilities at Launch Complex 34, Cape Canaveral, and test facilities (including a dynamic test tower) at MSFC in Huntsville.

In May 1961, President Kennedy, in his State of the Union address to the Congress, emphasized that major effort be directed toward circumlunar flights and manned landings on the Moon. Because of the high priority of this effort, MSFC thoroughly reviewed the Saturn program. This review showed that low orbital missions in support of the Apollo program were of primary importance. A two-stage Saturn would provide the performance needed to orbit an Apollo spacecraft and possess the safety requirements required for a manned mission.

Further, it was found that, as lunar mission weight requirements had increased, a vehicle configuration of even greater performance than the C-2 was desirable. These findings were followed on June 23, 1961, by redirection of design effort on the C-2 clarifying concepts of the C-3 and Nova configurations.

While these configuration studies were proceeding, the C-1 ten-vehicle R&D program was being revised. Because of the prime importance of the Apollo project, the mission required for Saturn was reoriented toward the injection of unmanned and manned Apollo spacecraft into earth orbits. As a result of this redirection, development of the S-V stage was deferred because it had been planned for other missions and was not required for the Apollo flights.

Essentially, the present Saturn program will develop a two-stage vehicle capable of supporting the manned mission. The flights will secure experience in the development of multiple-engine stages, launching equipment, procedures, and facilities. This experience will provide the technical basis for design data required for later members of the heavy launch vehicle family.

The C-1 R&D program has been divided into two blocks of vehicles (Fig. 1.5). In Block I, four vehicles (SA-1 through SA-4) will be flown. These will be composed of a live S-I stage, with inert S-IV and S-V stages. Such tests will define flight operation of the booster and explore control and environmental conditions, rf and tracking problems, and procedures for the operation of large vehicles.

The Block II Saturn vehicles (SA-5 through SA-10) will contain design modifications to support the Apollo mission more effectively. Tanks will be lengthened to accommodate a greater volume of propellants. Fins will be added to provide increased vehicle stability. For an extra measure of control, a more flexible and universal guidance and control system is being readied to support the manned mission.

The Block II vehicle will consist of a live, modified S-I stage, a live S-IV stage, a new instrument unit, and payload. Initial flight tests will be designed to study S-I and S-IV staging, S-IV operation, and system guidance and control. Operational procedures will be proved out for the new liquid hydrogen loading facilities at the launch site. Additional flight experience will be secured with the booster and associated facilities and tracking networks.

During the latter portion of Block II testing, Apollo "boiler plate" spacecraft will be tested under actual flight and reentry conditions. Apollo-Saturn interface events or compatibility and detail requirements of reentry heat shielding will be studied.

All these elements represent the evolution of MSFC's basic approach to vehicle development. Each stage is flight tested and thoroughly proved out before proceeding to flight tests of the next higher stage. As a result, desirable design changes can be fully defined and incorporated at a specific cutoff point. Mandatory changes are introduced as required.

Because of the complexity of the Saturn program, its unique development characteristics, and the large costs involved, the stages and associated components must be qualified and tested to a greater extent than in previous programs. Vehicle components must have the same high quality as the first items received for qualification testing. This need illustrates one of industry's main contributions to the program, for industry has played a responsible role not only in S-I component fabrication but in the design and development of stages and engines.

This responsibility is increased many times when the development program puts into practice such innovations as liquid hydrogen technology. A constant effort must be maintained to secure reliable, high quality components produced in response to the latest research developments. To assist the contractor, MSFC has established lines of intraprogram coordination between similar R&D efforts. For instance, details of

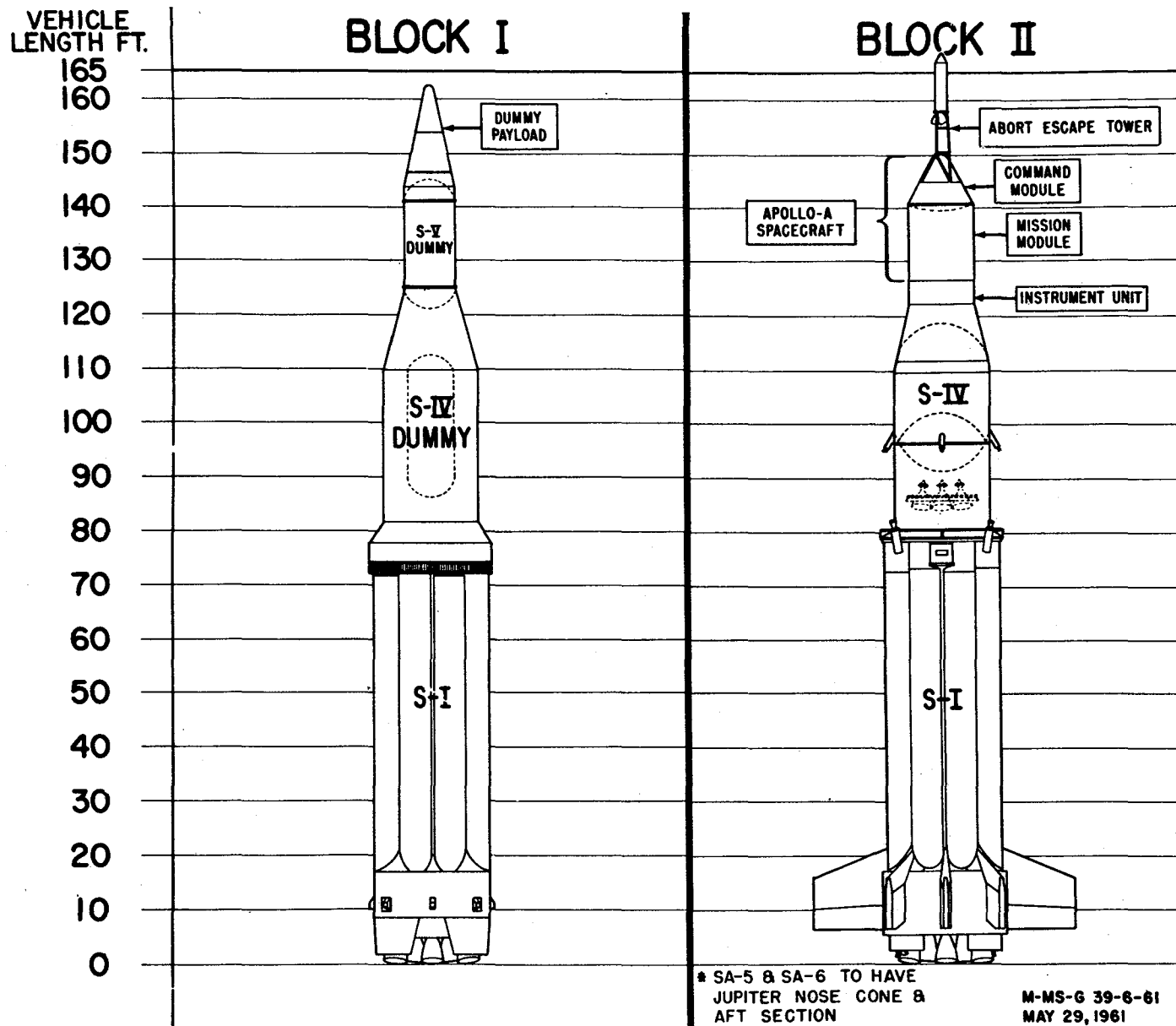


Fig. 1.5 C-1 development vehicle configurations, blocks I and II.

rapidly advancing liquid hydrogen technology were shared by Convair and DAC. In the same way, coordination has been established between DAC and North American Aviation, the latter contractor having been selected in September 1961 to develop and build a four-engine S-II stage for an advanced launch vehicle.

As the C-1 configuration moves toward operational status, industry's participation is secured not only for the research and development phase, but for production. The government-owned Michoud Plant was secured for this purpose early in September 1961. At this plant, operated by industry under the technical direction of MSFC, the C-1 vehicle first stage will be produced along with the F-1 powered booster for an advanced Saturn configuration.

Support for booster static testing, an essential part of the production program, led NASA to announce in October 1961 that a test site would be developed near the plant. Facilities included at this site will permit static firing qualification tests of both the C-1 and the advanced vehicle boosters before release to Cape Canaveral.

NASA Headquarters announced in September, 1961, the selection of Cape Canaveral as the base for all manned lunar flights and other advanced space vehicle missions. Approximately 80,000 acres north of Cape Canaveral will be secured for the development of these sites. This expansion was required because of the excessive vibration and noise anticipated with these vehicles.

Throughout 1961 planning of industrial booster production continued, S-II stage development was initiated, and investigations of advanced vehicle configurations to support the lunar missions proceeded. During the same period, preparations were completed for the launch of the first Saturn vehicle.

Static testing of the SA-1 flight booster was concluded in May, 1961. Booster checkout was completed in August, at about the same time when the second flight booster was transferred from the assembly area to checkout. The SA-1 booster, the inert S-IV stages, and the inert payload body were then transferred to Launch Complex 34. (The inert S-V stage had been delivered in April.) In the latter part of August, assembly of the SA-1 flight vehicle began at the launch site.

Between completion of assembly and actual launch, an exhaustive series of checkout tests were performed to assure that every required operation and function could be performed. Specifically, checkout consists of the application of a series of operational and calibration tests performed in a certain sequence. The response to each of these tests must be within a predetermined tolerance.

The checkout includes continuity testing, to assure that circuits have not been interrupted; component tests, to determine the satisfactory operation of individual parts; and overall testing, to evaluate power plant cutoff and other functions associated with the general vehicle network. Steering testing verifies the gimbaling response, attitude control, guidance, and special device systems of the vehicle. During calibration, the various vehicle measuring devices are adjusted. All of these tests are performed to check the sequences of operations required to bring the vehicle through the point of liftoff.

On October 27, 1961, the Saturn program reached its first major milestone with the successful SA-1 flight test (Fig. 1.6). The 162-ft tall vehicle weighed about 460 tons, with both inert upper stages filled with water to simulate fuel loading. Automatic fueling and sequencing processes were satisfactorily carried out. The 600-min countdown was uninterrupted by holds for technical reasons, although two holds were called because of weather.

The booster produced the 1,300,000 lb of thrust intended for the first four vehicle flights. (Later vehicles, using more powerful engines, will generate 1,500,000 lb of thrust.) Overall performance of the booster during flight was highly satisfactory. Structural integrity was maintained throughout powered flight. Wind shear, encountered near the region of maximum dynamic pressure, resulted in a 4.5-deg engine deflection, which was handled by the control system without difficulty.

Inboard engine cutoff occurred after 109 sec of burning, slightly earlier than anticipated. Analysis of telemetry data indicates the cause was propellant sloshing amplitudes, rather than performance deviations of the engines. Outboard engine cutoff occurred at about 115 sec. All engine thrust decays appeared smooth. The vehicle experienced practically no disturbance torques at cutoff and flew without pronounced tumbling motion through loss of the uprange signal.

During its trajectory, the SA-1 reached a height of about 137 km (85 statute miles). The vehicle flew for approximately 8 min, attaining a speed of almost 5800 km/hr (3600 statute mph), and impacted 345 km (185 nautical miles) downrange. Throughout the flight, more than 500 telemetry measurements were transmitted back to the ground station.

The flight of any vehicle is followed by an exhaustive evaluation of telemetry records. From these evaluations come the design improvements to be made on the next flight vehicle. As a result of the SA-1 flight findings, certain modifications are being made to the Block I vehicles, including additional slosh baffles in the propellant tanks to improve vehicle controllability in the latter phase of flight.



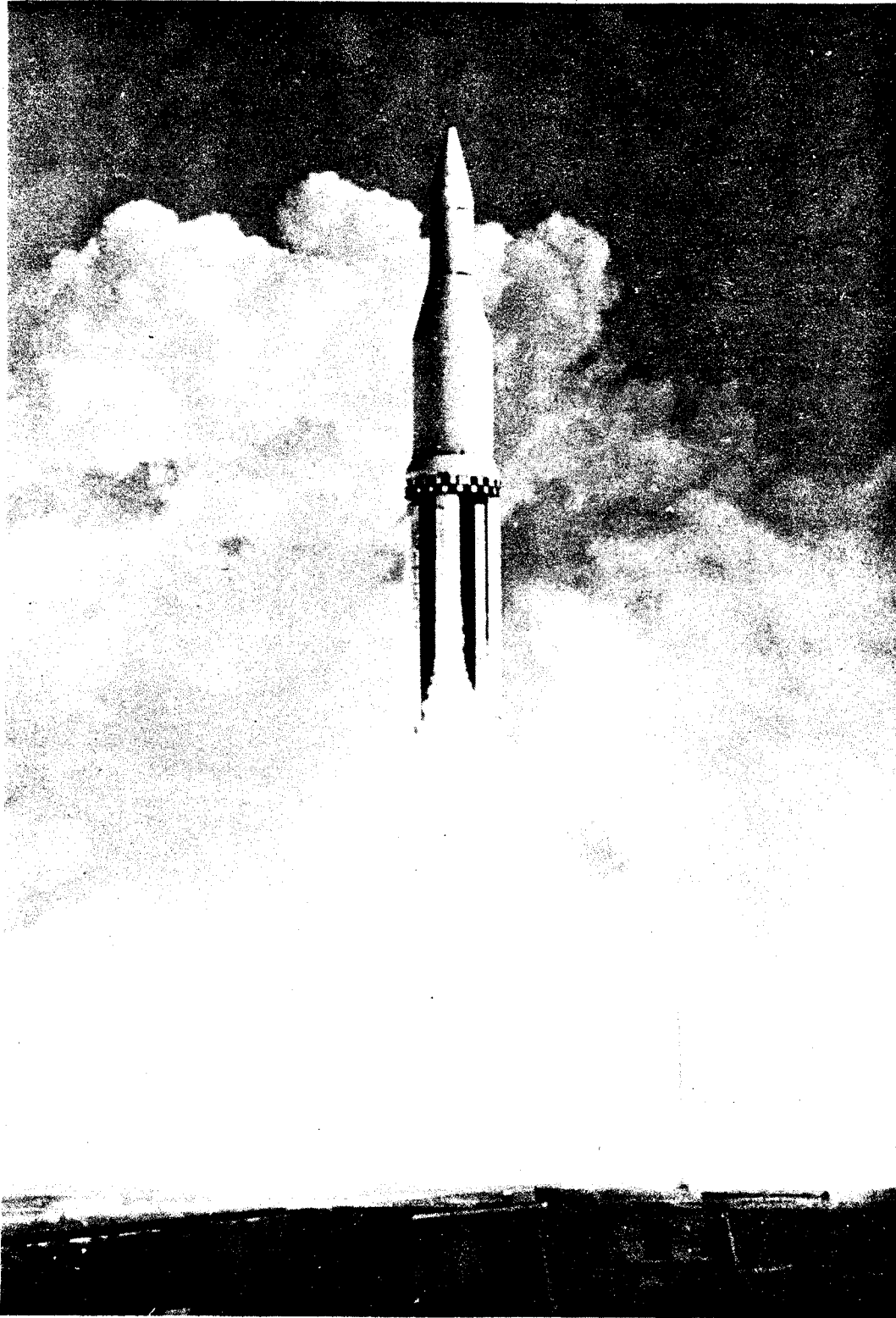


Fig. 1.6 Liftoff of the SA-1.

The flight disclosed that all major vehicle subsystems performed satisfactorily - structure, propulsion, control instrumentation, and heat protection. Ground equipment also performed satisfactorily, both during launch preparation and during the automatic sequence prior to liftoff.

The first milestone in Saturn history has been passed, leading to other steps in the development of the Saturn system. As testing and design improvement continue at MSFC for the Block I and Block II vehicles, parallel planning is also carried on to define the advanced vehicle, a step up from the C-1.

The advances in technology, methods, and procedures secured during the C-1 program provide a solid basis for the advanced configuration. Technical gains have already been realized in many fields: metals, instrumentation, facilities, handling and fabrication techniques. A large portion of advanced vehicle manufacturing can be accomplished in existing facilities with available tooling. Improved methods of handling the thicker metals of the advanced stages can be developed from fabrication methods defined during the C-1 program. C-1 assembly and checkout methods will be revised to meet new needs. Automated checkout, performed at the production plant, the test site, and the launch area, can be extended to meet the more comprehensive needs of the advanced vehicle program.

The C-1 and the advanced vehicle research and development programs merge inseparably, a continuity of effort based on and extending our present knowledge. Aerodynamic studies of advanced designs logically follow those studies performed on the C-1 vehicle. Liquid hydrogen technology, developed during the C-1 upper-stage programs, is extended in a logical development sequence through the S-II stage program.

In the same way, the high-thrust F-1 engine, developed during the course of the initial Saturn program, provides the foundation for developing a booster of greatly increased performance. In lieu of a booster providing 1,500,000 lb of thrust, future boosters are expected to provide thrust to magnitudes of 3,000,000 to 7,500,000 lb.

The advanced launch vehicles with the mature results of past plans and advances in research and development will directly support the manned lunar missions late in this decade. They will be capable of orbiting over 250,000 lb around Earth or sending 90,000 lb of payload on escape missions for lunar and interplanetary flights.

Of equal importance, the vehicles will be able to support essential R&D testing of spacecraft within flight and space environments. They provide the means for developing orbital rendezvous and mating techniques and for carrying payloads to the Moon for exploration of it prior to manned landings. Furthermore, the vehicles can carry nuclear upper stages, developed during the Rift program, for required flight testing in space.

The history of Saturn development to date illustrates some often unseen factors governing final vehicle design. In response to progressively more demanding missions and the steady advancement of scientific and technical knowledge, vehicle capabilities have constantly increased along with increasing performance.

In the space of little more than 3 years, we have progressed from the concept of a vehicle using relatively small clustered engines and ICBM-adapted hardware to the immense four- or five-stage vehicles, with F-1 clustered engines, upper stages using the most advanced liquid technology known, and capped with nuclear stages.

These programs have demanded the full measure of ingenuity and skills. Advanced programs, carrying men into still unexplored environments, demand that we provide even more; the history of Saturn development is still in the process of being created.

Robert L. Smith, Jr.

Quality Division  
George C. Marshall Space Flight Center  
National Aeronautics and Space Administration  
Huntsville, Alabama

In the past, propulsion vehicles for space payloads in some degree have been adaptations of available military missiles; two notable exceptions to this are the Vanguard and the Scout. This practice will no doubt continue for some time with such vehicles as the Agena (Thor and Atlas), Centaur (Atlas), and Delta (Thor); however, payload requirements for larger size and complexity, manned operation, and more exotic orbits and trajectories are dictating the development of a new generation of space vehicles designed specifically for space work. These vehicles are becoming larger and more complicated than those previously used. They are correspondingly more expensive and more difficult to handle, transport, and launch. It would be extremely optimistic to assume that these vehicles can be readied for launch without having gone through a thorough examination and testing operation corresponding to their degree of complexity and cost. For this reason, a review of the methods and, particularly, the principles of providing their flight readiness seems appropriate.

Certain things must be considered regarding methods of operation, and these may then be taken as basic assumptions, from which a projection may be made to determine testing approaches and philosophies. The amount of testing to be done at the launch pad will be directly determined by the pads available and the vehicles to be launched. The number of vehicles per year to be launched is, in turn, determined by the missions. Vehicle missions will therefore be examined first.

The following types of missions can probably be assumed:

1. Manned orbital--single man, training and observation; multiman, short time; multiman, long time.
  2. Circumlunar--unmanned observational and manned.
  3. Lunar landing--unmanned observational; manned, short time; manned, base operation.
  4. Unmanned orbital--small space station and large space station.
- Of these, unmanned circumlunar, lunar, and orbital missions could

probably be handled by existing vehicles. For the others, use of the larger Saturn-class vehicles seems indicated. However, multiman, long-time; orbital; and lunar manned-base missions would appear to require several firings per year for support. Depending on how much payload is required, manned circumlunar and short-time lunar landing operations could possibly require a close firing rate of two or three vehicles with orbital rendezvous. Several firings per year for each of these cases would result in a large total number of annual firings. Therefore, test time on the pad must be kept to a minimum. This time limitation would also make it very dangerous to assume, especially early in the program, that stages manufactured thousands of miles apart could be properly and safely mated in the allowable time.

These facts are obvious when one considers the following illustrations. Figure 2.1 illustrates the determination of available pad time starting with the missions to be accomplished. Figures 2.2 and 2.3 show the pad and time requirements for manned orbital and manned lunar operations, respectively, with the values arrived at in the same manner. Figure 2.4 is a summation of Figs. 2.2 and 2.3. The number of launchings assumed in each case is intended to be illustrative only. Many factors will influence this, not the least of which is the ability of the national economy to support the entire program.

It appears, however, that the requirement for stringent flight-readiness operations before moving to the launch area is realistic. Let us examine what could be considered good current practice and project some possibilities into the future.

## 2.1 Pretest Requirements

Regardless of the methods employed in testing vehicles, poor firing results will occur if certain pretesting and posttesting action is not taken. Therefore, an examination of what is right and wrong in test philosophy must be preceded by an examination of those other factors. They may be listed as follows:

1. Design qualification testing
2. Flight qualification testing
3. Reliability testing
4. Quality control
5. Inspection
6. Component functional testing
7. Failure reporting and follow-up

Only when these seven areas are properly covered in manufacture and test of a vehicle does the area of vehicle functional testing take its rightful place in the pattern of delivering the best possible vehicle to the firing site. If one of the seven is neglected, then functional testing must do more than its share to insure good vehicle delivery.

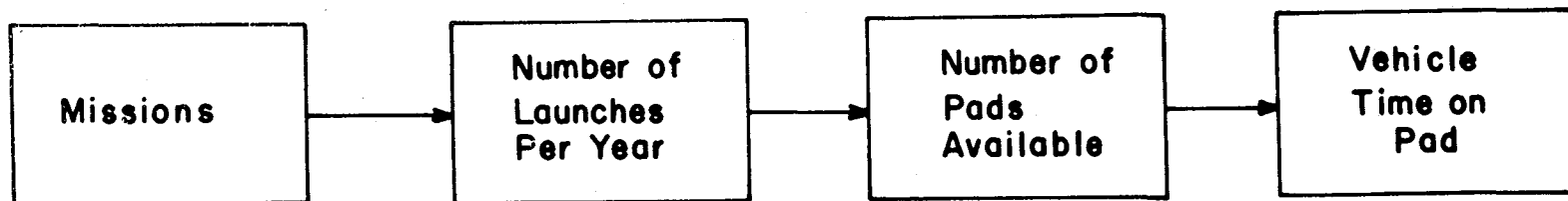


Fig. 2.1 Determination of available pad time.

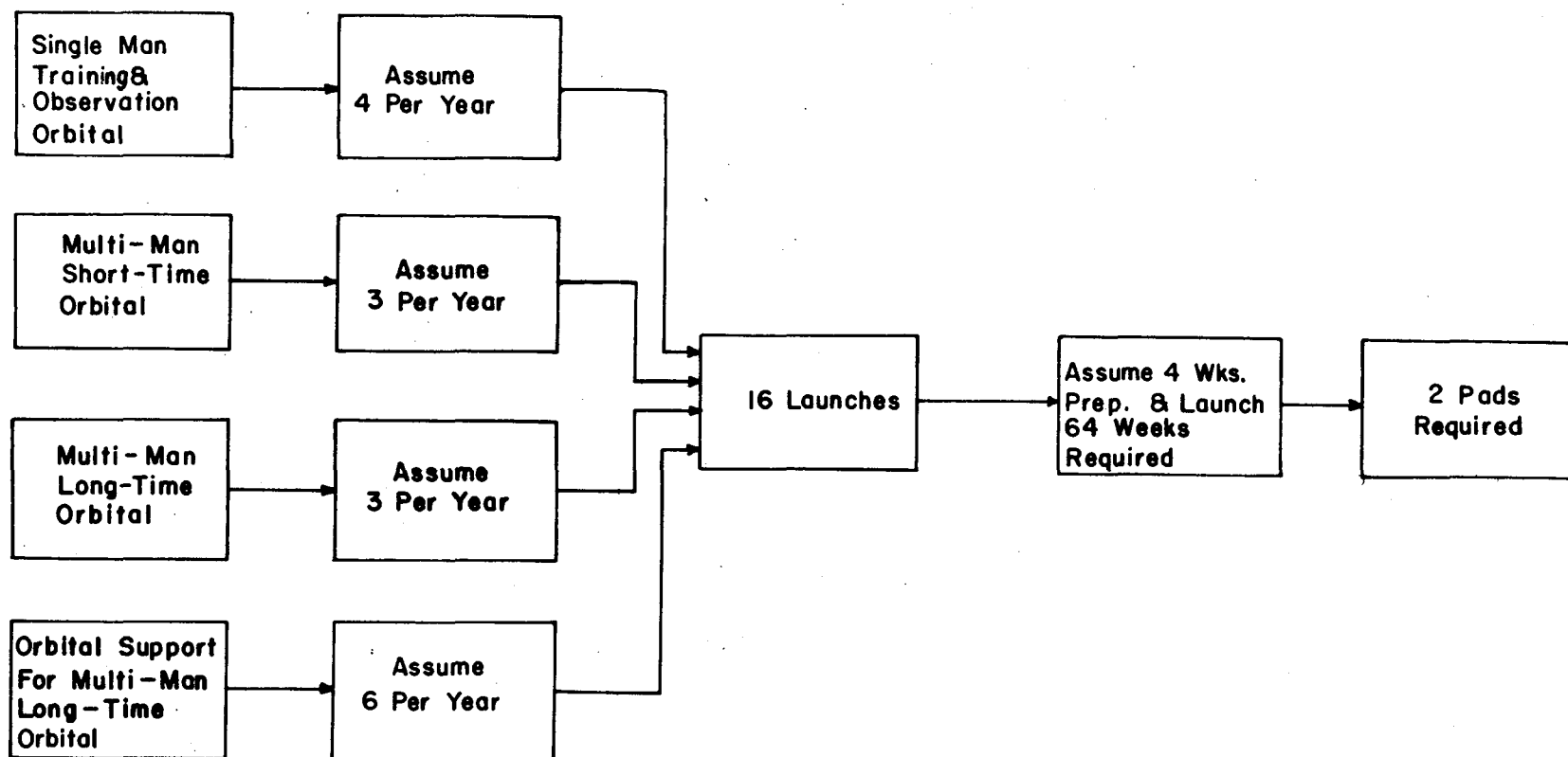


Fig. 2.2 Pad and time requirements for manned orbital operations.

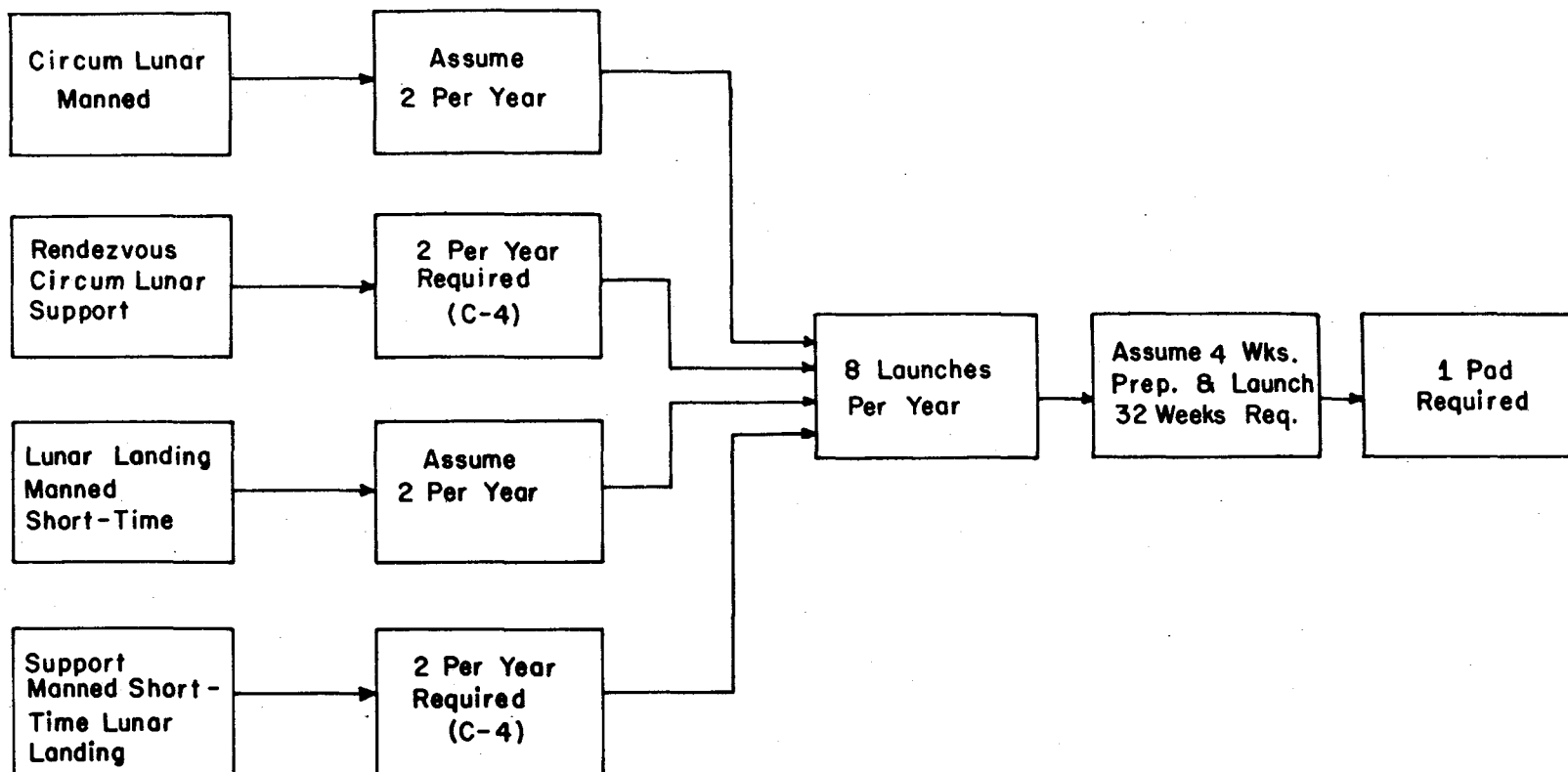


Fig. 2.3 Pad and time requirements for manned lunar operations.



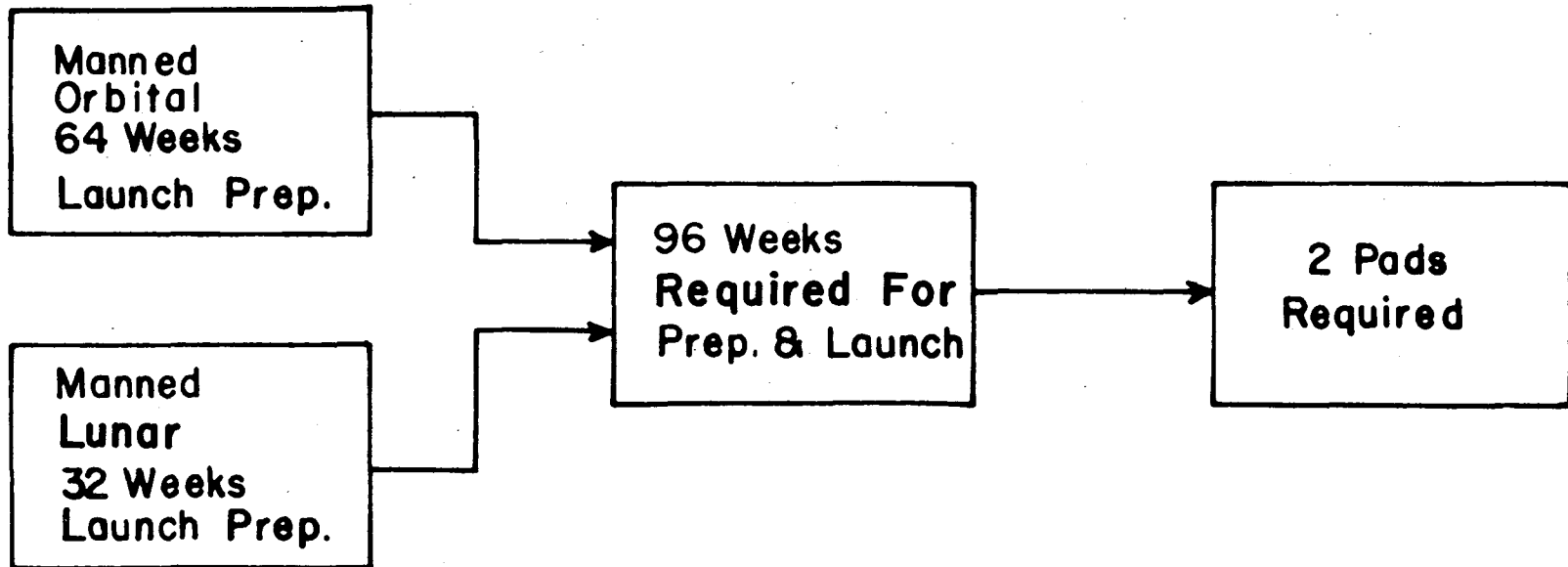


Fig. 2.4 Summary of pad and time requirements for manned orbital and manned lunar operations.

The degree to which this is accomplished becomes dependent on many variables, not the least of which is the skill and attitude of those performing the functional tests.

The first three of the seven auxiliary areas have been thoroughly discussed in literature over several years; no attempt will be made here to do more than define them with a few qualifying remarks as to the author's understanding of what is encompassed. Their virtues seem apparent to all; quarrels arise in terms of methods and times for obtaining these virtues.

#### 2.1.1 Design Qualification Testing

This is the testing necessary to determine that a component, assembly, or system will perform according to design.

#### 2.1.2 Flight Qualification Testing

Testing necessary to assure functioning according to design under the flight environment and loading falls within this category.

#### 2.1.3 Reliability Testing

This is the testing necessary to assure that a satisfactory level of confidence is achieved for the component, assembly, or system to perform as required.

In other words, if the device will not perform its function, there is no point in building it; if it will not perform in the vehicle, there is no point in flying it; if it will not endure long enough to accomplish its mission, there is no point in establishing that mission. We therefore assume in all subsequent discussion that the three requirements indicated above are met.

Having established that a basic design is supplied which, if followed, will accomplish its purposes, we must now establish that the materials, methods of manufacture, and handling and installation of the components will not so detract from the design that the useful life of the component will be limited. It is assumed in the three testing areas mentioned above that tolerances have been established for the four areas for which we propose to control the quality.

Since there is no sure method of knowing that a screw is correctly threaded or a joint is properly soldered, our reliance must be placed on empirical methods using trained people for the major effort in control of quality. Thus we need inspection. And, as a final check of quality, we perform a test on the bench to determine that a device can go through one or several functional operations, having no special

environmental parameters imposed. Having controlled the quality of all components, assemblies, and systems going to make up our space vehicle by means of methods control, inspection, and functional testing, we may now feel that all areas are safely covered and functional vehicle testing may begin. Before this is discussed, however, a further word concerning component functional testing is in order.

There are two schools of thought on component functional testing on the bench. One contends that environmental testing should be applied; that is, the component should be put under a flight-type environment while it is being operated. The other says that no special environment should be applied. The argument of the former approach is that since flight requirements must be undergone anyway, it is better to test the component on the bench. The latter holds that adding flight environment can weaken the component under test so that it may pass the bench test but fail during flight. An interesting point in the whole controversy is that, in almost every case, the only environment in question is vibration. Seldom does anyone attempt to apply any other environment during acceptance functional testing of components. When a query arises as to why "environmental testing" is specified when "shake testing" is meant, the answer generally boils down to "something might shake loose." This "something" is described as loose parts, bad solder joints, or trash, all of which can be controlled by thorough inspection procedures.

Here, two things should be pointed out: (1) a thorough program in the qualification and reliability test area first mentioned could include an accounting for this type of "environmental" testing, and thus relieve worry of fatigue failure, and (2) a thorough and complete quality control and inspection program could prevent any possible occurrences of the nature sought in such an "environment." Neither of these can be achieved without a great deal of effort and determination.

## 2.2 Vehicle Testing Operation

### 2.2.1 The Systems Approach

A launch program of maximum efficiency must utilize a minimum of testing time at the launch site and must recognize equipment modification only as the primary mission or safety of the flight are affected. Such a proposal is a drastic change from past practice in most programs, although it is agreed that these are admirable aims. Too often, unfortunately, those who made the decisions as to whether these aims should become an actuality were unwilling or unable, politically or technically, to hold the line.

If test time at the launch site is held to a minimum, testing at the factory level must be comprehensive enough to insure delivery of a vehicle that does not require exhaustive launch site examination.

Having accepted that the requirements set forth in the previous section have been satisfied, an examination of what constitutes proper factory testing is in order.

**Mechanical Testing.** A major problem may lie in mechanical components and systems. This particular area is more subject than any other to the argument that the design is so good, no testing need be done. This is especially true if it becomes necessary to break into closed lines and systems for test purposes. However, detailed investigation into most systems reveals that testing and checking is reasonable and proper to insure correct performance later.

It is necessary, for example, to ascertain that alignment of stages, singly and to one another, is proper; that flight control devices are properly mounted and aligned; and that rocket engines have the thrust vectors aligned within tolerances that will not allow a marginal flight control system to be overpowered. In fact, all alignment checking is for the purpose of insuring a good flight by knowing in advance that design tolerances built into the flight control system will not be stretched because of something relatively easily determined and corrected.

In the same manner, the integrity of pressure-tight systems should be determined at a place where difficulties may be most easily and inexpensively corrected. Proper functioning of these systems should also be checked. For example, such components as flowmeters, pneumatic valves, and hydraulic systems can cause severe problems at the launch site if an unverified stage leaves the manufacturer's plant.

**Electrical Testing.** The area of electrical testing probably offers the best possibility of doing a thorough testing job. Having verified components individually, it is imperative that their system be verified for assurance of operation of the flight vehicle. This means that a system-by-system verification, followed by an all-systems operational test for proper compatibility and sequencing, becomes logical. An all-systems test, by-passing individual systems, appears to offer short cuts saving much time and is most often proposed. However, the all-systems test generally involves about four major subsystems. It is cumbersome in terms of time and methods of operation; difficulty with one or more of the major subsystems, or even components, causes reruns and build-up of operating time on flight hardware. In the long run, no time is saved, and a less thorough look at operation is obtained. The result is a vehicle released for shipment in very nearly the same amount of time but with much less assurance of proper operation.

**Electro-Mechanical Testing.** It is not always easy to determine whether testing should be approached on a mechanical or electrical basis, since many devices on space vehicles lie somewhere between the

two. The decision must be made whether the major function lies in either area, or both, and where compatibility with the rest of the vehicle may best be assured. Thus, redundancy in testing becomes a necessity offset by the advantage of assuring proper compatibility. In most cases the redundancy may be covered by allowing and observing one or two extra functions in existing tests. The main factor is to see that such test coverage is obtained in every case.

### 2.3 Substitutes and Simulators

On past occasions, with heavy schedule pressures and crucial deadlines, it has been facetiously suggested that a substitute vehicle and a substitute set of ground support equipment be kept on hand for test. When a vehicle comes off the assembly line, the two substitutes are run through a test; then the flight vehicle is shipped to the launch site with the statement that it must work properly because the substitutes did. This approach, of course, represents the extreme in substitution, and allows the maximum of time for preparing flight hardware.

A lesser extreme, often proposed, is that several of the more complex system components, generally not completely ready at checkout time in R&D programs, be substituted either completely or by use of a nonflight dummy. The thinking is that the flight item, when ready, can be bench tested for correctness, then installed and expected to work properly. Experience demonstrates many times over, however, that a component that works on the bench does not necessarily work in the vehicle. It therefore becomes imperative that flight hardware be used for flight vehicle testing except in cases where not feasible. An example of infeasibility is the test firing of ordnance devices. The question, then, is what is proper and reasonable in the way of substitution and simulation.

#### 2.3.1 The Simulator

A simulator may be defined as a device utilized in place of a flight item to supply the responses expected. The responses result from stimuli, perhaps intended for the flight item. The word perhaps is used because it is not always practical to utilize the same stimuli; in many cases, this is what determines whether the device is a simulator rather than a substitute. A good example is a relay used to simulate operation of a pressure switch for indicating the level of propellant tank pressure. In the operation, a signal, possibly to a solenoid, starts pressurization of the propellant tank; when the proper level is reached, the pressure switch contacts close, providing a second signal that permits the sequence to proceed normally. In the checkout, the propellant tank cannot be pressurized because of safety requirements. The relay is therefore substituted for the pressure switch to simulate its action. The signal to the solenoid for pressurization, perhaps with a time delay, is routed to the relay coil. Closure of the relay contacts then simulates action of the pressure switch to allow the sequence to proceed. Such a checkout illustrates proper use of simulation techniques.

Improper use of such techniques is easily illustrated. Consider, for example, the same relay, except that now the pressure switch actuation source is a pneumatic control system, which can safely use the operating pressure required for actuation and can be pressurized as an adjunct to a normal testing operation. Although this is a simple example, such unrealistic simulation techniques exist or are proposed many times to "save" schedule time when a device is not ready for checkout. The lack of realism is generally obscured by a more complex situation in these cases.

### 2.3.2 The Substitute

A substitute is a device that may be utilized in place of a flight item and may receive stimuli and supplies responses in the same manner as the flight item. By this definition, a nonflight version of a flight item is a substitute. Therefore, in some cases, the difference between a simulator and a substitute is a very fine line. The intention is not to propose a universal definition as outlined here, but rather to identify the uses separately for discussion.

The close resemblance of the substitute to a flight item often results in the use of it in final checkout when the pressure is being applied to produce a flight item by the same time. The answer, of course, is obvious. If the substitute were exactly like the flight item, it would be a flight item. Since it is not, a complete test is impossible. Therefore the decision to use or not use a substitute must be resolved in terms of whether it is actually possible or not to produce the flight item for final checkout or whether the reason is hardware readiness, size, or relative immobility, or perhaps a combination of factors.

## 2.4 Types and Thoroughness

### 2.4.1 Types of Tests

The types of tests that should be performed during a final vehicle checkout are divided into the two general categories of mechanical and electrical testing. These are discussed to some extent above. Whether all testing is done in a single location at or away from the assembly area must be determined, among other things, by the facilities available and the size and mobility of the test vehicle. Generally, however, it appears that a single location not at the assembly area is more desirable.

The first operation should be a hardware check against documentation to determine status of the vehicle. Allowances can then be made in the testing operation for things that are not as they should be. All such problems need to be resolved, however, and the problem areas checked before the testing is finished and the vehicle released. If this is not done, complexities are introduced into the launching operation before the vehicle leaves the factory.

Next, mechanical systems need to be cleared so that electrical testing can be done safely. Whether such things as weight and alignment are checked before or after electrical testing is a moot point. However, it appears that clearing all mechanical testing at the same time is desirable since a different crew would probably be involved in electrical testing. This course would not preclude a follow-up check at the end of testing to assure that no incidental damage incurred during the testing operation.

Since a particular type and arrangement of electrical ground support equipment is used for launching and since the vehicle must mate with that equipment, the equipment at the final checkout location must be as nearly like the launch equipment as possible. Thus the checkout will not only insure a good vehicle but also insure compatibility at the launch site. This ground support equipment must also be verified with the associated facility prior to connection for checkout. A vehicle simulator is perhaps the simplest way of accomplishing this, although it presents some up-dating problems from one vehicle to the next in an R&D program. Further, a complete vehicle cable continuity check prior to connection for testing is essential to insure elimination of "ghost" troubles later, most of which result from wire problems. After these checks, the vehicle is ready for testing.

Further electrical testing should not be built up from simple system testing to a gradual combination of systems. The order of these is generally dependent on what must be cleared before additional work may be done. For instance, it is necessary to know that the power and electrical network systems are functioning properly before testing of the guidance and control system can begin. And proper functioning of the guidance and control system should be checked before attempting to calibrate the measuring instrumentation associated with that system (i.e., those measurements for flight information rather than for flight control). It is also useful to know as early as possible that a transfer to internal power and umbilical drop-flight sequence can be accomplished. This becomes increasingly important as automatic sequences are involved.

All electrical testing should culminate in the all-systems or simulated flight test. This test should include umbilical drop and operations during the part of the flight time that includes significant operations. In general, this will include the time of engine burning and stage separation, although in some cases reentry functioning may become involved. Testing of systems prior to the simulated flight test should be sufficient to insure reasonable confidence that everything will function properly during test, barring such unpredictables as wearout and human error, and that it will only be necessary to make one run of the test. The simulated flight test should be accepted as satisfactory only if there are no discrepancies or questionable occurrences during the test; a minor exception

can be made for difficulties with a system or component that can be simply rechecked or corrected after the test and that are independent of the sequencing and of other systems. Judgment of these must be based on individual cases. A simple example is a case where a recorder does not record a function, but it is clearly established that the proper line was not connected and the function is verified by another source.

#### 2.4.2 Thoroughness in Testing

The more that schedule pressure is applied, the more likely it becomes that thorough testing will suffer in favor of short cuts. Short cuts in testing are not necessarily to be avoided as long as the requirement for complete verification is kept in mind. However, verification of a vehicle costing several millions of dollars should not go wanting because of the desire to save a few days or weeks established by a tight schedule. Somehow a reasonable balance must be struck between the two.

One type of short cut often taken is the verification of a change made by incorporating the necessary extra steps into a major test already scheduled. The risk here is small of having the test ruined by a failure due to the change if the change is minor. However, if it is a major one, special precautions must be taken to prevent the loss of the test in case of failure. Loss of a major test, particularly if it results in damaged equipment, can cost more time than that necessary to check the change before proceeding.

A worse type of short cut is that involving a change proposed or made at such a time that testing becomes necessary at the launch site. A worse danger lies in saying that a component or system is highly reliable and not checking it will save time.

From this brief discussion it is clear that thoroughness in testing depends not only on the testing organization but to a great extent on the designers and schedulers.

### 2.5 Integrity of Testing

#### 2.5.1 The People

Merely going through a test procedure with a vehicle does not insure that the results of the test, or the procedure for that matter, will guarantee a good vehicle. In space vehicle work, particularly, a large production line usually does not exist; and engineering evaluation of test results, cross-correlation between tests, writing of test procedures, analysis of operating methods among other things, play an important role in determining whether a vehicle is acceptable. For these reasons, the emphasis in selection of test personnel should be on building an experienced, engineering-oriented test organization. This



is not to say that good technicians do not play a part in such an organization but rather to emphasize the engineering analysis.

The personnel selected should be sold on the necessity for the achievement of a successful flight. With an organization so oriented, it is desirable and practical for those doing the testing to write the test procedures. This provides an independent look at systems by the people who know why and how the test was designed and its relationship to other tests.

### 2.5.2 Parts Swapping at the Launch Site

It is obvious that replacing components and initiating changes to systems during a preparation for launch is deleterious for a vehicle that has checked out good. Yet such things as component failure, human errors during testing, and information development late in the schedule make such practices inevitable. To preserve the integrity of the vehicle, however, a regulation of these practices is mandatory.

The first means of reducing these practices is by cutting down on component failures. This problem can be alleviated by providing spares that have themselves been checked on the vehicle in which they may be used.

The second means is by eliminating as many components as possible for which spares are not provided and by taking a hard look at all unanticipated system change requirements. These changes should be examined carefully to determine whether they are really necessary. If such proves to be the case, then the exchanged components and their installation must be verified. Modifications sometimes tend to be of the "like-to-have" variety rather than the "necessary-for-safety or mission accomplishment" kind. However, a firm management program can minimize or eliminate most of these by a careful technical review of proposed changes.

The third means lies in having a good feedback reporting system to show, on paper, all changes made, reasons for changes, and, perhaps, verification of changes. This means is particularly important, of course, from the design standpoint because in many cases a comparatively simple design modification can prevent the necessity for future changes. Further, a correlation of such reports over several firings can clearly indicate a troublesome trend, if such exists. Such a trend could even indicate things that are being overlooked in final testing before shipment, and the reports should therefore be distributed to all concerned.

## 2.6 Record Keeping

The role of testing is, on the surface, satisfied when a good vehicle that operates properly with the ground support equipment is delivered to the launch site. Nevertheless, information developed during testing can have a bearing on both basic design and launch operations. Adequate record keeping and reporting is essential not only in the interest of efficiency but also for the sake of continuity in the launch site test and flight operation. The types of that should be kept, in most cases, can be determined from an examination of the data generated during testing.

Table 2.1 illustrates the type of record keeping that proves valuable. It is indicative rather than definitive and does not show in any case the magnitude of the material involved. This is particularly true of the measuring instrument calibration where a separate curve is involved for each measurement. Although many of the individual gages can be identified by the original laboratory calibration curve, many others have curves that are generated as a result of the calibration associated with testing. The necessity for furnishing this type of curve to the launch site is obvious.

Feedback of failures and discrepancies to design groups appears obvious, although in practice it often happens that organizations exist that provide a sufficient buffer between test and design groups to obscure details of difficulties. The necessity for correlating failures with past and future occurrences provides the impetus for this; care must be taken to insure that complete information is currently available while satisfying the correlation necessity. A design discrepancy, of course, must be remedied immediately, and subsequent testing should clearly establish that it is adequate. Since communication for establishing changes exists between the design and launch groups, no indication of a feedback to the launch group is suggested from the group where checkout is the primary consideration. An in-house feedback is indicated in both of these cases, however, since future problems could easily be linked to an existing one.

Two other areas of feedback are suggested that, although important, are easily overlooked. "As-is" schematic drawings accompanying the vehicle (and possibly ground support equipment) represent the hardware actually delivered. This practice, in itself, helps reduce the possibility of error introduced through other documentation channels. The test report on daily activities provides a historical source for checking on questionable areas appearing during a launch operation. If a history of a "ghost" trouble exists in a certain system and if it is persistent, then time must be taken to remove it. The whole problem should be solved in the preshipment testing. This is always limited by the apparently persistent conflict between checkout time and shipment date. If one is inflexible, the other will suffer accordingly when unforeseen problems arise.

Finally, nothing can surpass close coordination between test people and launch people and the use of the telephone as a reporting source. This procedure does not eliminate other reporting but does supplement it.

## 2.7 Who Does the Testing?

The group that performs the final test on a missile or space vehicle varies rather widely in its organizational parenthood, which ranges from design (engineering) through manufacturing to launch personnel. There are desirable features in all of these approaches; and whatever group does the testing, the others should have the prerogative of being present.

If the test organization is a part of manufacturing, there will be a considerable preknowledge of manufacturing difficulties. For this reason, there will be a tendency to take these difficulties into account. At the same time, to avoid unfavorable investigation, feedback on problems could be something less than vigorous. The same general statements can apply to a design organization responsible for final testing. Thus testing by a group other than these two has much to recommend it.

Assuming that the launch group is a separate organization from design and manufacturing, it is possible for this group to look independently at the systems. In this case, however, many of the test group would probably be utilized at the launch site for checkout and firing. If allowed, this practice would reduce considerably the validity of the independent look that can be taken during the launch operation.

In conclusion, then, it seems that the group performing the final checkout should be a separate entity. This organizational separation would result in test procedure design, although to some extent dictated by the nature of the equipment, gained independently during test and launch that could uncover difficulties missed elsewhere. It would mean, too, that those performing the tests are the same people who are responsible for generating them. A complete understanding of both tests and equipment would exist among the personnel performing them. The launch group would serve as backup by providing another, perhaps less rigid, look at the systems from a slightly different and objective view.

It is perfectly clear that any of the other three approaches to checkout is entirely valid, and that, in the long run, the results are a function of the quality and integrity of those performing the tests. Nevertheless, removal of possible hidden obstacles before the fact can do much to contribute to smoothness in the overall operation.

## 2.8 Role of the Government

At the present time, the government is the only customer for space vehicles. In this role, however, the customer is different from those in, say, retail aircraft sales. A retail customer has available what

is on the market and may pick and choose or buy nothing if he does not like what is offered. The government, however, cannot refuse to buy, because it must have what it is seeking. What is offered is a group of ideas that, if accepted, must be developed into hardware. Further, all the ideas may not prove feasible; and a very expensive purchase may grow more expensive by having to replace old hardware that did not develop from the original ideas.

Therefore, the government, as a different type of customer, must participate with the vendor by providing competent people and a comprehensive definition of its needs and by working with him to achieve the desired product. It is gross simplification to say that the definition of requirements must be sufficiently comprehensive that the vendor can achieve the product without participation by the government or that the skill of the vendor is so superior to the government representatives that no advantage is gained.

In final checkout, therefore, the government must participate with the vendor in determining whether proper prerequisites are met, whether testing and reporting of testing are sufficiently comprehensive, and whether objectives have been met. These are things that must be accomplished in a mood of mutual trust in a field where hidden costs can mount rapidly and where the life of pioneers in space depend upon whether the objectives are accomplished.

Table 2.1 Record Keeping Activity

Information Source	Type of Information	Type of Record	Feedback to		
			Design	Test	Launch
Component Failure	Data/Method of Failure	Failure Report	x	x	x
Design Discrepancy	Corrective Action Required	Unsatisfactory Condition Report	x	x	
Operational System Calibration	Data	Test Report	x		x
Measuring Instrument Calibration	Data	Calibration Curves			x
Telemetry Calibration	Data	Curves or Report			x
"As-Is" Drawings	Current Status	Schematic, Etc., Drawings			x
Daily Activities Peculiar Troubles	"Ghost" Troubles, Seq. of Test, Etc.	Daily Log Test Report			x
	Any	Report/Telephone	x		x

## 3

## EVOLUTION OF LAUNCH CONCEPTS AND SPACE FLIGHT OPERATIONS

Kurt H. Debus

Launch Operations Directorate  
George C. Marshall Space Flight Center  
National Aeronautics and Space Administration  
Huntsville, Alabama

New concepts evolve from the inventory of available knowledge and frequently become the building blocks for future concepts. The concepts of rocket launching and space flight operation are not exceptions. The simple concept of one man using a trough or forked stick to launch a hand-made rocket for his own amusement or to awe and injure an enemy has evolved into a highly complex operation employing the varied skills and capabilities of many people.

Knowledge, originally acquired for other purposes, is applied to the development of new skills and specialized fields of knowledge directly related to the evolution of new concepts. These concepts, in turn, contribute to the evolution of new skills and technologies and the creation of an ever-increasing pool of knowledge.

### 3.1 History

The first historical rocket was developed by the Chinese in the 13th Century. Known as the "Arrow of Flying Fire," it consisted of a quantity of gunpowder wrapped into paper and tied to an arrow which was ignited and shot from a bow. Two-men teams were used to launch the fire arrows: one man held the arrow on a drawn bow while the other man ignited it. It was soon observed that the arrows were self-propelled after ignition, and the bow was replaced by a variety of simple launchers. The most common of these consisted of one or two forked sticks, wooden or earthen troughs, or hollow tubes (Fig. 3.1). Each of these methods used the simple expedient of adjusting the elevation and azimuth angles of the launcher to achieve the desired rocket trajectories and ranges.

Before World War II, launch and space flight concepts remained relatively unchanged. They could be comprehended and implemented by a single individual. Experimentation and research were emphasized; the more distant goal of manned interplanetary flight spurred the experimenters to achieve the more immediate goal of atmospheric exploration.

**Preceding page blank**

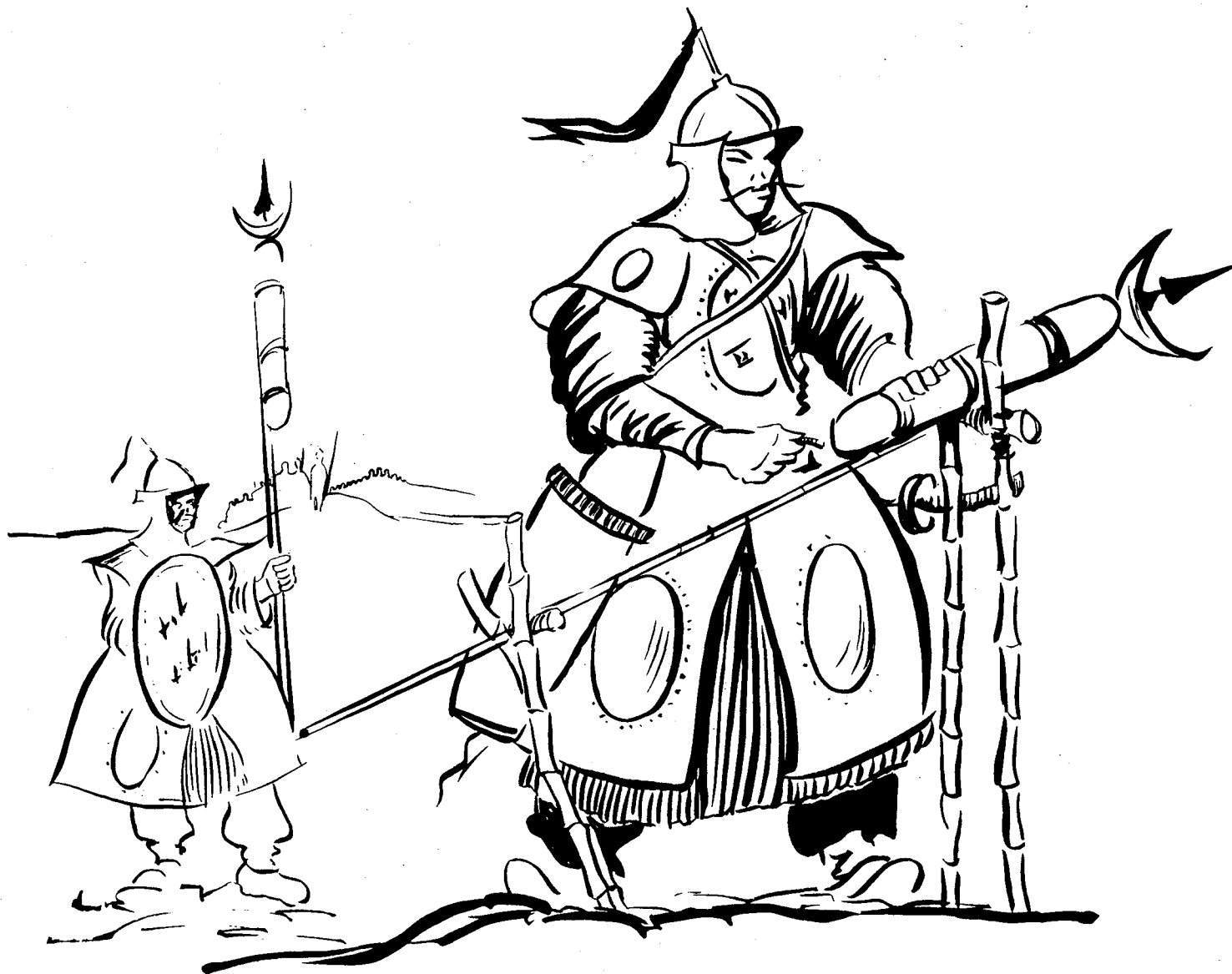


Fig. 3.1 Early Chinese rocket launcher.

Military requirements dictated new rocket concepts during World War II and launch operations began to assume an identity of its own. German rocket development paced similar development in other countries, culminating in the A-4 or V-2 rocket. A brief description of the V-2 and its launch complex indicates its generic relationship to present and future launch and rocket concepts.

The V-2 was approximately 46 ft long, 11.5 ft in diameter and, fully fueled, weighed 34,000 lb. It was powered by a single engine that developed 69,100 lb of thrust. It burned liquid oxygen and a mixture of alcohol and water. The range was determined by combustion cutoff, and the direction of flight was controlled by preadjusted steering devices, supplemented in special cases by radio control. The V-2 was transported by rail or truck, erected hydraulically, and launched from quickly prepared sites (Fig. 3.2).

Approximately 30 vehicles and trailers supported the V-2 by supplying the necessary fuel and oxidizer, communications and checkout equipment, and maintenance facilities. Included also were the hydraulic transporter and erector with umbilical connections, and the mobile subswitching and relay centers. The V-2 trucks and trailers were forerunners of the ground support equipment required to service and equip today's intercontinental ballistic missiles. Their principles are employed in many of today's fixed complexes, including the launch service structure, the launch control center, umbilical connections, and fuel and oxidizer storage and supply.

### 3.2 Current Development

Military requirements provided initial impetus to the development of new launch concepts and space flight operations. Many of the skills and capabilities required to successfully pursue these developments, however, were recruited from outside the military community. The organization of teams of scientists, engineers, and technicians evolved from the need to consolidate and coordinate a variety of talents to achieve a common goal: the successful launching and operation of space flight vehicles.

The evolution of the V-2 vehicular complex produced the highly instrumented and functional Saturn C-1 launch complex designed to achieve maximum efficiency and safety (Fig. 3.3). A brief examination of the Saturn C-1 vehicle and launch complex (LC 34) illustrates the varied technologies that have been brought to bear to achieve the initial Saturn launching.

On the launching pad the Saturn C-1 is approximately 163 ft high. Its liftoff weight is about 1,000,000 lb and with three stages activated, it will orbit more than 20,000 lb. The first stage has eight engines

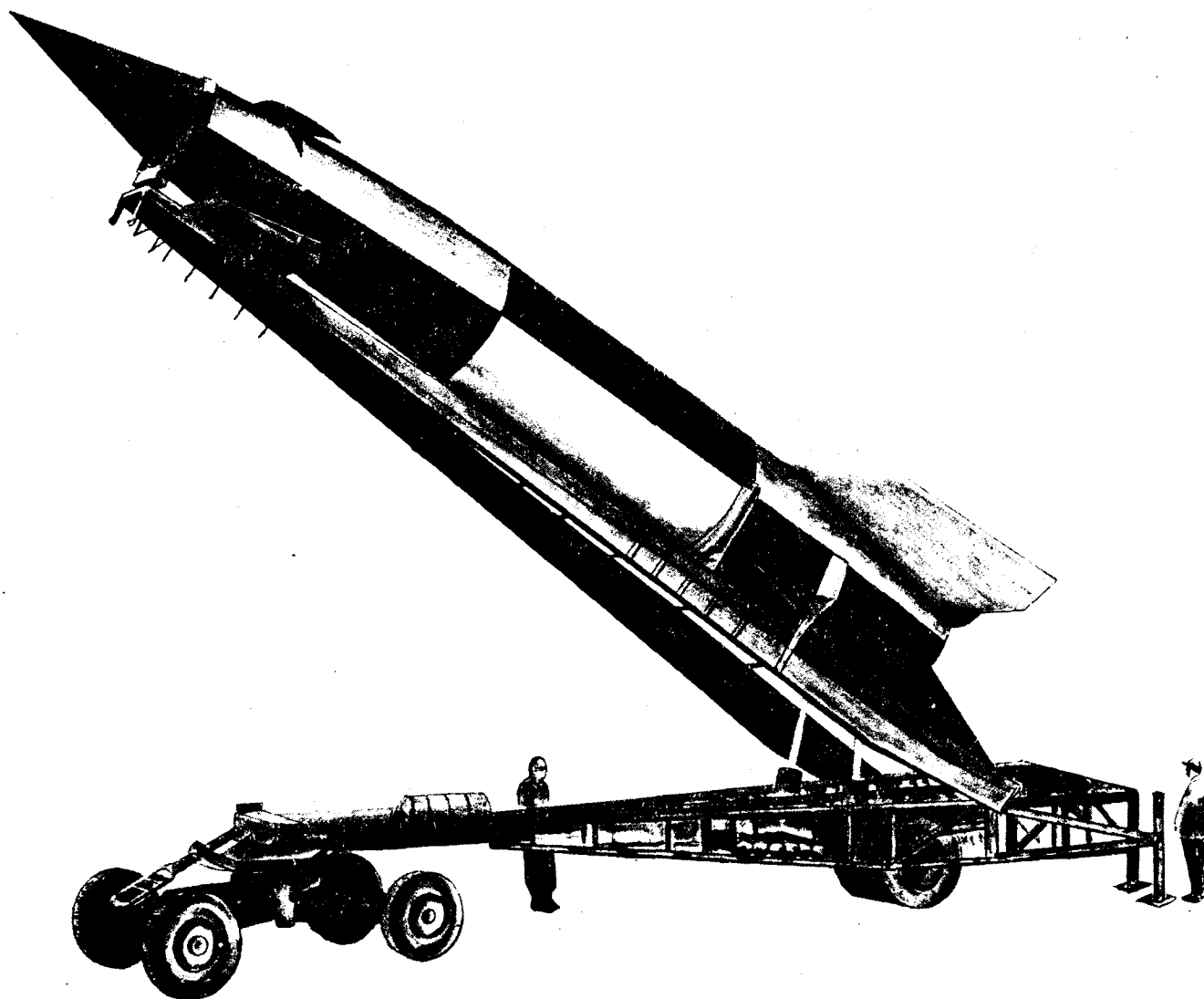


Fig. 3.2 V-2 shown mounted on mobile launcher.



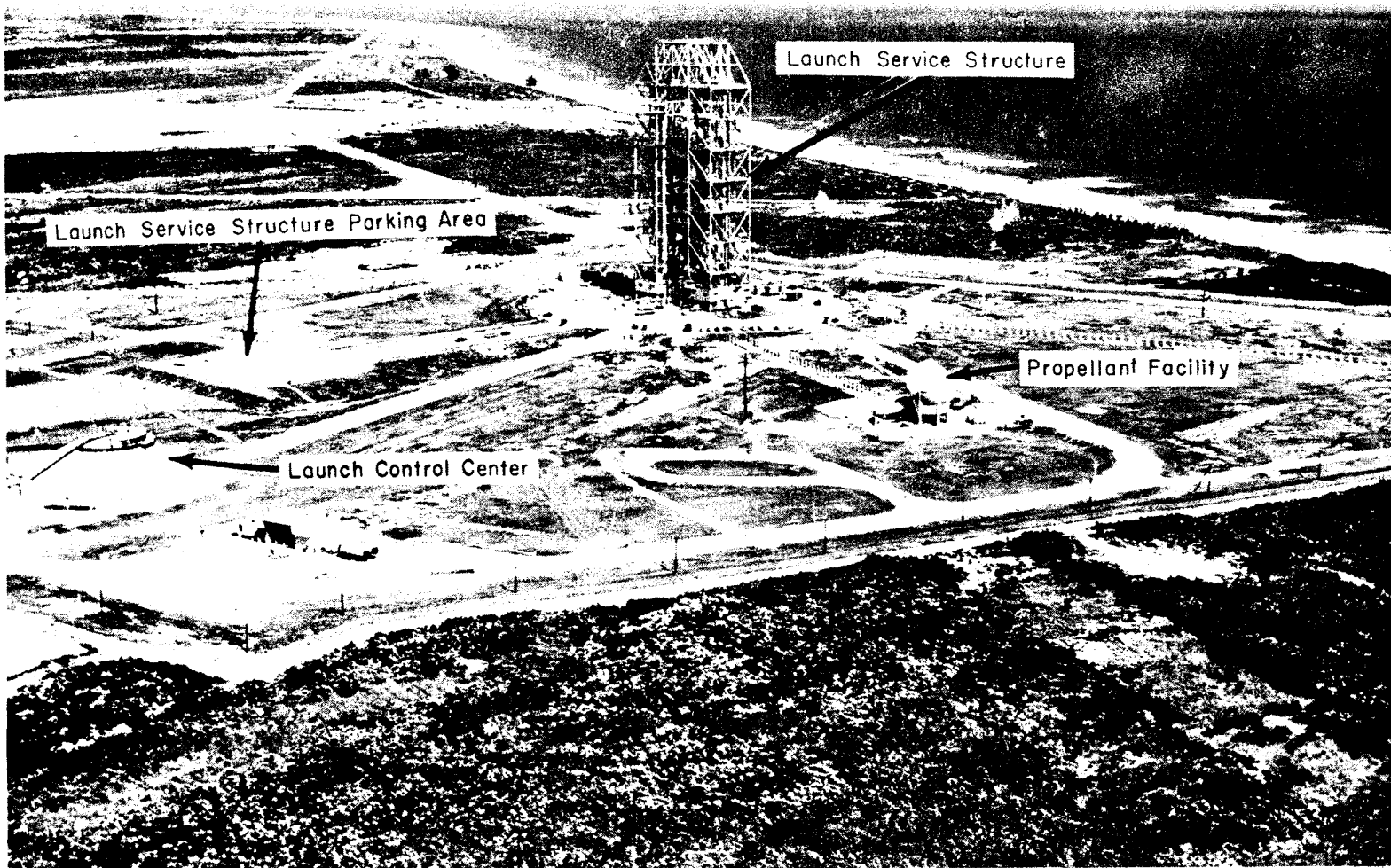


Fig. 3.3 Saturn C-1 launch complex LC 34.

burning RP-1 and LOX with a total thrust of 1,500,000 lb. Four of the engines are gimballed to provide control during first-stage powered flight. The second stage develops 90,000 lb of thrust with six liquid-hydrogen/LOX engines. The third stage has two liquid-hydrogen/LOX engines that develop 30,000 lb thrust. The Saturn uses all-inertial guidance. A high-speed digital computer will ultimately be incorporated to provide a universal guidance system capable of performing a variety of mission requirements to meet differing payload objectives.

Launch complex 34, at Cape Canaveral, Florida, used for the first Saturn launching, is a 45-acre facility expressly built for launching America's first space vehicle developed for the peaceful exploration of space. The main functional elements of the launch complex are the launch control center, launch service structure, launch pad, and propellant and pressurization facilities.

The launch control center is housed in a domed building, 120 ft in diameter (Fig. 3.4). The inner dome is of 5-ft thick reinforced concrete. On top of the inner dome is an earth fill which varies from 7 ft in the center to 14 ft at the edges. The final layer is 4 in. of gunite. The building is designed to withstand a blast pressure of 311,000 psi.

The service structure, used to erect and checkout the vehicle on the launch pedestal, is 310 ft high and weighs 2800 tons. Said to be the world's largest wheeled structure, it is mounted on four carriages powered by four 100-hp motors. It is capable of moving from 1.5 to 40 ft/min. It is anchored to steel piers by large wedges, enabling it and the vehicle it protects to withstand hurricane winds up to 125 mph.

The launch pad, 430 ft in diameter, is constructed of 8 in. thick, reinforced concrete. Located in the center of the pad, the launch pedestal is used to support and retain the vehicle during checkout and launch operations. Bolted to the top of the pedestal are eight steel arms, four to support the vehicle and four others to support and hold it down until proper ignition is attained. The foundation of the pedestal is a 160 ft by 106 ft concrete block set 9.5 feet below the surface of the pad.

The propellant facilities include an RP-1 system, LOX system, and a liquid hydrogen system. Two 30,000-gal cylindrical tanks are used for RP-1 fuel storage. The transfer system and associated plumbing includes two 1000-gal/min pumps, a recirculation pump, a filter-separator unit and miscellaneous valves, pipes, and controls. The main LOX storage tank is a sphere with an outside diameter of 43 ft. A smaller LOX vessel is used for replenishing the oxygen which boils off during the latter stages of launch preparation. The liquid hydrogen facility consists of a vacuum-jacketed, 125,000-gal sphere, pneumatic and electrical consoles, and the necessary plumbing and valves.

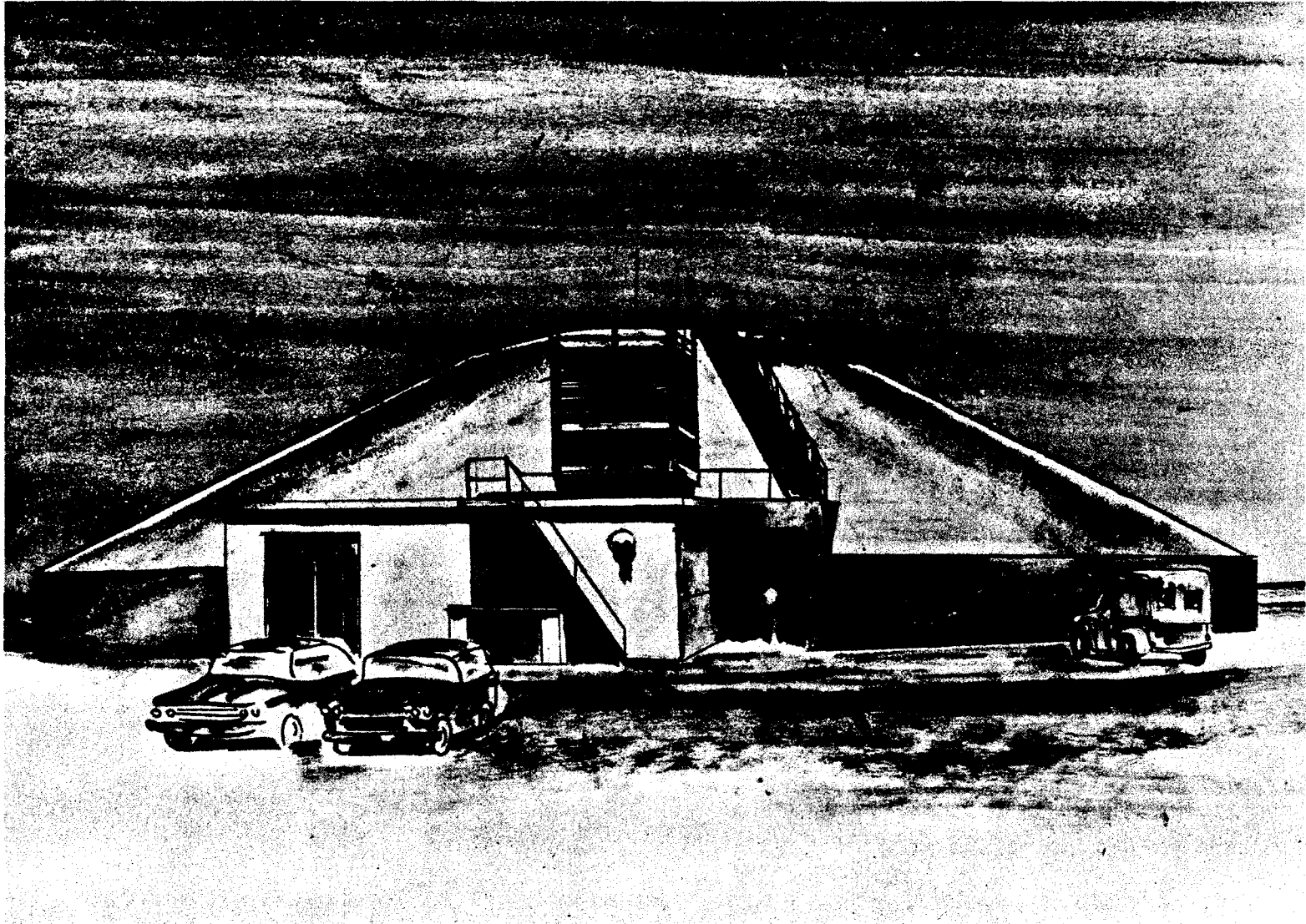


Fig. 3.4 Launch control center of LC 34.

High-pressure helium and nitrogen gases are required for the vehicle. The helium is used for bubbling the LOX tanks in the vehicle to keep the oxidizer from forming strata of different temperatures. The nitrogen is used for purging propellant lines, engine, and instrument compartments; for air bearings; and for pressure-operated components. The high-pressure system receives helium at 3000 psi pressure and boosts it to 6000 psi. The nitrogen is procured in liquid form and converted to gas before it is supplied to the vehicle.

In addition, a complex water system is available for safety and protection purposes. A comprehensive voice communications network and a closed-circuit television loop are used for intercommunication and monitoring the checkout and launching.

### 3.3 Skill Utilization

Until recently, missiles and space vehicles could be designed without too much consideration being given to the means for launching them. Launch preparations had to conform to vehicle design and were adapted to vehicle configurations and specifications which often prevented efficient launch operations.

This policy of tailoring launch procedures to vehicle design is no longer feasible with the advent of large space vehicles. The complexity of their configurations and the initial expense of their design and fabrication makes it apparent that all phases of a space program require design coordination at all stages of system development to insure success. Two significant trends have gradually emerged with the evolution of launch operations. As launch facilities and procedures became larger and more comprehensive, a need was created for professional, scientific, and technical services and skills that had been developed in other fields. At the same time, the exigencies of launch and space flight developments were reshaping these skills and capabilities into new fields of specialization that, in turn, gave birth to new professions and skills.

The many technologies, skills, and professions required for launch operations include such diversified and apparently unrelated fields as electrical, mechanical, and civil engineering, medicine, meteorology, law, psychology, and mathematics. Engineers design the complicated circuits for computers and checkout equipment, structural elements, and launch pads; space doctors study the preflight and postflight behavior characteristics of animals and men; meteorologists determine flight feasibility in terms of weather; lawyers busy themselves with the legal aspects of land acquisition; physiologists and psychologists study in-flight effects on human and animal behavior; mathematicians program computers, calculate trajectories, and analyze data transmissions. These are but a few of the technological and professional contributions required to sustain space activities.

Backing up the technical specialists are administrative and service specialists in such fields as public information, protocol, industrial relations, security, and publications. Many trades and professions are called upon to staff these important support functions. Among those contributing their skills and abilities are policemen, photographers, writers, and clerks. Their abilities, however, are shaped by the particular problems they encounter that are peculiar to launch operations.

Industrial relations provide a good example of how a support service can be shaped into a form somewhat different from the classic mold. In private industry, the industrial relations specialist must concern himself primarily with the labor unions that represent the workers of his company. Quite often there is only one man with whom an agreement must be reached. A similar situation does not exist for the industrial relations office of a large government-operated launch facility. Numerous unions and contractors are involved in the design, construction, and maintenance of space vehicles and launch facilities; and the industrial relations office must consider each contractor's relationship to the government and to the unions with whom they have bargaining agreements. It must also consider other government agencies engaged in launch operations and in the construction of launch facilities.

In the process of working with unions, contractors, and government agencies, the industrial relations specialist becomes a launch operations industrial relations specialist. He is in the anomalous position of representing an employer who hires employers. Instead of the classic company-union relationship, it has become a government-company-union triangle.

All the specialized fields and subfunctions necessary to launch a space vehicle into orbit or on a deep space mission cannot be completely envisioned by one person. The interdependent network of information and services is, for all its complexity and self-contained features, dependent upon a continuous incoming flow of materials, services, and information.

In the development of complex space vehicles and associated launching systems, nearly all fields of knowledge are called upon. This utilization, however, is not a unilateral benefit; the application of these fields of knowledge to specialized launch and space flight problems has contributed to their advancement in other applications. For example, the requirement for lightweight, reliable instrumentation for guidance and control and for exploratory scientific experimentation in space accelerated the development and production of subminiature components such as transistors. The application of transistors to communications, computers, and automated equipment has become widespread.

Radar, telemetry, and optical instrumentation supply the major portion of the information on each space vehicle launching and flight. Applications arising from radar and telemetry requirements for space vehicles include improved landing and flight controls for commercial aircraft, astronomical tracking and observation of the Sun and other radio stars, and additional navigation safeguards. Increasingly accurate, long-focal length cameras have also been developed that determine vehicle position in flight as related to a stellar background. These cameras are currently being used in geodetic surveys. In addition, the use of cryogenic propellants such as liquid hydrogen and liquid oxygen, contribute to the development of new equipment and techniques used in manufacturing, handling, storage operations, and have recently found application in the food preservation industry.

### 3.4 Future Concepts

As indicated by the comprehensive Saturn C-1 launching installations must be designed to provide maximum operating efficiency for a particular type of space vehicle. Several versions of the Saturn vehicle were planned, consecutively designated C-1, C-4. Each succeeding one was to be a more powerful and logical follow-on to its predecessor. However, the success achieved with the first version, C-1, has advanced the Saturn program to the projected C-5 version. The initial concept of the Saturn C-5 is a three-stage vehicle with 7,500,000-lb thrust first stage, a 1,000,000-lb thrust second stage, and a 200,000-lb thrust third stage. The three stages are expected to place 110-ton payloads into an Earth orbit to accomplish in-space rendezvous for manned lunar flights.

The higher launching rates, greater thrust, and increased acoustic disturbance inherent in the advanced Saturn are a few of the factors that are shaping a new concept for launch facilities. The launch complex for the Saturn C-5 now being planned (Fig. 3.5) will incorporate features of this concept; these include a separate vertical assembly building, a transporter/launcher complete with umbilical tower, an arming tower, fueling facilities, and a minimum pad.

The vertical assembly building will provide the space and equipment necessary to assemble and checkout the entire space vehicle. This will eliminate the necessity for long periods of time on the launching pad for checkout and assembly. It will also provide a controlled environment where assembly and checkout operations can be conducted under favorable conditions.

The transporter/launcher (Fig. 3.6) serves as a platform for vertical assembly, checkout, transport and launch. It also contains the umbilical tower so that umbilical connections will remain intact while the vehicle is being transported; this will eliminate repeated checkout procedures at the launch site. In addition to reducing checkout

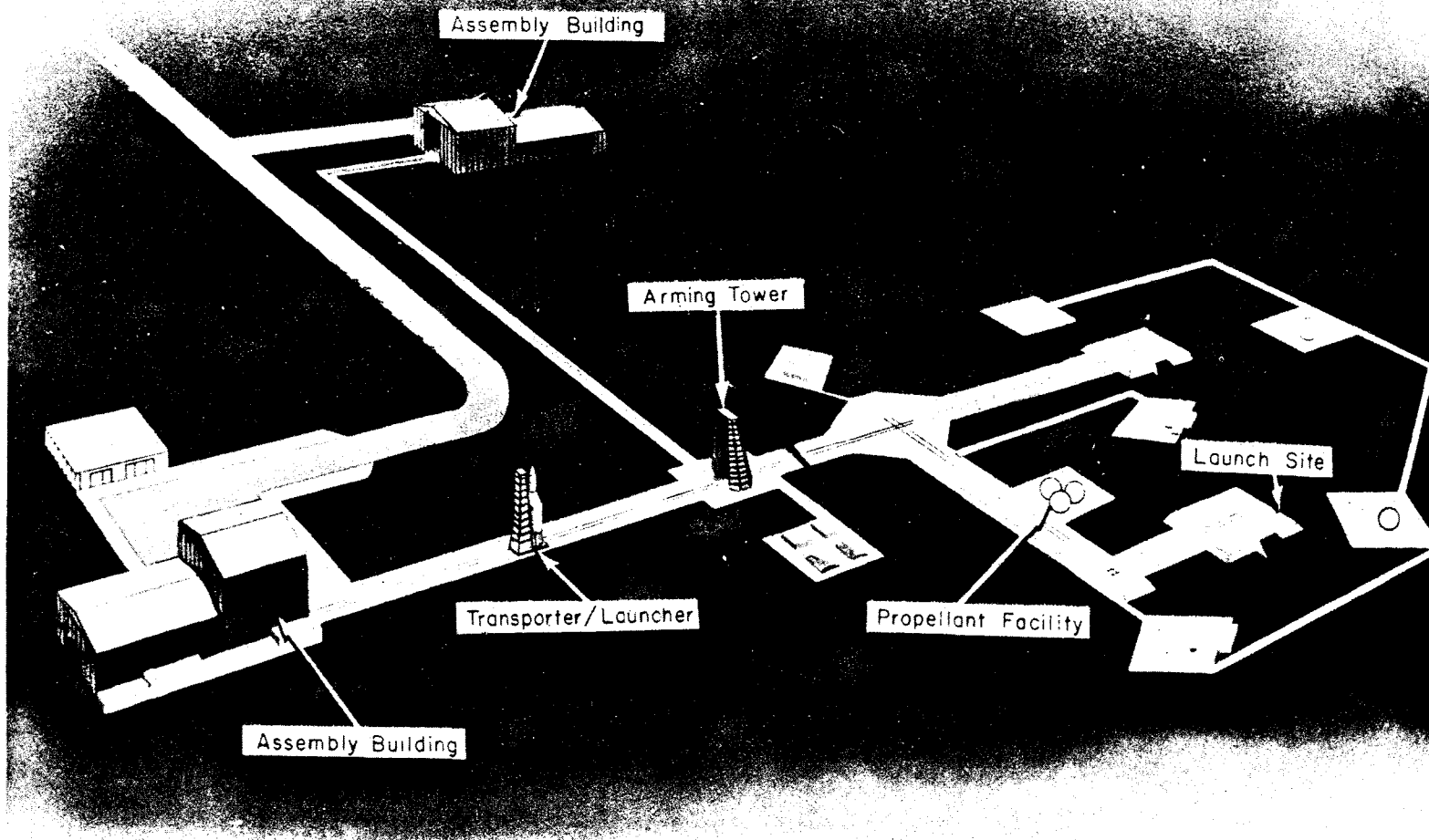


Fig. 3.5 Planned launch complex for Saturn C-5.

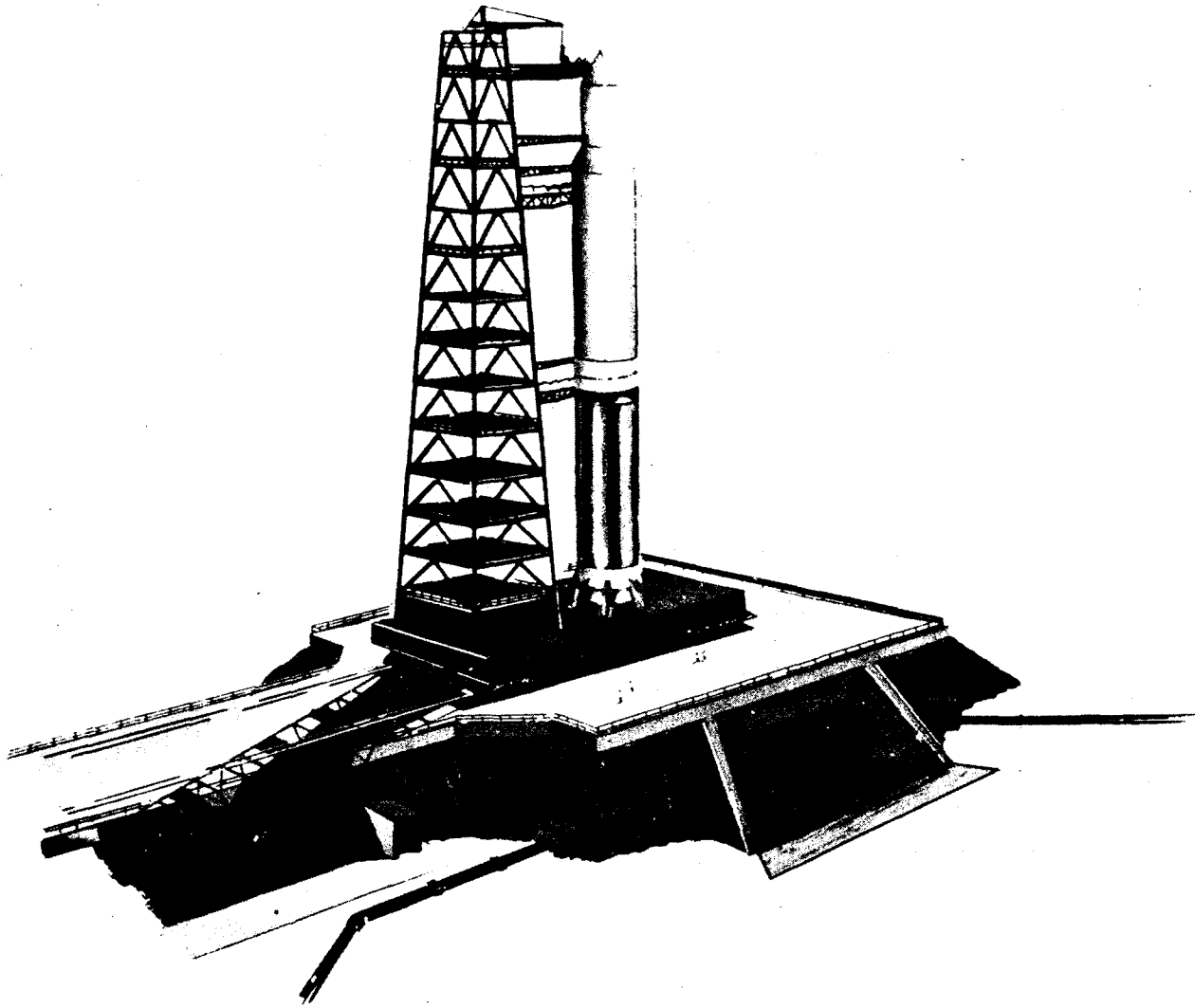


Fig. 3.6 Proposed Saturn C-5 transporter-launcher.



time on the pad, the transporter/launcher may be used to return the vehicle to the assembly building if a hurricane or other threatening weather is imminent. The transporter/launcher and assembly building eliminate the requirement for individual launch service structures. Two approaches to the development of the transporter/launcher are under study. The first is the use of wheeled vehicles operating on rails, and the second is the use of barges for water transport. Precise control of movement, vibration, and stability are essential factors in the development of the transporter/launcher.

The arming tower will provide a facility where explosive items such as retrorockets, squibs, and igniters can be installed while the vehicle is protected from environmental hazards. The arming tower will be so located that vehicles from one or more assembly buildings may be serviced.

The minimum launch pad (Fig. 3.7) will consist essentially of compacted earth covered with concrete. A flame deflector will be positioned under the pad. The complex pad facilities previously required will be eliminated through use of the vertical assembly building, the transporter/launcher, and the arming tower. This new concept is based on a high launch rate and consideration of the complexity of future space vehicle configurations. It is less expensive, operates more efficiently, and is capable of launching space vehicles at a more rapid rate than is now possible. The advantages of this new concept in launch complexes include a higher launching rate and the resultant reduction in initial construction costs and amount of real estate required for individual launches.

In addition to the savings in money and real estate, there are several other advantages that will accrue from the application of the new launch concept. One advantage is that umbilical connections will remain intact while the vehicle is being transported to the minimum pad, thereby preserving the validity of tests made in the assembly area. An interconnecting cable, carrying digital information and commands, will be the only connection between the launch control center and the space vehicle on the pad. The disconnection and reconnection of components, the principal reason checkout procedures are now repeated at the launch site, will no longer be necessary. This will result in reduction of operational work time and effectively reduce launch operations costs.

One factor that makes this concept possible is the use of automatic and digital equipment. Much of the present checkout and launch equipment consists of analog computers whose findings are affected by the voltage drops encountered over long transmission circuits. This led to the development of the blockhouse, near the launch pad, to reduce the distance between the information source and the analog computers. With digital computers, which record by impulse, variable voltage is not a factor; therefore, data received from a long distance retains its validity.

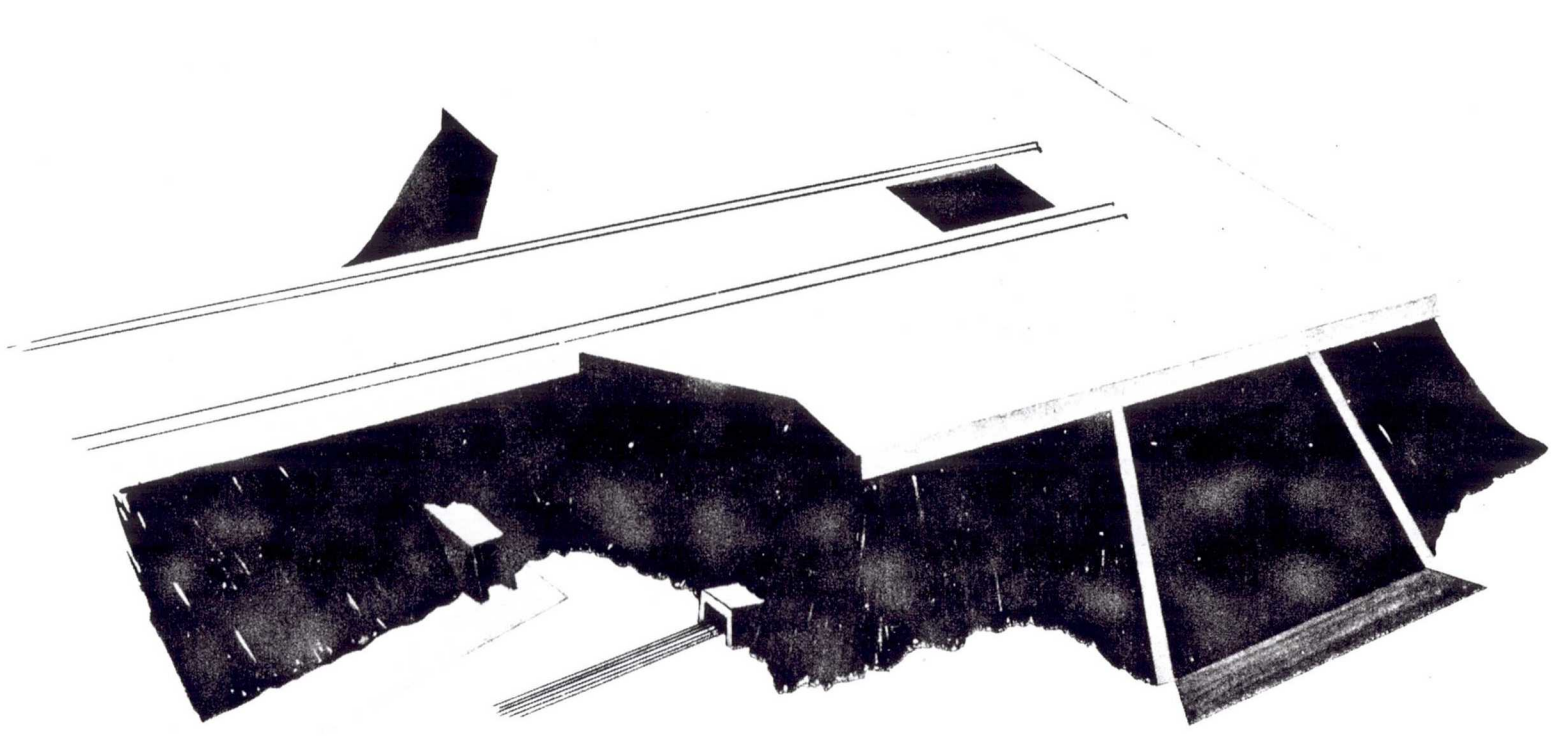


Fig. 3.7 Minimum launch pad.

This situation eliminates the need for a blockhouse and makes it possible to checkout and launch the space vehicle with one set of equipment located in the assembly building.

The need for individual service structures will also be eliminated by this new concept. These structures are now used to assemble the vehicles and to protect them from hurricanes. The vehicles, under the new concept, can be assembled before they reach the pad and can be removed from the pad area before a hurricane strikes. This factor alone will result in great savings in time and money, because the service structures are heavy and impose tremendous loads on their means of transport. The elimination of the service structure and the blockhouse will also result in a reduction of acoustical and explosive hazard areas.

One of the most rewarding aspects of this concept is the short stay time at the launch site. Instead of occupying an expensive launch complex for several weeks, the vehicle will remain at the relatively inexpensive pad area for less than 1 week. This concept will allow the assembly building to operate at full capacity, and thereby increase the launching rate.

The flexibility of this concept is another of the major advantages. Separate assembly buildings for liquid and solid propelled space vehicles can be located on the same complex. By modifying the transporter/launchers and their umbilical towers to fit individual configurations, these buildings become adaptable to various manned and unmanned space vehicles. This flexibility is also demonstrated by the capability of moving vehicles to the pad and back into the assembly building in a few hours, while maintaining their flight readiness even under hurricane conditions; this mobility, in turn, will reduce the hazard of weather-induced corrosion.

The concept also provides increased flexibility in scheduling the launching of vehicles that may or may not be able to meet a precise launch schedule. If a particular space probe, for example, can only be fired within a restricted time frame, the delay of a previously scheduled launch at the same pad area will not interfere with the mission. The earlier scheduled vehicle can be held in the assembly building on its transporter/launcher until after completion of the priority program. This concept also demonstrates how facility configurations, checkout and launch procedures, and vehicle design and development combine to become one synchronized and integrated effort.

Many other concepts vie with the dispersed-fixed concept as embodied in the proposed C-5 complex. Included are the underground silo and the fixed above-ground concepts, as well as several versions of the mobile concept. The underground silo concept is already being employed (Fig. 3.8).

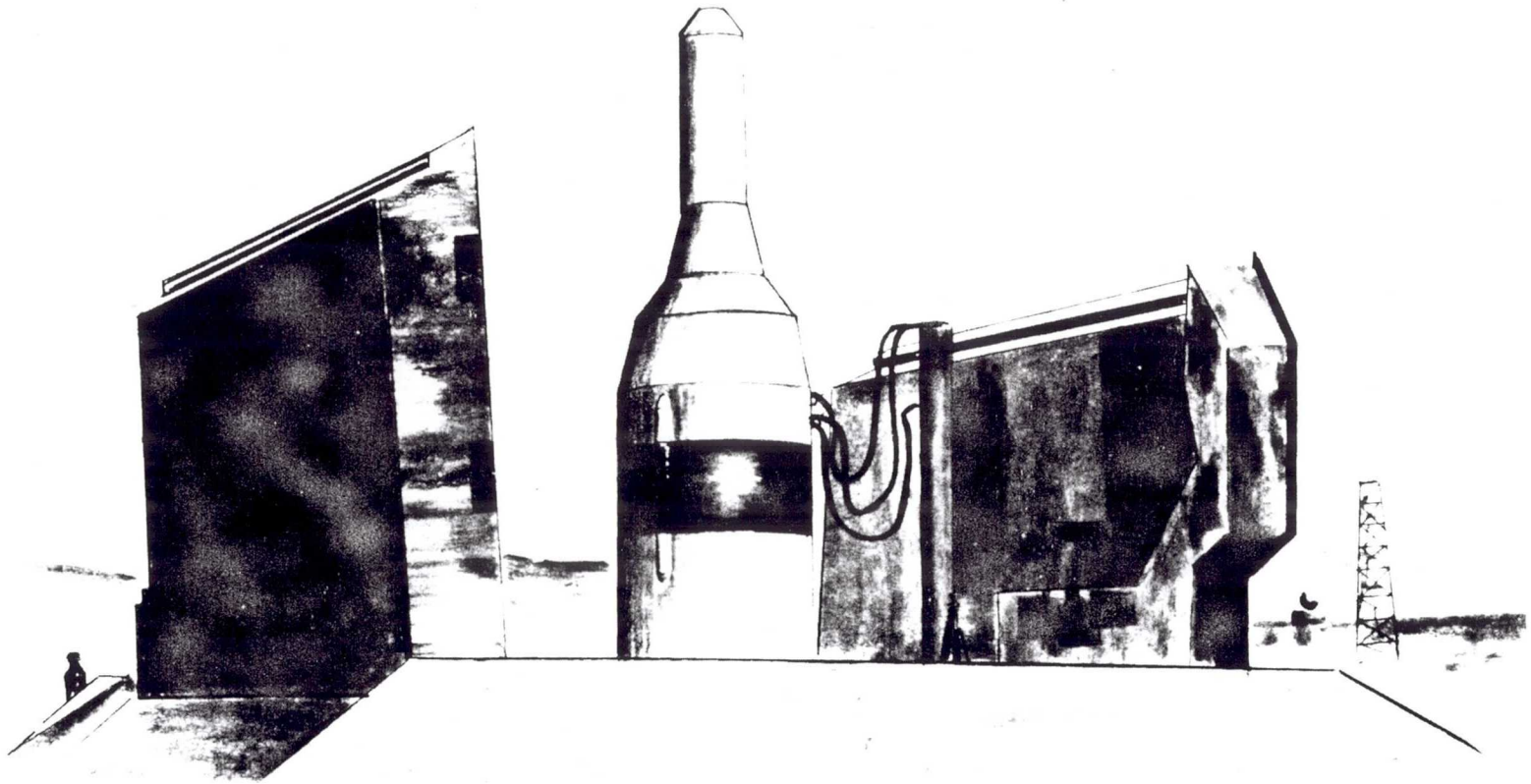


Fig. 3.8 Underground silo shown with ICBM.

Operational Atlas ICBMs are deployed in strategically located underground silos throughout the country. The underground silo launch site has several advantages. It is easily concealed, protected from the elements, relatively invulnerable to air attack, and comparatively easy to maintain after construction. In addition to the Atlas sites, the underground silo concept is planned for Titan and Minuteman ICBMs. Since the Minuteman is a solid fuel missile, its silo will not require contiguous underground fueling facilities.

Future space vehicles may dictate a variation of the fixed-vehicle/fixed-tower concept, wherein vehicles are assembled at the launch site and launched directly from the assembly structure. The nature of their missions eliminates the "shoot and scoot" or "shoot and hide" requirements so necessary for military missiles. Neither will they be required to maintain the high launch rate planned for the Saturn C-5s. The fixed-missile/mobile-tower concept, whereby vehicles are also assembled at the launch site but launched after the assembly structure has been moved, is the basic concept in use today, especially at missile and vehicle test centers.

The mobile concept is actually several concepts, but all of them have in common the idea of launching missiles and space vehicles from a moving site or from a site which can be moved. The main advantage is the relative invulnerability they provide against enemy attack. For this reason, the military has taken the lead in translating these ideas into reality.

Several nuclear submarines capable of launching Polaris missiles while continuously on the move are already on station (Fig. 3.9). This will require tactical, rather than strategic intelligence of their whereabouts by a potential enemy. Nonmilitary applications of the mobile launch concept will be used for other than security reasons. Launches from orbit are already being seriously considered for manned space probes. This concept would have space vehicles outfitted and refueled from orbiting modules.

These are a few of the concepts that have been employed, are being employed, and will be employed to launch missiles and space vehicles. In the meantime, feasibility studies of other concepts will be made as they are conceived.

Intimately associated with launch operations is the burgeoning area of space flight operations. The elaborate measures and precautions that are taken before a flight are not concluded upon the successful liftoff of the space vehicle. The environment of space must be probed and explored to resolve many of the technical and human problems that will be encountered in manned space flight operations. Space navigation, inflight maintenance and checkout, orbital rendezvous, refueling and

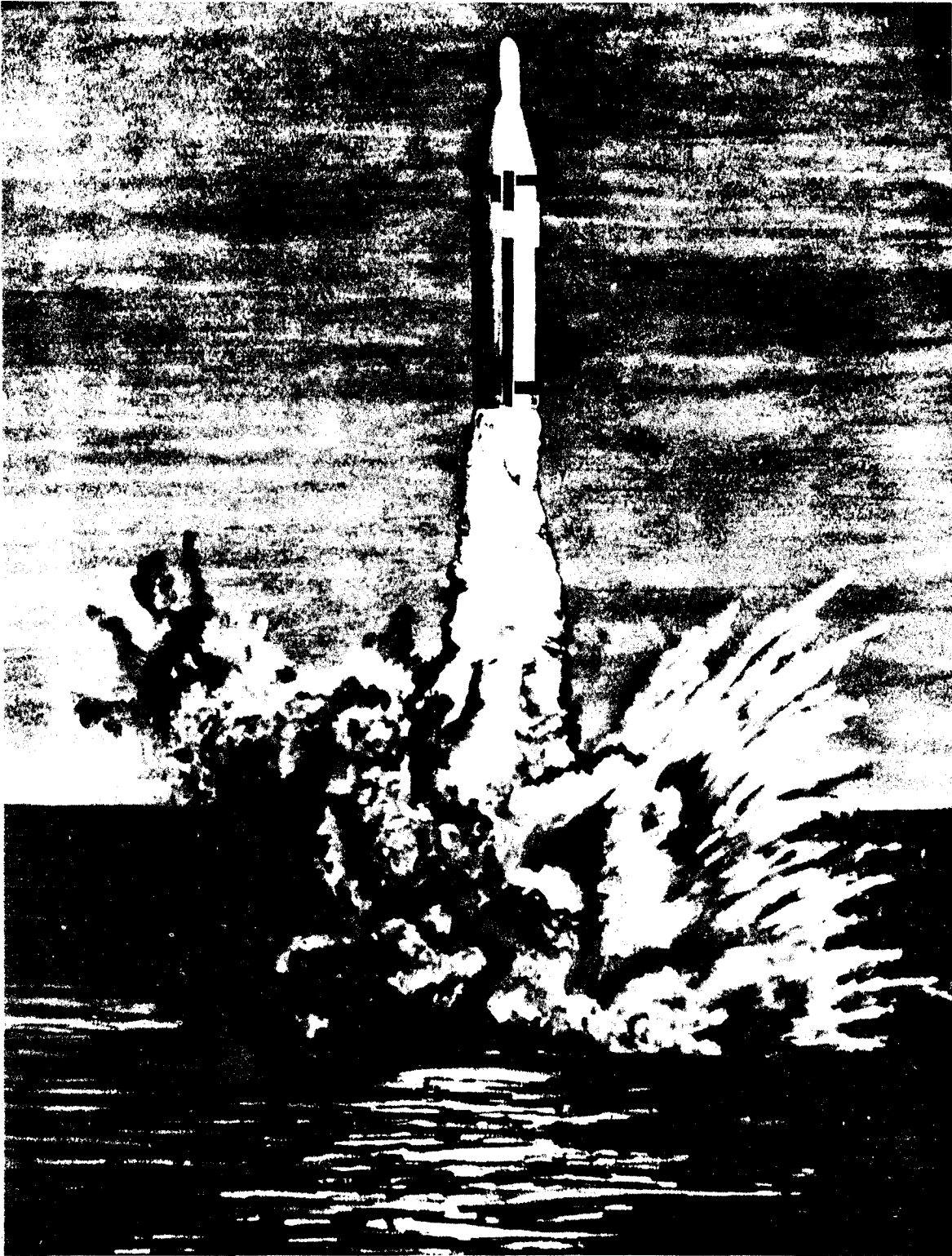


Fig. 3.9 Underwater missile launching.

docking, escape velocities, nutrition, and on-board equipment are a few of the areas where these problems will be encountered.

Manned lunar and planetary space probes will create an interesting paradox. Many facilities, services, supplies, professions and skills are required to launch a space vehicle; yet one man, or a few men at the most, will be expected to duplicate the function of this vast apparatus without having direct access to it. Flight and launch operations, which ordinarily would take weeks or months of advance preparation and planning, may require nearly instantaneous execution simultaneous with, or soon after, the decision to launch has been made.

Several methods are now available to provide an astronaut or flight crew the vast amount of information necessary for quick execution of flight and launch decisions. Other methods will be developed through experience. Television, telemetered information, ground analysis, and automatic identification of trouble can be employed. After automatic sensing devices locate a trouble area, telemetered information can be sent to ground stations for analysis. If necessary, specialists may be consulted for solutions that can be transmitted back to the spacecraft. Television may also be employed to spot trouble or to communicate with ground stations.

Some problems, such as those connected with long periods of weightlessness and inflight nutrition, will require extended space flight experience before they can be satisfactorily resolved. Procedures for emergency repairs on lunar or planetary surfaces will also improve with experience. A continuation of the aggressive pursuit of space exploration will take brains, imagination, rare skills, management, engineering know-how, salesmanship, and the cooperative efforts of many individuals and groups of people. These efforts, if properly applied, will continue the evolution of launch and space flight concepts and will contribute to the development of unexplored fields of knowledge.

## 4

## SPACE CARRIER VEHICLE FIRING HISTORIES

Frederick I. Ordway, III

Space Systems Information Branch  
George C. Marshall Space Flight Center  
National Aeronautics and Space Administration  
Huntsville, Alabama

Within the context of this paper a space carrier is defined as a rocket-propelled vehicle designed to place payloads (1) in orbit around the Earth, (2) along escape trajectories, or (3) to vertical altitudes of at least 300 miles. Vehicles lifting payloads to lower altitudes are considered atmospheric sounding rockets and are not discussed herein.

The characteristics and specifications of virtually all known space carriers are given in [1, 2, 3 and 4].

Carriers are conveniently classified into four categories, namely (1) small carriers, (2) IRBM-based carriers, (3) ICBM-based carriers, and (4) carriers based on first stages developing in excess of a million pounds of thrust.\* Firing histories through the end of 1961 for all major carriers are tabulated and arranged in alphabetical order for ease of reference.

Included in the small space carrier category are the early liquid rocket motor-propelled Juno 1 and Vanguard. These carriers were used by the United States to orbit Explorer and Vanguard satellites weighing from 18 to 53 lb. The Juno 1 was based on a Redstone ballistic missile first stage and three upper stages powered by clusters of small solid rocket motors. It was successful in 3 out of 6 orbital attempts. Vanguards were three-stage carriers, with single liquid rocket motors powering the first and second stages and a solid motor the third. One small test satellite and two full scale satellites were orbited out of a total of 11 attempts. Juno 1 and Vanguard carriers were retired from service in 1958 and 1959, respectively.

Today, all-solid propelled carriers have taken over the functions of these two obsolete liquid propelled vehicles. In the Argo series, the D-4, D-8, and E-5 have been used repeatedly to lift payloads in the 50- to 150-lb range from 400 to 1200 miles from the surface. NASA Scouts and U. S. Air Force Blue Scouts increasingly are being employed to

---

\*A fifth category includes vehicles launched from balloons. The only known examples of such carriers are the Far Sides fired 6 times during 1957 with 3- to 5-lb payloads. Two of these may have reached 4000 miles altitude, but transmitter failures prevented confirmation of performance.



carry relatively small payloads hundreds and often thousands of miles from the Earth, and to orbit satellites in the 100- to 200-lb class. The first Astrobe 1500 was fired in a flare experiment in December 1961. Seven five-stage, all-solid Strongarms were launched through 1961. British Black Knights were fired from Woomera, Australia beginning in 1958.

The second category is made up of carriers whose first stages are powered by intermediate range ballistic missiles. Included are one Jupiter-based carrier, the Juno 2; the five Thor-based carriers, namely Thor Able, Thor Agena A, Thor Agena B, Thor Delta, and Thor Epsilon (Able Star). The Juno 2, Thor Able, and Thor Agena A are no longer used; the remaining three Thor-based carriers are in constant service. The Soviets apparently used a T2 IRBM-based carrier once--to launch Sputnik 1 on October 1957.

To develop the four-stage Juno 2 it was necessary to substitute the newer Jupiter for the Juno 1's Redstone first stage. The upper staging for both vehicles was essentially the same. The Juno 2 launched two space probes, one 63,580 miles into space and the other along a lunar by-pass trajectory into orbit around the Sun. It also orbited 3 satellites out of 8 attempts.

The three-stage Thor Able used a Thor first stage and Vanguard-derived upper stages. It was employed in 3 early unsuccessful lunar firings, 1 of which soared 70,700 miles into space. It successfully powered Pioneer 5 into orbit around the Sun and out of 3 attempts launched 2 artificial Earth satellites.

The Thor Agena A was a two-stage carrier used exclusively in the Discoverer program. It orbited 10 satellites out of 15 launchings, and provided valuable flight experience for the follow-up Thor Agena B program.

The Thor Agena B is similar to the Thor Agena A, except that the Agena B second stage contains double the quantity of propellants and its single chamber engines possess the capability of being shut off and restarted in space. This feature provides the Thor Agena B with a greater flexibility to conduct orbital operations. Through December 1961, it had orbited 15 Discoverers in 21 attempts.

The Thor Delta is, like the Thor Able, a three-stage carrier with somewhat higher performance. It has been fired 6 times and succeeded in orbiting 5 satellites. The Thor Epsilon, also known as the Thor Able Star, is a two-stage carrier used to orbit Navy Transit navigation, Courier communication, and piggyback scientific satellites. It was successful in 6 out of 8 firings.

Of the American ICBM-based space carrier vehicles the Atlas was used exclusively through 1961. It has been employed without powered upper stages, in several two-stage configurations, and in a three-stage version. The two-stage Titan 1 and 2 ICBMs possess the capability to carry space payloads but as of the end of 1961 had not been used for this purpose. The Titan 3, which is a Titan 2 with two 120-in. solid wrap-around boosters attached to the first stage, has been selected to orbit Dynasoar manned gliders.

Atlas Score was fired once in the Score communication satellite configuration in which the entire empty shell of the Atlas (minus booster engines and shrouds) entered into orbit. In Atlas Mercury suborbital flights long range trajectory capsule recovery techniques were worked out. Later, when Mercury capsules were fired into orbit, they were accompanied by the empty Atlas shell as in the Score firing. By 31 December 1961, two Atlases without active upper stages had been successfully fired in Mercury orbital attempts.

Three Atlas Ables were launched, all meeting with failure. If successful, they would have placed fairly heavy payloads into orbit around the Moon. These were the only three-stage Atlas-based carriers built; following its unsuccessful firing history the program was cancelled.

Atlas-based carriers have been rather successful in two-stage configurations. Four Atlas Agena A firings resulted in two orbital achievements prior to the time the larger Agena B stage was available. Of the 7 Atlas Agena B firings, 6 resulted in orbits being achieved. In its military applications, the Agena B stage houses the complete payload, but in such space exploration applications as Ranger the probe separates from the stage and travels along the desired trajectory.

The final two-stage Atlas-based carrier is the Atlas Centaur. Possessing more than twice the power of the Agena B stage, the Centaur is still under development. As of January 1962 no Atlas Centaur firings had occurred.

The Soviet ICBM-based space carrier program is far less understood than that of the U. S. Firing histories are only known for successful launches; no data are available for space carrier vehicle firings which have not resulted in a completed mission.

It is believed that Sputniks 2 and 3 were orbited by early T3-type carriers, following which larger, more powerful, T3As were placed in operation. The latter vehicles succeeded in launching 3 lunar probes in 1959 and a series of large satellites in 1960 and 1961. From one of these (Sputnik 5) a Venus probe was fired. Two of the satellites were manned, Vostoks 1 and 2. The first stage thrust developed by these carriers is unknown but is probably about 800,000 lb, and possibly as much as 1,200,000 lb.

In the greater-than-a-million-pound-first-stage-thrust category the only definitely known development is the U. S. Saturn. However, as noted above, the Soviets may already be firing carriers at this high thrust level.

The first Saturn configuration, known as the C1, has an eight-engine first stage plus one or two high energy upper stages, depending on the mission requirements. By the end of 1961 a single test vehicle had been fired with inert upper stages. The advanced C5 version of Saturn, now under development, has a first stage powered by five engines which provide a total stage thrust of 7,500,000 lb.

Beyond Saturn would come Nova-type vehicles with first stages developing at least 10,000,000 lb of first stage thrust. A Nova developing 12,000,000 lb of first stage thrust with high energy upper stages could place approximately twice the payload into orbit around the Earth as could the Saturn C5.

#### REFERENCES

1. Ordway, Frederick I., III, and Ronald C. Wakeford, "International Missile and Spacecraft Guide," McGraw-Hill Book Company, Inc., New York, 1960.
2. Ordway, Frederick I., III, and B. Spencer Isbell, "United States Space Carrier Vehicle and Spacecraft Developments," Astronautica Acta, 7, Nos. 2-3, 1961.
3. Ordway, Frederick I., III, Space Carrier Vehicles, in "Handbook of Astronautical Engineering," ed. H. H. Koelle, McGraw-Hill Book Company, Inc., New York, 1961.
4. Ordway, Frederick I., III, James P. Gardner, Mitchell R. Sharpe, and Ronald C. Wakeford, "Applied Astronautics," Prentice-Hall, Inc., New York (in press).

#### Firing Site Location Abbreviations

AMR	Atlantic Missile Range, Florida
PMR	Pacific Missile Range, California (including Vandenberg AFB)
Ramey	Ramey AFB, Aguadilla, Puerto Rico
Wallops	Wallops Station, Wallops Island, Virginia
Woomera	Australian Guided Weapons Range, Woomera, South Australia

Table 4.1 Argo D-4 (Javelin) Firing History

<u>No.</u>	<u>Date</u>	<u>Firing Range</u>	<u>Remarks</u>
1	7 July 59	Wallops	Vehicle JV-1 lifted payload to altitude of 620 miles.
2	21 July 59	Wallops	Vehicle JV-2 broke up after takeoff.
3	22 Dec 59	Wallops	Vehicle 8.01 lifted payload to altitude of 560 miles.
4	14 Jan 60	Wallops	Vehicle JV-3 lifted payload to altitude of about 800 miles.
5	26 Jan 60	Wallops	Vehicle 8.02 lifted payload to altitude of 591 miles.
6	30 June 60	Wallops	Vehicle 8.07 broke up after third stage burnout.
7	9 Nov 60	Wallops	Vehicle 8.04 lifted payload to altitude of 610 miles.
8	10 Dec 60	Wallops	Vehicle 8.05 lifted payload to altitude of 450 miles.
9	12 Dec 60	Wallops	Vehicle 8.08 lifted payload to altitude of 720 miles.
10	27 Apr 61	Wallops	Vehicle 8.10 lifted payload to altitude of 472 miles.
11	13 June 61	Wallops	Vehicle 8.09 lifted payload to altitude of 539 miles.
12	14 June 61	Wallops	Vehicle 8.13 lifted 62-lb payload to altitude of 561 miles.
13	24 June 61	Wallops	Vehicle 8.15 lifted payload to altitude of 633 miles.
14	10 Oct 61	Wallops	Vehicle 8.23 lifted payload to altitude of 585 miles.
15	14 Oct 61	Wallops	Vehicle 8.17 lifted 109-lb top-side sounder to altitude of 560 miles.

Table 4.2 Argo D-8 (Journeyman) Firing History

<u>No.</u>	<u>Date</u>	<u>Firing Range</u>	<u>Remarks</u>
1	19 Sept 60	PMR	Vehicle 11.01 carried 83.5-lb Nerv 1 to an altitude of 1260 miles.
2	15 Nov 61	PMR	Bios 1 flight failed because carrier veered to right 57 sec after launch.
3	18 Nov 61	PMR	Vehicle carried 83-lb Bios 2 to a range of approximately 600 miles (tracking signals were erratic).

Table 4.3 Argo E-5 (Jason) Firing History

<u>No.</u>	<u>Date</u>	<u>Firing Range</u>	<u>Remarks</u>
1	11 Jul 58	Wallops	Vehicle J-A flight failed.
2	16 Jul 58	Wallops	Vehicle J-B flight failed.
3	1 Aug 58	Wallops	Vehicle J-CX carried 50-lb payload to altitude of 470 miles.
4	14 Aug 58	AMR	Vehicle 1822* carried 50-lb payload to altitude of 432 miles.
5	19 Aug 58	Ramey	Vehicle 1841* flight failed.
6	25 Aug 58	Wallops	Vehicle J-14 flight failed.
7	27 Aug 58	AMR	Vehicle 1909* carried 50-lb payload to altitude of 585 miles.
8	27 Aug 58	Ramey	Vehicle 1914* flight failed.
9	28 Aug 58	Ramey	Vehicle 1917* carried 50-lb payload to altitude of 510 miles.
10	28 Aug 58	Wallops	Vehicle J-15 flight failed.
11	29 Aug 58	Wallops	Vehicle J-16 carried 50-lb payload to altitude of 510 miles.
12	29 Aug 58	AMR	Vehicle 2022* carried 50-lb payload to altitude of 547 miles.
13	30 Aug 58	Wallops	Vehicle J-17 carried 50-lb payload to altitude of 518 miles.
14	30 Aug 58	Ramey	Vehicle 2023* carried 50-lb payload to altitude of 515 miles.

Table 4.3 Argo E-5 (Jason) Firing History (Cont'd)

<u>No.</u>	<u>Date</u>	<u>Firing Range</u>	<u>Remarks</u>
15	30 Aug 58	AMR	Vehicle 2025* carried 50-lb payload to altitude of 435 miles.
16	30 Aug 58	Wallops	Vehicle J-18 carried 50-lb payload to altitude of 510 miles.
17	30 Aug 58	Wallops	Vehicle J-19 carried 50-lb payload to altitude of 480 miles.
18	30 Aug 58	Ramey	Vehicle 2026* flight failed.
19	30 Aug 58	AMR	Vehicle 2020* carried 50-lb payload to altitude of 500 miles.
20	2 Sept 58	Ramey	Vehicle 2041* flight failed.
21	2 Setp 58	Wallops	Vehicle J-20 carried 50-lb payload to altitude of 490 miles.
22	2 Sept 58	AMR	Vehicle 2043* carried 50-lb payload to altitude of 492 miles.

\*Patrick Air Force Base flight number; vehicle number not available.

Table 4.4 Astrobee 1500 Firing History

<u>No.</u>	<u>Date</u>	<u>Firing Range</u>	<u>Remarks</u>
1	8 Dec 61	PMR	Vehicle lofted 3 sets of 7 flares to altitude of 1361 miles.

Table 4.5 Atlas Able Firing History

<u>No.</u>	<u>Date</u>	<u>Firing Range</u>	<u>Remarks</u>
1	26 Nov 59	AMR	Lunar flight attempt failed due to upper stage malfunctions.
2	25 Sept 60	AMR	Lunar flight attempt failed due to abnormal second stage ignition.
3	15 Dec 60	AMR	Lunar flight attempt failed due to carrier explosion.

Table 4.6 Atlas Agena A Firing History

<u>No.</u>	<u>Date</u>	<u>Firing Range</u>	<u>Remarks</u>
1	26 Feb 60	AMR	Midas 1 satellite flight failed; second stage separation probably did not occur.
2	24 May 60	AMR	Vehicle orbited 5000-1b Midas 2 at an apogee of 320 miles and a perigee of 300.1 miles.
3	11 Oct 60	AMR	Satellite flight failed.
4	31 Jan 61	AMR	Vehicle orbited satellite at an apogee of 344 miles and a perigee of 295 miles.



Table 4.7 Atlas Agena B Firing History

<u>No.</u>	<u>Date</u>	<u>Firing Range</u>	<u>Remarks</u>
1	12 Jul 61	PMR	Vehicle orbited 3500-1b Midas 3 at an apogee of 2129 miles and a perigee of 2153 miles.
2	23 Aug 61	AMR	Vehicle orbited 675-1b Ranger 1 at an apogee of 313 miles and a perigee of 105 miles.
3	9 Sept 61	PMR	Satellite flight failed; carrier exploded on pad.
4	21 Oct 61	PMR	Vehicle orbited 3500-1b Midas 4 (apogee and perigee not available) together with 75-1b Project West Ford payload.
5	18 Nov 61	AMR	Vehicle orbited 675-1b Ranger 2 at an apogee of 146 miles and a perigee of 95 miles.
6	22 Nov 61	PMR	Vehicle orbited unknown satellite (orbital data not available).
7	22 Dec 61	PMR	Vehicle orbited unknown satellite (orbital data not available).

Table 4.8 Atlas Mercury Firing History

<u>No.</u>	<u>Date</u>	<u>Firing Range</u>	<u>Remarks</u>
1	9 Sept 59	AMR	Vehicle carried a capsule to altitude of 100 miles in down range test.
2	29 July 60	AMR	Flight failed due to explosion 65 sec after takeoff.
3	21 Feb 60	AMR	Vehicle carried payload to altitude of 113 miles in down range test.
4	25 Apr 61	AMR	Vehicle was exploded by range safety due to failure in Atlas flight programmer.
5	13 Sept 61	AMR	Vehicle orbited unmanned 2700-1b MR4 capsule at an apogee of 159 miles and a perigee of 100 miles.
6	29 Nov 61	AMR	Vehicle orbited unmanned 2900-1b MR5 capsule (with chimp "Enos" aboard) at an apogee of 148 miles and a perigee of 100 miles.

Table 4.9 Atlas Score Firing History

<u>No.</u>	<u>Date</u>	<u>Firing Range</u>	<u>Remarks</u>
1	18 Dec 58	AMR	Vehicle orbited 8661-lb Score 1 at an apogee of 911 miles and a perigee of 110 miles.

Table 4.10 Black Knight Firing History

<u>No.</u>	<u>Date</u>	<u>Firing Range</u>	<u>Remarks</u>
1	7 Sept 58	Woomera	Flight was successful.
2	Mar 59	Woomera	Vehicle reached altitude of 350 miles.
3	10 June 59	Woomera	Vehicle reached altitude of 500 miles.
4	29 June 59	Woomera	Vehicle reached altitude of 500 miles.
5	10 Nov 59	Woomera	Vehicle reached altitude of 450 miles.
6	24 May 60	Woomera	Vehicle fired along "low trajectory."
7	21 June 60	Woomera	Vehicle reached altitude of 300 miles.

Table 4.11 Blue Scout Firing History

<u>No.</u>	<u>Date</u>	<u>Firing Range</u>	<u>Remarks</u>
1 ("Jr.")	21 Sept 60	AMR	Vehicle D-1 carried 32.8-lb payload to altitude of 16,600 miles.
2 ("Jr.")	8 Nov 60	AMR	Vehicle D-2 failed because the second stage blew up.
3	7 Jan 61	AMR	Vehicle D-3 carried 392-lb payload to altitude of 1000 miles.
4	3 Mar 61	AMR	Vehicle D-4 carried 172-lb payload to altitude of 1580 miles.
5	12 Apr 61	AMR	Vehicle D-5 carried 365-lb payload to altitude of 1200 miles.
6	9 May 61	AMR	Vehicle D-6 veered due to severe first stage separation and was destroyed by range safety.
7 ("Jr.")	17 Aug 61	AMR	Radio contact lost after fourth stage ignition. Vehicle 0-1 may have carried 27-lb payload to altitude of 140,000 miles.
8	1 Nov 61	AMR	Vehicle D-8 satellite flight attempt failed due to first and second stage explosion; third stage was destroyed by range safety.
9 ("Jr.")	4 Dec 61	PMR	Vehicle 0-2 carried 29-lb payload to altitude of 27,600 miles.

Table 4.12 Juno 1 Firing History

<u>No.</u>	<u>Date</u>	<u>Firing Range</u>	<u>Remarks</u>
1	31 Jan 58	AMR	Vehicle orbited 18.13-1b Explorer 1 at apogee of 1575 miles and a perigee of 224 miles.
2	5 Mar 58	AMR	Satellite flight attempt failed because the vehicle's fourth stage did not ignite.
3	26 Mar 58	AMR	Vehicle orbited 18.53-1b Explorer 3 at an apogee of 1740 miles and a perigee of 119 miles.
4	26 July 58	AMR	Vehicle orbited 25.76-1b Explorer 4 at an apogee of 1373 miles and a perigee of 163 miles.
5	24 Aug 58	AMR	Explorer 5 satellite flight attempt failed because of improper guidance. Booster collided with upper stages after separation.
6	22 Oct 58	AMR	Flight attempt failed because the 18.3-1b Beacon 1 satellite broke off from upper stage cluster.

Table 4.13 Juno 2 Firing History

<u>No.</u>	<u>Date</u>	<u>Firing Range</u>	<u>Remarks</u>
1	6 Dec 58	AMR	Vehicle lifted Pioneer 3 to 63,580 mile altitude.
2	3 Mar 59	AMR	Vehicle fired 13.4-1b Pioneer 4 past Moon and into orbit around the Sun at an aphelion of 107.9 million miles and a perihelion of 91.7 million miles.
3	16 July 59	AMR	Satellite flight attempt failed because the main power inverter shorted.
4	14 Aug 59	AMR	Beacon 2 satellite flight attempt failed due to premature propellant depletion in the first stage.
5	13 Oct 59	AMR	Vehicle orbited 91.5-1b Explorer 7 at an apogee of 681 miles and a perigee of 345 miles.
6	23 Mar 60	AMR	Satellite flight attempt failed due to upper stage malfunction.
7	3 Nov 60	AMR	Vehicle orbited 90.14-1b Explorer 8 at an apogee of 1422 miles and a perigee of 258 miles.
8	24 Feb 61	AMR	Satellite flight attempt failed due to premature separation of third and fourth stages. Interaction between payload and shroud caused loss of inertial reference. Second stage fired at proper time; third stage did not fire.
9	27 Apr 61	AMR	Vehicle orbited 82-1b Explorer 11 at an apogee of 1113 miles and a perigee of 310 miles.
10	24 May 61	AMR	Satellite flight attempt failed because the second stage did not ignite.

Table 4.14 Saturn C-1 Firing History

<u>No.</u>	<u>Date</u>	<u>Firing Range</u>	<u>Remarks</u>
1	27 Oct 61	AMR	Test vehicle reached an altitude of 84.8 miles; first stage only fired (upper two stages were dummies).

Table 4.15 Scout Firing History

<u>No.</u>	<u>Date</u>	<u>Firing Range</u>	<u>Remarks</u>
Test	18 Apr 60	Wallops	Vehicle reached altitude of 30 miles; third stage did not ignite.
1	1 Jul 60	Wallops	Vehicle carried 193-lb payload to altitude of 860 miles; ignition of fourth stage prevented by command signal as vehicle veered off course.
2	4 Oct 60	Wallops	Vehicle carried 78-lb payload to an altitude of 3500 miles.
3	4 Dec 60	Wallops	Beacon 3 satellite launch attempt failed because second stage did not ignite.
4	16 Feb 61	Wallops	Vehicle orbited 87-lb Explorer 9 at an apogee of 1607 miles and a perigee of 394 miles.
5	30 Jun 61	Wallops	Flight failed because the third stage did not fire; the 187-lb payload was carried to an altitude of 107 miles.
6	25 Aug 61	Wallops	Vehicle orbited 187-lb Explorer 13 at an apogee of 606 miles and a perigee of 174 miles.
7	19 Oct 61	Wallops	Vehicle carried a 94-lb P21 payload to an altitude of 4261 miles.



Table 4.16 Strongarm Firing History

<u>No.</u>	<u>Date</u>	<u>Firing Range</u>	<u>Remarks</u>
1	10 Nov 59	Wallops	Vehicle OB11.01 carried 15-lb payload to altitude of 1050 miles.
2	18 Nov 59	Wallops	Flight vehicle OB11.02 failed because of third stage ignition malfunction.
3	13 July 60	Wallops	Vehicle OB11.03 secured some useful data although fourth stage did not ignite. Attained 416-mile altitude.
4	13 July 60	Wallops	Vehicle OB11.04 secured some useful measurements but fifth stage failed to ignite. 441-mile altitude attained.
5	1 Aug 60	Wallops	Vehicle OB11.05 broke up during fourth stage burning. Telemetry also lost then.
6	14 Feb 61	Wallops	Vehicle E22-H1-1 successfully fired but failed to achieve desired apogee due to low fifth stage performance.
7	17 Feb 61	Wallops	Vehicle E22-H1-2 carried payload to a 1260-mile altitude.

Table 4.17 T2-Type Carrier Vehicle Firing History

<u>No.</u>	<u>Date</u>	<u>Firing Range</u>	<u>Remarks</u>
1	4 Oct 57	Tyura Tam (Aral Sea Region)	Vehicle orbited 184-lb Sputnik 1 at an apogee of 588 miles and a perigee of 142 miles.

Table 4.18 T3-Type Carrier Vehicle Firing History

<u>No.</u>	<u>Date</u>	<u>Firing Range</u>	<u>Remarks</u>
1	3 Nov 57	Tyura Tam (Aral Sea Region)	Vehicle orbited 1120-lb Sputnik 2 at an apogee of 1038 miles and a perigee of 140 miles.
2	15 May 58	Tyura Tam (Aral Sea Region)	Vehicle orbited 2925-lb Sputnik 3 at an apogee of 1167 miles and a perigee of 135 miles.

Table 4.19 T3A-Type Carrier Vehicle Firing History

<u>No.</u>	<u>Date</u>	<u>Firing Range</u>	<u>Remarks</u>
1	2 Jan 59	Tyura Tam (Aral Sea Region)	Vehicle launched 793-lb Mechta <sup>a</sup> payload past Moon and into orbit around Sun, at an aphelion of 120 million miles and a perihelion of 91 million miles.
2	12 Sept 59	Tyura Tam (Aral Sea Region)	Vehicle impacted 860.4-lb Lunnaya Raketa <sup>b</sup> on Moon when it was 236,875 miles from Earth.
3	4 Oct 59	Tyura Tam (Aral Sea Region)	Vehicle orbited 614-lb Auto- maticeskaya Mezplanetnaya Stantsiya 1 <sup>c</sup> on circumlunar trajectory; apogee was 292,000 miles and perigee 24,840 miles; closest approach to Moon: 3828 miles.
4	15 May 60	Tyura Tam (Aral Sea Region)	Vehicle orbited 10,008-lb Kosmicheskij Korabl-Sputnik 1 at an apogee of 228 miles and a perigee of 188 miles. After firing retrorockets 180° out of phase on 19 May 60, apogee was 430 miles and perigee was 191 miles.
5	19 Aug 60	Tyura Tam (Aral Sea Region)	Vehicle orbited 10,120-lb Kosmicheskij Korabl-Sputnik 2 at an apogee of 210 miles and a perigee of 190 miles.
6	1 Dec 60	Tyura Tam (Aral Sea Region)	Vehicle orbited 10,060-lb Kosmicheskij Korabl-Sputnik 3 at an apogee of 154 miles and a perigee of 116 miles.
7	4 Feb 61	Tyura Tam (Aral Sea Region)	Vehicle orbited 14,292-lb Sputnik 4 at an apogee of 204 miles and a perigee of 139 miles.

Table 4.19 T3A-Type Carrier Vehicle Firing History (Cont'd)

<u>No.</u>	<u>Date</u>	<u>Firing Range</u>	<u>Remarks</u>
8	12 Feb 61	Tyura Tam (Aral Sea Region)	Vehicle orbited 14,000-lb Sputnik 5 at an apogee of 201 miles and a perigee of 125 miles. From this satel- lite the 1419-lb Automatic- heskaya Mezhplanetnaya Stantsiya 2 probe was fired toward Venus; it went into orbit around the Sun with an aphelion of 92.8 million miles and a perihelion of 65.9 million miles.
9	9 Mar 61	Tyura Tam (Aral Sea Region)	Vehicle orbited 10,363-lb Kosmicheskij Korabl-Sputnik 4 at an apogee of 155 miles and a perigee of 115 miles.
10	25 Mar 61	Tyura Tam (Aral Sea Region)	Vehicle orbited 10,352-lb Kosmicheskij Korabl-Sputnik 5 at an apogee of 154 miles and a perigee of 111 miles.
11	12 Apr 61	Baykonur (northeast of Aral Sea)	Vehicle orbited 10,418-lb Vostok 1 at an apogee of 188 miles and a perigee of 109 miles. Cosmonaut Yuri Gagarin aboard.
12	6 Aug 61	Baykonur (northeast of Aral Sea)	Vehicle orbited 10,431-lb Vostok 2 at an apogee of 159 miles and a perigee of 110 miles. Cosmonaut Gherman Titov aboard.

<sup>a</sup>Total weight in trajectory: 3245 lb

<sup>b</sup>Total weight in trajectory: 3332 lb

<sup>c</sup>Total weight in trajectory: 3247 lb

Table 4.20 Thor Able Space Carrier Firing History

<u>No.</u>	<u>Date</u>	<u>Firing Range</u>	<u>Remarks</u>
1	17 Aug 58	AMR	Lunar flight attempt failed due to first stage malfunction.
2	11 Oct 58	AMR	Vehicle carried 84.4-lb Pioneer 1 to an altitude of 70,700 miles.
3	8 Nov 58	AMR	Vehicle carried 87.3-lb Pioneer 2 to an altitude of 963 miles; third stage failed to ignite.
4	7 Aug 59	AMR	Vehicle orbited 142-lb Explorer 6 at an apogee of 26,357 miles and a perigee of 156 miles.
5	17 Sept 59	AMR	Flight failed to orbit Transit 1A because the third stage did not fire.
6	11 Mar 60	AMR	Vehicle orbited 94.8-lb Pioneer 5 around Sun at an aphelion of 92.3 million miles and a perihelion of 74.9 million miles.
7	1 Apr 60	AMR	Vehicle orbited 270-lb Tiros 1 at an apogee of 468 miles and a perigee of 435 miles.

Table 4.21 Thor Agena A Firing History

<u>No.</u>	<u>Date</u>	<u>Firing Range</u>	<u>Remarks</u>
1	28 Feb 59	PMR	Vehicle orbited 1450-lb Discoverer 1 at an apogee of 519 miles and a perigee of 176 miles.
2	13 Apr 59	PMR	Vehicle orbited 1600-lb Discoverer 2 at an apogee of 224 miles and a perigee of 152 miles.
3	3 June 59	PMR	Discoverer 3 flight failed due to incorrect injection angle.
4	25 June 59	PMR	Discoverer 4 flight failed due to insufficient velocity.
5	13 Aug 59	PMR	Vehicle orbited 1700-lb Discoverer 5 at an apogee of 718 miles and a perigee of 120 miles.
6	19 Aug 59	PMR	Vehicle orbited 1700-lb Discoverer 6 at an apogee of 527 miles and a perigee of 130 miles.
7	7 Nov 59	PMR	Vehicle orbited 1700-lb Discoverer 7 at an apogee of 520 miles and a perigee of 98 miles.
8	20 Nov 59	PMR	Vehicle orbited 1700-lb Discoverer 8 at an apogee of 1030 miles and a perigee of 120 miles.
9	4 Feb 60	PMR	Discoverer 9 flight failed due to lack of sufficient velocity.
10	19 Feb 60	PMR	Discoverer 10 flight failed due to malfunction in the first stage. Veered off course; destroyed by range safety at 52 sec.

Table 4.21 Thor Agena A Firing History (Cont'd)

<u>No.</u>	<u>Date</u>	<u>Firing Range</u>	<u>Remarks</u>
11	15 Apr 60	PMR	Vehicle orbited 1700-lb Discoverer 11 at an apogee of 380 miles and a perigee of 109 miles.
12	29 June 60	PMR	Discoverer 12 flight failed because of incorrect injection angle.
13	10 Aug 60	PMR	Vehicle orbited 1700-lb Discoverer 13 at an apogee of 436 miles and a perigee of 161 miles. Capsule recovered from sea on 11 Aug.
14	18 Aug 60	PMR	Vehicle orbited 1700-lb Discoverer 14 at an apogee of 502 miles and a perigee of 116 miles. Capsule snatched in mid-air by C-119 aircraft.
15	13 Sept 60	PMR	Vehicle orbited 1700-lb Discoverer 15 at an apogee of 472 miles and a perigee of 124 miles.

Table 4.22 Thor Agena B Firing History

<u>No.</u>	<u>Date</u>	<u>Firing Range</u>	<u>Remarks</u>
1	26 Oct 60	PMR	Discoverer 16 flight failed because the first and second stages did not separate.
2	12 Nov 60	PMR	Vehicle orbited 2100-lb Discoverer 17 at an apogee of 616 miles and a perigee of 116 miles. Capsule snatched in mid-air by C-119 aircraft.
3	7 Dec 60	PMR	Vehicle orbited 2100-lb Discoverer 18 at an apogee of 459 miles and a perigee of 154 miles. Capsule snatched in mid-air by C-119 aircraft.
4	20 Dec 60	PMR	Vehicle orbited 2100-lb Discoverer 19 at an apogee of 323 miles and a perigee of 128 miles.
5	17 Feb 61	PMR	Vehicle orbited 2450-lb Discoverer 20 at an apogee of 486 miles and a perigee of 177 miles.
6	18 Feb 61	PMR	Vehicle orbited 2100-lb Discoverer 21 at an apogee of 659 miles and a perigee of 149 miles; after restart of Agena B engine values were 670 and 155, respectively.
7	30 Mar 61	PMR	Discoverer 22 flight failed due to mechanical malfunction.
8	8 Apr 61	PMR	Vehicle orbited 2100-lb Discoverer 23 at an apogee of 402 miles and a perigee of 183 miles. Capsule was ejected and entered new orbit with values of 882 and 126, respectively.



Table 4. 22 Thor Agena B Firing History (Cont'd)

<u>No.</u>	<u>Date</u>	<u>Firing Range</u>	<u>Remarks</u>
9	8 June 61	PMR	Discoverer 24 flight failed due to ignition malfunction of second stage.
10	16 June 61	PMR	Vehicle orbited 2100-lb Discoverer 25 at an apogee of 252 miles and a perigee of 139 miles. Capsule recovered from sea same day.
11	7 July 61	PMR	Vehicle orbited 2100-lb Discoverer 26 at an apogee of 503 miles and a perigee of 146 miles.
12	21 July 61	PMR	Discoverer 27 flight failed; carrier was destroyed by range safety after veering off course.
13	3 Aug 61	PMR	Discoverer 28 flight failed due to insufficient velocity after the first and second stage ignition and separation.
14	30 Aug 61	PMR	Vehicle orbited 2100-lb Discoverer 29 at an apogee of 345 miles and a perigee of 140 miles. Capsule recovered from sea.
15	12 Sept 61	PMR	Vehicle orbited 2100-lb Discoverer 30 at an apogee of 345 miles and a perigee of 154 miles. Capsule recovered in mid-air by C-119 aircraft.
16	17 Sept 61	PMR	Vehicle orbited 2100-lb Discoverer 31 at an apogee of 255 miles and a perigee of 152 miles.

Table 4.22 Thor Agena B Firing History (Cont'd)

<u>No.</u>	<u>Date</u>	<u>Firing Range</u>	<u>Remarks</u>
17	13 Oct 61	PMR	Vehicle orbited 2100-lb Discoverer 32 at an apogee of 246 miles and a perigee of 147 miles. Capsule recovered in mid-air.
18	23 Oct 61	PMR	Discoverer 33 flight failed due to premature shut off of second stage.
19	5 Nov 61	PMR	Vehicle orbited 2100-lb Discoverer 34 at an apogee of 637 miles and a perigee of 134 miles.
20	15 Nov 61	PMR	Vehicle orbited 2100-lb Discoverer 35 at an apogee of 173 miles and a perigee of 147 miles.
21	12 Dec 61	PMR	Vehicle orbited 2100-lb Discoverer 36 at an apogee of 297 miles and a perigee of 146 miles. It also orbited 10-lb Oscar 1 at an apogee of 289 miles and a perigee of 146 miles.

Table 4.23 Thor Delta Firing History

<u>No.</u>	<u>Date</u>	<u>Firing Range</u>	<u>Remarks</u>
1	13 May 60	AMR	Echo flight failed due to malfunction of altitude controls, and failure of third stage to ignite.
2	12 Aug 60	AMR	Vehicle orbited 132-1b Echo 1 at an apogee of 1050 miles and a perigee of 945 miles.
3	23 Nov 60	AMR	Vehicle orbited 280-1b Tiros 2 at an apogee of 451 miles and a perigee of 387 miles.
4	25 Mar 61	AMR	Vehicle orbited 79-1b Explorer 10 at an apogee of 112,500 miles and a perigee of 110 miles.
5	12 July 61	AMR	Vehicle orbited 285-1b Tiros 3 at an apogee of 511 miles and a perigee of 457 miles.
6	15 Aug 61	AMR	Vehicle orbited 83-1b Explorer 12 at an apogee of 47,858 miles and a perigee of 165 miles.

Table 4.24 Thor Epsilon (Able Star) Firing History

<u>No.</u>	<u>Date</u>	<u>Firing Range</u>	<u>Remarks</u>
1	13 Apr 60	AMR	Vehicle orbited 265-lb Transit 1B at an apogee of 479 miles and a perigee of 233 miles.
2	22 June 60	AMR	Vehicle orbited 223-lb Transit 2A at an apogee of 657 miles and a perigee of 389 miles. It also orbited 42-lb Greb 1 at an apogee of 657 miles and a perigee of 382 miles.
3	18 Aug 60	AMR	Courier 1A flight failed due to first stage malfunction.
4	4 Oct 60	AMR	Vehicle orbited 500-lb Courier 1B at an apogee of 770 miles and a perigee of 587 miles.
5	30 Nov 60	AMR	Transit 3A and Greb 2 flight failed; carrier was destroyed by range safety after first stage prematurely shut down.
6	21 Feb 61	AMR	Vehicle orbited 250-lb Transit 3B and 57-lb Lofti 1 to an apogee of 511 miles and a perigee of 117 miles (the two satellites failed to separate).
7	29 June 61	AMR	Vehicle orbited a triple payload weighing a total of 270 lb. The apogee of 175-lb Transit 4A was 623 miles and the perigee was 534 miles. The apogee of 55-lb Greb 3 and 40-lb Injun 1 was 634 miles and the perigee was 534 miles (these two satellites did not separate).

Table 4.24 Thor Epsilon (Able Star) Firing History (Cont'd)

<u>No.</u>	<u>Date</u>	<u>Firing Range</u>	<u>Remarks</u>
8	15 Nov 61	AMR	Vehicle orbited 190-lb Transit 4B, whose apogee was 694 miles and perigee was 586 miles; and 240-lb Traac I, whose apogee was 701 miles and perigee was 581 miles.

Table 4.25 Vanguard Space Carrier Firing History

<u>No.</u>	<u>Date</u>	<u>Firing Range</u>	<u>Remarks</u>
Test	23 Oct 57	AMR	Test vehicle carried dummy second and third stages.
1	6 Dec 57	AMR	Flight failed due to malfunction in the first stage.
2	5 Feb 58	AMR	Flight failed; the vehicle veered off course and broke up.
3	17 Mar 58	AMR	Vehicle orbited 3.25-lb Vanguard 1 at an apogee of 2463 miles and a perigee of 406 miles.
4	28 Apr 58	AMR	Flight failed because of control sequence malfunctions.
5	27 May 58	AMR	Flight failed because of incorrect injection angle and improper second stage cutoff.
6	26 June 58	AMR	Flight failed because the second stage engine cut off prematurely.
7	26 Sept 58	AMR	Flight failed because of insufficient velocity, due to contamination in fuel system.
8	17 Feb 59	AMR	Vehicle orbited 23.7-lb Vanguard 2 at an apogee of 2046 miles and a perigee of 347 miles.
9	13 Apr 59	AMR	Flight failed due to second stage engine actuator lug malfunction.
10	22 June 59	AMR	Flight failed due to second stage helium regulator malfunction.
11	18 Sept 59	AMR	Vehicle orbited 53-lb Vanguard 3 at an apogee of 2329 miles and a perigee of 319 miles.

## 5

## AUTOMATION IN ORBITAL AND SPACE MISSIONS

William L. Mitchell and Charles O. Brooks

Quality Assurance Division  
George C. Marshall Space Flight Center  
National Aeronautics and Space Administration  
Huntsville, Alabama

The advent of the space age has been a major factor in the rapid development of those scientific areas involved with measurement, data handling, and error analysis. By the use of various techniques of sampling, feedback, and decision making, which can be attained through the use of automatic machines under the direction of internally stored programs, it becomes practical to provide positive and continuous control of those processes necessary for successful completion of a mission or operational requirement. The automatic processing of such stimuli with the derived control therefrom is expressed by the word automation. This is not to say that developments in automation have not been successfully applied for some time in many other areas, but only to indicate that in the realm of space one finds a unique field in which the capabilities of automation can be fully utilized.

The need for the application of automation in orbital missions and in space missions is first of all reflected in the amount and complexity of both onboard and ground support equipment (GSE) involved. In order for this equipment to function as designed (whether the operations be sequential, concurrent, or a combination of both) it is mandatory that these multiple functions be monitored continuously and/or by controlled sampling. Automation, under the control of its computer complex and directed by its internally stored program, can without undue strain and at great speed look at a thousand different and interrelated situations. It can analyze them according to the internal program, and then act on its derived decision to manipulate the system in accordance to need. In addition, the job is handled with a consistency and accuracy not ordinarily obtained by any other means.

The effort in space has resulted in many significant discoveries and breakthroughs, which in turn have had a noteworthy influence on the effort. Such a rapidly changing technology poses special problems. In order that the total approach remain versatile and competent amid these changes, one must minimize such effects as drastic changeover of support

**Preceding page blank**

equipment, mass retooling effort, and a leftover complement of noncompatible equipment. Automation as a total approach furnishes the best answer, since it cannot become obsolete in theory at least. In fact, its advantages will increase as the needs become more severe.

For the sake of completeness, it must be said that automation for space began in a limited way when the first steps toward space flight were taken as a by-product of the guided missile effort. Automation made possible the early success of unmanned, self-contained missiles. It was substituted for man under circumstances of adverse environmental conditions and one-way mission requirements. The interesting point is that where automation made possible the elimination of man as a passenger in the missile area, it will reinstate him in the space effort. This clearly illustrates the versatility and capability of automation. One must at the same time be aware that this new way of accomplishing the impossible in space contains within itself many characteristic problems which are not easily solved, not the least of which is the additional total complexity of an automated system.

Automation has begun in the space application with the partial or piecemeal approach and is evolving toward the total system concept. This is logical. Ultimate success will depend upon total system automation. The application of particular automation techniques will be determined by the changing needs of the space missions and the development of those concepts which will satisfy the needs.

It seems fitting at this point to examine certain areas in the overall program where automation is either well established already, or is now being introduced, and then to project application into other areas.

The events in any space mission, whether orbital, probe, or rendezvous, are basically sequential in time. Thus, it can be easily seen that the control of the order and duration of many interdependent events on board the vehicle is a very important and critical requirement. Success or failure of the mission depends primarily on the attainment of this timing sequence. Consequently, automation of this function has been basic from the beginning.

Current developments indicate that in the near future the need will arise for the correlation and control of multiple sequences on separate vehicles in order to produce or prevent rendezvous through internal or external control of trajectories, or both. Here one finds sophistication of a high order, but it will be quite practical for future automation. This concept of vehicle control will at first relate particularly to orbital missions where the multiple missions require simultaneous operation of many vehicles successfully for an indeterminate time. Figure 5.1 illustrates one possibility for the automated operation of an unmanned vehicle. While general in nature, it is yet characteristic, since the



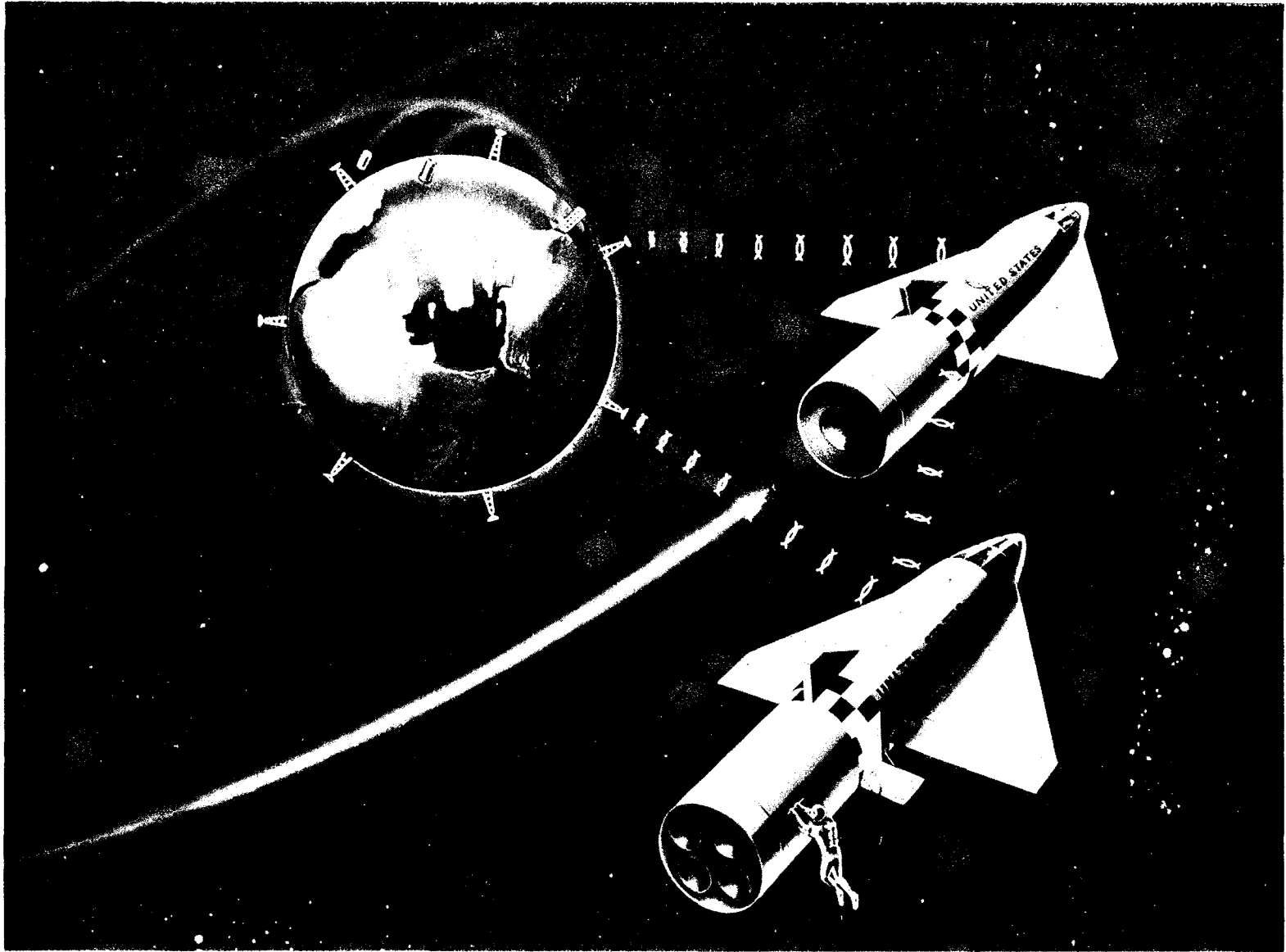


Fig. 5.1 One method of automated control of unmanned vehicle.

basic vehicular requirements of most missions contain many areas of similarity. Details depend among other things upon particular modes of mechanization.

This system is controlled during countdown by a master-slave combination of the launch control center computer and the on-board computer. The vehicle computer presents predigested vehicle data to the central computer for overall system coordination. After launch, the vehicle is capable of independent operation under control of its own computer. The core of the spacecraft system is the digital computer. By means of its program, the computer is in a command position in relation to both stage operation and control of the total vehicle. Controlled selection of characteristic stimuli is made by the computer through matrix switching. Inputs from the rf command link and programmed outputs from the PCM transmitters are sequenced as required by mission. Test routines are applied and guidance sequencing along with control demands are met as determined by system response. The ground based, central computer complex then acts in a back-up capacity and as monitor for total system operation. The requirement for such activity on the part of the central computer necessitates programming which contains complete mission information including vehicle computer scheduling. PCM data link would insure continuous and up-to-date information as to status of the flight. The ground-based computer would also be able to modify the vehicle program via rf command link after launch, if such action be needed. Reserve capacity for additional vehicle requirements is available if the on-board computer is overtaxed by some unusual demand. Some similar type of closed-loop operation as described will mark the next step forward in the space effort.

The sequence operations mentioned earlier tie in very closely with guidance and control, since some of the sequence output serve as input to that area. Once again one finds automation at the heart of a critically important function. In fact, it may be said that current missiles and space vehicles operate because they really are automated systems. Future systems will be even more dependent upon this concept and more and better approaches will permit greater control and realization of design goals. This is to say that present automatic control, internally at least, represents a concept which in more advanced situations will differ in degree rather than in kind.

Future requirements will probably include need for specialized repair of the vehicle itself by the astronaut under direction of the automatic program. Other needs will include celestial navigation by on-board means without human intervention; onboard environmental control as needed for survival by the astronaut; trajectory modification and calculation of transfer trajectories; collision course prediction and alarm; optimization and control of fuel consumption; landing and shutdown control with subsequent liftoff; generating control instructions for automated, mobile subsystems used to sample and explore; and continuous surveillance

of the state of the total system by self-contained methods with alarm for prefailure conditions and automatic log keeping for review and study. When needs reach this stage, it will become mandatory that the on-board system be a slave system to a large, ground based, central-control complex. This will dictate new communication links with possibly radio, radar, and light capabilities as well as television links for visual contact.

Figure 5.2 outlines a general approach to a manned spacecraft mission. Many, if not most, of the automated functions described for the unmanned vehicle are also applicable here. The presence of a human passenger adds greatly to total system requirements, especially as related to safety measures. However, the total system capacity is increased significantly at the same time. Missile behavior, in general, still depends upon the mission, as in the case of unmanned flight. The computer retains its key position in the automatic concept despite the presence of the astronaut. In reality, its problems are now more specialized and its total work load increased. Provision must be made for astronaut intervention of both program and control, for it is in this area that man finds his best utilization.

The master-slave relation of ground-based computer and vehicle computer is deepened by the new system demands. Communication at voice or visual levels, or both, is now desirable in addition to the digital flow of information already provided between computers. A look at the control position of the vehicle indicates the presence of man once again in the system. His function as part of the automatic system will probably relate to the overall program in a parallel manner. That is, the closed-loop part of the operation must not be directly dependent on human response, since man's reaction time and lack of objectivity would be a serious handicap.

Current attempts to put automatic vehicles on the Moon illustrate one phase of such an advanced program. Man must first remotely explore, sample, study, and evaluate the phenomena available without actually being there in person. He can then understand the limitations and possibilities related to later personal visits. The implications are clear that only via automation can such goals be realized. Initially, automation takes man's place; later it allows him to come along too.

Figure 5.3 illustrates an episode during a future manned Moon trip. Two spacecraft have effected a lunar orbital rendezvous in order to repair damage to one of the vehicles. The astronauts are able to communicate with each other and central control on Earth while inspection and repair are underway. Positive control of this situation is made possible through the complex automated systems involved. The delay in program caused by the malfunction of one vehicle is introduced by data link into the master program control on Earth. This allows the effects

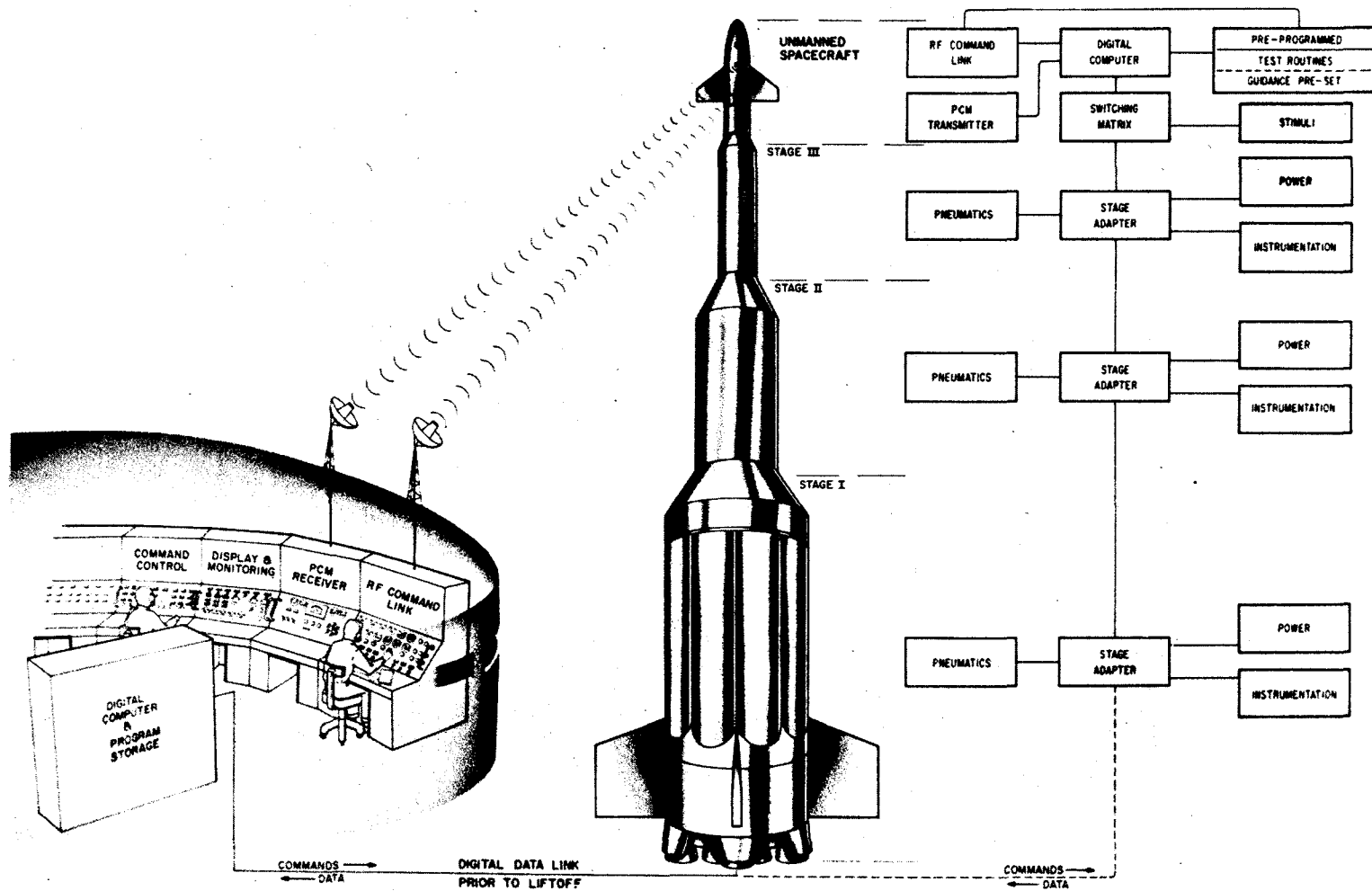


Fig. 5.2 General approach to a manned spacecraft mission.

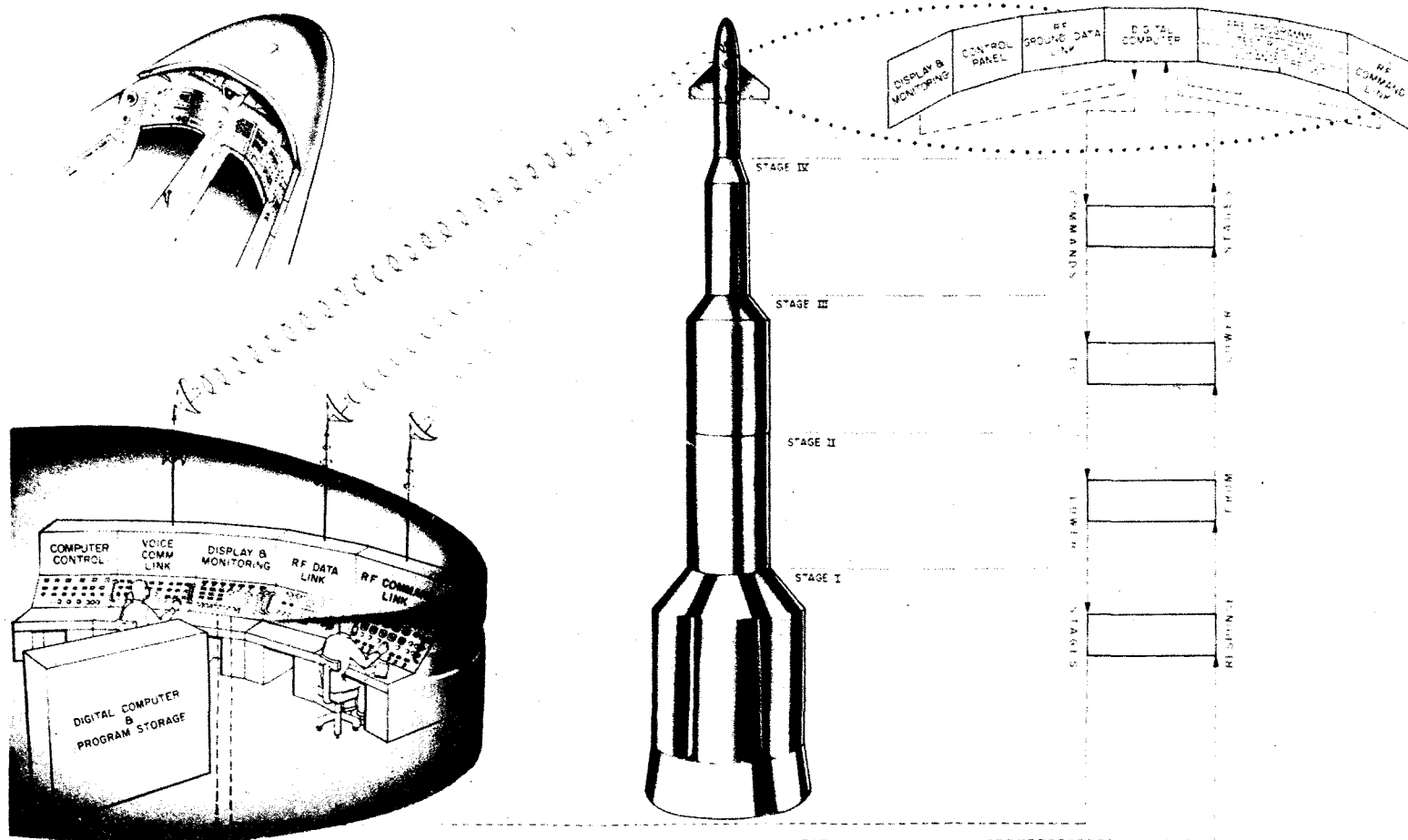


Fig. 5.3 Space rendezvous for repairs.

of the new situation to be evaluated and the program to be updated for both vehicles and total system. A point of significance here is the existence of a complex and world-wide communication network. Future control concepts for spacecraft may require such a facility for the positive control of remotely operating systems. The task of control beyond certain limits may prove to be so difficult by remote link that it will only be practical to place sole reliance on the internal spacecraft computer. The magnitude of such a task will probably await a major computer breakthrough. Molecular electronics may furnish the answer.

Thus far we have operated on the premise that we will have satisfactory systems to perform our missions. The availability of these systems or vehicles depends upon the successful completion of many time consuming and delicate operations prior to countdown time zero. Months and years go into the preparation for a possible few minutes operation. Here lies one of the most fertile areas for introduction and expansion of the automation concept. It is at this point that current efforts are being expended.

Throughout the long, tedious, and exacting period of vehicle preparation, the most pressing need is that of establishing system integrity by means of exhaustive checkout during various stages of effort. Variations and bottlenecks in checkout are indeed critical since they can make or break the effort. Automation can add a unifying influence to checkout that is characterized by consistency, accuracy, speed, versatility, and direction, which is not otherwise possible.

Adoption of automatic procedures for the checkout of missile systems has been employed in varying degrees for some time. Realization of a truly automatic checkout system has awaited the proper state-of-the-art condition in the missile field as well as in the field of automation. There exist many approaches to the problem of checkout automation; it is not within the scope of this paper to review and evaluate the various methods. It should be pointed out that it is now possible to clearly define all areas and modes of action. As in any new endeavor, best utilization awaits further system application.

One critical area remains for brief examination before proceeding to more particular details. Due to the existence of a computer at the heart of any automated system, it is fitting to examine very briefly a simplified expression of the computer concept. All digital computers have in common the following basic requirements:

1. Input/output equipment, which may feature cards, paper tape, magnetic tape and/or others.
2. The memory unit which contains the working data.
3. The arithmetic unit which performs prescribed operations on the data.
4. The control unit which determines the activities of the other units.

The input equipment permits communication between the machine and the operator. It feeds data and instructions to the memory unit. The output furnishes a permanent record of the end results of the computation. The memory unit contains all the working data and program instructions and makes them available to the arithmetic processing unit at very high speeds. After processing, the results are stored in the memory pending further computation or output as required. The arithmetic unit contains the circuits which perform the internal arithmetic operations. The control unit controls the operations of all the other units in the computer in a fully automatic way after initial input by the operator. Now we can apply these computer capacities to the problem at hand.

The automation process can be coordinated and controlled through one central computer or a multiple computer complex. Figure 5.4 illustrates a multiple-computer approach to the central control area of an automatic checkout system. The system being presently set up for automated checkout of Saturn space carrier vehicles utilizes this approach and consists of a central computer complex composed of a multiple array of Packard Bell type 250 computers for system control. One master computer will be able to control up to nine slave computers as a maximum. Satellite test stations for the various test requirements can be coupled into this control up to a maximum of 32 stations in the fully expanded system.

The operational central computer facility will be coupled through a buffering system to various satellite stations located in areas remote from central control. These remote stations are located in their particular area of application and must be linked to central control. Coupling through buffer systems is required to accommodate test objective rates and internal computer rates. Data-transmission signals are also conditioned and improved in the process. By means of such a system arrangement, programmed control of test sequences is achieved and in addition the necessary computation on measured data can be performed for components, subsystems, and the total system.

A multiple computer complex may consist in its initial or basic configuration of a master computer and one or more slave computers. The number of slaves would be increased commensurate with the task. The multiple-computer approach probably represents some advantages in cost and computer simplicity. Various peripheral units would be tied into the central complex for purposes of input and output. These devices may include among others, various magnetic tape units, paper tape readers, and punches, and high-speed on-line output units. The central station communicates with the various satellite units under program control through certain distribution matrices. The matrices may be relay, diode, or cross-bar types, either singly or in combination. They are addressable for program selection under computer direction.

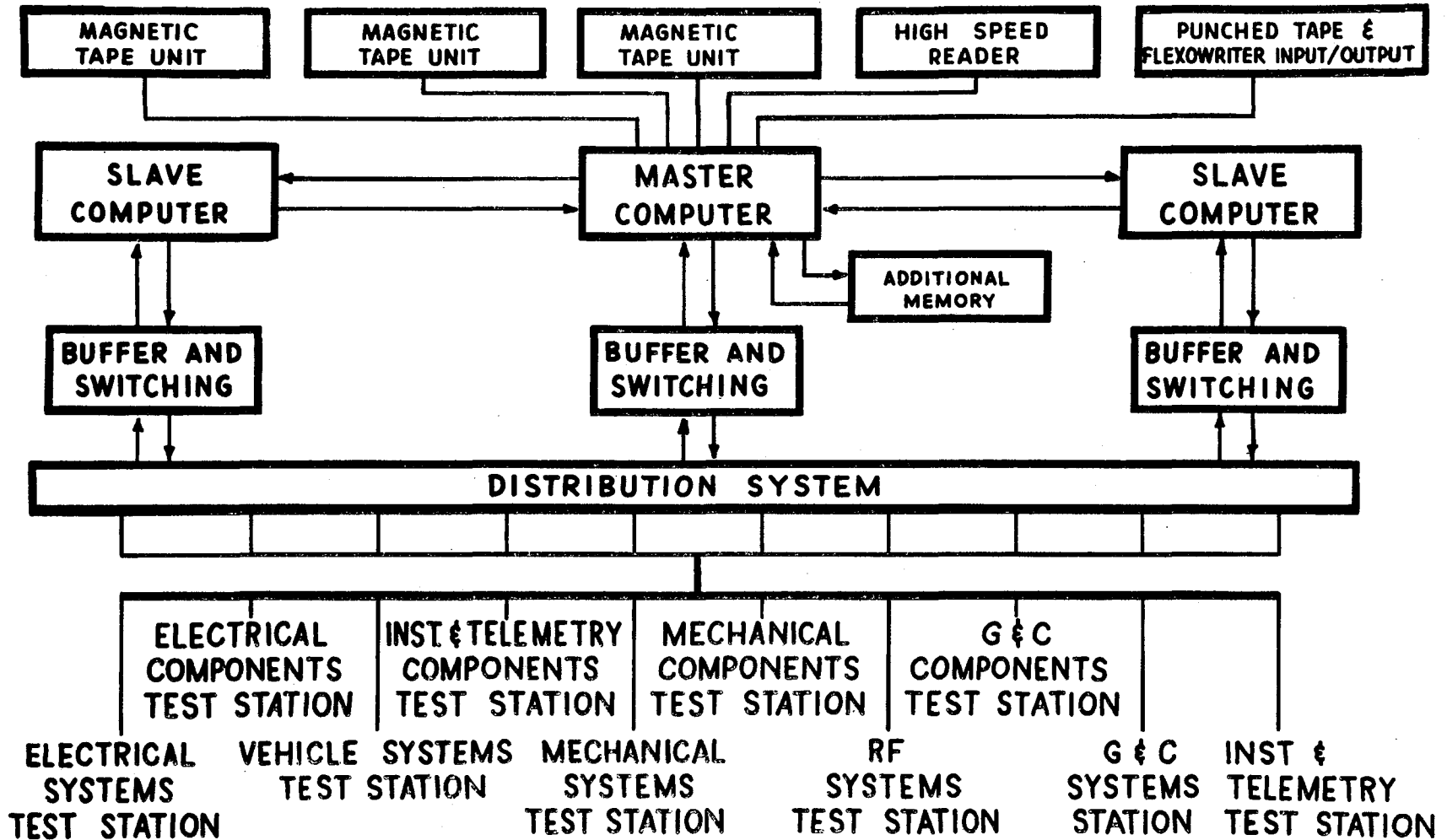


Fig. 5.4 Multiple-computer approach to the central control area of an automatic checkout system.



The nature of a satellite station is determined by its area of operation. A unit to test the guidance system would necessarily differ from that used to test the electrical system. Another consideration is the fact that in testing there are two areas in question. First, there are the individual components which must be tested for tolerance and second, there is the system performance to be verified. At this point we can examine briefly a simplified test sequence to see what computer operations are involved.

A test sequence will include a check of transducer response to computer-controlled stimuli; a comparison of the response with a predetermined calibration curve stored in the computer; means to halt the program for calibration adjustments if the response is not as desired; and finally a comparison between direct hardware measurements and the same measurements received through the rf link. This is done in order to prove rf system performance. The internally stored computer program contains all the instructions which enable the computer to initiate and control all test operations. The selection of the test point, control of the variable under test (such as pressure), and the identification of the measurement being taken, are all sequenced as required. The actual correction of the unit under test is a manual operation. A remote indicator coupled into the automatic system permits a visual check of measurement status to the technician. As he makes the required adjustments, the remote indicator follows the progress made and will signal a good test when the desired point is reached. A signal which originates from the remote unit allows the computer to then advance control to the next point in question. A display of the test status is also available at the console of the satellite unit to furnish visual assurance of test progress.

This simplified look at one test point is multiplied in complexity many times as the level of test rises through subsystems to the total system. It will not be easy to instigate such sweeping changes, but the requirements force the issue. Experience to date indicates difficult areas, yet at the same time shows that such an approach does indeed offer fulfillment. Future automation in checkout may lead to a situation where the self-contained system maintains, throughout its life, an up-to-the-minute report of its condition; this system could be interrogated to supply diagnostic information. It would even be conceivable for the vehicle to display the condition and area of trouble on a visual screen without external interrogation. This may be realized as an ultimate goal.

The impact of total system automation on orbital and space missions, as well as on technology in general, will produce profound changes. Even though the ultimate level of mechanization will increase gradually, the effect will be drastic. The addition of space to the area of man's activity has already opened new avenues of search. Automation has been the door through which space exploration has entered and it will continue to supply the key to the future in space. This is true because the nature of the elements involved is such that man cannot manipulate them properly without help, -- and this help is automation.

## ON THE THEORY OF OPTIMIZATION OF STEP ROCKETS

Harry O. Ruppe

Future Projects Office  
George C. Marshall Space Flight Center  
National Aeronautics and Space Administration  
Huntsville, Alabama

Usually, the goal of optimization of a space transportation program is either to obtain the greatest transportation capability within a given time frame for minimum cost, or to obtain the greatest transportation capability at the earliest time for a given total cost. Evidently, no analytic solution can be expected regarding such an extremely complex task. Therefore, only a more limited problem shall be investigated; namely the criteria will be developed for which the ratio of payload over launch weight is maximized for a given mission. For analytical methods, further simplification is required: "To perform a specific mission" is interpreted to mean "to provide one specific ideal speed." \*

In this limited respect, several methods of vehicle optimization are discussed. It is shown that under certain conditions an optimum number of steps does exist. A short discussion is included on the influence of the trajectory upon optimization and on a different criterion of optimization. Finally, some critical remarks are given concerning practical aspects of vehicle design.

Assuming given propulsion systems for the vehicle being optimized, the question of maximum payload ratio (or minimum growth factor, as, by definition, the product of growth factor and payload ratio is one) is reduced to the problem of optimum staging of step rockets. This sub-problem provides one input to the solution of the general problem of designing the best or most economic space transportation system. Many other inputs must be considered to obtain an optimized space transportation system [1].

---

\* Ideal speed of a one-step rocket is defined in the usual manner; see, for example, Sec. 6.1.1 of this paper.

**Preceding page blank**

Unless otherwise noted, two main assumptions shall be made:

1. The availability of engines or stages is disregarded.
2. The best vehicle is one which carries maximum payload weight for a given initial weight to a given characteristic speed.

The first assumption is necessary to develop an analytic theory while the second assumption is sufficiently simple and is useful because a close correspondence exists between the mission and its speed requirement [2].

The discussion is limited to the case of high-acceleration vehicles. For low-acceleration vehicles, a corresponding problem of optimum weight distribution between major subsystems does exist [3]. Indeed, the analytic results appear to have more direct applicability than in the high-acceleration case, where, as described in Sec. 6.2 there is a strong effect from realistic considerations. Recently, the theoretically interesting case of engine-staging for low-acceleration vehicles was investigated [4].

Historically, in the now classic paper [5], the basic case of optimization of high-acceleration step rockets was stated and solved. H. Oberth treated a more general case earlier, but his paper [6] was not available openly. H.H. Koelle found the existence of an optimum step number and developed a graphic method for its determination. This method was refined and presented very elegantly in analytic form in [7]. An extensive bibliography and a survey of the present status of the analytic theory is contained in [8].

## 6.1 Theory

### 6.1.1 Minimum Liftoff Weight

Simplest Case for Liquid-Propellant Vehicles: Zero Gravity, Two Given Parameters. Optimum weight distribution. For a step-rocket vehicle, the following is given

1. Number of steps:  $n$
2. Linear motion in zero gravity field.
3. Total ideal speed capability:  $V$
4. Weight of payload.
5. Exhaust speed of step  $i$ :  $c_i$
6. Structure ratio of step  $i$ :  $\epsilon_i$

$c_i$  and  $\epsilon_i$  are the two parameters mentioned in the subtitle. The other parameters either describe the mission (3, 4) or will be treated later (1, 2).

Some definitions are now presented.

Mass ratio of step i

$$r_i = \frac{W_{o(i)}}{W_{c(i)}} = \frac{\text{weight of vehicle at ignition of step } i}{\text{weight of vehicle at cutoff of step } i}$$

Payload ratio of step i

$$\lambda_i = \frac{W_{i(i)}}{W_{o(i)}} = \frac{\text{weight of payload of step } i \text{ equals weight of vehicle at ignition of step } (i+1)}{\text{weight of vehicle at ignition of step } i}$$

Structure ratio of step i

$$\epsilon_i = \frac{W_{s(i)}}{W_{o(i)}} = \frac{\text{weight of vehicle at cutoff of step } i \text{ minus weight of payload of step } i}{\text{weight of vehicle at ignition of step } i}$$

We ask for the vehicle which has minimum launch weight and is in agreement with conditions 1 through 6.

For a solution, the following equations can be derived

$$V = \sum_i^n c_i \ln r_i$$

$$\frac{1}{r_i} = \epsilon_i + \lambda_i$$

$$\text{Growth factor } G = \frac{\text{launching weight}}{\text{payload weight}} = \frac{W_{o(1)}}{W_{l(n)}} = \left\{ \prod_i^n \lambda_i \right\}^{-1}$$

The problem is now reduced to finding a choice for the  $\lambda_i$  so that G

becomes a minimum. Let us introduce  $c = \frac{1}{n} \sum_i^n c_i$

Then

$$V = c \ln r_1^{\frac{c_1}{c}} \cdot r_2^{\frac{c_2}{c}} \cdot r_3^{\frac{c_3}{c}} \dots r_n^{\frac{c_n}{c}} = c \ln r$$

or

$$R = \prod_i^n r_i^{\frac{c_i}{c}} = \left\{ \prod_i^n (\epsilon_i + \lambda_i)^{\frac{c_i}{c}} \right\}^{-1}$$

R can be called the effective mass ratio of the step rocket under consideration. A maximum of  $G^{-1}$  under the condition of  $R^{-1} = \text{constant}$  follows with the Lagrangian multiplier  $\alpha$  from

$$\frac{\partial}{\partial \lambda_j} (G^{-1}) + \alpha \frac{\partial}{\partial \lambda_j} (R^{-1}) = 0, \quad j = 1, 2, \dots, n, \quad \text{and above equation for } R^{-1}.$$

The solution is

$$\epsilon_i + \lambda_i = \frac{\epsilon_i}{1 - \frac{c_n \lambda_n}{c_i \epsilon_n + \lambda_n}}$$

From this equation  $\lambda_i$  is found, when  $\lambda_n$  is known.  $\lambda_n$  follows from

$$R = \frac{\prod_{i=1}^n \left( 1 - \frac{c_n \lambda_n}{c_i \epsilon_n + \lambda_n} \right)^{\frac{c_i}{c}}}{\prod_{i=1}^n \frac{c_i}{c}}$$

If all  $c_i$  and  $\epsilon_i$  are equal, then

$$\lambda_i = \lambda_n$$

or

$$\lambda_1 = \lambda_2 = \lambda_3 = \dots = \lambda_n = \lambda$$

Then immediately

$$G^{-1} = \lambda^n$$

and

$$R^{-1} = (\epsilon + \lambda)^n$$

This is the well known case of equality of corresponding weight ratios.

Optimum Step Number. To determine the optimum step number  $N$  so that  $G$  is a minimum, the optimum vehicle as discussed in connection with optimum weight distribution is taken, and  $n$  is treated as a continuous variable. The value  $n = N$  is asked for which minimizes  $G$ .

To treat  $n$  as a continuous variable is feasible only when the parameters  $c$ ,  $\epsilon$ , and  $\lambda$  are the same in each stage. If these parameters are not identical in each stage, the optimum step number can be determined by numerical computing and comparing the various optimized configurations. It is possible, then, that by omitting a low-performance first stage a better overall configuration results. The analytic development is as follows:

From the two final equations on optimum weight distribution, the following can be written

$$\ln G = \frac{\ln R \cdot \ln \lambda}{\ln (\lambda + \epsilon)}$$

From  $\frac{\partial}{\partial \lambda} (\ln G) = 0$ , we have

$$\lambda_{\text{opt}}^{\lambda_{\text{opt}}} = (\lambda_{\text{opt}} + \epsilon)^{\lambda_{\text{opt}} + \epsilon}$$

With the aid of a curve  $f(x) = x^x$  this Krause equation can be solved easily.

An approximation for  $0 < \epsilon < 0.4$  is

$$\lambda_{\text{opt}} \approx 0.366 - 0.460 \cdot \epsilon$$

After  $\lambda_{\text{opt}}$  is found, there is easily

$$r_{\text{opt}} = (\epsilon + \lambda_{\text{opt}})^{-1}$$

and

$$n_{\text{opt}} = N = \frac{V}{c \ln r_{\text{opt}}}$$

A Refined Case: The Third Parameter  $\mu$ . Whereas it was written in the first subsection of 6.1.1,  $W_s(i) = \epsilon_i W_o(i)$ , now, more refined, it is written

$$\begin{aligned} W_s(i) &= \epsilon_i W_o(i) + \mu_i \left[ W_o(i) - W_c(i) \right] = (\epsilon_i + \mu_i) W_o(i) - \mu_i W_c(i) \\ &= \bar{\epsilon}_i W_o(i) - \mu_i W_c(i) \end{aligned}$$

where  $\bar{\epsilon}_i = \epsilon_i + \mu_i$  has been introduced. The physical meaning of this refinement is quite obvious. Whereas in the previous case the structural weight of a stage (as defined by cutoff weight of the step under consideration minus its payload weight) has been considered to be proportional to the ignition weight of that stage, it is now assumed to be proportional to a linear combination of ignition weight and weight of the propellant used. The previous factor of proportionality  $\epsilon_i$  is replaced by

$\bar{\epsilon}_i = \epsilon_i + \mu_i$ , and the new factor  $\mu_i$  is introduced. For the special case of  $\mu_i = 0$ , the results of the previous case apply. We shall not go into any mathematical detail. Suffice it to say that again for the case of  $c_1 = c_2 = \dots = c_n$ ,  $\epsilon_1 = \epsilon_2 = \dots = \epsilon_n$  and  $\mu_1 = \mu_2 = \dots = \mu_n$ , the solution is  $\lambda_1 = \lambda_2 = \dots = \lambda_n$ , and for the special case of  $\epsilon_1 = \epsilon_2 = \dots = \epsilon_n = 0^*$  comes  $n_{\text{opt}} = N = \infty$ . This erroneously led at times to

\* This choice puts structural weight proportional to the weight of propellant used, that is, as can be seen from the limiting case of zero propellant weight independent of structural elements, e.g. engines, being neglected.

the conclusion that an optimum step number did not exist.

An important general result can be written using the symbol  $N(\frac{\epsilon}{\mu})$  for the optimum step number for given  $\epsilon$ ,  $\mu$  values

$$0 < N(\frac{0}{0}) < N(\frac{\epsilon}{0}) < N(\frac{\epsilon+\mu}{\mu}) < N(\frac{\epsilon+\mu}{0}) < N(\frac{0}{\mu}) = \infty$$

if both  $\epsilon$  and  $\mu$  are not zero. Comparing  $N(\frac{\bar{\epsilon}}{0})$  and  $N(\frac{\bar{\epsilon}}{\mu})$ , we conclude that the introduction of  $\mu$  reduces the optimum step number. This can be understood, because keeping  $\bar{\epsilon}$  constant the structure  $W_s$  is reduced by increasing  $\mu$ .

Simplest Case for Solid-Propellant Vehicles: Zero Gravity, Two Given Parameters. A somewhat different choice of parameters appears to be more convenient for solid-propellant rocket vehicles [9]:

The first step is called module number one, etc., until the payload is module number  $n$ . The launch weight then is  $W_0 = \sum_{i=1}^n W_i$ ; a module

fraction is introduced,  $f_i = \frac{W_i}{W_0}$ , and evidently  $\sum_{i=1}^n f_i = 1$ . If  $W_{pi}$  is the

weight of the usable propellant in module number  $i$ , then  $\Lambda_i = \frac{W_{pi}}{W_i}$  is the

propellant fraction. As usual,  $c_i$  is the jet speed pertaining to module number  $i$ . The growth factor is simply  $G = \frac{1}{f_n}$ . This nomenclature leads

to the result that the optimum step number is  $N = \infty$ . Again, this is due to neglecting engine weights.

The simple case ( $\Lambda_i = \Lambda$ ,  $c_i = c$ ) leads, for a three-stage or four-module vehicle, to the familiar result of weight similarity

$$\lambda_1 = \lambda_2 = \lambda_3 = \lambda = 1 - f_1$$

$$\epsilon_1 = \epsilon_2 = \epsilon_3 = \epsilon = (1 - \Lambda) f_1$$

$$\frac{1}{r_1} = \frac{1}{r_2} = \frac{1}{r_3} = \frac{1}{r} = 1 - \Lambda f_1$$

In the variable  $f_1$ , this weight similarity cannot be seen easily

$$f_2 = f_1 (1 - f_1)$$

$$f_3 = f_1 (1 - f_1)^2$$

$$f_4 = (1 - f_1)^3$$

$f_1$  is the free parameter which must be determined so that the mission is fulfilled; that is, a given mass ratio  $R = e^{V/c} = r^3$  results, or explicitly  $f_1 = \frac{1 - R^{-1/3}}{1}$ . More detail and more general cases as well as helpful graphs can be found in [9].

A Simple Case Including a Gravitational Field. Let us return to the problem of the simplest case for liquid-propellant vehicles, but refine it by considering a vertical ascent in a constant gravitational field of acceleration  $g$ . We want to maximize the cutoff speed  $V$ . Introducing the burning time  $\Delta T_i$  of stage number  $i$  yields

$$V = \sum_{i=1}^n c_i \ln \frac{1}{\epsilon_i + \lambda_i} - g \sum \Delta T_i$$

Using some new symbols

$a_i$  = Initial thrust acceleration of stage number  $i$ ,

measured in units of  $g$

$$c = \frac{1}{n} \sum_{i=1}^n c_i$$

$$C_i = \frac{c_i}{c}$$

$$A_i = \frac{c_i}{a_i c}$$

then easily

$$e^{-V/c} = R^{-1} = \prod_{i=1}^n (\epsilon_i + \lambda_i)^{C_i} \frac{e^{A_i}}{e^{A_i(\epsilon_i + \lambda_i)}}$$

and as usual

$$G^{-1} = \prod_{i=1}^n \lambda_i$$



We want  $G^{-1}$  to be a maximum. The usual method of solution results in

$$\epsilon_i + \lambda_i = \frac{\epsilon_i}{1 - \frac{c_n}{c_i} \frac{\lambda_n}{\epsilon_n + \lambda_n} + \left( \frac{A_n \lambda_n}{c_i} - \frac{A_i \lambda_i}{c_i} \right) c}$$

This equation is written in this form to show that for  $A_i = 0$ , the result for optimum weight distribution is again obtained.

A simple special case is

$$\begin{aligned} c_i &= c \\ C_i &= 1 \\ A_i &= \frac{1}{a_i} \\ \epsilon_i &= \epsilon \end{aligned}$$

Then

$$\epsilon + \lambda_i = \frac{\epsilon}{1 - \frac{\lambda_n}{\epsilon + \lambda_n} + \frac{\lambda_n}{a_n} - \frac{\lambda_i}{a_i}}$$

and from this

$$\lambda_i = f(\epsilon, \lambda_n, a_n, a_i)$$

where  $f$  means a function of. So corresponding weight ratios are no longer equal for different stages. Only if  $a_i = a_n$ , then we have  $\lambda_i = f(\epsilon, \lambda_n, a_n)$ ; hence  $\lambda_1 = \lambda_2 = \dots = \lambda_n$ .

The method indicated here can be generalized by introducing an average flight path angle  $\alpha_i$  for the stage number  $i$ . The mathematically correct result is to obtain a higher speed contribution from those stages which thrust close to the horizontal direction. The real situation is not described by this result. The physical fallacy originates from the fact that  $\alpha_i$  depends upon the result of the staging computation; therefore, the average flight-path angle is not independent of staging. This example shows clearly that exact investigations into optimum staging of rocket vehicles have to include the areas of trajectory shaping and flight mechanics.

### 6.1.2 Minimum Cost Vehicle

The investigations outlined in Sec. 6.1.1 lead to a vehicle of least launch weight for a given task. This is a coarse approximation to the minimum cost vehicle. Let us consider some improvements.

**Minimum Hardware Weight.** Under the present condition of nonrecovery of stages, a better approximation to least cost may be obtained by minimizing component weight instead of launch weight.

We define a total structure ratio  $\epsilon_T$ , using the same nomenclature as has been used in the discussion of optimum weight distribution (Sec. 6.1.1)

$$\epsilon_T = \frac{1}{W_o(1)} \sum_{i=1}^n \epsilon_i W_o(i) = \sum_{k=1}^n \lambda_o \lambda_1 \lambda_2 \cdots \lambda_{k-1} \epsilon_k, \text{ with } \lambda_o = 1$$

The structure factor can be written  $S = \frac{\text{total structure weight}}{\text{payload weight}} = \epsilon_T G$ ,

where  $G$  is the growth factor. So finally

$$S = \sum_{k=1}^n \frac{\epsilon_k}{\lambda_k \cdot \lambda_{k+1} \cdots \lambda_n}$$

The first problem can be outlined exactly as in Sec. 6.1.1. The vehicle should be designed so that it is in agreement with the six conditions given for optimum weight distribution, and  $S$  should be minimized.

The solution is quite complicated and is not given here. A more detailed discussion can be found in [7]. Some important results are that even for the simplest case of  $c_i = c$ ,  $\epsilon_i = \epsilon$ , it then follows that  $\lambda_1 < \lambda_2 < \lambda_3 \cdots < \lambda_n$ , and the optimum step number turns out to be somewhat smaller than it was in the case of determination of the optimum step number (Sec. 6.1.1).

**Inclusion of Stage Reliability.** Only the simplest case for liquid propellant vehicles discussed in Sec. 6.1.1 is investigated, and this in its simplest version:  $c_i = c$ ,  $\epsilon_i = \epsilon$ . But a factor  $\rho < 1$  for stage reliability will be included. Then comes  $G^{-1} = \rho^n \lambda^n$ , for the most probable growth factor and all other equations remain unchanged. The result for optimization of weight distribution for given step number  $n$  is again  $\lambda_1 = \lambda_2 = \cdots = \lambda_n = \lambda$ . Thus we again find the equality of corresponding weight ratios. But what about optimum step number? The investigation leads here to the equation  $\rho \lambda \lambda \lambda = (\epsilon + \lambda)^{\epsilon + \lambda}$ , instead of the simpler  $\lambda \lambda = (\epsilon + \lambda)^{\epsilon + \lambda}$ , which we found in determination of the optimum step number. Assuming that  $\lambda_o$  is the solution to the simpler second equation, then a first approximation to the solution of the first, or more complicated, is

$$\lambda \approx \lambda_0 \left[ 1 - (1 - \rho) \frac{\lambda_0}{\epsilon} \right]$$

from which

$$\lambda < \lambda_0$$

$$r > r_0$$

$$N < N_0$$

This is the analytic proof of what one would guess anyway, namely, that inclusion of stage reliability pushes the optimum step number toward a lower value.

Inclusion of Cost. Let us write  $C$  for the cost of a launched vehicle. We then want to maximize

$$G_c^{-1} = \frac{\text{most probable payload weight delivered}}{\text{cost}} = \frac{\rho^n W_0(1) \cdot \prod_{i=1}^n \lambda_i}{C}$$

Writing for the cost the following plausible equation and changing it in the manner shown, which is permitted only under the assumption  $B/A < 1$ , we obtain

$$G_c^{-1} \approx \frac{1}{A} \cdot \left( \frac{\rho}{1 + \frac{B}{A}} \right)^n \cdot \prod_{i=1}^n \lambda_i = \frac{1}{A} \cdot \rho'^n \cdot \prod_{i=1}^n \lambda_i, \text{ where } \rho' = \frac{\rho}{1 + \frac{B}{A}} < \rho$$

Thus, neglecting the constant  $A$ , the problem has been, again, reduced to the case shown previously, where simply the reduced reliability  $\rho'$  is substituted for  $\rho$ . All results from the above paragraphs on stage reliability apply.

A typical numerical example is

$$V = 9.5 \text{ km /sec}$$

$$c = 3.65 \text{ km/sec}$$

$$\epsilon = 0.10$$

Then

$$\lambda_{\text{opt}} = 0.32$$

$$N = 3$$

$$G_c^{-1} = 30.47$$

Introducing  $\rho = 0.935$ , and

$$C = A \cdot 1.1^N, \text{ thus}$$

$$\rho' = 0.85 \text{ comes}$$

$$G_{\rho'}^{-1} = 49.6 \text{ for } N = 3$$

Going to a two-stage vehicle, it follows that

$$\lambda = 0.1722$$

$$G^{-1} = 33.73$$

$$G_{\rho'}^{-1} = 47.2$$

In this rather typical case, the three-stage vehicle is best as judged on the basis of  $G$ , whereas judged on the more valid basis of  $G_{\rho}$ , the two-stage vehicle is the optimum solution.

For large vehicles,  $A$  may be \$10/lb of launch weight. As the example describes a typical orbital carrier, we see that realistically the two-stage vehicle may do the job for \$472/lb of delivered payload, whereas the three-stage version would demand \$496/lb in spite of its higher payload per successful flight.

## 6.2 Critical Remarks

After this survey of several analytic methods of step rocket optimization, some critical remarks are in order.

1. Often, cutoff energy is a more valid measure of performance than the characteristic speed  $V$  used in this paper.

2. The optimum step number  $N$  must be a whole number, and the practical step number  $n$  is determined often by the mission rather than by the optimization criterion. Furthermore, the stage parameters  $c$  and  $e$  are usually not the same for each stage. It is not economically sound to develop an optimum vehicle for each conceivable mission. The correct procedure is rather to develop a vehicle which can be made attractive for other missions, for example, by adding one more stage.

3. Another variable for optimization is the initial acceleration, which again is influenced by certain reliability demands (e.g., engine-out capability for a multiengine carrier) and launch restrictions (e.g., wind). For the upper stages, trajectory shaping and crew escape compatibility must be considered.

4. Available components (engines, stages) obviously will influence the choice of the most economic space carrier vehicle. But the larger the expected transportation volume and the longer the expected lifetime of the vehicle, the less important becomes the available component restriction.

5. Finally, attention should again be drawn to the important interaction between trajectory shape, flight mechanics, and vehicle optimization [10]. Except for the simple case including a gravitational field discussed in Sec. 6.1.1, this interaction was neglected.

### 6.3 Conclusions

Several methods to optimize the weight distribution and the step number of staged rocket vehicles have been described. The four main conclusions are:

1. Analytical methods are available to give a "first cut" to the solution.
2. An optimum step number  $N$  exists with respect to maximized payload capability of the vehicle. Some practical criteria push toward a reduction of  $N$  for the truly best vehicle. (See discussion of the third parameter  $\mu$  in Sec. 6.1.1 and Sec. 6.1.2.)
3. The widely used criterion of optimization, namely maximize payload capability, does not generally result in the most economic transportation system. The latter one will have a smaller number of stages than the former one.
4. Certain practical aspects, summarized in Sec. 6.2, reduce the value of results of analytical vehicle optimization studies. Still the analytical theories show areas of interest, trends, and areas of potential improvement. Furthermore, upper performance limits are established.

The methods and procedures described in this paper are of value especially in the early planning phase with regard to the introduction of a new space carrier vehicle. Whereas the maximization of performance can be handled quite straight forwardly, more subtle considerations such as reliability and economy can be included. Once the vehicle is sufficiently well defined, the analytic methods become less useful, and more and more detailed computations must be made and evaluated.

### REFERENCES

1. Huber, W. G. and H. H. Koelle, Economy of Space Flight, in "Handbook of Engineering," H. H. Koelle, ed., McGraw-Hill Book Co., New York, 1961.
2. Ruppe, H. O., Minimum Energy Requirements for Space Travel, in "Xth International Astronautical Congress Proceedings," F. Hecht, ed., Springer-Verlag, Vienna, 1960.
3. Stuhlinger, E. and R. N. Seitz, Electrostatic Propulsion Systems for Space Vehicles, in "Advances in Space Science, Vol. 2," Frederick I. Ordway, III, ed., Academic Press, New York, 1960.
4. Martelly, J., "Optimisation de la Propulsion Trans-Satellite," to be published in the "XIIth International Astronautical Congress Proceedings."

5. Malina, F. M. and M. Summerfield, The Problem of Escape from Earth by Rocket, Journal of the Aeronautical Sciences, 14:471 (August 1947).
6. Über die beste Teilung von Stufenaggregaten, Peenemünde Archiv No. 68/22, 1942.
7. Krause, H. G. L., Allgemeine Theorie der Stufenraketen, Forschungsbericht No. 11, Gesellschaft für Weltraumforschung, Germany (September 1953).
8. Krause, H. G. L., "General Theory of Multistage Rockets," Preprint No. 2073, American Rocket Society, New York, 1961.
9. Thackwell, Jr., H. L. and J. A. Nanderkerchoje, Optimum Staging of Solid-Propellant Rocket Vehicles, Astronautica Acta, 7:190 (1961).
10. Weber, R. J., Optimization of Multistage Rockets, ARS Journal, 31:849 (June 1961).

7

## EVOLUTION OF EARTH-LUNAR TRANSPORTATION SYSTEMS

H. H. Koelle

Future Projects Office  
George C. Marshall Space Flight Center  
National Aeronautics and Space Administration  
Huntsville, Alabama

Manned Earth-lunar transportation systems moved closer to reality with the initiation of a program to land man on the lunar surface in this decade. This will be the beginning of a transportation system connecting the Earth and the Moon, which will be improved continuously to a point where commercial traffic between these two celestial bodies becomes economically feasible. While the emphasis will be on the first manned lunar landing, it is not too early to take closer look at what might possibly follow this first landing and what refinements in the transportation system can be expected through about 1980. This is as far as one would dare to extrapolate advancement of the technology with any degree of confidence. It is quite probable that any prediction of today will be pessimistic, as new unpredictable discoveries will be made in the development of space technology.

Therefore, this study is only an attempt to develop a typical model of a lunar transportation system which will gradually be improved by incorporation of more efficient elements, such as high energy propellants, nuclear propulsion systems, and fully reusable space vehicles. Finally, it does not seem impossible to produce propellants on the surface of the Moon; this would enable space vehicles to be refueled before they return to Earth. It should be recognized, however, that this model is a hypothetical one only and has no other basis than that of imagination and a fair knowledge of the state of the art. Thus, the results of this study must be considered as very preliminary and only as describing the general trend in the evolution of Earth-lunar transportation systems.

## 7.1 Discussion

### 7.1.1 Assumptions

Modes of Operation. Seven different modes of operation will be considered which cover two decades. They can be briefly described as:

1. A large Earth launch vehicle, with two expendable chemical stages,

Preceding page blank

provides the transportation from the surface of Earth to a low-altitude orbit about it. The vehicle assumed in this example has five liquid propellant engines, each of 1,500,000 lb thrust, in the booster, and four liquid propellant engines of 200,000 lb thrust in the second stage. The orbital launch vehicle is assembled with the help of one rendezvous and docking maneuver and consists of a launch stage and a lunar landing stage, both using the hydrogen/oxygen propellant combination. The thrust levels are approximately 200,000 lb and 30,000 lb respectively. The return from the Moon is accomplished by a single stage employing conventional propellants (solid or liquid) and a direct entry into Earth's atmosphere with orbital entry velocity. This mode of operation is very close to the mission profile which probably will be employed for the first Apollo flight (stages 1, 2, 3, 4 and 5 of Table 7.1).

2. The second mode of operation is identical to the first with the exception of the lunar launch vehicle, which employs high-energy propellants instead of conventional propellants, thus reducing the take-off weight of the lunar launch vehicle by one-third. This eliminates the rendezvous requirement, as the basic launch vehicle has a direct capability within the given payload limit. It also seems advantageous to integrate the lunar landing and launch requirements into one single stage (stages 1, 2, 3 and 6 of Table 7.1).

3. The third mode of operation envisions the same ground launch vehicle to Earth orbit. The third stage, however, is now a nuclear stage that is used for the escape leg from the Earth orbit and is restarted upon arrival near the Moon for the braking maneuver into the lunar orbit. The fourth stage is a high-energy chemical propellant stage and accomplishes the lunar landing, as well as the lunar take-off, with direct entry of the manned capsule into Earth's atmosphere (stages 1, 2, 7 and 6b of Table 7.1).

4. The fourth mode of operation introduces a recoverable and reusable Earth ground launch vehicle that replaces the expendable orbital carrier vehicle used in modes 1 through 3. The thrust of this new vehicle is the same as modes 1 through 3 and, therefore, the payload capability is reduced because of the added weight for the recovery gear. This, then, requires the introduction of one rendezvous and docking maneuver as used in mode 1 (stages 8, 9, 7 and 6b of Table 7.1).

5. The fifth mode of operation uses the same reusable Earth launch vehicle as mode 4 and in addition uses a nuclear ferry vehicle capable of making a full round trip between Earth orbit and Moon orbit. It is refueled in Earth orbit by the reusable Earth launch vehicle. The local lunar transportation is provided by a single-stage chemical propellant vehicle that is refueled in lunar orbit by the lunar ferry vehicle. Its job is to transfer the cargo and crew from the lunar orbit down to the lunar surface and return the relief crew to the lunar orbit, from where



Table 7.1 Fundamental Vehicle Data

STAGE IDENTIFICATION	1	2	3	4	5	6	6a	6b	7	8	9	
STAGE DESCRIPTION	Nova Jr.	(expendable)	Orbit Launch Vehicle	Lunar Landing Vehicle	Lunar Launch Vehicle	Lunar Landing & Launch Veh.	Lunar Landing Veh. for Nuc. Ferry	Lunar Landing Vehicle	Restart for Take-off	Nuc. Orbit Launch Veh.	Nova Jr.	recoverable
	1st Stage	2nd Stage									1st Stage	2nd Stage
$F_0$ , thrust	$7.5 \times 10^6$	800,000	200,000	200/215,000	30,000	30,000		(Cargo Only)	30,000	70,000	$7.5 \times 10^6$	$1.0 \times 10^6$
$W_0$ , initial weight	$6.0 \times 10^6$	1,110,000	450,000	225,000	49,000	100,000	131,800	131,800	45,900	275,000	6.0	$1.3 \times 10^6$
$F_0/W_0$	1.25	0.721	0.444	0.89	0.61/3.88	0.30	0.23	0.23	0.65/3.82	0.25	1.25	0.77
$W_{11}$ useful payload	-	225,000	-	59,000	3 Men	3 Men	70,000	34,700 +	3 Men	(125,200)	-	150,000
$W_1$ , total payload	1,110,000	250,000	225,000	62,200	(12,500)	(13,600)	(73,700)	36,500 +	(12,500)	131,800	$1.3 \times 10^6$	158,000
$W_8$ , structure weight	345,000	59,300	32,000	23,000	5200	9640	8200	9200	9200	24,600	660,000	161,000
$W_6$ , residuals	45,000	7700	2000	1400	300	760	500	24,200	700	1200	40,000	10,000
$W_w$ , stage wet weight	390,000	67,000	34,000	24,400	5500	10,400	8700	33,400	9900	25,800	700,000	171,000
$W_8$ , useful propellant weight	$4.5 \times 10^6$	768,000	191,000	138,400	31,000	76,000	49,400	49,400 +	23,500	117,400	$4.0 \times 10^6$	971,000
$W_c$ , cutoff weight	$1.5 \times 10^6$	317,000	259,000	86,600	18,000	24,000	82,400	82,400	22,400	157,600	$2.0 \times 10^6$	329,000
$\mu = \frac{W_8}{W_w + W_8}$ , mass fraction	0.92	0.92	0.85	0.85	0.85	0.88	0.85	0.88	0.88	0.825	0.85	0.85
$\bar{I}_{sp}$ , specific impulse	300	425	425	434	315	434	434	434	434	800	300	450
r, mass ratio	4.000	3.500	1.737	2.600	2.722	4.170	1.600	1.600	2.050	1.745	3.000	3.950
$\Delta v$ , velocity increment	4085	5215	2310	4065	3080	6040	2000	2000	3050	4370	3240	6060
$M_{11} = \frac{W_0}{W_1 c}$ , growth factor	24			7.23	3.920	7.35	1.79	(1.81)		2.09		3.70
$M_1 = \frac{W_0}{W_{11}}$ , eff. growth factor	26.7			7.62	-	-	1.88	-				40.0
Reliability	1965-68: 80% -69: 85% -70: 90%		95%	90%	1968:90% -69:95%	85%	1969:90% -70:95%	1969:85% -70:90%		1969:85% -70:90%		1971:83.3% -78:96%

Table 7.1 Fundamental Vehicle Data (continued)

STAGE IDENTIFICATION	10		10a		6c		11		8a	12	
STAGE DESCRIPTION	Nuclear Round-Trip Ferry		Nuclear Ferry with Lunar Refueling		Lunar Shuttle (Orbit Fueled)		Lunar Shuttle (Lunar Surface Fueled)		Chemical Booster	Nuclear Ship	Nuclear Return
					From Orbit	To Orbit	To Orbit	From Orbit			
F <sub>0</sub> , thrust	200,000		200,000		30,000	30,000	230,000	230,000	7.5 x 10 <sup>6</sup>	3 x 10 <sup>6</sup>	
W <sub>0</sub> , initial weight	300,000	78,800	300,000	78,800	110,000	30,400	198,500	251,000	6 x 10 <sup>6</sup>	3,175,000	3,045,000
F <sub>0</sub> /W <sub>0</sub>	0.67	2.54	0.67	2.54	0.273	0.99	1.16	0.92	1.25	0.94	0.99
W <sub>11</sub> , useful payload	88,500	3 Men	120,000	3 Men	36,400	3 Men	-	120,000	-	30,000	-
W <sub>1</sub> , total payload	93,200	10,000	127,000	10,000	38,300	10,000	10,000	127,000	3,175,000	150,000	-
W <sub>s</sub> , structure weight	33,400	33,400	33,400	33,400	8500	8500	18,300	18,300	400,000	30,000	30,000
W <sub>6</sub> , residuals	35,400	1600	1600	1600	11,900	500	1700	1700	25,000	160,000	490,000
W <sub>w</sub>	68,800	35,000	35,000	35,000	20,400	9000	114,000	20,000	425,000	490,000	490,000
W <sub>8</sub> , useful propellant weight	128,000	33,800	128,000	33,800	41,800	11,400	74,500	94,000	2,400,000	25,000	25,000
W <sub>c</sub> , cutoff weight	172,000	45,000	172,000	45,000	68,700	19,000	124,000	157,000	3,600,000	2,500,000	2,500,000
$\mu = \frac{W_8}{W_w + W_8}$ , mass fraction	0.82		0.82		0.855		0.894		0.85	0.84	
$\bar{I}_{sp}$ , specific impulse	800		800		434		434		400	900	
r, mass ratio	1.745	1.745	1.745	1.745	1.600	1.600	1.600	1.600	1.663	4.700	5.580
$\Delta v$ , velocity increment	4350	4350	4350	4350	2000	2000	2000	2000	2000	13,670	15,200
$M_{11} = \frac{W_0}{W_1}$ , growth factor	2.19	-	2.19	7.88	1.87	3.04	1.91	1.97	1.89	17.5	101
$M_1 = \frac{W_0}{W_{11}}$ , eff.growth factor	-	-	2.31	-	-	-	-	2.09	-	-	-
Reliability	1972: 75%		1972: 75%		1972: 75%		1975: 81%				
	1978: 91%		1978: 91%		1974: 86%		1978: 91%				

\*Individual columns are arranged according to vehicles rather than stages.

they are taken back to Earth orbit by the nuclear orbit ferry vehicle. In this mode, all vehicles are reusable several times. Obviously the efficiency of the operation will improve with time as the number of reuses is increased by the learning factor and improved reliability (stages 8, 9, 10 and 6c of Table 7.1).

6. The sixth mode of operation is of interest only if it becomes possible to produce propellants on the Moon. Under conditions yet to be determined, it might be more economical to refuel with propellants produced on the Moon; thus, the lunar shuttle vehicle could be refueled on the lunar surface instead of in Earth orbit. The lunar shuttle vehicle has to double in size to carry the increased payload of the ferry, if the rendezvous mode in Earth orbit is employed; or the rendezvous can be eliminated if the size of the lunar shuttle remains the same. The first of these two options is used in this calculation (stages 8, 9, 10a and 11 of Table 7.1).

7. The seventh and last mode of operation is entirely different and might be of interest if large amounts of liquid hydrogen become available on the Moon. The total space transportation system may then be reduced to two vehicles - a chemical, reusable booster that transports the second stage, a nuclear spaceship, beyond the atmosphere and returns to Earth. The nuclear stage then makes the entire trip to the lunar surface, eliminating lunar orbital operations entirely, and is refueled on the Moon. The return trip is performed in one sweep; the nuclear engine is restarted upon entry into Earth's atmosphere to reduce the peak deceleration loads to a tolerable level of perhaps not more than 1.5 G. The landing can then take place under power or with the assistance of a flex wing deployed in the subsonic range at an altitude of about 10 km. The nuclear ship can be overhauled and reused for a new trip (stages 8a and 12 of Table 7.1).

8. An arbitrarily selected schedule for the development and operational cycle of these seven modes of operation is shown in Fig. 7.1.

Space Vehicles. The space vehicles required for these seven basic modes of operations are listed in Table 7.1. There are essentially twelve basic component units (stages) and a few modifications thereof. The essential weight data of these stages are compiled. The first two columns represent the two stages of the first generation, expendable, Earth launch vehicle. The third and fourth columns represent the chemical propellant, orbital launch, and the lunar landing stages, respectively, used in the first mode of operation. Vehicle 5 is the conventional lunar launch stage and 6 is the integrated lunar landing and launch stage used in the second mode of operation. A modification of the last is needed, as soon as the nuclear orbit launch stage is introduced, to adjust to the increased payload capability. Two versions are listed, one for cargo transportation only (6a) and one for mixed cargo and personnel transportation (6b). The

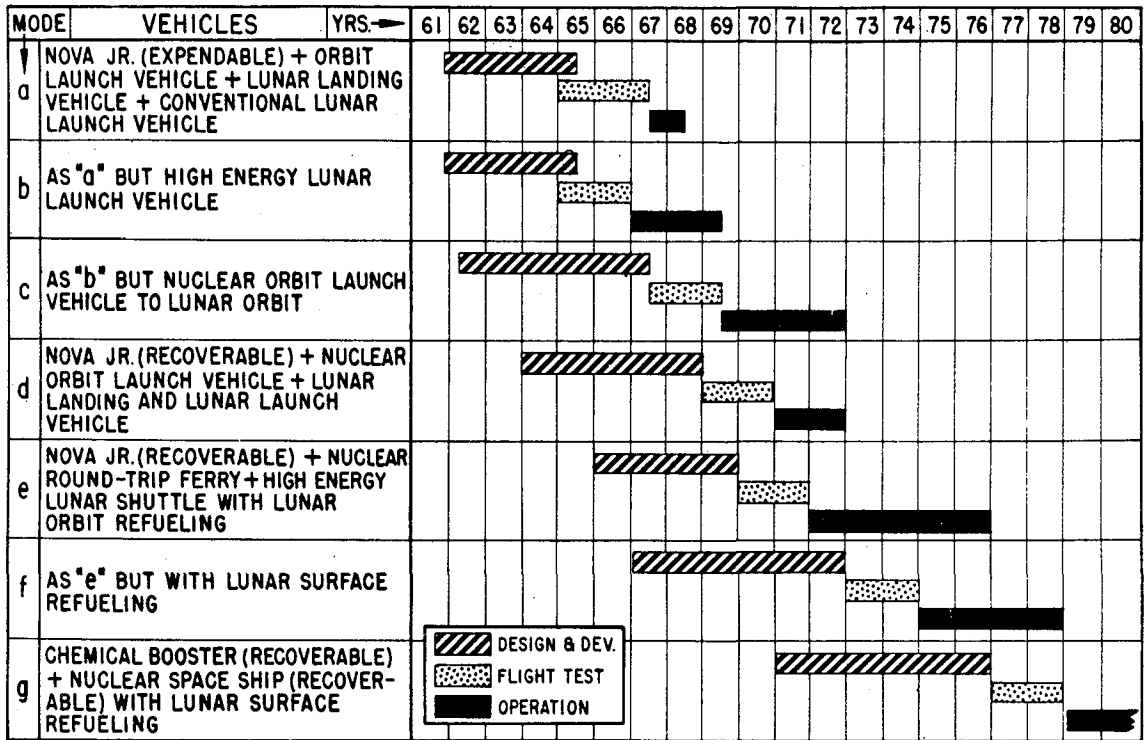


Fig. 7.1 Assumed time table for individual modes of operation.

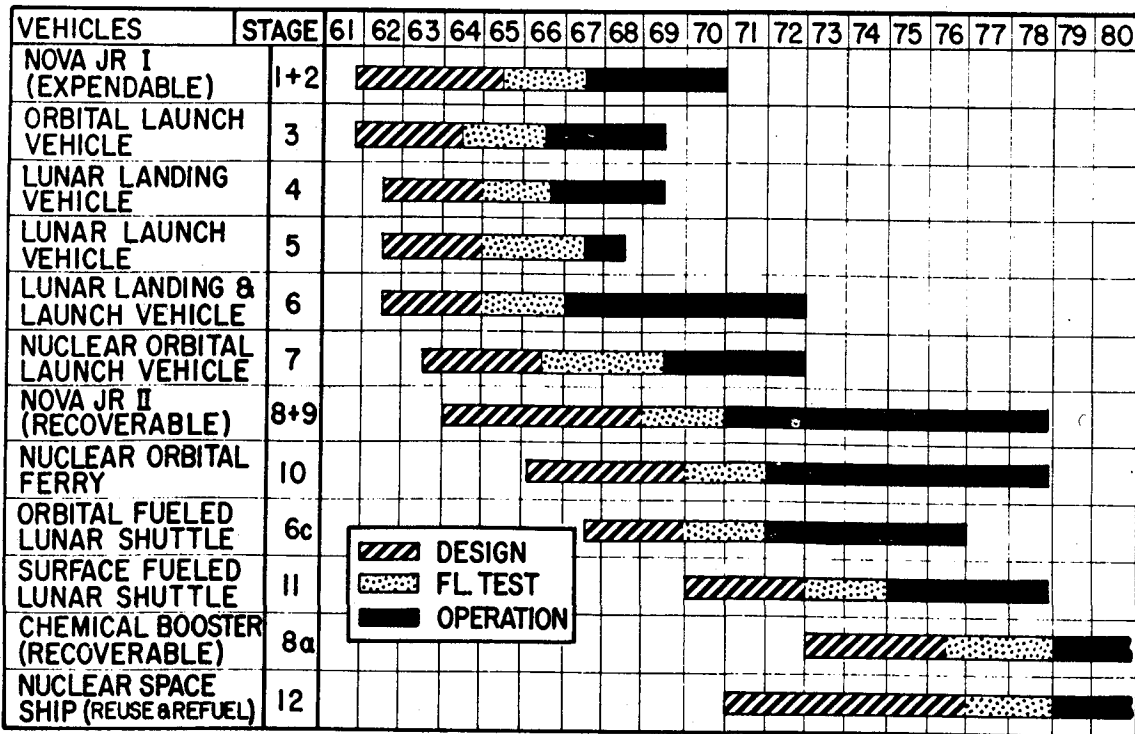


Fig. 7.2 Assumed time tables for individual hardware units.

nuclear orbit launch vehicle, which is reusable, appears in columns 8 and 9, first and second stages, respectively. Column 10 shows some of the data of the nuclear ferry vehicle capable of making a full round trip. A modification of this vehicle, resulting from the introduction of refueling in the lunar orbit, is listed in column 10a. The lunar shuttle vehicle, when refueled in the lunar orbit, is a modification of the original lunar landing and launch vehicle 6 and is listed in column 6c. With the introduction of refueling on the lunar surface, this vehicle grows in size and requires a more powerful engine. Except for this change, it is similar to 6 but is listed separately in column 11. A modification of the reusable booster (8) is used for launching the nuclear spaceship, column 12. The basic change is a reduction in propellant volume; its weights are listed in column 8a. Column 12 represents the nuclear spaceship for the outbound and return legs of the lunar trip.

The horizontal lines represent the initial thrust, several weights, propellant mass fraction  $\mu$ , the specific impulse, mass ratio, velocity increment and growth factors. An assumption of mission reliability in a particular year is listed in the last line of Table 7.1.

Typical schedules and time periods, where the various stages and space vehicle will be in operational use, are shown in Fig. 7.2.

Cost and Mission Reliability. Table 7.2 summarizes the cost of individual stages, spare parts, and launch operations as a function of time for all seven modes of operation. The second part indicates the assumptions made for the individual mission reliability of single stages, as well as the total mode of transportation of each system under consideration. Dividing the cost by reliability and payload (or number of personnel) weight yields the specific transportation cost per pound payload or per round trip. These figures can also be used to determine the direct operating cost for Earth-to-orbit transportation resulting from these examples.

### 7.1.2 Results

Specific Transportation Cost for Personnel. If the results of Table 7.2, with consideration of the schedules given in Fig. 7.1, are plotted versus time, the curves shown in Fig. 7.3 results. It is interesting to note that the round-trip cost for the first astronauts (excluding the development cost) should be close to \$40,000,000/man. It is obvious that the introduction of high-energy propellants for the return trip pays off nicely, and the trip costs are reduced to about 50 per cent in mode 2. Therefore, it seems that mode 1 will have only very temporary importance and should not be pursued unless a higher probability of success can be expected. Fig. 7.3 further shows that a nuclear propulsion system should be used as early as possible, since it promises an additional reduction of the round-trip cost by 50 per cent in mode 3. This mode is the best that can be expected with expendable systems. The introduction of a reusable Earth-to-orbit carrier vehicle will not pay off before 1972 (mode 4) because of

Table 7.2 Cost and Reliability Estimates for Lunar Mission

MODE OF OPERATION	a				b			c			d		e					f					g		
	1967 Pers.	1967 Cargo	1968 Pers.	1968 Cargo	1967 Personnel	1968	1969	1969	1970	1971	1971	1972	1972	1973	1974	1975	1976	1977	1978	1979	1980	1981			
Vehicle cost per launch:																									
Stage I	35.0	35.0	34.0	34.0	17.5	17.0	16.5	16.5	16.3	16.0	26.6	18.6	18.6	15.5	14.0	6.5	5.9	5.4	5.0	2.6	2.4	2.1			
Stage II	8.3	8.3	8.0	8.0	4.2	4.1	4.0	4.0	3.9	3.8									21	11.5	10				
Stage III	3.5	3.5	3.5	3.5	3.5	3.4	3.3	5.4	5.2	5.0	5.0	4.8	4.6	4.3	3.8	3.5	3.2	3.0	2.8						
Stage IV	3.8	3.8	3.8	3.8	6.2	6.1	6.0	4.3	4.2	4.1	4.1	4.0	1.0	0.6	0.4										
Stage V	5.8	-	5.8	-	-	-	-	-	-	-	-	-	-	-	-	-	-	-	-	-	-				
Spare parts	10	-	9.0	-	10.0	9.0	8.8	8.8	8.6	8.4	8.2	8.0	1.8	0.9	0.6	0.6	0.5	0.4	0.3	2	2	2			
Launch operations	8	8	7.9	7	-	-	-	-	-	-	4.5	4.5	0.6	0.6	0.6	0.6	0.6	0.6	0.6	1	1	1			
\$10 <sup>6</sup>	74.4	58.6	72	57.2	41.4	39.6	38.6	39.0	38.2	37.3	48.4	37.9	26.6	21.9	19.4	11.2	10.2	9.4	8.7	26.6	16.9	15.1			
Stage I Reliability	.86	.86	.90	.90	.86	.90	.92	.93	.94	.95	.833	.909	.909	.937	.947	.952	.957	.959	.960	.95	.96	.97			
Stage II	.85	.85	.88	.88	.85	.88	.90	.91	.92	.93									.90	.93	.94				
Stage III	.95	.95	.96	.96	.95	.96	.97	.97	.98	.98	.98	.98	.80	.833	.856	.875	.889	.90	.91	.90	.93	.94			
Stage IV	.90	.90	.91	.91	.95	.96	.97	.97	.98	.98	.98	.98	.86	.91	.933	.947	.954	.958	.960	-	-	-			
Stage V	.95	-	.96	-	-	-	-	-	-	-	-	-	-	-	-	-	-	-	-	-	-	-			
Mission Reliability	.60	.63	.664	.692	.66	.73	.78	.796	.831	.850	.80	.873	.626	.71	.756	.789	.815	.826	.840	.77	.83	.86			
Payload weight		59,000		59,000				34,700	34,700	34,700	34,700	34,700	36,400	36,400	36,400	120 K	120 K	120 K	120 K	150 K	150 K	150 K			
Crew number	3				3	3	3	3	3	3	3	3	3	3	3	3	3	3	3	10	10	10			
\$/lb		1576		17600				677	636	607	837	600	583	424	352	95	83	76	69	150	88	76			
10 <sup>6</sup> \$/man	41.3		36.1		20.9	18.1	16.5	8.5	7.96	7.60	10.5	7.5	7.1	5.15	4.28	0.95	0.83	0.76	0.69	1.20	0.7	0.61			

a K signifies x 10<sup>3</sup>

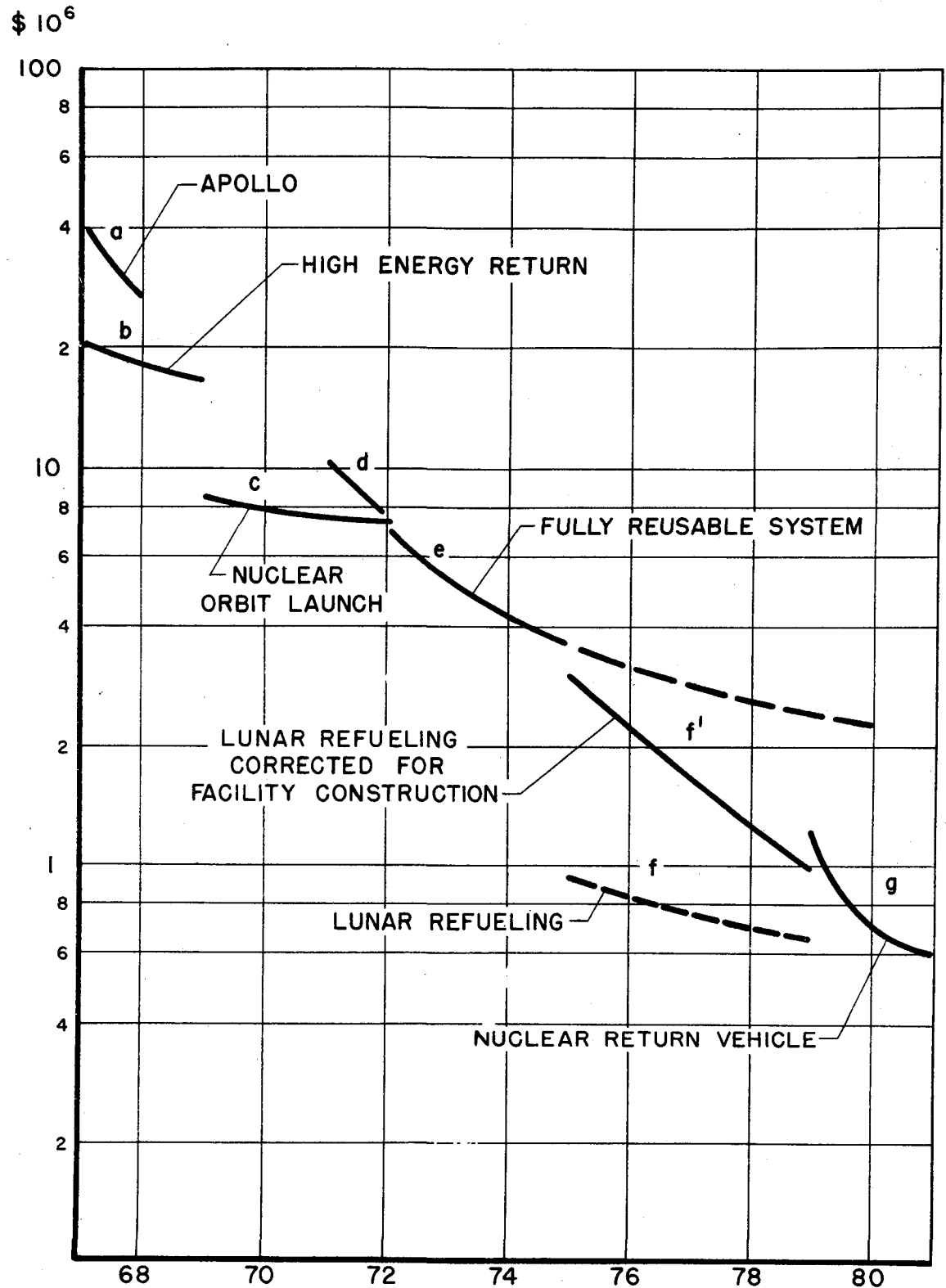


Fig. 7.3 Lunar round-trip cost trends.

the small reuse rates and low reliability.

Later, however, especially in connection with reusable nuclear ferry and lunar shuttle vehicles (mode 5), the reusable launch vehicle should reduce substantially the round-trip cost to less than \$40,000,000/man by about 1975, and less than \$2,000,000/man by 1980. This cost is as low as we can hope to go, unless a way can be found to produce propellants on the Moon. The lower line indicated for mode 6 is of a hypothetical nature. It would be valid only if propellant production facilities can be erected on the Moon at no cost. The upper line for mode 6 is arbitrarily drawn to indicate the trend desired. The difference between these two lines is the equivalent of the funding available for the establishment and operation of lunar propellant production facilities. Should these expenses be much larger, mode 5 would do as well. Finally, mode 7 indicates what can be expected by the introduction of first-class transportation, represented by a chemically boosted, all-nuclear spaceship for the round trip. This would, however, require the production of huge amounts of liquid hydrogen on the Moon, which at this time does not appear feasible. From Fig. 7.3, it is seen that three phases of manned lunar transportation systems will be of particular interest in the next 15 years:

1. 1967 - 69: All-chemical expendable systems with direct hyperbolic entry (mode 2)
2. 1970 - 72: Expendable systems with a nuclear orbit-to-orbit stage and direct hyperbolic entry (mode 3)
3. 1973 - 75: All-chemical, reusable, orbital carrier vehicle with nuclear ferry vehicle from orbit-to-orbit and return, and chemical, lunar round-trip shuttle vehicle, with return through Earth orbit at orbital entry velocity (mode 5)

Specific Transportation Cost for Cargo. A similar picture emerges for cargo transportation, and is shown in Fig. 7.4. The second mode of operation (2) does not apply because high-energy propellants are introduced in the return stage only. Thus, a drop from about \$1600/lb of payload to about \$650/lb can be expected by the introduction of a nuclear propulsion system in the orbit-to-orbit leg. The next big improvement comes with the fully reusable system (mode 5), which reduces the cost to \$300/lb during the 1975-'76 period. The only known way to reduce it further is by propellant production and refueling on the lunar surface. If this is at all feasible, a cost of \$100/lb can be achieved. The same three phases shown above as desirable for personnel transportation are equally suitable for cargo transportation.

Also of interest for general comparison is the specific transportation cost for the Earth-to-orbit phase resulting from these assumptions. The trend of this cost is shown in Fig. 7.5. Starting with a \$132/lb cost in 1967 for expendable systems, there is a cross-over point in 1971 at



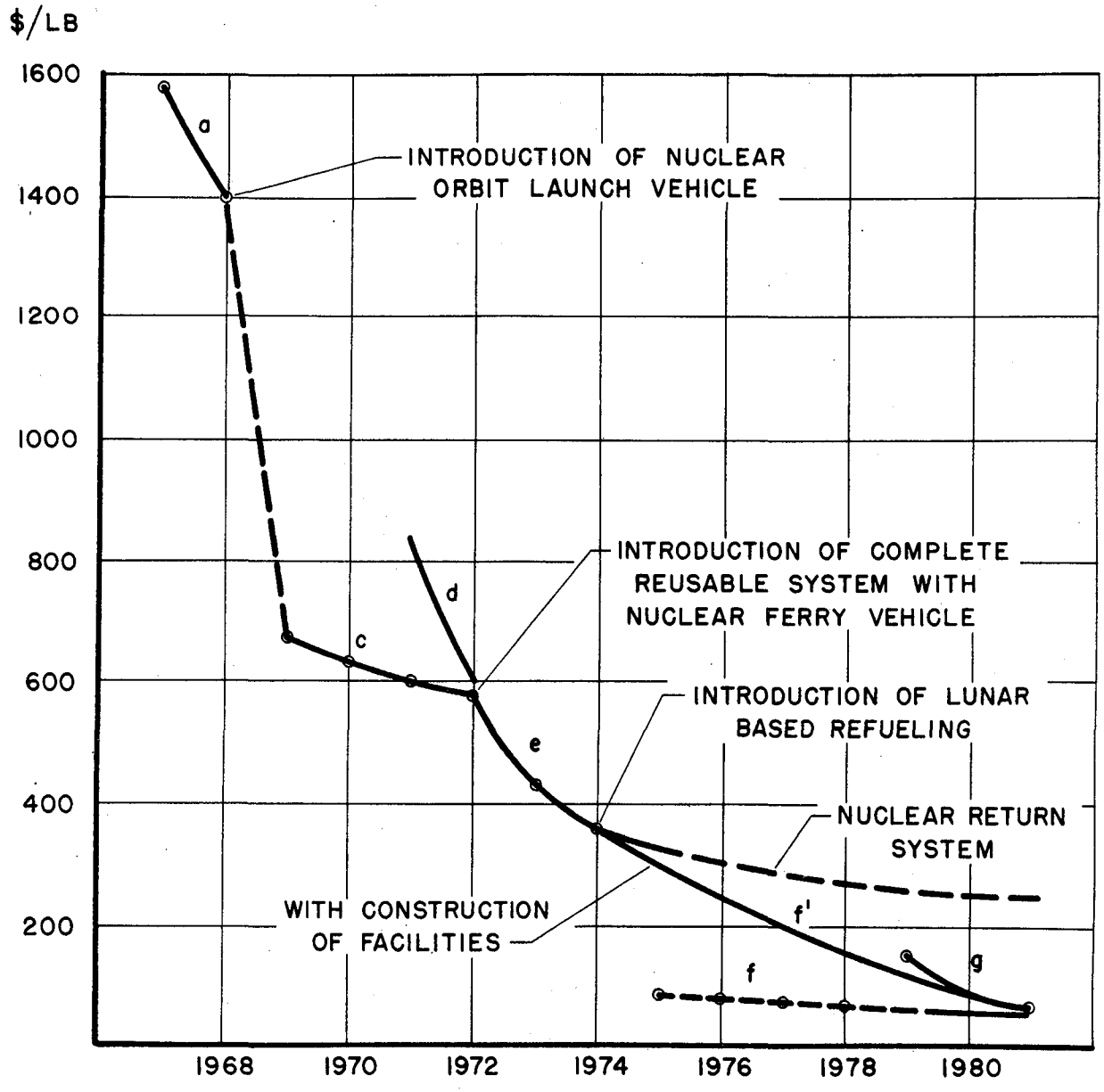


Fig. 7.4 Trends of cargo transportation cost to the Moon.

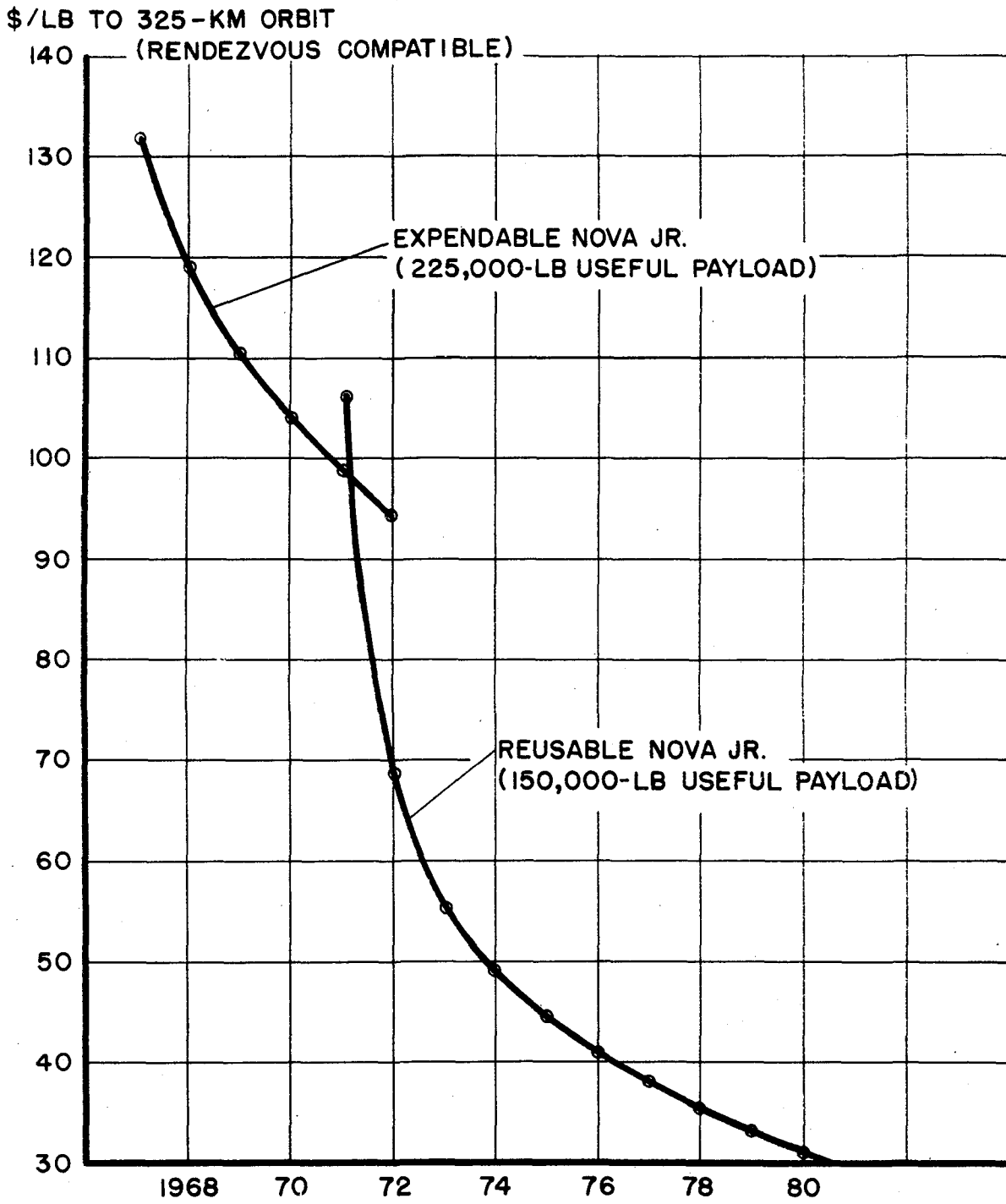


Fig. 7.5 Earth-to-orbit cost trends.

about \$100/lb with the reusable orbital carrier vehicle. As the efficiency of the reusable vehicle improves, the specific transportation cost comes down to about \$30/lb by 1980. It should be kept in mind, however, that this is only the direct operating cost and does not include development cost and other fixed costs.

Expected Transport Volume. In this chapter it is necessary to make an assumption of the total amount of traffic or transport volume, for this influences the cost assumptions. For this purpose a model of a typical Earth-lunar transport volume is developed.

The basic assumption is that from 1967 to 1980 a constant share of the gross national product (GNP) will be used for the development and operation of the Earth-lunar transportation system and a lunar base. This was assumed to be 0.25 per cent of the total GNP. Assuming further that the growth of the GNP is 3.5 per cent per year, and that half of the lunar operation funds (e.g., 0.125 per cent) is used for research and development plus the operation of the lunar base itself; the other half is available for the procurement and operation of the space vehicles needed to operate the transportation system between Earth and Moon. This results in the amounts given in column 2 of Table 7.3, starting with \$790,000,000 in 1967 and growing to \$1,280,000,000 in 1981. Using the preferred mode of operation in each particular year, and the specific transportation cost shown in Figs. 7.3 and 7.4, the number of annual flights as shown in column 3 of Table 7.3 results. From this, the total number of personnel transported to and from the Moon can be derived (column 4) as well as the total weight of the cargo actually delivered to the Moon. Only the successful flights are listed here.

There is a big increase in transport volume (personnel and cargo) in 1975 with the introduction of lunar refueling. Whether this is feasible or desirable remains to be seen. It can be assumed, however, that this additional capacity is available for the assembly and operation of the lunar propellant production site. These figures are used to determine the amount of facility weight that can be afforded to make this scheme pay off. It was found that the propellant production facility (roughly) should not exceed 1 lb if facility weight for each pound of propellant produced each year, to make this economically attractive. If this figure should be larger, it might be preferable to retain the fully reusable mode with refueling in Earth orbit. To show the available manpower and cargo for the lunar production facility a little more clearly, Figs. 7.6 and 7.7 have been included.

## 7.2 Conclusions

From the results of this study, the following three phases of development in Earth-lunar transportation systems can be foreseen clearly:

Table 7.3 Expected Transport Volume of Lunar Transportation Systems

1	2	3	4	5
Year	Lunar Transport. Funds Per Year	No. Flights Per Year (successful)	No. of Passenger Round Trips Per Year	Annual Cargo Delivered
	[10 <sup>6</sup> \$]			10 <sup>6</sup> lb
1967	790	6	12	0.342
1968	818	8	12	0.429
1969	845	14	42	0.472
1970	875	19	56	0.674
1971	905	21	62	0.712
1972	937	22	68	0.778
1973	972	32	96	1.136
1974	1005	39	118	1.421
1975	1040	73	220	8.750
1976	1078	86	260	10.380
1977	1115	97	297	11.700
1978	1155	112	335	13.380
1979	1195	60	390	7.930
1980	1235	88	572	11.890
1981	1280	73	730	11.210

ANNUAL PASSENGER ROUNDTrips

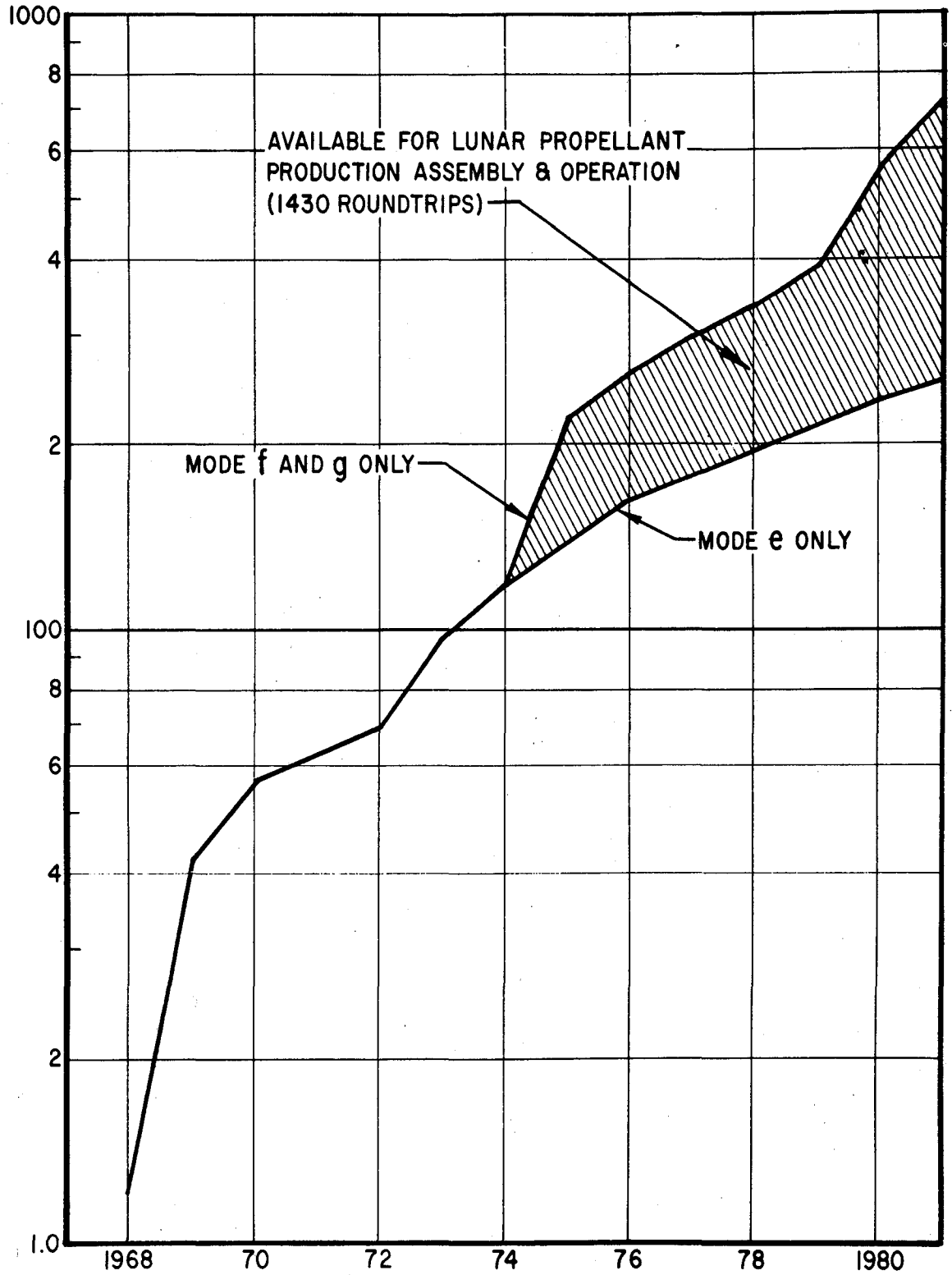


Fig. 7.6 Earth-Moon annual transport volume vs. time (0.125 per cent of GNP).

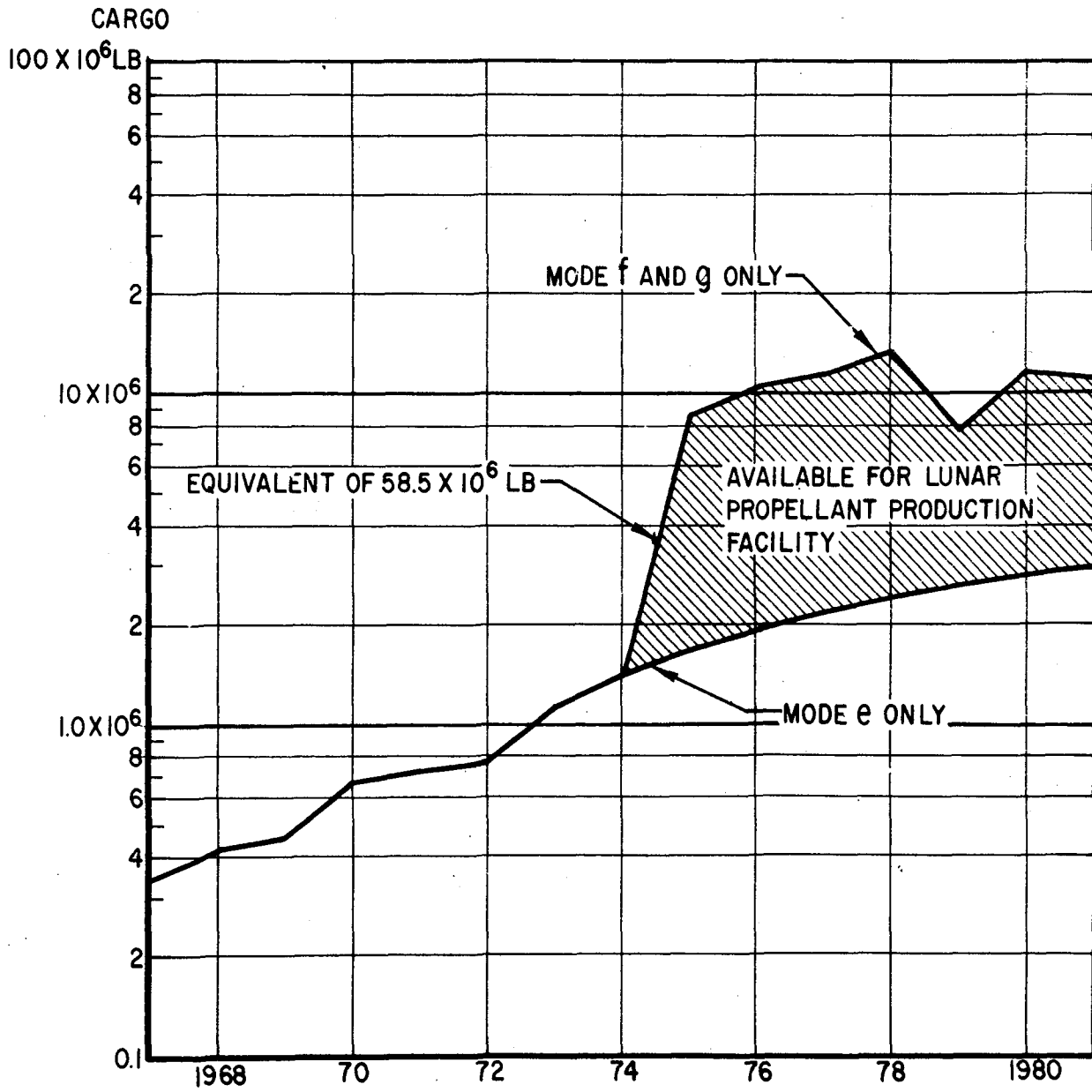


Fig. 7.7 Earth-Moon annual cargo transport volume vs. time (0.125 per cent of GNP).

1. 1967 - 69: All-chemical, expendable, rocket vehicles with direct hyperbolic entry into Earth's atmosphere
2. 1969 - 72: Expendable space vehicles with a nuclear, orbit-to-orbit stage and direct entry into Earth's atmosphere
3. 1972 - 75: All-chemical, reusable, orbital carrier vehicle with reusable, nuclear, ferry vehicle from orbit-to-orbit (and return) and chemical, reusable, lunar-round-trip (shuttle) vehicle. This mode of operation requires Earth and lunar orbital operations and eliminates the hazardous hyperbolic entry into Earth's atmosphere. Return of the personnel is accomplished with orbital velocity with moderate deceleration and good control at the landing site

Additional conclusions are as follows:

1. The round-trip cost is expected to drop by one order of magnitude from \$40,000,000/man to \$4,000,000/man between 1968 and 1975.
2. The specific transportation cost (direct operating cost only) for cargo to the lunar surface is expected to drop from \$1600/lb in 1967 to about \$300/lb in 1976.
3. The production of propellants on the Moon and refueling on the lunar surface, if feasible, would reduce the cost of personnel transportation to less than \$1,000,000/man and the specific cargo transportation cost to less than \$100/lb.
4. A propellant accumulator in Earth orbit (Profac) does not seem to offer any economical advantages over a nuclear ferry vehicle if it is limited in its applications to chemical rockets only.
5. It appears that transport volumes of approximately 150 round trips per year to the lunar surface and cargo at the rate of about 1,500,000 lb/yr will be economically feasible by the middle of 1970.

## HISTORY OF THE CLUSTER SYSTEM

William H. Pickering

Director, Jet Propulsion Laboratory  
California Institute of Technology  
Pasadena, California

## 8.1 Introduction

The free World's first Earth satellite evolved from the joint effort of two engineering and scientific teams: one under the direction of Dr. Wernher von Braun in Huntsville, Ala., and the other under the direction of the Jet Propulsion Laboratory (JPL) in Pasadena, California. These two teams effectively shared the responsibilities for the development of the high-performance vehicles used in the early Explorer satellites (Fig. 8.1) and Pioneer space probes.

In 1954, the Army Ordnance Corps requested JPL to review a satellite proposal by Dr. von Braun; in this proposal, Dr. von Braun first suggested the use of clustered, solid-propellant rockets for the high-speed stages of an Earth satellite carrier vehicle. This original proposal and the JPL counter proposal led eventually to the first U.S. space achievement.

## 8.2 The Initial Proposal—Project Orbiter

In the fall of 1954, the joint Army/Navy Project Orbiter was established with the ultimate objective of placing a minimum satellite in orbit around the Earth. The project was based on a proposal by the Army's Redstone Arsenal to develop a four-stage vehicle that would use existing, proved, reliable rocket boosters. The proposed four-stage vehicle was to consist of a modified Redstone missile as the main stage and clusters of Loki solid propellant rockets for the three-stage, spin-stabilized, high-speed assembly. A single-rocket fourth stage was to carry the satellite payload. Design modifications to the Redstone were already under study as part of a concurrent reentry test program.

In support of the Orbiter program, JPL performed a feasibility study that eventually resulted in substituting scaled-down Sergeant solid propellant motors for the Loki rockets. The study indicated that the superior performance of the Sergeant motors would increase the payload capability of the vehicle and at the same time increase overall reliability. A significant characteristic of the feasibility proposal was that the high-speed assembly could be adapted for use with a reentry test vehicle (RTV). As part of the feasibility study, a scheme was also proposed for determining the trajectory of the satellite by radio techniques.



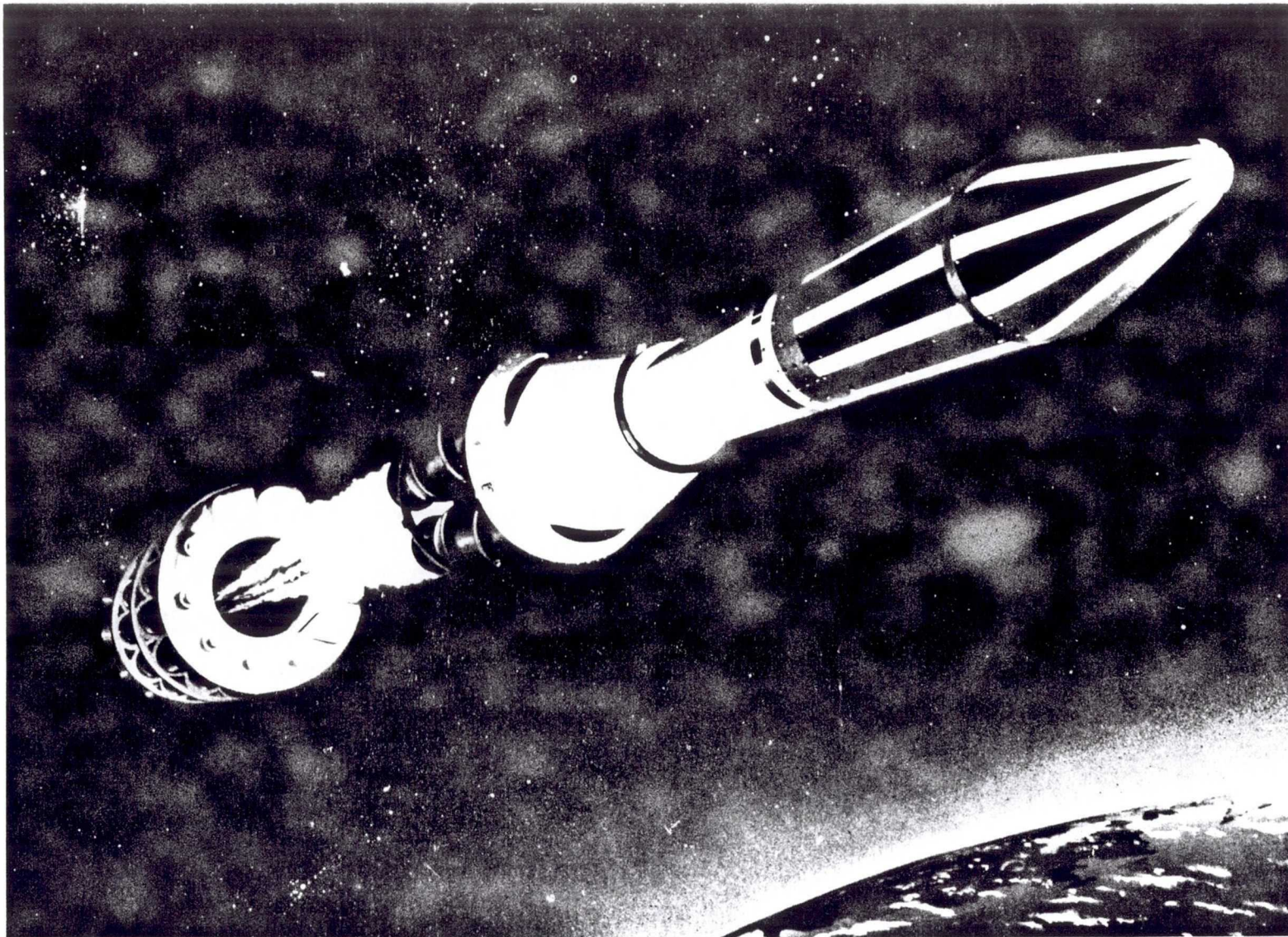


Fig. 8.1 The spinning cluster — third stage firing after burnout of second stage.

Project Orbiter was terminated in August, 1955, before the preliminary design phase was completed. Development effort on the high-speed stages and the radio trajectory-determining system was redirected toward the RTV objective.

### 8.3 Accelerated Development for the RTV

The reentry test vehicle was designated Jupiter C (a variation of the Redstone) and was to be used for design verification of an ablation nose cone for the Jupiter IREB. Official authorization to proceed with the RTV development was given in September 1955. Final design of the high-speed stages had to be established by January 1956, to meet the first firing date in September 1956.

The Jupiter C for the RTV program consisted of a high-performance version of the Redstone ballistic missile and two clustered stages of a scaled version of the solid propellant Sergeant motors.

The standard Redstone warhead hull and nose cone were replaced by an instrument compartment atop which was mounted a rotational launching tub containing the high-speed assembly (Fig. 8.2). To reduce the effects of thrust dispersion, the high-speed assembly was rotated about its longitudinal axis by two electric motors mounted in the instrument compartment.

The Redstone was designated as the first stage, and the high-speed clusters as the second and third stages. The originally proposed fourth stage was replaced by an inert motor and beacon payload for the first RTV flight (Round 27), and by the scale Jupiter nose cone and a recovery package for the second and third RTV flights (Rounds 34 and 40). This basic Jupiter C, with the activation of the fourth stage, was later used for launching Earth satellites in the 15-to 30-lb class.

The first high-speed stage consisted of 11 motors (Figs. 8.3 and 8.4) assembled in a cylindrical ring formation by three transverse bulkheads and attached to the rotational launching tub by an inner-circumference tube. Within this tube was nested the third stage, consisting of three motors bundled together by transverse bulkheads. The fourth stage was designed to have a single orbiting motor and payload attached in tandem, and to be mounted to a hollow truncated cone on the forward end of the third stage. For the RTV mission, the recovery nose cone was attached to an adapter (replacing the truncated cone) mounted on the forward end of the third stage.

The solid propellant was a case-bonded, radial-burning type with a star-shaped hole running nearly the full length of the 4.5 ft diameter motor.

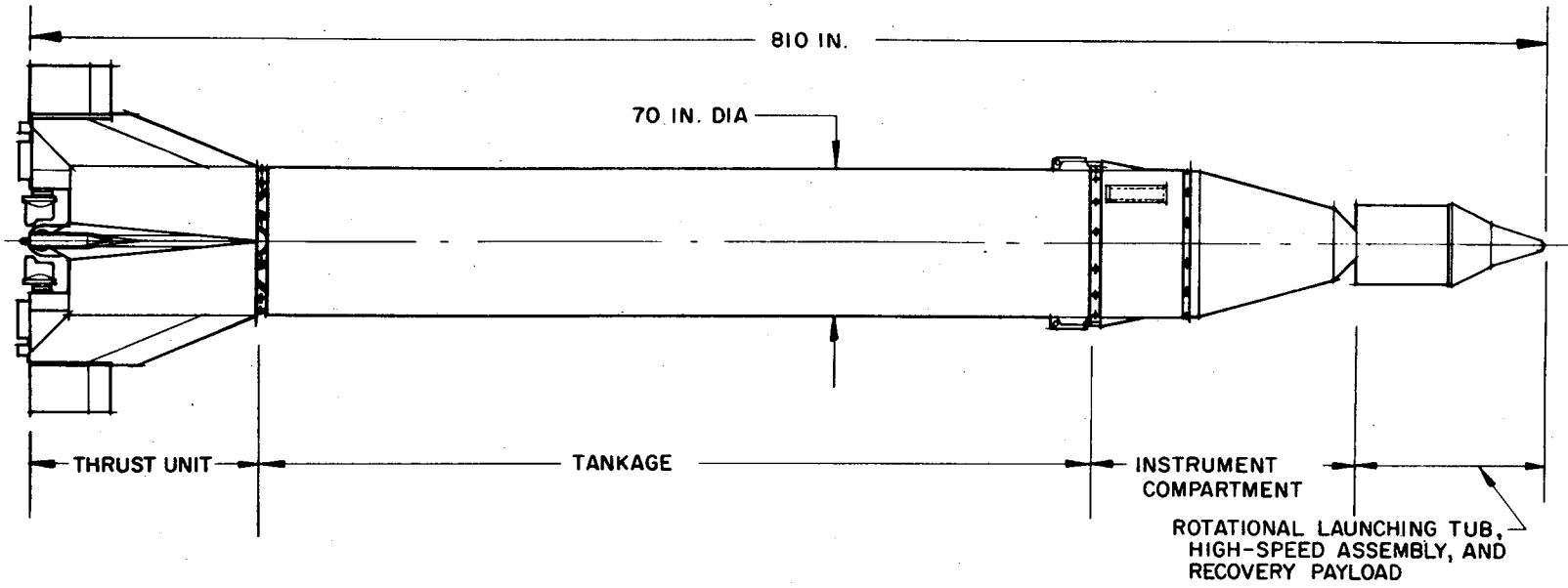


Fig. 8.2 The Jupiter C space carrier vehicle.

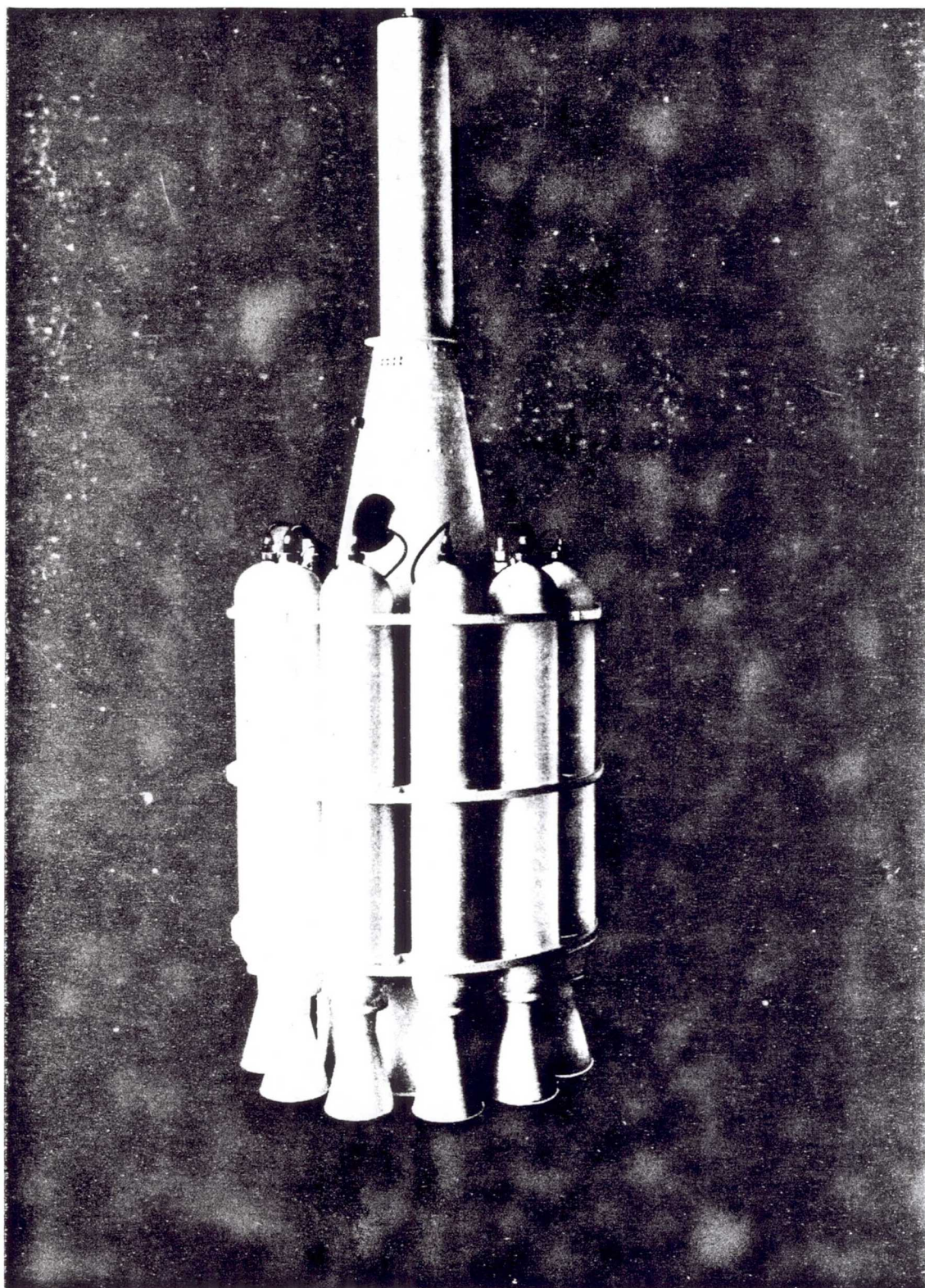


Fig. 8.3 The 3-stage cluster-assembly configuration without a payload.

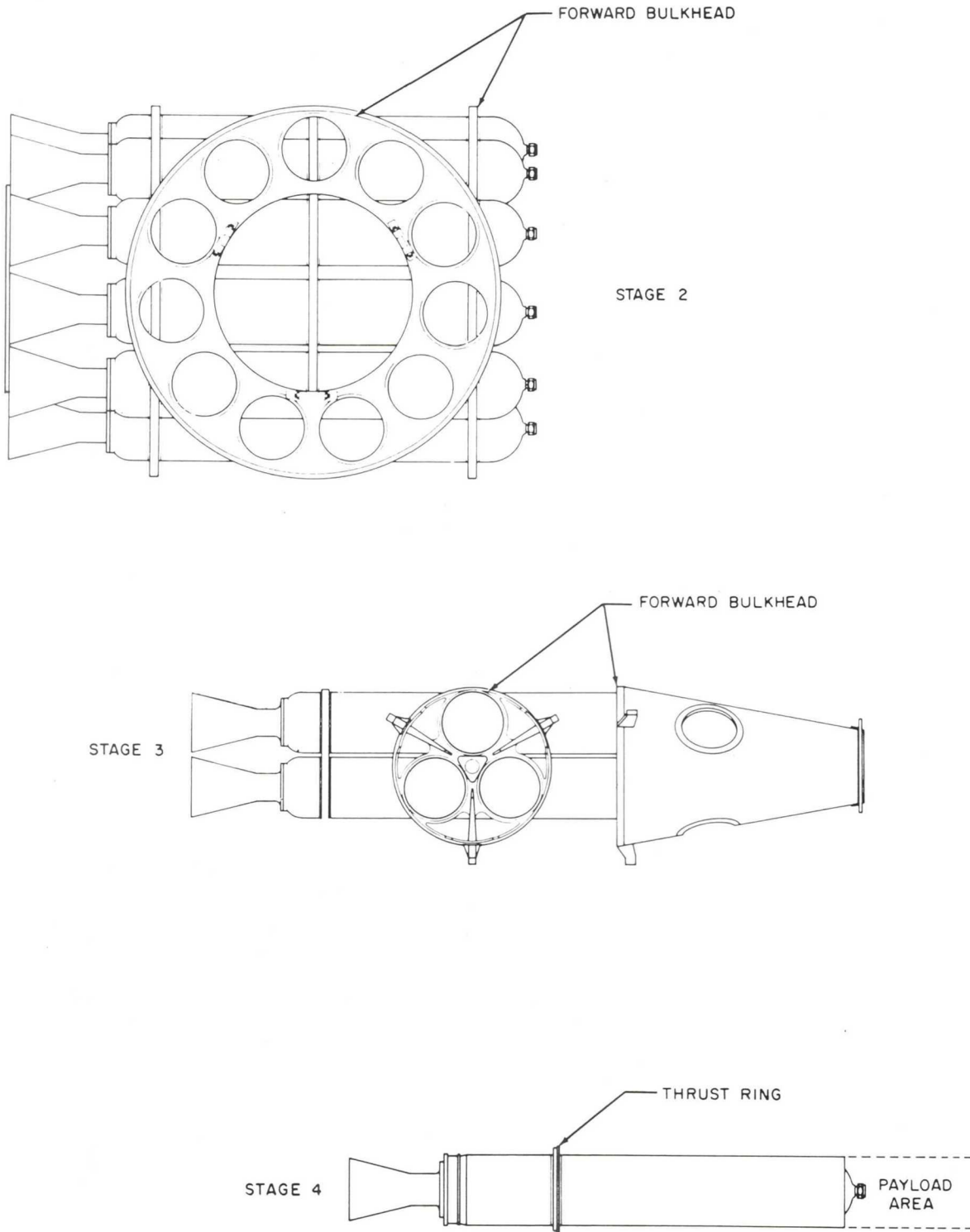


Fig. 8.4 Cluster staging definition.

Axial thrust loads were carried from the floor of the launching tub to the inner-circumference tube and forward bulkhead of the second stage, to the forward bulkhead and truncated cone of the third stage, and then to the motor case of the fourth stage. Thrust loads for the early satellite firings were transmitted to the payload through the fourth-stage motor case; thrust loads of the later and heavier satellites were carried to the payload through a rigid support tube attached to a truncated-cone adapter of the third stage. The middle and aft bulkheads, as well as the forward bulkhead, of both the second and third stages supported the motors against radial (transverse) loads induced by the spinning.

Spinup was initiated before launch and programmed during the main stage's burning; the spin rate was varied to avoid exciting the several resonant modes this stage generated as a function of fuel depletion. After separation from the main stage after burnout, the instrument compartment and high-speed assembly coasted in free flight. During the coast phase, attitude-control gas jets were programmed to aim the cluster properly for the firing of the second stage at a preselected point. Each stage was then fired sequentially after burnout of the previous stages, thereby attaining sufficient velocity for a reentry trajectory or satellite when using the fourth stage.

Development of the high-speed stages was influenced by several significant factors: the extremely short time schedule reliability requirements maintenance of a duplicate orbiting capability and minimum budget.

These factors dictated the course of the design; no opportunity existed for component state-of-the-art advancement, or for stage, inter-stage, or complete cluster environmental tests. These circumstances required reliance on a fundamentally simple design and on proven engineering techniques.

Choice of the propulsion units was based primarily on a consideration of the reliability and performance of scaled Sergeant motors proven in some 200 static tests. A no-change attitude was assumed with respect to the propellant grain composition and geometry in order to apply the available statistical information to an analysis of cluster performance and dispersion. An exception to the no-change attitude was made in later higher-performance versions when propellant and hardware improvements were incorporated into the fourth stage.

The clustering of many motors created a serious problem of thrust dispersion control. The accuracy with which such a system could follow a preset flight path was probably the only facet of the design to which the proven-techniques philosophy could not be applied completely; accurate

analysis and prediction was impossible by methods and facilities available at the time. Great efforts were taken to control, within narrow limits, the factors affecting dispersion.

The launcher tub and cluster assembly were rotated about their axis of symmetry in order to average the thrust dispersion effects of the individual motors and to provide gyroscopic stability to the flight direction. The telescoped and spinning stages introduced additional dispersion problems that led to the following launcher criteria: (1) a zero-length launcher was required, since a single-point attachment between the separating stages could have caused unwanted side forces during separation; (2) support points were to be located as far apart as possible to minimize the angular deviations introduced by the clearances required for separation; (3) the support structure was to be rigid to ensure that structural deformations did not affect the launching direction; and (4) the design should permit fabrication to close mechanical tolerances.

Perhaps the greatest problem presented by the clustering of several small solid-propellant rocket motors was the uniformity of thrust as a function of time. The interior ballistics of each motor had to be held within an extremely narrow tolerance. From the engineering standpoint, the problem was resolved to reproducibility and reliability. Reproducibility was maintained by rigid dimensional control of all metal parts and by rigid quality control methods to reduce in-batch and batch-to-batch variations of the propellant mix. To further reduce the effect of batch-to-batch variations, two batches of propellant were equally distributed in three motors; one set of three motors was used for the third stage and four sets of three motors (less one motor) were appropriately distributed in the second stage. Ignition reliability was attained by using two completely redundant igniter systems and by sealing each motor to atmospheric pressure by a thin copper diaphragm over the nozzle.

The RTV and potential orbiting missions required a minimum-weight, low-signal-level detecting, tracking and telemetering system. To meet this requirement a microlock phase-locked-loop radio system was developed. The main feature of the receiver system was its ability to lock to an extremely low-level signal. The lightweight missile-payload transmitter consisted of a crystal-controlled oscillator that was phase modulated by telemetering signals.

The primary unit of the ground station was a phase-locked receiver designed to detect the beacon signal and to track the Doppler shift automatically. The microlock antenna system used fixed helical antennas either singly, in multiple array, or in conjunction with a two-antenna interferometer system for determining angular position. Microlock stations were located at strategic points throughout the world along the payload trajectories to determine quickly and accurately their flight paths and record their telemetered data.

#### 8.4 The RTV Firing Program

The first proof-test version of the Jupiter C was successfully fired on schedule; just 1 year from the official authorization to proceed. The RTV program concluded in August 1957, with the first successful recovery of a reentry nose cone. This test proved the application of the ablation technique for protection against the effects of hypersonic reentry velocities.

On September 20, 1956, Jupiter C (Round 27) was launched through a heavy cloud cover to climb nearly 700 miles into space and plunge over 3000 miles down the Atlantic Missile Range. All stages of the reentry test vehicle performed satisfactorily, and communication was maintained with the payload throughout the flight. The mission was a success on the first firing. Principal objectives of the firing were to proof-test the staging techniques and structures of the three-stage Jupiter C configurations, and to investigate operation of a miniature transponder and the microlock instrumentation payload. The payload was attached to an inert fourth-stage motor and hollow truncated cone.

Round 34 was launched May 15, 1957, and was the first missile to carry a scale Jupiter nose cone. Although the cluster performed as expected, the missile did not follow the predicted trajectory due to guidance malfunction; consequently, recovery of the nose cone was not accomplished.

Jupiter C (Round 40) was launched on August 8, 1957. Payload for this flight was a second scale Jupiter IRBM nose cone, being tested for reentry survival; third stage of the recovery configuration had a conical section that supported the nose cone and enclosed the recovery package. The nose cone was successfully recovered, fulfilling the mission of the RTV program.

#### 8.5 Explorer Satellites In Orbit—Juno 1

On November 8, 1957, the Secretary of Defense announced that the Army was to participate in the IGY program. The code name Juno 1 was given to the satellite program and launch vehicles for the initial series of experiments, Explorers 1 through 5 and Beacon. The purposes of the experiments were to provide scientific information regarding satellite temperature, micrometeoroid impact and erosion, cosmic ray count, geomagnetic field intensity, and atmospheric density.

The Juno 1 launch vehicles were the same basic Jupiter C developed under the RTV program with the addition of a fourth-stage motor and payload. The first three Explorers utilized existing boosters left over from the highly successful RTV tests of 1956 and 1957.



In just 84 days from the announced authorization, at 5 sec past 2255 EST, January 31, 1958, Explorer 1, the free World's first Earth satellite, was placed in orbit (Fig. 8.5, and Table 8.1). All phases of the launch vehicle performed satisfactorily; the satellite was accelerated to an orbital velocity of 18,740 mph. Original estimates were the Explorer 1 would continue to circle the Earth for 6 years.

Explorer 1 was 6 in. in diameter and 80 in. long and included the payload and the empty fourth-stage motor case (Fig. 8.6). The payload was divided by a Fiberglas ring into two compartments, a cylindrical instrumentation section and an aerodynamic nose cone. The exterior of the stainless steel payload casing was sandblasted and striped with a white aluminum oxide coating to aid in thermal balance.

A midsection Fiberglas ring served a multiple purpose, as support for the turnstile-antenna wires of the high-power transmitter, the dipole-antenna gap for the low-power transmitter, and thermal insulation against the fourth-stage motor.

Two completely redundant and transistorized transmitters were used with a total of eight telemetering channels to relay the environmental data to the ground tracking and communication stations. Mercury batteries were used as the power source. A long-life, 10-mw low-power transmitter was used in conjunction with the highly-sensitive microlock system as the primary source of telemetered data. The 60-mw high-power transmitter was used primarily for orbit determination.

The scientific instrumentation of the payload was divided into three categories: (1) cosmic ray, (2) micrometeoroid, and (3) temperature.

The cosmic ray experiment consisted basically of a counting tube to measure, as a function of time and position, the cosmic ray intensity outside Earth's atmosphere. Explorer 1 made the initial discovery of the intense upper-altitude radiation belts.

The micrometeoroid experiment used an impact microphone and a set of 12 fracturable, wire-grid erosion gages to determine the statistical distribution of the space density and the relative momentum of micrometeoroids.

Temperature measurements were made at four locations to verify the application of surface coating for passive temperature control.

Ionospheric polarization effect, geomagnetic field intensity and atmospheric density information were determined by ground observation of the received radio signal and satellite orbital motions.

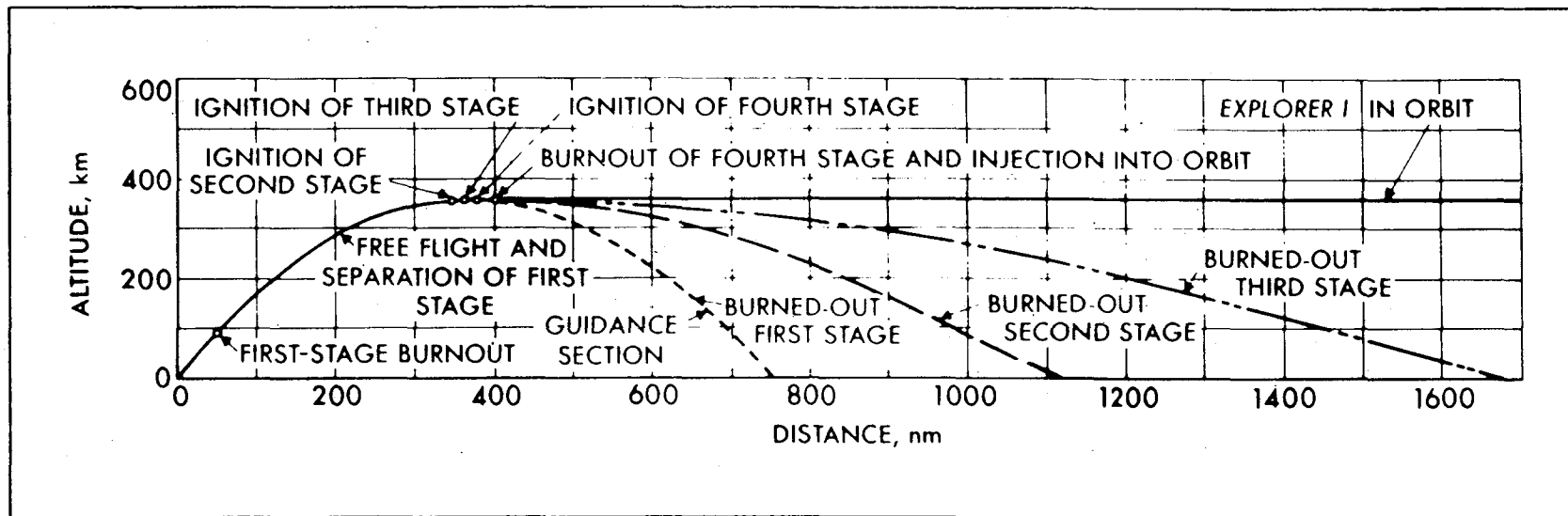


Fig. 8.5 Trajectory profile of Explorer 1 and propulsion stages.

Table 8.1. Initial Orbital Parameters- Explorers 1, 3, and 4

Initial Orbital Parameters	Explorer		
	1	3	4
Perigee (km)	360	188	262
Apogee (km)	2551	2801	2210
Eccentricity	0.1387	0.1660	0.1279
Inclination (deg)	33.3	33.5	50.1
Period (min)	114.7	114.7	110.1

Table 8.2. Initial Orbital parameters- Explorers 7, 8, and 11

Initial Orbital Parameters	Explorer		
	7	8	11
Perigee (km)	557	459	497
Apogee (km)	1069	2289	1793
Eccentricity	0.0356	0.1211	--
Inclination (deg)	50.3	50.0	28.5
Period (min)	101.2	112.7	108.1

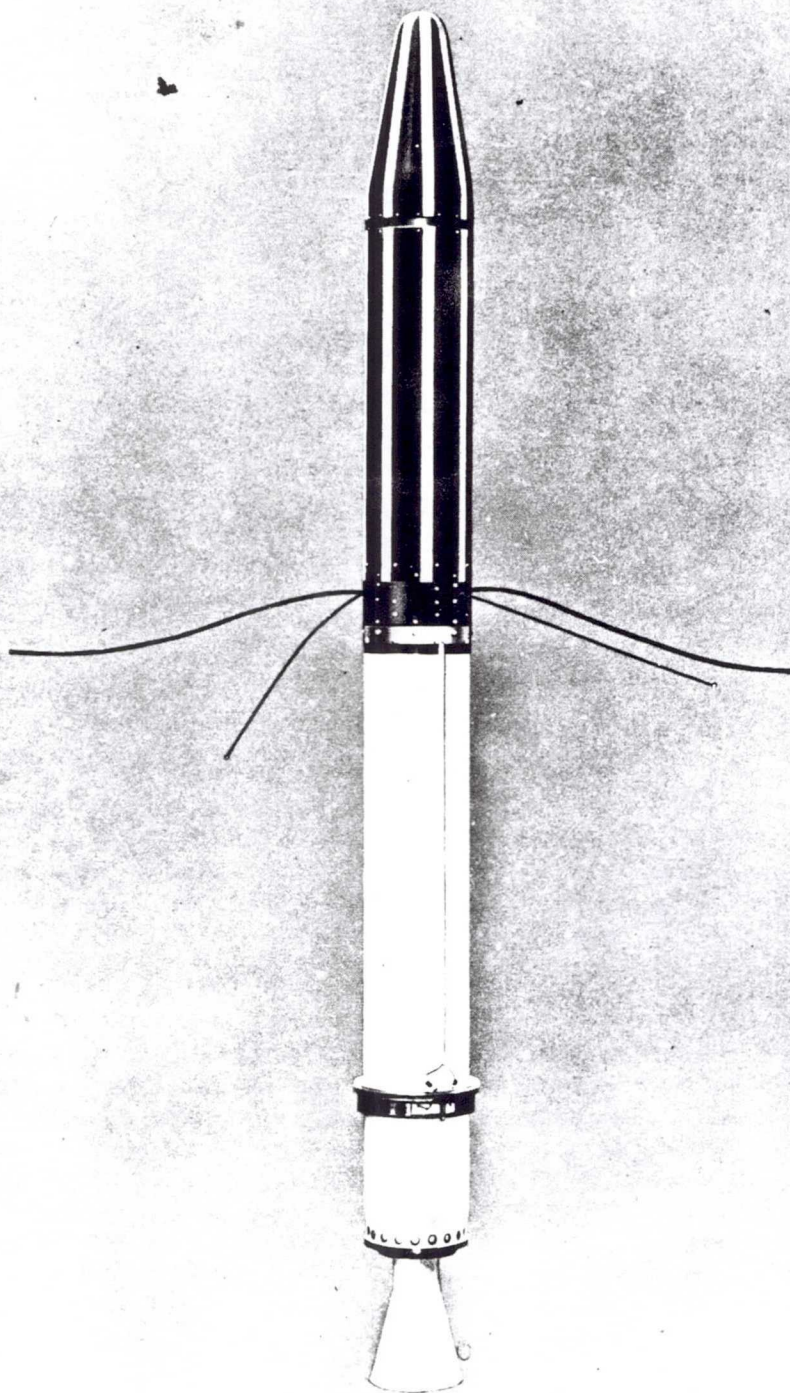


Fig. 8.6 Explorer 1.

Explorer 2 (Juno 1, Round 26) was launched on schedule March 5, 1958, and was intended to place Explorer 2 into orbit. Orbital velocity was not attained due to the lack of fourth-stage ignition. The Explorer 2 configuration was nearly identical with Explorer 1, with the addition of a tape recorder for cosmic ray data storage.

Explorer 3, the satellite with a memory, was injected into orbit (Table 8.1) March 26, 1958, by Juno 1 (Round 24). The Explorer 3 payload instrumentation was similar to Explorer 1. The principal difference was the addition of a miniature tape recorder for storage and interrogation of cosmic ray data and the elimination of the impact microphone and turnstile antenna. Valuable information was obtained regarding micro-meteoroid clouds and cosmic ray intensities. A large deviation in the local path angle at injection resulted in a high orbital eccentricity and limited the satellite lifetime to 93 days.

Explorer 4 was injected into orbit (Table 8.1) July 26, 1958, by Juno 1 (Round 44). The fourth-stage motor was loaded with a new, high-performance propellant which allowed a payload weight nearly twice that of any previous Explorer. The payload was given over entirely to radiation studies. Lifetime of the satellite was 455 days.

Juno 1 (Round 47) was launched on August 24, 1958, but was unsuccessful in placing Explorer 5 in orbit. The first stage's performance was successful, but during the coast phase the separated Redstone thrust unit collided with the instrument compartment causing the cluster to be launched in the wrong direction.

Juno 1 (Beacon, Round 49) was launched on October 22, 1958, but failed to place the Beacon (originally designated Explorer 6) payload into orbit because an inadvertent separation of the payload from the fourth-stage motor after liftoff.

## 8.6 Pioneering Deep Space—Juno 2

The Juno 2 (phase I) program was the result of a request in early 1958 for ABMA and JPL to utilize the higher-energy capabilities of the Army's Jupiter IREM stage to launch a space probe, Pioneer 3 and 4, as part of the United States participation in the IGY.

The basic objectives of the program were to measure cosmic radiation, to establish the probe trajectory that was to verify the design of the tracking and communication system and to permit more accurate determination of the Moon's mass by observing near-Moon trajectory deviations.

The vehicle for the Juno 2 (phase I) mission (Fig. 8.7) consisted of a modified production Jupiter first stage, instrument compartment and rotational launcher, and the three-stage, high-speed assembly. The

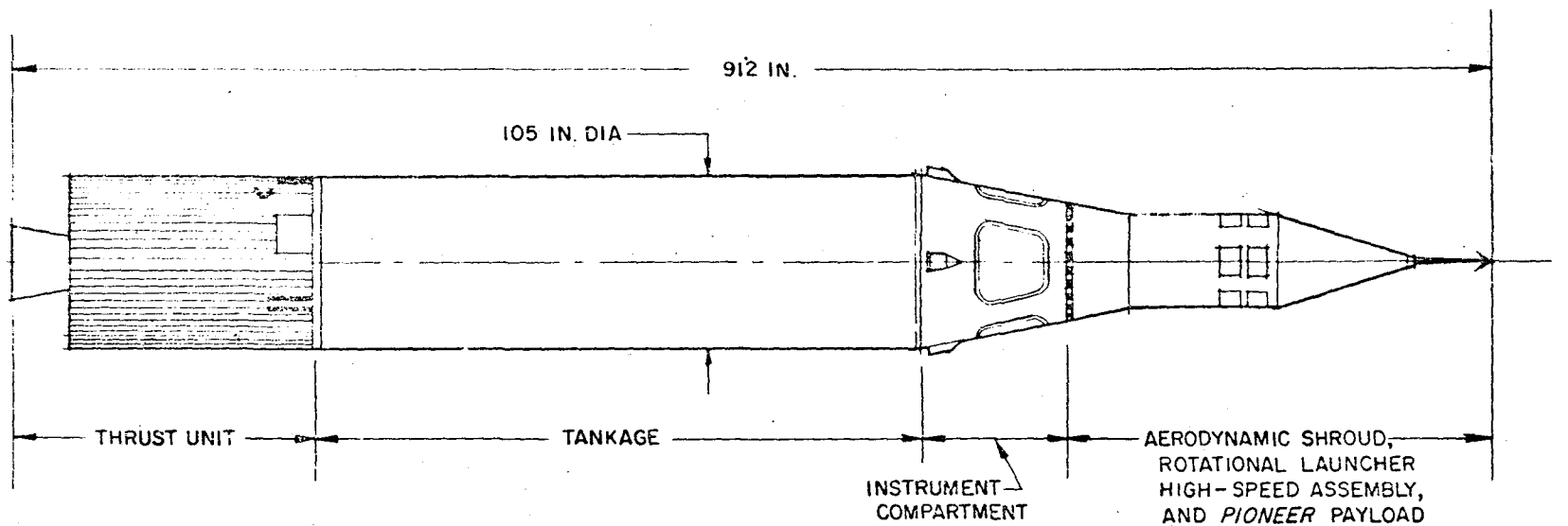


Fig. 8.7 The Juno 2 vehicle.

high-speed assembly was covered by a large aerodynamic shroud fastened to the instrument compartment. The instrument compartment housed the guidance spatial control, the events programmer and cluster drive motors and had the rotational launcher permanently attached.

The flight plan required separation of the instrument compartment and high-speed assembly combination from the booster after burnout, shroud-cap ejection during the early coast period, proper attitude stabilization, ignition of the high-speed stages, and, finally, separation and despin of the payload after fourth-stage burnout.

The tracking and communication system used for Pioneers 3 and 4 involved the early components of the presently established Deep Space Instrumentation Facility (DSIF), then referred to as the World Tracking Net. In operation at that time was the equatorially mounted, 85-ft diameter radio telescope at the Goldstone Station, Camp Irwin, California. Stations were also established at the Cape Canaveral launch site and at Mayaguez, Puerto Rico, for tracking and communication during the early phases of the probe flight into space.

The Goldstone and Puerto Rico tracking systems were basically the same except for their permanency and range capability, as differentiated by the size of their tracking antennas, an 85-ft diameter compared to 10-ft diameter. Both systems utilized simultaneous lobing antenna beams, automatic tracking, and narrow-band, phase-locked receivers. The vehicle coordinates (angular position), one-way Doppler (velocity), and telemetry data were channeled by telephone and teletype to the JPL computing center for trajectory determination and prediction.

Pioneer 3 (Juno 2, Round AM-11) was launched on December 6, 1958. Initial acquisition of the probe by Goldstone, as it rose above the eastern horizon, was performed precisely from the spatial coordinate data supplied by the Puerto Rico station and converted by the computing center.

Due to a premature cutoff of the first stage and angular dispersion in the high-speed stages, the probe failed to achieve escape velocity. A distance of 63,500 miles was achieved, however, leading to the discovery of the second high-intensity Van Allen radiation belt.

Pioneer 4 (Juno 2, Round AM-14) was launched on March 3, 1959, and achieved Earth-escape velocity (24,611 mph). It continued out into the Solar System to become an artificial planetoid of the Sun. Vehicle performance was such that at injection the velocity was below nominal, the pitch angle was low, and the azimuth angle was slightly to the south. These errors resulted in the probe's closest approach to the Moon being 37,300 miles.

A new tracking communication record was established by Pioneer 4. Up to the time that the probe signal was lost due to battery depletion at 407,000 miles, the signal level at the Goldstone site was sufficiently high to indicate the capacity for tracking the payload to a distance of more than 700,000 miles.

The Pioneer space probe (Fig. 8.8) was 20-in. long and a gold-plated cone, that included a 9-in. diameter instrument base and 3-in. insulated antenna spike. The thin Fiberglas conical surface, as well as the instrument base, were striped with paint for thermal control. The gold plating made the conical surface electrically conductive in order to serve as an unsymmetrical dipole antenna element in conjunction with the 3-in. spike.

Wrapped around the base was a two-wire mechanism for despinning the payload, which was necessary for operation of an optical trigger experiment. The despin mechanism was a set of two 60-in. weighted wires, wrapped in a direction opposite to that of the spin. When the weights were released, they flew outward due to centrifugal force, causing the cables to unwind, thus slowing down the payload spin. The wires were released upon full deployment. Although failing to operate on Pioneer 3, the spin rate of Pioneer 4 was reduced from 415 to 11 rpm.

The payload contained a tiny, transistorized, 1.1-lb. transmitter with a total effective radiated power, including telemetry modulation, of 180 mw. Three standard telemetry channels were used for relaying environmental and operational data. Power to operate the telemetry oscillators and transmitter (as well as the radiation circuits) was furnished by a battery of 18 mercury cells mounted peripherally in the payload base.

Two Geiger-Müller tubes were used, in conjunction with scalars, high-voltage power supply, and associated circuitry to further explore the upper-altitude radiation regions that were discovered by earlier Explorers. The purpose of the experiment was to obtain a quantitative space profile nominally between the Earth and Moon, and possibly beyond. The telemetered data revealed two distinct belts of radiation at approximately 3000 and 10,000 miles altitude and a series of narrow belts in a region between 30,000 and 60,000 miles.

### 8.7 The Heavy Earth Satellite Firings--Juno 2

The Juno 2 (phase II) program was established to utilize the increased capabilities of the Jupiter booster for Earth satellite (100-lb class) firings as part of the IGY. The vehicle for the satellite phase was the same Juno 2 modified Jupiter and four-stage configuration used in the phase I Pioneer series, with the addition of a support tube attached to the third stage to accommodate heavier payloads. Various agencies supplied the satellite payloads for a total of eight firings. The three successfully orbited payloads were designated Explorers 7, 8, and 11 (Table 8.2).



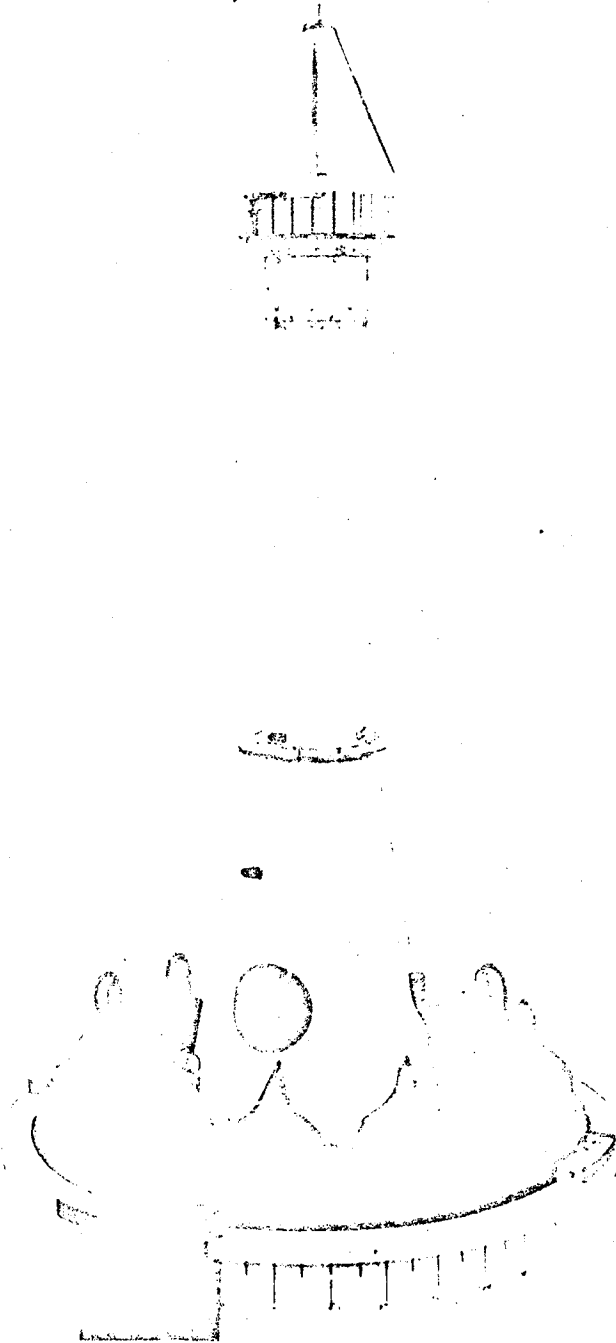


Fig. 8.8 The Pioneer space probe mated with high-speed cluster assembly.

Liftoff of Juno 2 (Round AM-16) occurred on July 16, 1959. The missile was destroyed by range safety after 5.5 sec due to a malfunction in the booster electrical system. The 91.5-lb multi-experiment, scientific payload was similar to the one successfully orbited by Round AM-19A later in October.

Juno 2 (Round AM-19B) was launched on August 14, 1959, but, due to guidance malfunctions, failed to orbit a 12-ft diameter inflatable sphere and beacon instrumentation. The experiment was to determine the characteristics of the upper atmosphere in a region between 100,000 and 500,000 ft. The sphere was to be released from a blunt-ended, 7-in. diameter, cylindrical case mounted on the third stage.

Juno 2 (Round AM-19A) was launched on October 13, 1959, and successfully placed the 91.5-lb multiexperiment Explorer 7 into orbit. The scientific experiments included cosmic ray, Lyman-Alpha, X-ray, and radiation and heat balance detectors, a micrometeoroid experiment, and a heavy nuclei chamber.

Juno 2 (Round AM-19C) was launched on March 23, 1960, in an unsuccessful attempt, due to a cluster malfunction, to place a 22.5-lb payload into a highly elliptical orbit. The purpose of the experiment was to make a detailed study of the two intense radiation zones. The intensity distribution was to be monitored over an extended period of time to establish the origin, buildup, and decay as related to solar activity. Also the experiment was designed to study the radiation composition, nature of the penetrating components and energy spectrum of the less penetrating components, and total energy flux in the trapped regions.

Juno 2 (Round AM-19D) was launched on November 3, 1960, and successfully placed into orbit Explorer 8, instrumented to study and report the temporal and spatial distribution of the ionospheric parameters existing between 200 and 1200 km above Earth. Correlative data comprised of measurements of the charge accumulations on the surface of the satellite and the relation of this data to electrical drag and density of the medium; also, measurements of the frequency, momentum and energy of micrometeoroid impacts were taken.

Juno 2 (Round AM-19F) was launched on February 24, 1961, in an unsuccessful attempt to place a 75-lb ionosphere beacon into orbit. The payload was similar to that launched by Round AM-19G. Failure to orbit was apparently caused by a malfunction of a shroud component.

Juno 2 (Round AM-19E) on April 27, 1961, successfully placed into orbit the 85-lb gamma-ray astronomy satellite, Explorer 11. The primary objective was to detect and map the high-energy gamma rays resulting from neutral pi-meson (pion) decay and to relate these data with the

density of cosmic ray flux and interstellar matter. The secondary objective was to measure the ratio of the high-energy gamma rays reflected by the Earth's atmosphere to the quantity of gamma rays falling upon the Earth.

Juno 2 (Round AM-19G) was launched on May 24, 1961, in a second unsuccessful attempt to place a 75-lb ionosphere beacon into orbit. The payload was designed to provide a means of studying the ionosphere by propagating signals through the ionosphere. These signals would enable the acquisition of data relative to ionosphere absorption, anomalies, integrated electron density, and Faraday rotation measurements and possible transmission time delays.

### 8.8 Conclusion

The solution for technical problems of the cluster system was based on proven engineering techniques and a fundamentally simple design. The soundness of this approach was demonstrated on the RTV flights and the Explorer 1 satellite mission. The flight tests were conducted on schedule and the cluster system performance was completely successful. Out of the total 19 mission attempts (Table 8.3), only two failures were attributed to the three-stage cluster system.

Table 8.3. Firing Resume for the RTV - Juno 1, and Juno 2 Program

Payload	Vehicle	Round	Firing date	Mission	Results
Microlock beacon	Jupiter C	27	Sept. 20, 1956	System proof test	Successful
Nose cone	Jupiter C	34	May 15, 1957	Reentry test	Unsuccessful
Nose cone	Jupiter C	40	Aug. 8, 1957	Reentry test	Successful
Explorer 1	Juno 1	29	Jan. 31, 1958	Earth orbit	Successful
Explorer 2 <sup>a</sup>	Juno 1	26	March 5, 1958	Earth orbit	Unsuccessful
Explorer 3	Juno 1	24	March 26, 1958	Earth orbit	Successful
Explorer 4	Juno 1	44	July 26, 1958	Earth orbit	Successful
Explorer 5	Juno 1	47	Aug. 24, 1958	Earth orbit	Unsuccessful
Beacon	Juno 1	49	Oct. 22, 1958	Earth orbit	Unsuccessful
Pioneer 3	Juno 2	AM-11	Dec. 6, 1958	Deep space probe	Unsuccessful
Pioneer 4	Juno 2	AM-14	March 3, 1959	Deep space probe	Successful
--	Juno 2	AM-16	July 16, 1959	Earth orbit	Unsuccessful
--	Juno 2	AM-19B	Aug. 14, 1959	Earth orbit	Unsuccessful
Explorer 7	Juno 2	AM-19A	Oct. 13, 1959	Earth orbit	Successful
-- <u>a</u>	Juno 2	AM-19C	March 23, 1960	Earth orbit	Unsuccessful
Explorer 8	Juno 2	AM-19D	Nov. 3, 1959	Earth orbit	Successful
--	Juno 2	AM-19F	Feb. 24, 1961	Earth orbit	Unsuccessful
Explorer 11	Juno 2	AM-19E	April 27, 1961	Earth orbit	Successful
--	Juno 2	AM-19G	May 24, 1961	Earth orbit	Unsuccessful

<sup>a</sup>Unsuccessful mission attributed to cluster malfunction.

## BIBLIOGRAPHY

1. Froehlich, Jack E., and Albert R. Hibbs, Contributions of the Explorer to Space Technology, Progress Report 20-359, (September 3, 1958).
2. Hibbs, Albert R., Notes on Project Deal, External Publication 471, California Institute of Technology, Jet Propulsion Laboratory (March 14, 1958).
3. Robillard, G., The Explorer Rocket Research Program, Publication 145 (October 31, 1958).
4. Van Allen, J. A., First Public Lecture on the Discovery of the Geomagnetically-Trapped Radiation, SUI 60-13, State University of Iowa (May 1, 1958).
5. Victor, W. K., H. L. Richter, and J. P. Eyraud, Explorer Satellite Electronics, TR 34-12, California Institute of Technology, Jet Propulsion Laboratory (January 29, 1960).
6. Victor, W. K., U.S. Explorer Satellites, External Publication 491, California Institute of Technology, Jet Propulsion Laboratory (May 1, 1958).
7. van Roos, O. H., Motion of a Spinning Rocket Cluster, Progress Report 20-376, California Institute of Technology, Jet Propulsion Laboratory (December 31, 1958).
8. Explorer 1, External Publication 461, California Institute of Technology, Jet Propulsion Laboratory (February 28, 1958).
9. Juno Brochure, Library Number 109, Jet Propulsion Laboratory (1961).
10. Radiation Observations with Satellite 1958 Alpha (Explorer 1), Volumes I through IV, SUI 61-3, State University of Iowa (March 1961).

## 9

## EXPLORER SATELLITES LAUNCHED BY JUNO 1 AND JUNO 2 VEHICLES

J. Boehm, H. J. Fichtner, and Otto A. Hoberg

Astrionics Division  
George C. Marshall Space Flight Center  
National Aeronautics and Space Administration  
Huntsville, Alabama

In the early 1950's rocket technology had advanced to such a state of the art that a project for orbiting an artificial moon around the Earth became feasible. At that time Dr. Wernher von Braun--well cognizant of this situation--began to shape solutions for the realization of the satellite concept. His great ability to combine ingenious fantasy with realistic engineering thinking was set forth in the paper "A Minimum Satellite Vehicle Based on Components Available from Missile Development of the Army Ordnance Corps, Guided Missile Development Division, Ordnance Missile Laboratories" [1]. This report contains the basic scheme for the Juno 1 and Juno 2 vehicles.

The efforts and planning for a satellite mission resulted in the first U. S. satellite project, Orbiter. The Vanguard, a purely scientific project, soon succeeded the Orbiter. In parallel to the Vanguard program a multistage rocket system, known as Jupiter C, was developed by the Army in Huntsville, Alabama, under Dr. von Braun's direction, for the investigation of reentry nose cones. Satellite capabilities were also inherent in this vehicle which, when somewhat modified, was used to place the first U. S. satellite in orbit on January 31, 1958 (only 84 days after the order was given).

This chapter covers the development of Explorer satellites and is preceded by a brief discussion of the carrier vehicles and their satellite lifting capabilities. General design objectives which were of essential influence to the layout of the mechanical satellite systems are presented. Miniaturization of components, lightweight structure, and utmost design symmetry were necessary because of the low payload capabilities and the spin applied to the upper stages.

Consideration is given to the dynamics involved to maintain prescribed orientation of the satellites in orbit. It is shown how the satellite program produced many new problems in the field of instrumentation, tracking, design, and systems engineering. Another part of this

chapter deals with the power supply systems, the electrical networks, and the timing devices applied in the satellites. Particular emphasis is given to the solution for solar cell battery power supply systems.

The concluding part refers to the broad and thorough test program which helped to achieve the indispensable reliability necessary for space missions.

## 9.1 The Carrier Vehicles

The Juno 1 and Juno 2 vehicles, both four-stage rocket systems, were conceived as fast and thrifty solutions for launching satellites and space probes. Both were developed by the former Development Operations Division of the Army Ballistic Missile Agency (contributing the first stages, guidance and control systems, and the launching) and by the Jet Propulsion Laboratory (contributing the high-speed upper stage assembly).

The composition of these multistage carrier vehicles was characterized by the choice of thoroughly proven components. It was intended that required modifications of existing hardware would not impair the reliability of the vehicles. Thus it became possible to provide, with existing means, a workable rocket system carrying payloads ranging from a maximum of 25 lb for Juno 1 to a maximum of 92 lb for Juno 2 (Table 9.1). Both vehicles evolved from the Jupiter C, a composite reentry test vehicle developed by the Army for investigating the aerodynamic heating of missile nose cones when diving into the Earth's atmosphere. The main difference between Juno 1 and Juno 2 was in the first stage (Figs. 9.1 and 9.2). Juno 1's main stage was a modified Redstone ballistic missile while a modified version of the more powerful Jupiter ICBM was Juno 2's main stage.

Both vehicles had the same arrangement of high-speed solid propellant stages. Their second stages were powered by 11 solid propellant motors, and the third stages consisted of three such motors; a single motor was used on their fourth stages. The payload was attached directly to the top of the fourth stage. The high-speed stage motors were clustered symmetrically about the longitudinal vehicle axis and housed in a cylindrical launcher. With a concentrically arranged shaft, this launcher could rotate in ball bearings, supported by the forward end of the first stage instrument compartment. Spinning of the high-speed stages was mandatory to minimize slight thrust differences between the motors. A shroud was introduced for the Juno 2 vehicle for protection from greater aerodynamic heating during the ascending part of the trajectory and for support of an angle-of-attack meter located in front.

1540

# **SPACECRAFT DESIGN AND ENGINEERING**



Table 9.1 Data Pertaining to Launched Satellites

Satellite	Vehicle	Firing Date	Perigee	Apogee	Eccentricity	Inclination (deg)	Period (min)	Weight Without 4th Stage	Initial Spin (rpm)	Orientation Required	Separation of 4th Stage
Explorer 1	Juno 1	Jan. 31, 1958	360	2552	0.139	33.2	114.7	18.1	750	none	none
Explorer 2	Juno 1	Mar. 5, 1958	-----	-----	-----	-----	-----	18.1	750	none	none
Explorer 3	Juno 1	Mar. 26, 1958	195	2810	0.166	33.4	144.7	18.1	750	none	none
Explorer 4	Juno 1	Jul. 26, 1958	267	2219	0.128	50.3	110.1	25.8	750	none	none
Explorer 5	Juno 1	Aug. 24, 1958	-----	-----	-----	-----	-----	25.8	750	none	none
Beacon 1	Juno 1	Oct. 22, 1958	-----	-----	-----	-----	-----	28.5	---	none	none
Payload AM-16	Juno 2	Jul. 16, 1959	-----	-----	-----	-----	-----	87.5	---	yes	yes
Payload AM-19B	Juno 2	Aug. 14, 1959	-----	-----	-----	-----	-----	26.0	600	none	none
Explorer 7	Juno 2	Oct. 13, 1959	555	1091	0.037	50.4	101.2	92.3	425	yes	yes
Payload AM-19C	Juno 2	Mar. 23, 1960	-----	-----	-----	-----	-----	22.5	525	none	none
Explorer 8	Juno 2	Nov. 3, 1960	420	2295	0.121	49.9	112.7	87.7	445	yes	yes
Payload AM-19F	Juno 2	Feb. 24, 1961	-----	-----	-----	-----	-----	75	---	yes	yes
Explorer 11	Juno 2	Apr. 27, 1961	490	1799	0.087	28.8	108.1	85	390	yes	none
Payload AM-19G	Juno 2	May 24, 1961	-----	-----	-----	-----	-----	75	460	yes	yes

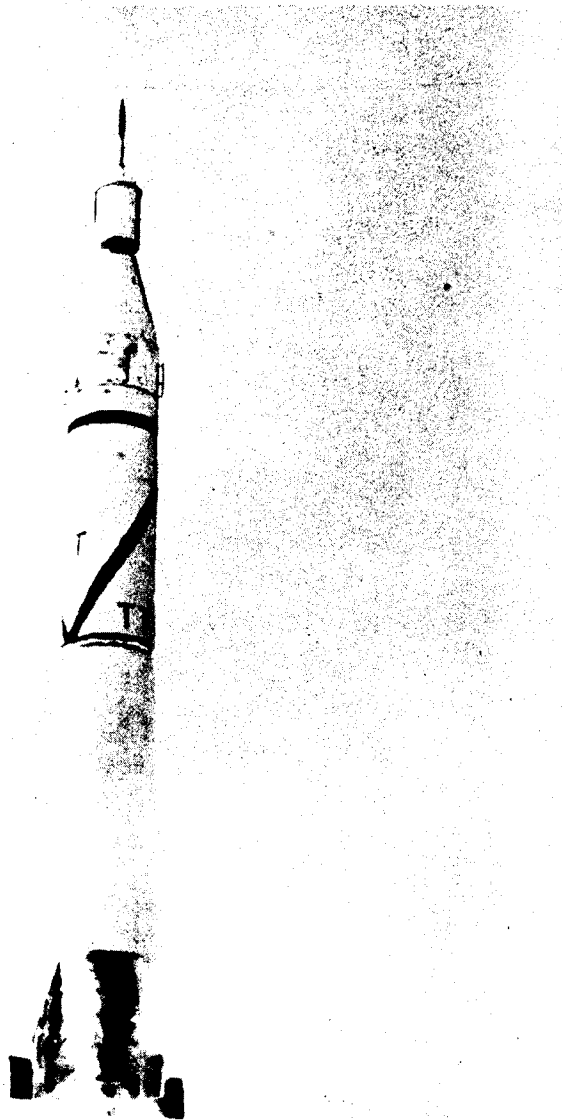


Fig. 9.1 Juno 1 configuration.

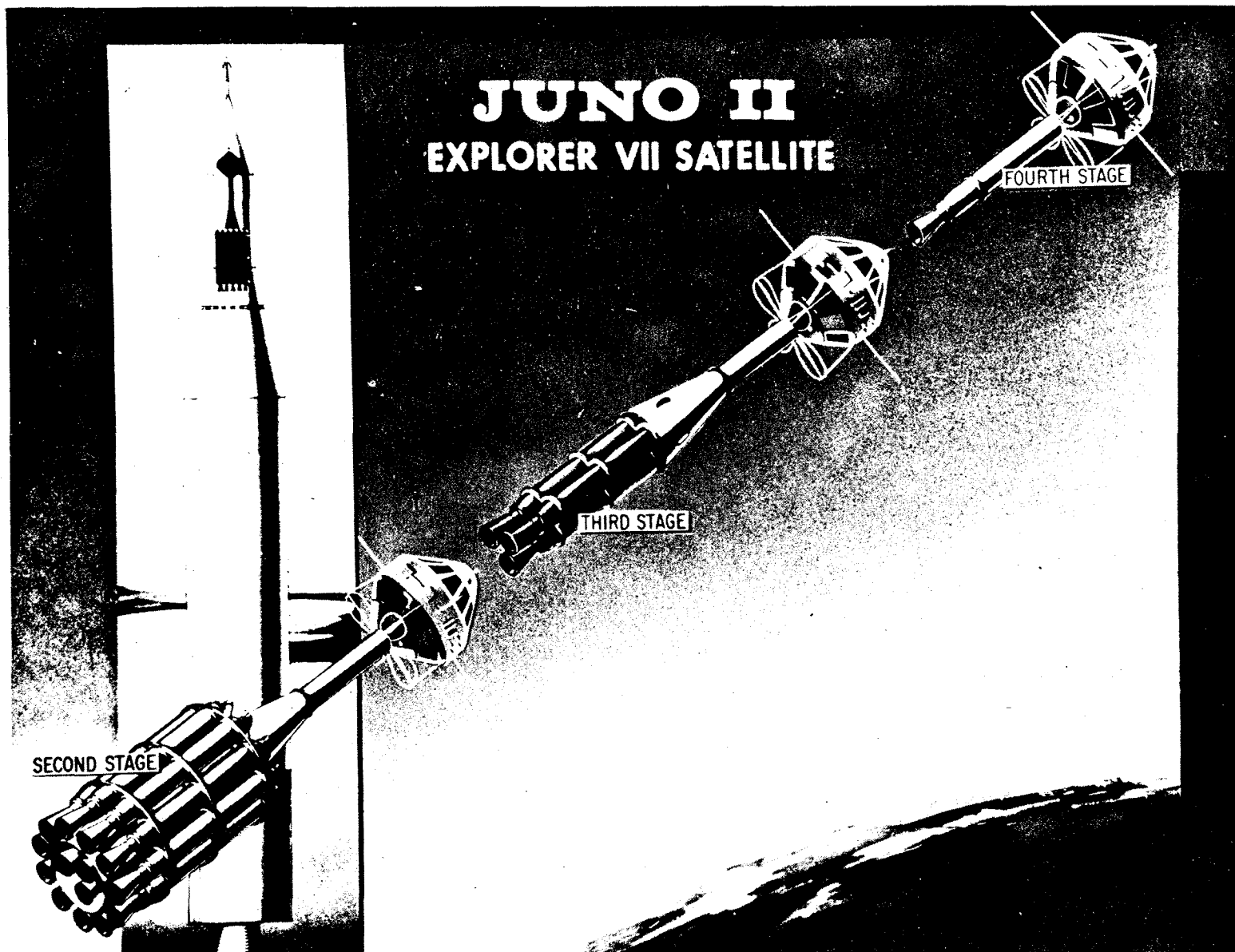


Fig. 9.2 Juno 2 vehicle and stage separation.

The flight patterns of both Juno vehicles were quite similar. The multistage rocket first rose vertically and then was tilted into the trajectory during the burning time of the first stage. Then, the instrument compartment and the launcher with the clustered upper stages were separated shortly after burnout.

To avoid bumping or other impairment of the first stage with the separated high-speed stages, the main stage was slowed down and displaced to one side by "kick" rockets. A few seconds after separation, the cone-shaped upper part of the shroud was detached by explosive bolts and springs. Again by kick-rocket action, the cone was moved sidewise to clear the path for the upper stages. During the coasting flight that followed, the instrument compartment with the spinning cluster launcher was being tilted to align the main axis of the system to a nearly horizontal position at apex. The tilting was imparted to an assembly with the spinning launcher and upper stages acting as a giant gyro [ 2 ]. During coasting flight, the attitude control was achieved by four pairs of air-jet nozzles with variable thrust. These nozzle pairs were properly arranged on the aft end of the instrument compartment. The ignition of the second stage was actuated by the program device in the first stage. The firing of the third stage followed approximately 9 sec later, and after the same interval, the fourth stage was ignited. In cases where separation of the payload from the empty shell of the fourth stage was required, a special separation device was inserted between payload and fourth stage.

The Juno 1 program began with the launching of Explorer 1 on January 31, 1958, and ended on October 22, 1958 with an attempt to launch Beacon 1. Pioneer 3, a space probe, launched on December 6, 1958, was the first flight of the Juno 2 series. The launching of payload AM-19G on May 24, 1961 completed this series (Table 9.1).

An optimum staging was not inherent in both vehicle types. Time and costs established limitations. Excessive static and dynamic accelerations of the upper stages imposed severe problems upon the payload developer. It was extremely difficult to fulfill the injection requirements for exact orbits since the amount of the spin speed of the cluster could not be chosen as high as desirable because of definite limitations prescribed by the overall configuration of this four-stage rocket.

Nevertheless, expectations were met that confirmed hopes for the Juno 1 and Juno 2 vehicles. The most significant accomplishment was the launching of the free world's first satellite.

## 9.2 The Mechanical System of the Satellites and Their Layout

The satellites were engineered to provide suitable structures for the great variety of scientific experiments presented by the different missions (Table 9.2). The rather low payload lifting capabilities of

Table 9.2 Satellite Missions

Satellite	Scientific Experiments On Board	Results
Explorer 1 (RS-29)	<ol style="list-style-type: none"> <li>1. Cosmic ray experiment. Cosmic ray intensity surrounding the Earth's atmosphere is measured by counter.</li> <li>2. Micrometeoroid experiment. Statistical distribution of the space density and the momentum of micrometeoroids is measured by means of an impact microphone and an arrangement of fracturable wire erosion gages.</li> <li>3. Temperature measurements. At four typical locations to check the effectiveness of passive temperature control (surface coating).</li> </ol>	Successful
Explorer 2 (RS-26)	Equipped like Explorer 1, but with a tape recorder for cosmic ray data storage.	Failed
Explorer 3 (RS-24)	Equipped like Explorer 1, but with a miniature tape recorder for storage and interrogation of cosmic ray data and without impact microphone.	Successful
Explorer 4 (RS-44)	Radiation experiments. Two Geiger-Mueller counters and two scintillation counters.	Successful
Explorer 5 (RS-47)	Similar to that of Explorer 4.	Failed
Beacon (RS-49)	High-altitude atmospheric density experiment. Evaluation by observation of the orbital characteristics. Orbit to be as circular as possible.	Failed
Payload AM-16	<ol style="list-style-type: none"> <li>1. Cosmic ray experiment. For monitoring of total cosmic ray intensity, geomagnetically trapped corpuscular radiation, and solar protons by two Geiger-Mueller counters.</li> <li>2. Lyman-Alpha and X-ray experiments for monitoring of the intensity of ionizing radiation striking the Earth's atmosphere by means of two specially designed gas ionization chambers.</li> </ol>	Failed

Table 9.2 (continued)

Satellite	Scientific Experiments On Board	Results
	<p>3. Thermal radiation balance experiment. To determine the driving force behind the circulation of the atmosphere. Measurements of three components of radiation: (1) incident radiation from the Sun; (2) reflected sunlight which never enters the Earth's thermodynamic system; (3) infrared heat radiation from the Earth and its atmosphere and measuring the temperatures of various bolometers.</p> <p>4. Heavy primary cosmic ray experiment. For monitoring the heavy nuclei content of the primary cosmic radiation by argon filled ionization chamber.</p> <p>5. Micrometeorite penetration experiment. To measure micrometeorite penetration and molecular sputtering by means of photo conducting CdS cells.</p> <p>6. Temperature measurements.</p> <p>7. Unprotected solar cell experiment.</p>	
Payload AM-19B	High-altitude atmosphere experiment. To find the characteristics of the upper atmosphere by an orbiting 12-ft diameter inflatable sphere and beacon.	Failed
Explorer 7	Repetition of Payload AM-16	Successful
Payload AM-19C	Van Allen radiation belts experiments. To study the radiation composition, nature of the penetrating components and energy spectrum of the less penetrating components, and total energy flux in the trapped region.	Failed
Explorer 8 (AM-19D) (S-30)	Direct ionosphere measurements experiment. To study the characteristics of the ionosphere by means of onboard detectors.	Successful

Table 9.2 (continued)

Satellite	Scientific Experiments On Board	Results
Payload AM-19F (AM-19F) (S-45)	Indirect ionosphere measurements experiment. To study the characteristics of the ionosphere by propagating signals through the ionosphere.	Failed
Explorer 11 (AM-19E) (S-15)	Gamma ray astronomy experiment. To detect the high-energy gamma rays and to measure the ratio between reflected (by Earth's atmosphere) and nonreflected high-energy gamma rays by means of a gamma ray telescope capable of discriminating against neutron interaction and charged cosmic ray particles.	Successful
Payload AM-19G (S-45)	Similar to that of Payload AM-19F	Failed

the carrier vehicles forced design from the very outset toward miniaturization of components and extremely lightweight satellite structure. This apparent disadvantage offered a unique opportunity to develop sophisticated payloads with increased reliability [3, 4].

By following this prescribed development philosophy, the design was shaped by consideration of a series of parameters emanating partly from the various mission objectives and partly from the multistage carrier vehicles. Requirements for mission objectives included satellite orientation in space, appropriate mounting possibilities for the sensors, sufficient area for solar cell arrays, temperature control, and antenna arrangements. The first stage system subjected the satellites to high static, dynamic, and centrifugal accelerations. Weight limitation prohibited excessive balancing weights; therefore, the satellites had to be designed as symmetrical as possible about the spin axis. The shell of the satellites for the Juno 1 vehicles took the aerodynamic heating, since the payload was not covered by a protective shroud.

Several satellites required maintaining the spin axis as established at injection for scientific experiments and antenna orientation (Table 9.1), accomplished by spin-stabilization. Because of weight and power limitations, the use of an active attitude-control system was eliminated. An oblate inertia distribution about the spin axis was chosen to assure stable orientation of the satellite during energy dissipation. To nullify nutation, special damping was artificially introduced. The antenna systems, with their long flexible elements, lent themselves very favorably to the generation of additional nutation damping. Spin stabilization was achieved this way for Explorers 7, 8, and 11. The moment of inertia ratio with respect to the spin axis and a lateral axis through the center of gravity was 1.24:1 for Explorer 7, 1.32:1 for Explorer 8, and 1.44:1 for payload AM-19F\*. These ratios were realized by separating the empty shell of the fourth-stage motor from the satellite body (Table 9.1).

The orientation of the spin axis can be preserved only under the assumption that no external torques are acting on the satellite. This assumption does not fully correspond to the actual conditions. The perturbing torques resulting from such forces as magnetic induction and differential gravity will produce a slowly increasing deviation from the original orientation of the spin axis. The rate of change is hard to predict. It is anticipated that the orientation change can be established to a reasonable degree of accuracy by comparison of the analytical results with corresponding satellite orientation measurements.

---

\* Indirect ionosphere measurement satellite, which failed to orbit.



Another interesting dynamical task was offered in the spin reduction of Explorer 8 [5, 6]. The initial spin of 445 rpm had to be reduced to approximately 25 rpm to ascertain proper operation of the experiments. For maximum spin lifetime, the spin was to be reduced while full angular momentum was conserved. This could have been accomplished solely by attaching masses to the ends of the ends of the extensible dipole antenna, thereby diminishing the rpm by increasing the moment of inertia. Since weight limitation prohibited this solution, a two-step rpm reduction was applied, presenting an optimum compromise between weight penalty and loss of angular momentum. The concept chosen for the first phase consisted of two wires wound around the circumference of the satellite in a direction opposite of the direction of the spin (Fig. 9.3). Masses were connected to the outer wire ends and the wires were allowed to unwind. When completely unwound, the wires were released to allow a reduction to 100 rpm. The second step brought a spin reduction from 100 rpm to approximately 25 rpm. The second reduction was obtained by a combined antenna-release and de-spin system, which applied a special braking device to control the unreeling velocity of the wires.

A particularly intriguing dynamic problem occurred with the orientation requirement for Explorer 11. The satellite was placed into orbit with a spin velocity of 390 rpm about the minimum moment of inertia axis. The mission demanded a transfer of the spin about this axis to spin about the axis of maximum moment of inertia by dissipation of internal mechanical energy. A special energy dissipator was developed for this spin-to-tumble transfer [7]

The satellites launched with the Juno 1 vehicle may be referred to as first generation payloads. In December 1954, the authors were assigned the task of developing an instrumentation payload for the Jupiter C multistage vehicle (Fig. 9.4). The objectives of the successful first firing of this Jupiter C (RS-27) were to flight test the upper solid propellant stage arrangement, the structure of the three stages, and a check on the function of a miniature Dovap transponder and the microlock. The payload was mounted on top of the inert fourth stage. This payload became the forerunner of the first satellite generation. Jet Propulsion Laboratory used the basic configuration of this payload for the Van Allen radiation experiment, called Explorer 1, when it was in orbit.

Correspondingly, the satellites developed for the Juno 2 carrier vehicle may be classified as second generation payloads. The configuration of both satellite types was established within the former Army Ballistic Missile Agency (ABMA). The first generation satellites had a cylindrical shape with 6-in. diameters and were approximately 36 in. long. The stainless steel shell was covered at its forward end by an aerodynamic blunt nose cone and was connected to the fourth stage by a fiber glass ring which served as a dipole antenna gap as thermal insulator against the last stage. For easy installation and accessibility,

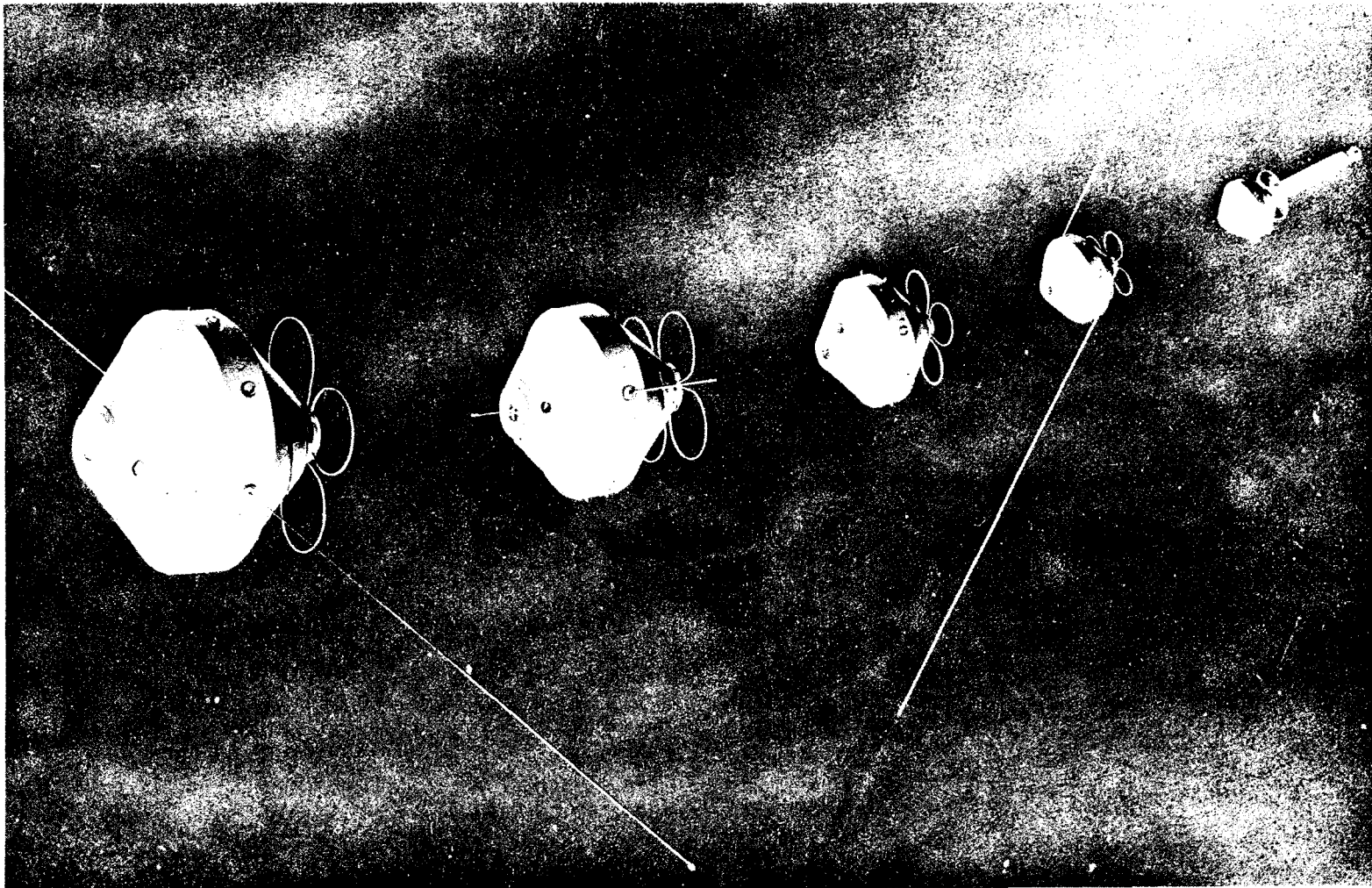


Fig. 9.3 Five flight phases of Explorer 8. (a) last stage separation; (b) first step spin reduction; (c) antennas begin to extend; (d) spin reduction continues; (e) orbiting satellite.

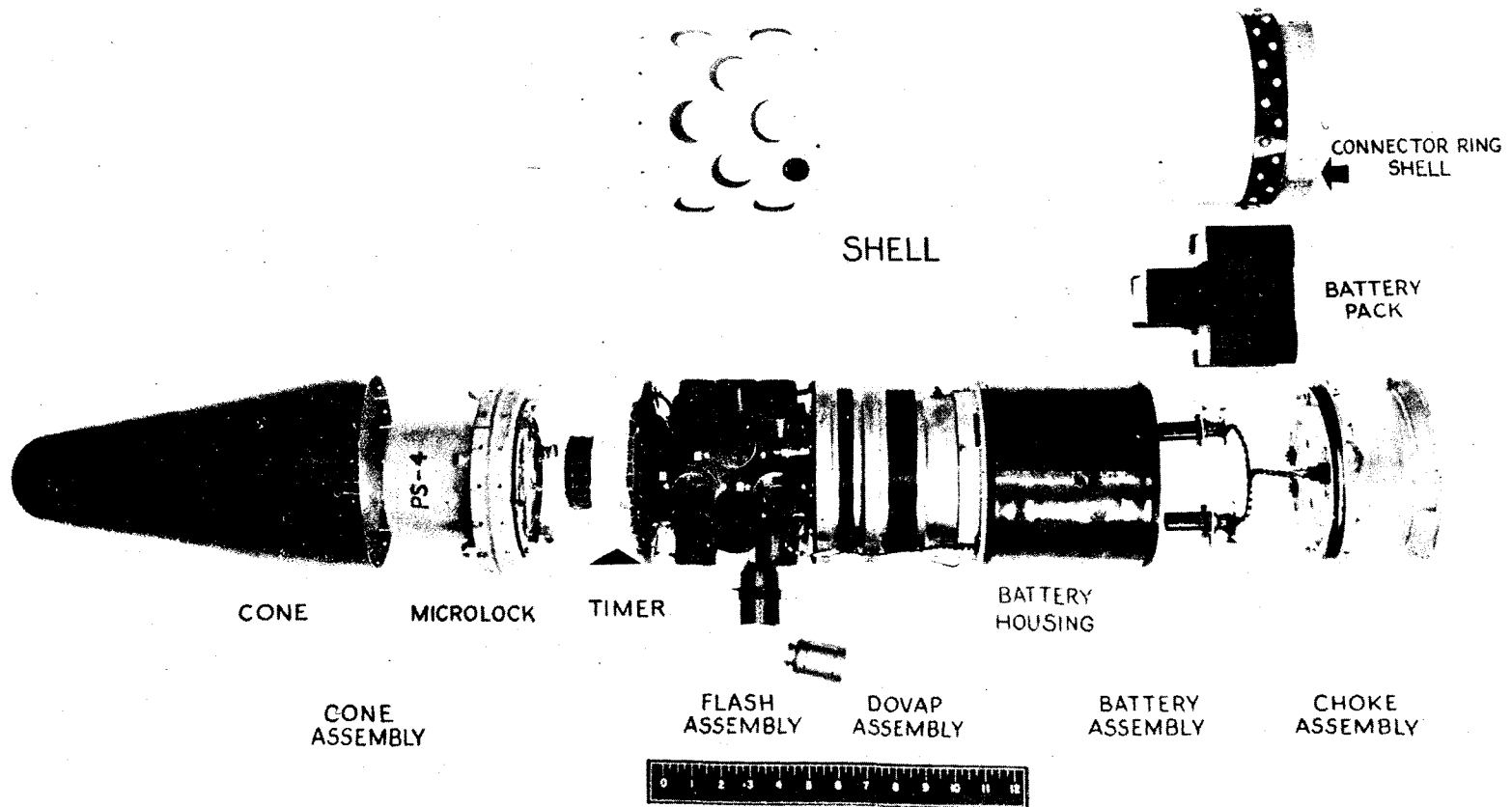


Fig. 9.4 Instrumentation payload for Jupiter C.

most of the instrumentation components were packaged so that they formed a column which exactly fitted the inside diameter of the satellite shell. The column design with its modules of 6-in. diameter and of varying thickness was also introduced into the second generation satellites, e.g., Explorer 7, 8, 11 and payload AM-19F (Figs. 9.5 and 9.6a, 9.6b). The instrument column was concentrically arranged about the spin axis (Fig. 9.7).

For the second generation satellites (excluding Explorer 11) the guiding design objective was to obtain an oblate mass distribution about the main axis of the spin-stabilized body (Fig. 9.8). The desired moment of inertia ratio was obtained by placing the relatively heavy batteries at the greatest possible distance from the spin axis (Fig. 9.7). In the following descriptions, Explorer 7 is used as a typical example. The external overall configuration was composed of a truncated double cone joined by a cylindrical center section. The connection between the centrally-placed instrument housing and the outer center ring was obtained by four spokes which sustained the centrifugal forces caused by spin, and also furnished support for the battery packs which were equally distributed at an equal radial distance from the spin axis.

The top and the lower truncated conical shell, made of polyester fiberglass, had to hold the center ring in position, and therewith the heavy batteries, during the impact of the thrust forces. The truncated cones were attached at the narrow opening to the rigid center column. At the wide opening, the cones were connected to profiled aluminum rings providing good transition of thrust through the center ring and sustaining the centrifugal load at the same time. The overall dimensions of the orbital carrier were 30 in. in diameter at the equator and approximately 30 in. in length. This method of packaging the instrumentation proved to be a noticeable advantage with respect to accessibility and exchangeability of components.

The required dynamic stability made it mandatory that separation of the empty shell of the last-stage rocket motor from the satellite occur after burnout. Because of tiny impulses generated by outgassing and afterburning, it was decided to set the separation approximately 2 min after burnout to avoid any collision with the shell or antenna wires. The timing was initiated by a timer in the third-stage rocket cluster. After 2 min, the delay timer caused the explosive charges in the separation device to ignite. It was necessary to assure instantaneous separation that would not produce an undue reaction to the satellite. A separation device was designed to this specification and was installed as a package, preloaded and sealed, between the satellite and the fourth-stage rocket motor. Material for the shell cones was either fiberglass or aluminum. The selection of the material greatly influenced the spin decay as a result of the generated eddy currents caused by the satellite's spin in the Earth's magnetic field.

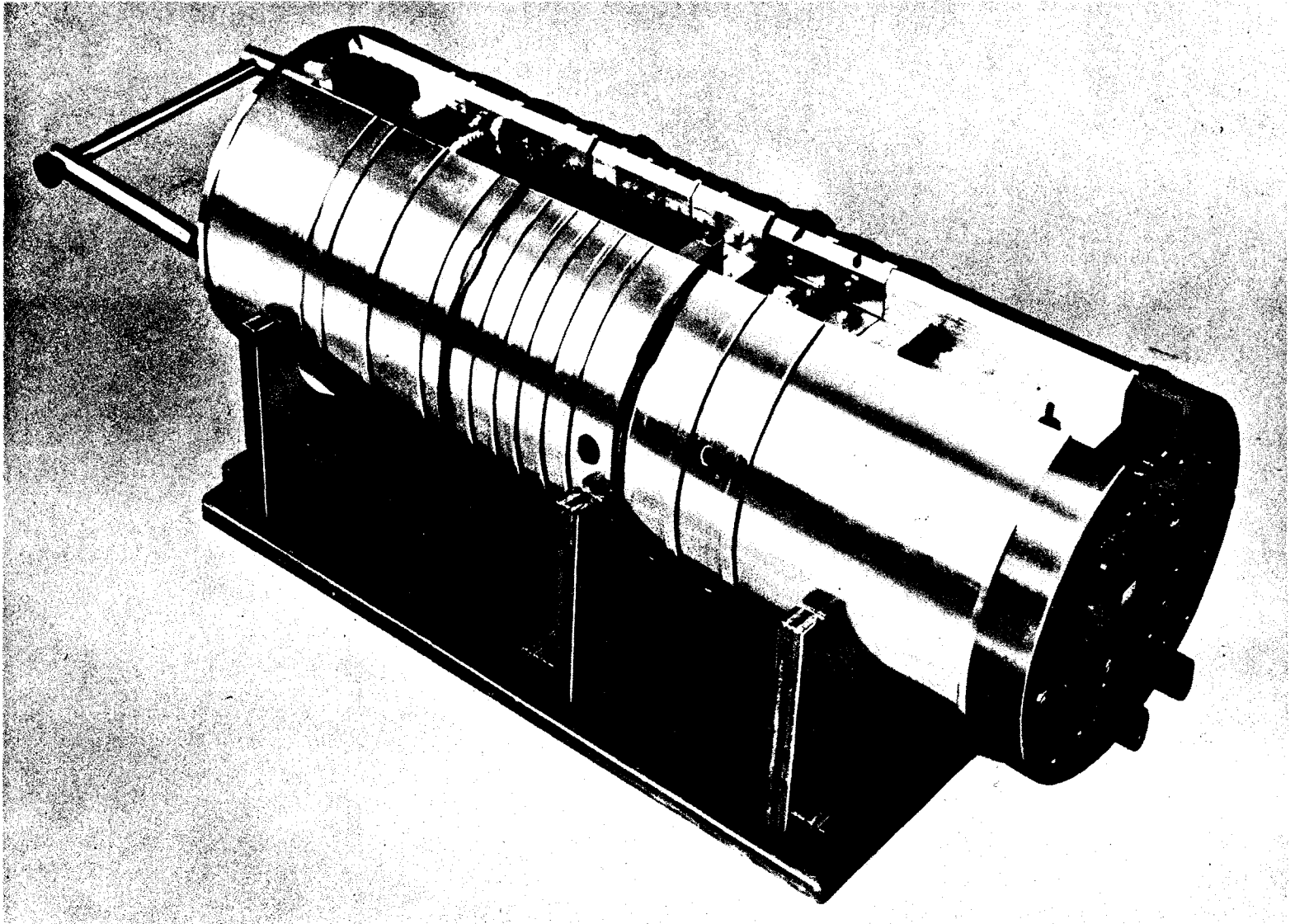
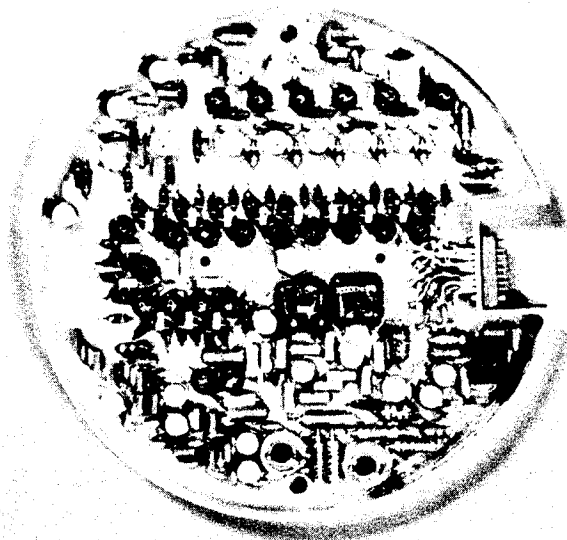
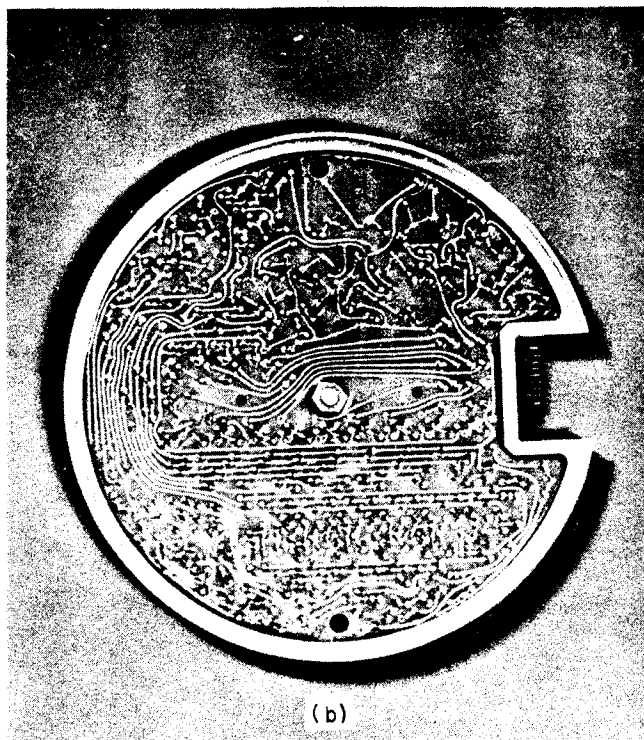


Fig. 9.5 Typical instrument column Explorer II.



(a)



(b)

Fig. 9.6a Bottom view of typical module (telemetry of payload AM-19F).

Fig. 9.6b Top view of typical module (telemetry of payload AM-19F).

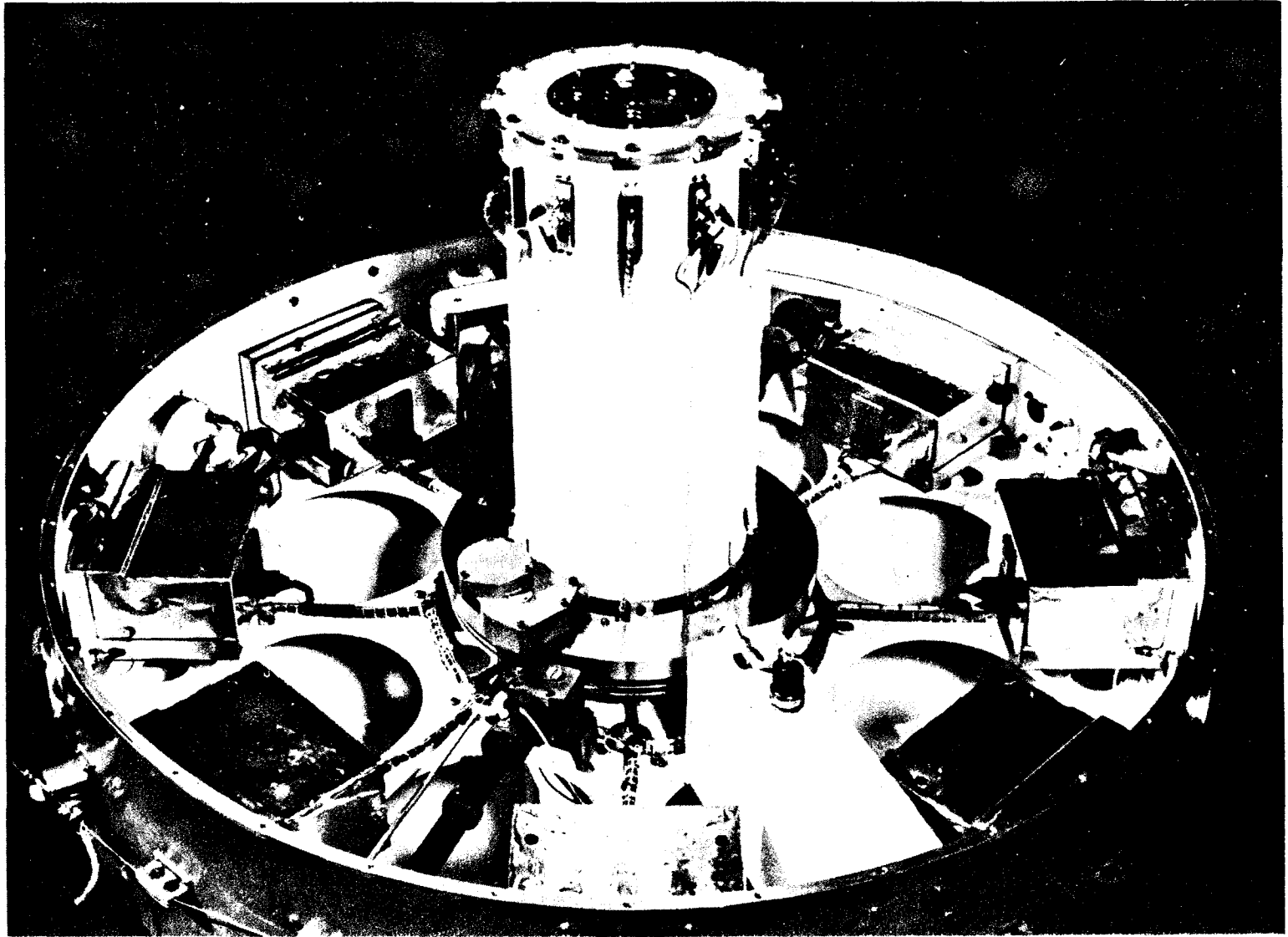


Fig. 9.7 Inside view of Explorer 8; top removed.

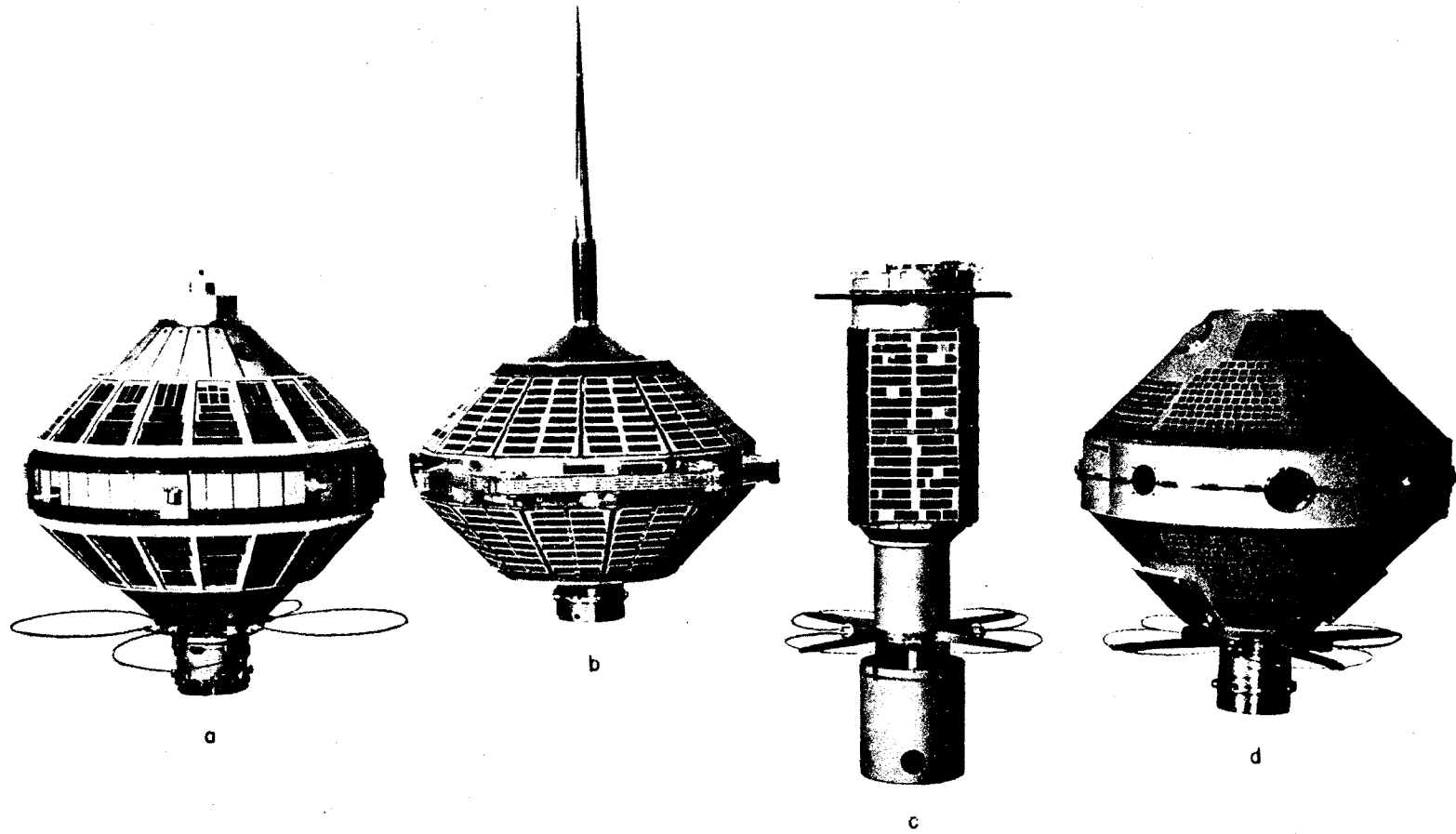


Fig. 9.8 Group of second generation satellites: (a) Explorer 7; (b) payload AM-19F; (c) Explorer 11; (d) Explorer 8.



The thermal calculations and testing had a decisive influence on the design by yielding satisfactory radiation and conductivity conditions for the satellite [8]. Sensing elements, instrumentation, and power supplies imposed temperature restrictions upon the orbiting satellite. Proper operation was guaranteed only when temperature fluctuations were held within prescribed ranges. Therefore, the instrumentation and batteries could not be exposed to temperatures lower than 0°C or higher than 60°C. The design of the satellites was influenced by thermal considerations. In Explorer 7, for instance, the thermal considerations affected the design in the following manner. The internal instruments and the batteries were insulated from the exterior hull of the carrier. The batteries were in thermal contact with the instrument column by four spokes. However, they were thermally detached from the satellite skin by Kel-F spacers, placed between the battery boxes and an aluminum ring composing a main structural element of the satellite shell at the equator.

With suitable emissivities on the outer skin surfaces, the desired thermal balance was achieved, indicating that acceptable internal average temperatures could be expected. Since the material of the shell was a thermal insulator, the outside of the shell had to be covered by a metal foil to reduce the temperature gradients along the skin and secure the necessary emissivities. The satellite configuration and the shell material made it necessary that the radiation exchange was directed to: (1) increase to the utmost the internal radiation exchange between the two truncated cones, and (2) diminish as much as possible undesirable energy exchange between the cones and the instrument column and batteries. To attain this controlled radiation exchange, the inside of the truncated cones was coated with titanium dioxide (TiO<sub>2</sub>). All surfaces of the instrument column, battery supports, and battery boxes were covered with gold foil and were made of polished aluminum. A passive temperature control system was obtained in this way; the simplicity in this system meant greater reliability.

The various antenna systems developed for the different missions presented interesting mechanical design problems. To obtain efficient transmission for the 20-Mc transmitter of Explorer 7, an antenna of a radial wire length of approximately 12 ft was required. During the ascending, propelled flight phase, the space around the payload was limited by the protective shroud; therefore, an extended antenna system of desired dimensions was not applicable. Furthermore, the accelerations would not permit even the use of a lightweight rigid antenna of such size. Only an extensible antenna system was acceptable. The four antenna wires were stored by winding them into separate grooves on a common drum which was bearing-supported and motor-driven. The wires were unreeled simultaneously at nearly constant speed. The release started exactly when the separation of the last-stage shell took place.

For the indirect ionosphere measurements payload (AM-19F), a special circular and erectile loop antenna of 6 ft in diameter was the optimum solution for the transmission of three continuous frequencies (20, 40, and 41 Mc). The antenna consisted basically of four rigid arms and four flexible tape sections[ 9]. In the collapsed position, the arms, pivoted near the equator area, were tangentially arranged to the satellite body. The antenna was held in the collapsed position by means of restraining cords. At erection, the tape sections moved under velocity control so the final arrangement was a circular pattern, with the four arms swung out and locked in their outward positions.

### 9.3 The Satellite Instrumentation and Tracking Systems

The satellite program presented many new problems in the fields of instrumentation and tracking design and systems engineering. The instrumentation was determined by the specific mission; a basic problem was the design of circuits with very low power drains. This problem was solved with the use of switching transistors. By potting the printed circuit boards and mounting them together the problem of environments and physical space was solved.

The power output of the Juno 1 Explorer series satellites did not exceed 30 mw due primarily to the state of the art in transistors. The modulation used was determined by the ground receiving stations (microlock and minitrack). This was phase modulation of the tracking or low-power transmitter and amplitude modulation of the telemetry (communication) or high-power transmitter. The telemetry used low-frequency IRIG channels.

During the launchings of Explorers 1, 2, and 3, ABMA used for tracking a modified Dovap receiver with a sensitivity of approximately -128 dbm. The antenna system consisted of two stacks of four each Channel-6 TV antennas cut to 108 Mc. It had a gain of approximately 12 db and was motor driven in azimuth and elevation as well as in the plane of polarization.

During launch and the early weeks of orbiting, Doppler data were of primary interest. A digital print-out was made of the Doppler beat as well as recording it on tape with WWV time. Calculations were also made of the spin rate for the first few weeks. Of interest was the Faraday effect observed as the satellite passed over the horizons.

Experimentation was conducted during evening and night passes to see if the effect\* of WWV transmissions reflected from ionized clouds which surrounded the satellite could be detected. This was never

---

\* First noticed by Dr. J. D. Krauss of Ohio State University.

achieved, perhaps because not much time was devoted to the experiment. It must be pointed out that the indications Dr. Krauss observed coincided with the time the satellite passed overhead.

Recordings of the telemetry signals were also transcribed with reference to time at the ABMA station; however, the quality of the telemetry signal was only fair. There was no attempt to demodulate the telemetry signal at the station. The average length of a pass was between 6 and 7 min with a maximum signal strength of approximately minus 118 dbm.

The Juno 2 satellites presented a more difficult problem in system engineering than the Juno 1 series since the systems were much more complicated. Figure 9.9 is a typical system block diagram [10, 11, 12, 13].

For the second generation Explorers, several new ideas were used to aid both tracking and telemetry systems. A new method of phase modulation was developed to increase the reliability of the tracking signal (less phase jitter). A 1-w (nominal) AM telemetry transmitter operating at 20 Mc was developed; this was pushing the frontier of state of the art in transistors.

A novel crossed dipole antenna for this transmitter was extended after orbit was achieved. Very low frequency subcarrier oscillators were developed for Explorer 11 to allow information to be placed on a tape recorder which had a record playback ratio of 1 : 50; a whole orbit of information (100 min) was compressed into 2 min [14]. Other novel circuits used on this satellite were the command system (7-channel) and the pulse height-to-width converter for measuring very fast pulses [15]. See Figs. 9.6a and 9.6b for a typical instrumentation module. The use of the recorder multiplied the subcarrier oscillator frequencies by 50, thereby requiring wide bandwidth modulators and amplifiers. The S-45 satellite was unique among satellite systems because of the number of phase-correlated rf signals and the control of the basic oscillator frequency. The frequency was controlled by a crystal placed in a passive oven that used the heat of the Sun and the cold of space in the Earth's shadow for temperature regulation. Frequency stability was better than one part in  $10^8$  at  $0.002^\circ$  F temperature change per orbit [16].

For the launching of the Juno 2 Explorer series, phase-lock receivers were used for launch and orbital tracking. These receivers had a sensitivity of approximately -150 dbm. Antenna systems for 108 Mc consisted of colinear arrays with horizontal and vertical polarization with a gain of approximately 17 db and two quad-helix arrays with circular polarization and a gain of 20 db.

# SATELLITE INSTRUMENTATION BLOCK DIAGRAM

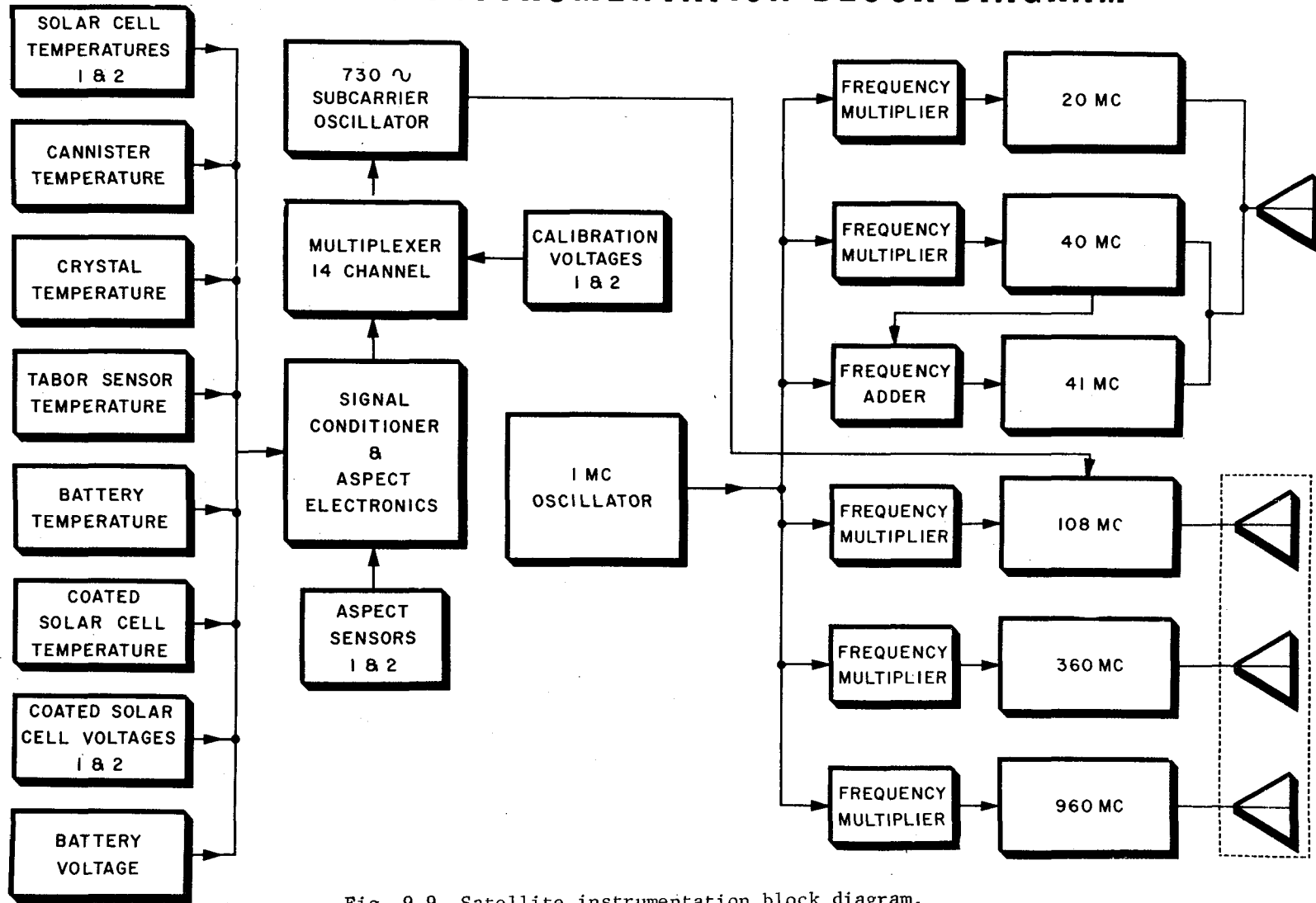


Fig. 9.9 Satellite instrumentation block diagram.

The antenna system used at 960 Mc included 14-ft and 10-ft parabolic dishes, each fed with a helix. The gain of the 14-ft dish was 30 db and the 10-ft dish was 27 db. The positioning and control system for the 108 Mc and 960 Mc antenna systems were modified SCR 584 radar control systems. The antennas have the capability of being positioned in azimuth and elevation.

Doppler data were recorded in digital and analog form; the Doppler beat was recorded on magnetic tape. Signal strength was recorded in analog form on a strip chart recorder and on magnetic tape. The composite telemetry signal was recorded on magnetic tape and it was also demodulated and recorded on a strip chart recorder. WWV time was recorded on magnetic tape and a strip chart recorder. A digital clock synchronized with WWV was recorded with the digital doppler print-out.

Modifications were made on the basic tracking system to optimize the system depending on satellite characteristics. In the case of the Pioneer 3 a converter was designed for 960 Mc which required multiplying the voltage control oscillator by 18. A Doppler count modification kit was also designed which converted the Doppler frequency suitable for use with an electronic counter while still maintaining the required accuracy.

A parametric amplifier was used to track Pioneer 4 to approximately 168,000 miles. It is believed the system held lock to approximately minus 153 dbm.

Explorer 7 was equipped with two transmitters, one at 20 Mc and amplitude modulated; the other transmitter was at 108 mc and was phase modulated. A Collins R-390 receiver was used to receive the 20 Mc signal with a low noise preamplifier added to the rf stage. A Yagi antenna with 6db gain, capable of being positioned in azimuth only, was used for receiving the 20 Mc signal. The 20 Mc receiver had a sensitivity of approximately minus 125 dbm. The receiver for 108 Mc and the recording system were described in previous paragraphs.

Explorers 8 and 11 used wide-band telemetry systems. The phase lock receivers had a predetection bandwidth of 3 kc; therefore, it was necessary to modify the 455-kc amplifier as well as the phase detector to pass the information. The bandwidth was modified to 50 kc.

The AM-19F and AM-19G satellites (S-45) presented a problem in ground receiving system design. These satellites were designed to transmit low power, phase coherent signals at frequencies of 20, 40, 41, 108, 360, and 960 Mc. These frequencies were chosen for determining the propagation characteristics of the ionosphere by measuring the relative

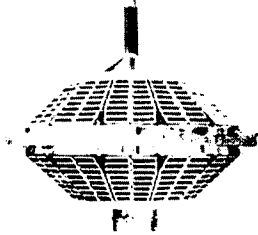
phase delay of signals transmitted through the ionosphere from a satellite by the differential Doppler technique and Faraday rotation.

A receiving system capable of accurately measuring the phase difference between any two pairs of the six frequencies and maintaining phase coherence with the received signal was needed. Such a system was designed, based on the phase lock principle. The Doppler shift was tracked by the locked loop and normalized in all receivers so its effect does not appear in the phase difference information channel. Drift in the transmitter oscillator frequency as well as drift in the local oscillator frequencies are also cancelled in the ground system. The sensitivity of the system was approximately -150 dbm. Due to such a high sensitivity, the system required very careful attention in filtering and shielding because the local and reference oscillators are multiples of 1 Mc, and the harmonic and mixer products generated in the system may fall on or near the signal frequency. Therefore, careful shielding and filtering were employed to avoid desensitization of the system and false locking.

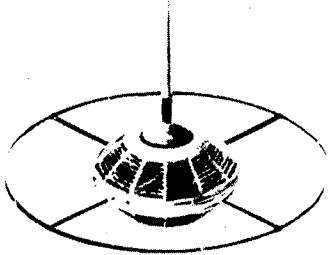
Several unusual problems were encountered in the design of antennas for the satellite payloads orbited by the Jupiter C., Juno 1, and Juno 2 vehicles. Weight and space requirements necessitated the use of electrically small antennas in many cases, and the resulting problems of bandwidth and efficiency, together with restrictions on solar cell shadowing, continued to produce some rather novel antenna designs. The use of spin stabilization on these satellites also imposed certain pattern requirements to avoid modulation of transmissions by the spinning motion of the satellite. Probably the most elaborate and unusual antenna system used in the satellite program was that employed by the AM-19F and AM-19G ionosphere beacons (S-45). The satellites were designed to transmit six continuous frequencies over a wide frequency range with linear polarization, constant amplitude, wide angular coverage, and high efficiency. The two antenna assemblies used to transmit these frequencies consisted of a multifrequency loop and a composite arrangement of linear elements, all of which were packaged inside the small space permitted by the Juno 2 shroud. Figure 9.10 shows several satellite antenna configurations [17].

#### 9.4 The Power Supply System, Electrical Networks, and Timing Devices Of the Satellites

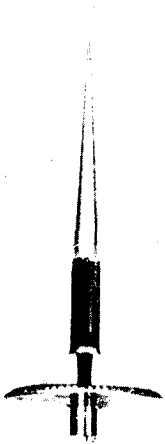
To make various satellite configurations operational in space, electrical power is needed. Electrical power has to serve the communications and tracking systems, the measuring instruments, timers for switching functions, separation devices, and antenna release mechanisms.



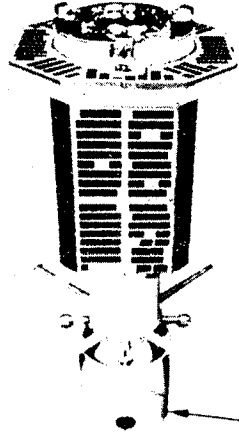
S-45 SATELLITE  
LOOP ANTENNA FOLDED



S-45 LOOP ANTENNA  
EXTENDED



S-45 HIGH FREQUENCY  
ANTENNA



S-15 SATELLITE

SLEEVE ANTENNA



S-15 QUADRILOOP  
ANTENNA

# PAYLOAD ANTENNAS

Fig. 9.10 Satellite antenna configurations.

Dependent on the desired operational lifetime of an experiment, the power source has to be selected. Mercury batteries can operate experiments for a lifetime of up to 8 weeks. If the expected lifetime is longer, other means of electrical power supplies must be chosen. Solar power conversion was used in several satellite systems and excellent results were achieved. Solar cells in conjunction with nickel cadmium batteries for storage of electrical energy were the power supply system in many applications. Table 9.3 shows the power sources for different satellites, the overall power consumption, and designed life time. To describe a typical design approach of a solar cell power supply system, the S-46 satellite design approach will be shown [18].

Within given weight limitations and configuration requirements, several approaches had to be studied. Various configurations were considered, including three- and four-finned cylinders. Preliminary calculations showed that the requirements of a light weight, constant-power output system could be met by placing an equal group of cells on each side of a rectangular body. This application required that the rectangular body be placed around the cylindrical instrument housing.

To prevent reverse current flow between the cells illuminated by the Sun and the cells on the dark side, diodes had to be inserted in series with each group of solar cells. The loss of about 0.7 v per diode had to be considered for the overall voltage output. Several power and voltage outputs were required for transmitter, subcarrier oscillator, and instrumentation totaling about 1300 mw. The operational voltages were established considering nickel cadmium batteries continuously connected to the solar cell power system during charge and discharge cycle. The maximum charging voltage was limited by zener diodes and a certain cell deterioration was assumed during discharge. This gave a voltage variation of  $\pm 11.5$  per cent about the nominal value.

Calculations indicated an orbit period of about 10 hr with about 2 hr of Earth shadow for the satellite as a maximum. There would be periods of 100 per cent sunlight orbit, giving a maximum solar cell temperature of about 80°C. Subsequent studies also indicated more than 2 hr shadow time and required a careful selected firing time to stay within the 2 hr of Earth shadow time for adequate design of the power supply. The solar cell arrangement was based on the maximum temperature of 80°C, and cell losses had to be considered for this temperature.

To obtain extremely long cycle life (over 5000 cycles) from sealed nickel cadmium batteries, it was necessary to limit the discharge to about 10 per cent of total battery capacity. Eight



Table 9.3 Satellite Power Sources

Satellite	Power Source	Power Consumption (milliwatts)	Designed Lifetime
Explorer 7	Solar cells paralleled with nickel cadmium batteries (6 different voltages)	2642	Transmitter cutoff by timer after 1 year.
	Mercury batteries (3 different voltages)	94	
S-46	Solar cells paralleled with nickel cadmium batteries (3 different voltages)	1328	Transmitter cutoff by timer after 1 year.
Explorer 8 (S-30)	Mercury batteries (33 different voltages)	946 continuous 3157 intermittent	Approximately 1.5 months.
S-45 (Payloads AM 19F & 19G)	Solar cells paralleled with nickel cadmium batteries (1 voltage)	2639	Transmitter cutoff by timer after 1 year.
Explorer 9 (S-15)	Solar Cells paralleled with nickel cadmium batteries (4 different voltages)	1616	Expected life of satellite was 1 year; transmitter can be turned off by ground command. Last minute change of orbit revised power source life expectancy to 4 months, since the satellite will be exposed to radiation belt with no solar cell protection.

hundred and sixty orbits for 1 yr of operation of S-46 were expected with more than 50 percent of the orbits in full sunlight. This meant not more than 400 to 450 cycles for the batteries.

At very low charging rates, about 150 per cent of the ampere-hours delivered on discharge must be returned to the battery during charge. The average charging current to return the battery to the fully charged condition is given by

$$I_c = \frac{I_1 \times T_1}{T_c \times \eta_{ah}}$$

where

$I_c$  = Average battery charging current required from solar cells

$I_1$  = Average electronic load current

$T_1$  = Maximum time per orbit battery is under load

$T_c$  = Minimum time per orbit battery is receiving charge

$\eta_{ah}$  = Ratio of ampere-hours delivered from battery under load to ampere-hours required to return battery to fully charged condition

The incident solar radiation outside the Earth's atmosphere is approximately  $140 \text{ mw/cm}^2$ . This value can vary by plus or minus 3.4 per cent as the Earth moves from perihelion to aphelion. The spectral distribution of the solar radiation approximates that of a  $5900^\circ\text{K}$  black body. A plot of the distribution of this radiation is shown in Fig. 9.11 together with the spectral response plot of a silicon solar cell. It shows that the solar cell responds to the wave lengths between approximately 0.4 and  $1.2 \mu$ . Integration of the solar energy distribution curve shows that this wave length band contains approximately 55 per cent of the total solar energy available. Other factors, such as reflection losses, internal resistance losses, and junction property restrictions, limit the maximum theoretical conversion efficiency of silicon solar cells. In connecting solar cells in series, mismatch in voltage-current characteristics and connection resistance reduces the over-all efficiency of groups of cells even further. For the predicted cell temperature of  $80^\circ\text{C}$ , the efficiency has to be further reduced. It is 71 per cent of its value at  $30^\circ\text{C}$ .

ENERGY CAL.  $\text{CM}^{-2} \text{MIN}^{-1}$  PER 0.01 MICRON WAVELENGTH BAND

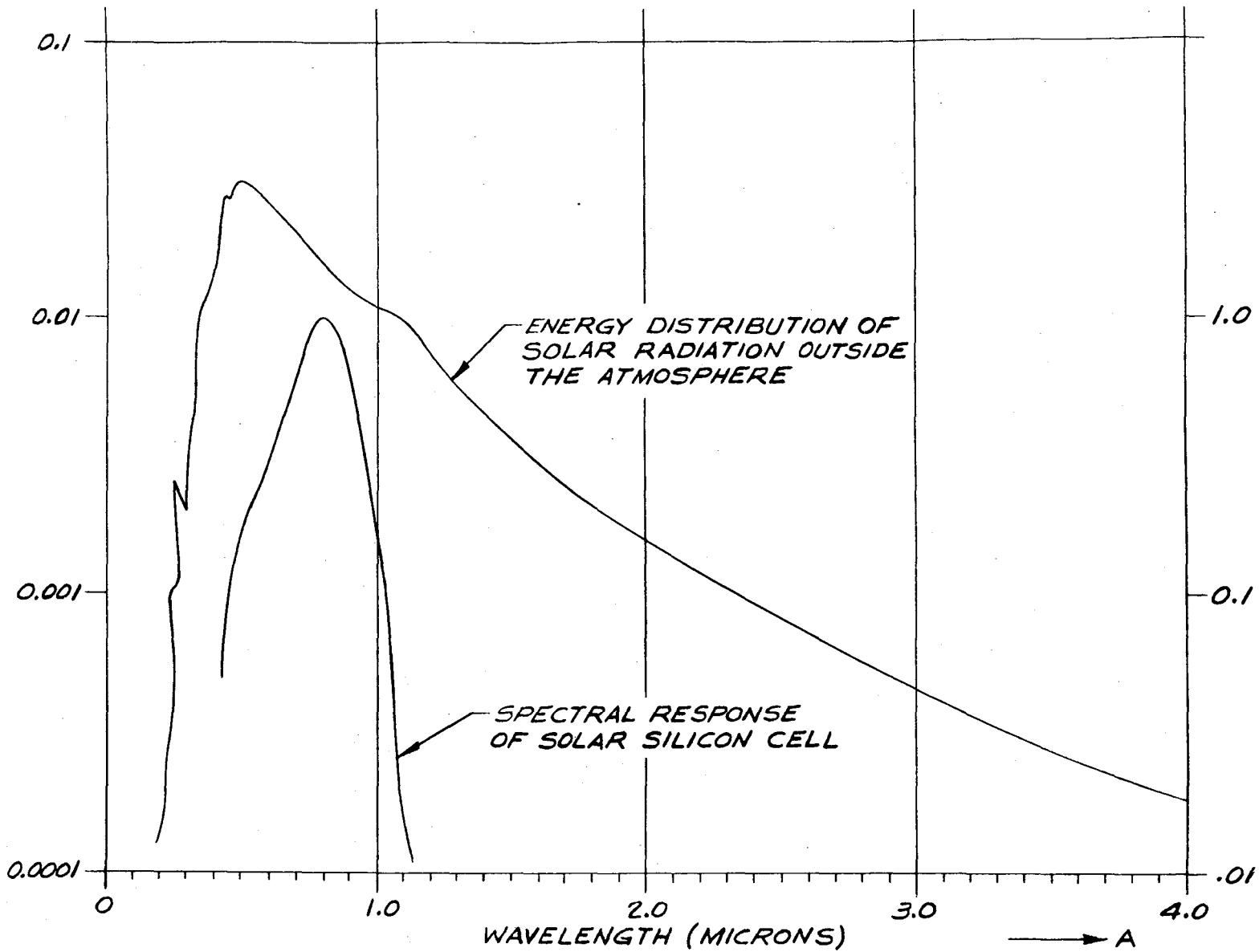


Fig. 9.11 Spectral distribution of solar energy and spectral response of solar cells.

The required power output of the solar cells is given by

$$P_o = I_o V_o$$

where  $P_o$  = power output of solar cells in milliwatts  
 $I_o$  = sum of electronic load current and battery charging current in milliamperes  
 $V_o$  = sum of average system voltage and voltage drop across blocking diode

The number of series connected cells required for each voltage was determined by dividing  $V_o$  by the optimum cell voltage at the maximum expected temperature.

With the solar cell surface perpendicular to the Sun, the total solar cell area needed to produce the required power is given by

$$A = \frac{P_o}{\eta K}$$

where  $A$  = active solar cell area in sq cm  
 $\eta$  = group solar cell efficiency at design temperature  
 $K$  = solar constant in mw per sq cm

From this equation, the number and type of cells for each power supply was determined.

To completely analyze a solar cell system layout for a nonoriented satellite, it is necessary to evaluate the design for the effects of variation in light incidence on the power output that results from:

1. Aspect of axes with respect to the Sun.
2. Tumble.
3. Rotation or spin.
4. Shadow from protruding parts.

In the case of S-46, the satellite was a cylindrical body of the diameter of the last-stage rocket. A rectangular box was required to provide adequate area to mount solar cells for the mission. After the battery capacity was established, the solar cell groups were designed. The layout provided for proper distribution on each of the six sides of the structure. Special care had to be taken in cell

placement on top and bottom plates to avoid undue shadowing of any cell group by the instrument housing or the fourth-stage rocket protruding through the solar cell box assembly.

The general equation for analyzing the effect of satellite rotational position on the solar cell system output can be based on the assumption that the power generated varies directly with the cosine of the angle between a line normal to the cell surface and the incident light vector. The curves shown in Fig. 9.12 relate the power output of a typical silicon solar cell to the angle of incidence of light for a fixed load. Although the curve for optimum power would follow closely the true cosine curve, the fixed load curve must be used for this type of analysis. This is not reflected in the general equation to be derived. Corrections for deviations from the true cosine function are to be made when the problem is fed into the computer.

To utilize an analog computer for plotting all possible satellite positions which may occur, some equations can be established using Fig. 9.13 for the geometric relations.

For side 1

$$\cos \gamma_1 = (\cos \phi \sin \beta \cos \theta + \sin \phi \sin \theta)$$

For side 2

$$\cos \gamma_2 = \cos \phi \sin \beta (\theta - 90^\circ) + \sin \phi \sin (\theta - 90^\circ)$$

For side 3

$$\cos \gamma_3 = \cos \beta \cos \phi$$

The results of this analog computer simulation of the problem are shown in Figs. 9.14 and 9.15. The average relative power per cycle of tumble rotation was plotted against the spin rotation angle  $\theta$  to demonstrate the effect of spin superimposed on tumble for fixed values of  $\phi$  (the angle of the Sun with respect to the plane of tumble rotation). By integrating the curves for  $\phi = 0$  deg and  $\phi = 90$  deg, the minimum and maximum average relative power for the system was obtained for simultaneous spin and tumble.

One of the major problems in establishing a functional satellite is the integration of various assemblies, sensors, and power supplies into a complete functional system. This requires the cooperation of the electronic, structural, electrical and thermal designers.

The electrical network combines all electrical components into the desired operational system as defined by the mission. Careful

POWER  
OUTPUT IN  
PERCENT

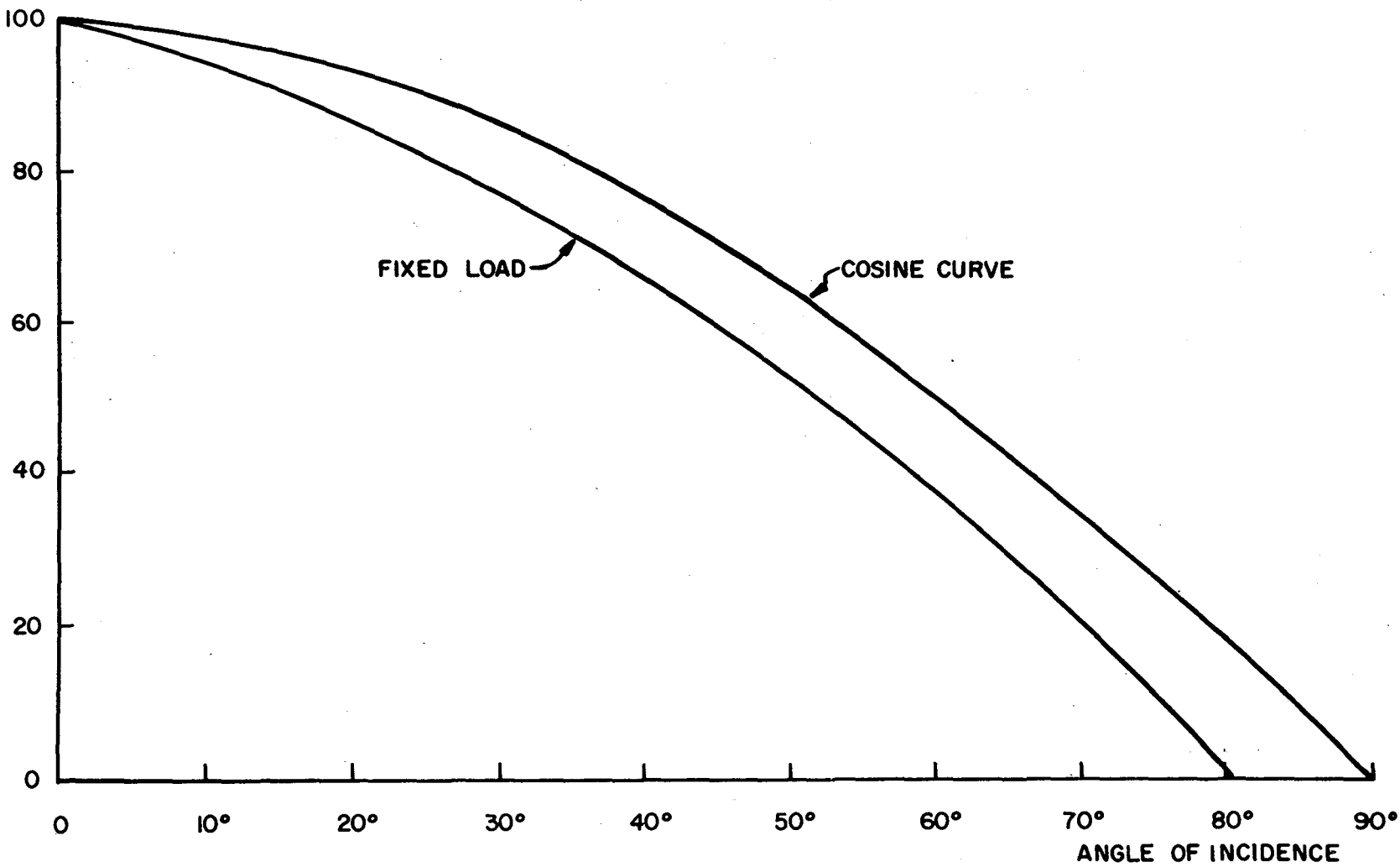


Fig. 9.12 Silicon solar cell output versus light incidence.

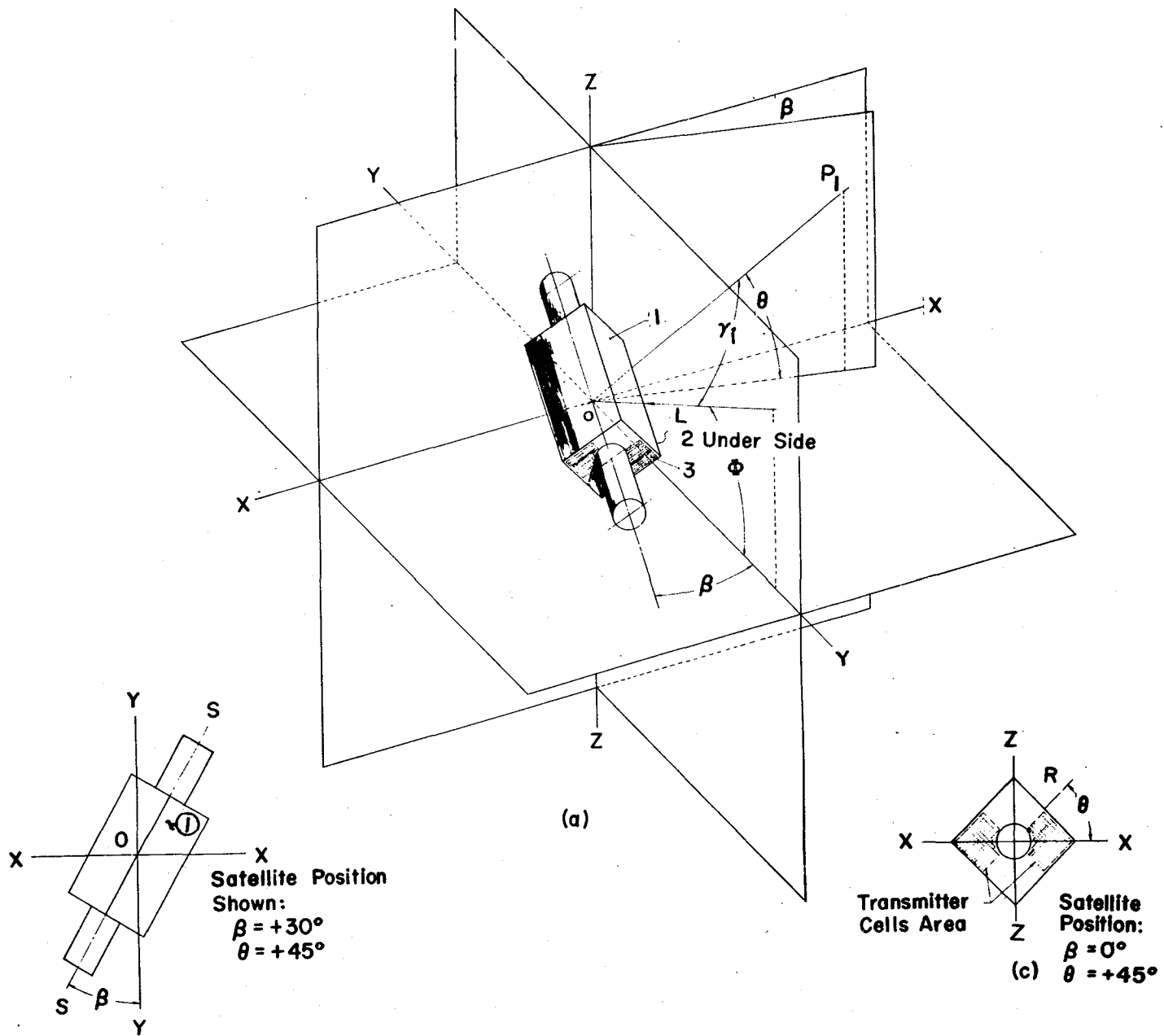


Fig. 9.13 Arbitrary space position of satellite S-46 for establishing satellite position equations.

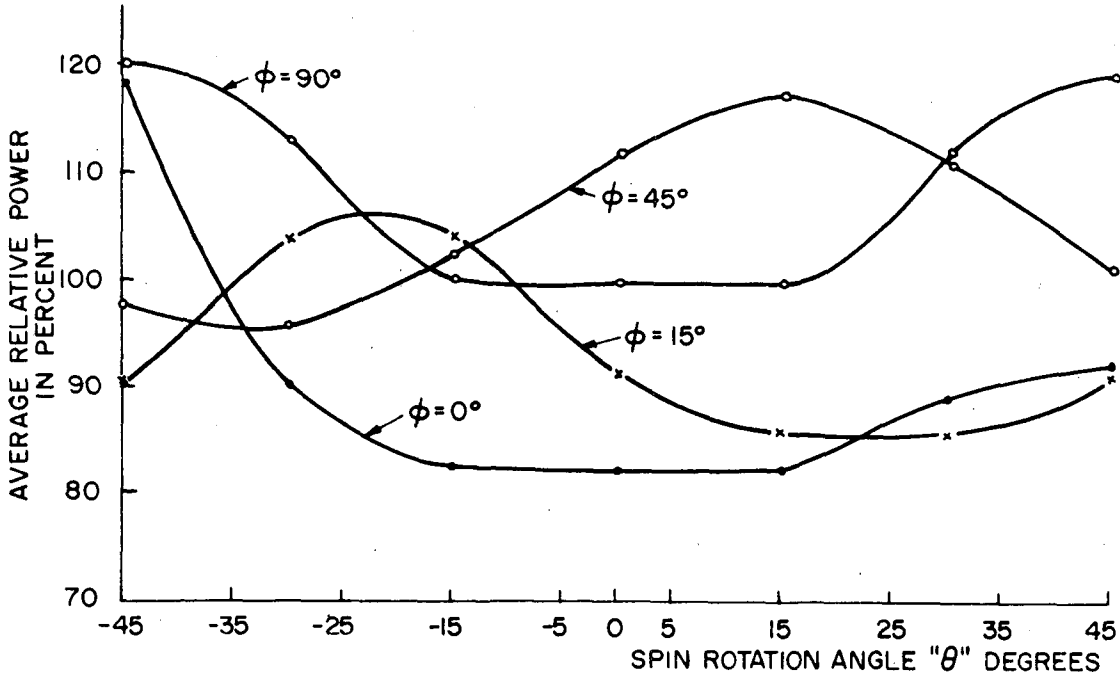


Fig. 9.14 Relative average power per tumble cycle as a function of spin rotation at  $0^\circ$ ,  $15^\circ$ ,  $45^\circ$ , and  $90^\circ$ .

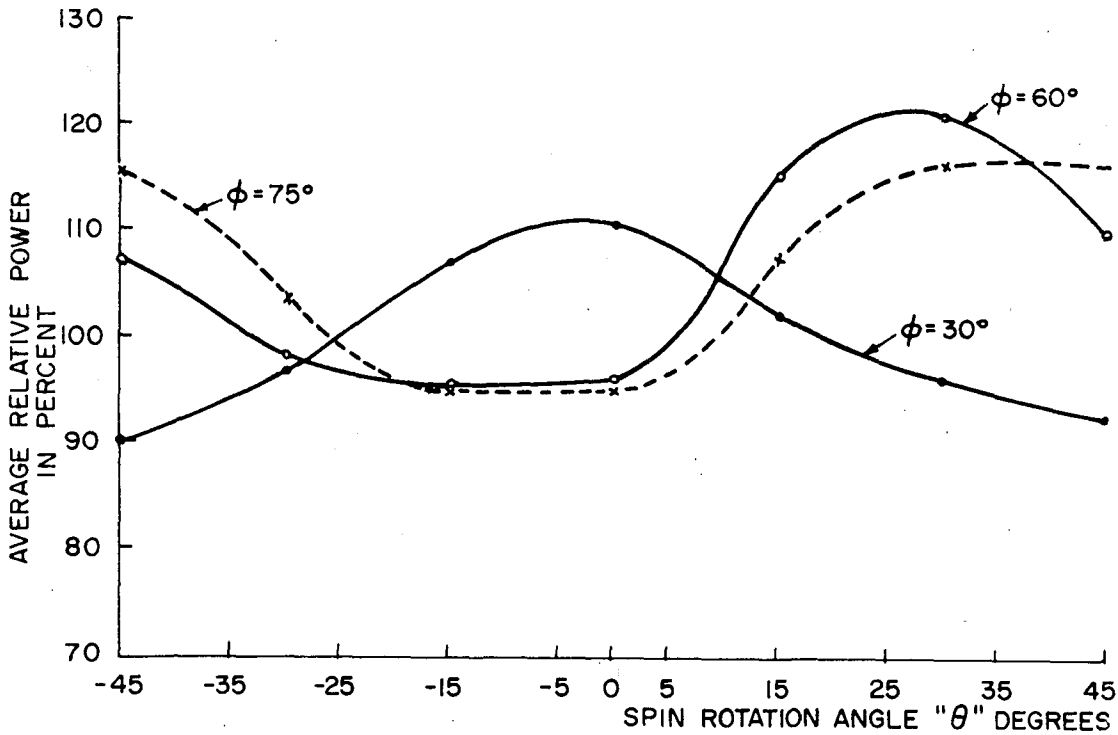


Fig. 9.15 Relative average power per tumble cycle as a function of spin rotation at  $30^\circ$ ,  $60^\circ$ , and  $75^\circ$ .



planning is necessary to assure functional compatibility of the entire system. Power requirements define the power sources. To save weight, these sources must be shared by several consumers. Still, interference-free operation has to be achieved. The systems design has to be approached with a great amount of flexibility to allow modification of the different subassemblies, if required by the advancement of design or development. The electrical system is designed by utilizing a modular construction. A distribution center will provide the flexibility for changes and serve as a central point for power distribution, timing, and sequencing functions. The various modules should be connected to the distributor by cables and connectors to maintain ease of module exchange.

The S-46 satellite again can serve as a typical example for this design philosophy as utilized in the different satellite configurations launched under our assigned program.

Checkout and preflight monitoring is an important part of electrical systems design. An assembled satellite has limited access for operational checking. This access is even less after mating with the overall space carrier vehicle. The status has to be monitored during preflight and actual launch countdown to assure satisfactory systems performance prior to launch. Timing devices, a part of most satellite electrical systems, were used to sequence proper payload separation from the last stage, unreel antennas, blow off shrouds, etc. The RC timers were part of the network and could execute several functions in sequence. For satellites powered by solar cell systems, another long duration timer was developed to cut off the entire system at a desired preset time. To avoid saturating a frequency band with useless radio signals, it was necessary to include such a timer to shut off the transmitter on Explorer 7 after 1 yr of operation. Otherwise, the transmitter could possibly operate as long as the solar cell power system continued to function.

A 1-yr electronic timer was developed by Bulova for this special purpose, operating on its own power source. The timer had no escapement; it operated on a transistor switch-operated tuning fork mechanism, with an accuracy of better than 0.1 per cent.

#### 9.5 Environmental and Functional Testing of the Satellites

A vital prerequisite for the successful performance of the satellites was comprehensive and rigorous testing with respect to functions and environmental conditions. The test program gave optimum simulation of all expected environmental conditions to be encountered by the satellites during the ascending phase of its trajectory and while in orbit. In particular, exhaustive functional tests were performed with individual component systems.

The applied test procedure provided tests with prototype models, and also flight acceptance tests with the actual flight satellite. The prototype models completely resembled the satellite to be launched. Accordingly, separate test specifications were prepared for prototype acceptance containing well-founded safety factors. The satellites to be launched were subjected to basically the same series of tests under substantially less rigorous conditions. The main intent of these tests was to investigate the satellites after final assembly in order to determine the extent of human error.

Several prototypes were manufactured for mechanical, electrical, and other tests, which were often run in parallel. Findings of the prototype testing were evaluated and, where necessary, led to corresponding modifications which were considered before the manufacture of the flight satellite.

The Juno 1 and Juno 2 rocket systems, with the cluster rotating up to 750 rpm and 450 rpm, respectively, imposed stringent requirements on balancing the satellites. For example, the radial distance of the center of gravity from the spin axis of the 92.3 lb Explorer 7 satellite was to be smaller than 0.005 in. The dynamic tests were performed with a highly sensitive special balancing apparatus. Because the design is rotationally symmetric, the balancing weights which had to be added resulted in only a small weight penalty.

Another essential phase of the test program represented the testing of the effects of static and dynamic accelerations produced by spin, thrust, initial shock, and vibrations. The satellites were spun on a mechanism at a rate of 600 rpm for at least 5 min. Functional operation of the payload instrumentation was monitored during the spin period. This was to prove: (1) the structural adequacy of the satellites; and (2) the perfect functioning of instrumentation and the complete power supply under spin.

The complete satellite assemblies were mounted on a centrifuge and subjected to accelerations caused by first stage thrust and the cluster rockets. Instrumentation and power supply were checked before and after a 3-min exposure to acceleration. By spinning the satellites on the centrifuge, centrifugal acceleration was superimposed on thrust acceleration.

To simulate the acceleration conditions during propelled flight, the entire payload of the Juno 1 missions was spun on the revolving centrifuge. It was necessary to abstain from exposing the entire satellite of Juno 2 missions because of unacceptable gyroscopic torques. Therefore only the instrument column of these satellites was subjected to the superimposed accelerations. The initial shock resulting from the three solid propellant rocket stages was checked by a linear accelerator. Thirty shock exposures to about 25g and 10 msec duration

were imparted to the instrument column. The test apparatus used was a newly developed linear accelerator, working cyclically on a pneumatic principle. The behavior of the satellite was tested, with regard to the structure and the operation of the instrumentation under the impact of rocket vibrations, by vibrating the satellite in three directions about three mutually perpendicular axes, one of which was the spin axis.

The orbital environments were simulated with respect to vacuum and temperature, after the satellites were exposed to launch environments. For obvious reasons, the condition of weightlessness could not be simulated. The instrumentation and power supply (except solar cells) worked in near vacuum over the anticipated range of temperature. The thermal characteristics of the satellite were determined to enable prediction of orbital temperature ranges by analysis. Liquid nitrogen and a special electric heating blanket were used in a vacuum chamber to cool the satellites to a low temperature and to heat it up by a heat-step which could be directed to all or part of the satellite's surface. In this way, internal conductive and radiative coefficients of the satellite were determined and evaluated in order to calculate, in connection with the surface emissivity ratios, the temperatures for certain orbital data.

The satellite's capability to operate over longer periods in space was investigated by subjecting the satellite to a vacuum of  $5 \times 10^{-5}$  mm of mercury at instrumentation temperatures between  $5^{\circ}$  and  $55^{\circ} \text{C} \pm 5^{\circ} \text{C}$ , respectively, for 2 weeks. For 1 week, each of the extreme temperatures was applied; they represent the extremes of the permissible temperature range. During this vacuum-temperature "soak" test, the functioning of all the experiments (except the solar cells) was continuously monitored.

Spin decay was investigated by means of a specially developed apparatus for generation of a highly homogeneous magnetic field. After completion of satellite assembly, electrical tests were performed to verify the circuitry and the capability of the power supply to operate the various electronic components. Operational tests were run to certify the antenna patterns, field intensity and compatibility of transmitters with the microlock stations.

Typical of the way functional testing was executed were the following two tests performed with component systems. Both elements had to operate perfectly, the separation device which was applied in all cases when the empty shell of the fourth-stage motor was disconnected from the satellite, and the 20-Mc antenna release mechanism as flown with Explorer 7. The malfunction of either one of these components during the actual flight would have resulted in a total failure of the mission.

The separation device, after all its parts had been checked rigorously, was tested under closely simulated flight conditions so that the dynamic behavior of the complete system, consisting of satellite and empty shell of last-stage motor, could be observed. A satellite mock-up of true mass distribution was suspended at its center of gravity, with low friction, by a cord. In this way, the six degrees of motion freedom were approximately simulated. A rocket dummy, also representing an actual mass distribution, was attached to the dummy satellite by the separation device to be tested. After the system was spun up to the cluster rpm of 450 and nutation was artificially imparted, the separation mechanism was actuated. It was found that the applied mechanical scheme was sound and reliable. The separation was instantaneous and without noticeable reaction to the satellite body.

The extensible 20 Mc antenna system of Explorer 7 was also tested under a close simulation of possible flight conditions. The test program was based on full-scale operation of the antenna system in a large vacuum chamber, a 41-ft diameter sphere, at 1 to 2 mm of mercury. The satellite was suspended as it was for the separation test. The motion of the wires and the satellite was observed. Nutation of a varying amount was generated by the dropping of weights onto the simulated satellite. The operation of the mechanical system to full wire extension with and without nutation, the damping capability of the extended wires, the wire release velocity, and the spin decrease caused by inertia increase by change of mass distribution, were studied and checked. The antenna release system was accepted for flight after a considerable number of operations had been performed satisfactorily in every respect.

The test program outlined above was based on the philosophy that high reliability is achieved not only by suitable design but also by the quality of the tests.

## REFERENCES

1. von Braun, Wernher, A Minimum Satellite Vehicle Based on Components Available from Missile Development of Army Ordnance Corps, Guided Missile Development Division Ordnance Missile Laboratories, (Redstone Arsenal), Huntsville, Alabama, September 15, 1954.
2. Haeussermann, Walter, Spatial Attitude Control of a Spinning Rocket Cluster, ARS Journal, 20: 56-58 (January 1959).
3. Explorer 1, prepared by Jet Propulsion Laboratory, Astronautics 3: 20 (April 1958).
4. Boehm, Josef, Considerations to the Development of Explorer 7 Satellite, IRE Transactions on Military Electronics, MIL-4: 86-92 (April-July 1960).
5. Pfaff, Helmuth, Combined Antenna - Release and Despin - System (Second Phase) for Payload 19D (S-30), Rept. MM-M-G&C-2-60, NASA-Marshall Space Flight Center, Huntsville, Alabama, August 10, 1960.
6. Counter, Duane N., Spin Reduction for Low Probe Satellite S-30 (19 D), Rept. MNN-M-G&C-5-60, NASA-Marshall Space Flight Center, Huntsville, Alabama, September 12, 1960.
7. Kuebler, M. E., Tumble Transfer of Satellite S-15 (Explorer 11), Rept. MTP-G&C-61-30, NASA-Marshall Space Flight Center, Huntsville, Alabama, July 10, 1961
8. Heller, Gerhard, Problems Concerning the Thermal Design of Explorer Satellites, Rept. No. DV-TM-11-60, Army Ballistic Missile Agency, Huntsville, Alabama, May 17, 1960.
9. Wagner, Hermann R., Payload S-45 Development Report (Mechanical), Memo M-G&C-MM, NASA-Marshall Space Flight Center, Huntsville, Alabama, July 25, 1961
10. Instrumentation Description and Checkout Procedures for the Gamma Ray Satellite, S-15, Rept. MTP-M-G&C-61-16, NASA-Marshall Space Flight Center, Huntsville, Alabama, March 17, 1961.
11. Checkout Procedure for Missile 16-S Payload, ABMA Report, G&C Laboratory, Huntsville, Alabama, February 11, 1959.
12. S-46 Satellite Instrumentation, ABMA Report, G&C Laboratory, Huntsville, Alabama, February 9, 1960.

## REFERENCES (Cont'd)

13. Instrumentation for the Ionosphere Beacon Satellite S-45, Rept. MTP-M-G&C-61-4, NASA-Marshall Space Flight Center, Huntsville, Alabama, February 8, 1961.
14. King, Olin and Frank, Emens, Data Transmission System for the Gamma Ray Astronomy Satellite, Proceedings of National Telemetering Conference, Chicago, Illinois, Paper 4-37, May 1961.
15. Malone, Lee, Radio Command System for the Gamma Ray Satellite Experiment S-15, Rept. MNN-M-G&C-2-60, NASA-Marshall Space Flight Center, Huntsville, Alabama, July 20, 1960.
16. Fisher, Alan J., Final Engineering Report Satellite S-45 Ionosphere Beacon Transmitter, Rept. MTP-M-G&C-61-16, NASA-Marshall Space Flight Center, Huntsville, Alabama, March 10, 1961.
17. Harper, J. W., and Swindall, P. M., Final Engineering Report on Satellite S-45 Antenna Systems, Rept. MTP-G&C-I-61-40, NASA-Marshall Space Flight Center, Huntsville, Alabama, September 15, 1961.
18. E. Cagle, P. Youngblood, R. Boehme, S-46 Satellite, Vol. II of Summary Project Report, TN D-608, NASA-Marshall Space Flight Center, Huntsville, Alabama, April 1961.

## 10

CORRELATION OF THE THERMAL BEHAVIOR OF SATELLITES AND THE ROTATIONAL  
MOMENTUM VECTOR

Gerhard B. Heller, Billy P. Jones, Robert J. Naumann, and William C. Snoddy

Research Projects Division  
George C. Marshall Space Flight Center  
National Aeronautics and Space Administration  
Huntsville, Alabama

Satellites and spacecraft instrumentation operate properly only in the particular temperature range for which they are designed. The lower limit is in most cases 0°C and is determined by the efficiency of primary or secondary batteries. The upper limit is between 50°C and 70°C; it is determined primarily by the temperature limit of electronic components and by lifetime requirements of batteries.

This paper describes the method of passive thermal control developed for the series of Explorer satellites which has already proved very successful in Explorer 1. The more refined methods required by the later Explorers were developed by a thorough evaluation of data from the previous Explorers. Temperature measurements allowed conclusions to be drawn on the spinning mode and the direction and magnitude of the rotational momentum vector. Methods have been developed to determine the rotational characteristics of the Explorer satellites from radio signal strength measurements.

The correlation between the thermal behavior and the attitude of the satellites is shown including the latest results of all successful Explorer satellites of the Juno 1 and 2 series, i.e., 1, 3, 4, 7, 8, and 11. Conclusions from the evaluation of the last three satellites are still tentative.

### 10.1 Theoretical Temperatures

Investigations were carried out to determine the parameters that influence the temperature on board a satellite. From such studies, the variables were placed into three main groups: (1) satellite environment, including general radiation environment, orbital characteristics, position of Sun, and satellite attitude; (2) satellite configuration and its detailed design aspects; and (3) thermal properties of satellite

materials. In this paper, emphasis is placed on the theoretical aspects of the temperature, attitude calculation and their correlation with flight data. The thermal design of the Explorers may be found in [1, 2, 8].

The time-dependent temperature of an isothermal element  $j$  of a satellite can be determined from a general heat balance equation which summarizes all heat fluxes due to conduction, radiation, and storage in the thermal capacity of the element,  $j$  [4, 5, 6].

$$\sum_{k, j=1}^n \left[ c_{k,j} (T_k - T_j) + r_{k,j} (T_k^4 - T_j^4) \right] + q_j + A_{1j} \epsilon_{1j} S D_1 + A_{2j} \epsilon_{1j} B S g D_2 + A_{3j} \epsilon_{2j} E S g - A_j \epsilon_{2j} \sigma T_j^4 - c_j \dot{T}_j = 0 \quad (10.1)$$

where

- $T_j, T_k$  = temperature of satellite elements  $j$  or  $k$
- $c_{kj}$  = conductive transfer coefficient from  $k$  to  $j$
- $r_{kj}$  = radiative transfer coefficient from  $k$  to  $j$
- $q_j$  = internal heat release
- $A_{1j}$  = effective area of element  $j$  for solar radiation
- $A_{2j}$  = effective area of element  $j$  for albedo radiation
- $A_{3j}$  = effective area of element  $j$  for Earth radiation
- $A_j$  = effective area of element  $j$  for radiation to space
- $\epsilon_1$  = emissivity with respect to solar radiation
- $\epsilon_2$  = emissivity with respect to infrared radiation
- $\sigma$  = Boltzmann constant
- $c_j$  = heat capacity of element  $j$

$k$  applies to all elements for which thermal coupling to the element  $j$  exists.



Equation (10.1) defines a set of  $n$  simultaneous, nonlinear differential equations in  $n$  dependent variables and one independent variable. The first term is the sum of all coupling energy fluxes between satellite elements; the second term is the internal heat release. Terms 3 to 6 account for the energy exchange with the radiation environment due to Sun and Earth. For other celestial bodies additional similar terms can be introduced. Term 7 accounts for the effect of heat capacity.

The equations were solved numerically by the use of digital computers. The less complex satellites in the Explorer series, such as 1 through 4, required only two simultaneous equations which yielded the time-dependent temperatures of the instrument column and the concentrically placed and thermally insulated outer shell [7, 8]. Explorers 7 and 8 required the solution of 12 temperatures [9]. The validity of the program has to be checked by a detailed analysis of the conductive  $c_{kj}$  and radiative  $r_{ki}$  transfer coefficients. The geometry factors of radiation between internal surfaces have to be determined. The coefficients are checked in a vacuum chamber during the ground testing program. One type of such tests is conducted by applying heat input in the form of a step function on one-half shell of the satellite. The other half shell can radiate freely to the liquid nitrogen-cooled wall of the vacuum tank [10]. The same type of digital computer program used for analyzing the ground tests is used for the prediction of the temperature variations in space and for the analysis and correlation of telemetered temperature records.

$A$  is the effective area for radiation from the element to space. The areas  $A_1, A_2, A_3$  are effective areas of an isothermal surface element with respect to received Sun radiation ( $A_1$ ), received albedo ( $A_2$ ) and received infrared Earth radiation ( $A_3$ ). The emissivity  $\epsilon_1$  refers to the Sun radiation and is also valid for albedo. The emissivity  $\epsilon_2$  refers to infrared radiation. In most cases, it is permissible to use the same emissivity value for radiation from the surface of the Earth, from the atmosphere, and from the surface of the satellite area element.

The function  $g$  is determined from

$$g = 1 - \sqrt{\frac{R^2 - R_0^2}{R^2}} \quad (10.2)$$

where  $R_0$  = radius of Earth. The radius vector  $R$  is given by [11]

$$R = \frac{R_p}{1-e} - \frac{e}{1-e} R_p \cos M + \frac{e^2}{1-e} R_p \sin^2 M + \dots \quad (10.3)$$

where

$R_p$  = radius at perigee

$e$  = eccentricity

$M$  = mean anomaly determined by

$$M = \frac{2\pi t}{p} = \frac{R_o \sqrt{g_o} t}{\left(\frac{R_p}{1-e}\right)^{3/2}} \quad \text{radians} \quad (10.4)$$

where

$t$  = time measured from perigee

$p$  = period

$g_o$  = standard acceleration due to gravity

The step function  $D_2$  is

$D_2 = 1$  (if satellite is above the illuminated hemisphere of the Earth)

$D_2 = 0$  (if satellite is over the nightside of the Earth)

The step function  $D_1$  determines the time in sunlight, i.e.

$D_1 = 1$  for the satellite in the Sun

$D_1 = 0$  for the satellite eclipsed by the Earth

The point of egress from and ingress into the shadow cylinder can be determined from the orbital characteristics and the position of the Sun. If we define the point of egress or ingress by an angle  $\chi$  measured within the orbital plane from the intersection of the shadow circle at the Earth's surface with the orbital plane, we can write

$$\sin \chi = \frac{\sqrt{1 - \left(\frac{R_o}{R_p}\right)^2 \left(\frac{1 + e \cos v}{1 + e}\right)^2}}{\cos \delta} \quad (10.5)$$

where

$v$  = true anomaly

$\delta$  = distance from Sun to orbital plane

Using the standard astronomical spherical coordinate systems, we can write

$$\sin \delta = \sin j \sin (L - L_{\odot}) \quad (10.6)$$

$$\cos j = \cos i \cos \epsilon + \sin i \sin \epsilon \cos \Omega \quad (10.7)$$

$$\cos L = \cos E_{\odot} \cos \Omega - \sin E_{\odot} \sin \Omega \sin i \quad (10.8)$$

where

$$E_{\odot} = \sin \epsilon \frac{\sin \Omega}{\sin j} \quad (10.9)$$

and

$j$  = inclination of orbit to ecliptic

$L$  = longitude of ascending node in spherical ecliptic coordinates

$L_{\odot}$  = longitude of Sun

$\epsilon$  = inclination of ecliptic to Earth equator

If we define an angle  $\phi$  measured in the orbit plane from perigee to the shadow line, we can write for the true anomaly from perigee to egress and ingress

$$v_1 = \phi - \chi_1 \quad (10.10)$$

$$v_2 = \phi + 180 + \chi_2 \quad (10.11)$$

Using Kepler's mathematical treatment, we obtain for the eccentric anomaly  $E$

$$E = 2 \tan^{-1} \left[ \sqrt{\frac{1-e}{1+e}} \tan \frac{v}{2} \right] \quad (10.12)$$

and for the mean anomaly  $M$

$$M = E - e \sin E \quad (10.13)$$

The time in sunlight becomes

$$T_x = \frac{M_2 - M_1}{360} 100\% \quad (10.14)$$

Orbital elements and the Sun position are time variables; the time in sunlight will change both with the day and the hour of launching. This is used to determine the proper firing window, together with other criteria connected with the mission of the satellite.

The right ascension of the ascending node of the satellite orbit at injection (index o) is

$$\Omega_o = \Omega_{oo} + \sigma_o - 90^\circ + \alpha_\odot \quad (10.15)$$

where

$$\Omega_{oo} = \tan^{-1} [-\sin(\text{Lat}) \tan Z] \quad (10.16)$$

where

$$\sigma_o = \text{hour angle} = 15 (H_o - \sigma)$$

$$\alpha_\odot = \text{right ascension of Sun} = \tan^{-1} [\tan L_\odot \cos \epsilon] \text{ rad}$$

Lat = geocentric latitude

Z = azimuth

The argument of perigee is given by

$$\omega_o = \pi - \tan^{-1} \left[ \frac{\tan \text{Lat}}{\cos(180-Z)} \right] \text{ radians} \quad (10.17)$$

The variation of the orbital characteristics with time after launching is considered by the equations

$$\dot{\Omega} = \dot{\Omega}_o + \dot{\Omega}t \quad (10.18)$$

$$\dot{\omega} = \dot{\omega}_o + \dot{\omega}t \quad (10.19)$$

$\dot{\Omega}$  and  $\dot{\omega}$  are the changes of the orbital elements due to the Earth's equatorial bulge. They are obtained from [11].

$$\dot{\Omega} = -\frac{2\pi}{P} \cos i \left[ 3 \frac{k_1}{\left[ \frac{R_p}{(1+e)} \right]^2} + 10 \frac{k_2}{\left[ \frac{R_p}{(1+e)} \right]^4} \left( 1 + \frac{3}{2} e^2 \right) \left( 1 - \frac{7}{4} \sin^2 i \right) + \dots \right] \quad (10.20)$$

$$\dot{\omega} = \frac{2\pi}{P} \left[ 3 \frac{k_1}{\left[ \frac{R_p}{(1+e)} \right]^2} \left( 1 - \frac{3}{2} \sin^2 i \right) + 10 \frac{k_2}{\left[ \frac{R_p}{(1+e)} \right]^4} \left( 1 + \frac{3}{4} e^2 \right) \left( 1 - 5 \sin^2 i + \frac{35}{8} \sin^4 i \right) + \dots \right] - \dot{\Omega} \cos i \quad (10.21)$$

The motion of the Earth-Sun vector is defined by the longitude,  $L_{\odot}$ , which can be approximated by the series

$$L_{\odot} = k_1 (D + 77) + k_2 \sin [k_1 (D + 77)] + k_3 \sin 2 [k_1 (D + 77)] - (360 - k_4) + \dots \quad (10.22)$$

where

$D$  = days after vernal equinox

$k_1$  = mean motion of Sun = 0.9856 deg/day

$k_2 = 1.9481^{\circ}$ ,  $k_3 = 0.0207^{\circ}$ ,  $k_4 = 281.616^{\circ}$

A digital computer program comprising Eq. (10.5) through (10.22) allows the prediction of time in sunlight conditions throughout the lifetime of a satellite. [12, 13]. Figure 10.1 shows the predicted time in sunlight curve for Explorer 7, and the measured temperatures of the batteries and the 20-Mc transmitter from telemeter recorded through 320 days of operation.

Figure 10.2 shows a predicted temperature curve for Explorer 1 using a computer program based on Eq. (10.1) through (10.4) with results from the time in sunlight determination. The dip in the sunlight portion of the curve is due to the decrease of albedo and infrared radiation from the Earth at the apogee of the satellite orbit. The time in sunlight was 73 per cent.

## 10.2 Dependence of Temperature on Satellite Attitude

The effective areas for the various radiation terms in the energy flux Eq. (10.1) have a strong influence on the temperature. They, in turn, are functions of the satellite attitude.

If the spin axis of the satellite is aligned parallel to the surface of the Earth at the injection point and, as such, aligned with the velocity vector, we can compute the angle  $\gamma$  between the rotational vector to the Sun vector from the dot product of these two vectors

$$\cos \gamma = \vec{S} \cdot \vec{V} \quad (10.23)$$

where the Sun vector

$$\vec{S} = \begin{pmatrix} \cos L_{\odot} \\ \sin L_{\odot} \cos \epsilon \\ \sin L_{\odot} \sin \epsilon \end{pmatrix} \quad (10.24)$$

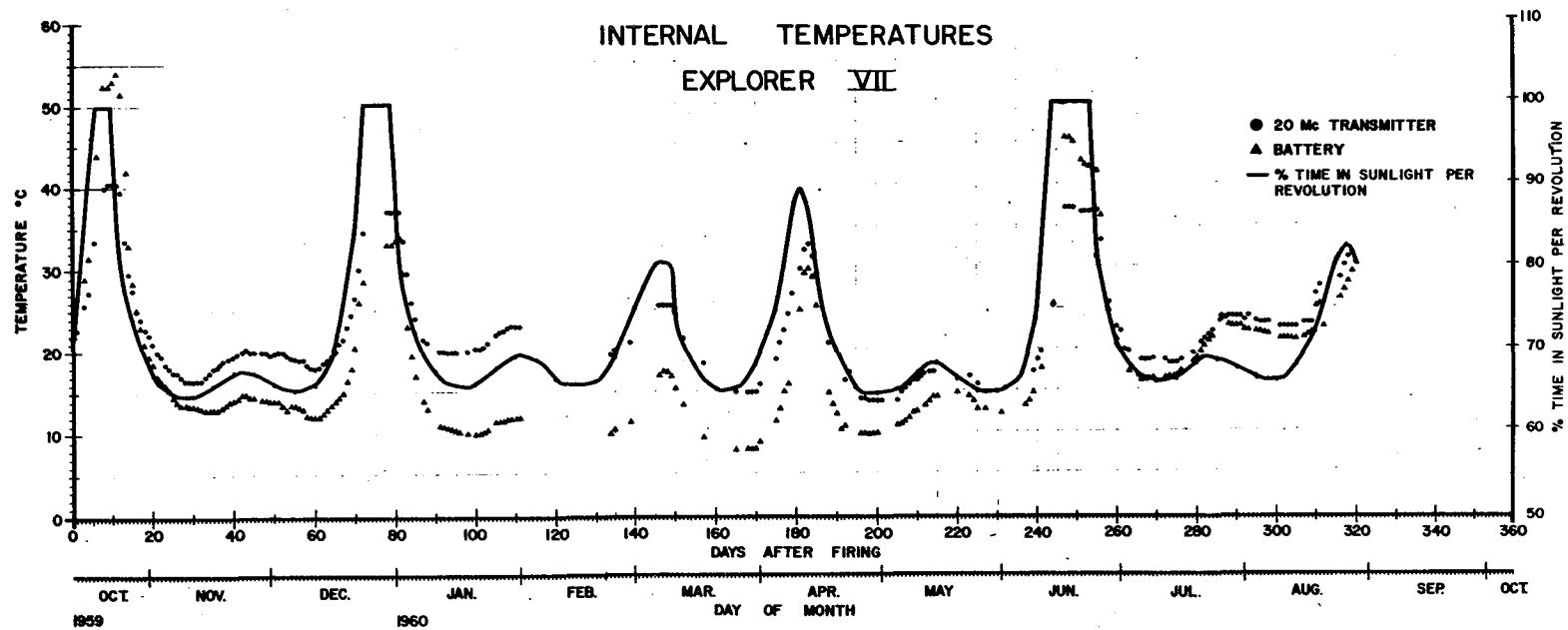


Fig. 10.1 Internal temperature and per cent time spent in sunlight per revolution of Explorer 7.

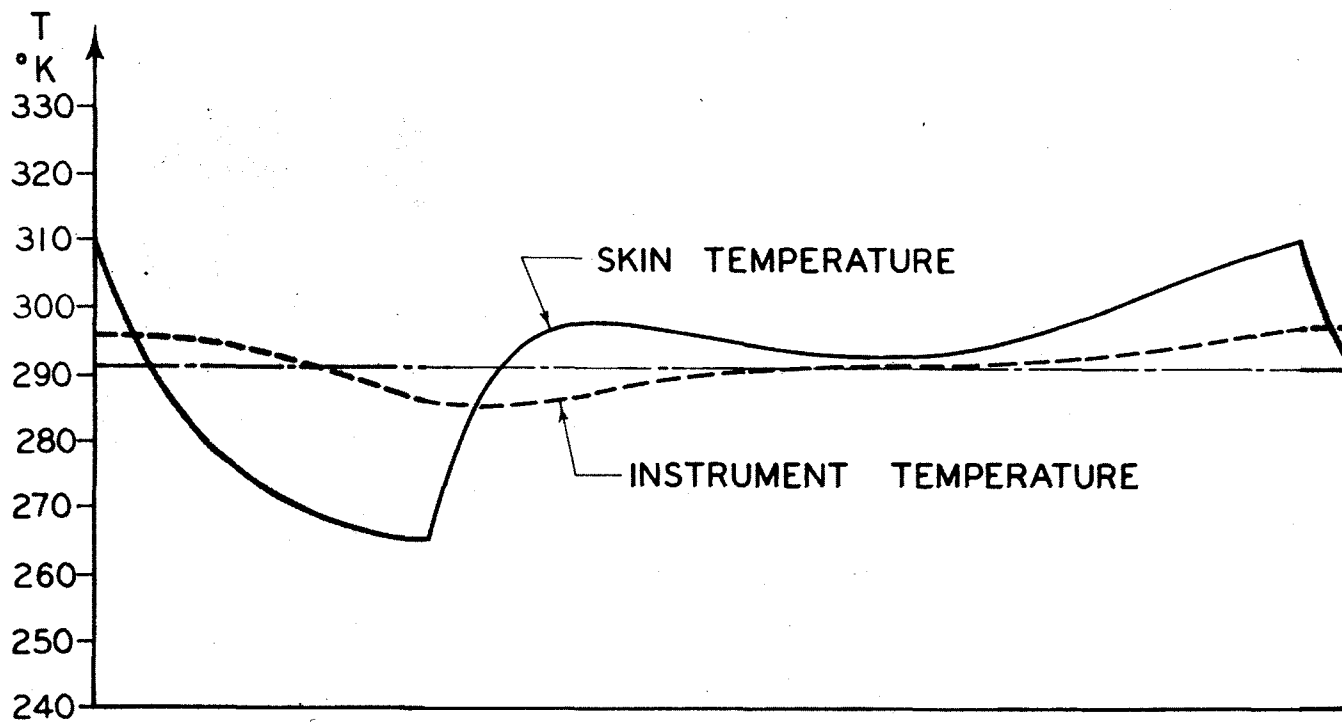


Fig. 10.2 Temperature of Explorer 1 during one sunlight and shadow cycle.

and the initial velocity vector

$$\vec{V} = \begin{pmatrix} -\sin \omega_0 \cos \Omega_0 - \cos i \sin \Omega_0 \cos \omega_0 \\ -\sin \omega_0 \sin \Omega_0 + \cos i \cos \Omega_0 \cos \omega_0 \\ \sin i \cos \omega_0 \end{pmatrix} \quad (10.25)$$

From this,

$$\begin{aligned} \cos \gamma = & \cos L_0 (-\sin \omega \cos \Omega - \cos i \sin \Omega \cos \omega) \\ & + \sin L_0 \cos \epsilon (-\sin \omega \sin \Omega + \cos i \cos \Omega \cos \omega) \\ & + \sin L_0 \sin \epsilon \sin i \cos \omega \end{aligned} \quad (10.26)$$

where

$\omega$  = argument of perigee

$\Omega$  = right ascension of ascending node

$i$  = inclination of satellite orbit to equator

$L_0$  = longitude of Sun

$\epsilon$  = inclination of ecliptic to equator [14].

Explorer 1 had a pencil-like shape and was initially spinning about its longitudinal axis. The initial angle of its axis to the Sun vector was 73 deg. The initial spinning mode was not about a stable axis. However, transition to the stable mode about a transverse axis can only take place if momentum is transferred from one axis to the other, and if the difference in rotational energy is dissipated. Prior to the launching of Explorer 1, it was not predictable when tumbling would start and when a propeller-like mode would finally be reached. The thermal design was based on two extreme cases: (1) spin unchanged, and (2) complete transition to propeller mode. Analysis showed that for case (1) the predicted satellite temperature would drop below 0°C after 45 days, due to the effect of the rotation of the Earth-Sun vector. If transition did not occur prior to this, the batteries were expected to freeze out and terminate the experiment.

Figure 10.3 shows the predicted and measured temperatures for Explorer 1 for cases (1) and (2). An analysis of the decay of the satellite spin rate, using the modulation of the signal strength, determined



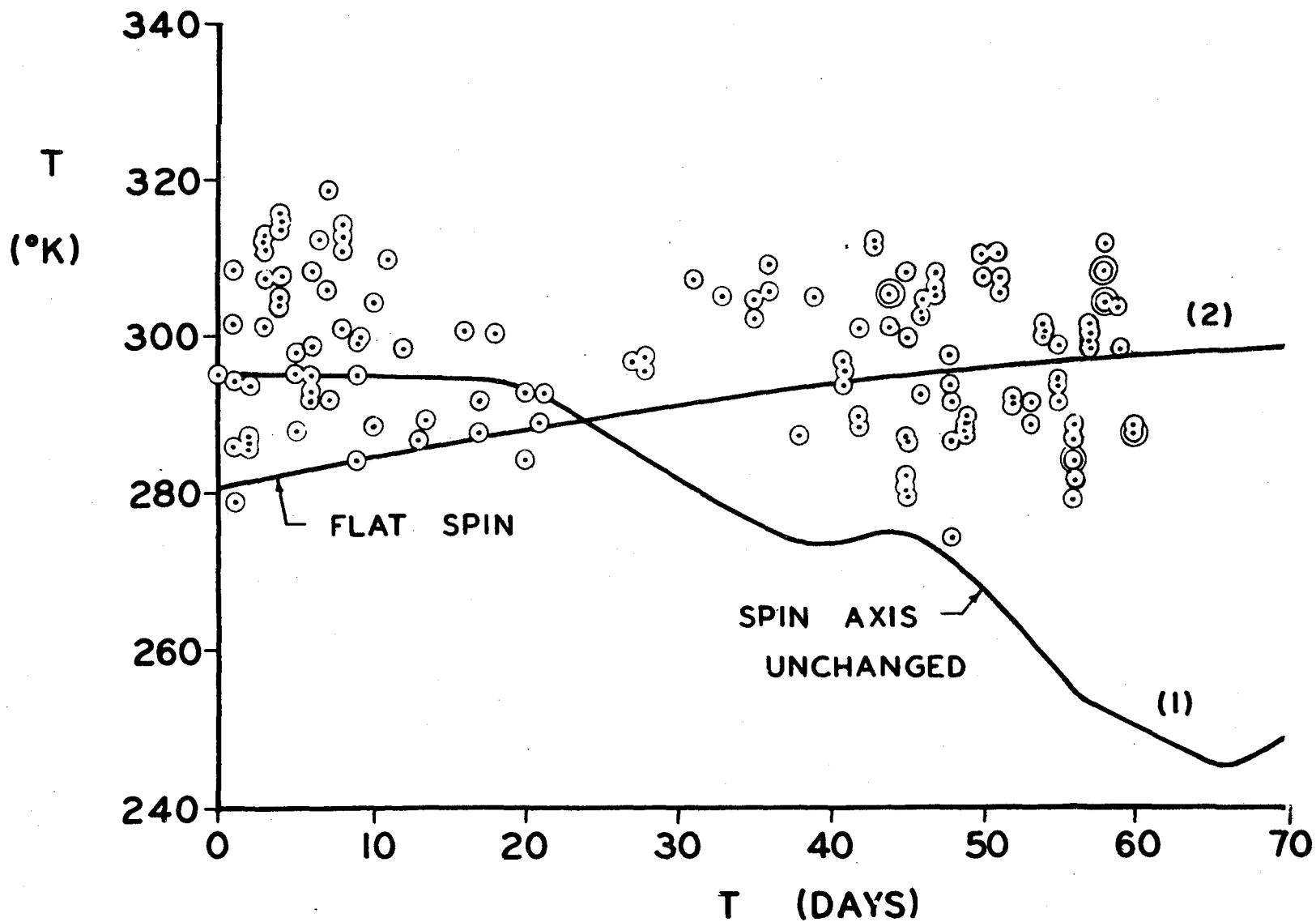


Fig. 10.3 Temperature of Explorer 1 (nose cone instrument temperature).

that the transition to the propeller mode took place during the first two orbits. This is the first example of a correlation between rotation spin modes and satellite temperatures in the Explorer series of satellites.

### 10.3 Analysis of Transition of the Spinning Mode of the Explorer 1-Type Satellites

Explorer 1 had four wire antennas whose flexing provided a plausible mechanism for energy dissipation. A theoretical investigation leads to a second-order linear differential equation for the motion of a mass element under the influence of damping forces, restoring forces due to stiffening and centrifugal forces, and driving forces (i.e., centrifugal and Coriolis).

Based on the work of Wells cited in [17], the differential equation relating the opening angle  $\theta$  of the precession cone to time is

$$\frac{d\theta}{dt} = \frac{P}{L (R-1)^4} \frac{\sin \theta [1 + 2 (R-1) \cos \theta]^2}{[c_1 \cos^2 \theta + c_3]^2 + c_4^2} \quad (10.27)$$

where

$P$  = energy dissipation of antennas per radian of satellite rotation per radian of bending amplitude squared (the value is determined experimentally)

$L$  = angular momentum

$R$  = ratio of transverse to polar moment of inertia

The coefficients are

$$c_1 = 1 + \frac{2}{R-1} - \frac{ml^2}{B} - \frac{\rho l^2}{3B} \quad (10.28)$$

$$c_3 = \frac{\alpha R^2}{Bl (R-1)^2 \omega_0^2} + \frac{1}{(R-1)^2} \quad (10.29)$$

$$c_4 = \frac{2PR^2}{Bl (R-1)^2 \omega_0^2} \quad (10.30)$$

where

$l$  = length of antenna

$m$  = mass of antenna tip

$\alpha$  = stiffness of antenna

$\rho$  = linear density of antenna

$\omega_0$  = initial body-fixed rotation rate

$$B = m(a + 1) + \frac{\rho a l^2}{2} + \frac{\rho l^2}{3} \quad (10.31)$$

with  $a$  equal to the pivot radius of antenna.

Figure 10.4 shows the computed results and some measured angles from Explorer 1. The opening time is  $\infty$  for 0 initial angle. This fact makes an accurate prediction of the opening time difficult unless the initial error angle at satellite injection is known. As Fig. 10.4 shows, the fit between measured and theoretical values is quite good and this correlation, in turn, allows an estimate of the initial angle at  $t = 0$ .

Explorer 3 is similar to Explorer 1 except for elimination of the wire antennas. Energy dissipation is possible due to flexing of the shell and other relative motions inside the satellite. Therefore, the transition of the spinning was slower by about a factor of 100 compared to Explorer 1. Explorer 3 was designed for a mean temperature of 20°C. The firing time was selected such that it went through a cycle of 100 per cent sunlight. Figure 10.5 shows the temperature versus days after launch for 3 cases, i. e., spin unchanged, random attitude, and flat spin [15]. The firing time was selected such that the temperature for the initial spinning mode would stay higher than for all other modes in the 2-month instrumented lifetime. The transmitter ceased to operate after 43 days, which was considered to be caused by battery freeze-out. A destructive hit by a meteoroid is unlikely because the transmitter operated again on the 62nd and 71st days. The signals, however, were too noisy for telemetry. The thawing of the batteries, which requires an increase of temperature above the theoretical curve for the flat spin, could not be explained at that time for Explorer 3, because it would require a change of the rotational momentum vector, and measurements of Explorer 3 did not allow an analysis of this effect.

#### 10.4 Correlation of Satellite Temperature with Attitude Determination

The thermal design of Explorer 4 was based on previous experience. The case of 100 per cent sunlight was excluded; the mean temperature was raised to 38°C, and the satellite was designed to stay in the temperature range of 0° to 60°C, regardless of attitude, provided the transition of the rotational mode occurred during the first 10 to 20 days.

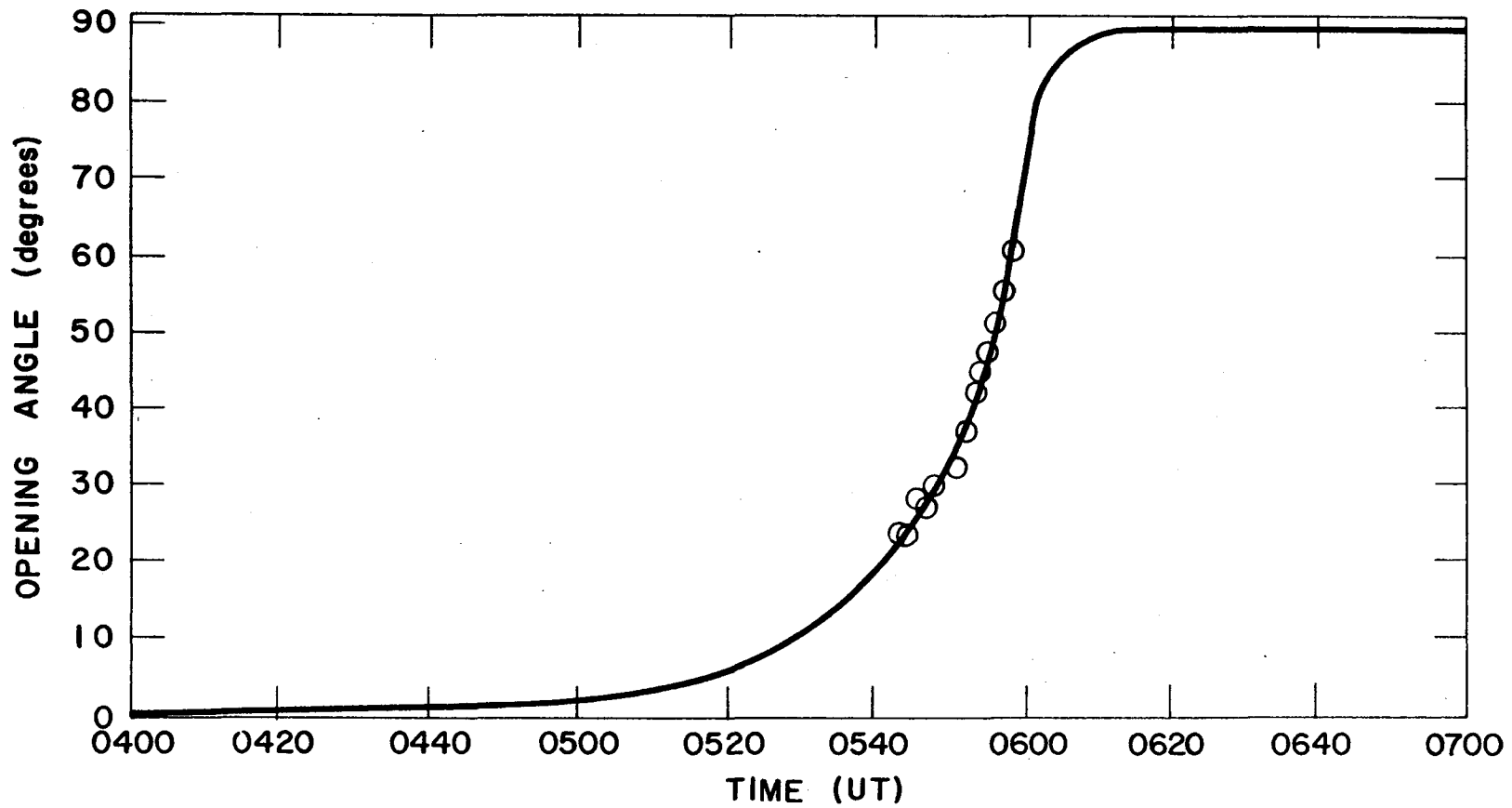


Fig. 10.4 The opening angle of the precession cone of Explorer 1.

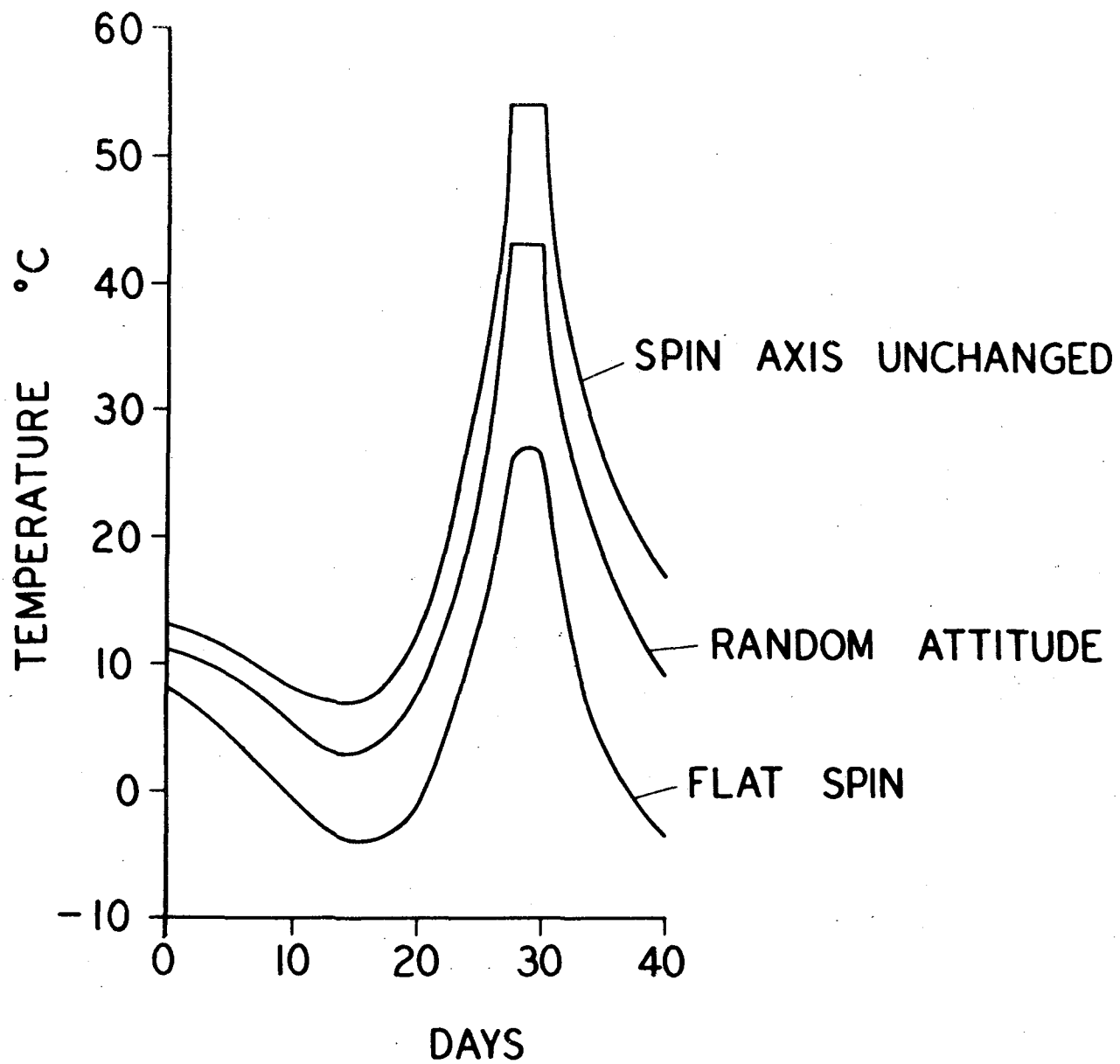


Fig. 10.5 Explorer 3 theoretical temperature versus days after firing for different attitudes.

The temperature sensitivity of the subcarrier oscillator frequency had been calibrated prior to launch. Two sets of useful data were obtained as shown in Fig. 10.6 [17]. Both sets follow the same distinct temperature pattern. The apparent zero shift could be resolved by matching to the initial temperature at satellite injection. It is very close to the arithmetic mean of the two temperature points.

Figure 10.7 shows the measured temperature superimposed on a grid of theoretical temperatures that consider the variation in time of sunlight, orbital characteristics and show the projected area to the Sun as a parameter. For a satellite in a flat spin, the average area can change between 63.7 and 100 per cent.

The initial temperature drop from 322°K to 301°K can be explained by the transition of the spinning mode. However, the changes after this are not compatible with the assumption of a space-fixed rotational momentum vector. The temperature rise between the 6th and 12th day corresponds to a precession of the momentum vector by 10°K per day. This requires torques acting on the satellite of the order of 100 cm.

An independent method for determining the satellite orientation was developed from variations in the signal strength received from the 108.00 Mc microlock transmitter [18] through [23].

Figure 10.8 shows the antenna patterns for the 180.00 Mc and 108.03 Mc transmitters of Explorer 4. It can be seen that the 108.00 Mc antenna has a minor lobe on the side of the nose cone, whereas, the 108.03 Mc antenna shows the typical symmetrical dipole pattern. In both cases the radiation is linearly polarized in a plane containing the symmetry axis. If the satellite is spinning in a propeller-type rotation, the rotational momentum vector is perpendicular to the satellite axis. If viewed along the momentum vector with a linearly polarized receiving antenna, nulls will be observed at twice the frequency of rotation about the lateral moment of inertia. This is due to the rotation of the plane of polarization. On the other hand, the plane of polarization of electromagnetic radiation is also rotated by the Faraday effect resulting from magnetoionic-splitting as the signal traverses the ionosphere. The rotational frequency of the Faraday effect is small at the 108.00 Mc frequency and, therefore, does not seriously affect the observed pattern of signal strength variations.

If the satellite is viewed in the plane perpendicular to the momentum vector, 4 nulls will occur in the 108.00 Mc pattern due to the four-lobed pattern. This effect will occur at angles of the viewing vector to the momentum vector  $\psi$  smaller than 90 deg, but will disappear at  $\psi$  below 20 deg, as can be inferred from Fig. 10.8.

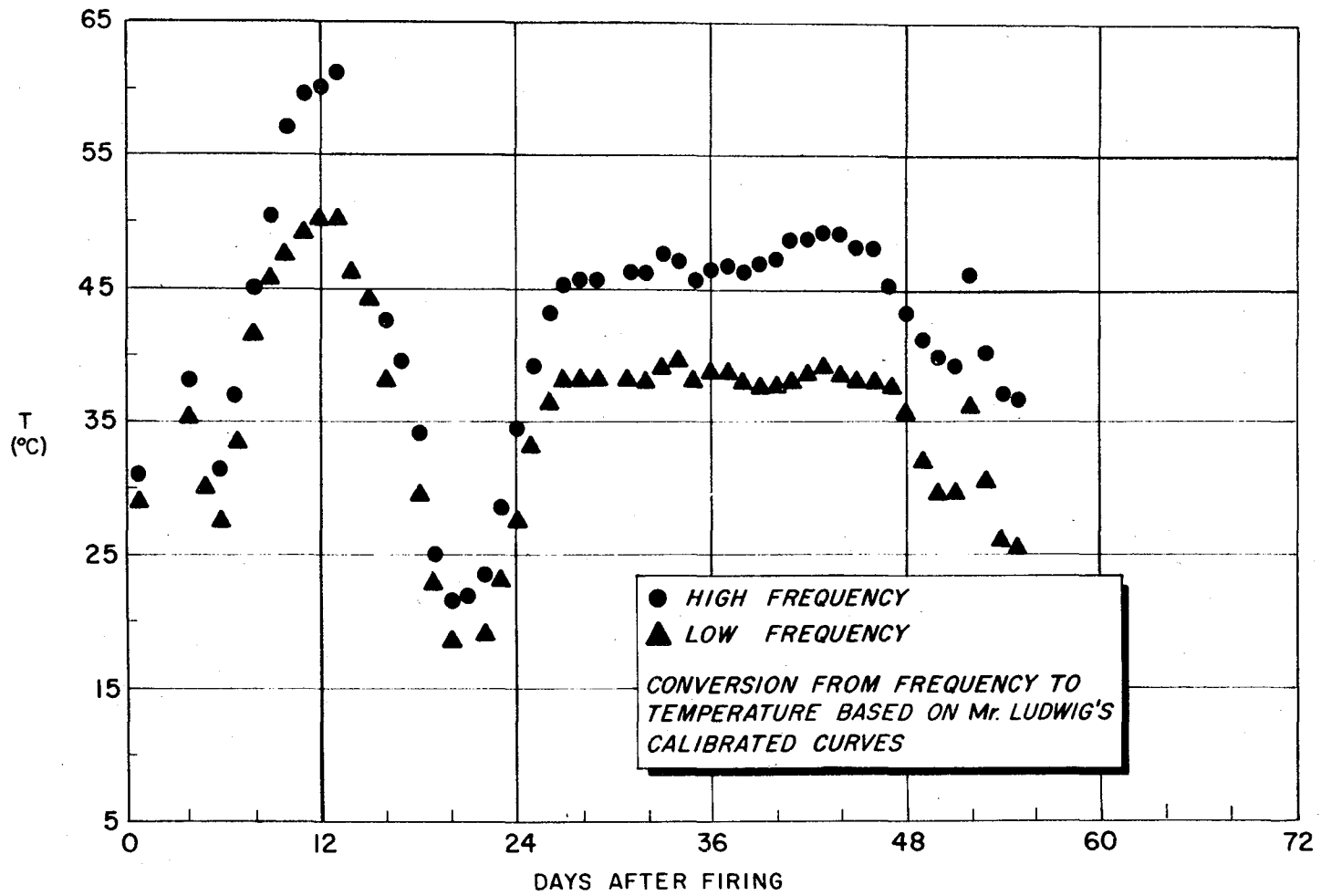


Fig. 10.6 Temperature of Explorer 4 based on channel 3 frequencies received by ABMA tracking station.

# MEASURED TEMPERATURE OF EXPLORER IV SUPERIMPOSED ON THEORETICAL CURVES

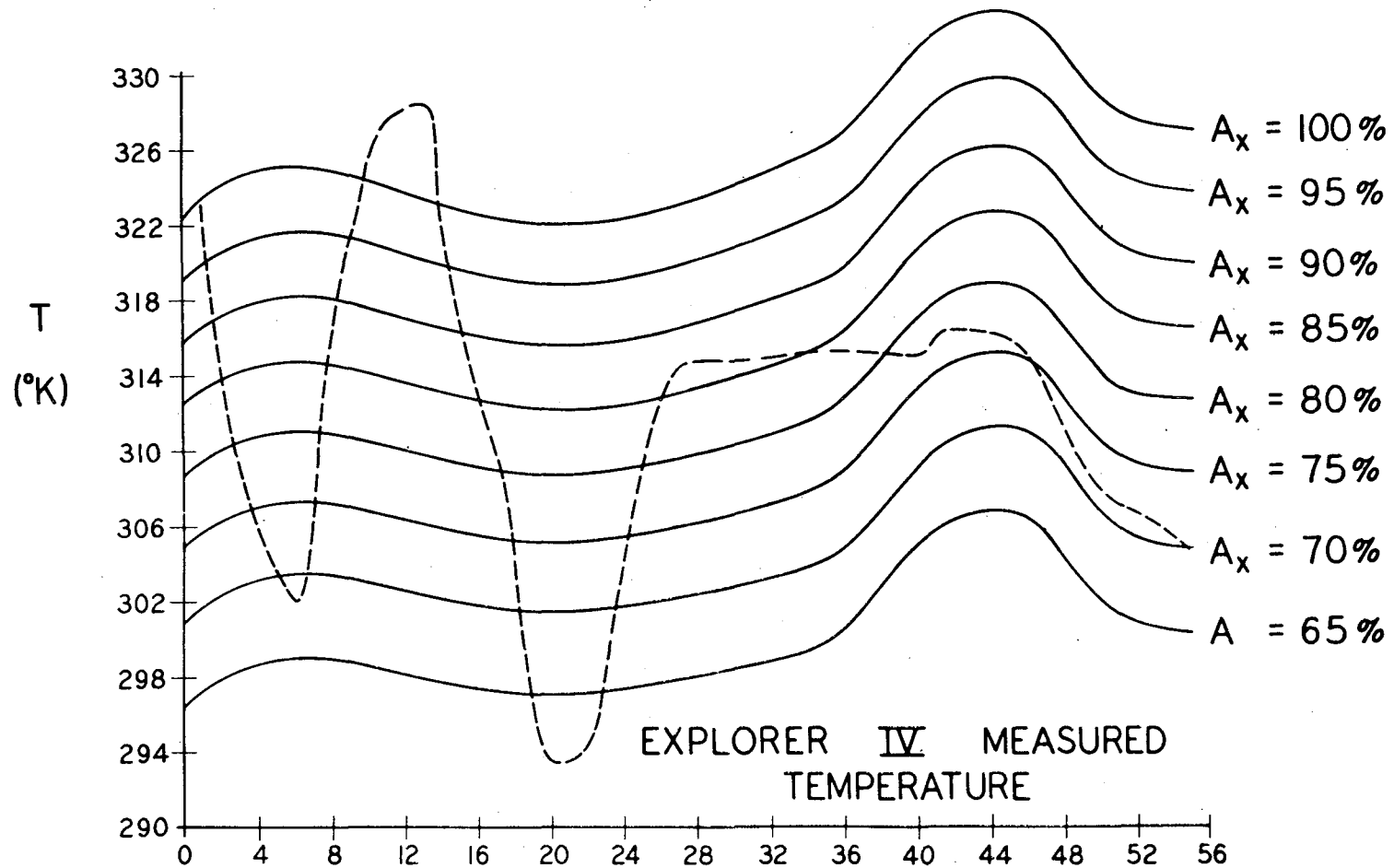
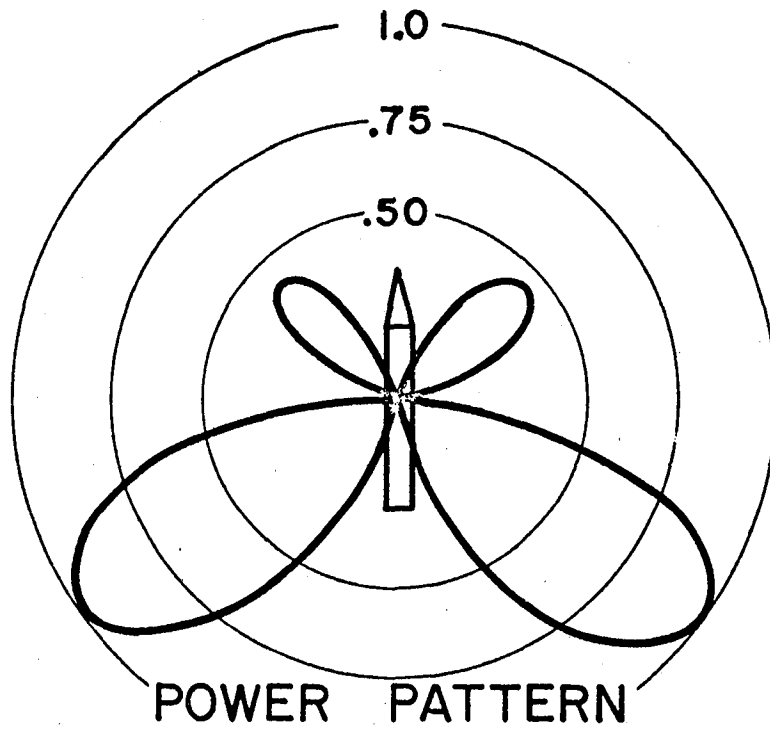
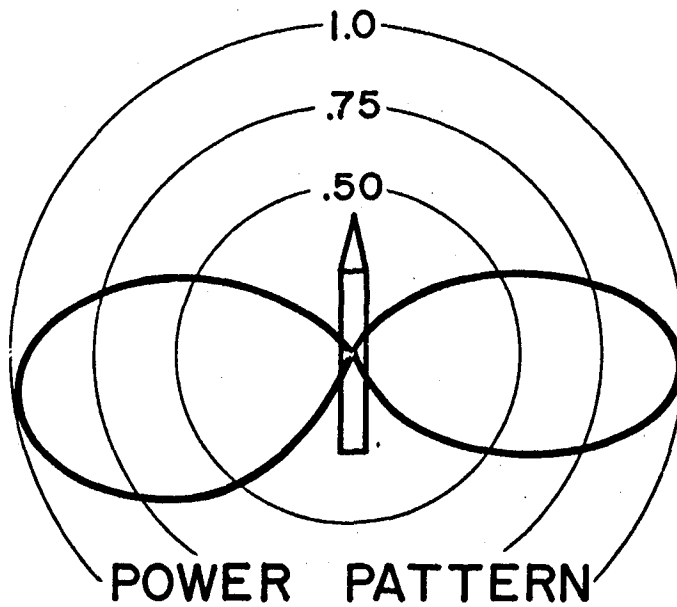


Fig. 10.7 Measured temperature of Explorer 4 superimposed on theoretical curves.





108.00 mc



108.03 mc

Fig. 10.8 Explorer 4 antenna radiation patterns which may be considered figures of revolutions about the longitudinal axis.

By observing the times when the look angle  $\psi$  is less than 20 deg, the rotational momentum vector may be determined as the center of a circle on the celestial sphere defined by the viewing vector when the look angle becomes 20 deg. The viewing vector  $\vec{U}$  is obtained from

$$\vec{U} = \vec{R} - \vec{R}_{st} \quad (10.32)$$

where

$\vec{R}_{st}$  = vector from center of Earth to tracking station

$\vec{R}$  = radius vector of satellite

$\vec{R}_{st}$  is known from the geocentric coordinates of the station and  $\vec{R}$  is found from the geocentric position of the satellite which is listed in 1-min intervals in the Smithsonian Astrophysical Observatory ephemeris. It is convenient to transform the obtained vectors into an Earth-centered, right-handed, space-fixed coordinate system in which the x-axis is in the direction of the vernal equinox and the z-axis in the direction of the north celestial pole. A further transformation into spherical celestial coordinates using right ascension, R.A., and declination,  $\delta$ , allows two-dimensional plotting and correlation to fixed stars on the celestial sphere.

It turned out that the number of passes received by the Huntsville Tracking Station for which  $\psi$  is less than 20 deg was not very great. Because of the rapid changes of the momentum vector inferred from temperature measurements, it was desirable to derive a different method. About 3 weeks after the launching date (July 26, 1958), the Huntsville Tracking Station changed its receiving antenna system from a single dipole array to a combination of two dipole arrays with crossed polarization. The two antenna arrays were mounted separately and placed about 50 m apart. Their outputs were added by a "T" junction and then detected by a single Hallamore receiver. As the satellite passed, the path length to the two antennas changed, and as a consequence, the phase angle between the two antenna outputs changed. This produced an interferometer effect which altered the effective polarization of the receiving antenna. If the two output voltages are in phase, the array is effectively plane polarized at 45 deg to each element. If the phase angle becomes 90 deg, the array becomes circularly polarized. The distance of the antennas was such that the polarization change was usually slow compared to the tumble rate. Several rotations of the satellite could be observed at nearly constant polarization.

The signal strength of the 108.03 Mc transmitter as received by the described array showed different patterns, depending on the range of the viewing angle  $\psi$ . The type of fading observed is summarized in the following table:

<u>Look Angle (deg)</u>	<u>Observed Pattern</u>
0 - 30	No fades when antenna is circularly polarized - polarization fading when antenna is linearly polarized.
30 - 45	Slight fading when antenna is circularly polarized.
45 - 60	Mixture of slight and severe fading due to combination of polarization and antenna nulls.
60 - 75	Predominantly antenna pattern fades, only slightly affected by polarization changes.
75 - 90	Severe fading due entirely to antenna pattern regardless of polarization of the receiving antenna.

It should be pointed out that the look angle  $\psi$  usually varies more than 90 deg during a satellite pass over a station and, therefore, in most cases, all indicated patterns occur. Graphical methods were used to determine the rotational momentum vector from these patterns and from the depth of the nulls. The results are plotted in Fig. 10.9. The correlation between this method and the temperature measurements shows agreement within  $\pm 2^\circ\text{C}$ .

The origin of the torques causing the observed precession has been investigated. A fully acceptable theory has not yet been found to explain these motions. Gravitational torques appear to be an order of magnitude too small. Preliminary calculations indicate that magnetic coupling resulting from a permanent magnetic dipole moment inherent in the satellite may be responsible, but this cannot yet be affirmed.

#### 10.5 Behavior of Satellites Rotating About the Stable Axes of Explorers 7 and 8

Explorer 7 was planned for an instrumented lifetime of 1 year. The thermal design had to consider time in sunlight values between 65 and 100 per cent and any attitude. For a spin-stabilized satellite, this requirement can be achieved by using a nearly spherical shape and a disk-type mass distribution. Interaction with light pressure and with gas molecules, ions, and electrons of the outer atmosphere, are thus minimized. The effects of the Earth's magnetic field are minimized by the use of a fiberglass shell. Any possible current loop was interrupted where practical to prevent, or minimize, induced currents. The firing

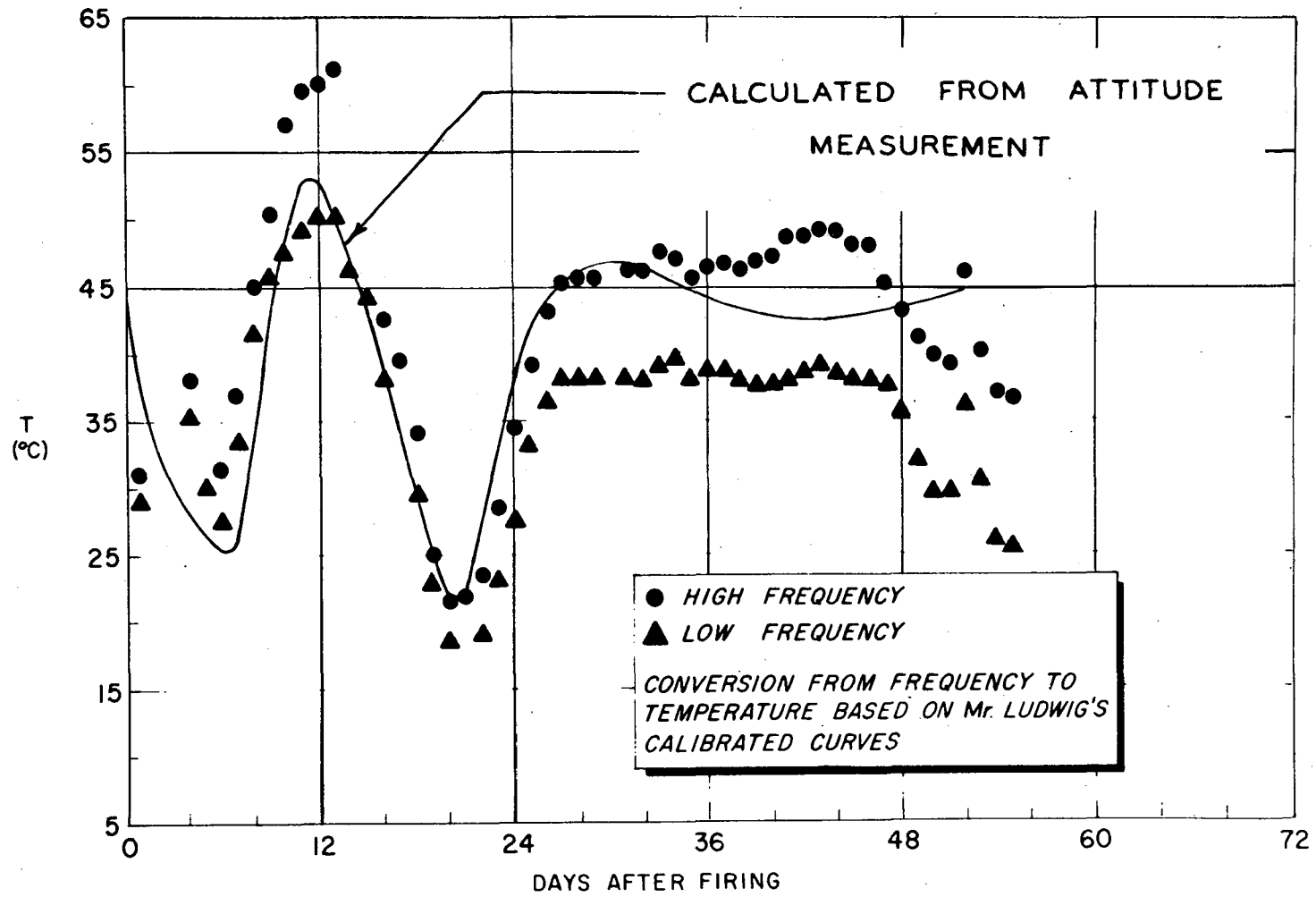


Fig. 10.9 Comparison of temperatures obtained from telemetry and calculated temperatures from attitude measurements.

time was selected such that the angle between the Sun vector and spin axis would never become less than 42 deg, and the minimum angle would not coincide with a 100 per cent sunlight period. Figure 10.1 shows that the internal temperature of the transmitter stayed between 14° and 41° C, and the batteries between 8° and 54° C. Explorer 7 had five temperature sensors in the package and an additional seven temperature sensors connected with the heat balance experiment of Dr. Suomi of the University of Wisconsin.

Attitude information can be derived from the skin temperature measurements and from the temperature differences between the various sensors. Figure 10.8 shows the ratio in count rates which are a measure of the temperatures of a black sensor located on the forward axis of the satellite (B-6), and a black sensor located on the satellite equator (B-1) [24]. Under equal illumination conditions, sensor B-6 is shadowed by various portions of the satellite of the Sun position deviates from the equator toward the rearward by more than 42 deg. A distinct discontinuity occurs if the angle reaches 44.2 deg. This is the angle where the sensor B-6 goes from the partial shadow of the housing to the Van Allen box into the shadow of the solar cell assembly. The count rate goes to zero when B-6 is completely in the shadow. Figure 10.10 shows also for comparison the time in sunlight curve. It can be seen that the variation of  $T_x$  is small and has little influence. This method is very sensitive. It showed that the angle between the rotational momentum vector was the same after 300 days as it was at injection.

The coordinates of the momentum vector were determined by analysis of signal strength measurements [25]. During most passes, the field strength of the 20-Mc transmitter showed very distinct patterns during an interval of 1 min. It had the appearance of a broad maximum with sharply pointed nulls. The nulls were 10 to 15 db deep. The period was constant in the middle of the interval, but changed over larger time periods. The frequency is about one-half cycle/sec and is not connected to the rotational frequency of the satellite which was 6.0 cps. A careful analysis revealed that the fluctuation was due to Faraday rotation. The 20-Mc signals were received by a horizontally polarized Yagi antenna. Since Explorer 7 was equipped with turnstile antennas, the radiation pattern should be omnidirectional. However, the polarization is dependent on the viewing angle. The signal in the direction of the spin axis is circularly polarized, becoming elliptically polarized for any angle deviating from the spin axis until at an angle of 90 deg the waves are plane polarized. A plane-polarized wave may be considered as two components: the ordinary wave and the extraordinary wave. These two waves rotate in opposite directions and differ in their interaction with a conducting medium such as the plasma of the ionosphere. A phase angle develops between the two waves which are directly proportional to the total amount of electrons between the

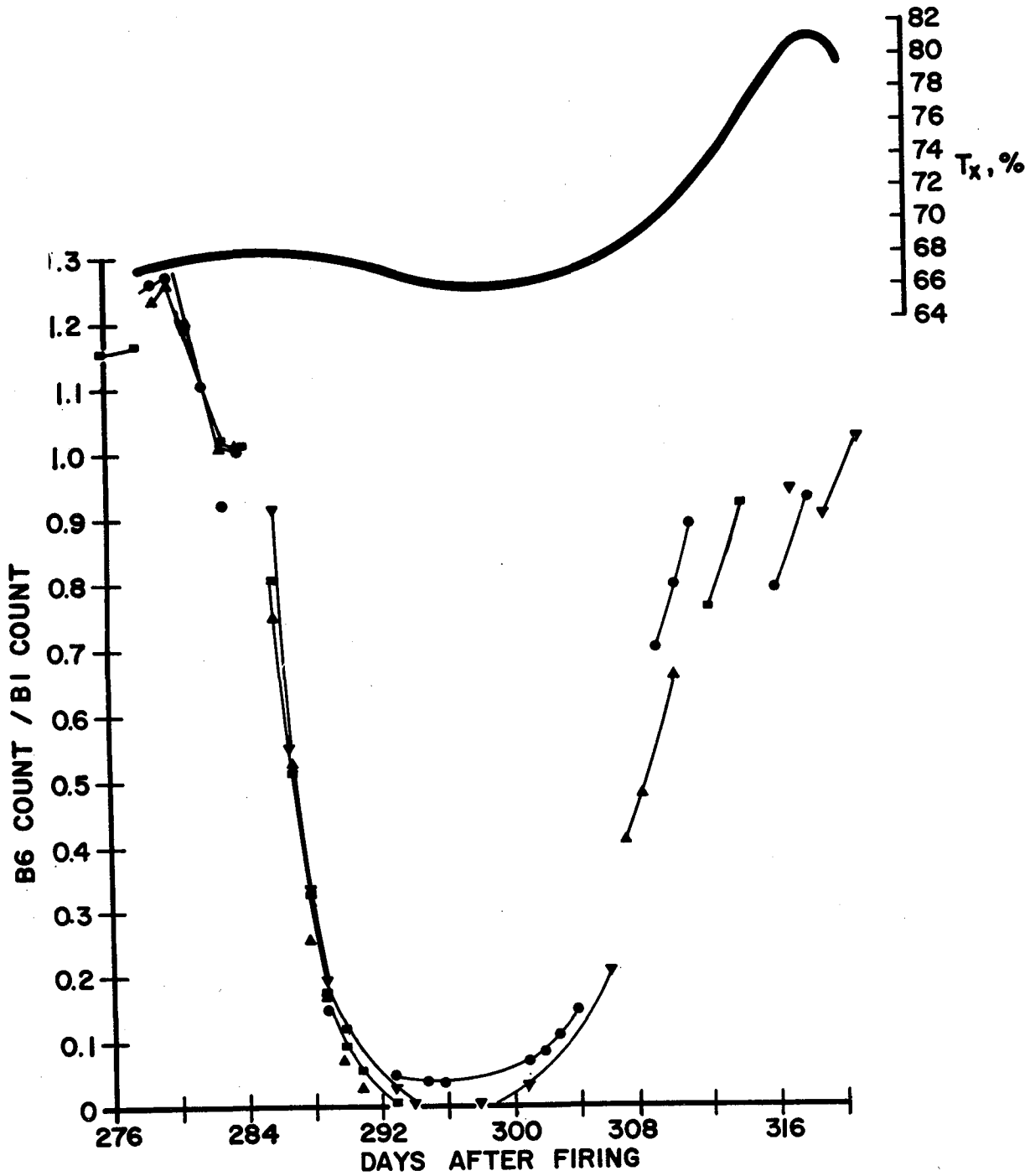


Fig. 10.10 Count ratio of black sensors B6 on spin axis and B1 on satellite equator during period of maximum Sun angle.

observer and the source of radiation. It is, therefore, a function of the relative motion of the satellite with respect to the ground antenna. A maximum received field strength is obtained when the major axis of the polarization ellipse is parallel with the plane of the receiving antenna; a minimum occurs when the minor axis is parallel to the receiving antenna. Thus, by comparing the ratio of maximum to minimum signals during a Faraday rotation, the ratio of the axes of the polarization ellipse is found. From the previous discussion, it follows that this axis ratio is determined by the look angle  $\psi$ .

The method of determining the look angle directly from the depth of the null is not very accurate because of the uncertainties in propagation effects and receiver calibration. However, as discussed previously, the deepest null is expected when the satellite is viewed from its equator. The time of the cross-over of the view vector over the satellite equator can be found from comparison of a whole series of nulls and is fairly accurate. The line-of-sight vector is obtained by subtracting the station coordinates in a space-fixed system from the satellite position coordinate computed in the same coordinate system. If we use the customary Cartesian coordinate system with the x-axis in the direction of the vernal equinox, we can write for the right ascension R.A.

$$\text{R.A.} = \tan^{-1} \frac{U_y}{U_x} \quad (10.33)$$

and for the declination

$$\delta = \sin^{-1} U_z \quad (10.34)$$

where  $U_{xyz}$  is the space-fixed line of sight vector.

Each of these vectors determines a point on the celestial sphere corresponding to the satellite equator projected on the celestial sphere. The rotational momentum vector is at 90 deg from any point of this circle and is determined by a graphical best fit to the observed points. The point found is given by the following spherical equatorial coordinates

$$\text{R. A.} = 305 \text{ deg} \pm 5 \text{ deg}$$

$$\delta = 32 \text{ deg} \pm 2 \text{ deg}$$

It coincides within the measuring accuracy range with the initial velocity vector at injection into orbit, and it did not change within this range during the first 4 months of operation. The ambiguity into which hemisphere of the celestial sphere the momentum vector is pointing is easily resolved by the condition at injection.

Additional determinations of the attitude of Explorer 7 were made from solar cell output measurements, from solar cell temperatures, and from differences between the temperatures of the instrument compartment and the batteries [24, 26]. Since the rotational momentum vector did not change measurably throughout the first year of operation, the Sun vector oscillated nearly sinusoidally around the equator. Figure 10.11 shows the attitude of the Sun with respect to the satellite equator and the difference between measured internal temperatures. It is significant that the maximum temperature difference maintained by an internal heat flux through the spokes connecting the battery housing with the instrument column is 10.2°C. It can be seen that this maximum coincides with the maximum attitude angle of the Sun with respect to the satellite equator.

The thermal design of Explorer 8 had some unique problems [12, 27]. The firing time was determined mainly by thermal considerations. It was desirable to avoid rapid changes of the instrument temperatures, and to maintain the temperature within 0° and 50°C throughout the instrument lifetime. The firing time was selected such that 100 per cent sunlight would occur only in the last 10 days of the 60-day lifetime. The shell of Explorer 8 was similar in shape to Explorer 7, but consisted of aluminum alloy with a sandblasted surface. Results of emissivity tests obtained 4 weeks prior to firing indicated a ratio of emissivities  $\epsilon_1$  to  $\epsilon_2$  to be too high. The satellite temperature would exceed the upper limit of 50°C. The surface chosen and finally applied 1 week prior to the launching was a combination of a conductive silver paint of an emissivity ratio of  $\epsilon_1/\epsilon_2 = 0.33/0.47$  and a red iron oxide paint with an emissivity ratio of  $\epsilon_1/\epsilon_2 = 0.73/0.80$ . Since the iron oxide paint was nonconductive, it could not be applied in one coherent surface. Some of the sensors mounted in the satellite surface for ionosphere measurements required an equipotential surface. The red paint was, therefore, applied in a pattern of square dots whose sides were smaller than the Debye length in the ionosphere, which is of the order of magnitude of a few centimeters.

Unlike Explorer 7, the ionosphere satellite (Explorer 8) was affected by external forces and changed its rotational momentum vector. According to Bordeau, Donley, and Whipple [28], the torques were due to the interaction of the satellite with the Earth's magnetic field. However, no quantitative correlation and comparison of their effects with temperature variations have yet been established.

Temperature measurements made on board the satellite (Fig. 10.12) indicate that the temperature remained well within the 0° to 50°C range.



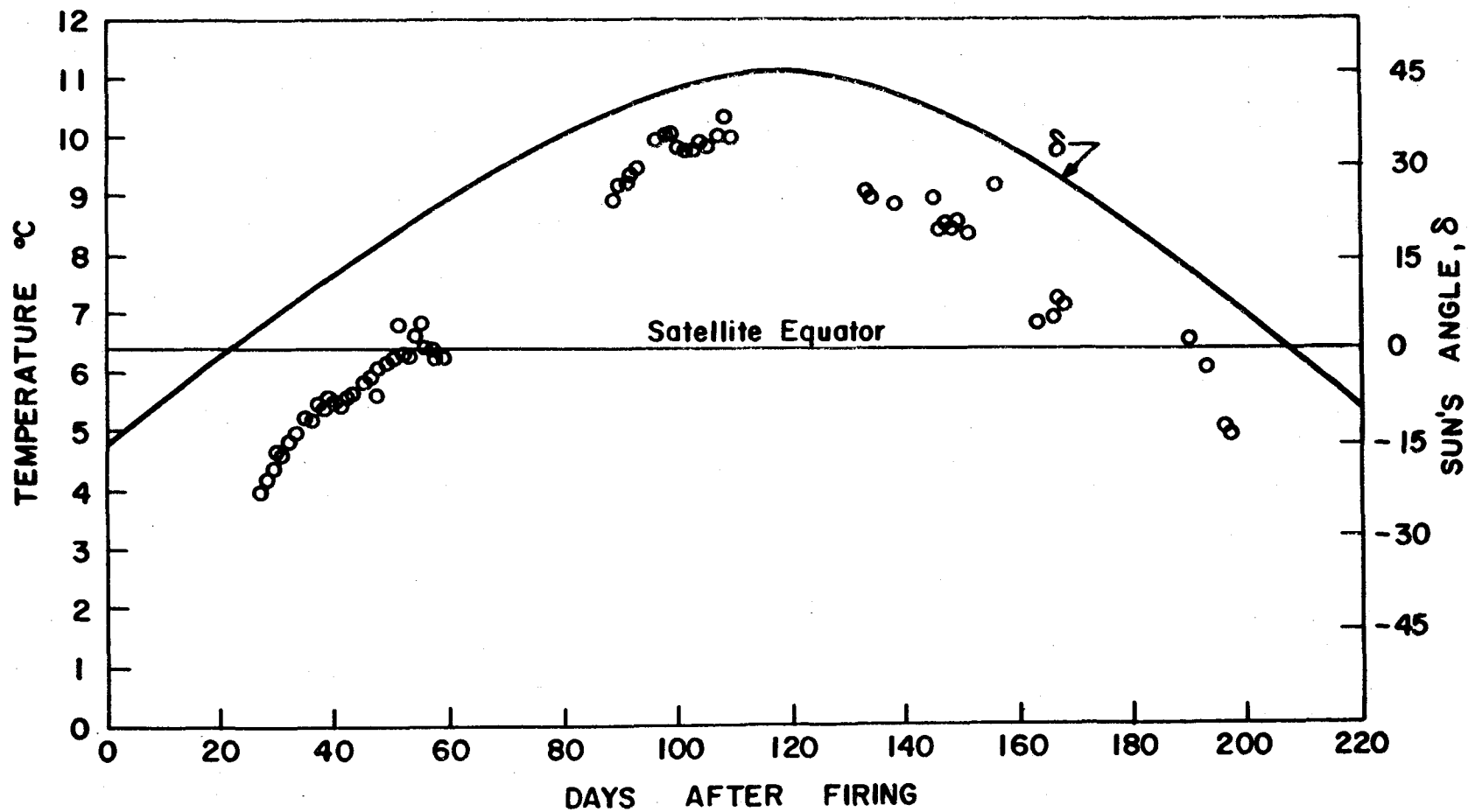


Fig. 10.11 Difference between the temperature of the instrument compartment and the batteries.

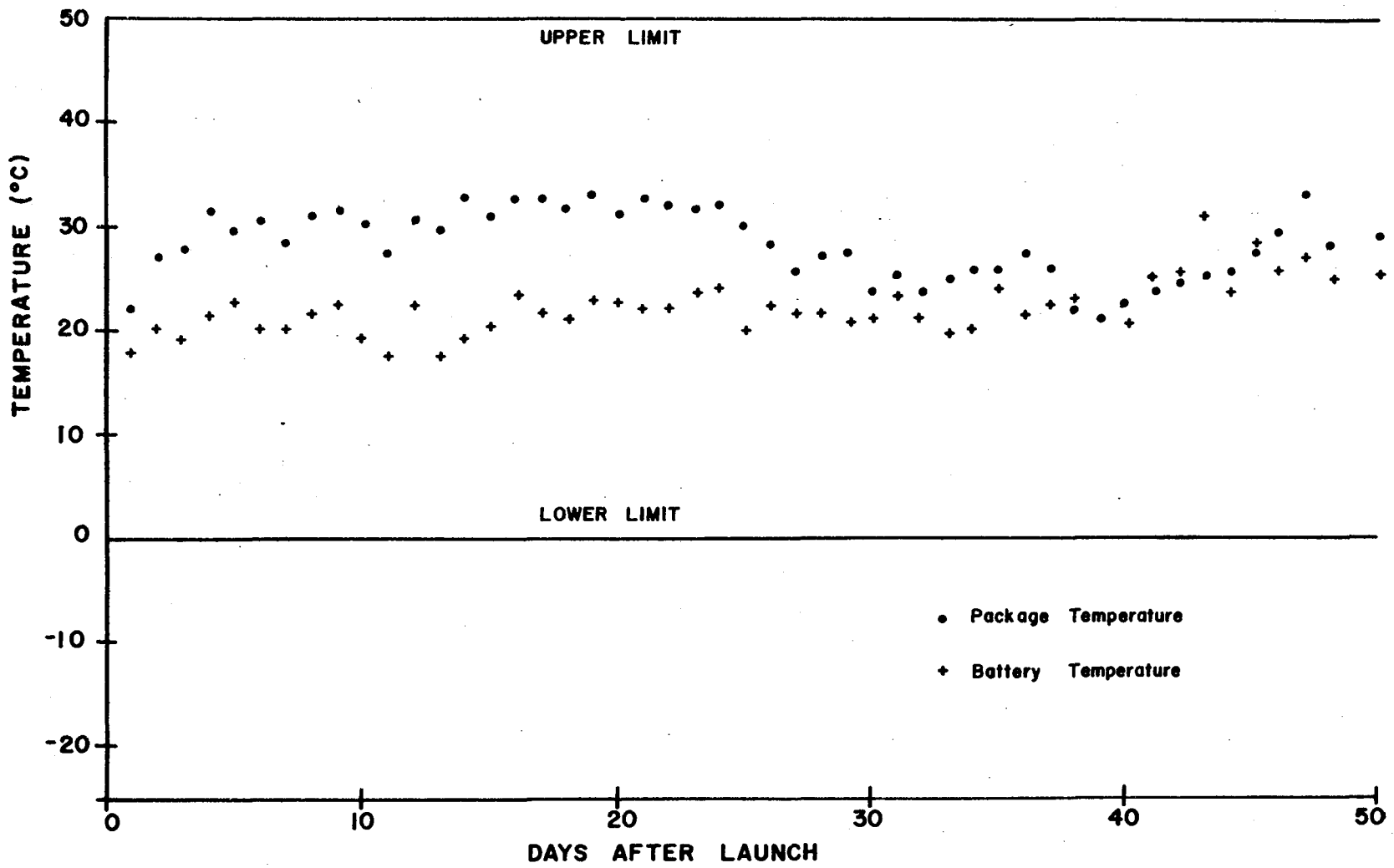


Fig. 10.12 Instrumental package and battery temperature versus days after launch for S-30.

## 10.6 Explorer 11

Figure 10.13 shows the configuration of the Explorer 11 gamma ray telescope satellite (S-15), which was launched by a Juno 2 on April 27, 1961. It is solar cell-powered with an expected instrument lifetime of 1 year.

This satellite shows a number of interesting aspects from the thermal design viewpoint [29]. Like Explorers 1 through 5, it is spin-stabilized about an axis with the least moment of inertia. A transition to a flat spin was supposed to be effected in the first 4 days of orbiting by a damper containing mercury [30]. It could be expected that the spin about the longitudinal axis would be damped out completely, eliminating the equalizing effect of the rotation; this, in turn, could cause strong temperature gradients up to 120°C between sunlit and dark surfaces.

The instrument lifetime of 1 year made it necessary to design the payload for variation of the time in sunlight between about 65 and 85 per cent. The initial goal for the temperature limit was 0° to 50° C, however, the limit was extended to the range 0° to 60°C because of the imposed requirements. The thermal design based on these requirements and the ground testing of the payload is described in [29].

## 10.7 Results

Explorer 11 has eight temperature measurements, their purpose being to monitor the functioning of the on-board equipment. A special thermally isolated disk was to determine the long-time behavior of a surface with a high emissivity ratio  $\epsilon_1/\epsilon_2$  of about 8 in the space environment. Results are still preliminary and have to be analyzed further.

Figure 10.14 shows the temperatures in the MIT instrument compartment and the MSFC package. The steep decrease at the beginning was completely unexpected and was caused by two events:

1. The satellite maintained its initial spin axis for about 14 days before it started to tumble.
2. The satellite changed its rotational momentum vector such that the satellite axis came very close to the Sun vector.

The case in which the satellite tip points toward the Sun results in a temperature drop to less than -40°C and is not covered by the thermal design. The later maximum of the temperature was caused by the Sun becoming perpendicular to the axis of the satellite and the orbit passing through a situation of maximum per cent in sunlight. During this maximum, the payload went into flat spin and the temperature fluctuations were greatly reduced from this point on. The analysis of

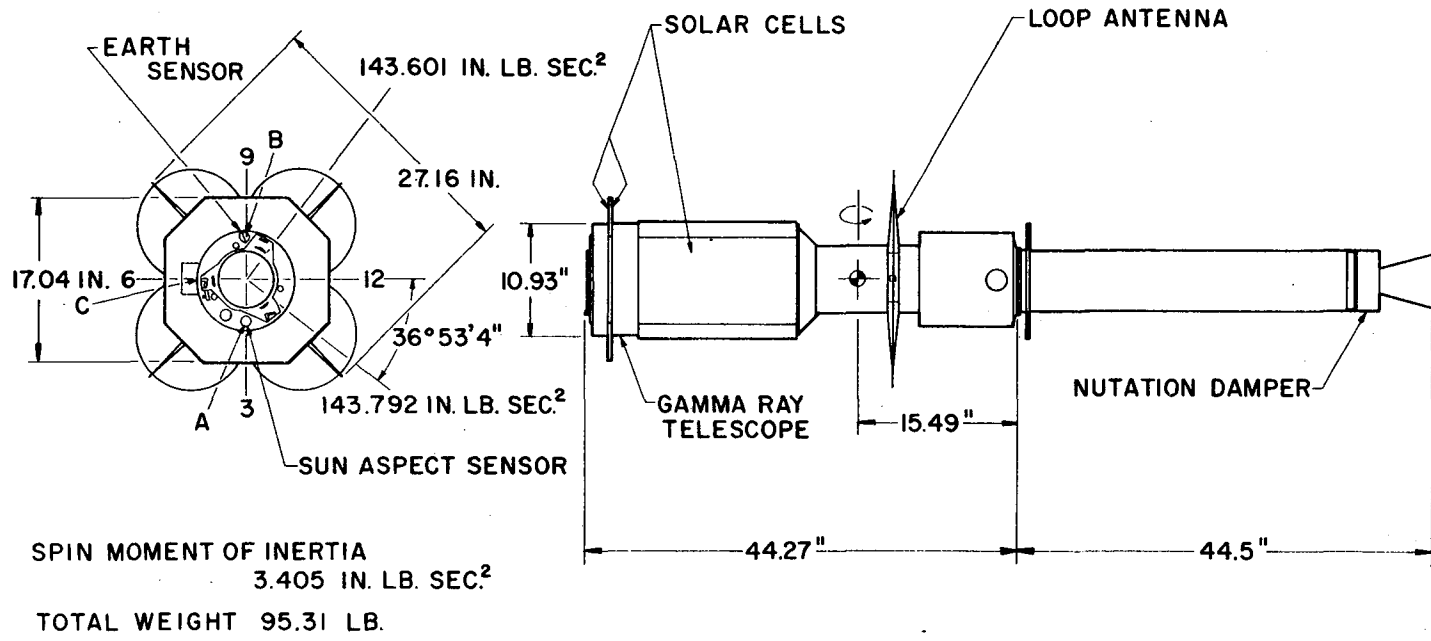
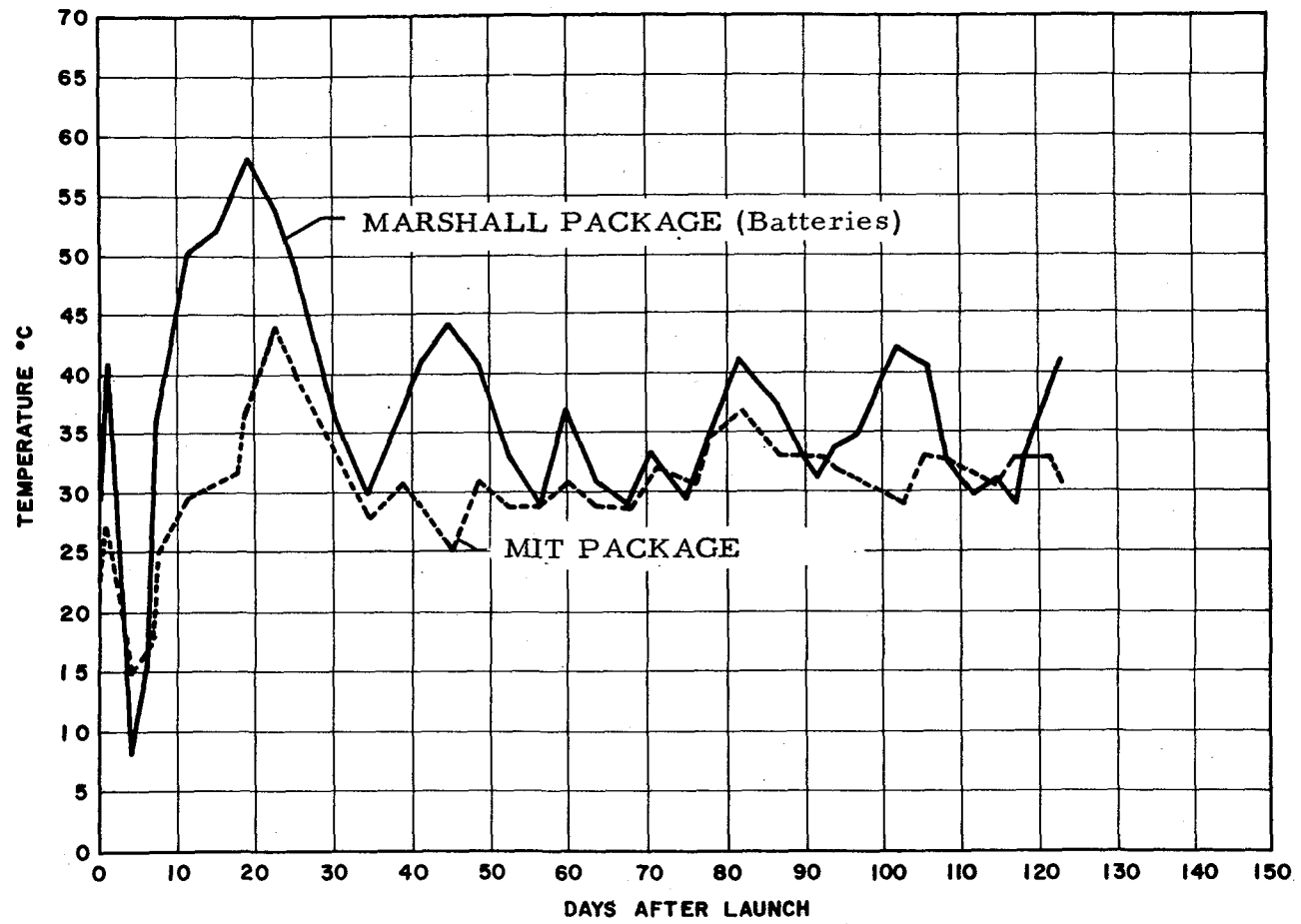


Fig. 10.13 S-15 configuration.



Fig, 10.14 Measured temperatures of payload S-15 (Explorer 9).

rf signal strength from Explorer 11 again furnished an independent method for correlating the thermal behavior [31, 32]. Two features of the antenna pattern (Fig. 10.15) are significant for the analysis:

1. The forward lobes are 6 db lower than the major lobes.
2. The side nulls between the forward and rearward lobes are 74 deg from the symmetry axis. The signal as received by a steerable array of helices on the Green Mountain Station in Huntsville, Alabama, is not affected by polarization effects. This fact is important because signal nulls can be clearly linked with the geometry of the antenna lobes.

The nose lobe can be recognized because its ratio to a half cycle is 0.41, if the look angle  $\psi$  is 90 deg.

In a coordinate system, defined such that the angular momentum vector is along the z-axis and the viewing vector  $\vec{u}$  is in the x-z plane, the viewing vector may be expressed by

$$\vec{u} = \begin{pmatrix} \sin \psi \\ 0 \\ \cos \psi \end{pmatrix} \quad (10.35)$$

The satellite symmetry axis  $\vec{A}$  is given by

$$\vec{A} = \begin{pmatrix} \cos \emptyset \sin \alpha \\ \sin \emptyset \sin \alpha \\ \cos \alpha \end{pmatrix} \quad (10.36)$$

where  $\emptyset$  is the angular displacement of the x-y projection of  $\vec{A}$  from the x-axis, and  $\alpha$  is the opening angle or the half angle of the precession cone.

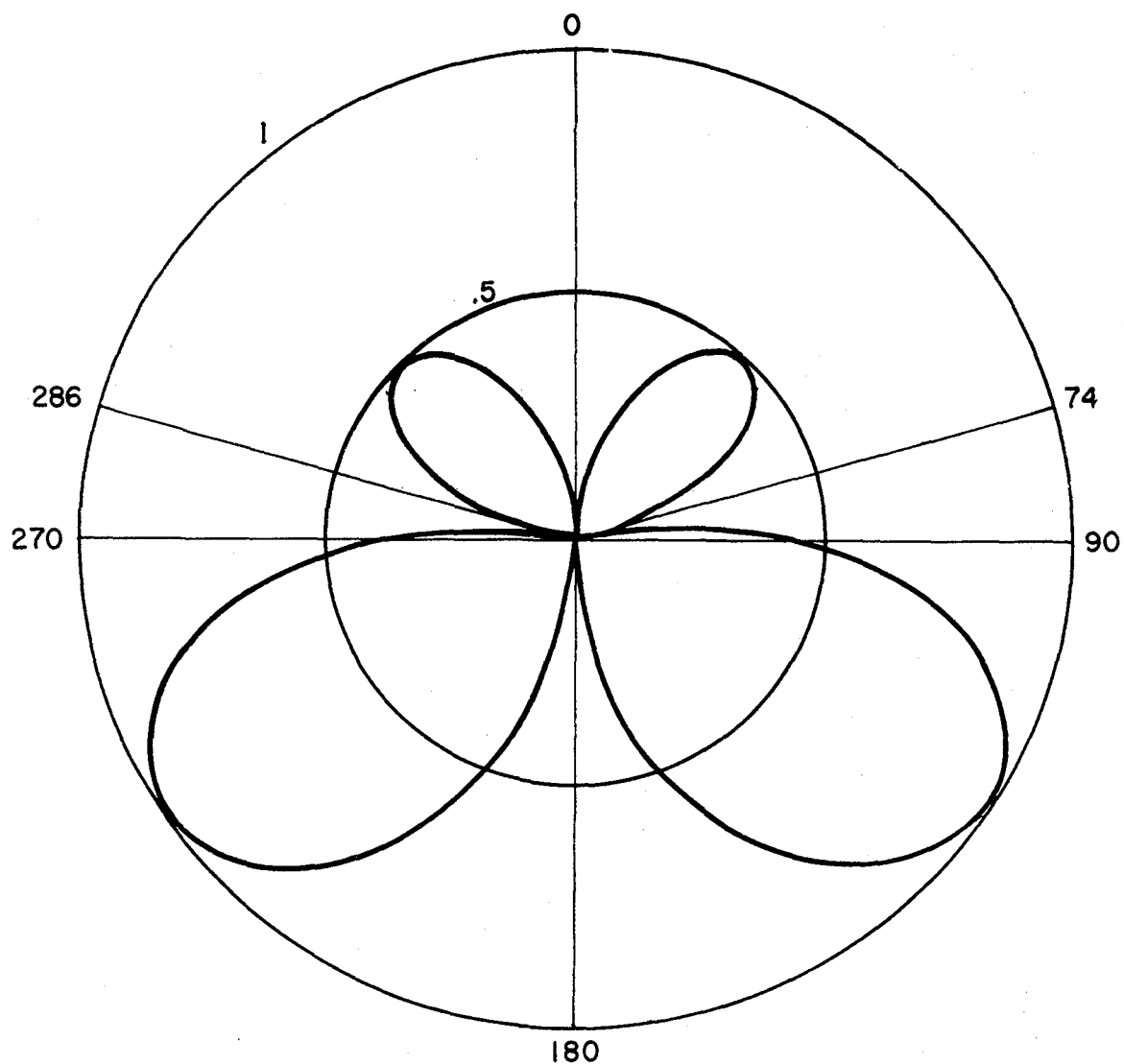
When the side null is observed, the vector  $\vec{A}$  must be

$$\cos 74 \text{ deg} = \vec{A} \cdot \vec{u} \quad (10.37)$$

or

$$\cos 74 = \sin \psi \cos \emptyset \sin \alpha + \cos \psi \cos \alpha \quad (10.37a)$$

This equation has the three unknowns  $\psi$ ,  $\emptyset$ , and  $\alpha$ . The opening angle can be considered a constant during any pass. The angle  $\emptyset$  can be determined from the measured time of the nose lobe compared to a half cycle. The equation can then be solved for cases where  $\psi = \alpha$ . This occurs when during a pass the nose or tail points toward the station. In analyzing the signal strength records, it is only necessary to look for the deep nulls connected with this situation. Both  $\psi$  and  $\alpha$  are determined this way. Since the opening angle  $\alpha$  is practically a constant during a pass, further analysis of the other portions of the



ANTENNA RADIATION PATTERN FOR  
TRACKING TRANSMITTER (108.06 MC)

Fig. 10.15 Polar plot of S-15 antenna radiation pattern for the 108.06 Mc tracking beacon.

record allow the determination of a series of  $\psi$  values from the record of such a pass. From the two or more values of  $\psi$  and the corresponding viewing vectors  $\underline{u}$  the orientation of the rotational momentum vector  $\underline{L}$  may be found from

$$\begin{aligned} u_1 \cdot L &= \cos \psi_1 \\ u_2 \cdot L &= \cos \psi_2 \\ &\vdots \\ u_i \cdot L &= \cos \psi_i \end{aligned}$$

and  $|\underline{L}| = 1$

The method has the advantage that the relative time intervals between nulls can be determined with between accuracy than the relative depth of nulls. Many redundant determinations can be used for a least square fit. Figure 10.16 shows the result of a determination. The intersection of the rotational momentum vector with the celestial sphere is plotted in spherical equatorial coordinates. The investigation of the torques causing the change of the direction of the angular momentum vector continues.

#### REFERENCES

1. Heller, G., The Explorer, in "Ten steps Into Space", Monograph No. 6, Franklin Institute, Philadelphia, 1958.
2. Heller, G., Thermal Problems of Satellites, Rept. DV-TN-73-58, Army Ballistic Missile Agency, Huntsville, Alabama, September, 1958.
3. Heller, G., Thermal Control of the Explorer Satellites, ARS Journal, 30:344 (April, 1960).
4. Heller, G., and B.P. Jones, Thermal Properties of Explorer VII, Chap. 6, TN-D-608, Juno II Summary Project Report, National Aeronautics and Space Administration, Huntsville, Alabama, July, 1961.
5. Snoddy, W.C., Temperature Control of the S-30 Payload (Explorer VIII), Rept. MTP-RP-61-14, NASA-Marshall Space Flight Center, Huntsville, Alabama, August, 1961.
6. Jones, B.P., Same Ordinary Differential Equations Associated with the Thermal Problems of Space Vehicles, Rept. M-RP-INT-1-60, NASA-Marshall Space Flight Center, Huntsville, Alabama, November, 1960.



DECLINATION (DEG)

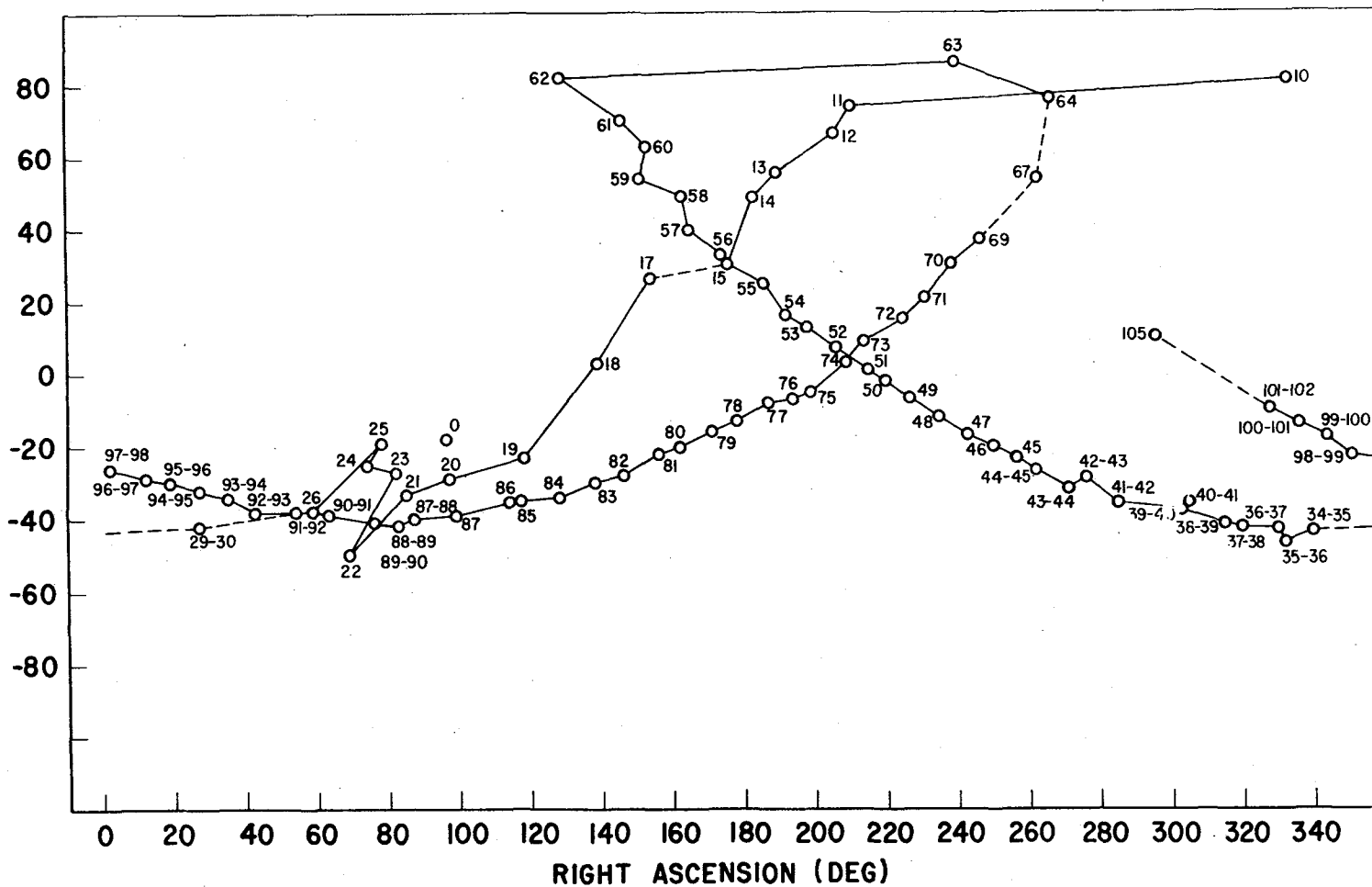


Fig. 10.16 The observed excursion of the momentum axis in celestial coordinates with the days after launch as a parameter.

7. Snoddy, W.C., Theoretical and Measured Temperatures of Explorer IV, Rept. No. DV-TN-6-59, Army Ballistic Missile Agency, Huntsville, Alabama, March, 1959.
8. Heller, G., Problems Concerning the Thermal Design of Explorer Satellites, IRE Transactions on Military Electronics, MIL-4: 98 (April-May, 1960).
9. Snoddy, W.C., Theoretical Orbital Temperatures of IGY Satellite No. 16, Rept. No. DV-TN-18-59, Army Ballistic Missile Agency, Huntsville, Alabama, June, 1959.
10. Jones, B.P., Thermal Design Tests of the IGY Satellite (Payload for Missile No. 16), Rept. No. DV-TM-23-59, Army Ballistic Missile Agency, Huntsville, Alabama, August, 1959.
11. Krause, H. G. L., The Secular and Periodic Perturbations of the Orbit of an Artificial Earth Satellite, in VII th International Astronautical Congress Proceedings, Associazione Italiana Razzi, Rome; 1956.
12. Informal data on Theoretical Temperature Program on IBM 7090 for S-30 Payload (19-D), generated by W.C. Snoddy, September, 1960.
13. Snoddy, W.C., Calculations Concerning the Passage of a Satellite Through the Earth's Shadow, Rept. No. MTP-RP-61-1, NASA-Marshall Space Flight Center, Huntsville, Alabama, February, 1961.
14. Cochran, D., Attitude of the Spin Axis of Satellites with Respect to the Direction of the Sun, Rept. No. DV-TN-11-59, Army Ballistic Missile Agency, Huntsville, Alabama, March, 1959.
15. Heller, G., and B.P. Jones, A Comparison of Experimental and Theoretical Temperatures of Explorer III, Rept. No. DV-TN-76-58, Army Ballistic Missile Agency, Huntsville, Alabama, October, 1958.
16. Snoddy, W.C., Theoretical and Measured Temperatures of Explorer IV, Rept. No. DV-TN-6-59, Army Ballistic Missile Agency, Huntsville, Alabama, March 1959.
17. Pilkington, W.C., Vehicle Motions as Inferred from Radio Signal Strength, Extension Report No. 51, Jet Propulsion Laboratory, California Institute of Technology, Pasadena, California, September, 1958.

18. Naumann, R.J., Attitude Determination of Explorer IV, Rept. No. DV-TN-19-59, Army Ballistic Missile Agency, Huntsville, Alabama, June, 1959.
19. Naumann, R.J., Recent Information Gained from Satellite Orientation Measurements, in "Advances in Ballistic Missile and Space Technology," ed. C.T. Morrow, D.P. LeGalley, and L.D. Ely, Pergamon Press, New York (1961).
20. Naumann, R.J., Directional Dependence of Counting Rates from Explorer IV, Presented to the 3rd Argna Working Group, SRI, January, 1961 (also published as a Masters Thesis by Physics Dept., Graduate School of the University of Alabama, May, 1961).
21. Lundquist, C.A., R.J. Naumann, and S.A. Fields, Recovery of Further Data from 1958 Epsilon, in "Space Research," ed. H.K. Kallman-Bijl, North Holland Publishing Co., Amsterdam, 1960.
22. Weber, A.H., C.A. Lundquist, and R.J. Naumann, "Directional Flux Densities and Mirror Point Distribution of Geomagnetically Trapped Charged Particles from Satellite 1958 Epsilon Measurements," presented to American Geophysical Union, First Western National Meeting, UCLA, Los Angeles, December, 1961.
23. Lundquist, C.A. and R.J. Naumann, Orbital and Rotational Motion of a Rigid Satellites Seminar Proceedings: Tracking Program and Orbit Determination, Jet Propulsion Laboratory, California Institute of Technology, Pasadena, California, (1960).
24. Jones, B.P., Solar Aspect of Explorer VII Compared with Certain Measured Temperatures, Rept. No. MTP-RP-60-2, NASA-Marshall Space Flight Center, Huntsville, Alabama, November, 1960.
25. Naumann, R.J., Orientation of Explorer VII, Rept. No. DV-TN-13-60, Army Ballistic Missile Agency, June, 1960.
26. Heller, G., Thermal Problems of the Payload of Missile AM-16, Rept. No. DV-TM-20-59, Army Ballistic Missile Agency, Huntsville, Alabama, July, 1959.
27. Snoddy, W.C., Temperature Control of the S-30 Payload (Explorer VIII), Rept. No. MTP-RP-61-14, NASA-Marshall Space Flight Center, Huntsville, Alabama, August, 1961.
28. Borduea, R.E., J.L. Donley, and E.C. Whipple, Jr., "The Ionosphere Direct Measurements Satellite Instrumentation (Explorer VIII)," paper presented at the Institute of Radio Engineers-American Rocket Society Meeting, June, 1961.

29. Snoddy, W.C., Temperature Control of the SA-15 Payload (Explorer XI), Rept. No. MTP-RP-61-17, NASA-Marshall Space Flight Center, Huntsville, Alabama October, 1961.
30. Kuebler, M.E., Spin-Tumble Transfer of Satellite S-15 (Explorer XI), Rept. No. MTP-G&C-61-30, NASA-Marshall Space Flight Center, Huntsville, Alabama, July, 1961.
31. Naumann, R.J., S.A. Fields, and R.L. Holland, Determination of the Angular Momentum Vector for the S-15 Payload (Explorer XI), to be published as a National Aeronautics and Space Administration Technical Note.
32. Holland, R.L., and R.J. Naumann, A Solution for the Orientation of the Angular Momentum Vector of a Satellite from R.F. Look Angle Measurements, Rept. No. M-RP-INP-61-22, NASA-Marshall Space Flight Center, Huntsville, Alabama, October, 1961.

||

## PROBLEMS IN RADIATION SHIELDING FOR SPACE VEHICLES

J. W. Keller, M. O. Burrell, R. D. Shelton, and J. A. Downey, III

Research Projects Division  
George O. Marshall Space Flight Center  
National Aeronautics and Space Administration  
Huntsville, Alabama

The interest in manned exploration of space has resulted in a rather clear definition of the requirements for propulsion systems. Either the specific impulse must be increased or else very large vehicles must be developed. It is probable that deep space exploration by mankind will be seriously inhibited if the big-booster approach alone is followed, simply because of propellant, cost, structure, manufacture, transportation, and launch. The strong economic motivation to avoid large vehicles has resulted in several efforts to produce propulsion systems with high specific impulse. Perhaps the most direct application is that promoted under the Orion project, which would use the rapid expansion of fission bomb material to provide propulsion. The nuclear heat exchanger rocket, while less direct or dramatic, would use a nuclear fission reactor to heat the propellant which would drive electric thrust units. Because all of these schemes use nuclear fission as an energy source and because all fission of heavy nuclei results in penetrating radiation, all of these systems must have adequate shielding of some kind if man is to be aboard the spacecraft.

Whether or not the propulsion system uses nuclear energy, there is still a radiation problem. It is probable that every magnetic field in space is filled with energy-charged particle radiation of high penetrating power. Since Hess discovered cosmic rays in 1913, man has broadened his knowledge of space radiation to the extent that he can discuss the radiation belt of Jupiter or the solar flare production of high-energy protons. Space explorers will be concerned with great radiation belts upon leaving the Earth, with the background of cosmic radiation that pervades all space, with the violent particle radiation storms associated with solar activity, and with the radiation belts around planets to be visited.

The physics of the radiation problem has been studied most thoroughly in a number of areas. The stopping of charged particle radiation has been

of interest since nuclear physics began. By studying the tracks of charged particles in cloud chambers and emulsions, the physicist could determine the products of nuclear reactions and their energies. Many Nobel laureates studied the interaction of charged particles with matter [1, 2].

Later, when massive accelerators were designed to accelerate charged particles, special studies were made [3] to determine methods for protection of laboratory personnel from radiation. In such applications, special efforts were made to minimize the cost of shielding. These studies, however, were not concerned with minimum-weight systems, and often postulated the appropriate location of a mountainside.

Nuclear radiation shielding has been studied extensively in the past 15 years. The weapons effort, the nuclear submarine program [4], and the nuclear powered airplane program [5], in particular, have contributed tremendously to our knowledge concerning the interaction of neutrons and gamma rays with matter. However, because of environmental and system differences, the nuclear radiation problem for submarines, aircraft, nuclear rocket stages, Orion ships, and electrically-propelled spacecraft are all quite different.

Despite the effort expended in the study of radiation, there are several areas in which there is a decided lack of information: how radiation affects humans; the production of secondary radiation by charged particles; the statistics on solar flares; the radiation belts surrounding the bodies in the solar system. Our satellite instrumentation provides only the crudest sort of measurements. The huge accumulation of information concerning radiation is quite valuable, but far from sufficient for the design of space vehicles.

### 11.1 Radiation from Nuclear Reactors

The utilization of nuclear reactors in space flight is very probable within the next 10 years. Future experience will define more clearly the ultimate role of nuclear power in space. Nuclear reactors will be employed to furnish the primary power for certain types of space vehicles and will also find application as auxiliary power units.

Typically, the fissioning of a single  $U^{235}$  nucleus yields approximately 195 Mev of energy. Some 83 per cent of the fission energy is released in the form of kinetic energy of the two primary fission fragments. The fission fragments are heavy, highly ionizing particles, and their kinetic energy is rapidly dissipated within the reactor in the form of heat. The other 17 per cent of the fission energy is accounted for in the neutrons and gamma radiation that are released instantaneously upon fission, and in the betas, gammas, and neutrinos that are emitted during the decay of the radioactive fission fragments. The shield

designer is concerned with highly penetrating neutron and gamma radiation, a large percentage of which escapes from the reactor core.

Neutrons normally account for 5 or 6 Mev per fission. The weighted average of the energies of fission neutrons is approximately 2 Mev. Neutrons having energies of 0.01 to 18 Mev are released during the fission process.

Prompt gamma rays provide a total of about 6 Mev per fission. Energies of 0.1 Mev to 10 Mev are represented; the average energy of prompt gamma radiation is about 1 Mev.

Gamma radiation from radioactive fission products provides about 6 Mev per fission. This radiation is released some time after fission occurs. The quantity of radioactive fission products contained in a reactor core increases during operation. Under constant power operation an equilibrium condition will ultimately be attained where radioactive fission products are decaying at the same rate that they are being formed. The energy of gamma radiation emitted from fission products ranges from about 0.2 to 7 Mev, depending on the parent nuclide. The average energy of decay gammas will vary somewhat since the relative percentage of long-lived fission products increases with reactor operation. Generally, the average energy of fission product gamma radiation is roughly 1 Mev.

To evaluate the total radiation energy released by a reactor, it is necessary to know that there are about  $3.1 \times 10^{16}$  fissions per sec per Mw of reactor heat. From the above energy contributions it is apparent that about  $5 \times 10^{17}$  Mev of energy per sec per Mw of reactor energy are released from neutrons, prompt gammas, and fission product gammas. This is equivalent to 75 Btu/sec.

A discussion of nuclear radiation is incomplete without considering the neutron-induced secondary gammas generated in the surrounding media and reactor shields. The secondaries from a highly shielded reactor may be more important than the primary radiation in calculating the dose at the payload. The reason for this is that the capture gammas generated in many shielding and structural materials are characterized by 6 to 10 Mev gamma rays and if the cross section for neutron capture is relatively high (for example, 2.6 barns in iron), a large fraction of the slow neutrons will be converted into high-energy gamma rays. One solution to this problem is to alloy or intermix the shield with boron, which has a very high cross section for neutron absorption (750 barns) but emits only alpha rays and 0.5 Mev gamma rays which are readily stopped. For instance, a 2 per cent alloy of boron in iron will virtually eliminate the capture gammas.

Gamma rays from neutron inelastic collisions are also an important source of secondary radiation, but in most shielding problems are considered to be of less importance than the capture gammas. This assumption is based on the following properties of inelastic collisions by neutrons. Gamma rays from inelastic neutron collisions are usually characterized by 0.5 to 2 Mev gammas, which are attenuated rapidly in dense shields. Another consideration is that the threshold energy for inelastic scattering is usually near or above 1 Mev. Thus, if a neutron has an inelastic collision with a nucleus, there is a good likelihood that the resulting neutron energy will be near the threshold for inelastic scattering and consequently will not undergo another inelastic collision. Also, if a hydrogenous material is used in the shield, most of the neutrons are quickly degraded in energy below the inelastic threshold energy.

The methods used in shielding neutrons and gamma rays are essentially independent of their origin. The dominating principle is reduction of radiation flux and the associated energy by choosing a shield to absorb as much of the energy as feasible and reduce the transmitted flux. For neutrons the ideal shielding material is hydrogen because on a single collision the neutron energy may be theoretically reduced to zero, regardless of initial energy. On the average, a neutron scattered by hydrogen is degraded to approximately one-half its initial energy. However, the scattering of neutrons by hydrogen is always into the forward hemisphere. Hence, if one seeks a material which scatters the neutron flux out of the beam, some other element such as carbon would be better.

For gamma rays, the ideal shielding materials are those which provide a large number of electrons per unit volume, along with a large photoelectric cross section, such as lead. For such elements, the principal mechanism for the energy reduction of the gamma rays between 0.5 Mev and 5 Mev is Compton scattering on electrons. Photoelectric absorption is the principal means of energy absorption below 0.5 Mev, while pair production is the primary mechanism of energy absorption above 5 Mev. In the latter case, a pair of 0.51 Mev gammas results from the annihilation of a positron and an electron, but these are usually neglected in shielding calculations because they are readily absorbed in the typical gamma shield.

It is seen that the materials which are needed for the proper shielding of reactor radiation have conflicting requirements. Thus, hydrogen or light elements, in general, are needed to shield neutrons and lead, or dense materials, are needed to shield gamma rays. How these difficulties are compromised is a large part of the shielding technology and no attempt will be made here to go into the details of the methods. It is apparent that neutrons slowed down by hydrogenous material will be more readily captured by the heavier elements which are very likely to emit energy secondary gammas. The inelastic scattering



of neutrons, however, is minimized by having a hydrogenous material which reduces the neutron energy below the threshold for inelastic collisions. Since the hydrogen seems to provide more advantages than disadvantages as a neutron shield, the problem of capture gammas is solved by adding an element such as boron to absorb most of the slow neutrons, and consequently minimize the high-energy capture gammas.

Some of the major problems encountered in shielding against nuclear radiation have been discussed here. However, the radiation problems encountered in space are likely to be quite different from those in the Earth's atmosphere. For example, air scattering is a major source of radiation dose at the payload if a nuclear-powered vehicle is operated in the atmosphere. Radiation escaping from a nuclear rocket into space may be completely ignored. Hence, the use of a reactor shadow shield and shields designed to scatter the radiation away from the rocket may play an important role in space shielding.

One of the controlling factors in determining the shielding necessary for nuclear rockets may be the problem of radiation heating of the propellant. Such heating may be of sufficient severity to cause boiling of the propellant (liquid hydrogen) with subsequent propellant loss and cavitation of the pump resulting; or pressurization of the propellant tank to prevent such boiling may result in unduly thick walls.

Theoretical treatment of the propellant heating problem may be broken down into two main problem areas: (1) the accurate determination of the rate of heat deposition in the propellant as a function of position and time, and (2) the proper treatment of the circulation of the heated propellant (due to both natural and forced convection) within the tank during the heating period which will determine the maximum temperature attained. Problem (1) is being attacked using Monte-Carlo statistical techniques, an approach which should be adequate. Problem (2), however, is far from being resolved. Adequate theoretical treatment appears unlikely. The experimental approach is very difficult without performing full-scale experiments.

Recent Monte-Carlo calculations [6] of radiation heat deposition in cylindrical tanks, 30 ft in diameter and 50 ft long, have shown that for incident 2 Mev neutrons and gammas 97 and 65 per cent, respectively, of the total incident energy was absorbed within the full tank. The difference between the above percentages is attributed to the fact that the mean free path of 2 Mev neutrons in liquid hydrogen is about 3 in. while that for 2 Mev gammas is above 5 ft. The rate of energy deposition as a function of depth into liquid hydrogen is illustrated for both neutrons and gammas in Fig. 11.1.

Another important factor in determining heat deposition in the propellant is the consideration of the secondary gamma radiation resulting from neutron capture in the hydrogen (one 2.23 Mev gamma per capture). For

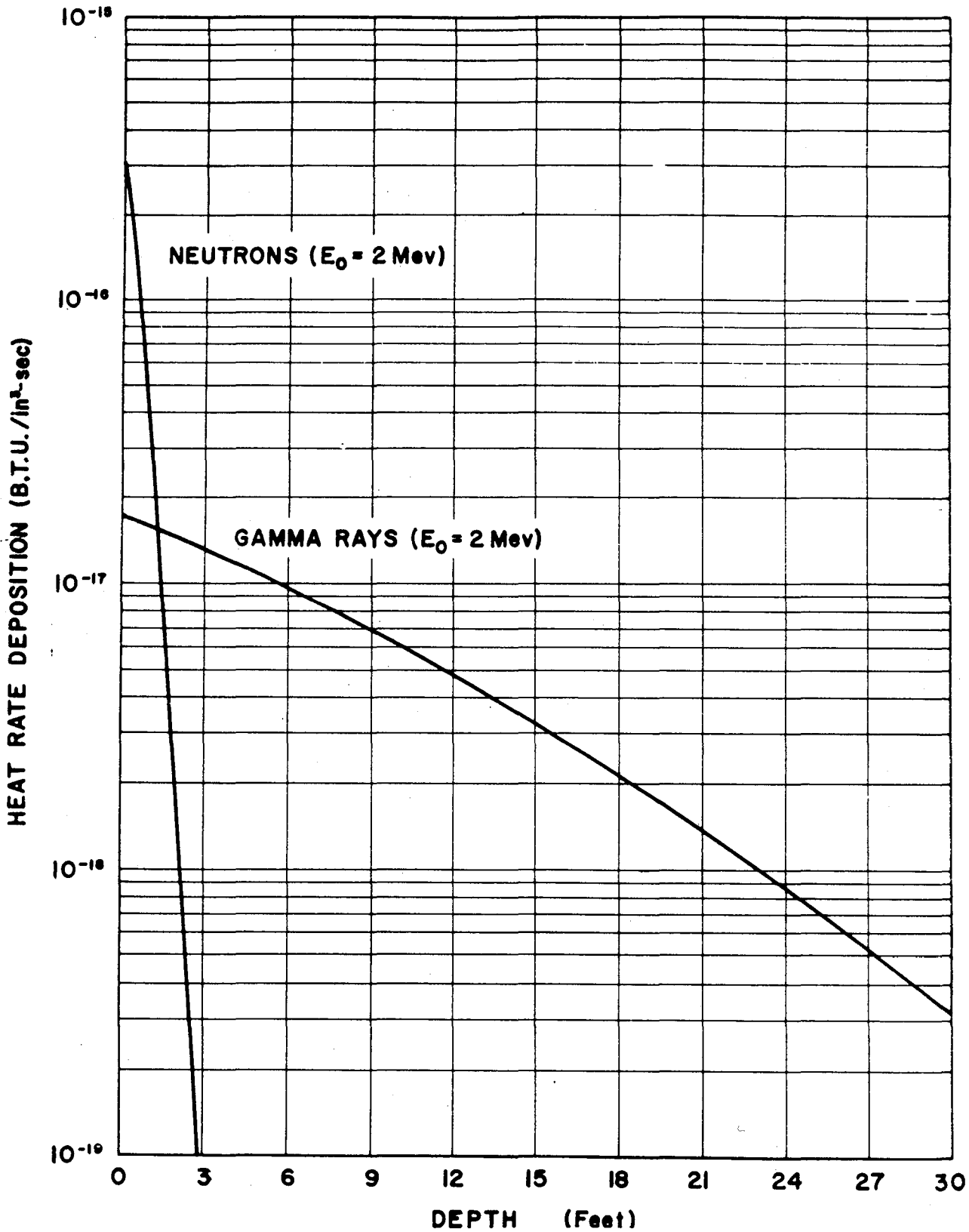


FIG. 11.1 Rate of energy deposition as a function of depth into liquid hydrogen for normally incident neutrons and gamma rays.

this problem the spatial distribution of the neutron captures must be known. Monte-Carlo calculations have been made [6] to determine this distribution as a function of depth in liquid hydrogen for various incident neutron energies. A sample of these results are shown in Fig. 11.2. While these curves give the distribution of neutrons slowed only to 0.5 Mev, they are probably representative of the thermal flux distribution.

It appears that the most satisfactory solution to the propellant heating problem is to shield the reactor sufficiently so that the incident energy will not cause an intolerable temperature rise (within tank pressurization limitations). On the basis of present techniques for determining propellant temperature rise, attempts at system weight optimization are of doubtful value.

Consideration of manned applications for nuclear rockets presents an additional shielding problem. In this case, it is not clear whether the problem of shielding man, or that of shielding the propellant, will be the controlling factor in the design of the reactor shield. If the manned considerations are the controlling factor, then the propellant problem as outlined above is minimized. However, with vehicles becoming larger and larger in diameter, some shielding may be placed so that the outer portions of the propellant tank will be protected from radiation emitted from the sides of the reactor. This shielding would not be effective for protecting the crew.

It is quite impossible to assess fully the shielding problem for manned applications at this time. This is partly because tolerant dose levels for reactor and natural radiations have not been established for manned missions.

## 11.2 Natural Radiation in Space

The problem presented by the existence of ionizing radiations in space is a serious one to all proponents of manned space flight. Radiation levels are seen to exist which will be dangerous for an unshielded man; hence, the problem of providing protection with as small a weight penalty as possible. It does not appear that these radiations will have a significant effect on the components of space vehicles, with the exception perhaps of solar cells, which are exposed on outside surfaces.

Since the Van Allen belts are confined to a relatively small region of space which can be rapidly traversed by high-thrust vehicles, they present the limiting problem only for vehicles orbiting in that region, or for low-thrust vehicles spiralling out through the belts. The protons in the inner belt have been found to present a very formidable shielding problem for such vehicles. The electrons in the Van Allen belts, although of high intensity, are relatively easily shielded against because of their low energies. Most of the electrons are stopped in the vehicle shell with only the resulting bremsstrahlung presenting a problem within the vehicle.

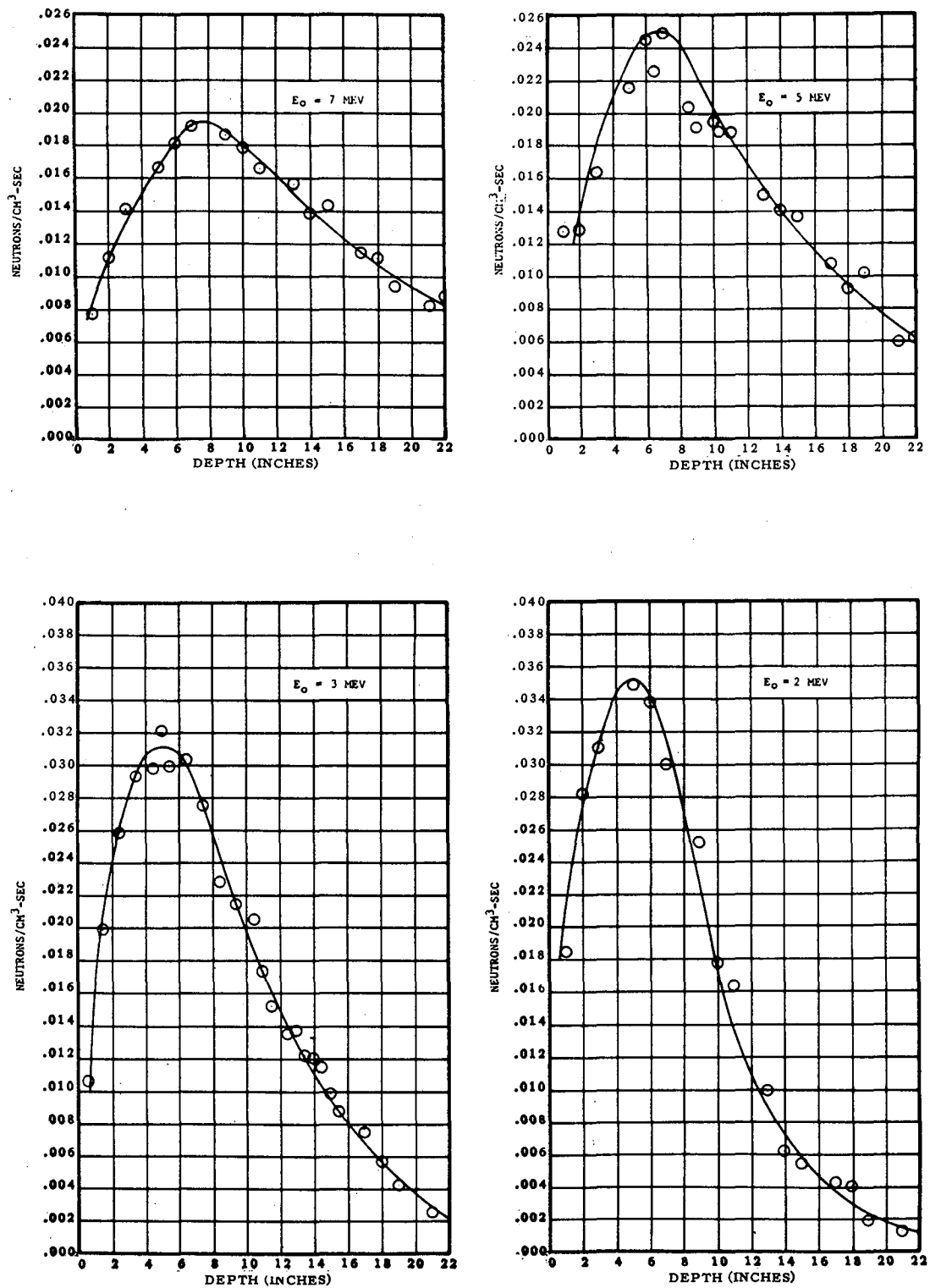


Fig. 11.2 Spatial distribution of 0.5 eV neutrons in liquid hydrogen slabs due to normal-incident monoenergetic neutrons ( $1 \text{ neutron/cm}^2 \text{ - sec}$ ).

For high-thrust vehicles with missions taking them far beyond the Van Allen belts, solar proton outbursts are considered to present the most severe potential hazard from a radiation standpoint. The seriousness of this problem is as yet undecided, primarily because of uncertainties in the time profile for these events. Since the mechanisms for the acceleration and propagation of solar protons are not understood at this time, all considerations of the shielding problem are based upon past observations with no assurance that the worst case possible has been observed. Also, the period of time over which intensive observations have been made represents a rather short sample time upon which to base statistical estimates of encounter probabilities.

All vehicles operating outside the protection of the Earth's magnetic field will be subjected to the full intensity of the background cosmic radiation. It appears that for long missions, on the order of several years, this component may be of significance, with dose estimates of 25 rem/yr having been made [7].

For electrons in the energy range of interest in the Van Allen belts (less than a few Mev) the energy loss in penetration through matter is principally due to electronic excitation and ionization of the atoms in the stopping substance. However, a portion of the energy is lost through radiative collisions (bremsstrahlung). In both types of collisions, the electron may suffer significant deflections in direction. Also, a large number of deflections result from elastic scattering. Consequently, the actual path length of the electron may be considerably greater than the thickness of the absorber being traversed. For electrons, large fractions of the total energy may be transferred in a single collision, resulting in a wide variation in the actual path length for electrons of the same energy. The thickness of shielding needed for stopping the electrons in the Van Allen belts is seen to be quite small with the maximum path length for a 1-Mev electron in aluminum being  $0.545 \text{ gm/cm}^2$ , a thickness less than that expected for most space vehicle shells.

As the incident electrons are so readily shielded, the only problem within a vehicle would result from the bremsstrahlung radiation produced in the shield. The fraction,  $f$ , of the total electron energy,  $E$ , which is given up as bremsstrahlung by an electron in the energy range of interest and stopped in a material having atomic number  $Z$  may be represented [8] approximately as

$$f \approx kZE$$

where  $k$  is a semi-empirical constant having a value  $\sim 7 \times 10^{-4} \text{ Mev}^{-1}$ . This equation shows that the fraction of the energy lost in this way by Van Allen belt electrons is quite small. However, the large intensity of incident electrons presents a potential hazard. Also, the production of bremsstrahlung is held to a minimum by using a low- $Z$  material for stopping the electrons.

An approximate energy spectrum of the bremsstrahlung is given by [8]

$$N(E_\gamma)d(E_\gamma) \simeq \frac{2 k Z (E-E_\gamma)}{E_\gamma} d(E_\gamma)$$

where  $N(E_\gamma)d(E_\gamma)$  is the number of photons having energies between  $E_\gamma$  and  $E_\gamma + dE_\gamma$ . It is seen from this equation that the spectrum is quite soft; consequently, a material having a high photoelectric cross section would constitute a very effective shield. The most efficient shield for electrons in the Van Allen belt would be composed of a layer of low-Z material to stop the primary particles followed by a layer of high-Z material to attenuate the bremsstrahlung.

Protons, which constitute the chief shielding problem in space, lose energy mainly through inelastic collisions with bound electrons, causing excitation and ionization. This process results in a practically continuous reduction of energy as the protons penetrate through a medium. As a result of the relative masses of the colliding particles, the protons are not appreciably deflected by such collisions and, therefore, follow essentially straight paths through the material. The maximum energy loss in such a collision is 1/460 of the initial energy so that there is very little variation in the range through a given material for monoenergetic protons (since so many collisions are required to stop the particle). Tabulations of the mean proton range as a function of proton energy for a variety of materials are contained [9].

Plots of the range-energy curves for several materials covering a range of atomic numbers are shown in Fig. 11.3. It is obvious from a comparison on this basis that low-Z materials, hydrogen and hydrogenous materials in particular, are superior because of a greater electron density per unit weight. In actual practice, however, extremely low density materials such as  $H_2$  may not be desirable because of geometric factors.

In shielding against protons in the energy range of interest (up to several Bev), the range of the primary particles is not the only factor which must be taken into consideration. The secondary radiation caused by the interactions of the incident protons with the stopping material must also be considered. The largest dose contribution from secondary radiation originating in the shield should be that due to nucleons emitted as a result of nonelastic collisions with nuclei of the shielding material. Such nonelastic reactions of high-energy nucleons with atomic nuclei are generally thought to take place in two phases. The first phase is the rapid development of a nucleonic cascade; the second is the deexcitation of the thermally excited nucleus by the process of evaporation. The cascade develops through the incident nucleon colliding with nucleons

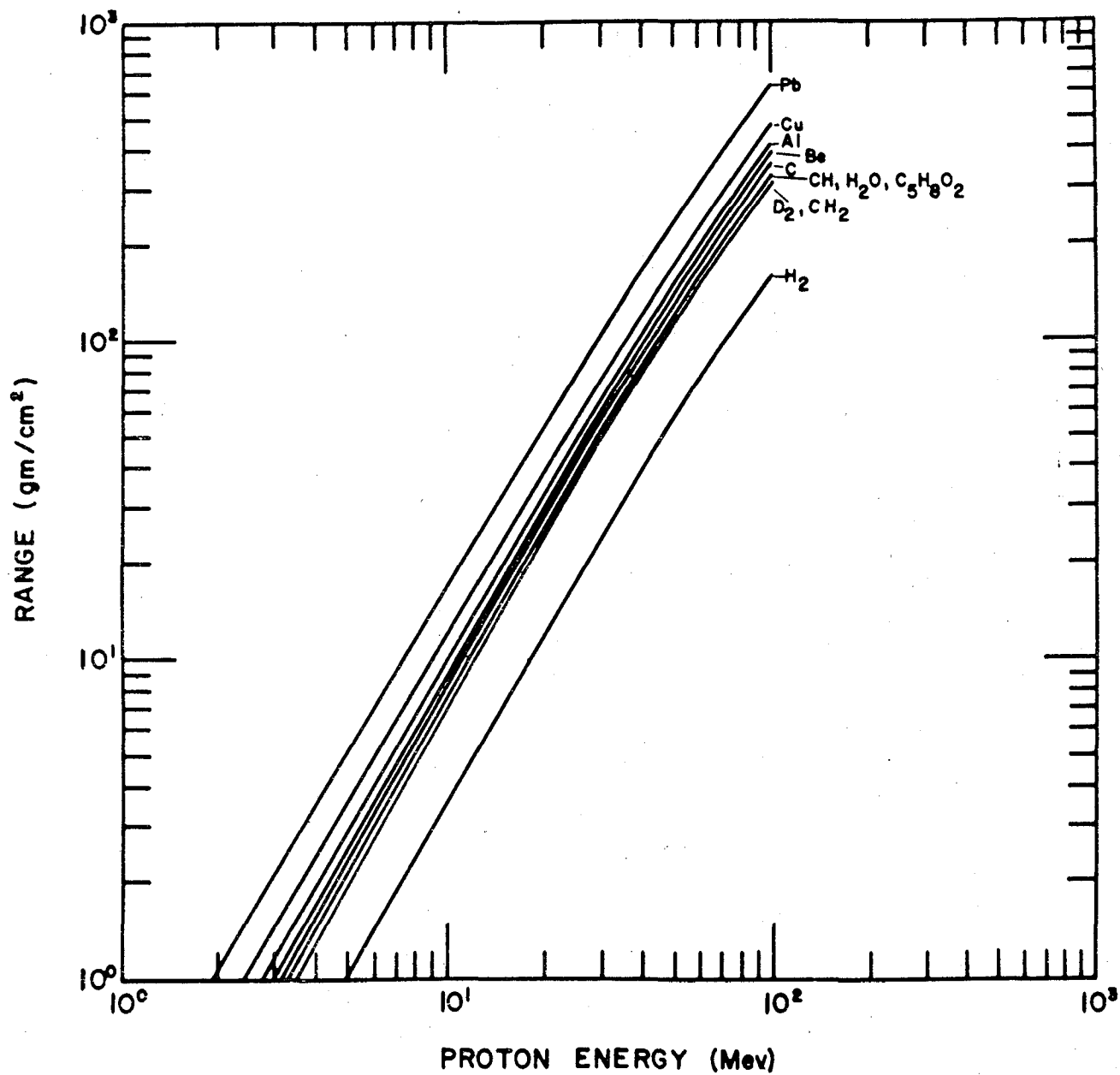


Fig. 11.3 Range-energy curves for protons.

of the target nucleus; the recoil nucleons either escape from the nucleus or collide with other nucleons which, in turn, either escape or collide with still other nucleons. The nucleons that do not escape are assumed to share their energy with the entire residual nucleus from which lower-energy nucleons boil off in the process of deexcitation. The most important particles released by such reactions, from the standpoint of dose behind a shield, should be the neutrons since they do not lose energy by ionization in getting out of the shield as do the released protons.

Considering a beam of protons incident normally on a slab of shielding material, the spectrum of the primary radiation emerging from a thickness,  $x$ , may be determined [10] by the equation

$$\phi(E, x) dE = \phi(E'; 0) \frac{S(E')}{S(E)} \exp \left[ - \int_0^x \Sigma(E'_s) ds \right] dE$$

where  $\phi(E, x) dE$  is the flux of protons between  $E$  and  $E + dE$  at a distance,  $x$ , from the shield surface,  $S(E)$  is the stopping power of the shield material for protons of energy  $E$ ,  $E'$  is the incident energy of protons degraded to energy  $E$  in traversing a distance  $x$  in the shield material, and  $\Sigma(E'_s)$  is the reaction cross section at a distance  $s$  into the shield for protons which entered the shield with energy  $E'$ . The calculation of the secondary component of the radiation is much more difficult, since several nucleons may be emitted at various angles and energies following a nonelastic collision, the energy of the cascade particles being high enough to produce tertiary effects in many cases. Also, basic experimental cross section and yield data for such reactions are quite scarce. Most of the estimates of secondaries which have been published have involved the use of extrapolations and interpolations of theoretical determinations of yields from nuclear reactions. Some calculations have assumed straight-ahead production of secondaries [10], while others have considered an angular distribution but have neglected tertiary effects [11]. Proton penetration codes are being formulated based on Monte-Carlo techniques capable of handling these problems more accurately. Also, improved theoretical yield data are being generated for use in these codes. Final application of the codes using the theoretical cross sections will be checked out in a series of accelerator experiments.

Figure 11.4 (taken from [11]) shows estimates of the dose rate as a function of shield thickness at the center of a 4-ft inner radius carbon shield in the most intense portion of the Van Allen proton belt for both the primary protons and the secondary neutrons. In this case, the contribution from tertiary interactions were neglected; however, the relative biological effectiveness (RBE) values used for the neutrons were probably conservative (5 for cascade neutrons and 10 for evaporation neutrons).



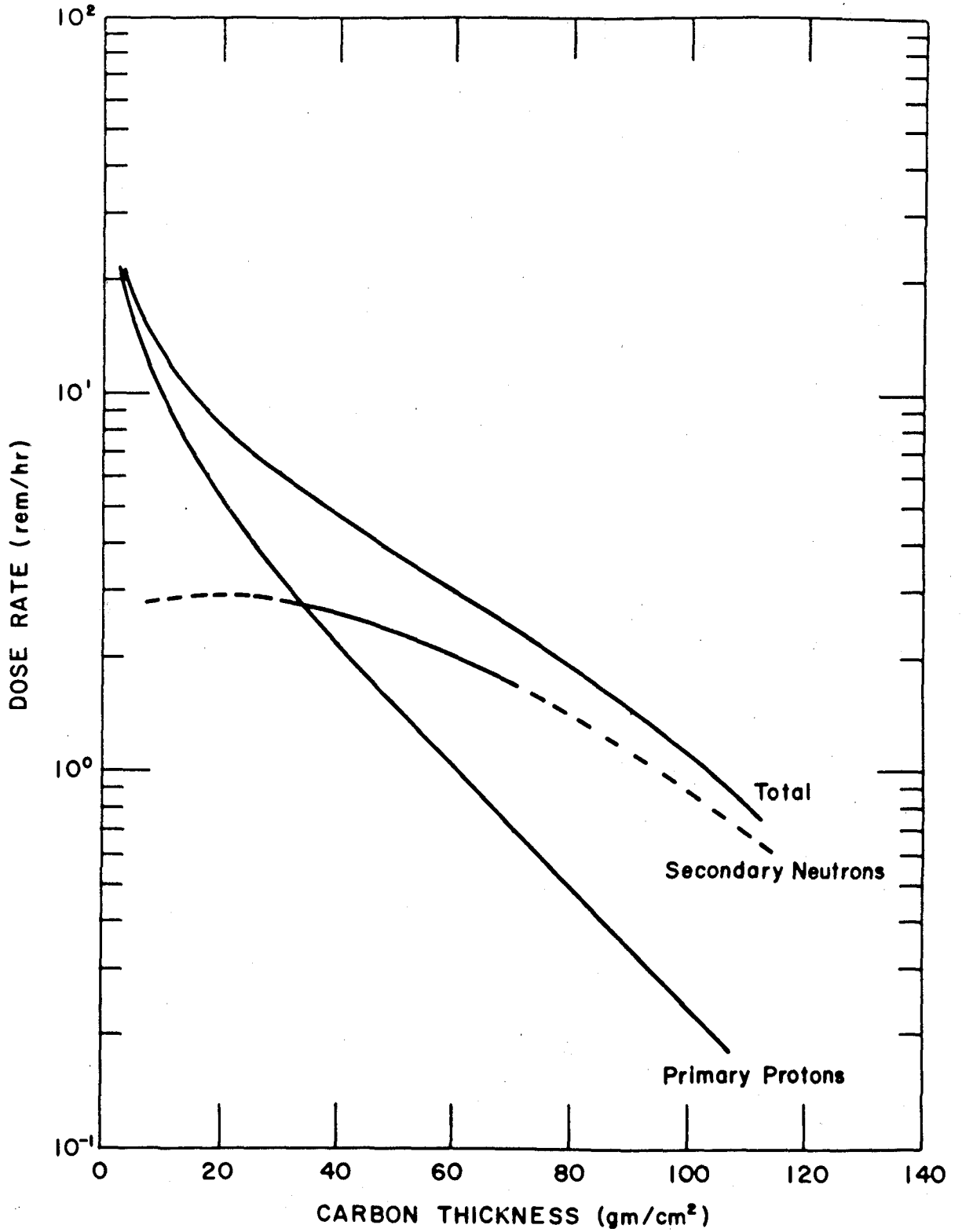


Fig. 11.4 Effect of secondary neutrons on total dose rate for carbon shield (heart of inner van Allen belt).

The cascade neutrons were assumed to have a cosine distribution in the laboratory system while evaporation particles were assumed to be emitted isotropically. The resulting shield thicknesses are seen to be quite formidable with  $\sim 100$  gm/cm<sup>2</sup> needed to reduce the total dose rate to  $\sim 1$  r/hr. Consequently, due to the very large shielding penalty involved, the intense regions of the inner Van Allen belt will probably be a forbidden region for manned orbiting vehicles.

Contrary to what might be expected, much of the radiation encountered in solar proton outbursts appears to reach the vicinity of the Earth with an isotropic distribution, thus necessitating protection from all directions. Figure 11.5 (taken from [12]) shows one set of rough upper and lower estimates of the integrated dose as a function of water shield thickness for the low-energy flare events of August 1958, May 1959, July 1959, the intermediate energy event of November 1960, and the high-energy event of February 1956. While the dose is given in rep, the RBE for high-energy protons is close to 1 and, therefore, the units may be considered as rem with little error. However, these curves consider primary radiation alone. Some estimates of the secondary problem for such flares have been made [13].

It is seen that the first few gm/cm<sup>2</sup> of shielding result in a very rapid decrease of the dose, with the addition of subsequent shielding seen to be less and less effective. This is a result of the hardening of the spectrum as more and more material is penetrated. Uncertainties in shield weight increase as thicker shields are used since it requires larger and larger additions of shielding to effect a given percentage change in dose [14].

There are two philosophies which may be applied to the solar flare problem for short duration missions. One is to shield against possible solar flares, the other is to predict flare-free periods during which the mission can be carried out. Satisfactory flare prediction techniques have not been developed as yet and the progress in this area is slow. Consequently, it appears that at least for the early manned flights, shielding may be necessary. For long-duration missions, shielding will undoubtedly be necessary since such long flare-free periods will be rare. Also, the possible hazard from primary cosmic radiation arises.

It is evident that quite heavy shielding will be required in manned space vehicles. Since the addition of such weights will reduce performance, it is important that the shield weight be minimized. Consequently, a number of possible vehicle shielding concepts have been suggested.

One possible means of reducing the shield weight for vehicles operating in the Van Allen region, suggested in [15], takes advantage of the angular distribution of the radiation. It is suggested that, since the radiation is peaked in a direction perpendicular to the lines of force

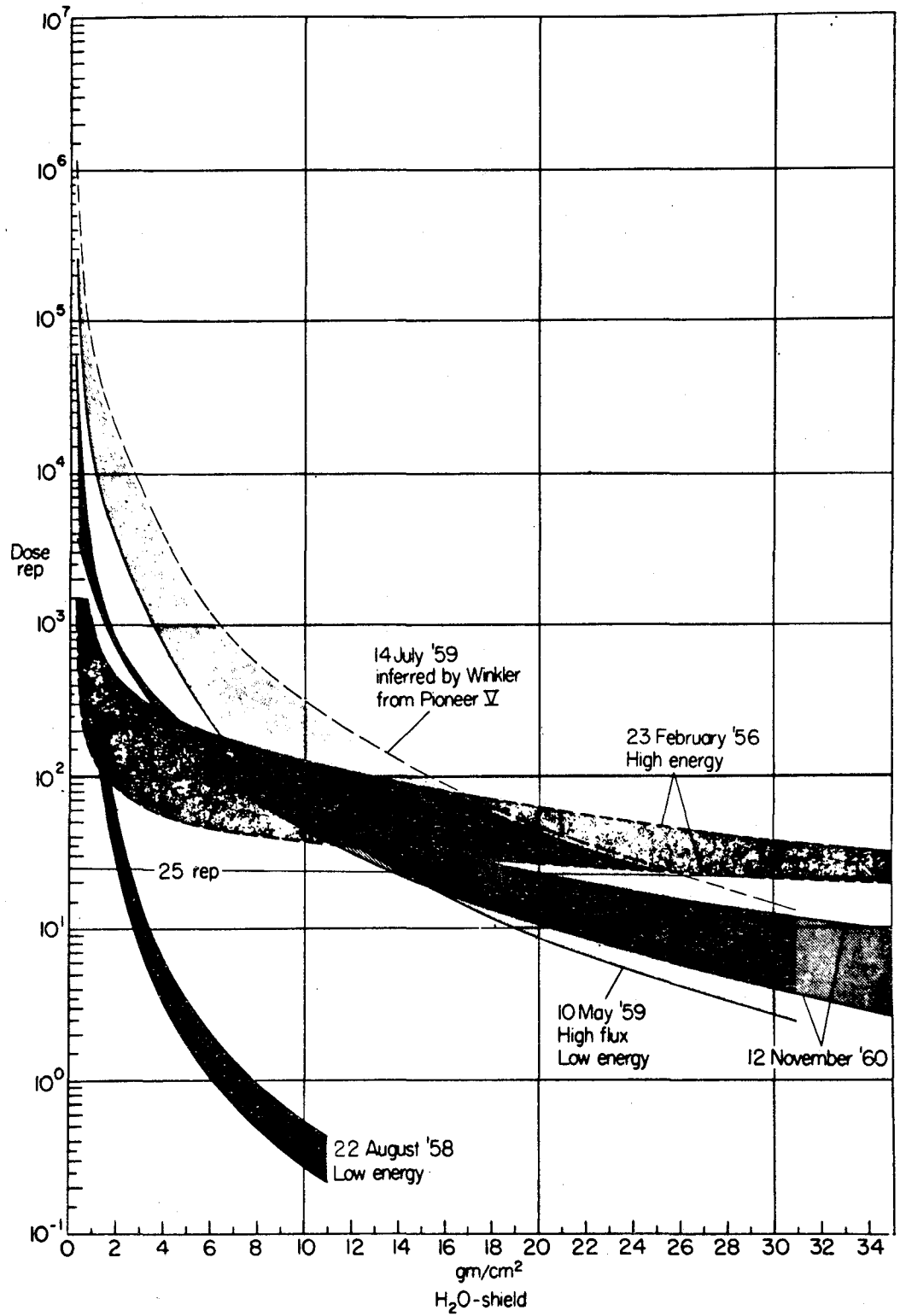


Fig. 11.5 Integrated proton doses versus shield thickness for solar proton events (upper and lower limits).

of the Earth's magnetic field, the crew compartment might be protected by a ring of shielding whose axis is kept parallel to the lines of force at all times. This idea, besides presenting many orientation problems, might not be practical since the angular spread of the radiation may be such that to shield a given volume will require almost the same weight as it would to surround it.

For deep space missions, the fact that one may traverse the Van Allen belts rapidly plus the fact that solar proton outbursts are intermittent in nature, suggests that a possible weight advantage could be realized by using two crew compartments, one large compartment for normal operations during quiet periods and a much smaller heavily shielded compartment for occupation during relatively short periods following large solar flares. The use of a liquid shielding material might allow the shielding to be moved about so as to surround either compartment, making it possible to place a shield of less thickness about the larger compartment. Such an arrangement would reduce the length of stay in the smaller compartment.

An interesting variation [16] of the storm cellar concept would be to place the small heavily shielded compartment between any on-board reactor power source and the large compartment. The shielding surrounding the small compartment would then serve as a reactor shadow shield for the large compartment.

In nuclear as well as nonnuclear vehicles, employment of equipment and stores as shielding could be a means of reducing necessary shield weights. The most obvious application of this concept is the use of propellants as shielding. Such an application should be examined carefully, since fuel depletion would decrease the shielding, perhaps leaving inadequate shielding when needed for a large solar proton outburst. Also, as a result of the low density of such fuels as liquid hydrogen, and the correspondingly large thicknesses of shielding needed for many applications, the shapes assumed by the vehicles utilizing such shielding might not be acceptable aerodynamically for ground launch.

Many persons have suggested the use of active shields such as magnetic fields for protection from the charged particles. Early results of such studies [17] indicate that the scheme is practical only if superconductors are used. Even then, it shows advantages over passive shielding only if very large volumes are to be shielded and a quite high cutoff energy is required. Even in this case, if all the engineering problems such as maintaining cryogenic temperatures are considered, any advantage may disappear. Also, the reliability of such a system is not a problem encountered in the case of bulk shielding. Study in this field, however, is continuing.

One of the most important factors in the shielding problem is the establishment of tolerant dose levels for astronauts. Shield weight will be very strongly dependent upon this parameter since the dose reduction factor obtained with the addition of a given thickness becomes less and less as one shields to lower and lower doses (not to mention geometrical effects). It does not appear unrealistic to assume that the tolerant dose, within limits, may vary from mission to mission depending upon the importance of the mission and the weight available for shielding.

The entire problem area of biological effects of high-energy particles on humans will require much more study before dose limits can be established with confidence.

### 11.3 Summary

In the exploration of space, many different sources of radiation will be encountered. Of greatest significance will be the energetic protons emitted during certain solar disturbances, the electrons and protons in the Van Allen belts and in radiation belts around other planets, and to a lesser extent the primary galactic cosmic radiation. In addition to the natural radiation environment, on certain missions astronauts will be exposed to neutron and gamma radiation from on-board nuclear reactor sources. Radiation shielding will be required on manned space vehicles, except perhaps during very short flights. The shield designer is confronted with the problem of providing an adequate and structurally sound shield of minimum weight for a particular mission.

The mechanisms of interaction of charged particles (protons and electrons); neutrons, and gamma radiation with matter are quite different. Charged particles ( $E \lesssim 1$  Bev) are attenuated primarily through ionization and excitation processes involving bound electrons in the target materials. Low atomic number elements which have a larger number of electrons per unit weight are optimum from a weight standpoint for shielding against charged particles. Low-Z materials also serve as excellent neutron moderators.

A neutron can lose a large percentage of its original energy on a single collision with a nucleus of a light element. In a neutron shield, it is desirable also to include a material such as boron, which has a high absorption cross section for thermal neutrons. It is particularly desirable to reduce the leakage of slow neutrons from a reactor shield to minimize the production of secondary gamma radiation resulting from  $(n, \gamma)$  processes in adjacent materials. A judicious selection of structural materials in a nuclear powered space vehicle can serve to minimize further the production of secondary gammas.

Gamma radiation is attenuated in matter primarily through the processes of photoelectric absorption, Compton scattering, and pair production. The relative importance of these processes on the energy of the

incident gamma radiation and on the material through which the radiation is passing. The photoelectric and Compton processes dominate at low energies. The threshold for pair production is 1.02 Mev, and attenuation by pair production becomes increasingly important at higher energies. In general, high atomic number materials are desirable for attenuating gamma radiation.

There will be many different sources of gamma radiation in nuclear-powered space vehicles. Prompt gammas are emitted during the fission process. Gammas are also given off by highly radioactive fission fragments; this radiation necessitates the requirement for reactor shielding after shutdown of a reactor, particularly if the period of operation has been long and there is a large accumulation of fission products. Gamma radiation will be emitted from vehicle components in which radioactivity has been induced by neutron absorption. Gammas will also be formed through nonelastic neutron scattering events. A beam of electrons passing through matter will lose some of its energy through the production of gamma radiation while in the vicinity of a nuclear field - the bremsstrahlung process. Bremsstrahlung radiation may constitute a significant natural radiation hazard for vehicles operating in the outer Van Allen zone (electron belt). It can be seen that there will be numerous potential sources of gamma radiation that must be considered in the shield design of a nuclear powered space vehicle.

Fluxes of known natural space radiation are not sufficiently high to cause damage to space vehicle materials, except for certain radiation sensitive materials exposed on the vehicle's surface, for example, solar cells. On the contrary, nuclear heat-exchanger rockets will operate at very high-power levels, and shielding may be required even on unmanned flights for protection of certain materials and to reduce radiation heating of the propellant.

The design of minimum weight reactor shielding was studied extensively during the nuclear powered aircraft program. However, before the discovery of the Van Allen belts, extensive studies of charged particle shielding were not made except in connection with high-energy accelerator installations where the cost of the shield, not its size or weight, was of primary importance. The ranges of protons and electrons having energies of a few Kev to several hundred Mev can be predicted quite accurately. Thick shields may be required to afford astronauts protection from the energetic protons in space. A certain fraction of the protons entering the shield will encounter high-energy nuclear collisions resulting in the emission of secondary neutrons, protons, and gamma radiation. The yields, direction of emission, and energies of the reaction byproducts can at present only be crudely estimated. These secondary particles will dominate the design of very thick shields, and much more information must be generated on these nuclear collision processes to permit reasonable certainty in the design of shielding for solar flare and Van Allen protons.

Since Van Allen-type radiation is confined to a restricted region in the vicinity of a planetary magnetic field, the solar flare protons will constitute the greatest natural radiation hazard to exploration of the solar system. Satisfactory techniques for the prediction of solar flare events have not been developed. The intensity of radiation, the time profile of the event, and the spectrum of the emitted radiation can vary greatly from flare to flare. There will be serious uncertainties in the design of shielding for space vehicles unless our present knowledge of the natural radiation environment is vastly improved. There is also a dearth of information on the biological effects of radiation, particularly the high-energy protons and secondary neutrons and protons that will be encountered from Van Allen and solar flare radiation. Furthermore, extremely careful and realistic consideration must be given to the establishment of allowable dosages for various classes of missions.

#### REFERENCES

1. Haliday, D., "Introductory Nuclear Physics," 2nd Edition, Wiley & Sons, Inc., New York, 1955.
2. Bethe, H., Zeitschrift für Physik, 76:293 (1938).
3. Sternheimer, R. M., The Physical Review, 115:137 (1959).
4. Rockwell, III, T., "Reactor Shielding Design Manual," McGraw-Hill Book Co., Inc., New York, 1956.
5. Branch, I. F., Nucleonics, 19:8:27 (1961).
6. Burrell, M. O., Nuclear Radiation Transfer and Heat Deposition Rates in Liquid Hydrogen, MSFC Report (to be published).
7. Tobias, C. A., Radiation Hazards in High Altitude Aviation, Wright Air Development Center Tech. Rep. 52:119 (May 1952)
8. Evans, R. D., "The Atomic Nucleus," McGraw-Hill Book Co., Inc., New York, 1955
9. Rich, M. and R. Madey, Range-Energy Tables, Univ. of Calif. Radiation Lab Rpt. UCRL-2301 (1954).
10. Perkins, J. F., et al, Shielding Problems in Manned Space Vehicles (1st Semi-Annual Report), Lockheed Nuclear Products Rpt. No. NR-104 (July 1960).
11. Keller, J. W., A Study of Shielding Requirements for Manned Space Missions, Convair-Ft. Worth Rpt. FZK-124, (Oct. 1960).

12. Foelsche, T., "Radiation Hazards in Space," a paper presented at Fall Central General Meeting of AIEE, Detroit, Michigan, October 1961.
13. Allen, R. I., et al, Shielding Problems in Manned Space Vehicles (Annual Report, 1960), Lockheed Nuclear Products Rpt. NR-140, (September 1961).
14. Keller, J. W., "Uncertainties in Space Radiation Shielding Calculations," a paper presented at the ARS Space Flight Report to the Nation Meeting, New York (October 1961).
15. Singer, S. F., "Some Consequences of a Theory of the Radiation Belt," a paper presented at the IX IAF Congress, Amsterdam (1958).
16. Keller, J. W. and N. M. Schaeffer, Radiation Shielding for Space Vehicles, Electrical Engineering, 79:1049-1053 (December 1960).
17. Levy, R. H., Radiation Shielding of Space Vehicles by Means of Superconducting Coils, Avco Everett Res. Lab Rpt. 106 (AFBSD-TN-61-7) (April 1961).



## EVAPORATIVE FILM COOLING FOR HYPERSONIC REENTRY VEHICLES\*

Rudolf Hermann

Director, University of Alabama Research Institute  
Huntsville, Alabama

## 12.1 Evaporative Film Cooling Application for High Heat Transfer Cases

Extremely high heat transfer rates are encountered by reentering vehicles and in rocket engines, which require great effort in efficient cooling of the walls. Mass transfer cooling is a means of controlling the heat transfer in cases where conventional backside cooling of the walls is insufficient. Various schemes of mass transfer cooling have been studied and applied during the last few years. Among them ablation cooling has received particular attention. In this method, the outer layers of the skin material melt and vaporize or often sublime directly with simultaneous chemical processes. The process was developed and first applied successfully by the Army Ballistic Missile Agency for the Jupiter IRBM nosecone. Another scheme of mass transfer cooling is evaporative film cooling or applying a liquid coolant. This method was used for cooling rocket engines much earlier than ablation cooling for nosecone reentry. It was first applied successfully, under the technical direction of Dr. Wernher von Braun, in the development of the rocket engine for the A4 missile at Peenemünde, Germany, during World War II.

Hence, it seems appropriate in this volume to report research on liquid evaporative film cooling as applied to hypersonic reentry vehicles. This research was performed by the author and his associates at the University of Minnesota. It is a logical extension of previous investigations on liquid evaporative film cooling of high-temperature, hypersonic wind tunnel nozzles, which started in 1954 [1, 2, 3, 4,]. Such a system was developed and successfully used in the hypersonic wind tunnel of the Rosemount Aeronautical Laboratories of the University of Minnesota. Since 1957, evaporative film cooling has been applied to the blunt bodies in hypersonic flow in wind tunnel experiments and the analysis of this method has been advanced considerably [5, 6, 7,].

---

\*The research covered in this chapter was supported by the Office of Scientific Research, U.S. Air Force, Contract 49(638)-190, while the author was Technical Director, Hypersonic Facilities, Rosemount Aeronautical Laboratories, University of Minnesota.

Possible future applications of the use of film cooling appear to be in electric arc chambers used for air heating of high-temperature wind tunnels or for the production of plasma jets for propulsion.

The evaporative film cooling method consists, in principle, of a one-spot injection of an evaporating liquid coolant in or near the stagnation point region of a blunt body or somewhat upstream of the throat of a wind tunnel Laval nozzle. A very thin liquid film, which is of the order of 0.001 to 0.01 in., is produced by the high shear stress exerted by the flow. Evaporation of this coolant film takes place because of heat transfer from the gas and is self-regulating according to the local heat transfer conditions. Obviously a large enthalpy of evaporation is desired for this method. In our investigations to date we have used water as a coolant since it has well-known thermodynamic characteristics and is convenient to handle; however, other coolants may be used.

One other scheme of mass transfer cooling, studied extensively during the last few years, is transpiration cooling, where air or a light gas such as helium or hydrogen is injected through porous walls. The porosity must be very fine and extend over the whole surface to be cooled. To use only the theoretical minimum of coolant flow, the porosity should actually be tailored according to the local heat transfer. In contrast, evaporative film cooling is self-regulating and requires only a small number of relatively large holes or slots for injection of the coolant. The inherent advantage of evaporative film cooling for hypersonic reentry vehicles from the aspect of simplicity in manufacturing and safety against clogging during the operational use is obvious. Several other advantages of evaporative film cooling are discussed in Sec. 12.4.

## 12.2 Experimental Investigation on Blunt Bodies in Hypersonic Wind Tunnel Flow

### 12.2.1 Models and Wind Tunnel

The experimental investigation was conducted on two hemisphere-cylinder models and one cone with either pointed or blunt nose. A 3-in. diameter hemisphere-cylinder model, instrumented with 15 pressure orifices on the hemisphere, 10 pressure orifices on the cylinder, and 4 thermocouples, was used for pressure distribution and preliminary experiments with water injection. The final 3-in. diameter hemisphere-cylinder model (Fig. 12.1) contained 25 pressure orifices and 66 thermocouples to determine the wetted area of the evaporating film. The large hemisphere models permitted the determination of details of the temperature distribution along the hemisphere. The blunted cone was investigated as a prototype for reentry nosecones or fuselages. Also, it provided flow condition with approximately constant pressure

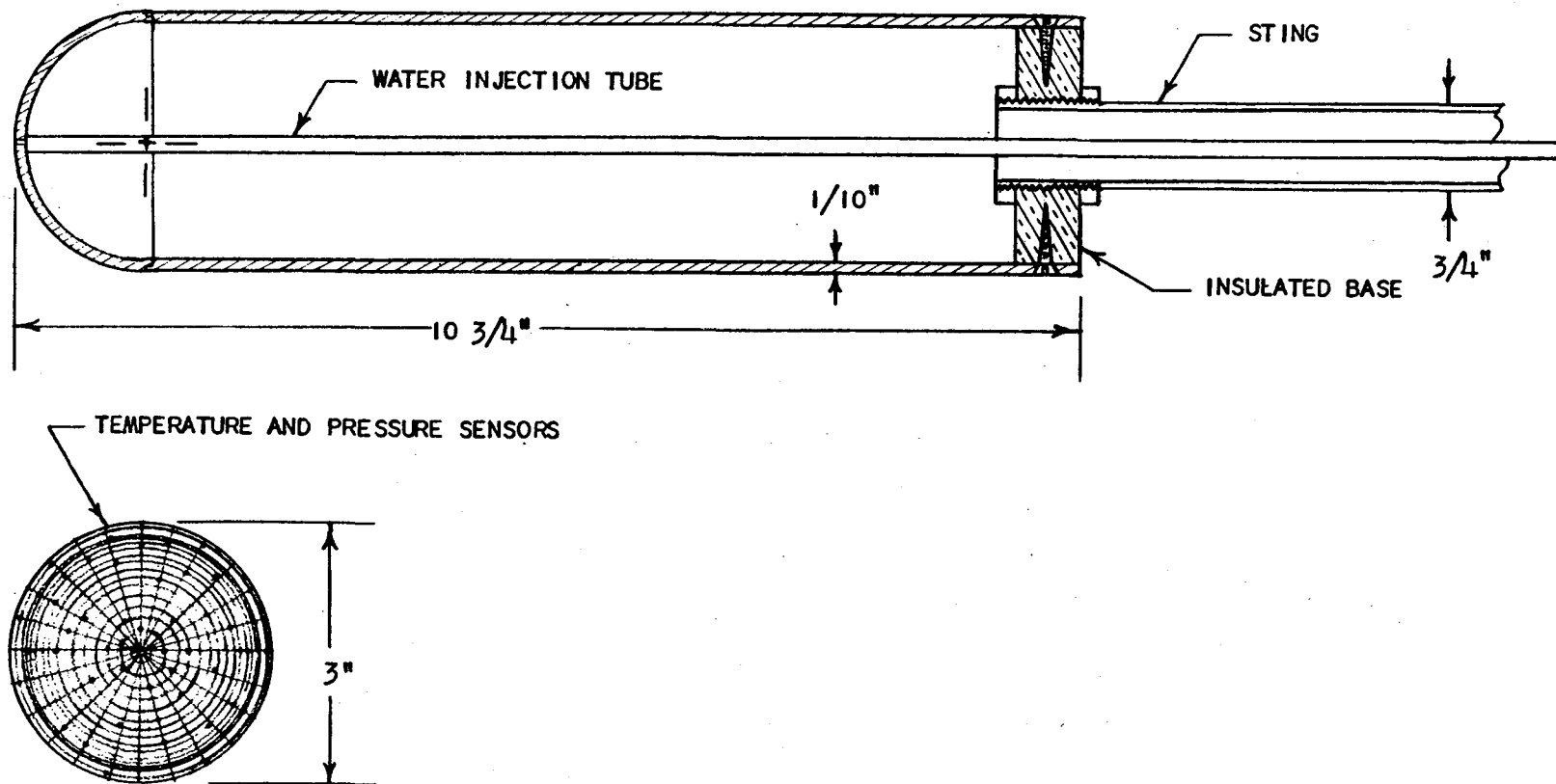


Fig. 12.1 Hemisphere-cylinder model for film cooling investigations with instrumentation.

and Mach number along the surface at distances sufficiently downstream from the blunt nose. The half angle of the cone is 10 deg, its base diameter is 5.5 in., and its length is 15.6 in. The cone can be used alternately with a pointed tip or a spherical nose with 0.5-in. diameter. The water mass flow can be controlled by a bevel gear drive operated from the outside of the wind tunnel. Using the pointed cone, the water is injected through a slot some distance downstream from the tip. Using the blunt tip, injection is at the stagnation point.

The models have been investigated at Mach 7 in the hypersonic blowdown wind tunnel of the Rosemount Aeronautical Laboratories described in detail in [8]. A gas-fired pebble-bed storage heater can produce stagnation temperatures up to 2600°R in the test section at nominal stagnation pressures of 10 atm. The test section contains a two-dimensional contoured Laval nozzle with 12 in. by 12 in. cross section, producing a uniform hypersonic stream of  $M = 7$ . The running time is 2 min. The film cooling investigation was carried out for stagnation temperatures from 1100° to 2500°R. Typical stagnation point heat transfer rate was  $\dot{q} = 25 \text{ Btu/ft}^2 \text{ sec.}^*$

#### 12.2.2 Measured Wall Temperature and Comparison with Analysis

One primary objective of the investigation was to determine the effectiveness of the method, that is the extent to which the wall can be cooled, when film cooling is applied. Figure 12.2 shows the measured wall temperature of the final hemispher-cylinder model for  $M_\infty = 7$ ,  $p_\infty = 10 \text{ atm}$ ,  $T_\infty = 1740^\circ\text{R}$  as a function of the dimensionless arc length  $s/b$ . The similarity analysis, presented in Sec. 12.3.2, has been evaluated for the same conditions and compared with the experiments in Fig. 12.2. It shows the calculated temperatures  $T_i$  of the gas-liquid interface as a function of the arc length. Near the stagnation point the calculated interface temperature is 552°R while the average measured wall temperature is 558° with a scatter of  $\pm 13^\circ\text{R}$ . Comparing this value with the stagnation temperature  $T_\infty$ , it is evident that the film-cooling method is very effective. The average difference between experimental wall temperatures and analytical interface temperature around the sphere is about 10°F. Hence, the theory predicts the temperature of the interface near the stagnation point and its variation around the sphere very well. The analytical value of the mass fraction at the interface  $K_i$  does not depend on the arc length up to  $\theta = 80 \text{ deg}$ , as expected from Eq. (12.1). The  $K_i$  values calculated from experimental  $T_w$  values show a large scattering due to the high sensitivity of  $K_i$  as a function of  $T_w$ , but agree in general with the theoretical curve.

---

\* See p. 282 for list of symbols used in this chapter.

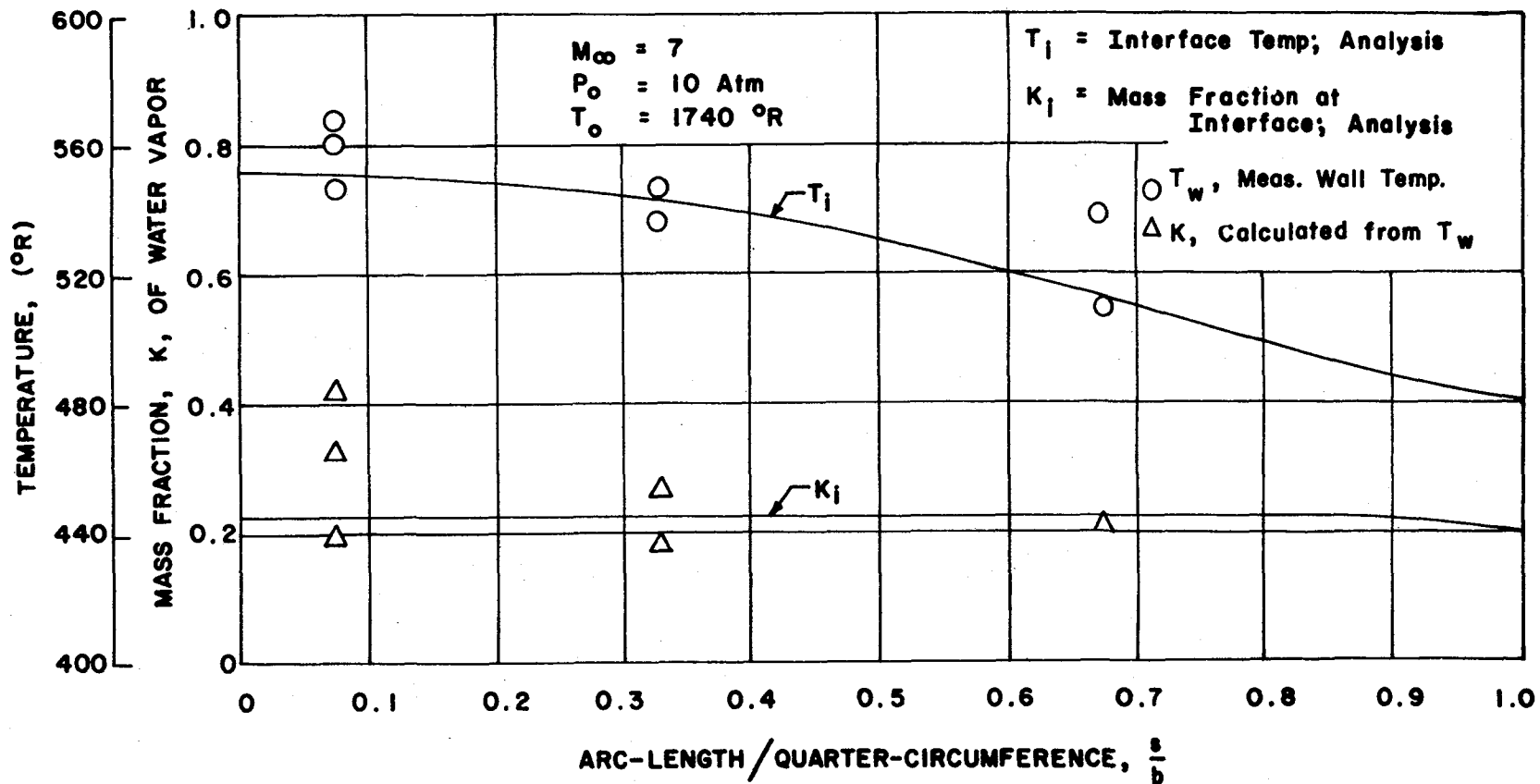


Fig. 12.2 Comparison between measured temperature on wall surface of hemisphere and calculated temperature of gas-liquid interface; also mass fraction  $K_i$  at interface.

The measured wall temperatures have been analyzed in a thermodynamic state diagram, common to the air flow and the evaporating water film [5]. A similar diagram is presented in Fig. 12.7 showing the experimental points measured on the hemisphere model in the wind tunnel presented in Fig. 12.2. Also included are two measured throat wall temperatures, obtained in the application of evaporative film cooling to Laval nozzles. One value refers to the nozzle throat of our hypersonic wind tunnel [2, 3,] the other to the nozzle throat attached to a jet engine combustion chamber [1]. They will be discussed in Sec. 12.4.3.

### 12.3 Basic Concepts and Analysis

#### 12.3.1 Basic Concepts

At a blunt body, the coolant is injected over a small area near the stagnation point and the liquid film develops along the solid wall with the thickness  $\delta_L$  due to the shear stress on the interface exerted by the gas boundary layer with the thickness  $\delta_g$ . Typical calculated values of  $\delta_L$  for our experiments are about 0.008 and 0.001 in. in the stagnation point region of the hemisphere or blunt cone, respectively, and between 0.002 and 0.001 in. along the cone surface. Due to the small dimension, the film thickness has not been measured on the wind tunnel models, but rather obtained by calculation. In the case of evaporative film cooling in the wind tunnel nozzle, we obtain a film thickness of 0.002 in. by a corresponding calculation for turbulent boundary layer. Experiments showed that the film thickness was less than 0.001 in., for otherwise its effect on the Mach number distribution could have been detected [2, 4,]. Evaporation occurs at the interface between liquid film and gas boundary layer. We deal with a binary which consists of one, two, or sometimes three phases. Water exists in the vapor form, liquid form, and sometimes in the solid state.

With the following basic concepts, analytical understanding has been obtained, a similarity analysis was developed, and numerical calculations could be performed.

1. The flow in the liquid film is laminar. This is justified because the Reynolds number of the film  $Re_L$  is in the order of 20 near the stagnation point of a sphere and has typical values on the cone of 100 near the tip, and of 10 near the base. Waves at the interface should not occur due to the small values of  $Re_L$ . They have been observed [9] at  $Re_L \sim 5000$ . In a flow without pressure gradient, we should then have the familiar Couette flow with linear velocity distribution. Although this condition is no longer exactly true in the neighborhood of the stagnation point, it has been used in the following analysis for simplicity.

2. The shear stress  $T_i$  at the interface is equal to the one calculated for the gaseous boundary layer at a porous wall at rest with mass addition equal to the evaporation from the film. This is justified by the fact that the velocity of the liquid at the interface is very small compared with the velocity at the edge of the boundary layer, in the order of  $10^{-2}$  near the stagnation point and of  $10^{-3}$  along the cone. These values have been obtained by evaluation of the analysis [5].

3. The gaseous boundary layer is laminar, which simplifies the analytical treatment considerably. The assumption is justified by the magnitude of Reynolds number of the experimental investigations presented here; that is, for the hemisphere  $Re_R = 60,000$  and for the length of the cone  $Re_x = 1 \times 10^6$ .

The assumption of laminar gaseous boundary layer refers only to our wind tunnel experiments. It does not restrict the application of evaporative film cooling to this type of flow. In fact, the flow near the Laval nozzle throat and in the test section of the wind tunnel is turbulent and similar calculations for film cooling have been carried out [3, 4,]. A corresponding analysis for evaporative film cooling at turbulent boundary layer flow around a blunt body could probably be accomplished, as well.

4. The profiles of velocity  $u$ , total enthalpy  $H$ , and water vapor mass fraction  $K$  are shown in Fig. 12.3. If we assume  $Pr = 1$  and also the Lewis number of diffusion of the water vapor into the air  $Le = 1$ , the profiles are similar and have equal boundary layer thickness. The profile for the mass fraction is similar but reversed with respect to the two others. The similarity is only valid for the profile of the total enthalpy, not for the static enthalpy or static temperature. Observe that film cooling corresponds to the case of a strongly cooled wall; the interface temperature is much smaller than the recovery temperature, or  $T_i \ll T_r$ . For reentering vehicles, the interface temperature is usually somewhat above the free stream temperature and has values between  $500^\circ$  to about  $960^\circ R$  (Fig. 12.7). Note that the heat flux with evaporative film cooling is directed from the gas boundary layer towards the liquid interface, which is opposite to the conventional application of evaporation.

### 12.3.2 Similarity Analysis of Evaporative Film Cooling for Bodies of Revolution

With the established concepts of heat and mass transfer, an analysis has been developed which permits the calculation of the temperature and water vapor mass fraction at the interface, the film velocity and thickness, and the mass flux of evaporation. For the analytical treatment of the two-phase boundary layer, we have used the concepts and

Definitions:  $Pr = \frac{u c_p}{k} = \frac{V}{\alpha}$  ;  $Le = \frac{D_{1,2} c_p \rho}{k} = \frac{D_{1,2}}{\alpha}$

Assumptions:  $Pr = 1$  ;  $Le = 1$

Results:  $\frac{u}{u_e} = \frac{H - H_i}{H_e - H_i} = \frac{K_i - K}{K_i}$  ;  $\delta_u = \delta_H = \delta_K$

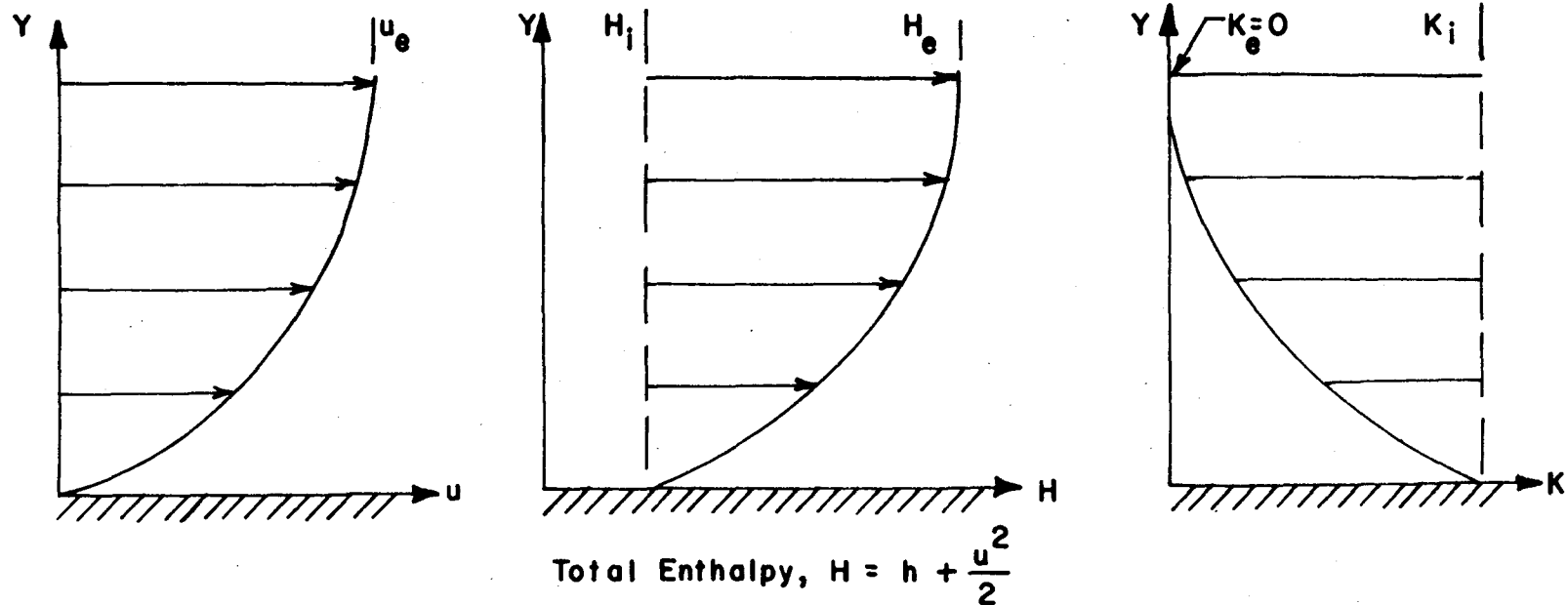


Fig. 12.3 Velocity  $u$ , total enthalpy  $H$ , and water vapor mass fraction  $K$ ; similar profiles in gaseous boundary layer for  $Pr = 1$  and  $Le = 1$ .



assumptions stated in Sec. 12.3.1. We have followed the lines of Lee's analysis of ablation [10], but have taken into account the effect of heat blockage by the mass addition to the gas boundary layer. The analysis is described in more detail elsewhere [6, 7]. Here only a few important results and equations will be quoted.

The most important parameter is the mass fraction  $K_i$  of the water vapor at the interface. It is found to be

$$K_i = \frac{H_e - H_i}{L_v + (H_e - H_i)} \quad (12.1)$$

Here,  $L_v$  is the sum of the enthalpy  $i'$  for heating the coolant from the injection temperature to the interface temperature  $T_i$  and the enthalpy  $r$  for evaporation at  $T_i$ , or

$$L_v = i' + r \quad (12.2)$$

For low injection temperatures (near  $0^\circ\text{C}$ ),  $L_v$  varies only between about 600 and 660 cal/g (1100 to 1200 Btu/lb<sub>m</sub>) in a wide range of temperature ( $T_i = 0^\circ\text{C}$  to  $330^\circ\text{C}$ ) or pressure ( $p_{vi} = 4.5$  mm mercury to about 100 atm). Hence, it is seen from Eq. (12.1) that  $K_i$  depends essentially on  $\Delta H$ . It is interesting that  $K_i$  does not depend on the particular body shape or location, or on the coolant flow  $\dot{m}_c$  applied, or on the mass flux of the main stream. Our experiments have been conducted up to  $T_o = 2300^\circ\text{R}$ , which furnishes  $K_i \sim 0.25$ . For  $\Delta H \gg L_v$ ,  $K_i \rightarrow 1$ . The variation of  $K_i$  as a function of stagnation enthalpy for reentry vehicles will be discussed in Sec. 12.4.1. Using Dalton's law, which relates the mass fraction  $K_i$  with the partial vapor pressure,  $p_{vi}$ , one obtains

$$\frac{M_2}{M_1} \left( \frac{p_e}{p_{vi}} - 1 \right) = \frac{L_v}{H_e - H_i} \quad (12.3)$$

This equation permits the calculation of the interface temperature  $T_i$ , if  $H_e$  and  $p_e$  are given. Since  $p_{vi}$ ,  $L_v$ , and  $H_i$  are functions of  $T_i$ , this is an implicit relationship for  $T_i$ . An important effect of the evaporation is that the mass flux  $(\rho v)_i$ , which evaporates from the liquid film into the gas boundary layer, reduces the heat flux and shear stress at the gas-liquid interface. The ratio of those parameters with and without mass transfer is called the heat blockage factor

$$\psi = \frac{\dot{q}_{gi}}{\dot{q}_o} = \frac{\tau_{gi}}{\tau_o} \quad (12.4)$$

For laminar stagnation point flow, this parameter has been correlated [11] from boundary layer calculations by the relation

$$\psi = 1 - 0.68 \left( \frac{M_2}{M_1} \right)^{0.26} \frac{H_e - H_i}{\dot{q}_o} (\rho v)_i \quad (12.5)$$

The heat flux  $\dot{q}_o$  in the stagnation point region without mass transfer can be obtained from various formulas available in the literature. Now the evaporating mass flux  $(\rho v)_i$  can be calculated. Also, equations for the velocity  $u_i$  at the gas-liquid interface and the film thickness  $\delta_L$  have been obtained from the continuity equation for the liquid film and shear stress relation [6].

### 12.3.3 Evaluation and Conclusions

The analysis has been evaluated for a hemispherical ( $R = 0.5$ -in.) nose of a cone with a water flow rate  $\dot{m}_c = 2.2 \times 10^{-4}$  lb<sub>m</sub>/sec, for  $T_o = 1200^\circ\text{R}$  and  $2000^\circ\text{R}$ . Figure 12.4 shows two interesting parameters as an example. The coolant film thickness  $\delta_L$  is presented as a function of the arc length; it has a maximum value of about 0.001 in. near the stagnation point and then decreases at first rather sharply. The following increase in  $\delta_L$  is due to the decreasing shear stress in the region of fast decreasing density. The mass flux of evaporation  $(\rho v)_i$  shows a trend similar to the known  $\dot{q}$ -variation with azimuth around a sphere. If made dimensionless by the mass flux of the free stream  $(\rho v)_\infty$ , it has typical values of  $10^{-2}$ , however it increases very much with the total temperature.

It has been shown (Sec. 12.2.2), that we are able to predict analytically, without any empirical information, the temperature and water vapor mass fraction at the gas liquid interface for the flow near the stagnation point and around the hemisphere. Our experiments on blunt bodies in the hypersonic wind tunnel are in agreement with those predictions and have demonstrated the effectiveness of evaporative film cooling.

Another important objective was to compare the amount of coolant flow required experimentally to cool a particular body from the stagnation point to a certain downstream location with the integrated value of the theoretical local mass flux  $(\rho v)_i$ . This ratio shall be called

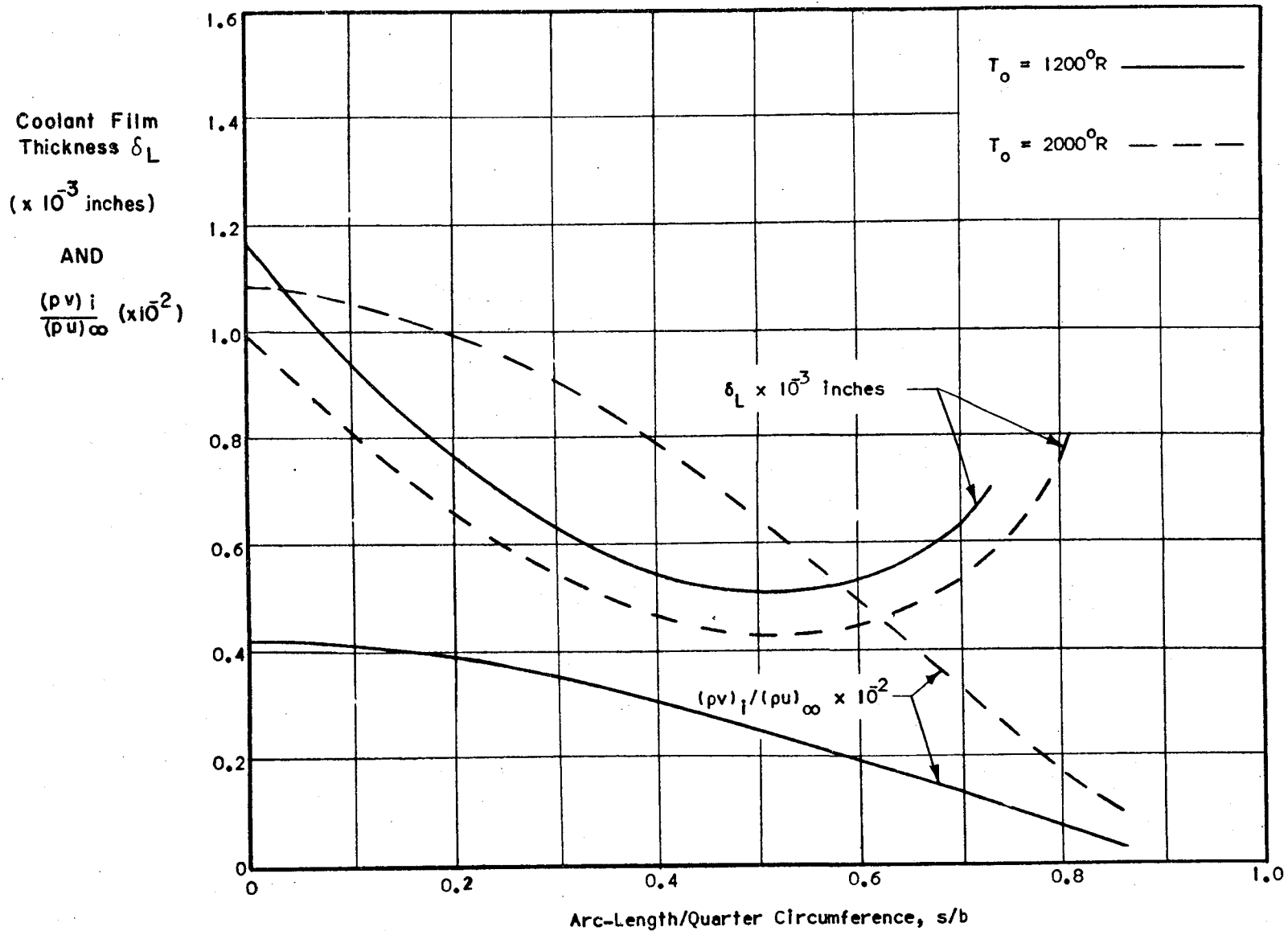


Fig. 12.4 Coolant film thickness  $\delta_L$  and local mass flux of evaporation  $(pv)_i$  as function of azimuth for the blunt cone hemisphere.

coolant usage factor. To date we were not able to determine the minimum amount of cooling needed, due to experimental difficulties in the determination of the length of the film. Limited funds did not permit continuation of extensive experiments. Hence, the coolant usage factor of the method is not sufficiently known. Most of the experiments have been run with a surplus of coolant flow, corresponding to usage factors of 4 or 2. It is felt that with more refined experimental technique the minimum usage factor will be somewhere between 1 and 2.

Although this part of the analysis lacks confirmation, it is felt that the theoretical understanding of the processes involved is sufficiently advanced. Hence, the application of the analysis to extreme reentry conditions (Sec. 12.4), which are beyond the ones measured in the hypersonic wind tunnel, is justified.

#### 12.4 Film Cooling at Velocity Reentry

##### 12.4.1 Water Vapor Mass Fraction and Heat Blockage Parameter

The application of evaporative film cooling for reentry vehicles up to circular speeds is investigated. In particular, we discuss an equilibrium gliding vehicle with a value of the lift area loading  $W/SC_L = 80$  (psf). The coordinates of the trajectory correspond to one of the upper boundaries of the corridor of permanent flight. The stagnation pressure at about 290,000 ft. altitude is 0.003 atm, while the maximum stagnation pressure is about 0.07 atm, a factor 1000 smaller than the maximum values occurring in ballistic missile reentry.

Calculation of the water vapor mass fraction at the interface  $K_i$  is based on Eq. (12.1) of the analysis. The total enthalpy  $H_e$ , at the edge of the boundary layer, near the stagnation point is identical to the stagnation enthalpy  $H_o$ , which is essentially a function of velocity only.  $H_i$  must be interpreted carefully. Its value is small compared to  $H_e$  for large velocities. The static pressure  $p_e$  at the edge of the boundary layer near the stagnation point is equal to the pitot pressure behind the normal shock. The water vapor mass fraction  $K_i$  is presented in Fig. 12.5 as a function of reentry velocity with pressure at the stagnation point (pitot pressure,  $p_p$ ) as parameter.  $K_i$  is increasing strongly with velocity. For velocities near circular velocity,  $K_i \sim 0.91$ . For very small velocities,  $K_i \rightarrow 0$ . It can be seen that the influence of the pressure on  $K_i$  is very small for pressure ranging from near the ice point to near the critical point of water vapor. This covers reentry vehicles from the Dynasoar type to ballistic missiles.

The heat blockage parameter  $\psi$ , which can be calculated from the analysis, is of great importance because it characterizes the reduction in heat transfer due to the effect of the mass transfer occurring perpendicular to and away from the interface. From Eq. (12.5), it

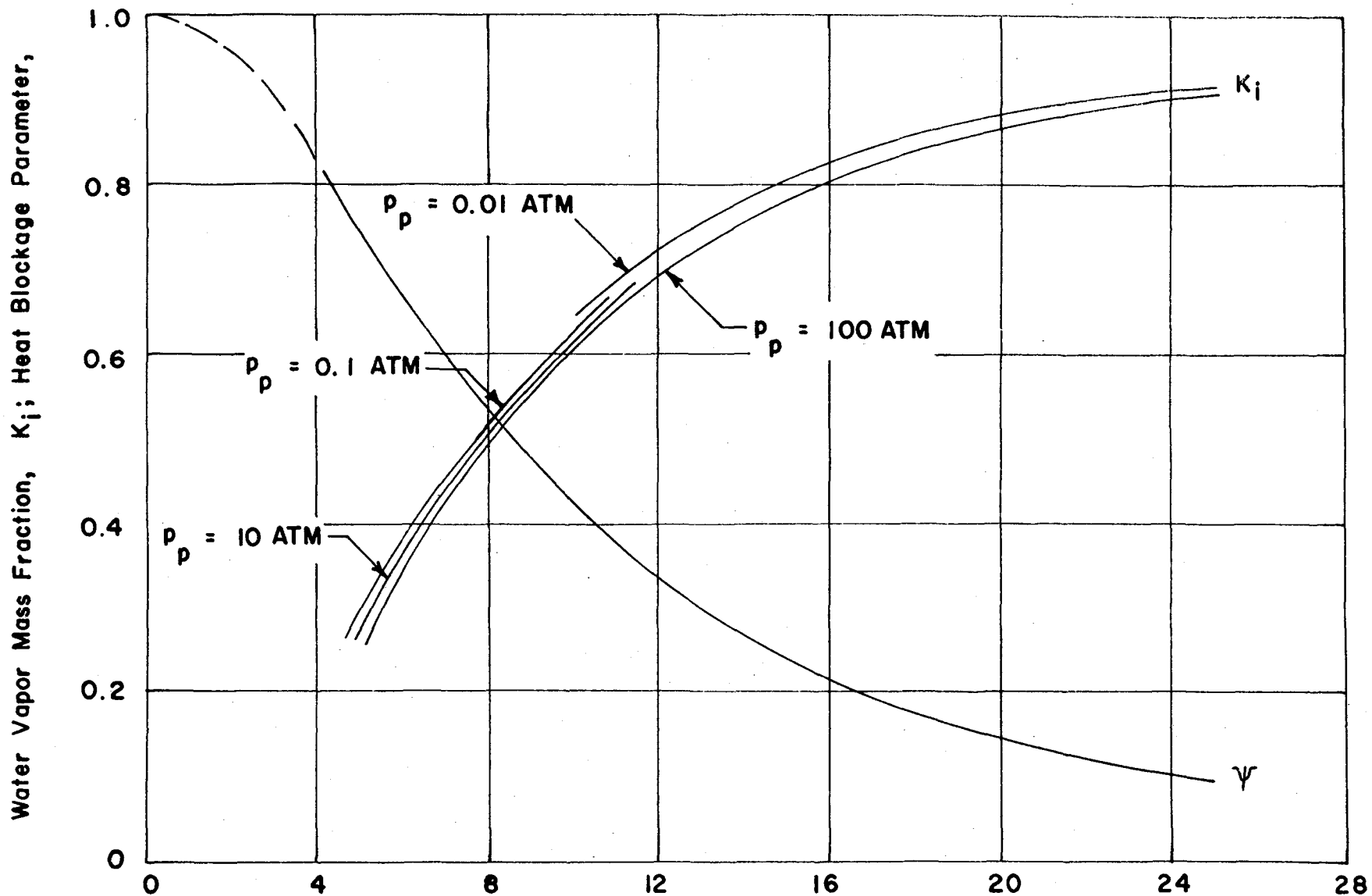


Fig. 12.5 Water vapor mass fraction at interface as function of arbitrary vehicle velocity and stagnation pressure and heat blockage parameter as function of velocity of a particular gliding vehicle ( $W/SC_L = 80$  psf).

can be transformed into

$$\frac{1}{\psi} = 1 + 0.68 \left( \frac{M_2}{M_1} \right)^{0.26} \frac{H_e - H_i}{L_v} \quad (12.6)$$

Inserting the numerical factor 1.61 for the ratio of the molecular weights of air and water and introducing  $K_i$ , one obtains

$$\frac{1}{\psi} = 1 + 0.775 \frac{K_i}{1 - K_i} \quad (12.7)$$

Figure 12.5 shows the heat blockage parameter  $\psi$  as a function of the flight velocity for the particular gliding vehicle trajectory. At low velocities it is close to unity while at reentry velocities the blockage factor decreases to 0.11 as a consequence of the large rate of evaporation. It means that the actual heat transfer  $\dot{q}_o$  is only 11 per cent of the heat transfer  $\dot{q}_o$  without mass transfer. Correspondingly, the amount of coolant needed for the evaporative film cooling is also reduced to 11 per cent.

#### 12.4.2 Evaporative Film Cooling Compared to Ablation Cooling

To compare various mass transfer schemes together with respective materials or fluids, it has become customary to introduce a so-called effective heat of the mass transfer process, particularly for ablation. Here, we introduce the equivalent effective heat of evaporation of the water for the film cooling process. The effective heat is defined by

$$Q_{\text{eff}} = \frac{\dot{q}_o}{(\rho v)_i} \quad (12.8)$$

With the aid of the heat balance equation, this can be transformed into the convenient form

$$Q_{\text{eff}} = \frac{L_v}{\psi} \quad (12.9)$$

The units of  $Q_{\text{eff}}$  are obviously those used for  $L_v$ , for instance Btu/lb<sub>m</sub>. Introducing for  $\psi$  the value from Eq. (12.6) we obtain

$$Q_{\text{eff}} = L_v \left[ 1 + 0.68 \left( \frac{M_2}{M_1} \right)^{0.26} \frac{H_e - H_i}{L_v} \right] \quad (12.10)$$

For small enthalpy difference,  $Q_{\text{eff}}$  is nearly equal to  $L_v$ , then increases with  $\Delta H$ , and finally is nearly proportional to the enthalpy difference ( $H_e - H_i$ ).  $Q_{\text{eff}}$  can also be expressed by  $K_i$ , yielding

$$Q_{\text{eff}} = L_v \left( 1 + 0.775 \frac{K_i}{1 - K_i} \right) \quad (12.11)$$

The effective heat of evaporation is shown in Fig. 12.6 as a function of the velocity. For small velocities it is only somewhat larger than 1100 Btu/lb<sub>m</sub>, while at circular reentry velocities it increases tenfold to 11,000 Btu/lb<sub>m</sub>. In the velocity range from 14,000 ft/sec to 26,000 ft/sec  $Q_{\text{eff}}$  of evaporation is about 1.5 to 2 times the effective heat of ablation of teflon and about 2 times that of quartz (values were taken from [12]). Hence, from the standpoint of mass needed for the cooling process, evaporative film cooling using water is definitely superior to the cooling using ablation of quartz or teflon.

#### 12.4.3 Wall Conditions for Various Vehicles

The pressure-temperature conditions which occur at the interface for evaporative film cooling during reentry for various vehicle trajectories can best be analyzed in a thermodynamic stage diagram (Fig. 12.7), plotting log pressure vs triple point, which occurs at 0.01°C at a vapor pressure of 4.5 mm Hg. Above the triple point, the saturation line divides the gas from the liquid phase; below, it divides the gas from the solid phase. Also included is the boundary between liquid and solid state above the triple point which is very nearly a vertical line at 0°C. The saturation follows approximately the equation of Clausius and Clapeyron. More accurately the numerical values for water vapor are found in tables. The saturation line ends at the critical point, which occurs at  $T = 374.15^\circ\text{C}$  and  $P = 218.39 \text{ atm}$ . Beyond this point water in the liquid and vapor state cannot be distinguished. The slope in the equation mentioned above is proportional to the heat of evaporation  $r$ , that is, for the change of state across the saturation line. Above the triple point,  $r$  varies somewhat with temperature and has a typical value (at 100°C) or  $r = 540 \text{ cal/gm}$  or  $1000 \text{ Btu/lb}_m$ . At the triple point its slope has a finite change.

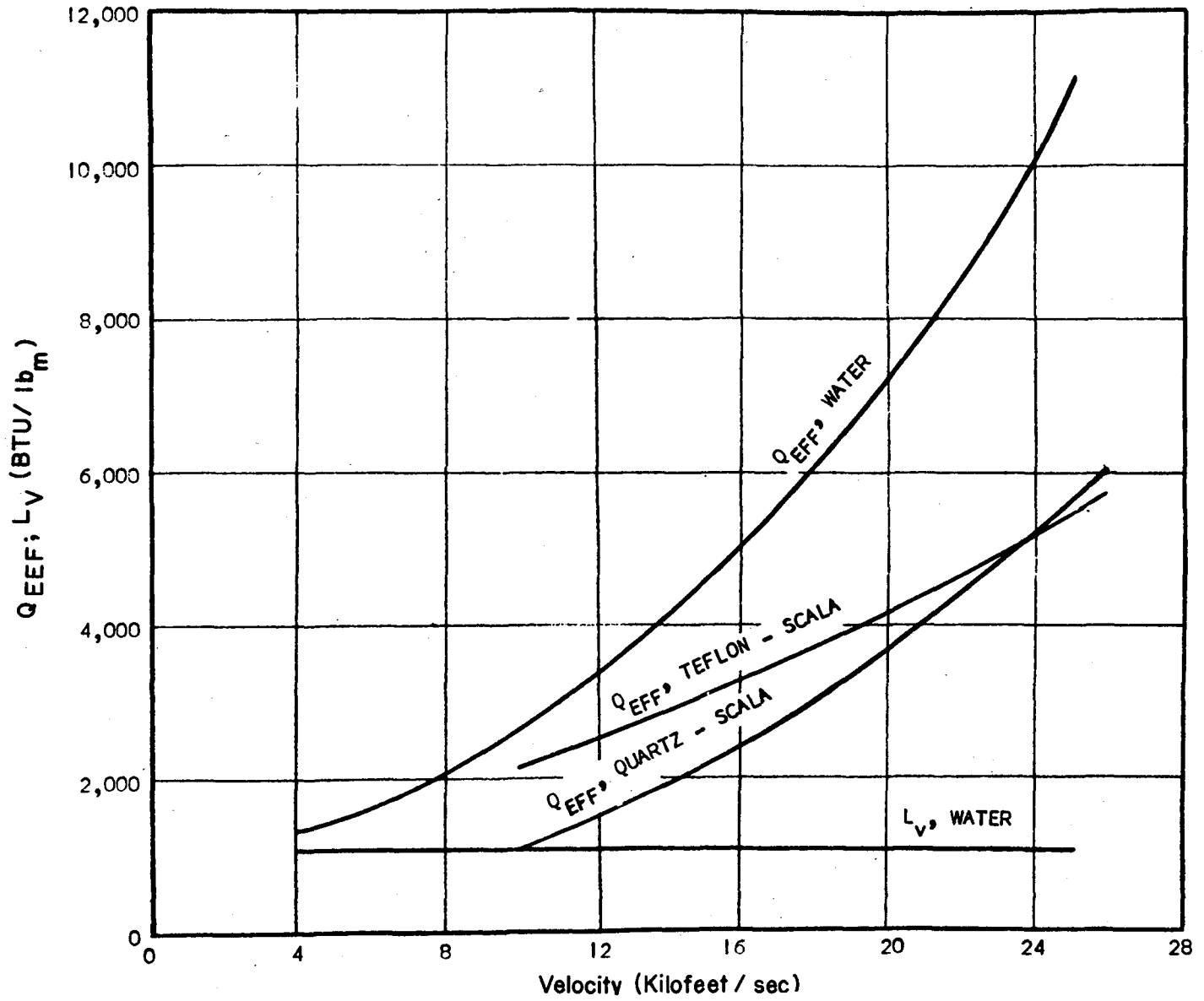


Fig. 12.6 Effective heat of evaporation of water in a film cooling process compared with the effective heat of ablation for teflon and quartz.



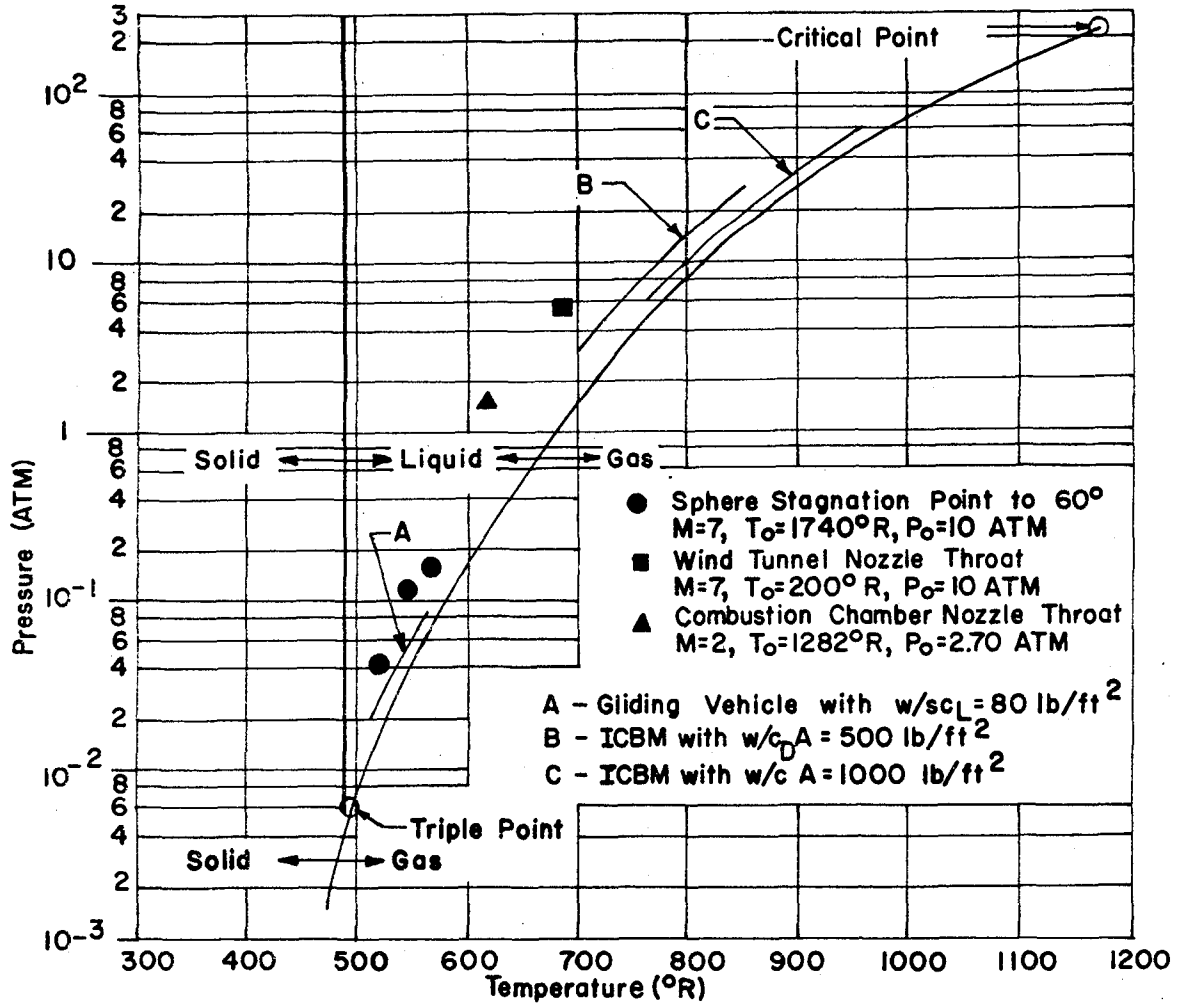


Fig. 12.7 Pressure-temperature state diagram with saturation and ice line for water and interface conditions for three typical reentry vehicles and hypersonic wind tunnel results.

Inserted in the state diagram are experimental points using evaporative film cooling. They represent measurements by the author on the hemisphere model in the hypersonic wind tunnel and in the throat of nozzles installed in a hypersonic wind tunnel or attached to a combustion chamber, as discussed in Sec. 12.2.2. The experimental points are measured wall temperatures  $T_w$ . They can be interpreted as being nearly equal to the temperature of the interface  $T_i$ , because the temperature change through the thin coolant film is very small. The experimental points are plotted at the measured wall temperature  $T_w$  and the measured wall pressure  $p_w$ . Here,  $p_w$  represents the sum of the water vapor partial pressure plus the air partial pressure, hence a total pressure in thermodynamic terminology. It is an important finding that all experimental points  $(T_w, p_w)$  are located somewhat above the saturation line. Since the pressure is constant through the boundary layer, we have  $p_w = p_e$ .

The thermodynamic state of the interface must lie on the saturation line (within a negligible difference due to a finite net evaporation rate). Hence, the pressure which is obtained at the saturation line for  $T = T_w = T_i$  represents the vapor pressure  $p_{vi}$  at the interface. The vertical distance between the experimental point  $(T_w, p_w)$  and the saturation line is representative of the ratio of partial vapor pressure to total pressure  $p_{vi}/p_w$ . The mass fraction  $K_i$  at the interface can be calculated from  $p_{vi}/p_e$  using Dalton's law.

Included in Fig. 12.7 are the ranges for the conditions at the interface for three typical reentry vehicles (A,B,C). The distance of the characteristic lines from the saturation line is not entirely to scale. The regime for the gliding vehicle (A) with  $W/SC_L = 80$  psf is obtained from its range of stagnation pressure and the resulting  $K_i$  presented in Fig. 12.5. The distance between the characteristic line (A) from the saturation line depends upon the water vapor mass fraction at the interface,  $K_i$ . For the lowest stagnation pressure, corresponding to the highest altitudes and largest velocities, the mass fraction is high,  $K_i \sim 0.9$ , and the line will be very close to the saturation line (within 10 per cent of pressure). For higher pressure, that is, lower velocities, the mass fraction is smaller,  $K_i \sim 0.2$ , and the characteristic line is more remote from the saturation line. It can be noted that the wall temperature occurring on the gliding vehicle stagnation point will stay below  $560^\circ\text{R}$ . At the highest speeds and altitudes, the interface conditions will come rather close to the ice region but will not reach it.

The characteristic regions for the ICBM with various ballistic parameters (B,C) are obtained from typical stagnation pressure ranges which are covered by those ICBM's. Of course, the ICBM with the highest area loading (C) reaches the highest stagnation pressure ( $\sim 60$  atm) and therefore also the highest temperatures. But even for this extreme case, the conditions at the interface are still below the critical point, and its wall temperature does not exceed  $950^\circ\text{R}$ .

#### 12.4.4 Total Amount of Coolant Needed

Often the question is raised concerning how much coolant will be needed by a reentering vehicle when using evaporative cooling. No specific answer can be given to such a general question. It depends on the type of the vehicle and on the trajectory selected. However, it can be stated generally, that the amount of water used with film cooling will be only half the mass of material lost using a scheme of ablation cooling. To calculate the total amount of coolant exactly, the total heat input to the vehicle must be known at a given velocity. Then, if the effective heat of evaporation at the particular velocity is taken from Fig. 12.5, the amount of coolant needed each second in that portion of the trajectory is determined. From this value, the total amount can be calculated by integrating over the whole trajectory.

For illustrating how much coolant would be used, a specific example is given. It refers to a super-circular reentry and recovery of a manned vehicle [13]. For a lifting vehicle with a wing loading  $W/S = 42$  psf and a lift-over-drag ratio  $L/D = 2$ , the total amount of heat entering the wing per unit area is given as  $q_{tot} = 12,200$  Btu/ft<sup>2</sup>. The important heat pulse is only 90 sec. The temperature of the wing is assumed to be kept at 2500°F and that of the nose at 4000°F. The effective heat of evaporation at circular velocity is about 11,000 Btu/lb<sub>m</sub> (Fig. 12.6) and increases considerably with higher velocity. We assume conservatively that during all the super-circular reentry  $Q_{eff}$  is only 10,000 Btu/lb<sub>m</sub>. Using the relation

$$\frac{\text{mass of coolant}}{\text{mass of vehicle}} = \frac{q_{tot} \cdot S}{Q_{eff} \cdot M} \quad (12.12)$$

where  $M$  = mass of the vehicle. For the above example, we obtain a ratio of 0.03, or the mass of coolant we need for the total mission is 3 per cent of the mass of the airplane. If it turns out that the coolant usage factor of the liquid would be two, due to imperfections of the injection system, twice that amount (6 per cent of the total vehicle mass) would be needed. The heat input per unit area in the nose of the fuselage is given with 80,000 Btu/ft<sup>2</sup>. Estimating the frontal area of the fuselage to be 2 ft<sup>2</sup> and the vehicle mass  $M = 10,000$  lb<sub>m</sub>, the relative amount of coolant needed will be 0.3 per cent which is only one-tenth of the amount needed for the wing. Obviously those figures are very attractive from the stand point of weight. They do not present any optimum case but are selected because this example has been published.

#### 12.4.5 Additional Advantages of Evaporative Film Cooling Method

We have seen that during reentry from circular velocities the walls of a vehicle protected by evaporative film cooling encounter temperatures which are very moderate, with a high value of  $950^{\circ}\text{R}$  for ballistic missiles and a low value of  $510^{\circ}$  to  $560^{\circ}\text{R}$  for gliding vehicles. This fact presents one of the greatest advantages of evaporative film cooling compared with other mass transfer schemes. However, it is obvious that there are a number of additional advantages and benefits which are a consequence of the stated numbers.

Since the skin of the vehicles and its underlying structure are kept at low temperatures, thermal stresses can be avoided and will permit simpler and lighter construction and the use of less costly materials.

Because the cool skin and structure prevent any heat input into the interior of the vehicle, instrumentation and human passengers are placed automatically in a comfortable temperature. Hence, no large additional internal cooling efforts will be needed in the case of a gliding vehicle. For other vehicles, the amount of internal cooling needed should be drastically reduced. This is an important consideration if a whole system is considered.

Other benefits are seen from the standpoint of aerodynamics and control. With evaporative film cooling, the aerodynamic shape of the leading edge of wings and control surfaces and of the nose of the fuselage are fixed and kept intact. This is in contrast to ablation and a most important factor for gliding vehicles with controlled reentry and landing. It will also be of particular importance for gliding vehicles designed for multiple use.

Further, due to cooling of the boundary layer, there will be a reduction of ionization in the flow around antennas which will improve radio communication and telemetering in cases where it is now difficult or impossible.

#### 12.5 Summary and Conclusions

1. Evaporative film cooling experiments have been conducted in the hypersonic wind tunnel of the University of Minnesota under moderate hypersonic conditions ( $M = 7$ ,  $T_o = 3000^{\circ}\text{R}$ ,  $P_o = 10$  atm,  $\dot{q} = 25$  Btu/ft<sup>2</sup> sec) on axisymmetric blunt bodies at zero angle of attack.

2. A similarity analysis has been developed for laminar stagnation point flow which predicts, without any empirical information, the temperature and water vapor mass fraction at the gas-liquid interface, the local mass flux of evaporation, the coolant film thickness, and the

velocity at the interface. It is in very good agreement with measured wall temperature around the hemisphere. The experimentally needed coolant mass flow so far is about twice the analytical value.

3. The analysis, extended to circular reentry condition, furnishes the following results:

a. Evaporative film cooling is thermodynamically feasible for typical reentry vehicles, such as Dynasoar gliding vehicles or ballistic missiles. This method uses evaporation of water between the ice point and its critical point.

b. It produces typical low temperatures of the skin, from  $560^{\circ}\text{R}$  for Dynasoar to  $950^{\circ}\text{R}$  for ICBM's.

c. The total coolant mass needed compares favorably with the mass lost using ablation cooling.  $Q_{\text{eff}}$  for evaporation of water is nearly twice that for ablation at circular velocities ( $11,000 \text{ Btu/lb}_m$ ).

## DEFINITION OF SYMBOLS

SYMBOLS	DEFINITION
b	arc length from zero to 90°
$C_L$	lift coefficient, referred to Area S
H	total or stagnation enthalpy
i	enthalpy for heating the coolant from 0°C to the temperature of evaporation
K	mass fraction of water vapor
Le	Lewis number
$L_v$	enthalpy of formation of vapor (including heating of liquid)
M	Mach number; molecular weight
$\dot{m}$	mass flow
P	total pressure
p	pressure
$p_p$	pitot pressure
Pr	Prandtl number
$\dot{q}$	local heat flux
$Q_{eff}$	effective heat of evaporation for water in film cooling process
r	heat of evaporation at temperature T
Re	Reynolds number
S	reference area of vehicle
s	distance along gas liquid interface, measured from stagnation point
T	absolute temperature
u, v	components of velocity parallel and normal to gas liquid interface
W	weight of vehicle
$\delta_g$	boundary layer thickness of gas
$\delta_L$	film thickness of coolant
$\theta$	azimuth

## DEFINITION OF SYMBOLS (Cont'd)

SYMBOL	DEFINITION
$\rho$	mass density
$(\rho u)_e$	mass flux at the outer edge of boundary layer
$(\rho v)_i$	mass flux of evaporation (mass addition to gas phase)
$\tau$	shear stress
$\psi$	heat blockage parameter

Subscripts

c	coolant
e	outer edge of gas boundary layer
g	gas
i	gas liquid interface
L	liquid
o	stagnation condition in the reservoir; evaluated for zero mass addition
R	radius of curvature of blunt body
r	recovery
v	vapor
w	body wall
x	length in flow direction
1	foreign component (evaporated coolant) in gas boundary layer
$\infty$	undisturbed free stream
m	mass

## ACKNOWLEDGEMENT

The author sincerely acknowledges the great efforts and contributions of W. Melnik, Principal Engineer, in the theoretical treatment and evaluation of experimental results; of J. Stankevics, Senior Engineer, in the earlier phase; and of K. Thompson, Principal Engineer, and M. Luger, Engineer, in the later phase of the experimental investigation.



## REFERENCES

1. Hermann, R., H. Leitinger, and W. L. Melnik, Design and Construction Problems of a Hypersonic Facility and Preliminary Investigation of Liquid Film Cooling, University of Minnesota, Rosemount Aeronautical Laboratories Research Report No. 127 (March 1955) or Wright Air Development Center TN 55-507.
2. Hermann, R., H. Leitinger, and W. L. Melnik, Design and Construction of a Gasfired Storage Heater and Investigation of Evaporative Film Cooling on Typical Hypersonic Nozzle Throat Sections, University of Minnesota, Rosemount Aeronautical Laboratories Research Report No. 148 (July 1958) or Wright Air Development Center TR 58-376 under similar title.
3. Hermann, R., W. L. Melnik, and J. O. A. Stankevics, Research on Evaporative Film Cooling of a Mach Number 7 Contoured Wind Tunnel Nozzle in the Rosemount Aeronautical Laboratories Hypersonic Facility, University of Minnesota, Rosemount Aeronautical Laboratories Research Report No. 173 (October 1959), or Wright Air Development Division TR 60-251.
4. Leitinger, H., An Estimate of the Thickness of the Coolant Film on an Evaporative Film Cooled Laval Nozzle Throat Section for Mach Number 7, Department of Aeronautical Engineering, University of Minnesota, Research Paper, September 1957.
5. Hermann, R., Evaporative Film Cooling of Blunt Bodies in Hypersonic Flow and its Application to Reentry Vehicles, in XIth International Astronautical Congress Proceedings, Carl C. W. Rentersward, ed., Springer Verlag, Vienna (1961).
6. Hermann, R., "Evaporative Film Cooling at Hypersonic Velocities for Reentry Vehicles", Presented at the 1961 Air Force Ballistic Missile Division/Aerospace Corporation Symposium, Los Angeles, California, (August 1961).
7. Hermann, R., W. L. Melnik, and K. O. Thompson, Two Air Force Office of Scientific Research- technical notes are in preparation covering the subjects of Refs. [5] and [6] in greater detail.
8. Hermann, R., J. O. A. Stankevics, W. L. Melnik, and M. A. Luger, Design, Calibration, and Simulation Capability of the Rosemount Aeronautical Laboratories' High Temperature Hypersonic Facility, University of Minnesota, Rosemount Aeronautical Laboratories Research Report No. 172 (October 1959) or Wright Air Development Division TN 60-108, Dayton, Ohio.

## REFERENCES (Cont'd)

9. McManus, H. N., Jr., Film Characteristics and Dimensions in Annular Two-Phase Flow, Proceedings of the 6th Midwestern Conference on Fluid Mechanics, University of Texas, (1959).
10. Lees, Lester, Similarity Parameters for Surface Melting of a Blunt Nosed Body in a High Velocity Gas Stream, American Rocket Society Journal, Vol. 29, No. 5, pp. 345-354, (May 1959).
11. Bethe, H. A., and Mac C. Adams, A Theory for the Ablation of Glassy Materials, Avco Research Laboratory, Research Report 38, (November 1958).
12. Scala, Sinclair M., A Study of Hypersonic Ablation, General Electric, Department R59SD438, (September 30, 1959).
13. Smith, Robert H., and J. Menard, "Supercircular Reentry and Recovery with Maneuverable Manned Vehicles," Institute of Aerospace Sciences - American Rocket Society Paper No. 61-114, 1808 (June 1961).

297

## **PROPULSION**

## DEVELOPMENT TRENDS OF LIQUID PROPELLANT ENGINES

A. A. McCool and Keith B. Chandler

Propulsion & Vehicle Engineering Division  
George C. Marshall Space Flight Center  
National Aeronautics and Space Administration  
Huntsville, Alabama

The exact origin of the liquid-fueled rocket engine remains questionable, even though pioneering efforts in this field have been documented. A practical design for such an engine existed as far back as 1895. In 1927, Pedro E. Paulet, Peruvian engineer, published accounts of a liquid engine he constructed in 1895 [1]. Other early experimenters who made significant contributions to development included Robert Esnault-Pelterie, French aviation pioneer, and K. E. Tsiolkovsky, a Russian teacher who published an article in 1903 on the possibilities of space exploration. This paper represented the first real attempt to deal mathematically with the problems of space flight. He also proposed the use of a De Laval divergent expansion nozzle and suggested the use of liquid oxygen and liquid hydrogen as propellants in a constant pressure combustion chamber.

Dr. Robert A. Goddard, often called the father of American rocketry, began active experiments in 1920 with liquid propellants for rocket engines. By 1923, he had already developed a practical liquid oxygen and gasoline engine; and on March 16, 1926, one of his rockets made a short flight. Although crude in comparison with his later models, this engine was amazingly simple in design, employing concepts still embodied in today's huge and complex space vehicles. Among Dr. Goddard's "firsts" are: firing a rocket with a speed faster than sound, using vanes in the rocket exhaust for steering purposes, and attaining a record rocket altitude of 2000 ft.

During the period of Dr. Goddard's pioneering efforts in America, Professor Hermann Oberth in Germany was also pioneering the cause of the rocket. In his By Rocket to Planetary Space (published in 1923) he developed a detailed mathematical theory of trajectories, and he also proposed a number of striking new ideas on rocket construction. He proposed the first concept of a regeneratively cooled thrust chamber, one that allowed the propellants to pass through a cooling jacket prior to injection into the combustion zone. He also presented the use of pumps for propellant feed systems and the concept of a two-stage rocket using two propulsion units.

Oberth's studies led to further experiments, but it was not until 1927, when a group of German amateur enthusiasts formed the Society of Space Travel, that group experimentation began to supplement individual efforts. The society tested various rocket engines using liquid oxygen in combination with gasoline or alcohol in most of their experiments. Some of the thrust chambers were jacketed to allow cooling with water. The experiments continued until 1933 when the society was dissolved, and the work was continued secretly by the German Army.

By 1938, preliminary calculations for the A-4 rocket were complete and detailed design began in 1940. The A-4 rocket was better known as the V-2. With the first successful flight test in 1942, a new era in rocketry had truly arrived.

The V-2 engine incorporated many of the features still used in present day engines. Figure 13.1 shows a representative group of engines developed between 1942 and 1961. The V-2 developed a thrust of 56,000 lb at sea level and operated for 62 sec. The system included: a thrust frame, turbopump assembly, thrust chamber, gas generator, heat exchanger and propellant valves. The thrust frame provided for mating the engine to the missile structure and transferred the thrust vector to the missile skin. Two centrifugal pumps for propellant feed were provided for the fuel and oxidizer, and a turbine mounted on the same shaft as the pumps were used as a power source. Steam obtained from decomposition of hydrogen peroxide in a gas generator turned the turbine. Sodium permanganate provided the catalytic reaction of the hydrogen peroxide to form steam. The thrust chamber assembly consisted of a chamber body and an injector welded into a single unit. Two concentric shells with a coolant passage between them made up the chamber body.

The start sequence was begun by energizing a pyrotechnic igniter. Partial opening of the main oxidizer and fuel valves allowed both oxidizer and fuel to flow by gravity into the combustion chamber. If burning was satisfactory, the observer then signaled main stage operation. Sequencing of the control valves allowed the permanganate catalyst to flow to the decomposition chamber prior to the peroxide. Once the peroxide and catalyst reacted, steam and gaseous oxygen powered the turbopump. As the pumps accelerated, the main valves were fully opened allowing full propellant flow into the oxidizer and fuel headed and injector elements. The oxidizer and fuel elements were concentric, and mixing began as the oxygen and alcohol emerged, thereby establishing full thrust in the combustion chamber.

The development of large liquid-propellant rocket engines in America was initiated in 1947 by the Air Force for the Navaho project. The original engine proposed for this program was to produce a thrust of 75,000 lb. Liquid oxygen and an alcohol-water mixture were the propellants. While early V-2 concepts were incorporated in this engine,

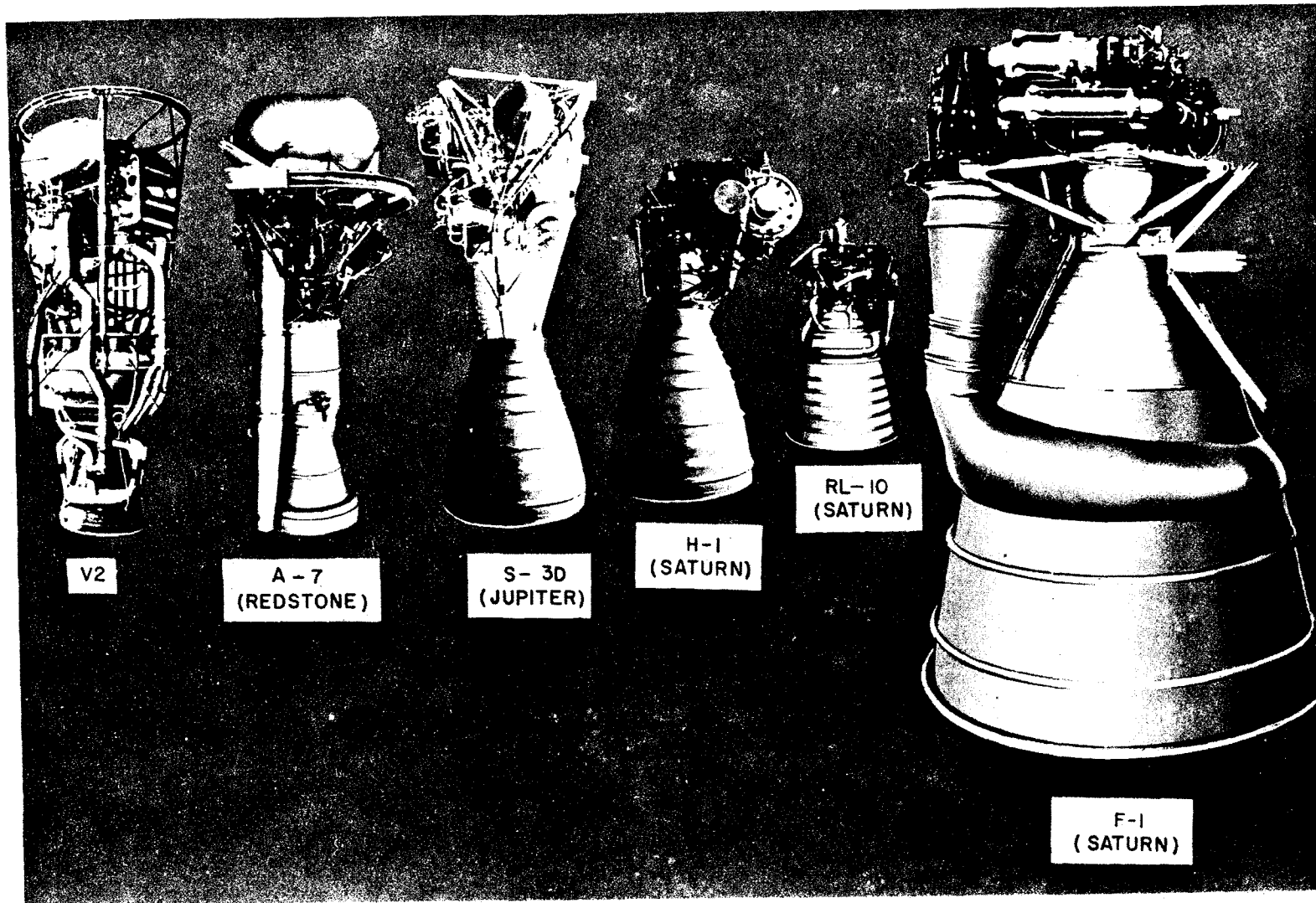


Fig. 13.1 A representative group of liquid propellant engines developed between 1942 and 1961.

many new design features and improvements were brought in. A new thrust chamber design provided better cooling for the higher heat transfer rate. An improved single injector replaced the 18 separate injectors, thus providing simplicity. Figure 13.2 compares the injector configurations. A simplified control system eliminated the complicated interlock of controls.

The A-series engine utilized a cylindrical combustion chamber as compared with the bulky spherical V-2 chamber. The A-series engine turbopump was capable of producing 850 hp; the V-2 turbopump produced only 460 hp. Power for the turbine was provided by a similar hydrogen-peroxide gas generator. Here in the power system, another advance had been made over the V-2 engine. The A-series engine utilized a decomposition chamber containing potassium permanganate for a catalyst, whereas the V-2 engine used sodium permanganate as the catalyst. High-pressure gas fed the hydrogen peroxide into the decomposition chamber, where it reacted with the catalyst to form high-pressure super-heated steam. The sodium permanganate used in the V-2 was a liquid which required an additional tank. Both the hydrogen peroxide and catalyst were pressurized and fed into a reaction chamber, thus requiring additional valving and sequencing over the later A-series engine.

The engine incorporated a closed loop thrust control system in which the chamber pressure was sensed and compared to a reference pressure. Any difference between the chamber and reference pressures caused an error signal which was amplified to control a valve in the hydrogen peroxide line thereby controlling pump speed, flowrates, and thrust. Thrust could be controlled to better than 2.0 per cent of nominal at any time during flight, and this control reduced the guidance requirements for range accuracy.

In 1951, the Army was moving rapidly toward the design of the Redstone missile. The propulsion requirements for this missile were met by the A-series engine, so continued development of the engine was sponsored by the Army. Production was begun in 1952, and the first successful flight was completed in August 1953. Since then, about 75 launchings have been made through 1961. The Redstone missile, with its A-7 engine, became the "reliable workhorse" for America's space accomplishments. As an example of the versatility of this missile system, a high-energy fuel consisting of unsymmetrical-dimethylhydrazine and diethylenetriamine was substituted for the alcohol to provide additional performance. A performance gain of about 12 per cent was obtained. No major changes to the engine or missile were required to use this fuel, which was utilized in the booster for Explorer 1, the first American satellite. Other successful accomplishments of this reliable system were the Mercury suborbital launches, including America's first astronaut flight on May 5, 1961.

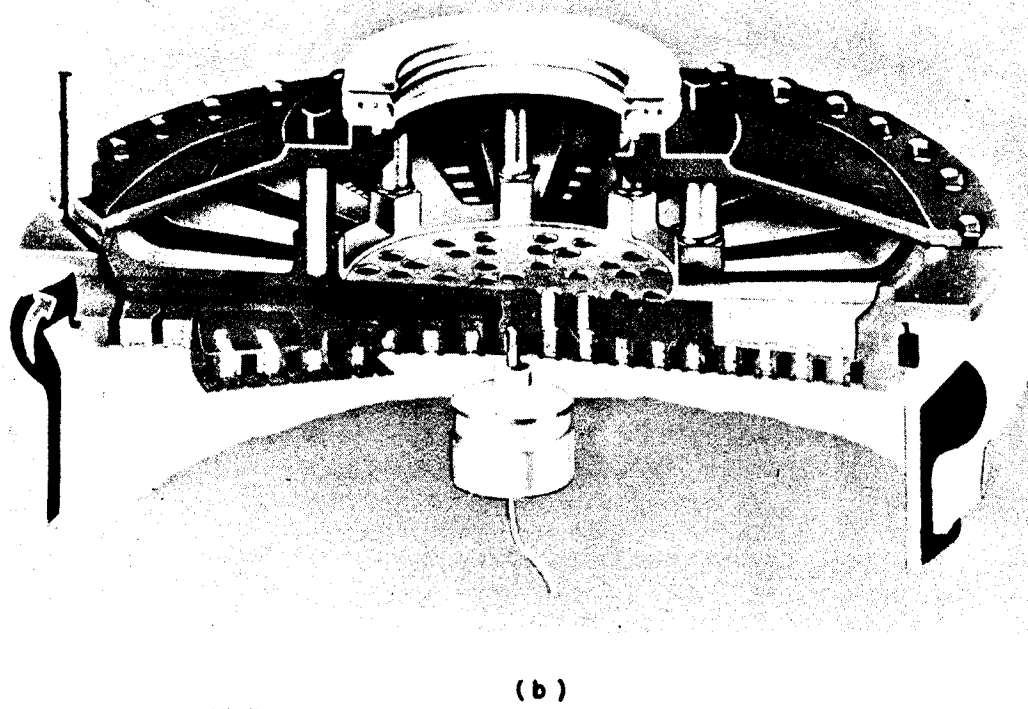
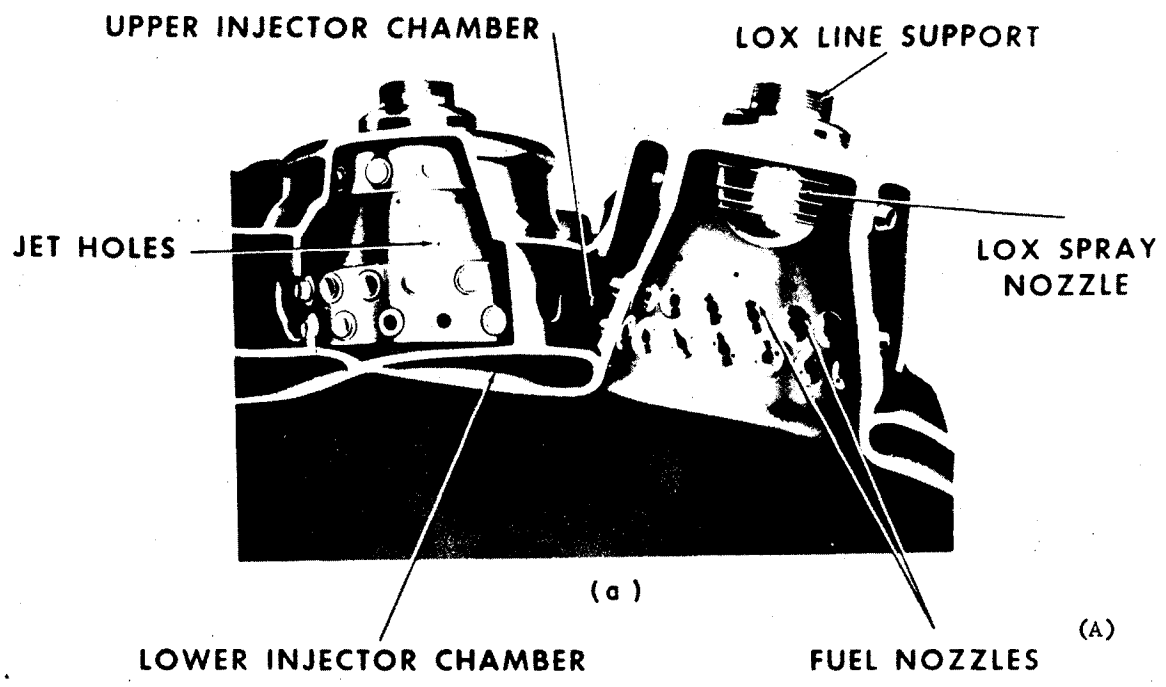


Fig. 13.2 Injection systems of liquid propellant engines (a) V2, (b) A7 used with the Redstone IRBM.



In 1955, development efforts were progressing at Rocketdyne Division of North American Aviation, Inc., to modify the Atlas S-3 engine for use in the Jupiter missile. This S-3D engine produced a thrust of 150,000 lb, using liquid oxygen RP-1, a refined kerosene fuel. Major components of the propulsion system include a thrust chamber assembly, turbopump, gas generator, control system, and a thrust vector control system. Related S-3D systems include the following: an external start system; an electro-pneumatic system to start, sustain, and stop propellant flow; and a thrust control system that operates by throttling the flow of oxygen to the gas generator, thus controlling power to the turbopump.

Many advances in state of the art were incorporated in this engine. The first advance was the propellant performance gain (about 7 per cent) attained by switching from oxygen and alcohol to oxygen and kerosene. A bipropellant gas generator utilizing the same propellants as the combustion chamber eliminated the need for a steam generating system. In starting, propellants are furnished to the engine from auxiliary start tanks and then bootstrap takes place. In the bootstrap design, propellants are bled to the gas generator from a point downstream from the pumps. Once power is attained and the pumps come up to speed, the propellants are bootstrapped from the pumps, and flow from the start tanks ceases.

This engine utilized a tubular-wall regeneratively cooled thrust chamber, which provided a major reduction in weight, cost, and fabrication time, as compared to the double-walled chamber (Fig. 13.3). A bell-type nozzle replaced the 15-deg half-angle conical nozzle used in the Redstone. The S-3D thrust chamber utilized an 80 per cent bell on the divergent portion of the nozzle, which means that the nozzle is 80 per cent of the length of a conical nozzle for the same expansion ratio. The major advantage of the bell nozzle is in the reduction of length and weight. Better performance is also obtained. This is true because the flow of the combustion gases is allowed to expand more in a radial direction from the sonic throat and is then turned or straightened into approximately axial flow at the exhaust.

A gimbal bearing design allowed swivelling of the thrust chamber for thrust vector control, and hydraulic actuators moved the chamber upon receipt of signals from the vehicle guidance system. The effective gimbal angle was  $\pm 7\frac{1}{2}$  deg. This system was a distinct improvement over the carbon vanes used in the jet streams of V-2 and Redstone missiles, and provided a real gain in performance and controllability.

The S-3D engine demanded higher pressures and flowrates for the higher thrust. This in turn made substantial increases in the turbopump horsepower requirements. Inducer design and cavitation characteristics were not well known at that time. Consequently, the pumps were

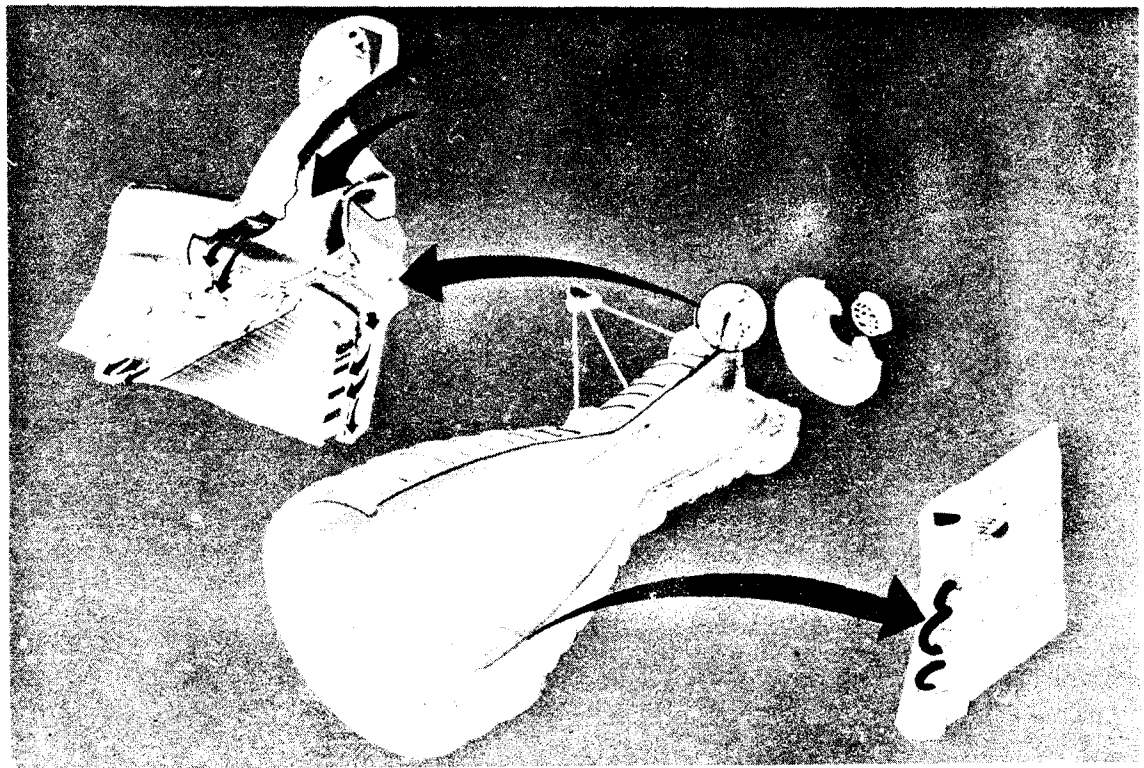
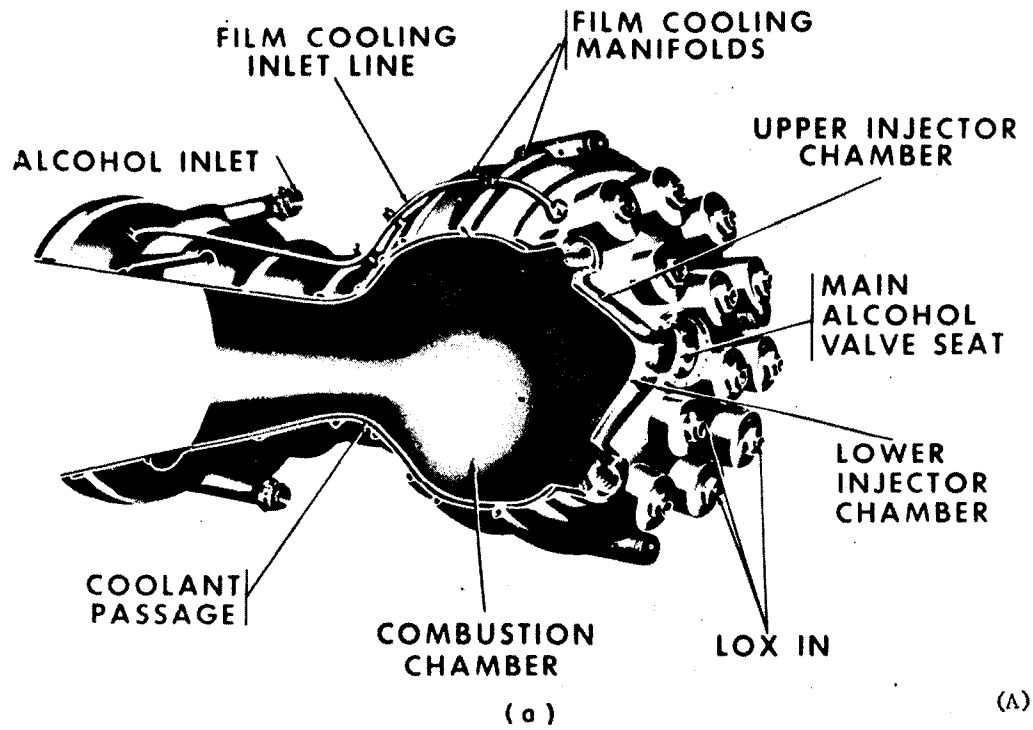


Fig. 13.3 Thrust chamber configurations of liquid propellant engines (a) V2 (b) S-3D.

designed to operate at low speeds. An efficient direct-drive turbine would require a large diameter turbine wheel, so a gear train was provided to allow the turbine to run at higher speeds than the pumps. An accessory pad for auxiliary power was provided in the gearbox for driving accessory components. The gearbox received additional lubrication by means of a pressurized oil tank.

The first Jupiter missile launching, using a S-3D engine, was made in March, 1957. Both the Atlas and Thor missile systems use a closely related S-3 type engine.

Development of the H-1 engine was begun by Rocketdyne in 1958 and was based on the Jupiter S-3D engine. It is a fixed-thrust (188,000 lb) engine, utilizing oxygen and RP-1. The H-1 was successfully used in a cluster of eight engines in the booster, or first stage, of the Saturn launch vehicle on October 27, 1961. Since the H-1 was a direct outgrowth of the S-3 series used in the Jupiter, Thor, and Atlas missiles, full utilization has been made of the technology developed in these programs.

Many innovations were incorporated in the H-1 engine which not only changed engine configuration but brought about greater simplification and increased reliability. The turbopump assembly is mounted directly on the thrust chamber in a piggyback fashion. Such positioning eliminates the need for flexible sections in the high-pressure propellant lines between the pumps and the thrust chamber. Since thrust vector control is attained by gimbaling the entire engine, flexible sections are required in the suction lines, but the pressure is fairly low and reliability is not so difficult to achieve. The H-1 does not have a device for thrust control as was used in the S-3D engine. Instead, the thrust is calibrated by the manufacturer during acceptance testing by the selection of proper orifices which are inserted in the lines supplying propellant to the gas generator.

The starting sequence has been greatly simplified. Auxiliary pressurized oxidizer and fuel start tanks have been eliminated by the use of a solid propellant turbine spinner to accelerate the turbopump. Replacement of the complex electrical interlock system and solenoid valves has been accomplished by a pressure-ladder sequence that utilizes fuel pump discharge pressure as the actuating force for opening the various valves. The igniter formerly used in the combustion chamber has been replaced by a hypergol slug in the fuel line.

The engine is started by energizing a pyrotechnic squib in the solid propellant gas generator, or turbine spinner, and the resulting combustion gases accelerate the turbopump. Fuel pump discharge pressure is utilized to open the main oxidizer valve and the main fuel valve in sequence. A slug of triethyl aluminum precedes the fuel flow into the

combustion chamber and ignites hypergolically with the oxidizer. Pressure in the propellant lines forces propellant into the gas generator, with a slight oxidizer lead. Ignition is accomplished by hot gases from the turbine spinner, and after about 200 msec of combined turbine spinner and gas generator operation, the turbine spinner dies out and the engine has bootstrapped into main stage operation. The entire sequence has been accomplished in less than 1 sec.

All need for special lubricating fluid for the turbopump gearbox has been eliminated by utilizing engine fuel, in conjunction with an additive. The pressurized lubricating tank is no longer necessary, as the fuel for lubrication is tapped off downstream from the fuel pump.

Engine shutdown is initiated by firing a pyrotechnic squib associated with the main oxidizer valve. The main oxidizer flow stops very quickly, the combustion in the gas generator decays, and the turbopump decelerates. The main fuel valve closes, and the engine is thus shut down in a fuel-rich condition. Thrust decay, or tail-off, is minimized by this rapid sequence, which is desirable for accurate guidance and flight prediction.

The trend toward system simplification is illustrated in Fig. 13.4 which compares the S-3D and H-1 engines.

In 1958 the need for a large engine for space vehicle boosters was recognized, and early in 1959, a contract was signed with Rocketdyne to develop an engine with 1.5 million lb of thrust. This engine, known as the F-1, will operate on oxygen and RP-1 propellants. Preliminary flight rating tests are scheduled for early 1963, and the first flights could be achieved in 1964. The F-1 is to be used in clusters of from 2 to 8 engines in vehicles of the Saturn and Nova classes.

Basically, the F-1 is an outgrowth of the H-1, but the difference in size is tremendous. The cooled portion of the thrust chamber is 11 ft long, 40 in. in diameter at the chamber throat, and 9.5 ft in diameter at the exit. The turbopump generates 60,000 hp, weighs almost 3000 lb, and moves propellant at a rate of 3 tons each second. Enough oxygen is used in 1 sec of F-1 operation to supply the breathing requirements of an average person for 3 yr!

The features of the F-1 that are similar to those of the H-1 include the piggyback turbopump, hypergolic ignition, pressure-ladder start sequence, tubular construction of the thrust chamber, hydraulically operated gimbal system, fixed orifice propellant control, and baffled injector. Simplification of the hydraulic system has been attained, however, by using the on-board fuel for hydraulic fluid and the main fuel pump as the source of pressure.

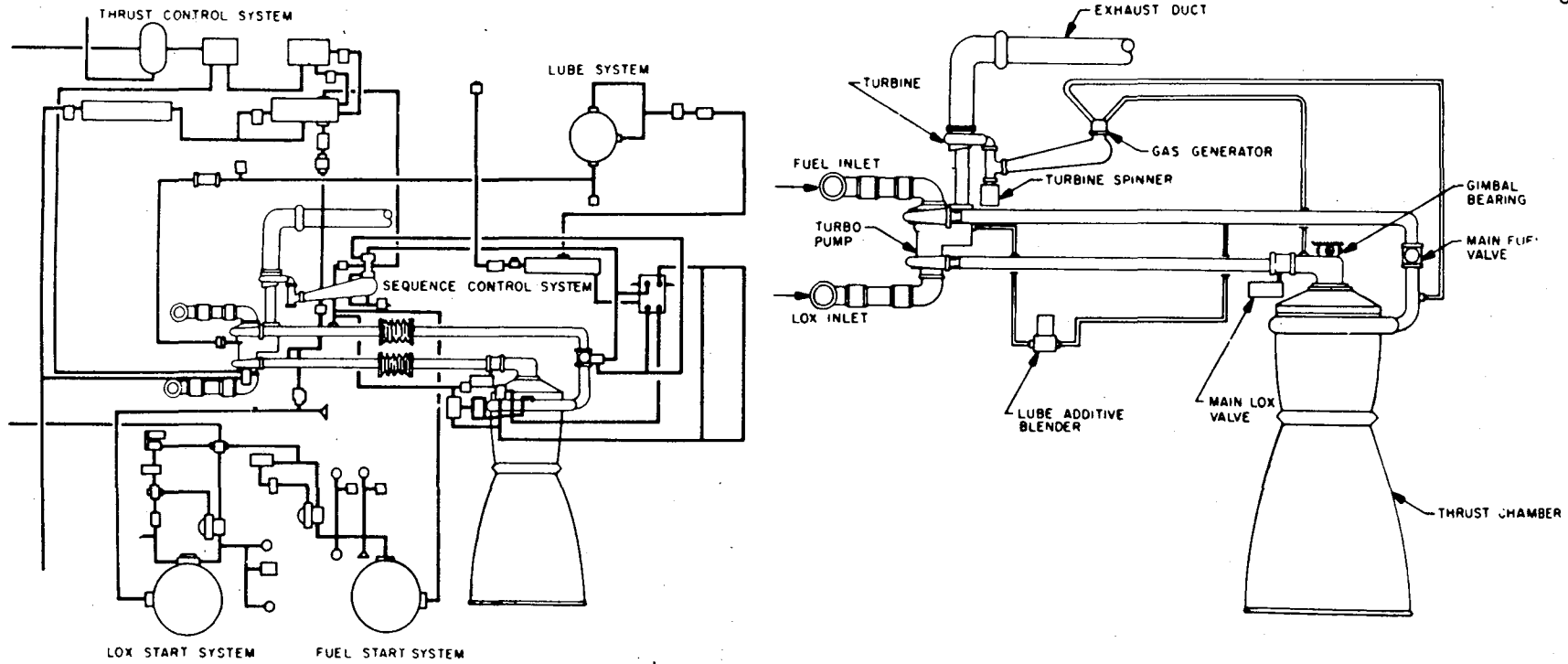


Fig. 13.4 System schematics of an early (left) and modern (right) liquid propellant engines.

The gas generator is regeneratively cooled and operates fuel-rich with the main on-board propellants, oxygen and RP-1. After passing through the two-stage turbine, exhaust gases are ducted to the exhaust nozzle at a point where the expansion ratio equals 10 to 1. Cooling the gas generator alleviates the possibility of hot spots that could ignite fuel vapors. Ignition is accomplished in the gas generator by electrical spark. The turbine is accelerated by flowing main propellants under tank pressure into the gas generator rather than by using an auxiliary turbine spinner or some other temporary source of gas. This method is known as tank head start.

Engines that are gimbaled or swivelled must have provisions for flexing the suction lines, and special bellows have been designed for the F-1. The H-1 system has two bellows in each suction line, one for each plane of engine movement. Although this arrangement requires only flexing capability and no axial movement, it does require a fairly cumbersome wrap-around configuration in the suction lines. The bellows used on the F-1 combine both flexing and axial movement, which facilitates a direct routing of propellant to the engines. It is capable of a change in length of  $\pm 10$  in., and it provides compensation of pressure and volume, thus preventing excessive loads on the pump and actuators and pump cavitation.

The exhaust nozzle is regeneratively cooled with fuel to a point where the expansion ratio equals 10 to 1. Additional expansion to 16 to 1 is achieved by the use of a sectional skirt that is bolted on in the field. The bolted-on feature was incorporated to facilitate the use of conventional means for transporting the engine to the launch site. The skirt is composed of a double wall, with the interior wall being perforated. Cooling is accomplished by flowing turbine exhaust gases between these two walls and through the perforations into the nozzle.

The thrust of a rocket engine is a function of the exhaust velocity of the combustion gases, and the exhaust velocity is an inverse function of the molecular weight. Thus, propellants of low molecular weight are most efficient. An average molecular weight of the oxygen and kerosene combination is above 20, while oxygen and hydrogen is about 9.8. Fluorine and hydrogen is even less at 9.1. These latter two high-energy propellant combinations have always been considered the ultimate. Because of its toxicity, however, fluorine has not yet been accepted sufficiently to be included for use in production engines. Although the oxygen and hydrogen combination has also been approached with considerable hesitancy because of the explosion hazard, current testing has shown that with proper precautions it can be used safely.

The first production engine to use the high-energy propellant combination of oxygen and hydrogen is the RL10 being built by the Pratt and Whitney Aircraft Company at West Palm Beach, Florida. There are

two versions of this engine, namely, the RL10A-1 and RL10A-3. The former is to be used in the Centaur launch vehicle and is designed to operate with separate boost pumps. The latter is to be used in the S-IV stage of the Saturn launch vehicle and will use propellants directly from the vehicle tanks. Other differences are minor. Since the RL10A-3 will eventually be used exclusively, the following discussion will be limited to the RL10A-3 model.

This engine develops 15,000 lb of thrust (vacuum) and operates at a specific impulse of over 400 lb-sec/lb. The thrust chamber is a conventional tube bundle construction, and it is regeneratively cooled by circulating the liquid hydrogen propellant. A most unusual aspect of the system is the absence of a gas generator. Figure 13.5 illustrates how the topping cycle takes advantage of the peculiar properties of hydrogen fuel: low critical pressure, high specific heat, and low initial temperature ( $-420^{\circ}\text{F}$ ). In passing through the tubular cooling jacket of the thrust chamber, the fuel is heated to about  $-100^{\circ}\text{F}$  and expanded in the process. This provides enough energy to drive the two-stage partial-admission aluminum turbine, which drives the two centrifugal pumps. The fuel pump is driven directly from the turbine, and the oxygen pump is driven on a parallel shaft through a spur gear train. No lubricant is used in the engine. The gears and bearings are cooled by fuel bled from the pump. For a certain operating condition, this cycle is thermodynamically more efficient than a gas generator drive.

The RL10A-3 engine utilizes a spark ignition system and has a multiple start capability, with relatively long coast periods between operating cycles. Residual heat in the thrust chamber jacket, even when initially at  $-300^{\circ}\text{F}$ , is sufficient to cause the fuel to spin the turbine fast enough to initiate the start sequence. Propellants flow to the combustion chamber, where they are ignited by the spark igniter located in the center of the injector face. The resulting combustion provides additional heat to rapidly accelerate the turbopump to operating speed. Operating speed is varied to provide thrust control by varying the amount of fuel bypassing the turbine in response to chamber pressure signals. Propellant mixture ratio can be controlled during flight in order to provide maximum utilization of propellants. The control valve responds to signals to achieve simultaneous depletion of both propellants. Valve control and operation are accomplished by solenoids and helium pneumatic pressure.

The propellant injector face is made from a porous welded steel mesh and is cooled by transpiration of hydrogen through it. Oxidizer is supplied through a machined tube which projects through the injector face and whose outside diameter is considerably smaller than the hole. Each element of the injector thus consists of a nozzle of liquid oxygen and a concentric annulus for the gaseous hydrogen. The concentric jet design brings the fuel and oxidizer into immediate contact upon leaving the injector face, which tends to shorten the required mixing length and prevent combustion instability.

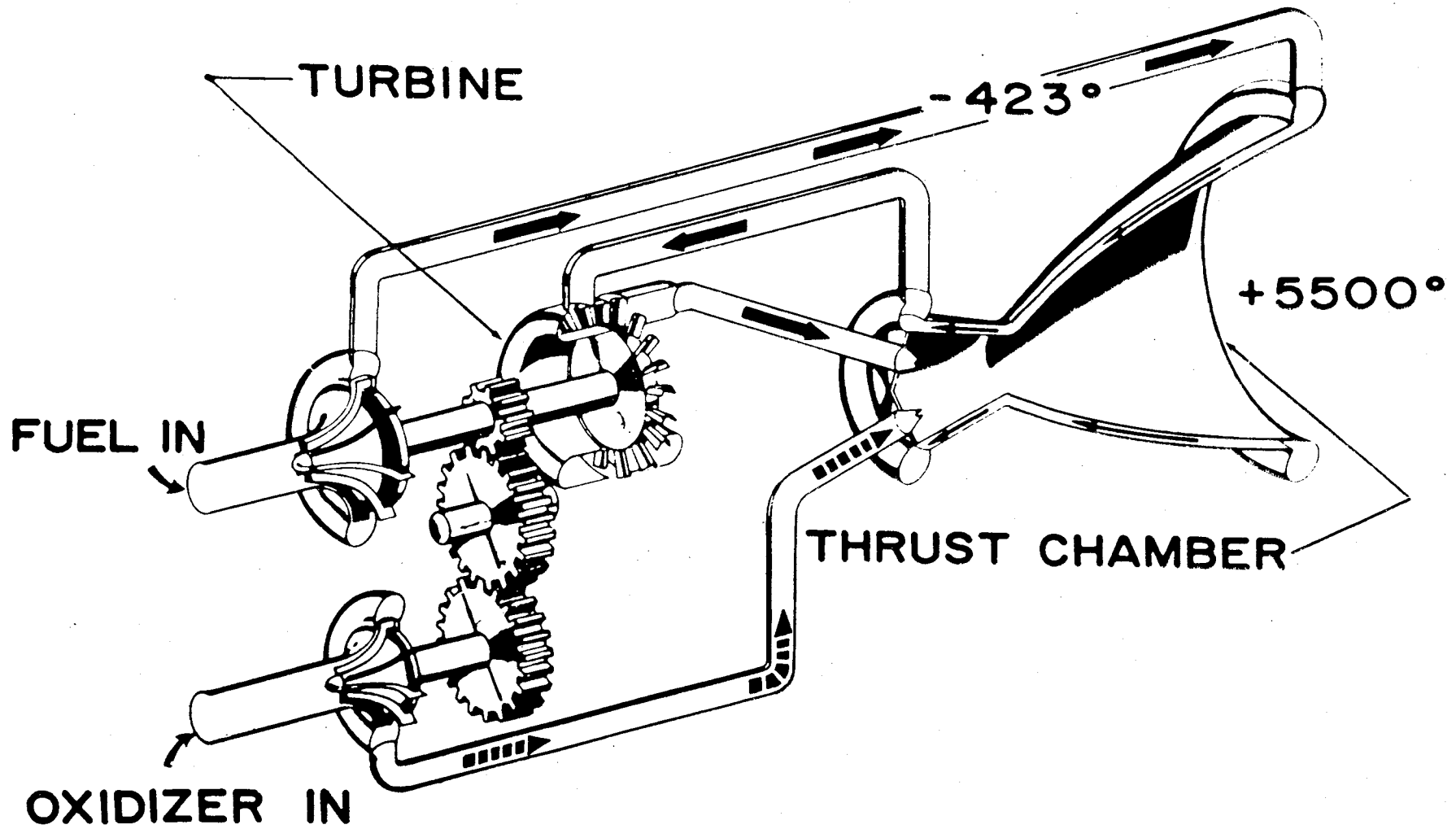


Fig. 13.5 The RL10A propellant feed system topping cycle.



A conventional gimbal system is used for thrust vector control. The actuation force is supplied by a hydraulic system that is powered from an accessory pad on the oxidizer pump. An electric motor is used for circulating the hydraulic fluid during checkout and coast periods.

In September of 1960, a contract was signed with Rocketdyne for the development of a 200,000-lb thrust rocket engine known as the J-2 (see Fig. 13.6). This engine is to be used for upper stages of the Saturn vehicle, and will utilize liquid oxygen and liquid hydrogen. Its thrust chamber is of tubular wall design and is regeneratively cooled with hydrogen. Propellants are fed by two turbopumps, each of which is driven by its own turbine. In this manner, each pump operates at an optimum speed, without the use of a gearbox. The fuel pump is an axial flow type; the oxygen pump is centrifugal. Power for the two pumps is furnished by a single gas generator that utilizes the main propellants of the engine. Hot gases from the generator flow through the fuel pump turbine and the oxygen pump turbine and are then routed through ports into the exhaust nozzle.

The J-2 has an expansion ratio of 27.5 to 1 for altitude operation, but it is designed to flow full at sea level. Thus, at a nominal cost in performance, there is no need for expensive and cumbersome equipment to simulate altitude conditions during sea level testing.

An electrical spark ignition is used in the gas generator and in the main combustion chamber. In the latter, the ignition spark is augmented by an auxiliary ignition flame. Hydrogen gas, stored in a 4-cu ft bottle at 210°R and 800 psi, is used to spin up the turbines during the start sequence. To provide restart capability, the storage bottle is recharged by tapping gas from the fuel manifold. Only three starts are possible, however, due to the limited quantity of helium that is provided for pneumatic valve actuation and purging. The start sequence is controlled by a combination electrical system and pressure-ladder sequence in the pneumatic system.

Control of the J-2 thrust vector is governed by gimbaling the entire engine, including the piggyback turbopumps and gas generator. The gimbal actuators are operated by a hydraulic system whose pump is driven from an accessory pad on the oxygen pump. During checkout and coast periods, the hydraulic fluid is circulated by an electric pump. There are no requirements for special lubricant fluids.

Leakage of fluid connectors in rocket engines has received considerable attention in past development programs, and this program is no exception. All critical connections are either brazed or provided with a collection device so that any leakage can be safely bled overboard.

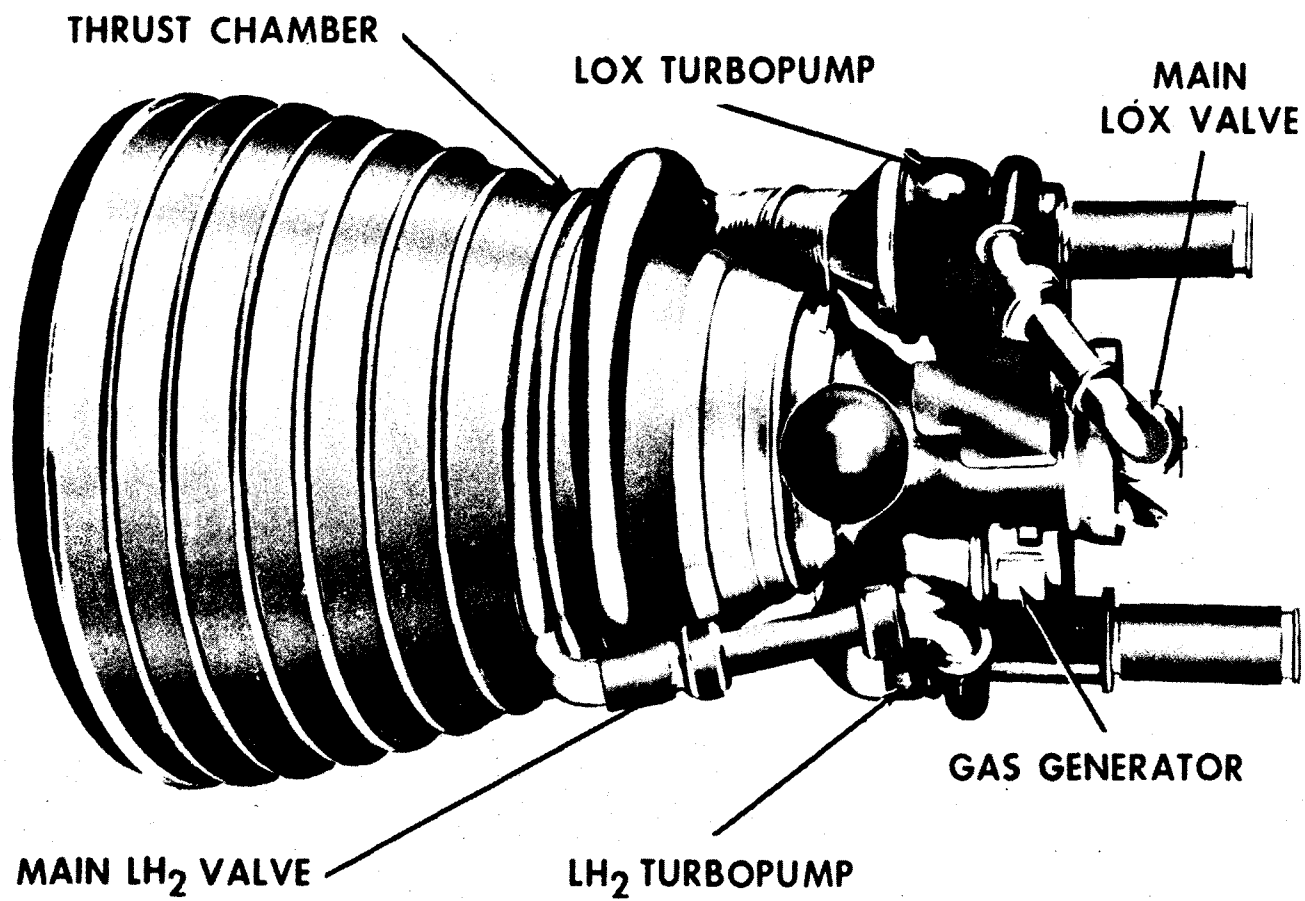


Fig. 13.6 The J-2 liquid propellant engine.

The J-2 engine is more complex than the current oxygen-RP engines, and one might conclude that the state of the art in developing simplicity has taken a set-back. It must be remembered, however, that it is only the second production engine to utilize the oxygen and hydrogen propellant combination, which represents a new technology. The original concept, for instance, used a tank head start sequence, but the fuel dumped overboard produced a potential hazard for explosion. The 4-cu ft sphere of hydrogen was added for spinning up the turbine, but undoubtedly the system can be simplified during future development. This matter of simplification was put rather succinctly by a British engineer named Bill Stout in 1930. He said, "What you don't put in an airplane don't give no trouble/simplicate, and adds more lightness."

Many dreams of the early pioneers in rocketry are rapidly becoming realities. Man has thrown off the shackles of gravity, and in the foreseeable future, he will be accomplishing the ultimate in adventure--travel to other planets. In a few short years, liquid-rocket engines have become sophisticated and reliable power plants, capable of tremendous bursts of power and of operating under the most difficult environmental conditions.

A summary of the progress made during the last 20 years is shown in Fig. 13.7. The specific impulse ( $I_{sp}$ ) is a ratio of the lb-sec of impulse produced per lb of propellant consumed and is used to measure engine efficiency. Generally speaking, the upward trend of this parameter has been due to the use of progressively higher energy propellant combinations. Engines currently under development use oxygen and hydrogen, which is very near the ultimate for chemical systems.

The thrust-to-weight ratio (engine thrust divided by dry weight) has increased steadily by improvements in the state-of-the-art until the F-1. This engine is larger than its predecessors by about one order of magnitude, and it truly represents a new generation. The H-1 ratio is high because it enjoys the benefits from a series of upratings and simplifications that began with the Navaho engine. Design of the F-1 is quite conservative, however, and it is reasonable to expect that the thrust-to-weight ratio will improve as its development progresses.

Thrust, of course, has been increased a most significant amount with the development of the F-1, but we cannot expect to see another step as large as one order of magnitude. Chamber pressure has increased rather steadily, and in spite of the fact that higher chamber pressures will create new problems, the gains to be realized are sufficient to justify the effort. We can expect this parameter to level off at about 2500 psia because of the law of diminishing returns.

In future liquid-propellant engines, further improvements in simplification can be expected. For example, considerable effort has already been devoted to elimination of the gas generator by utilization

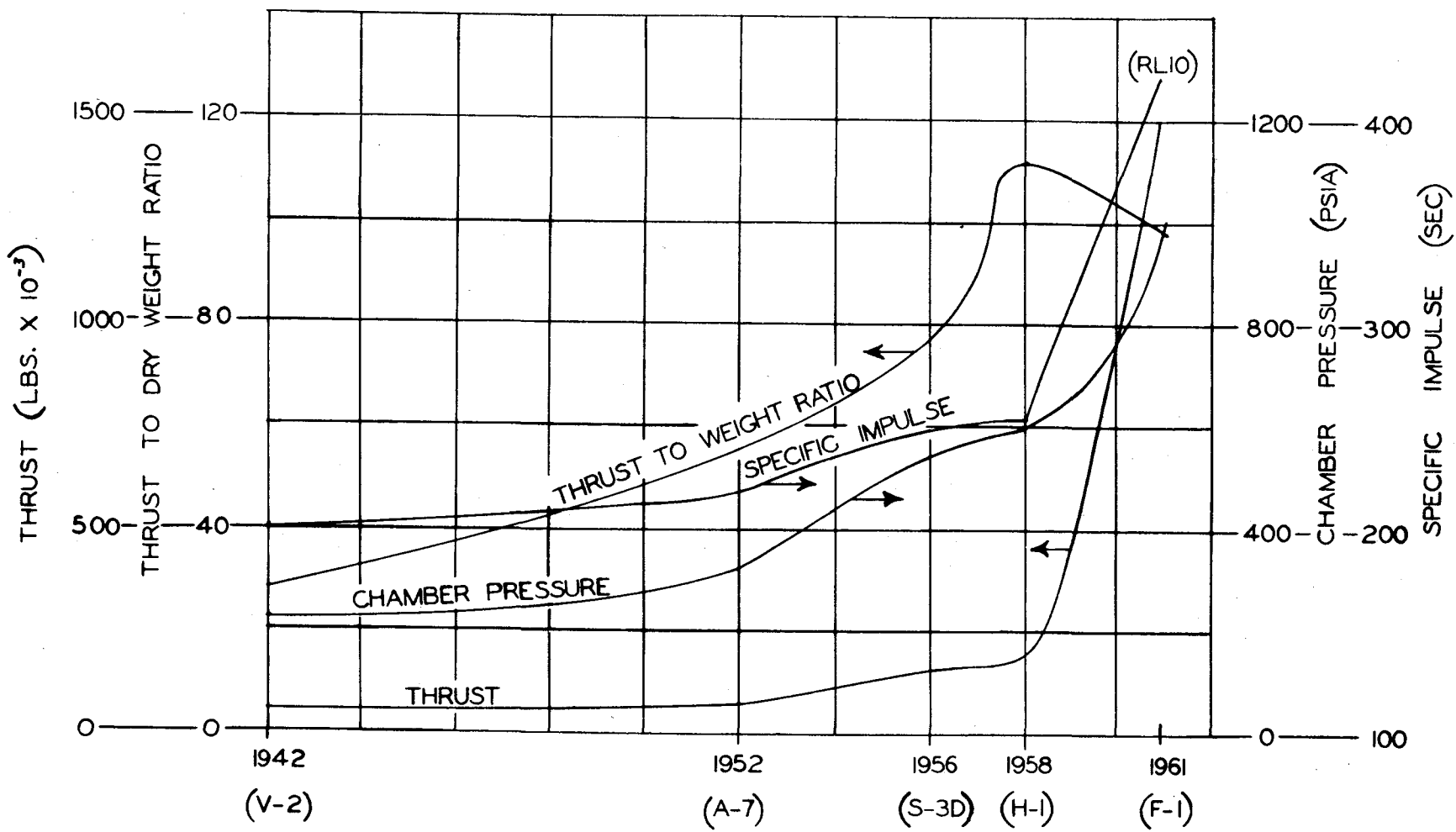


Fig. 13.7 Engine performance improvement during past 20 years.

of the tap-off principle. In this concept, hot gases for driving the turbopump are tapped off the main combustion chamber. Sufficient testing has been conducted to indicate the feasibility of this principle. New methods for achieving thrust vector control are being investigated, but the most popular method, known as secondary injection, is one which utilizes an adverse pressure gradient in the exhaust nozzle. In this concept, the engine would not be gimbaled, but rather, the effective direction of the exhaust gases would be altered by injecting a fluid (liquid or gas) into the nozzle through a port in the wall. The resulting thrust vector is thereby deflected from the axis of symmetry providing a component of side thrust.

Many new concepts are being considered as a replacement for the De Laval nozzle. Included in this group are: the plug or spike nozzle, reverse flow nozzle, and tank integrated nozzle (where the nozzle actually forms a portion of the tank bottom). Initial studies have shown that the integrated nozzle appears especially promising for use in upper-stage applications where large interstage savings are introduced. Studies in which this concept have been considered for boosters have not been conclusive.

## REFERENCES

1. Sutton, G. P., "Rocket Propulsion Elements" 2nd ed., John Wiley & Sons, Inc., New York (1958).

## ÜBER BALLISTISCHE UND AERONAUTISCHE RAUMFAHRT

Eugen Sänger

Forschungsinstitut für Physik der Strahlantriebe e.v. Stuttgart  
Stuttgart West Germany

Die ersten Erfolge bemannter Raumfahrt sind mit Raketentriebwerken mässigen spezifischen Impulses durch vielstufige ballistische Geräte im wesentlichen nach den Vorschlägen von Hermann Oberth und auf Grund der bahnbrechenden praktischen Arbeiten von Wernher von Braun aus militärischen Entwicklungen erzielt worden.

Der Übergang zur zivilen bemannten Raumfahrt fordert nun höhere Wirtschaftlichkeit und Flugsicherheit und damit den Übergang von ballistischen zu aeronautischen Raumfahrtgeräten.

Diese Entwicklung wird durch die allmähliche Verfügbarkeit von Raketentriebwerken wesentlich höherer spezifischer Impulse gefördert und mündet in Zukunft offenbar in einstufige aeronautische Raumflugzeuge ähnlicher Flugtechnik, Wirtschaftlichkeit und Flugsicherheit, wie übliche Verkehrsflugzeuge sie haben.

### 14.1 Die vier Generationen der Raketentriebwerke.

Die technischen Erfolge des Hyperschallfluges und der Raumfahrt im letzten Jahrzehnt gehen in erster Linie auf die Entwicklung der Raketentriebwerke zurück.

Die derzeitige Situation dieser Triebwerke stellt sich etwa in der in Abb. 1 skizzierten Weise dar, wobei bekanntlich zur technischen Kennzeichnung an Stelle von Leistung und Wirkungsgrad üblicher Motoren bei Raketentriebwerken die Begriffe Schub und spezifischer Impuls völlig analog verwendet werden.

Grundlage der jetzigen Raumfahrzeuge sind die Flüssigkeits-Raketentriebwerke der derzeitigen Generation mit einem spezifischen Impuls im Vakuum bis etwa 280 sec, Schüben bis etwa 750 Tonnen und den häufigsten Treibstoffkombinationen Kohlenwasserstoff-Flüssigsauerstoff oder Stickstoffwasserstoff-Stickstofftetroxyd. Die meisten Triebwerke dieser Generation sind in Serienfertigung und Fluganwendung.

**Preceding page blank**

Eine zweite Triebwerksgeneration mit spezifischem Vakuumimpuls bis etwa 450 sec steht in technischer Entwicklung, mit Schubgrößen von wenigen Tonnen bis etwa 500 Tonnen, und unter Verwendung der Treibstoffe Flüssigwasserstoff oder Hydrazin als Brennstoff und Flüssigsauerstoff oder Flüssigfluor als Verbrennungstoff.

Diese zweite Triebwerksgeneration stellt offenbar die letzte Grenze chemischer Raketenmotoren dar und scheint das Bild im vor uns liegenden Jahrzehnt zu beherrschen.

Die erwähnten beiden Triebwerksgenerationen bedienen sich überwiegend der vor und während des Weltkrieges von der deutschen Luftfahrtforschung in Trauen entwickelten Technologie\*:

1. Zwanglaufkühlung der feuerberührten Wände, die aus Rohren aufgebaut sind. (Deutsches Reichspatent 716 175)
2. Öffnungswinkel der Feuerdüsen über 25 Grad (Deutsches Reichspatent 689 124).
3. Verbrennung von Kohlenwasserstoffen bzw. Wasserstoff mit Sauerstoff.
4. Feuergasdrücke über 40 atm.
5. Zündung der Triebwerke durch Einspritzung von Metallalkylen.
6. In neueren Entwicklungen Antrieb der Förderpumpen der Treibstoffe durch das verdampfte Kühlmittel aus der Zwanglaufkühlung (Deutsches Patent 380/40).

Eine dritte Generation von Raumfahrttriebwerken mit spezifischen Impulsen zwischen etwa 800 sec und 3000 sec ist im Forschungs- und teilweise im Entwicklungsstadium und bedient sich der Kernenergie zur Aufheizung von Arbeitsgasen, wie Wasser, Ammoniak oder Wasserstoff, dadurch, dass die Wärmeenergie der Kernreaktion durch Wärmeaustauscher oder durch Vermischung mit den Reaktionsschwaden auf die Arbeitsgase übertragen wird.

Kernenergietriebwerke der ersten Art ("konvektive Fissionsraketen") sollen um die Mitte dieses Jahrzehnts zum Fliegen kommen, mit spezifischen Impulsen zwischen 800 und 1200 sec.

---

\*Mitt. 13 des Forschungsinstitutes für Physik der Strahlantriebe (FPS), Verlag E.v.Olnhausen, Stuttgart, bzw. "A Rocket Drive for Long Range Bombers", Ed. Cornog, 990 Cheltenham Rd., Santa Barbara, California.



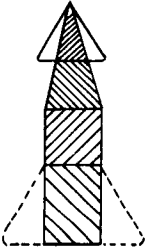


Triebwerke	Zellen
<p><u>Derzeitige Generation</u></p> <p>Spez Vakuumpuls <span style="border: 1px solid black; padding: 2px;">~280 sek</span></p> <p>(Kerosin-Flüssigsauerstoff, oder Hydrazin-Stickstofftetroxyd)</p> <p>(In Serienproduktion)</p>	<p>Drei-bis Vier-Stufig</p>  <p>letzte Stufe bemannt und geflügelt (x15,Dyna Soar,TIVA)</p> <p>3. Stufe, verloren</p> <p>2. Stufe, verloren</p> <p>1. Stufe, ev. wiedergewinnb. (bemannt und geflügelt)</p>
<p><u>Zweite Triebwerks-Generation</u></p> <p>Spez. Vakuumpuls <span style="border: 1px solid black; padding: 2px;">~450 sek</span></p> <p>(Flüssigwasserstoff-Flüssigsauerstoff oder Flüssigwasserstoff-Flüssigfluor)</p> <p>(In technischer Entwicklung)</p>	<p>Zweistufig</p>  <p>1. Stufe, bleibt ev. am Boden</p> <p>2. Stufe geflügelt, bemannt</p>
<p><u>Dritte Triebwerks-Generation</u></p> <p>Spez. Vakuumpuls <span style="border: 1px solid black; padding: 2px;">800-3000 sek</span></p> <p>(Kernfission mit Wasserstoff, Wasser oder Ammoniak)</p> <p>(In Erforschung, teilweise in technischer Entwicklung)</p>	<p>Einstufig, »Aerospace-Vehicle«</p>  <p>Gesamtflugvorgang wie Flugzeug</p>
<p><u>Vierte Triebwerks-Generation</u></p> <p>Spezimpuls <span style="border: 1px solid black; padding: 2px;">3000-30 000 000 sek</span></p> <p>(Kernfission, Kernfusion, Materiezerstrahlung)</p> <p>(In Erforschung)</p>	<p>Reine Raumfahrzeuge interplanetarer und interstellarer Natur</p>

Fig. 14.1

Kernenergietriebwerke der zweiten Art ("Misch-Fissionsraketen") erzeugen die thermische Kernenergie entweder auf kontinuierliche Weise in gasförmigen Reaktoren oder in diskontinuierlicher Weise durch rasch aufeinanderfolgende Explosionen kleiner Atombomben, wobei in beiden Fällen die Fissionsschwaden mit den eigentlichen, den Antriebsstrahl bildenden Arbeitgasen gemischt werden. Diese Triebwerke sind noch im Forschungsstadium und lassen die höheren spezifischen Impulse und sehr hohe Schübe erwarten.

Schliesslich werden in einer vierten Triebwerksgeneration eine grössere Zahl geplanter Raketensysteme mit spezifischen Impulsen zwischen 3000 und 30.000.000 sec zusammengefasst, die sich sämtlich im Stadium der Erforschung, teilweise der ersten Grundlagenforschung befinden, und zu denen beispielsweise elektrostatische Ionenraketen, elektromagnetische Plasmaraketen, reine Fissionsraketen, photonische Raketensysteme etc. zählen. Die Mehrzahl dieser Raketentriebwerke vierter Generation dürfte nicht innerhalb der Atmosphäre, sondern nur im freien Weltraum verwendbar sein, entweder wegen der nur sehr geringen zu erwartenden Schübe, oder wegen der Schädlichkeit des Antriebsstrahles für die Umgebung oder aus anderen Gründen, so dass sie mehr für reine Raumfahrzeuge als für die hier zu untersuchende Frage der erdnahen ballistischen und aeronautischen Raumfahrzeuge in Betracht kommen werden.

14.2 Die Zellen der Raumfahrzeuge auf Grund der ersten Triebwerksgeneration.

Aus dem dauernd als Motorkennzahl erwähnten spezifischen Impuls in Sekunden ergibt sich durch Multiplikation mit der Erdbeschleunigung  $g = 9.81 \text{ m/sec}^2$  (also mit rund 10) die wirksame Auspuffgeschwindigkeit  $w$  in  $\text{m/sec}$  des Motors, bzw. als tausendfacher Kehrwert des spezifischen Impulses der spezifische Treibstoffverbrauch in  $\text{kg/sec ton}$ .

Den spezifischen Impulsen der erwähnten Triebwerksgenerationen entsprechen daher rund folgende Auspuffgeschwindigkeiten

- 1. Generation. . . . .  $w \sim 2800 \text{ m/sec}$
- 2. Generation. . . . .  $w \sim 4500 \text{ m/sec}$
- 3. Generation. . . . .  $w \sim 8000 \text{ bis } 30.000 \text{ m/sec}$
- 4. Generation. . . . .  $w \sim 30.000 \text{ m/sec bis}$   
Lichtgeschwindigk.

Im schwerefreien und luftwiderstandsfreien Raum ist das Verhältnis  $G_0/G$  des Startgewichtes des Fahrzeuges zum Fahrzeuggewicht  $G$  nach Verbrauch aller Treibstoffe verbunden mit der erreichbaren Flugeschwindigkeitssteigerung  $v$  und der Auspuffgeschwindigkeit  $w$  durch die sogenannte Raketengrundgleichung

$$v/w = \ln G_0/G$$

Die Gewichtsverhältnisse  $G_0/G$  gehen bei ballistischen Geräten ohne Nutzlast bis zu  $G_0/G = 15$ . Bei geflügelten aeronautischen Geräten hofft man, bis etwa  $G_0/G = 10$  zu kommen. Mit jeweiliger Nutzlast gehen die Gewichtsverhältnisse erdnaheer Raumfahrzeuge kaum über  $G_0/G \sim 7$ , d.h.  $\ln G_0/G$  ist rund 2, die erreichbare Fluggeschwindigkeitssteigerung einer Raketenstufe wird höchstens gleich der doppelten Auspuffgeschwindigkeit des Raketenmotors.

Erdschwere und Luftwiderstand vermindern dieses Ergebnis noch beträchtlich, in praktischen Fällen um 1000 bis 2000 m/sec.

Die Zirkulargeschwindigkeit einer Erdaussenstation liegt in der Grössenordnung 8000 m/sec, die Fluchtgeschwindigkeit bei rund 11.000 m/sec.

Man sieht ohne weiteres, dass mit Triebwerken der ersten Generation oft drei bis vier Raketenstufen nötig sind, um diese Fluggeschwindigkeiten zu erreichen, wie dies Abb. 1 ebenfalls andeutet.

Derartige vielstufige Geräte mit Startgewichten bis 500 Tonnen sind im Bau und bis 6000 Tonnen geplant, wobei die oberste Stufe bemannt sein soll (Mercury, Wostok, Apollo, Dyna Soar, TIVA etc.) und nach Möglichkeit mit Flügeln ausgestattet ist, um sie wie ein Flugzeug an die Erdoberfläche zurückbringen, landen und bergen zu können.

Alle bisherigen und weiteren unbemannten Raumfahrzeuge werden daneben im wesentlichen nur als Vorarbeiten für solche bemannte Raumfahrzeuge angesehen und dienen der technischen Entwicklung der bemannten Geräte und der Voraufklärung des "Fahrwassers" und der "Landeziele" bemannter Raumfahrzeuge, z. B. in Form der geophysikalischen und astrophysikalischen Forschungsraketen.

Diese unbemannten Raumfahrzeuge haben nur in Ausnahmefällen bleibende, eigenständige Bedeutung, etwa als militärisch Waffen oder als wirtschaftliche Nachrichtensatelliten oder dergleichen.

Die Zellenentwicklung strebt nun dahin, nicht nur die letzte Stufe wiedergewinnbar und wiederverwendbar zu machen, weil sie Menschen und Nutzlasten enthält, sondern die Wiederbenutzbarkeit auch auf die schweren und sehr teuren Grundstufen auszudehnen, indem diese ebenfalls zu einer Art von Hyperschallflugzeugen ausgebildet werden, sodass zunächst nur noch die mittleren Stufen verloren gegeben werden sollen.

Die Gründe für diesen angestrebten Übergang von der ballistischen zur aeronautischen Raumfahrttechnik auch in den ersten Stufen sind insbesondere:

Wesentliche Verminderung der Kosten eines Startes von derzeit etwa 35 bis 100 \$ je Kilogramm Startgewicht auf die bei Flugzeugen üblichen Kosten in Höhe eines geringen Vielfachen der Treibstoffkosten von unter 0,1 \$/kg, dadurch, dass auch die sehr teure Erststufe, die im Aufwand mit einem modernen Strahlverkehrsflugzeug vergleichbar ist, nicht bei jeder Anwendung verloren geht, sondern wie ein Flugzeug immer wieder benützt wird.

Ermöglichung der Flugzeugerprobung jedes aus der Fabrik kommenden neuen Fahrzeuges vor der endgültigen Verwendung, wodurch die heute oft nur 50% betragende Verlässlichkeit sich auf jene von üblichen Flugzeugen erhöhen lassen dürfte, eine gerade für den bemannten Raumflug unabdingbare Forderung.

Ermöglichung der Start- und Landevorgänge auch in dichtbesiedelten Ländern, etwa Europas, von mehr oder weniger üblichen Flugplätzen, während derzeit die Startmöglichkeiten noch auf wenige Erdpunkte (Cape Canaveral, Woomera etc.) mit ausserordentlich teuren Bodeneinrichtungen beschränkt und in Europa gar nicht möglich sind.

Ermöglichung der Transporte der Raumfahrzeuge von der Fabrikationsstätte nach dem Startplatz, die gegenwärtig mit der Vergrößerung der Raumfahrzeuge in Richtung der Gewichte von Hochseeschiffen immer schwieriger werden und sich schliesslich nur noch dadurch ermöglichen lassen, dass die Raumfahrzeuge selbst als Flugzeuge ausgebildet sind.

Der katastrophale Rückgang der Luftfahrtindustrie auch in den grossen Industrieländern wie USA durch den meteorhaften Aufstieg der ballistischen Missiles und Raumfahrzeuge kann durch technische Rückführung der letzteren, der Raumfahrzeuge, auf den aeronautischen Weg wieder aufgefangen werden. In den zahlreichen Ländern, zu denen auch Deutschland gehört, mit geringer Erfahrung in ballistischen Geräten, aber Potential im Bau von Luftfahrzeugen, kann die Aufnahme von Arbeiten an aeronautischem Raumfahrtgerät wesentlich leichter vorgehen.

#### 14.3 Die Zellen der Raumfahrzeuge auf Grund der zweiten Triebwerksgeneration.

Diese Gesamtsituation der auf die erste Triebwerksgeneration abgestellten Raumfahrzeuge erfährt nun mit dem Heranreifen der zweiten Triebwerksgeneration mit Auspuffgeschwindigkeiten über 4000 m/sec am Boden, bis 4750 m/sec im Vakuum und vielleicht etwa 4500 m/sec im Durchschnitt eine entscheidende Erleichterung.

Die doppelte durchschnittliche Auspuffgeschwindigkeit beträgt nun 9000 m/sec und nach Abzug von 2000 m/sec für Schwere- und Luftwiderstandsverluste bleibt noch ein möglicher Fluggeschwindigkeitsgewinn von  $v \sim 7000$  m/sec einer einzigen Raketenstufe.

Gemessen an der Zirkulargeschwindigkeit von etwa 8000 m/sec und der Fluchtgeschwindigkeit von etwa 11.000 m/sec erkennt man, dass nurmehr zweistufige Geräte bzw, einstufige Geräte mit einer kleinen Vorstufe notwendig sind, um diese Fluggeschwindigkeiten zu erreichen.

Damit zeichnet sich eine erhebliche Vereinfachung und Verbilligung der Raumfahrten ab, insbesondere werden in diesem Fall keine verlorenen Zwischenstufen mehr existieren.

Der Start könnte unter solchen Bedingungen genau wie bisher in vertikaler Richtung erfolgen, es ergibt sich nun aber auch die Möglichkeit eines flugzeugartigen Horizontalstartes, gegebenenfalls von einer katapultähnlichen Startschlittenbahn, wobei die erwähnte kleine Vorstufe des eigentlichen Raumflugzeuges auf dieser Startschlittenbahn und damit am Boden bleibt und somit von vornherein wiedergewinnbar und wiederwendbar ist.\*

Diese Phase der Entwicklung wirtschaftlicher Raumfahrzeuge wird in USA unter dem Sammelbegriff "Aerospace-Vehicle" noch zögernd beschritten, es scheint, dass sie in USSR mit Hilfe grosser Schienenstartbahnen schon intensiver bearbeitet wird.

Dabei handelt es sich im wesentlichen um flugzeugartige Geräte, die zunächst katapultartig von der Erdoberfläche gestartet werden, später mit Triebwerken der dritten Generation vielleicht völlig mit eigener Kraft wie Flugzeuge starten, die Atmosphäre durchfliegen, in den Weltraum eindringen, dort manövrieren und im Gleitflug wieder an die Erdoberfläche zurückkehren können, um dort wie Segelflugzeuge zu landen, und die voraussichtlich auch als Hyperschallflugzeuge die endgültig schnellstmöglichen irdischen Verkehrsaufgaben durchführen können.

Diese Geräte scheinen auch für die Aufnahme europäischer Raumfahrtentwicklungen sehr vielversprechend zu sein, da sich die Lage Europas von jener der USA in dieser Hinsicht besonders dadurch unterscheidet, dass Europa nicht in einem politischen Wettbewerb mit einem mächtigen Konkurrenten im Raum steht.

Wenn daher die USA gegenwärtig gezwungen sind, durch kurzfristige Gewaltprogramme mit Hilfe verllorener ballistischer Geräte und möglicherweise unter Einsatz von Feststoffraketen mit Schüben bis 10.000 Tonnen ohne Rücksicht auf wirtschaftlichen Aufwand ihre Wettbewerbsfähigkeit im Raum unter Beweis zu stellen, so kann Europa den ruhigeren Weg langfristiger Planung wirtschaftlicher Geräte der beschriebenen Art bevorzugen.

Für diese Geräte kommen Feststoffraketen aus mehreren Gründen nicht in Frage.

---

\*l.c.

Wirtschaftliche und betriebssichere Raumflugzeuge setzen, wie gesagt, jedenfalls Wiederverwendbarkeit in der Art normaler Flugzeuge voraus. Während bei Flüssigkeitsraketen die Treibstoffkosten niedrig (0,05-0,20 \$/kg) und die Baukosten hoch sind, liegen bei Feststoffraketen die Treibstoffkosten hoch (2.5 - 4.0 \$/kg), während die Baukosten niedrig bleiben. Da Wiederverwendbarkeit nun die Baukosten auf viele Flüge verteilt, sind in diesem Zusammenhang Feststofftriebwerke ohne Interesse, weil bei ihnen oftmalige Verwendung desselben Gerätes den Gesamtaufwand wegen des hohen Treibstoffpreises nicht merkbar senken, sondern im oben angegebenen Verhältnis hoch halten würde.

Sobald jedoch Flüssigkeitstriebwerke der zweiten Generation mit spezifischem Impuls um 450 sec zur Verfügung stehen, ist deren Überlegenheit gegenüber dem spezifischen Impuls der Feststoffraketen von 250 bis 280 sec der ausschlaggebende Grund für die Verwendung der Flüssigkeitstriebwerke.

#### 14.5 Raumflugzeuge.

Die durch den hohen Treibstoffanteil am Startgewicht bedingte hohe Anfangsflächenbelastung der Raketenflugzeuge und der noch immer beschränkte spezifische Impuls der Raketentriebwerke zweiter Generation verlangen einen Katapultstart dieser Raumflugzeuge, gegebenenfalls in horizontaler Richtung auf eine Anfangsfluggeschwindigkeit von vielleicht 500 m/sec.

Ein derartiger Katapultstart eines Raumflugzeuges von beispielsweise 100 Tonnen Anfangsfluggewicht auf einer etwa 7 km langen Schlittenbahn mittels besonderen Startraketenantriebes des Startschlittens würde bei Verwendung von Feststoff-Startraketen etwa 10.000 Tonnensekunden Startimpuls mit Gesamtkosten von vielleicht 150.000 \$ erfordern, bei Verwendung von Heisswasser-Startraketen dagegen etwa 15.000 Tonnensekunden Startimpuls mit Gesamtkosten von vielleicht 500 \$ bei höherer Betriebssicherheit.

Hier zeichnet sich deutlich die Notwendigkeit der Entwicklung besonders wirtschaftlicher und betriebssicherer Startraketenantriebe ab, die in ihren Eigenschaften völlig verschieden von den bisher behandelten Flugraketenantrieben sein können\*.

Das nach dem Katapultstart mit einer Anfangsgeschwindigkeit von z.B. 500 m/sec fliegende Raumflugzeug steigert seine Geschwindigkeit mit Hilfe der an Bord mitgeführten Treibstoffe und seines Raketentriebwerkes in der Art wie das amerikanische Versuchsflugzeug X 15, bis zum Verbrauch aller Bordtreibstoffe, um dann weiterhin entweder eine Gleitflugbahn

---

\*FPS-Berichte 6, 11 und 20, Verlag E.v.Olnhausen, Stuttgart.

innerhalb der Atmosphäre, oder schliesslich reine Trägheitsbahnen im Weltraum zu beschreiben. Mit Triebwerken der zweiten Generation lassen sich beispielsweise folgende Flugbahnen erwarten:

Bei 65% Treibstoffanteil am Startgewicht des Raumflugzeuges beträgt die Flugbahnlänge 6800 km, ausreichend für interkontinentale Flüge, die Gesamtflugdauer ist 62 Minuten, also die mittlere Fluggeschwindigkeit 6500 km/h, und die grösste stationäre Flughöhe 32 km.

Bei 76% Treibstoffanteil beträgt die Flugbahnlänge 20.000 km, entsprechend einem Nonstop-Flug über die grösstmöglichen irdischen Entfernungen, die Gesamtflugdauer 92 Minuten, die mittlere Fluggeschwindigkeit 13.000 km/h, und die grösste stationäre Flughöhe 43 km.

Bei 87% Treibstoffanteil geht das Raumflugzeug in eine niedrige Erdsatellitenbahn, die Flugbahnlänge wird unendlich, die Fluggeschwindigkeit 13.000 km/h, und die grösste stationäre Flughöhe 43 km.

Diese Untersuchungen zeigen sehr plastisch, wie eng Luftfahrt und Raumfahrt sachlich zusammenhängen, und wie das rasche Heranreifen der Raumflugzeuge mit Raketentriebwerken der zweiten Generation sowohl die weitere Entwicklung der Luftfahrt, als auch jene der Raumfahrt zu beeinflussen beginnt.

In Form der Hyperschall-Raketenflugzeuge sind diese Geräte geeignet, schon heute die Arbeiten an Überschall-Flugzeugen des Machzahlbereiches 3 bis 4, wie sie als militärische und zivile Transportflugzeuge, insbesondere als Überschall-Verkehrsflugzeuge gepflegt werden, grundsätzlich zu überholen und selbst die letzte, nicht mehr überholbare Endstufe des schnellen irdischen Luftverkehrs vorzubereiten.

In Form der Raumflugzeuge sind diese Geräte geeignet, in der bemannten Raumfahrt die heutigen ballistischen Raumfahrzeuge, die ein primitives, unwirtschaftliches und unsicheres Erststadium der technischen Entwicklung darstellen, abzulösen und die Raumfahrt auf eine ähnlich wirtschaftliche und verlässliche Basis zu stellen, wie sie die Luftfahrt bereits erlangt hat.

## 15

## ELECTRIC PROPULSION: A NEW TECHNOLOGY

Ernst Stuhlinger, Gerhard B. Heller, Robert N. Seitz  
and George C. Bucher

Research Projects Division  
George C. Marshall Space Flight Center  
National Aeronautics and Space Administration  
Huntsville, Alabama

Within the past 3 years, electric thrust devices have passed from the first exploratory feasibility experiments to the flight-engineered hardware phase. This rapid surge of development has been punctuated by equally rapid improvements in the performance figures of electrical thrust devices. The most spectacular advances were made in ion engine technology. Total energy expenditure per ion pair has gone from 35,000 ev in 1958 to about 600 ev at the present time leading to power utilization efficiencies of up to 80 per cent, depending upon the specific impulse. The percentage of the particles intercepting the accelerating and focusing electrodes has been reduced from more than 50 per cent in 1958 to less than 0.01 per cent at the present time. Great improvements in ion current per unit area have also been realized, leading to greater thrust "pressures."

The feasibility of arc engines was a widely accepted belief in 1958. At that time, arcs were operated for reentry simulation, and their conversion to propulsion devices was considered easy. Most conversion effort centered upon engineering modifications to render the arcs capable of flight, at the expense of fundamental research leading to improved performance. Only during the past year have the research problems been recognized, and work started on the specific problems of arc propulsion. Due to this late start, progress has been less spectacular than in ion engine research. Nevertheless, the period from 1958 to the present has seen the development of an engine with an overall power conversion efficiency of 56 per cent using hydrogen as a propellant; of an ac operated engine; the first radiation-cooled flight engine; and of an associated technology including propellant feed systems, current control systems, and ignition circuits.

Electromagnetic, or plasma, accelerators remain in an earlier phase of research compared with arc and ion engines. Reliable thrust and efficiency measurements are difficult with plasma accelerators, but efficiencies of 30 to 40 per cent are within the present state of the art. One "pinch plasma engine" is presently being engineered for flight test in the 1962-1963 period.

Preceding page blank



The three principal types of thrust devices will now be discussed in greater detail.

## 15.1 Principal Types of Electric Thrust Devices

### 15.1.1 Ion Engines

Ion engines contain four major components: the feed system, the ion source, the ion accelerator, and the beam neutralization system. To be suitable for an ion engine, an ion source must possess special characteristics. It must be designed so that the average current density drawn from an array of these sources is high enough to keep the total area of the engine to a reasonable size. It should be sufficiently light that its mass is a small fraction of the total vehicle mass. It should convert the electrical power output of the power supply into ion kinetic energy with the highest possible power efficiency. It must have a long and reliable lifetime of the order of a few years. It should convert virtually all of the propellant atoms into ions. High propellant efficiency is desirable not only for flight economy, but also because neutral atoms which escape from the ion source accumulate in the accelerator where they may cause scattering, erosion, and voltage breakdown. Finally, it should produce ions of high atomic weight.

During the past 3 years, several types of ion sources have been developed which meet the above specifications to a greater or lesser degree. These include the surface ionization source, and several modified duoplasmatron and Penning discharge sources. Propellant efficiencies of some of the different ion sources are listed in Table 15.1.

Table 15.1 Propellant and Power Efficiencies of Ion Engines

Ion Source	Propellant Efficiency (%)	Power Efficiency (%) ( $I_{sp}=10,000$ sec)
Electron Bombardment	80	78 [Ref. <u>1</u> ]
Duoplasmatron	90	90 [Ref. <u>2</u> ]
Surface Ionization	98.5	77 [Ref. <u>3</u> ]

The surface ionization source relies upon the principle that, in theory, a high work function material like tungsten can catalytically ionize more than 99 per cent of a propellant such as cesium whose ionization potential is considerably less than the work function of tungsten. Unavoidable radiation from hot ionizing surfaces accounts for the major power loss with surface ionization sources.

The modified duoplasmatron sources utilize a magnetically pinched glow discharge to ionize mercury as a propellant. In the laboratory, these types of sources have achieved the lowest ionization energy expenditures of any sources tested so far, at propellant efficiencies (with mercury) in excess of 90 per cent.

Another promising collision source which has been developed into a complete engine is an electron bombardment source developed by H. Kaufmann at the Lewis Research Center, (NASA). This source offers ionization energies as low as 1100 ev per ion with propellant efficiencies of about 80 per cent.

Once the ions have been produced, acceleration is necessary. The ion accelerators must meet certain specialized requirements. Since ion emission is generally uniform across the surface of the source, the accelerator must provide a uniform electric field across the source to extract ions as rapidly as they are formed. The accelerator must have as low an ion interception as possible since high-energy ion bombardment sputters the electrodes rapidly and results in deterioration of the ion optics.

Two approaches are commonly taken in the difficult job of designing an ion acceleration and focusing system. One consists of specifying electrode shapes and attempting to determine the space-charge flow pattern which results. The electrode configurations are adjusted by trial and error to get a desired flow pattern.

Another approach consists of trying to determine analytically the electrode configurations required to produce any given beam. This is a more difficult problem; solutions do not always exist. For simple rectilinear flow (planar, cylindrical, or spherical geometries), the Pierce principle is used as a first approximation to a more defined design. However, more advanced techniques have been developed for guns employing curvilinear flow.

The ion accelerator should draw off all the ions which the ion source can provide. Space charge effects impose a limitation on ion current density. To increase the maximum current density and thereby enhance the thrust pressure, it is customary to employ an accel-decel system in which the ions are first accelerated to a high velocity, and then decelerated to the desired exhaust velocity.

One of the most controversial questions relating to ion engines is that of the neutralization of the ion beam once it leaves the source. The beam must be neutralized to avoid an accumulation of charge on the space vehicle. It must be neutralized close to the vehicle to avoid the buildup of large potentials in the ion beam which would cause it to spread excessively, and even to reflect some of the ions back to the

negatively charged accelerator electrode. All of the present theoretical and experimental results indicate that ion beam neutralization may not be a severe problem [4, 5]. However, the crudeness of the theoretical treatments, and the great difficulty of simulating the unlimited conditions of outer space in laboratory experiments render space tests mandatory to answer the beam neutralization question. Preferably, several neutralization techniques should be tried in these tests, since the stability characteristics of the plasma are quite sensitive to the geometry of its boundaries.

#### 15.1.2 Arc Engines

Arc engines consist of a propellant storage tank, a flow control system, an arc chamber, and a convergent-divergent expansion nozzle. Propellant storage is a significant problem with hydrogen or helium because of low atomic weights and low boiling points, especially when radiation absorption from an onboard nuclear reactor is involved. Other promising propellants are ammonia and a hydrogen-lithium mixture.

Within the arc chamber and the nozzle, the principal problems are erosion of the walls and electrodes and dissociation, or "frozen flow," losses in the nozzle which reduce arc engine power efficiencies. The latter term refers to the energy lost when gases, dissociated and ionized in the arc chamber, fail to recombine in the nozzle to give up their recombination energy and enhance the expansion process.

Careful attention to electrode design and effective cooling techniques can relieve internal erosion. Rotating the arc electrically to vary its point of attachment to the electrodes also helps. Recent experiments with a mixture of hydrogen and lithium as propellants suggest another approach to reducing erosion [6]. The lower ionization potential of this bipropellant means a lower arc voltage, and hence reduced electrode erosion rates. The heat transfer losses can be reduced considerably by careful arrangement of the gas flow pattern, by optimizing the length and shape of the arc, and by employing regenerative cooling. Heat losses to the walls decrease with increasing engine size, simply because the surface-to-volume ratio of engines becomes more favorable as they increase in magnitude.

Much theoretical and experimental effort has been spent recently to learn more about recombination and reassociation in high temperature arc [7]. Helium would be an ideal propellant from the standpoint of dissociation losses--there would be none; however, the storage problem offsets the gain in power efficiency by far. Higher specific impulse means higher chamber temperatures, greater heat losses, and lower efficiency.

Another attractive possibility is the use of ac power instead of dc power. The use of ac permits stable operation with only a negligible ballast resistance and without power rectification losses.

Among the arc engines currently under development are 30 kw dc engines (AF and NASA) and a small 1 kw arc engine (NASA) for flight test late in 1962. Characteristics of these engines are shown in Table 15.2.

Table 15.2 Power Efficiencies of Arc Engines

Specific Impulse (sec)	Propellant	Power (kw)	Efficiency (%)	Company
780	NH <sub>3</sub>	1	24	Plasmadyne
900	H <sub>2</sub>	3	40	Avco
1000	H <sub>2</sub>	30	38	Avco
1000	NH <sub>3</sub>	30	40	Avco
1000	H <sub>2</sub>	30	56	Plasmadyne
1100	H <sub>2</sub>	1	38	Plasmadyne
1100	H <sub>2</sub>	30 (ac)	45	GE
1350	H <sub>2</sub>	30	41	Avco
2000	H <sub>2</sub>	30	20	Plasmadyne

### 15.1.3 Plasma Accelerators

The majority of plasma propulsion devices currently being explored can be classified into three major categories. These are pulsed plasma accelerators, crossed-field accelerators, and traveling wave accelerators.

The pulsed plasma accelerators depend upon the interaction of a pulsed current discharge in a plasma with either its self-generated magnetic field, or with the magnetic field generated by the external return circuit for the discharge current. The T-tube, rail, and button guns fall in this category, as does the pinch plasma engine presently planned for space flight testing in 1963.

Crossed-field accelerators are steady state devices in which plasma from an arc is accelerated by the  $\vec{j} \times \vec{B}$  force which arises when external electric and magnetic fields are applied to the plasma perpendicular to the streaming direction and perpendicular to each other. In the low specific impulse regime (less than 1400 sec), power conversion efficiencies around 30 to 40 per cent have been achieved with various gases as propellants.

Traveling wave accelerators utilize a moving, recurrent magnetic field which accelerates an ionized gas. The field is generated by one of the following methods: (1) a polyphase resonant radio frequency

circuit generates a succession of traveling waves in field coils (the induction motor principle); (2) a delay line gives the desired velocity of propagation; or (3) a series of timed, pulsed capacitor discharges energize the field coils.

Each of the above devices has its own specific limitations. The pulsed devices require the development of lightweight reliable condenser banks and of associated equipment to improve power coupling efficiency into the plasma. Nevertheless, plasma accelerator technology is making headway and offers certain advantages over other contenders, provided technical development is successful.

## 15.2 Future Improvements in Electrical Propulsion Systems

While the first phase of electrical propulsion development is drawing to a close, the next phase has begun to take shape. Very characteristically, this next phase is concerned with improved efficiency and increased lifetime. As a rule, these properties are not in the focus of endeavor during the feasibility demonstration phase of a technical development, but they must receive growing attention as soon as the basic soundness of a concept is assured.

Judging from the present status of ion engine development, it is very likely that future ion engines will have propellant efficiencies between 80 and 98 per cent, and power efficiencies--depending on their specific impulses--between 60 and 90 per cent. Once the efficiencies are in the 90 per cent region, their influence on overall performance is less significant than their influence on secondary effects such as lifetime of ion sources, erosion of electrodes and structural elements, and voltage breakdown across insulators. From this viewpoint, surface ionization sources look promising because of their high propellant efficiency. A very substantial gain in the power efficiency of surface ionization sources would be obtained if the ionizing surface were not heated by precious electric power, but by cheap heat directly from the nuclear reactor. Studies in this direction are underway.

Accumulated operating times of individual electric engines are presently not longer than a few hundred hours. Even though results are promising in general, a number of areas require continued development effort before the desired lifetimes of 20,000 or 30,000 hr can be guaranteed. Among them are the design of electrodes and filaments; the fabrication of homogeneous, large-area porous tungsten ionizers; the development of propellant feed systems; and the design of beam neutralization systems.

Arc engines have been operated up to 50 hr at efficiencies of 40 per cent. The goals for future developments are extension of the specific impulse to 2000 sec, increase of lifetimes, and an improvement

of efficiencies. At 1000 sec, specific impulse efficiencies up to 80 per cent seem feasible. Other areas where improvements will be made include high-temperature insulators and materials, electrode geometries, heat transfer analyses, better arc dynamics, and minimization of leakage losses.

Besides the engineering work that must still go into the improvement of thrust-producing engines, a considerable effort will be required for developing nuclear-electric power supplies. One of the first nuclear-electric power generators for space use, the Snap 8, will begin its flight testing phase in 1965. With 30 kw output power and a specific power of about  $0.03 \text{ kw kg}^{-1}$ , it is marginal for electric propulsion. Power supplies of 100 to 300 kw, 1 to 4 Mw, and about 20 to 40 Mw power, and specific power figures of 0.3 to  $1 \text{ kw kg}^{-1}$  are desirable for future space missions. Most likely from about 1970 on, power supplies will not be based on turbo-electric generators, but on thermionic or plasma dynamic converters.

The engineering development of electric propulsion should be paralleled continuously by vigorous research programs. Although present technologies will be adequate to make electrically propelled vehicles equivalent, and even superior, to nuclear rockets on planetary flight, further research is urgently needed for improved and refined problem solutions, for more economic performance, and to assure reliability under long-time operation.

### 15.3 Flight Testing of Electric Engines

Plans and preparations for space flight testing of electric propulsion systems have become firm within the past year and a half. Tests for ion engines are necessary to settle the ion beam neutralization question; they are also necessary as mission-rating tests for all types of electric thrust devices before actual space missions with more expensive power supplies. Present NASA plans call for two test flights in late 1962; four small engines, delivering only a few millipounds of thrust, will be tested. The payloads will incorporate two surface ionization engines, one collision-type ion engine, and one arc engine. The four engines and the flight test capsule are shown in Fig. 15.1.

These engines will be launched by Scout vehicles into nearly vertical trajectories with peak altitudes of about 8000 km and total flight times of well over 1 hr. This will allow each engine about 35 min of operating time under space conditions. Power will be provided by batteries.

Testing on satellites may begin in late 1963, using power supplies like Snap 2 and Sunflower. It seems probable that soon after these tests are completed, arc engine propulsion systems will be harnessed

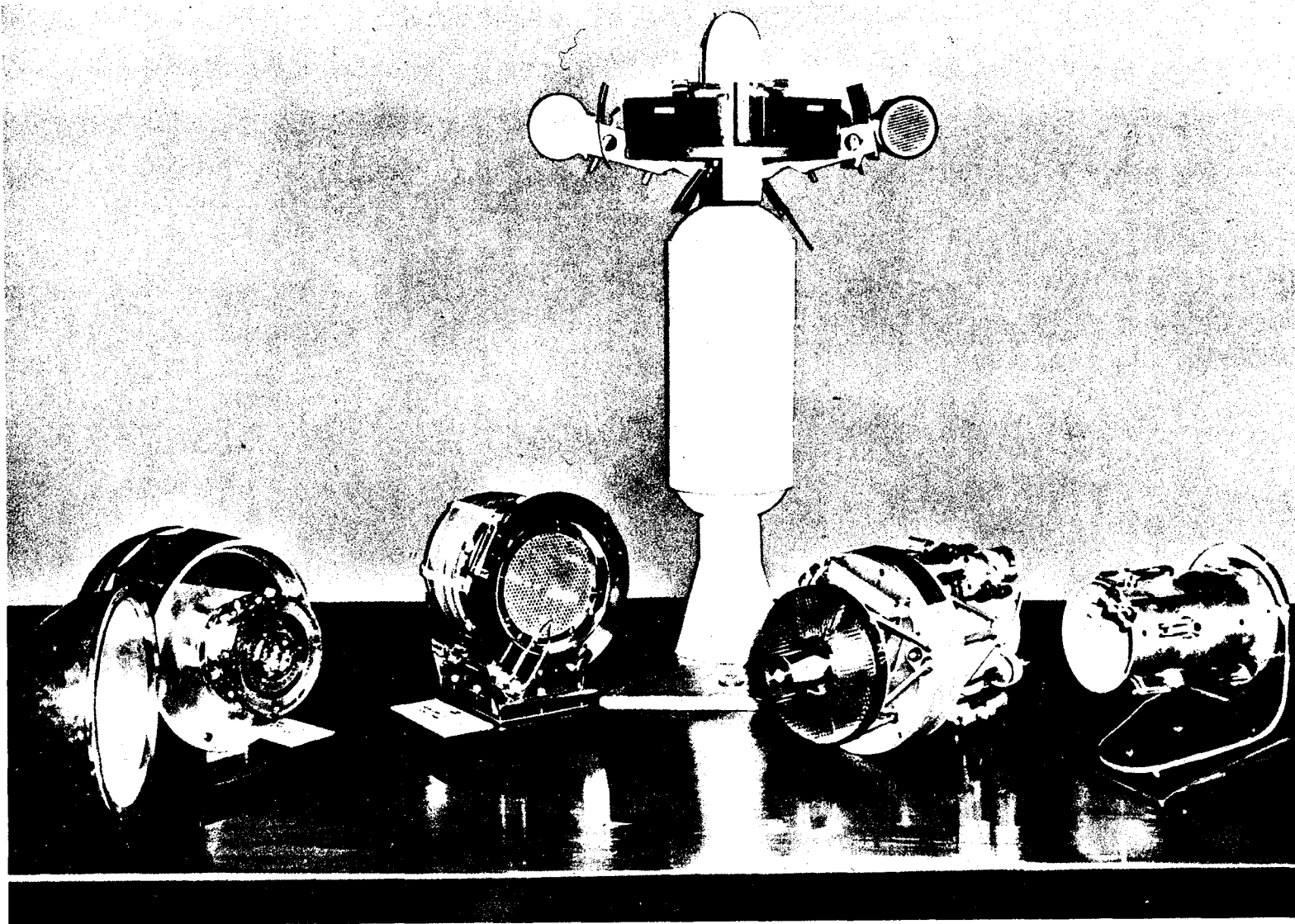


Fig. 15.1 Electric propulsion engines and test capsule for flight testing in late 1962.

for the transfer of satellites from low to high orbits, for the correction of orbital launching errors, and for other applications where fine control of total impulse is required. The next major milestone in the flight test program will be the testing of 30 kw engines in conjunction with the 30 kw Snap 8 power supply in 1965-1966. After that, ion propulsion may be applied to the propulsion of probes to the planets, for out-of-the-ecliptic flights, for deep space missions, and ultimately, in the 1975 to 1985 period, for manned flights to Mars. All of these missions will be discussed below in more detail.

#### 15.4 Power Supplies

Until thermionic and plasma dynamic converters with sufficiently high efficiencies become available, the nuclear turbo-electric power supply system will probably be used. The nuclear fission reactor is the most attractive source of primary energy for the long lifetimes associated with missions employing electric propulsion.

Studies have indicated that the Rankine vapor heat cycle is superior to the Brayton gas cycle in the conversion process. The efficiencies of the Rankine vapor cycle are close to the efficiencies attainable with the ideal Carnot cycle. Figure 15.2 illustrates the cycle efficiencies of the Carnot, ideal Rankine (no system inefficiencies), and the actual Rankine (turbine inefficient) cycles, using potassium as a working fluid.

The fast reactor is best suited for space power applications because of lower core and reflector size and weight. A recent report [8] describes a fast reactor designed by Atomics International for use in a 300 kw (electric) space power plant. It is fueled by uranium monocarbide, cooled by rubidium boiling at 1800°F, produces 2.4 Mw (thermal) energy for more than a year at continuous full-power operation, and weighs approximately 500 lb. Reflectors are made of beryllium oxide and control is provided by moving the reflectors.

The selection of working fluids for a nuclear turbo-electric system is governed by factors such as material temperature limitations, materials compatibility, stability during prolonged nuclear radiation and high-temperature operation, physical and thermal properties of the fluid, and others. Elements, and in particular alkali metals, are most attractive as working fluids. When upper- and lower-temperature and pressure limitations are imposed on the cycle, the most suitable working fluids for nuclear turbo-electric systems are found to be sodium, potassium, cesium, and rubidium.

To reject the thermal energy not converted into electrical energy, a waste heat rejection system must be employed. In a space environment, radiation is the only known method for rejecting heat. Since the



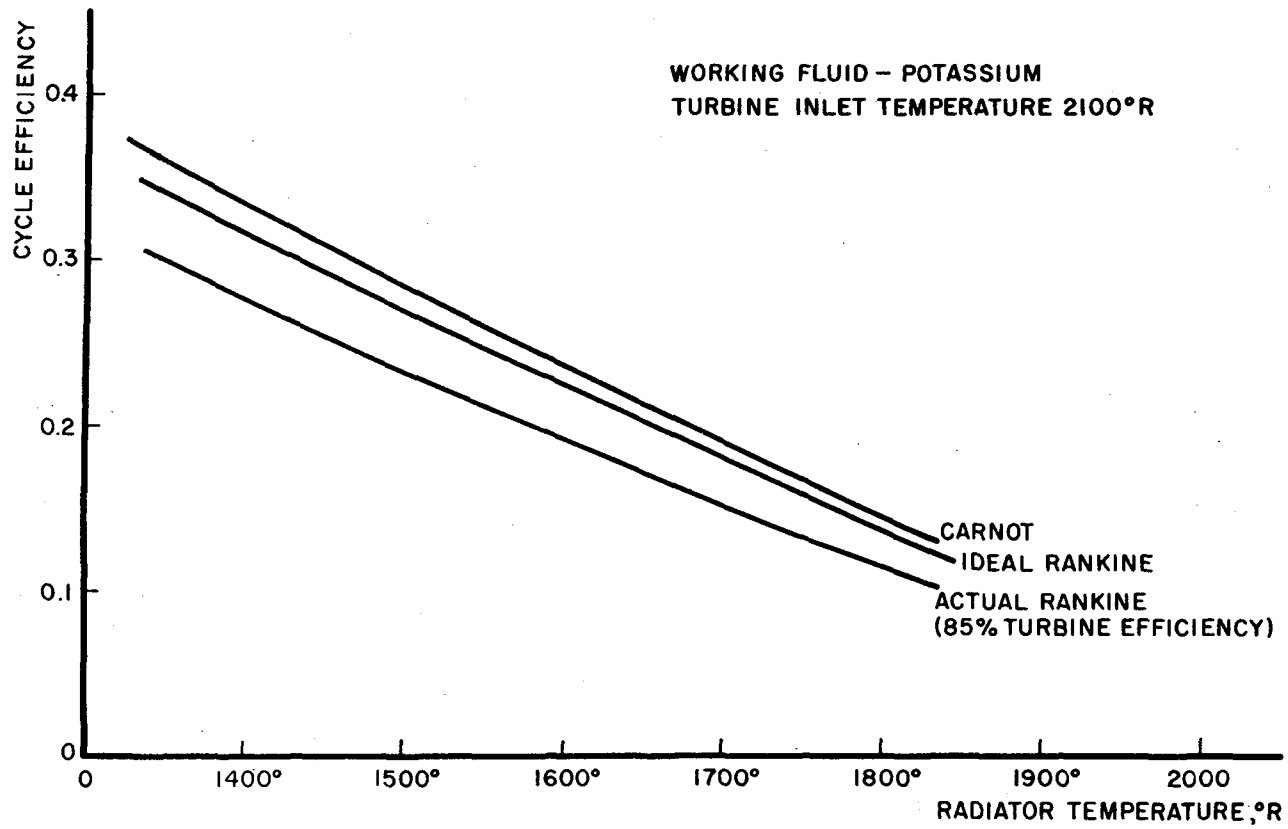


Fig. 15.2 Cycle efficiency versus radiator temperatures for Carnot, ideal Rankine and actual Rankine cycles.

Rankine cycle efficiency is around 20 per cent, the thermal energy to be rejected is significant; the radiator is by necessity very large. In fact, it is the heaviest part of the power supply system.

The heat radiated from a body in uniform surroundings is given by the Stefan-Boltzmann equation

$$Q_R = \sigma \epsilon A_R (T_R^4 - T_S^4) \quad (15.1)$$

where  $Q_R$  = heat radiated

$\sigma$  = Stefan-Boltzmann constant

$\epsilon$  = emissivity of radiator

$A_R$  = area of radiator

$T_R$  = absolute temperature of radiator

$T_S$  = absolute temperature of surroundings

Away from a planet, for all practical purposes,  $T_S$  is absolute zero, and can be dropped from Eq. (15.1). Since the heat radiated varies as the fourth power of the radiator temperature, a high temperature is desirable. For the actual Rankine cycle, there is a definite relationship between the temperature of the working fluid entering the turbine,  $T_A$ , and the temperature of the working fluid in the radiator,  $T_R$ , which results in optimum cycle efficiency and minimum radiator area. This relationship is given by

$$\frac{T_R}{T_A} = 1 - \frac{5}{8k} + \frac{1}{8k} (25-16k)^{\frac{1}{2}} \quad (15.2)$$

where  $k = \frac{\text{Rankine cycle efficiency}}{\text{Carnot cycle efficiency}}$

The ratio  $\frac{T_R}{T_A}$  ranges between 0.75 and 0.80, and it can easily be remem-

bered that the heat rejection temperature,  $T_R$ , is always approximately 3/4 of the turbine inlet temperature,  $T_A$ , when the radiator area is at a minimum. The relationship in Eq. (15.2) presumes that the radiator is at a uniform overall temperature, and this is essentially the case in Rankine cycle where the working fluid gives up its heat while condensing in the radiator at temperature  $T_R$ . The turbine inlet temperature,  $T_A$ , is the highest temperature reached by the working fluid, and its upper limit is determined by material temperature limitations in the reactor core. At the present time, around 2500°F (2960°R) is considered the upper limit.

Since the radiator temperature varies almost directly with the turbine inlet temperature in an optimized system Eq. (15.2), a higher turbine inlet temperature will result in a higher radiator temperature and a smaller radiator area. This relationship is illustrated in Fig. 15.3. It is interesting to note that for minimum radiator areas, the radiator temperature is always approximately 3/4 the turbine inlet temperature, as mentioned above. Figure 15.3 is based upon a 1 Mw (electric) power system using potassium for the working fluid, a value of 1.0 for the radiator emissivity, and a uniform radiator temperature.

The materials for radiator construction should be light weight and have good heat transfer properties, and the flow passages must be of a material compatible with the working fluid. To reduce radiator weight, a fin-tube configuration can be used. The fin-tube configuration results in a larger radiator area but the overall weight is reduced because the fins can be selected of a low-density material. Meteoroid puncture protection is required only over the fluid flow passages. Cornog [9] has investigated materials suitable for fin construction. He found that beryllium, graphite, and copper, in that order, have the most attractive thermal conductivity to density ratios at operating temperatures above 1200°F. Beryllium is usually considered to be the best fin material. If an alkali metal is used as the working fluid, the most suitable tube material will be the refractory metals molybdenum, columbium, tantalum, and tungsten, or selected stainless steels and alloys.

As may be seen from Eq. (15.1), the value of  $\epsilon$ , the emissivity of the radiator, should be high in the temperature range in which it operates. Since the emissivity of beryllium is low, a suitable surface coating is required. Aluminum oxide will be a favorable coating with emissivity values approaching that of a black body in the infrared.

An important design consideration for the power supply is protection from meteoroid impacts. To date, there have not been sufficient measurements in space to accurately determine the meteoroid flux and the mass, velocity, and density distributions. Experiments in the laboratory are now limited by inability to reproduce meteorite velocities. The thickness of meteoroid protection material over tubes in the fin-tube configuration is dependent upon the material used, the exposed area, the mission lifetime, and the desired probability of no punctures. One rather disheartening fact is that as the power levels for electric propulsion systems go higher in the future, the weight per unit radiator area will increase. This happens because as the power level increases, more heat must be rejected, thus greater radiator areas are required, and thus the thickness of the protective material must be increased in order to maintain the same degree of total improbability of puncture.

Meteorite "bumpers" have been proposed as a means of protecting vulnerable areas. The penetration resistance increases substantially if a given thickness of material is divided into more than one sheet

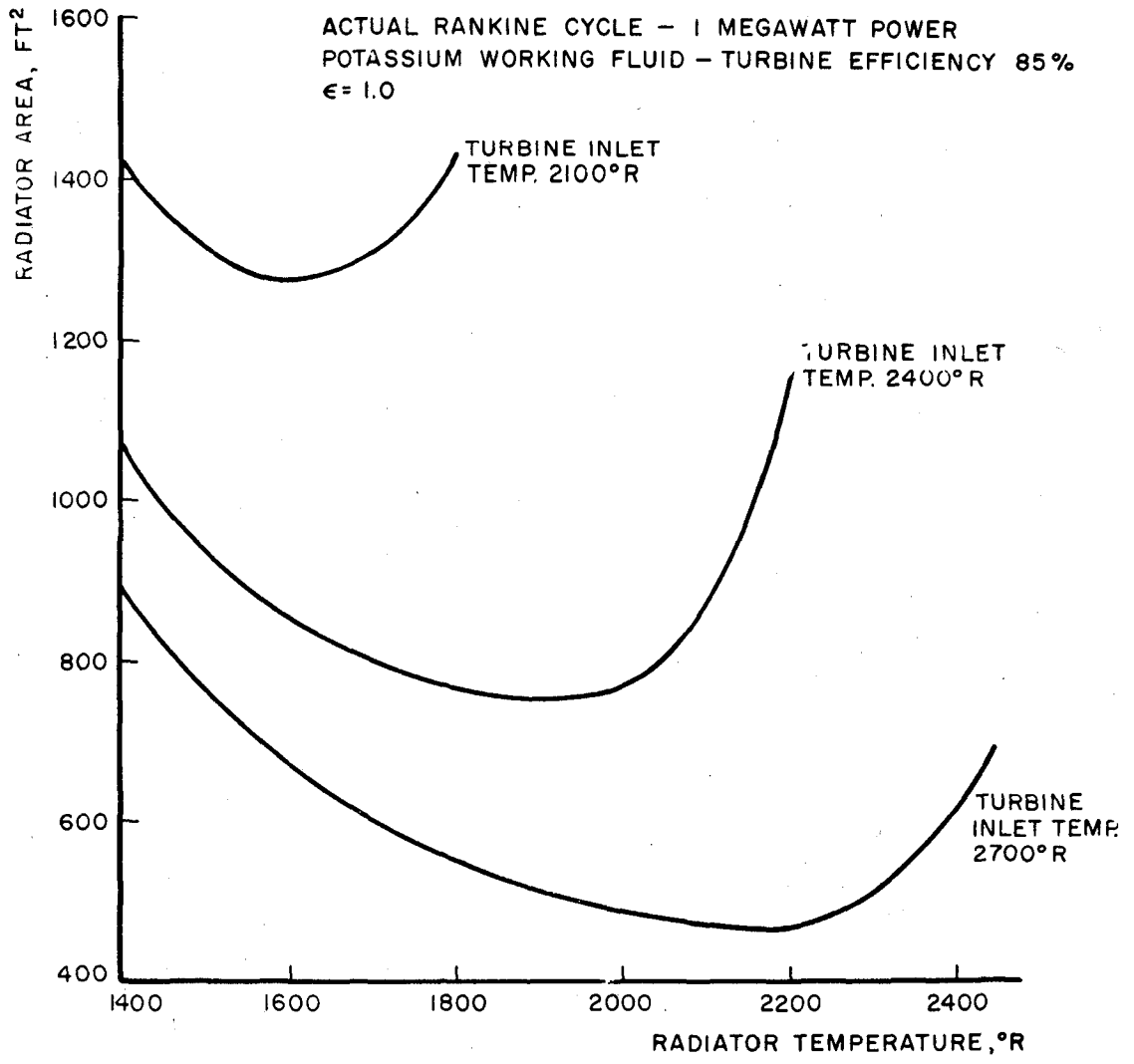


Fig. 15.3 Radiator area versus radiator temperature for varying turbine inlet temperatures.

and separated. Using Pyrex glass spheres, 1/8-in. diameter at velocities up to 11,000 ft/sec., Nysmith and Summers [10] found that the penetration resistance increased by a factor of 1.75 when a single sheet was replaced by two sheets (each 1/2 thickness of the original) with 1/2 in. spacing, and by a factor of 2.2 with 1 in. spacing. Even though "bumpers" may dissipate the energy of impacting meteoroids, their use will result in a definite loss of thermal performance, thus requiring a trade-off until minimum weight is achieved.

When the Snap 8 system is proved operational in space, it will provide valuable information for designing future power supply systems. As thermionic and plasma dynamic converters become competitive with turbo-electric converters, the systems will become lighter, simpler and more reliable.

### 15.5 First Missions: 1966-1970

Early missions for electric propulsion are expected to begin in 1966, provided electric engines and nuclear-electric power supplies are vigorously developed. After flight testing of arc and ion engines with the 30 kw Snap 8, proven engines will use the Snap 8 for mission flights until about 1970.

Electric propulsion systems depend upon a number of parameters that are unique for these systems [11]. The most important ones are the specific power of the power source,  $\alpha$ , the propulsion time,  $\tau$ , the specific impulse,  $I_{sp}$ , and the energy conversion efficiency,  $\eta$ , of the engine. For each set of  $\alpha$ ,  $\tau$ , and terminal velocity,  $\mu$ , an optimum specific impulse is found to make the payload ratio a maximum. Figure 15.4 shows the relationship between the total velocity increment and propulsion time, using specific impulse and payload weight as parameters, based upon specific space ship characteristics taken from Ref. [12]. The velocity increments required for specific missions are functions of propulsion time, launch site, time of flight and flight plan, but these factors are assumed specified in Fig. 15.4. This figure shows that electric propulsion provides a great flexibility for fulfilling specific missions. For any given mission, there is a trade-off between propulsion time and payload weight.

Early missions with arc engines may have propulsion times of 50 to 100 days, as shown in Table 15.3.

Electric engines do not operate with a constant energy conversion efficiency over a full range of specific impulse. Figure 15.5 illustrates the thrust attainable from present-day electric engines as a function of specific impulse. The ideal theoretical electric engine should produce a hyperbolic relationship, but actual engines show lower thrust values at specific impulses between 1200 and 4000 sec. This does not necessarily

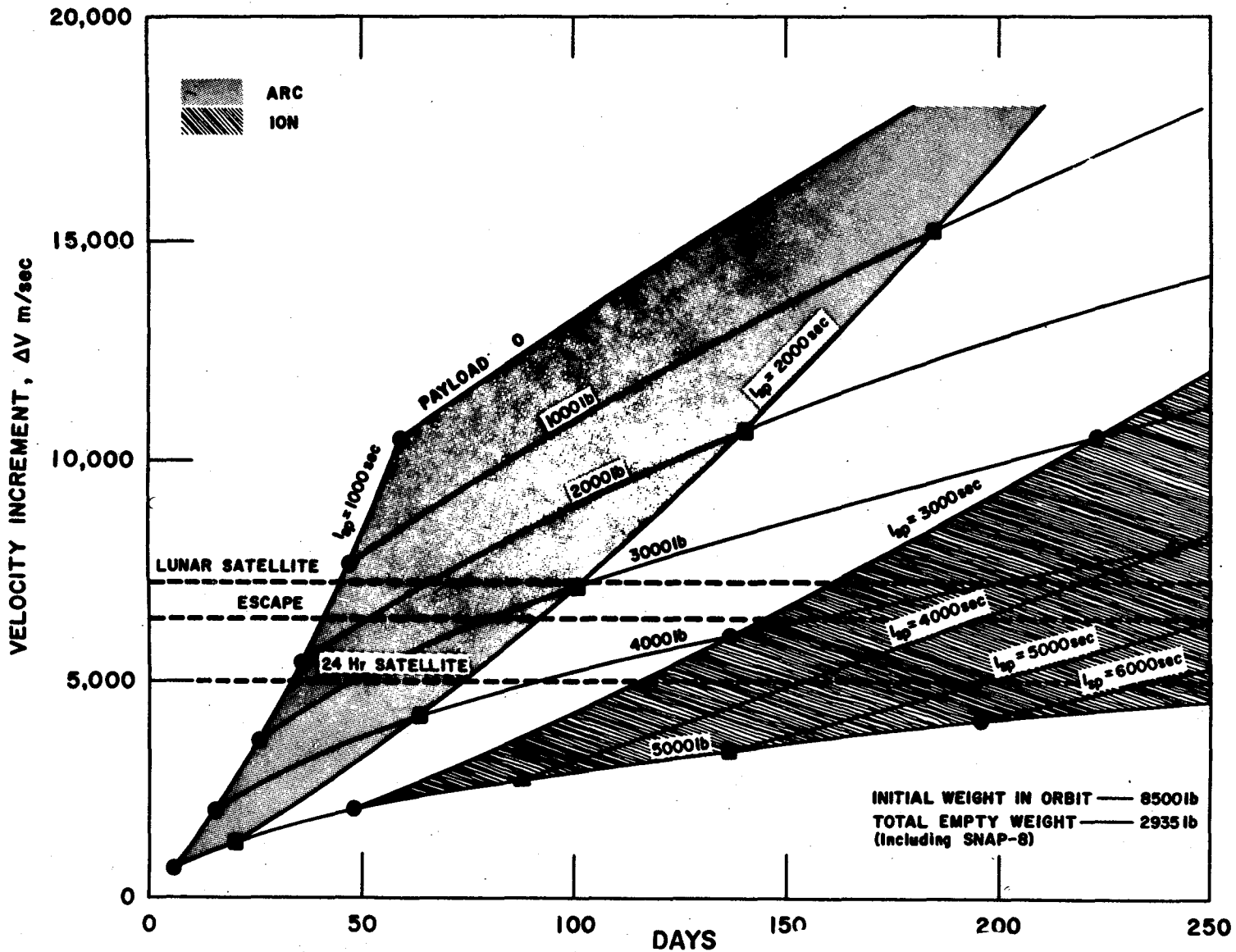


Fig. 15.4 Early mission capabilities of electric propulsion using 30 kw Snap-8 nuclear electric power supply.

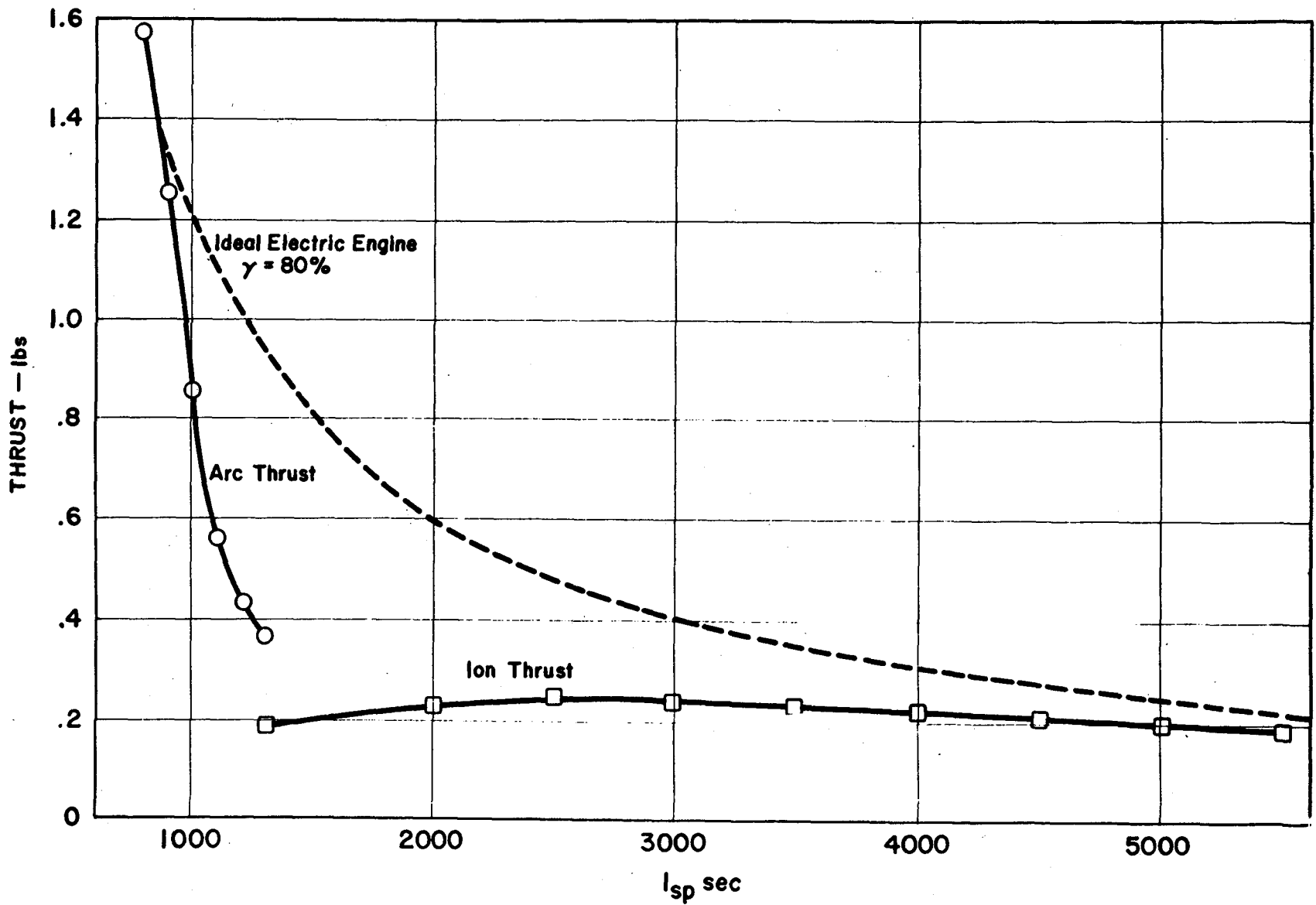


Fig. 15.5 Thrust versus specific impulse for 30 kw electric engines (existing state-of-the-art, December, 1961).

reduce the payload capability, but for a given payload the time of propulsion increases as the characteristics of the actual engines depart from those of the ideal engine. This illustrates the need to increase the energy conversion efficiencies of electric engines. Equally important is the need to increase the specific power of the power source, which would have the same effect on the overall mission.

Table 15.3 Typical Early Arc Engine Missions  
(Snap 8 Power Supply, Engine Efficiency = 80%, Start From 485 km Orbit With 8500 lb)

Mission	$I_{sp}$ (sec)	Final Weights (lb)		Propulsion Time (days)
		Useful Payload	Total	
Transfer to 24-hr orbit	1500	3140	6075	65
Transfer to 24-hr orbit	2000	3675	6610	75
Transfer to lunar orbit	2000	3000	5935	100

Specific early missions for which some details have been determined and discussed include:

1. Orbital transfer from 485-km nonequatorial orbit to 36,000 km-equatorial orbit (24-hr communications satellite). The power source can be used for operation of satellite equipment after transfer. Possible with 30 kw arc engine with  $I_{sp}$  of 1200 to 1600 sec [12 - 18].
2. Attitude control of satellites, using several 1 kw arc engines with  $I_{sp}$  of 700 to 1000 sec [15].
3. Mapping of radiation belts, solar corpuscular radiation and magnetic field between Earth and Moon, using 30 kw arc engine [15].
4. Lunar ferry, between Earth orbit and lunar orbit [19]. This mission requires specific power figures higher than are now available. Improved power sources would increase the likelihood of this mission.
5. Planetary missions using the 60 kw version of the Snap 8 and ion engines with specific impulses of 3000 to 5000 sec. These missions include Mars or Venus flyby, Mars or Venus capture, Mars orbiter, 15-deg out-of-the-ecliptic probe Refs. [18, 20 - 24].

The Snap 8 power supply will be the limiting factor in many of the above missions. Its lifetime of 10,000 hr will be an upper limit for propulsion times.

#### 15.6 Advanced Missions: 1970-1980

The potential of electric propulsion will be fully utilized only if nuclear electric power sources are developed in progressive steps



such as 100 to 300 kw, 1 to 4 Mw, and about 20 to 40 Mw. Lifetimes must be extended to several years and specific powers should be increased to 0.5 or 1 kw kg<sup>-1</sup>, and possibly even higher.

Advanced missions for electric propulsion will include uses in Earth orbits, between the Earth and Moon, and to the planets or other targets in the solar system. Some of the proposed missions, in the approximate order of increasing total velocity increment are:

Attitude and position control of space vehicles	Ref. [15, 25]
Orbit correction for low-altitude satellite	Ref. [25]
Orbital transfer	Ref. [15, 25]
Supplies to space station	Ref. [25]
Lunar supply mission	Ref. [19, 25]
Mars or Venus flyby	Ref. [26]
One-way trip to Mars or Venus	Ref. [26 - 27]
15-deg out-of-the-ecliptic probe	Ref. [26, 29]
Manned trips to Mars or Venus	Ref. [25, 28]
Mercury satellite	Ref. [26]
Jupiter flyby	Ref. [20, 26, 27, 28]
Jupiter orbiter	Ref. [25 - 26]
45-deg out-of-the-ecliptic probe	Ref. [22]
Pluto flyby	Ref. [25]
Probe to 100 A.U. distance	Ref. [29]

Reference [13] also discusses these missions. Some of the more ambitious missions can be accomplished only by electric propulsion. It provides a unique propulsion concept for the unmanned and manned exploration of the solar system.

In cislunar space, electric engines can be used for ferries. Many trips will be made between the close Earth orbital supply station and the low lunar orbital station. These missions will require fairly high thrust, so the lower range of the specific impulse spectrum of electric engines is favored. Table 15.4 lists characteristics of electric engines and nuclear power supplies considered feasible for a lunar ferry during the 1970-1980 period.

Table 15.4 Characteristics of a Lunar Ferry  
Using Electric Propulsion

Earth Orbit Altitude	485 km
Lunar Orbit Altitude	32 km
Total Weight Leaving Earth Orbit (including payload and fuel)	400,000 lb
Total Weight of Propulsion Module (including electric engines, nuclear electric power supply, tanks, structure, etc.)	40,000 lb
Power Supply Output	4 Mw
Specific Power of Power Supply	0.3 kw kg <sup>-1</sup>
Energy Conversion Efficiency of Engine	50%

The ferry will meet the Earth orbital supply stations and take on supplies and propellant for the electric engines. The electric engines will be started and the ship will spiral out until it reaches escape velocity. Then it will coast without propulsion to the neighborhood of the Moon, where the engines will be started again for the spiral inward until the final lunar circular orbit is achieved. During the engine-off periods the power is consumed by a ballast resistor and radiated to space. The low thrust of the ship will facilitate a rendezvous with the lunar orbital supply station. After delivering the supplies, the ferry reverses the flight plan. Adjustment of inclination to the orbital plane is performed during the propulsion spirals by thrust vectoring. The optimum supply-carrying capability is achieved at a specific impulse around 1300 sec. Since this maximum is very broad, especially on the high-impulse side, electric engines with impulses up to 2000 sec look promising for this mission. The maximum payload per year shifts to higher  $I_{sp}$  values with an increase of the power source weight. With a 60,000-lb propulsion module, the optimum  $I_{sp}$  is 1540 sec. The payloads for this ferry may consist of scientific instruments, food, tools, propellants, etc. It will be brought down to the surface of the Moon by soft landing vehicles using high-energy chemical propellants.

Payload capabilities and travel times are summarized in Table 15.5.

Table 15.5 Payloads and Travel Times for Lunar Ferry

Time for Single Round Trip	$\frac{V}{g_0}$	Payload for Single Round Trip with Engine Efficiency ( $\eta = 0.5$ )	Payload per Year With Engine Efficiency ( $\eta = 0.5$ )	Payload per Year with Efficiency of Advanced Electric Engine ( $\eta = 0.75$ )
(days)	(sec)	(lb)	(lb)	(lb)
33	1103	129,000	1,430,000	2,145,000
40	1310	159,000	1,460,000	2,190,000
50	1600	189,000	1,395,000	2,090,000
60	1882	212,000	1,295,000	1,940,000
70	2165	230,000	1,200,000	1,800,000
80	2450	243,000	1,110,000	1,665,000
90	2727	253,000	1,025,000	1,540,000
100	3006	263,000	950,000	1,425,000

The weight of propellant consumed decreases with increasing specific impulse, while the payload capability on a yearly basis shows a maximum at 1300 sec impulse.

Reference [19] discusses a flight plan for a lunar ferry with a spiral from the low Earth orbit out to the vicinity of the Moon, a capture maneuver to a lunar orbit and an immediate descent of each detached payload ship to the surface of the Moon.

For space exploration beyond the Moon, ion or magnetofluiddynamic (MFD) engines with specific impulses of 3000 to 30,000 sec will be used. The MFD engines are not as far advanced in their development as ion engines. However, in the period of 1970 to 1980 these engines should reach an advanced stage of development. Selection of the best engine for each mission must be made on the basis of performance and mission requirements. Arc engines are not considered for prime propulsion in interplanetary space. However, they have been discussed in connection with so-called high-powered maneuvers during the approach to a planet and for the initial spiralling out from a low Earth orbit to escape.

### 15.7 Manned Planetary Vehicles

The most intriguing challenge to the space flight planner is the conceptual design of a manned vehicle for planetary exploration. Electrically propelled vehicles will be particularly suited for this mission because of their liberal payload ration which will allow ample equipment for the crew, and will also allow the necessary shielding against solar protons and Van Allen radiation.

Design studies of electrically powered spaceships for manned planetary flight will probably begin toward the end of this decade. By that time, nuclear-electric power supplies of the 20 to 40 Mw class will have entered the planning stage; our knowledge of meteor fluxes and space radiation will be more realistic than it is now, and many details of the atmosphere and the surface of Venus and Mars will be known from exploratory probes.

The following paragraphs contain, in a very condensed form, the results of a study for a conceptual design of a Mars expedition. More details, including arguments for the selection of certain parameters and schemes, may be found in Ref. [30].

#### 15.7.1 The Master Plan

The objective of the planetary expedition will be manned surface exploration of Mars. A fleet of five electrically propelled vehicles, assembled and checked out in a 320 km orbit around Earth, will travel together toward the planet Mars and establish a satellite orbit at an altitude of 300 km where the atmospheric pressure is  $10^{-6}$  mm Hg. Atmospheric drag will be overcome by continuing low-level operation of the ion engines. Each ship will carry three passengers and their equipment. The basic design of all ships will be identical; however, three ships

(type A) will carry landing craft for Mars and a smaller amount of propellant than the other two (type B). The first landing craft to descend will carry only equipment such as surface vehicles, shelters, and tools. The second will transport a small crew, while the third will serve as a backup for the second. Each of the landing craft has the capability of transporting all landing crew members back to the orbiting ships.

The design of the interplanetary vehicle will provide for rotation of the crew compartments at a rate which results in a simulated gravity of about 0.1g. The radius should be large enough to keep Coriolis forces small. It is anticipated that sufficient experience with orbital operations will be accumulated by 1970 or 1975 to confirm, or to improve, the suitability of this assumed gravity.

Each vehicle will contain a radiation shelter to afford protection for the crew members against solar proton outburst and against Van Allen radiation. The shelter will consist of thick layers of shielding material, surrounded by equipment and other supplies such as drinking water, oxygen tanks, propellant for the return flight, samples from Mars, etc. (Fig. 15.7 insert). Solar outbursts will require shelter protection for not more than a few hours; traveling through the Van Allen belts will make it necessary that the crew members stay "in the doghouse" for 22 or 23 hours a day for a period of several days.

It is planned that all five ships will make the complete round trip back to the 320-km Earth orbit. In case of failures, two ships could conveniently accommodate the 15 crew members; in an emergency, one ship could carry the crew back into the Earth orbit.

#### 15.7.2 Flight Plan

The flight plan of a Martian round-trip vehicle depends upon the acceleration of the vehicle, and also upon the relative motions of Earth and Mars. As shown by Moeckel [31], the total round-trip time is shortest when the return leg passes around the Sun inside the Earth's orbit to catch the Earth on the other side (Fig. 15.6). In this way, a propulsion system with a specific power of  $0.5 \text{ kw kg}^{-1}$  can achieve a complete round trip to Mars, including a waiting time of 40 days in the Martian orbit, in about 560 days. Spiralling around the Earth until escape will take about 48 days, while spiralling down to Mars will require 21 days. The Earth-Mars transfer takes about 140 days, or roughly one half of the Hohmann transfer time. The return transfer time is almost twice as long because of the indirect approach, but a direct transfer after 40 days of Martian exploration would not result in a rendezvous between ship and Earth.

The thrust vector will be tangential to the flight path and constant in magnitude during the spiralling periods. A program of variable thrust may be applied for the planetary transfer periods, optimized for

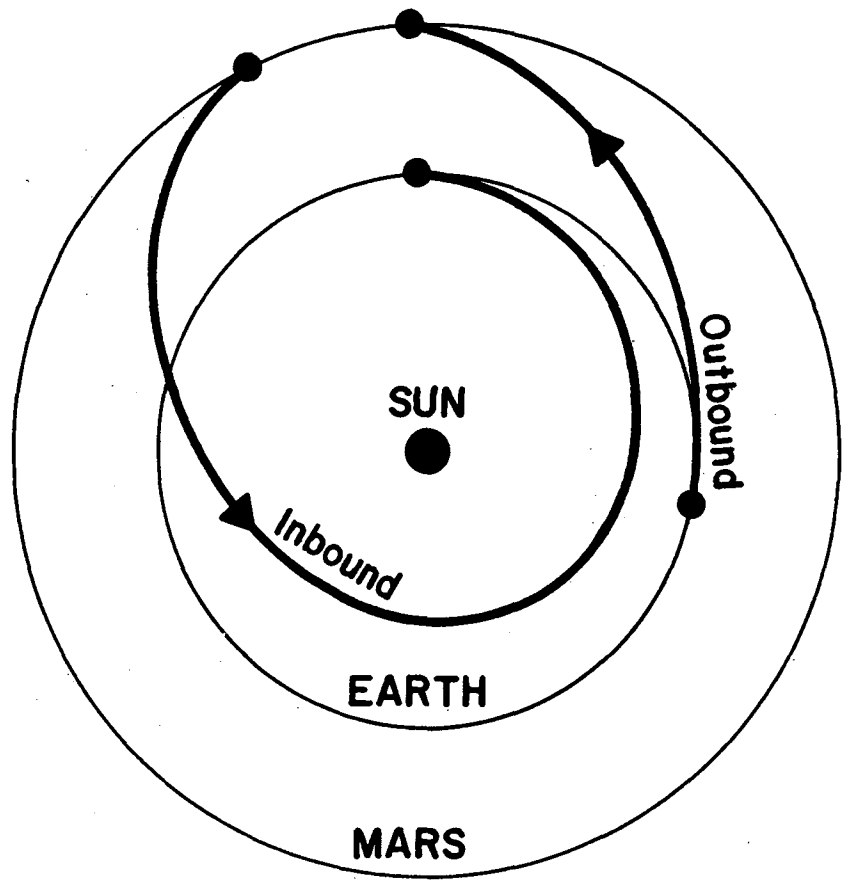


Fig. 15.6 Trajectories of Martian round trip. Direct outbound and indirect inbound legs (Moeckel, Ref. 33 ).

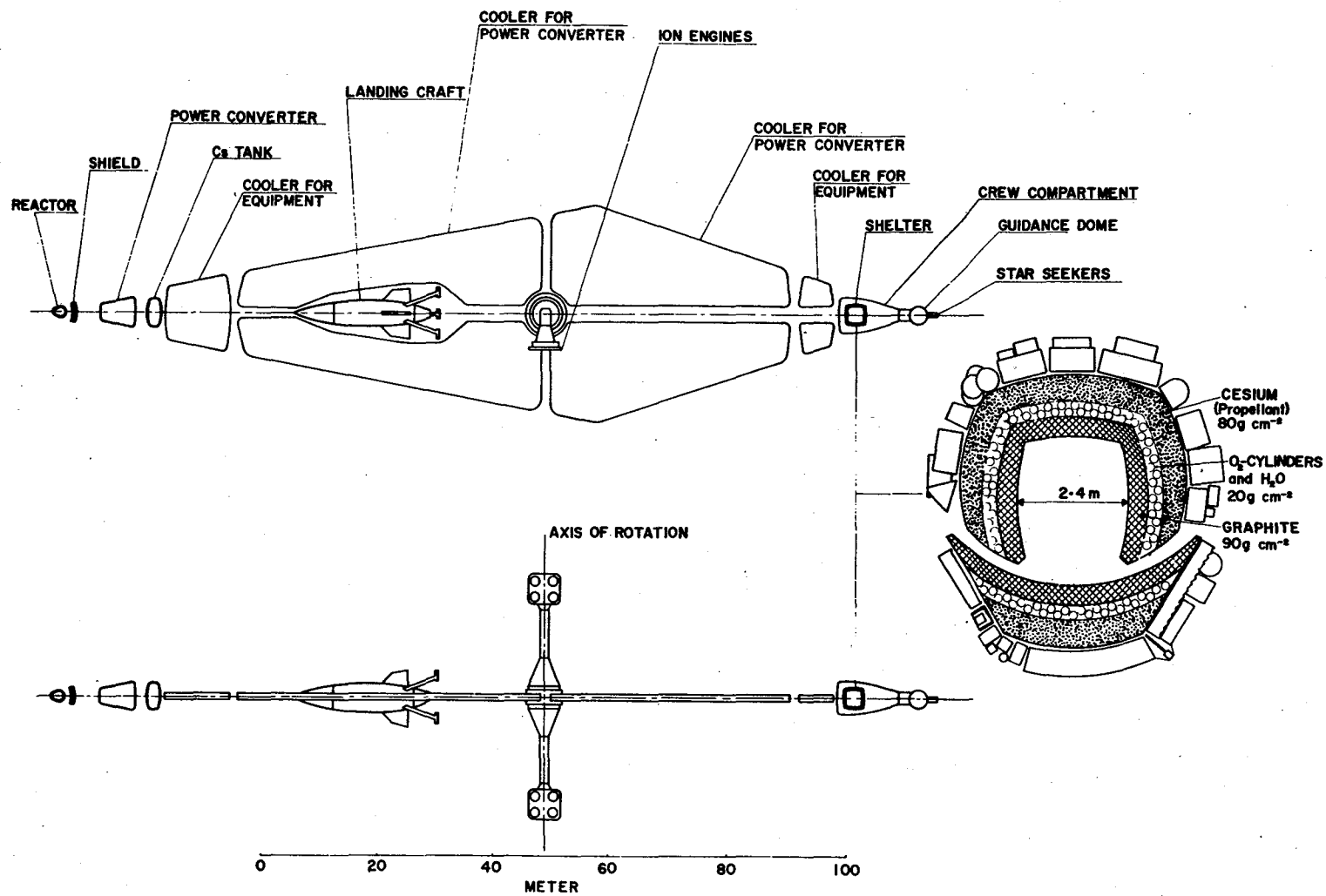


Fig. 15.7 Manned electric spaceship for Martian round trip.

maximum payload on the round trip. It has been shown that a variable thrust program on planetary transfer trajectories results in slightly greater payload capabilities than a constant thrust program [32]; however, the gain is not too great and may not justify the added complexity of a variable thrust system [33]. This Mars project assumes constant thrust throughout the flight, with several brief thrustless periods during the transfer phases. The direction of the thrust vector with respect to the path tangent, however, varies according to a preset program.

Guidance of the spacecraft is achieved by a system of planet and star seekers which constantly read the angles to the planets with reference to a fixed star system. These angles, together with the known positions of the planets as functions of time, permit accurate determination of the ship's location in three-dimensional space. Comparison of this location with the predetermined trajectory will show deviations, if any should develop. Corrective maneuvers will then be initiated immediately by a change of thrust vector direction.

Besides the planet and star seeker system, the ship will carry accelerometers and integrators in three directions to give direct readings of accelerations, velocities, and distances. These readings will enable the crew to monitor constantly the performance of the propulsion system.

Note that the continuous propulsion of an electric planetary vehicle renders the guidance problem relatively easy. Comparing it with the guidance of a chemically propelled planetary vehicle is like comparing the guidance of an airplane flown under visual flight rules over familiar territory with the guidance of a ballistic missile to the same target.

### 15.7.3 Performance and Design Data

The principle data of each of the five ships are listed in Table 15.6 and Table 15.7.

Table 15.6 Mass Requirements of Proposed Manned Mars Ship

Mass	Type A (tons)	Type B (tons)
Power Plant	80	80
Shelter	55	55
Landing Craft	70	--
Pure Payload	40	40
Propellant	115	185
Total	360	360

Table 15.7 Performance and Design Data of Manned Mars Ship

Parameter	Quantity or Rate
Specific Power	0.5 kw kg <sup>-1</sup>
Total Power	40 Mw
Initial Acceleration	1.5 x 10 <sup>-4</sup> G
Exhaust Velocity	140 km sec <sup>-1</sup>
Characteristic Velocity	90 km sec <sup>-1</sup>
Voltage	14,500 v
Current	2740 amp
Total Trip Time	560 days
Thrust	56 kg
Propellant Flow Rate	3.75 g sec <sup>-1</sup>
Active Ion Motor Area (20 ma cm <sup>-2</sup> )	14 m <sup>2</sup>
Rotational Rate of Ship	1 rev/40 sec
Artificial Gravity in Crew Compartment	0.1g

Overall efficiency of the propulsion systems has been assumed as 80 per cent. During the escape spiral around the Earth, the propellant for return will be used as additional shielding mass around the shelter. On the return trip, samples from Mars will be stacked around the shelter. The time within the Van Allen belts during return will be only about one half as long as the time on the outbound leg.

The vehicle must be designed and equipped to meet the following requirements: living and working accommodations for three, and, in case of emergency, for up to 15 crew members; separation between reactor and crew compartments of about 150 m; rotation of crew compartments to provide approximately 0.1g acceleration; thrust vector direction through center of mass; Martian landing vehicle to be carried on outbound leg only.

It is assumed that the electric power generator will be of the thermionic or of the plasma dynamic type. Rotation of the vehicle will be initiated at the beginning of the trip by solid spin rockets and will be sustained by an occasional boost from solid rockets. Figure 15.7 shows a sketch of the ship, illustrating the arrangements of the major components. Propellants will flow from the two tanks at such rates that the center of mass of the vehicle remains fixed. Prior to the return trip, propellants from around the shelter will be distributed between the two tanks to preserve the center of mass.

The orientation of the ship will be such that its rotational plane coincides with the plane of the trajectory. In this case, the rotational axis need not change when flight direction changes. Necessary changes



of the rotational plane will be effected by varying the thrust vector directions of the two thrust units. A model of the manned Mars ship is shown in Fig. 15.8.

It is anticipated that a manned Martian expedition of this kind will be feasible during the 1980-1985 period. Ten years ago, a mission of this type would have been considered impossible. Within the past few years, however, great strides have been taken in the development of electric engines; the remaining problems are clearly foreseen and appear surmountable; progress is being made in the development of larger power supplies with higher specific powers; missions have been defined and analyzed. Electric propulsion is indeed a new technology and one with vast potential for the exploration of outer space.

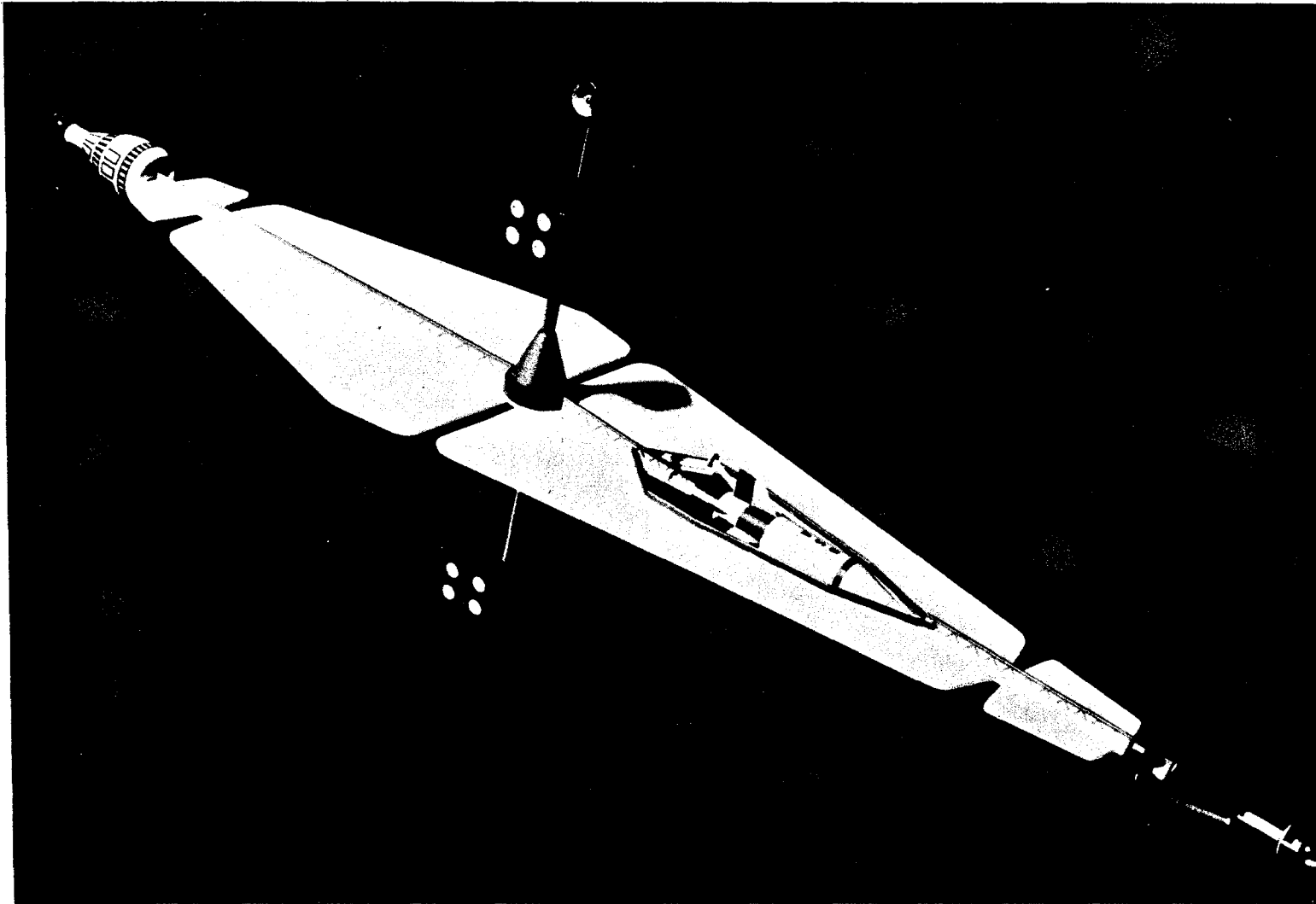


Fig. 15.8 Model of manned Martian electric spaceship.

## REFERENCES

1. Personal communication from H. Kaufmann, NASA, Lewis Research Center.
2. Thompson-Ramo-Wooldridge (TAPCO), Cleveland, Ohio, Progress Report on Contract NAS 8-42, 1961.
3. Personal communication from H. Childs, NASA, Lewis Research Center.
4. Sellen, T. M. and H. Shelton, Transient and Steady State Behavior in Cesium Ion Beams, Air Force Office of Scientific Research Report 60-1395, Washington, D. C., 1960.
5. Sellen, T. M. and R. F. Kemp, Cesium Ion Beam Neutralization in Vehicular Simulation, Air Force Office of Scientific Research Report 937, Washington, D. C., June 1961.
6. Noeske, H. O. and R. R. Kassner, Analytical Investigation of a Bi-propellant Arcjet, American Rocket Society Space Flight Report to the Nation, New York, 1961.
7. Heller, G. and B. P. Jones, "Survey of Arc Propulsion," American Rocket Society--Oak Ridge National Laboratory Space-Nuclear Conference, Gatlinberg, Tennessee, May 1961.
8. Molitor, J. H. and T. M. Littman, Analytical Studies in Ion Propulsion, USAF, Aeronautical Research Laboratory Report 60-320, April 1961.
9. Cornog, R., "Design Optimization of Thermal Radiators for Space Vehicles," paper presented at the American Astronautical Society Meeting, Los Angeles, August 4-5, 1959.
10. Nysmith, C. R. and J. L. Summers, Preliminary Investigations of Impact on Multiple-Sheet Structures and an Evaluation of the Meteoroid Hazard to Space Vehicles, NASA TN-D-1039, September 1961.
11. Stuhlinger, E., "Possibilities of Electric Spaceship Propulsion," in "Bericht über den V Internationalen Astronautischen Kongress," F. Hecht, ed., Springer-Verlag, Vienna, 1955.
12. DeWeiss, F. A., D. W. Grunditz, and V. W. Miselis, "Design of a Multipurpose Arc Jet Space Vehicle," paper presented at the American Rocket Society Space Flight Report to the Nation, October 1961.
13. Heller, G., "The Electric Engine as a Propulsion System for the Exploration of Space," paper presented at the International Symposium on Space Age Astronomy, California Institute of Technology, August 7-9, 1961.
14. Yarymovych, M. I., F. J. Davidson, J. Lambert, and A. Mironer, "The Arc Jet Propelled Space Vehicle," paper presented at the American Rocket Society Space Flight Report to the Nation, October 1961.
15. Dangle, E. E., J. D. Gossett, and W. D. Hibbard, Jr., "Earth Satellite Missions for Electrical Propulsion," paper presented at the American Rocket Society Space Flight Report to the Nation, October 1961.
16. Rosener, J., Summary of Electrothermal Thrustor Mission Applications, Plasmadyne Corporation Report PLR-89, December 6, 1961.
17. Heller, G., "The Plasma Jet as an Electric Propulsion System for Space Application," paper presented at the 14th Annual American Rocket Society Meeting, November 1959.

18. Edelbaum, T. N., Study of Applicability of Ion Propulsion Engines for Space Missions, United Aircraft Corporation Research Laboratory, Report UAR-0869, March 6, 1961.
19. Stuhlinger, E., "Lunar Ferry with Electric Propulsion System," First Symposium (International) on Rockets and Astronautics, Tokyo 1959 Proceedings, M. Sanuki, ed., Tokyo, Japan June 1959.
20. Speiser, E. W., A Preliminary Study of Advanced Propulsion Spacecraft Payload Capabilities, Jet Propulsion Laboratory Technical Memo 33-42, NASA Contract NAS 4-6, May 10, 1961.
21. Edelbaum, T. N., et al, Mission Capability of Ion Engine Using Snap 8 Power Supplies, Contract NAS 5-935, Phase I - Summary Report, August 1961.
22. Stearns, Jr., J. W., Applications for Electric Propulsion Systems, Jet Propulsion Laboratory Technical Memo 33-47, April 10, 1961.
23. Edelbaum, T. N., et al, "Applications of Electric Propulsion to NASA Missions," paper presented at the American Rocket Society Space Flight Report to the Nation, October 1961.
24. Speiser, E. W., "Performance of Nuclear Electric Propulsion Systems in Space Exploration," paper presented at the American Rocket Society Space Flight Report to the Nation, October 1961.
25. Stuhlinger, E. and R. N. Seitz, "Electrostatic Propulsion Systems for Space Vehicles," in "Advances in Space Science," V. 2: F. I. Ordway, III, ed., Academic Press, New York, 1960.
26. Melbourne, W. G., Interplanetary Trajectories and Payload Capabilities of Advanced Propulsion Vehicles, Jet Propulsion Laboratory Tech. Report 32-68, March 31, 1961.
27. Koerner, T. W. and J. J. Paulson, Nuclear Electric Power for Space Missions, Jet Propulsion Laboratory Tech. Release 34-230, January 5, 1961.
28. Moeckel, W. E., Fast Interplanetary Missions with Low-Thrust Propulsion Systems, NASA TR R-79, 1961.
29. Dyson, F. J., "Proposal for High Velocity Space Probe Carrying Parallax Telescope," Institute of Advanced Studies, Princeton, New Jersey, 1961.
30. King, J. and E. Stuhlinger, "Conceptual Design Study of a Manned Return Trip to Mars with an Electric Space Ship," paper to be presented at the Electric Propulsion Specialists Conference, Berkeley, California, March 14-17, 1962.
31. Moeckel, W., Interplanetary Trajectories for Electrically Propelled Space Vehicles, NASA, Lewis Research Center Report E-1336, June 1961.
32. Irving, J. H., "Low-Thrust Flight: Variable Exhaust Velocity in Gravitational Fields," in "Space Technology," H. Seifert, ed., John Wiley and Sons, New York, 1959.
33. Downey, J., S. Fields, and E. Stuhlinger, "Optimization of Electric Propulsion Systems," paper to be presented at the Electric Propulsion Specialists Conference, Berkeley, California, March 14-16, 1962.

## A PERFORMANCE ANALYSIS OF ELECTRICAL PROPULSION SYSTEMS

R. D. Shelton, W. G. Johnson, Billy P. Jones, and J. C. King

Research Projects Division  
George C. Marshall Space Flight Center  
National Aeronautics and Space Administration  
Huntsville, Alabama

The electrical propulsion systems used for space exploration will be composed of a group of relatively complex subsystems. In developing the systems for practical application, it will be necessary to give attention not only to the characteristics of the individual subsystems, but also to the characteristics of the total system. The purpose of this discussion is to identify the primary parameters which characterize system performance, evaluate their influence on the general mission capability, and resolve them into factors associated with particular subsystem development.

The typical electric propulsion system has four major subsystems: (1) a source of prime electric energy; (2) a thruster which converts the electric energy into kinetic energy of an expellant stream; (3) a fuel or expellant source and control system; and (4) a payload defined as the remainder of the spacecraft. A basic requirement of the space electric propulsion system is that it be reliable and longlived in the space environment. This discussion, however, is concerned with improving performance levels and not with the development of the engineering ramifications of this basic requirement of reliability and lifetime, except to point out areas in which increases in performance might reasonably be expected to result in a reduction in reliability and lifetime.

Analysis and evaluation of probable deficiencies in electric propulsion systems in terms of the primary parameters is useful in determining the areas in which research and development are needed and the benefits may be derived. The standard for this analysis and evaluation will be an ideal system undergoing rectilinear acceleration from rest, with limitations on the power and propellant supply. The thrust unit of this ideal system is assumed to be constant in operating characteristics during the propulsion time and to eject propellant at a single velocity, with the total power input to the thrust unit appearing as kinetic energy in the propellant stream leaving the system.

**Preceding page blank**

Several variations make the performance of an actual system different from the ideal. Some of the electrical power delivered to the thrust unit will not appear as kinetic energy in the propellant stream. The propellant stream itself, because of departures from a single velocity of propellant ejection, will not produce maximum thrust. The power supply may suffer weight increases and power losses associated with the requirements of particular thrust systems. Components of the propulsion system may degenerate with time and may even need replacement during an extended mission. It is with the details of these departures from the ideal system that the following discussion is concerned.

### 16.1 System Performance

It is convenient to approach the subject of propulsion system analysis by considering the factors influencing overall vehicle performance. The primary parameters in this category may be classified according to whether they are related to the mission or the vehicle. The velocity change  $u$  which the propulsion system must produce in the vehicle and the allowable propulsion time  $\tau$  are mission parameters. To define the vehicle parameters, it is necessary to make certain assumptions regarding the vehicle in advance. If we assume a model vehicle, consisting initially of a propulsion system of mass,  $M_P$ ; propellant tanks and associated structure,  $M_S$ ; a propellant loading,  $M_F$ ; and a remainder,  $M_R$  (composed primarily of payload), the initial mass is

$$M_0 = M_P + M_S + M_F + M_R \quad (16.1)$$

The design objective will be to apportion the component weights to maximize the payload fraction,  $M_R/M_0$ . It is evident that the mass fractions allotted to  $M_P$ ,  $M_S$ , and  $M_F$  should be as small as possible; their values will be constrained by design factors and performance requirements. For the present analysis,  $M_P$  will be considered proportional to the power  $P_0$  delivered to the terminals of the thrust unit, defining a proportionality factor  $\alpha$  (the specific power) by

$$M_P = \frac{P_0}{\alpha} \quad (16.2)$$

It is reasonable also to assume that  $M_S$  will be proportional to the propellant loading  $M_F$ , or

$$M_S = sM_F \quad (16.3)$$

Thus, the minimization of  $M_p$  and  $M_s$  will be subject to the engineering limitations on  $\alpha$  and  $s$ .

Other vehicle characteristics are related to the thrust unit. Consider, for example, a rocket system of mass  $M$  ejecting propellant with a relative velocity distribution  $\dot{M}(\bar{v})$  that is assumed to be a positive definite function expressing the spread in speed and direction of the propellant leaving the rocket. If rectilinear acceleration from rest is assumed, the basic equation of motion is

$$M \frac{d\bar{u}}{dt} = \iiint \dot{M}(\bar{v}) \bar{v} \, d\omega \, dv \quad (16.4)$$

where  $M$  is the mass being accelerated;  $\bar{u}$  is the rocket velocity;  $\bar{v}$  is the propellant velocity vector;  $t$  is the time variable;  $d\omega$  is the element of solid angle; and  $dv$  is the increment in propellant speed. Equation (16.4) is Newton's second law for rocket motion for the case of propellant ejection with a spread in speed and may be expressed in the more usual form

$$M \frac{d\bar{u}}{dt} = M \langle \bar{v} \rangle \quad (16.5)$$

by the definitions

$$M = \iiint \dot{M}(\bar{v}) \, d\omega \, dv \quad (16.6)$$

$$\langle \bar{v} \rangle = \iiint \dot{M}(\bar{v}) \bar{v} \, d\omega \, dv / \iiint \dot{M}(\bar{v}) \, d\omega \, dv \quad (16.7)$$

where  $\dot{M}$  is the total mass flow rate, and  $\langle \bar{v} \rangle$  is an average velocity of propellant ejection. The right-hand side of Eq. (16.4) is the thrust arising from the acceleration of propellant mass relative to the rocket system. The kinetic beam power  $P$  of the propellant stream is given by

$$P = \frac{1}{2} \iiint \dot{M}(\bar{v}) \bar{v} \cdot \bar{v} \, d\omega \, dv \quad (16.8)$$

If the average of the square of the velocity is defined as

$$\langle v^2 \rangle = \iiint \dot{M}(\bar{v}) \bar{v} \cdot \bar{v} \, d\omega \, dv / \iiint \dot{M}(\bar{v}) \, d\omega \, dv \quad (16.9)$$

Eq. (16.8) may be written as

$$P = \frac{1}{2} \dot{M} \langle \vec{v} \cdot \vec{v} \rangle = \frac{1}{2} \dot{M} \langle v^2 \rangle \quad (16.10)$$

In discussing the thrust available from the kinetic energy of the propellant stream, it is useful to define a parameter K (the propellant stream efficiency factor) by the relationship

$$K \equiv \frac{\langle \vec{v} \rangle \cdot \langle \vec{v} \rangle}{\langle \vec{v} \rangle \cdot \langle \vec{v} \rangle} = \frac{\langle v \rangle^2}{\langle v^2 \rangle} \quad (16.11)$$

The losses from velocity distributions arising from beam divergence, neutral efflux, and multiple ionization are conveniently expressed in terms of the parameter, K. K varies between 0 and 1, being unity for the ideal case of a single velocity of propellant ejection.

Only a fraction  $\eta$  of the power  $P_0$  delivered to the thrust unit is available as kinetic beam power P. Thus  $\eta$ , defined by

$$\eta = \frac{P}{P_0} \quad (16.12)$$

is a convenient parameter in which to lump losses associated with heating ionizers, maintaining magnetic fields, pumping and control power requirements, etc. These losses will be discussed in more detail.

From the foregoing discussion, the basic equations governing rectilinear acceleration from rest in field-free space are:

$$M \frac{du}{dt} = \dot{M}^* \langle v \rangle \quad (16.13)$$

$$P = \eta P_0 = \frac{1}{2} \dot{M} \langle v^2 \rangle \quad (16.14)$$

$$\langle v \rangle^2 = K \langle v^2 \rangle \quad (16.15)$$

---

\* For convenience,  $\dot{M}$  is assumed to be positive throughout this discussion. Since  $M$  is considered positive and is decreasing, however,  $\dot{M}$  is actually negative in Eq. (16.13), and requires a minus sign to obtain equality ( $du/dt$  and  $\langle v \rangle$  are taken positive as usual). The minus sign is needed in the direct integration of Eq. (16.13) to obtain Eq. (16.25).



$$\dot{M}\tau = M_F \quad (16.16)$$

$$M_0 = M_P + M_S + M_F + M_R \quad (16.17)$$

$$\alpha \equiv P_0/M_P \quad (16.18)$$

$$M_S = sM_F \quad (16.19)$$

Equation (16.13) is the usual equation of motion generalized to include a velocity distribution in the propellant stream leaving the thrust unit. The vector character of  $\bar{u}$  and  $\langle \bar{v} \rangle$  has been removed by assuming a one-dimensional translational problem. The scalar  $\langle v \rangle$  is the average of the axial component of velocity in a thrust unit. Equation (16.14) expresses the efficiency with which the power  $P_0$  delivered to the thrust unit is converted to kinetic beam power  $P$  in the propellant stream, where  $P$  is related to the velocity distribution function  $\dot{M}(\bar{v})$ . The relation between beam kinetic power and useful thrust is contained in Eq. (16.15). Equation (16.16) contains the assumption that the propellant mass  $M_F$  is ejected at a uniform rate during the propulsion time  $\tau$ . The total initial mass  $M_0$  is expressed in Eq. (16.17) as the sum of the constituents already defined. Equation (16.18) defines the very important specific power parameter for the propulsion system. Equation (16.19) relates the tank structural mass,  $M_S$ , to the propellant loading,  $M_F$ .

We have now identified the basic quantities involved in the performance evaluation of the elements of a propulsion system. Specifically, we wish to find a relationship involving  $u$ ,  $K$ ,  $\eta$ ,  $\tau$ ,  $\alpha$ ,  $s$ , and  $\langle v \rangle$  which maximizes  $M_R/M_0$ . This can be done by eliminating  $M_F$ ,  $M_S$ , and  $M_P$  in Eq. (16.17). From Eqs. (16.17) and (16.19) we can write

$$M_F = M_0 - M_P - sM_F - M_R \quad (16.20)$$

From Eqs. (16.14) and (16.15)

$$\dot{M} = \frac{2\eta P_0}{\langle v^2 \rangle} = \frac{2\eta K P_0}{\langle v \rangle^2} \quad (16.21)$$

From Eqs. (16.16) and (16.21)

$$\dot{M} = \frac{M_F}{\tau} = \frac{2\eta K P_0}{\langle v \rangle^2} \quad (16.22)$$

From Eqs. (16.18) and (16.22)

$$M_P = \frac{P_0}{\alpha} = \frac{M_F \langle v \rangle^2}{2\eta K \alpha \tau} \quad (16.23)$$

Substituting this expression into Eq. (16.20) and solving for  $M_F$ , we have

$$M_F = \frac{M_0 - M_R}{1 + \frac{\langle v \rangle^2}{2\eta K \alpha \tau} + s} \quad (16.24)$$

The integration of Eq. (16.13) results in

$$u = \langle v \rangle \ln \frac{M_0}{M_0 - M_F} \quad (16.25)$$

By substituting Eq. (16.24) into Eq. (16.25) and solving for  $M_R/M_0$ , we obtain\*

$$\frac{M_R}{M_0} = \left( 1 - 1 - e^{-u/\langle v \rangle} \right) \left( 1 + s + \frac{\langle v \rangle^2}{2\eta K \alpha \tau} \right) \quad (16.26)$$

The required optimum value of  $\langle v \rangle$  is found by maximizing  $M_R/M_0$  with respect to  $\langle v \rangle$  (equating  $\partial(M_R/M_0)/\partial\langle v \rangle$  to zero). This process yields, after some manipulation, the desired condition for optimum exhaust velocity

$$e^{u/\langle v \rangle} = 1 + \frac{u}{\langle v \rangle} \left[ \frac{\eta K \alpha \tau}{\langle v \rangle^2} (1+s) + \frac{1}{2} \right] \quad (16.27)$$

After substituting appropriate values for  $u$ ,  $\eta K \alpha \tau$ , and  $s$ , Eq. (16.27) can be solved for the optimum average velocity of propellant ejection (Fig 16.1).

The parameters in the product  $\eta K \alpha \tau$  occur together in Eq. (16.27). Therefore, they are of equal weight and can be collected, for purposes of general analyses, into a single constant with units of velocity squared.

\* A similar equation, omitting the parameter  $s$ , is given in [1].

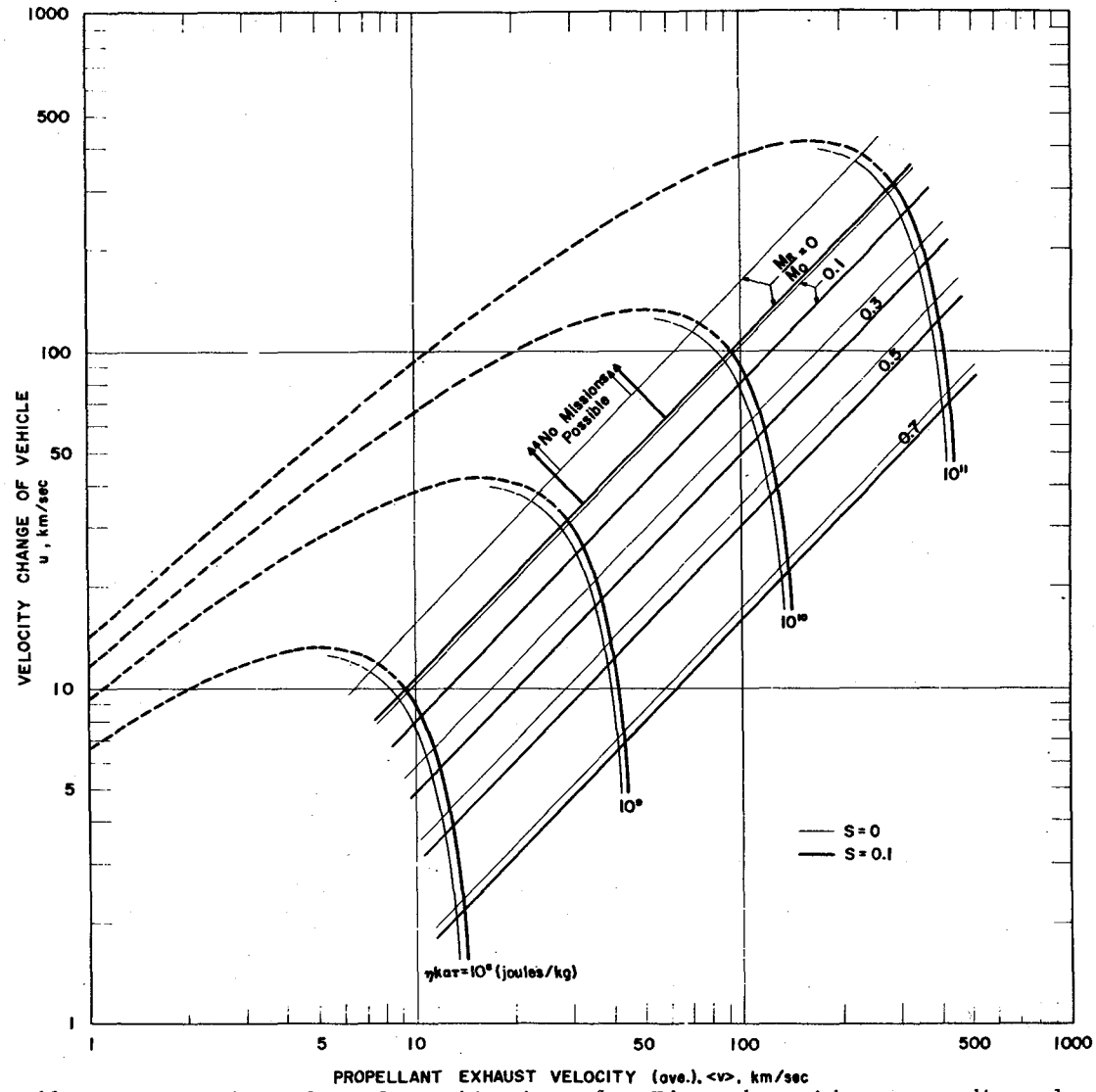


Fig. 16.1 Optimum values of  $\langle v \rangle$  for combinations of  $\eta K_{tr}$ , and  $s$ , with corresponding values of "payload" fraction,  $M_R/M_0$

## 16.2 The Power Supply

The source of primary electrical power will most likely consist of a nuclear reactor to provide thermal power, a power converter to produce electrical power from the thermal power, a waste heat disposal system, and equipment for distribution, control and conditioning of electrical power. The parameter  $\eta_c$ , defined by

$$\eta_c \equiv \frac{P_o}{P_t} \quad (16.28)$$

expresses the efficiency with which thermal power of the reactor  $P_t$  is converted to electrical power  $P_o$  at the terminals of the thrust unit. The constant  $\alpha$ , defined in Eq. (16.2) as

$$\alpha = \frac{P_o}{M_p} = \frac{\eta_c P_t}{M_p} \quad (16.29)$$

is the most widely distributed of the primary parameters, since it involves the reactor, the conversion and distribution system, the fuel storage and control system, and the thrust system.

The problem of improving the level of performance of the system can be readily considered in terms of two complementary problems. The first is that of improving the utilization efficiency of both available prime electric power and fuel. The second is that of increasing the ratio of available prime power to vehicle mass. Obviously, the two problems are related but center about different subsystems. The first will be solved primarily through improvement in thrusters; the second, through improvement in prime electric power sources and spacecraft designs. Both areas are given detailed consideration in this section.

The largest electric propulsion system under development now must be considered a forerunner or engineering development step toward electric propulsion systems for space exploration. It will utilize the Snap 8 operating at a nominal 30 kw output power level in conjunction with compatible thrusters. Although such a system has only limited capacity for space exploration, it is an interesting one with which to start an engineering analysis. It is the first system which promises usefully long lifetime at power levels sufficient to be of interest to mission planners.

The critical subsystem currently appears to be the prime electric power source. It consists of a nuclear reactor weighing in the neighborhood of 400 lb and producing 300 to 600 kw thermal power. An alkali

metal, sodium-potassium amalgam, is used as a reactor coolant and as a heat transport medium in a primary loop. The NaK leaves the reactor at a temperature somewhat above 1000°F, is pumped through a shell and tube boiler and reenters the reactor at approximately 200°F cooler than the temperature at which it was discharged. The second loop working fluid is mercury, employed in a modified Rankine cycle. It enters the heat exchanger as a liquid, is vaporized, and superheated. As a high-quality vapor it is used to drive a multistage turbine, to the shaft of which is affixed both an electric generator and the mercury pump. The exhausted vapor flows to a radiator-condenser element and the condensed mercury is pumped back to the boiler. System lubrication is provided by the mercury. The alternator is a three-phase unit producing about 37.5 kw of electric power at about 75 v, 1000 cps.

Estimates of usable electric power range from slightly less than 30 ekw to about 3 ekw and subsystem efficiency estimates range from about 9 per cent to 12 per cent. When the electrical conditioning equipment required to match alternator output and thruster input is included in the system, efficiency of the order of 7 per cent to 10 per cent is estimated. The total weight of the power generation equipment, exclusive of reactor, is approximately 1100 lb, of which about half is represented by the radiator-condenser unit. The reactor, nuclear shielding, and supporting structure can be expected to add an additional 900 to 1100 lb. Weight estimates for the power conditioning equipment range from about 150 lb to an amount in excess of 400 lb, depending upon the amount of thermal conditioning required to assure reliable operation of the circuitry.

There are two possible avenues for improving the level of performance of this particular subsystem. The first is to improve the efficiency of conversion of the available thermal power to usable electrical power, and the second is to improve the specific power ratio  $\alpha$ .

The problems involved in improving efficiency primarily concern materials. In the system currently under development, for example, mercury has been chosen as the working fluid in the secondary loop. The selection of this particular working fluid was dictated by several factors. One of the main determining considerations was that sufficient information was available on the behavior of mercury in contact with turbine structural materials at the temperatures of interest to indicate that while the corrosion problem was severe, it was surmountable without an extensive materials research. The upper temperature limit to which the mercury vapor can be raised is dictated largely by pressure considerations. The temperature at which it must be exhausted from the turbine is determined by the lowest vapor quality at which the turbine can be operated without deterioration of performance and loss of reliability. Because of the difficulties and inefficiencies involved in attempting to pump a vapor back into the boiler, a Rankine cycle is used. Two penalties are incurred; the heat required to vaporize the fluid is unavailable for further use and a radiator is required to assure condensation. However, vapor pumping is sufficiently inefficient to make the described operation attractive.

The turbine efficiency is currently estimated at 65 per cent to 70 per cent, alternator efficiency at about 90 per cent and mercury pump power requirements at perhaps 1.5 kw. The cycle efficiency, using mercury at the design temperatures, is of the order of 16 per cent. Quite obviously, while improvements in efficiency of the rotating equipment are always worthwhile, the only area through which manifold increases in  $\eta_c$  can be effected is in the improvement of thermal cycle efficiency. As an example of the course such an improvement program might take, one might consider the use of alkali metals and alkali metal amalgams for the reactor coolant and the turbine working fluid. The basic requirement to be met by the coolant is that it remain liquid to high temperatures (e.g., 2000°F); that the driving fluid vaporize at relatively high temperature (1000°F to 1400°F); that its latent heat of vaporization be low; that specific heat of its vapor be high, and that in the liquid phase it impose no stringent pumping requirements. From a thermodynamic standpoint, such a system appears attractive; however, solutions to the problems arising from incompatibilities of materials do not appear within immediate reach of the current state of technical knowledge. Undoubtedly, these problems will be solved for future systems, and the rate of solution will most likely be determined by the emphasis placed on attacking the problems.

In addition to the attractiveness of higher temperature systems for thermodynamical efficiency, such systems are also attractive from the standpoint of weight saving. The mechanism by which heat must be rejected from the system in space is purely radiative. Assuming constant emissivity as a function of temperature, and applying the Stefan-Boltzmann law

$$S = aT^4 \quad (16.30)$$

where  $S$  is the radiation energy density,  $a$  is a constant, and  $T$  is the radiator temperature. It is evident that for the rejection of fixed quantities of heat, relatively modest increases in the temperature of the radiator will result in an appreciable decrease in required radiator area and weight.

Even if the problems about the compatibility of a high-temperature working fluid with the loop structural materials were solved, it would not be possible to go to high-temperature operation with complete impunity. Operation at high temperature imposes severe environmental conditions on parts of the system not immediately in the working fluid loop. These can be effectively met only through improvement in materials. For example, the materials currently utilized in the construction of reactors for flight systems are not capable of reliably withstanding the thermal environment which would be imposed by operation at an outlet temperature

of, e.g., 2000°F for periods of the order of 10,000 hr. Further, increasing the turbine temperature results immediately in increased alternator temperature. Again, the materials required for efficient and reliable operation at, say, 1400°F are not yet available.

Of perhaps greater importance is the thermal environment in which the electronic components and power conditioning components of the system can be expected to operate. Even in the system currently under design, it is anticipated that some active thermal control may be necessary to assure the reliability of such components. In the most pessimistic estimates, conditioning conversion efficiency of 60 per cent to 65 per cent with a maximum allowed operating temperature of 175°F, the weight of the components required to maintain the thermal environment range upward from the order of 400 lb. Estimates of the weight of the equipment actively utilized for power conditioning range from about 45 lb to perhaps 150 lb. In considering systems of higher power, this is an area in which much attention might be profitably devoted.

Following the successful demonstration of the Snap 8 in space flight, there is one step that can be taken immediately to improve the specific power ratio. The reactor is being developed to operate at power levels up to 600 kw, thermal. Thus, with no increase in reactor weight, and with only minor increase in nuclear shielding weight, the output power can be doubled by providing parallel power conversion units. It is generally true that even without technological improvements the level of generated power can be increased more rapidly than the system weight required to effect such increase in power. The specific power ratio of the system currently under construction is of the order of  $2 \times 10^{-2}$  kw/kg. With a twofold increase in power,  $P_o$ ,  $\alpha$  should rise to about  $3 \times 10^{-2}$  kw/kg.

As will be shown, there presently seems little possibility of producing the electric power in a form completely usable by the electric engines without certain conditioning. Since, because of the thermal control requirements imposed by some of the components, power losses entailed in the conditioning circuitry are expensive in terms of system weight, rather extensive effort should be made to improve the compatibility between the "raw" output of the power conversion unit and the power requirements of the thruster and to increase the efficiency and reliability of power conditioning equipment at temperatures appreciably higher than 175 to 225°F at which such systems can now be expected to work reliably.

In addition to the turboelectric power converters, thermoelectro, thermionic, magnetofluidynamic, and photovoltaic devices are also under development. At present, the photovoltaic devices seem limited to power levels below a few (perhaps 3) kilowatts, while magnetofluidynamic (MFD) devices seem limited in efficient use to powers above a few (perhaps 2)

megawatts. These more direct techniques are quite appealing. Because they involve, in theory, no rotating machinery, it can be argued that they are inherently more reliable and more long-lived than is the turboelectric converter. Theoretically, the methods required to bring to useful form such a system as the thermoelectric converter are well understood. The problems involved in reducing the art to practice—particularly at power levels above a few tens of kilowatts—are largely the same type of materials problems encountered with turboelectric converters. Materials capable of withstanding the anticipated thermal environment and of functioning satisfactorily for extended periods do not yet exist.

Figure 16.2 shows the anticipated trends in specific power as a function of prime power generated. The improvements indicated are predicated upon the success met in material improvement programs. It is interesting to note that at levels above about 1 Mw generated power, the specific power estimated on the basis of total system weight remains essentially constant. It depends as much upon the weight of tankage, thrusters, fuel control equipment and structure, as upon the ratio of power to power conversion system weight. Thus, while at 1 Mw output power level the thermionic conversion system might be expected to represent perhaps 40 per cent of the weight of a turboelectric system of similar power rating, the total system weights (the values of  $\alpha$ ) are nearly equal. Hence, the choice of system to be employed at these levels appears to be dependent more upon such parameters as reliability, lifetime, engineering ease, etc., than on differences in system weight.

### 16.3 The Thrust Unit

The evaluation of the electric thrust unit requires several careful measurements, the laboratory techniques for which are still highly debatable. From Eq. (16.2), the specific power  $\alpha$  may be written

$$\alpha = \frac{P_0}{M_p} \quad (16.31)$$

where  $P_0$  is the power delivered to the terminals of the thrust unit and  $M_p$  is the mass of the propulsion system, which may be divided into reactor, conversion equipment, and thrust units. The mass of the thrust unit is therefore a part of the primary parameter  $\alpha$ .

In Eq. (16.31), it is seen that the mass of the thruster is important in determining  $\alpha$ . In addition, the power input requirements of the thruster are quite important in determining  $\alpha$ . For example, in the plans to flight test ion engines, it was found that the thrust units alone required six to eight separate power inputs. Each power input was achieved



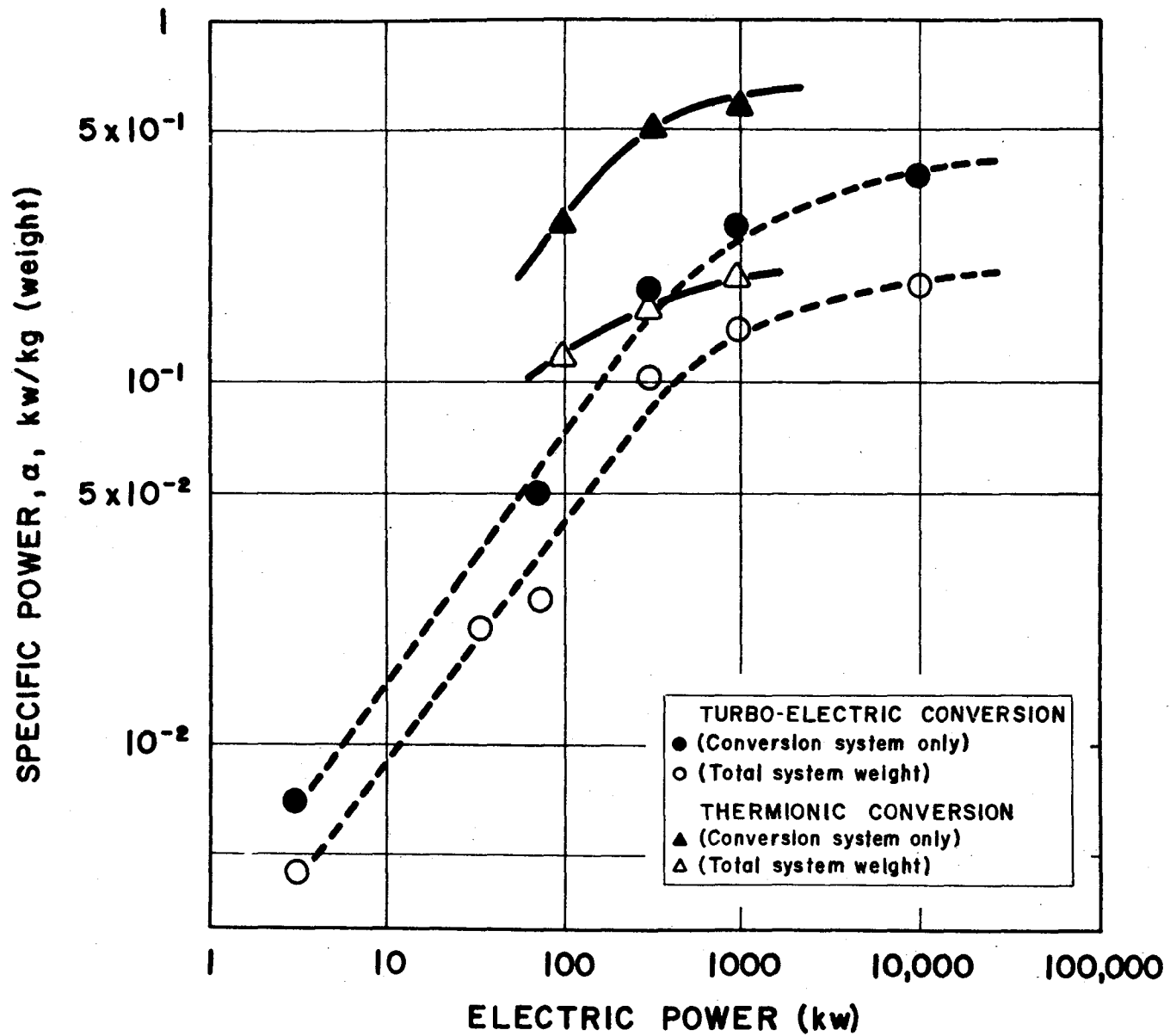


Fig. 16.2 Estimated specific power as a function of generated power.

by increasing the system mass and lowering the total efficiency of the propulsion system, and it was seen clearly that two of the engineering areas important to electric propulsion would be the development of efficient power conversion and distribution systems and the reduction of the number of power input requirements to the thrust unit.

The constants,  $\eta$  and  $K$  can be related to laboratory measurements by calculating the ratio of the actual thrust  $F$ , measured experimentally, to the thrust  $F_0$  of an ideal engine consuming the same power  $P_0$  and having the same mass flow rate  $\dot{M}$ . For the ideal thruster

$$P_0 = \frac{1}{2} \dot{M} v^2 \quad (16.32)$$

$$v = \left( \frac{2 P_0}{\dot{M}} \right)^{\frac{1}{2}}, \quad (16.33)$$

and

$$F_0 = \dot{M} v = (2 P_0 \dot{M})^{\frac{1}{2}} \quad (16.34)$$

In the actual case, using Eqs. (16.13), (16.14), and (16.15)

$$P = \eta P_0 = \frac{1}{2} \dot{M} \langle v^2 \rangle \quad (16.35)$$

$$\langle v^2 \rangle = K \langle v^2 \rangle \quad (16.36)$$

$$\langle v \rangle = \left( \frac{2 \eta K P_0}{\dot{M}} \right)^{\frac{1}{2}} \quad (16.37)$$

and

$$F = \dot{M} \langle v \rangle = 2 \eta K P_0 \dot{M} \quad (16.38)$$

The thrust ratio is, therefore

$$\frac{F}{F_0} = \left( \frac{2 \eta K P_0 \dot{M}}{2 P_0 \dot{M}} \right)^{\frac{1}{2}} = \frac{F}{(2 P_0 \dot{M})^{\frac{1}{2}}} = (\eta K)^{\frac{1}{2}} \quad (16.39)$$

or

$$\eta K = \frac{F^2}{2 P_o \dot{M}} = \frac{\dot{M} \langle v \rangle^2}{2 P_o} \quad (16.40)$$

Equation (16.40) relates the primary engine efficiency parameters,  $\eta$  and  $K$ , of an electric thrust unit to the measurable quantities of thrust, input power, and mass flow rate. If  $\eta K$  is a function of the conditions under which the thrust unit is operated,  $\eta K$  of Eq. (16.27) must be replaced with a proper function of  $\langle v \rangle$  before the optimization for  $M_R/M_O$ .

The parameters,  $\eta$  and  $K$ , are rather general and can be applied to any type of electric thrust unit. They are independent by definition, but appear together in the equation for payload optimization (Eq. 16.27), and in the equation defining the measurements to be made for the evaluation of thrust units (Eq. 16.40). However, the parameters are basically quite different. The parameter  $\eta$  is a measure of the efficiency with which electrical energy is converted to kinetic energy, and  $K$  is a measure of the efficiency with which the kinetic energy produced in the propellant stream is converted to thrust.

#### 16.3.1 The Ion Thrust Unit

In the ion engine, the losses that make the kinetic efficiency factor  $\eta$  less than unity may be associated with propellant feed and control, ion production, acceleration, and neutralization. All types of electric units will require power for propellant feed and control, and efforts to curtail this loss can proceed on a fairly general basis independent of the type of thrust unit being developed.

The collision type of ion source will expend power to heat an electron emitter and to accelerate the electrons to energies sufficient to produce ionization by collision. In some types of collision sources, power is required for a magnetic field. In the surface ionization source, the hot ionizer loses heat by conduction and radiation. The broad effort to produce more efficient ion sources includes an engineering attack on all the major loss factors. Lightweight, permanent magnets may be used to provide magnetic fields in some cases. Because of its low ionization potential and other excellent properties, cesium may be used as propellant to increase efficiency in all types of ion sources. Heat reflectors and insulators are being studied. New types of ion sources are being tried, and their efficiencies are often expressed in terms of the electron volts of energy required to produce an ion-electron pair.

Accelerator losses are closely associated with lifetime and performance. In general, ions and electrons which are accelerated and stopped in the thrust unit expend energy uselessly, although it may be

argued that some stray electrons may be accelerated and used to create useful heat in surface ionizers. Stray ions not only waste heat but sputter electrodes away from the optimum shape, create secondary electrons, and cause insulator breakdown.

For electron emission, most neutralization schemes include a hot filament to which a potential is sometimes applied. This source of loss is expected to be small.

The beam efficiency factor  $K$  is kinematic in nature and is a function of the properties of the propellant stream. However, the factors that make  $K$  less than unity can be related easily to the operation of the thrust unit. In the ion engine, for example, Eq (16.11) may be used to compute the dependence of  $K$  on neutral efflux (Fig. 16.3), or the dependence of  $K$  on the percentage of doubly ionized atoms (Fig. 16.4). If the distribution in speed is Gaussian,  $K$  is a function of the standard deviation  $\sigma$  (Fig. 16.5). The effect of poor beam focussing is shown in Fig. 16.6. All of these illustrations [3] show the losses that are incurred when there is a velocity spread in the propellant stream.

In terms of mission capability, the neutral efflux effect on  $K$  is secondary to the problems in lifetime and reliability caused by the slow migration of the unaccelerated propellant through the thrust unit. Many of the good propellants, such as Cs and Hg, are good conductors and can cause insulation breakdown. The charge exchange process, which is one of the principal reasons for the impingement of fast ions on the accelerator structure, is proportional to the density of neutral atoms that accumulate in the ion stream, either by leakage from the source or by ion beam impingement on the electrodes.

Although Fig. 16.4 shows that multiple ionization is not a great problem if the optimum accelerating voltage is applied, it should be recognized as an important design factor. The small loss shown in Fig. 16.4 results only if the accelerative potential is varied as shown in Fig. 16.7, which indicates the need for an understanding of what is emitted from the thrust unit. Cesium is thought to make the multiple ionization problem much less severe in collision sources, since it has a low first ionization potential and a relatively high second ionization potential.

The acceleration of heavy particles usually involves a wide distribution in charge-to-mass ratios. Although Fig. 16.5 is not typical of heavy particle accelerators, it does illustrate the problem of general speed distributions.

Stream divergence is common in all thrust systems. In the ion thrusters, it could result from poor optics or neutralization problems. In the latter case, the computation of the beam divergence contribution to  $K$  must be based on measurements sufficiently far downstream to insure that the beam beyond does not exert forces on the spacecraft.

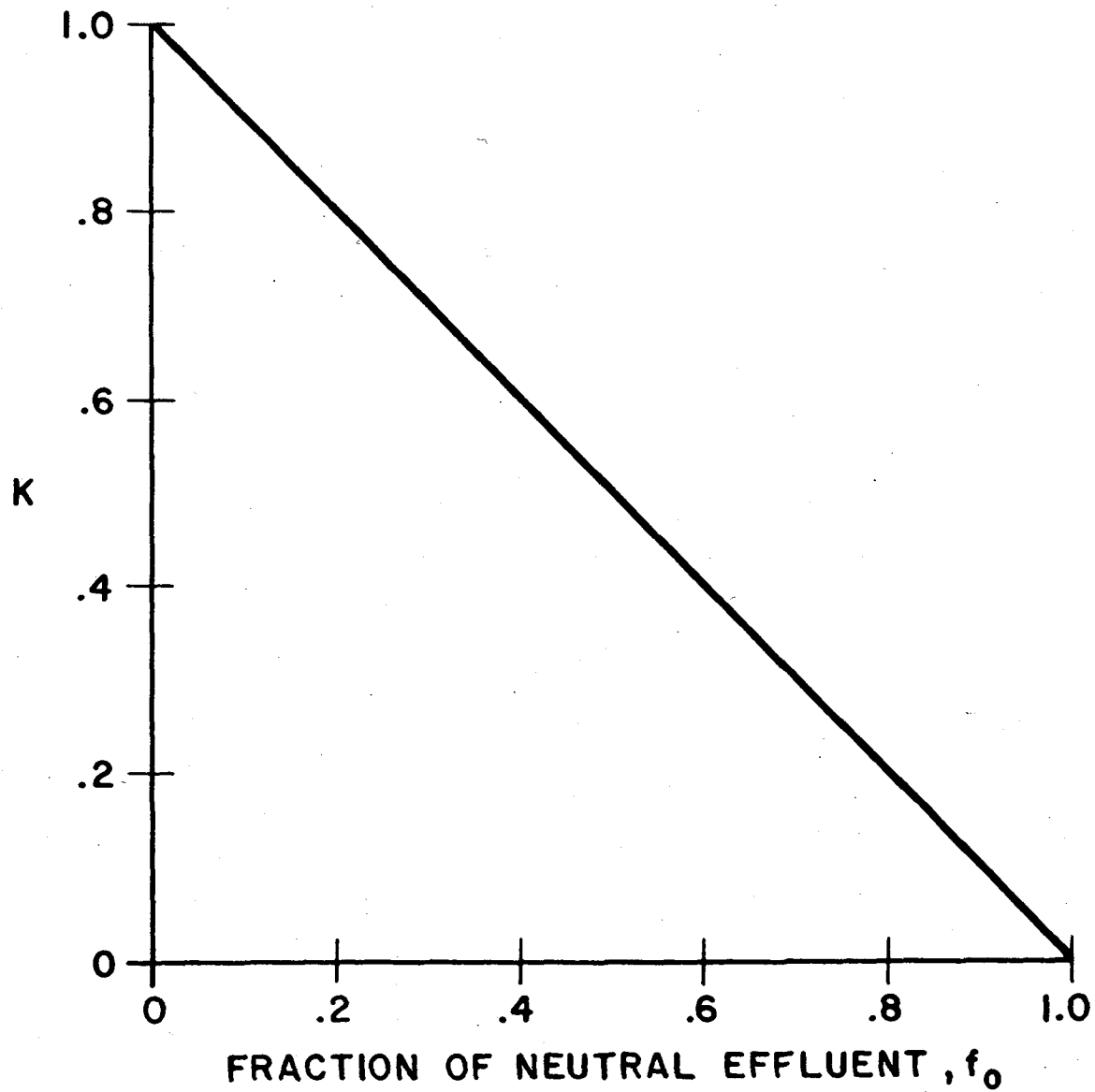


Fig. 16.3 K as a function of neutral efflux for an ion thrust unit emitting neutral and singly ionized atoms.

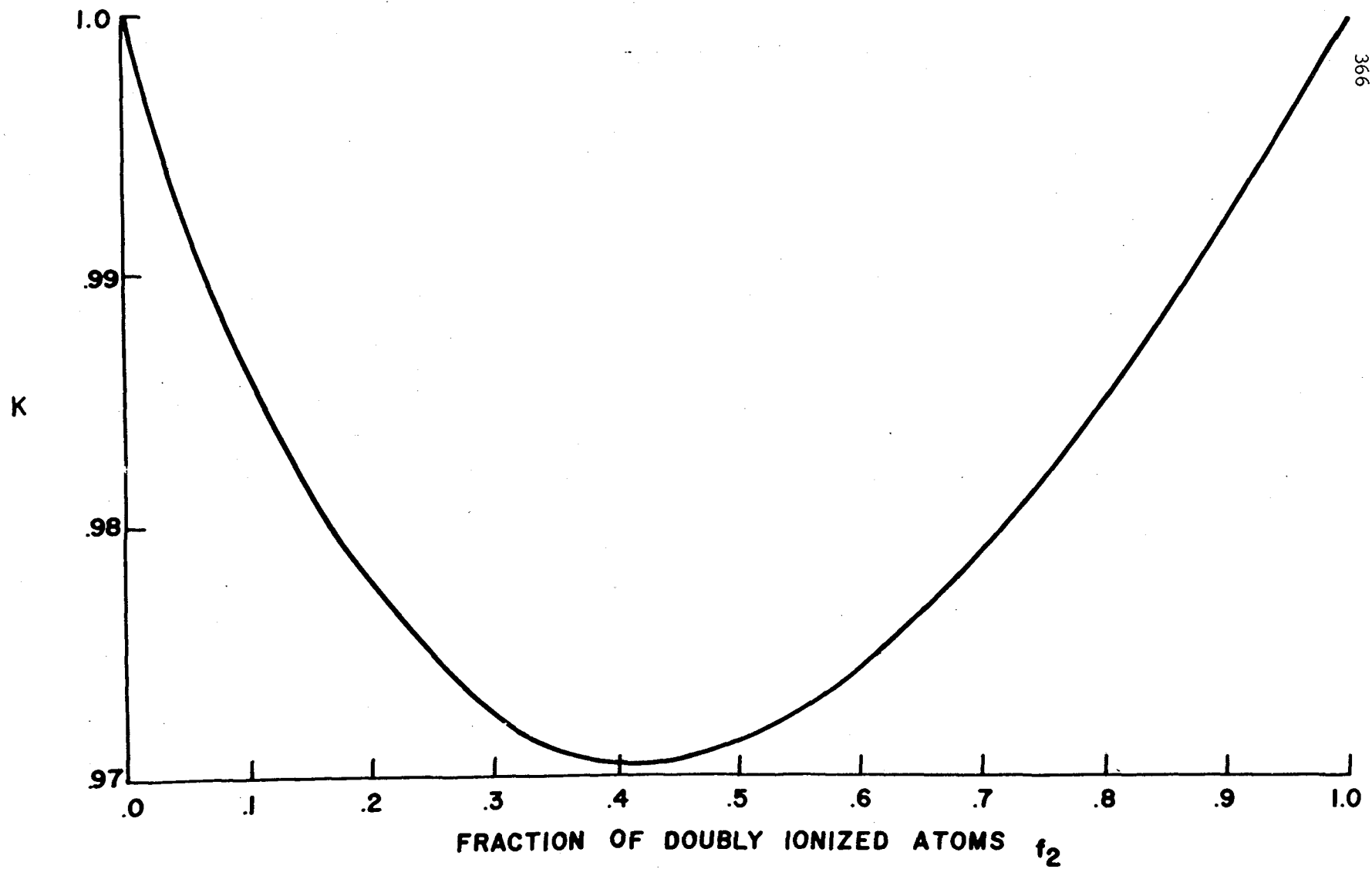


Fig. 16.4  $K$  as a function of double ionization for an ion gun emitting singly and doubly ionized atoms.

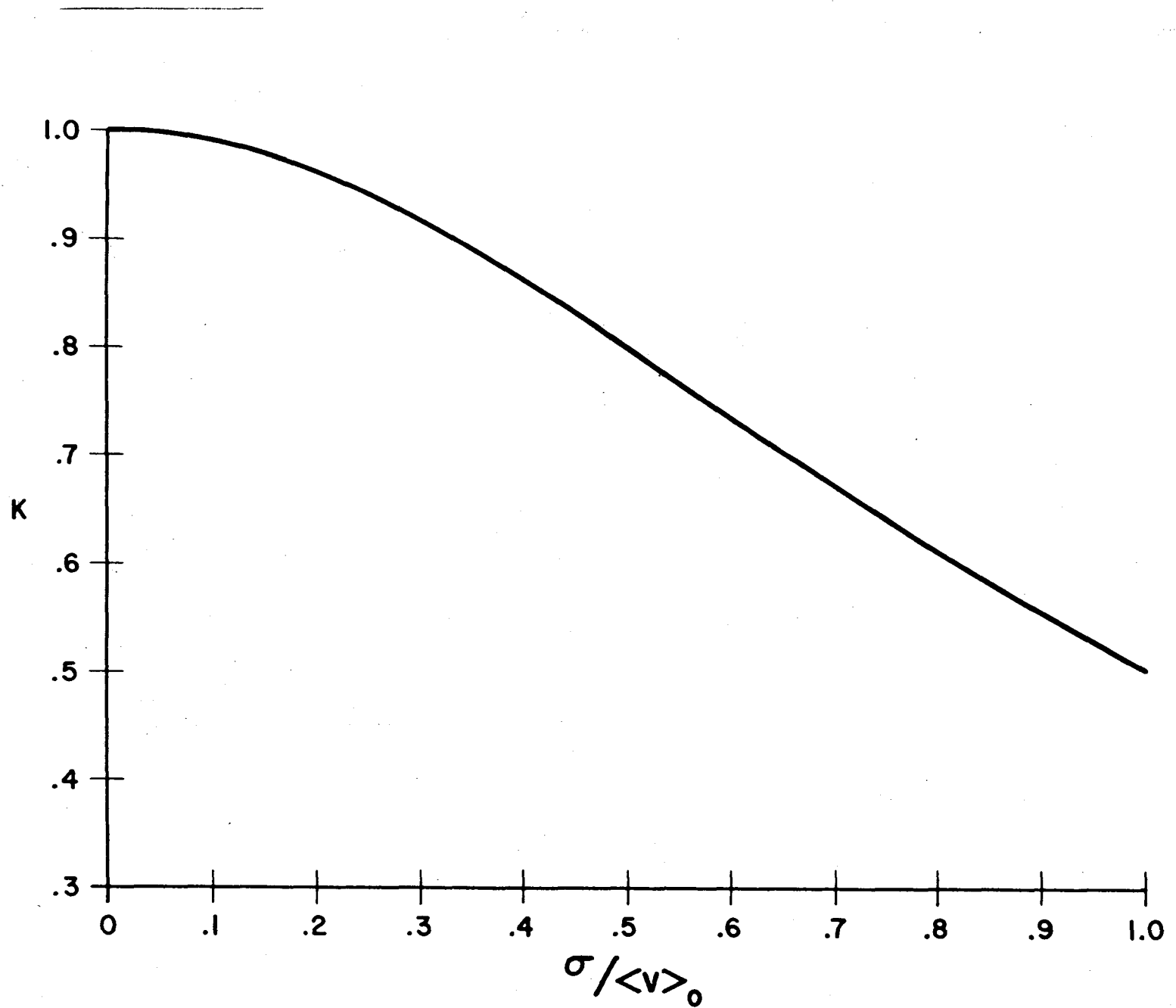


Fig. 16.5 K versus standard deviation/average velocity ratio.

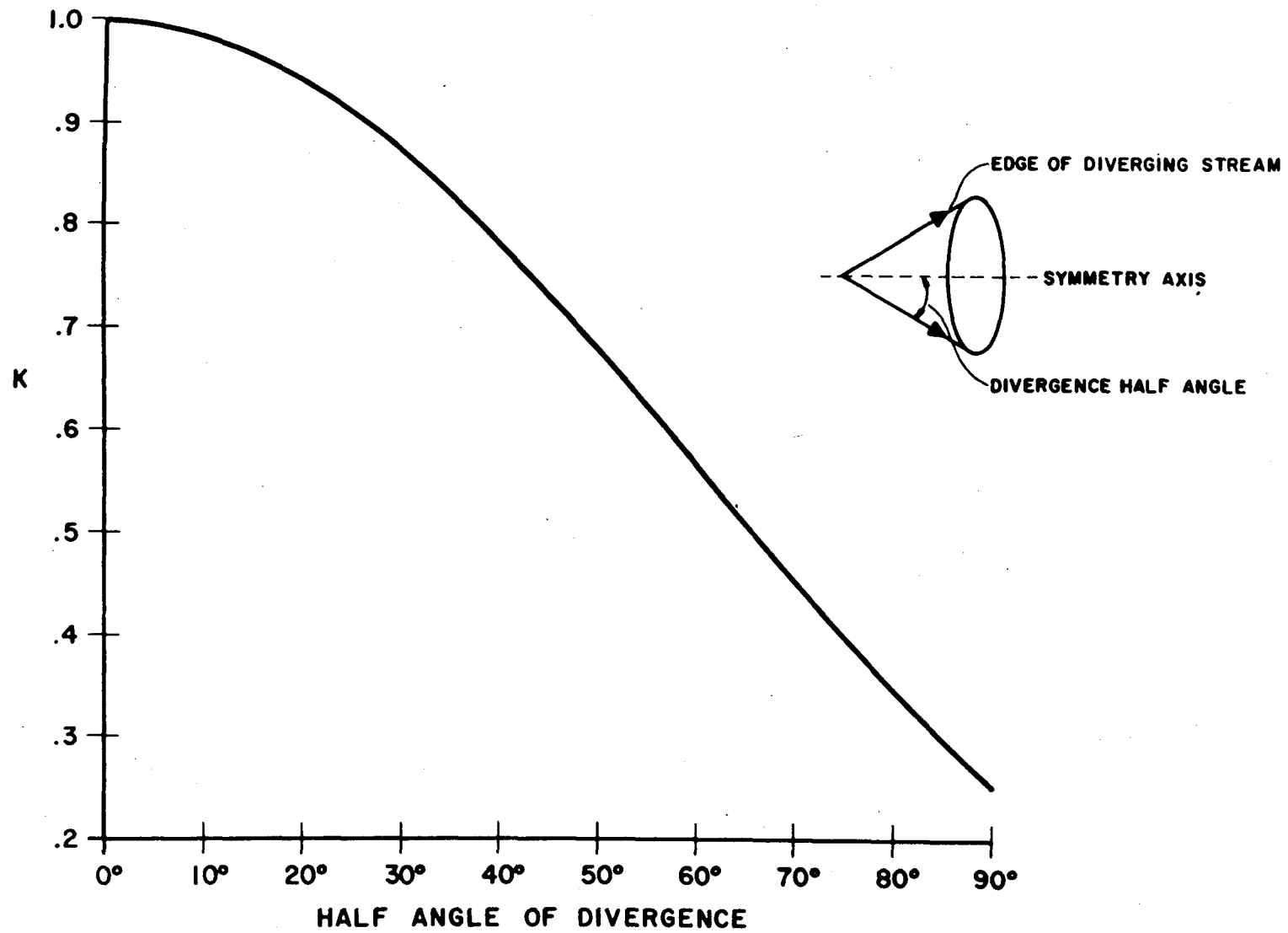


Fig. 16.6 The dependence of  $K$  on the divergence half angle.



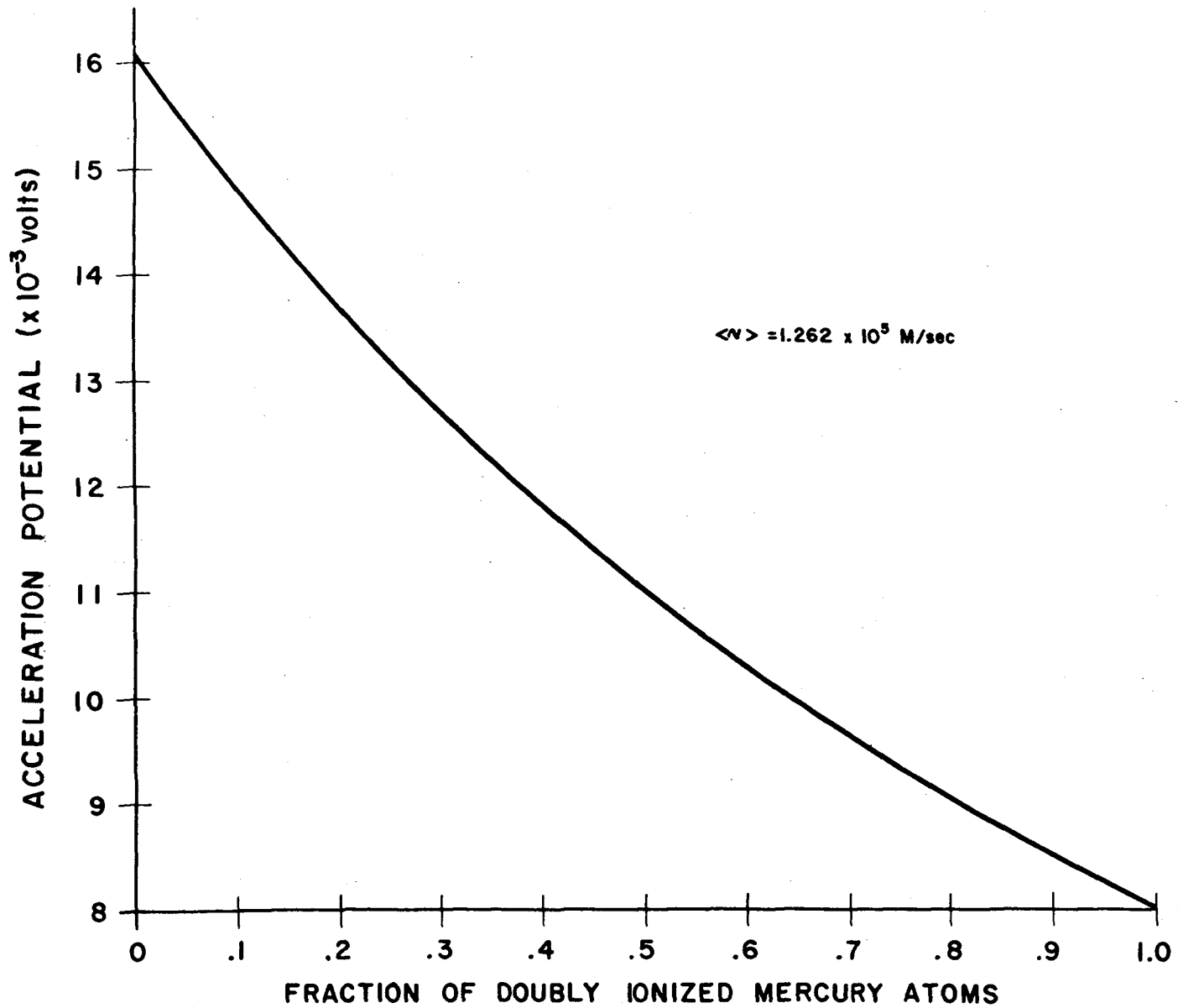


Fig. 16.7 The required acceleration potential of the doubly ionized fraction of Hg.

### 16.3.2 The Arc Thrust Unit

It would be desirable to be able to predict the performance of an arc engine analytically within a few per cent of the measured performance. The main objective is to calculate the thrust of the engine, given the electric power delivered to the thrust unit and the propellant on which the unit is to operate. Since the arc engine is similar to the combustion rocket in the sense that a gas is heated and expanded through a nozzle, it is appropriate to approach the problem on the basis of thermodynamic analysis. A careful examination of the assumptions is in order, however.

Basic Equations. From the conservation of momentum, the classical equation for thrust produced by gas expansion is [4]

$$F = \dot{M} \langle v \rangle + (p_e - p_o)A_e \quad (16.41)$$

where  $F$  is the thrust;  $\dot{M}$  is the mass flow rate;  $\langle v \rangle$  is the average axial component of velocity, where  $p_e$  is the average pressure at the exit plane of the nozzle;  $A_e$  is the exit area; and  $p_o$  is the ambient pressure. The equation assumes steady-state conditions; that is, the pressure, density, and velocity of the gases are constant. For most arc engines  $p_o = 0$ , since their application is most likely to be outside any appreciable planetary atmosphere. Making the same steady-state assumptions, the classical correction factor for the divergence angle of a conical nozzle expansion section to make allowance for the nonaxial component is

$$\lambda = \frac{\langle v \rangle}{v} = \frac{1}{2} + \frac{1}{2} \cos \epsilon \quad (16.42)$$

where  $\epsilon$  is the cone half-angle. The factor also assumes that  $v$ , the velocity magnitude, is uniform across a section of the cone. Equation (16.41) becomes

$$F = \lambda \dot{M} v + p_e A_e \quad (16.43)$$

In addition, if one-dimensional flow is assumed and the last term of Eq. (16.43) is made negligible by almost complete expansion of the gas,\* then

$$F = \dot{M} v \quad (16.44)$$

\*Complete expansion requires an infinitely large nozzle exit area.

By rearranging Eq. (16.44), we define specific impulse as

$$\frac{\frac{F}{\dot{M}}}{g} = \frac{v}{g} = I_{sp} \quad (16.45)$$

It is useful here to repeat Eq. (16.33)

$$v = \sqrt{\frac{2P_o}{\dot{M}}} \quad (16.46)$$

Equation (16.46) gives the exhaust velocity as a function of power. It implicitly assumes that all power goes into the gas to produce thrust. It represents an upper limit to exhaust velocity obtainable for a given power.

Thermodynamic Process. If  $dQ$  denotes the quantity of heat added to the gas from all sources and  $1/JdW$  is the heat equivalent of work removed from the gas, the first law of thermodynamics requires that for a steadily flowing gas [5]

$$\begin{aligned} dQ = dU + \frac{1}{J} Vdp + \frac{1}{J} pdV + \frac{1}{Jg} wdw \\ + \frac{1}{J} dW + \frac{1}{J} dE_F \end{aligned} \quad (16.47)$$

The last term in Eq. (16.47) accounts for energy loss due to friction and assumes that all friction effects can be combined into one term. From the definition of enthalpy, the change in enthalpy is

$$dh = du + \frac{1}{J} (pdV + Vdp)$$

so that

$$dQ = dh + \frac{1}{Jg} wdw + \frac{1}{J} dE_F + \frac{1}{J} dW \quad (16.48)$$

Integrating Eq. (16.47) between reference planes 1 and 2 gives

$$\begin{aligned} {}_1Q_2 = h_2 - h_1 + \frac{1}{2gJ} (w_2^2 - w_1^2) + \frac{1}{J} (E_P)_2 \\ + \frac{1}{J} {}_1W_2 \end{aligned} \quad (16.49)$$

which is the general statement of the first law of thermodynamics for any flow passage of any fluid between two reference planes (states) with the restriction that there is no energy storage and no energy added from an external source during the passage. It also assumes no potential energy change due to a change in elevation between two states.

If it is assumed that the process is reversible, adiabatic, and no work energy is removed from the gas,  $dE_P = 0$ ,  $dQ = 0$ ,  $dW = 0$ , and Eq. (16.48) becomes

$$dh + \frac{1}{Jg} wdw = 0 \quad (16.50)$$

Integrating between reference states 1 and 2 yields

$$h_2' - h_1 + \frac{1}{2gJ} (w_2'^2 - w_1^2) = 0 \quad (16.51)$$

and if the entrance velocity is zero

$$w_2'^2 = 2gJ (h_1 - h_2')$$

or

$$w_2' = \sqrt{2gJ (h_1 - h_2')} \quad (16.52)$$

Equation (16.52) represents the idealized conversion of stagnation enthalpy into kinetic energy in the gas [6]. The form is the same as that of Eq. (16.46). In this equation,  $w_2'$  is the isentropic exhaust velocity. The ratio of Eq. (16.52) to Eq. (16.46) gives the efficiency with which the electric power is converted to total enthalpy in the gas in the limit where  $h_2'$  approaches zero.

$$\left(\frac{w_2'}{v}\right)^2 = C \left[ \frac{(h_1 - h_2') \dot{M}}{P_0} \right]$$

(16.53)

$$\eta_{\text{arc}} = \lim_{h_2' \rightarrow 0} \left(\frac{w_2'}{v}\right)^2 = C \left(\frac{h_1 \dot{M}}{P_0}\right)$$

$\eta_{\text{arc}}$  different from unity represents losses to the electrodes and thermal losses through the walls prior to the process; that is to say, all energy that does not become convertible to total stagnation enthalpy. The efficiency with which this total enthalpy is converted to kinetic energy in the gas, including recovery of dissociation and ionization enthalpy, is another matter. Part of the losses represented by Eq. (16.53) can be recovered by proper utilization of the gas flow and, in the case of the electrode loss, will aid also in extending the life of the electrodes.

Discussion. At this point, it might be revealing to list the assumptions that were made and to discuss them as they relate to an arc thruster. The assumptions were

1. There is no energy storage in the process
2. There is no energy added during the gas flow from state 1 to state 2
3. There is no potential energy change due to a difference in elevation between states 1 and 2
4. The process is reversible and adiabatic, that is, it is isentropic,  $ds = 0$ . This includes the assumption that there is no heat transfer through the nozzle walls
5. The flow is steady, that is, the static pressure  $p$ , the specific weight of the fluid, and the velocity  $w$  are constant with respect to time at each flow station
6. The flow is one-dimensional, that is, all exhaust gases have an axially directed velocity and the gas velocity is uniform across any section normal to the flow up to and including the exit section
7. The process is frictionless, both with respect to the nozzle walls and internal to the gas, consistent with the assumption that  $ds = 0$
8. The gas entrance velocity is zero

The classical combustion rocket motor theory makes the following additional assumptions ([4])

1. The working fluid behaves as an ideal gas
2. Chemical equilibrium is established in the combustion chamber and does not shift in the nozzle, that is, the working substance is homogeneous and invariant in composition throughout the flow process.

The assumptions of no energy storage could be interpreted to include no energy loss to dissociation and ionization as well as no energy stored in electric and magnetic fields; so that if the assumptions were removed, these losses and their possible recovery would have to be incorporated explicitly in the analysis. Their partial explicit recovery during the process requires the removal of the assumption of no energy addition between states 1 and 2. This latter assumption is not as appropriate if the arc extends through the nozzle throat. Considering the fact that arc thrusters are red to white hot even with regenerative cooling, and in view of the losses at the electrodes, the process is far from reversible and adiabatic. The assumption is much worse than the equivalent assumption for chemical rocket motors. Whether the flow is one-dimensional and laminar is also subject to question since the arc strikes through the gas, presumably causing more turbulence, with the arc being a hot-ionized core. The assumption that there is no change in potential energy is certainly reasonable. If the last two additional assumptions are made, the classical idealized exhaust velocity equation for the converging-diverging nozzle results

$$v = \left\{ 2g \cdot \frac{RT}{m} \cdot \frac{\gamma}{\gamma-1} \left[ 1 - \left( \frac{p_2}{p_1} \right)^{\frac{\gamma-1}{\gamma}} \right] \right\}^{\frac{1}{2}} \quad (16.54)$$

where

R = universal gas constant

T = effective combustion flame temperature

$\gamma$  = adiabatic coefficient

m = molecular weight of propellant gas

The foregoing equation does not seem appropriate for arc thrusters, since it assumes an ideal gas and equilibrium throughout the process. Finding the equivalent equation for arc thrusters becomes the problem of estimating the change in enthalpy for real gases in nonequilibrium flow.

#### DEFINITION OF SYMBOLS

u            velocity change of vehicle  
 $\tau$             propulsion time  
 $M_p$             propulsion system mass

$M_S$	tankage and associated structural mass
$M_F$	propellant loading mass
$M_0$	initial mass of vehicle
$M_R$	$M_0 - M_p - M_S - M_F$ (primarily payload)
$P_0$	electric power input to thrust unit
$\alpha$	$P_0/M_p$ (specific power)
$s$	$M_S/M_F$ (tankage structure factor)
$M$	instantaneous mass of vehicle
$\vec{v}$	velocity of expellant particle
$\dot{M}(\vec{v})$	expellant velocity distribution function
$d\omega$	element of solid angle
$\dot{M}$	total mass flow rate
$\langle \vec{v} \rangle$	average velocity of propellant ejection
$P$	kinetic beam power
$K$	$\langle v \rangle^2 / \langle v^2 \rangle$ (propellant stream efficiency factor)
$\eta$	$P/P_0$ (electrical to kinetic energy conversion efficiency)
$\langle v \rangle$	average of axial component of expellant velocity
$P_t$	thermal power of reactor
$\eta_c$	$P_0/P_t$ (thermal to electric power conversion efficiency)
$S$	radiation energy density
$T$	temperature
$a$	$S/T^4$ (constant)
$F$	thrust (actual)
$F_0$	thrust (ideal)
$\sigma$	standard deviation (Gaussian speed distribution)
$P_e$	average pressure at exit plane of nozzle
$P_0$	ambient pressure
$A_e$	nozzle exit area
$\epsilon$	nozzle cone half angle
$\lambda$	thrust correction factor for nozzles assuming no dispersion in particle velocity magnitude
$g$	acceleration of gravity
$I_{sp}$	specific impulse
$Q$	heat
$J$	Joule equivalent
$W$	work
$U$	internal energy
$V$	volume
$w$	velocity in nozzle
$E_f$	frictional energy loss
$h$	enthalpy
$\eta_{arc}$	arc efficiency (electric energy to gas enthalpy)
$R$	universal gas constant
$m$	molecular weight of gas
$\gamma$	adiabatic coefficient

## REFERENCES

1. Stuhlinger, E., and R. N. Seitz, Electrostatic Propulsion Systems for Space Vehicles, in "Advances in Space Science, Vol. 2," F. I. Ordway, III, ed., Academic Press, New York, 1960.
2. Advanced Propulsion Studies and Recommendations, Jet Propulsion Laboratory, January 31, 1961.
3. Stuhlinger, E., R. D. Shelton, R. A. Potter, and L. Lacy, "The Effect of Velocity Distributions on a Power-Limited Propulsion System," paper presented to the ARS Electric Propulsion Conference, Berkeley, California, March 14-16, 1961.
4. Sutton, G. P., "Rocket Propulsion Elements," John Wiley & Sons, Inc., New York, 1956.
5. Zucrow, M. J., "Principles of Jet Propulsion and Gas Turbines," John Wiley & Sons, Inc., New York, 1948.
6. Heller, G., "Propulsion of Space Vehicles by the Thermodynamic Process," paper presented to the IXth Tripartite AXP Conference, Quebec, Canada, 1959.



17

## A PROPOSED ELECTRIC SPACESHIP ENGINE

Hermann Oberth

Feucht b. Nürnberg  
West Germany

This paper describes an electric spaceship engine which ejects electrons and ions and creates an electric wind consisting of particles of colloidal size. The design is shown followed by the presentation of some relatively simple and approximate formulas together with estimates of their accuracy. Consideration is then given to the losses by dispersion, ionization, scattering, and inequalities in particle mass. An estimate of the efficiency of such a propulsion system is provided, as well as a discussion of useful missions for colloiddally propelled spaceships.

## 17.1 Description

In the schematic design shown in Fig. 17.1 the various components are numbered to aid in identification. The members denoted by (1) are the electrodes. Since the electrodes serve as the charging stage for the colloidal dispersion, it is advisable to also use them as propellant containers to eliminate the extremely high voltage differential which would exist across the feed system if it were at vehicle ground potential while the electrodes were at their necessarily high potential.

Each electrode is a thin metal cylindrical plate (2), which is shown with exaggerated thickness in Fig. 17.1 with a layer of insulating cloth (3). The front wall (4) consists of a conducting porous (or at least permeable) disk, recessed somewhat from the end of the tube so that an antechamber (5) remains. The disk (4) is also insulated from the cylindrical electrode (2) and is biased by a power supply to a higher voltage than the latter. The optimum voltage must be determined by experiment.

The propellant, designated by (6), can be almost any type of liquid. Furthermore, it is also possible to use solid substances as propellants, provided their vapor pressure is high enough to allow sufficient flow rates through the perfusing emitter (4). If necessary, they can be electrically heated to increase their vapor pressure. It might even be feasible to turn some solid materials into a gas by means of controllable chemical processes. There is also the possibility of using external mechanical means for slinging fine powder onto the charging disk (4).

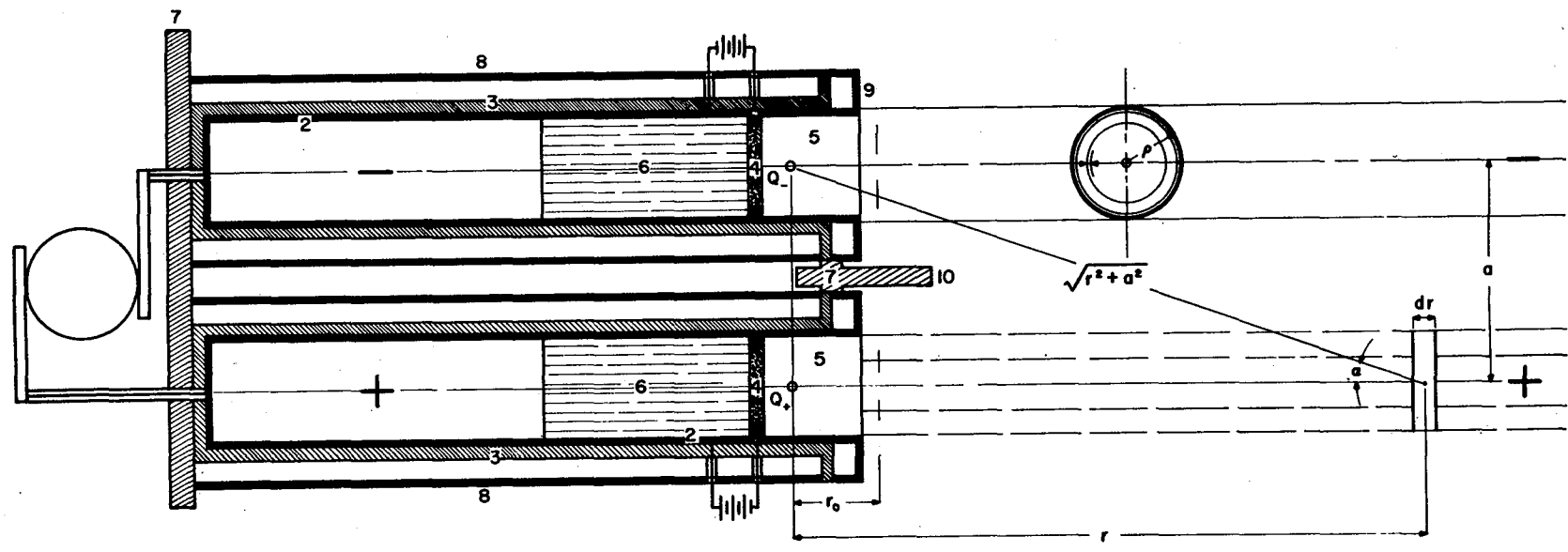


Fig. 17.1 Schematic of electric propulsion engine.

The powder will then become charged and will be repelled. The electrode supports (7) are made of insulating material. The repulsion electrodes are protected against micrometeors by the protective casing (8). Micrometeorites that might hit the meteor bumper (8) would be crushed and vaporized and would no longer be able to penetrate the insulating layer (3). The protective casing (8) is thin.

Because of the flight mechanical acceleration, the propellant (6) is drawn to the porous plug (4) and acquires an electric charge when it penetrates the disk. Whether it might be necessary to augment this process with a piston will still have to be investigated. However, a piston should not be necessary in space.

In passing through the porous disk, the propellant carries an electric charge with it. It seems probable that a film of liquid will develop over the front face of the porous plug (4) and that charged particles perfusing through the plug will collect some of the liquid and form droplets. Neutral droplets will be unable to leave the electrodes; only charged droplets will be able to leave them. However, a few molecules will be ionized on the anode and a few electrons will be ejected from the cathode. Because of the small potential difference between the electrodes (2) and the porous disk (4), the electrons and ions remain for a relatively long time in the plenum chamber (5) and have sufficient time to serve as condensation centers for uncharged vapor molecules drifting through the chamber. The longer the resulting agglomerates can linger here, the less they will differ in size and mass. It is not until they pass to the end of the cylinder and beyond that the full force of the electric field will be exerted upon them.

Component (9) is a metallic ring which is electrically tied to the cylindrical electrode (2). It is intended to serve as a focusing ring which collimates the beam. Component (10) is an insulating plate between the two electrodes.

## 17.2 Derivation of Equations

Some simple methods of calculating the efficiency are presented. Only one beam is considered. Let us assume that the particles of the other beam have negligible mass. The smaller their mass-to-charge ratio, the faster they will travel for a given acceleration voltage. (Inasmuch as positive and negative particles will be ejected at the same rate in the steady state, to prevent the buildup of net charge on the vehicle, it follows that the density of the negative beam will be so small that it can be neglected.) The Coulomb force between two charges is given by the equation

$$F = \frac{Q_1 Q_2}{r^2}$$

If  $q$  is the charge per unit length of the beam, then the volume element of length  $dr$  contains the total charge  $qdr$ . If the charge on the anode is  $Q_+$ , then the force contribution made by  $qdr$  (which is designated  $dF_+$ ) is

$$dF_+ = \frac{Q_+ qdr}{r^2} \quad (17.1)$$

This force is evinced on the one hand in the acceleration of the electrically charged particles, and on the other hand, in the acceleration of the spaceship. The total force of repulsion exerted on the anode by a beam extending from the anode to a distance  $r_1$ , amounts to

$$F_+ = Q_+ q \int_{r_0}^{r_1} \frac{dr}{r^2} = Q_+ q \left( \frac{1}{r_0} - \frac{1}{r_1} \right) \quad (17.1a)$$

The term  $r_0$  is taken here to signify the distance of the equipotential surface at which the repulsion begins from the apparent center of the charge  $Q_+$ . However, this equipotential surface as well as  $r_0$  are only to be regarded as convenient concepts for purposes of calculation. At large distances from the electrode, both  $r_0$  and  $r_1$  appear somewhat larger than they would if measured at small distances, but smaller than they would if measured from the centerpoint of the electrode, because the majority of the charge is repelled by the beam to the rear of the electrode. Consequently,  $r_0$  represents an approximate average of all the center-of-charge to electrode aperture distances corresponding to different beam lengths.

If the cathode contains the charge  $Q_-$ , it is attracted by the beam element  $qdr$  with a differential force

$$dF_- = Q_- q \frac{dr}{r^2 + a^2} \quad (17.2)$$

where  $a$  is the distance between the positive and negative centers-of-charge. For simplicity, it is assumed here that components (2) and (8) of Fig. 17.1 are at the same potential.

This differential force is directed at an angle to the direction of propagation of the beam given by

$$\alpha = \arccos \frac{r}{\sqrt{r^2 + a^2}}$$

as shown in Fig. 17.1. Therefore, it can be decomposed into two components, one perpendicular to the beam and one parallel to the beam of which

$$dF_{\perp} = dF_{\parallel} \frac{a}{\sqrt{r^2 + a^2}}$$

represents the force which attempts to pull the cathode to the anode. This motion is, of course, prevented by the supports (7) in Fig. 17.1. The other component, designated  $dF_{\parallel}$ , is effective along the direction of motion of the beam and tends to reduce the thrust. It amounts to

$$dF_{\parallel} = Q_{\parallel} q \left( \frac{dr}{r^2 + a^2} - \frac{r}{\sqrt{r^2 + a^2}} \right) = Q_{\parallel} q (r^2 + a^2)^{-\frac{3}{2}} r dr \quad (17.2a)$$

The integrated retarding force is derived therefrom by integration

$$F_{\parallel} = Q_{\parallel} q \left( \frac{1}{\sqrt{r_0^2 + a^2}} - \frac{1}{\sqrt{r_1^2 + a^2}} \right) \quad (17.2b)$$

This force is to be subtracted from  $F_{\perp}$ , and the expression for the total force ( $F = F_{\perp} - F_{\parallel}$ ) then follows from Eqs. (17.1a and 17.1b) and is given by

$$F = q \left[ Q_{\perp} \left( \frac{1}{r_0} - \frac{1}{r_1} \right) - Q_{\parallel} \left( \frac{1}{\sqrt{r_0^2 + a^2}} - \frac{1}{\sqrt{r_1^2 + a^2}} \right) \right] \quad (17.3)$$

If  $r_1 = \infty$ , this expression reduces to

$$F = q \left[ \frac{Q_{\perp}}{r_0} - \frac{Q_{\parallel}}{\sqrt{r_0^2 + a^2}} \right] \quad (17.3a)$$

and if we set

$$\frac{a}{r_0} = k \quad (17.3b)$$

and if  $|Q_-| = |Q_+|$ , there results

$$F = q \frac{Q}{a} k \left[ 1 - \frac{1}{\sqrt{1 + k^2}} \right] \quad (17.3c)$$

### 17.2.1 The First Limiting Case ( $q_- = 0$ )

An electric charge  $Q$  generates an electric potential field about itself given by  $Q/r$ . The contribution  $d\phi_A^*$  to the anode potential which is made by a beam of length  $dr$  and charge per unit length  $q$  amounts to

$$d\phi_A = q \frac{dr}{r} \quad (17.4)$$

The net potential  $\phi_A$  at the anode may now be found by an integration over  $r$

$$\phi_A = q \ln \frac{r_1}{r_0} \quad (17.4a)$$

This potential can increase without limit as the beam length increases without limit but the performance of the propulsion system is not affected by this. Moreover, the beam is not infinitely long and the anode potential will increase very slowly once  $r_1/r_0$  becomes large.

At the location of the cathode, the voltage induced by the negative beam amounts to

$$\phi_C = q \int_{r_0}^{r_1} \frac{dr}{\sqrt{r^2 + a^2}} = q \ln \frac{r_1 + \sqrt{r_1^2 + a^2}}{r_0 + \sqrt{r_0^2 + a^2}} \quad (17.4b)$$

A comparison of Eqs. (17.4a) and (17.4b) shows that  $\phi_A > \phi_C$ . Therefore, if a constant current is to be drawn from the engine, it must provide for this voltage difference. It should be observed that some power is initially required to establish the electrostatic field, as well as to impart kinetic energy to the repelled particles, whereas power is

---

\*The subscript A refers to the anode; the subscript C refers to the cathode.

invested almost solely in the kinetic energy of the particles once the system has come into steady-state equilibrium. Consequently, the power efficiency can only be profitably defined for steady-state operation. The required engine potential is expressed by

$$\begin{aligned}
 U = \phi_A - \phi_C &= q \ln \frac{r_1}{r_0} \frac{r_0 + \sqrt{r_0^2 + a^2}}{r_1 + \sqrt{r_1^2 + a^2}} \\
 &= q \ln \frac{1 + \sqrt{1 + a^2/r_0^2}}{1 + \sqrt{1 + a^2/r_1^2}}
 \end{aligned}
 \tag{17.5}$$

If  $r_1$  is much longer than  $a$ , Eq. (17.5) can be simplified to

$$U = q \ln \frac{1 + \sqrt{1 + k^2}}{2}
 \tag{17.5a}$$

### 17.2.2 The Second Limiting Case (both beams carry the same charge per unit length)

This condition is highly desirable. For the same internal efficiency of the engine as that which characterized the first case, the thrust is maximized and the fuel consumption is minimized.

It is possible to be quite brief in the establishment of the equations appropriate to case two if we observe that we may apply the same geometrical proportions which we applied in case one. However, most of the results are to be doubled, to accommodate for the presence of both the positive and the negative beams. Some terms may also be dropped now such as the absolute space potential. We find

$$\begin{aligned}
 F_A &= qQ_+ \left( \int_{r_0}^{r_1} r^{-2} dr - \int_{r_0}^{r_1} (r^2 + a^2)^{-\frac{3}{2}} r dr \right) \\
 &= qQ_+ \left( \frac{1}{r_0} - \frac{1}{r_1} - \frac{1}{\sqrt{r_0^2 + a^2}} + \frac{1}{\sqrt{r_1^2 + a^2}} \right)
 \end{aligned}$$

For the cathode, the following relation holds

$$F_C = qQ_- \left( \frac{1}{r_0} - \frac{1}{r_1} - \frac{1}{\sqrt{r_0^2 + a^2}} + \frac{1}{\sqrt{r_1^2 + a^2}} \right)$$

Both forces must be added.

$$F = F_A + F_C = q(|Q_+| + |Q_-|) \left( \frac{1}{r_0} - \frac{1}{r_1} - \frac{1}{\sqrt{r_0^2 + a^2}} + \frac{1}{\sqrt{r_1^2 + a^2}} \right) \quad (17.6)$$

For  $r = \infty$  and  $|Q_-| = |Q_+| = Q$ , this expression transforms into

$$F = 2 \frac{qQ}{r_0} \left( 1 - \frac{1}{\sqrt{1 + k^2}} \right) \quad (17.6a)$$

The potential at the anode amounts to

$$\begin{aligned} \phi_A &= q \left( \int_{r_0}^{r_1} \frac{dr}{r} - \int_{r_0}^{r_1} \frac{dr}{\sqrt{r^2 + a^2}} \right) \\ &= q \left( \ln \frac{r_1}{r_0} - \ln \frac{r_1 + \sqrt{r_1^2 + a^2}}{r_0 + \sqrt{r_0^2 + a^2}} \right) \end{aligned} \quad (17.7)$$

Equation (17.7) was derived in a manner analogous to Eqs. (17.4) and (17.5). The potential at the cathode  $\phi_C$  is just as large but of opposite sign.

For the case  $r_1 = \infty$ , the potential to be overcome by the device is

$$U = 2\phi = 2q \ln \frac{1 + \sqrt{1 + k^2}}{2} \quad (17.7a)$$



while the rest of the spaceship remains neutral, or to say it more accurately, does not alter the potential which is inherent to that point in space (for our Milky Way galaxy will have an absolute negative potential of some millions to billions of volts, anyway, which we have no way of determining since we are a part of this system).

If Eq. (17.6a) is divided by Eq. (17.7a), the result is

$$\frac{F}{U} = \frac{Q}{r_0} \frac{1 - \frac{1}{\sqrt{1+k^2}}}{\ln \left[ \frac{1}{2} (1 + \sqrt{1+k^2}) \right]} \quad (17.8)$$

and since, as a result of the net neutrality of the couplet  $Q_+$  and  $Q_-$ , both are equal to the capacity of the electrodes multiplied by half their potential difference (for simplicity's sake, let us assume the capacities of the electrodes to be equal and call this capacity C), we can also record this as

$$F = \frac{CU^2}{2r_0} K \quad (17.8a)$$

wherein

$$K(k) \equiv \frac{1 - \frac{1}{\sqrt{1+k^2}}}{\ln \left[ \frac{1}{2} (1 + \sqrt{1+k^2}) \right]} \quad (17.9)$$

### 17.3 Discussion of the Equations

From Eqs. (17.7) and (17.7a), we conclude:

This value is directly proportional to the linear charge density of the beam. The portion of the applied voltage U required for ejection and acceleration of the electrically charged particles increases with increasing beam length up to a specific limiting value.

Furthermore, this limiting value is dependent upon the ratio

$$K = \frac{a}{r_0}$$

where  $r_0$  is the distance at which the repulsion begins. For very large values of  $k$ , the ratio

$$\frac{2q}{U} \ln \frac{k}{2}$$

approaches the value 1 asymptotically.

Moreover, Eqs. (17.6), (17.8), and (17.8b) show that  $F$  (and, therefore,  $F/U$ ) vary inversely with  $r_0$ . If we increase  $r_0$ , we reduce  $k$ , while only slightly increasing  $K$ . Also, the capacity increases as the beam length increases. However, the rates of improvement in  $K$  and in the total beam capacity are not sufficient to offset the rate of decrease of  $F$  and  $F/U$  as  $r_0$  increases. Therefore,  $r_0$  should be made no larger than is absolutely necessary. From Eq. (17.8) it follows that

$$U = \sqrt{\frac{2r_0 F}{CK}} \quad (17.10)$$

and from Eq. (17.7) we have

$$q = \frac{U}{2 \ln \frac{1}{2} (1 + \sqrt{1 + k^2})} \quad (17.11)$$

With regard to these two equations, it is interesting to note that the required voltage  $U$  as well as the charge per unit length  $q$  of the beam depend (aside from the thrust device constants  $a$ ,  $r_0$ , and  $C$ , and the constants  $K$  and  $k$  derived from this) only upon the required reaction force and not directly upon the density and the velocity of the beam. Only in calculating the current density and the efficiency do we also need to know the average velocity of the particles.

We can probably control the rate of propellant feed by simply heating or cooling the propellant chamber of an electrode so that the pressure increases and the viscosity decreases, or vice versa, without requiring a transfer of gas into or out of the chamber opposite (4) in Fig. 17.1 to increase or decrease the pressure. But in any event, we can certainly control it if the propellant chamber contains a movable piston or an expandable balloon into which gas can be inducted or from which it can be ejected. In such a case, it is evident that each voltage  $U$  requires a unique mass discharge rate  $\dot{m} = dm/dt$  so that the charge particles, flying off with the desired velocity, form a beam with the linear charge density  $q$ . Consequently, there is a functional relationship among the variables  $C$ ,  $U$ , and  $\dot{m}$ , so that if any two of them are fixed, the third is determined.

The electrical energy  $E_e$  in the beam can be expressed as

$$E_e = UI = Uqc \quad (17.12)$$

Since the electrical energy is, to first order approximation, converted entirely into the kinetic energy  $E_K$  of the two beams, we must have

$$E_e = E_K = 2 \times \frac{1}{2} mc^2 = mc^2 \quad (17.12a)$$

With the aid of Eqs. (17.10), (17.11), and (17.9), we obtain for  $E_e$

$$E_e = \frac{U^2}{2} \frac{c}{\ln \frac{1}{2} (1 + k^2)} = \frac{r_0 F c}{C} \frac{1}{1 - \frac{1}{\sqrt{1 + k^2}}} = E_k$$

But  $F = mc$  and therefore, according to Eq. (17.12a),  $E_k = Fc$ . From this, it follows that

$$r_0 = C \left( 1 - \frac{1}{\sqrt{1 + k^2}} \right) \quad (17.13)$$

The reason  $r_0$  is directly proportional to the capacity  $C$  for a fixed value of  $k$  is that, for the assumed charge of the electrode (1) and the protective cover (8) (Fig. 17.1), and with the same electrode proportions, their capacities (and overall sizes) increase linearly with  $r_0$ . The expression in parentheses in Eq. (17.13) contains implicitly the change of the electric induction effects and of the values of  $C$  and  $Q$  which occur when the ratio  $K = a/r_0$  changes. Naturally,  $r_0$  can never exceed the electrode's length even for the largest possible value of the capacity. Then the expression in parentheses simply becomes correspondingly small.

It is evident from Eq. (17.13) that  $C$  is readily expressible as an explicit function of  $r_0$  and  $k$ . Also, there are no great difficulties in expressing  $k$  or  $a = kr_0$  as a function of  $r_0$  and  $C$ . However, when we attempt  $r_0$  as a function of  $a$  and  $C$ , we are led to a quartic equation in  $r_0$

$$\frac{r_0^4}{C^2} - \frac{2r_0^3}{C} + \frac{a^2 r_0^2}{C^2} - \frac{2a^2 r_0}{C} + a^2 = 0$$

Although it is possible in principle to solve the above equation by means of the Euler technique, it is so cumbersome that I prefer to use approximation techniques, either graphically or in accordance with the Regula Falsi. In the latter case, Eq. (17.13) may be reformulated as

$$\left(1 - \frac{r_0}{C}\right)^2 \left[1 + \left(\frac{a}{r_0}\right)^2\right] = 1 \quad (17.13a)$$

By way of illustration, a numerical example is provided. It is not intended to be a design proposal but to provide a complete set of order-of-magnitude specifications of the mass, acceleration, capacity, etc., of a complete system as well as a schematic design layout. Since this is an electrostatic problem, the cgs system of units will be used as is customary in the field of physics, although ultimately the results will be expressed in practical units to which the engineer is accustomed.

The two electrodes in Fig. 17.1 are assumed to be of equal size, each being 3 m long and, together with the meteorite covering, 1 m in diameter. The axes of the cylinder are spaced 105 cm apart, so that we will be able to set  $a = 100$  cm since, as a result of electrostatic induction, the charge density on the side next to the neighboring electrode is somewhat enhanced. In consideration of their mutual electrostatic induction, their capacity is estimated at 120 cm each.

If we utilize these values in Eq. (17.13a), we find that the left side of the equation has a double root for  $r_0 = C$ . The value of the left-hand side of Eq. (17.13a) increases on either side of  $(C - r_0)^2 = 0$ , but values of  $r_0$  greater than 120 C do not need to be considered because the left side of Eq. (17.13a) would equal one only for  $r_0 = \infty$ , whereas  $r_0$  cannot logically be greater than the electrode length. However, for  $r_0 = 59.006$ , the left side of the above equation will be 1.00027 so that we can take it to be unity with sufficient accuracy for our purposes. It thereby follows that

$$\begin{aligned} k &= 1.695 \sqrt{1 + k^2} = 1.968 \\ \frac{1}{2} (1 + \sqrt{1 + k^2}) &= 1.484 \\ \ln \left[ \frac{1}{2} (1 + \sqrt{1 + k^2}) \right] &= 0.3947 \quad (4) \end{aligned}$$

Now we wish to obtain from each electrode a thrust of 98.06 newtons (22.04 lb) at an exhaust velocity  $c$  of 10 km/sec (a specific impulse of 1020 lb-sec/lb). Thus, the total thrust from both electrodes is 196.12 newtons (44.08 lb).

If we insert next the value of  $r_0$  from Eq. (17.13) into Eq. (17.10), we obtain, with the aid of Eq. (17.9)

$$U = \sqrt{2F \ln \left[ \frac{1}{2} (1 + \sqrt{1 + k^2}) \right]} \quad (17.14)$$

There follows from this

$$V = \sqrt{1.9612 \times 10^7 \times 0.3947} = 2782.4 \text{ statvolts} \\ = 835,000 \text{ v}$$

Electrostatic induction machines designed according to the Wommelsdorff principle can reach such voltages when a hydrocarbon atmosphere is used instead of air (p. 114 of Ref. [1]). But we probably do not need to design induction machines for such high voltages, for it is possible to connect them in series if the mechanical concept of [1, page 221] is heeded.

The linear charge density  $q$  of the beams can be found from Eq. (17.11)

$$q = \frac{2782.4}{2} \cdot \frac{1}{0.3947 (4)} = 3524 \text{ statcoulombs}$$

For  $c = 10 \text{ km/sec}$ , the total current is

$$I = qc = 3524 \times 10^6 \text{ cm}^{\frac{1}{2}} \text{ g}^{\frac{1}{2}}/\text{sec} = 3.524 \times 10^9 \text{ statcoulombs-cm/sec} \\ = 1.175 \text{ amp}$$

The total beam power output of the accelerator therefore amounts to

$$VI = 835,000 \text{ v} \times 1.175 \text{ amp} \\ = 9.806 \times 10^{12} \text{ erg/sec} = 980.6 \text{ kw} \\ = 1333 \text{ hp}$$

The associated fuel consumption is

$$2 \times 9.806 \text{ g/sec}$$

Thus, each electrode ejects 9.806 g/sec. Naturally, we could also have arrived at these figures through purely mechanical considerations. The total mechanical power output of a rocket motor is given by

$$\begin{aligned} \frac{1}{2} \dot{m}c^2 &= \frac{1}{2} \times 19.612 \text{ g/sec} \times (10^8 \text{ cm/sec})^2 \\ &= 9.806 \times 10^{12} \text{ erg/sec} = 980.6 \text{ kw} \end{aligned}$$

Consider that the same pair of electrodes is supposed to furnish the same thrust force of 196.12 newtons but at the reduced exhaust velocity of 7 km/sec =  $7 \times 10^5$  cm/sec = 15,659 mph.

It is evident that most of the other thrust device parameters do not change from those of the first example. In accordance with Eq. (17.14), the voltage  $U$  will remain the same; also, in accordance with Eq. (17.11), the linear charge density  $q$  will remain unaltered. Only the current consumption will decrease

$$3524 \text{ statcoulombs} \times 700,000 \text{ cm/sec} =$$

$$2467 \times 10^9 \text{ statcoulomb-cm/sec} = 0.8223 \text{ amp}$$

The kinetic power decreases to 686.4 kw or about 933 hp. We find the fuel ejection rate to be  $2 \times 14.009$  g/sec; i.e., the pressure or the temperature in the propellant chamber must increase to such an extent that 14 g/sec diffuse through the front wall.

I consider it a distinct advantage of my thrust device that the exhaust velocity can be changed without requiring a change in the acceleration voltage or amperage.

#### 17.4 Nonuniform Charge Distribution in the Propellant Beam

Until now, we have assumed a uniform charge distribution in all parts of the propellant beam. We must now ask: Is this really the case?

As an electrode begins to operate, it ejects the first droplets at a velocity that results from the charge  $Q$  of the electrode and the charges and masses of the droplets. Later, as a longer beam is generated, its space charge will repel the droplets just leaving the electrode, somewhat reducing their velocity in that region. The charge density near the electrode will be somewhat enhanced while at the far end of the beam the velocity of the particles will be increased by the thrust that the beam itself exerts on them.

As we have seen, the charge of the beam causes not only an acceleration of the particles parallel to the axis, but also a spreading of the beam away from the axis. However, the axial acceleration exceeds the transverse acceleration (at least near the end  $r_1$ ), as may easily be understood when comparing the length of the beam with its width. Consequently, in the vicinity of the electrode, the particles will move somewhat slower and will be more densely crowded together while at a greater distance from the electrode, the particles will initially move somewhat faster than conservation of energy would predict (a result of acceleration by the moving space charge in the beam, giving rise to non-conservative forces). Eventually, when the length of the beam has become practically infinite, the final velocity will correspond to the ideal velocity which the thrust device could provide minus a correction term for the aforementioned energy losses.

This situation is self-regulating. This homeostatic characteristic can be shown mathematically, but may also be understood without mathematics. If the droplets near the electrode were to be repelled by the space charge of the previously ejected particles so much that they could not leave the electrode, then the motion and acceleration of the previously ejected particles would cause them to disperse very rapidly, the repelling force caused by their space charge cloud would decrease and emission would begin again. Similarly, if for any reason, the electrostatic back pressure of the beam should decrease, then the particle ejection rate would increase until the buildup of space charge restored the repelling force to its equilibrium value.

As  $r_1$  increases, the repelling force of the beam will increase with it, but it must approach a limit, varying with the operating conditions, since its relative potential cannot exceed the value indicated by Eqs. (17.6a) and (17.7a).

#### 17.5 The Construction and Assembly of an Electric Spaceship

Figure 17.2 shows my proposed design for an electric spaceship suitable for missions to the inner planets. It is powered by solar energy converted into kinetic beam power with the aid of gas turbines and induction machines. These systems promise a net power conversion efficiency of 38 to 50 per cent. Solar batteries would be less effective for electric spaceships. Firstly, they would afford a lower power-to-weight ratio, and secondly, it would be difficult for them to supply the necessary high voltages.

As with all other outer space structures, the electric spaceship should be lightweight and quite large. Such a structure cannot be assembled on Earth. On Earth, only small parts, light metal rolls, etc.,

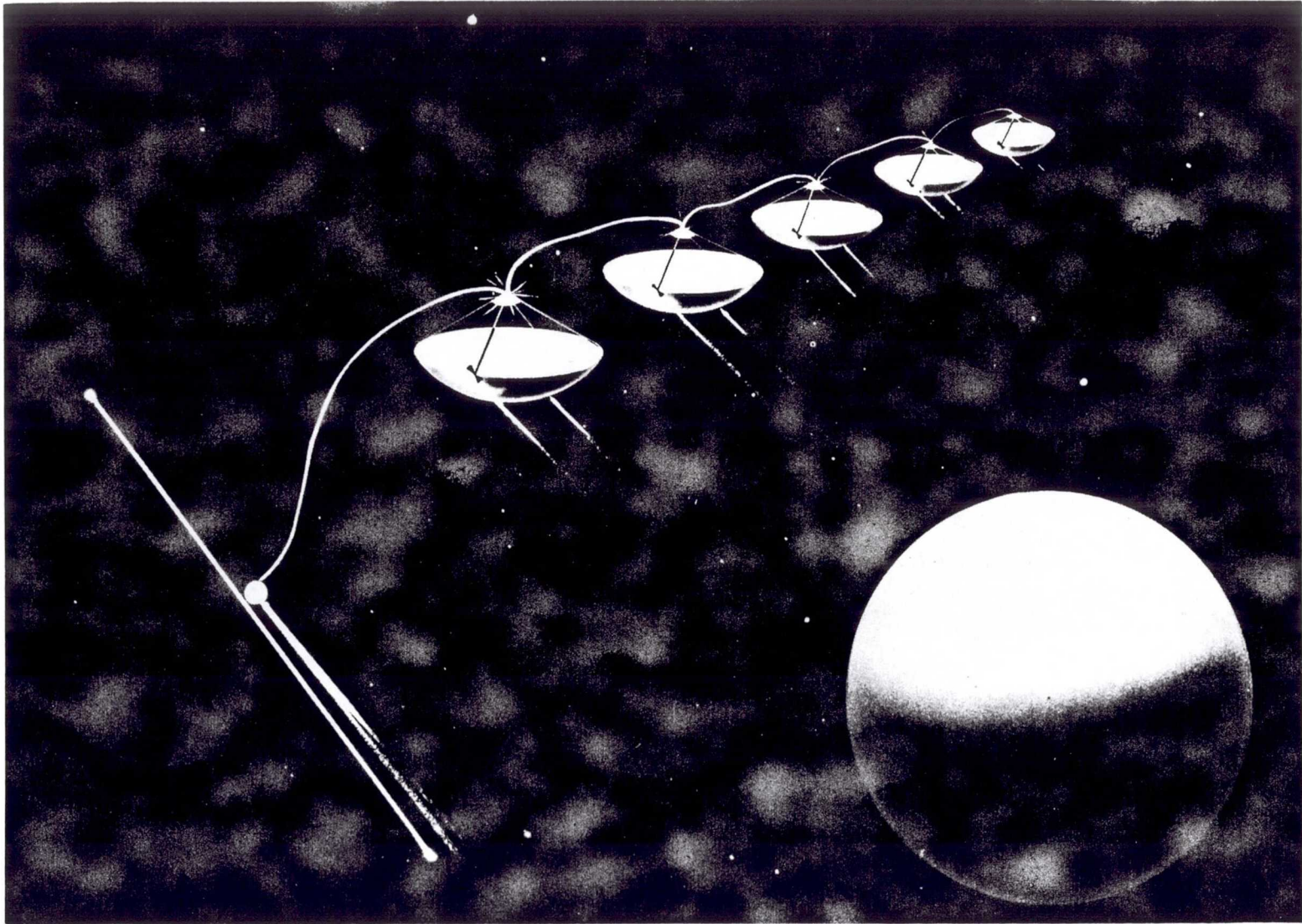


Fig. 17.2 Electric spaceship for planetary travel.



could be produced and transported by rocket. The most suitable assembly site would be the space station previously described in [1, pp. 81-85].\*

Absolutely essential for this space construction work is a space suit which will allow human beings to work in outer space. For this purpose, the space suit recommended in Chap. III of [1, p. 34f] could be developed. However, it would be even better to use a space robot as suggested by Dr. von Braun with gyroscopic reaction rotors and gripping devices which can be operated by a man on the inside. The upper part should be made of transparent material to enable the space worker to get an unobstructed view at all angles.

At greater distances from the Sun, nuclear reactors would be more advantageous than solar power generation systems. However, for the inner planetary regime, nuclear reactors would be an unnecessary luxury. The tubes and fins of the power plant's inevitable radiator, through which the expanded gas would stream, must be shadowed from the Sun so that the radiator can dissipate heat. In the range of the inner planets, the solar collector concentrating solar energy on the working fluid need not be larger than the shadow shield which shields the radiator from sunlight. Thus, the solar collector can be used as a shadow shield.

The machines are connected to each other and with the main switch cell by electrical cables. These serve

1. to remotely control the machines,
2. to power the repulsion electrodes at the main switch cell,
3. to provide emergency power for the electrodes if one of the electrostatic generators should breakdown.

Reference [1, p. 221 ff.], shows how to insure reliable start-up of the induction machines, and how to insure that one pole is always positive and one pole is always negative. This prevents one machine from acting as a motor consuming all of the electricity which the other induction machine generates when they are connected in series or in parallel.

The induction machine is started by a battery which is switched off when the generator voltage surpasses the battery voltage and is again switched on, if the generator axle counterrotates; i.e., if its poles are inverted so that the induction machine consumes current instead of generating current.

---

\*Two spaceships are placed in orbit and then connected to one another by a long steel cable. They then revolve around their common center-of-mass to provide artificial gravity for the spaceship's inhabitants. At the center, a sphere of wire gauze is constructed, serving as an assembly chamber.

Until now, no particular emphasis has been placed upon the development of lightweight induction machines. However, using suitable materials and taking advantage of all possibilities, it should be possible to reduce the weight of these machines to about 0.3 kg (0.66 lb)/kw. Also, a properly constructed hydrogen or helium turbine to drive the generator need not be very heavy.

The total power output of the generator must be from 10 to 30 per cent greater than the idealized kinetic beam power which we would have if all the particles acquired the same exhaust velocity  $c$  and if all other losses were eliminated. To return to the second sample calculation (for which the two electrodes should have a thrust of 98.06 newtons each at an exhaust velocity of  $c = 7000$  m/sec), the generator would have to produce about 890 kw instead of 686.4 kw if the thrust level were  $2 \times 98.06$  newtons at an average exhaust of  $c = 7000$  m/sec.

The above power level would correspond to a generator weight of 535 kg. To be on the conservative side, we will round off this figure to 600 kg. The additional components might weigh another 200 kg and the portion of the live payload which these two electrodes would have to propel would amount to about 200 kg. Excluding the fuel, the part of the space vehicle for which these two electrodes would be responsible would amount to 1000 kg.

The electrodes might contain a total of 4000 kg of propellant. This can be accommodated by the 1 x 3 m electrodes if we assume a specific gravity of 1.27 for the propellant. Alternatively, the electrodes could be slightly enlarged, or the space (5) of Fig. 17.1 could be shortened somewhat. With the above set of values, the initial mass is 5000 kg and the final mass is 1000 kg. This leads to an initial acceleration of 20 cm/sec<sup>2</sup>.

Since 28 g of fuel are ejected each second, the propulsion system would be able to operate for a total period of 142,857 sec or, for 1 day, 15 hr, 40 min and 57 sec. Of course, the operation need not be continuous.

The characteristic velocity capability is

$$c \ln \frac{M_0}{M_f} = 7000 \ln 5 = 11,266 \text{ m/sec}$$

It would therefore be possible for a spaceship of this type to leave a space station and go into orbit around the Moon within a few days and then return to the space station.

## 17.6 Experimental Preparatory Work

The development of a suitable induction machine would be of first importance. The machine is based upon the principle of the Wommelsdorff

induction machine and is called the Womella. In the Womella, a series of rotor plates rotate between a set of stator plates. In contrast to this, not only the rotor but also the stator plates would rotate. The stator plates would support the outer casting of the generator.

With this technique the unbalanced torque of the Womella which would affect the entire space vehicle whenever the generator changed its rpm in space would be avoided. The relative velocity of the plates would be twice that of the Womella for the same shaft and countershaft rotation speeds, thereby doubling the current intensity without increasing the size or weight of the generator.

Fortunately, this machine could be constructed on the ground and tested in the laboratory. The following questions would then have to be answered experimentally:

1. If  $n$  smaller electrostatic generators are series-connected i.e., if the negative pole of one generator is connected to the positive pole of the next, and if precautions are taken to prevent the poles from becoming inverted [1, p. 221, item 20] we will obtain an  $n$ -fold increase in voltage across the output terminals of the series-connected generators. The total weight of the series-connected generators will be  $n$  times their individual weight. If we also desire an  $n$ -fold increase in current output, we must connect  $n$  of the series strings in parallel, leading to a total system weight which is  $n^2$  times the weight of an individual generator. By contrast, if we wish to build a single electrostatic generator with the same number of plates which supplies  $n$ -times the current at  $n$ -times the voltage of an individual generator, the weight of the larger generator will be  $n^3$  times the weight of the smaller, and the reliability of the larger generator will be less than that of the smaller.

Series-connection of small electrostatic generators will require extra components which will not be necessary with the larger generator, so the optimum size of the electrostatic generator will have to be determined experimentally.

Of course, this question can also be answered on the basis of theoretical reasoning, but experimental confirmation must still be obtained. Also, the operating procedure would have to be determined experimentally.

2. With manned spaceships, we must demand not only light weight, but also absolute reliability of these generators, and this can be achieved only through practical testing.

3. In addition, testing of materials would have to be conducted. The Womella plates are made of ebonite, which is an especially hard, vulcanized rubber. Since this device was designed, it appears that materials have been discovered which would be even more suitable for our induction machine. For a given generator weight, the maximum operating voltage increases with the bulk resistivity and the dielectric constant

of the dielectric between the plates. But the current also increases for a given size generator with the rotational speed and with the dielectric breakdown length. The power output equals the product of voltage and current, but only experimental measurements can show which materials will be best with regard to the product of the bulk resistivity multiplied by the dielectric constant multiplied by the square root of the dielectric breakdown constant and divided by the material's specific gravity.

4. The casing of the Womella contains dry air. As shown, dry methane gas would have superior insulation qualities, and perhaps there are other gases which are even more suitable. But apart from its insulating properties, it would also be necessary to test methane to determine whether the sparks that would jump across the contacts would carbonize the gas. Also, the dielectric constant increases with the density of the gas. But then the frictional drag coefficient and the temperature of the gas would also increase. Where does the optimum value lie? What would be the optimum working temperature? With an electrical spaceship, any operating temperature can be realized but the correct operating temperature must be known! Finally, how compatible are the structural materials with the gaseous dielectric?

In the course of this development activity, additional questions will probably arise that have not been mentioned here. For this reason, the development work should begin as soon as possible.

As mentioned, the effects of space charge can be calculated rather exactly by electronic computers and can be simulated experimentally by two conducting plates which might, for example, form part of a funnel-shaped collector which would collect the beams at the far end of a laboratory vacuum chamber.

#### 17.7 Conclusion

The laboratory measurement and testing techniques are well known and widely used, e.g., techniques for measuring the size, charge, and velocity of droplets by electrostatic, electromagnetic, and luminous effects, methods of measuring the force of repulsion, etc. It is only necessary to select instruments with the proper operating characteristics.

#### REFERENCES

1. Oberth, H., "Man Into Space," Harper and Brothers, New York, 1957.

## 18

## INERTIAL GUIDANCE, ITS EVOLUTION AND FUTURE POTENTIAL

J. S. Farrior

Lockheed Missiles & Space Co.  
Sunnyvale, Calif.

## 18.1 Introduction

Guidance, or navigation, is defined here as the art, science, or act of making some form of physical measurements, using these measurements along with certain initial conditions and stored data to compute information in some specified form, and using the computed information as a basis for commands to the vehicle control system to cause the vehicle center of gravity to move in a desired way. The vehicle can be a ship, submarine, land vehicle, airplane, missile, or spacecraft.

The physical measurements required for guidance can be made by any method or combination of methods that will permit determination of the vehicle's motion, such as optical sighting, or radio tracking, or inertial measurements. The measurements and computations can be performed either aboard the vehicle, on another vehicle, on Earth or other celestial body, or partially aboard the vehicle and partially at other locations.

Processing the data and solving the guidance equations can require a rather complex computer, since a number of constraints exist limiting the number of acceptable solutions to the guidance problem. The constraints are imposed by propulsion performance, vehicle maneuver capability, aerodynamic lift, drag, heating, necessity for obtaining high, overall performance, and the tolerances of the required terminal conditions.

If desired, the computed data can be displayed as vehicle velocity and position so that manual adjustment of speed and course can be made or as signals causing automatic pitch and yaw corrections, propulsion thrust control, or thrust termination.

The control system, considered here as separate from the guidance system, is the system that manipulates the thrust vector to maintain stability of vehicle attitude in the presence of disturbances, timed attitude commands, and guidance commands. However, for stability and performance analyses, they must be considered together, since the guidance system and control system are part of the same closed loop.

Considering the above points, historical development of guidance techniques generally, inertial guidance in particular, and important

applications for future use will be reviewed.

## 18.2 The Guidance Problem and Its Historical Development

The guidance, or navigation, problem began when life on Earth reached a stage of development that permitted certain species to exert a significant control over their travels. Instead of being pushed aimlessly about by the elements, they had the ability to follow some desired path. Guidance capability in the animal increased from the simple ability to return to its home after seeking food or a mate, to the more difficult problem of long-range migration, long-range homing, and "blind" guidance. The navigational techniques employed, where understood, are, in some cases, found to be highly sophisticated [1, 2].

Since man's speed is relatively low when relying on his legs, his instinctive ability to navigate is poorly developed. In navigating over land, primitive man could nearly always return the way he came, because he could blaze a trail or remember the terrain over which he had passed. When he had developed to the point of building boats that would cover broad expanses of water, he experienced a much more difficult navigation problem because he traveled over a surface having few, if any, characteristics which permitted fixing his geographical position. He relied upon many simple, and frequently inaccurate, methods of estimating course and position based on observation of the wind, waves, birds, heavenly bodies, soundings, and crude dead reckoning.

The invention of the compass, possibly by the Arabs, was a major breakthrough in navigation. Celestial navigation has its origins in man's remotest antiquity, but accurate latitude determinations could not be made before instruments were perfected with which to measure the altitude of Polaris above the horizon. The ancient astrolabe of the Greeks was followed by the quadrant and the sextant.

The determination of longitude requires an accurate knowledge of time, and another major breakthrough came with the invention of a satisfactory shipboard chronometer in the late eighteenth century. Shortly after the invention of the chronometer, navigation was put on a scientific basis by the publication of a nautical almanac in 1767 by the Naval Observatory at Greenwich, and by the appearance of textbooks on navigation, an excellent example of which was Bowditch's American Practical Navigator, first published in 1806.

For many years, efforts to improve navigation were directed toward improving the existing devices and techniques. As a consequence, there appeared better maps, more lighthouses, lightships, foghorns, more accurate chronometers, sextants, better textbooks and almanacs.

With the arrival of the electronic age, new devices and techniques

were introduced. The development of the airplane brought new navigational problems, due mostly to its speed and limited flying time. Radio beacons, gyroscopic compasses, radio time signals, and electronic sounders and altimeters were perfected. Finally, more sophisticated devices such as radar, loran, and inertial navigation equipment were introduced.

Perhaps the most significant stimulus for the improvement in navigational techniques came with the development of the ballistic missile by the Germans during World War II [3] which led to extensive postwar development first of missiles and finally of space vehicles.

### 18.3 Why Inertial Guidance?

From the early days of the science of vehicle guidance to the present, there have existed two schools of thought concerning vehicle guidance techniques. One school, who are proponents of radio systems, claims high accuracy as well as low cost and weight for the vehicle-borne components as the primary advantages. Before the perfection of accurate inertial components, they insisted that radio techniques had the highest probability of demonstrating satisfactory results.

The other school, advocates of inertial systems, points out that the small amount of ground equipment required and the freedom from counter-measures as being important advantages of inertial systems. They observe that there were perhaps serious problems associated with the radio systems, such as unknown propagation errors and a probable difficulty in obtaining accurate velocity measurements in real time for providing lateral steering and thrust cutoff. There were also some who thought that, ideally, a combination radio-inertial system should be used wherein on-board inertial components would provide smoothing of the radio-derived data and that the low-frequency drift of the inertial components could be eliminated by use of the radio-derived data. It was claimed that such a system should be extremely accurate and should require only moderately accurate inertial components, permitting relatively simple and inexpensive missile-borne equipment [4]. In the face of all the evidence pro and con, it was difficult or impossible to select a single approach, and extensive developments took place on all types of systems.

The situation at present is that pure inertial systems have won out as far as ballistic missiles are concerned. Redstone, Jupiter, Thor, Sergeant, Atlas, Titan, Polaris, Pershing, and Minuteman all employ such systems, although radio systems had originally been considered for some of these missiles. Satisfactory performance has been demonstrated in flight tests.

The details of inertial guidance components and systems have been described in literature [5, 6, 7, 8].

#### 18.4 The Birth of Inertial Guidance

It is difficult to trace a subject to its real beginning. Many early contributions were made to the many sciences that are basic to the field of inertial guidance. However, before inertial guidance could become a recognized technology, a special impetus was required; that impetus was supplied by the beginning of World War II.

A meeting of influential scientific people, mostly professors from universities, was held at Peenemünde, Germany, on September 28-30, 1939, to discuss the problems associated with the rapid development of a rocket-propelled missile. At this meeting, called "Der Tag Der Weisheit" (the day of know-how), Dr. Wernher von Braun, the technical director of Peenemünde, addressed the group, explaining the many problems that existed. Among those present were Prof. Buchhold, of Darmstadt, and Prof. Schuler, of Goettingen. The guidance problem was discussed and it was decided that if good effectiveness were to be achieved, guidance equipment must provide thrust termination with an accuracy of at least one part in a thousand.

All agreed that this specification would be extremely difficult to achieve, and both doppler and inertial schemes were proposed as possible solutions. The majority believed that doppler techniques were most likely to succeed, but a few recognized that inertial techniques had many advantages and should be developed. The participants were allowed to select for their work certain of the problems which were presented, and these were taken back to their organizations. Thus a number of development programs were initiated that attempted to exploit both doppler and inertial techniques to solve the guidance problem for the missile that later became the V2.

It is a credit to the early German investigators that in spite of the almost insurmountable difficulties, they fully recognized the potential of inertial guidance. In synthesizing various schemes to solve the inertial guidance problem, they came up with almost all of the basic devices which are in use to day [9].

The basic concept of a three-axis stabilized platform, complete with gyroscopes, accelerometers, servo-mechanisms, and associated electronics, was itself a considerable contribution. However, there were serious deficiencies in the supporting technologies that prevented a rapid realization of sophisticated hardware having high accuracy.

Precision inertial systems, such as those currently available, required the ultimate in precision machining, optimum utilization of materials, highly specialized and proven design concepts, application of advance theory, use of high-gain electronic amplifiers having stability and reliability, and the availability of reliable and accurate computers. The



equipment must also be small and light, consume little power, and operate in the difficult vehicle environment.

The early designers had little opportunity of going directly to a sophisticated inertial guidance system design. Although the basic concepts were understood, it was necessary to begin within the constraints that existed at the time. Consequently, developments were begun on the simplest possible system that would permit the application of inertial techniques.

The first inertial guidance system developed for the V2, called the LEV-3, is seen in Fig. 18.1. It consisted of two free gyroscopes, leveling pendulums, and an integrating gyro-accelerometer with a velocity-presetting device. This simple device provided attitude control signals and a cutoff signal when the preset longitudinal velocity had been reached. Although providing only about 1 per cent accuracy, the device was reliable and was manufactured in quantity.

Other developments promising more accuracy were also carried out. Prof. Buchhold developed the BMK (Buchhold Messkopf), which consisted of an unbalanced, moving coil with an inductive pickoff and a feedback system. The coil current, which was proportional to the acceleration, was sent through a properly charged electrolytic cell that, upon becoming discharged, developed a voltage jump to trigger thrust cutoff. The electrolytic cell was developed by Prof. C. Wagner. This device had an accuracy of about 0.1 per cent and was intended to be mounted on a stabilized platform. It was used with reduced accuracy attached to the missile.

Dr. H. Schlitt developed an interesting accelerometer having a pivoted, mechanically unbalanced, coil mounted in a magnetic gap very much like the voice coil of a loud speaker. Instead of having proportional pickoff, it had a low-force contact so that the system oscillated when measuring an acceleration. The average coil current was proportional to the acceleration. This development did not become operational due to its late development.

At Kreissel Geraete GmbH, F. Müller worked on a three-axis platform, the SG-66 (Fig. 18.2), which contained most of the features of a modern stabilized platform. This platform, with a BMK accelerometer and an electrolytic integrator, would have produced very good accuracy, but its late development precluded its achieving operational status.

#### 18.5 Post War Developments

After the end of World War II, a number of inertial system developments were started in the United States, including those undertaken by a group under Dr. von Braun at Ft. Bliss, Texas, and by American industrial organizations.

The von Braun group, which moved to Huntsville, Alabama in 1950, began

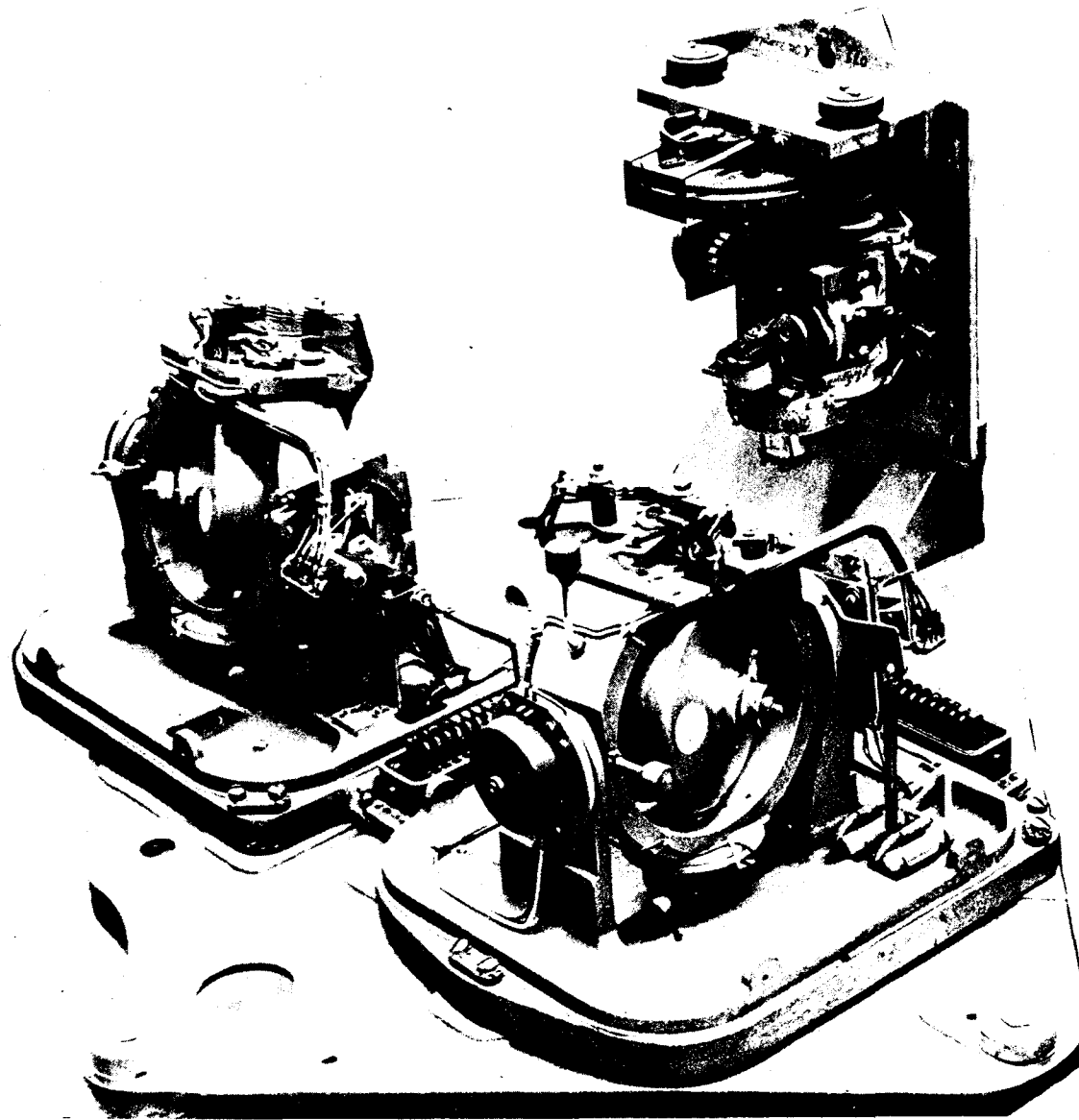


Fig. 18.1 LEV-3 inertial guidance system developed for V-2 guided missile.

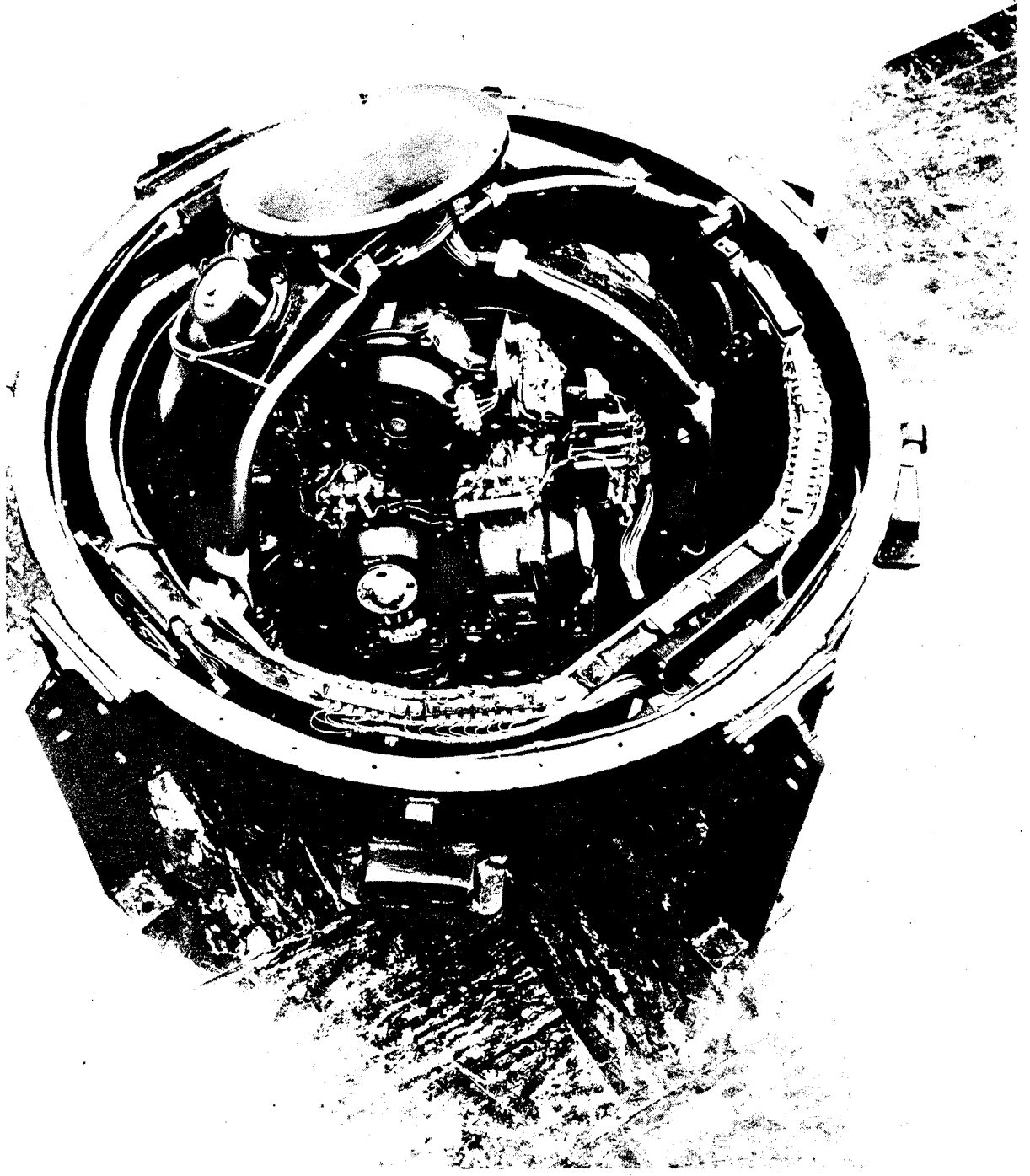


Fig. 18.2 SG-66 stabilized platform developed by F. Muller.

work for the U. S. Army on a three-axis, stabilized platform having an inside-out gimbal system and three single-degree-of-freedom gyroscopes. A significant contribution was the development of a low-torque air bearing for the output axis of the gyroscope. This work was done under the direction of F. Müller. Prof. Buchhold, at that time head of the guidance and control laboratory, decreed that no vacuum tubes would be used due to their unreliability, and at first this meant that magnetic amplifiers having high performance had to be used. When transistors first became available, they could be employed only for the input stages of the amplifiers due to their low power ratings, and magnetic amplifiers were still required for the output stages.

Dr. Schlitt directed development of a motor-reaction-torque double-integrating accelerometer and a small integrating accelerometer consisting of a single-turn unbalanced galvanometer coil in which the current was generated by induction. Both accelerometers utilized air bearings. A small dc-integrating tachometer was also developed which had a linearity of approximately 0.01 per cent. Dr. Schlitt developed a guidance scheme based on the above components.

When development of a guidance system for the Redstone missile was started, Prof. Buchhold and Dr. Haüssermann made a decision to drop all accelerometer work except for an air-bearing, integrating gyro-accelerometer development. Under the direction of J. S. Farrior, an analog guidance computer was developed, the main feature of which was highly accurate ball-and-disk integrator. Due principally to Prof. Buchhold, a new and simpler guidance scheme based on the use of the new devices was developed.

The Redstone inertial guidance system was initially flight-tested in 1954, becoming the first accurate inertial ballistic missile guidance system to complete a flight evaluation program. The results were sufficient to dispel any doubts as to the capability of inertial guidance systems and allowed work on more advanced systems to proceed with confidence. The Redstone stabilized platform, the ST-80, was improved upon and reduced in size to provide the ST-90 for the Jupiter missile. In the investigations made by the Department of Defence to determine whether the Jupiter or the Thor IRBM should be continued, the superiority of the Jupiter guidance scheme and hardware was evident. Flight tests on the Jupiter guidance system, which started in 1957, also indicated a high level of performance, and Dr. Haüssermann coined the descriptive name delta-minimum to describe the guidance scheme being used [10]. The Ford Instrument Company manufactured the Redstone and Jupiter guidance equipment.

The ST-90 was further improved and miniaturized, thereby generating the ST-120 for the guidance system of the Pershing missile. Figure 18.3 shows the relative sizes of the ST-80, ST-90 and ST-120. The difficult time schedules for development of the Pershing missile were met by applying techniques similar to those used for the Jupiter, but in a considerably

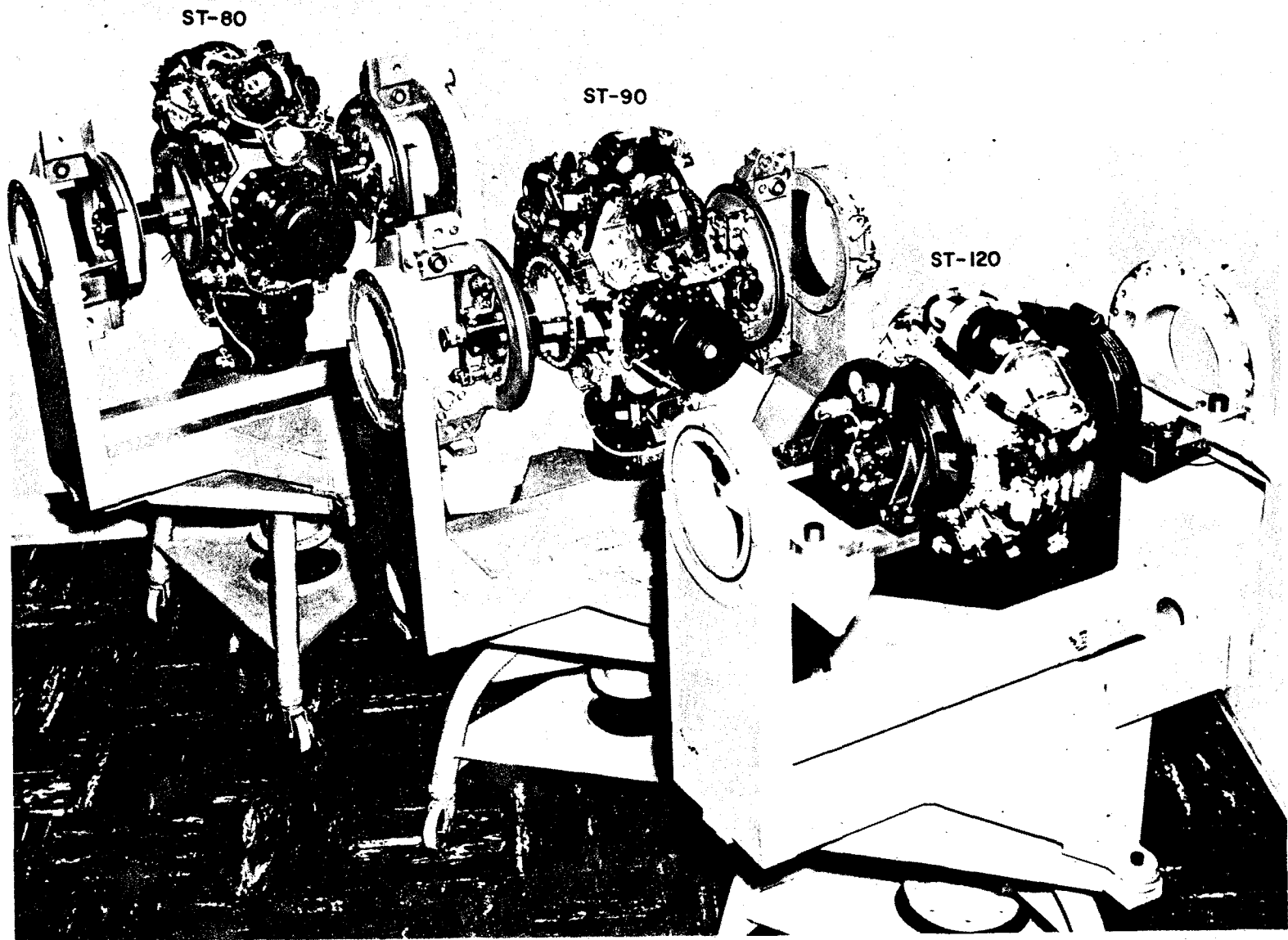


Fig. 18.3 Relative sizes of the ST-80, ST-90 and ST-120 stabilized platforms.

miniaturized and improved version. Pershing flight tests of the guidance system, which began early in 1961, demonstrated the accuracy of the equipment. This system was subsequently manufactured by the Eclipse Pioneer Division of the Bendix Corporation.

At the present time, the George C. Marshall Space Flight Center is developing, under the direction of Dr. Haüssermann, an advanced guidance system for the Saturn vehicle.

Other organizations in the United States also pioneered in the postwar development of inertial guidance systems. It is impossible to recognize here all of the contributors, and the following discussion is limited to the most significant of which the author has personal knowledge.

In 1945, North American Aviation set up a small guided missile group under Dr. William Bollay. After evaluation of alternate methods of guidance, the conclusion was reached that the inertial method was the only one having the required accuracy and invulnerability. Because of skepticism in other quarters, it was necessary to continue work on a radio system for two or three years. Early developments include a double-integrating accelerometer and an accurate gyro, both of which used air bearings of an original design.

The North American Aviation-designed G-1 gyroscope DM-1 distance meter went into laboratory tests in 1949. The instruments were assembled on a platform of unique design, utilizing a central, gas-lubricated ball support in lieu of gimbals and gas-jet reaction torquers in lieu of gimbal motors. This system, including an analog computer, went into flight test in 1950. The flight tests were approximately two to three hours in length, corresponding to the intended flight time of the missile as then contemplated. Although not actually tested in a missile, North American claims these tests to be the first successful flight tests of a pure inertial navigator for non-ballistic missiles. Among the more recent North American developments have been the development of the autolubricated, gas-spin bearing, the Submarine Inertial Navigation System (SINS), and the Minuteman guidance system. Much successful, early, developmental work was done on digital computers.

Shortly after World War II, the Arma Division of the American Bosch Arma Corporation became active in inertial system developments. They pioneered in some original developments that include a stabilized platform making use of two floated gyroscopes with two degrees of freedom with unique design. They also developed a completely transistorized digital computer and a vibrating-string accelerometer. The latter device, attributed mainly to Dr. C. D. Bock, demonstrated exceptional accuracy and had the advantage of supplying a digital output. These devices have become the heart of the successfully demonstrated Atlas inertial guidance system, designed and manufactured by Bosch Arma.

As a result of their wartime work in gyroscopic devices, the Massachusetts Institute of Technology's Instrumentation Laboratory, under the direction of Dr. C. S. Draper, began the development of inertial guidance system [5]. The laboratory's work on inertial guidance for ballistic missiles, which started in 1954, became the basis of the Thor missile's guidance system, manufactured by the AC Spark Plug Division of General Motors Corporation. The Titan guidance system, which was the responsibility of AC Spark Plug and International Business Machines Corporation, is also based on a MIT design.

In 1951, MIT started the design of SINS. The successful demonstration of this equipment led to the development, by Sperry Gyroscope Co. and North American Aviation, Inc., of SINS equipment for use on submarines designed to fire Polaris missiles. The inertial guidance system for the Polaris missile was designed and the prototypes built by MIT.

In 1946, the Northrop Corporation, another pioneer, began the development of a stellar-aided, inertial guidance system for the Snark missile. This and other successful developments by Northrop have contributed much to the state of the art of astro-inertial systems.

#### 18.6 The Future of Inertial Guidance

Inertial guidance is well established as a technique for the guidance of ballistic missiles. It appears to be the only answer to the guidance of missiles such as Polaris, which must be launched from submerged submarines. The submarine guidance problem also seems to be best solved by inertial means, although other techniques such as the Transit Navigation System may be used to obtain periodic fixes. The future will see an increased use of inertial guidance systems for ships, airplanes, and land navigation systems.

Guidance for the injection phase of the space mission is very similar to that for ballistic missiles. Due to the ability in some missions to make post-injection corrections, it may be considered less severe. Radio systems are presently being applied successfully to part of this phase. The General Electric Co. tracking system and the Burroughs computer, used with the Atlas booster and the Bell Telephone Laboratory tracking system and Remington Rand computer, used with the Thor booster, are examples. A major difficulty with radio systems is the distance covered during the complete injection phase, in which the vehicle is carried beyond the reach of the up-range tracking station. However, after injection, radio methods may be employed for post-injection corrections by employing a number of properly located tracking stations.

It is probable that inertial guidance will become the principal technique for injection guidance. While it may be used for complete missions such as the establishment of 24-hr. satellites in orbit, tracking methods

may be used to correct for the effects of drifts and accumulated inaccuracies. Used in conjunction with star-trackers, it will provide for accurate mid-course corrections.

Inertial equipment probably will play an important part in the guidance of lunar-landing vehicles. In addition to maintaining a reference system, it will measure the accelerations during the retro-thrust phase. Together with star-trackers, it will provide injection and mid-course guidance for return to Earth, and during the reentry phase, it will measure lift and drag forces to assure a satisfactory descent trajectory.

Increasingly powerful forces are being brought to bear on the navigation problem. Sophisticated mathematical techniques of analysis are being applied to derive guidance schemes providing optimum performance and greater accuracy. A vast force of engineers and scientists skilled in the guidance and control field are available. A conference on guidance, control, and navigation was held recently at Stanford University, and over 800 specialists attended.

Many new devices are being developed. Cryogenic and electrostatically supported gyroscopes promise exceptional accuracy. Digital computers in combination with miniaturized packaging techniques permit more sophisticated schemes to be employed. In short, inertial techniques, both pure and in combination with other techniques, will have a most important place in tomorrow's guidance technology.



## REFERENCES

- 1 Sauer, E. G. F., Celestial Navigation by Birds, Scientific American 199:42 (1958).
- 2 Griffin, D. R., More about Bat Radar, Scientific American, 199:40 (1958).
- 3 Dornberger, W., "V2- Der Schuss ins Weltall," Bechtle Verlag, Esslingen, 1952.
- 4 Parks, R. J., Guidance Schemes and Systems, in "Handbook of Astronautical Engineering," H. H. Koelle, ed., McGraw-Hill Book Company, New York, 1961.
- 5 Draper, C. S.; Wrigley, W.; Hovorka, J.; "Inertial Guidance," Pergamon Press, Oxford, England.
- 6 Savet, P. H., "Gyroscopes," McGraw-Hill Book Company, Inc., New York, 1961.
- 7 Slater, J. M., Guidance and Control Components, in "Handbook of Astronautical Engineering," ed., H. H. Koelle, McGraw-Hill Book Company, New York, 1961.
- 8 Farrior, J. S., Full Inertial and Stellar-monitored Inertial Guidance, in "Handbook of Astronautical Engineering," H. H. Koelle, ed., McGraw-Hill Book Company, New York, 1961.
- 9 Müller, F. K., "A History of Inertial Guidance," Army Ballistic Missile Agency, Redstone Arsenal, Alabama, 1960.
- 10 Häussermann, W., "Delta Minimum Inertial Guidance Scheme," Army Ballistic Missile Agency, Redstone Arsenal, Alabama, April 13, 1959.

# **GUIDANCE AND CONTROL**



## GUIDANCE AND CONTROL SYSTEMS FOR SPACE CARRIER VEHICLES

W. Haeussermann, G. G. Gassaway, and F. B. Moore

Astrionics Division  
George C. Marshall Space Flight Center  
National Aeronautics and Space Administration  
Huntsville, Alabama

In the past, the requirements of a guidance and control system were defined by clearly specified military characteristics for a particular missile system. In contrast, today's large space carrier (launch) vehicles must be developed for a variety of missions which cannot be completely defined early enough to be used as design criteria.

The design aspects of the guidance and control systems of large carrier vehicles are given, beyond the former aspects on ballistic missiles, by new, partially anticipated mission requirements, by the new vehicle properties and capabilities, and by stronger reliability demands.

In the following considerations, the C-4\* configurations of the Saturn class vehicles will be used to illustrate the system engineering viewpoints on the guidance and control system of the most powerful launch vehicles visualized today. The viewpoints, however, are applicable to any large carrier vehicle regardless of size, maximum thrust, number of stages, or mission.

Only the operations of the carrier vehicle and its different stages are considered in this paper. Navigational requirements, as they arise after injection into escape paths either by direct ascent or from orbit, have been disregarded.

#### 19.1 System Engineering Requirements

##### 19.1 Missions

The missions to be fulfilled by the large carrier vehicle have a direct influence on the guidance and control system design. Each phase

---

\* The C-4 and C-5 configurations may be used interchangeably throughout this discussion, except that certain performance and structural data have not been set for the C-5 at the time of this writing.

of the operation, which the carrier must complete between launch from Earth and final fulfillment of its mission, places different requirements on the system.

One factor influencing the design is the nature of the vehicle maneuvers which the system must direct during the various phases of flight required to fulfill a given mission. Since the size of the vehicle and its supporting launch pad structure do not permit prelaunch azimuth alignment, it is necessary on most missions to roll the vehicle into the proper azimuth after launch. This is a factor in the required stabilized platform gimbals freedom.

Maneuver requirements during the later stages of the injection phase also contribute heavily to the necessary platform freedom and gimbal arrangement. On some missions, it is impossible to confine the launch trajectory to a plane. Injection of a payload into an equatorial orbit from available launch sites, for instance, requires a propelled "dog-legging" maneuver.

The phases of the mission which greatly influence the required maneuverability are orbital operations [1]. Since these phases are distinctly different from the familiar orbital or escape injection operations, a more detailed description is given.

Orbital operations include multiple launchings to place parts of a space vehicle in orbit; the subsequent connecting or fueling operations while coasting in orbit; and the launching of the vehicle from orbit. Table 19.1 lists some of the characteristics of those Saturn C-4 vehicle configurations that are planned for two types of orbital operations designed for lunar landing with return missions. The first type, termed the fueling mode, requires the launch of a tanker containing liquid oxygen into a high-altitude parking orbit. A second launch carries a similar tanker into a chasing ellipse. These tankers rendezvous and are checked out. The third launch consists of injecting a two-stage escape vehicle with spacecraft into a chasing ellipse. The escape vehicle stages are fully fueled. The spacecraft and escape vehicle rendezvous with the tankers and the liquid oxygen is transferred in orbit. After transfer of the liquid oxygen, the vehicle is checked out and launched from orbit using the R-1 stage. The second stage (R-II) is used for lunar landing. The spacecraft carries its lunar launch system. Typical trajectories for each launch are shown in Fig. 19.1. The second type, termed the connecting mode, requires one launch of the first stage of the orbital carrier vehicle with all propellants loaded into the high-altitude orbit. The second carrier brings in the second stage loaded with propellants and the spacecraft into a chasing ellipse. After rendezvous and docking, the vehicle is checked out and launched from orbit as previously described. Figure 19.2 shows typical trajectories for these orbital operations. A third application of orbital operations still in the early planning stage is the construction of a space station in orbit.

Table 19.1  
 Orbital Operations Summary Using C-4 Vehicle  
 For Manned Lunar Landing and Return

<u>Mode</u>	<u>Payload</u>	<u>1st Stage</u>	<u>2nd Stage</u>	<u>Vehicle Length</u>
Fueling mode 1st & 2nd launch	Tanker	S-IC F-1 engine (4) 1,500,000 lb	S-II J-2 engine (4) 200,000 k lb	253 ft
Fueling mode 3rd launch	R-II stage, unfueled; R-I stage, fueled, with spacecraft			325 ft
Connecting mode 1st launch	R-I stage fueled; J-2 engine (1)	"	"	295 ft
Connecting mode 2nd launch	R-II stage, with spacecraft J-2 engine (1)	"	"	263 ft

Note: The fueling mode gives a 25% gain in weight for the spacecraft.

FUELING MODE

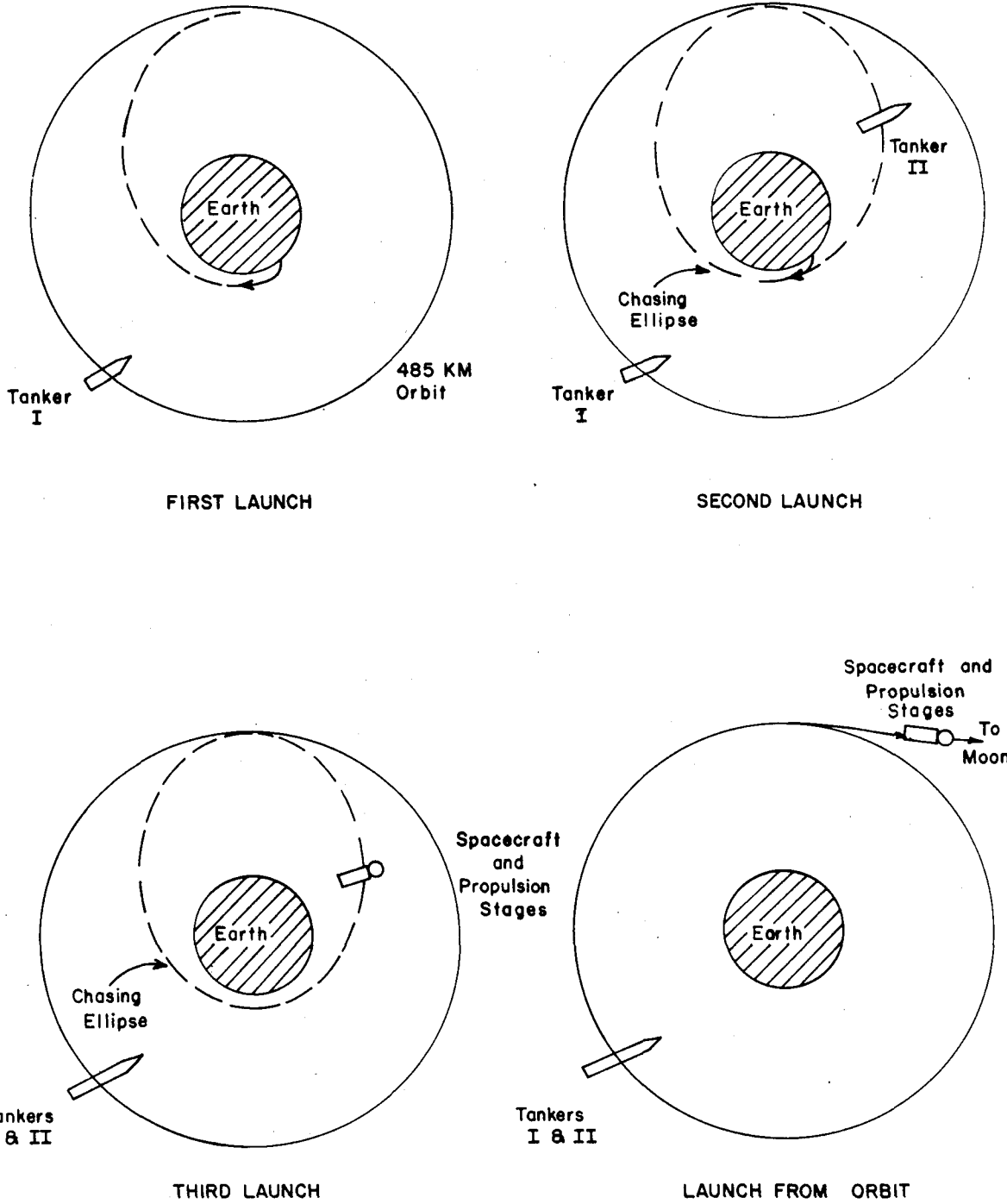


Fig. 19.1 Typical trajectories - fueling mode.

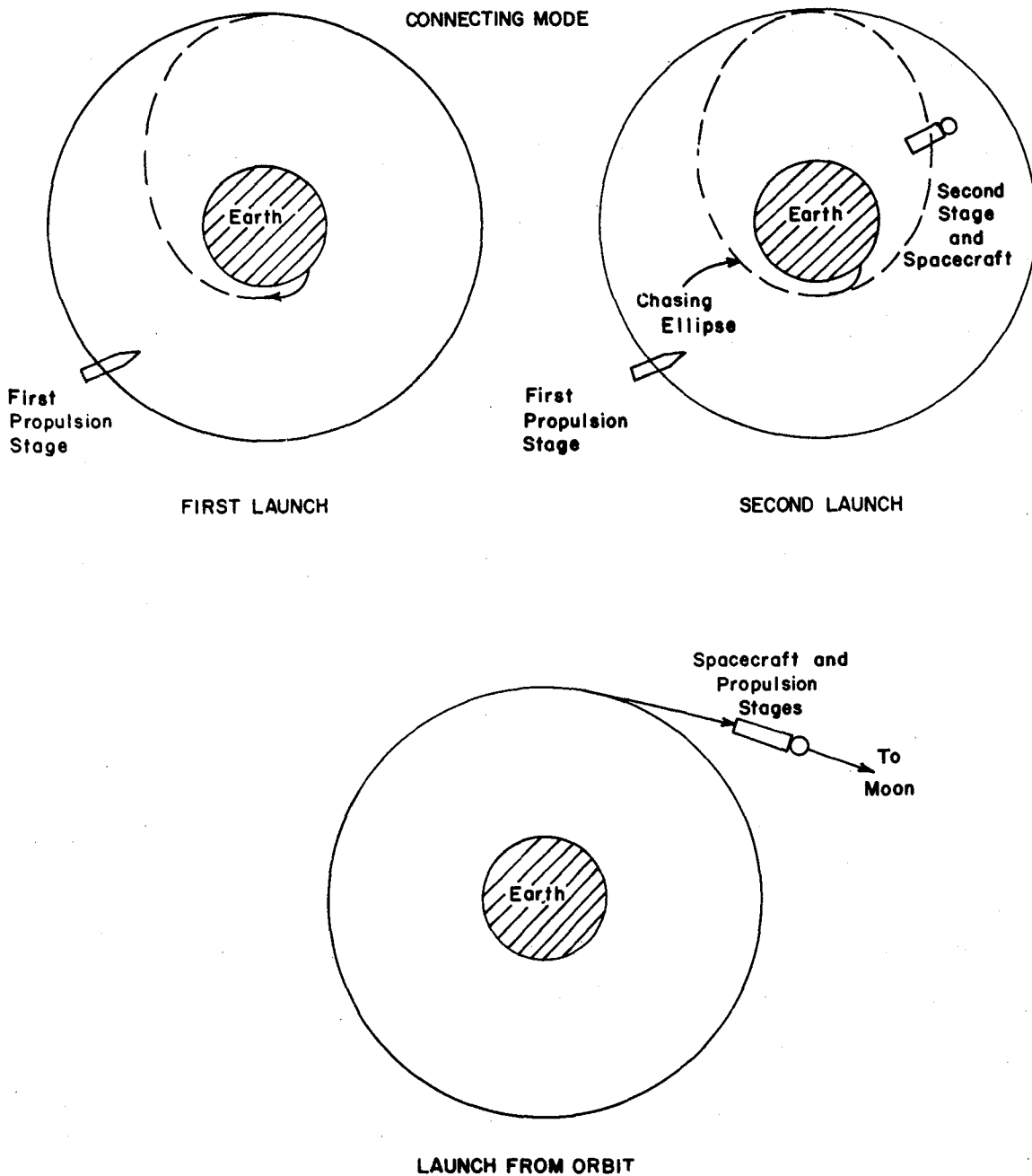


Fig. 19.2 Typical trajectories - connecting mode.

During some coasting phases, it may be desirable to allow the vehicle to tumble in an arbitrary manner or to maintain attitude or attitude rate control. The inertial reference should be maintained for use in the later powered phases, if possible. During the docking phase, it appears that situations can exist to make unlimited maneuverability of both target and chaser vehicles a definite asset. Orientation may be required for antenna coverage or heat protection during some phases. The guidance and control system must, therefore, be capable of orienting the vehicle in any attitude without disturbing the position of the inertial platform.

For final rendezvous maneuvers, the system must be capable of accepting inputs from sensors other than those used for injection guidance and control. During long coasting phases, the system must be capable of accepting inputs from sun sensors, horizon seekers, or star trackers for correcting the inertial sensors.

Punctual launching is a requirement for escape missions. An appreciable hold may cause a lunar shot postponement for a month or a planetary flight delay of years. The number of launch time windows can be doubled by inserting an orbital flight period. The window itself can be widened by plane change maneuvers; however, large angular changes are expensive in propellant requirements. Very small launch time windows are imposed on launch from orbit, but here the space carrier vehicle system is reduced by one or two stages and the first orbital propulsion stage must possess, for most applications, an automatic reignition capability.

A single guidance and control system is planned for launch guidance of vehicles carrying manned spacecraft as well as scientific payloads. The system must therefore have the reliability required for manned missions. In manned missions, the system must be capable of providing information to the pilot for decision making or for use in navigation.

For the accuracy required of a space carrier vehicle guidance system, the all-inertial method is completely adequate. It is also preferable because it is self-contained and independent of ground bases which, depending on the ascent flight path, might be installed on remote islands; this would create communication and interference problems.

#### 19.1.2 Vehicles

Most vehicle influences on the guidance system are indirect. The guidance function must be accomplished in the optimum manner with large ranges of initial conditions that are imposed as a result of over-riding control considerations. Inability of the control system to impose large control torques, because of limited deflection capability of the engines plus the inability of the vehicle to withstand these forces due to stability and structural characteristics, makes the use of guidance impractical during the first stage. In the presence of large thrust



dispersions or winds, the velocity and displacement deviations at the initiation of second stage burning may be quite large. These deviations make a guidance system that constrains the vehicle to a standard trajectory (delta minimum guidance scheme) impractical.

The study of these initial conditions and the varied end conditions imposed by the various missions influence the guidance scheme and the guidance system.

Size and shape of the vehicle have an appreciable influence on control system design. Within the limited available controlling torques, the system must overcome inherent aerodynamic instability and compensate for wind disturbances and thrust misalignments, while avoiding the excitation of structural and sloshing mode instability.

Since the vehicle is long and flexible, the characteristics of the bending modes must be determined and considered in the control system design. The control sensors detect motion of the vehicle at their particular locations, regardless of whether the motion is true vehicle response to an external disturbance or because of local flexure of the vehicle. Since the bending modes can be excited by the applied control torques, a closed loop through the flexible structure exists. If the control sensors are not properly located, and if the information signal is not adequately filtered and shaped within the control system, the loop may be unstable and lead to catastrophic structural failure of the vehicle.

With the vehicle control loop frequency and the first structural bending mode frequency close together, the desired shaping and filtering are difficult. On large carrier vehicles, the control frequency cannot safely be made lower than 0.1 cps to 0.3 cps because of the uncertainty of aerodynamic and propulsion system characteristics and because of the required rate of response to disturbances such as wind gusts. The first bending frequency of approximately 1 to 2 cps cannot be pushed higher without a severe weight penalty. Figure 19.3 shows a preliminary frequency spectrum for the Saturn C-5 vehicle.

Until more accurate analytical methods of describing the vehicle structural dynamics are realized, full scale dynamic testing or scaled testing, which can be accurately interpreted, will have to be continued.

In liquid-propelled carrier vehicles, the sloshing mode characteristics of the propellants influence the control system design. Because of the close proximity of the control and sloshing frequencies, it is not always possible to provide adequate damping in the control system of all modes simultaneously. Therefore, the sloshing problems are alleviated by use of baffles in the tanks if weight considerations permit. This reduces the restraints which would otherwise be placed on the control system.

## 1st Mode Sloshing

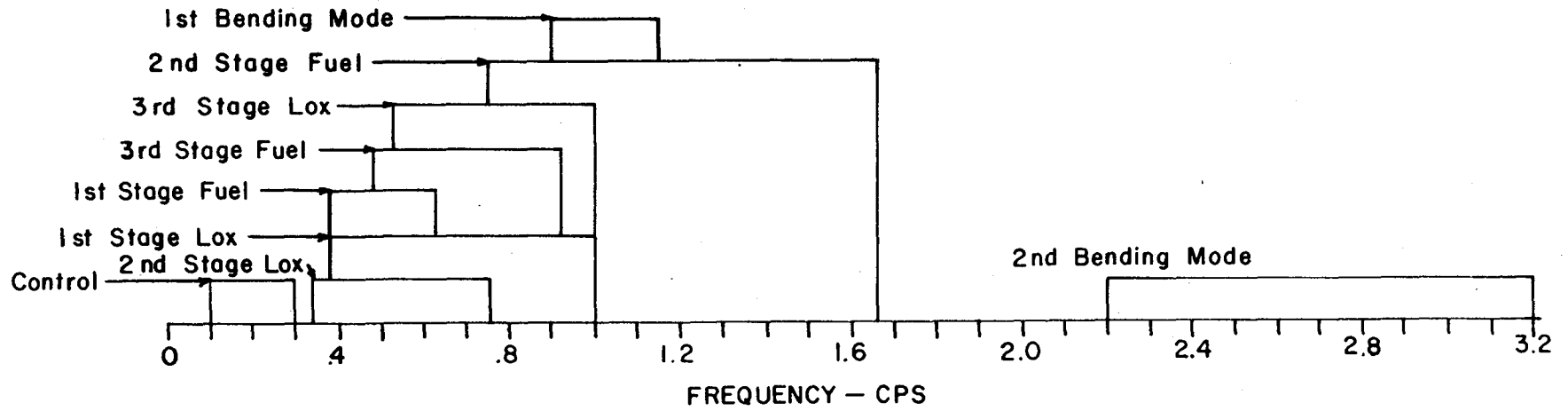


Fig. 19.3 Preliminary frequency spectrum for Saturn C-5.

The vehicle shape directly influences the control system requirements in a distinctly different manner also. Since the center of pressure on the Saturn C-4, just as on the Saturn C-1, is located forward of the center of gravity over portions of the flight, artificial stabilization by a controlled angle of attack will be required. If this technique is not employed, the control torques required to overcome wind disturbances and the lateral forces applied to the vehicle structure are prohibitively large. With angle of attack control, the vehicle attitude is so directed that the upsetting and compensating torques are reduced because of the smaller angles of attack.

In a large space carrier vehicle such as Saturn C-4, an automatic check-out is required for reasonable launch preparation time and launch-on-time capability. All inputs to the automatic checkout system and the outputs must be accommodated in the guidance and control system. In prelaunch checkout, the data must be available on the ground. Stimuli to facilitate the checkout are sent to the guidance and control system from the ground via rf command links or hard line. The constants for the guidance and cutoff equations must be changed periodically to allow for large launch delays beyond the first planned launch window. The design of the guidance and control system must be compatible with the checkout philosophy.

In orbital operations, the guidance and control system must be compatible with the orbital checkout scheme.

### 19.1.3 Reliability

One significant physical design feature apparent in the sensing and computing components of the guidance and control system of large space carrier vehicles is the departure from microminiaturization. Volume and weight are no longer overriding considerations as was the case in past rocket development programs. Microminiaturization was a necessity in the past because of the severely limited payload capability of pre-Saturn launch vehicles. Although volume and weight considerations cannot be ignored in the future, they can be made subservient to such prime considerations as accuracy, reliability, flexibility, and repairability. Considering future missions, flexibility for employment in a wide variety of applications is needed to eliminate multiple, almost parallel developments resulting in unnecessary expenditure of funds and technical effort. Repairability is important not only from the standpoint of economical, reliable maintenance during the development, testing, and launching phases, but also from the more critical aspect of repair in orbit. Simple, straightforward means of checking and repairing components on board in orbit must be provided. The repair crew, whether vehicle technicians or astronauts, must be limited in number. Experienced technicians in all fields cannot be available for orbital repairs.

The considerations discussed lead to system layouts which enhance isolation of malfunction to a single black box. Within each black box, modular construction with throw-away modules will be emphasized.

In the design and development of the guidance and control system for large carrier vehicles, high reliability must be the overriding consideration. The tremendous cost of each vehicle and the limited development and manufacturing facilities available limit the number of vehicles available for operational use and for research and development (R&D) testing. Thus, it is even more important that each vehicle fulfill its assigned mission. The ultimate reason for the emphasis on reliability, however, is that the vehicle must be "man-rated."

Reliability is emphasized through proper attention to the system design and to the conservative design of the individual components in the system. The key to reliable system design, as well as reliable component design, is emphasis on simplicity.

The carrier vehicle is simplified through the use of an integrated guidance and control system. By using only one complete set of sensing and computing elements, rather than a complete system in each stage, unnecessary duplication is avoided. Only those portions of the system which must be an integral part of each stage, for example, the actuation system, are duplicated.

The system is further simplified by attention to the design of each component so that it offers maximum utilization with a minimum of complexity. For instance, the stabilized platform, the basic purpose of which is to provide an inertial reference for the guidance accelerometers, also serves to furnish attitude information to the control system. The additional resolvers involved effectively replace autopilot gyros which would have many more moving parts.

Another typical example of simplification is the use of differentiation of the attitude signal for control stabilization instead of rate gyro signals. In this case, the complexity comparison is between a simple capacitor and a rate gyro of many electrical and moving mechanical parts. In some instances, depending on the platform location and the specific structural bending problem, the differentiation technique cannot be used. The more complex solution is utilized only where simpler solutions are inadequate.

Reliability is further improved by designing the guidance and control system to be adequate for all Saturn missions. Improved reliability is achieved through more flight experience on equipment, even though the number of vehicles flown on any given mission may be small. The employment of systems or components used for military programs further improves the experience and thereby the reliability for Saturn.

## 19.2 System Description

### 19.2.1 Guidance Scheme

The adaptive guidance mode provides the guidance and cutoff equations to be implemented by the guidance and control components [2, 3]. The scheme is the prime influence on the design of the guidance portion of the guidance and control system. The equations derived from this scheme are given in Table 19.2.

The guidance and control system must provide the data needed as inputs to the guidance and cutoff equations, the equipment for computing the equations during each phase of flight, and the equipment for executing the commands derived as a result of the equations. A block diagram of the guidance and control system is shown in Figure 19.4.

The displacement and velocity information ( $x$ ,  $y$ ,  $\dot{x}$ ,  $\dot{y}$ ) needed for these equations is derived from measurements by the accelerometers on the stabilized platform. Since the acceleration data are inertial and the adaptive guidance mode is best described in a coordinate system that is space-fixed in position and direction at a standard reference point, these data must be transformed during the computation process to provide velocity and displacement data in this coordinate system. These data are transformed in the digital computer by adding the acceleration of gravity which has been computed as a function of the vehicle position to the inertial acceleration. The term  $F/m$  needed in the equations is the thrust to mass ratio of the vehicle and is derived by taking the root sum square of the outputs of all the accelerometers on the stable platform. This is an approximation to  $F/m$  during any maneuvers, but is sufficiently accurate since the angular dispersions are small. Time ( $t$ ) is derived from the computer clock.

The cutoff computation is performed during the final stage only, and its output is a signal used to give shutdown of the engines of this stage. Engines of all previous stages are burned to fuel depletion.

The guidance equation is used during all stages. In the first stage, this equation is simplified to a function of time alone by setting the coefficients of all other terms to zero. This provides the first stage with a time referenced tilt program in pitch. This simplification is required since the vehicle could not maneuver enough to follow the general equation in the presence of large thrust deviations or aerodynamic disturbances because of the aerodynamic instability and structural limitations previously mentioned.

After cutoff of the first stage, the thrust direction equation is solved continuously in terms of Euler angles in the space-fixed coordinate system. These Euler angles define the desired orientation of the

Table 19.2  
Guidance and Cutoff Equations

Thrust Direction:

$$\begin{aligned}
 X &= A_0 + A_1 X + A_2 Y + A_3 \dot{X} + A_4 \dot{Y} + A_5 t + A_6 \frac{F}{m} \\
 &+ A_7 \dot{X}^2 + A_8 XY + A_9 XX + A_{10} \dot{XY} + A_{11} X t + A_{12} X \frac{F}{m} \\
 &+ A_{13} Y^2 + A_{14} Y \dot{X} + A_{15} \dot{Y} \dot{Y} + A_{16} Y t + A_{17} t \frac{F}{m} + A_{18} \dot{X}^2 \\
 &+ A_{19} \ddot{XY} + A_{20} \dot{X} t + A_{21} \dot{X} \frac{F}{m} + A_{22} \dot{Y}^2 + A_{23} \dot{Y} t + A_{24} \dot{Y} \frac{F}{m} \\
 &+ A_{25} t^2 + A_{26} t \frac{F}{m} + A_{27} \frac{F}{m}
 \end{aligned}$$

Where  $A_i$  ( $i = 0, 1, 2, \dots, 27$ ) are stored constants different for each stage.

Cutoff Equation:

$$\begin{aligned}
 t_c &= B_0 + B_1 X + B_2 Y + B_3 \dot{X} + B_4 \dot{Y} + B_5 t + B_6 \frac{F}{m} \\
 &+ B_7 \dot{X}^2 + B_8 XY + B_9 XX + B_{10} \dot{XY} + B_{11} X t + B_{12} X \frac{F}{m} \\
 &+ B_{13} Y^2 + B_{14} Y \dot{X} + B_{15} \dot{Y} \dot{Y} + B_{16} Y t + B_{17} t \frac{F}{m} + B_{18} \dot{X}^2 \\
 &+ B_{19} \ddot{XY} + B_{20} \dot{X} t + B_{21} \dot{X} \frac{F}{m} + B_{22} \dot{Y}^2 + B_{23} \dot{Y} t + B_{24} \dot{Y} \frac{F}{m} \\
 &+ B_{25} t^2 + B_{26} t \frac{F}{m} + B_{27} \frac{F}{m}
 \end{aligned}$$

Where  $B_i$  ( $i = 0, 1, 2, \dots, 27$ ) are stored constants.

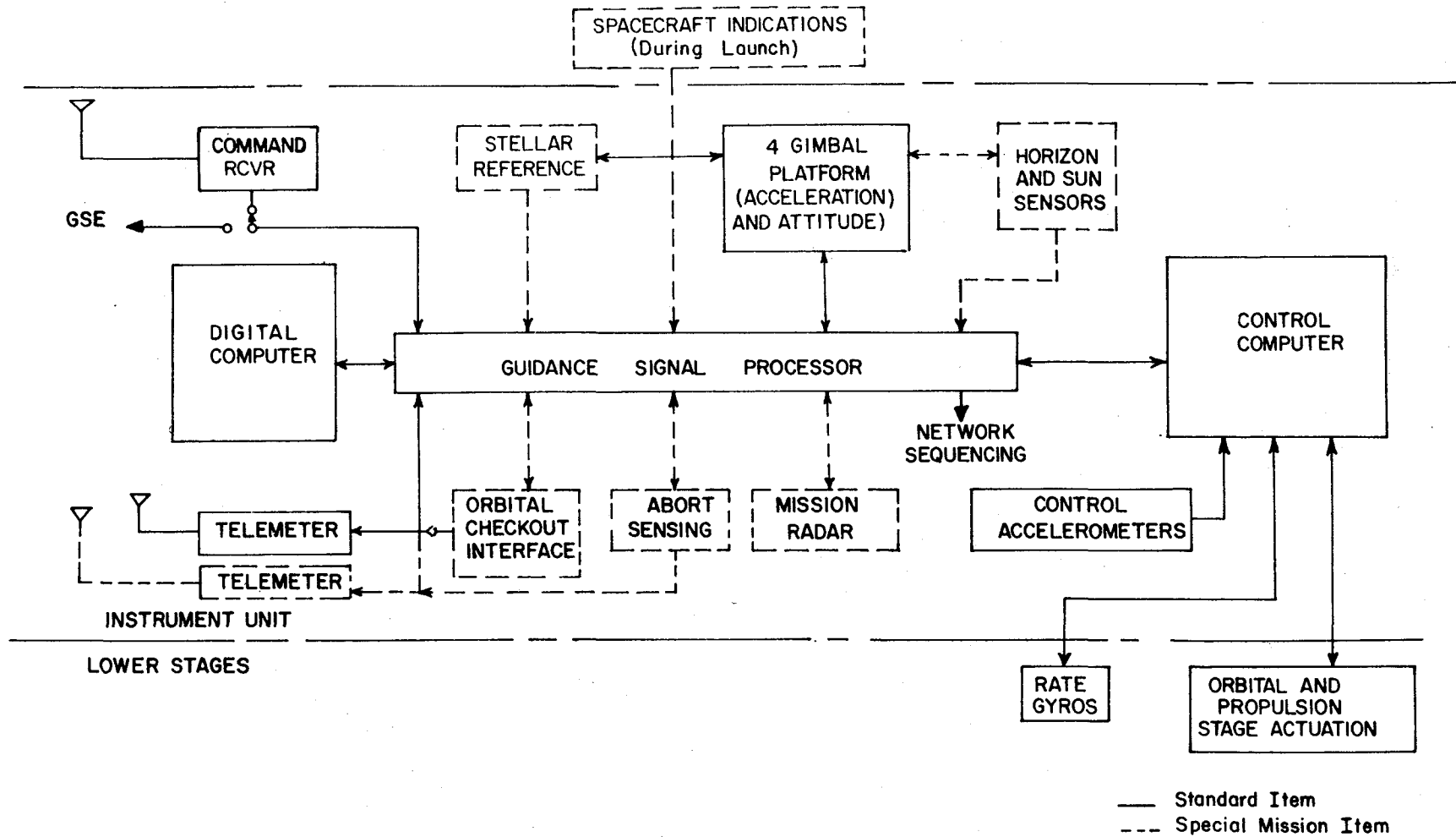


Fig. 19.4 Block diagram of guidance and control system for advanced Saturn configuration.

vehicle in the space-fixed system. Unit vectors along the axes of the desired vehicle coordinate system are transformed by means of the Euler angles into components in the space-fixed coordinate system. These components are then transformed into the actual vehicle coordinate system using the platform gimbal angles. These outputs provide error signals which are sent to the vehicle control system. When these error signals are reduced to zero, the actual vehicle coordinate system is aligned with the desired vehicle coordinate system; therefore, the thrust is placed along the optimum direction. The guidance of the vehicle is accomplished when this optimum thrust direction is maintained until the cutoff equation gives its signal for shutdown of the main engines.

The vehicle may be constrained to the reference path in cross range as in a delta minimum guidance method, or the adaptive guidance mode equations may be expanded to provide cross range guidance.

#### 19.2.2 Control Scheme

The Saturn control system is included in the block diagram shown in Figure 19.4. The structural dynamics must be evaluated and locations of the control sensors carefully determined to insure stability. The structural stability problem becomes more severe on larger carrier vehicles where the bending frequencies are proportionately lower. Each configuration will present a different problem and no simple overall solution can be expected. In some cases it may be necessary to locate control sensors, such as rate gyros, at a number of different locations along the vehicle, with the signals from the various sensors being phased in and out as a function of the varying nature of the problem. The accurate determination of the vehicle characteristics will remain a difficult and critical item that will influence the control system design. This design will be made simpler and the components less complex as the knowledge of these characteristics is improved.

On the Saturn C-4 attitude rate information for stabilization will be derived from rate gyros during the first stage operation. In all subsequent stages, the attitude rate information will be achieved by differentiating the attitude error signals from the stabilized platform.

In the first Saturn configurations, wind disturbances will be sensed directly by local angle of attack transducers. The signal output of these transducers are fed into the control system with a polarity such that the resultant engine deflections reduce the angle of attack. It is possible that body-fixed accelerometers will be used instead of direct angle of attack control in later Saturn configurations; accelerometers are preferred since the instruments can be located in an enclosed environment within the vehicle rather than exposed to the elements as are angle of attack transducers. The accelerometer is aligned with the sensitive axis perpendicular to the vehicle longitudinal reference axis



and senses lateral accelerations caused by angle of attack. In addition, the accelerometers sense lateral accelerations caused by control deflections and tangential accelerations, as well as accelerations from structural bending. This makes the system analysis more complicated than for direct angle of attack control.

The idealized control equations for the yaw, pitch, and roll axes are

$$\beta_y = a_{oy} (\chi_y - \phi_y) + a_{1y} \dot{\phi}_y + b_{oy} \alpha_y$$

$$\beta_p = a_{op} (\chi_p - \phi_p) + a_{1p} \dot{\phi}_p + b_{op} \alpha_p$$

$$\beta_r = a_{or} (\chi_r - \phi_r) + a_{1r} \dot{\phi}_r$$

The control equation provides control of the attitude  $\phi$ ; the time rate of change of attitude  $\dot{\phi}$ ; the angle of attack  $\alpha$ ; and  $\chi$ , the attitude direction commanded from the guidance system. The control system is designed with a view toward satisfying the ideal control equation at the control frequency. This equation is not satisfied at higher frequencies because of hardware lags and body-bending filters.

Implementation of the control equations is accomplished through the application of the commanded torques to the vehicle, as described in the next section. Where the control torquing technique is compatible between the various stages of the multistage vehicle, for instance, by gimbaling four engines in each stage, the control commands are switched to each stage in turn as it becomes the propelling stage.

### 19.2.3 Vehicle Control Torquing Techniques

The torques necessary to stabilize and direct the course of a space vehicle can be derived by controlling the magnitude or direction of the thrust generated by the primary propulsion system, by auxiliary propulsion systems, or by the manipulation of aerodynamic surfaces. Control by the latter method is somewhat limited in application since it can only be applied throughout those portions of the trajectory where a relatively high aerodynamic pressure exists. Even in isolated instances where aerodynamic control is used in the space vehicle, thrust vector control is a necessary supplement.

Thrust vector control has been widely accomplished in the liquid propelled stages by gimbaling the main propulsion engines. Many other methods of deflecting the thrust vector have been investigated, and

some have been successfully applied. For example, jet vanes, jetavators, or even a portion of the nozzle itself can be deflected in the jet stream to derive the desired torques; however, these techniques do not look promising for application on large launch vehicle stages because of the structural and environmental problems associated with material exposed to the jet exhaust to utilize this type of control.

Another method of thrust vector control fundamentally different from the gimballed engine technique involves the separation of the jet stream from the nozzle wall in an unsymmetrical pattern by influencing the boundary layer adjacent to the walls. The jet can be caused to separate from the chamber walls in a desired manner by injecting gas or liquid at some point downstream of the throat. This disturbance in the normal flow pattern causes a change in direction of the exhaust gas flow and a consequent deflection of the thrust vector. This technique, known as secondary injection, shows some promise from the standpoint of the control engineer. Derivation of large control torques by merely manipulating the valves which determine the flow rate of the secondary injectant holds some definite attractions when compared with, for instance, the problems associated with the gimbaling of a large liquid propellant engine. Depending on the characteristics of the gas or liquid injected, however, the flow rate requirements can be quite large and may even approach the flow rates of the primary propellants. The problems associated with supplying the secondary injectant, piping it to the proper location on the chamber, and controlling its flow are therefore not minor. The system would have to be an integral part of the propulsion system and would certainly complicate the engine design. Since the engine, rather than the control system, is the pacing item in the carrier vehicle development, it seems unwise to further complicate its design and development. It appears, therefore, that secondary injection will not play an important role in thrust vector control of large space carrier vehicles within the next few years.

Another scheme of control which must also be an integral part of the propulsion system is thrust vector magnitude control. On a vehicle propelled by four axially aligned engines, for instance, the necessary pitch and yaw maneuvering and controlling torques could be obtained from the thrust level differential between the four engines. This scheme can only be applied to produce control torques on multiengine vehicles; its effectiveness is directly dependent upon the location and arrangement of the engines. In addition, an auxiliary roll control system is required. Since thrust level controllers of limited range are a necessary part of most engine developments, the problem is to extend the range of control without lowering the specific impulse and the rated thrust level of the engine.

Although thrust level control appears a candidate to control the launch vehicle of the future, its application must await the age of

truly throttleable engines. The F-1 engines of the Saturn C-4, do not lend themselves to this technique. It appears, therefore, that liquid propelled carrier vehicles of today must employ the technique of gimbaling the engine to obtain the desired thrust vector direction.

Most of the previous comments refer primarily to the control of liquid propelled vehicles. Solid propelled carrier vehicles obviously cannot be controlled by gimbaling the engine since the solid propellant, its container, and the chamber are structurally integral. No simple approach to thrust level control is available, either. Currently, it appears that the solid propelled carrier vehicle can be controlled best by means other than manipulation of the primary thrust vector. Utilization of auxiliary control engines to produce the desired torques seems most promising. The engines could be either liquid or solid propelled, but the latter would be preferable to retain the simplicity advantages of the solid propulsion system. The number, thrust level, and location of the auxiliary engines, as well as the determination of the required degrees of freedom of rotation of each, depends entirely on the configuration to be controlled.

In addition to techniques for vehicle control during the propelled phases, some means of controlling the attitude of the orbiting stage during the coast and rendezvous phases must be provided. The coast phases require only modest accuracy; for example, limit cycles of several degrees are satisfactory to obtain heat protection against sun radiation for the cryogenic propellants. The coasting phases are expected to last less than a month. Rendezvous maneuvers require closer attitude control, but their duration is less than 30 min. Thus the application of control jets for torquing the vehicle is most feasible; a weight, volume, and power comparison shows that rotation reaction systems, such as flywheel and gyroscopic actuation devices, are not compatible. A multiple-jet auxiliary system seems the best solution for the control of large propulsion and tanker stages envisioned for orbital operations. A favorable characteristic of the multiple-jet system is that through proper location and activation of the jets small translational corrections, as well as rotary motion, can be accomplished.

### 19.3 Component Description

A brief description is given of some of the components used in the guidance and control system illustrated in Figure 19.4. These components are applicable to any carrier of the Saturn class and any other carrier vehicle, present or future. It should be pointed out that the guidance and control scheme, the implementation, and most of the components described in this paper can be moved into the spacecraft and used for both the launch guidance and control and subsequently, the spacecraft guidance and control. The design, in all possible cases, considered this ultimate capability as part of the system engineering requirements.

### 19.3.1 Stabilized Platform

The stabilized platform, shown in Figure 19.5, had four gimbals which allow unlimited rotational freedom in all directions. Three single degree-of-freedom air bearing gyroscopes with direct current torque motors on the platform gimbals and the necessary electronics maintain the inner element stable and space fixed in direction after launch. A resolver chain on the gimbals provides the coordinate transformations necessary to generate error signals to implement the guidance and control scheme already discussed. Some basic specifications on this platform are given in Table 19.3.

### 19.3.2 Digital Computer

Two versions of the general purpose digital computer are planned. The first, for early application, is the IBM ASC-15 Titan computer. The second, for use on later vehicles, is a computer in which an advanced packaging technology, such as deposited thin films, is applied. Some characteristics are given in Table 19.4.

### 19.3.3 Control Computer

The control computer derives from the error signals received from the guidance system and the control sensors the control commands to be executed by the vehicle torquing mechanisms. The operations include filtering and shaping of the incoming error signals, summing them in the proper ratio and generating the command signals at the necessary power level to operate the actuating mechanisms. The shaping and filtering is accomplished by passive networks composed of resistors, capacitors, and inductors. Because of the low frequencies involved, relatively large inductance and capacitance values are required. Typical networks include inductors and capacitors ranging up to 800 and 25  $\mu\text{f}$ .

The signals are summed by multi-input magnetic amplifiers. Magnetic amplifiers are used since they accomplish with a minimum of active components the desired computing, phasing, and signal isolation. Transistor amplifiers are utilized to bring the command signals to the required power level. The control computers used in the early Saturn vehicles have a volume of 0.5  $\text{ft}^3$ , a weight of 30 lb, and a power requirement of 150 w.

As presently visualized, the Saturn C-4 class control computer will have no major functional differences from those previously described. Although certain functions, such as the generation of the proper gain ratios, may employ digital computation, the primary functions in the control loop will be accomplished by analog techniques. This technique is simpler and more reliable and the obtainable accuracy of 5 to 10 per cent is sufficient. The major improvements will be in the area of

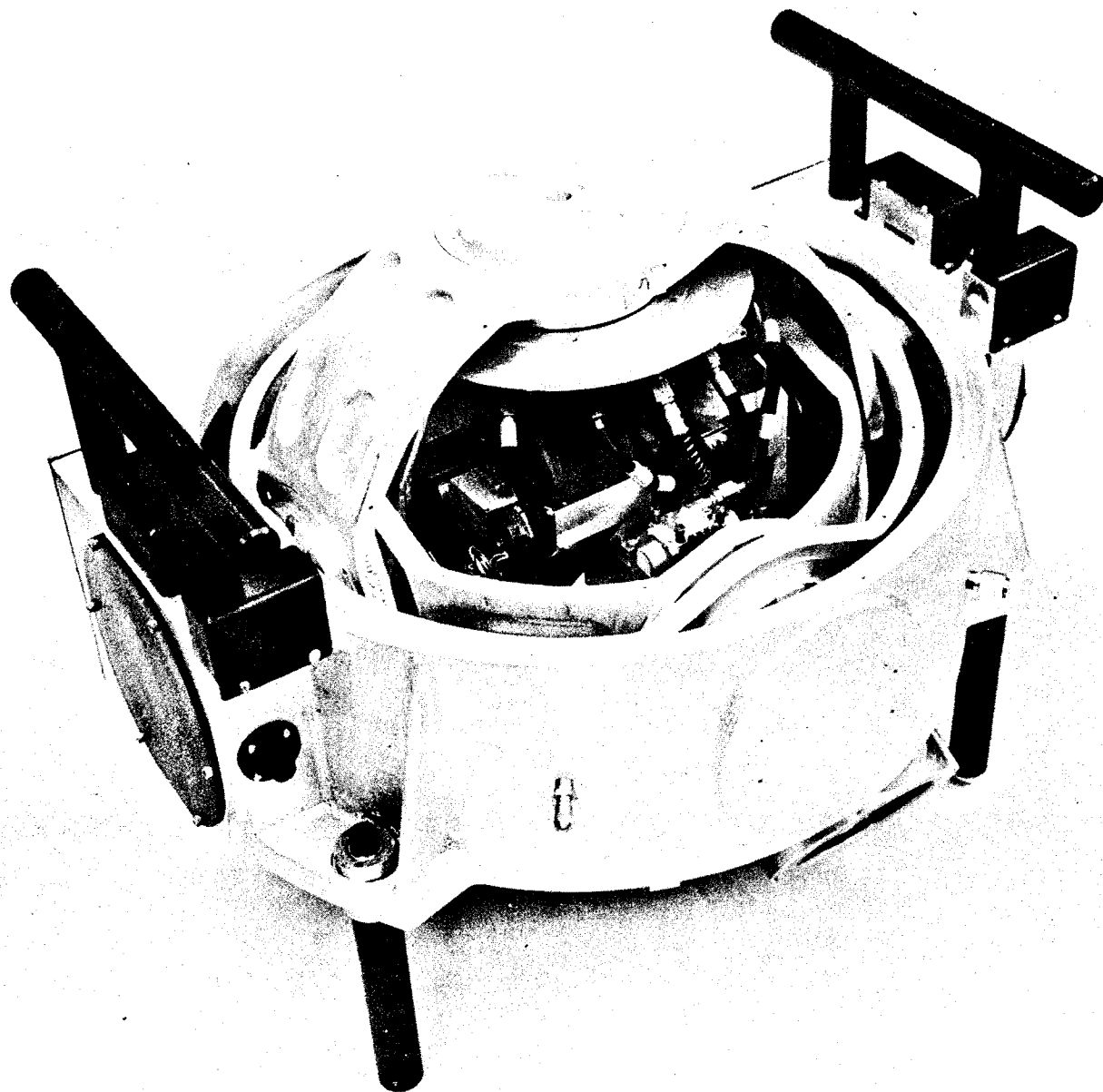


Fig. 19.5 Saturn stabilized platform.

Table 19.3  
Some Basic Specifications for the Stabilized Platform

Size	Platform, 19-in sphere with mounting ring electronics box, 0.22 ft <sup>3</sup>	
Weight	Platform, 85 lb electronics box, 18 lb	
Power	115 v $\pm$ 1 v, 400 $\pm$ 0.025 cycle 3 phase, 120 w 28 v, dc; 110 w	
Leveling Accuracy	$\pm$ 10 sec of arc	
Resolver Chain Accuracy	$\pm$ 0.1 deg	
Azimuth Alignment Accuracy	$\pm$ 10 sec of arc	
Gyro Performance	Constant drift	0.075 deg/hr
	Acceleration sensitive drift	0.05 deg/hr/g
	Acceleration squared sensitive drift	0.05 deg/hr/g <sup>2</sup>
Accelerometer Performance	Scale factor	$5 \times 10^{-6}$ g
	Bias	$5 \times 10^{-5}$ g
	Nonorthogonality	$\pm$ 15 sec of arc
	Base alignment	$\pm$ 5 sec of arc
	Threshold sensitivity	$10^{-5}$ g

Table 19.4  
Digital Computer Characteristics

<u>ASC-15</u>	<u>Characteristic</u>	<u>Advanced</u>
Serial	Operation	Serial, whole value
172.8 kc	Bit rate	0.5 to 1.0 mc
23 or 24 bits + sign	Word length	22-30 bits + double precision
Drum, 6000 words	Memory	Solid state; 6000-8000 words, nondestructive random access
312 $\mu$ sec	Add/sub times	50-100 $\mu$ sec
1.87 msec (23 bit accy)	Multiply times	400-800 $\mu$ sec
23 ms (subroutine)	Divide times	0.7 to 1.5 msec
89 lb	Weight	20-30 lb
2.75 ft <sup>3</sup>	Size	0.2 to 0.3 ft <sup>3</sup>
70 w ac	Power	20-40 w
190 w dc		

subcomponents, detailed circuitry design, and packaging to incorporate advancements in the state of the art. Although these advancements are expected to decrease the size, weight, and power requirements considerably, this is a by-product as the changes will be primarily for improved reliability.

#### 19.3.4 Actuators

Because of the large mass of the engines, the structural compliance of the engine and thrust frame, thrust vector alignment tolerances, the severe environment, and many other factors, engine gimbaling is difficult. The specific actuation problems and consequently the resulting design are unique for each stage of the various Saturn configurations.

Control of the H-1 engine on the Saturn S-1 stage requires use of pressure feedback stabilization within the hydraulic system to overcome the inherent instability caused by the mass and compliance of the gimbal system. A similar problem, though more severe, will be encountered in the gimbal system of the F-1 engine in the first stage of the Saturn C-4 vehicle. In addition, the much larger torques involved will further complicate the problem. The actuator designed for use with the F-1 engine must produce a torque of 4,600,000 in. lb at an operating gimbal velocity of 10 deg/sec, equivalent to a power output of 120 hp. A hydraulic flow rate of 150 gpm is required. A hydraulic valve having three stages of amplification, rather than the one and two stage varieties employed on most vehicles, will be necessary. Simple pressure feedback within the hydraulic system will probably not provide the necessary stabilization while maintaining adequate stiffness. Frequency and load sensitive hydraulic feedback and/or electrical feedback within the gimbal loop will be used to obtain the desired degree of stability and stiffness.

Gimbaling of the J-2 engine employed in the upper stages of the Saturn C-4 does not present so severe a stiffness and stabilization problem as does the F-1 since the masses and torques are much lower. Preignition environment is much more severe, since the hydrogen-oxygen engine must be prechilled to a temperature incompatible with a conventional hydraulic system. The solution lies in the development of a hydraulic system which can be insulated and heated as required or in the development of a system; for example, a pneumatic system which is compatible with the low temperatures. The former solution requires less development and will probably be employed on earlier vehicles where the J-2 engine will be used only on the S-II stage. In such an application, wherein the engine and control system must operate after coasting phases in orbit, a pneumatic system may be the best solution.

For control in orbit and rendezvous maneuvers, an attitude control system for the orbiting stages is required. On a typical Saturn C-4



injected stage, a system composed of 10 thrust units in the 5 lb to 200 lb class provides adequate control. The jets would be fixed-direction on-off liquid-propellant thrust units. Although nitrogen gas and hydrogen peroxide thrust units have been used extensively in the past, the development status is such that hypergolic units with the advantage of higher specific impulse will be available for Saturn C-4 missions.

#### 19.4 Conclusions

Guidance and control systems for large future space carriers will evolve by a gradual improvement of today's inertial guidance and control systems of ballistic missiles rather than by the adaptation of radically new methods and components.

The authors do not believe that many of the futuristic schemes, such as those employing nongimbaled inertial components, or inertial sensors applying electrostatic suspension or cryogenic principles, can be used for the first generation of large space carrier vehicles. Likewise, complex adaptive control techniques are not seriously considered at this time since in most proposed systems the additional complexity more than offsets the advantages gained. Analyses of digital filtering techniques as applied to the structural bending problem are not sufficiently advanced to determine the relative merits as compared with analog filtering techniques. Analyses leading to the development of such techniques will be continued, however, in the hope that practicable approaches will evolve.

In certain other areas, the development is more advanced and, with some additional development effort, components which can be gainfully employed will be available. Examples include the application of thin-film circuitry and new packaging techniques in the area of digital computers and the use of digital command systems. It is expected that some of these advanced techniques will be applied in the large carrier vehicles discussed in this paper.

Power supplies require additional development effort at the present time. A large portion of the weight allowance given to guidance and control components for the large space carrier vehicles is used for the power supply. The development of power supplies, which have a better weight to energy ratio than can be obtained from currently available sources or from current developments, will result in a significant weight saving that can be applied directly to payload capability. An example to be studied in this area is nuclear power conversion.

## References

1. Orbital Operations Preliminary Project Development Plan, Compiled by Marshall Space Flight Center, Committee for Orbital Operations, Huntsville, Alabama, September 15, 1961.
2. Miner, W. E. and D. H. Schmieder, The Path-Adaptive Mode for Guiding Space Flight Vehicles, American Rocket Society preprint 1944-61 (August 1961), New York.
3. Schmieder, D. H., and N. J. Braud, Implementation of the Path-Adaptive Guidance Mode in the Steering Techniques for Saturn Multi-Stage Vehicles, American Rocket Society preprint 1945-61 (August 1961), New York.

## 20

## FLIGHT SIMULATION OF ROCKETS AND SPACECRAFT

H. H. Hosenthien and J. Boehm

Astrionics Division  
George C. Marshall Space Flight Center  
National Aeronautics and Space Administration  
Huntsville, Alabama

### 20.1 Historical Remarks and General Considerations

Research and development costs for rocket and spacecraft navigation systems would be exorbitantly high if the feasibility, performance, and reliability of these systems and their components had to be proven only by real flight tests. This fact was, by necessity, fully recognized at the very beginning of the guided rocket development at the German Rocket Center in Peenemünde. Apparatus was developed to simulate rocket flight in the laboratory enabling stability ranges, navigation characteristics, influence of nonlinearities, etc. to be studied.

As early as 1939, a one-axis, mechanical simulator was conceived for imitating the motion of the rocket about its center of gravity. This first simulator of the differential equation of motion about the rocket center of gravity was followed, in 1941, by a second generation type consisting of mechanical, electrical, and electronic elements. It was capable of simulating the combined attitude control and trajectory guidance dynamics throughout the powered flight of the rocket. The development time of the V2 navigation system was sharply reduced by the use of these devices [1].

During the past two decades one could observe that simulation techniques in rocket flight adhered closely to a pattern of work phases discussed below. The requirements to be fulfilled during the development of a navigation system for a guided rocket are inferred from the specific rocket type, the chosen rocket path, the aerodynamic coefficients, the structural limitations (stress), and several other limiting factors. The behavior of the guided rocket in flight is comprehensively presented by a set of complicated differential equations which mostly contain nonlinearities originating from such effects as hysteresis, saturation, and backlash.

The solution of these differential equations furnishes essential design characteristics for the layout of the system and its components. The difficulties in evaluating the rocket flight equations are mastered by

simulation techniques. First, a plain mathematical approach is taken to the simulation of the problem by pursuing a step-by-step procedure. Simplified versions of the problem are formulated, and then are simulated by analog computers in which the physical system quantities are substituted by electrical analogs. These simulations facilitate study of the type of problem involved. The simulators have five advantageous qualities which are used extensively during the investigation: (1) a high rate of test repetition; (2) relief from complete mathematical statement of the problem; (3) simple coefficient variations; (4) simple introduction of modifications or changes; and (5) important reduction of investigation time.

Based on the results of the mathematical simulation, the investigation is carried on by a second simulation phase during which actual flight components are introduced into the simulation circuit. Thus, the navigation system is flown in the laboratory by an arrangement which combines simulation and functioning of flight components. This phase of simulation is particularly helpful in gaining judgement and experience on how the selected navigation system and its components will behave in real rocket flight. It is also possible to check available components for their system suitability, and to test newly developed components against prescribed performance requirements.

Astronautics has opened a broad new field of simulation applications. A great variety of simulators capable of testing both men and space vehicles is necessary to prepare thoroughly for space flight. In addition to simulation of the space environment, simulation of space flight navigation is also important. The rotary dynamics aspect of weightlessness is simulated by supporting the imitated spacecraft on spherical air bearings. Space motion simulators and simulation systems are either available or under development for studies of three-axis attitude control studies, unmanned and manned orbital rendezvous maneuvers spacecraft reorientation lunar orbits etc. Navigational training simulators will prepare the space pilot for his later tasks in outer space.

## 20.2 Simulation of the Differential Equation of Motion About One Axis Through the Rocket's Center of Gravity

Pressing time schedules and navigation problems in the development of an adequate, reliable control system soon demanded laboratory simulation of flight conditions to overcome principle difficulties. This chapter presents the evolution of the motion simulator for study of dynamic rocket behavior in motions about the center of gravity.

The apparatus to be provided was to simulate the moment equation of the rocket

$$M_{\theta} + M_D + M_1 = M_2 + \sum M_{\text{Dist}} \quad (20.1)$$

$$\ddot{\phi} + d\dot{\phi} + c_1\phi = c_2\beta + \sum \frac{M_{\text{Dist}}}{\theta} \quad (20.1a)$$

The following quantities are included:  $\theta$  = moment of inertia;  $M_{\theta}$  = inertial reaction moment;  $M_D$  = damping moment;  $M_1$  = restoring moment;  $M_2$  = control moment;  $M_{\text{Dist}}$  = disturbing moments;  $\ddot{\phi}$  = angular acceleration;  $\dot{\phi}$  = angular velocity;  $\phi$  = attitude angle;  $\beta$  = vane deflection;  $d$  = damping coefficient;  $c_1$  = restoring moment coefficient; and  $c_2$  = control moment coefficient.

As early as May 1940, stability investigations of control systems were started with the help of a simulation device. The mechanical apparatus conceived for this purpose is shown schematically in Fig. 20.1a and 20.1b. Nearly all control system components are arranged on a platform which is balanced on knife-edges. The moment of inertia  $\theta$  is given by the mass distribution of all moving parts about the rotation axis. The restoring moment  $M_1 = c_1\phi$  and the control moment  $M_2 = c_2\beta$  are generated by pairs of tension springs which are located symmetrically to the rotation axis. Springs were applied to obtain the moments instantaneously. Fig. 20.1a presents the simulator at the reference attitude position,  $\phi = 0$  deg.; the platform is illustrated in a deflected position in Fig. 20.1b. At a deflection of the platform, the  $c_1$ -pair of springs produces, as desired, a moment proportional to the attitude angle  $\phi$ . The lower ends of the  $c_2$ -pair of springs are attached to the frame by a swing. The upper ends are hinged to a carriage which can be displaced relative to the simulator platform. The carriage motion occurs in response to the actual servo drive of the control system. The displacement of the carriage is directly proportional to the output angle  $\beta$  (vane deflection) of the servo actuator shaft. Therefore, the moment produced by the  $c_2$ -springs is proportional to the vane deflection, thus representing the control moment  $M_2$ . It is apparent from Fig. 20.1b that the restoring moment  $M_1$  is obtained by varying the tension force in the  $c_1$ -springs caused by the motion of the platform. The control moment  $M_2$  is mainly generated by changing the leverage of both  $c_2$ -springs at roughly equal tension force. At a counterclockwise motion of the servo output shaft, Fig. 20.1b, the carriage moves to the right, thus increasing the lever arm of the right spring and simultaneously decreasing the lever arm of the left spring by the same amount. This change of the lever arms causes a clockwise acting moment  $M_2$ . Because of both the finite length of all the springs and the geometry of the simulation device, exact proportionality between the moments  $M_1$  and  $M_2$ , and the angles  $\phi$  and  $\beta$  does not exist. But for practical purposes, proportionality can be assumed within the machine's angular range of mobility.

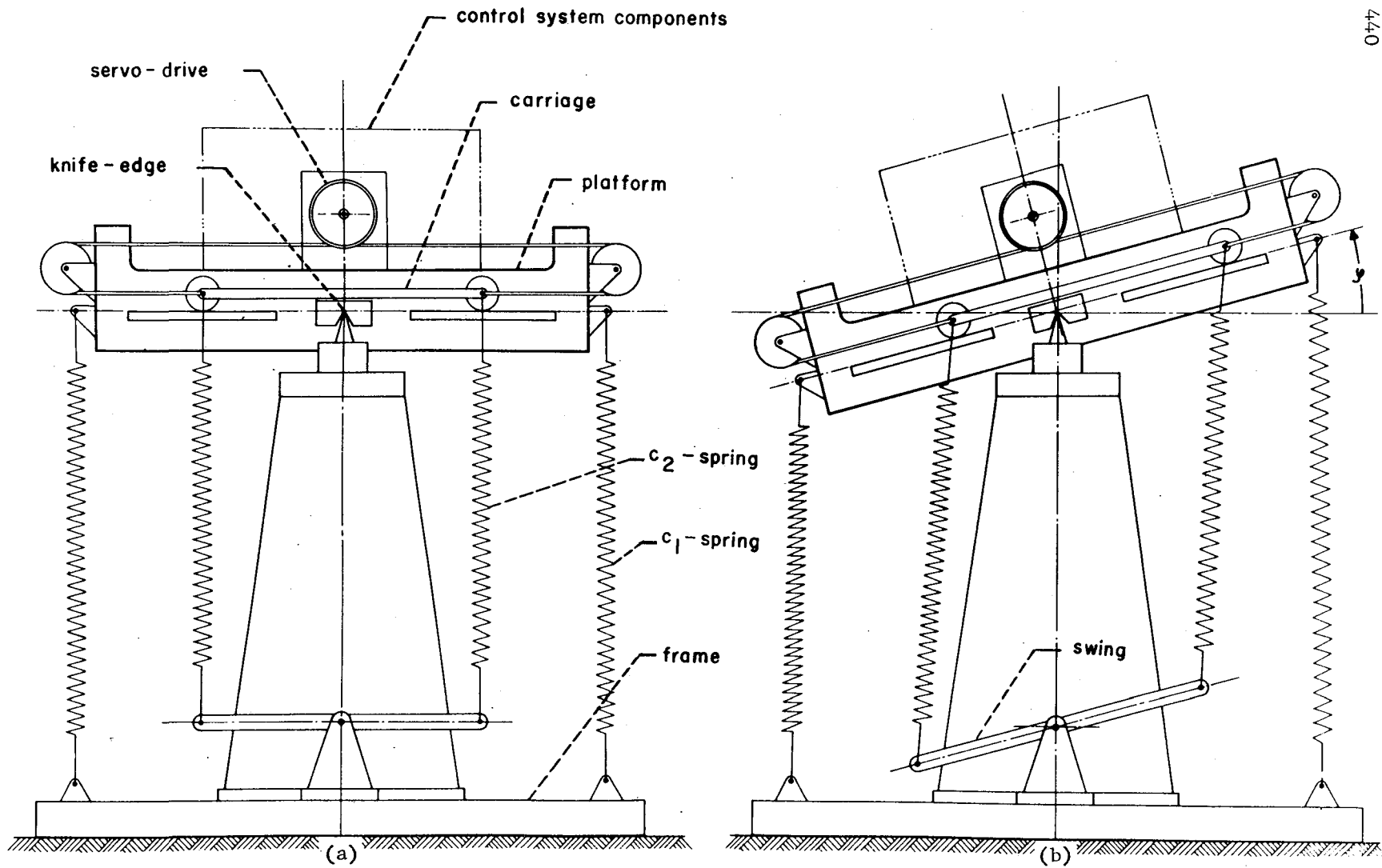


Fig. 20.1 Scheme of first mechanical motion simulator (one axis).

The friction moment in the support elements, predominantly constant in magnitude and changing in direction with directional changes in angular velocity of the platform, was to be made negligible since this moment had no equivalent in actual flight. To minimize undesirable friction, the platform was supported on specially shaped and treated knife edges. The moments  $M_D$  and  $M_{Dist}$  were not considered by this simulator.

In spite of its shortcomings, this simulator furnished valuable assistance in the study of navigation systems in the early days of guided rocket development.

A proposal came forth which suggested the stationary mounting of the servo drive (cf. R. Schubert [2]). A new grouping of two pairs of springs was suggested. The transformation of

$$\text{yields} \quad \ddot{\varphi} + c_1 \dot{\varphi} + c_2 \beta = 0 \quad (20.2)$$

$$\ddot{\varphi} + (c_1 - c_2) \dot{\varphi} + c_2(\varphi + \beta) = 0 \quad (20.3)$$

The new spring arrangement was to concur with Eq. (20.3). The pivoted platform now carries only a position sensing device, and is suspended by two pairs of springs. By the action of these springs, the motion of the platform obeys Eq. (20.3). The platform requires from the servo drive a moment which, in opposition to reality, is dependent not only on the vane deflection  $\beta$  but also on the attitude angle  $\varphi$ . The part of the moment proportional to  $\varphi$  appears negligible in relation to the hinge moment acting on the servo drive. The mentioned proposal also points out the need for developing smaller simulation devices by using mechanical and electrical elements.

An improved simulation device by W. Haeussermann considerably advanced the technique of simulation. The scheme of this apparatus is based on a physical pendulum and can be described as follows [3]: The homogeneous part of Eq. (20.1a)

$$\ddot{\varphi} + d \dot{\varphi} + c_1 \varphi = 0 \quad (20.4)$$

is represented by a physical pendulum and an eddy current brake. The size of the damping moment is controlled by changing the field excitation of the eddy current brake shown in Fig. 20.2. At constant moment of inertia  $\theta$ , the restoring moment  $M_1$  is varied by tilting the plane of motion of the pendulum about a horizontal axis. The coefficient  $c_1$  is then proportional to the sine of the tilt angle. To produce the inhomogeneous part of Eq. (20.1a),  $c_2 \beta + \sum \frac{M_{Dist}}{\theta}$ , a moment is imparted

about the pendulum axis by a torquer such as a high performance D' Arsonval movement which can be driven directly by potentiometers or electronic

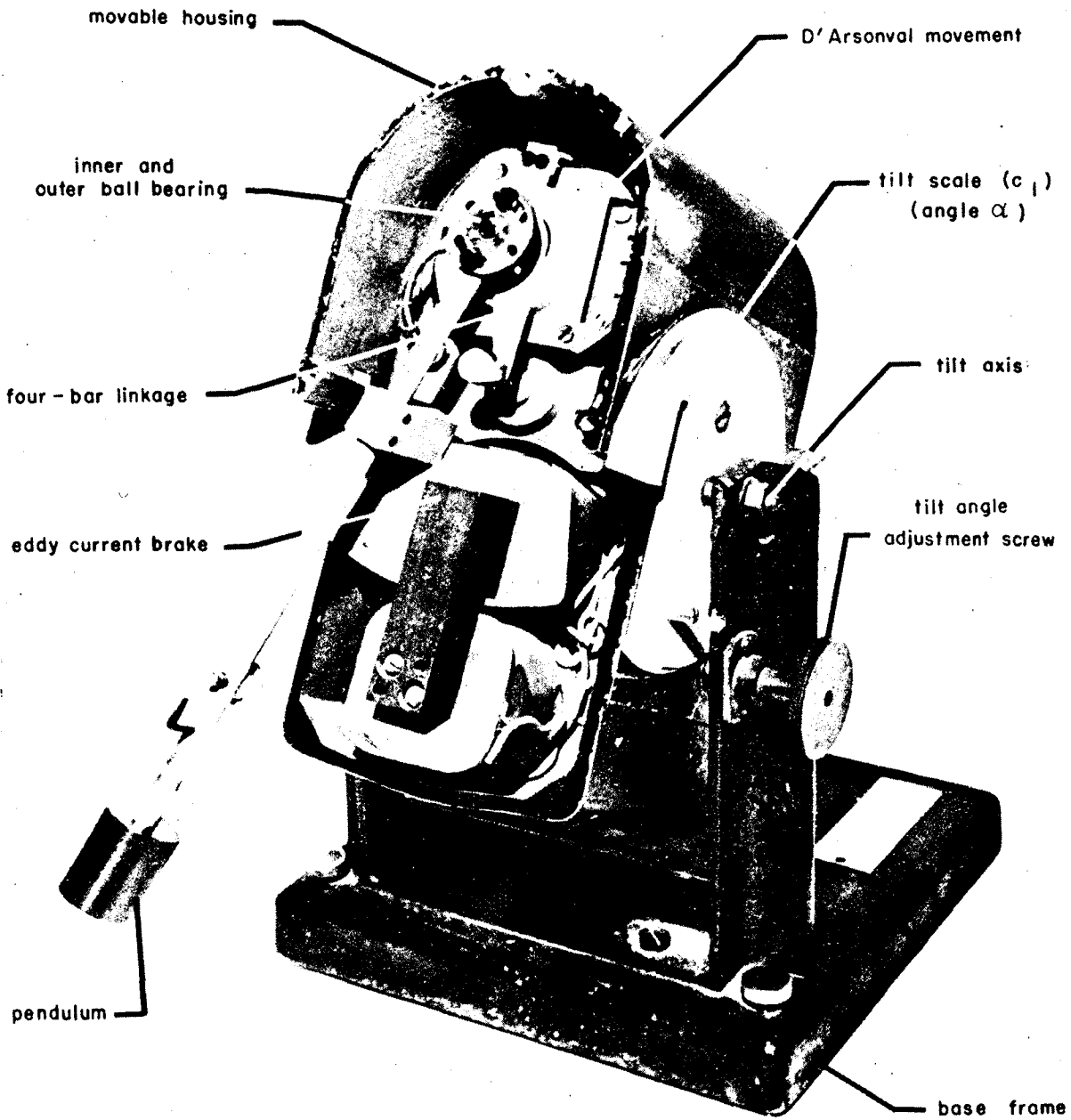


Fig. 20.2a Pendulum motion simulator.



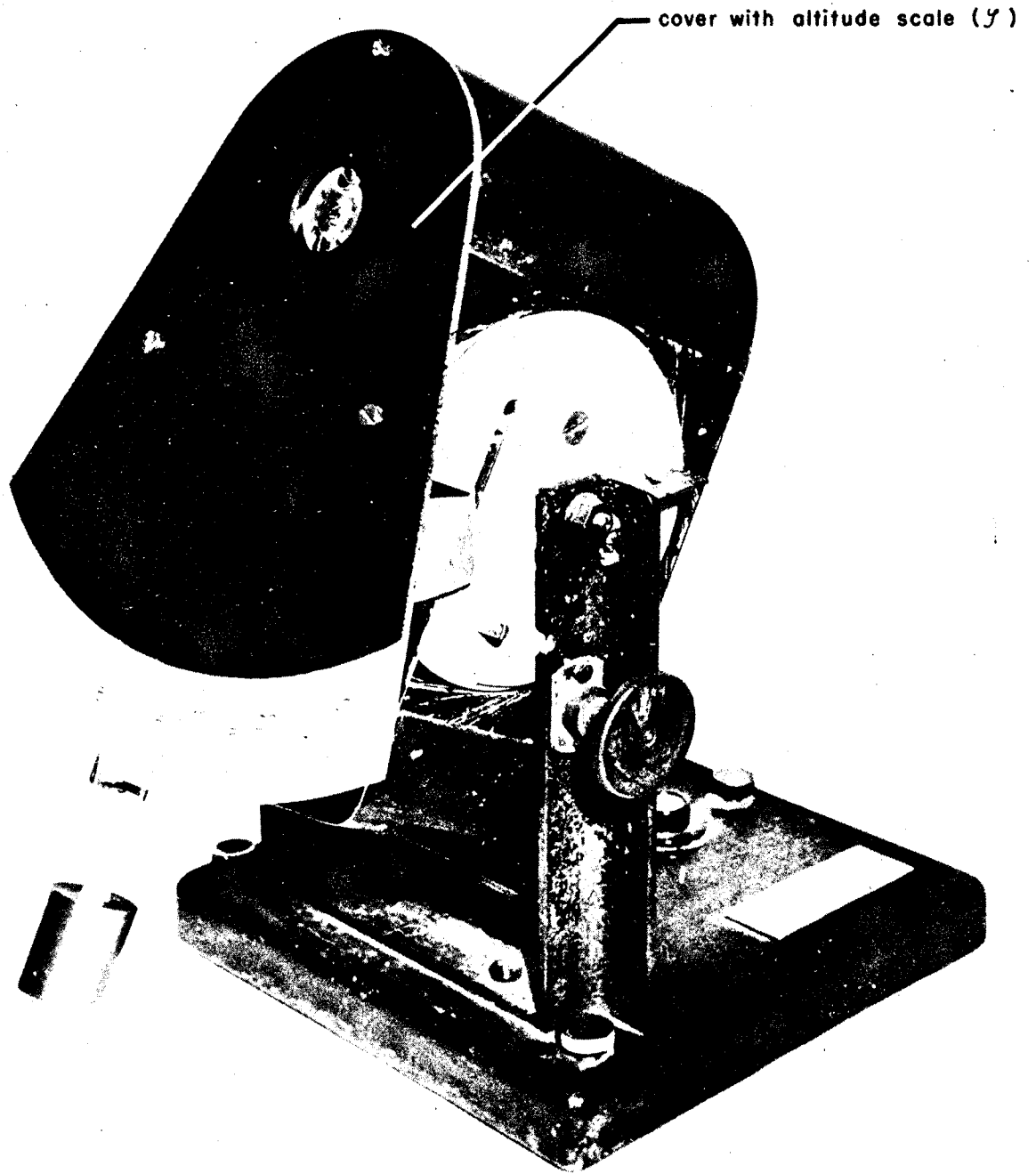


Fig. 20.2b Pendulum motion simulator.

amplifiers. During the development of this simulator, particular care was exercised to minimize the friction in the bearing of the pendulum. The bearing was designed so that the friction moments, constant and dependent only upon the direction of rotation, are transformed almost completely into damping torques which can be included in the calibration of the eddy current brake. To achieve this transformation, one ball bearing is placed inside another ball bearing. The connecting element for these two high-quality ball bearings is a cylindrical sleeve which is rigidly connected by press fit with the outer race ring of the inner ball bearing and the inner race ring of the outer ball bearing. This sleeve is subjected to an oscillating motion which is introduced by a motor-driven, four-bar linkage (eccentric). The sleeve is part of the oscillating follower member of this linkage. When the pendulum is at rest, the clockwise and counterclockwise friction moments cancel on an average. If the pendulum is in motion, the average friction moment is proportional to the pendulum velocity if the frequency and the amplitudes of the oscillating follower member are appropriately chosen. The pendulum simulator excludes the use of attitude sensors in the simulation loop. The attitude information  $\phi$  is provided by a potentiometer, which has the same characteristics as the gyroscope pick-up.

Among the many advantages of this motion simulator are: (1) true and accurate simulation; (2) continuous and convenient variation of the coefficients of the differential equation; (3) perfect calibration; and (4) small size and weight. This pendulum device also allows the simulation of aerodynamically unstable rockets (negative  $c_1$ -values).

An application of this moment equation simulator is illustrated by a block diagram, Fig. 20.3. This diagram of the entire control loop shows the incorporation of the pendulum simulator into the complete laboratory setup. The pendulum attitude ( $\phi$ ) is supplied to the control system; the vane deflection  $\beta$ , appearing at the output of the servo drive, is fed by its electrical analog into the torquer of the pendulum simulator to close the control loop. Figure 20.3 also points out the different inputs such as variation of aerodynamic coefficients and variation of signal ratios and disturbances (wind), for study and investigation of such subjects as the stability ranges of a rocket control system.

Several development trends are shown in the evolution of this motion simulator. The components of the control system were separated from the mass taking part in the simulated motion. This enabled the developers to build smaller and handier simulators. At the same time, the detrimental friction moment in the platform bearings could be diminished. The quality of simulation was improved until reality was closely approximated. Optimum methods of modifying and adjusting coefficients within wide ranges were devised. Continuous variation became possible, and these improvements resulted in a drastic reduction of simulation time.

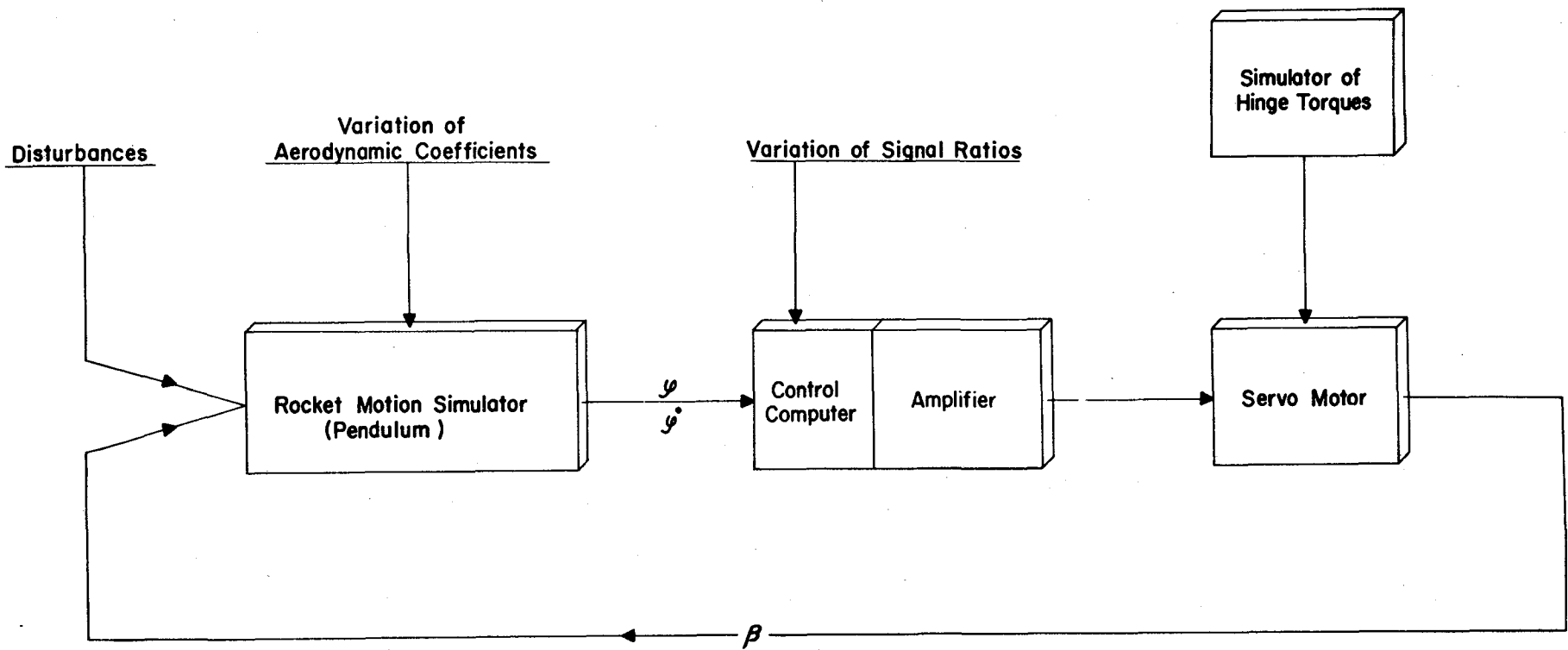


Fig. 20.3 Block diagram of rocket motion simulation about the center of gravity (one axis).

### 20.3 Electronic Rocket Motion Simulation

The development of the world's first guided rocket, the V2 presents an interesting historical study of the viewpoints mentioned previously (cf. Sec. 20.1) The reader can find this story in Ref. [1]. Here the emphasis is placed on the development of simulation techniques which led to a useful rocket control and guidance system.

After successful preliminary test flights of the automatically controlled, small-scale rocket A5, the electromechanical simulation of the anticipated behavior of the full-scale rocket A4 (V2) was started in 1940. The method of attitude stabilization of the V2 rocket by resistor-capacitor networks (rc networks) was successfully demonstrated on the mechanical rocket-motion simulator in mid-1940.

Prior to flight testing, this system was further investigated in a static firing of the V2 in mid-1941. This test may be termed a closed-loop attitude control test of the rocket under static firing. For this test, the rocket was suspended by gimbal joints about its center of gravity within the static firing tower. The V2 was free to perform small angular motions in pitch and yaw during this test. It was successfully demonstrated that the rc stabilizing networks provided the necessary attitude-rate feedback to the carbon jet vanes to damp out the pitch and yaw pendulum motions of the suspended V2. This test was repeated for four different control schemes and equipment for performance comparison. The one system using stabilization by electrical rc networks, proposed and developed by Helmut Hoelzer, was found to be feasible and was selected for the operational V2.

Motivated by this success and experience gained with rc stabilizing networks, Dr. Hoelzer proposed the development of a special purpose analog computer that was to become vital in the simulation of the control and guidance dynamics of the V2. It was finished in bread-board form by Otto Hirschler in 1941, and was finally extended to simulate translational motions.

The following account of the development of flight-dynamical simulation of the V2 by using an electronic analog computer, covering the period from 1941 to 1945, is based on Helmut Hoelzer's dissertation [4].

Radio beam guidance and full inertial guidance were under investigation; both types had been actively pursued, and both were well advanced in their theoretical and component development by the end of World War II. However, radio beam guidance will be used here to illustrate the state of development of flight-dynamical simulation during that time.

The radio-beam guidance of the V2 acted in the yaw plane only. Since the attitude control in the pitch, yaw, and roll axes was chosen, tight coupling effects between them could be neglected. The following system of differential equations, obtained from first-order perturbation of the standard trajectory, describes the flight mechanics of the V2 in the yaw plane with an accuracy sufficient for simulation. From balance of forces in yaw,

$$\ddot{\epsilon} + k'\dot{\epsilon} = c_2^1\phi + c_2^1\beta + W_\epsilon W \quad (20.5)$$

From balance of moments in yaw,

$$\ddot{\phi} + d\dot{\phi} = -c_1\phi - c_2\beta + k\dot{\epsilon} + W_\phi W \quad (20.6)$$

The symbols in Eq (20.5) and (20.6) are defined as follows:

$\epsilon$  = deviation of trajectory with respect to reference radio guidance surface, obtained as an output signal from the on-board guidance receiver.

$\phi$  = yaw attitude deviation angle of the rocket axis with respect to a space fixed direction of the yaw attitude gyro.

$\beta$  = control vane deflection angle, obtained as an electrical signal from a potentiometer attached to control vane.

$W$  = wind velocity.

$k'$  = lateral acceleration per unit lateral deviation velocity.

$c_1^1$  = lateral acceleration per radian yaw attitude angle.

$c_2^1$  = lateral acceleration per radian yaw vane deflection.

$W_\epsilon$  = lateral acceleration per unit lateral wind velocity  $W$ .

$k$  = yaw angular acceleration per unit deviation velocity.

$c_1$  = yaw angular acceleration per radian attitude angle.

$c_2$  = yaw angular acceleration per radian vane deflection.

$W_\phi$  = yaw angular acceleration per unit wind velocity  $W$ .

$d$  = yaw angular acceleration per radian/sec attitude rate (aerodynamic damping coefficient).

It is the task of the control and guidance system to command the control vanes so that attitude error,  $\phi$ , and path deviation,  $\epsilon$ , are kept within tolerable limits under disturbances (winds) and under the influence of misalignments (of vanes, fins, etc.) to restrict the residual errors at the end of a flight phase (at cutoff) to limits prescribed by the rocket's mission. This task has to be performed in such a manner that the rocket is stable at all times while in flight with respect to attitude control and path guidance dynamics. To meet these requirements, the following control equation is used in the on-board control and guidance computers

$$\dot{\beta} + m_0\beta = e_0\epsilon + e_1\dot{\epsilon} + e_{-1} \int \epsilon dt + a_0\phi + a_1\dot{\phi} + a_2\ddot{\phi} \quad (20.7)$$

where:

$a_0$  = attitude control gain

$a_1$  = attitude-rate control gain

$a_2$  = attitude-acceleration control gain

$e_0$  = path-deviation control gain

$e_1$  = path-deviation rate control gain

$e_{-1}$  = path-deviation integral control gain

$m_0$  = gain of control vane servo drive

Control Eq. (20.7) is presented in idealized form, neglecting additional time constants and nonlinearities of the actual equipment.

A block diagram for dynamical simulation of the V2 navigation system (including radio-guidance and control hardware) is presented in Fig. 20.4. The top section of Fig. 20.4 represents the electronic simulation of lateral force Eq. (20.5); the middle section of Fig. 20.4 represents the electronic simulation of moment Eq. (20.6); and the right bottom section contains the on-board equipment: the control computer, the guidance computer, and the hydraulic vane drives. By the inclusion of the on-board equipment in the simulation, the representation of control Eq.

20.7 is physically extended to the actual case comprising nonlinearities and additional time lags. Two major feedback loops are represented in Fig. 20.4.

1. The attitude control loop from the yaw-gyro through the control computer, vane drive, vane position ( $\beta$ ), and back through the moment equation simulator to the yaw gyro.

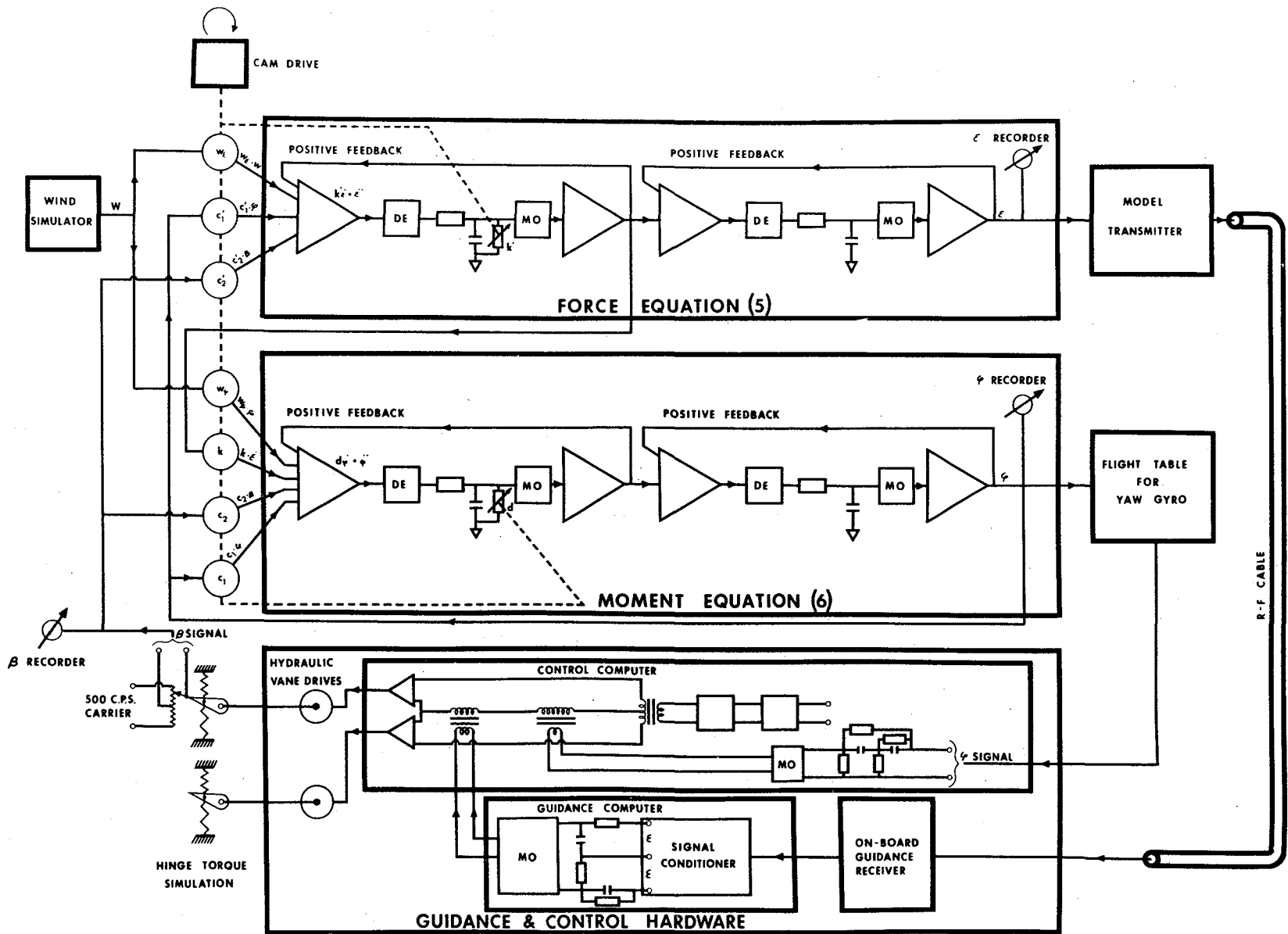


Fig. 20.4 Block diagram of dynamical simulation of V2 navigation system (yaw).

2. The radio-guidance loop from the model transmitter (simulating the radio-guidance ground station) through the rf cable, on board guidance receiver, guidance computer, control computer, vane drive and vane position ( $\beta$ ), and back through the lateral-force simulator to the model transmitter. The lower left section of Fig. 20.4 shows schematically the hinge-torque simulation by means of springs restraining the deflection of the vanes. To introduce wind disturbances similar to in-flight condition (wind profiles versus altitude as well as wind gusts), a wind simulator is shown on the left of the top section of Fig. 20.4.

Principally, the electronic simulation of force and moment Eq. (20.5) and Eq. (20.6) is accomplished, respectively, by integrating  $\ddot{\epsilon}$  and  $\ddot{\phi}$  twice. To obtain  $\dot{\epsilon}$  and  $\dot{\phi}$  alone, the effect of the terms  $k'\dot{\epsilon}$  and  $d\dot{\phi}$  were eliminated by deliberately imperfect integration in the first integrators. This is shown by the variable leakage resistors, marked  $k'$  and  $d$ , respectively, across the integrating capacitors.

To simulate the time-variation (due to changes of air density, velocity, mass, moment of inertia, center of gravity and center of pressure position, jet vane erosion, etc. with real flight time) of the coefficients ( $W_{\epsilon}$ ,  $c_1^i$ ,  $c_2^i$ ,  $k_1^i$ ,  $W_{\phi}$ ,  $c_1$ ,  $c_2$ ,  $k$ , and  $d$ ), a set of properly cut cams arranged on a common shaft is driven by an adjustable constant-speed drive in real flight time. Each cam actuates a variable resistor or potentiometer to produce the desired gain variation in the simulation loops.

A photograph of the electronic motion simulator of the V2 is shown in Fig. 20.5. The upper part of the simulator contains the electronic analog computer components; timer; wind simulator; model transmitter; meters for  $\epsilon$ ,  $\phi$ ,  $\beta$ , and flight time; operational and calibration controls; etc. The cam drive for variable coefficient simulation is shown in the lower section of the photograph. In the bottom section are power supplies and a rotating inverter to produce the 500 cps carrier frequency signal.

The signals used in the force-equation and moment-equation simulation, Fig. 20.4, are suppressed-carrier amplitude modulated, except inside the four integrators where the signals are demodulated prior to application to the rc integrating networks. After integration the signals are modulated again upon the 500 cps reference carrier. The demodulators and modulators are indicated in the block diagram, Fig. 20.4. An ac carrier was employed instead of dc, which modern simulators use, because modern high-gain, zero-drift stabilized dc amplifiers were not available during the period from 1941 to 1945. However, good ac amplifiers were available during design of the V2 simulator. The summation of the right-hand terms of Eq. (20.5) and Eq. (20.6) was accomplished by means of transformers, with the secondary windings connected in series in the grid circuit of a high-quality ac amplifier.

The integration of the demodulated ac signal by the rc lag networks shown in Fig. 20.4 (for integration of  $\dot{\epsilon}$  and  $\dot{\phi}$ , respectively), is



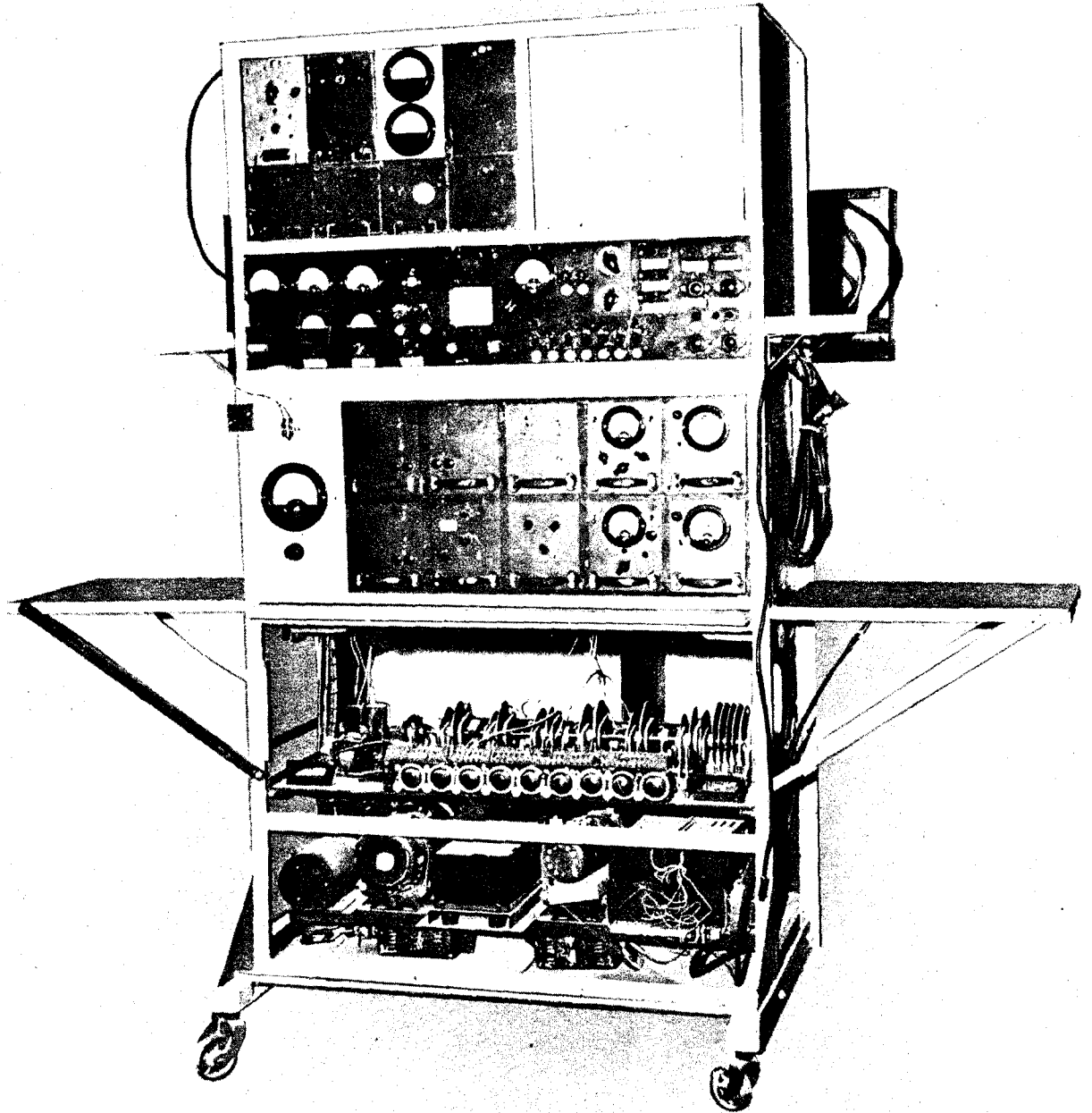


Fig. 20.5 Analog computer for rocket (V2) motion simulation.

imperfect because the capacitor voltage influences the charging current. This effect makes the integrand (the current through the series resistor) dependent on the integral. However, if by means of positive feedback (as shown in Fig. 20.4) the capacitor voltage is added to the input voltage, the effect of the capacitor voltage upon the charging current can be cancelled, leading to nearly perfect mathematical integration within bounds set by the accuracy of the positive feedback adjustment and amplifier linearity.

The accuracy of the electronic V2 motion simulator was checked by comparing numerically calculated rocket response with the simulated response; it was found to be about 5 per cent [4]

The electronic V2 motion simulator, Figs. 20.4 and 20.5, played a very important role in the layout of the V2 control and guidance system, particularly with regard to the best compromise in the choice of control and guidance gains. Several thousand simulation runs were made prior to the end of World War II. All these investigations were carried out in close cooperation with the system designers and flight-mechanical specialists. This cooperation was necessary to ensure maximum utilization of the simulator by flight-mechanics specialists. The designers assisted in calibration and adaptation to the varying requirements of this newly developed device.

A discussion of the results of the V2 simulation has been omitted. However, a full account of these results can be found in [5], which is divided into three parts:

Part I: Tolerances for the radio-guidance system Victoria II;

Part II: Shape of the guidance gain program, performance and limitations of the combined attitude-control and radio-guidance system ..., with special regard to lateral wind response;

Part III: Influence of the vane servo-drive (Lrm 5) characteristics upon trajectory shape and stability of the V2 rocket ....

During the interim period from 1945 to 1950, the von Braun group continued rocket development work on a limited scale at Fort Bliss, Texas. A development unit headed by O. Hirschler started work on a rocket motion simulation facility in 1946. The task of this unit was twofold:

1. Repair and reactivate the V2 motion simulator (Figs. 20.4 and 20.5) which the U. S. Army had shipped from Germany to the United States.
2. Develop a newer, larger, and more flexible rocket motion simulator to be used in the guidance and control studies of anticipated guided missile projects of the Army, using the experience gained in the development of the V2 simulator.

This new development appeared necessary since electronic analog computers were not commercially available at that time.

The reconditioned V2 rocket-motion simulator was very instrumental in the dynamical analysis of the Hermes 2 project. The new simulator was not operational until 1950.

In the following discussion, the new rocket-motion simulator will be termed ac analog computer. It borrowed the following features from the old V2 simulator:

1. The use of suppressed-carrier amplitude modulated computer signals.
2. The application of multi-cam operated function generator to simulate the time-varying coefficients.

The old V2 simulator was strictly a special-purpose machine. Its amplifiers, integrators, cam unit, etc., were permanently interconnected. The increased flexibility of the new ac analog computer was achieved by the following main features:

1. Individual summing amplifiers, integrators, and cam-function channels are available which can be patched together on the front side of the computer to adapt to varying simulation problems.
2. A push-button matrix and relays serve to separate remotely or connect the simulated equation system.
3. Improved ac summing amplifier performing summation of terms by resistor networks connected to negative-feedback amplifiers (as in modern dc analog computers); these summing amplifiers allow continuously variable gain adjustment for setting the coefficients of the equations to be simulated.
4. Improved ac integrator design employing integrating capacitors which are electronically switched at carrier frequency in the negative feedback loop of an ac amplifier [6]. This technique eliminates the need of separate modulator and demodulator as in the old ac integrator (Fig. 20.4).

To analyze properly the ac analog computer behavior, an analytical method was developed, based on direct relations among the modulating signals representing the computer variables [7].

The end of the interim period marked the beginning of a new era in electronic simulation technique; an effective zerodrift stabilization method for dc analog computer amplifiers was invented in 1950 [8].

About this same time, an upswing in guided missile development effort occurred. Commercial production provided improved and drift-stabilized dc analog computers needed to speed up the missile projects. Extensive literature on dc analog computers and simulation methods also became available (cf. [9], [10], [11], [12]).

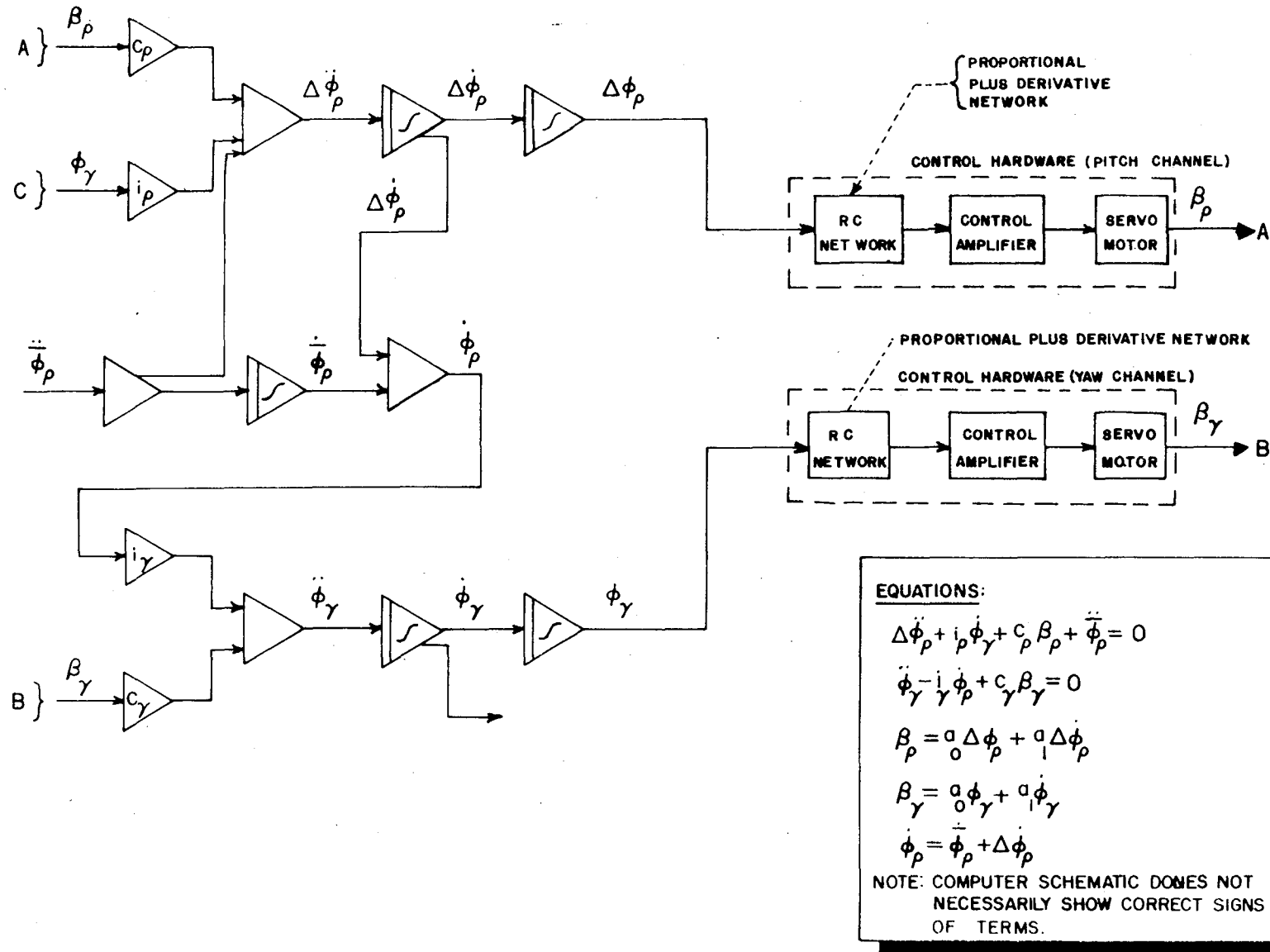


Fig. 20.6 Simulation of injection attitude control of Explorer 1.

As an interesting example of the application of the ac analog computer, the spatial attitude control simulation of Explorer 1 performed by Fred E. Digesu [13] will be described briefly with reference to Fig. 20.6. The problem was to design an attitude control system which would gradually tilt the top unit of the Jupiter C rocket, after separation from the Redstone first stage, into the injection attitude and hold this attitude until firing of the second stage.

The equations simulated are shown in Fig. 20.6, where the subscripts  $\dot{p}$  and  $\dot{y}$  indicate pitch and yaw. The first pair of equations represent the equilibrium of torques in pitch and yaw; that is, the inertial reaction torque, the gyroscopic torque, and the control torque. The second pair of equations express the linearized control equations mechanized by actual control components as shown in Fig. 20.6. The last equation relates pitch rate,  $\dot{\phi}_p$ , to programmed pitch rate,  $\dot{\Phi}_p$  and pitch rate error,  $\Delta\phi_p$ . By means of the derivative of this relation, the first equation has been modified so that the simulation of the large pitch attitude angle,  $\phi_p$ , is avoided.  $\Delta\phi_p$  was used in the simulation instead of  $\phi_p$ . This substitution improves the accuracy and resolution of the pitch simulation to better than 0.1 deg. The gyroscopic moments are caused by the spinning cluster of solid propellant rockets used to launch the Explorer 1 satellite. The gyroscopic moment terms produce a mutual coupling between pitch and yaw, indicated by the terms  $+i_p\dot{\phi}_y$  and  $-i_y\dot{\phi}_p$ . The simulation showed that proper control gains,  $a_0$  and  $a_1$ , could be found that made it unnecessary to decouple the pitch and yaw motions by additional terms and driving functions in the control equations. This highly simplified the control system.

This chapter will be concluded with a brief description of the guidance and control simulation (including flight components) of an IRBM (Jupiter) in the pitch plane. This simulation was to determine the final guidance and control scheme and component design with regard to stability and response, and was to serve as a functional test prior to actual flight. Figure 20.7 shows the simulation arrangement in block form, including only the essential variables and devices arranged in three sections: simulated missile dynamics, special simulation devices, and guidance and control flight components.

The left section, simulated missile dynamics, represents the analog computer setup simulating:

1. Rigid body dynamics: the equations of translational and rotational motions of the rigid missile body in pitch;
2. Elastic body dynamics: the equations describing bending modes referenced to the rigid (neutral) missile longitudinal axis;
3. Sloshing dynamics: the equations describing translational and rotational motions of the propellants in pitch.

The rigid body, the elastic body, and the sloshing dynamics form a system of coupled differential equations, the time-varying coefficients being simulated by the real time arbitrary function generator (such as a constant-speed cam device).

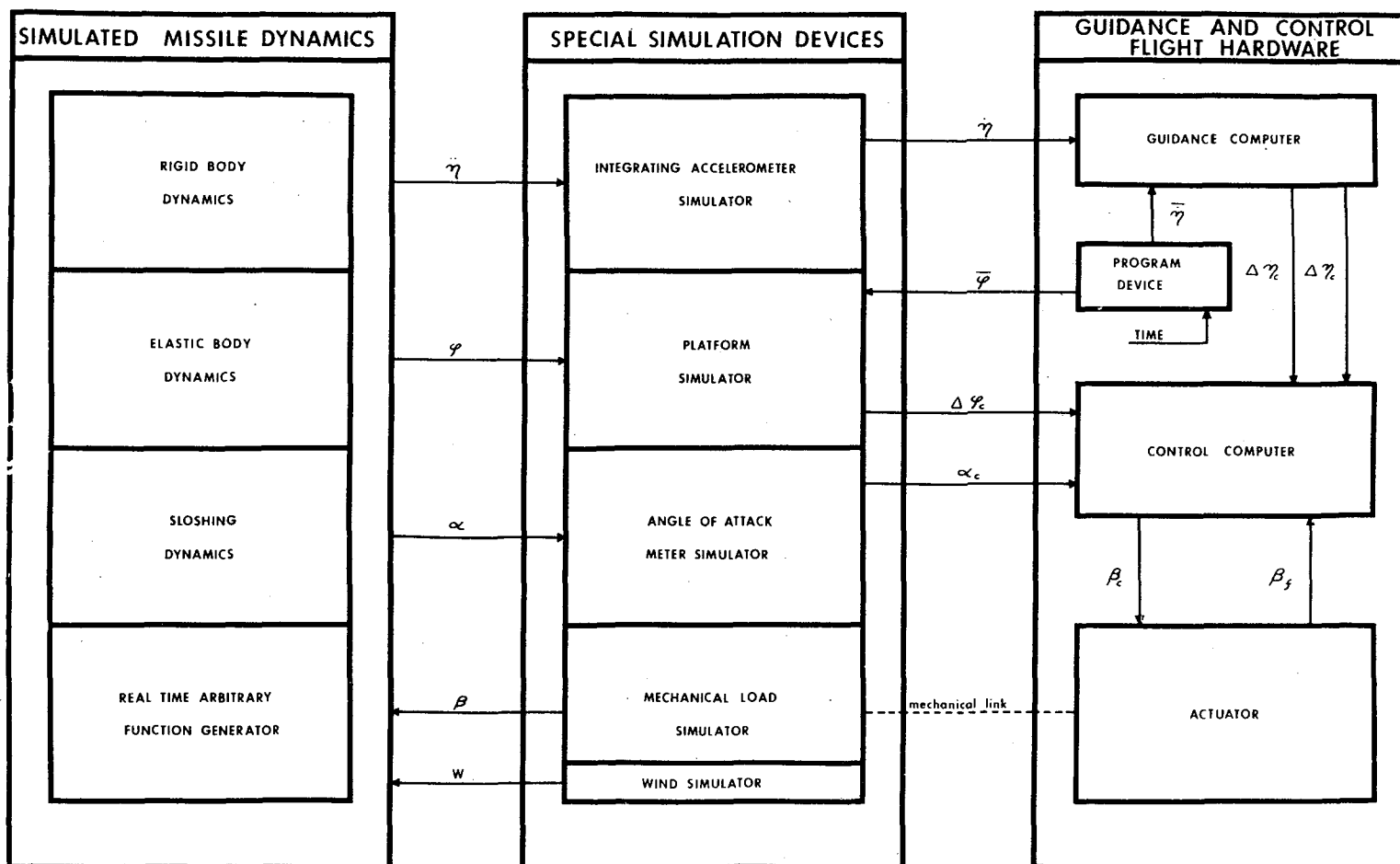


Fig. 20.7 Block diagram of Jupiter IRBM guidance and control (pitch).

Two inputs are applied to the simulated missile dynamics:

1. Simulated swivel-engine deflection,  $\beta$ , obtained electrically from the mechanical load simulator (cf. Figs. 20.8a and 20.8b);
2. Wind velocity,  $w$ , obtained from the wind simulator.

Three outputs are furnished by the simulated missile dynamics:

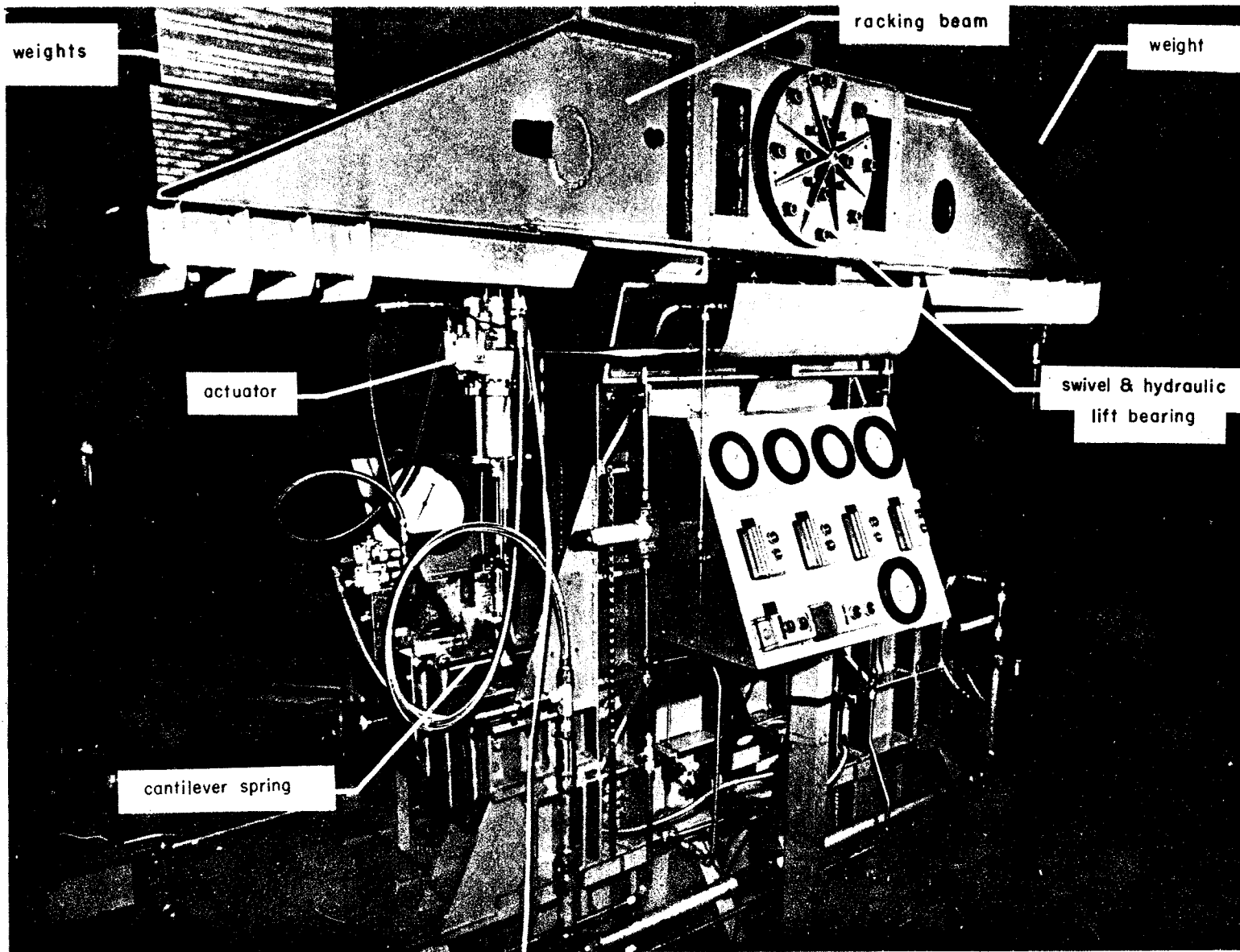
1. Slant-altitude acceleration,  $\ddot{\eta}$ , to be integrated by the integrating accelerometer simulator before application to the guidance computer;
2. Total attitude angle,  $\phi$  (including the effect of body bending), to be processed by the platform simulator before application to the control computer;
3. Angle of attack,  $\alpha$  (including effects from body bending), to be applied to the angle-of-attack meter simulator feeding the control computer.

The guidance computer receives the slant-altitude velocity,  $\dot{\eta}$ , as a synchro shaft position, compares it with the programmed standard velocity  $\bar{\eta}$  from the magnetic-tape programmer, and applies the guidance velocity error command,  $\Delta\eta_c$ ; then after integration the displacement error command,  $\Delta\eta_c$ , to the control computer.

The pitch attitude error command,  $\Delta\phi_c$ , is obtained by comparing total attitude,  $\phi$ , with programmed attitude,  $\bar{\phi}$ , in the platform simulator and is furnished to the control computer. The indicated angle of attack,  $\alpha_c$ , from the angle-of-attack meter simulator is fed to the control computer.

Within the control computer, the guidance, attitude, and angle-of-attack commands are modified by a control gain programmer. In addition, the attitude and angle-of-attack commands are shaped by electrical networks to insure stability of rigid and elastic body modes. The modified signals are summed and compared to the control position feedback signal,  $\beta_f$ , to produce the error command,  $\beta_c$ , which is applied to the swivel-engine control actuator.

The hydraulic actuator drives the mechanical load simulator, Figs. 20.8a and 20.8b, which simulates (by rocking beam with weights attached) the inertial properties of the swivel engine as well as the compliance of the thrust frame (by cantilever spring at lower tiepoint of actuator). The load simulator consists of a horizontal beam supported at the center by a hydraulic lift bearing (to simulate swivel bearing friction). This bearing is a true replica of the actual swivel bearing, used here in only one plane. In Fig. 20.8b the mechanical brake can be seen which is linked to the rocking beam to adjust the damping of the gimbal resonance mode.



458

Fig. 20.8a Mechanical load simulator for IRBM hydraulic actuators.



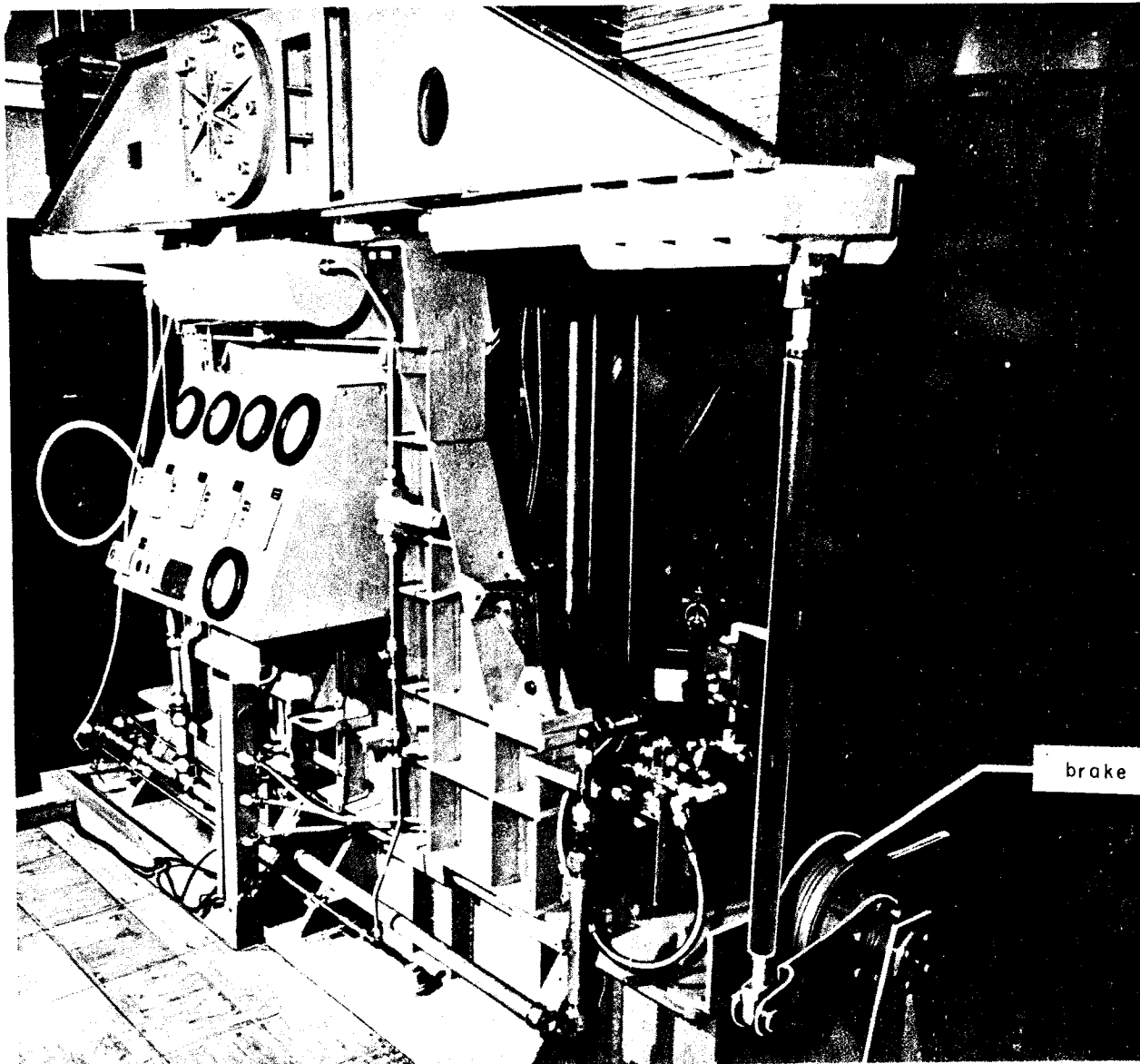


Fig. 20.8b Mechanical load simulator for IRBM hydraulic actuators.

## 20.4 Simulation of Space Flight

The advent of space technology gave strong incentive for the development of simulation techniques. The requirements of space flight demand swift advances in the field of simulation. The evolving simulation tasks may be classified into the following three principal types: (1) simulation of attitude control and guidance systems; (2) simulation of space environment for testing and checking the reliable functioning of the system's components under space environmental conditions; and (3) simulation of both craft and environmental conditions for training the space pilot. This section will be devoted to some considerations of simulation for the study of space flight navigation systems.

The scope of these simulation tasks is rather extensive. Problems to be studied and investigated using simulation techniques pertain to flight phases such as orbital rendezvous maneuvers, lunar or planetary midcourse guidance, reorientation of satellites and spacecraft, lunar and planetary orbits, etc. Within the limits of this paper, only two simulation projects are discussed, the simulation of weightlessness for rotary dynamics and the simulation of orbital rendezvous maneuvers within the confines of a laboratory. Both areas dealt with in this section can be considered as typical cases. The first simulation task deals with a basic simulation detail required for nearly all laboratory investigations in matters of space flight, and the second value presents a characteristic system simulation.

To simulate for rotary dynamics investigations (the state a spacecraft encounters while coasting in orbit or on a deep space path), a frictionless suspension of a platform (duplicating the spacecraft) with full angular freedom of motion about three mutually perpendicular axes is to be devised. Moments of inertia, neutral equilibrium at any attitude, and absence of undesirable external moments are required characteristics of an ideal simulator. It is impossible to meet completely all these requirements with a simulation apparatus. Therefore, a simulation device with acceptable and controllable deviations from the ideal conditions will be developed.

In 1959, W. Haeussermann conceived a motion simulator scheme which lent itself remarkably well to simulated weightlessness. First, the simulator was planned for studies of integrated spatial attitude control systems. The scheme of this simulation device, which was designated Satellite Motion Simulator, is based on the use of a spherical air bearing for suspension of the simulated spacecraft at practically negligible friction.\*

\* This apparatus was successfully developed at the Guidance and Control Laboratory of the former Army Ballistic Missile Agency, Huntsville, Alabama, later to become Astrionics Division of the George C. Marshall Space Flight Center [14].

The two outstanding elements of this space motion simulator are the platform, simulating the spacecraft, and the spherical air bearing, giving frictionless suspension. The design characteristics for the layout of the platform are established by considering quantities such as representation of suitable moments of inertia (pitch, yaw and roll), size, weight, angular mobility ranges about three mutually perpendicular axes (pitch, yaw and roll), appropriate mounting surfaces for both systems and auxiliary components, isoelasticity, antimagnetism, and immunity from temperature variations. The particular shape of the platform shown in Fig. 20.9 resulted from the great mobility ranges necessary (pitch  $\pm 120$  deg, roll  $\pm 120$  deg and yaw unlimited) and given movement of inertia ratios. A symmetrically shaped, circular, disk-like, platform offers better mounting surfaces, a box design for higher rigidity (which is most desirable to minimize unbalance moments), and less dependence upon temperature influences. Such a design can be applied when the mobility ranges in pitch and roll are reduced to approximately  $\pm 90$  deg. The platform is built from nonmagnetic material, and special treatment prevents warping.

Great attention must be given to the layout and manufacture of the spherical air bearing. In several similar motion simulators, built at various research and development centers, a stainless steel sphere of 10-in. diameter is applied. To avoid unbalance because of imperfect spherical shape, the sphericity must be correct to very small limits of tolerance. By special manufacturing techniques, it was possible to produce spherical air bearings with a tolerance of 0.000001-in. These tolerances must be fulfilled for both the steel sphere and the supporting cup. The air cushion of the bearing is approximately 0.002-in. thick, and the air pressure used is approximately 100 psi. The bearing is designed and manufactured to float smoothly as a stable body within its 6-in. rim diameter supporting cup. The cup has tiny holes which are equally spaced in two concentric circles. The simulator of Fig. 20.9 shows the rotatable and specially shaped support leg of the platform. To prevent collision between the platform and the support leg, the support leg should have a servo-driven automatic displacement. In this way, the area can be cleared for all possible deflections of the platform.

Even with very refined means of compensation, the unbalances cannot be completely eliminated. The efficient operation of the simulator required a reduction of unbalances to approximately two to three magnitudes under the maximum control moment furnished by the system. Since this moment is diminutive, it is not to exceed approximately 3 g-cm at any attitude of the platform. Such small total unbalance torque has been accomplished in praxis. The compensation of predictable unbalances was achieved by means of an adjustable mass on a cantilevered leaf spring which is fastened to the platform [14]. This device was used for the three rotation axes to simplify the adjusting procedure according to the established compensation curve. The temperature compensation device uses

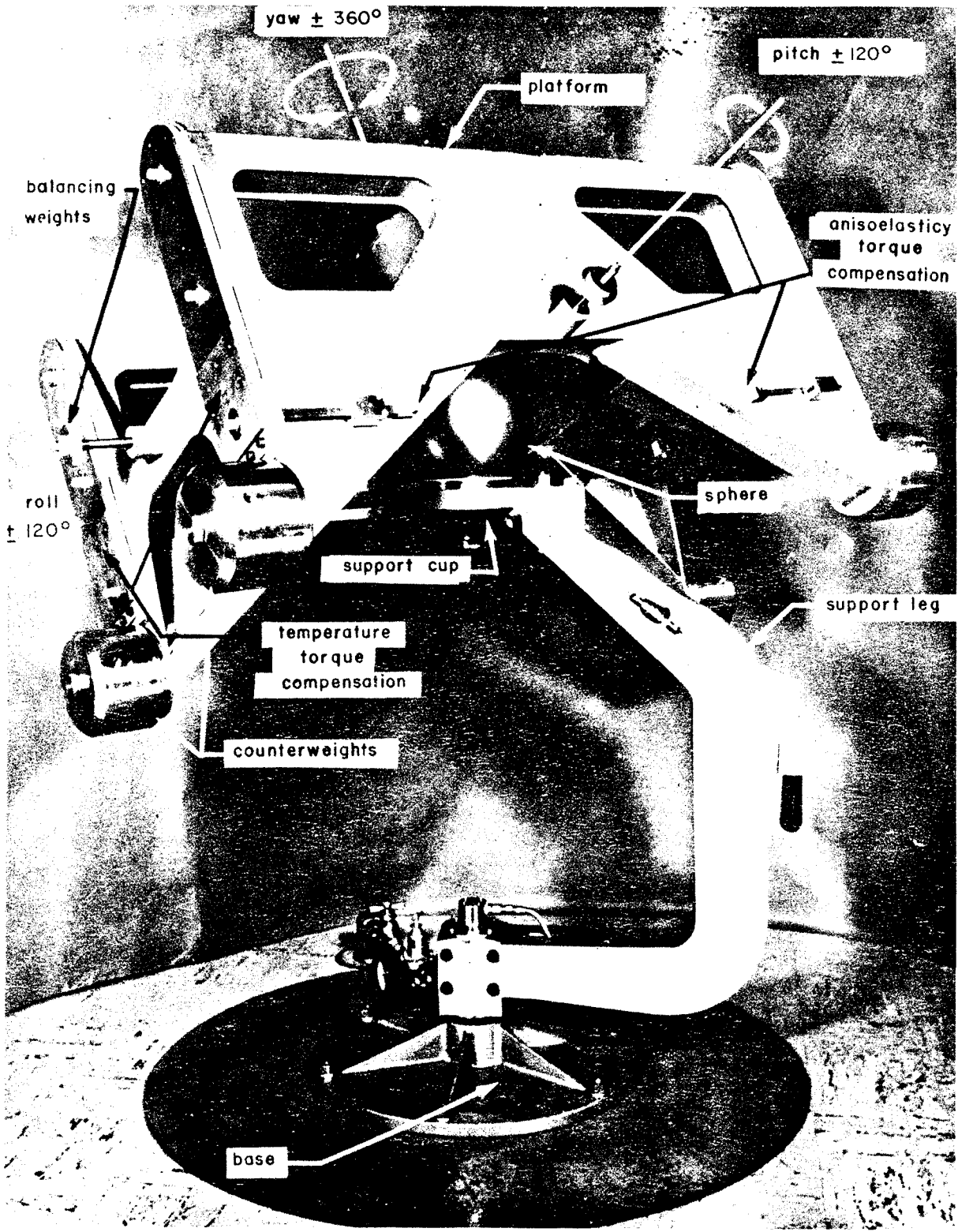


Fig. 20.9 Space motion (angular) simulator.

a relative mass shift that is actuated by properly arranged parts with different thermal linear expansion coefficients. The proper operation of the motion simulator requires protection from air currents and limitation of temperature changes within the area surrounding the device. Both requirements can be taken care of by a special enclosure.

The development of this space motion simulator has reached such a perfection of balancing the nearly frictionless floating platform that it would move noticeably should a small swarm of flies land on it.

Preparations for forthcoming orbital rendezvous operations are well underway. The rendezvous technique must be developed to solve problems in refueling, crew exchange, replenishment of food stores, emergency situations, etc. Refueling in space may decisively influence the date that a manned lunar landing will be achieved; we would not have to wait for the readiness of a super space carrier vehicle.

Efforts toward perfecting the rendezvous technique must be supported by an equally emphasized development of sophisticated and highly reliable guidance and attitude control systems which can cope with the known requirements.

Research and development work in the field of space navigation can be greatly accelerated if rendezvous maneuvers are efficiently simulated in the laboratory. The use of flight components within the simulation loop will be of particular value in preparing the actual rendezvous maneuver. The following discussion concerns the practical (for efficient operation) limit between electro-mechanical and electronic analog simulation for orbital rendezvous maneuvers.

Laboratory simulation of rendezvous operations will probably always be incomplete to a certain extent. The following kinematic-dynamic consideration clearly expresses a basic limitation. When coasting in orbit, the spacecraft is weightless and frictionless within the gravisphere of our planet. To simulate this condition in the laboratory, the development of a scaled-down gravisphere would be necessary. Since this does not seem feasible, mechanical simulation where translational motion is involved cannot correspond to reality. It will be shown that in spite of such limitations, simulation of rendezvous operations can still be a precious tool of development.

Several requirements are fundamental to the simulation system. A rendezvous operation is composed of three distinct phases, namely: (1) the acquisition phase, encompassing the distance between the existing orbiting vehicle and the ascending vehicle from approximately 20,000 ft to 4500 ft; (2) the docking approach phase, extending from approximately 4500 ft to 100 ft; and (3) the final docking phase, reaching from approximately 100 ft to the mechanical joining of the spacecraft. Each of these phases must be given special consideration for simulation. The sequence of

guidance and control functions during the three phases of rendezvous operations are to be simulated so that they occur in the same order and for the same length of time as they do in actual orbital maneuvers.

Later advantages are obtained by applying a time scale factor  $k_t = 1$ . First, a true, full scale attitude control operation (except for the absolute amounts of the mass moments of inertia) for the spacecraft will be possible. Then, by considering the dimensions of the laboratory area, the scale factors  $k_d$ ,  $k_v$  and  $k_a$  for the translational displacement, the translational velocity and the translational acceleration of the spacecrafts can be determined. For the sake of simulation system simplicity, it will be necessary to maintain the practically unchanged three-dimensional angular relations (geometry) of the relative attitude of the two spacecrafts in their respective orbits. This will render the most accurate true angular velocities and angular accelerations.

The dimensions and the weight of the actual spacecraft force a scaling down to smaller configurations for the laboratory simulation; however, the simulated spacecraft must at least meet the following two objectives. First, it must possess the same mass moment of inertia ratio as the actual spacecraft. This requirement is established for the dynamics of the attitude control system of the spacecraft. Second, sufficient room for attachments for the operation of actual guidance and control components must be provided.

The equipment used for guidance and control of rendezvous maneuvers helps determine how much laboratory simulation can be undertaken. For the task of guiding the approach of the two spacecraft and controlling their orientation about their centers of gravity, three main groups of systems are required: (1) sensing system; (2) onboard computers; and (3) actuating systems.

The sensing components are mainly optical and radar types. Actual components will have attitude sensors. Sensors for range and velocity (or both) cause serious difficulties in laboratory simulation. In particular radar, which will be one of the important components of the whole orbital operation system, cannot be included in the simulation loop. Preliminary investigation has shown that reflections from the laboratory building, multipath propagation, etc., will impair the functioning of the radar system.

The on-board computers of the guidance and control systems for rendezvous maneuvers should not be a hindrance to incorporating as many actual components as possible into the laboratory simulation system.

It looks quite different for actuation systems that generate impulses for the guidance and control of the spacecraft. The attitude control could be achieved easily by real actuation; however, the actuation system for translational motion of the simulated spacecraft will probably be substituted. The two spacecraft will have to be slaved along each of their computed paths. Propelling these bodies within the laboratory by rocket thrust seems tedious even when simulation is reduced from three- to two-dimensional displacements.

The final docking phase may be divided into two parts. First, simulate the approach until the imitated spacecraft are almost touching. The behavior of the attitude control system will be of particular interest during this simulation section. The second and final part of the docking phase can be simulated by suspending both vehicles with pendulums. Now the operation of the actual docking mechanism can be observed and investigated.

For rendezvous maneuver simulation, several schemes for generating the spatial motion of the spacecraft with six degrees of freedom have been proposed. One of these suggestions proposes the floating of the simulated craft in a water tank. Another suggestion is based on a suspension by means of an overhead carriage system which furnishes the x and y translational motions. The supporting spherical air bearing is moved along a vertical guide, mounted to the lower carriage, thus producing the third translational motion (z direction). Furthermore, a scheme was presented which uses a spatial path simulator for the generation of six degrees of freedom in motion [15]. This path simulator is a self-contained apparatus. The only mechanical connection with the laboratory is the wheel contact on the floor to support the simulator weight. The three translational motions are produced by superimposing a horizontal motion (x and y component) with a vertical motion (z component). The horizontal motion is obtained by equipping the path simulator with a set of three wheels, the axes of which are simultaneously rotated and driven by remote control. The vertical component is produced by a hydraulic lift system. A spherical support air bearing on top of the hydraulic piston rod provides the three required angular motions.

The schemes mentioned offer optimum mobility for the target vehicle and the chasing vehicle. The proposals appear to be feasible, but their systems are objectionably complex. Therefore, simplification must be effected by reducing the number of degrees of motion freedom. This is theoretically and practically possible. A considerable simplification can be made when the orbital path of the target is considered fixed. In this case, it is sufficient to simulate only the motion of the chasing vehicle relative to the target vehicle, which means that the simulation of target translational motion can be dropped. A proposal dealing with such a simulation is presented in a recent report [16].

One simulator is subjected to two degrees of translational freedom by means of a flat air bearing (moving parallel to a special floor which is flat and smooth), and the third degree of relative translational motion is imparted by means of a hydraulic lift to the second simulator which is arranged stationary (no horizontal displacement). Both simulators provide three degrees of rotary freedom by spherical air bearings.

The striving for systems simplification, supported by analytical studies and evaluation of proposed simulation schemes, [17], [18], drastically reduced the systems's complexity. The result was a simulation laboratory with simulation equipment as illustrated in Fig. 20.10 [19]. This space flight facility will provide the following simulation equipment: (1) a spacecraft motion simulator (with a circular, symmetrical, disk-shaped platform); (2) a three-axis attitude indicator (for accurate determination of the platform attitude as a function of time); (3) reference sources such as room-fixed references for attitude control studies (optical reference is given by a collimated light beam, simulating a star infinitely far away); (4) moveable references (two servo-driven references are computer-controlled in such a manner that each can be independently slaved to approximately any position over a hemisphere as a function of time) [20], (5) projection system references (simulation of moveable attitude reference sources during maneuvers in space, achieved by a spherical projection screen located with the sphere center coincident with the center of rotation of the spherical air bearing of the spacecraft motion simulator); (6) and computers (analog and/or digital to solve a complete six-degrees of freedom problem, three degrees for target rotation and three degrees for relative translation between target craft and chasing craft).

These devices will allow simulated studies of attitude control, spacecraft tracking dynamics, spacecraft search and reorientation dynamics, axes cross coupling, etc. The simulation efforts which can be exercised in a laboratory with the described equipment or with similar facilities will offer the assistance necessary in the development of a thoroughly proven and adequate attitude control and guidance system for orbital rendezvous operations.

#### REFERENCES

1. Dornberger, W., "V-2", Viking Press Inc., New York, 1959 (Translation of "V2- Der Schuss ins Weltall", 1952), See chapter "Peenemünde at work." Note: J. Boehm brought the development of the first rocket motion simulator to a successful conclusion in April 1940.
2. Schubert, R., Neues Schwingtischmodell (New motion simulation). Peenemünde Archives Report #115/18, October, 1942.



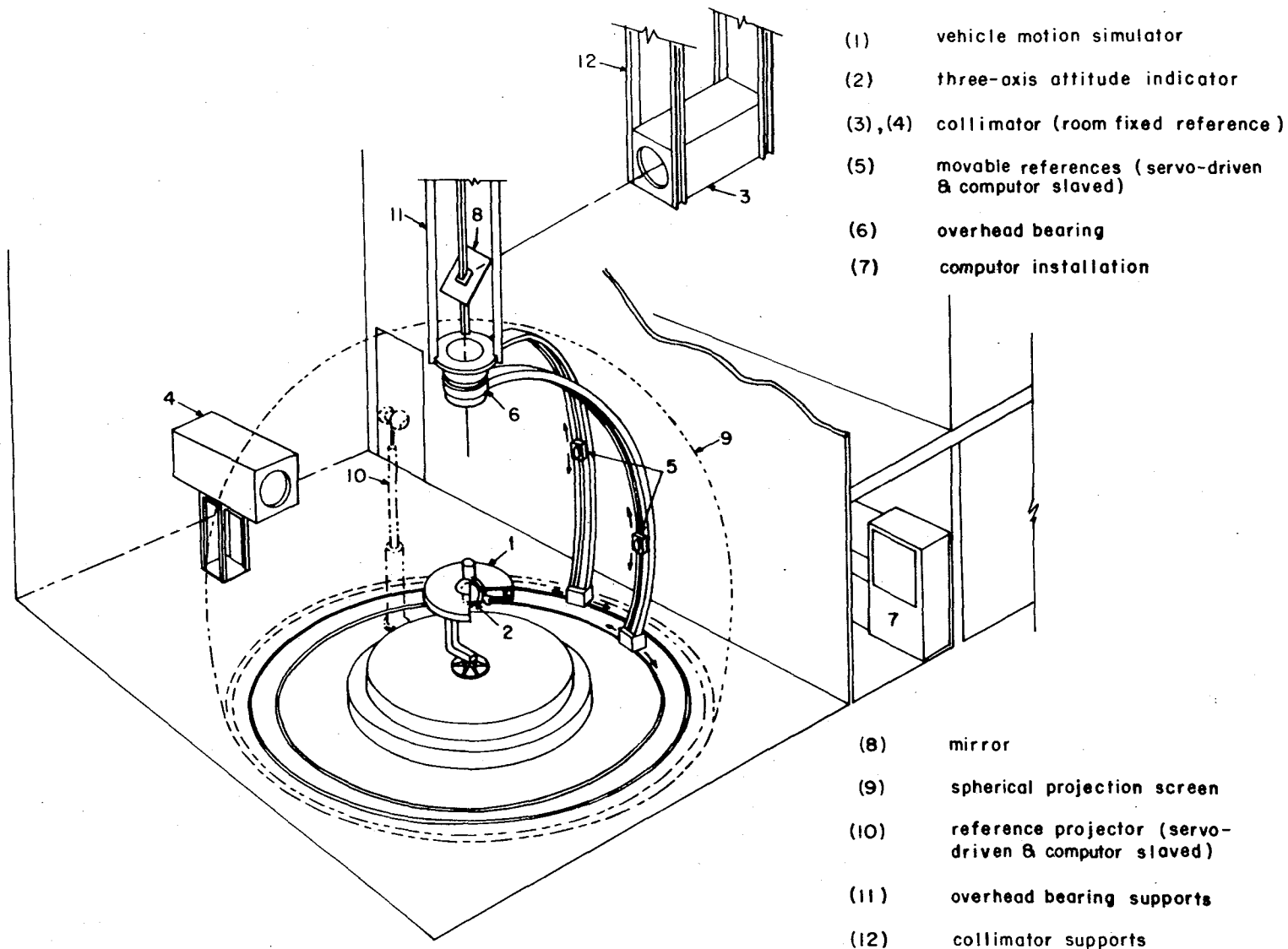


Fig. 20.10 Space flight simulation system.

3. Haeussermann, W., Entwicklung eines Schwingtischmodells (Development of a motion simulator), Peenemünde Archives Report #73/1, November, 1942.
4. Hoelzer, H., Anwendung elektrischer Netzwerke zur Lösung von Differential-gleichungen und zur Stabilisierung von Regelorganen (Application of electrical networks to the solution of differential equations and to the stabilization of control systems). Doctor's thesis submitted to the Departments of Mathematics and Physics, January, 1946.
5. Hoelker, R., Untersuchungen am Bahnmodell (V2 Motion Simulator Investigations), Consisting of Part I, II, and III, Peenemünde Archives Reports #86/150, April, 1944; #86/155, June, 1944; and #86/158, August, 1944.
6. Hosenthien, H.H., Reflected Nonlinear Modulators in Alternating Current Electrical Analog Computers, U.S. Patent No. 2,961,610 filed Aug. 18, 1949, issued Nov. 22, 1960.
7. Hosenthien, H.H., Analysis of Carrier Systems by Modulation - Equivalent Transfer Matrices, Army Ballistic Missile Agency, Report IR10, Huntsville, Alabama, March, 1956.
8. Goldberg, E.A., Stabilization of D-C Amplifiers, RCA Rev., 2: 296 (1950).
9. Korn, G.A., and Th. M. Korn, "Electronic Analog Computers", McGraw-Hill, Book Co., Inc., New York, 1952.
10. Soroka, W.W., "Analog Methods in Computation and Simulation", McGraw-Hill, Book Co., Inc., New York, 1954.
11. Wass, C.A.A., "Introduction to Electronic Analogue Computers", McGraw-Hill, Book Co., Inc., New York, 1956.
12. Jackson, A.S., "Analog Computation", McGraw-Hill, Book Co., Inc., New York, 1960.
13. Digesu, F.E., Spatial Attitude Control of Explorer I, Rept. No. DG-M-128-58, Army Ballistic Missile Agency, Huntsville, Alabama, May, 1958.
14. Haeussermann, W. and H. Kennel, A. Satellite Motion Simulator, Astronautics, 5: 22-23 (December 1960).
15. Boehm, J., Scheme for Laboratory Simulation of Orbital Rendezvous Maneuvers, Rept. #MTC-M-G&C-61-26, NASA-Marshall Space Flight Center, Huntsville, Alabama, May, 1961.

16. Schultz, D.N., and D.D. Sweitzer, Feasibility Study for Simulating Orbital Rendezvous, Rept. #M-ASTR-IN-62-1, NASA-Marshall Space Flight Center, Huntsville, Alabama, 1962.
17. Kuebler, M.E., Limitations of Orbital Rendezvous Simulation in the Laboratory, Rept. MTP-ASTR-M-62-2, NASA-Marshall Space Flight Center, Huntsville, Alabama, 1962.
18. Kennel, H.F., Evaluation of Rendezvous Simulation Studies, Rept. #M-G&C-NC, NASA-Marshall Space Flight Center, Huntsville, Alabama, September, 1961.
19. Committee for Flight Simulation Facility, Flight Simulation Facility, ASTR-IN-61-26, NASA-Marshall Space Flight Center, Huntsville, Alabama, December, 1961.
20. Celestial Simulator Facilities, Space Program Summary No. 37-5, Jet Propulsion Laboratory, Pasadena, California, pp. 47-55, October 1, 1960.

N63-15997

A COMPARISON OF TWO SUPERCONDUCTIVE BEARING PRINCIPLES

T. A. Buchhold  
Consulting Engineer  
General Electric, Co.  
Schenectady, N. Y.

The phenomenon of superconductivity can be used to build bearings that are virtually frictionless and can operate in vacuum. Such bearings are of interest for cryogenic gyroscopes, accelerometers, and other cryogenic mechanical devices.

The resistance of certain metals and alloys, such as lead, tin, niobium, niobium-tin, etc., virtually goes to zero at very low temperature; hence, by definition the material is a superconductor. Niobium becomes superconductive at 9°K. It is generally operated at 4.2°K, which is the temperature of liquid helium at normal atmospheric pressure. If a superconductor such as niobium is exposed to a magnetic field, the flux cannot penetrate the bulk metal surface and the flux lines are therefore constrained in a direction parallel to this surface and the resultant flux compression produces a pressure on the surface [1]. (A surface penetration in the order of 10<sup>-4</sup> to 10<sup>-5</sup> mm can be ignored for most practical bearing applications.)

This phenomenon is used for superconductive bearings; however, the critical magnetic field H<sub>c</sub> must not be exceeded (about 1500 oe for niobium) since to do so would be to destroy the superconductivity and make the material resistive.

Two design principles used in superconducting bearings will be compared in the following discussion. Figure 21.1 shows the cross-section of a flat cylinder of iron (a) with a superconductive coil (b) made of niobium wire. Above the coil is a disk of niobium (c) guided by a mechanical bearing (d). If the coil is excited, a flux  $\phi$  is produced that cannot penetrate the superconductive disk. According to the Maxwell's theory, the flux lines, which are then parallel to the surface, have the specific repelling force of

$$f = \frac{1}{2} HB, \text{ or if } f \text{ is in } \frac{\text{kg}}{\text{cm}^2}, f = \left(\frac{B}{5000}\right)^2$$

Preceding page blank

and the entire force  $F$  can be expressed by

$$F = f A = \left( \frac{B}{5000} \right)^2 A \quad (21.1)$$

where  $B$  is the flux density in gauss and  $A$  the effective area in  $\text{cm}^2$ . This repelling force makes it possible to design a stable bearing, which is not possible with conventional magnetic materials and circuits.

To obtain  $F$  for the bearing of Fig. 21.1, an average flux density  $B$  must be used, and can be computed as

$$B = \frac{4 \pi}{10} \frac{IN}{L} \quad (21.1b)$$

where  $IN$  is the ampere turns and  $L$  the length of the magnetic lines in the gap  $x$ . The reluctance of the iron is neglected. The area is

$$A = \pi DL$$

where  $D$  is the average diameter. This force acts on the disk (c) upwards. The coil (b) in which a current  $I$  flows can now be short-circuited by a superconductive switch. For a normal coil circuit with the linked flux  $\phi$ , current  $I$ , and resistance  $R$ , we have

$$\frac{d\phi}{dt} = - IR$$

since in our circuit  $R = 0$  and

$$\frac{d\phi}{dt} = 0 \text{ or } \phi = \text{constant} = \phi_0 \quad (21.2)$$

The flux  $\phi_g$  that goes through the gap  $x$  is

$$\phi_g = kBx \quad (21.3)$$

where  $k$  is a constant. The leakage flux  $\phi_L$  through the coil is also proportional to the current  $I$  and thus the flux density  $B$ , and therefore can be expressed for convenience as

$$\phi_L = kBx_i \quad (21.4)$$

where  $x_i$  is a constant and can be thought of as an imaginary fixed gap.

The entire linked flux  $\phi_0$ , which is constant, as shown in Eq. (21.2), is

$$\phi_0 = \phi_g + \phi_L = kB(x + x_i) \quad (21.5)$$

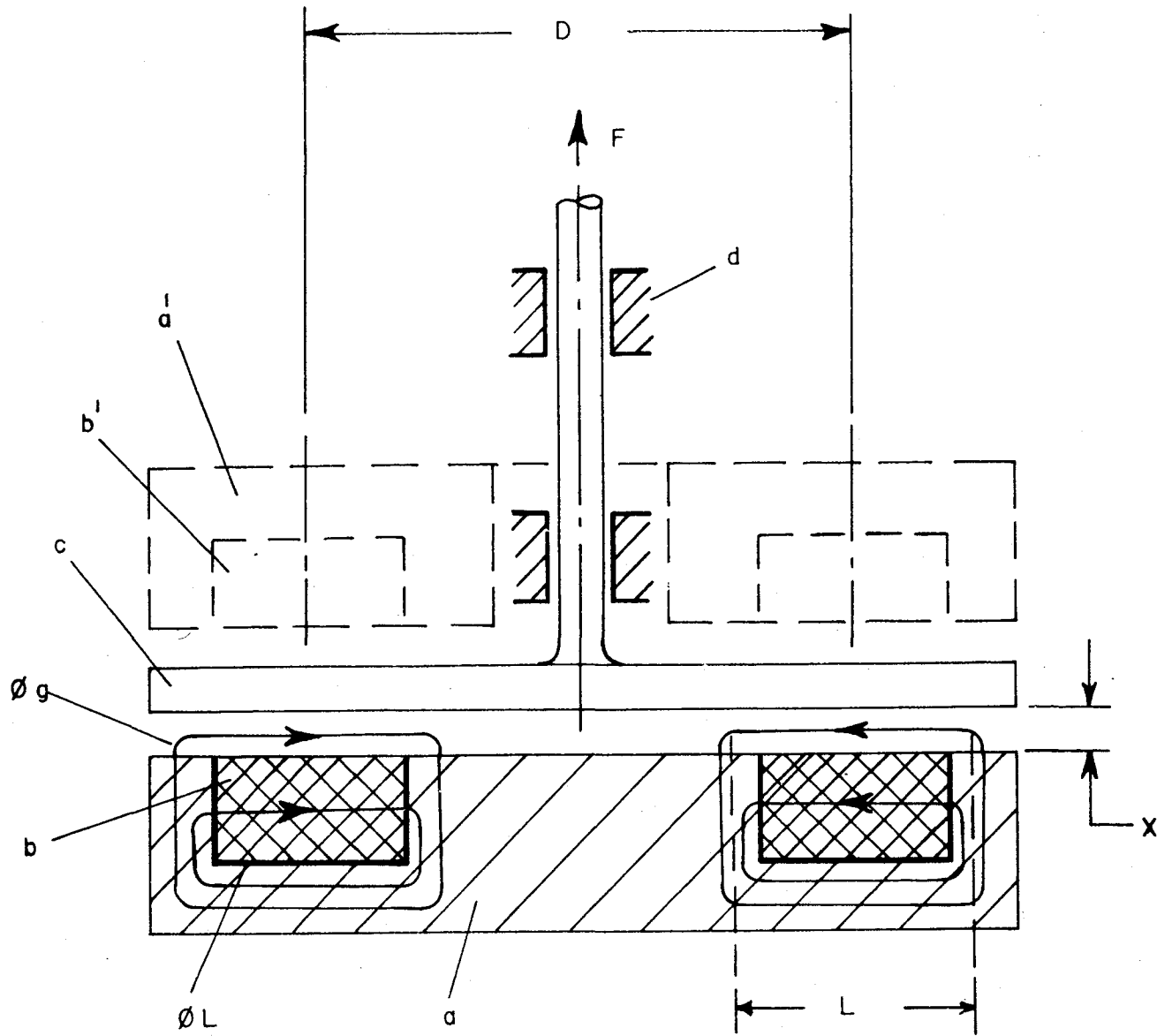


Fig. 21.1 Cross-sectional view of superconductive bearing.

or

$$B = \frac{\phi_0}{k(x + x_i)} \quad (21.6)$$

Since B is proportional to the coil current, this current changes with varying gap x in spite of  $\phi_0$  being constant. The force F, which is proportional to  $B^2$  as shown in Eq. (21.1), is

$$F = \frac{K}{(x + x_i)^2} \quad (21.7)$$

where K is another constant.

Figure 21.2a shows two curves for the force F as a function of the gap x. Curve (a) assumes  $x_i = 0$  (no coil leakage); and curve (b) with a finite leakage, expressed by a finite  $x_i$ , shows that the curve has a smaller slope (less stiffness).

In order to obtain the stiffness or the spring constant c of the bearing positioned in the vicinity of  $x = x_0$ ,  $\frac{dF}{dx}$  is formed

$$c = \frac{dF}{dx} = - \frac{K}{(x + x_i)^3}$$

using Eq. (21.7) for the initial force and displacement values  $x_0$  and  $F_0$ , and neglecting the minus sign

$$c = \frac{2 F_0}{x_0 + x_i} = \frac{2 F_0}{x_0 \left(1 + \frac{x_i}{x_0}\right)}$$

The magnetic reluctance  $r_0$  of the magnetic path through the gap  $x_0$  is proportional to  $\frac{1}{x_0}$ , and the reluctance  $r_2$  through the imaginary gap  $x_i$  is proportional to  $\frac{1}{x_i}$ ; therefore the previous equation can be written

$$c = \frac{2 F_0}{x_0 + x_i} = \frac{2 F_0}{x_0 \left(1 + \frac{r_0}{r_2}\right)} \quad (21.8)$$

If a second cylinder (a') with coil (b') is placed above the disk, the resulting force  $F_r$  is shown in Fig. 21.2b and is the force difference between the lower and upper coils. For the stiffness around  $x = 0$ , twice the value of Eq. (21.8) must be used. The bearing is stable in the vertical

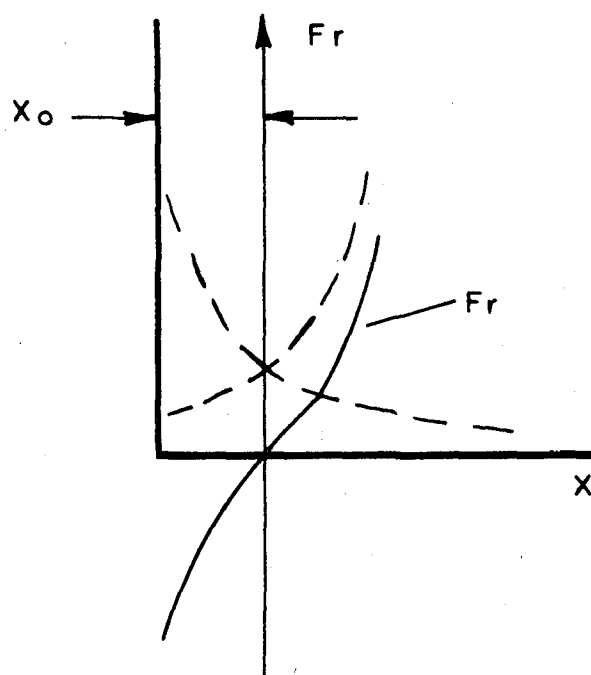
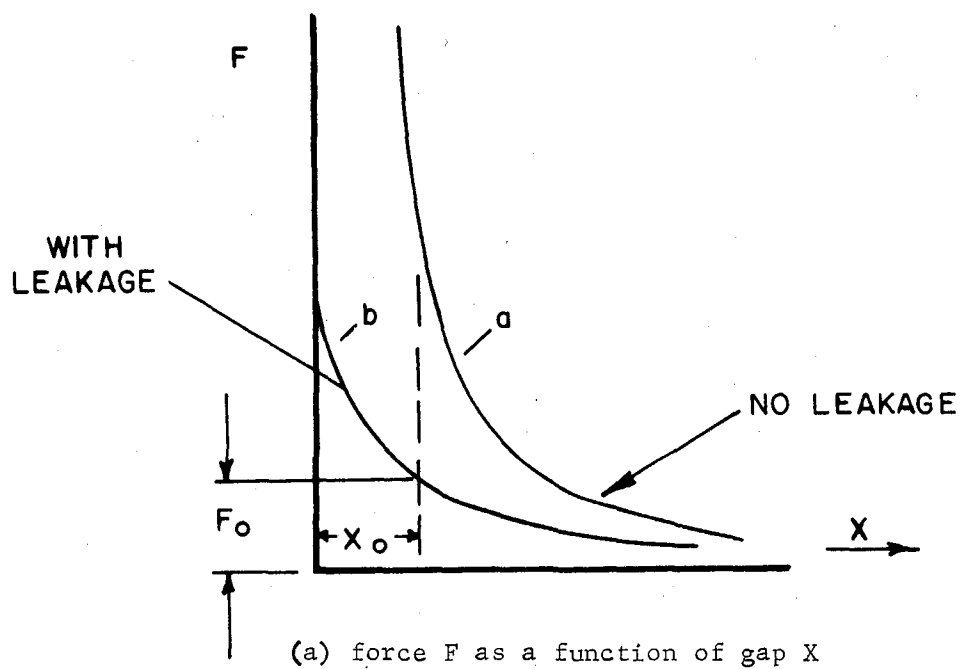


Fig. 21.2 Typical force curves



direction. Figure 21.3 shows a cryogenic bearing carrying a sphere (c). The housing (a) of iron contains the coils  $b_1$  and  $b_1'$  analogous to those of Fig. 21.1. The coils  $b_2$  and  $b_2'$  provide stability in the horizontal direction and the coils  $b_3$  and  $b_3'$  (not shown) take care of forces perpendicular to the plane of paper.

Equation (21.8) shows that in order to obtain a high stiffness, both the gap  $x_0$  and the leakage gap  $x_1$  should be made as small as possible. The variable gap clearance  $x_0$  can be controlled relatively easily, but the leakage flux  $x_1$ , which depends mainly on the insulation thickness separating the wires, cannot be easily controlled. By using thick, rectangular wire and making coils with only one layer, the coil leakage will be reduced; however, to produce the required high bearing flux density, very large currents are needed. These currents are not easy to handle, and the additional leakage in the high current leads connecting the coils becomes considerable. In addition, rectangular wire has a disadvantage in that its corners become field stress points where the critical field may be exceeded initially.

In the following discussion, a second bearing design principle will be investigated that avoids the foregoing disadvantages. In Fig. 21.4a, the iron cylinder (a) contains the coil (b) which has a ring-shaped niobium cover (c). The cover has a thin radial slit (not shown) in order to avoid a superconductive short circuit. The magnetic flux path goes through the variable gap  $x$  of length  $L$  which has the reluctance

$$r = \frac{L}{\mu_0 \pi D x} \quad (21.9a)$$

where

$$\mu_0 = \frac{4\pi}{10}$$

and  $\pi D x$  is the average cross section for the flux (Fig. 21.4a). The magnetic flux path then goes through the gap  $x_2$  of constant reluctance

$$r_2 = \frac{L_2}{\mu_0 \pi D_2 x_2} \quad (21.9b)$$

which is formed by the cover (e) and an additional niobium cylinder (f). The vertical force is

$$F = kB^2 \quad (21.10)$$

where  $k$  is a constant.

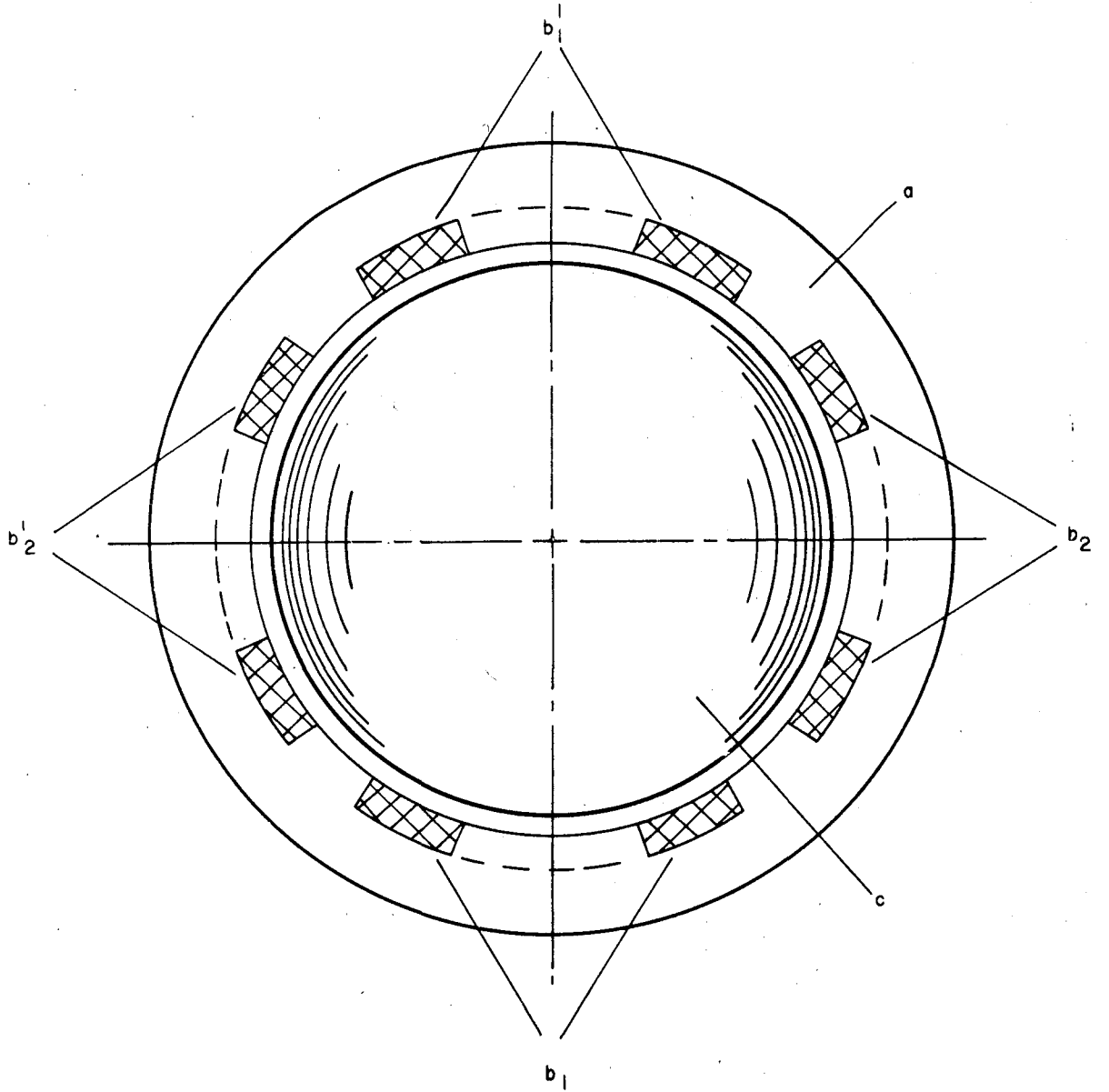


Fig. 21.3 Cryogenic bearing carrying a sphere.



The spring constant is

$$c = \frac{dF}{dx} = 2kB \frac{dB}{dx} = 2(kB^2) \frac{1}{B} \frac{dB}{dx} \quad (21.11)$$

or

$$c = \frac{2F}{B} \frac{dB}{dx}$$

The flux density in the gap  $x$  is

$$B = \frac{\mu_0 IN}{L} \frac{r}{r + r_2} \quad (21.12)$$

therefore

$$dB = \frac{\mu_0 IN}{L} \frac{r_2}{(r + r_2)^2} dr \quad (21.13)$$

since

$$\frac{dr}{r} = - \frac{dx}{x}$$

Equations (21.12) and (21.13) yield (minus sign is omitted)

$$\frac{dB}{B} = \frac{dx}{x} \frac{1}{1 + \frac{r}{r_2}}$$

Substituting in Eq. (21.11)

$$c = \frac{2F}{x \left(1 + \frac{r}{r_2}\right)} \quad (21.14)$$

The spring constant in the vicinity of  $x = x_0$ ,  $r = r_0$ , and  $F = F_0$ , becomes

$$c = \frac{2 F_0}{x_0 \left(1 + \frac{r_0}{r_2}\right)} \quad (21.15)$$

Equation (21.15) shows that  $c$  is not influenced by the leakage flux  $x_i$  of the coil. The schematic Fig. 21.4b explains the bearing action of Fig. 21.4a. It shows the constant magnetomotive force  $IN$  and the two reluctances  $r$  and  $r_2$ . If the variable reluctance  $r$  is increased (gap becomes smaller) the flux  $\phi$  decreases; however, the ampere turns along the reluctance increase. Consequently, the flux density  $B$  within the gap increases. Therefore, the force  $F$  also increases.

A coil leakage can be represented by the reluctance  $r_L$ , parallel to  $IN$ , which does not influence the flux  $\Phi$  or the flux density  $B$  in the magnetic circuit of the gaps. Equations (21.8) and (21.15) show on a theoretically mathematical basis that the spring constant  $c$  is the same for both bearing principles; however, in reality there is a great practical difference. If in the first bearing (Fig. 21.1) the gap  $x_0$  becomes smaller, Eq. 21.8 shows that the spring constant  $c$  depends more on the value  $x_1$ , which expresses the coil leakage and which is subject to practical design disadvantages.

For the second bearing principle (Fig. 21.4), the conditions are different. If both gaps  $x_0$  and  $x_2$  are made proportionally smaller ( $r_0/r_2$  equals  $K$ ), spring constant becomes larger and the bearing very stiff.<sup>2</sup> From Eq. (21.15) it follows that a large fixed reluctance  $r_2$  also increases the stiffness. However, Eq. (21.12) shows that increasing  $r_2$  increases the required ampere turns  $IN$ , and here practical limitations are ultimately reached.

The sleeve bearing shown in Fig. 21.5a consists of an iron housing (a) containing the coil (b) with the niobium cover (e) having a small radial slit (not shown) in order to avoid a superconductive short circuit. A superconductive shaft  $c$  with a radius  $R$  is to be supported. With the shaft centered, the flux goes through the gap  $x_0$  and then through the fixed gap  $x_2$  formed by the cover (e) and the superconductive niobium ring (f). The shaft (c) is displaced vertically an amount  $\Delta x$ . Along the circumference of the shaft (Fig. 21.5b), the gap changes as a function of the angle  $\alpha$ .

For a small displacement of  $x$

$$x_2 = x \cos \alpha \quad (21.16)$$

For the incremental area  $LRd\alpha$ , the increase in force  $dF$  perpendicular to the surface is

$$dF = c(\Delta x \cos \alpha) = \frac{2 dF_0}{x_0 \left(1 + \frac{r_0}{r_2}\right)} \Delta x \cos \alpha = \frac{2 f_0 LRd\alpha}{x_0 \left(1 + \frac{r_0}{r_2}\right)} \Delta x \cos \alpha$$

when  $F_0$  is replaced by  $dF_0$ , as shown in Eq. (21.15),

where  $f_0$  is the force

$$f_0 = \frac{B^2}{5000} \quad \text{in kg/cm}^2$$



In order to obtain the total vertical force change  $\Delta F$ , the component  $dF \cos \alpha$  must be integrated from  $\alpha = 0$  to  $\alpha = 2\pi$ .

$$\Delta F = \frac{2 f_o RL}{x_o \left(1 + \frac{r_o}{r_2}\right)} \times \int_0^{2\pi} \cos^2 \alpha \, d\alpha$$

$$\Delta F = \frac{2\pi RL f_o}{x_o \left(1 + \frac{r_o}{r_2}\right)} \Delta x$$

Let

$$F_o = 2\pi RL f_o \quad (21.17)$$

then the spring constant  $c$  becomes

$$c = \frac{F_o}{x_o \left(1 + \frac{r_o}{r_2}\right)} \quad (21.18)$$

The derivation of Eq. 21.18 assumes that the magnetic lines in the gap  $x_o$  are parallel to the axis of the shaft. This is approximately the case if  $L$  in Fig. 21.5 is small compared with  $\pi R$ , which is half of the shaft circumference.

By using the two bearing elements shown in Fig. 21.4 and Fig. 21.5, any type of bearing can be built. Figure 21.6 shows a bearing supporting a sphere that could be used for a cryogenic gyro. The housing (a) is iron and contains the two coils ( $b_1$ ) and ( $b_2$ ) with the two niobium bearing sockets ( $e_1$ ) and ( $e_2$ ), which have at least one vertical, thin slit to avoid a superconductive short. The flux  $\phi$  follows a path through the gap formed by the superconductive ball and the bearing socket (e) and then through the constant gap formed by the bearing (e) and the superconductive ring (f). This bearing stably supports the sphere in all directions and is a combination of the characteristics explained in Fig. 21.4 and Fig. 21.5. The mathematical analysis of this bearing is somewhat more complicated but again shows that the effectiveness of the bearing is independent of the coil leakage and that the bearing stiffness increases with decreasing gaps.

In summary, two superconductive magnetic bearing principles are compared. The first principle keeps the total flux constant as the coil current changes with a changing bearing gap. The leakage flux of the

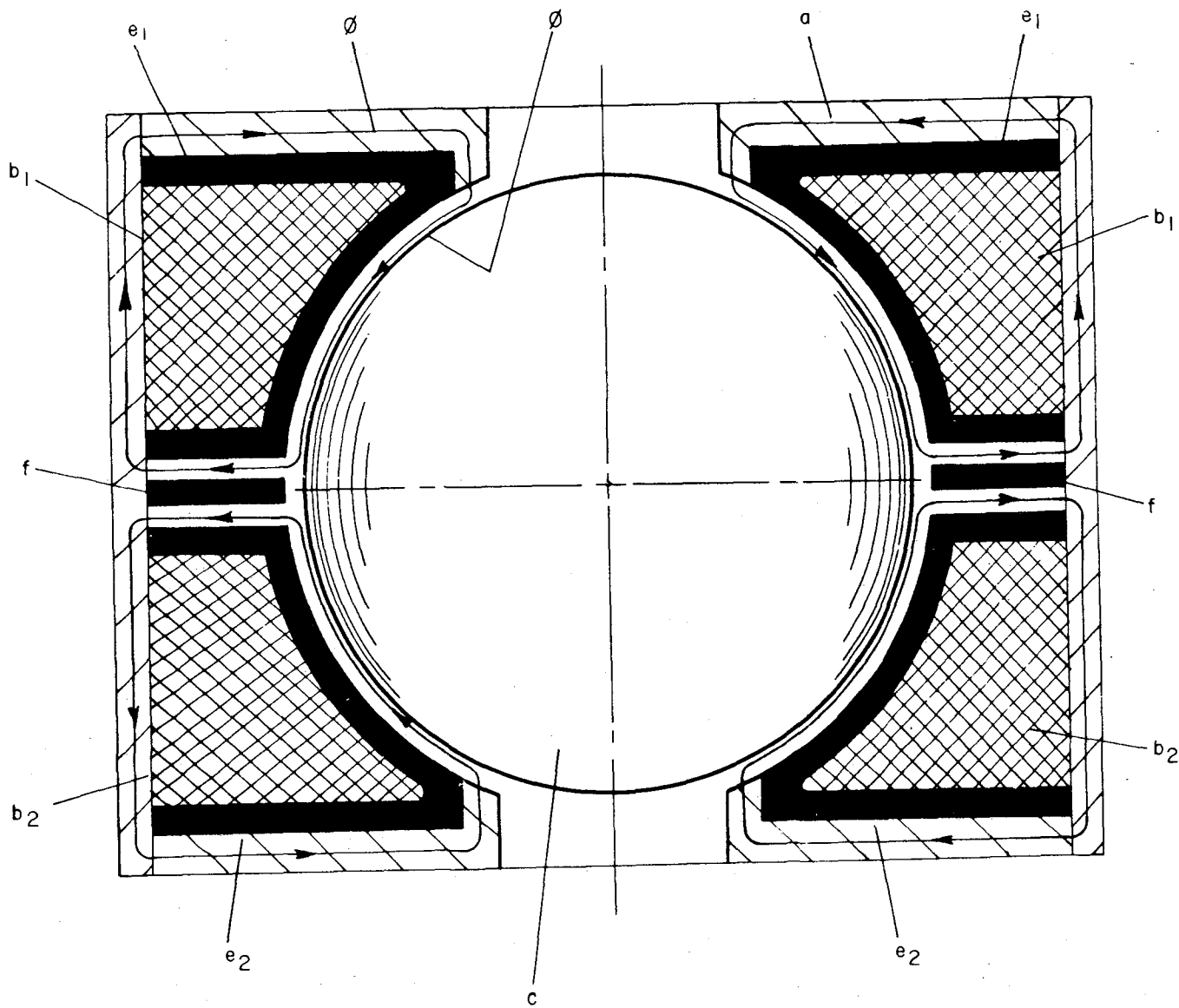


Fig. 21.6 Bearing supporting a sphere that could be used as a cryogenic gyroscope.



coil circuit limits the bearing stiffness. The second principle keeps the total ampere-turns constant when an additional fixed reluctance is inserted in the magnetic path. The bearing stiffness, which can be made large by using small gaps easily incorporated into the bearing design, is not influenced by coil leakage.

#### REFERENCES

1. Buchold, T. A., The Magnetic Forces on Superconductors and Their Applications to Magnetic Bearings, Cryogenics, 1: 203 (1961).

26/10

# **INSTRUMENTATION AND TRACKING**

|

22

## Preceding page blank

TELEMETRY DEVELOPMENT FOR LARGE GUIDED MISSILES AND SPACE CARRIER  
VEHICLES

Otto A. Hoberg and James E. Rorex

Astrionics Division  
George C. Marshall Space Flight Center  
National Aeronautics and Space Administration  
Huntsville, Alabama

Telemetry development must parallel or precede the development of the missiles or space vehicles, because without a progressive development program of instrumentation and telemetry techniques, the vehicle development program would falter from a lack of reliable, accurate, and comprehensive data. Telemetry data are used to optimize the vehicle design, and on these data the majority of vehicle engineering decisions are based. As vehicles have become more complex and sophisticated, the telemetry systems have necessarily become more complex and sophisticated. The team headed by Dr. Wernher von Braun has written history in missile and vehicle development from the V2 to the Saturn, and the development of instrumentation and telemetry systems has been parallel and complementary to the development of the vehicles.

The importance of flight test evaluation was documented in December 1939 by the successful flight test of the German A5 test missile, which preceded the development of the V2. For 77 sec of flight, 9 parameters, such as position of platform in 3 planes, rudder positions, pressure combustion chamber, takeoff and cutoff, were recorded. Figure 22.1 shows a sample of these recorded flight data. Since the missile was designed to be recovered, only on-board recording was required. This recording system consisted of a camera which synchronously photographed performance information as it was mechanically transferred to the deflection plate of an oscilloscope (Fig. 22.2).

Advancing from the A5 to the A4 (V2) required solving a number of instrumentation problems connected with the employment of an rf data link instead of recovery of recorded data on film. In reading the Peenemünde archive reports, one can find practically all presently known methods and techniques proposed by universities and research institutes in Germany. After these proposed techniques were applied to an established V2 development schedule, a moderate telemetry system evolved. Characteristics of electrical components, filter techniques, and performance of voltage controlled oscillators were obviously limiting

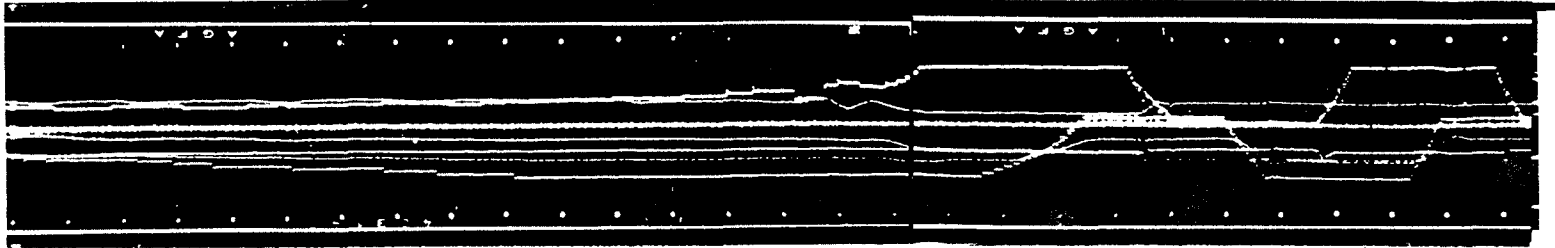


Fig. 22.1 Recorded flight data.

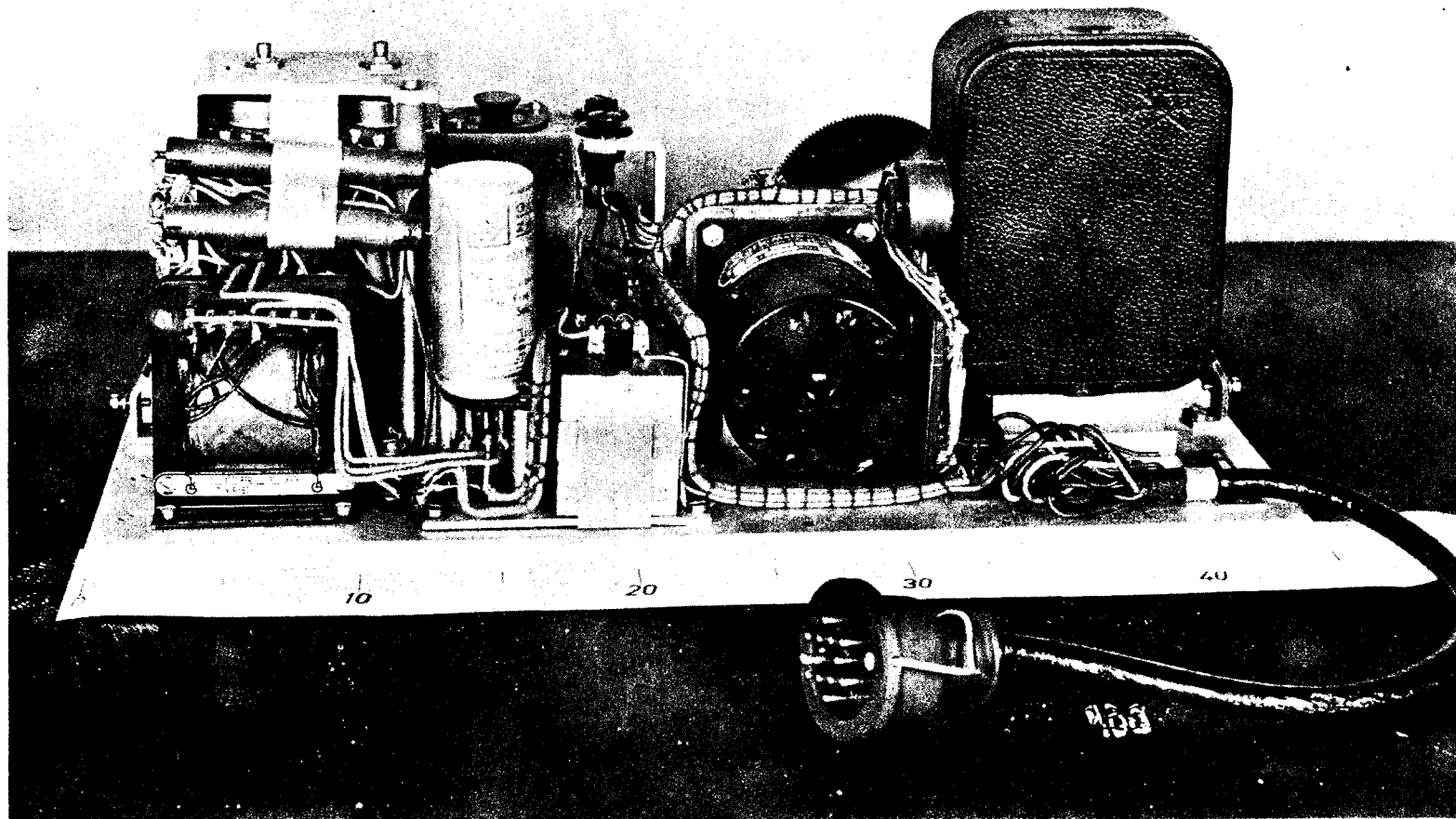


Fig. 22.2 Recording system (camera and oscilloscope) of A-5 rocket.

factors. This development resulted in the Messina I telemetry system, with total capability of 9 FM/AM channels on a 61.8-Mc carrier frequency, as the basic system for the V2. Accuracy, linearity, frequency response, and reliability were far from adequate. Realizing these shortcomings, the development of a Messina II was started. Although this system was not used for research development flights, its basic characteristic will be mentioned here briefly. Figure 22.3 shows the block diagram of the advanced telemetry system for the V2 project. The system had a capacity of 12 information channels. Each information-input amplitude modulates a common 500-kc carrier which is fed to a gate, triggered by pulses in sequence, and phase shifted with reference to a 500-cps repetition frequency. Internal calibration is provided during each frame. Figure 22.4 shows a sample of such a frame.

Unfortunately, the development had not been completed by the end of 1945; however, a number of features contained in the system can still be considered "modern" within present telemetry designs.

From 1947 until 1950, a telemetry system developed by the U.S. Naval Research Laboratory was used for flight tests for the V2 and Hermes 2 at White Sands Missile Range. The system was a pulse-position AM type which employed mechanical commutation.

### 22.1 Redstone

When the Redstone missile program was initiated in 1950, commercially available telemetry equipment was limited. The Research Development Board (RDB) created standards for telemetry systems and a few manufacturers had started to develop and manufacture building-block components for telemetry systems. Most of these components were bulky, inefficient, and unreliable. At Redstone Arsenal, with only a few engineers and technicians assigned to instrumentation, a program was started to evaluate existing telemetry equipment and to develop a telemetry system which could adequately handle a relatively comprehensive measuring program.

After considerable evaluation and experimentation, it was decided to employ a PAM/FM/FM system on the Redstone. The system flown on Redstone No. 1 utilized 16 of the 18 standard RDB, Inter-Range Instrumentation Group (IRIG), subcarrier bands. The 400-cycle band was not used, because this frequency coincided with the frequencies the inverters generated as a power source for the guidance platform. The 40-kc subcarrier band was not used in this particular system, because this frequency was used for magnetic tape speed compensation in the telemetry ground station. The compensation was later moved to 100 kc, and the 40-kc channel was used for data transmission. The 30-kc and the 22-kc subcarriers were modulated by 30 x 10 mechanical commutators, which were driven by dynamotors that supplied B+ voltage to the transmitter

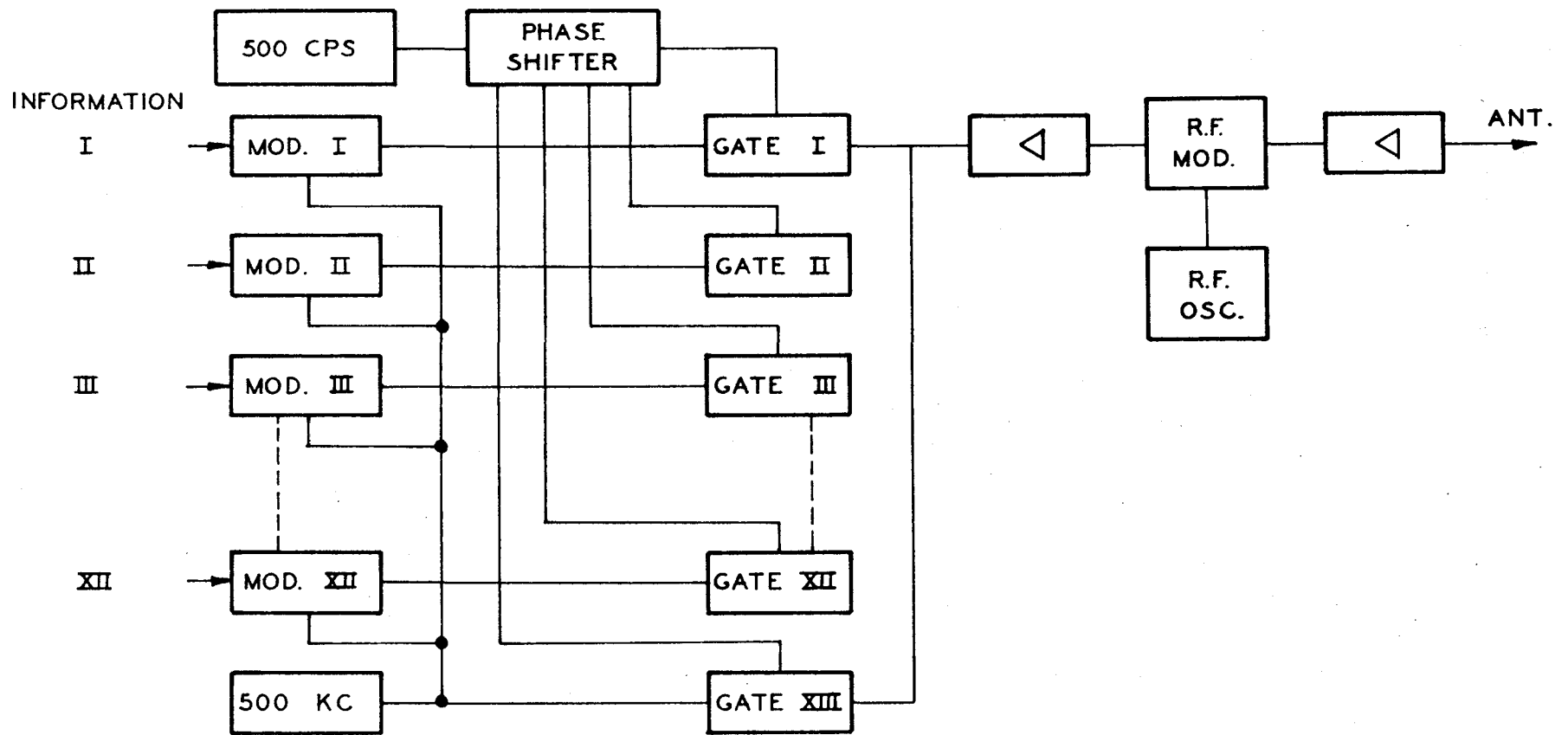


Fig. 22.3 Block diagram of advanced telemetry system for V-2 (Messina II).

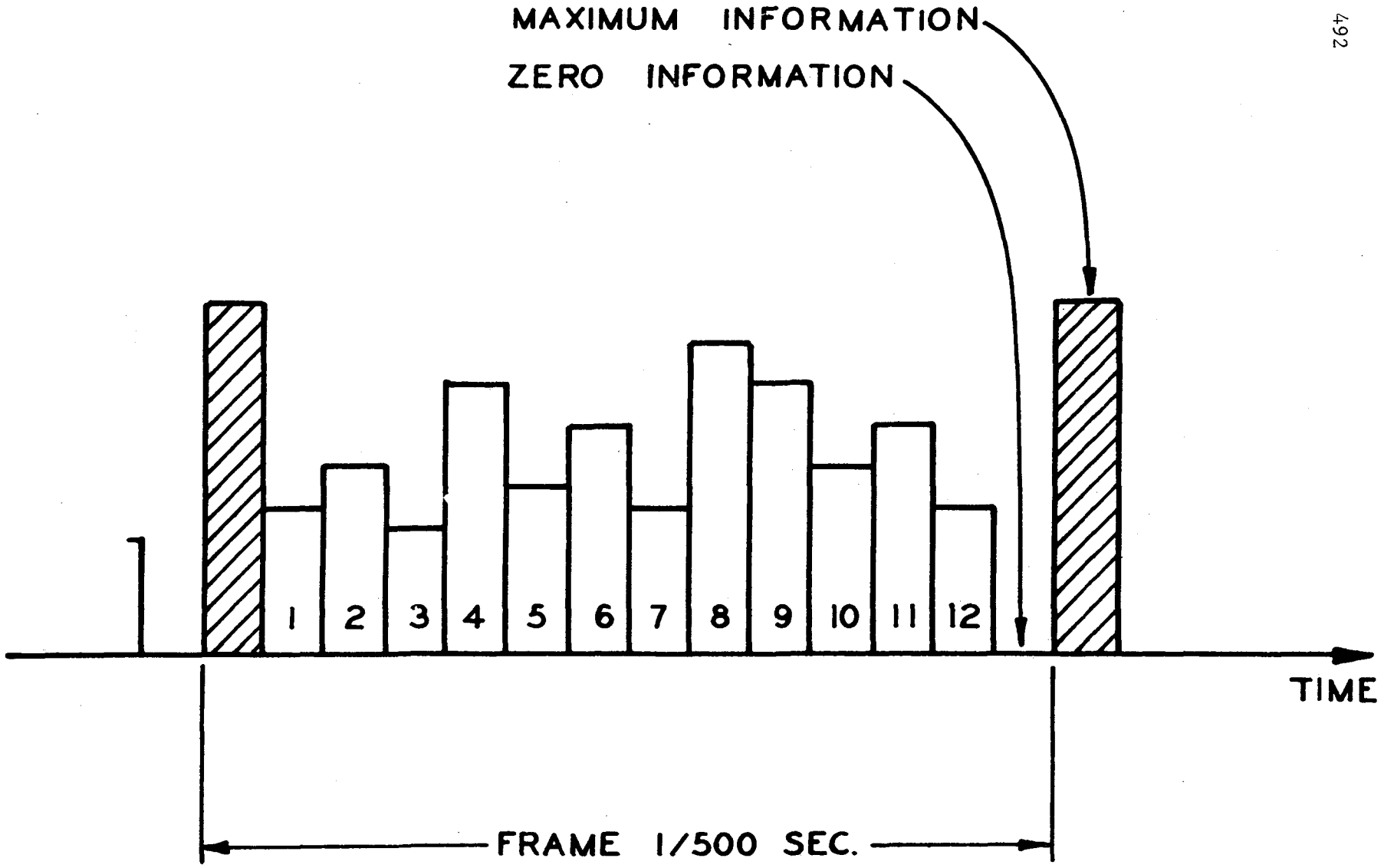


Fig. 22.4 Internal calibration - frame.



and subcarrier oscillators. Voltage to the 30-w power amplifier was supplied by a separate dynamotor unit. The inflight calibrator injected 5 precision voltage steps at 20-sec intervals. The steps were programmed by motor driven cams which were offset a few degrees to prevent calibration from occurring on two channels simultaneously. The first system was developed in 1952, and was flown on the first Redstone in August 1953. All of the components were bolted to a large, flat, aluminum chassis. Interconnection of components was made on terminal strips. The unit was appropriately called the flying breadboard.

The components for Redstones No. 2 through 8 were arranged and assembled to permit easy removal by using interconnecting plugs. This unit weighed about 130 lb. It should be pointed out that weight was not an important factor in the early versions since these missiles contained concrete ballasts. The flight records of the early missiles which carried these systems were very satisfactory from a telemetry standpoint. These telemetry units proved to be reliable, serviceable, and capable of accurate data transmission. The front and rear view of this package is shown in Figs. 22.5 and 22.6.

A second unit was designed in 1954 to attempt a reduction in size and weight because of the bulkiness of this package. Size and weight were reduced. Many characteristics of the resulting design, however, were considered undesirable because servicing was difficult, and mechanical and electrical designs were far from ideal. The choice of components was based on the previous design and were not considered optimum. This package, called the XO-1 (Fig. 22.7), weighed about 110 lb and occupied 4080 in.<sup>3</sup>. The number of measurements on the Redstone varied from about 100 to 150, and the missile carried one or two of these packages, depending upon the mission.

Weight reduction was considered a secondary design criteria in these early systems; other design goals, such as reliability, accuracy, flexibility, and serviceability, were considered primary.

Reliability was achieved by a comprehensive program of component evaluation and testing, as well as careful design consideration, meticulous inspection and checkout procedures, and individual integrity in all phases of design, testing, and checkout.

Careful component selection and calibration, noise filtering, design for low intermodulation, use of preflight and inflight calibration, and proper checkout procedures—all these attributed to an unprecedented high degree of accuracy for an FM/FM system.

To achieve flexibility, all channel input impedances were standardized at 100,000 ohms, and input voltages were 0 to 5 v full scale. All

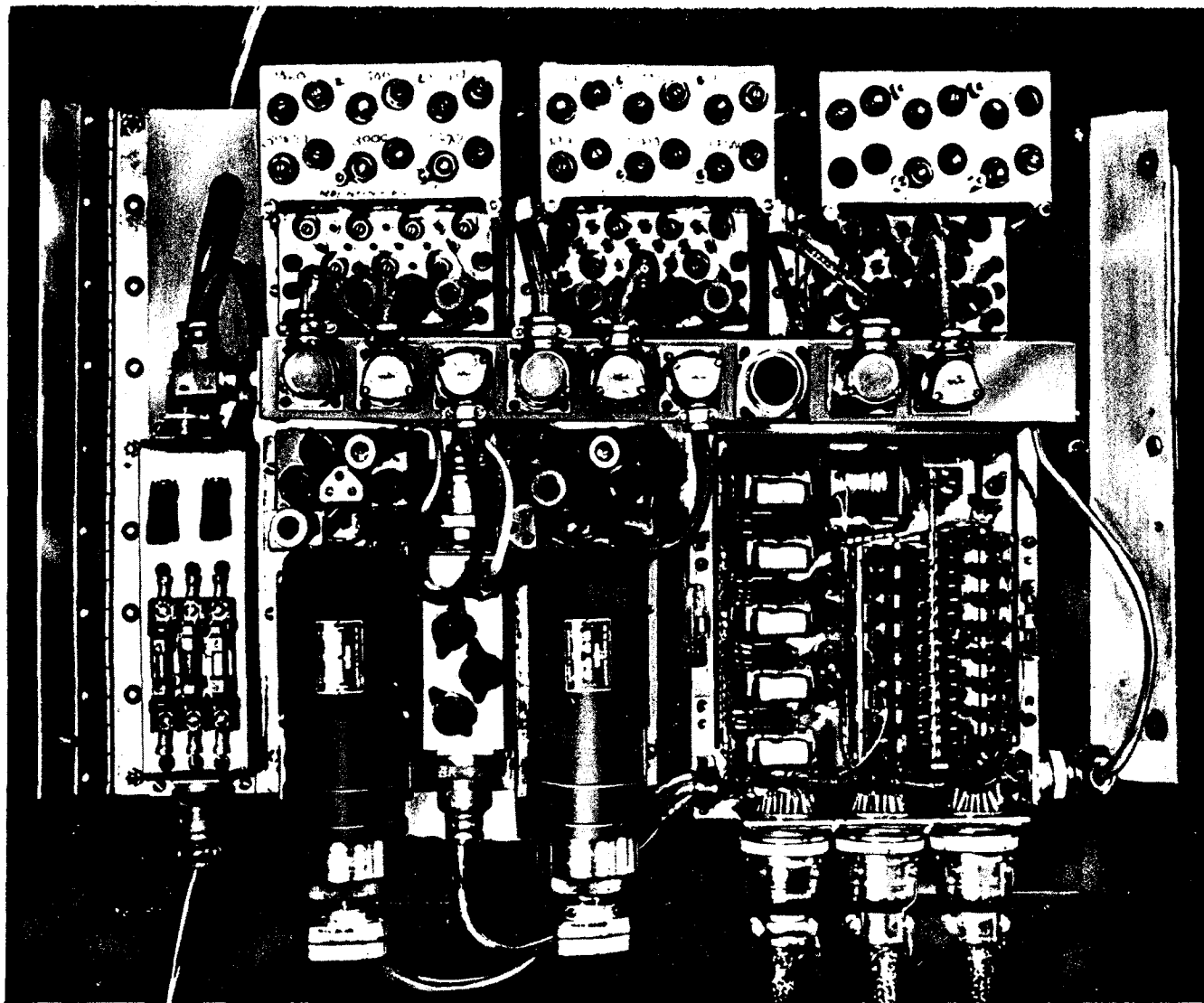


Fig. 22.5 Front view of telemetry units of Redstones 2 through 8.

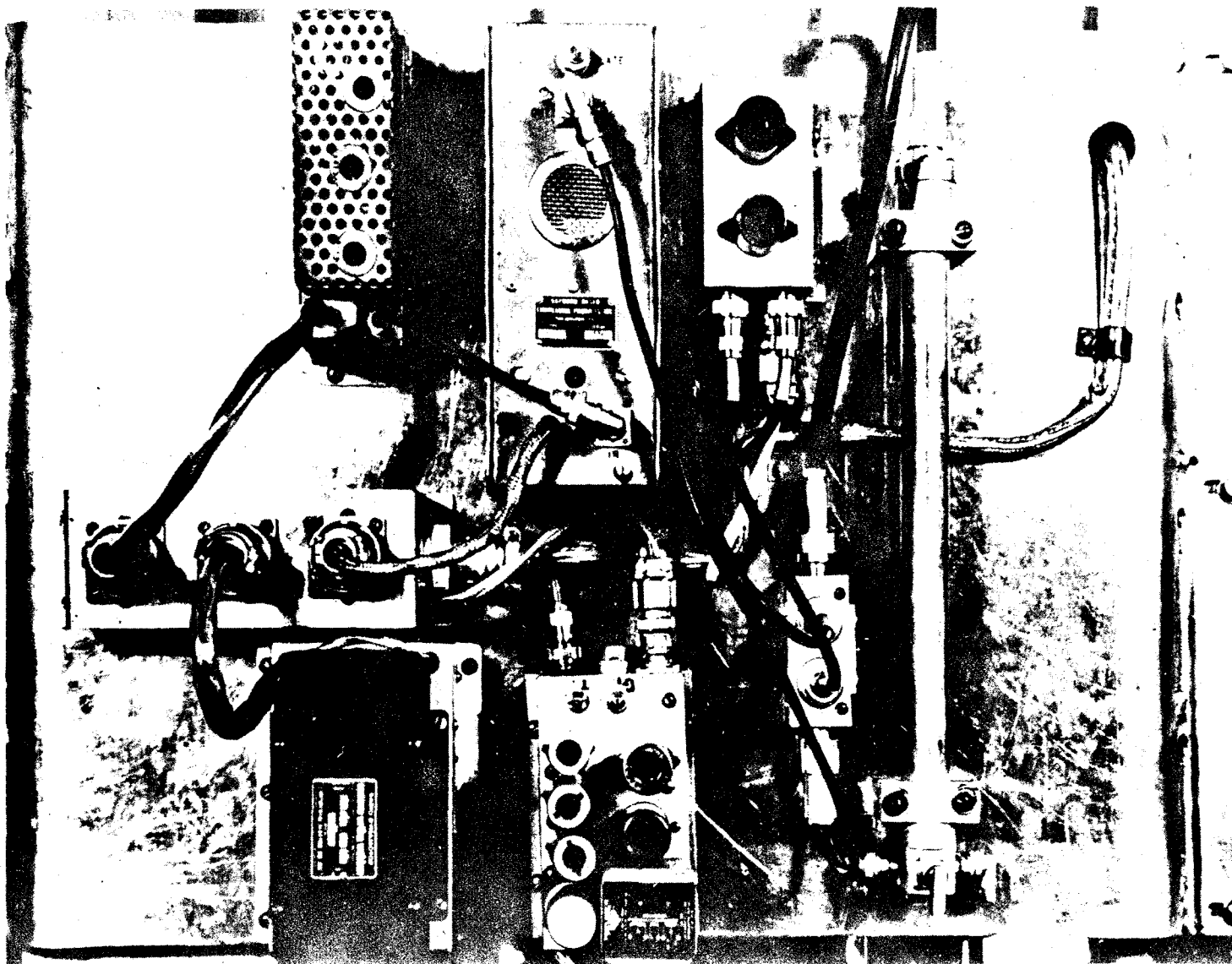


Fig. 22.6 Rear view of telemetry units of Redstones 2 through 8.

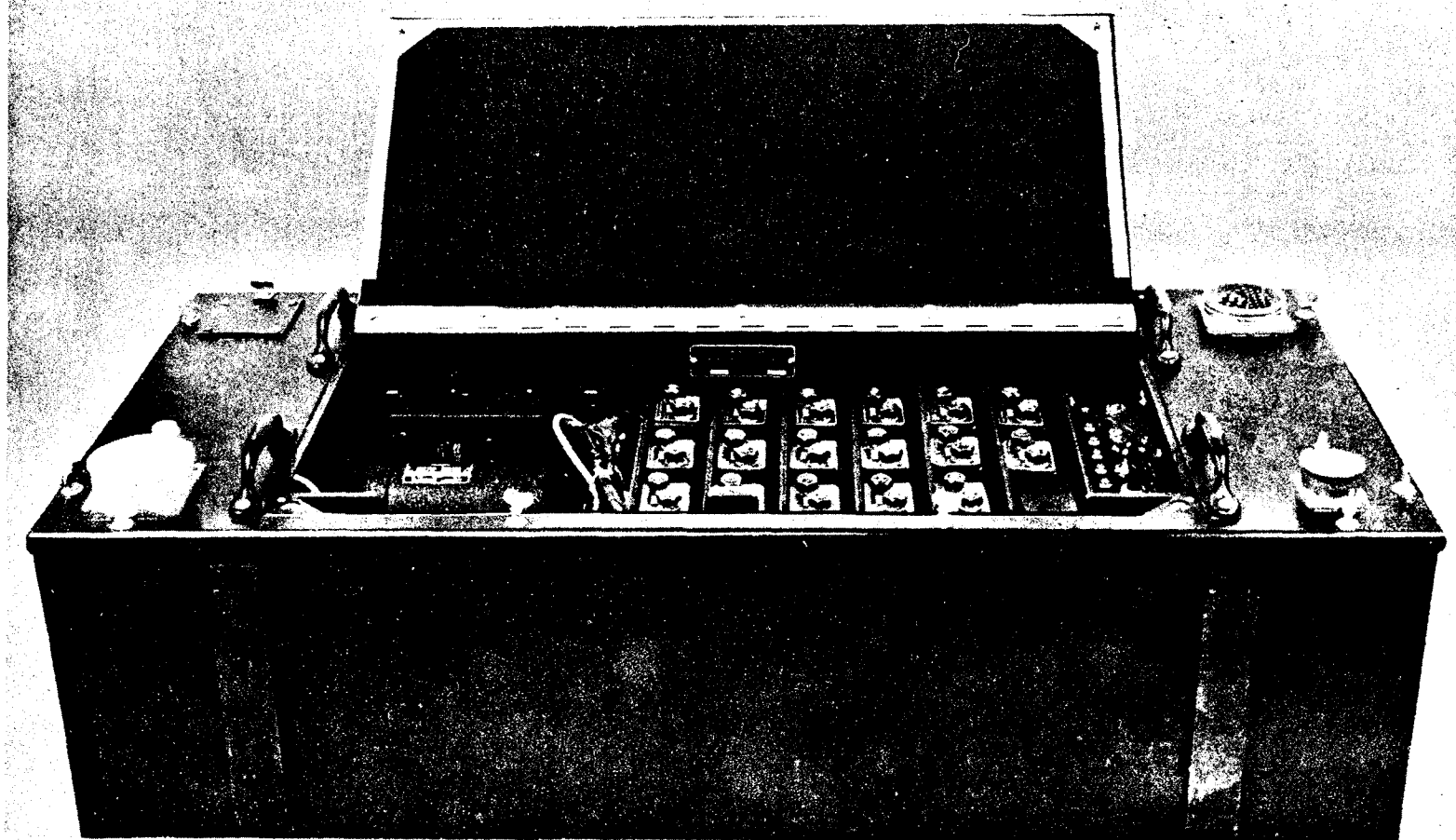


Fig. 22.7 X0-1 telemetry package.

measuring devices could be calibrated into a 100,000 ohm load, permitting convenient changes to be made in the measuring program with no redesign in the system. These program changes are often made to concentrate measurements in some critical area of the missile for convenience of diagnosing the effect of design changes which are made on the missile to improve performance.

Serviceability was achieved by modular construction and layout of component parts to facilitate rapid exchange of components. Packaging was designed for easy accessibility; adjustments could be made without removing equipment from the missile. Reliability and accuracy were enhanced by serviceability.

The approach taken on the telemetry design of the Redstone proved to be very sound; there was no significant loss of data in the Redstone development program. The only data losses that occurred during Redstone flight tests were caused by minor component failures. The data, in most cases, could be recovered by hand evaluation, as was the failure of a commutator gating unit on one flight. Although the data could not be decommutated by standard means, they were extracted by hand and recovered.

## 22.2 Jupiter

During the development of the Redstone, a continuous component evaluation program had been underway and it was obvious that the design of the XO-1 could be improved. A new unit designated the XO-2 was designed in 1956 and used on the early Jupiter IRBM and tactical Redstone missiles.

Although the XO-2 was characteristically similar to those previously described, it reflected a considerable improvement with respect to size, weight, and serviceability; for example, semiconductor power supplies replaced dynamotors; the 40-kc subcarrier was added, making a total of 17 subcarrier bands; and an improved mechanical commutator was used and the inflight calibrator was redesigned. This package, including a 30-w power amplifier, weighed 77 lb and had a volume of approximately 3560 in.<sup>3</sup>. The early Jupiters carried two of these packages with about 150 to 200 measurements being made. Figure 22.8 shows a view of one of these packages.

The model XO-3 transmitting set was a package redesign of the XO-2 to facilitate mounting for a special purpose and warrants little mention.

Although these units had proved to be excellent from the standpoint of reliability and accuracy, it seemed to be both practical and essential to implement a further reduction in size, weight, and power consumption without sacrificing any of the desirable characteristics. Early in 1958, another telemetry transmitting set, designated the XO-4, was

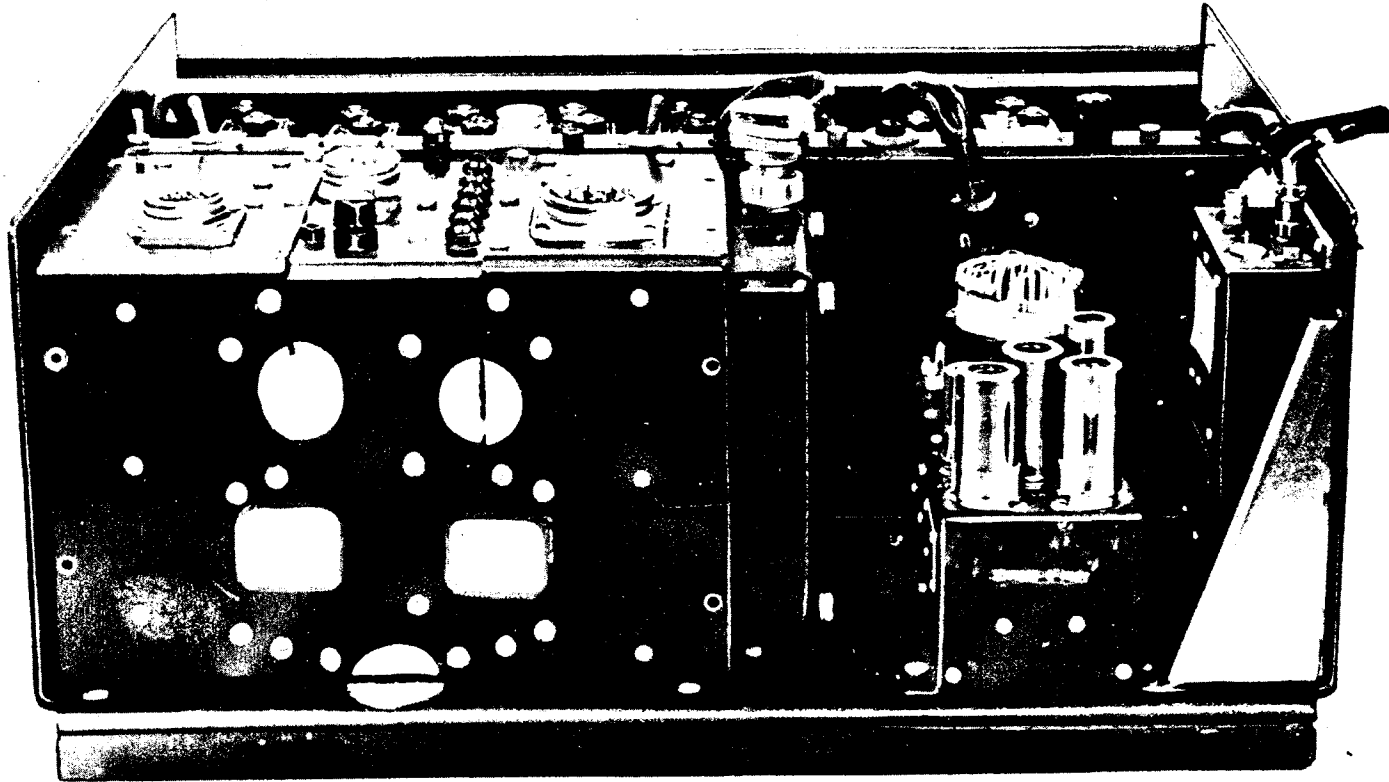


Fig. 22.8 X0-2 telemetry package.

designed. Again, the latest state-of-the-art advances available in components were applied. Primary considerations of the design in the order of emphasis applied were: reliability, accuracy, minimum size and weight, flexibility, and serviceability.

Considerable emphasis was now placed on size and weight reduction, since the previous design had been very satisfactory in other characteristics. No sacrifice in reliability or system accuracy would be tolerated to conserve space and weight, although some reduction in serviceability compared to previous design was necessary. However, because of increased reliability of component parts, serviceability could now be compromised to some degree without adverse effects. Some transistorized components were on the market at that time, but they were not in mass production. Therefore, transistorization was not a primary goal in the design, and transistors were used only in applications where the resulting characteristics of the set would definitely be an improvement over the use of vacuum tubes.

Figure 22.9 shows a view of the XO-4. The total weight of the XO-4, including a 35-w rf power amplifier, is 37 lb; and the volume is approximately 900 in.<sup>3</sup> Two or three of these units were flown on each of the later development flights of the Jupiter and have proven to be 100 per cent reliable.

### 22.3 Juno 1 and Juno 2

With the advent of satellites and deep space probes, weight and space limitations became of paramount importance in the design of payload telemetry systems. For example, on a space vehicle, a 1-lb addition in weight to the third-stage payload has approximately the same effect as 100 lb additional weight on the first stage.

Power consumption is another very important factor that affects the weight of the payload. A ballistic missile or a space carrier vehicle will have a flight duration of a few minutes, whereas, a satellite payload will transmit data for months. If a payload uses solar cells to sustain the battery charge over such a long duration, it requires from 125 to 600 times as much weight per unit of power in a payload as in a ballistic missile.

Because of the long operating time and the weight limitations, the main considerations in payload design are reliability, power consumption, and weight. Accuracy, serviceability, and flexibility are secondary. To conserve weight and power, the experiments and the telemetry system were an integral design and the parts were hand selected for close tolerances, thus reducing power consumption and increasing reliability.

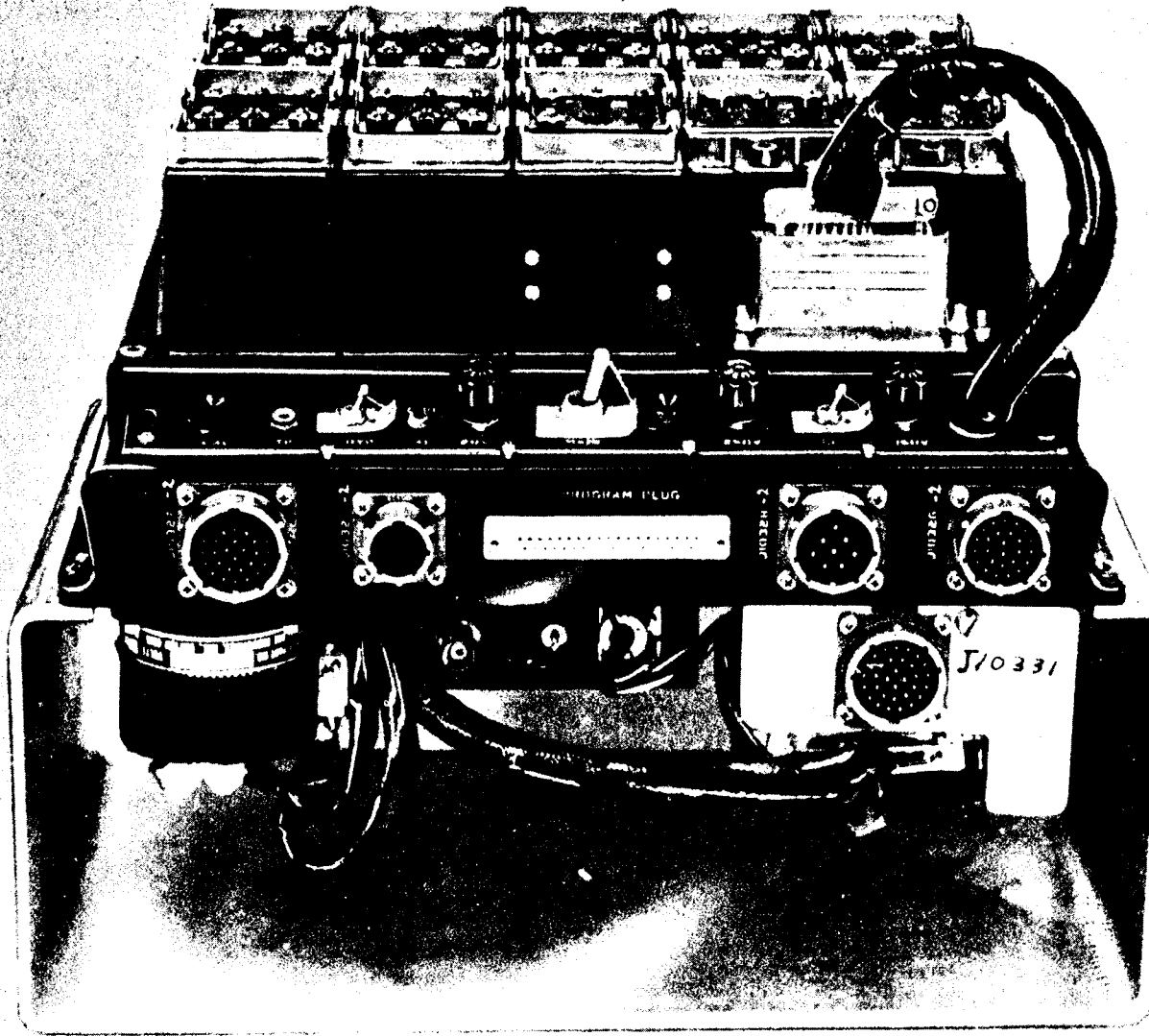


Fig. 22.9 XO-4 telemetry package.



Although each payload telemetry system was different in circuitry and configuration, some typical decks may be seen in Fig. 22.10. These decks were circular printed circuit cards sandwiched into a cylindrical configuration with interconnecting cables joining each deck.

Table 22.1 is a comparison of some of the characteristics of a ballistic missile or carrier vehicle telemetry system with those of a typical payload system. It should be noted that the data capacity of the payload telemetry is much less than that of the carrier vehicle.

Table 22.1 System Characteristics

Characteristic	AN/DKT(XO-4) Jupiter Telemetry System	Explorer 7 Telemetry
Weight, lb	37	3.2
Volume, in. <sup>3</sup>	900	108
Number of measurements	100 (approx.)	25
Total power consumption, w	315	2.21
Accuracy specification, per cent	1	3
Data bandwidth, cps	4000	53
Total expected operating life, hr	20	9000
RF power output, w	35	0.6

The Juno 1 carrier vehicle, based on an elongated Redstone, carried one of the previously mentioned XO-2 transmitting sets. The Juno 2 was based on a modified Jupiter missile with one XO-4 telemetry package used to transmit essential vehicle performance data.

#### 22.4 Pershing

The Pershing solid-propellant medium-range ballistic missile uses two modified XO-4 transmitting sets on the first stage. These sets are electrically identical to the ones used on the Jupiter except for a package modification to facilitate mounting.

When the Pershing warhead is subjected to reentry tests, another change in telemetry configuration is required. To better utilize

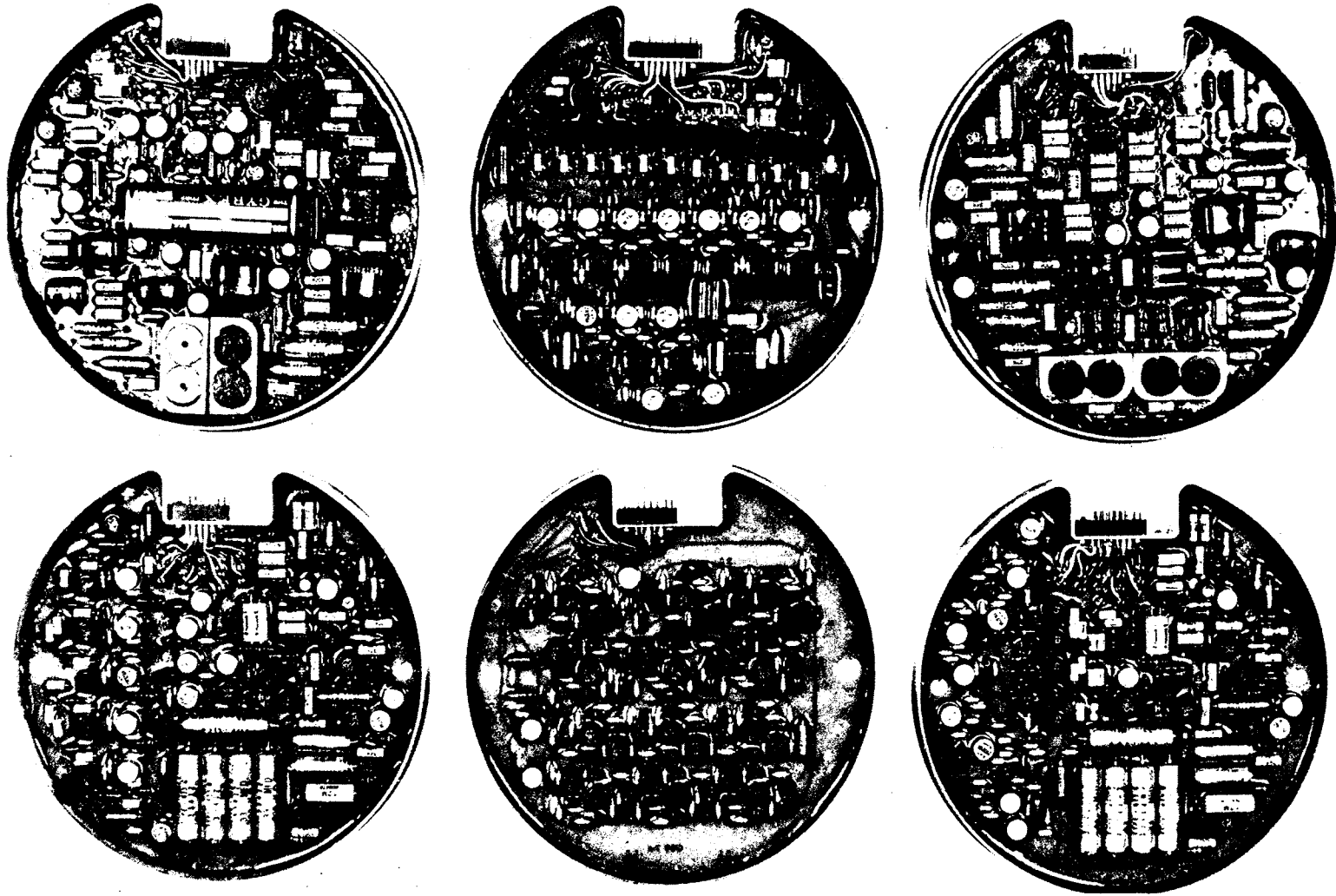


Fig. 22.10 Some typical decks.

available space, two links are mounted on one chassis. Each link utilizes only 10 standard subcarrier oscillators. The components are similar to those used in the XO-4. The history of telemetry performance on the Pershing shows as high a telemeter reliability as that of the Redstone and Jupiter.

## 22.5 Saturn

The Saturn C-1, with its cluster of eight liquid-fueled engines, compounded the data transmission problems. The magnitude of the Saturn as compared to the Jupiter increased the requirements for telemetry channels by a comparable magnitude.

An approximate comparison of the measurements required on the Saturn with respect to earlier ballistic missiles, is shown in Table 22.2.

Table 22.2 Telemetry Measurements on Space Vehicles

Vehicle	Total Measurements (approx. average)	Vibration Measurements (50 to 3000 cps data)
Redstone	100	4
Jupiter	150	9
Pershing	150	9
Saturn C-1		
S-I Stage	550	40-50
S-IV Stage	250	6
Instrumentation Unit	150	30
(Other stages will be comparable in magnitude to the S-IV stage).		

It was obvious that additional systems would have to be developed to supplement the FM/FM system, and that this system should be further improved. In solving the problem, the same criteria of previous designs will be followed, as well as these additional considerations:

1. New modulation techniques will be considered to facilitate handling the vastly increased number of vibration data required.
2. A more intensified effort will be made to reduce the power consumption and weight of the systems without sacrificing any desirable characteristics.
3. The equipment will be designed for increased reliability and longer operating times.
4. The system and the equipment will be designed for use as a utility link for automatic calibration and automatic checkout schemes

necessary in rapid checkout for consecutive firings in orbital and docking operations.

5. A digital link (PCM) will be considered to handle those data particularly adaptable or advantageous to this technique.

6. Because of the magnitude and complexity of the eventual multi-stage vehicle, a data systems approach will be taken for the total vehicle.

After an extensive study of practical modulation techniques and an investigation of component developments, it was decided to undertake the following development programs:

1. Redesign the FM/FM system using the latest solid components where practical.

2. Develop a solid-state high-capacity multiplexer capable of being used on both PAM and PCM systems, as well as operating synchronously with other multiplexers for serializing checkout data.

3. Develop both high- and low-level solid-state gates capable of remote multiplexing into a mixed high-low level system.

4. Develop an improved decommutator for separating the multiplexed data.

5. Develop a single-sideband AM/FM system, designated SS/FM, for more efficient transmission of vibration data.

6. Develop a state-of-the-art analog-to-digital (A to D) converter and programmer to be used in PCM systems, as well as digital automatic checkout systems.

7. Investigate the use of core memory devices or magnetic tape for on-vehicle data storage, or both.

8. Investigate the use of predetection recording for future applications.

9. Investigate the problems and advantages of UHF for telemetry transmission.

10. Investigate the use of adaptive telemetry techniques for bandwidth reduction and, consequently, power conservation.

11. Maintain a continuous program of component evaluation and development for system improvement from the standpoint of reliability, accuracy and efficiency.

12. Develop a PCM demodulator capable of interfacing with an electronic computer for use in automatic checkout and calibration.

13. Develop a more efficient rf power amplifier.

A new, transistorized version of the FM/FM system was developed in 1961. This package, designated the XO-5, is similar in characteristics to the previous model except components are transistorized where practical.

Excluding the rf power amplifier, the unit weighs 13 lb, is 320 in.<sup>3</sup> in volume and consumes 24 w of power. Including the 35 w rf power amplifier, the total system weighs 23 lb, is 565 in.<sup>3</sup> in volume and consumes

185 w of power. The XO-5 package is shown in Fig. 22.11. Figure 22.12 is a pictorial comparison of the XO-1, 2, 4, and 5 while Fig. 22.13 is a similar comparison in the form of a bar graph. Since these units use modulation techniques and have the same data bandwidth, the comparison indicates the relative state-of-the-art telemetry hardware development advances over a period of approximately 8 yr.

Figure 22.14 is a 216-channel solid-state multiplexer (commutator) developed in 1960. This multiplexer operates at a rate of 3600 pps, each channel being sampled 12 times per sec. The unit weighs 18 lb, is 650 in.<sup>3</sup> in volume, and consumes approximately 5 w of power. This unit was successfully flown on the first Saturn C-1 flight. The multiplexer was designed to be compatible with existing decommutators; as a result, extra synchronizing pulses were necessary to subdecommutate the data. A decommutator has been developed that will allow subframe synchronization without the use of the extra pulses. Elimination of these pulses will allow the system to be expanded to 270 data channels at the speed it now operates. Other refinements of the system will allow remote subcommutation with either low-level, high-level, or mixed inputs. The units can operate independently, or two or more can be operated synchronously. For PAM applications, the output of the multiplexer modulates a wideband (70 kc  $\pm$  30 per cent) SCO and is mixed with IRIG channels 2-14 in a PAM/FM/FM system. This package, the XO-6, is shown in Fig. 22.15.

A decommutator that was developed to be used with the multiplexer is shown in Fig. 22.16. The multiplexer uses a crystal stable clock which allows ringing filter techniques to be used for synchronizing the decommutator to the multiplexer. The decommutator is all solid-state, using shift registers for gating logic. It is extremely simple to set up and operate. A convenient patch panel is located on the front panel, allowing any one of the 270 data channels to be patched into the output demodulators. The unit has 10 demodulators built in, but as many others may be added as are desired.

An SS/FM system has been developed to be used for wideband data, particularly vibration. Figure 22.17 depicts the vehicle-borne portion of this system while Fig. 22.18 shows the demodulator. Development of this system began early in 1959, and the first units will be flown on the second Saturn C-1 flight in the spring of 1962. Fifteen channels of wideband data (vibration), each with 50 to 3000 cps data bandwidth, may be transmitted in the same rf bandwidth as a standard FM/FM system with a full complement of subcarriers. This represents better than a 10 to 1 improvement in data bandwidth to rf bandwidth over the standard FM/FM system. The SS/FM package weighs about 18 lb, is 750 in.<sup>3</sup> in volume and consumes 23 w of power; this does not include the power amplifier.

Since early in 1961, a digital telemetry system (PCM) has been under development and is scheduled for a test flight on the third Saturn

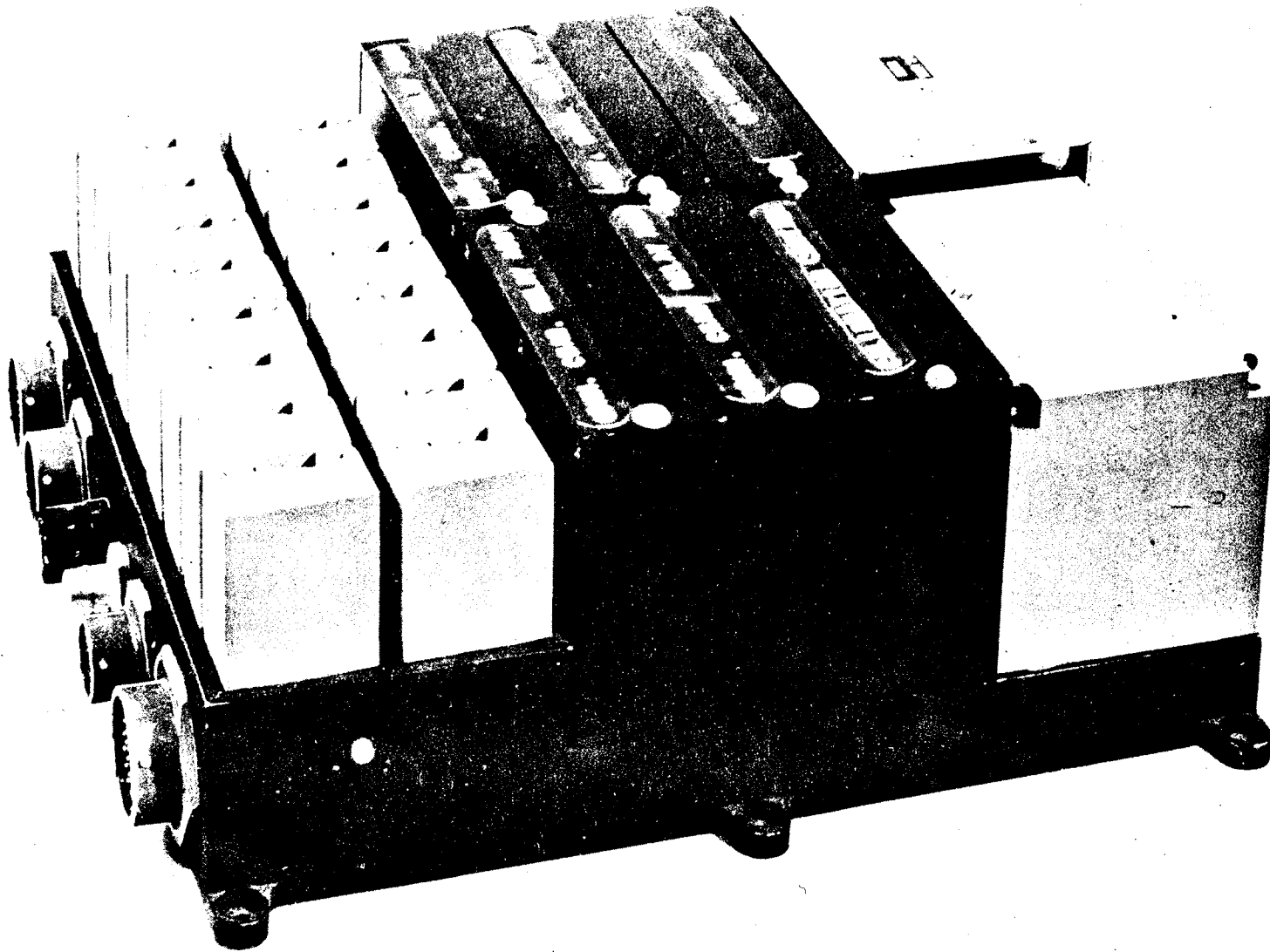


Fig. 22.11 X0-5 telemetry package (Saturn).

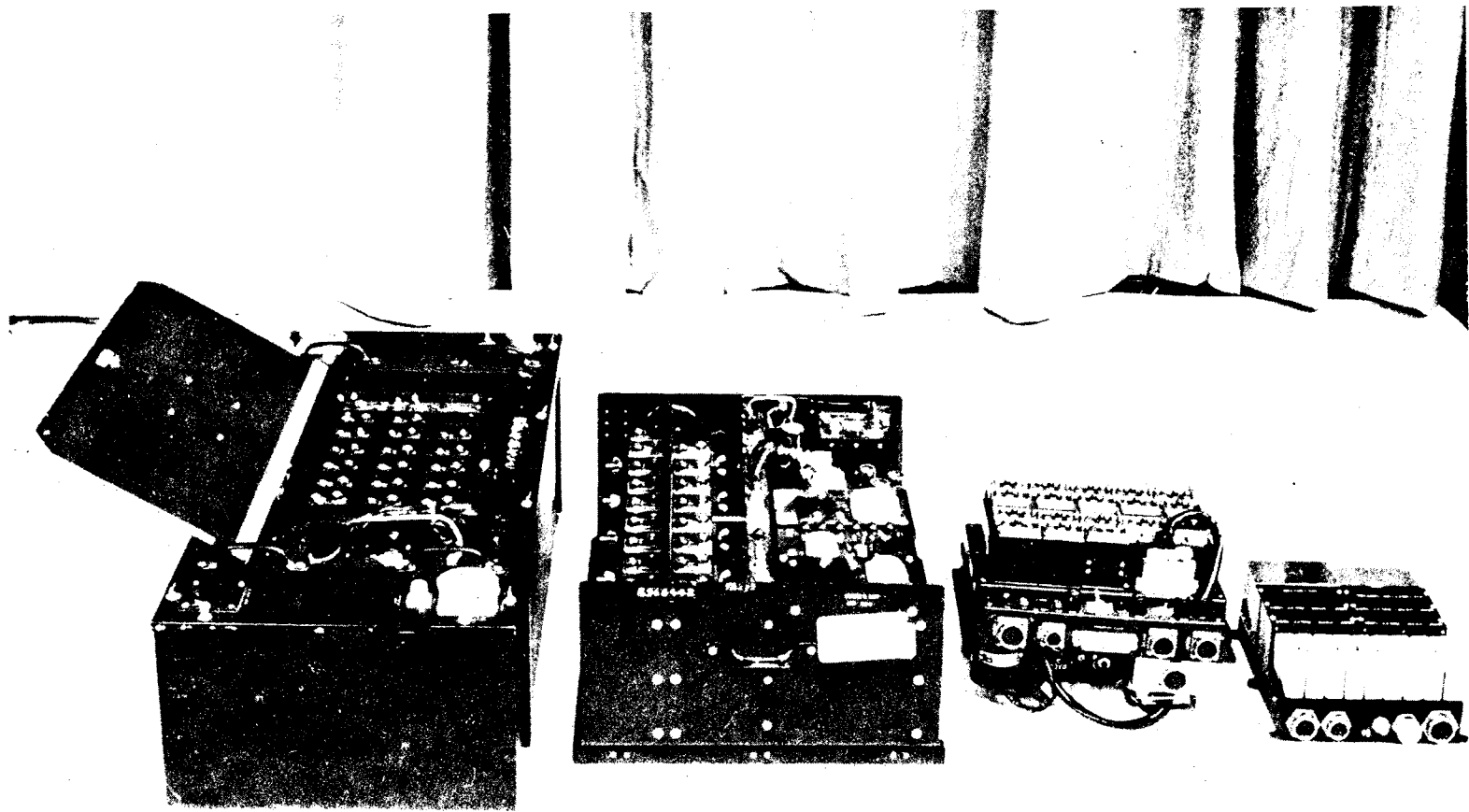


Fig. 22.12 Pictorial comparison of X0-1, -2, -4, and -5.

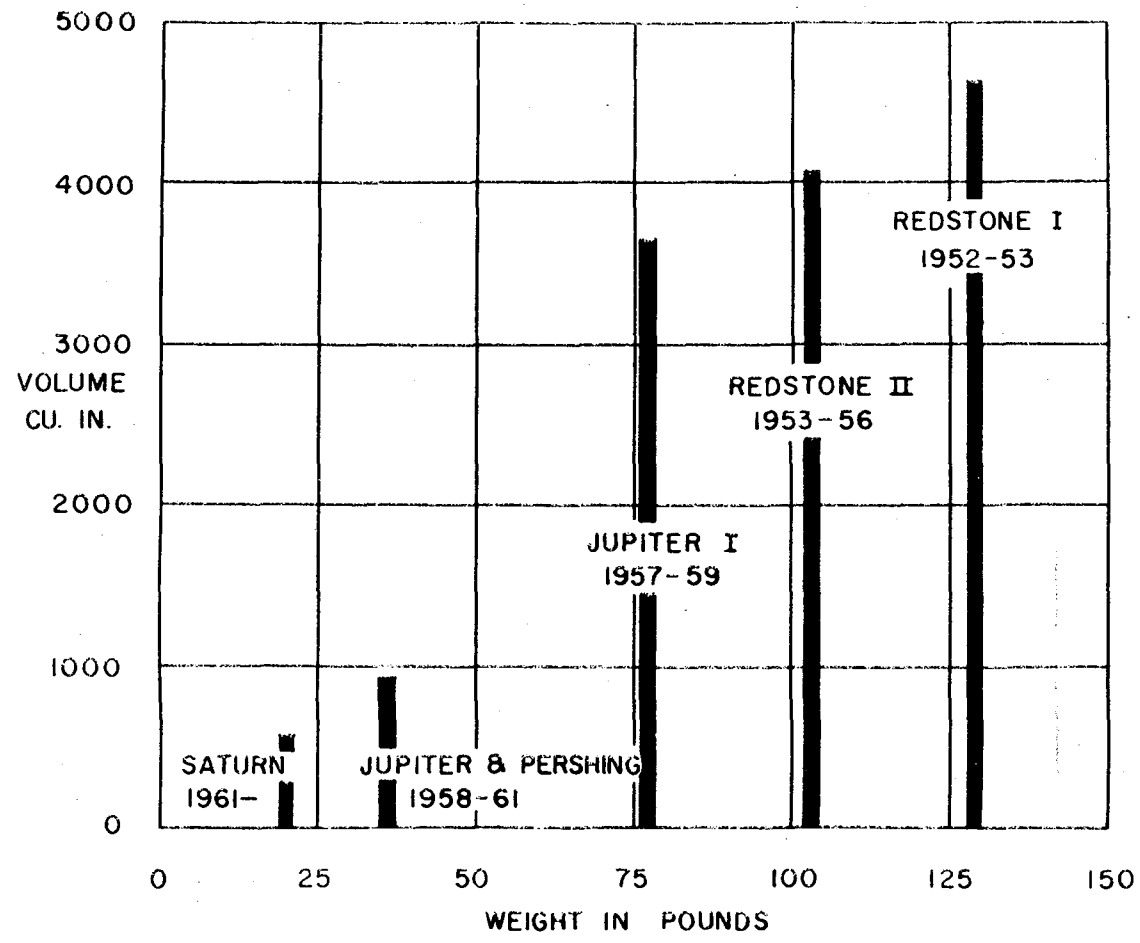


Fig. 22.13 Bar graph comparison of XO-1, -2, -4, and -5.



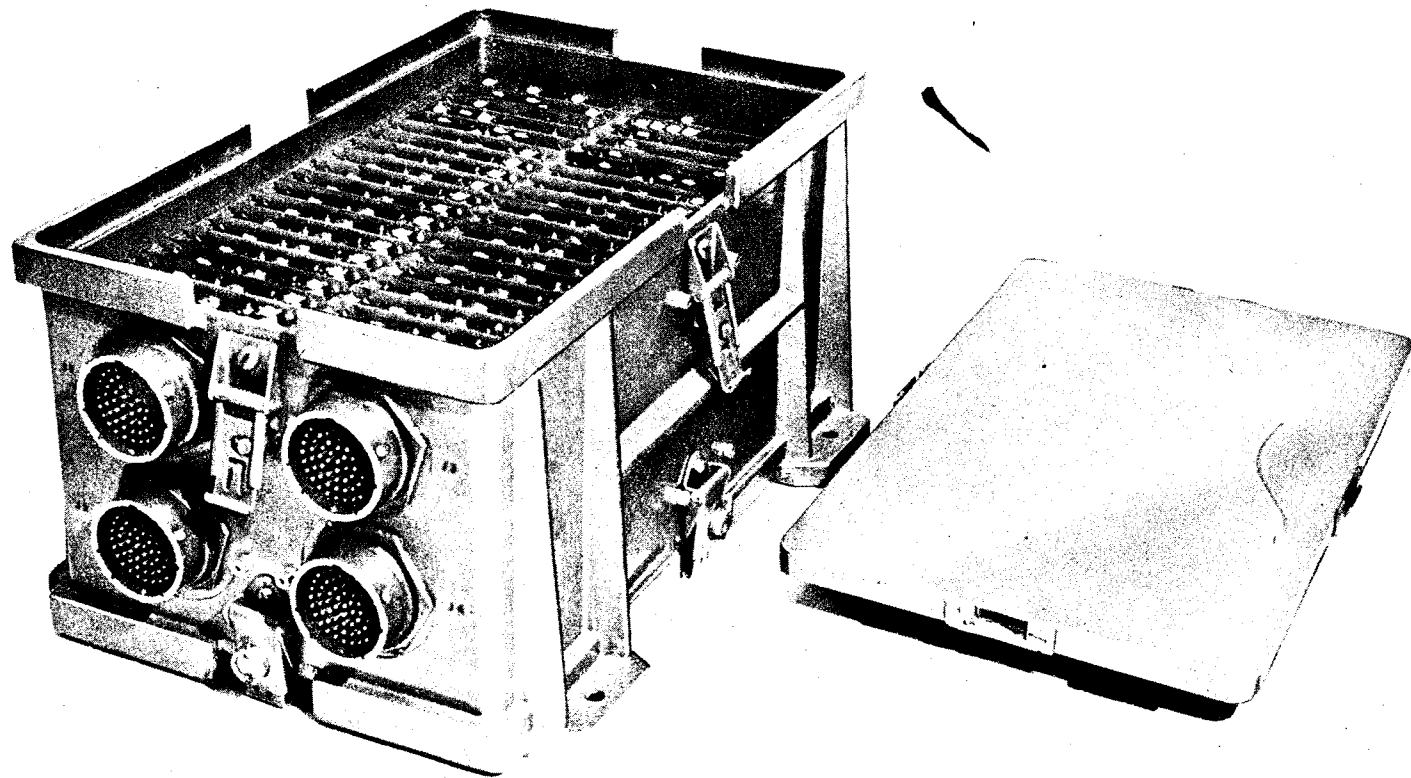


Fig. 22.14 216-channel solid-state multiplexer(commutator).

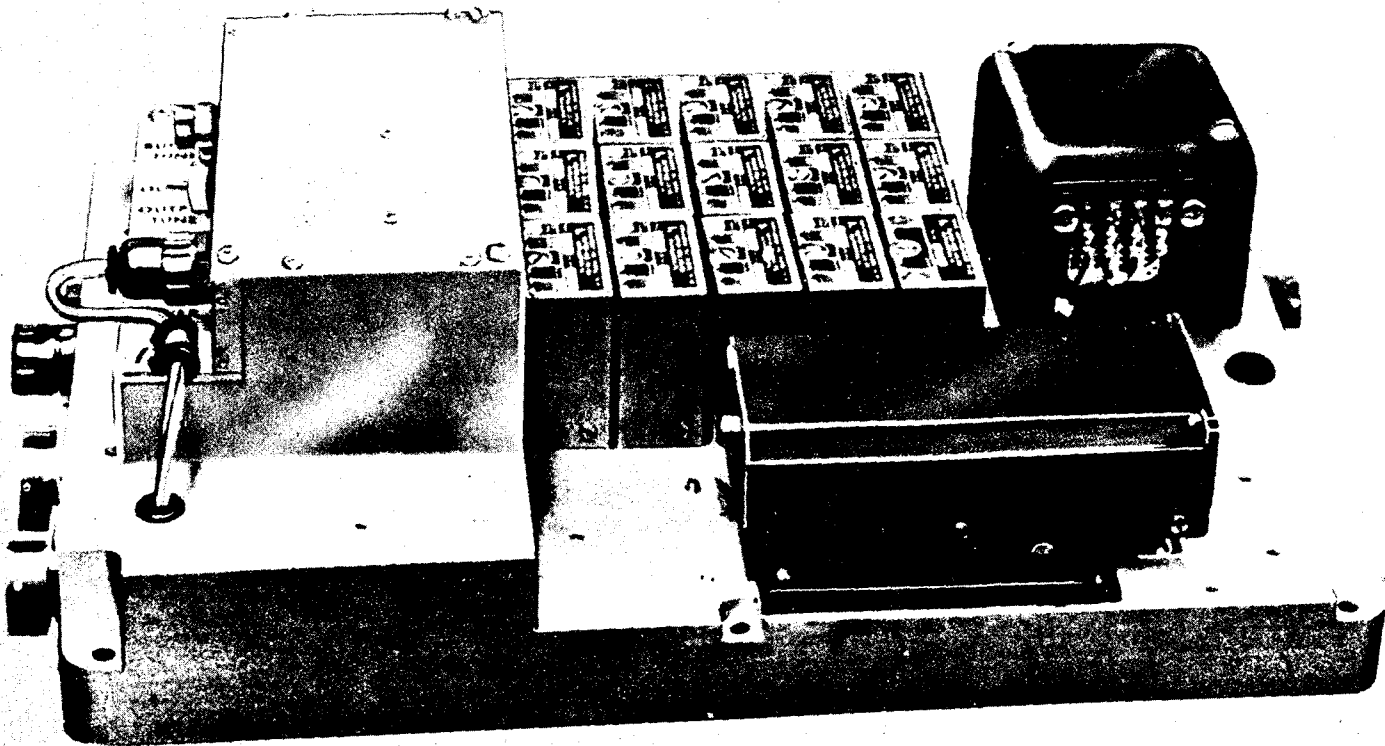


Fig. 22.15 X0-6 telemetry package.

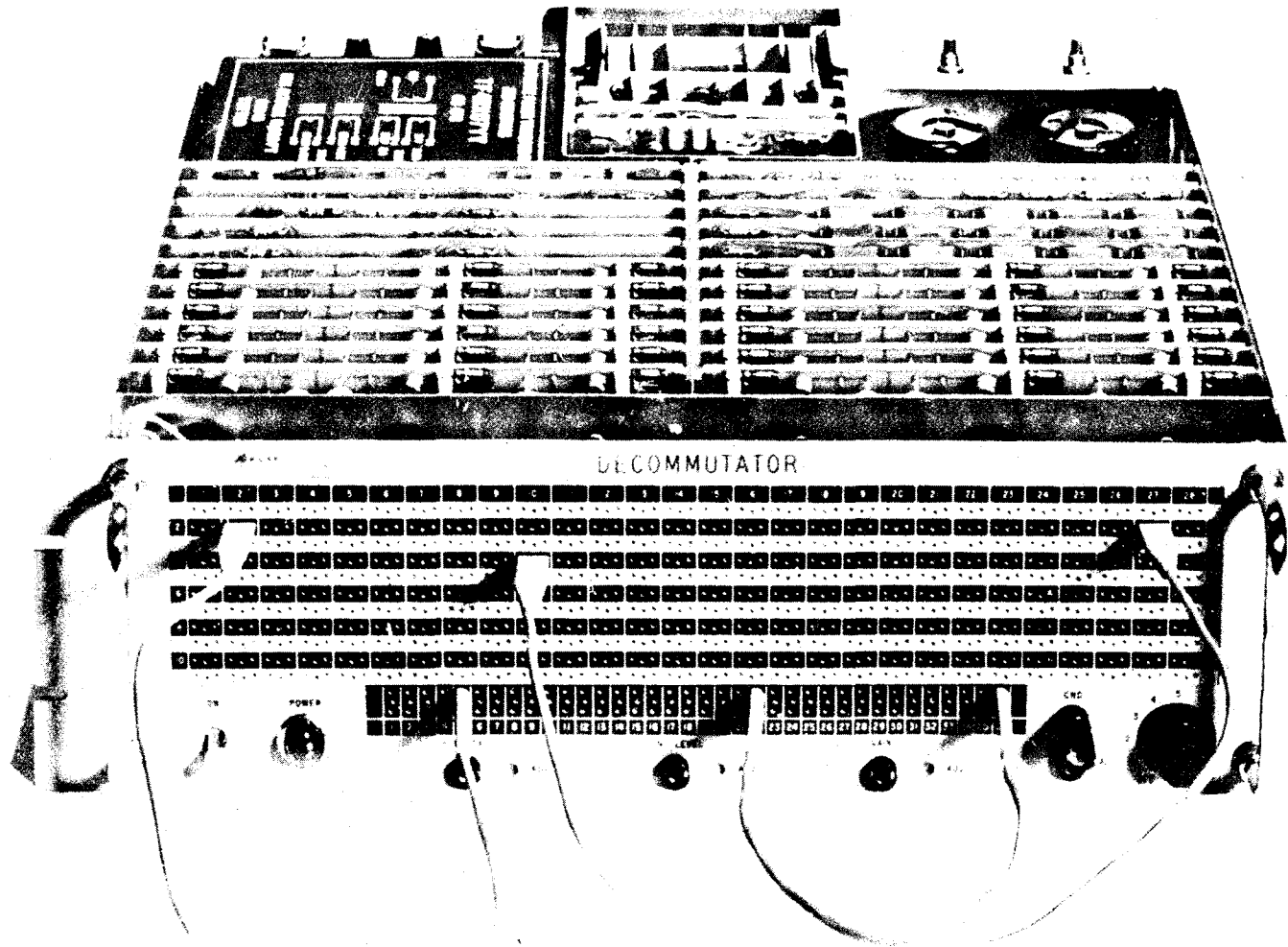


Fig. 22,16 Decommutator to be used with X0-6 multiplexer.

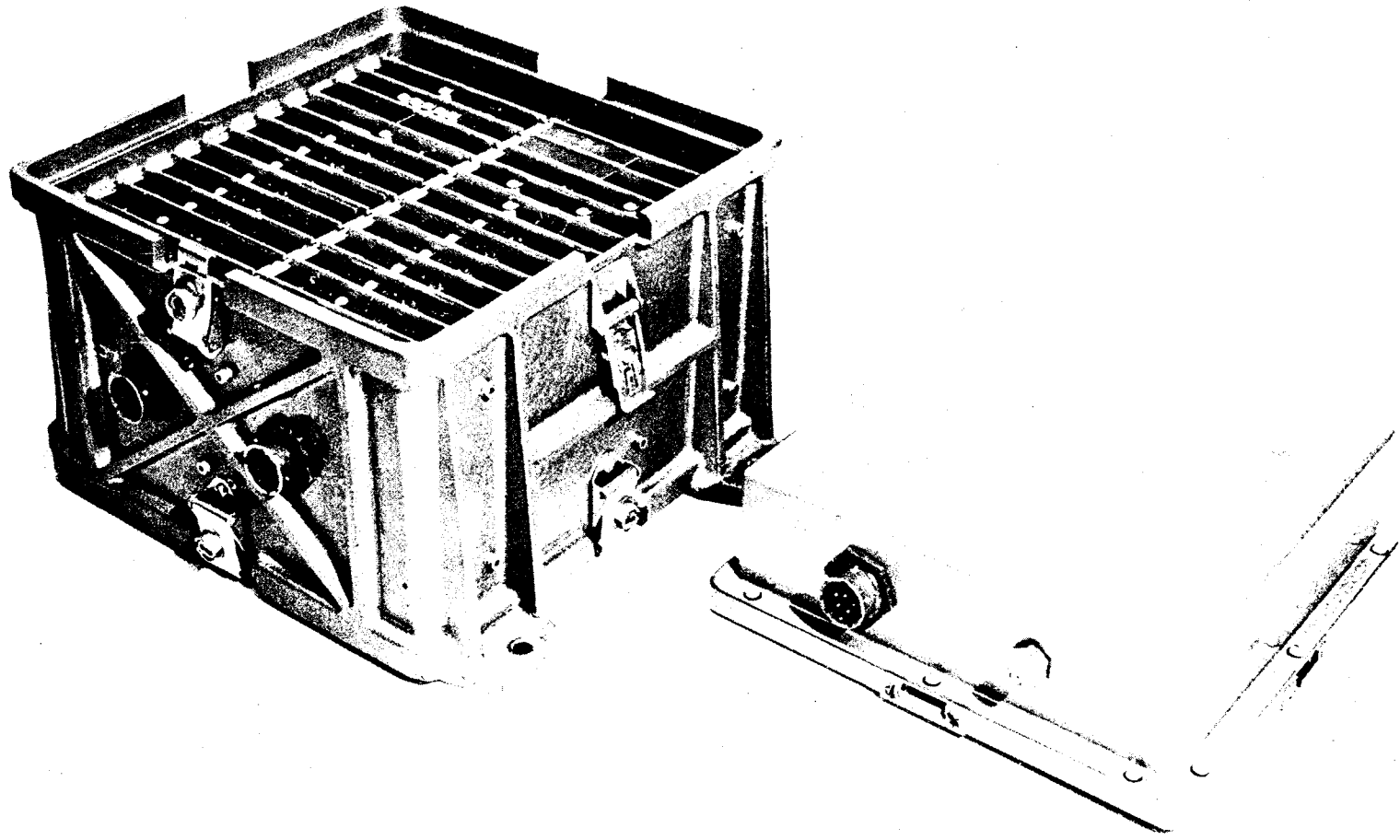


Fig. 22.17 Vehicle-borne portion of SS/FM system.

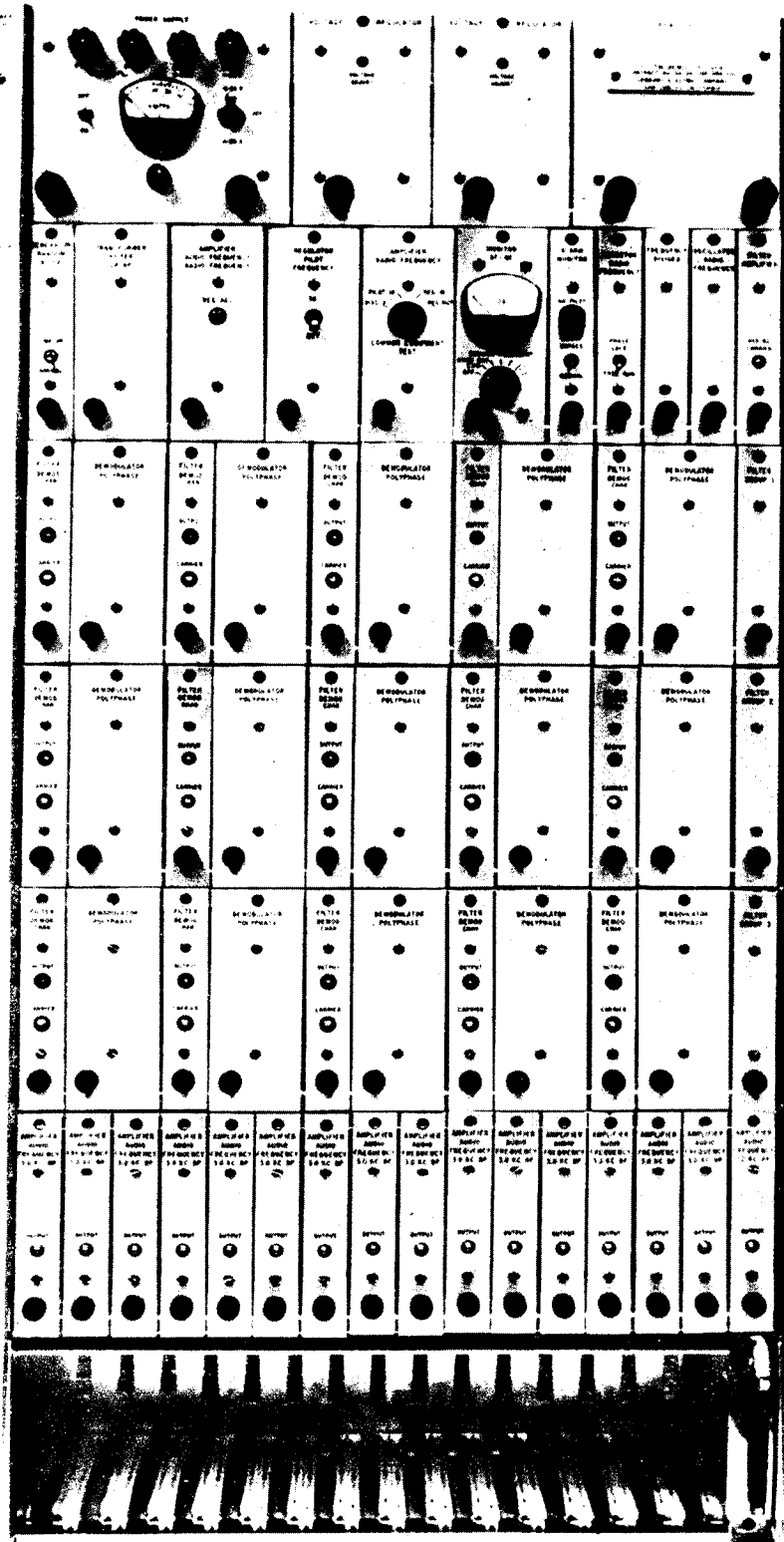


Fig. 22.18 Demodulator of SS/FM system.

flight. The vehicle-borne PCM system will consist of one or more of the 270-channel multiplexers previously described, an A to D converter, a programmer, and an FM transmitter unit. The A to D converter is capable of obtaining accuracies of up to 0.1 per cent. A high degree of flexibility in bits per word, bit rate, word and frame identification, and input format has been designed into the unit, thus making it adaptable to a variety of formats. The size of the A to D converter and programmer is approximately the size of one multiplexer. The system size will depend upon the number of multiplexers used.

Although the PCM system will be used for a portion of the flight data transmission, it will also be employed to digitize data for automatic calibration and checkout. Digitizing data aboard the vehicle for this purpose increases the accuracy and considerably reduces the number of wires on the vehicle, as well as from the vehicle to the checkout area. The system is simple and requires little additional equipment in that the multiplexers and A to D converter are already necessary for transmission of flight data. The equipment will operate in two modes, one for checkout and one for flight. In the checkout mode, all data will be serialized and put into digital form for transmission to the checkout computer. At the receiving end, the data will be processed, paralleled, and stored for instantaneous access by the computer. The analog output of the telemetry ground station may be digitized and fed to the computer for comparison. A complete instrumentation and telemetry calibration and checkout can be made in this manner. Portions of the automatic checkout system will be tested on the Saturn configuration 5; it is planned to have the entire system in operation before completion of the Saturn configuration 10.

To increase flexibility, auxiliary equipment has been designed that may be used with the other systems. This equipment includes vibration and flow rate multiplexers, preflight and inflight calibrators, and sub-carrier packages for triple FM applications. Figure 22.19 shows a typical auxiliary package which contains flow-rate and vibration multiplexers for taking spectral samples of the data. It also contains preflight and inflight calibrators for injecting precision voltages into the telemetry systems at programmed intervals. The package is of sandwich construction and can be expanded or reduced as required.

## 22.6 Conclusions

An intensive program of telemetry component development has been carried on from the early V2 and Redstone missiles through the Saturn space carrier vehicle. Each system has become progressively better and more sophisticated. With each new system, the reliability, accuracy, and bandwidth utilization have been increased, whereas the size, weight, and power requirements have been reduced.

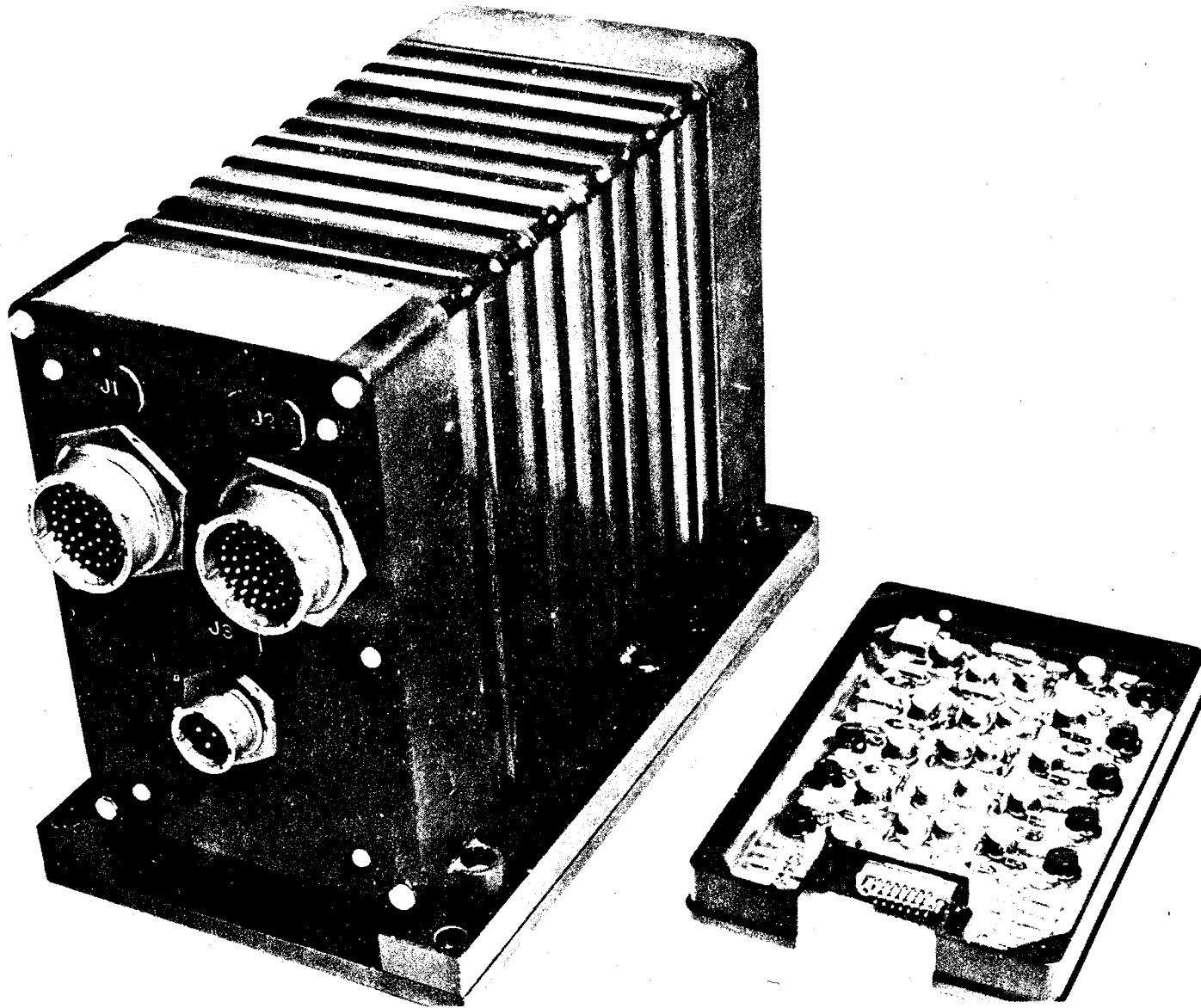


Fig. 22.19 Typical auxiliary package.

Telemetry and instrumentation engineers have applied innovations such as printed circuits and solid-state devices to the design of components and systems in advancing the telemetry state of the art. These advances have been made through the concentrated effort of engineers and technicians working on systems and components from the first concept to the final design, checkout, and modification. The ideas from numerous organizations, private companies, and individuals have been blended into the total systems concept. To maintain a competent technical approach, certain development has been performed inhouse, but many areas of development have been performed by contractual support of private companies. Except for some prototype systems, all manufacturing is performed by private industry.

A good comparison of progress over an 8-yr span, 1953 to 1961, would be to compare a Redstone telemetry system with that of a Saturn S-1 stage. The total telemetry system for an S-1 stage has a data bandwidth of about 100,000 cycles, requires 6 telemetry links with a total weight of approximately 196 lb, has a volume of 5,500 in.<sup>3</sup>, and consumes 1100 w of power. The telemetry system for an early Redstone had a data bandwidth of about 4000 cycles, required one link with a total weight of 130 lb, had a volume of 4600 in.<sup>3</sup>, and consumed 476 w of power. If the system used in the Redstone were used for the data on the Saturn S-1 stage, it would require a total of 20 links at a weight of 2600 lb, a volume of 92,000 in.<sup>3</sup>, and would consume 9529 w of power. The number of rf links or bandwidth utilization has been improved by a factor of 3.3. The equipment weight has been improved by a factor of 13, and the power consumption has been improved by a factor of 8.6. If the Redstone equipment were used for the S-1, the cost of the equipment would be approximately \$300,000. The cost of the telemetry equipment now used on an S-1 stage is about \$150,000; thus, a cost saving of one-half is achieved.

The systems of tomorrow will be further improved, using such techniques as micromodules and improved modulation techniques with more efficient carriers, receivers and antennas. There is still room for vast improvement. A continuing program is necessary to improve the components and subsystems which will be used to build better data systems in the future.



## 23

## APPLICATION OF THE DOPPLER PRINCIPLE TO ROCKETRY

Karl Sendler, James R. White, and Rudolf Bruns

Launch Operations Directorate  
George C. Marshall Space Flight Center  
National Aeronautics and Space Administration  
Huntsville, Alabama

## 23.1 The Doppler Effect

The frequency shift due to relative motion was first measured by Christian Doppler at Prague in 1842. In this experiment, the sound from a moving bell was compared with that of a stationary tuning fork. The sound arrived at a higher pitch than that of the tuning fork when the bell was moved rapidly toward the observer and a lower pitch when the bell was moved in the opposite direction. Similar results were obtained when the observer moved while the bell remained stationary. It was later shown that Doppler's principle is applicable to light and radio waves as well as to sound waves.

In the simplest application of this principle to modern tracking problems, the bell is replaced by a crystal-controlled transmitter in the moving vehicle and the frequency of the signal received at a ground station is compared with that of a crystal reference oscillator. The difference is directly proportional to the rate of change of distance between the vehicle and the station. Such measurements are limited in accuracy by the fact that two crystals cannot be ground to exactly the same frequency. In spite of this limitation, however, the system is frequently used when weight limitations preclude the use of more complicated on-board equipment.

The accuracy of the measurement can be greatly increased by the use of an on-board transponder that receives a signal from a ground transmitter and reradiates it to a ground receiver. The return signal, which has been subjected to a Doppler shift on the way up to the vehicle and again on the way down, is then compared with a sample of the original signal from the ground transmitter. The difference is proportional to the loop velocity or the rate of change of the loop distance from the transmitter to the vehicle and back to the receiver. For the special case in which the vehicle is known to be traveling directly away from the ground transmitter and receiver, the velocity of the vehicle is half the loop velocity.

## 23.2 Philosophy of Doppler Tracking Systems

An electronic system that makes direct use of the Doppler effect is especially suitable for rocket development. The development of ballistic missiles and space vehicles requires a highly accurate, reliable, and all-weather instrumentation system. Most rockets are powered only during a relatively short portion of the flight; therefore, exceptionally high accuracy is required for that portion of the trajectory. To evaluate guidance and control systems and power plants while the vehicle is in the research and development phase, it is necessary to determine the trajectory to an even greater accuracy. The more common electronic tracking systems, such as radar, are not considered adequate.

Some optical systems, such as ballistic cameras with star calibration, produce the required position accuracy; but they are limited by their dependence on atmospheric conditions. Another serious objection, both to optical and radar tracking systems, is the fact that they are basically position measuring devices. Minor imperfections of the engines or the guidance and control systems are most often detected by comparing the observed velocity or acceleration with predicted values. Velocity can be determined from radar and optical data only by differentiating the position data; double differentiation is required in order to find acceleration. Slight noise in the position information is thus greatly magnified by this process, while Doppler systems yield velocity information without differentiation and require only one differentiation to obtain acceleration.

The demand for accurate and reliable trajectory data is further increased by the stringent flight safety requirements that must be fulfilled when ballistic missiles are fired. If it becomes necessary for one of the slower, air-breathing missiles to be destroyed for safety reasons, emergency measures can be taken to bring a winged vehicle to Earth near the point at which the malfunction occurred. Such is not the case when the offender is a ballistic missile far outside the atmosphere. If the vehicle is destroyed by radio command, the pieces will continue in a ballistic trajectory and may impact hundreds or even thousands of miles away. It is necessary to know when the potential impact point (the point at which the rocket would impact if thrust should terminate at a given instant) reaches the edge of the danger area, so that emergency action can be taken before life or property is endangered. Reliability is even more important in flight safety instrumentation than in systems used to properly evaluate vehicle performance. A failure in this equipment can result in the destruction of a perfectly good vehicle.

In the early stages of rocket development, it was sometimes necessary to make use of ground tracking stations as part of the guidance system. The velocity was measured by tracking stations in the launch area, and when it reached the value required to produce the desired range, the engine was cut off by radio command.

The original Doppler velocity cutoff system contained a ground transmitter and receiver, both located behind the launch site on a line tangent to the trajectory at the cutoff point. The on-board transponder received a signal from the ground transmitter, doubled the frequency, and retransmitted the resulting signal to the ground station. A signal from the same ground transmitter was doubled and compared with that returning from the missile. Before liftoff these two frequencies were exactly the same; but as velocity increased, the frequency received from the missile was shifted downward due to the Doppler effect, producing an audible beat between this signal and the second harmonic of the ground transmitter. When the beat reached a precalculated frequency, the cutoff command was initiated.

### 23.3 The Dovap System

A one-station system like that described above can measure only one component of velocity -- the component toward the station. In order to evaluate the performance of a missile, all components of both velocity and position are required. A Dovap (Doppler velocity and position) system was formed by adding additional stations to one of these velocity cutoff systems.

A typical Dovap system consists of a reference transmitter, three or more receiver stations, and a recording station. The transmitter, which operates on a frequency of about 37 Mc with an output power of 2 to 4 kw, radiates an unmodulated signal to the missile and to each of the receiver stations. A transponder in the missile receives the signal, amplifies it, doubles the frequency, and retransmits the second harmonic to the ground receiver stations. At each of these sites, the signal from the missile transponder and that from the ground reference transmitter are received and compared. The beat between the missile signal and the second harmonic of the reference is recorded at a central station.

Although the reference signal  $f_t$  is a constant 37 Mc, the signal received by the transponder is altered by the Doppler effect when the missile is in motion. If the missile is moving away from the transmitter the frequency received is  $f_t - d$  where  $d$  is the Doppler shift. This frequency is doubled and retransmitted as  $2f_t - 2d$ . The return signal suffers an additional Doppler shift so that station  $R_1$  receives a frequency of  $2f_t - 2d - d_1$ .

Station  $R_1$  also receives the reference signal direct from the transmitter site. This reference is unaffected by the Doppler shift, as both the transmitter and receiver stations are stationary. The reference frequency is doubled at the receiver site and is beat with the missile signal to produce

$$2f_t - (2f_t - 2d - d_1) = 2d + d_1 \quad (23.1)$$

This is an audio frequency that is proportional to the rate of change of the loop distance from transmitter to site  $R_1$ . The actual loop distance is found by integrating this frequency.

The receiver used to compare the signal from the missile with the frequency of the reference transmitter is a dual-channel, superheterodyne receiver with a common local oscillator shared by the two channels. The local oscillator frequency used by the 37 Mc channel is doubled and supplied to the mixer stage of the 75 Mc channel, producing an i.f. of 5 Mc for the data channel and 2.5 Mc for the reference channel. The 2.5 Mc i.f. is doubled and the two subtracted to form the Doppler beat.

The beat frequency from each station is recorded on 35-mm film together with coded timing pulses. As most of the stations are in remote locations, it is considered more convenient to relay the beat frequency to a central recording station, where accurate timing is available, than to relay the timing signals to the various sites and record each beat locally. This places all of the recording equipment in a central, easily accessible, location and reduces the remote receiver stations to relatively simple installations. It also has the advantage that one recorder can serve several sites.

The beat frequencies are transmitted to the recording station over telephone lines where the distances are short and where such lines are available. However, it is often found to be more economical to use an rf link. In the case of some of the more critical stations, rf links are used even when land lines are available, due to the increased reliability and improved frequency response. The rf link employs standard FM-FM telemetry equipment. A subcarrier oscillator, usually 52.5 or 70 kc, is frequency modulated with the audio beat and the resulting signal is then frequency modulated on an rf carrier in the 70 to 100 Mc range and transmitted to the recording site. There it is received and discriminated one time with a wide-band FM receiver to recover the modulated subcarrier, which is again discriminated to produce the original Doppler beat. Unlike the FM-FM system used for missile to ground telemetry, each carrier is usually modulated with only one subcarrier. The double modulation technique is necessary, however, in order to handle the extremely low beat frequencies encountered at liftoff.

At the recording station, beat signals varying in frequency from zero to about 2000 cycles are displayed on cathode-ray tubes and photographed with an oscillograph recording camera. The signal is placed on the horizontal axis with no sweep on the vertical axis. The time base is provided by the motion of the film, which is driven by a synchronous motor governed by a crystal controlled oscillator. Four cathode-ray tubes, presenting the beats from four stations, are mounted in front of each camera. Lamps, fed by coded timing pulses, are mounted between the cathode-ray tubes. The resulting films show four sine waves and several rows of dots and dashes produced by the timing lamps.

The beats are also recorded on magnetic tape, using FM recorders to extend the frequency range to zero. Originally these recorders were only used as back up for the cameras. In case of a camera failure, the tape record could be played back into the camera recording equipment to reconstruct the film. Equipment to read the magnetic tape directly was later developed, with the result that the cameras became secondary in importance to the tape recorders.

The film record is read by a stroboscopic film reader that counts the total number of cycles in each trace on the film and punches an IBM card, showing the subtotal and the time for every 0.5 sec of flight. The cycle counters used to reduce the magnetic tape produce a subtotal read-out on digital tape for each 0.1 sec of flight. In both cases, the subtotal is read to 0.1 cycle.

The total number of cycles that have occurred up to a given time constitutes the integral of frequency and, therefore, indicates the total change in loop distance from liftoff to the given time. As the original loop distance at liftoff is known from a first order survey of the stations and of the launching pad, the actual loop distance from the transmitter to the missile to any receiver station can be determined at any time. The loop distance measurement from each receiver defines an ellipsoid with one of its foci at the receiver station and the other at the ground transmitter. Three such ellipsoids define a point in space. It is desirable, however, to use more than three receivers to allow a redundant calculation of  $x$ ,  $y$ ,  $z$ ,  $\dot{x}$ ,  $\dot{y}$ , and  $\dot{z}$  for each point of the trajectory.

The Dovap system installed at Cape Canaveral to track the Redstone missile consists of eight receiver stations, all located within 20 miles of the launching pad at Cape Canaveral, and one transmitter station and one recording station, both located at the Cape. Another complete system of five receiver stations, a transmitter, and a recording station, on Grand Bahama Island and the nearby Cays, was used to cover the terminal portion of the trajectory. As each missile carried only one transponder, the two systems were not operated simultaneously. A switchover to the Dovap on Grand Bahama was made when the missile reached the point at which the geometry of that system became more favorable.

One limitation of the system is the ambiguity of its data. Dovap is basically a velocity measuring system; position data are obtained by integration. Therefore, to determine the constants of integration, one point of the trajectory must be known. This may be the liftoff point or some other point obtained from an independent system. The system on Grand Bahama, which cannot see the missile at liftoff, must rely on the Cape Canaveral Dovap or ballistic cameras for a tie-in. Furthermore, a momentary equipment failure could render subsequent data useless unless a tie-in can be obtained by extrapolating through the dropout. Fortunately, however, the system is so uncomplicated that equipment failures are extremely rare.

The accuracy of Dovap is difficult to express. The raw data give loop range measurements, and the accuracy of the position data calculated from these is a function of the position of the missile and the geometrical configuration of the stations. Experience indicates that loop distances can be measured to an accuracy of about 5:1,000,000. With the station layout used at Cape Canaveral, this can produce position errors to the order of 10 m when the missile is 100,000 m from the stations. Velocity accuracies of about 0.5 m/sec can be obtained up to that distance from the station complex, independent of the rocket velocity.

#### 23.4 The Udop System

Dovap was a satisfactory tracking system for short range missiles (up to 200 miles range) and is still used extensively in the development of missiles of that type. When longer range missiles appeared, however, more accurate guidance was required and more accurate tracking was necessary to observe the performance of these new guidance systems. Dovap was obviously incapable of measuring velocity to the accuracy required for the Jupiter IRBM. An ultra-high-frequency Doppler (Udop) system was developed to meet these new accuracy requirements.

A major limitation of the Dovap system is its resolution, or the accuracy to which the best cycles can be counted. Each cycle represents a loop change of one wavelength or about 4 m. The beat can be counted to the nearest 0.1 cps, corresponding to 0.4 m of loop distance. If better resolution is required, it is desirable to use a shorter wavelength.

Dovap is again limited in that a single transmitter is used to supply a reference signal to the missile and also to the ground stations. It is desirable that the antenna that radiates the signal to the missile be located very near the ground to prevent multipath reception in the missile. If the antenna is located on a tower, two signals will reach the transponder — one directly from the antenna on the tower and another reflected from the ground or sea. The relative length of these two paths varies as the elevation of the missile changes. The reference signals to the receiver stations are not disturbed by this type of multipath because the elevations of the ground stations are fixed. Therefore it would be desirable to use a different antenna to supply reference to the receiver stations. This antenna could be located on a pole or tower, providing line-of-sight transmission to receiver sites beyond the horizon from the transmitter. Use of two antennas is impractical, however, when both reference signals are of the same frequency.

It is impossible to build an antenna that would radiate a signal to all the receiver stations without also radiating some energy to the missile, where it would interfere with the signal from the other antenna on the ground. A more practical approach uses two harmonically related

reference signals, both derived from the same crystal oscillator but radiated at different frequencies. For example, an 18.5 Mc transmitter with an antenna on a pole might supply reference to the Dovap ground stations, while a 37 Mc transmitter, using the same exciter, interrogates the missile from an antenna on the ground. The transponder doubles the 37 Mc (less any Doppler shift), and the receivers multiply the 18.5 Mc reference by four to produce 74 Mc. Unfortunately, 18.5 Mc and all other frequencies below 30 Mc are too noisy for this type of service. The plan works much better if the whole system operates at much higher frequencies.

Another objection to Dovap frequencies is encountered when missiles begin to travel higher into the ionosphere. Vhf frequencies suffer severe phase shifts when they pass through the ionosphere. It is known that uhf frequencies, on the other hand, are only slightly affected. Flame effects are also less severe at higher frequencies.

In addition to the phase shifts caused by ionosphere and flame, these two effects combine to produce rapid variations in attenuation, both in the transmitter-to-missile path and in the missile-to-receiver path. If actual dropouts occur, they are usually of sufficiently short duration to permit extrapolation of data through them; but fluctuations in signal level are difficult to handle by the present Dovap receiver. Changes in signal strength, even when they do not constitute a complete dropout, cause phase shifts in the receiver. It is possible, at the present state of the art, to develop a receiver with phase shift substantially independent of signal strength. However, because of other limitations of the system, it is considered impractical to invest in a research and development project to produce a new Doppler receiver at these frequencies.

The most urgent need was for a more accurate measurement of cutoff velocity for the Jupiter missile. A single station was installed to produce these velocity data and, at the same time, to investigate the feasibility of a uhf Doppler position measuring system. A uhf transmitter, transponder, and ground receiver, developed as part of the Corporal missile system, was available. The first station was an interrogator transmitter with a frequency of about 450-Mc. This signal was doubled by the missile transponder and reradiated to a ground receiver that was located near the transmitter. A sample of the 450-Mc reference was doubled and sent to the receiver over a cable. Only one receiver station could be used because the receiver did not have a reference channel and required a high level reference signal. Results were very encouraging. The system produced the resolution necessary for the velocity and proved that the combined effects of flame and ionosphere were greatly reduced.

The first Udop system could only measure one loop range, however, and as mentioned above, three or more loop measurements are required for position and velocity calculations. It was necessary to combine this loop measurement with others from the Dovap stations in order to determine the three components of velocity. The site for the one station was selected so that it would be almost directly behind the missile at cutoff and would become the strongest station in the system during that critical portion of the flight.

Before more stations could be added, a receiver with a reference channel had to be built. A contract was let for the development of a dual-channel uhf receiver which would not produce objectional phase shifts for changes in signal strength. The reference channel made it possible for widely separated Udop receiver stations to be supplied with a common reference frequency, coherent with the signal used to interrogate the transponder.

Unlike the Dovap system, Udop does not attempt to make a single reference transmitter perform the dual function of interrogating the on-board transponder and supplying reference to ground receiver stations in all directions, but uses a dual-reference transmitter that produces a 50-Mc and a 450-Mc reference system from the same 25-Mc source. One antenna, located on the ground, radiates 1000 w at 450 Mc to interrogate the missile transponder, which doubles the frequency and reradiates 900 Mc, plus or minus Doppler shift, to all ground receiver stations. Another antenna, located on an 80-ft pole at the transmitter station, radiates 1000 w at 50 Mc to all receiver stations. Each receiver picks up the 50-Mc reference, multiplies it by 18, and compares the resulting 900 Mc with the 900 Mc, plus or minus Doppler, from the transponder. The difference between these two frequencies is the Udop beat, a tone which varies from zero at liftoff to about 30 kc at the cutoff velocity of a missile.

The beat frequency is transmitted to a central station where the beats from all stations are recorded on magnetic tape. For this data link, a data transmitter with a frequency response substantially flat from 1 cps to 60 kc was developed. To cover the first few seconds, before the beat rises to 1 cps, the outputs of the receivers near the launch site are transmitted to the recording station over land lines during the early part of the flight. The more distant stations do not encounter this problem, as they did in the Dovap system, because the Udop beat is already above 1 cps when the missile appears on the station horizon.

The configuration of the Cape Canaveral Udop system is the same as that used for Dovap, and the two systems share the same stations. One receiver is always located within a few hundred meters of the launch pad. In some cases, when very accurate data are required for the liftoff phase,



a ground station antenna is also placed on the pad near the base of the missile. Three more stations are located within 5 km of the launch pad and three others at distances of 20 to 30 km. Although only three receivers are required to determine position and velocity, the optimum configuration of a three station system varies with the position of the missile. The close-in stations are of more value in the early part of the flight; the extended base line stations become more significant as the distance of the missile increases. Furthermore, a redundant solution, using all stations, yields higher accuracy than can be obtained from the optimum combination of three. Also an indication of the accuracy of the final results can be obtained from internal agreement of the redundant data. An error in counting the cycles from one station can be spotted immediately by this method. A redundant system has the additional advantage that the loss of any one station can be tolerated with only slight loss of accuracy. The Udop system is designed so that failure of any one component in the ground system cannot cause a complete loss of data.

In addition to the Udop stations mentioned above, there is another Udop system in the Bahama Islands 200 miles downrange from Cape Canaveral. This system consists of a transmitter station, a recording station, and five receiver stations, located on Grand Bahama Island and the smaller islands of the Little Bahama Bank. This system was installed primarily for missiles that impact in that area, but also supplements the uprange system on some other flights.

The two Udop systems do not interrogate the transponder at the same time. A switchover is performed during flight. At a preselected time, a voice command is given to switch off the uprange interrogator and turn on the 450-Mc transmitter of the Grand Bahama system. The uprange and downrange stations cannot function as a single giant Udop system because neither of the 50-Mc transmitters can supply a reference signal to stations in the other system. Both 50-Mc transmitters remain on throughout the flight (they are not switched as are the 450-Mc interrogators), but they do not have exactly the same frequency and phase, so the two systems are not coherent. After switchover, the downrange stations become an elliptical system (i.e., each station measures loop distance and defines an ellipsoid in space); and the uprange configuration, which no longer controls the transponder, becomes a hyperbolic system. The loop range measurement from each uprange station now contains an error, namely the phase and frequency difference between the uprange and downrange reference transmitters — but the error is the same for each receiver station. By subtracting the cycle counts from two such stations, a loop difference can be determined. Three loop differences (four receiver stations) can determine a point in space.

A hyperbolic system is less accurate than an elliptical system, except for velocity components in certain directions preferred by the

system geometry; but when data from the two systems (uprange and downrange) are combined, there is a resulting increase in overall accuracy. It should be noted, though, that another tie-in point is required after the interrogator switchover.

The error between the two reference transmitters is greatly reduced by use of atomic clocks to provide the excitation for the transmitters. The accuracy obtainable from atomic frequency standards, at present, is not sufficient to enable the two systems to be considered coherent, however.

Another method of combining widely separated stations into one system was tried using Dovap stations. Some of the downrange sites near the submarine cable were supplied with a reference tone from the cable and the uprange interrogator signal was derived from the same tone. The resulting increase in accuracy was somewhat less than expected, presumably due to phase shifts in the cable.

Improvements in the Udop system are directed toward increased sensitivity of the receiving equipment. A phase-locked receiver has been developed for Udop, making possible the use of smaller on-board packages and greatly extending the distances over which the system can operate. Phase-locked receivers are now installed at four of the uprange stations and are being installed at some of the downrange stations.

### 23.5 The Beat-Beat System

The Dovap and Udop tracking systems are not real time systems. Emphasis is placed on accuracy rather than speed of reduction. The raw data are recorded on tape and several days may be required for the data reduction process before velocity and position information are available. This delay is not too objectionable when the data are to be used for evaluation of vehicle performance, but there is a need for some trajectory information in real time so the Flight Safety Officer may know immediately whether the path being followed is one that could result in an impact in populated areas. It is necessary that the time required for processing these data be limited to a fraction of a second. The Beat-Beat system is a simplified Doppler tracking facility designed to provide this type of information.

The original Beat-Beat system consisted of a pair of Dovap receiver stations placed symmetrically about the flight line and modified to give the angle off course in real time. A later model of the system uses tunable receivers and can track telemetry transmitters or almost any rf source between 55 and 960 Mc. As long as the vehicle remains in a plane equidistant from the two stations, the Doppler beat frequency at each station is exactly the same. When the vehicle deviates to the left or right, one beat frequency will increase and the other will decrease.

The difference between these two beats, or the Beat-Beat, is a function of lateral velocity. The total number of cycles of the difference

$$F = \int_0^t (f_1 - f_2) dt \quad (23.2)$$

is directly proportional to the difference between the distances from the vehicle to the two stations. If the distance is great enough to allow the lines from the vehicle to the Beat-Beat sites to be considered parallel, it can be seen from Fig. 23.1 that  $\sin \epsilon = \frac{\lambda F}{B}$ , where B is the distance between stations,  $\epsilon$  is the angle between the direction to the missile and the reference plane, and  $\lambda$  is the wavelength. The base line B is normally 200  $\lambda$ . Therefore  $\sin \epsilon = \frac{F}{200}$ .

The beat output from a normal Dovap receiver will vary from zero to several hundred cycles per second during a missile flight. In Beat-Beat it is necessary to subtract the two beat frequencies in real time, using the simplest and most reliable method available. To simplify this task, a bias frequency is added to the two Dovap beats. This is accomplished by supplying 37.001 Mc from a crystal-controlled generator to the two Beat-Beat receivers over coax cable to replace the 37 Mc reference signal normally received from the Dovap transmitter. The receiver outputs will then remain at least 2 kc when the vehicle is on the pad and will increase in frequency as the velocity increases. The difference between the two beats, however, is unaffected by the bias.

The two beats are fed into a ring modulator that produces the Beat-Beat. A second ring modulator is fed by the same two signals after one of them has been shifted 90 deg. The result is a second Beat-Beat, 90 deg out of phase with the first. The two ring modulators drive a two-phase synchronous motor geared to a data potentiometer. Strip chart recorders, fed by this potentiometer, are used to display the angle off course in the blockhouse and at the safety officer's console in central control.

The original installation used standard Dovap receivers and was only capable of tracking the Dovap transponder; but Beat-Beat is a hyperbolic system and does not make use of the fact that the transponder is coherent. It can track a free-running beacon. The error in the beacon frequency is cancelled when the two beats are subtracted to produce the Beat-Beat frequency. A more versatile Beat-Beat system was required — one which could track a telemetry package on missiles not carrying a Dovap transponder. Most missiles carry several telemetry transmitters, so it would be desirable to change frequencies quickly in the event of a failure of an

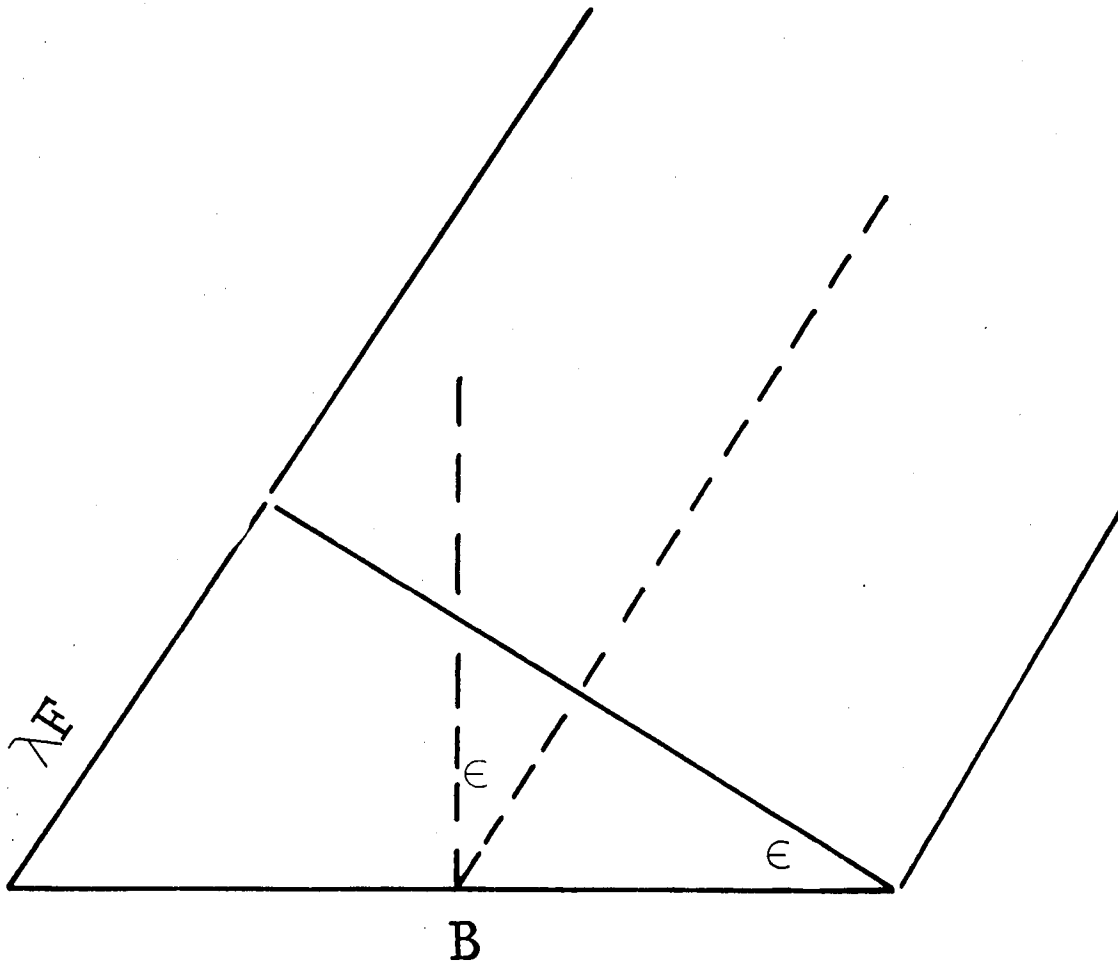


Fig. 23.1 Diagram illustrating  $\sin \epsilon = \frac{\lambda F}{B}$ .

on-board package, or to operate a backup system that would track a different rf source. After the Dovap Beat-Beat had proved its worth as a flight safety system, Beat-Beat Mark II was developed.

A manufacturer of telemetry receivers was asked to repackage two of his standard models on a single chassis, sharing a common local oscillator so that the two channels would be coherent. A mechanical servo has been developed that compares the two i.f. signals from the new receiver and causes a motor to rotate at the difference frequency. The modulation is removed and the two i.f. frequencies are converted to 400 cps by a synchronous detection process. A control transformer shifts the phase of one of the 400 cycle i.f. signals to keep it in phase with the i.f. from the other channel of the receiver. The resulting phase error (if any) is detected and used to drive the servo motor that positions the control transformer. A data potentiometer, geared to the same servo motor, feeds the recorders at the safety officer's console as it did in the earlier system.

To determine whether a vehicle will impact outside the target area, the safety officer must know the angle off course and the rate of change of the angle. To assist him in determining this, the predicted curve and a family of curves, indicating the maximum slope which the recorder trace can be allowed to assume for each value of  $\epsilon$  for each second of flight, are calculated and drawn on the chart before the firing.

Another cause for concern to the safety officer is the possibility that a vertical takeoff vehicle will continue in vertical flight or program in the opposite direction. To guard against this type of malfunction, another Beat-Beat baseline was installed symmetrically about a plane passing through the launching pad, perpendicular to the flight line. This system detects any slight deviation forward or backward from the vertical. A predrawn curve indicates the path which the missile is expected to follow, and a family of curves, similar to that mentioned above, indicates the slope which the recorder trace can assume without endangering the area behind the pad.

Beat-Beat is less accurate than Dovap because of the shorter baseline. Because reliability, rather than high accuracy, is the primary concern in flight safety instrumentation, the system was designed for an accuracy of 1 mil. Comparison of Beat-Beat data with trajectory information from more accurate systems, operating during actual flights, indicates that the accuracy achieved is well within this limit.

### 23.6 The Radop Concept

It was stated earlier that Doppler systems have the unique capability of measuring rocket velocity directly, thereby having definite advantages over other instrumentation types. However, the Doppler systems

actually measure loop velocities only and are not able to produce velocity resolution into specified coordinate directions, unless provided with some information extraneous to the system. In the classical solution, this extraneous information is the tie-in point mentioned above. Two conditions must be met to make the introduction of the tie-in point effective throughout the entire period of Doppler tracking coverage. No signal dropout must occur, or the entire remaining portion of a station recording becomes worthless. Extremely high position accuracy, usually obtainable only by optical triangulation, is required for the tie-in point. Geometry deterioration increases as the rocket travels away from the station complex.

For a Jupiter missile trajectory, the position error of a tie-in point provided at about 40 sec flight time causes a tenfold position error at the time of missile cutoff. On the other hand, the inherent simplicity and reliability of Doppler instrumentation has raised the desire to employ such systems in places other than heavily instrumented missile launch areas to support vehicle programs requiring world-wide tracking. In such applications, it is usually impossible to obtain a tie-in point of the required accuracy, and an uninterrupted signal cannot be postulated. Two ways are open to overcome the difficulties. By employing at least six Doppler receiver stations simultaneously, rocket position and velocity can be determined analytically from the six observed loop velocities. Analysis shows, however, that at least a dozen receiver stations are required to achieve acceptable data accuracy. The reason for this is that position accuracy is determined largely by the ability of the system to resolve observed loop velocities into specified coordinate directions. Because the number of stations required to do this with greater accuracy is prohibitive in terms of real estate, logistics and operating effort, position determination by this method is rather weak.

At this point, the Radop (Radar, Doppler) concept is introduced to show a feasible solution. Radop is called a concept, rather than a system, because the necessary tracking equipment has been available all the time. The only new aspect is a novel method of raw data reduction using results of existing instrumentation systems.

As pointed out above, any Doppler system requires some extraneous vehicle position information. In the Radop concept, radar position data are used for this purpose. Admittedly, position accuracy so obtained will be inferior if compared with the classical Doppler data reduction method employing a tie-in point. It can be shown that, for suitable station configurations, the limited position accuracy has negligible effect on the process of resolving Doppler loop velocities into specified coordinate directions. Furthermore, tracking data requirements emphasize velocity accuracy rather than position accuracy. The mathematical solution employs azimuth, elevation angle, and slant range from

at least one radar, as well as loop velocities from at least three Doppler receiver stations. Any additional radar on Doppler station available allows a least-squares solution for vehicle position and velocity. Tentative computations using Cape Canaveral Udop and C-band radar data have affirmed the feasibility of the Radop concept by comparison with results of standard data reduction methods employed by the Atlantic Missile Range.

In addition to being more suitable for instrumenting remote tracking complexes abroad, the Radop concept has a great potential as a flight safety tracking scheme with virtually instantaneous output. Already, C-band radar data are being accepted in real time by a high-speed computer at the Atlantic Missile Range to compute the instantaneous impact point. Necessary smoothing of radar position data, however, causes a delay of several seconds between reception of data and impact point output. Any such delay poses a substantial limitation on the allowable flight azimuth, a restriction being felt more and more as lunar and planetary missions increase in number and significance. Provided that the output of three or more Udop receivers could be digitized and fed into the same computer along with the radar data, unsmoothed radar and Doppler data would provide sufficiently accurate position and velocity data to calculate the instantaneous impact point. The only delay so encountered would be a fraction of a second spent for the computation process.

### 23.7 Orbital and Deep Space Applications

Doppler tracking systems have been used for the development of ballistic missiles for almost two decades. Weight and size of on-board equipment such as transponders, antennas, and power supplies were almost unlimited due to the payload capability of such a vehicle. Furthermore, distances to be covered were very short compared with requirements of orbital, lunar, and interplanetary missions.

A radical change from the old concept was required with the firing of the first satellites, with very limited payload capabilities. For best weight utilization, a one-way Doppler system was used with a solid-state transmitter providing about 10 mw of radiated power. To achieve a very narrow noise bandwidth, a highly sensitive receiver, using phase lock technique, was necessary. In addition, two interferometer systems, arranged 90 deg from each other, provided angle measurements. Such data, obtained from ground stations with a favorable station geometry, furnished position and velocity as well as orbital parameters.

As missions become more sophisticated, corresponding improvements are required for both the on-board and the ground instrumentation. To eliminate any drift in frequency of the on-board oscillator, a two-way Doppler tracking system must be employed. The use of a transponder will guarantee highly accurate Doppler data because of the coherent receiving

capability. To keep size and weight within an acceptable limit, a solid-state transponder is preferred. In general, such a transponder consists of a complete receiver and a low-level transmitter. Deep space missions require additional amplifiers to increase the radiated power to the necessary level. Precise determination of spatial coordinates and orbital elements at interplanetary distances requires two-way Doppler data from a number of stations; and, whenever possible, station geometry should be such that continuous coverage is provided. However, the final arrangement of stations depends on such parameters as trajectory, accuracy requirements, and minimum trackable elevation angle.

A marked improvement is obtained by providing additional range data. This is accomplished by independent systems as described above in Radop or by measuring the Doppler shift of a modulation frequency on the cw carrier. For such a range measurement, the signal has to originate in the ground station that makes the two-way operation mandatory. The ultimate tracking system should be able to provide two angles, range, and range rate simultaneously.

Spacecraft transmitters of early satellites were also used for transmission of narrow-band telemetry information. Future missions will require an information bandwidth much wider than that needed for tracking purposes. This will make the use of a separate tracking transponder highly desirable.

Lunar and interplanetary distances can be covered, from the ground to the spacecraft, by narrow beam antennas with a transmitting power of 10 kw or more. Transmitting power as high as 100 kw is considered for future missions.

To guarantee the most reliable operation on a space mission, an extensive effort is necessary in the design of on-board antenna systems. Experience with early satellites shows that most missions require two different tracking antennas for satisfactory results. The near-Earth portion of the flight is best covered by an isotropic or omnidirectional antenna. Such a system consists of a number of antennas with overlapping patterns. The result is a radiation pattern reasonably isotropic. For lunar and interplanetary distances, a high-gain antenna on board the spacecraft is an absolute necessity. For most known missions, the high-gain antenna will be an erectable or inflatable parabolic antenna. Steerable parabolics are considered for some missions.

Because of serious limitations of weight, space, and power in a spacecraft, the radiated power of an on-board transponder is very limited. To compensate for these shortcomings and to guarantee reliable operation under the most severe conditions, a special effort is demanded at the receiver site. Two-turn helical antennas, used for tracking early satellites, have been replaced by parabolic reflectors with high gain and



narrow beamwidth for reduction of possible interference. Jet Propulsion Laboratory's Deep Space Instrumentation Facility uses steerable 85-ft, parabolic-reflector antennas that can be controlled manually or by error signals from the tracking receiver. New large aperture antenna systems are being planned. An advanced antenna system with a trackable dish approximately 250 ft in diameter would provide improvement of approximately 10 db over existing systems.

Very sensitive receivers applying phase lock technique were used for tracking the first satellites. For tracking lunar and interplanetary probes, the threshold of the ground receiver system must be further reduced if reliable data are to be expected. This assurance can be accomplished by the use of low-noise preamplifiers. Traveling wave tube amplifiers, parametric amplifiers, and maser amplifiers are used in tracking experiments with promising results. Jet Propulsion Laboratories was successful in receiving Venus-reflected Doppler and range signals using a maser amplifier followed by a parametric amplifier as a pre-amplifier. The receiver is phase coherent with a very narrow bandwidth. This experience shows that passive tracking of a probe with an ultra high sensitivity setup is possible. Satellites without transponders, or with transponders that fail to radiate, can be tracked passively and the reflected signal can provide velocity and range data.

Lunar and interplanetary missions will require manned or unmanned orbital operation for rendezvous or in-orbit assembly that will require an on-board range and range rate measuring system. Such a homing system will be necessary to operate as an acquisition system and for the final approach. Systems so developed might well prove to be an important part of the instrumentation for an actual landing maneuver.

Tracking of the first satellites was accomplished on a frequency of 108 Mc. This frequency was only used with a one-way system. When more accurate Doppler data became necessary, a coherent system with a frequency of 890 Mc to 960 Mc was employed. But even these frequencies will be replaced by an S-Band frequency in the future. The higher frequencies will allow the use of smaller antennas with better protection from interference due to a narrower beamwidth. Even higher frequencies in the X-Band are considered for Doppler measurements on orbital rendezvous and deep space missions.

Whatever the scientific requirements of a future space mission may be, Doppler data will always be of utmost importance. The state of the art will have to improve continually to meet more stringent requirements as future missions become more and more complex.

## 24

## SPACE VEHICLE TESTS AND MEASUREMENTS

Daniel H. Driscoll and Albert E. Schuler

Test Division  
George C. Marshall Space Flight Center  
National Aeronautics and Space Administration  
Huntsville, Alabama

### 24.1 Introduction

Rocket development includes a repetitive process of test and change based upon test results, the object being to mature the rocket's design. Implied in the word mature is a desired goal that must be determined before the process starts.

While design, development, and test have achieved popular usage only in the past few decades, the process of development is as old as man. Each man goes through a state of development with each new experience. The object that he seeks in those experiences, is to gain confidence so that when next he has a similar experience the result will be satisfactory. The development rate is determined by his efficiency in assimilating and applying his observations. Man develops by the mental observations, and adjustments he makes on the basis of experience. In rocket technology, this comes from the observations that are made when the rocket is subjected to an experience.

The rate at which a rocket matures depends upon the efficiency with which man produces the reality of experience for the rocket, the accuracy with which he can make observations, and his ability to draw correct conclusions. Measurements are needed to produce a standard for comparing observations of similar experiences made at different times by different men. To translate phenomena into measurable and recordable quantities, instrumentation is needed. Because man is limited in the number of things he can observe, retain, and assimilate accurately into an overall evaluation, it is necessary to provide means of recording the happenings of relatively short duration for future reference and evaluation. Being the product of the human mind, none of these developmental tools can replace the trained human mind. In short, rocket development includes the ability to test, measure, and communicate.

The rocket is, by nature, paradoxical. It must be very reliable because of high unit cost; yet the safety factors used must be low

**Preceding page blank**

(normally meaning low reliability) because high safety factors mean higher mass. Herein lies the major challenge to the engineer. As a result, the designer is continually treading close to the margin of reliability; a well-planned, comprehensive test program is essential. A rocket development schematic is shown in Fig. 24.1.

Two general types of test programs are involved in the development of a rocket: ground and flight testing. With ground testing, confidence is gained that the flight test has a reasonable chance of success (least reasonable risk). The freedom to take reasonable risks is a major factor in pacing the development program. Some factors which must be considered in establishing a reasonable risk are:

1. Value of payload.

2. Value of facility and hardware to program at the time risk is to be taken.

3. Precautions taken to minimize loss in the event of failure.

(Ground testing is more adaptable to precautionary measures than flight testing because of less stringent weight limitation.)

4. Design safety factors.

In each case, the potential loss must be weighed against the potential gain.

How then should a test program be formulated? The basis of the test program is the design, and the design is in turn based on expected experiences of the product. These experiences determine the environments for which the rocket and the associated ground support equipment are designed and therefore must be tested. The specific test plan depends upon the maturity of the design at the start of the development program. Some of the experiences to which a production copy, multistage rocket, and its components are exposed to may be:

1. Preassembly of components and materials
2. Inspection of the components
3. Storage of the components
4. Functional acceptance of components
5. Assembly of the stage
6. Preacceptance firing checkout (for liquids)
7. Acceptance firing (for liquids)
8. Postacceptance firing checkout (for liquids)
9. Stage storage and transport to launch site
10. Erection and assembly of multistage rocket
11. Prelaunch checkout
12. Launch preparation
13. Launch
14. Boosted flight
15. Booster recovery
16. Stage separations
17. Coast phase in space
18. Powered flight of stage in space

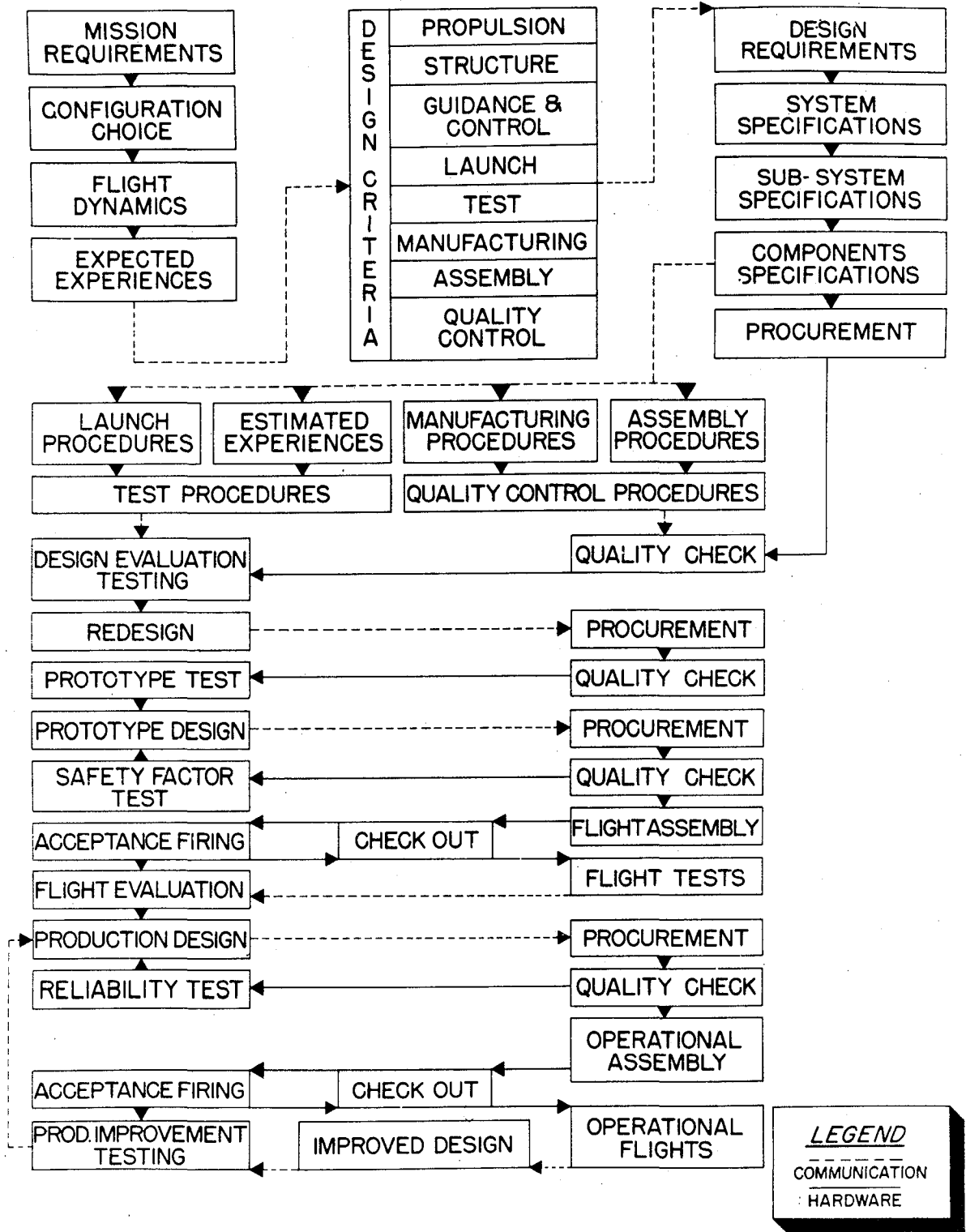


Fig.24.1 A development schematic.

While each of these experiences does not produce an environmental condition, each must be carefully reviewed to determine where a theory must be put to test. As much consideration must be given to ground support equipment, launch and test facilities, as is given to the rocket. A well-organized test program can only be devised after a careful review of all these experiences and the equipment associated with their support. This is the foundation upon which the gaining of real confidence is built.

The general types of ground testing are shown in Table 24.1. Components of contemporary rocket systems may experience the range of conditions shown in Table 24.2. All these conditions must be reliably measured and recorded. Only the rapid advances made in instrumentation, measuring, and automatic data reduction, and the ability to use this technology have made it possible to test complex rocket systems economically.

Advances in rocketry, as in all fields of technology, depend upon the ability to measure. Instruments are the indispensable tools and unifying elements of all research. Only when a thing is measured and expressed in numbers is something known about it. The rate of progress depends heavily upon the capability and skillful use of instruments to obtain accurate and reliable measurements.

Great efforts and advances in such measurements have been made during the 25 years of active rocket development. Many of the measurements could not be made with existing commercial instruments because of extreme physical values, new physical phenomena, high-accuracy requirements, or extreme environmental conditions. Consequently, modification and development of new instruments were necessary. These developments were performed by government, private industry, research institutes, and universities on initiative or research contracts. Many new techniques were required for the proper installation, calibration and operation of new instruments and the evaluation of measurements. The measurement engineers and technicians first must be convinced that the measurements are right and then substantiate the results, especially if results disagree with theory or fixed concepts.

During the past 25 years, the quality of instruments and measurements has steadily improved. Confidence in measurements has grown, and the importance and value of measurements have been recognized. During the V-2 development, less than 100 measurements per test were made. During a Saturn test, more than 1000 measurements are made. Today's schedule for preparing tests provides proper time to install and calibrate instrumentation.

This chapter presents a condensed survey of the principles, methods, and instruments used for ground measurement in rocket development and testing during the past 25 years. This survey shows the great progress, the present state of the art, and a look at the future.

Table 24.1 Types of Ground Testing

Datum	Applied Research	Design Evaluation	Prototype	Quality Check	Reliability
Object	Determine practicality of new techniques and materials	Determine performance characteristics, design criteria, and scale factors	Gain confidence in design, procedures, and specifications	Gain confidence that specific items meet standards	Gain confidence that design safety factors are being maintained
Relative status of design	Immature	Immature	Mature, but fluid	Production	Production
Basis for test	Theory	Theory and operational requirement	Operational and design requirement	Specification, procedure, and operational requirement	Design requirement
Type of information gained	Design concept	Design suitability	Design maturity status	Characteristic of test item	Statistical
Experience simulated relative	Phenomenon	Event or environment	Operational experience	Varies from none to flight operational	Exaggerated environment
Test item's identity in relation to production copy	None	Model and prototype of production copy	Prototype of production	Production copy	Production copy
Most emphasized assembly	Not applicable	Component and subsystem	All levels	All levels	Component and subsystem

Table 24.1 Types of Ground Testing (Cont'd)

Datum	Applied Research	Design Evaluation	Prototype	Quality Check	Reliability
Relative instrumentation requirements per test:					
quantity	Medium	High	Medium	Low	Low
quality:					
accuracy	High	High	Medium	Medium	Medium
percision	Medium	High	Medium	High	High
Test item scale	Often less than 1:1 for economic reasons	1:1	1:1	1:1	1:1
Relative number of like test items	Depends entirely on nature of test	1 to 3 (Minimum cost)	3 to 10 (Minimum cost)	Depends on number of items produced	Depends on number of items produced and disiring sampling rate

Table 24.2 Rocket Systems Range of Conditions.

Temperature, °R	20 to 6000
Pressure, psia	0.001 to 5000
Force, lb	0.5 to 1,500,000
Linear acceleration,	0 to 10
Vibration	
Acceleration,	0 to 100
Frequency, cps	0 to 2000
Sound pressure, db	0 to 163 (ref. to 0.0002 microbar)
Corrosive media	Air to Fluorine



## 24.2 Recording Systems

Most measurements for rocket development and testing must be recorded. This requires that transducers convert physical phenomena into electrical signals and that systems condition and record these signals. The conditioning equipment is comprised of bridges, amplifiers, attenuators, cathode followers or other impedance matching equipment, oscillators, demodulators, regulated dc power supplies, special circuits, and range balancing equipment.

Accurate and reliable measuring requires frequent calibration of the complete measuring system from transducers to recording equipment. The systems for very important measuring are calibrated before and after each test, while others are calibrated less frequently. Calibration in this context is a comparison with standard instruments. Sometimes the standard instruments are located at the test stand for calibrating. In other cases, field calibrations are made with master gages or secondary standards, which are calibrated frequently with the primary standards in the laboratory. In rare cases, transducers in the field are not calibrated by applying physical values, but their electrical output is simulated by unbalancing the bridge or by other external electrical means. This procedure is called shunt calibration and calibrates only the recording system. End-to-end calibrations are preferred, that is, the application of physical action and comparison of measured reaction values with standards or master gages.

Quantitative measurements with best accuracy, but not necessarily fastest response, are needed for the constant or slowly changing data during the steady-state period of the test. Less accuracy, but quick response, is required for qualitative measurements to study oscillations and buildup or decay during transient periods. Oscillographs have been used for most qualitative measurements throughout rocket development. In Germany, before 1945, both large and small oscillographs were available. The large oscillograph had a carbon arc lamp, eight galvanometers with individual magnets, and wire loops with mirrors. It used 12-cm wide paper located about 110 cm from the galvanometers. The paper speed was 0.02 to 2 m/sec and the highest natural frequency was 20,000 cps. The small, or portable, oscillograph had 3 galvanometers, an incandescent lamp and 9-cm wide paper. The accuracy was  $\pm 2$  to 3 per cent.

In the United States, before 1945, several different types and models with many different characteristics were available. Continuous development and improvement in these instruments have continued. The oscillographs are now much more compact and versatile. They have 36 or more separate galvanometer elements in one magnet block, finer lines, etc. The latest improvement is of instant visibility of the records on dry paper without chemical development. The accuracy is  $\pm 2$  to  $\pm 5$  per cent. Response is 3000 cps for modern, high-sensitivity galvanometers.

While oscillographs have been used for vibration and sound measurements, magnetic tape recorders are preferred because of the higher speed of response. They have the added advantage that the records can be played back into vibration analyzers. A one-channel tape recorder was available during the development of the V-2, but the quality needed improvement. Modern tape recorders have 14 channels, 0 to 20,000 cps response, low noise, and high linearity.

Strip-chart recorders have also been used for quantitative measurements. Before 1945, two types were available. One had a moving-coil measuring system with a pen arm attached to the coil. The other type had two crossed coils, one for the measuring signal and the other for restoring moment. This crossed coil recorder eliminated errors caused by changing supply voltages when the return coil and the transducers were energized by the same voltage supply. The accuracy of the recorders, with utmost care and maintenance, was 1 per cent.

Strip-chart recorders with zero balance and 0.25 per cent accuracy were a great advance in accuracy and reliability. Special circuits were developed to make measurements independent of change in supply voltage. Pen speeds of 4.5 sec for the full scale became available in 1947; today, speeds up to 0.25 sec for the full scale are available. Paper speeds up to 120 in./sec and accuracies of 0.2 per cent are offered.

About 1953, the first digital recording systems were developed and used for special applications. Since then, a large variety of analog-to-digital conversion systems have been developed; for example, shaft-position conversion, successive-approach methods and pulse-duration systems. The pulse-duration system generates a voltage with a saw-tooth curve, starts counting high frequencies at zero voltage, and stops counting when the voltage coincides with the measuring voltage. In 1957, a digital tape recorder with pulse-duration conversion became available. This system has a capacity of 1200 samples/sec, a relay commutator for 400 channels, and records about 200,000 values per test. Computers select certain data, for example, 10 consecutive values at certain slice times and convert them to temperature, pressure, or other parameters, based on calibrations with the same recording system. Several hours after the test, some 20 to 40,000 data points are printed on paper, including individual values, average values, and tabulations. Today, data handling systems are available that record more than 5,000,000 samples/sec; and it is expected that even faster, more automatic, and more reliable data handling equipment will be available for future measuring systems.

### 24.3 Pressure Measurements

About one-third of the measurements for development and testing of rockets are pressure measurements. Gage pressures, absolute pressures and differential pressures, ranging between several inches of water to

5000 psi must be measured at different environmental or operating conditions, and with different accuracy requirements. Quantitative measurements with best accuracy and qualitative measurements with high speed of response are both required.

A Bourdon tube pressure gage with wire potentiometers was used as a pressure transducer for quantitative measurements on the V-2 and smaller propulsion units. The circular potentiometer was attached to the front or back of the gage and coupled with the axis of the pointer in order to turn with the gage. Thus, the gage could be used as a transducer and as an indicator. The potentiometer was connected in a voltage divider to a crossed-coil recorder with an accuracy of  $\pm 1.5$  to 2 per cent.

For differential pressure measurements a commercial instrument, using the U-tube principle with float and gear in a heavy iron housing, was used for several years. However, it was too bulky, so a differential pressure transducer with bellows and differential transformer was developed. A variety of sensing elements based on different size bellows with integral helical springs was built. The bellows moved an iron core in a differential transformer. The differential transformer had one primary and two secondary coils with opposing voltages. The voltage difference in the two coils was proportional to the position of the iron core and the differential pressure. The output was recorded by the crossed-coil recorder with an overall accuracy of  $\pm 1.5$  to 2 per cent. The same principle, now very familiar, has been used since in commercial instruments.

Qualitative measurements were made with available variable capacitance transducers. The pressure bent one flexible plate of a capacitor, changing the distance between the plates and varying the capacitance. The output of the capacitive transducer was measured in an electronic unit comprised of an oscillator, bridge and amplifier; an oscillograph was used for recording. The accuracy of these qualitative transducers was  $\pm 1.5$  per cent, and the overall accuracy with the oscillograph was about  $\pm 3$  per cent.

After 1945, strain gages replaced the older types of transducers for qualitative measurements, but the potentiometer-type transducers were still preferred for several years for quantitative measurements. In the United States, industry continued to improve the transducers, using ultra-low torque potentiometers with vacuum-deposited, straight resistance strips to pick up motion of the sensing element directly. Around 1950, transducers with torsion tube and variable reluctance pickups became available. These transducers were fast enough for qualitative recording on oscillographs. They produced a larger signal and were less sensitive to line effects than the low-level, strain-gage transducers. As a result, the variable reluctance transducer has become the most widely used pressure sensor at the test stands. Laboratory accuracy is better than  $\pm 0.1$  per cent but the field accuracy is about  $\pm 0.5$  per cent. Where high

accuracy and high reliability are required (for example, the combustion chamber pressure), the value is measured during the test with several transducers and recording systems. The average of several measurements increases the accuracy by the square root of the number of measurements.

For very high response measurements, a flush-mounted capacitive transducer is used. This transducer is water-cooled and suited to high or low temperatures.

The ultimate pressure transducer will probably be a digital type. Transducers with digital output have been used, but their application is limited. Transducers with strain gage, capacitive, or variable reluctance pickups can be used with an oscillator, resulting in a digital output. Such systems can be used in some cases with an accuracy of better than  $\pm 0.1$  per cent but cannot be used as complete measuring systems. The perfect transducer is under development with a digital output that, when combined with the modern digital data handling equipment and computers, will produce accurate, reliable, and automatic pressure measurements.

For pressure calibrations, dead-weight testers and manometers were the only standards until about 1951. Manometers are low-pressure standards and use height times either specific weight of water, bromide, or mercury columns as measure of pressure. Dead-weight testers use weights on a piston floating on hydraulic fluid in a cylinder. Either the cylinder or piston must be rotated to overcome friction.

The need for more accurate reference pressures resulted in the development of the dead-weight pressure balance, operational since 1951. The pressure balance uses bellows or pistons to convert pressure into force, and an equal arm-balance compares the force with dead weight. Solenoid valves regulate inlet or outlet of compressed air to the piston-cylinder combination until pressure times effective area equals weight.

In 1960, an automatic pressure calibration system was developed that used the dead-weight pressure balance as a pressure standard. In this system, a programming device uses information from a punched tape to connect all transducers in a selected pressure range via solenoid valves and manifold from a missile to the pressure balance. The appropriate weight increment for the respective pressure is applied in the programmed calibration step, makes the pressure balance regulate the pressure, records the output of the transducer, applies weights for the next pressure step, and continues until the calibration of this group of transducers is complete. These transducers are reconnected to the missile and another group of transducers is connected to the pressure balance until all are calibrated. A tape can be punched for any desired calibration program. This fully automatic calibrator is especially useful for calibrations made immediately before and after tests.

In this instrumentation setup, frequent readjustments are necessary because the same recording systems are switched to other test stands between tests. Therefore, a semiautomatic calibrator has been designed (Fig. 24.2). This system offers the same automatic calibration described above and has in addition a push-button operation to select any individual odd value, to rock back and forth between zero and a selected pressure for slope adjustment or to perform automatic calibration of a selected pressure range in steps of 10 or 20 per cent. This system is already being used by rocket developers; it is expected to become a more useful tool for future rocket testing and automatic checkout systems.

#### 24.4 Thrust and Weight Measurements

Before 1945, in Germany, all quantitative thrust measurements were made with mechanical scales with capacitive or magneto-strictive load cells. The scales were an integral part of design and structure of the test stands. A lever system extended in conventional fashion to scale heads in the measuring bunker or blockhouse; recording was accomplished by film cameras. All efforts were made to avoid friction or erroneous forces caused by guides, fuel lines, gas supply lines, measuring lines, and cables. During rocket tests measurements had to be corrected for fuel consumption, which was measured by level gages. The accuracy of the thrust measurements was within  $\pm 0.25$  per cent. Calibration was accomplished by dead weights on a traveling railroad car provided by the German Bureau of Standards.

Capacitive or magneto-strictive load cells were used for qualitative measurements to study oscillations and transients. These load cells were commercially available, small, and could be included easily in any test arrangement where qualitative measurements were desired. The capacitive load cell worked on the same principle as the capacitive pressure transducer. The magneto-strictive load cell measured the impedance change of a coil around a ferromagnetic rod, changing its magnetic field under tension or compression force. The electronic unit consisted of an oscillator, bridge and amplifier, as described above for pressure measurements. The output was recorded on oscillographs with an overall accuracy of about  $\pm 3$  per cent. In the laboratory, the load cells were calibrated with a hydraulic testing machine and a test ring with an elliptical shape. At the test stand a jack was used.

Since 1945, thrust and other forces have been measured with load cells using strain gage pickups. Many commercial variations are available. Some use one load column, while others use several load columns, mostly of high quality steel. Still others use bonded strain gages or unbonded strain gage pickups. The moisture effect was eliminated by hermetically sealed housings. The temperature compensation is now 0.001 per cent/ $^{\circ}$ F for the slope and 0.005 per cent/ $^{\circ}$ F for zero shift. The repeatability is 0.25 per cent, and the highest range is now 500,000 lb.

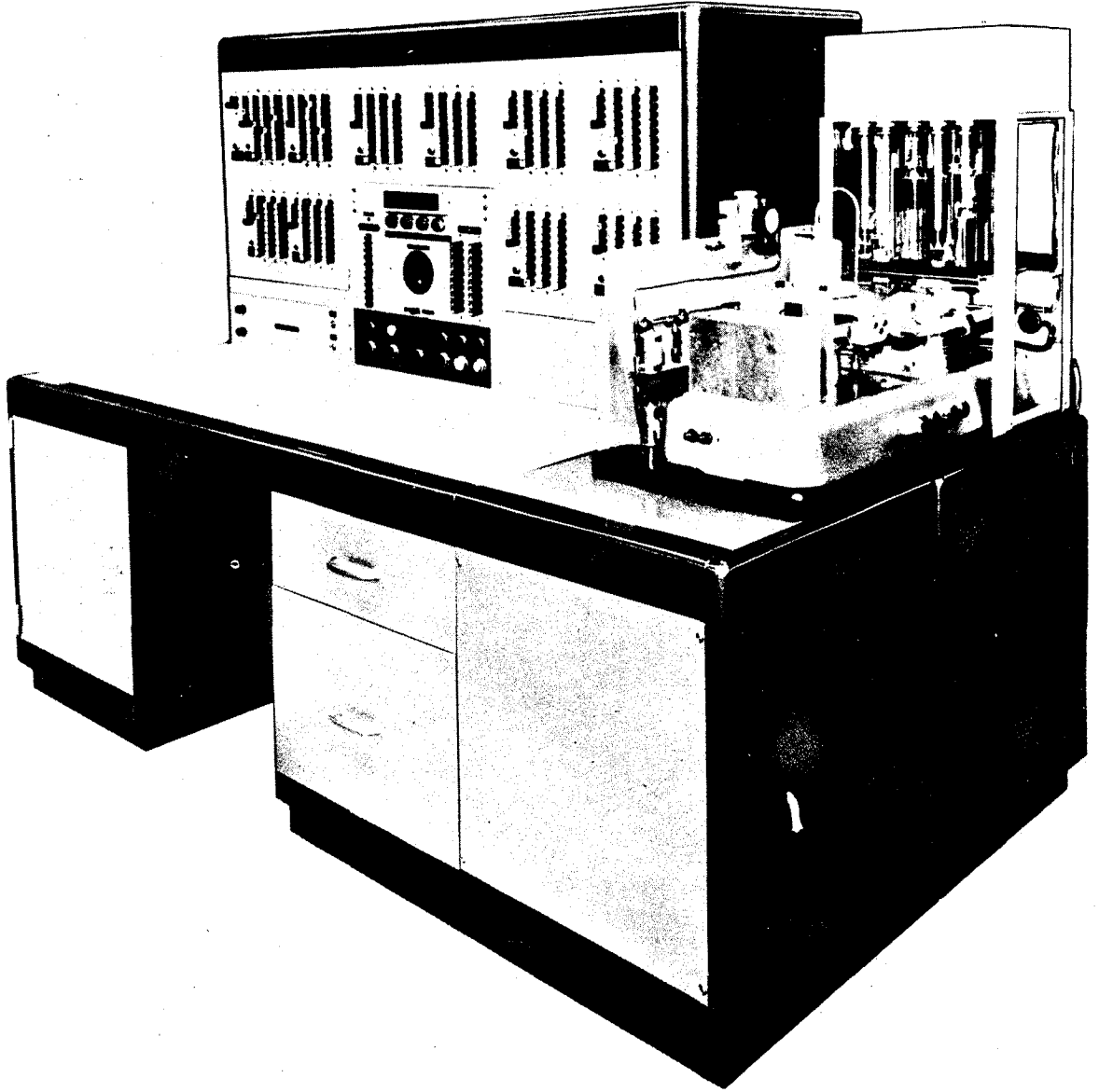


Fig. 24.2 Automatic pressure calibration system.

Calibration was first accomplished with testing machines using National Bureau of Standards (NBS) test rings as secondary standards, providing an accuracy of 0.1 per cent. Later, dead-weight calibrations were made to meet special requirements; but today laboratory calibrations are being done with a 200,000-lb calibrator, using a mechanical scale (Fig. 24.3). The traverse beam contains a push-pull hydraulic jack. Compression load cells are installed beneath the traverse beam, and the piston pushes them against the platform of the scale. Tension load cells are mounted above the traverse and the piston pulls the load cell and yoke down against the weighing system. The calibrator was tested with NBS-certified weights up to 500 lb, and the upper part of the range was checked with several NBS-certified test rings and standard load cells. The resulting accuracy is better than  $\pm 0.05$  per cent of the reading above 10 per cent of the range. The readability is 10 lb. Readings are accomplished with poised weights and a notched beam. A 1,500,000-lb calibration system with a similar principle is planned for the near future.

At the test stands, load cells are calibrated with hand-operated jacks and calibration kits comprised of a precise compression load cell and a hand-balanced bridge with digital indication. An automatic thrust calibration system has been developed and provides automatic loading from a hydraulic jack governed by the calibration load cells according to pre-set values. The slope stability of the load cells presently used as secondary standards is very good, but the poor zero stability requires rezeroing at each operation. A more stable and accurate field standard is now being developed.

Weighings are needed to determine the mass of components, capacity of the tanks, the volume versus height characteristics of tanks, tank shrinkage, density of fuels, center of gravity, as well as liftoff weight and mass. The mechanical scale is used for all these measurements whenever feasible. For weighing on a crane, spring scales were used until 1945; but load cells are now preferred. Because of their small size and convenient installation, load cells have replaced mechanical scales in many applications. For example, a scale on the launching pad is vulnerable to launch operation damage. The scale under the V-2 launching table was out of order after practically every firing. The scales in the Redstone and Jupiter firing pads were better protected, but for redundancy and possible field use, load cells were incorporated in the launching tables. The first installations were not reliable enough, due mainly to zero shift with a missile in place on the load cells for days or weeks. Because of weather conditions, no zero check was possible. The introduction of a sealed housing improved the zero stability, but the best solutions were found in new designs. These designs permitted temporary lifting of the rocket for zero check, and provided an unloaded position of the load cells below the rockets, thus raising the load cell or rocket only for occasional weight readings.

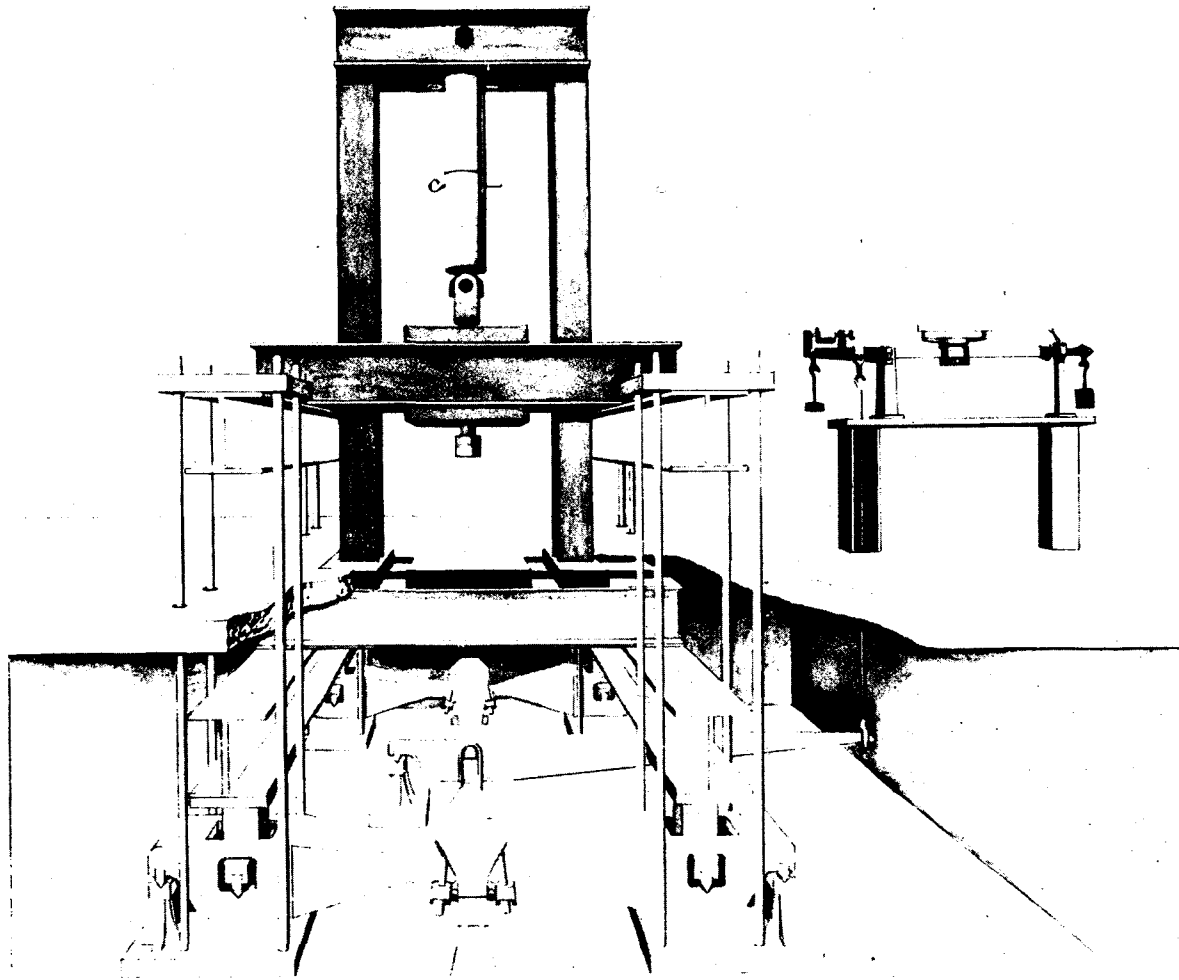


Fig. 24.3 200,000-pound load cell calibrator.



The weighing system at the launching site had often been used for filling control of propellants. Because of unfavorable capacities required for the total weight of the missile, the filling accuracy was poor compared with present methods of flow measurement.

Both the weight and mass of the rocket at liftoff and during flight are very important for analysis of the firing. The thrust less the lift-off weight equals the effective thrust, and effective thrust divided by mass determines the acceleration. The weight of the same body changes with the acceleration of gravity, which varies more than 0.5 per cent over the Earth, while the mass remains the same. Many engineers use the same units of mass and weight interchangeably. This becomes increasingly unacceptable with larger rockets and greater distances between operation sites. A standard procedure for using units of mass, weight, force, pressure, and acceleration was prepared to insure consistent and uniform terms and units. Mass and weight must not be confused in the space age when orbiting masses experience weightlessness.

#### 24.5 Flow Measurements

The measurement of flow rates is one of the most important in the development and testing of liquid rocket propulsion systems. Flow rate and thrust must be measured to determine the specific impulse of rocket engines. The mass flow rate, rather than volumetric flow rate is required, because engine thrust is a function of the mass of propellants undergoing combustion and the acceleration of the rocket is a function of its mass which changes 70 to 90 per cent during consumption of the propellants. Thus, the mass flow rate is doubly important for the rocket in flight, because the flight characteristic is determined by mass and thrust. The measurements of liquid level, density, propellant loading, and propellant utilization are functions of mass and thrust requirements.

During the early development of rocket engines, flow rate was determined by weighing with mechanical scales. For direct flow rate measurements, the well-known nozzle and orifice were used in several test arrangements. Generally they are not useful because of insufficient accuracy, high pressure drop, and stringent installation requirements. Consequently, the development of special flow meters was started in 1939. After several years, fairly accurate flow rate measurements were obtained with flow meters, based on the baffle-plate principle. This flow meter functioned somewhat like a rotameter. The main difference was that the force on the baffle plate was counteracted by springs instead of weights; and the displacement was transmitted for remote recording by linear, wirewound potentiometers. However, the potentiometers were immersed in the liquid and frequently out of order.

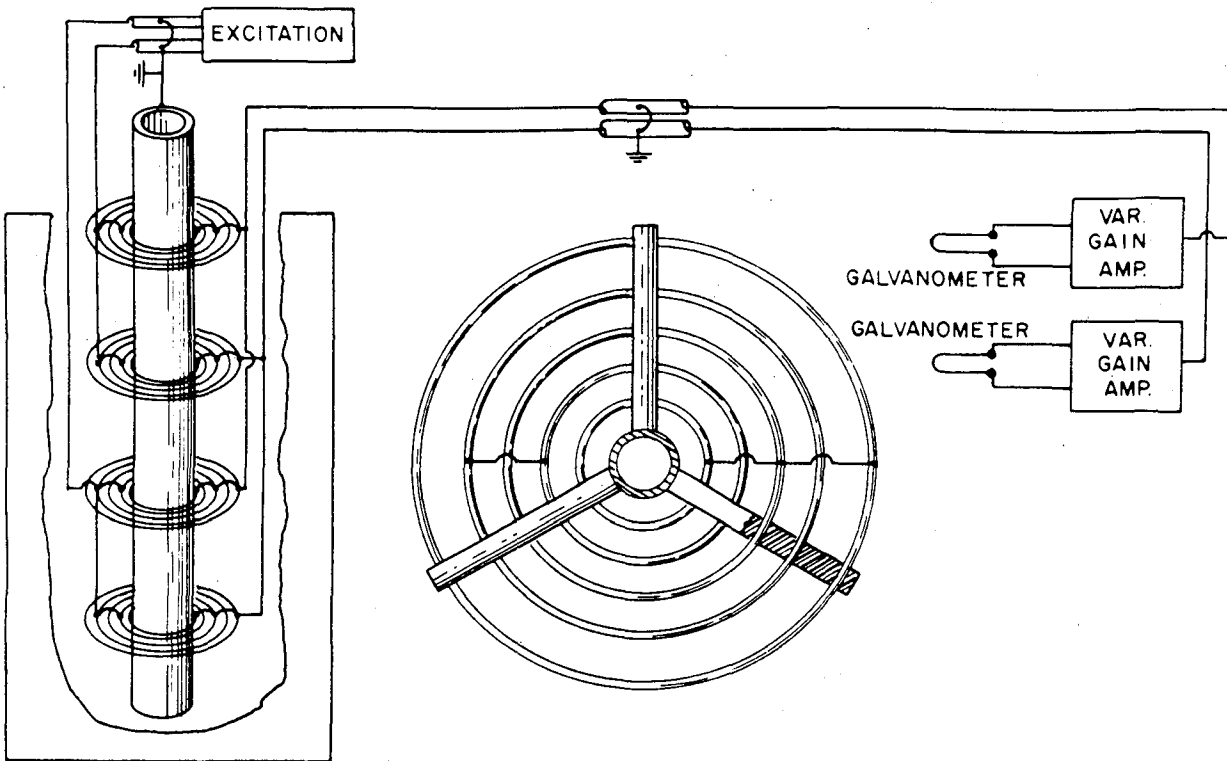
In later rocket systems, flow measurements were made with level gages in the propellant tanks. The capacitive level gage was found best

for continuous level measurements in liquid oxygen; an inductive level gage with a float was best for fuel. The capacitive level gage had a two-part inner tube, concentrically mounted in one outside tube, representing two capacitors in neighboring arms of a bridge. The output versus level progressed from zero to maximum and back to zero. The reversion point was at a certain level and provided a measure for changes in sensitivity and dielectric constant. The inductive gage consisted of a long iron core inside a ceramic tube with a coil of varying field strength as the primary winding. A torus aluminum float around the tube as a secondary winding changed the impedance of the primary as a function of the float position. These continuous-level gages had a repeatability of about 1.5 per cent of the range. The best accuracy for the flow rate was around  $\pm 2$  per cent for full duration tests or  $\pm 3.5$  per cent for half duration tests. This was not sufficiently accurate and started the development of level switches or discrete liquid level detectors. Such point sensors have the advantage that the repeatability is determined by an absolute height value, and the percentage accuracy grows with the height of the tanks.

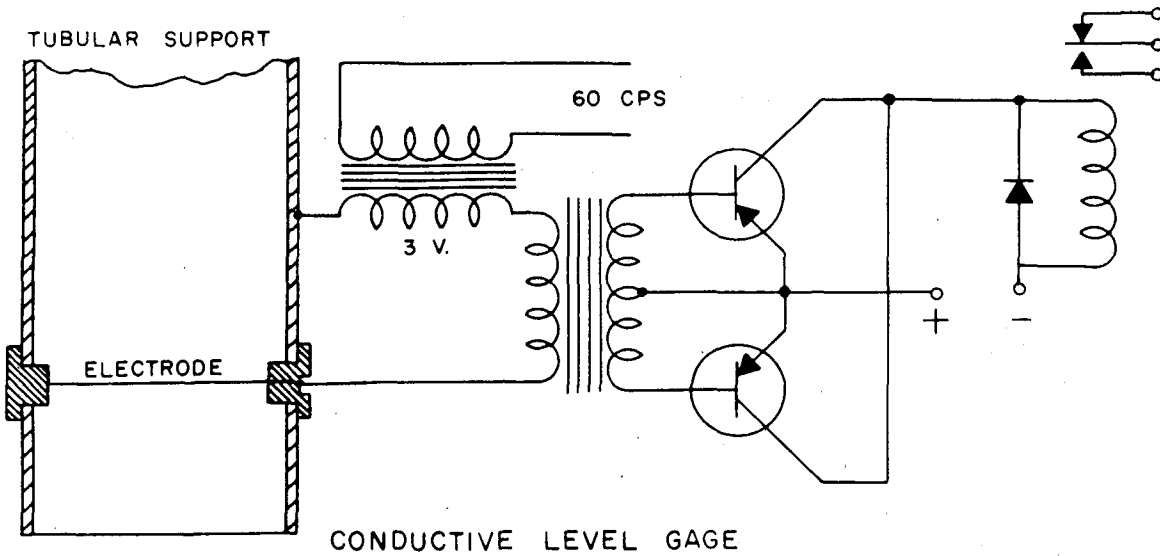
The first level switches were float-operated. A mercury switch was used in fuel, and a commutator-type switch was used in LOX. For nitric acid, the inductance of short coils in a ceramic tube was changed by torus aluminum floats, as in the continuous inductive level gage. The inductance change was used to operate a relay at a certain float position. These level switches were about 10 times as accurate as continuous level gages.

Later, the float switches were replaced by capacitance switches for LOX and JP fuel and by conductivity switches for water or other conducting liquids, such as the fuel in the Redstone missile. The capacitive switch consists of several concentric rings in the same plane, alternately connected to form the two plates of a capacitor, which varies its capacity when the dielectric between the rings changes from liquid to gas (Fig. 24.4). The conductivity switch has a 0.02-in. wire, mounted across a 2-in. tube in bushings. When the liquid level drops below the wire, the resistance between the wire and tube becomes infinite and a circuit operates a relay.

During recent years, the discrete liquid level sensors have been more in demand and the industry has developed about 15 different types using capacitive, optical, nuclear, damping, thermal and other principles. The capacitive sensors are similar, but the circuit is improved to permit smaller and thinner rings and to operate in water. The optical level switch uses a small light source. A light beam is reflected by a prism and detected by a solid-state detector. When the prism is touching liquid, the angle of reflection and the signal of the detector change. The nuclear switch uses the increase in detected radiation energy when the medium between radiation source and detector changes from liquid to gas. Provisions exist for mounting inside and outside the tank.



CAPACITIVE LEVEL GAGE



CONDUCTIVE LEVEL GAGE

Fig. 24.4 Capacitive and inductive level gages.

The damping effect of the liquid is employed by a large variety of discrete liquid level sensors. Some use crystals, either bonded to a metal housing or directly exposed to the liquid, oscillating at supersonic frequencies. Others use a thin diaphragm, oscillating at supersonic frequencies due to magneto-strictive force. Even the vibration of a pedal is being used. The touch of liquid, which dampens oscillation, is used for switching operation. Most of these switches demonstrate high repeatability in the laboratory, have a fast speed of response, and operate in most propellants, including LOX and liquid hydrogen.

In cryogenic propellants, the use of thermal sensors has been investigated. The hot-wire probe can be used in this environment for flow rate measurements. Thermistors or carbon resistors are too slow and are used for monitoring only. The same applies to float switches, still being manufactured and used in several versions.

When the turbine-type flow meter became available with reduced installation requirements, the frequency output increased the accuracy to make possible the inclusion of flow meters in rocket design. Continuous improvements in bearings, turbine shape and electrical pickup give the turbine flow meter extremely good repeatability. Its accuracy is as good as its calibration, provided the calibration is made with the same line configuration and with the same propellant condition as its expected use. This calibration is best accomplished at static test stands with contact level gages in the fuel tanks. The output of the turbine flow meters is counted electronically. The counters are switched on by level sensors at the upper part of the tank and switched off by level switches at the lower part of the tank, thus providing an automatic calibration procedure. The quantity of fuel between level switches is determined accurately by water calibrations. Accurate shrinkage corrections are determined in separate measuring series. For further increase in accuracy, the multiple sampling method is employed, whereby the calibration factor is determined several times during the same test by counting the cycles of the turbine meter between three to five pairs of level sensors at the upper and lower portions of the tank. With this method, flow rate measurements with better than  $\pm 0.1$  per cent accuracy were obtained for all propellants during static tests on the Redstone and Jupiter missiles. The combined use of level gage and turbine flow meter is ideal, giving very accurate calibration on the spot and during the same test for steady-state test periods. The turbine flow meter gives the accurate rate value for any part of the test, including transients.

Calibration of volumetric flow meters with contact level gages is also being used for calibrating rocket or other flow meters in the laboratory or at calibration stands. Small flow meters are less sensitive to line configuration and can be transferred to another place of operation with little loss in accuracy. The 8-in. flow meters for Saturn engines could not be calibrated in the original missile configuration. All

efforts were made to simulate the rocket configurations as closely as possible at other calibration stands. Still the uncertainty of these measurements increased to more than 1 per cent. Special efforts made these large flow meters less sensitive to line effects, and considerable improvements were accomplished by lightweight rotors and other small changes.

Level gages and turbine flow meters measure the volumetric flow rate, but the development and testing of rockets requires the measurement of mass flow rate, as stated before. Mass flow meters are also important for aircraft and for processing, quality control, or pricing throughout industry. Therefore, the instrument industry started the development of mass flow meters in 1952. There are now about 10 true mass flow meters on the market or under development.

Several mass flow meters use the angular momentum principle. They bring the liquid in rotation by a motor-driven impeller, duct or vane, and remove the rotation or angular momentum by a turbine or vane, measuring the created torque as a function of the mass flow rate.

Some angular momentum mass flow meters use a fluid conduit in the form of a loop or square, producing a flywheel effect. As with a mechanical gyroscope, a force perpendicular to the plane through the conduit produces a momentum perpendicular to the plane and force. An oscillating force simplifies the liquid conduits and mechanical design that is already rather complex.

Another version uses a synchronous motor and constant torque coupling to a turbine with no blade angle. The turbine rotates at a speed proportional to the reciprocal of mass flow rate.

The twin-turbine flow meter uses the different angular momentum generated by different plate angles on two turbines coupled by a spring. The angular displacement between the turbines is measured as a function of mass flow rate by interval counters or other methods. The speed of the rotor unit with the two turbines can be measured at the same time as function of the volumetric flow rate.

Other mass flow meters measure the drag on a reed or adjustable vane. Many inferential mass flow meters measure volumetric flow rate with turbines, magneto induction, propagation of sonic vibration, motion of nuclear effects, or differential pressure systems, and correct automatically for density.

A current research and development program is aimed at investigating mass flow meters based on the angular momentum principle. It is expected that a true mass flow meter with better than  $\pm 0.5$  per cent accuracy will soon be available for measurements on all propellants including LOX and liquid hydrogen.

Calibration of mass flow meters cannot be done with point level sensors. Several gravimetric methods are currently being refined. Mechanical scales and load cells are good primary instruments; but great effort is necessary to eliminate errors caused by fuel lines, guides, hydrodynamic impact, and jet effect of exhausts. Another method measures the change in buoyancy of a plummet in the propellant tank to determine the decrease of mass.

Until accurate and reliable mass flow meters are available, the volumetric flow rate must be measured and multiplied by the density as in the past. The density was usually determined as function of pressure and temperature from handbooks or data obtained in the chemical laboratory. However, it was found that the density of LOX in rocket tanks is less than the handbook values. A weighing system was necessary to investigate this density effect. Such a system was also needed to determine true shrinkage of the tank when filled with LOX. Therefore, the calibration stand was equipped with a precision weighing system, comprising five different sets of load measuring instrumentation for most accurate results with the multiple sampling method. On the platform of a mechanical scale were three hydraulic load cells, 120 deg apart. On top of these load cells were three electronic load cells and a "spider." Hanging on the center of the spider were the tanks with two different types of electronic load cells in series. With this weighing system, the average density of the LOX in the rocket tank was found to be 1.134 kg per liter, more than 0.5 per cent less than the handbook value.

A nuclear densitometer system was developed to measure the densities in the LOX tank and the suction line. The system used a monoenergetic gamma radiation source and a scintillation counter as detector. The mass absorption coefficients  $K = \frac{1}{\rho D} \log_e \frac{I_0}{ID}$  were measured for various materials:  $K_{H_2O} = 0.06405 \text{ cm}^2/\text{g}$ ;  $K_{O_2} = 0.05770$ ;  $K_{H_2} = 0.1145$ ;  $K_{N_2} = 0.05765$ ;  $K_{Al} = .00527$ .

Most of the nuclear densitometers use outside mounting of radiation source and detector. One prototype was modified so that the radiation source could be mounted in the liquid any distance up to 70 in. from the outside detector to enable some study of the density profile. Some of these instruments are satisfactory, others still need improvement.

With the addition of liquid hydrogen to the family of fuels, the need for density measurements increased considerably because the density of liquid hydrogen changes 0.06 per cent/ $^{\circ}\text{F}$ . How well liquid hydrogen in rockets follows the published density data must be investigated. New liquid hydrogen densitometers for outside mounting on a 5-in. fuel line and a 4 ft to 8 ft tank have been developed. A program has been started to develop small point sensors with beta radiation and solid-state

detectors for inside mounting to measure the density profile with a multitude of point densitometers distributed throughout the tank. Other NASA centers measure the density of liquid hydrogen by measuring the buoyancy of a float submerged in liquid hydrogen.

Industry also develops capacitive instruments similar to the continuous capacitive level gages; since the dielectric constant of hydrogen is a function of its density, these instruments measure the average density or mass of liquid plus gaseous hydrogen in the tank. Most of these instruments use servobalance of the capacity and are good for filling control and propellant utilization systems but are not accurate enough for flow rate measurements. Propellant utilization systems regulate the flow rate of propellants during flight with the end in view that both propellant tanks are empty at the end of combustion. The discrete liquid level gage, or a head pressure system, is also being used for propellant utilization in LOX and fuel tanks.

Another important measurement for rocket launching is filling control of the propellant tanks. The head pressure method is preferred for this purpose because the differential pressure is a function of the mass. The differential pressure gages have been refined from bromide-filled U-tubes on early missiles to force balance systems with an accuracy of better than  $\pm 0.05$  per cent.

The filling of noncryogenic liquids has been measured for many years with positive displacement flow meters. Current rotating piston meters have a repeatability of better than  $\pm 0.05$  per cent, and neck tanks or prover systems are used for calibration of these meters with an accuracy of  $\pm 0.02$  per cent. However, the positive displacement flow meter measures the volume, and attachments are available that automatically convert the volumetric readings to mass, using temperature or buoyancy effects for gear changes, or other conversions of the count. Another good total-mass flow meter is the volumetric turbine flow meter that counts every second for a part of a second, as determined by the buoyancy of a float submerged in the liquid.

#### 24.6 Temperature Measurements

About one-third of the measurements for rocket development and testing are for temperatures ranging from  $-255^{\circ}\text{C}$  to  $+2500^{\circ}\text{C}$ . Thermocouples have long been used for temperature measurements; and there is not much margin for improvement in these devices. Advancements were made by replacing the cumbersome ice bath with hot reference junctions, better techniques in making and attaching thermocouples, purer thermocouple materials, and new materials for higher temperatures; that is, Ir-Ir Rh or W-Re (tungsten-rhenium). The Ir-Ir Rh thermocouple is effective up to  $2000^{\circ}\text{C}$ , and the W-Re couple can be used for temperatures above  $2500^{\circ}\text{C}$ . Some research continues to improve their stability and to coat them for

oxidizing environments. Thermopiles were used for LOX, connecting three to four Cu-constantan thermocouples in series and having all reference junctions in a Dewar flask with LOX under atmospheric conditions. The true reference junction temperature in this instrument was often cause for doubts; consequently, resistance thermometers are now being used for all cryogenic liquids. The newest in this field is a germanium crystal thermometer with a much larger output per degree temperature.

For calibration, the thermocouples and resistance bulbs are compared with NBS-calibrated sensors. An automatic calibration system has been developed that regulates an oven at a set temperature and automatically prints the output of 10 thermocouples after temperature equilibrium is reached. For low temperatures, the boiling points of LOX and liquid nitrogen are used as additional standard values.

The optical pyrometer, total radiation pyrometer, and an infrared radiometer were used for surface temperature measurements in nose cone tests, jet vane studies, and similar tests. Efforts were made to determine true temperatures and emissivity with a two-color method using infrared detectors in the 1 to 3  $\mu$  region, but there was still room for improvement when the nose cone program and the development of instruments was discontinued at MSFC.

Calorimeters have been used for studies of heat flux and radiation on test stand structures, in the tail section of rockets, at different locations during separation tests with models to study design criteria for upper stages, etc. The calorimeters used had a copper block varying between 0.25 in. to 1 in. in diameter and 0.062 in. in thickness, blackened by platinum black or copper oxide with a thermocouple peened in the back. The temperature rise was recorded; and, from calibrations, the Btu/ft<sup>2</sup>/sec could be determined. The calibration was made with a black body at constant known temperature. The main trouble with the field measurement was the quick change in calibration or absorption coefficient of the black surface under test stand environments with water spray, smoke, and flame.

Flame temperature measurements were required to determine enthalpy and performance of the rocket engine. The sodium line reversal method was employed, using ribbon or carbon arc lamp as a calibrated light source, an optical wedge to change the brightness continuously, a lens to focus the light beam in the flame, other lenses and a prism to resolve the spectrum, and a drum with optical film to record the spectrum. When the decreasing brightness of the light became equal to and then less than the brightness of the flame, the sodium line reversed from dark to bright. Drum and wedge were coupled and the point of reversal was a measure for brightness and respective temperature of the flame. These measurements established the flame temperature relationship of the rocket engine. The emission-absorption principle with automatic balancing was developed for ramjet flames, a project discontinued in 1953.



## 24.7 Vibration and Sound

An instrument with a coil attached to a mass was used as a vibration transducer during the V-2 development. A permanent magnet around the coil induced voltage in the coil when vibrating. More recently piezoelectric accelerometers were developed for frequencies from 10 cps to 5000 cps, and strain gage accelerometers for frequencies from zero to 500 cps. The output of these transducers is recorded on oscillographs or more often on magnetic tapes for play-back and analysis.

The vibration analyzers use band pass filters to separate the components of composite waves on a frequency basis. Some analyzers have several filters covering one-third or one-half an octave and analyze continuously. Other analyzers have one filter and adjust the frequency manually or automatically, in steps or continuously. During the V-2 development a commercial instrument was used with about 20 one-third octave filters. The spectrum was shown on an oscilloscope as amplitude bars for the different frequencies, and a camera recorded the spectrum. The transducer output was analyzed and recorded during tests often without tape recording. After 1945, an analyzer was used with filter and continuous manual adjustment. A number of commercial filters with variable bandwidths were used to determine the vibration amplitude for certain frequencies. Later, application was found for analyzers with 32 band filters in one-third octaves for frequencies from 16 to 18,000 cps. For special studies, an analyzer was used with 422 narrow-band filters and three-dimensional recording, 10 times per second, on electric stylus paper. The standard instrument today is an analyzer with narrow-band filter and automatic, continuous adjustment through a selected frequency range of zero to 250 cps, zero to 2500 cps, or zero to 25,000 cps at constant bandwidth that can also be selected in seven filter types from 2 to 200 cps. The tape is prepared in the form of a loop and runs through the analyzer automatically several times while the frequency of the filter is constantly changed through the spectrum at constant bandwidth. The output is recorded on an X-Y plotter.

Rocket noise measurements were started in 1957 with studies of the noise characteristics in the Jupiter tail section, in ground support trailers, and around the launching pad. The Saturn rocket considerably increased concern about noise. A large-scale measuring program was started to study basic characteristics of acoustic environments, sound propagation, influence of weather on sound velocity profiles, etc. Piezoelectric crystal microphones, used as transducers and preamplifiers, were located near the microphone because of low output and distance to the recording system. The recording system consisted of a matching amplifier and a tape recorder. Calibrations were made before installation while spot checks were made in the field using a commercial calibrator. This calibrator had a small steel housing with a cavity for the microphone. A diaphragm on the bottom of the microphone was vibrated by an electric

magnet at 400 cps and varying calibrated voltages, producing rms sound pressure levels up to 130 db at 400 cps. The evaluation was done with special equipment following the principles described for vibration analysis. The tape was played back, and a set of one-third octave filters resolved the spectrum, squaring and integrating networks produced true rms values. A voltage recorder presented the rms values for the different frequency bands.

Near-and-far field measurements were made during tests on a model cluster of eight 500-lb engines, captive tests of the Saturn booster, controlled explosions, cannon shots and operations of a siren at different frequencies. The siren permitted more systematic studies under different weather conditions. Rawinsonde balloons were launched daily for the measurement of sound velocity profiles up to 10,000 ft. The basic characteristics of acoustic environments are now generally understood. The controlling effects of atmospheric conditions on sound propagation are generally known. Improved methods of measuring weather conditions are planned. In general, sound measurement and control is sufficiently advanced to permit tests of large thrust boosters without adverse noise effects in nearby communities.

#### 24.8 Other Measurements

Rpm. The principle of voltage generators has been used for many years, but pulse generators are now preferred for more accurate digital recording.

Displacement. Wirewound potentiometers have been used as transducers, and wax paper recorders have been used for direct displacement measurements. For many years, the differential transformer was used; but it has reached a status enabling full-scale displacement measurements to 0.01 in.

Cameras. Cameras have been frequently used to record indicating instruments. The camera is very important for observation of such things as tank depletion, liquid surface, and flames.

Gas analyzers. A variety of gas analyzers is used for different purposes; some examples include analysis of exhaust gases, percentage of ortho and para parts in liquid hydrogen, and the gas mixture in the tail section of missiles. A combustible-gas analyzer was moved up and down in the tail section of the vehicle to monitor dangerous gas mixtures.

Humidity. A compressed gas is used to operate valves in the rocket propulsion systems. This gas must be dry, otherwise the water vapor condenses and freezes. An electrolyzing cell was developed having a sensitivity of 0.1 ppm (parts per million). Gas is passed through the cell at constant flow rate and decomposed by long, helical electrodes. As a

standard for investigation and calibration, an NBS-developed principle was extended to measure lower water vapor content. This standard passes saturated gas over an absorbing film and measures the resistance. Then it passes the unknown gas over that film and increases the pressure until the resistance is the same as for the saturated gas. This pressure and the water vapor content of the saturated gas give the water vapor content of the unknown gas. A program is underway to combine an oil content monitor with the water vapor indicator.

#### 24.9 The Future

This chapter covers the major measurements made during the development and testing of rockets. Other measurements made on special occasions are too numerous to be discussed.

The survey shows how much the art of measurement has advanced during the last 25 years of rocket development. It is very gratifying to note that the complexity and importance of measurements in all fields are now fully realized and that several universities have introduced courses in the science of measurements.

## 25

TORQUE MODULATION AND MODULATION ERROR DETECTION CONCEPTS IN MODERN  
GUIDANCE INSTRUMENTS

H. Schlitt

Inertial Development Laboratories  
Bell Aerosystems Company  
North Tonawanda, New York

From a historical standpoint, the evolution of instrument concepts shows many parallels to the general progress of technology through the ages. This is only natural since the basis for all thoughts on instrument design and usage is dictated by the state of the art in all technical fields contributing to this area.

As a result, the evolution of instrument techniques follows very closely the thinking that prevailed throughout the design history of general machinery. Only since the beginning of this century have instrument techniques been decisively separated from all other areas of technology, and the necessity of extreme accuracy combined with rugged environmental requirements has given impetus to a greatly accelerated path of evolution in this field. This development was characterized by pronounced sophistication of the technical approaches and physical concepts such as the force balance principle and the Schuler tuning.

Furthermore, a decisive step was achieved with the introduction of the digital computation techniques to deal with the ever increasing volume and complexity of computations required. Simultaneously, the advance of precision electromechanics, the reduction of tolerances and the introduction of new materials such as beryllium and ceramics, greatly increased the possibility of achieving ultra-precision instruments.

Last but not least, the appearance of semiconductors finally moved many seemingly hopeless projects into reality by permitting instrumentation complexities to come into line with the performance requirements.

In the area of high performance instruments for guidance applications, we are today in a situation where the requirements in many cases still exceed to a significant extent the existing possibilities. This is reflected in unsatisfactory performance and marginal reliability of much equipment under development or in use.

Furthermore, increased usage of sophisticated and complex instrumentation in the military and commercial fields results in a mounting economical pressure for lower development, production, and above all, maintenance costs. The latter requires a drastic increase in reliability to achieve a significant cost reduction over the entire life of the equipment. Only if these goals can be achieved will a further extension of the market for precision instruments become economically feasible.

Under these conditions, it is only natural that different philosophies exist as to the best technical approach toward solving the existing and foreseeable tasks. These philosophies partially reflect the historical progress in the instrumentation field, from a period of rather crude analog simulation of physical laws where reliability and acceptable performance were easily attained, to today's sophistication, performance and complexity with all the adverse characteristics attached to these approaches.

Since conceptual technical advances in many cases provide new ways and means for the solution of today's severe requirements, the use of instrumentation schemes is suggested which differ radically from conventional concepts created in the first quarter of this century. This approach promises increased application of advanced technical concepts, rather than today's exclusive exploitation of the advance in precision mechanics for a decisive contribution to the solutions in this field. It opens the prospects for partial replacement of precision mechanics by electronics and a reduction of cost as well as improvement of performance and reliability. As such, it may form a new basis for instrument technology for the foreseeable future.

This paper is compiled on the basis of research and development activities carried out by Bell Aerosystems in areas of advanced design concepts to show a contribution to the application of conceptual advances in the instrument field.

### 25.1 Conventional Basic Instrument Concepts

In following the evolution of instrument design, it becomes apparent that the earliest attempts of measuring were based on the direct use of existing physical relationships. This extends from the use of the balance scale in ancient times through the introduction of the knot line for ship navigation to the application of the fly ball controller for the early steam engines. Even early barometers (using hydraulic principles), the gyro, the Foucault pendulum, etc., make use of a simulation of physical relationships and can be classified in the category of the present analog computer with analog sensors.

The accuracies of these instruments were defined by the existing state of the art of mechanical accomplishments and often allowed only a

qualitative demonstration of the desired effects. Needless to say, in most cases the complexity was extremely low; therefore the achieved reliability became acceptable even under consideration of the poor mechanical conditions that existed.

With the advent of the use of electricity, a whole new area of design possibilities for measuring instruments was opened. It permitted the design of many versatile instruments for industrial and military applications, based on the use of electromagnetic laws. It is important to realize that the electronic measuring methods are not distinguished by especially high accuracy; their most important feature is their versatility and ease of application for the accomplishment of certain tasks. However, only until extreme accuracy was required in missile and airplane guidance did the engineer devote his ingenuity to the creation of the very sophisticated guidance instrumentation we see today. Here two technical concepts proved extremely valuable: the feedback technique and the force balance method. Both of these concepts, together or individually, represent the basis for most instrumentation concepts that exist today. Without them, modern guidance instrument design is inconceivable.

The combination of these techniques allowed the extension of the force balance principle from the balance scale of ancient times to the precise conversion from mechanical into electrical measuring quantities used in missile and space vehicle guidance systems. It further permitted the realization of the gyroscopic accelerometer integrator, the double integrating distance meter and numerous other instrument concepts, all of which are of major importance for guidance applications.

Unfortunately, all uses of analog simulation techniques in the endeavor to create precise sensors for acceleration and angular displacement are confronted with a unique dilemma. This is the requirement of a torqueless suspension system of the sensing portion of the mechanism. Present day attempts, while representing extreme improvements compared to the techniques as they existed at the beginning of this century, have not yet solved this problem in a completely satisfactory manner. Even gas bearings, floated bearings, electrostatic suspension systems and sophisticated spring suspensions such as the two or three spring pivot, still leave much to be desired if low cost, extreme accuracy and reliability become mandatory. In fact, the complexity of the suspension system is in nearly all cases responsible for the high cost and maintenance problems of the instruments.

This area deserves most of our future attention if we want to improve performance, achieve simplicity and reduce costs. There are two approaches to this problem. One is the improvement of the existing general technical solutions by continuous refinement, increased precision of parts, and selection of new and better materials. This may be considered a conventional approach and its importance in conjunction with the general evolution of technology should not be underestimated. However, past experience

and foreseeable requirements make doubtful whether this approach alone will provide satisfactory progress in the instrumentation field. It appears that the stimulus of new conceptual ideas is required to complement the conventional approach if timely solutions are to be achieved.

The techniques described here attempt to complement the conventional instrument approaches and tend to indicate one such general direction for the design of a combination of high performance and low cost instrumentation in the future.

#### 25.1.1 The Torque Modulation Concept for Measuring Instruments

In the attempt to eliminate residual torque effects on instrument suspension systems, the technical concept of torque modulation was created in the early thirties of this century. As in so many instances, the science of precision mechanics was not available to make sufficient use of such an advanced and sophisticated concept; its potential for the design of precision instruments remained unexplored. Nevertheless, it was known both in this country and in Europe, and some attempts were made to apply this principle to precision instruments (e.g. the gyro compass).

The application of the torque modulation concept to gyroscopes with extremely low drift characteristics and high repeatability was not recognized until the mid-1950's, nor was the possibility of separating and eliminating various physical torque sources. At that time, Bell Aero-systems started a major program of investigation in this area. Today, based on the results of this program, it appears that this approach represents one of the most fruitful concepts for the design of precision instruments inasmuch as it replaces extremely accurate, expensive and comparatively unreliable precision mechanics by an operating technique that adds very little complexity to a system.

Torque modulation refers to periodic modulation of the null torque of a suspension system, which is achieved by continuous rotations of the system about an axis normal to the sensing axes of the instrument. This results in an averaging effect of all torque phenomena such that the low frequency content of the suspension null torque is eliminated. As a consequence, the entire suspension null torque effects are transformed to a higher frequency region around the rotation frequency where, in most cases, they exhibit only an insignificant effect on the performance of the instrument.

This approach in its concept can be compared to the chopper stabilization of the electrical null of dc amplifiers. Here a modulation from dc to ac is performed, followed by an ac amplification which is drift free. Finally, the amplified ac voltage is again demodulated. It is this process of modulation which removes the effects of changing null characteristics of the amplifier elements and therefore compares with the modulation of the suspension torque effects in the instrument case.

### 25.1.2 Application of the Torque Modulation Concept to High Performance Gyroscopes

A typical application of the torque modulation concept is the two-degree-of-freedom gyroscope with case rotation. Here the gyro torque effects are eliminated by a continuous rotation of the gyro housing about an axis parallel to the gyro spin axis. This results in an averaging effect of all torques of the suspension system, the flotation medium and the unbalances in the plane normal to the gyro spin axis.

The basic effect is shown in Fig. 25.1 which indicates the gyro torque of a conventional stationary two-degree-of-freedom gyro as a function of time (dotted line). The solid line indicates the effect of case rotation on the torque measured in one stationary axis. It is apparent that the averaging effect applies only to the extent that the torque under investigation remains constant. Any torque changes, especially as their frequency content approaches or exceeds the case rotation frequency, are not properly averaged anymore.

This can best be shown in the frequency domain by means of Fig. 25.2. This figure indicates the power density spectrum of a conventional stationary floated two-degree-of-freedom gyro, which exhibits a pole at zero frequency. The area under this curve represents the  $\delta$  - or RMS value.\* The application of case rotation to this gyro causes a drift which consists of a frequency  $\omega$  equal to the speed of housing rotation whose amplitude is instantaneously proportional to the drift the gyro exhibits as a stationary instrument. This means that the case rotation frequency  $\omega$  is amplitude modulated and therefore contains an upper and lower side band as indicated in Fig. 25.2. The total area of the modulated drift around the frequency  $\omega$  is equal to the area under the stationary drift curve, which means that the RMS values in both cases are equal.

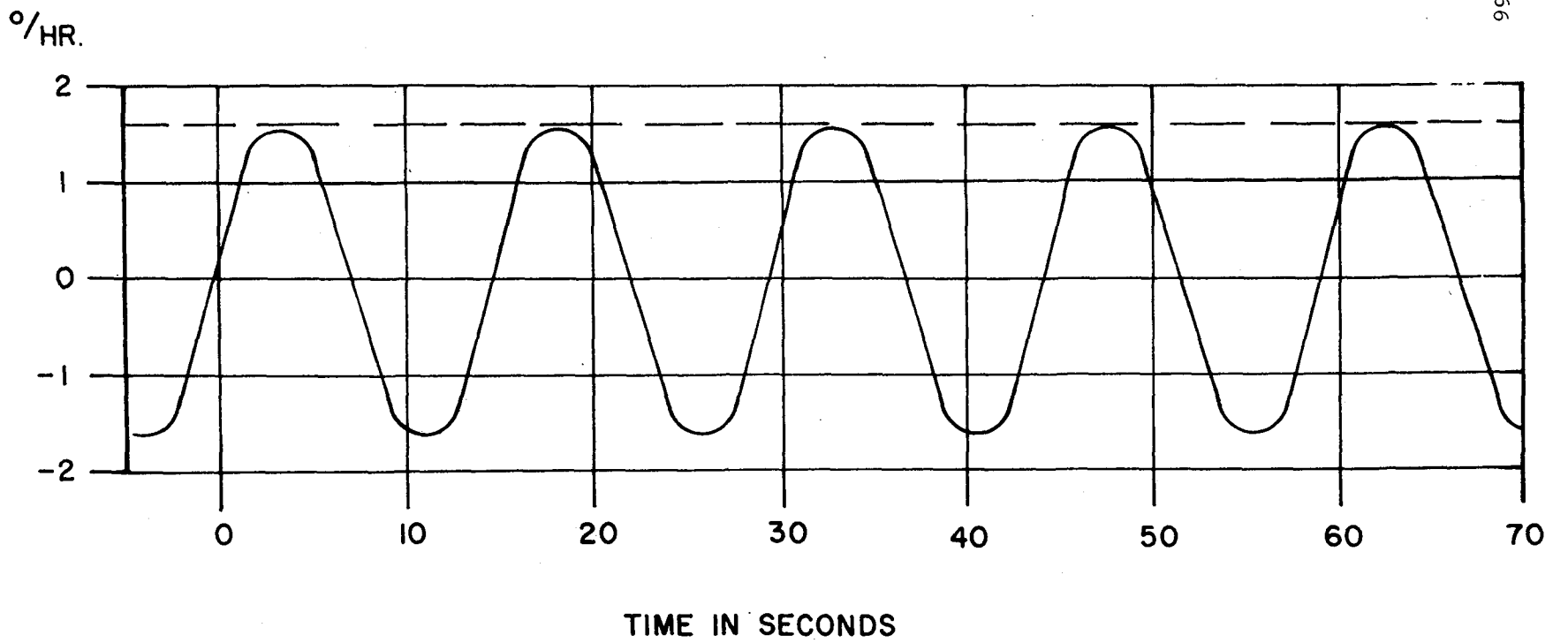
This indicates that the torque modulation does not reduce the RMS value of the basic gyro torque but only transforms its frequency content from the zero frequency region into a higher frequency domain where its effect on the system performance may differ.

To assess the benefits of such a suspension torque frequency transformation on the performance of a system, it becomes necessary to consider its transfer function. This means the function which relates the system output error to the gyro drift. A typical case is shown in Fig. 25.3 for an inertial navigation system where the square of the transfer function relating the azimuth gyro drift to the system's position error in the east coordinate is shown. The figure indicates poles of this transfer function at zero frequency; the frequency of Earth rotation  $\Omega = 0.262$  rad/hr and the Schuler frequency  $\omega_s = 4.5$  rad/hr. For all frequencies

---

\*Of the gyro drift; it amounts in this particular case to 0.7 deg/hr (RMS).





————— Drift of gyro in case rotation mode of operation  
- - - - - Drift of stationary gyro in conventional operational mode

Fig. 25.1 Oscillogram of drift data of two-degree-of-freedom gyro in rotating mode of operation.

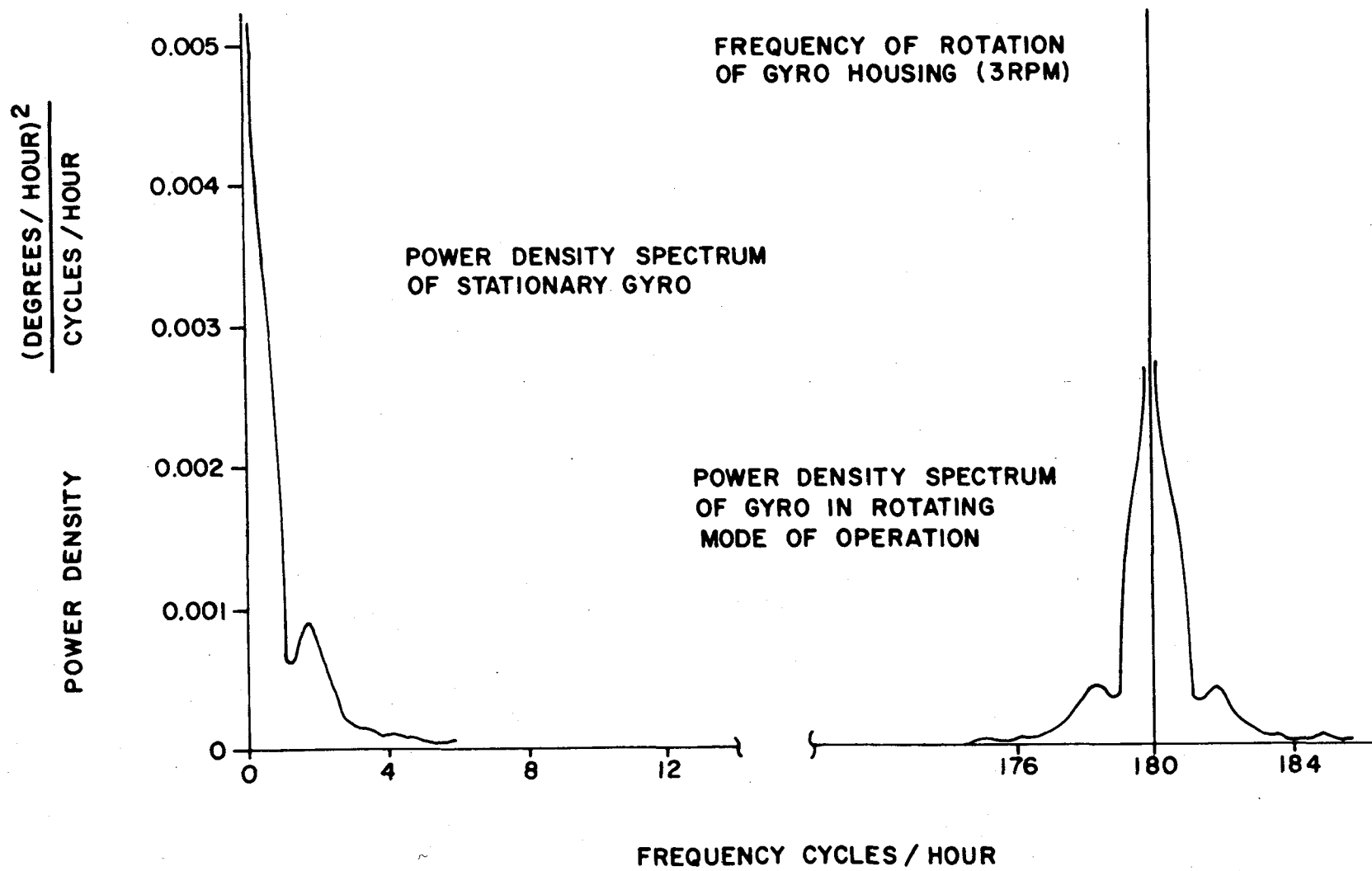


Fig. 25.2 Power spectra for stationary and rotating gyros.

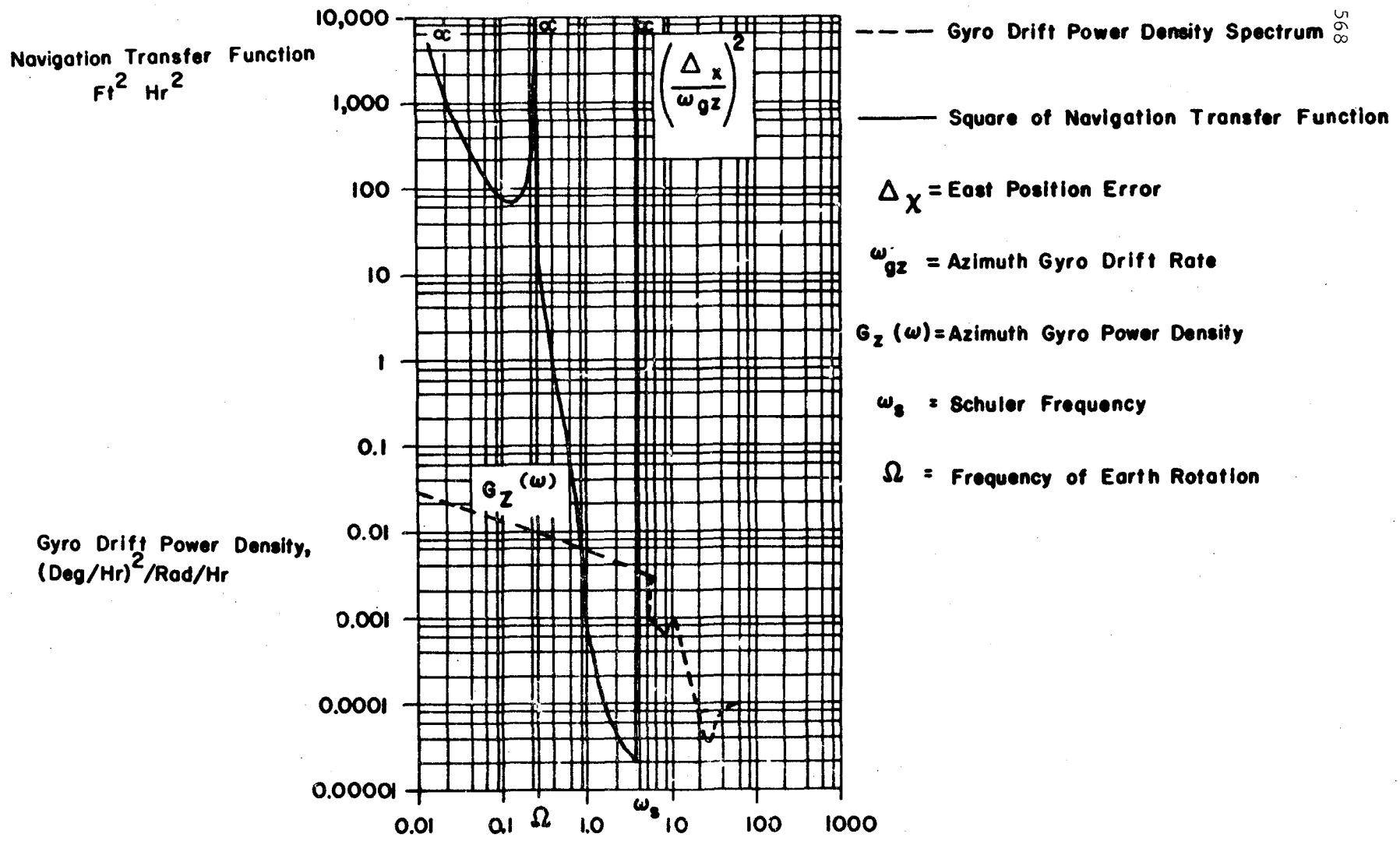


Fig. 25.3 Gyro drift power density spectrum and square of navigation transfer function versus frequency.

which exceed the Schuler frequency significantly, the transfer function becomes negligible. Fig. 25.3 furthermore presents the drift power density curve exhibited by a conventional stationary gyroscope (dotted line). It is apparent that the pole of this drift power density curve coincides with the zero pole of the system transfer function and that the two additional poles of this transfer function are located in a frequency region where considerable power density of the gyro drift exists. As a result, there is an appreciable position error building up as a consequence of the azimuth gyro drift.

The use of gyro case rotation, however, moves the gyro power spectrum so far to the right that only the residual effect of the lower side band of the spectrum has any effect on the system performance, while the major portion of the gyro drift is in a region where the system transfer function is negligible.

Caution has to be exercised in the design of the gyroscope to be case-rotated to avoid creating any periodic torque components in the gyro in the course of rotating the gyro housing. These components would appear in the stationary system as constant torques and degrade the performance of the instrument. Consequently, the gyro suspension system has to be designed so that its torque deflection characteristics are precisely linear.

Considering ballistic guidance application, it becomes important to adapt the case rotation technique to a vastly different environment. With this rather high and rapidly varying acceleration profile during the propelled phase, the case rotation speed has to be chosen faster than for an airplane navigation system. Airplane navigation systems housing rotations are in the order of 2 to 6 rpm; the ballistic applications require 20 to 40 rpm. As a result, the viscous restoring torque effect from the rotation of the housing develops into a rather pronounced characteristic, which becomes of major importance for the performance of the system.

It has to be recognized that the concept of case rotation does not eliminate the effects of all torque sources; there are three major torque categories which are not changed whatsoever: (1) effects from external magnetic fields, (2) anisoelasticity, and (3) mass unbalance along the gyro spin axis. The first category of torques can be reduced sufficiently and easily by proper shielding, the second category requires a proper design approach similar to all other gyros, and the third type of torque can easily and automatically be compensated for in the system preparation mode if conditions are created where the torques of category 1 and 2 are negligible. Since the mass unbalance under these conditions is the only remaining torque source, the compensation of the effect can be made acceleration dependent. This results in a compensation scheme true for all flight conditions.

### 25.1.3 Application of the Torque Modulation Concept to Accelerometers

Considering the null torque of a suspension system of an accelerometer, the problem of achieving sufficient null stability is very similar to the case of the gyro suspension. Again the torque modulation concept becomes applicable for a proper solution. In this case, a rotation of the accelerometer about an axis normal to the accelerometer input axes is required.

The concept is illustrated on the basis of a two-degree-of-freedom spring suspended accelerometer (Fig. 25.4). Here again, the instrument suspension system is continuously rotated so that any null torque will be modulated with the frequency of case rotation and averaged out. The same physical considerations described for the gyro suspension system apply here as far as the case rotation speed is concerned. It has to be noted that a resolution of the accelerometer output signal is required to obtain information in stationary coordinates. Limitations for the speed of case rotation are given by the residual centrifugal forces acting on the sensing mass as well as any viscous torques that may result from the suspension system.

As the null stability of accelerometers normally does not represent too big a problem area, the possible improvement of such an instrument appears mostly of importance for space guidance applications where extremely long times of operation are required. Especially if integration of low thrust accelerations of a space vehicle over extended periods of time is desired, a decisive improvement in accelerometer null stability is of importance.

### 25.2 The Modulation Error Detection Concept

As an extension of the technical philosophy underlying the torque modulation concept, a modulation error detection scheme was developed. This makes use of a periodic modulation of a major parameter of an instrument so that its output information appears modulated accordingly. If the instrument can be operated so that its input remains zero, any modulated output information is representative of the error which develops inside the instrument. This concept permits the removal of all instrument errors or torques, regardless of their origin and their characteristics. However, precautions have to be taken so that the modulation process does not create modulated errors with certain characteristics which cannot be detected. This requirement is not much different from the case rotation concept, where modulated suspension torques in the rotating system result in constant torque components in the stationary coordinate system.

The significance of the modulation error detection concept lies in the fact that it points for the first time to a solution which replaces

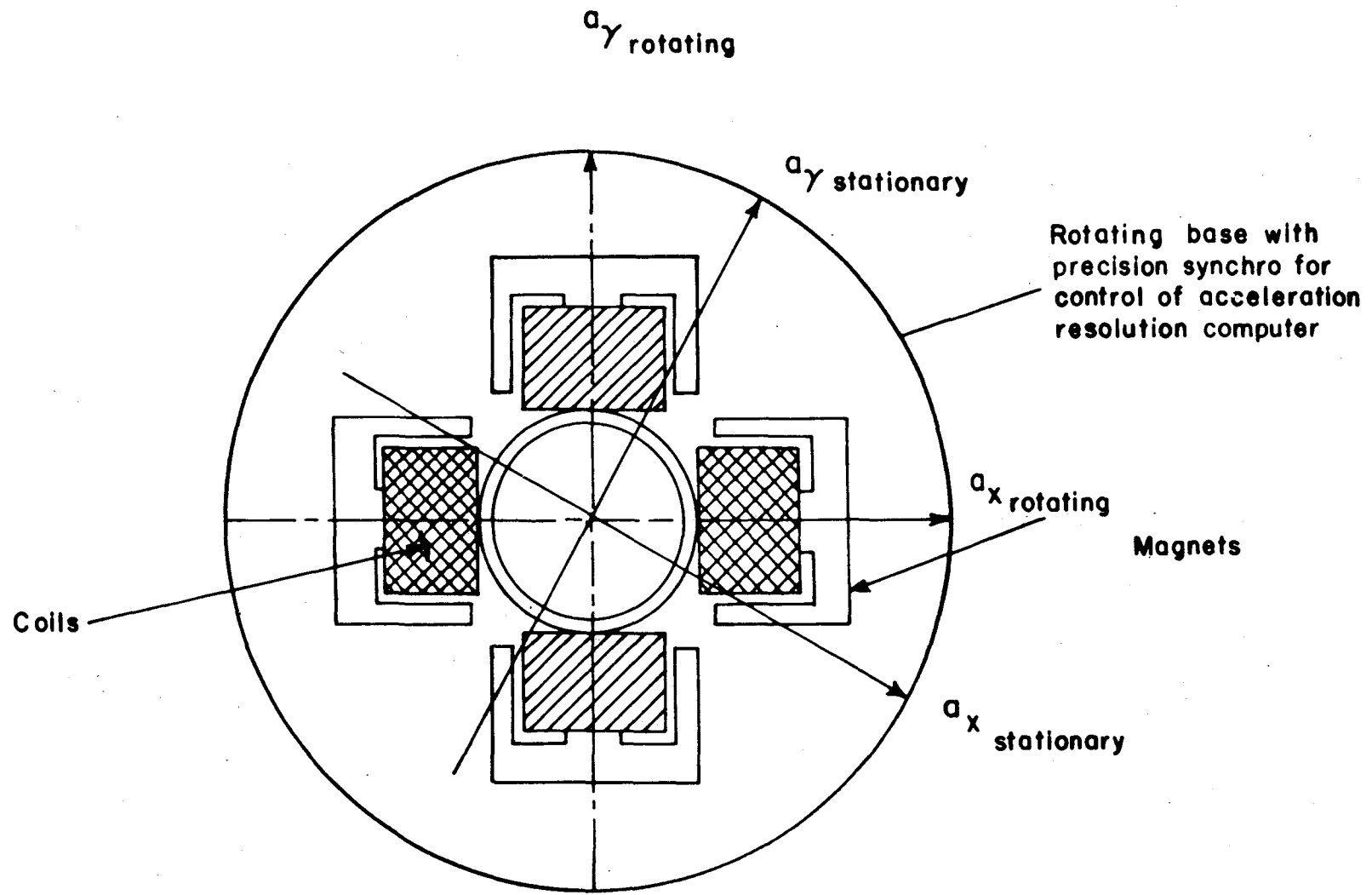


Fig. 25.4 Two axes, constrained pendulum-type accelerometer with rotating base.

precision mechanics on a large scale by electronic feedback techniques. Therefore, it shows a direction for improving performance while at the same time the complexity and cost may be reduced. It is this general outlook which makes this instrument concept so attractive in spite of the formidable problem areas yet to be resolved.

### 25.3 General Considerations for the Application of Modulation Error Detection Techniques

The modulation error detection technique, as described in the case of a gyro, can certainly be extended to numerous instrument designs. It is conceivable that with some instruments, the moment of inertia or the restoring forces are modulated accordingly. A successful application of this technique becomes possible in those areas where conventional approaches do not yield satisfactory performance results and/or precision mechanics is to be replaced by electronics.

### 25.4 Conclusions

The increasing requirements for economy, reliability, and high performance in the field of precision instruments necessitate the augmentation of conventional suspension approaches by advanced instrument operating concepts. Such concepts properly applied contain the promise of solving some of the existing and foreseeable requirements in the guidance instrumentation field.

Examples of some of these advanced techniques are the torque modulation technique and the modulation error detection concept. They are described in their application to some precision instruments to minimize various drift effects. However, their significance extends beyond this particular field of application and the methods used here can well be extended to numerous other instrument designs. It is felt that sufficient effort in these areas may contribute decisively in the long run to our capabilities in the precision instrument area.

## 26

## GROUND VERSUS ON-BOARD TRACKING FOR SPACE NAVIGATION

F. A. Speer and H. F. Kurtz.

Aeroballistics Division  
George C. Marshall Space Flight Center  
National Aeronautics and Space Administration  
Huntsville, Alabama

It is generally recognized that space missions of long duration will require instantaneous tracking measurements as direct input to the navigational scheme. Traditionally, it is thought that these measurements result from high-precision ground tracking. Present-day practical tracking applications include the monitoring and destruct command of ballistic missile flights and giving midcourse corrections of unmanned space probes.

As development progresses towards large, manned space vehicles designed to travel over lunar and interplanetary distances, there is a trend to place on-board some or all of the intelligence gathering systems. These would be under the direct control of the crew.

It is the purpose of this paper to assess the relative merits of the two extreme possibilities — exclusive ground tracking versus on-board tracking — for a spectrum of space missions including orbital, lunar, and escape. This comparison may be made from a general operational viewpoint or from the viewpoint of tracking accuracy and tracking speed. Both aspects are presented. The result of the comparison greatly depends on the tracking precision of the measured parameters used for the orbit determination. One common set of precision figures is used and is considered fairly representative for the present state of the art.

### 26.1 Principal Types of Tracking

Tracking accuracy in general depends on the basic measuring precision, the station location or configuration, electromagnetic propagation effects, and knowledge of the equations of motion. The interpretation of tracking results must properly account for all associated physical phenomena, such as transmitter frequency shifts, variations in refractive index, the motion of the observation point, and — at extreme conditions — even relativistic effects.

For the purpose of this study, the tracking accuracy is represented



by a simplified but reasonably realistic model. Most of the possible bias errors are removed including station location, station vertical, and gravitational and celestial constants. The only parameter considered biased and not solved for in the study is the propagation velocity of electromagnetic waves (light velocity). All instrumentation errors are assumed normally distributed with constant variances estimated to be achievable now, except for errors in the optical position angles of near celestial bodies which are functions of the distance from the bodies. A summary of all error assumptions used is shown in Table 26.1.

### 26.1 Ground Based Systems

Ground systems have the primary advantages of easy maintenance, unlimited power, and high-precision potential. The three major tracking quantities are discussed in turn.

**Range.** Range is measured by the travel time of a monopulse or a modulated coherent carrier from the ground station to the vehicle and return. The primary error sources are the uncertainty in light velocity, the short-term time error of the electronic equipment, and recording and reduction errors. The time and reduction errors are of a random nature while the propagation velocity causes a systematic (bias type) error which, if not accounted for, leads to misinterpretation of orbital observations. Both components are shown in Fig 26.1. It is noted that range error due to presently achievable timing errors (lower portion of the figure) is equal to the systematic error due to propagation velocity uncertainty (upper portion of figure) at a distance of about 5000 km. For distances from vehicle to stations less than 5000 km, the timing error dominates, while for greater distances, the systematic error dominates. The present uncertainty of the light velocity is in the order of  $800 \text{ m/sec}$  ( $\frac{\Delta c}{c} \approx 3 \cdot 10^{-6}$ ).

**Range Rate.** Range rate is measured by the Doppler effect of a radio source on-board the vehicle moving from the observer with a line of sight velocity component  $\dot{s}$

$$\Delta f = - f_0 \left[ \frac{\dot{s}}{c} + \frac{\dot{s}^2}{2c^2} \text{ ----} \right]$$

For simplicity, it is assumed that the velocity vector is essentially oriented along the line of sight. Twice the Doppler shift and higher accuracy can be obtained with two-way transmission from ground to a vehicle transponder and back to the ground. Major error sources are again the propagation velocity, the stability of the reference frequency ( $f_0$ ) of the vehicle transmitter, and reduction errors. Assumed accuracy for Doppler measurements over large distances is approximately  $0.3 \text{ m/sec}$  or  $1 \text{ cps}$  for  $960 \text{ Mc}$  [1].

Table 26.1. Summary of Assumed Errors

Tracking Quantity	Distance Function	Error Magnitude <sup>a</sup>
Ground		
Range	No	±15 m (Fig. 26.1)
	Yes	Moon distance bias error = ±1 km
Range Rate	No	±1 m/sec
Direction Angles	No	±0.03 deg
On-Board		
Altitude	No	±100 m
Relative range rate	No	±1 m/sec
Relative range	No	±15 m
Earth center direction	Yes	±0.07 to ±0.001 deg (Fig. 26.2)
Moon center direction	Yes	±0.07 to ±0.001 deg (Fig. 26.2)
Sun center direction	No	±0.07 deg
Star direction	No	± 0.001 deg

---

<sup>a</sup>All errors are assumed random errors, normally distributed except for the range bias error due to propagation velocity.

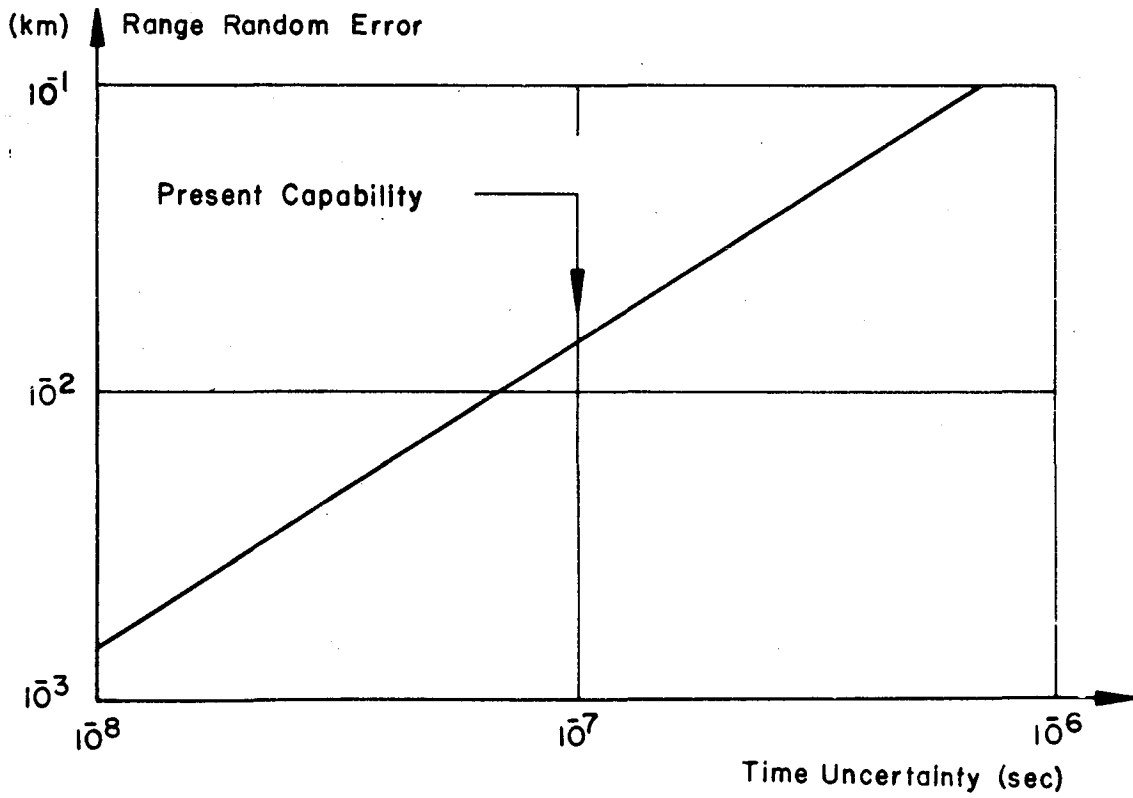
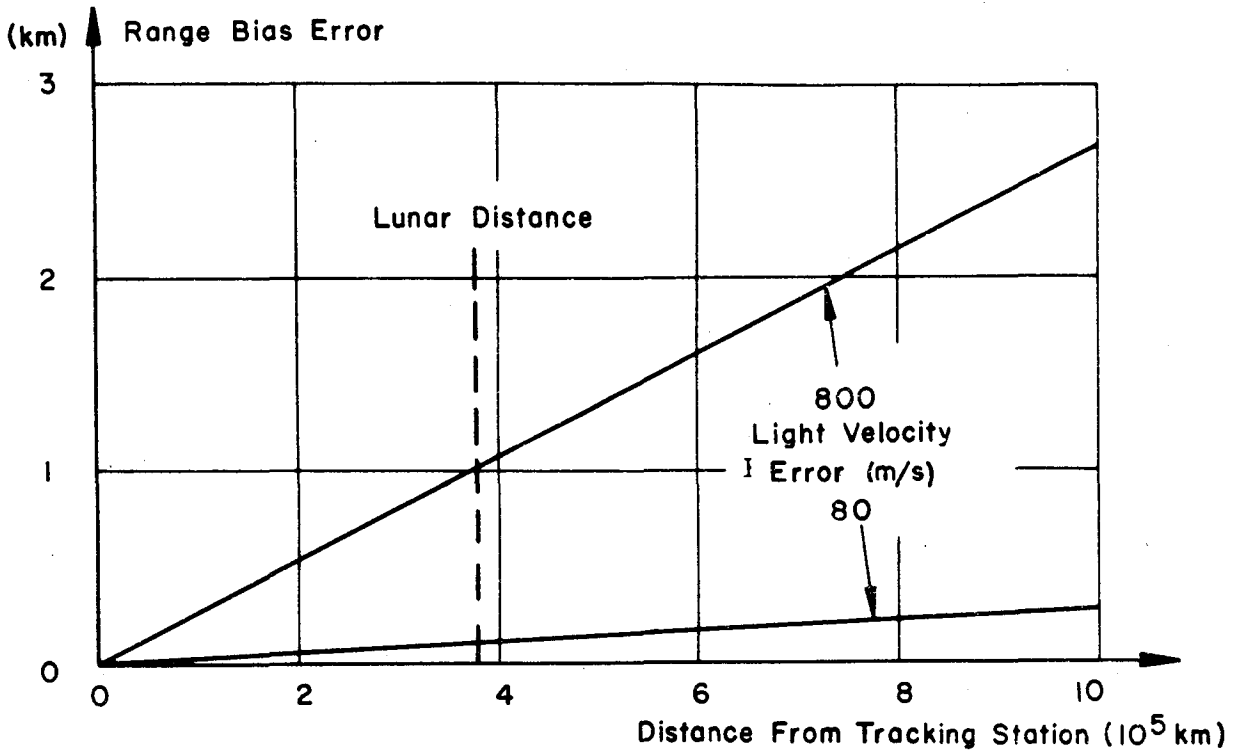


Fig. 26.1 Range error.

Direction. The direction vector of the space vehicle as seen from an observation point on Earth may be measured in two orthogonal angles (azimuth - elevation or hour angle - declination). There are two principal techniques of measurement, one using a single high-gain antenna of high-directional precision and the other using an interferometer array.

The random angle errors of a high-gain antenna consist primarily of: (1) the servo jitter which is a thermal noise dependent upon the signal level, (2) variations in refraction conditions, and (3) variations in the antenna structure due to heat and wind. Accuracies achieved at the Deep Space Instrumentation Facility (DSIF) are of the order of 0.01 deg. In case of interferometers four factors must be considered: (1) the strong dependence on geometry, (2) the possibility of ambiguities, (3) variations or uncertainties of the baseline, and (4) refraction errors.

#### 26.1.2 On-Board Systems

The primary advantage of on-board systems is that continuous tracking coverage with a single station is possible. In manned vehicles, the accessibility of hardware and the elimination of communication requirements are important considerations. The three major types of on-board measurements are discussed briefly below.

Radar Altimeters. The radar altimeter measures the travel time of radar pulses reflected by the Earth or planet surface. The range is limited to near orbital altitudes. The accuracy depends not only on instrumental and propagation errors but also on knowledge of surface conditions. A value in the order of  $\pm 100$  m appears to be a good estimate of achievable accuracies up to 300 km altitudes.

Optical Measurements. Optical instruments operating in the visible or near infrared spectrum may be used to determine the direction of the vehicle from suitable celestial bodies. There are two random error components in measuring these angular positions; these are the instrumental error and the error caused by the irregularity of the planet contour used to determine the center. This irregularity may be of geometrical or optical nature or both.

The sun-angle error is assumed constant since the distance from the Sun is essentially constant for the trajectories considered in this paper. The angle errors of Earth and Moon are functions of the distance from these bodies and are shown in Fig. 26.2. The peculiar shape of the two error curves in this figure is the result of combining the instrumental error ( $10^{-3}$  deg) with the error in knowledge of the observed body contour. For the uncertainty in the contour radii of the Earth and Moon, 20 km and 5 km were assumed. The angle error corresponding to these contour uncertainties decreases with increasing distance.

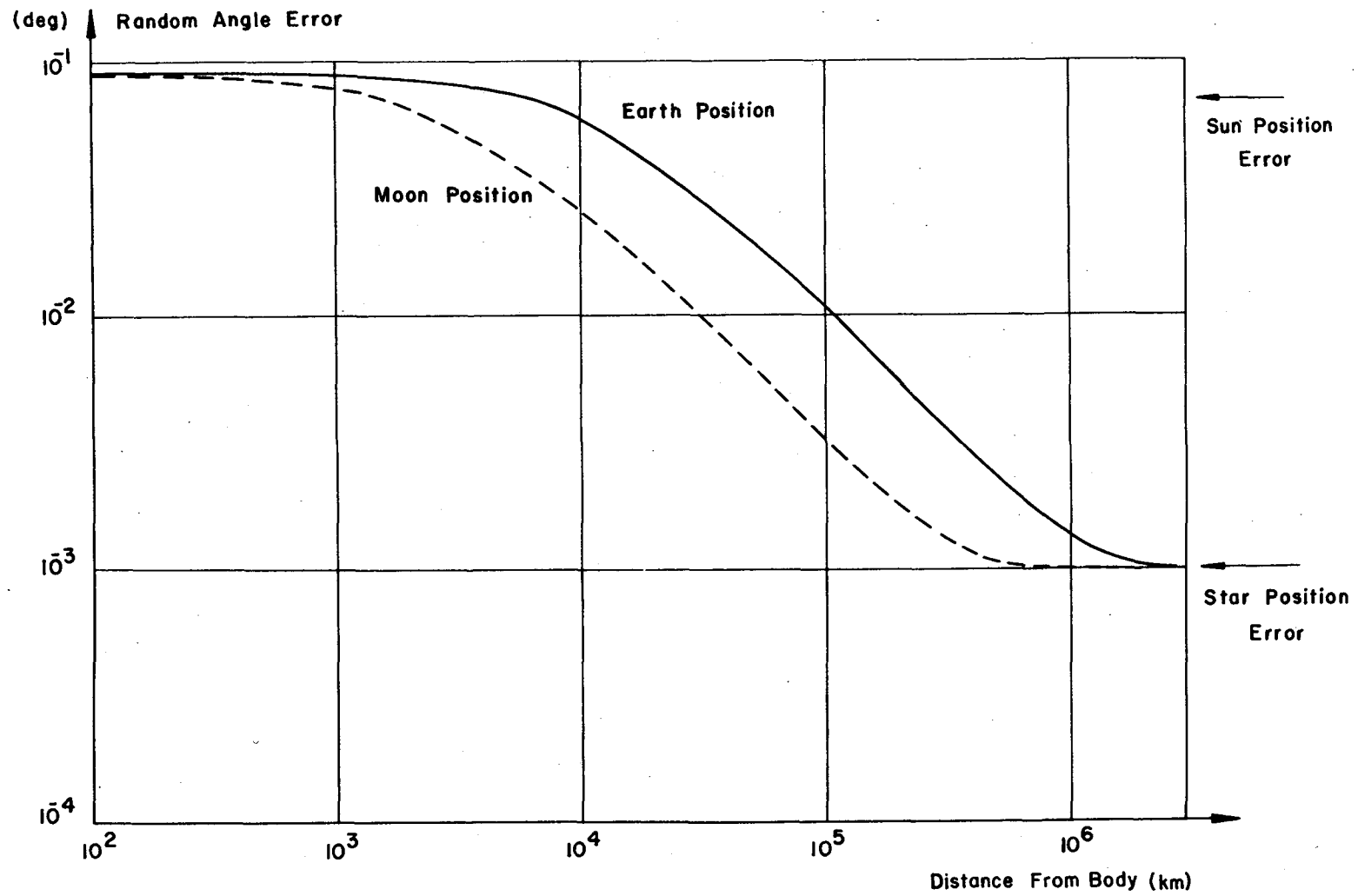


Fig. 26.2 Onboard angle error.

The error due to the contour uncertainty may be reduced through the use of map-matching techniques, using identifiable landmarks on the body surface rather than the body contour. By these techniques, which are of special interest for manned vehicles, the angle errors of Earth and Moon may be reduced to a few seconds of arc (approaching  $10^{-3}$  deg).

The position of a star, which appears as a point light source, exhibits only an instrumental error component of  $10^{-3}$  deg.

Relative Range and Range Rate. Range rate and range are applicable primarily to intersatellite tracking. Where one satellite ephemeris is known with high accuracy, range rate can then be measured between this reference satellite carrying a radio transmitter and the space vehicle. This approach appears promising in some applications for orbital operations. The accuracies are similar to ground tracking values.

## 26.2 Orbit Determination Process

Orbit determination is the process of obtaining from tracking data the actual orbital path of a vehicle. For navigational purposes, this path is defined to include not only the establishment of the post-flight history but the prediction of the vehicle's future path (assuming no additional thrust periods). Because random and biased errors are involved in the process, the true actual path can never be obtained, but only a best estimate of the actual trajectory with certain probable error limitations.

The orbit determination process is aided greatly by the relatively well-known form of the equations of celestial motion and of many of the constants entering these equations. If a limited number of unknown constants can be determined (including the position and velocity of the vehicle at some time), the complete past and future flight histories of the vehicle may be computed. A very large number of observations, spread over a long time period, can be processed to solve for a comparatively few unknown constants, initial conditions, and observational bias errors.

### 26.2.1 Parameter Correction

Through a knowledge of the equations of orbital motion, observations  $\alpha_i$  of a vehicle path (e.g., range) may be related to the unknown parameters  $p_j$  of the equation (e.g., initial velocity)

$$\alpha_i = f_i(p_j) \quad - \quad (26.1)$$

The problem in orbit determination is to find the set of parameters  $p_j$  which correspond uniquely to a set of given observations  $\alpha_i$ . Because actual observations are contaminated by both random and bias errors, it is not possible to match the observations exactly. The maximum likelihood values of the  $p_j$  must be found, defined as the values which minimize the

sum of the squares of the differences between actual observations and calculated observations after taking into account the relative errors of different types of observations, e.g., range vs range rate error.

The maximum likelihood values of the  $p_j$  are generally obtained by the method of differential corrections [2]. The covariance matrix  $C_p(\alpha)$  of errors in the  $p_j$  due to errors in the observations  $\alpha_i$  is found to be

$$C_p(\alpha) = \left[ (\gamma_{\alpha p})^T C_\alpha^{-1} (\gamma_{\alpha p}) \right]^{-1} \quad (26.2)$$

where  $C_\alpha$  is the covariance matrix of errors in the observations  $\alpha_i$  and  $(\gamma_{\alpha p})$  is the matrix of partials of the observed quantities  $\alpha_i$  with respect to the parameters  $p_j$ , obtained by differentiating Eq. (26.1).

The diagonal elements of the covariance matrix are the statistical variances of the parameters, and the off-diagonal elements are the covariances (correlation between errors in different parameters).

The total error in the parameters  $p_j$  is the sum of the component  $C_p(\alpha)$  due to the observational error and another component due to error in the assumed model of the observable functions  $f_i$ , Eq. (26.1). Any error in this model will create differences between the observations  $\alpha_i$  and the calculated values  $f_i(p_j)$  (e.g., the wrong value of the Moon's mass or neglected terms in the Earth's gravitational field). If these differences can be reduced by changes in the parameters  $p_j$ , an error in the determined values of the  $p_j$  will result. The covariance matrix of parameter errors due to the model error is, according to linear transformation theory

$$C'_p = (\gamma_{p\alpha})^T (\gamma_{\alpha q})^T C_q (\gamma_{\alpha q}) (\gamma_{p\alpha}) \quad (26.3)$$

where:  $C_q$  is the covariance matrix of errors in the parameters  $q$  of the equations of motion which are not solved for,  $(\gamma_{\alpha q})$  the matrix of partial derivatives of the observable functions with respect to the parameters  $q$ , and  $(\gamma_{p\alpha})$  the matrix of partial derivatives of the parameters  $p_j$  with respect to the observations.

The covariance matrix  $C_p$  of the total error in the parameters  $p_j$  due to errors both in the observations and in the orbit computation model is then the sum of the two error matrices  $C_p(\alpha)$  and  $C_p(q)$

$$C_p = C_p(\alpha) + C_p(q) \quad (26.4)$$

### 26.2.2 Prediction of Mission Parameter

For use in a navigation scheme, the orbital parameters  $p_j$  determined from observations of an orbit must be used to predict the orbit characteristics pertinent to the achievement of the mission. For purposes of error analysis, it is useful to characterize each mission by one or more mission parameters whose value must be controlled by the guidance system to accomplish the mission requirements. For example, the primary purpose of the guidance for a lunar landing mission may be to land within a given area on the lunar surface.

The covariance matrix  $C_m$  of the errors in the mission parameters  $m$  may be obtained by linear transformation theory

$$C_m = (\gamma_{mp})^T C_p (\gamma_{mp}) + (\gamma_{mq})^T C_q (\gamma_{mq}) \quad (26.5)$$

where  $(\gamma_{mp})$  represents the matrix of partials of the mission parameters with respect to the parameters  $p$ , and  $(\gamma_{mq})$  the partials with respect to the parameters  $q$ .

As previously indicated, some of the errors  $C_p$  may originate through the errors  $C_q$ , in which case the errors  $C_p$  and  $C_q$  are correlated and the relationship in Eq. (26.5) must be modified. The velocity of light enters the observational model for determining the parameters  $p$ , but does not directly affect the prediction of the mission parameters. The partial matrix  $(\gamma_{mq})$  is zero and the expressions given are valid.

Often the mission parameter of interest is the position of the vehicle, either in three-dimensional space or on a two-dimensional surface. The error distribution in space or on the surface is multivariate and is not completely characterized by a single parameter. The multivariate error probability surfaces are ellipsoids for a three-dimensional distribution or ellipses for a two-dimensional distribution. If only the distance from a nominal point is of interest, it may be said that 95 per cent of all errors lie closer to the nominal point than the length of the semimajor axis of the 95 per cent probability error surface (ellipse or ellipsoid). In fact, slightly more than 95 per cent of the errors will lie within this distance, depending upon the other dimensions of the ellipse (ellipsoid).

## 26.3 Comparison of Ground Versus On-Board Tracking

### 26.3.1 Operational Comparison

Space tracking must be considered an inherent part of the operational vehicle control exercised to monitor and guide the vehicle to the final mission point. This operational aspect makes the time requirement for the orbit determination and system reliability as important as tracking accuracy.

Table 26.2 presents, as concise a form as possible, the general



Table 26.2. Comparison Ground Versus On-board Tracking

	Ground	On-board
<b>Fundamental Limitations</b>		
Distance	Limited	Unlimited
Atmospheric effects	Affected	Unaffected
Ionospheric effects	Affected	Unaffected
<b>Design Limitations</b>		
Size	Unlimited	Limited
Power consumption	Unlimited	Limited
Redundancy	Unlimited	Limited
Present stage of the art	High	Low
<b>Station Configuration</b>		
Tracking visibility	Limited	Unlimited
Number of stations	3 (or greater)	1
Maximum base line	Earth diameter	Lunar, planet orbit diameter
Object of tracking	Space vehicle	Planets, Moon, Sun
Attitude of station	Stable	Artificial stabilization
<b>Operations</b>		
Space communication	Required	Not required <sup>a</sup>
Long Range Earth communications	Required	Not required
Real Time orbit determination	Required	Required
Preferred computer site	Central station	On-board

---

<sup>a</sup>Computer assumed to be on-board

viewpoints of a comparison between ground and on-board tracking. Although most of the items listed are self-explanatory, a few comments are added.

The ground station distance limitation is a function of power, receiver sensitivity, and antenna size. Although both power and size can be increased, it is obvious that optical star trackers are in a different category with regard to practical distance limits.

Tracking visibility refers to any geometrical constraints, such as Earth rotation or eclipses, which would impair the line of sight vector between tracking station and tracking object. For most of the on-board measurements, there is practically no constraint in the visibility. Therefore, only one station within the vehicle is required.

Figure 26.3 represents the minimum number of ground stations required so that an orbiting satellite of given altitude and inclination will always be visible from at least one station with the indicated elevation angle.\* It is not suggested that orbital missions, by necessity, require completely continuous tracking coverage; however, the number of stations is a good measure of tracking visibility and associated operational requirements.

The minimum number required for high altitudes at moderate inclinations is three stations. This number increases sharply with both decreasing orbital altitude and increasing inclination. The orbital inclination plays an important role in determining the northern and southern boundaries of the Earth's zone to be covered. Polar orbits would require covering the entire globe.

As the number of stations increases, the efficiency of station use becomes poorer. Each of the three stations required for coverage of a high-altitude or escape trajectory can track between one-third and one-half of the time. Each of the 30 stations required for continuous tracking of a circular orbit with an altitude of 450 km and inclination of 45 deg would function less than one-tenth of the time. In addition, the absolute tracking time per station is likewise reduced.

The maximum baseline enters the achievable accuracy in a rather indirect way. However, it is significant that the effective baseline of the DSIF net, for instance, is one Earth diameter. Similarly, on-board instrumentation can claim "baselines" essentially identical to the travel distances and therefore significantly larger than one Earth diameter.

The most predominant operational problem is that of communication. The tracking data (high density,  $\approx 10^3$  bits/sec) are transmitted from each ground station to a control center. Acquisition data (medium density,  $\approx 10^2$  bits/sec) are sent back to the tracking stations. Whenever required, command signals (low density,  $< 10$  bits/sec) are sent to that command

\* The special case of the Earth-synchronous orbit is excluded.

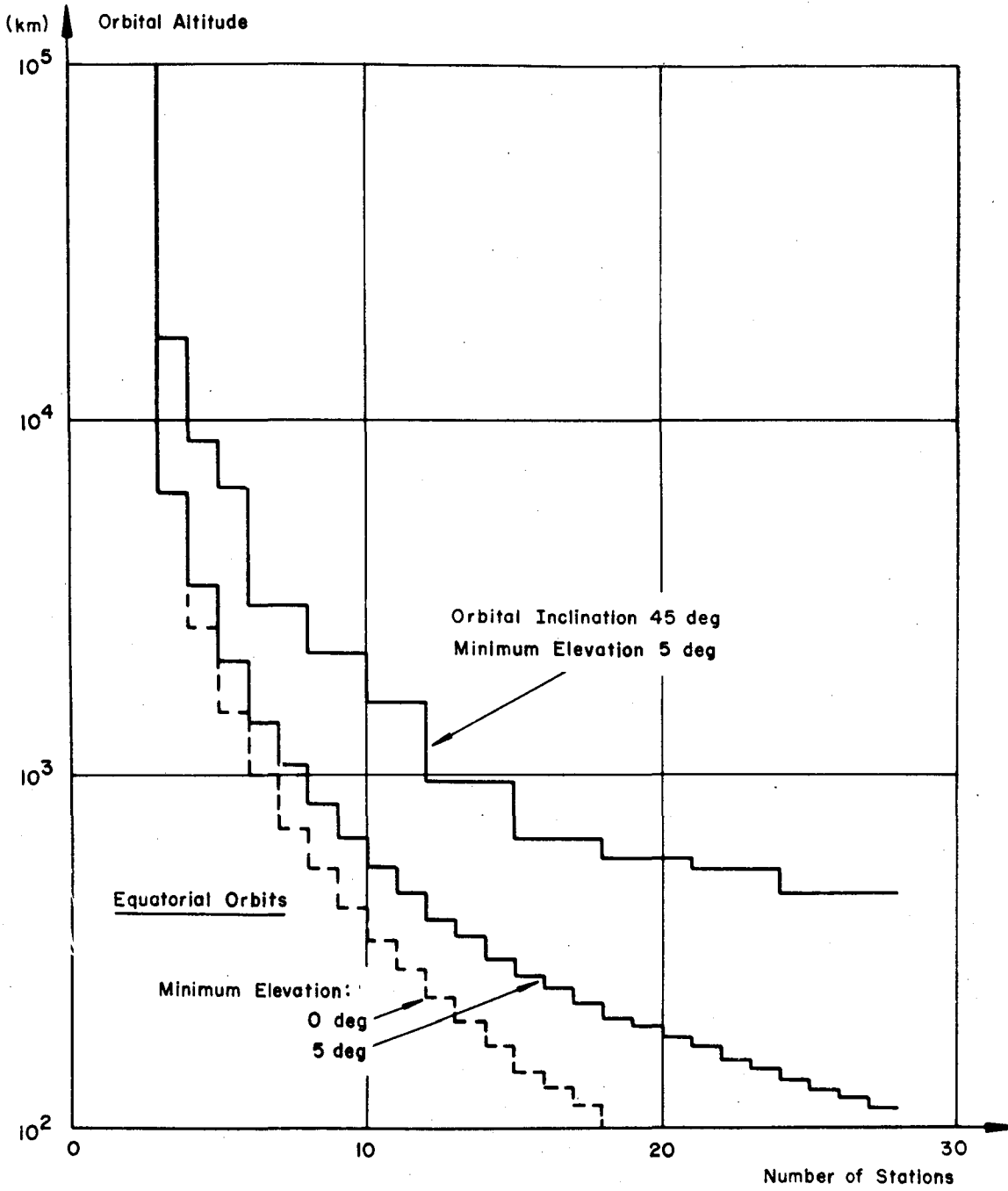


Fig. 26.3 Stations required for continuous tracking.

transmitter which is in sight of the space vehicle.

The left portion of Fig. 26.4 illustrates this situation for a lunar mission, which imposes heavy requirements on both space and global ground communications. Three ground tracking sites and associated command transmitters are considered. The control and computer center may be envisioned in the neighborhood of one of the tracking stations, reducing the number of long distance ground links to two.

A better solution of the communication problem suggested by the right portion of Fig. 26.4 utilizes a chain of communication satellites. In this approach all the unfavorable high-density ground links are avoided. The result is a significant increase in reliability. For limited distances, it may even be possible to replace the three command transmitters by one attached to the central computer and utilizing the communication satellites as command relay stations to the space vehicle.

In low-altitude orbits, the number of stations increases from 3 to 13 (Mercury net) or more, and the communication problem becomes even more serious. Again, three Earth-synchronous communication satellites or their equivalent would be the answer for a ground station network.

The ultimate simplicity in communication will be achieved by a closed loop, on-board system which is feasible in large, manned space vehicles. Both tracking instrumentation and the computer are located on-board; space and ground communications other than for monitoring are not required.

The comparison of communication requirements is also considered the key to the reliability comparison. The inherent design reliability of a global operational control network with its many independent links cannot approach that of an optimized on-board system of large, manned space vehicles.

Such a system would include only three major components: (1) electronic and optic tracking instruments, (2) electronic computer, and (3) vehicle navigation control system. The tracking data would flow continuously into the computer where the decisive mission parameters would be computed and displayed to the pilot. At predetermined time intervals, or when certain error thresholds are exceeded, the automatic navigation control system or the pilot, or both, can initiate a corrective maneuver.

This operational advantage of on-board instrumentation for manned space vehicles may be questioned for unmanned vehicles. The complex on-board tracking instrumentation will often require simple mechanical adjustments or maintenance, and its functioning will depend on vehicle attitude and internal environment. Human-control override should be required as in manned flights and can be exerted only from the ground. Therefore, a clear advantage for on-board tracking cannot be seen here. As long as tracking quality from the ground is sufficient, it appears to offer

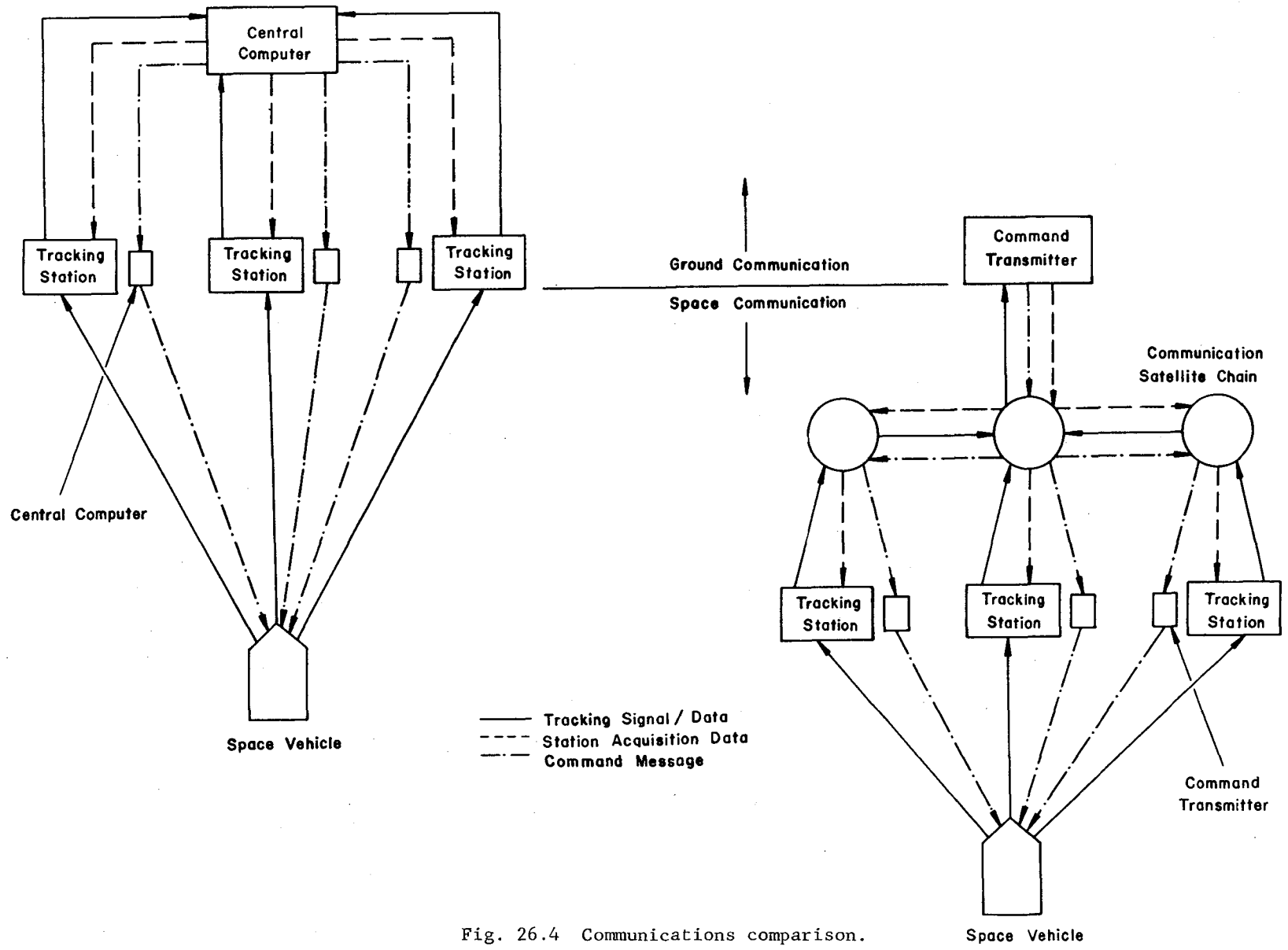


Fig. 26.4 Communications comparison.

the highest potential to do both the sensing and "thinking" for unmanned space probes in a ground control center and transmit to the vehicle only the brief coded messages of the necessary commands.

### 26.3.2 Accuracy Comparison

The relative accuracies of ground and on-board tracking are now developed with respect to three categories of missions: orbital, lunar, and escape. The attempt was made to investigate only those parameters which are most important with regard to the ground versus on-board comparison. Consequently, the completeness of the results had to be somewhat compromised. A truly complete analysis can be achieved only in very specific cases.

**Orbital Mission.** For the purpose of this paper, a 250-km-altitude circular orbit applicable for vehicle parking or rendezvous purposes was considered. The results should be somewhat characteristic of the large class of low-altitude (200 to 1000 km) and low-eccentricity ( $e < 0.1$ ) orbits.

The orbital inclination was considered to affect only the number of ground stations available. It was assumed for the present study that each orbital revolution was tracked by three stations measuring azimuth, elevation, and range (see Table 26.1 for characteristics). The stations were uniformly distributed around the orbit; each station had a maximum elevation angle of 60 deg, corresponding to a total tracking time per station pass of 5.5 min. The data sampling rate was 3600/hr. The mission parameter chosen for the orbital mission was the semimajor axis of the 95 per cent spatial position error ellipsoid at a time 1.5 hr (one revolution) after the end of tracking.

This characteristic mission error for ground and on-board tracking of a 250-km circular orbit is shown as a function of tracking time in Fig. 26.5. The ground track curve shows three sharp steps, as each of the three assumed stations acquires and tracks. During times of no tracking, the mission error propagates with two components, one oscillatory with approximately the orbital period, the other a secular trend upward (actually a very long period error) due to the error in determination of the orbital period [3]. This error propagation is shown as a dashed line after tracking with one, two and three stations; it represents the deterioration of orbital knowledge with time.

Two types of on-board tracking are represented. One consists of direct measurements of the orbit through an altitude measurement (altimeter), measurement of the angle between the center of the Earth and a star perpendicular to the orbital plane, and measurement of the angle between the Earth's center and a star in the orbital plane. The other type is the relative measurement of the position of one satellite with respect to another. This case is encountered in orbital rendezvous, where a space station might

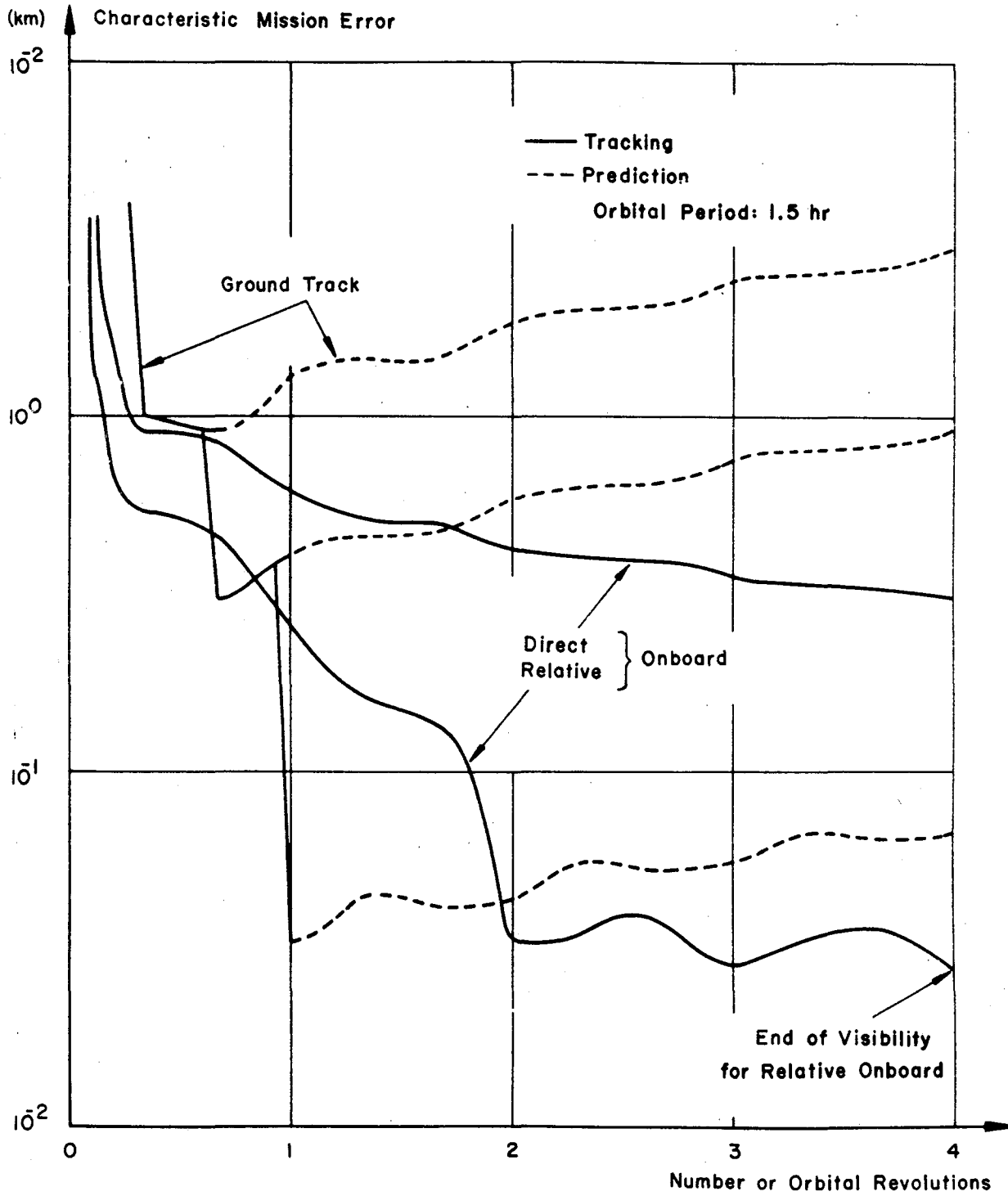


Fig. 26.5 Orbital tracking comparison.

track a ferry vehicle approaching it. It is assumed that the orbit of the reference satellite is high enough to avoid prediction uncertainties due to atmospheric drag, and is known with negligible error due to continuous updating of its ephemeris. The relative range and range rate between the known and unknown satellites are measured as well as the angle at the unknown satellite between the known satellite and a star perpendicular to the orbital plane. The latter measurement is necessary if the two orbits are nearly coplanar, as was the case in this study. The accuracies assumed are shown in Table 26.1. A sampling rate of 360/hr was used for the on-board data.

The known satellite was assumed to be in a 485-km circular orbit. Two coplanar satellites in 250-km and 485-km orbits will be visible to each other for periods of about 6 hr (4 revolutions) separated by periods of about 23 hr (15 revolutions) when the Earth is between the satellites. The relative tracking curve (lower solid line of Fig. 26.5), represents the accuracy attainable by tracking during an entire visibility period. During the nontracked period which follows (unless there is another known reference satellite) the mission error would propagate in the same fashion as for the ground track prediction curves.

It can be seen that the relative on-board measurements are increasingly better than the direct on-board measurements during the four revolutions shown. During following revolutions, however, the direct measurement error would continue to reduce as more data are accumulated. The error from relative tracking would increase during a nonvisible period.

Ground tracking requires three station passes to surpass clearly the direct on-board tracking and would require four passes to obtain a continuing advantage over relative on-board tracking.

Lunar Mission. Two types of lunar missions have been considered: a lunar landing and a circumlunar and Earth return. The trajectories are shown in Fig. 26.6.

The lunar landing (impact) trajectory has a 68-hr travel time corresponding to a velocity 50 m/sec below local escape at injection. The trajectory ends in near-perpendicular lunar impact when the Moon is near its minimum declination.

The characteristic mission parameter for lunar landing is the error in prediction of the impact position on the lunar surface in the absence of terminal maneuvers. The semimajor axis of the 95 per cent position error ellipse on the lunar surface was used.

The circumlunar and Earth-return trajectory is injected with a velocity 90 m/sec below local escape and approaches within 11,000 km (5.3 Moon radii) of the Moon after a travel time of 92 hr. The vehicle returns to Earth



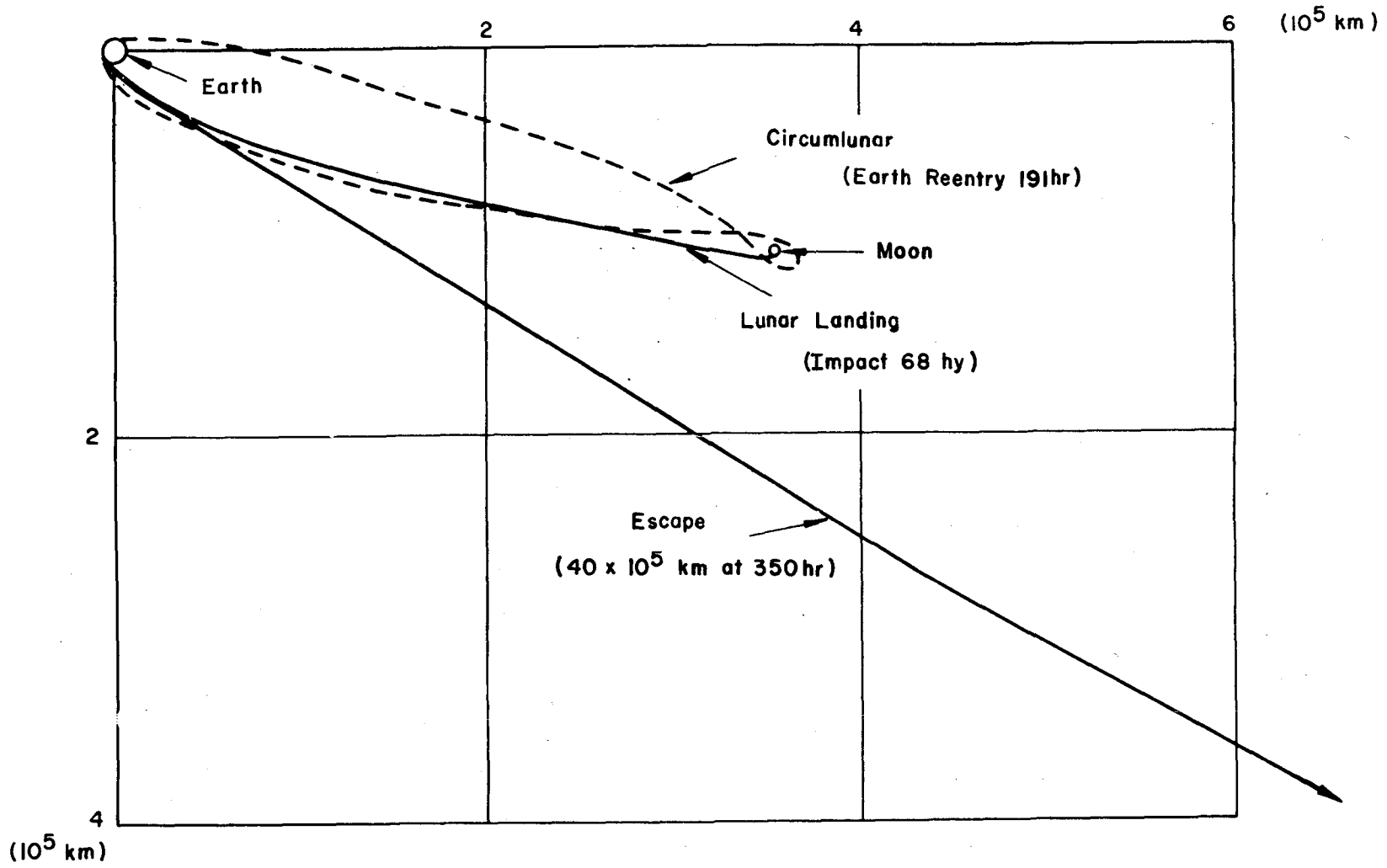


Fig. 26.6 Mission trajectories.

after 191 hr of travel time, and reenters the Earth's atmosphere within permissible limits for safe landing.

The circumlunar flight has been characterized by the error in prediction of the impact position on the Earth's surface, assuming a ballistic no-lift reentry. The semimajor axis of the 95 per cent position error ellipse on the Earth's surface was used.

The characteristic mission errors for the lunar impact and circumlunar missions are shown as a function of tracking time in Fig. 26.7. The on-board tracking assumed for both missions consists of measurements of the angles subtended at the vehicle between the Earth's center and the Moon's center, Earth center and the star Polaris, and Earth center and the Sun. The ground tracking is the measurement of range from the three DSIF stations. It has been reported previously that the addition of angle and range rate data does not alter substantially the results of range tracking only [4]. The data accuracies are shown in Table 26.1. A data sampling rate of 360/hr was used for both ground and on-board data.

The oscillatory nature of the ground track curves is a peculiar characteristic of the bias error in the velocity of light. The error due to the velocity of light strongly dominates the ground track results under the assumption of a measurement of the signal travel time to  $10^{-7}$  sec (15 m) and the present uncertainty in the velocity of light. If the light velocity uncertainty were reduced by a factor of 10, the ground track error curves would also be essentially reduced by a factor of 10.

Particularly striking in the mission error behavior is the sharp decrease leaving Earth and the sharp increase approaching it once more on the circumlunar mission. This effect means that a point is reached in the trajectory where accuracy may actually be decreased by the addition of more data. This is because a relatively high-accuracy level is reached at lunar approach. On the return leg very little significant additional knowledge is accumulated. The bias error with increasing total tracking time leaves more and more room for misinterpretation of the range observations. Even upon approaching the reentry altitude, the impact uncertainty would remain quite large in comparison to the range tracking error (15 m) because of error residuals in the velocity vector and because the orbit determination process tries to match all range observations, including those with large bias errors. A higher accuracy may be reached by throwing away the mass of data over the flight and using only the data after a certain time when the effect of the bias decreases, as illustrated by the circumlunar restart curve. The latter curve assumes that an orbital determination is begun without prior information about 2 hr before reentry.

In practice, the period of contaminating data would not be used. Consequently, during the portion of flight from 150 hr until reentry, the real

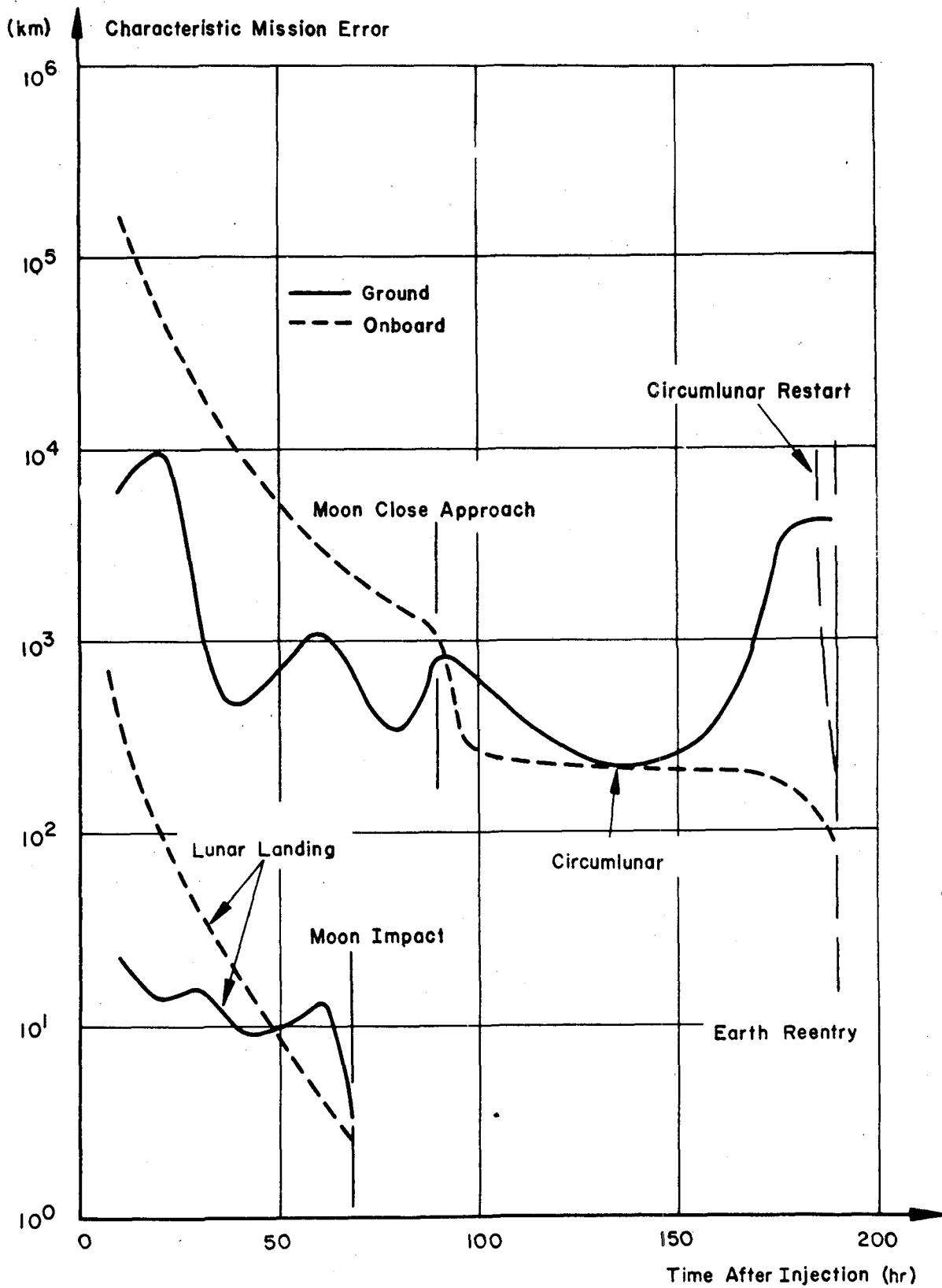


Fig. 26.7 Lunar tracking comparison.

ground track error curve would remain at a constant level, which is about equal to the on-board tracking error.

Escape Mission. The escape trajectories chosen have Earth inclinations near 14 deg and are designed with an approximate geometry with respect to the Sun for Venus probes. The velocity at injection was varied between 400 m/sec and 800 m/sec in excess of local escape. The trajectories were studied only to a travel time of 350 hr or distances of about 3.9 to  $5.5 \times 10^6$  km (10 times the Earth-Moon distance) from the Earth. The 400 m/sec excess trajectory is shown in Fig. 26.6.

The semimajor axis of the 95 per cent position error ellipsoid at a time 350 hr after injection was taken as the characteristic mission error. The velocity error ellipsoid at a corresponding time showed the same trend. This parameter would represent the accuracy of orbit determination at a time when a midcourse maneuver might be desired. The same ground and on-board tracking assumed for the lunar mission was also used for the escape mission.

With the present uncertainty in the velocity of light, on-board tracking surpasses ground tracking within 100 hr after injection (Fig. 26.8). Since the light velocity uncertainty is the dominant error factor in the ground tracking, any improvement in this uncertainty will reduce the ground-tracking error proportionally.

The effect of the energy of the trajectory on the tracking is also seen in Fig. 26.8. An increase from 400 m/sec in excess of local escape velocity to 800 m/sec causes an increase in the characteristic mission error from ground tracking by a factor of about 1.5. The same increase in energy causes a slight reduction in the error from on-board tracking before 100 hr but an increase in the error after 100 hr.

This behavior is explained by the combination of two effects. First, data obtained in the Earth-Moon dynamic region are of high geometric weight in the orbit determination. Since the 800 m/sec orbit leaves this dynamic region faster than the 400 m/sec orbit, the mission error for both ground and on-board tracking should tend to be larger for the 800 m/sec orbit. The second effect is the change in measuring accuracy with time and distance from the Earth. The range-measuring error increases with distance from the Earth (Fig. 26.1), which again tends to increase the mission error for ground tracking of the 800 m/sec orbit.

In the case of on-board tracking, the measuring error (Fig. 26.2) decreases with time and distance from Earth. This effect overcomes the first dynamic effect until 100 hr, resulting in a lower mission error for the 800 m/sec orbit. By 100 hr, however, the measuring error has reached its minimum, the dynamic effect dominates, and after 100 hr the mission error for on-board tracking is less for the 400 m/sec orbit.

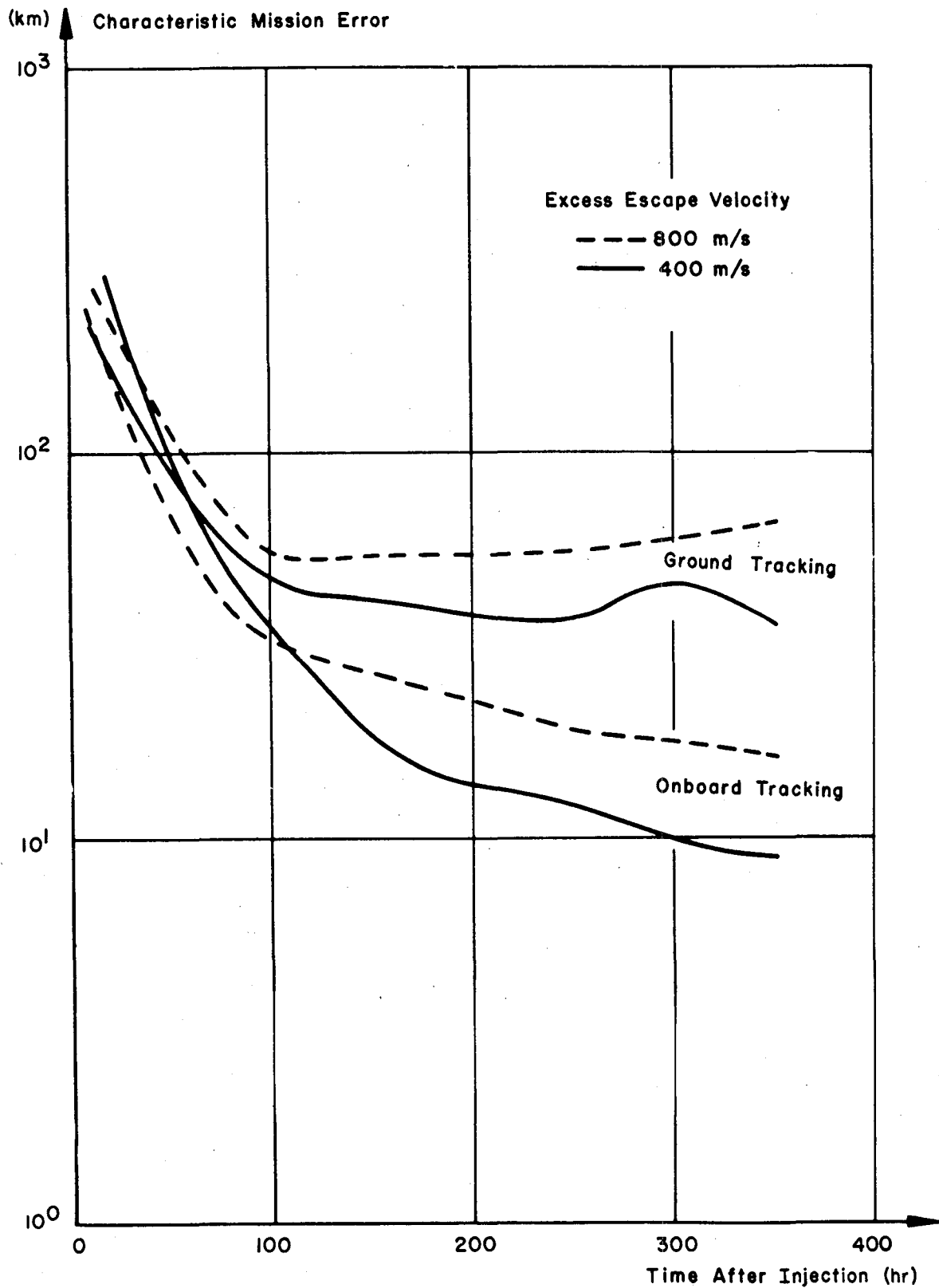


Fig. 26.8 Escape tracking comparison.

### 26.3.3 Comparison of Missions

The tracking-accuracy comparison between ground and on-board measurements is summarized in Fig. 26.9. Here the ratio of ground to on-board error is shown for the characteristic parameter of each mission. The abscissa is tracking time on a logarithmic scale. The order of magnitude difference between tracking times of the various missions should be noted. If the error ratio is less than 1, the error from ground tracking is less than the error from on-board, and ground is favored. If the ratio is greater than 1, on-board tracking is more accurate.

For the orbital mission, on-board (satellite-to-satellite tracking) has an advantage if the number of applicable ground stations is limited. As soon as a number of ground stations of the quality assumed can be used, (three in 1.5 hr) ground tracking becomes more accurate.

The lunar impact, circumlunar, and escape missions all show similar trends. Ground tracking has a strong early advantage in accuracy, but on-board tracking improves as flight time and distance from the ground stations increase. On-board accuracy surpasses or equals ground accuracy after 50 to 100 hr.

As noted before, the ground error and hence the ratio of errors for the lunar and escape missions in Fig. 26.9 are very sensitive to the uncertainty in the velocity of light. An improvement in the present knowledge of the velocity of light will shift the lunar and escape error ratio curves downward proportionally.

The question with regard to the velocity of light bias error is: If it is so important why not solve for it as another parameter in the orbit determination process? This is the logical way to improve our knowledge of such parameters. There are, however, many parameters which must be considered. Great practical problems are encountered in solving for all of these parameters fast enough for navigation purposes and with the data from only one mission. The uncertainty in the velocity of light is still a disadvantage for ground tracking.

In a similar fashion, improvements of the optical on-board system will shift the ratios upward. Such improvements may be anticipated, especially near the Earth and Moon, by referring to pronounced landmarks of small diameter on the surface. It is conceivable that angular accuracies in the order of seconds may be achieved, thus essentially flattening out the error curve of Fig. 26.2 to a nearly constant level of some  $10^{-3}$  deg.

The most convenient parameter with which to display the effects of tracking improvements is probably the time of equal accuracy (ratio one) in Fig. 26.9. Except for orbital missions (where the velocity of light

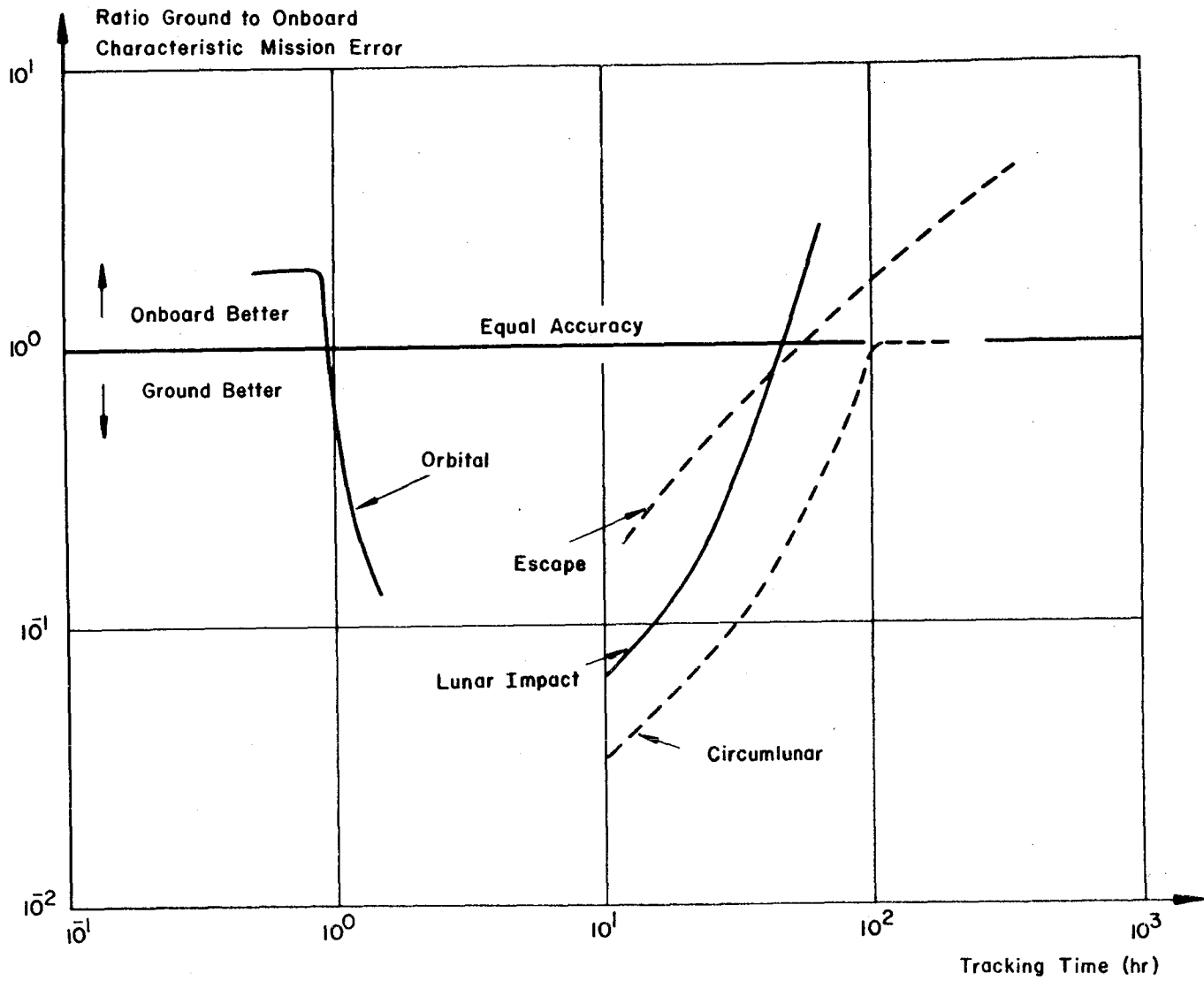


Fig. 26.9 Comparison of mission tracking.

is not the determining accuracy factor), increased on-board accuracy shifts the equal-accuracy-point to earlier times, while improved ground tracking (by reducing the uncertainty in the velocity of light) shifts that point to later times.

The effect of potential tracking improvements on the on-board vs ground equilibrium is shown in Fig. 26.10. The curves represent contours of equal accuracy for on-board and ground tracking. Several equal-accuracy times are shown as the contour parameter. The absolute uncertainty in the velocity of light (present value 800 m/sec is varied on the abscissa while the ordinate represents the initial angular error between celestial bodies, leaving the long distance value of  $10^{-3}$  (Fig. 26.2) unchanged.

According to Fig. 26.10, the 50-hr equal-accuracy-point for an escape mission exhibits the following equivalence: an improvement of the angular accuracy by two orders of magnitude corresponds to a reduction in the uncertainty of the velocity of light from 800 m/sec to 140 m/sec, less than one order of magnitude. Therefore, speaking in relative terms, for escape missions improvement in ground tracking appears to be more powerful than that of on-board.

Also shown in Fig. 26.10 is the case of the circumlunar mission (the lunar impact mission behaves in a similar fashion). Here, on-board and ground improvements yield approximately the same percentage accuracy increase. Improving on-board tracking by a factor of 10 will shift the equal-accuracy-point back to a time prior to closest approach. However, our knowledge of the velocity of light will increase as more lunar space probes are being tested. Therefore, it is felt that both on-board and ground tracking systems will stay as fully competitive partners.

#### 26.4 Conclusions

In an operational comparison of ground versus on-board tracking and orbit determination, it is shown that for large manned vehicles on-board instrumentation has several advantages. These advantages are primarily the great reduction of the communication problem between vehicle and ground computer, the lack of distance limitation for optical instrumentation, and the fact that only one tracking station (on-board) is required.

Comparing the tracking errors in terms of appropriate mission errors, it is found that in orbital missions on-board tracking has an advantage if the number of ground stations is limited. As soon as this number can be increased beyond four per orbit, ground tracking becomes superior.

The lunar impact, circumlunar, and escape missions all show similar trends. Ground tracking has a strong early advantage, but on-board tracking improves as flight time and distance increase. At the present state of the art, on-board accuracy surpasses or equals ground accuracy after 50



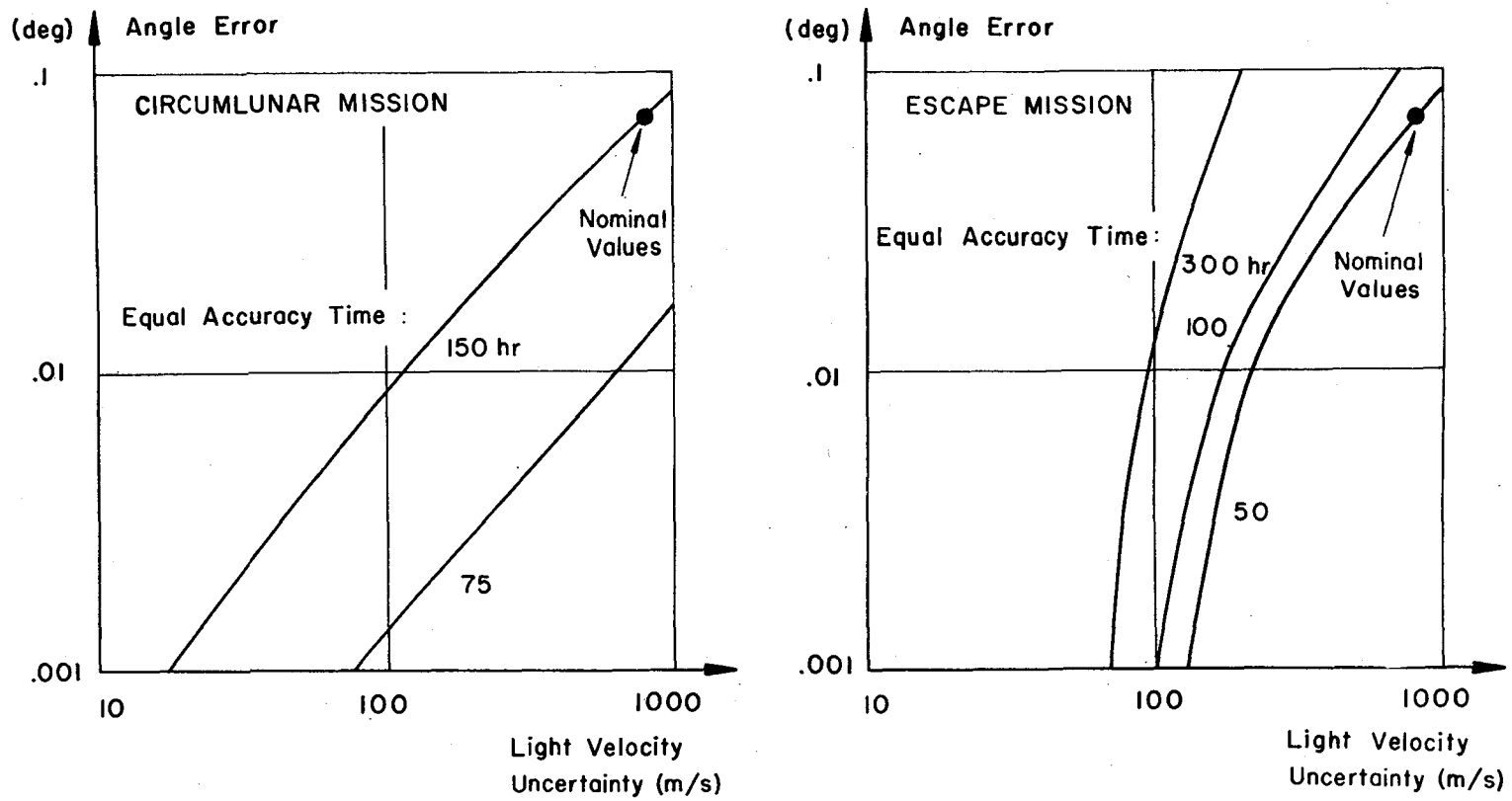


Fig. 26.10 Potential of improved range tracking.

to 100 hr tracking time.

The equal accuracy point depends essentially on both the uncertainty of the velocity of light and the initial on-board angle accuracy. The improvement of the on-board accuracy for escape missions by a factor of 100 is equivalent to a ground improvement factor of 7 and would seem to favor ground system development. However, long duration escape missions eventually will favor on-board tracking since the bias error in ground tracking increases with the distance from Earth, and operational difficulties exceed any slight advantage in accuracy.

In lunar missions there is no clear advantage for either one of the two potential system improvements. Most likely, on-board and ground tracking will remain fully competitive.

#### REFERENCE

1. Hall, J. R., System Capabilities and Development Schedule of the the Deep Space Instrumentation Facility, Jet Propulsion Laboratory Report October 1960. Jet Propulsion Laboratory, Pasadena, California.
2. Zurmuehl, R., "Praktische Mathematik für Ingenieure and Physiker," Springer-Verlag, Berlin, 1953.
3. Speer, F.A. and H. F. Kurtz, Tracking and Orbit Determination for Orbital Operations, MTP-AERO-61-86, October 25, 1961. George C. Marshall Space Flight Center, NASA, Huntsville, Alabama.
4. Kurtz, H. F. and F. A. Speer, Tracking Accuracies for Lunar Missions, MTP-AERO-61-3, January 18, 1961. George C. Marshall Space Flight Center, NASA, Huntsville, Alabama

## 27

## PILOT MANUFACTURING FOR SPACECRAFT

Wilhelm Angele

Astrionics Division  
George C. Marshall Space Flight Center  
National Aeronautics and Space Administration  
Huntsville, Alabama

## 27.1 Materials and Application Problems

The success of any electronic or mechanical device has always depended, in the final analysis, on finding the right material for the right job. In the missile and space industry, where electronics and mechanics must function together with a precision and complexity unimagined a few decades ago, the choice of materials is often uniquely challenging. Density, temperature expansion, heat conductivity, tensile strength, hardness, inertial damping, electrical qualities -- all of these are among the considerations which keep design specialists dissatisfied with present resources, and always on the lookout for unusual materials and for better combinations of existing materials.

The choice of a material is as demanding as the function that it is expected to perform. The task, for example, may be to assure uniform heat expansion of the components in spite of different temperatures -- as in the case of a sensitive gimbal-mounted gyro, where the inside is warmer than the outside. The design may call for equal temperature coefficients of a metal and an insulator, to be fused together as in the case of a high-speed gas bearing in which a special glass is combined with Kovar, a low-expansion alloy of iron, nickel, and cobalt. The flywheel of a gyro motor needs to be heavy; a machinable tungsten alloy, Mallory 1000, will serve the purpose. For low-heat conductivity and very high electrical insulation, beryllium oxide has been used. When stiffness, form stability, corrosion resistance, and light weight are important, electrically oxidized pure beryllium is appropriate. Air bearings of extremely high quality, with tolerances measured in  $\mu$ , are being made of fused quartz.

The severe environmental conditions under which spacecraft operate impose a difficult problem on plastics and adhesives. Years of storage, high humidity, low and high temperatures, vibration, vacuum, and cosmic radiation are some parameters which control the proper selection of plastics.

Preceding page blank

Thermoplastic or thermosetting plastics used for structural elements, electrical insulation, potting, ruggedizing, and conformative coatings form a never-ending line of newcomers. Even so, a plastic which can withstand radiation to a large degree is still missing.

Never before in history has the designer had such an enormous array of materials at his command, and never before have work shop personnel had such a multitude of machining, forming, molding, joining, and finishing problems as in today's missile age. Table 27.1 shows data of some unusual materials and, for comparison, data for a few common metals.

## 27.2 Tools and Equipment

The choice of material for a design often demands a special cutting tool. For high-tensile steels and fast stock removal, ceramic cutting tools are used. For cutting beryllium, carefully ground and lapped carbology bits are used. In special cases, for giving microfinishes without lapping nonferrous metals, cut and finished diamonds are necessary.

The use of diamond cutting tools makes special demands on the concepts of precision and tolerances. The cutting edge of the diamond must have no defects detectable by a 1000-power microscope; such a cutting edge is very sensitive to sudden pressure changes, shock, or vibrations in the machine tool. Temperature-controlled, tapered journal bearings are usually applied. The bearing clearance is adjustable to produce a wide gap for starting purposes. As the engine approaches speed and operating temperature, the gap is closed to the minimum workable dimension. This minimum is necessary to assure a stiff bearing film and a smooth function. The one serious danger is that bearing elasticity causes chatter and cutting tool breakage. Even so, the art of using diamond cutting tools has proven its reliability on materials such as magnesium, copper, brass, and, more recently, beryllium.

Special precautions must be taken in the machining of beryllium, as it is highly toxic. Certain people are allergic to it and may develop beryllium dermatitis. More serious is beryllium pneumonia, which takes a long time to cure. The most serious consequence is berylliosis, a lung disease similar to silicosis. Berylliosis causes a reduction of lung capacity and is at this time incurable. A precaution for nonallergic workers is an air suction system which removes beryllium chips and beryllium dust as quickly as formed. The workers are required to change all clothes daily and to take a complete shower at the end of their work day. Workers are given periodic medical examinations; their weights are taken biweekly. In spite of handling and machining difficulties, the advantages of beryllium to the space effort outweigh the disadvantages. The beryllium machine shop at the George C. Marshall Space Flight Center (MSFC) started operating May 1, 1958, and has operated with no ill effects to the present time.

Table 27.1 Selected Characteristics of Available Materials and Metals

	Dens. g/cm <sup>3</sup>	Tensile kg/cm <sup>2</sup> x 10 <sup>3</sup>	Mod. E kg/cm <sup>2</sup> x 10 <sup>5</sup>	Expan C. °C x 10 <sup>-6</sup>	Therm. C cal sec cm <sup>2</sup> sec	Melt T. °C	Electr. Res. μ Ω cm
Aluminum pure	2.7	0.8	7.0	23.8	0.50	660	2.7
Aluminum 7075-T6	2.8	5.7	7.3	23.6	0.29	600	5.7
Alnico V	7.3	0.4		11.3			47.0
Beryllium	1.85	2.5-5.5	31.0	11.6	0.35	1278	4.0
Be Oxide	3.0	1.3	31.5	5.5	0.19	2550	7 x 10 <sup>15</sup>
Copper el.	8.9	4.2	12.5	16.8	0.91	1083	1.69
Epoxy	1.2	0.6	0.3	5.0	0.0004		10 <sup>18</sup>
Glass Corning 7052	2.28	0.7	6.5	4.6	0.0023	820	10 <sup>23</sup>
Gold	19.3	1.4	8.1	14.3	0.70	1063	2.4
Invar	8.0	4.6	15.0	0.9	0.026	1425	81.0
Iron	7.8	2.9	20.0	12.1	0.16	1530	10.0
Kovar	8.36	5.5		5.0	0.40	1450	49.0
Lava Gr. A	2.3	0.2		3.3	0.003	1600	10 <sup>20</sup>

Table 27.1 (continued) Selected Characteristics of Available Materials and Metals

	Dens. g/cm <sup>3</sup>	Tensile kg/cm <sup>2</sup> x 10 <sup>3</sup>	Mod. E kg/cm <sup>2</sup> x 10 <sup>5</sup>	Expan C. °C x 10 <sup>-6</sup>	Therm. C. cal sec cm <sup>2</sup> sec	Metl T. °C	Electr. Res μ Ω cm
Magnesium	1.74	2.1	4.0	26.0	0.38	651	4.6
Mallory 1000	17.0	7.9	28.0	5.4	0.22		12.0
Monel	8.9	11.0	18.0	14.0	0.06	1300	42.0
Mylar	1.39	1.5	0.4	27.0	0.0004	250	10 <sup>25</sup>
Nickel	8.9	8.5	2.1	12.9	0.14	1455	6.8
Porcelain	2.3	0.2	7.0	4.1	0.0025	1550	3 x 10 <sup>20</sup>
Quartz fus.	2.2	0.5	5.0	0.6	0.003	1470	5 x 10 <sup>24</sup>
Sapphire	3.9	5.0	35.0	5.0	0.007	2030	10 <sup>17</sup>
Silver	10.5	3.0	7.0	18.8	1.00	960	1.6
Steel 1095	7.8	10.2	21.0	11.1	0.11	1430	22.0
Teflon	2.2	0.2	0.1	100.0	0.0002		10 <sup>22</sup>
Titanium	4.5	4.1	12.0	8.4	0.89	1800	42.0
Tungsten	19.3	30.0	35.0	4.6	0.40	3410	5.6

Machining of materials harder than Rockwell C60, or very brittle materials such as porcelain, glass, quartz, or bonded metal powder (magnet cores), is done efficiently by the ultrasonic method. For example, machining a 1-cm-square hole in a block of glass is accomplished easily by a soft steel or brass bar 1 cm square. This tool is firmly attached to one end of a stake of nickel lamination. A coil around the nickel stake excited with ultrasonic frequency causes the nickel to contract and extend (magnetostrictive principle). The frequency must be adjusted to the mass of the exponential tool holder and tool for resonance to gain the largest amplitudes and effectiveness. The face of the tool is brought into proximity with the glass block, which has a small gap where the hole is to be cut. Boron carbide and water are pumped into the gap. The boron particles are accelerated by the face of the tool and bounced back and forth between tool and glass. The cutting is a process of fatigue and erosion. A ferrite stator and rotor of an incremental encoder have been made by ultrasonic machining. The rotor has a 1-in diameter and 150 teeth. Attempts to mill and grind have failed due to the brittleness of the materials. Also, the ultrasonic cutting time is a small fraction of any other tooth-by-tooth machining method because, ultrasonically, all teeth were cut simultaneously by one form tool. In this specific case of cutting brittle powdered metal, the form tool will last for many cuttings.

While the ultrasonic method is restricted to hard or brittle materials, a tough metal such as Alnico cannot be cut in this way with acceptable speed. The electric erosion process, applicable only to electrical conductors, is one acceptable method. The principle of this process is the disintegration of metals by electric sparks. Several machine-tool builders here and abroad manufacture this high-precision equipment in varying sizes. Tolerances of 0.0002 in. and surface finishes of 20  $\mu$  in. are obtainable. This electric erosion principle is also used for grinding carboloy tools. It allows stock removal without stressing the base metal and produces materially sound cutting edges.

Considerable progress has been made in the art of drilling a large number of holes with accuracy. Drilling printed circuit boards is a problem of speed, accuracy, and versatility. The ordinary shop procedure of using a sensitive drill press and adjusting the workpiece to the drill by hand is not only fatiguing but not accurate enough. Tape-controlled or numerically-controlled machine tools are expensive, and the programming for such machines is too time-consuming for small numbers of boards. Full-size drill jigs, made in a jig borer, are costly for small quantities. Economical multiple-size templates to be used in pantograph-type machines are customary and helpful when contour milling is needed.

Drilling with optical magnification for hole placement is a new way to get accuracy and speed with no tool cost for templates. Figure 27.1 shows the principle, using surface projection with 10 or 20 times

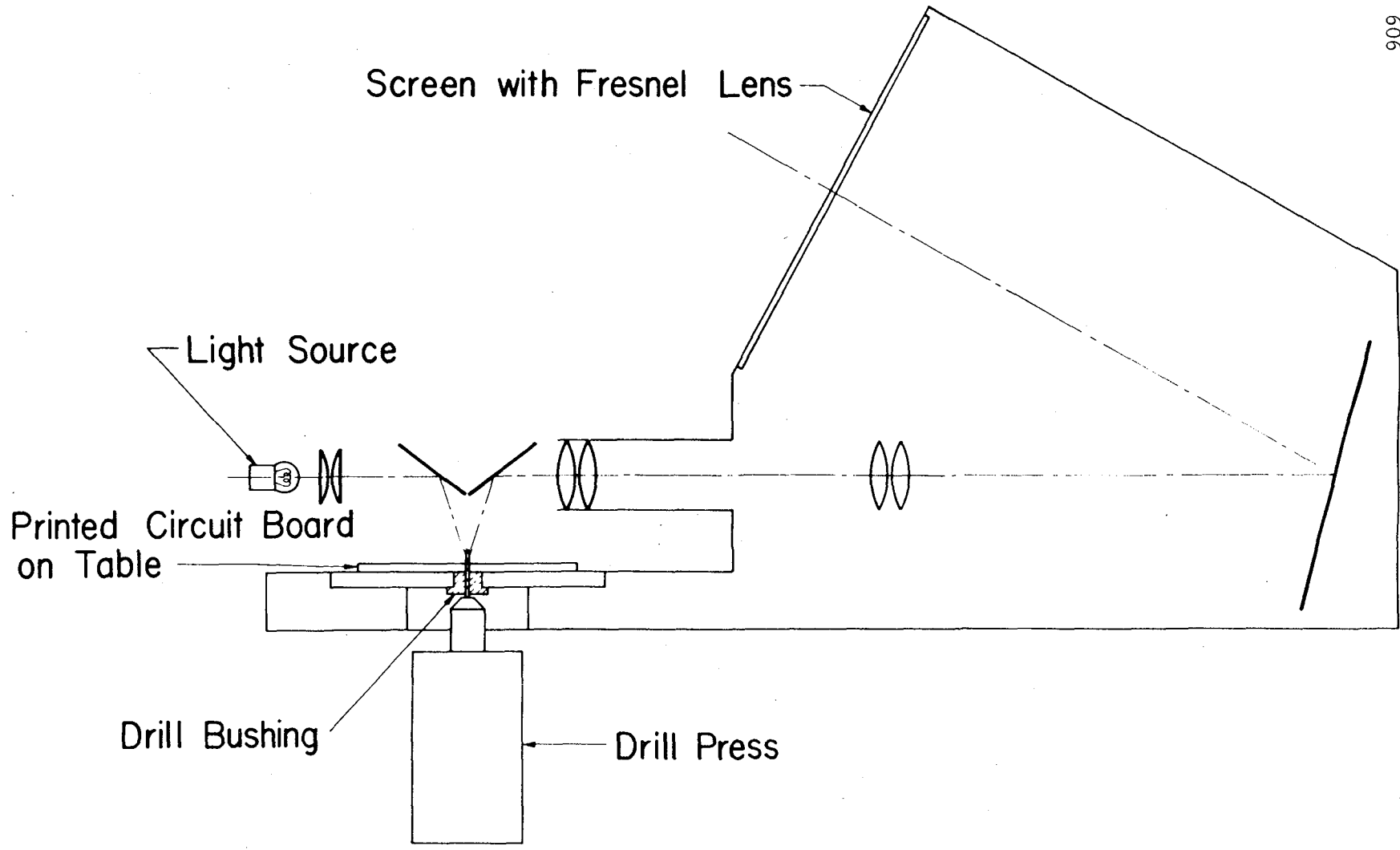


Fig. 27.1 Printed circuit drill with optical magnification.



enlargement of the eyelet to be drilled. The area of the hole to be drilled by a high-speed drill spindle from underneath is brightly illuminated by a light source, a condenser, and a mirror. An objective picks up the central beam over a second mirror and projects the image over an erection optic to the screen. Efficiency of the optical system is very high since the center of the light beam is reflected by the printed circuit board into the center of the projection optic. A Fresnel lens behind the frosted glass screen improves the brightness of the image so the system can be used in daylight with little shielding. Holes are located easily within  $\pm 0.001$ -in. accuracy. Thirty to 60 holes per minute can be drilled by an experienced operator.

In some cases, the time saved does not justify the expense of automation. However, there are times when quality and accuracy are overriding factors and automation is the best solution even for a single-run item. For example, an incremental encoder of an integrating accelerometer output required electric windings of repetitive patterns for its stator and rotor. The wire size of 0.001-in. diameter was too fine for manual handling and was especially tedious when used for the internal coils of the stators. An automated coil winder with tape control for the number of turns and change of coils to form the proper pattern was the answer to the problem. The coil winder and tape reader are shown in Figure 27.2. The new device made it possible to wind internal and external coils without stretching the wire and with good uniformity of the individual coils. With this new tape-controlled coil winder it takes 5 min. to wind an armature; by hand it took several days.

### 27.3 The Art of Measuring Mechanical Dimensions

Parallel to progress in machining and improvement of accuracy must go advancement in metrology, since we only know the quality of our product through exact measurement.

The accuracies attained by precision machine shops have been limited by the quality of machine tools and particularly by the lack of the proper measuring equipment. In addition, the training and experience required to deal with dimensions of the magnitude of light wavelengths was restricted to a few metrological laboratories. Today, well-equipped gage rooms have interferometers to measure gage blocks to 0.000001 in., and practical instruments capable of measuring 0.000010 in. are available for the tool rooms and precision shops. The latter meet the needs of the shop personnel, as the measurements are mostly relative; for example, concentricity and roundness. However, squareness and flatness are absolute. The easiest instrument of the group to apply is the electric pickup gage with 0.000010-in. accuracy, 0.001-in. range, and 1:10,000 magnification; in some cases 1:40,000 is used. The latest air gages reach magnifications of 1:100,000. This means 0.000001 in. is shown as large as 0.1 in. The range at such magnification is only 0.0001 in.

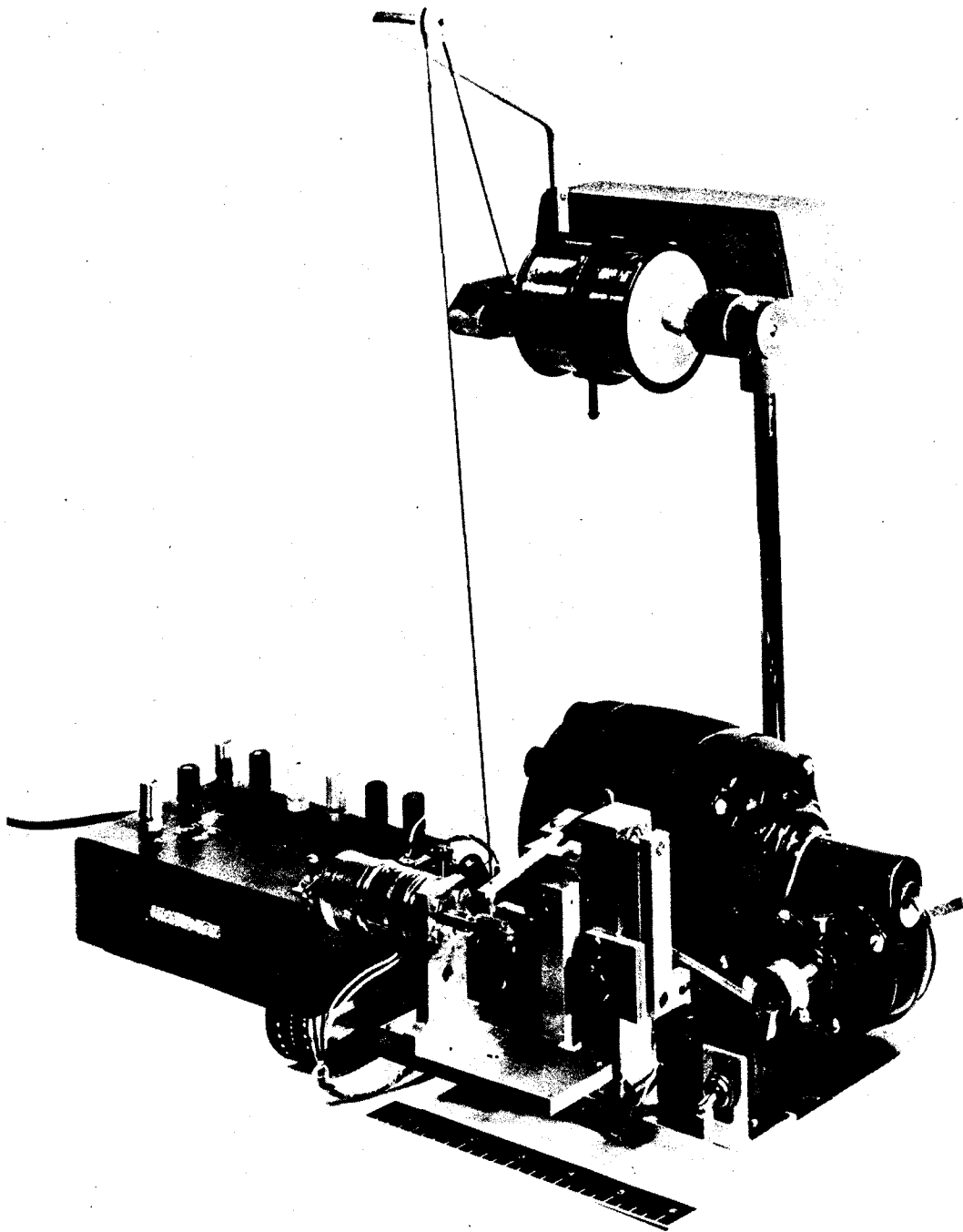


Fig. 27.2 Tape controlled coil winder

The principle of the air gage is based on volume measurement of airflow in a small gap formed by an air nozzle and the part to be measured. A flowmeter calibrated in hundred thousandths of an inch indicates the width of the gap and its variation. The flowmeter is a tapered glass tube with a small float. The air pressure and temperature of parts involved must remain constant. Air gages have had wide application, especially in the manufacturing of air bearings for gyroscopes where accuracy, close tolerances, and good surface finishes are mandatory. Figure 27.3 shows schematically how to measure the squareness of an air-bearing sleeve. The sleeve is air-centered and air-supported by spindle and base so that it can be rotated freely. The air gap between spindle and sleeve is less than 0.001 in., and the air pressure is set relatively high (up to about 50 psi) to achieve bearing film stiffness. A measuring orifice is placed close to the surface being measured.

When air-bearing support is not feasible, the part is placed on the turntable of an Indi-Ron, which has a very precise bearing guaranteed within  $3 \mu$  in. The part has to be centered and adjusted angularly coaxial on the table with an accuracy comparable to the accuracy expected from the measurement. Variations in radii (out of roundness) or squareness of faces or shoulders to the rotating axis, can be picked up simultaneously and in relation to each other with air gages or electric gages as shown in Figure 27.4. The readings can be recorded on polar coordinate paper.

Other precision measurements are performed by applying an autocollimator for small angular readings. Figure 27.5 illustrates the linearity check of a ball-and-disk integrator screw. A master screw is geared 1:1 with an idler to the test screw. Each screw carries a polygon mirror to assure equal angular motion of each screw between checkpoints. The autocollimator shows no deflection of the reflected crosshair image as long as two of the flats (one of each polygon) from a precise 90 deg. angle. Another mirror facing the autocollimator is mounted to the bridge over the two nuts which are guided by only one thread of each screw. A difference in pitch results in a slight tilt of the bridge. The crosshair image reflected by the bridge mirror will deviate from the polygon-reflected image. Assuming a screw distance of 4 in. and an autocollimator sensitivity of 0.2 sec of arc, a pitch error of  $2 \mu$  in. can be detected. For a fast check, the screws can be continually driven by motor since the polygons produce a stationary image when in synchronous rotation. No other fast and accurate check is known for a lead screw.

Here is another interesting optical check: the roller of a ball and disk integrator has to be checked for straightness (Fig. 27.6). An optical flat is laid on the roller and supported at the free end by a point. The mercury vapor light source produces an interference pattern at the contact line or points between the optical flat and the roller.

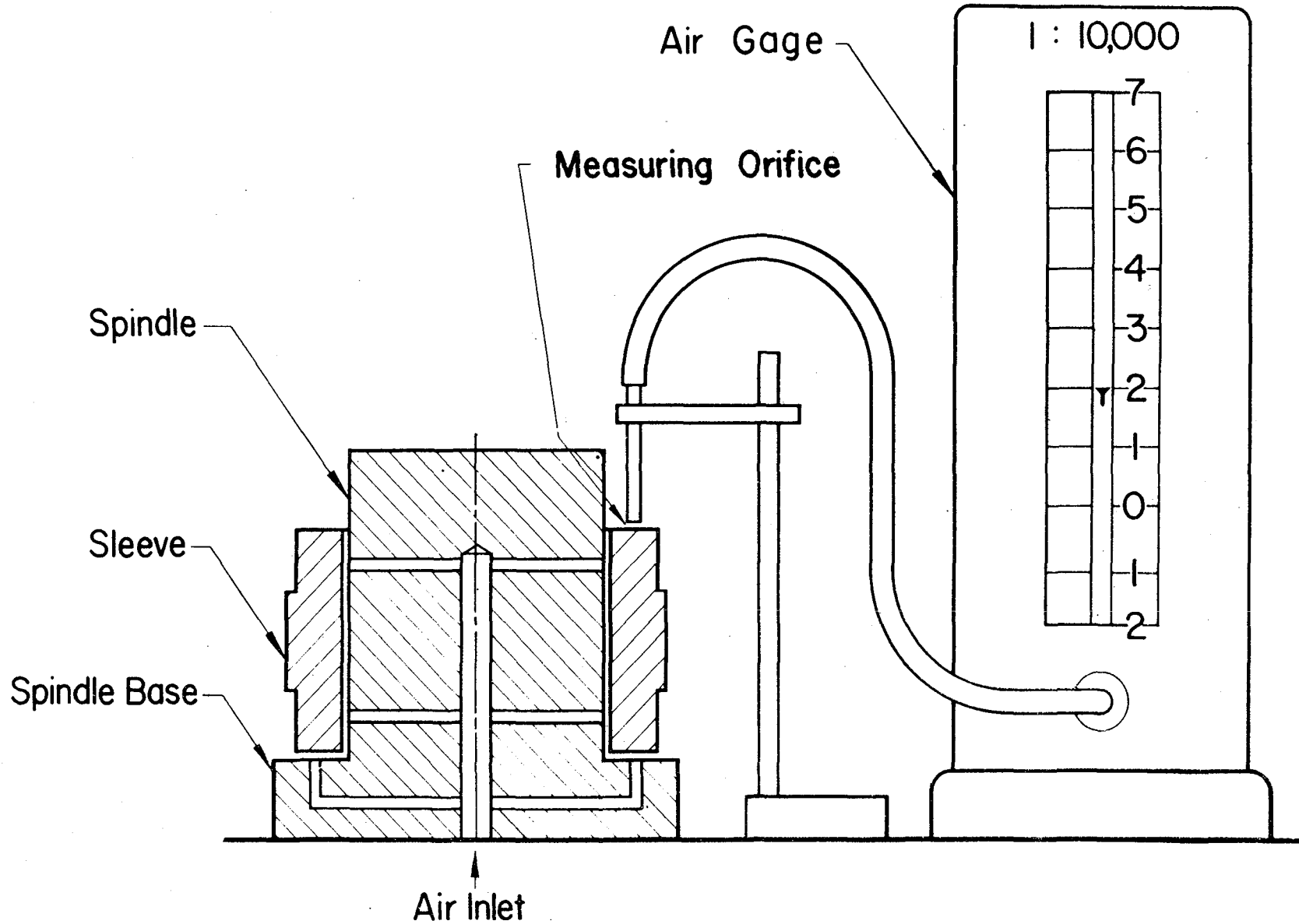


Fig. 27.3 Squareness measurement of air sleeve.

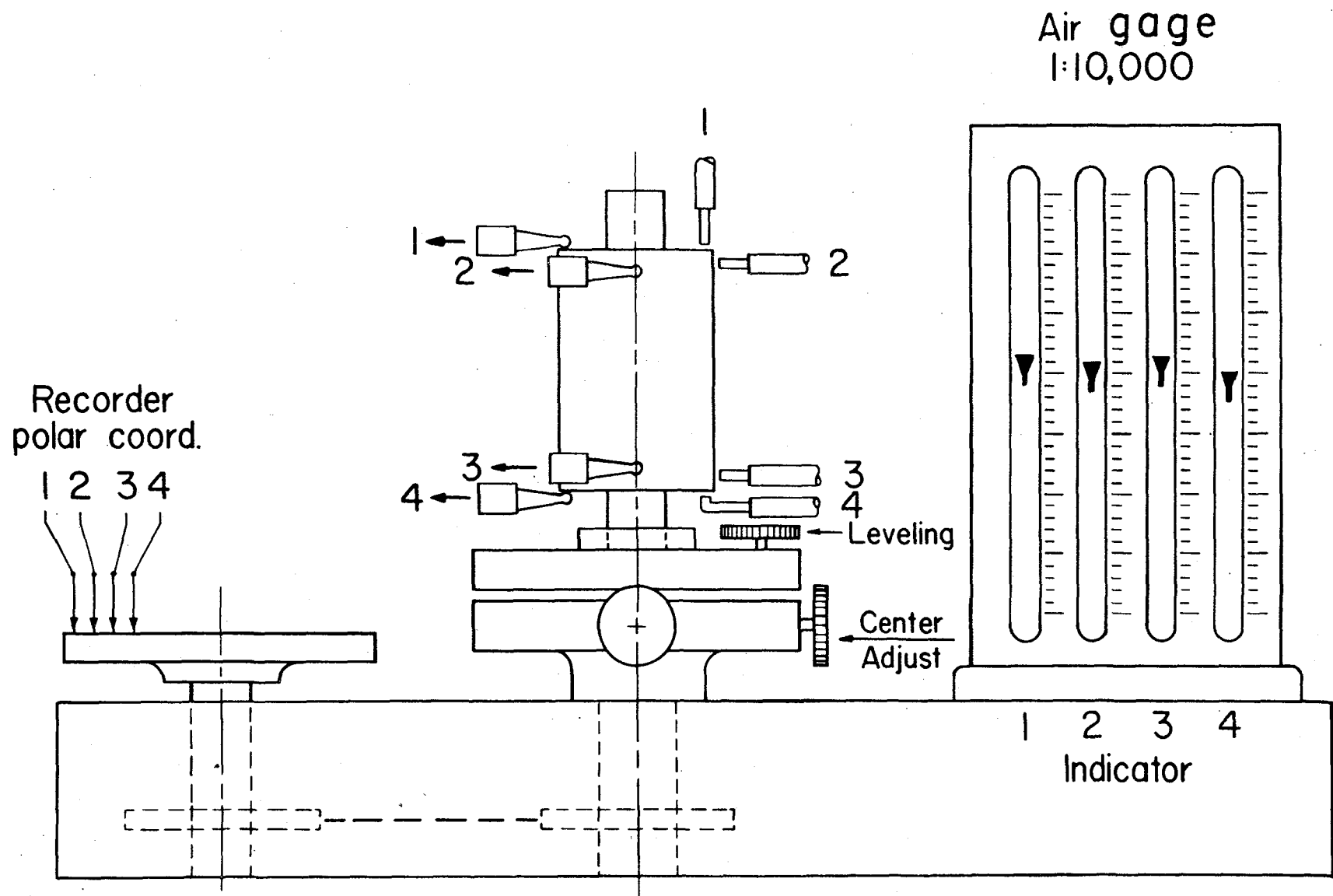


Fig. 27.4 Indi-Ron and recorder

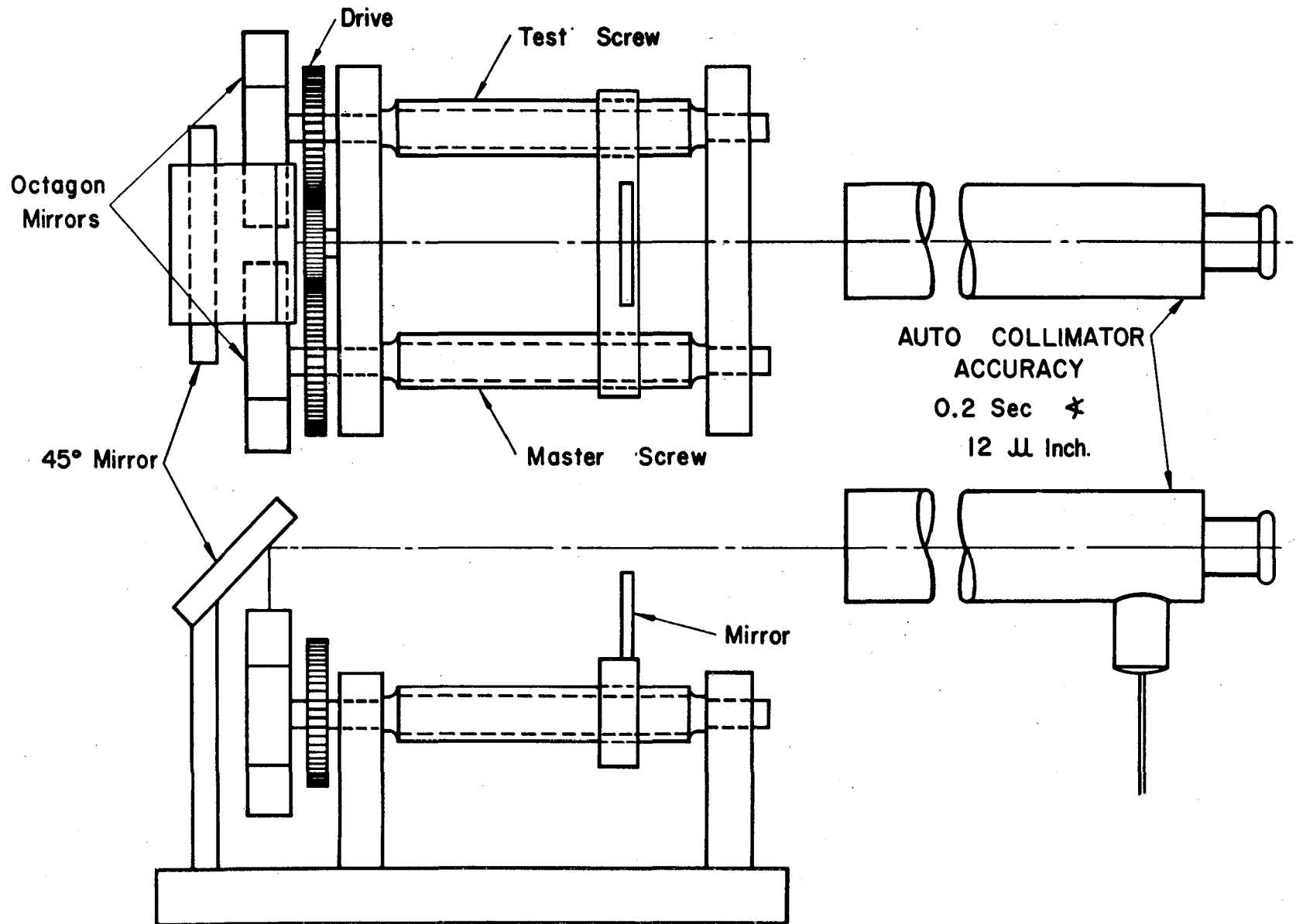


Fig. 27.5 Linearity check of integrator screw.

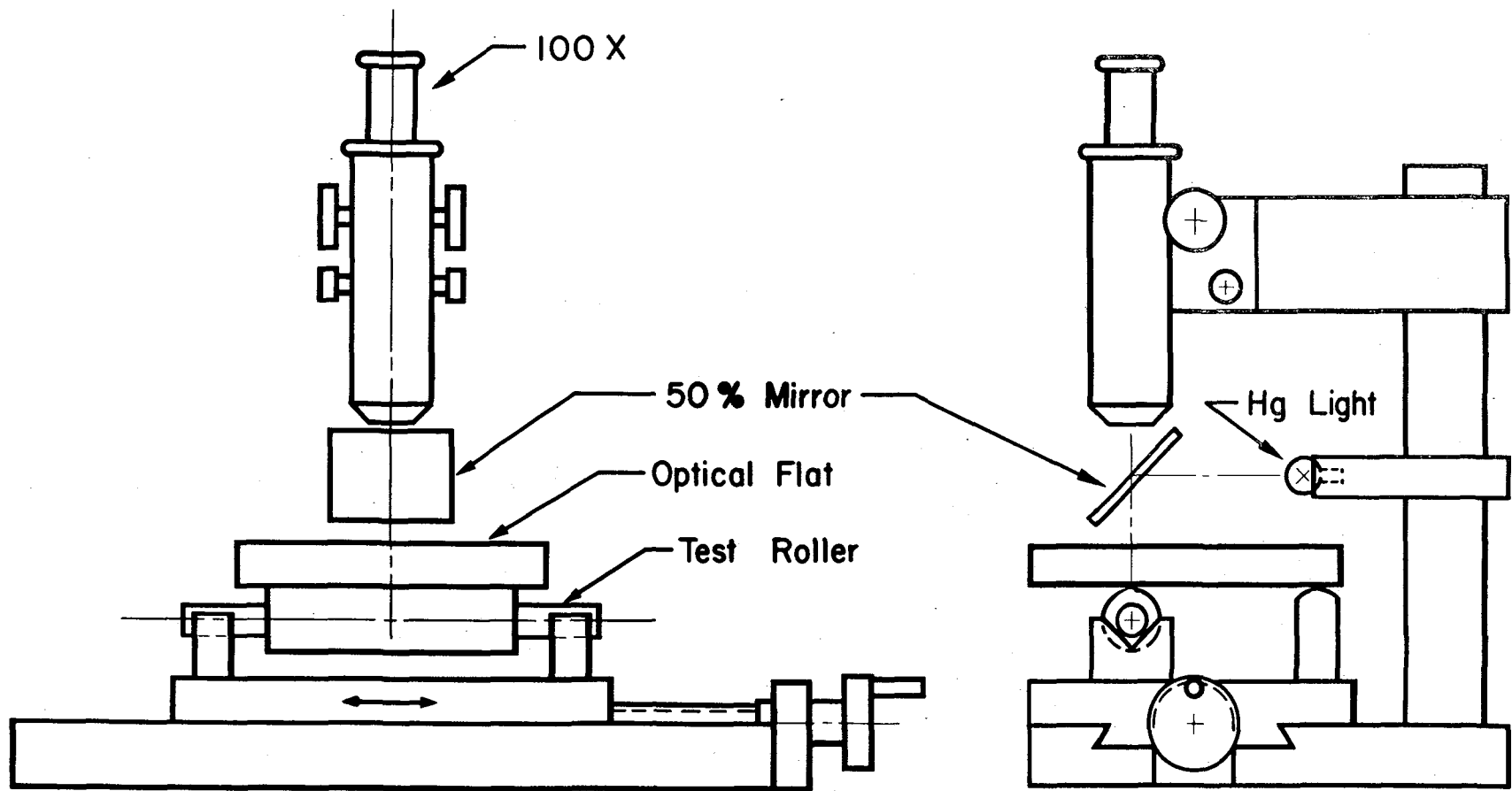


Fig. 27.6 Micro interferometric straightness test.

As the test roller is rotated, the interference pattern changes if the roller is not straight. The pattern can be seen only through a microscope because the cylindricality of the roller causes very narrow interference bands (microinterferometer).

#### 27.4 Frictionless Bearings

Universal machining and measuring abilities and material knowledge are prerequisites for the design and manufacture of frictionless, high-quality bearings. Considerable capability has been accumulated in this area since the beginning of air bearing design in 1944. Efforts have been devoted mostly to bearings for the precession axis of gyroscopes, where no friction is permitted and no torque allowed by the flow of the carrying gas or fluid. Such precision bearings should be dimensionally stable, and neither temperature nor time should influence their quality. Monel, titanium, aluminum, beryllium, and ceramics have been used to build bearings of required accuracy. Combinations of these materials are selected to match temperature expansions; better results are expected by the application of Pyrex or fused quartz. Small bearings could be made of sapphire. Pyrex, fused quartz, and sapphire have the outstanding properties of extremely low expansion due to temperature, form stability, and noncorrosiveness; above all, they can be machined to optical finishes and accuracies. Cleanliness is promoted by their transparency. Cleaning can be thorough, since no dirt is hidden in their surfaces as it is in the myriads of cavities of normal ceramics. Test pieces made of Pyrex glass and fused quartz show great promise.

The first quartz bearing designed and built by the Pilot Manufacturing Development Branch of the Astrionics Division of MSFC was dimensioned for a 5-cm gyro motor. Quartz shaft and bushings of 10-mm diameter and length were carefully finished to optical quality. The looseness at rest is less than  $50 \mu$  in. The coul friction torque with a simulated load of 250 g is 25 gcm; by applying increasing vibration, the friction is reduced to zero. The endurance test showed no signs of wear at the bearing surfaces after 5000 start-and-stop cycles of the rotor. The bearing needs no artificial lubrication; it uses the surrounding air and is self-lubricating. The shaft is in contact with the sleeve at rest. As soon as the rotating motion or vibration begins, air is wedged in between and the bearing is floating. This bearing has gas friction and needs no maintenance as long as the surrounding air is clean. For clean air, whiteroom specifications permit no particle larger than  $0.3 \mu$  or  $8 \mu$  in. The cleanness of the air has a direct influence on the lifetime of the bearing.

Gyro gimbal bearings represent a different concept and have different requirements. The air or gas is forced into the gap through pressure regulating nozzles. The airflow within the gap has to be very uniform and must not create torque. The airgap is larger (up to 0.001 in.)



than in spin axis bearings. The surface finishes need not be as good; a velvet finish of up to  $15 \mu$  in. is sufficient. Roundness and squareness of gas-lubricated gimbal bearings must have very close tolerances if low torque is expected. For reference, bearings with  $10 \mu$  in. of deviation from roundness and squareness had less than 10 d-cm torque. Also it is important that the air jets enter perpendicular to the gap and they are not disturbed by irregular edges or burrs. Adjustable compensation nozzles have been tried successfully.

Spherical bearings are somewhat easier to manufacture. There is no squareness problem. The method of optical lens finishing is quite old and established. Roundness, surface finish, air nozzle and jet perpendicularity requirements are the same. A spacecraft motion simulator based on a 10-in. spherical air bearing was built and now operates successfully. The roundness of the 10-in. steel ball was made to  $50 \mu$  in.

#### 27.5 Air Screw Accelerometer - Odometer

Many accelerometers measure vehicle acceleration during flight to determine its velocity and traversed distance. They apply different principles and fall into certain categories, such as the spring-mass type, the vibration-string type, and the integrating gyro type. Recent progress in the development of air bearings has made it possible to apply a completely new principle for an integrating accelerometer, the nut-screw configuration. A nut, when supported on a screw by a thin film of air, is practically without friction and can be used as an integrating accelerometer. A linear acceleration force acting parallel to the axis of the screw creates, due to the lead angle of the thread, a radial component force which causes angular acceleration of the nut. The angular acceleration is proportional to the linear acceleration, whereby the constant of proportionality is determined by the tangent of the lead angle, of the pitch diameter of the thread, and of the outer diameter of the nut. It is independent of the mass of the nut. The angular speed of the nut is also proportional to the velocity of the vehicle, and the total number of revolutions indicates the traversed distance. To prevent the nut from running off the screw, a servo system is employed, as shown in Fig. 27.7, so that the screw is rotated the same amount as the nut, thereby remaining stationary with respect to the nut.

Whether the nut floats on a driven screw (Fig. 27.8) or the screw floats within a driven nut, the basic principle is the same. The latter arrangement, as shown in Fig. 27.9, has the advantage that the screw can be provided with one thread only, so that the lead angle of the thread can be made extremely small for the measurement of very high velocities (escape velocity). A prototype of this accelerometer was designed and built by the Pilot Manufacturing Development Branch of the Astrionics Division of MSFC and worked very well. It has a measurement

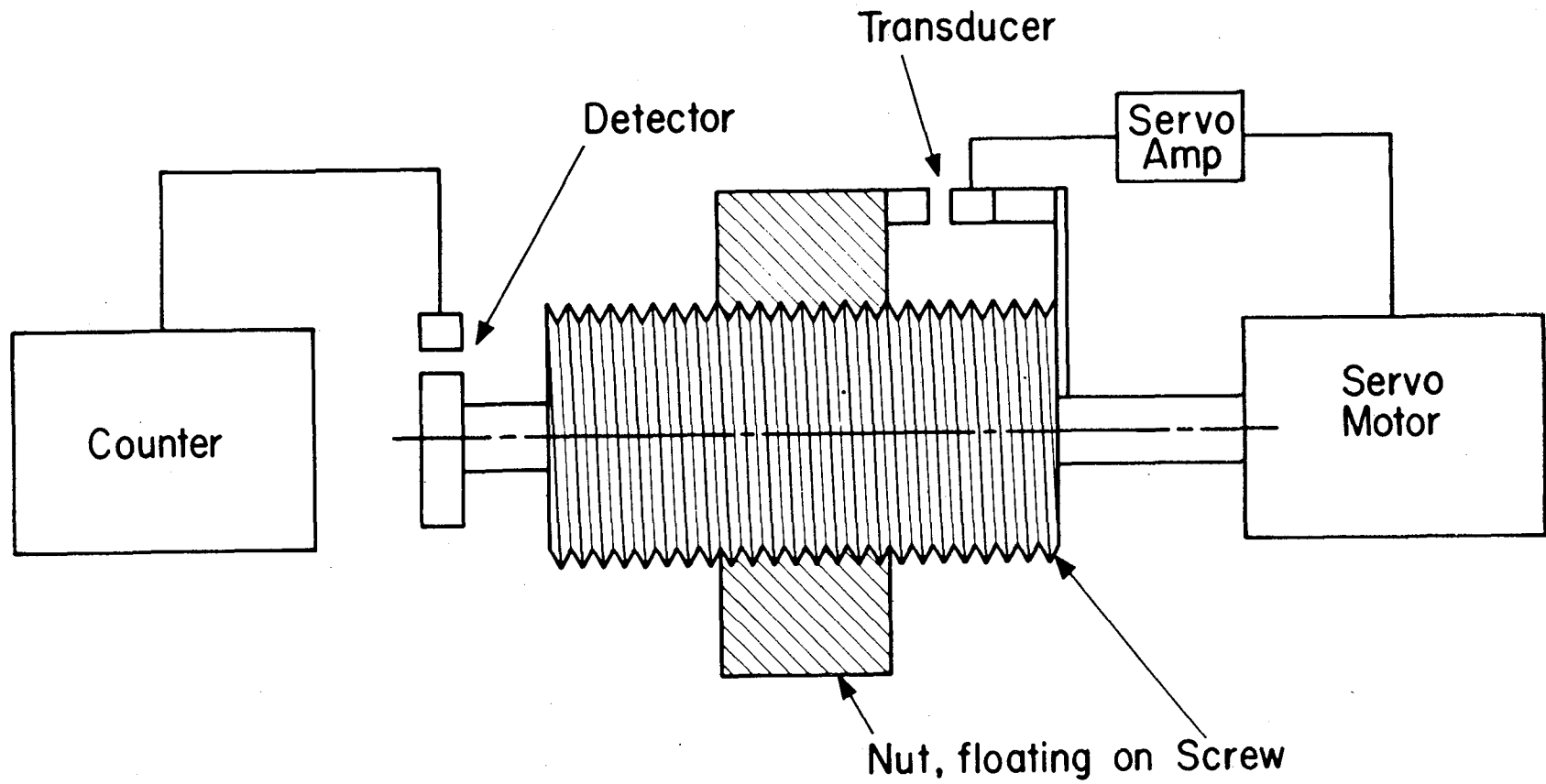


Fig. 27.7 Diagram of air screw accelerometer.

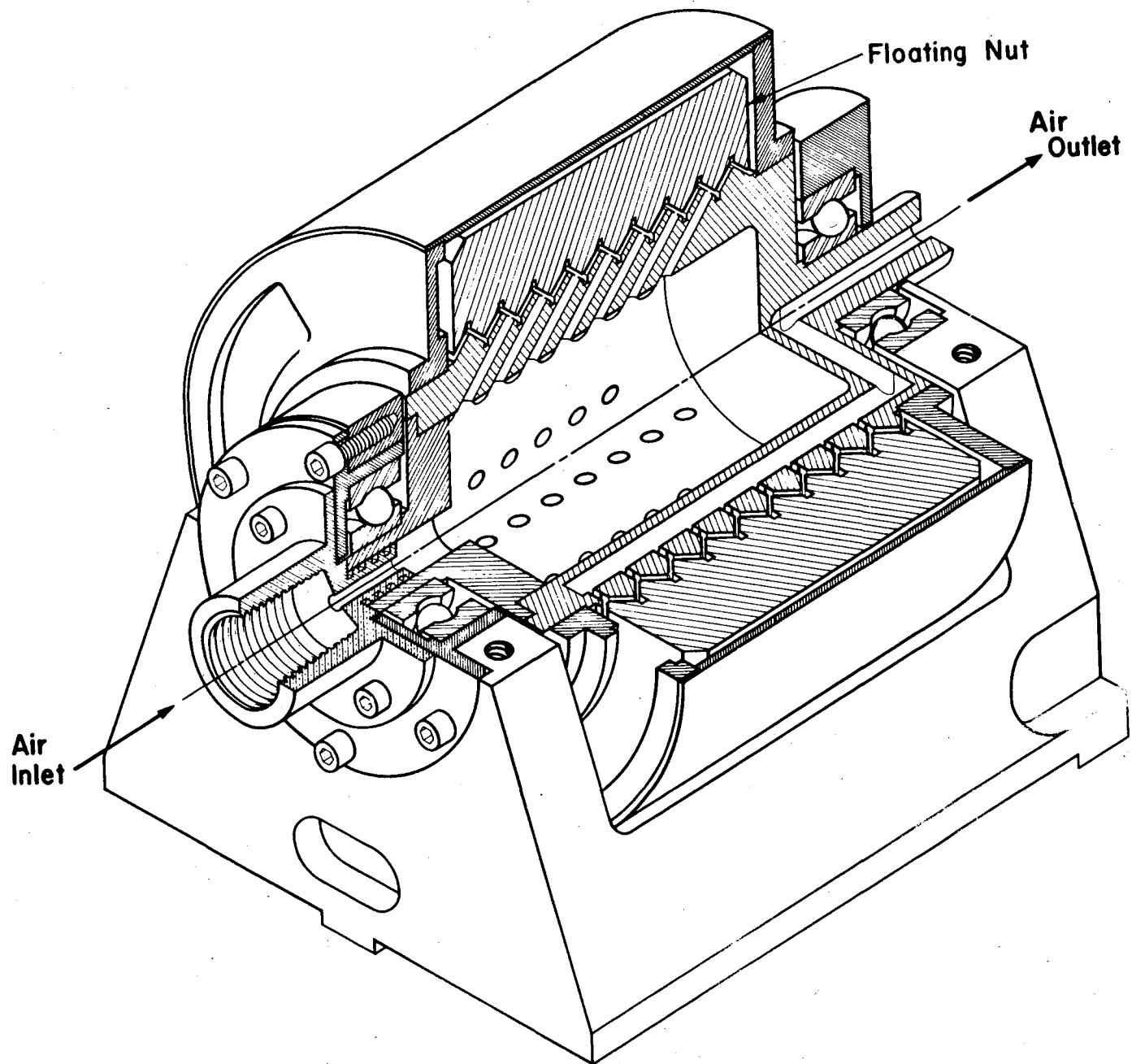


Fig. 27.8 Air bearing accelerometer multihelix.

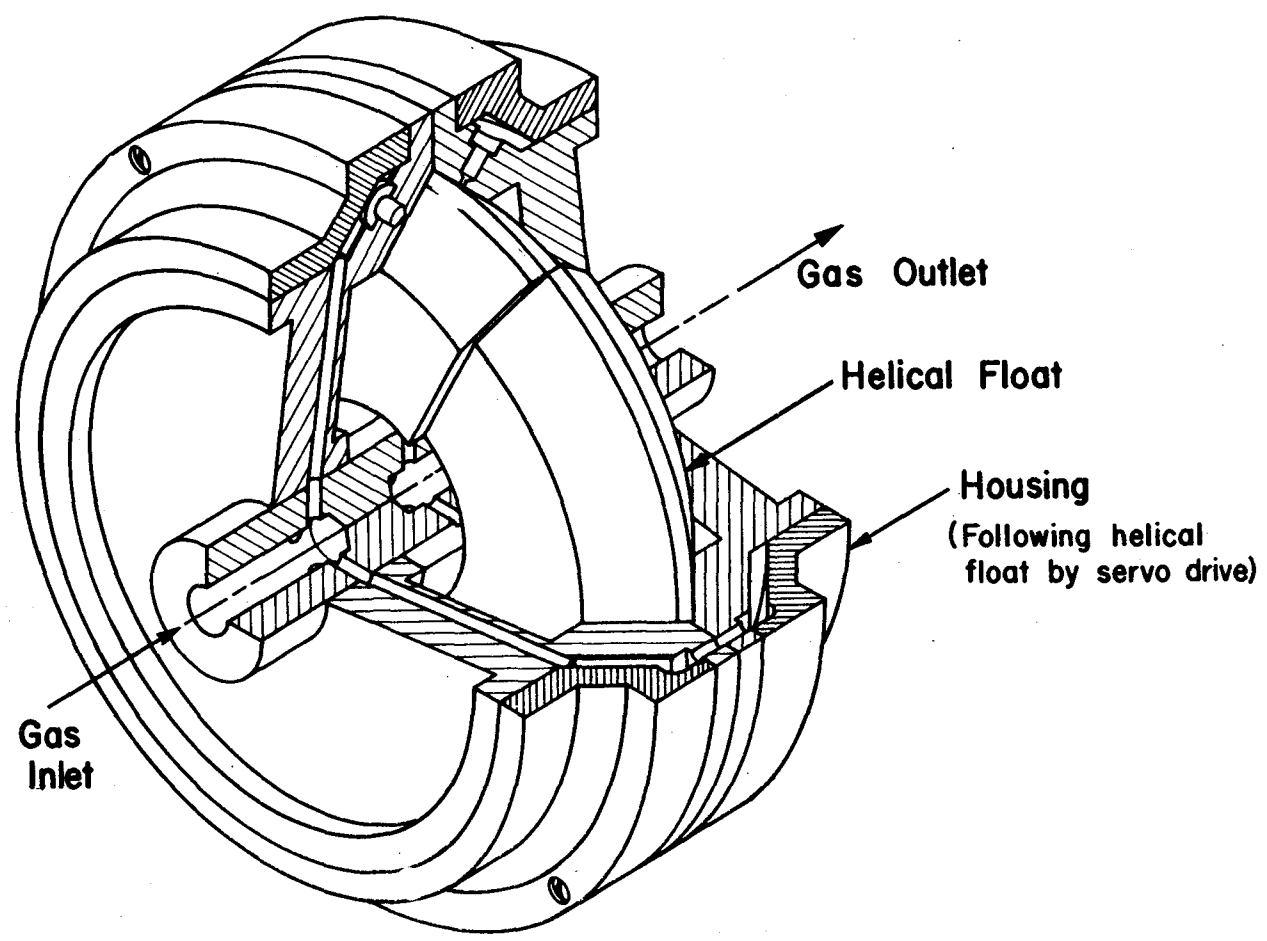


Fig. 27.9 Air bearing accelerometer (1 turn helix).

sensitivity of  $5 \times 10^{-5} \text{ G}$  and the repeatability is  $\pm 0.06$  per cent. The main source of error in this type of instrument is the turbine torque created by unsymmetrical airflow in the gap between nut and screw. The turbine torque was measured to be 3.6 d-cm/psi air pressure, too high for very accurate measurements but capable of reduction.

The outstanding features of this type of accelerometer are: (1) simplicity of design, (2) reliability, (3) compactness, and (4) its inherent ability to measure numerically vehicle velocity and traversed distance.

#### 27.6 Heavy Load Bearings

Air bearings can also be built for extremely heavy loads in flat, cylindrical, or spherical forms. When pressure of several hundred or a 1000 psi is required, it is safer to use water or servo oil instead of air. Such heavily loaded bearings are not intended for high speed; therefore, the viscosity of liquids is of no concern. The first large project was to study the possibility and feasibility of moving the entire service tower for the Saturn space carrier vehicle several hundred yards at the launching site. The weight was given as 3,000,000 lb including wind load. The structure was planned with three legs. The weight of 1,000,000 lb for each leg was to be carried by three flat bearings of 20-in. diameter. Figure 27.10 shows the arrangement in triplet fashion. Each pad has one nozzle, and the rim of the pad has a rubber-seal ring. Tests on a smaller scale showed satisfactory results. The main problem was the flatness of the track. It was suggested that a sufficiently wide, reinforced concrete foundation be built and covered with terrazzo or other suitable corrosion-proof top. A surface flatness of 0.001 in./ft should be possible by the use of large-diameter grinding disks and proper measuring tools for flatness. For cost and quality comparison, large-size granite surface plates for tool rooms, with 10 times better accuracy, cost \$35.00 per sq ft. The water supply could be drawn from a ditch parallel to the track and a motor, pump, and filter could be mounted at one leg. The multiple-pad flat water bearing system was not accepted for use.

#### 27.8 Saturn Floating Support

A frictionless and, if possible, weightless mechanical support is needed for the study of bending modes and dynamic behavior of the Saturn spacecraft. Here is another application for which large fluid bearings offer an ideal solution. The weight of 1,000,000 lb will be supported by 8 sets of bearings 16 in. in diameter. Each set has a flat and a spherical bearing to allow lateral and angular motion (Fig. 27.11). The center part, of plano-concave shape, has nozzles feeding both sides with liquid to float the load. The 8 sets of bearings will be supported by interconnected hydraulic pistons for equal load distribution.

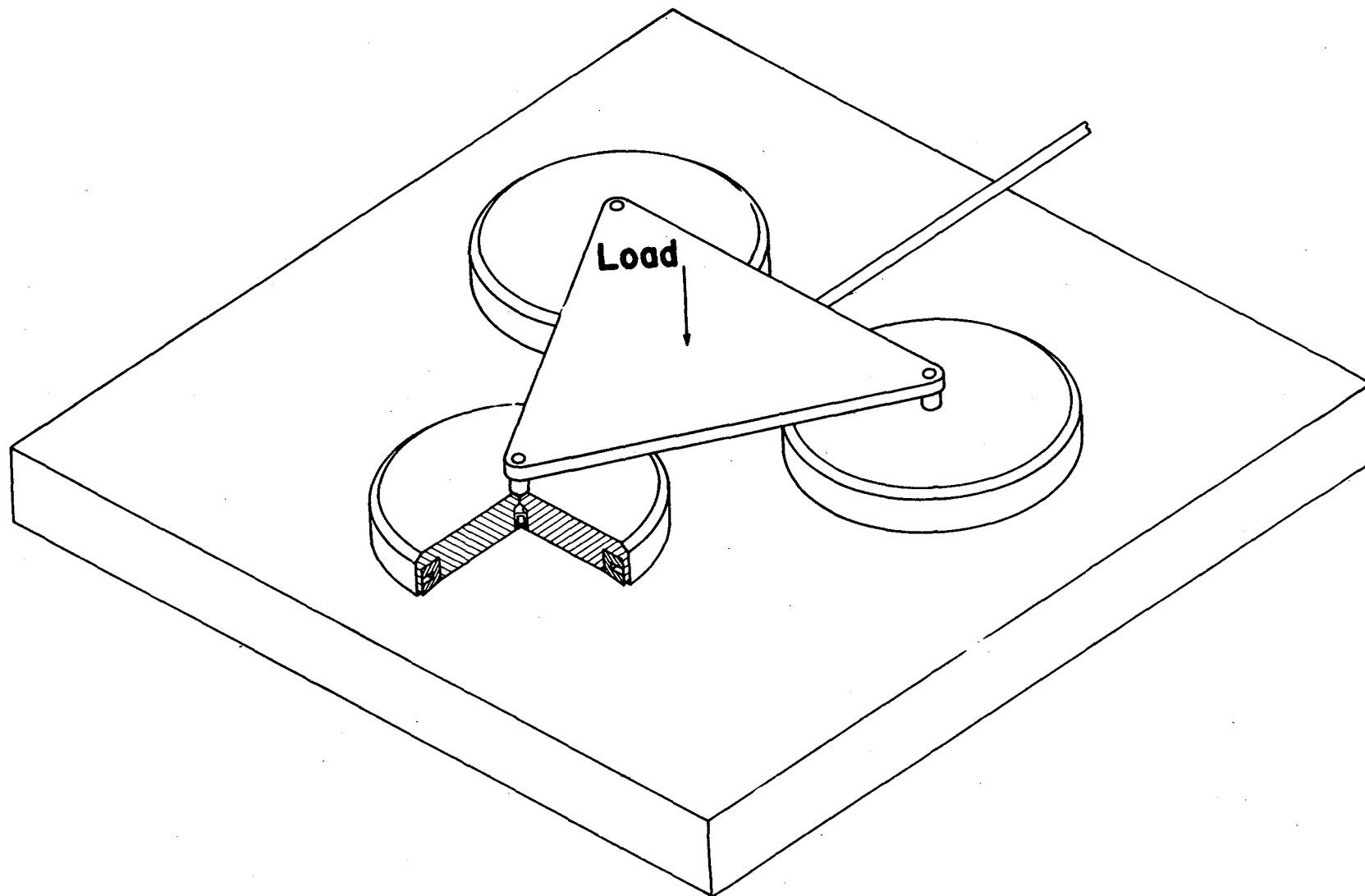


Fig. 27.10 Triple pad fluid bearing.

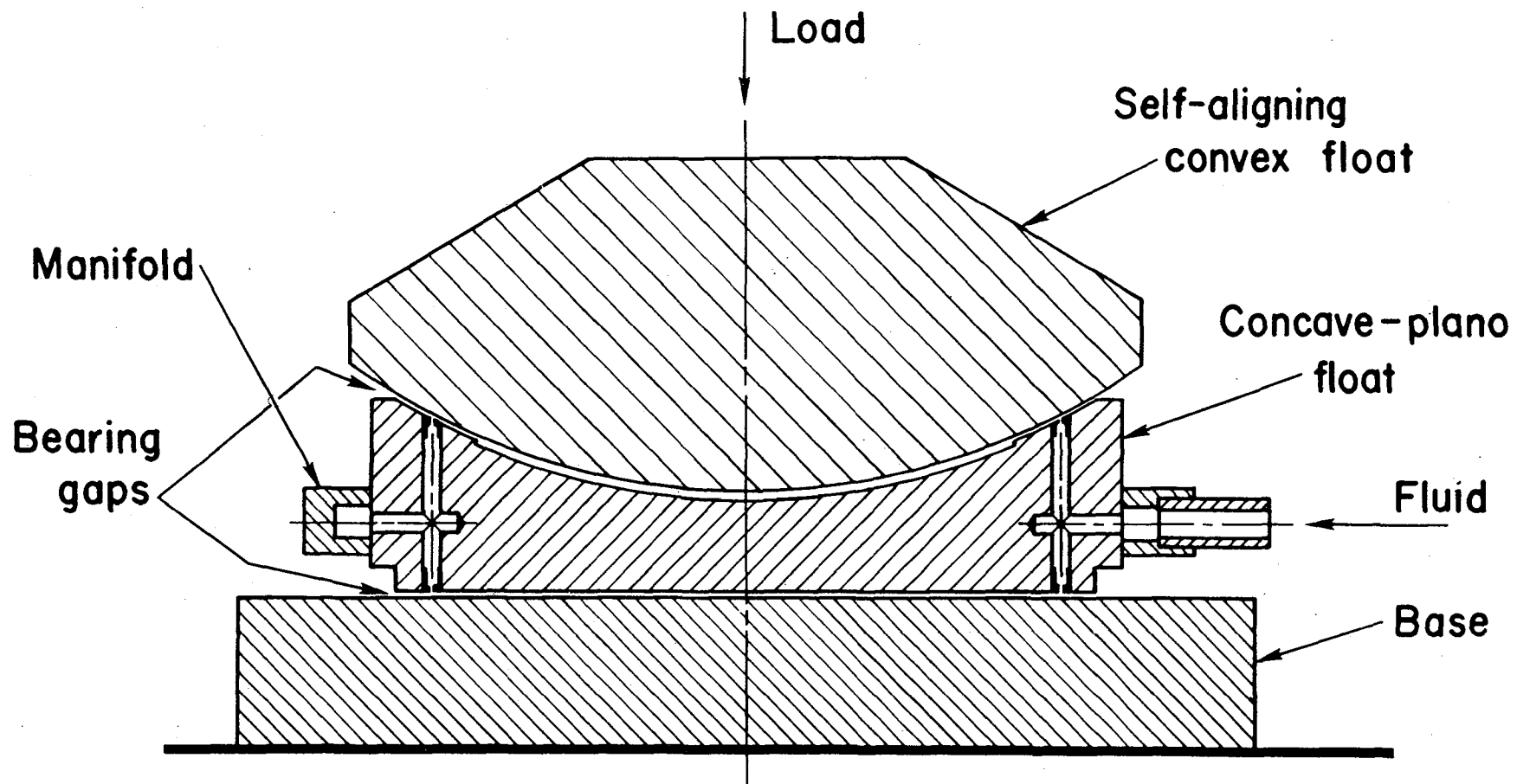


Fig. 27.11 Saturn dynamic test bearing.

One bearing set was built and load-tested with 90 tons in a hydraulic press. The airflow rate was about 1 gal per min at 1100 psi pressure with approximately 0.001-in. gap. The center plano-concave part of the fluid bearing floated freely. This gearing has been accepted by all concerned with the Saturn dynamics tests.

#### 27.9 Printed Cables and Connectors

Several years ago the development of a new electrical wiring system was started. It was intended to be used in missiles with the objective of saving weight and increasing reliability. Out of the original thin printed circuit strips grew a laminated flat conductor Mylar cable. The copper conductors are 0.040 in. wide, 0.004 in. thick, and 0.075 in. spaced between centers. The entire thickness is about 0.010 in. Four widths with 6, 12, 18, and 25 conductors are tentatively suggested as standards. The 25-conductor cable is about 2 in. wide. Flat conductor cables are now commercially produced in rolls of great length in steadily increasing quantities.

This new cable requires a fundamental change in the wiring concept. The previous laced, complicated round wire harness with all its many branches will be replaced by individual flat multiconductor strips which have a molded-on plug at each end and pressure-sensitive adhesive for ease of mounting. They connect electrical instrument boxes in straight runs in the simplest fashion possible. The connector-pin sequence at the corresponding boxes requires coordination or matching, since the flat cable does not permit circuit diagram changes; nor does it offer opportunities for miswiring.

The lack of a reliable, separable connector has retarded the application and broad use of printed cables. Considerable effort has been made to develop a connector which fulfills all the mechanical and electrical requirements and maintains them under severe environments. Many different approaches were undertaken, with varying degrees of success. One of our own promising developments is shown in Fig. 27.12. This connector can be used to connect a printed cable with another printed cable or with a printed circuit board. The plastic plug is molded permanently to the cable. The cable conductors are brought out to the surface of the plug to be used as contact areas. This is accomplished by stripping the cable ends and inserting a shuttle-type spacer between the conductors. Adjacent contact areas are staggered for the required (0.06-in. minimum) creepage path. The connection through the receptacle is made by individual contact springs of profiled beryllium copper wire. All contact surfaces are gold plated over nickel for protection against corrosion. The contact springs are designed to assure a uniform contact pressure (approx. 200 g) and are retained in a plastic housing (receptacle) which is enclosed in a metal shell. This shell gives mechanical protection against rough handling



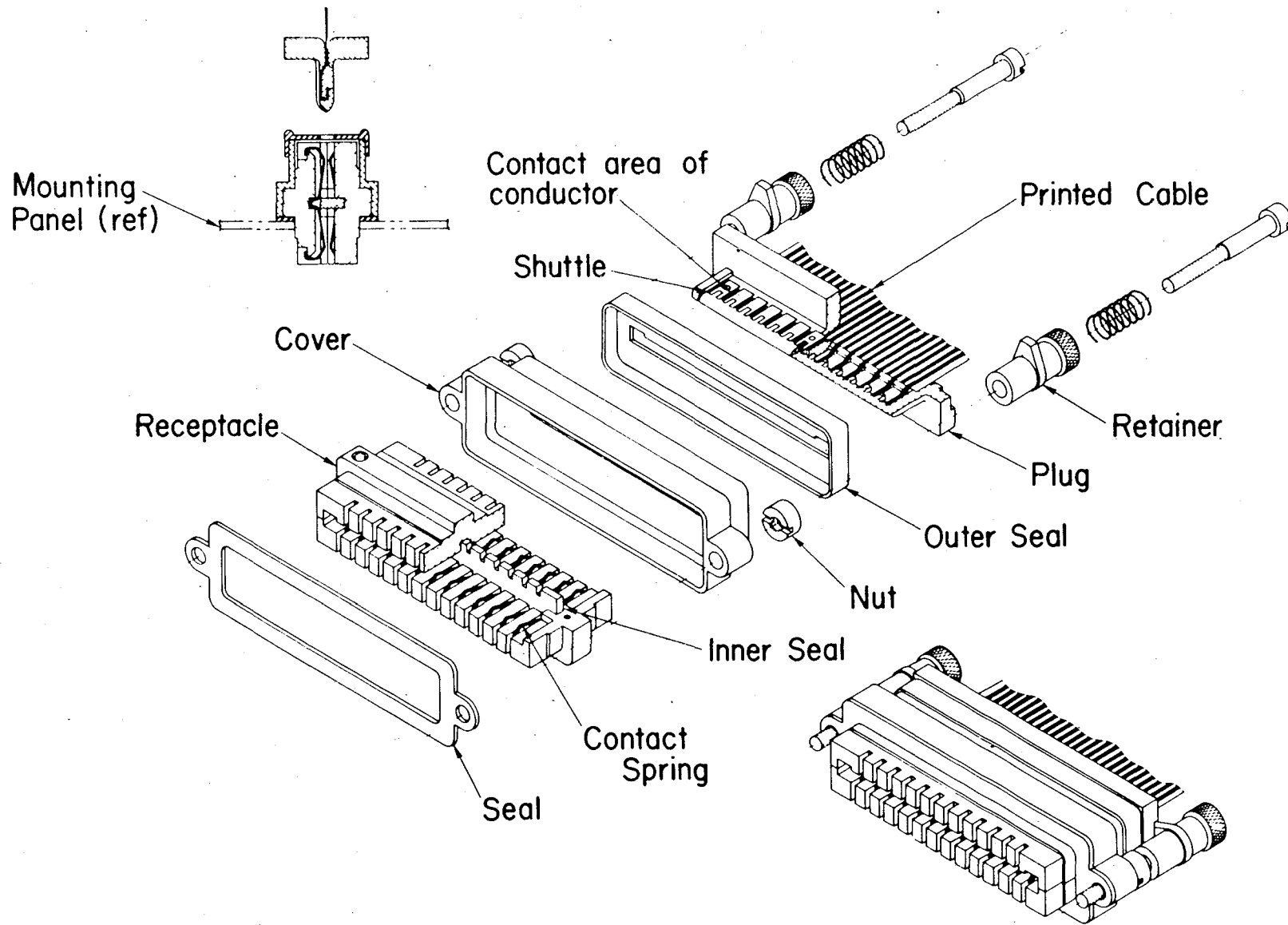


Fig. 27.12 Connector for flat conductor cable.

and hermetically seals the connector. Rubber seals are located between plug and receptacle and between receptacle and mounting surface. An additional dust seal is located permanently within the receptacle. Spring-loaded fasteners make a quick connect or disconnect possible without tools, and they also prevent separation of the plug and receptacle by vibration, shock, or accident. A number of prototypes are presently undergoing environmental testing. The advantages of the flat conductor cable over conventional round wire harnesses are as follows:

1. Time saving is unexpectedly high. Stripping a cable and molding a plug takes less than a minute, whereas the time needed for a round wire connector of the type presently used with an average number of contacts (25) for cutting, stripping, marking, soldering, inspecting, and potting is at least 1 hr. This does not include forming the cable on a nailboard and lacing. The installation time is also quite different. The flat conductor cable is fastened by pressure sensitive adhesive on the back of the cables, while the wire cable needs many clamps with screws and safety devices to secure it against vibration damages. The time advantage in installation is estimated at 5 to 1.

2. The flat cable represents vast improvements in reliability due to its ability to withstand vibration and flex tests far beyond the limits of round wires. No breakage has ever occurred during extreme shake tests, even at  $-80^{\circ}\text{C}$ . The connector design has incorporated manufacturing tolerances; dust, water, and corrosion protection; and a metal housing for limited rough handling. The plug is kept engaged by spring pressure. The contact springs of heat-treated beryllium copper have gold over nickel plating, a well-designed contact pressure of 150 to 200 g with 3000 psi specific pressure, achieved by contact radius to assure reliable contact quality (0.4 milliohm) and a sufficient lifetime of 500 insertions. The springs have a deflection of 0.020-in. minimum at insertion of the plug and a spring constant of 100 g/mm. The shortest leakage path length is 0.060 in., to satisfy high-voltage tests. The contact can carry 3 amp with only a small temperature increase. The present connector has two connections per line of the above described quality; the plug has none.

3. Weight and space saving is obvious. The cable derives added mechanical strength from the Mylar insulation (Mylar tensile strength is 20,000 psi). The cable has, in a sense, a cumulative strength because individual copper lines cannot be stretched. The copper gage need not be selected from mechanical handling but only for electrical requirements.

4. The electrical load capacity is higher by a factor of 2 to 3 due to its large heatsink, the mounting structure, and good convection when installed in single layers.

5. Electrical shielding is accomplished by a film of metal and is often handled sufficiently by the absorption of the metal mounting structure.

6. Inspection time is reduced, since miswiring is eliminated and visibility and accessibility is much better.

7. The cable preparation is engineered for mechanization in manufacturing without critical hand operations.

8. The flat conductor cable connects electric component boxes by parallel lines, thus excluding diagram changes within the cable. Alterations are made inside boxes where they are originated.

The development effort over the years has resulted in a well-engineered and superior cable system, established better specifications for connectors, and produced reliable connector hardware. The final result awaits only application and extensive flight testing.

#### 27.10 Outlook for New Materials and Manufacturing Techniques

The advancement of man into space poses many severe problems concerning materials and manufacturing techniques. The era of missiles and spacecraft is here. Its increasing influence in the various branches of science and technology is expected. The manufacturing engineer must be prepared to handle new problems in many new fields, including nuclear devices, cryogenic instruments, and solid state micro-miniaturized electronics. The machine shops will require new ways of machining, such as chemical treatment, explosive forming, and electromagnetic forming. Numerically-controlled automated machine tools of many kinds, microscopic dual manipulators for micro-assemblies, and many more tools, methods, and materials unknown today will be employed.

## **ENGINEERING AND COMPONENTS**

**Preceding page blank**

# 28      Preceding page blank

## MANRATING SPACE CARRIER VEHICLES

Joachim P. Kuettner

Saturn Systems Office  
George C. Marshall Space Flight Center  
National Aeronautics and Space Administration  
Huntsville, Alabama

"Manrating" is a new term. To manrate a space vehicle means to make it suitable for carrying a manned payload. The crux of the matter is that there is no agreement as yet on what is suitable. The first attempts to define manrating criteria are barely underway at a time when the pioneer astronauts are already circling the Earth in small satellites.

Historically, this is a surprising situation, for it always had been the primary goal of the rocket pioneers to develop rocket power for manned space travel. However, the winding road from Peenemünde to interplanetary space demonstrates that it was military requirements which have paced the difficult and costly rocket technology. With warheads as payloads, there was no manrating problem. Manrating has been the privilege of aviation technology which, until a few years ago, progressed on an entirely separate avenue and has lived with the manrating and escape problem from its birth.

While it is admittedly an oversimplification, the difference between the two technologies may be stated in the following general terms. From an aviation standpoint, man is not only the subject of transportation, and as such in need of protection as a passenger; but he is also a most important integral part of the machine over which he truly has control. His decisions in expected and unexpected situations are probably the greatest contributions to his own safety. Aviation, to the best of our knowledge, has never seen the necessity for a fully automatic initiation of emergency escape.

In contrast, rocket technology has been for 20 years a missile technology governed by the requirements of target accuracy and maximum range. As such, it had to develop automatic controls. Unlike a human payload, a warhead has no use except on the target. Once the missile fails, it may as well destroy itself during flight.\* There has been no need to save

---

\* For this reason, missilery has accepted aerodynamically unstable vehicles which, in case of loss of thrust, flip over and break apart destroying themselves in the air.

the payload after a successful flight or in case of a catastrophe.

The development of manned space flight is not just a matter of replacing a warhead by a manned cabin. Suddenly, a switch is thrown between two parallel tracks, those of missile technology and those of aviation technology, and an attempt is made to move the precious human payload from one track to the other. As in all last minute switchings, one has to be careful to assure that no derailment takes place.

Essentially, the manrating problem is one of human safety being concerned with both safety on the launching pad and safety during flight. Even if it were possible to design vehicle and pad operations to unprecedented reliability (taking human tolerance fully into account), it would still not obviate the necessity to provide means for emergency recovery both on the pad and during flight.

It is convenient to think of the manrating effort as covering four areas: (1) design, (2) quality assurance, (3) operations, and (4) emergency conditions. Before these points are discussed, it is pointed out that one question keeps coming up in all areas of the manrating problem, namely the role of the human occupant. Specifically, should he be an inactive passenger or should he take an active part in the operation of the vehicle?

The minimum role which every human occupant is bound to play is that of a living payload. Unfortunately, the human payload is quite sensitive and is in no way considered expendable. Thus he is strictly a problem as far as the missile engineer is concerned.

The maximum role of the occupant is that of a full-fledged pilot of the whole space vehicle. In this case the pilot would exercise full human control during powered flight; we are dealing here only with the space carrier or launch vehicle of the engineers, the electrical and control systems, the cutoff, and so forth. The minimum role he could play would be little above that of an instrumented payload.

On this widely discussed subject, there is agreement only on one point: both extremes are undesirable. To give the astronaut nothing but a panic button\* in powered flight is a waste of the outstanding skill and experience for which he was selected and trained (although this was the approach that had to be taken initially in the Mercury Project). It would also be technically unsound to discard the highly developed, precise automatic systems of missile technology only because pilots enjoy moving a stick.

---

\*To be pushed for initiation of the abort sequence in case the red "Mayday" light comes on.

A general trend is presently noticeable to phase in gradually the occupant in the role of an onboard flight supervisor who overrides failing systems, switches to backup systems, and decides on mission abort. For example, if the astronaut, in certain cases of automatic control failures, attempts to steer the vehicle into a parking orbit, however imperfect, rather than to abort the mission immediately at a point of the trajectory, it results in a severe reentry and landing in a remote and possibly dangerous portion of the Earth. In this function as a trouble shooter, man's unique capability is used to assess unexpected situation and then to react to it. For catastrophic situations developing too rapidly for an intelligent decision, automatic safety devices must be retained. Four key aspects of manrating are considered in the following paragraphs:

1. **Design Aspects.** In the design of space carriers, the sudden emergence of manned astronautical projects has forced both the US and the USSR to utilize available military rocket-powered missiles. In the past, manrating carrier vehicles was a matter of modifying existing hardware (and accepting many possibly undesirable fixed factors) rather than designing new vehicles. This situation is presently coming to an end, and it is already clearly recognized that precise manrating design criteria must be defined.

In the structural area, this refers to the establishment of yield and ultimate safety factors (values of 1.1 and 1.4, respectively are approximate figures) to vibrational restrictions, etc. The acceptance or rejection of pressure stabilized structures (balloon-type) for man-carrying carrier vehicles must be determined.

In flight mechanics and control, manrating favors a trend towards aerodynamic stability resulting, for example, in the reappearance of finned carriers such as the one seen in Fig. 28.1. The shaping of trajectories has to consider the acceleration tolerance of the human body, both during normal flight and in case of an abort.

In the propulsion area, the engine-out capability of clustered motors is an important manrating consideration. So are limiting noise and vibration levels and the selection of nontoxic propellants.\*

In the general design philosophy, special efforts are undertaken in the area of failure effect analysis. Once the critical components have been determined, a criticality ranking is established. The effort then is directed towards redesign; or if this is not feasible, towards redundancy and monitoring of the components with high criticality value.

2. **Quality Assurance.** For quality assurance, a manrated carrier vehicle requires firm criteria for the qualification and reliability test program, strict quality inspection procedures, and a carefully designed

---

\*In the Mercury-Redstone project we decided, for this reason, against the more powerful hydyne in favor of alcohol as the propellant.

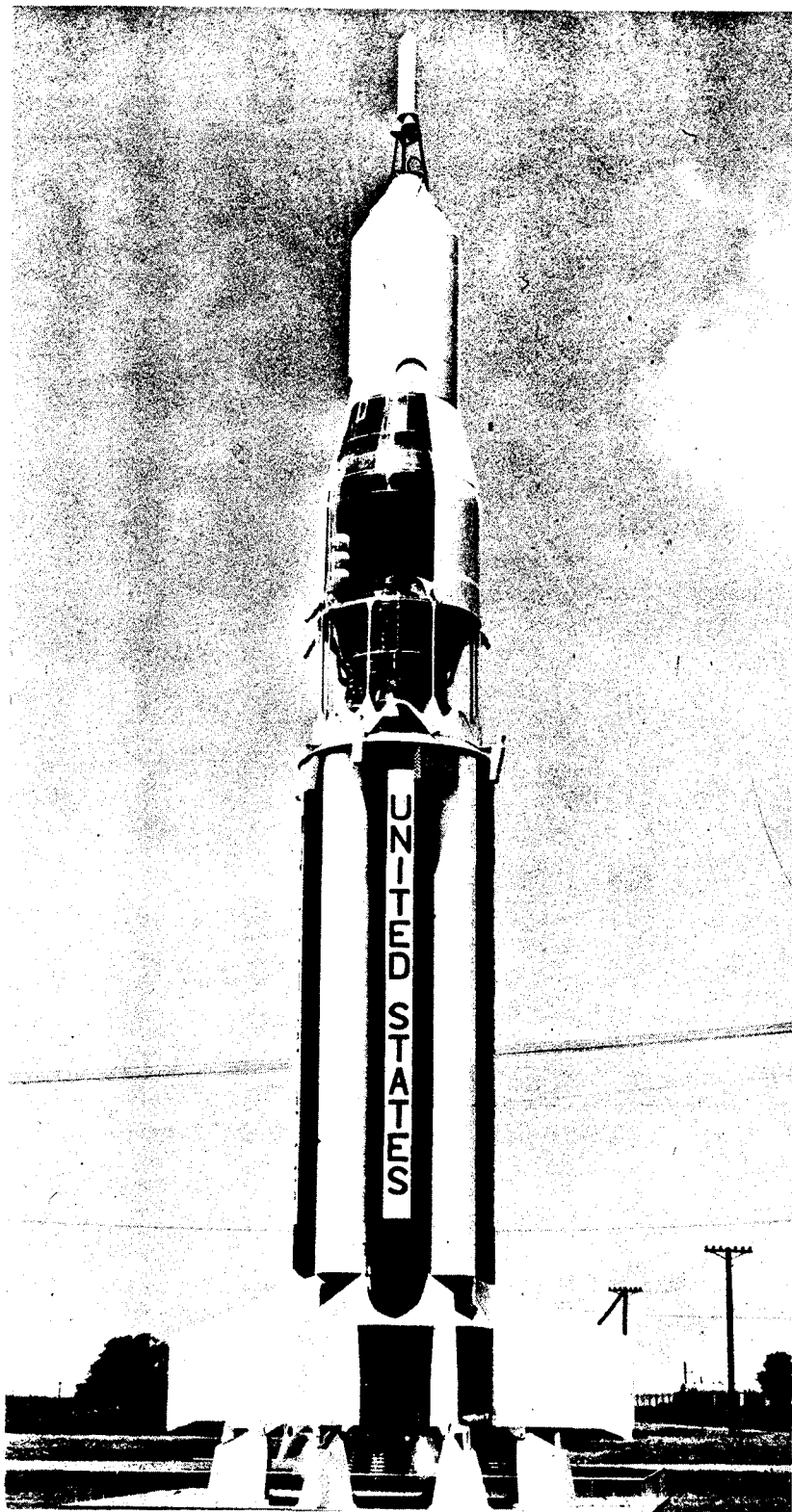


Fig. 28.1 Saturn C-1 with fins with Apollo payload



checkout program, especially in the area of interface and systems compatibility. In the Mercury-Redstone project, a special Mercury stamp was introduced on all components to be flown with a man aboard. An extensive reliability program conducted by Chrysler's Missile Division tested not only individual components and subsystems but whole missile sections (Fig. 28.2). The George C. Marshall Space Flight Center's Quality Assurance Division, during its compatibility tests, ran complete flight simulations with the entire space vehicle.

With regard to actual reliability figures, a distinction has to be made between mission reliability and escape reliability to arrive at a survival reliability value. Figure 28.3 illustrates the situation. The mission of the carrier vehicle is defined as the successful injection of the payload into the proper trajectory. A good compromise between obtainable and desirable reliability values may be an 85 per cent value at a confidence level of about 90 per cent. If the escape system fulfills the same condition, the survival probability is about 98 per cent.

In the Mercury-Redstone project, about 60 Redstone and Jupiter C flight records were at our disposal. Since configurations, missions, and components varied with individual flights, there were several ways to arrive at a reliability estimate. One of them used an artificial Mercury configuration composed of individual components flown on previous flights. This composite vehicle led us to an expected mission reliability from 85 to 90 per cent at a 75 per cent confidence level for the new Mercury-Redstone carrier vehicle. The actual flight record suggests this figure to be correct.

3. Operational Aspects. Manrating criteria must also apply to the operations at the launch site, specifically to the prelaunch checkout, the countdown, and the launch operations. Prior to the prelaunch checkout, the launch vehicle stages and the spacecraft must have undergone separate checkouts of such thoroughness that the total space vehicle should spend a minimum time of exposure on the launching pad. In the later phases of the Mercury-Redstone project, the time between the mating of spacecraft and its carrier vehicle and the actual launch was under 2 weeks.

The actual countdown has to be man-oriented, that is, it must be designed to insert the flight crew at the latest possible time and with a minimum of risk. This implies, for example, that rf checks with the on-board explosives armed, and the service structure removed, are made prior to crew boarding. The countdown should be conducted by one crew. Until automatic checkout procedures become routine, personnel fatigue during the long and complicated countdown will remain a serious problem. In the Mercury-Redstone project the 11-hr countdown was split into 2 days to promote mental acuity of the launching crews. The astronaut embarked 2 hr before nominal launch time. In practice, however, he spent

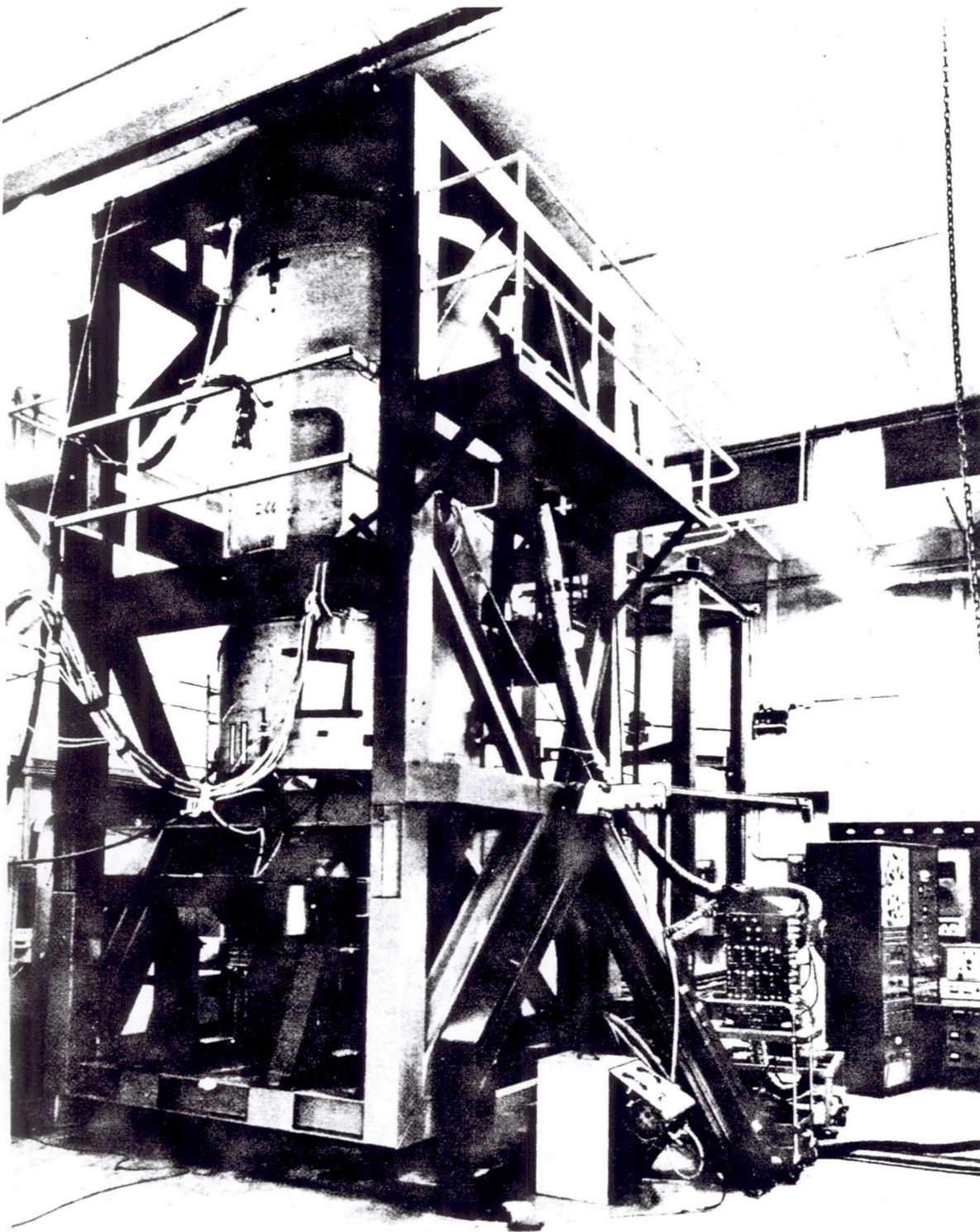
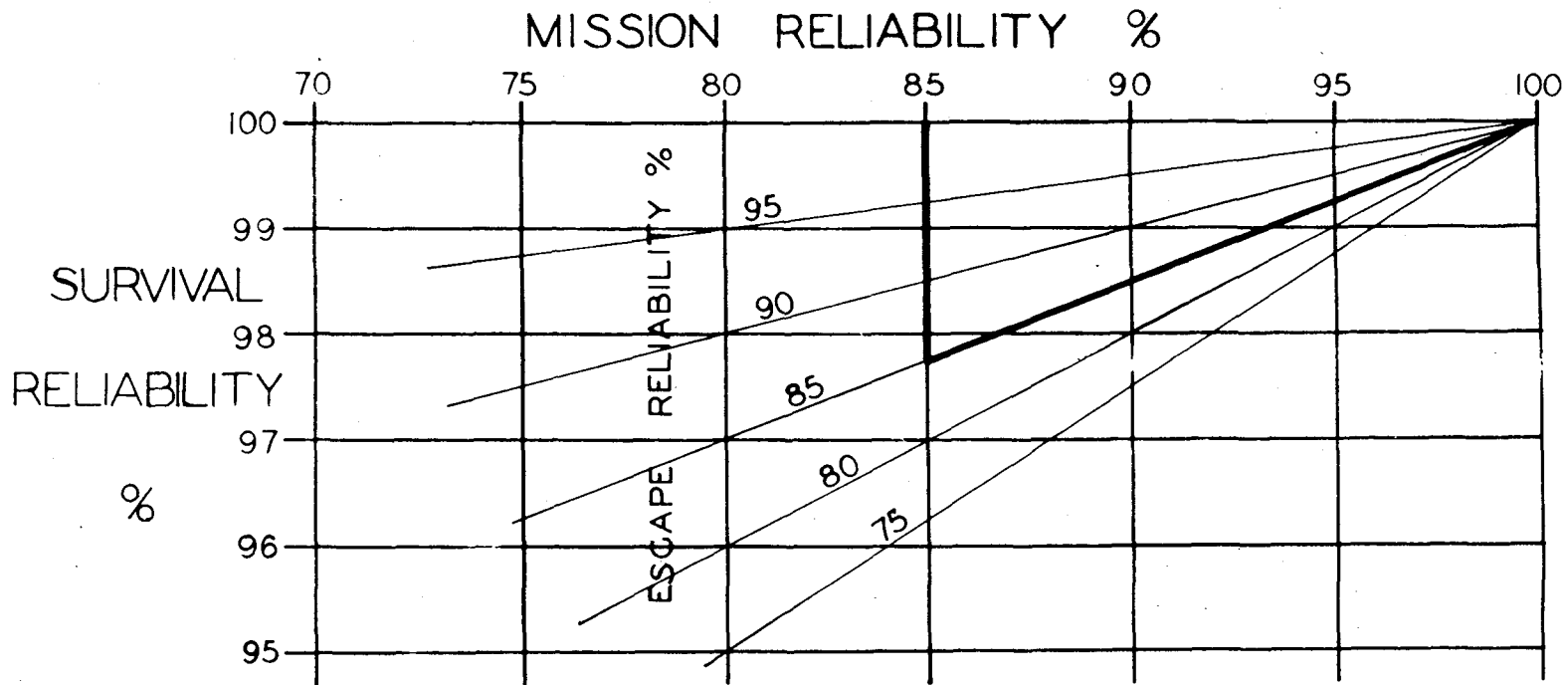


Fig. 28.2 Rocking and Shaking Fixture used for Complete Mercury-Redstone Top Section, including Instrument Compartment and Automatic Abort System. Courtesy Chrysler Missile Division.



$P_M$  &  $P_E$  - RELIABILITY VALUES AT 90% CONFIDENCE LEVEL

$$P_S = P_M + (1 - P_M) P_E$$

$P_E$  = ESCAPE RELIABILITY

$P_S$  = SURVIVAL RELIABILITY

INCLUDING ABORT SENSING,  
EJECTION AND RECOVERY

$P_M$  = MISSION RELIABILITY

Fig. 28.3 Mission Reliability vs. Survival Reliability as a Function of Escape Reliability.

over 4 hr in his capsule before the actual launch took place. This was probably close to the acceptable limit.

4. Emergencies. The last and most important aspect of manrating is in emergency conditions. Obviously, emergencies on the launching pad and during flight must be treated differently. Depending on the type and degree of the emergency, either an orderly egress of the crew on the pad may be considered, or an armed escape mechanism may be relied upon. After ignition, only the latter is available.

It has been mentioned before that catastrophic conditions may develop so fast that there is no time for the astronaut to make an intelligent decision. In this case, the escape system must be triggered by an automatic emergency detection system. Even if there is enough time, the astronaut needs some kind of an emergency monitoring system for his personal information. The emergency detection system (EDS) is therefore a focal point of the manrating problem.

The philosophy underlying the future development of an EDS at the George C. Marshall Space Flight Center distinguishes between catastrophic and critical conditions. Imminent vehicle disintegration, developing in less than  $t$  sec, represents the catastrophic case. It requires automatic abort. Delayed vehicle disintegration developing in more than  $t$  sec is the critical case and is reported to the astronaut for a decision, such as corrective action or manual abort. The time  $t$ , defined as the threshold for an intelligent decision (not of human reaction only), is probably of the order of several seconds and must be determined more precisely.

A thorough failure effect analysis is again the only sound way to find the correct classification. Present studies indicate that there are relatively few catastrophic conditions to be monitored by the EDS, and those that are expected will depend on the individual carrier vehicle and on its different flight phases. For example, loss of two out of eight engines will be in the critical category except immediately after liftoff where it may result in a catastrophic collision with the ground or ground structures.

Typical catastrophic situations are:

1. Excessive attitude deviations or turning rates, leading to high angles of attack during high dynamic pressures and resulting in a structural breakup.
2. Sudden loss of tank or bulkhead differential pressure in pressure-stabilized structures.
3. Loss of electrical power in the control and instrument system.
4. Loss of thrust immediately after liftoff.

Typical critical situations are:

1. Partial loss of thrust.
2. Development of a fire.
3. Flight-path deviation.
4. Loss of tank pressure.

To detect such situations, the EDS should have a higher reliability than the systems to be monitored. Threefold sensor redundancy with a majority-voting-logic is a possibility considered; selection of the simplest sensors and the cleanest parameters is another. Finally, the setting of abort limits is a matter of very careful analysis.

Figure 28.4 gives a block diagram of the automatic abort-sensing system used on the Mercury-Redstone vehicle. The normal sequence of events following an automatic abort is (1) engine cutoff (except during the initial flight over the launching site), (2) separation of spacecraft and carrier vehicle, (3) ignition of the escape rocket, (4) rapid escape of the spacecraft from carrier, and (5) recovery.

A well-organized emergency organization on the launching site is a necessity. Figure 28.5 shows one possibility of emergency egress used during the Mercury-Redstone project. The gondola of the cherry picker hovers near the spacecraft during the time between service structure removal and just before liftoff. Other equipment, such as armored cars, amphibious vehicles, and helicopters stand by for recovery from an on-the-pad abort.

While the astronaut and the launch director have the capability to initiate abort before the actual launching takes place, it is better not to arm the automatic abort system before liftoff. This is the procedure used in the Mercury-Redstone project.

Without going further into the numerous details which have to be observed during a manned launching, the pioneering work of the Mercury-Redstone project has shown the general direction in which the manrating effort will continue. Those directly connected with this effort know, however, that we have to progress rapidly if we want to see a truly man-rated carrier vehicle ready on the launch pad for the first manned trip to the Moon.

#### ACKNOWLEDGMENT

The author expresses his thanks to the many members of the von Braun team whose thoughts and efforts have been summarized in this chapter.

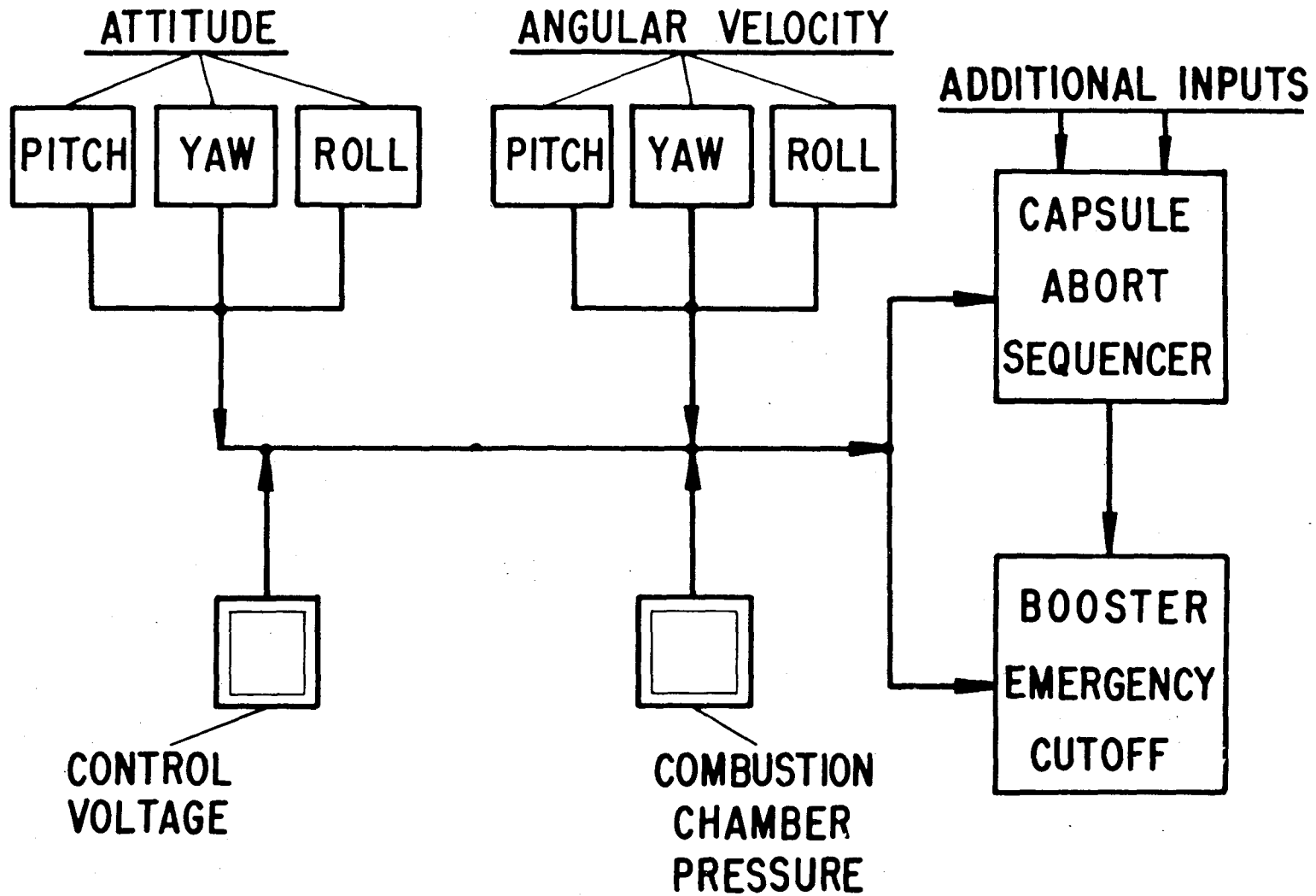


Fig. 28.4 Block Diagram of the Mercury-Redstone Automatic Abort Sensing System.

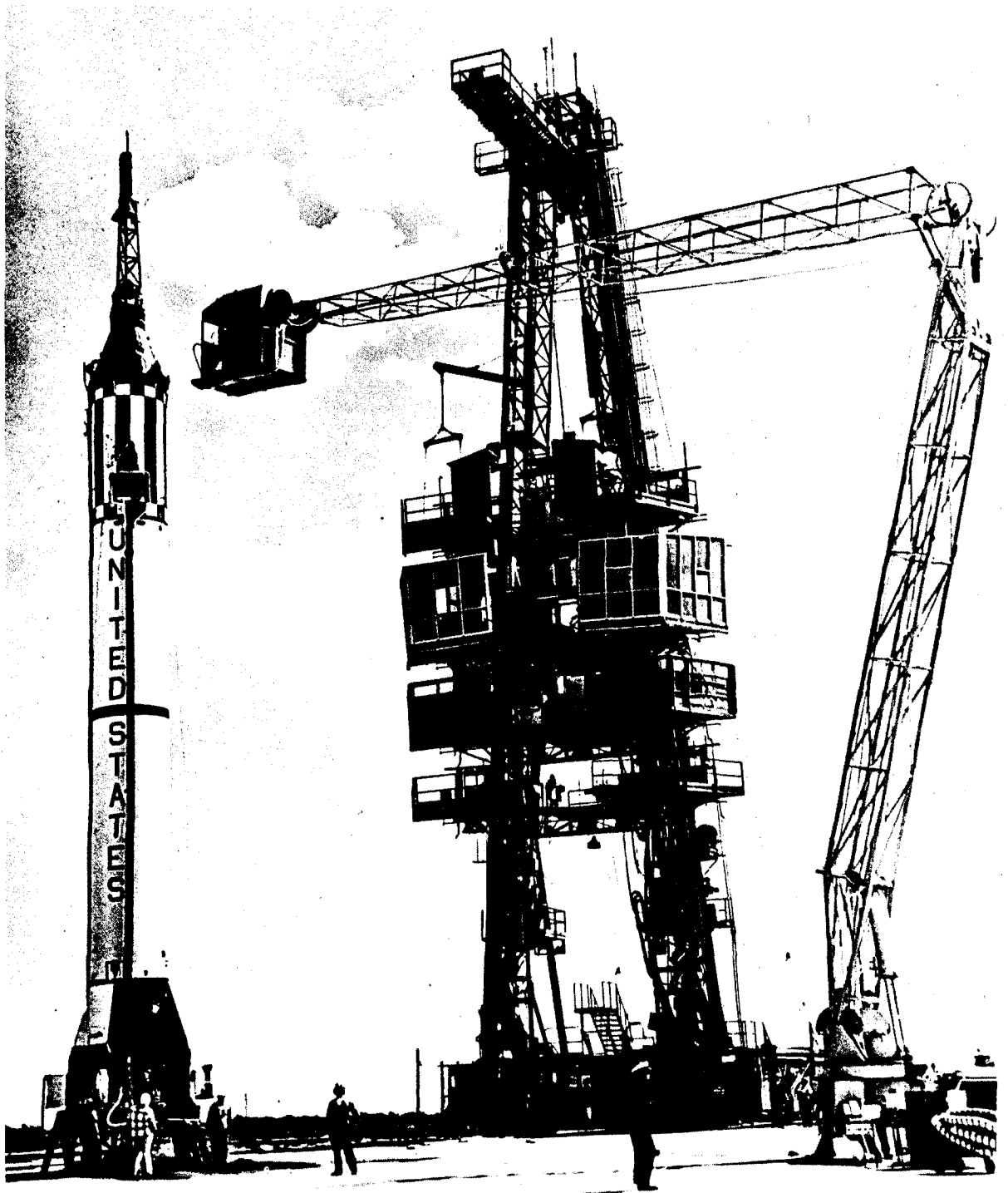


Fig. 28.5 Shepard's Mercury Capsule MR-3 on the Launching pad with Emergency Egress Structure ("Cherry Picker").

16005

29

ELECTRICAL SYSTEMS IN MISSILES AND SPACE VEHICLES

H. J. Fichtner

Astrionics Division  
George C. Marshall Space Flight Center  
National Aeronautics and Space Administration  
Huntsville, Alabama

Now that space operations have become a reality, it is appropriate to review the accomplishments of the past and to discuss what must be done in the future to insure the operational readiness of our large carrier vehicle systems. Well-planned overall systems engineering is the key to this task, with electrical systems engineering playing a major subsidiary role.

When missiles were introduced on a relatively large scale some 25 years ago overall electrical systems engineering did not exist as such, although with the V2 missile the systems approach was being utilized for the first time. In those days the designers of the propulsion system provided for the system's electrical needs by maintaining the required start and cutoff sequence. The designers of the guidance and control system worked their own electrical system and took care of the electrical equipment needed for the checkout and launch operations.

Missiles resulting from this parallel design effort were operational; but to build, checkout, and prepare them for launching was very expensive and time consuming. Relatively early in the research and development phase of the V2 program the entire system was evaluated for large-scale production. This evaluation showed that it was impossible to supply all the electrical components needed to achieve the requested production rates. For the first time, this created the need for a coordinated overall systems approach which considered checkout equipment and the missile as one system. Duplication of functional components, signals, power sources, etc., was avoided to simplify the system as much as possible. The requirements placed on the overall system created the need for a systems engineer who was required to have a thorough knowledge of the various subsystems, their operation, and functions. A philosophy was established which has been followed since: "Keep the missile system simple; wherever possible, keep components out of the missile, especially if they only function during pre-flight checkouts." Under these conditions, the entire V2 system was redesigned. Aside from production considerations,

Preceding page blank



operational simplicity was of major concern. Checkout and launch operations during the research and development phase were carried out by the designers themselves or by high-caliber, technically trained personnel. In combat application, the system being operated by troops had to be self-checking and automated in its launch sequence. The V2 system at the end of World War II was a classical example of functional simplicity with a minimum amount of components. The actual launch operation was simplified to only two pushbuttons: one to start the launch sequence, and one to start the full flow of propellants. The entire launch sequence was self-checking and returned the system to a safe condition if a malfunction was sensed during this time before launch. All operational missile systems today essentially follow this pattern of operational sequence.

Inflight instrumentation systems were refined more and more after World War II, and missile behavior as well as environmental conditions during the entire flight phase were observed through radio links. This possibility of telemetry coverage opened a new area for missile design engineers to obtain valuable data for further study programs. Theoretical data could be hardened by actual data, and values could be obtained for the anticipated new missile programs. Within the last 15 years, the measuring program expanded from between 30 and 40 measurements to between 500 and 600 measurements per test flight. All these measuring programs had to be incorporated into the overall system in such a way as to not interfere with the standard system necessary for proper flight performance. A malfunction in the instrumentation system should not influence in any way the behavior of the standard system. However, the instrumentation system was required to function as long as possible to record catastrophic failures, such as fire in the engine area, control failures, etc., that would eventually lead to a flight failure. This systems-approach worked very satisfactorily in programs like Redstone, Jupiter, and Pershing. There were few failures which could not be explained. The telemetry records gave perfect coverage and usually a quick explanation.

As the missile systems expanded in size and complexity, the checkout time and the time required for launch readiness also increased. The constant changes from one missile to a more advanced missile demanded exacting checkout, test, and firing procedures. Event sequencing had to be dictated that could be achieved only by designing all tests and sequence events into the system. Whenever possible, the human element was eliminated in all critical phases of checkout and launch. This effort was well spent, judging from the results of the various missile programs of the last 5 years. It is not a major problem today to prepare a satellite on a certain day, or even hour of the day, for firing and injection into orbit. It is taken for granted that the entire system is reliable enough to meet a specified countdown time. It cannot always be assumed, however, that a missile takes off from its launch pad and stays on its prescribed trajectory. Special precautions are necessary as directed by the safety officer of the missile range.

An entirely independent and redundant system has been designed over the years as a tool for the safety officer to maintain full control over the missile. He must be able at any time during the propelled flight phase to cutoff thrust or to destroy the entire missile if he decides that this is necessary for safety reasons. This system must work under any condition possible in the flying missile such as power failure, structure breakup, or other failures. The various requirements in the known missile programs, such as 15-min readiness, automation to any degree, and self-checking of subsystems and components, lead to standardization and refinement of the entire system to achieve reliability. Only after the achievement of this reliability was it possible to plan for the placing of man into space.

Project Mercury was established and funded based on reliable missile systems. The primary missions of Project Mercury are the orbiting of manned capsules around the Earth, the study of man's capabilities in space flight, and the safe return of the capsules and their occupants to the surface. The program was divided into two main phases: (1) to use the modified Redstone carrier for suborbital unmanned and manned capsule flights to help qualify the Mercury capsule in a space environment, and (2) to carry out unmanned and manned orbital flights with the qualified Mercury capsule being boosted by an Atlas ICBM.

It was necessary to analyze the entire flight history of the two systems to establish a malfunction study that showed where systems improvements were desirable and possible. Parallel to this study, an abort-sensing philosophy was established to provide, during the total countdown and flight, the utmost in safe abort for the man in the capsule and for the launch crew at the pad.

A new design aspect entered the overall systems design; this was the concern about the man. Electrical checkout and functional circuits, well established in previous flights, had to be reanalyzed and redesigned because the safety of a human life was involved. Automatic abort sensing during the countdown and carrier vehicle flight was to be incorporated into an existing system. Since two independent systems were involved, carrier vehicle and capsule, close technical coordination was essential. In the preflight condition, up to liftoff, any malfunction had to result in the "safing" of the entire system or ejection of the capsule from the carrier rocket. It was necessary to make all abort systems redundant and operational under all possible conditions. After liftoff, the range safety officer's requirements added to the complexity of the system.

Abort had to be possible over radio link at all times from the ground; the astronaut also had the ability to abort the mission. It was necessary to develop automatic abort sensing devices for the space carrier vehicle such as:

1. Attitude error sensors for pitch, roll, and yaw axes.
2. Angular velocity sensors for pitch, roll, and yaw.

3. Control voltage detectors to sense voltage failure.
4. Combustion chamber pressure switches to sense engine performance.

All these sensing devices could activate a common abort bus for both carrier vehicle and capsule. Elaborate tests were performed with the system to qualify all components and circuits for the stringent requirements.

The Mercury-Redstone's three, successful, unmanned, test flights and two, successful, manned, suborbital flights indicate that the systems approach is sound and that the concepts in systems design are advanced enough to be applied to larger space vehicles.

The experience gained in many missile systems over the past years was carefully applied to the present systems such as Saturn. The Saturn, a large, multistage, space carrier vehicle, demands an extremely well-coordinated engineering and design effort to fit all stages into one workable system. Overall systems design direction and standardization, within stages, are absolutely necessary. The first block of Saturn vehicles will show what this effort means.

The electrical interconnect diagram of the Saturn first stage shows the breakdown into 16 major areas. This breakdown was selected as a logical division into subassemblies and, in some cases, into subsystems. The interconnection diagram depicts the vehicle integration scheme and illustrates to some degree the complexity of the present Saturn electrical network; it is shown in Fig. 29.1.

The electrical system used in Block One Saturn vehicles serves to supply power for the operating and switching functions needed by the various vehicle subsystems. Primary vehicle power is provided by the main batteries, which in many cases furnish the necessary power directly through the distributors to the electrically operated components. In other cases, battery power is converted into other voltages and frequencies by power supplies and routed to the subsystems through the distributors.

The entire integrating electrical network consists of cables and distributor boxes. Integration of the subsystems requires approximately 500 cable assemblies and nine distributors, since almost all components are served through distributors. This system guarantees a high degree of flexibility to incorporate design changes. The entire system can be built and checked out on the bench prior to assembly into the vehicle. This means a high assurance of quality and reliability, since accessibility prior to vehicle assembly is provided.

The Block One Saturn subsystems are established as follows:

1. Electrical power. The electrical power system consists of two 28-v batteries supplying two independent busses; one bus handles all

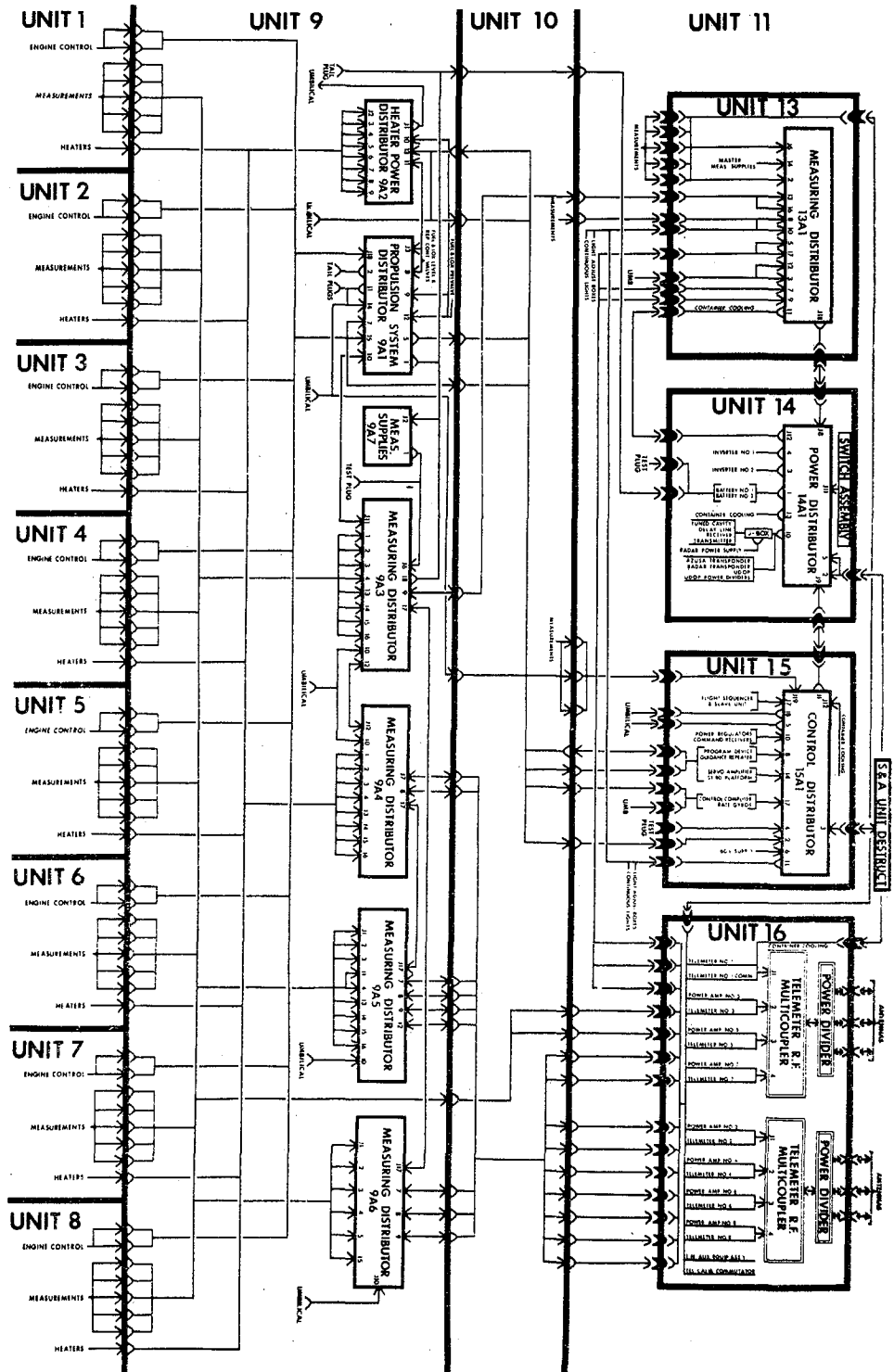


Fig. 29.1 Electrical interconnect diagram for first stage of Saturn.

steady loads, the other bus all variable loads. The steady loads are mainly the secondary power supplies, such as 5-v supplies for measuring voltage and the 60-v power supply for control components. The variable loads are heaters, relays, valves and cooling equipment. Each battery will carry its total load during flight after power switch-over from ground supply shortly before ignition of the engines.

2. Pressurization. The propellant tanks are pressurized by two pressurizing systems. Fuel tank pressurization is controlled by valves in the manifold system which regulate the nitrogen gas supply with pressure switches. The fuel tanks are initially pressurized by the ground system prior to ignition. Pressure level is maintained during powered flight by pressure switch sensing, which activates required valves in a controlled sequence as fuel is consumed.

The liquid oxygen tanks are initially pressurized by a ground pressure supply. After ignition, liquid oxygen is gasified by running it through a heat exchanger. The gas then maintains the desired pressure within the liquid oxygen tanks. Mechanical vent valves relieve excess pressure through the preset valve. These tanks may be electrically vented from the blockhouse at any time prior to liftoff.

3. Engine start and cutoff. The fuel and oxidizer are fed to the engine by turbine-powered pumps. Initial turbine momentum is given by the turbine spinner, which is started by squibs ignited by an electrical signal from the ground equipment. The turbine spinner is sustained by fuel and oxidizer burning in the gas generator. After initial startup, fuel pressure maintains engine operation. The eight Saturn engines are started with the ground equipment in a staggered sequence pattern. Only two engines are ignited simultaneously. The four groups of two engines are ignited 100 msec apart. All engines are monitored for combustion and proper build up of hydraulic fluid pressure needed for engine gimbaling. These criteria are monitored for 3.3 sec to ensure that all eight engines are running properly and that hydraulic pressure is maintained.

Only if these indications are satisfactory does the ground support equipment (GSE) continue the launch sequence with the thrust-commit signal. This signal deenergizes a relay in the vehicle to energize the one-engine out bus. Energizing this bus enables the vehicle to give cutoff automatically to one engine if the thrust falls below the specified limits. When one engine is cut off prior to liftoff, the remaining engines are also cut off in a given, patterned sequence. Should the thrust of any engine drop below the specified limits during the first 10 sec of flight, that engine will be cut off, and the engine out circuits will be deactivated to prevent the other engines from being cut off because of low thrust. This circuit is reactivated at liftoff-plus-10-sec so that the other engines with low thrust may be cut off. Emergency cutoff may be given from the ground by radio link, through the destruct command receivers, any time after liftoff. This signal will switch all engines

off at once. Normal cutoff sequence is provided by liquid level sensors in the fuel and oxidizer tanks. When fuel and oxidizer consumption reaches a preset low level, the cutoff for the four inboard engines is triggered. Derived from this signal 6 sec later, the outboard engines are also cut off. In the engine cutoff sequence, circuitry is provided to insure that there are more than two outboard engines running at one time.

4. Flight sequencing. The program device is the source of all in-flight sequence events. It provides accurate time pulses to initiate and execute guidance, control, and sequenced functions. The program device is a precise, six-channel, magnetic tape recorder, of which three channels are presently used:

- a. One channel provides the tilt program.
- b. One channel initiates telemeter inflight calibration.
- c. One channel stimulates the overall vehicle sequencing.

The program device is started from zero at liftoff, relating all sequence events of the channels to liftoff as the time base. Shortly before calculated inboard engine cutoff, the program device is stopped and restarted at the actual, inboard engine cutoff signal. This provides a new time base for the upper-stage operational sequence based on inboard engine cutoff. This has the advantage of eliminating the tolerances of carrier vehicle performance; cutoff predictions are theoretical values only.

All overall vehicle sequencing stimulated by the program device is executed by the flight sequencer; a chain of relays respond to pulses from the program device.

5. Control. The heart of the control system is the stabilized platform and its executing equipment. The stabilized platform serves as inflight reference for signals to the control system. The control system senses and corrects vehicle inflight inaccuracies through null-seeking devices that continuously compare actual flight information with the programmed flight path. The signals and values derived from the stabilized platform are transmitted to the control computer. The control computer in turn translates these signals into control signals. The output signals are executed by hydraulic servo actuators, which gimbal the four control engines accordingly.

6. Inflight cooling. To assure proper operation of some inflight equipment within the given tolerances, an inflight cooling system regulates the temperature within the pressurized canisters where this equipment is housed.

7. Heating. The air required by the air-bearing gyros is heated to maintain the stringent tolerances of the platform. A temperature sensing device monitors and maintains this temperature within the preset limits as the stabilized platform is in operation. The angle-of-attack meters used with the control system are also heated to prevent icing during flight.

8. Tracking. The Saturn tracking equipment consists of two radar units, Udop, Azusa, and their associated antennas. The equipment is powered and operated through vehicle circuitry. There are four continuously burning lights tracked by CZR cameras for a period after liftoff. The flight sequencer turns the lights off after the vehicle is out of camera reach.

9. Telemetry. The Saturn vehicle carries eight telemeter links which are used to transmit about 600 measurements back to ground receiving stations. These measurements are routed and signal-conditioned from all areas of the vehicle to the proper telemetry channel for transmission.

These short descriptions of the major areas to be combined into one overall system indicate the necessity of well-defined technical system coordination. A thorough knowledge of the system's functional operation is essential for the systems designer. The design must provide not only reliable, and in some areas redundant, operation during the flight application, but also the means of complete functional checkout after completion of assembly, preflight, and launch operations.

Before entering the area of ground checkout equipment, a few words should be said about some features in the vehicle system. Since eight engines have to be operated during the propelled flight phase, the probability of one engine failure cannot be overlooked. The engine start and cutoff sequences have been described before. If one engine is lost due to some malfunction, a hazardous condition may be created for the overall system. Since combustion chamber pressure is sensed as the criterion for proper engine behavior, this indication is utilized to cut a particular engine off. The eight engines are in individual compartments, and a fire in one compartment should be localized to that area. All propellant supply will be shut off properly by sequence; however, a fire or minor explosion may destroy all electrical lines in this engine compartment. The design provides short circuit protection; one short of any operational electrical line to another or to the vehicle structure below the fire wall will not affect the rest of the system. All measuring pickups in each engine area are also fed by its own measuring power supply. These pickups are protected by line resistors to maintain operation in this troubled area as long as possible while not affecting the measurements in other areas of the vehicle.

All circuits for vehicle destruction are completely redundant, from power source to explosive train. For future application, an exploding bridgewire system will be introduced for all ordnance items as substitutes for the present sensitive squibs in which elaborate protective circuitry complicates the system unnecessarily.

The function of the ground checkout system for the Saturn is not a new concept. As in previous projects, it is still designed to checkout

all vehicle circuits in various subsystem tests. All subsystems are checked out and qualified, then the overall system is operated with the same equipment, bypassing all inapplicable subsystems test circuits. The overall systems test, if fully automated in itself, creates signals in the ground checkout equipment and returns the resultant stimulus for the next step in the automated process. This method will consider all critical functions during the countdown, and a failure at any point of the sequence will stop the countdown and return the system to a safe condition.

Since the complexity of the entire system is considerably increased compared with other known systems, new methods of manufacturing are being established. The rack and panel concept was introduced to build up the entire system by use of modules. Distribution racks were designed on which standardized connectors are wired to an IBM patchboard. This results in standardization and a high degree of flexibility. The connectors will receive either an incoming or an outgoing cable. They will also receive standardized relay modules, diode modules, resistor modules, transistor modules, etc. Standardized modules and the racks with the connectors can be fabricated in quantity long before circuit definition. After the system circuits are established and detailed design is finished, the IBM patchwork will interconnect all modules. This patchboard can be defined late in the schedule to incorporate all design refinements or changes. In the area of control panels this system cannot be adapted readily; however, standardization of panels and components has been maintained throughout the program and stages involved so far. This has considerably shortened the design and manufacturing time, as well as lowering the cost.

For the present, the same equipment used for checkout will be used for stage static firings as well as for final checkout at the manufacturing site and launch site. The concept, as described, will serve the overall Saturn system as long as it stays with the present scheme of operation. The system proved itself to be extremely satisfactory at the first Saturn firing; no technical difficulties arose during the countdown and inflight operation.

The problem of increased distance between launch pad and blockhouse will dictate a different overall scheme for several reasons. The main reason is the safety distance in the case of a mishap. This and other considerations, such as increased firing density, quicker checkout, and better data retrieval, lead into a new scheme of vehicle electrical systems for the single stage as well as for the assembled configuration. A scheme will be chosen to standardize stage checkout at the manufacturer's site for all stages of the system, and to continue to launch operations. The scheme will make use of a digital method and the automation of all system checks.



The question may arise as to the necessity of automating to this degree, since the present automated countdown has worked satisfactorily. Before going into this major effort of generating a sophisticated automatic system, the advantages and disadvantages should be discussed. If a properly operating system is assumed, the biggest advantage to be gained will be improvement of the overall systems reliability, and an overall time saving for various phases of testing and launch preparation. The human error can be eliminated in the checkout procedure. Standardized testing will occur throughout the vehicle test program and complete test results will be printed out and available for design improvement studies. Since running time utilized for the testing procedure will be cut to a minimum, the effective mean time-to-failure ratio for the vehicle will be increased.

Once a system is correctly automated, more thorough testing can be achieved in much less time than in the manual case. Therefore, the confidence of firing personnel in the flight hardware can be increased. When a system failure has been noted, the exact condition under which the failure occurred can be easily duplicated. More complete data can be gathered at the instant of failure to aid in trouble-shooting and fault isolation. The anticipated schedules for Saturn flights will require automation of the checkout procedures to save time and to make the best use of personnel.

Since the advantages have been reviewed, we can now look at the disadvantages and the reasons of failure of some known automated systems. The first disadvantage is the complexity introduced in an overall system by adding automated features. The complexity in many cases has been generated, not because it was required, but rather because of conditions under which the design occurred. Lack of confidence in the system on part of the user in many cases has been another disadvantage for automated systems. Inadequate learning time for the user has resulted because of poor planning and crash program conditions. One of the major reasons for automatic checkout system failures has been inadequate planning in the area of checkout program generation—those instructions in machine language that tell each component exactly what to do. More than one program has resulted in capable, but ignorant, checkout hardware.

Another item that should not be overlooked is the degeneration of operator knowledge about the total system in the presence of working automation. A system may work so well that the operators lose touch with the actual process being carried out; when there is trouble, panic and lost time occur. Any well thought-out automation program must consider and overcome these disadvantages.

The state of the art in various types of checkout equipment, both analog and digital, has greatly improved over the last few years. It is possible to obtain reliable conversion and processing equipment to work

with digital intelligence equipment of greater reliability than ever before. It is now possible to foresee a checkout system made up of existing equipment that is reliable and accurate. In the Saturn program it will be possible to have checkout equipment operating in an air conditioned environment. It can be operated by engineering personnel and subjected to preventive maintenance, and it can achieve the reliability currently expected of industrial automation. Once a system is working, it can be expected to continue to do so. An automatic checkout system tailored specifically to the needs of the Saturn and Nova programs can be generated with a high degree of confidence that the system will work properly.

The following automation requirements should be followed for overall system:

1. The development must cover all foreseeable programs from Saturn C-1 through Nova.
2. The same technologies, in fact the same hardware wherever possible, should be used throughout the Saturn-Nova developments, just as vehicle technologies in hardware are being utilized from one vehicle configuration to another.
3. The hardware and techniques developed must fit into the plans and facilities of both the contractor and the launch site.
4. The system must provide for both manual and automatic operation in an either/or fashion until user confidence and training are adequate.
5. Maximum time should be provided for personnel training and systems design proofing.
6. The test programming of delivered hardware will be adequate and proven.
7. A systematic method of data processing must be developed to handle the large flow of test results and performance history generated by the automatic process.

Before discussing the various checkout configurations and plans, it is necessary to clarify and define certain operations and test conditions. The vehicle measurements and controls are separated into: (1) operational measurements and controls used to prepare and launch the vehicle; and (2) telemetry measurements used to evaluate flight performance.

Measurements of the state of the vehicle are needed for both vehicle operation and for measuring programs. Such measurements go both to the operational equipment and to the telemetry system. Prior to assembly, the stage also has operational and measuring and telemetry checkout requirements. Separate stage interface GSE is generated as an integral part of the stage design. The equipment may be no more than a standard electrical distribution system or, in some cases, it may contain controls and manual monitoring equipment. Some versions may have such items as analog to digital conversion equipment to allow proper mating with digital ground support equipment.

Stage interface GSE is broken into two main categories: circuitry concerned with the operational task, and circuitry utilized to manipulate and evaluate the measuring and telemetry hardware. Here the stage and its interface GSE are connected to the facility test equipment. Non-electrical stimuli, such as pressures, are fed directly from the facility test equipment to the vehicle. To properly simulate upper and lower interfaces, stage substitutes are provided so that the entire operation can be evaluated. In the case of liquid propulsion stages, most of this operation would be concerned with evaluating and calibrating the outputs of the various measuring adapters contained within the stage. The future development of an rf link can reduce the number of hard wires which travel through the stage interface GSE. Interface GSE for measuring and telemetry systems will consist of electrical measurement stimulation circuitry and a set of digital acquisitional equipment.

At the launch site all measuring and telemetry information can be received through an rf link from each stage or up to launch day through a coaxial cable to avoid radiation. All of the operational portions of the stage interface GSE are connected to the operational and launch equipment, thus completing the circuitry required to prepare and launch the vehicle. The intelligence and comparison units to handle the operational measurements and controls of the vehicle system will be the computer complex. The heart of this complex will be a medium-size general-purpose digital computer, which will handle the digital guidance equipment. The computer will be expanded to handle the various types of analog and digital equipment in operational checkout. It also will generate commands and data to preset and launch the vehicle.

As soon as the digital guidance system is introduced in the present Saturn C-1 configuration, automatic checkout equipment will be installed at the stage contractor site as well as at the launch site. For a number of vehicles, the dual capability of manual and automatic checkout possibilities will be available until the new digital checkout system can be proven. By the time the Saturn C-4 configuration is ready to be launched, it will be mandatory that the new automatic checkout scheme with the digital mode be operational because the distances between launch site and control room are so great that no other method will be possible.

The new automatic system will demand an extreme amount of engineering discipline, and enforcement of standardization at the stage contractor's plant as well as at the launch site, to make the system reliable and to achieve our goal.

## 30

## THE PROPELLANT MANAGEMENT FIELD

Helmut Zoike

Servomechanisms, Inc.  
Goleta, California

This paper details the development and evolution of the field of propellant management, especially that using the so-called differential pressure or  $\Delta p$  method.

It will deal with

1. Defining subsystems that make for propellant management
2. Problem and design considerations for these subsystems
3. Evolution of these subsystems (Treatment is of basic principles, with more detailed exposition in references.)

The reasons for the selection of the  $\Delta p$  approach over other competitive approaches are outlined in an extensive analysis [1] and as a short summary [2].

This study shows a clear advantage for the  $\Delta p$  method, particularly in accuracy, maintainability, ease of calibration, and real checkout of the system as well as basic flexibility of the system for changes due to later improvements. A report that compares other propellant management systems is [3].

Furthermore, 5 yrs of practical experience with the  $\Delta p$  method shows the advantages claimed for these systems. A continuing engineering and development program in the propellant management field assures further advantages and benefits.

### 30.1 Review of Propellant Management Problems

#### 30.1.1 What is Propellant Management?

Any system that secures or contributes to the goal of making sure that the propellants are handled in such a way that they are delivered into tanks and consumed at the right rate and in the right ratio so that the tanks are empty at the cutoff points is one concerned with propellant management. Only in this way will the chemical energy of the propellants be fully utilized. To accomplish this goal, several control functions have to be performed in several subsystems as follows:

Propellant Tanking. The propellant tanks must be filled within the limits of the required accuracy. This is a requirement that has two purposes:

1. To establish as accurately as possible the total takeoff weight of the vehicle, since the propellants constitute by far the major weight of the total vehicle. This is a very important factor, which, if controlled accurately, can bring a substantial payload increase.

2. To give the craft enough fuel and oxidizer, so that its powerplant can operate as efficiently as possible, and produce the total impulse expected.

Propellant Utilization. The tanks must be emptied so that nothing remains, but it is not mandatory to operate exactly at the optimum engine mixture ratio to attain optimum propellant utilization. In other words, it is more important to empty the tanks completely than to run the engine on optimum mixture ratio.

Thrust Control. To achieve the right rate of propellant consumption, a separate thrust control system is necessary. It attains the total mass-flow rates of the propellants needed to obtain the required thrust independent of the propellant utilization system. Actually, the system is misnamed as a thrust control system, since the variable that is controlled is the combustion chamber pressure and not the thrust directly. Thrust cannot be measured as easily or accurately as combustion chamber pressure and requires a complex and expensive measuring system. However, since the combustion chamber is test-fired and the relationship of combustion chamber pressure to thrust is determined quite accurately, it represents a very good secondary control signal for such a system.

Pressure Switches. In a complex, multi-engine power plant there are several control functions that can best be accomplished with simple, on-off control devices, the most important of which is the pressure switch. A few selected examples of its use will show the importance of this control element in propellant management systems. It is utilized as an indicator of proper operation of all engines in a cluster before takeoff before release of the missile from the launch platform. Furthermore, the same switch can be used as a control element for an "engine out" indication during flight.

A different control function of pressure switches is their use as overflow switches for the Saturn oxidizer and fuel tanks. They are safety devices that cut off the propellant supply valves in case of malfunction in the propellant tanking system. Another typical use of pressure switches is in tank pressurization control. The large quantity of pressurizing gas is delivered most efficiently through an electromagnetic valve controlled by a pressure switch.

### 30.1.2 Common Problems in Propellant Management

There are a number of problems common to several or all propellant management subsystems. In approximate order of importance, they are:

1. Reliability
2. Accuracy
3. Extreme environmental conditions
4. Maintainability
5. Tank shapes
6. Pressure transducers
7. Pressure sensing methods
8. Oxidizer fuel compatibility
9. Systems integration problems
10. Minimization of size, weight and power consumption

**Reliability.** The reliability of any propellant management subsystem must be considered foremost. This requirement is particularly true for subsystems used within a manned spacecraft. The complexity of large, multi-stage space vehicles leaves no room for subsystems that are marginal in performance or functional reliability. Everyone agrees upon the necessity for reliability, but the problem lies in its achievement. A discussion of reliability is not within the scope of this short chapter, but its importance is paramount. The organization of reliability procedures must be detailed in every phase of engineering and manufacturing as a guide for everyone to follow [4].

**Accuracy.** The required accuracy of any propellant subsystem is determined by the over-all system requirements. Not every vehicle system needs a propellant utilization control system, thrust control system, or propellant tanking system. This makes evident a basic difference in the methods available to the system engineer for achieving his desired results. These are called the open-loop to differentiate from the closed-loop approach. For many years, power plants of large vehicles were controlled by the open-loop method in which the desired performance was achieved by a preset or calibrated system. In this method one relies on the repeatability of a great number of components and processes in a power plant. This method has basic limitations in that the processes involved cannot always be made as repeatable as required, and it is inadequate for many missions. The solution lies in the use of a closed-loop system, in which a variable is compared to a desired value the difference used to reset the variable to a correct value that is independent of the variations of components and processes involved.

The accuracies attainable in the open-loop vary with the design and basic nature of the different subsystems as well as the integrity of the closed-loop system performance. But in general performance improvements by factors from 5 to as much as 20 have been achieved with several propellant management subsystem designs.

If a system can stand the inaccuracies of an open-loop system, there is no need to consider a closed-loop system. But high-performance systems need closed-loop controls, with consequent benefits in range and payload. There is an exception to this in certain clustered engine power plants such as the Saturn. The use of eight engines in this design effectively averages the engine tolerances, making it unnecessary to resort to a closed-loop control system.

As mentioned above, the systems discussed here are limited to  $\Delta p$  methods; and, therefore, pressure measuring devices are used as sensors for the control loops. One compelling reason for this use is that the art of pressure measuring is very advanced. Accuracies achievable for control purposes are as good as 0.02 to 0.03 per cent of full range. These are performances that, in earlier days, were hoped for in a calibration laboratory but not in a rocket power plant.

Extreme Environmental Conditions. It is generally agreed that the vibration produced by a vehicle is the prime enemy of instrumentation and control systems. The reason is that the vibration is, in comparison to that of aircraft, extremely high. This is true in G-level as well as in the frequency range. Levels up to 100 G's or higher are encountered. Frequencies up to 2000 or 3000 cps are typical. The vibration problem is made still greater because the acoustic noise is severe. This requires that test facilities be available for frequencies up to 20,000 or 50,000 cps and for high decibel values. The determination of the vibration frequency spectrum of a particular vehicle or power plant is a very cumbersome and painstaking task. However, because of the different suspension and couplings used between the vehicle and test stand and the actual flight condition, the value of these tests is at best questionable. In general, they represent maximum values. It is probable that vibrations are reduced in magnitude. Random noise testing of equipment has evolved more as representing test condition simulation than of actual frequency behavior of a power plant or vehicle.

The conventional method of solving vibration problems in aircraft instruments or equipment with shock mounts is not applicable to spacecraft since the proper design of a shock-mount suspension requires knowledge of a frequency spectrum before the spectrum is readily available from flight testing. In fact, a haphazard use of shock mounts in a missile can produce exactly the opposite results if the system resonates. Therefore, it should be considered only if no other possible solution can be found.

Temperatures encountered in a vehicle can vary within extreme values. The use of liquid oxygen or hydrogen as propellants makes possible temperatures of  $-200^{\circ}\text{F}$  or  $-300^{\circ}\text{F}$ . In the high-temperature range, aerodynamic heating and hot gases in the power plant or tail section can reach  $1000^{\circ}\text{F}$ . Proper design to protect against these extremes is necessary and can

reduce the limits in most cases to those acceptable by the instruments. Insulation against high and low temperature extremes is required; and active temperature control with heaters, electrical blankets, and ovens may be necessary. However, it is not always possible to reduce the ambient conditions for the instruments or control systems to the desired level. Then the instrument has to be designed for the extreme condition, such as pressure transducers or pressure switches capable of operating at temperatures down to  $-250^{\circ}\text{F}$  or transducers in high temperatures up to  $600^{\circ}\text{F}$ . This represents an advancement of the state of the art in transducer design [5].

Another problem in propellant management is the acceleration experienced during the flight. Accelerations up to 15 G's have to be considered. However, in comparison with the vibrational acceleration, they represent only a minor problem. The influence of acceleration, however, can be of importance if the required accuracies in the sensors are extremely high. Proper design of the sensors with a minimum of acceleration sensitivity provides a solution to the problem.

Maintainability will be a problem in a complex vehicle system as long as complete reliability is unattainable. Since this goal will take a long time to be realized, if at all, an easy and efficient way must be found to maintain the vehicle. Modular design with quickly exchangeable, functional modules is one answer; and automatic checkout is required, indicating the functional and operational readiness of the system. The checkout procedure must indicate the faulty component or module so that a quick exchange can be made.

In regard to propellant management, a problem exists in that a great number of systems requires the sensors to be placed within the tanks. If a malfunction occurs, it is impossible for long sensors within the tanks to be replaced without a total disassembly of the vehicle. This is particularly true in case of variable capacitance sensors. This becomes a problem of some magnitude in three or four-stage vehicles such as Saturn.

The  $\Delta p$  method, on the contrary, has no functional parts within the tanks. The sensor is located in a convenient position near the tank and is connected only through the pressure sensing lines. The sensor can be replaced within minutes, since only two pressure connections and one electrical plug are disconnected for each tank. This is one of the chief advantages of  $\Delta p$  method as opposed to a capacitance system or any other that requires sensors within the tanks. A further advantage of the  $\Delta p$  method is that it is easily calibrated and checked. The actual input to the sensors represents the actual pressure simulation of the liquid level in the tanks. In a capacitance system this is not possible since the tanks cannot be filled. Only a substitution of an equivalent electrical capacitance for the capacitance of fuel or oxidizer can be done. But this does not check the most important part of the system and is certainly



an undesirable feature. Particularly in a high-impedance, low-level signal system, such as a capacitor sensor, electrical leakage problems can be created that are not easily handled in a vehicle system.

Tank Shapes. Most of the better known propellant management systems require calibration of the tank volume against the sensing element. The  $\Delta p$  method is no exception. The basic equation that governs the operation of the system is  $\Delta p = \rho Gh$ , where  $\Delta p$  is pressure difference,  $\rho$  = density of propellant,  $G$  is the acceleration constant and  $h$  is the liquid level height from some reference point. If we consider the problem of propellant tanking in which the acceleration constant is known for the launching site, only the density and height are variables. These variables as are considered as the mass level as opposed to the volume level of other point sensing methods. Since the designer is interested in the total propellant mass, this method gives the desired quantity is a direct way. Thus, density variations through temperature or batch are of no consequence, since the height for an equal  $\Delta p$  would change accordingly. This is only true in a symmetrical tank that does not change in cross sections, as in a cylindrical tank without shaped bottom or top. Unfortunately, such a tank is impossible in a practical vehicle design. A shaped tank, however, brings in, by definition, a variable volume-to-height relationship. Density changes will not be corrected automatically, but as a function of the shape alone. This can be overcome by making the output of the  $\Delta p$  output transducer a function of tank shape.

To a certain degree, the shaped top or bottom can even be helpful since the same incremental pressure change may represent a much smaller propellant change. This, depending on shape, may be an increase of sensitivity of 1:2 or 1:3. In a propellant utilization system, a similar consideration exists. Since we are interested in the ratio of the two propellants, it is important only that the tank shapes at the bottom are similar. In most cases this is true. A good example is a system in which two spheres are used as propellant tanks. This is relatively easy, if the tanks are filled and emptied in the ratio of their respective volumes [6].

Pressure Sensing Methods. For several reasons, it is desirable that the pressure sensor not be directly in contact with the propellant. In some cases the propellants (for example, liquid fluorine) are highly toxic and corrosive. For liquid oxygen and liquid hydrogen, the low temperature of the liquids prohibits direct contact. In any case, it is advantageous to place the sensor where the ambient conditions are more favorable.

Several methods are available:

1. The gas balance method (purging method)
2. The gasifier method
3. The inverted bell method (Cartesian diver) [7]
4. Combinations of the above

The two methods most used are described briefly below.

**The Gas Balance Method.** In the gas balance method, a purging gas is used to balance the static pressure of the liquid to be measured with a gas pressure of equal value. This is done in the simplest form by placing a dip tube into the tank from the top to a depth considered the lowest point to be measured (reference level). Another pressure line is connected to the gas pressure on top of the liquid (Fig. 30.1A).

**The Gasifier Method.** In the gasifier method the natural properties of a cryogenic fluid are utilized to gasify the liquid before it is piped to the sensor. The pressure line connecting the tank to the sensor acts as a heat exchanger that gasifies the liquid at the entrance of the pressure line. Since the system represents a dead-end service, no flow is established that could transport liquid into the sensor.

Difficulties arise because the gasifying process is inherently unstable and provides a pulsating pressure not uniform enough to serve as a control system input. Suitable damping has to be provided to reduce the magnitude of the oscillating pressure to an acceptable level (Fig. 30.1B).

**Pressure Transducers.** All the systems described utilize, in one way or another, a pressure transducer as the sensing element for the desired control function. The transducer is the heart of each control system and has to have extremely good accuracy under severe environmental conditions. Two different methods have been employed to fulfill these requirements. One method is the force-balance method described in detail in Ref. [8]. The other is the Bourdon tube transducer described below.

Pressure transducers are composed of two basic components: a pressure sensitive element that converts pressure to mechanical displacement, and a pickoff that converts this displacement to a useful electrical output.

The configuration of the pressure sensitive element is a torsional Bourdon tube whose output is an angular motion of the free end of the element (Fig. 30.2). The torsional Bourdon tube is so designed that the sensitivity to pressure in this angular mode is far greater than the sensitivity to acceleration, shock, and vibration in linear modes. The tube is made of Ni-Span-C, a material which exhibits low hysteresis and, within a certain temperature range, has low temperature sensitivity. The tube is four-fluted, insuring uniform high rigidity in all linear directions.

The pickoff is a four-pole reluctance bridge. An armature composed of magnetic material attached to the free end of the tube changes the balance of the bridge as the tube rotates. The symmetrical design of the pickoff results in a sensitivity to angular rotation only; purely linear motions of the magnetic armature do not cause a bridge unbalance.

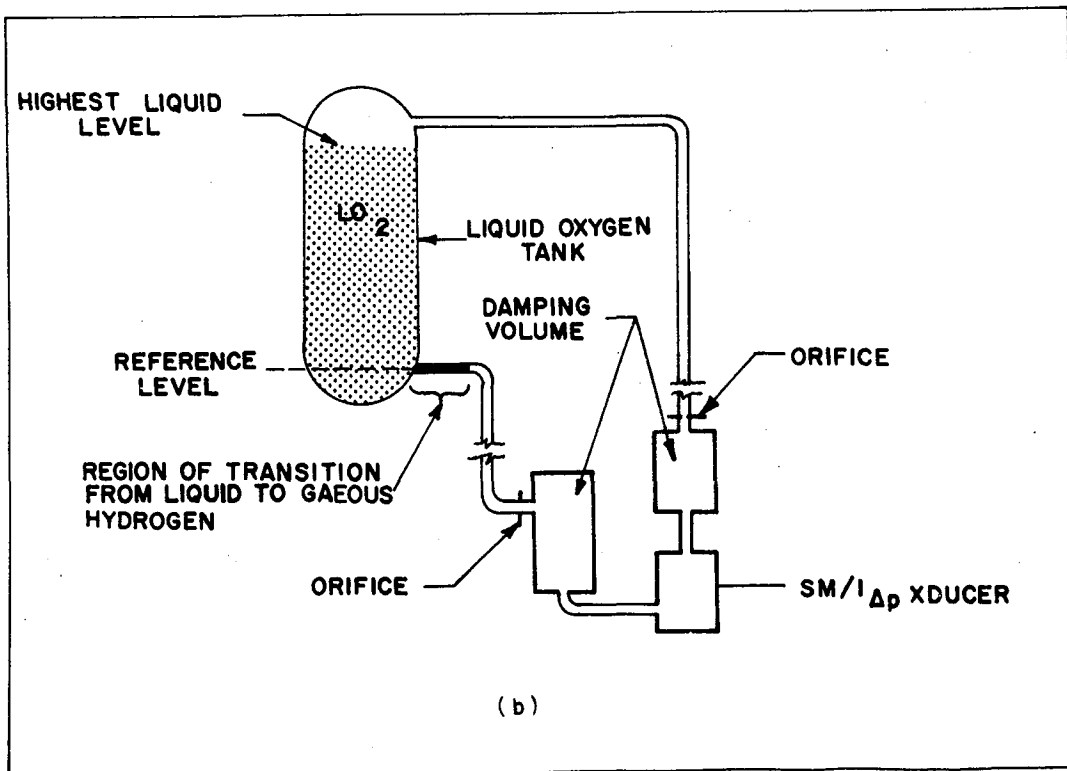
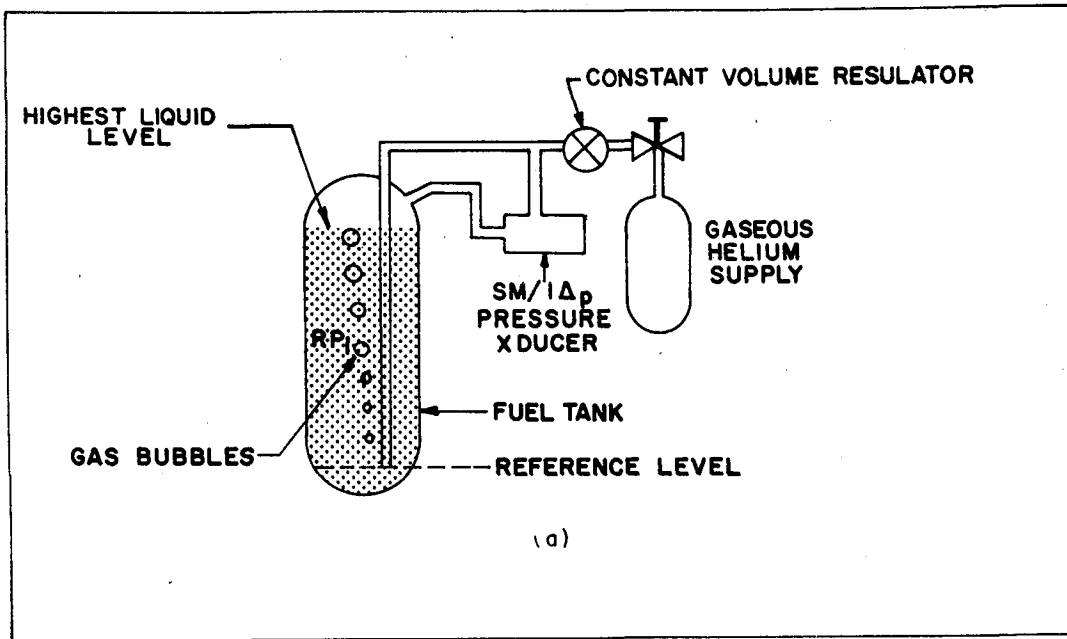


Fig. 30.1 The gas balance method (a) and the gasifier method (b).

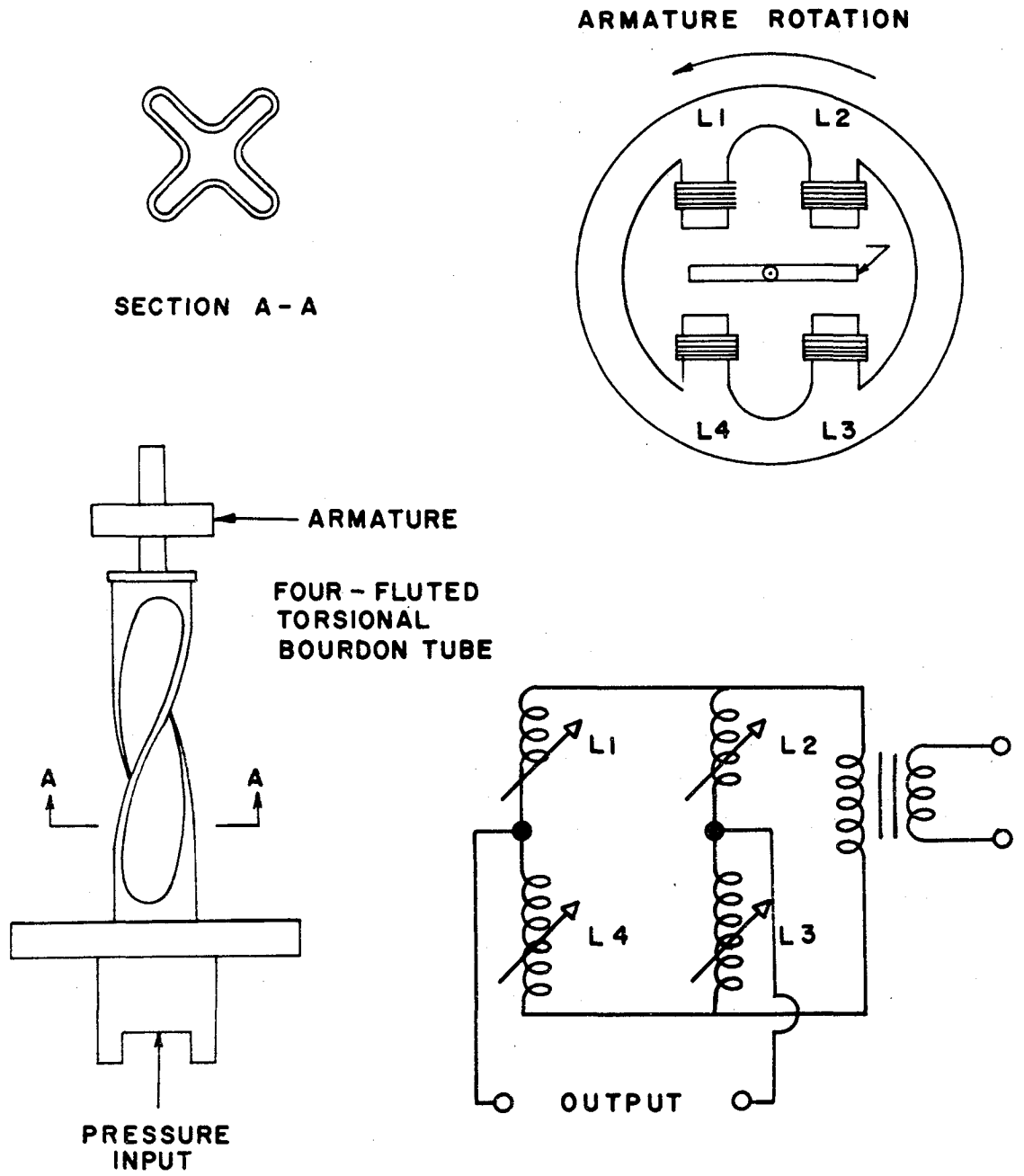


Fig. 30.2 Basic Bourdon tube transducer elements.

Compatibility of oxidizer and fuel with the pressure transducer is a requirement that poses a problem for the instrumentation designer. Oxygen compatibility is a particular problem, since it requires that the sensing elements in contact with liquid or gaseous oxygen be made of inorganic materials. This is not easy in an electrical transducer with organic insulation materials. The pickoff in a Bourdon tube transducer uses epoxy encapsulation materials. The transducer is plated with either cadmium or gold, and no part within the transducer is exposed to gaseous oxygen. Fuel compatibility in present systems does not present a problem. In future systems using corrosive fuels, it can probably be solved in the same way by goldplating the components.

**Systems Integration Problems.** One of the big problems of the designer of propellant management systems is that the systems are not considered early enough in the over-all vehicle design. The reason for this is twofold. In general, no ready components for such systems are available, and performance is doubtful, or at least not proven, so most systems for propellant management have to be initiated subsequently. This creates the problem of integrating the system into an existing power plant. Another problem comes from the fact that control systems, in most cases, are organizationally separate from the power plant. The control valve, however, is a part of the power plant. Hence, a competitive problem usually develops. Design of the valve by the power plant group, without adequate consideration of the control problems, usually fails. Often attempts are made to combine even the shutoff function with the control function. This creates a design limitation for each function and solves neither problem well. In any case, the two functions should always be performed by separate valves. Another consideration of importance is whether control should be done in the main line or the bypass line. This is also connected with the fail-safe design of the system. For example, if a propellant valve for a propellant utilization system is placed in the main line, then any malfunction will shut off the full power plant.

On the other hand, if control is accomplished with a bypass valve with capacity just sufficient to accommodate the maximum control range, then a malfunction of the valve or system can only cause the system to revert to an uncontrolled state. This situation is hardly catastrophic as a consequence of the fact that the control range is usually about 5 per cent to 10 per cent of the total flow. To drive a valve in the main line requires a much bigger control valve and more control power; thus, the whole system grows to the point of impracticality. A bypass control system can usually be built to a fraction of the size and to require a fraction of the power. In many cases a totally different drive system both simpler and more reliable, can be selected for a control valve in the bypass line.

**Small Size, Weight, and Power Consumption.** Since the main purpose of propellant management is to save weight and utilize all propellants, it is obvious that the additional weight of such a system should be as small as

possible; otherwise, such a system loses much of its appeal. Formerly it was expected that typical propellant utilization systems would weigh about 100 to 150 lb. However, propellant utilization systems using the  $\Delta t$  method are much lighter. Some systems weigh no more than 20 lb including all brackets and pipelines.

If bypass control valves are used, then power consumption is reduced considerably. This use requires a valve that minimizes the necessary friction and driving forces. For example, for the Saturn, a 2-in. fuel control valve was developed that can be driven by a 2-w motor. Consequently, the power amplifier and power supplies in such a system are much smaller than other valve designs. Therefore, it is possible to design a propellant utilization system with about 30 to 40 w of power consumption.

## 30.2 Propellant Tanking Systems

### 30.2.1 LOX Tanks

The simplest and oldest LOX tanking control is the so-called overflow pipe. This is a vertical pipe within the tank reaching to the desired level and open at the top. As soon as the LOX reaches the level, it overflows into the pipe, and is carried outside the tank. This system was used successfully in the V-2 rockets. The basic disadvantage is that it is fixed and suitable for only one particular fill level. Small variations in level are accomplished by using a variable-length fillpipe, the length of which is changed by a flexible bellows. An obvious disadvantage is that LOX spills around the vehicle when the pipe overflows.

A more sophisticated approach for a variable level was developed for the V-2 in the form of a temperature-sensitive bridge circuit. In this case, a balanced Wheatstone bridge was designed, one arm of which was placed in the LOX tank at a variable level. As soon as the LOX reached this flat coil, its resistance was changed by the temperature of the LOX. The unbalanced bridge switched a polarized relay. The relay contact then switched an indicator, and the operator shut off an electromagnetic control valve. With this system, reasonably good accuracies were achieved, but such an open-loop system left much to be desired.

The first closed-loop LOX control system was developed for the Jupiter guided missile. At the time of its conception not enough experience was available to predict the attainable accuracy. Two approaches were chosen. A Bourdon tube transducer was selected with an estimated accuracy of better than 0.5 per cent. However, the requirements at the time were to reach an accuracy of 0.1 per cent of the total LOX weight. Since no guarantee could be given that the long-term stability and repeatability of the Bourdon tube transducer would be that good, a parallel approach was selected and developed.

Beam Balance LOX Tanking System, AXC 2004. This approach utilized a beam-balance sensor, with a weight as the reference, balanced against a force created by the  $\Delta p$  in a pair of bellows. This system, having a highly suppressed zero point, reached an accuracy of better than 0.1 per cent; but, in comparison with the Bourdon tube transducer, it proved to be much more complex and expensive. Since the Bourdon tube transducer later also reached nearly the same performance as the much more sophisticated beam-balance method, it was logical to abandon the latter. A photograph of the force beam-balance, computer type, AXC 2004 is shown in Fig. 30.3.

Bourdon Tube LOX Tanking System, TMC 601. The LOX tanking system, TMC 601, finally used in the Jupiter system actually measures, controls, and indicates the level of LOX in the tank. The entire computer is encased in a protective cover designed to withstand the extreme conditions generated by a missile firing. The computer monitors the weight of the propellant aboard the missile, compares it with the desired weight, allows for tank diameter and propellant density correction, and controls the flow of propellants to the missile. The basic principle of the system is again the  $\Delta p$  method measuring the static head of the liquid in a tank by means of a highly refined pressure transducer. A two-mode control system (Fig. 30.4) facilitates the rapid and accurate loading of the missile. The first mode permits extremely high pumping rates until approximately 98 per cent capacity is reached. The second mode then takes over with much lower flow rates and controls the pneumatic proportional valve that adds the necessary LOX to fill the tanks completely. The second mode also provides for continuous topping, thus compensating for LOX evaporation losses during standby. The system furnishes local and remote indications, either as analog dial outputs or as a go and no-go system of lights [9, 10] (Fig. 30.5).

This system proved the  $\Delta p$  method beyond doubt. Actual comparison testing on a weight scale proved that the system had a maximum error of 0.15 per cent expected [11]. Several hundred of these computers were built and used in the field.

Wide-Range LOX Tanking Computers, TMC 602. The next step in tanking computers came with the requirement for the Jupiter-based space boosters. These vehicles differed in requirements from the operational computer for tactical use since the LOX level had to be variable over a much wider range of LOX weight. Furthermore, a digital indication was desirable, instead of the go and no-go signals. The wide-range computer, TMC 602, was developed. In principle, these computers were like the former type but had an output in the form of a digital ratiometer calibrated in per cent of the desired filling.

Saturn LOX Tanking Computer, TAC 605. After successful completion of this program, requirements for LOX tanking controls for the Saturn booster had to be developed. The same basic principle was used, although some refinements were incorporated. Because of the expected long standby time and

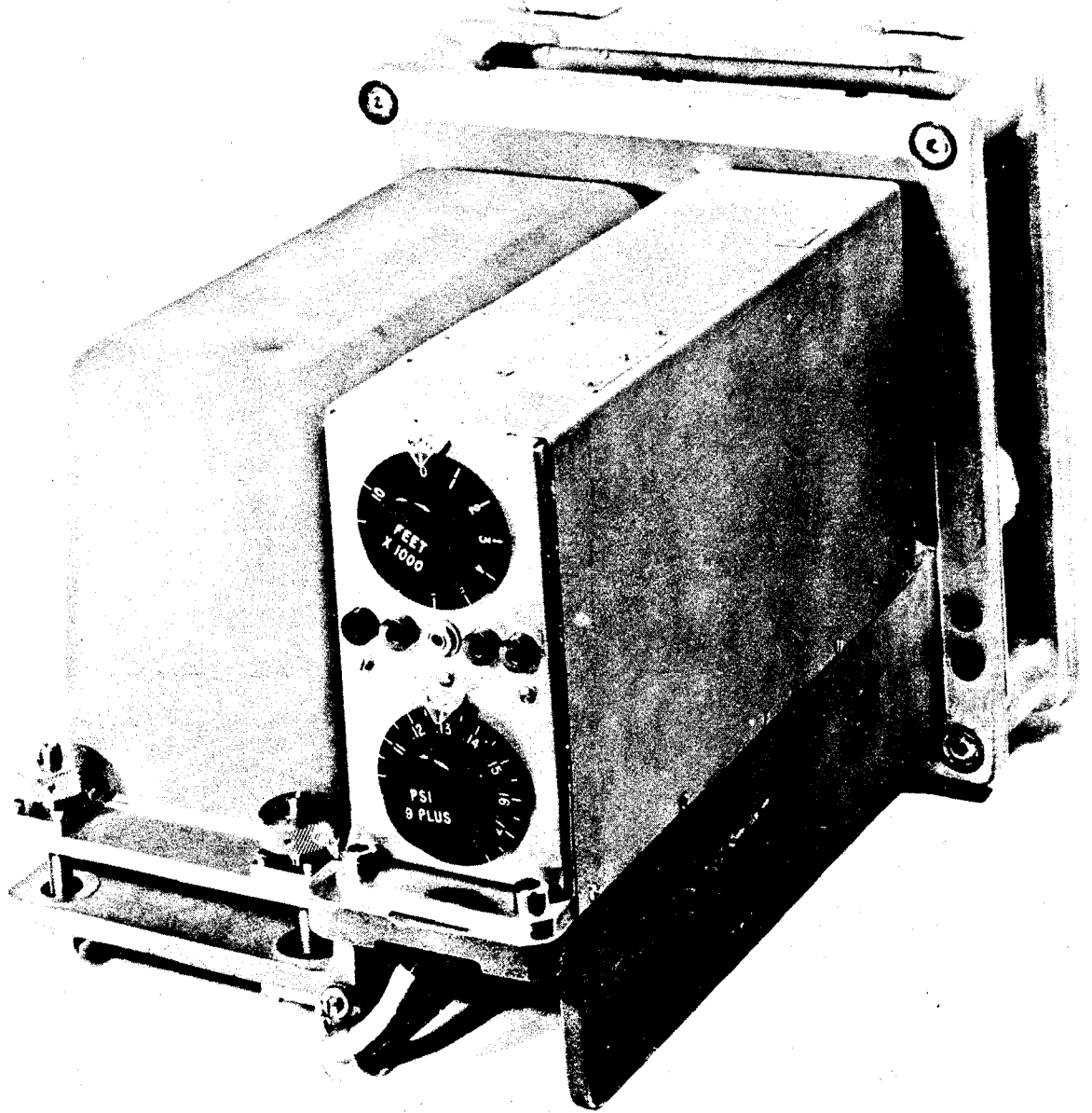


Fig. 30.3 Beam balance LOX tanking computer, AXC 2004.



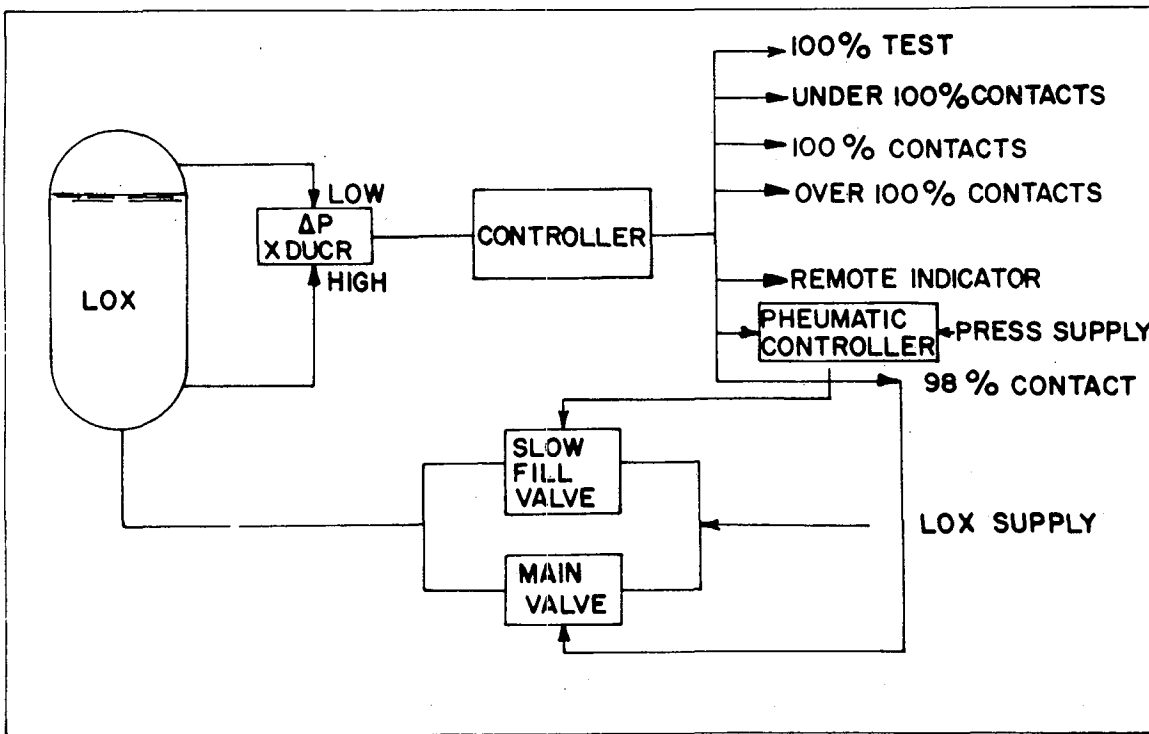
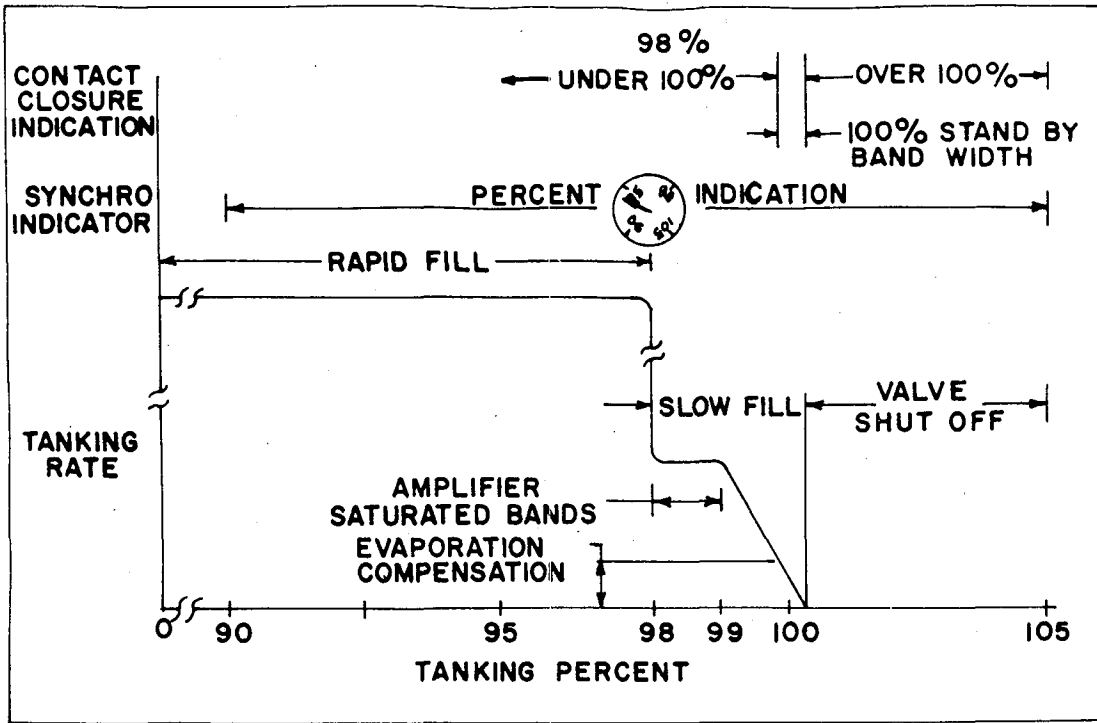


Fig. 30.4 Tanking control modes of TMC 601 (a) and overall system block diagramming of Jupiter (b).

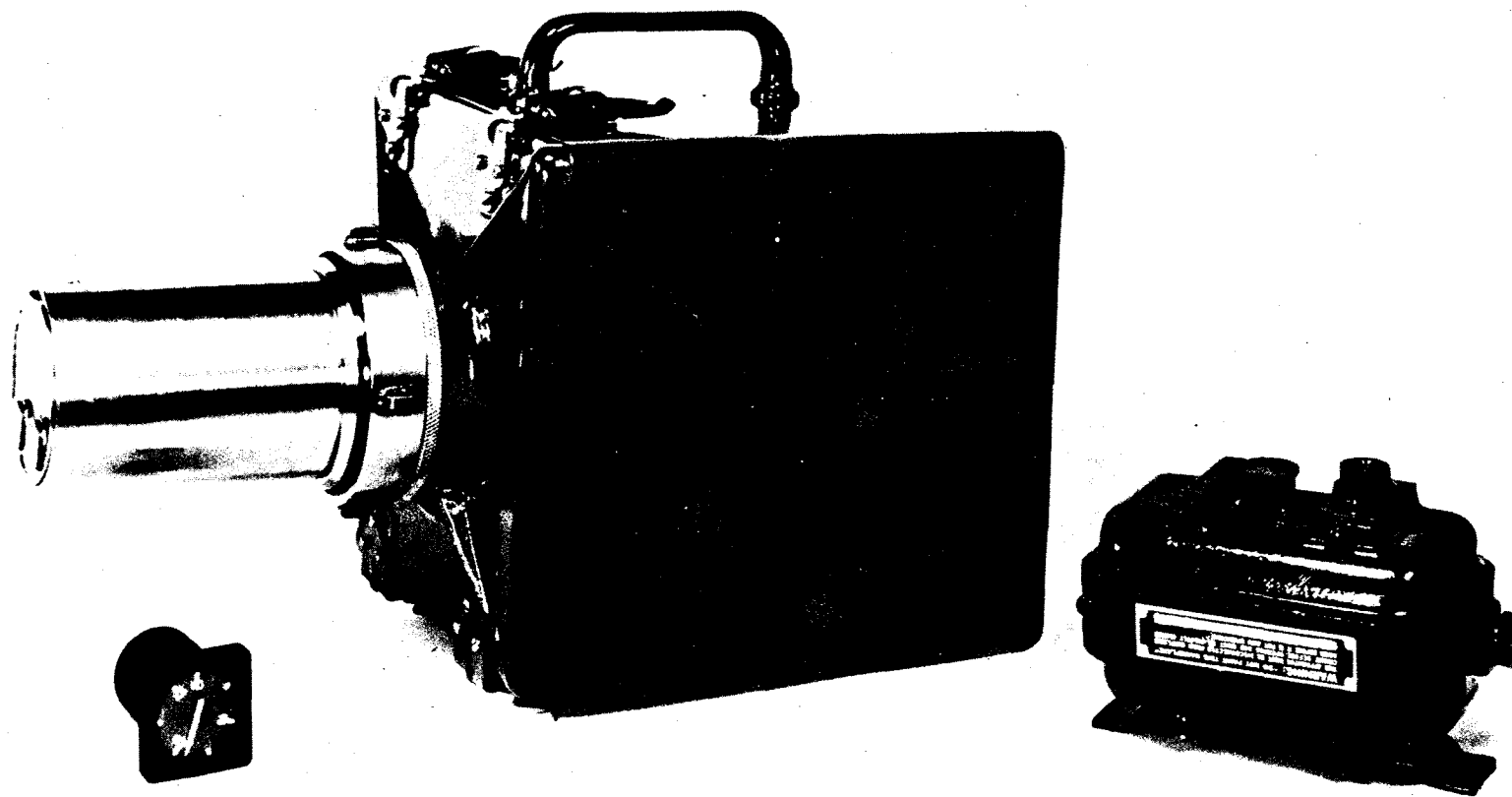


Fig. 30.5 Bourdon tube LOX tanking computer system, TMC 601.

undercooling of the fuel tanks, the ratio of LOX to fuel had to be changed. These changes are made remotely from the blockhouse. A remote dialing system for the pressure correction of the command value is incorporated (Fig. 30.6). This command value is represented in digital form by the nominal command value plus the dialed correction value. The actual control value is represented in a digital voltmeter in per cent of the command value. In addition, a manual adjustment of the LOX evaporation rate is used. This makes it possible to adjust over a wide range of expected evaporation rates without exceeding the control tolerances. Another feature is the automatic system checkout through a checkout signal generator. With help of this device, the system can be functionally checked out before the actual tanking process is under way. Finally, an improved accuracy of  $\pm 0.1$  per cent of the total control system is required. This calls for a pressure transducer stability and repeatability of better than 0.05 per cent. For a while great difficulties were encountered in the control of the material processing of the Ni-Span-C Bourdon tubes. However, after an extensive research and development program, transducers are now delivered that perform with over-all system accuracy of better than  $\pm 0.03$  per cent.

### 30.2.2 Fuel Tanks

Historically, the filling of a vehicle with common fuels such as alcohol and kerosene has never been a major problem. Volume displacement meters, commonly used in filling stations, have the necessary accuracy of 0.1 per cent. Because these meters were available, designers overlooked the small disadvantage: they measured only the volume. Correction for density, by measuring batch density as well as temperature variations, were a nuisance but not a problem. Mass flowmeters with automatic adjustment for density changes were developed. Automatic shutoff features were included by which the total amount of fuel required could be preset; automatic shutoff occurred when this value was reached.

Saturn Fuel Tanking Computer, TAC 606. With the advancement of LOX tanking methods for the Jupiter missile, it became apparent that the same system could be used to great advantage in fuel tanking. The main reason for not using the volume displacement meter method is the increase in size and flow rates of these meters. It is a major problem to calibrate them with the better than 0.1 per cent accuracies required. Test stands for calibration are expensive, and calibration procedures are very laborious.

### 30.2.3 Fuel Density Computer, TAC 607

In the Saturn, a unique problem exists in that the fuel tanks are surrounded on three sides by LOX tanks. In connection with the requirement of a long standby time, this proximity will change the fuel density. Therefore, a continuous measurement of the fuel density is necessary. Again, the same  $\Delta p$  method is utilized to obtain fuel density. Referring to the basic equation where  $\Delta p = \rho Gh$ , it can be seen that if a known

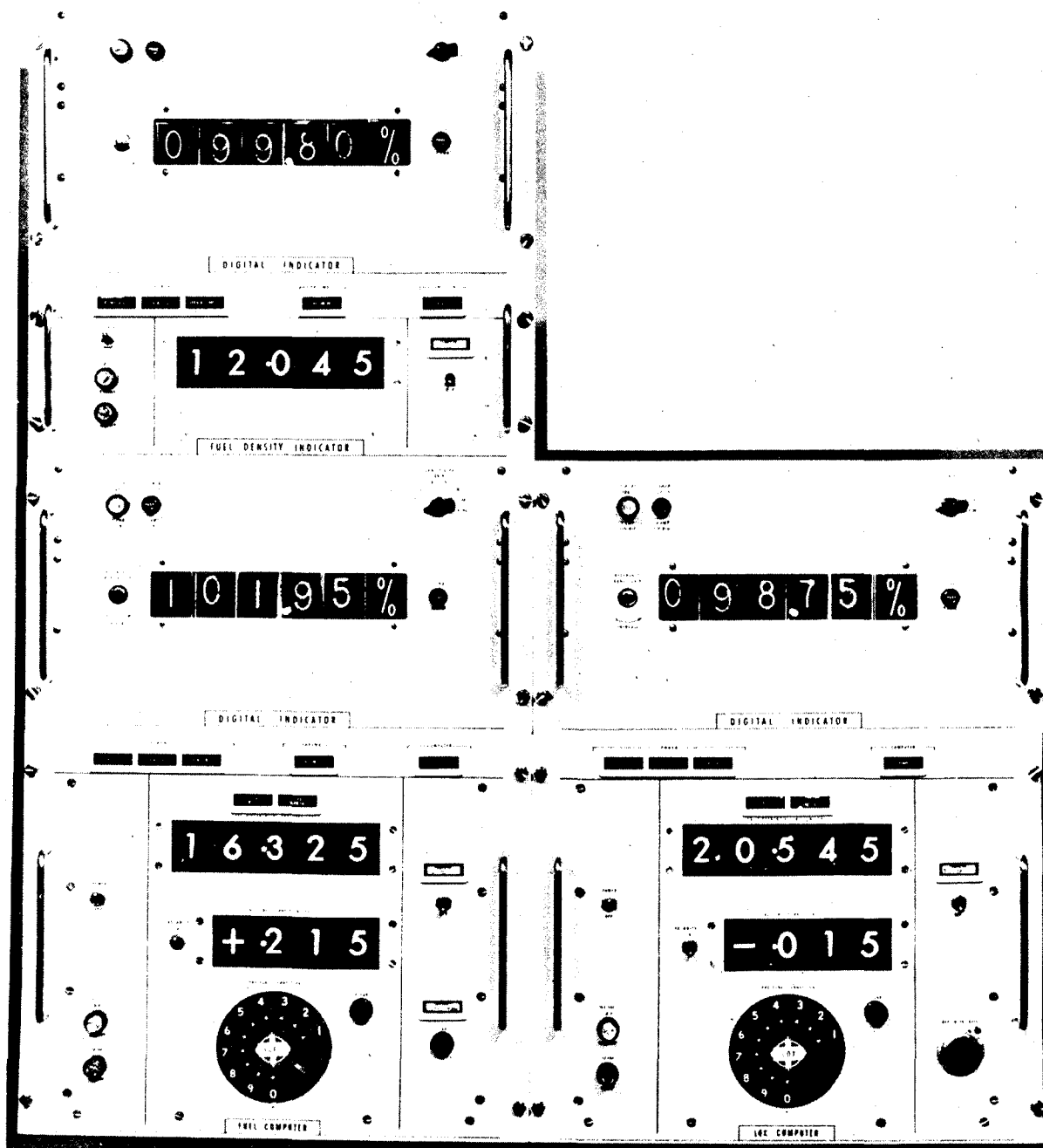


Fig. 30.6 Saturn tanking computers, TAC 605, TAC 606, TAC 607.

height is introduced into the system over which a  $\Delta p$  will be determined, and the acceleration constant for the launching site is known, then  $\Delta p$  measures directly the density of the fluid. One of the main features of determining density by the  $\Delta p$  method is that this method averages the density over the total length of the tank. This procedure is in contrast to other methods that determine the density of the fluid only at one point in the tank. Another requirement is that the tank mass should be variable from 75 per cent to 100 per cent of tank capacity. To get the best average under these conditions, four separate lengths of the upper reference tubes are provided, the most suitable one of which is selected.

#### 30.2.4 Future Propellant Tanking Problems

The propellant tanking system for the Saturn, representing the first model of such a complex system, has proven to be a very accurate and useful piece of equipment. There are still a number of design improvements that can reduce the complexity and increase the reliability.

Pressure Switch, On-Off, Tanking Control System. To increase reliability, studies were undertaken to see whether an on-off tanking control system could be used. The system will consist of two solid-state pressure switches with multiple switch output functions or signals. Each switch will have its own power supply and utilize the basic Bourdon tube transducer. The analog output signal is amplified in a solid-state circuit that finally switches the on-off control valves either directly through power transistors or through relays. The transducers in this case are located directly in the vehicle and only the electrical signal lines are connected to the tanking valves [12]. Besides the advantages in reliability and simplicity, this system will certainly be the cheapest conceivable LOX and fuel tanking system.

Hydrogen Tanking Problems. One of the problems existing in the field of hydrogen tanking is the low density of hydrogen and the resulting low pressure (0.5 to 1.0 psia) available to a sensor. A force-balance pressure transducer for altimeter purposes in flying aircraft [13] is available for application to this problem. A Bourdon tube transducer to cover a full range of 1 psi differential pressure is also under development.

Another problem exists in the pressure sensing lines. A study has shown the importance of achieving an accurate pressure presentation of the liquid hydrogen level. The gas density on top of the liquid hydrogen or in the connecting pressure lines is no longer negligible. One major requirement is that the line should be isothermal, preferably at higher temperatures. The gasifier method, as described earlier for LOX use, seems to be the most promising solution. However extensive experimentation in this area needs to be done.

Another problem of hydrogen tanking is that the gaseous hydrogen on top of the liquid hydrogen represents a proportionately large mass in itself. Since a tanking system should fulfill two requirements: (1) to tank the missile with a known mass of propellants; and (2) to secure enough total propellant for the propulsion system, a dilemma exists. The  $\Delta p$  system measures the total mass in liquid and gaseous form available in the tank, but it cannot directly measure the liquid level. The liquid level of the usable mass of hydrogen cannot be obtained without feeding into the system some other information. This is a problem with any system, since no system can measure the total mass as well as the usable liquid hydrogen level with one sensor. A study program under actual conditions with hydrogen tanks and tanking sensors should give the appropriate direction for a solution [14].

Exotic Fuel Tanking Computers. A future problem in propellant tanking is the handling of very corrosive exotic fuels. In general, the problem of compatibility of fuel with transducer can be avoided by the gas balance or purging method. This method prevents direct contact of the fuel with the pressure transducer. However, it is believed that this method will not always be applicable to storable propellants. The development of transducers that can stand prolonged exposure to exotic corrosive fuels seems to be the best solution. Isolating diaphragm devices compatible with the liquids are a possibility, but in general these devices add to unreliability and reduce accuracy. Some exotic fuels are so corrosive that the basic sensing element made out of Ni-Span-C will not stand prolonged exposure. An answer to this problem is the development of quartz Bourdon tube transducers. Fused quartz chemically withstands nearly all known rocket fuels and is very stable, thus it would improve the accuracy of the transducer.

### 30.3 Propellant Utilization Systems

The purpose of the propellant utilization system is to accomplish simultaneous depletion of the propellants. This goal was practically achieved during development of the V-2 through a preset, flow-control system. In this system, propellant flow was measured through an arrangement of Venturi tubes in the LOX and fuel lines and through differential pressure sensors with pneumatic outputs directly controlling bellows-driven bypass control valves. These valves were located between the high-pressure and low-pressure side of the centrifugal pumps, and by opening and closing, controlled the efficiency of the pump system. By setting the absolute flow rates of this controller to the desired engine mixture ratio and tanking the missile with the propellants in the same ratio, effective propellant utilization could be achieved. In addition, the total mass flow rate was selected to achieve the right thrust.

This system was developed and tested in late models of the V-2 power plant. However, shortcomings of this system led to extensive flow testing for calibration with the complex pipe system.

In 1944, a system was developed combining ratio flow control and a thrust control system in one combined pneumatic control system. This system had the advantage that a true ratio control was used, coincidentally controlling thrust through a pressure transducer by sensing combustion chamber pressure and varying the total mass flow rate.

In 1945, a study was made in which an acceleration control system would control the V-2 propellant valves in a preprogrammed acceleration program. The idea behind this system was that only through the final measurement of the thrust could accurate, repeatable performance of the power plant be achieved. In this way, all thrust and weight tolerances would be overcome by actually controlling the missile by the desired acceleration.

Early attempts at propellant utilization in the United States included a system that would control the flow rates of the two propellants. Turbine-type flowmeters were selected as basic sensors, and a ratio control system with electromagnetic control valves was considered. A scale model system was tested and found to be relatively satisfactory. However, it was recognized that all of these early attempts would never make an effective propellant utilization system. The tolerances in the tanking process, inaccuracies of the sensors, aerodynamic heating effects and density changes in the fuel would never allow for an accurate, simultaneous depletion. Accuracies of 1 to 2 per cent of the total tank mass could be achieved but would be insufficient for the existing requirements. It was concluded that only a closed-loop control system of the individual tank levels would fulfill the task. It was also recognized that no sensors with the required accuracy were available; liquid-level sensing devices from industrial instrumentation were not applicable for a guided missile. All effort was directed toward the development of such a sensor. The control problem was believed to be a smaller task and could be achieved with no great developmental effort.

### 30.3.1 Pneumatic Differential Pressure Propellant Utilization System

First attempts to design a true propellant utilization sensing system with level sensors used pneumatic differential transducers. These transducers are widely used in industry [15]. These sensors are basically a differential-pressure bellows system with a pneumatic amplifier for differential-pressure signal amplification. The output is a 3 to 15 psi pressure signal for comparison in a pneumatic ratio-sensing device, which in turn controls a pneumatic valve with a preset propellant ratio. These pneumatic differential transducers were investigated for stability, repeatability, accuracy, and susceptibility to environmental influences. They showed remarkable repeatability and accuracy under laboratory conditions, but under the expected acceleration and vibration environment they were not sufficiently stable.

### 30.3.2 Force-Balance Propellant Utilization Sensor, CA-568

In early 1956, design and development was started on propellant utilization sensors using the force-balance principle. Such force-balance pressure sensors had been developed for the aircraft industry. For example, mach number could be computed by measuring the ratio of pitot to static pressure, using two  $\Delta p$  capsules for driving the sensor. The basic advantage of such a system is that it measures the ratio of the two differential pressures directly, cancelling the effect of acceleration. This gives, at cutoff, an accuracy of 1 per cent of the ratio at 10 per cent of the total propellants.

The goal was reached but the environmental stability was not satisfactory under vibration. Shock mounts were required that made the assembly too big, heavy, and expensive. An improved design was substantially reduced in size and weight and had better over-all performance characteristics (Fig. 30.7), but it still had to be suspended in a vibration shock mount system [16].

One such sensor was flight tested on the Jupiter Missile AM-19 with good results.

### 30.3.3 Bourdon Tube Transducer Propellant Utilization Control System, TMC 609

This system has the most advanced sensor for propellant utilization. It was built to the Jupiter missile specification and later changed to satisfy the Saturn requirement. In principle, it operates as follows:

1. An adjustable solid state timer is used to change the desired control function on a time basis
2. Bourdon tube transducers are a new dc-dc type instead of ac as previously used. Better null stability and lower noise level is attained (Fig. 30.8).
3. The system incorporates a control valve. It has extremely low friction and force requirements, an interchangeable orifice to accommodate the required adaptable control function, and an electrical actuator with feedback and telemetering potentiometers. For fail-safe consideration, the valve is spring loaded in its midposition.

The advantages of this system are:

1. Small size and weight (20 lb maximum)
2. Considerable reduction in cost
3. Solid state timing device for improved reliability
4. Bourdon tube transducers do not require shock mounts



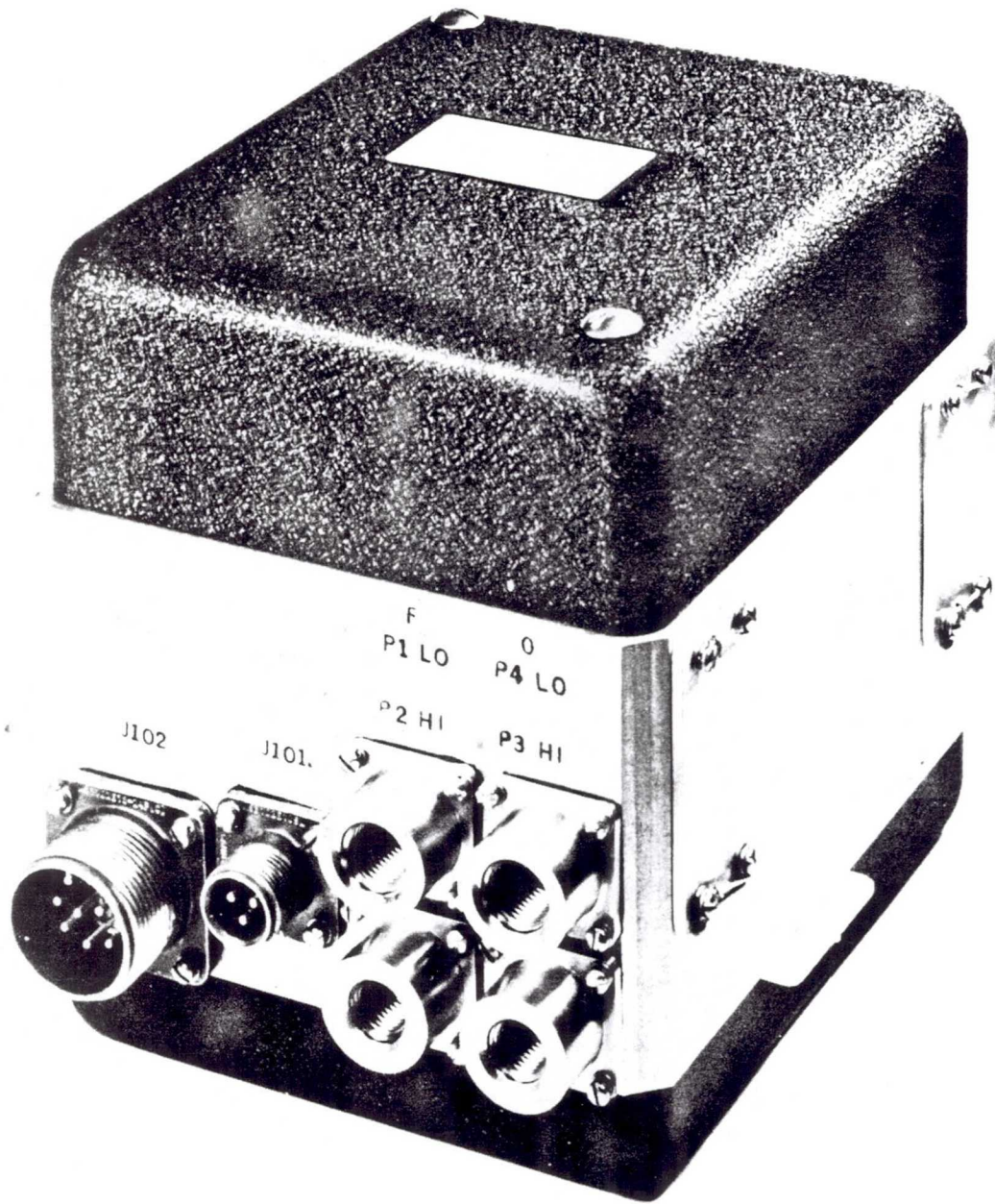


Fig. 30.7 Force balance propellant utilization sensor, CA # 568-1.

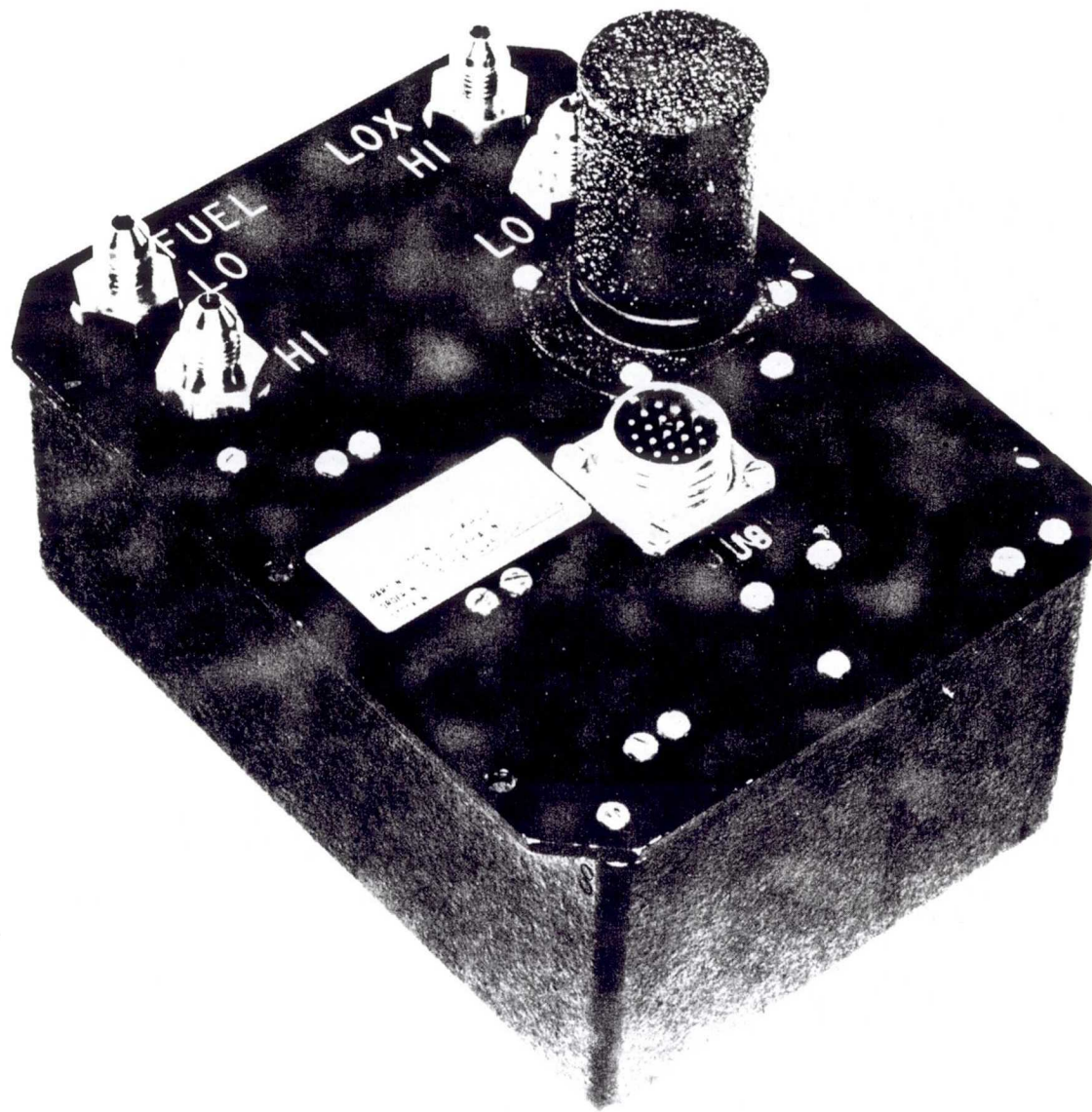


Fig. 30.8 Propellant utilization sensor for Saturn propellant utilization systems, C568-2.

### 30.3.4 Future Propellant Utilization Control System Problems

The problems confronting future propellant utilization systems are similar to the future propellant tanking problems. Solutions will have to be found for liquid hydrogen applications as well as exotic fuel requirements. One additional advance is desirable. Until now the system requirements usually have been met by a timed program for the LOX/fuel ratio to allow for the engine mixture ratio, tank shaping, and other variables. However, a study reveals that the accuracy can be greatly improved if an acceleration timing program is employed [17]. In this scheme, the  $\Delta p$  is multiplied by the output of an acceleration signal and the product used as a program signal for tank shape and other corrections.

### 30.4 Thrust Control Systems

In the past, most missiles used the open-loop approach for controlling the thrust of the missile. The accuracy of this method, in general, was between 2 and 3 per cent. Thrust variation can be tolerated to a certain degree, since the cutoff computer in the guidance system will adjust for this tolerance. However, the complexity of the guidance system can sometimes be greatly reduced in connection with a thrust control system; this was the case with the Redstone missile. Another advantage of a thrust control system is a great reduction of necessary hot test firings.

#### 30.4.1 Thrust Control System CC-506

This closed-loop thrust control system was used with the Redstone missile. In principle, the system is a combustion chamber, pressure-control system. It works in conjunction with the open-loop system in which the regulator for the hydrogen peroxide tank controls the coarse setting and the thrust control system represents the fine control.

A Bourdon tube pressure transducer senses the combustion chamber pressure and compares its electrical output to an electrical reference. This reference is variable and can be set to a calibrated, combustion-chamber pressure scale. The resultant error signal is amplified in a hybrid transistor-magnetic amplifier and powers a motor driven control valve. This gate valve is located in the hydrogen peroxide line and modulates the flow into the gas generator. It has a shaped orifice and a minimum flow capacity of 80 per cent. With this flow characteristic a fail-safe design feature is incorporated, making it impossible for the main flow to be blocked. Therefore, a malfunction is never catastrophic [18].

The system has a good reliability record. Combustion chamber pressure is controllable generally within 1 in 300 psi.

Dr. Haeussermann, Director of the Astrionics Division, George C. Marshall Space Flight Center, says, "Up to this point, we could fly out standard trajectories only on paper. With the use of the thrust controller we can now fly our standard trajectory in reality." Altogether, about 250 thrust control systems have been built, including some systems for the Mercury program (Fig. 30.9).

For liquid hydrogen propulsion systems, a new problem arises in thrust control. A typical example is that of the Pratt & Whitney engine, which, because of its characteristics, needs a high-speed control system. The new dc-dc Bourdon tube transducer, TR 2022, has been proposed to overcome some of the vibration problems encountered with mechanical sensors. The new problem will be to design an electromagnetic torquer, controlled by this Bourdon tube transducer, driving the pneumatic valve with a very fast time response [19].

### 30.5 Pressure Switch Control Functions for Propellant Management

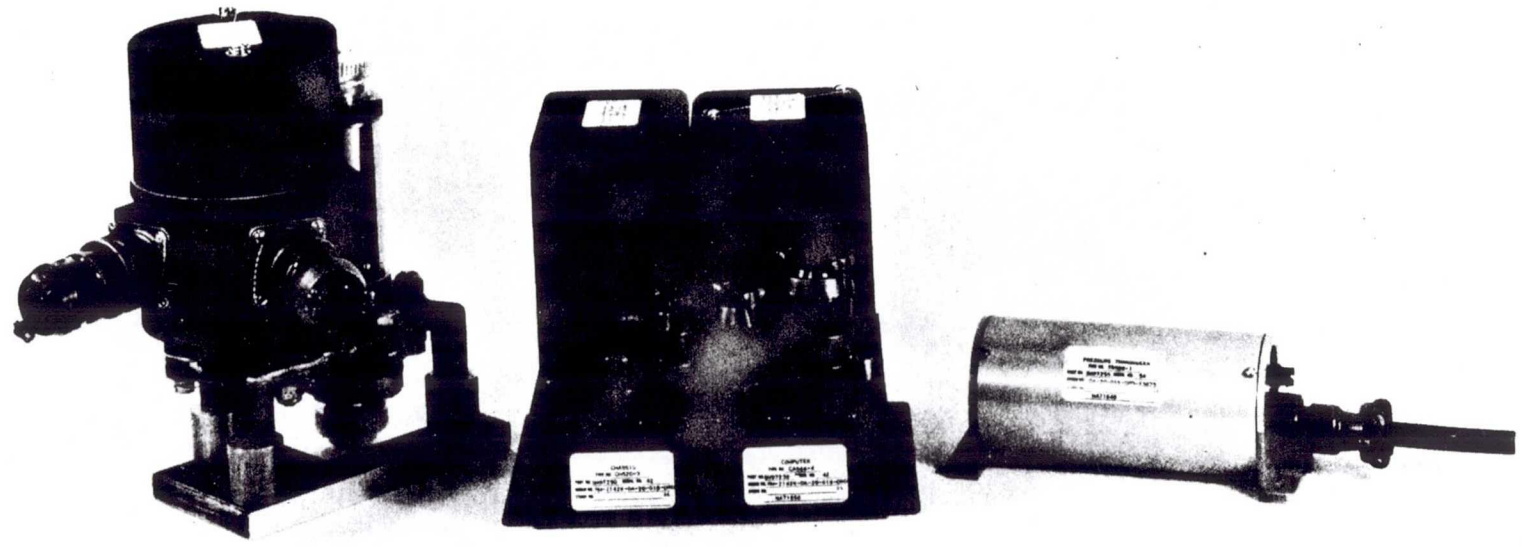
The pressure switch is one of the oldest control elements in propellant management. In general, it is a simple element consisting of a diaphragm or Bourdon tube and a switch; but seldom has one element given the power plant designer more trouble than this device. There are two basic reasons for these troubles:

1. The pressure switch is a measuring instrument delivering output in the form of switching power. Reliable switching under vehicle environmental conditions requires a snap action switch instead of a simple touch contact switch. The power required to activate this switch has to be taken from the diaphragm or Bourdon tube. The activating forces under vehicle environments vary with temperature, acceleration and vibration, creating inaccuracies and unreliable switching.

2. The simple diaphragm and snap action switch suffers from inability to compensate easily for changes in environmental influences such as temperature, acceleration, and vibration. A survey of 25 different pressure switch designs showed that none could be considered fully acceptable.

#### 30.5.1 LOX and Fuel Pressure Switch, TR 2124 and TR 2125

With the advance of solid-state switching techniques using transistors a new approach seems possible. It uses a Bourdon tube transducer with a twisted Bourdon tube and reluctance pickoff as the sensing and transducing elements (Fig. 30.2). The pickoff is supplied from an internal power supply; the output is fed into an amplifier and a phase-sensitive rectifier circuit. The electrical null of the pickoff is located at the switch point. The phase sensitive output controls a power switching transistor. In contrast to the mechanical diaphragm snap action switch, this switch uses practically no power from the sensing element but derives switching power from the power supply.



The TR 2124 and TR 2125 switches are the first designs of such a solid-state pressure switch and are used in the Saturn booster as fuel and LOX safety switches to prevent overflowing the tanks in case of malfunction of the tanking computers.

### 30.5.2 Pressure Switch, TR 2129

This device represents two years of development in solid-state pressure switch design [20]. It also uses the Bourdon tube transducer with its inherent design features (Fig. 30.10). Its advantages are:

1. Capable of withstanding vibrations of over 65 G's up to 2000 cps
2. Very small on-off differential (0.1 to 0.25 per cent)
3. Capable of withstanding temperature variation from 65°F to 165°F with a built-in heater and can also be temperature compensated over this range. The repeatability of the switch action is within 0.1 per cent
4. Designed for multiple switch points so that two or three output signals can be given by the same switch at different pressures
5. Capable of remote setting of switch points
6. Independent of line voltage variation with  $\pm 10$  per cent of supply voltage. A similar switch exists that can switch an electromagnetic solenoid valve directly, without the use of a relay [21].

### 30.5.3 Future Pressure Switch Developments

As in future transducer improvements, the use of pressure switches with new exotic fuels presents problems that can be solved as previously described. However, another requirement has become of major importance in space flight applications: the capability of operating under extremely low temperature conditions, down to -300°F. Preliminary investigations show that the electronic components needed in the switching circuit can be made to function. However, no component suppliers will guarantee operation at these low temperatures.

Increased reliability for the operation of pressure switches in manned space ships is another requirement. Pressure switches with redundant output signals can be designed so that no catastrophic destruction will result from malfunctions. Another requirement besides the switch output is an analog output for monitoring purposes. Reduction of the number of transducers through the multiple use of the basic Bourdon tube sensor as an analog transducer as well as for switch functions is advantageous. Experience shows that leakages in pipes and tubings are a major problem. A switch designed for a direct mounting, without tube connectors, is a future design objective. Improvement in reliability of spot-welded circuit techniques is also necessary.

The progress made in developing a solid-state pressure switch is considered a major technological break-through. Thus the confidence lost in pressure switches as a simple and reliable element can be restored.

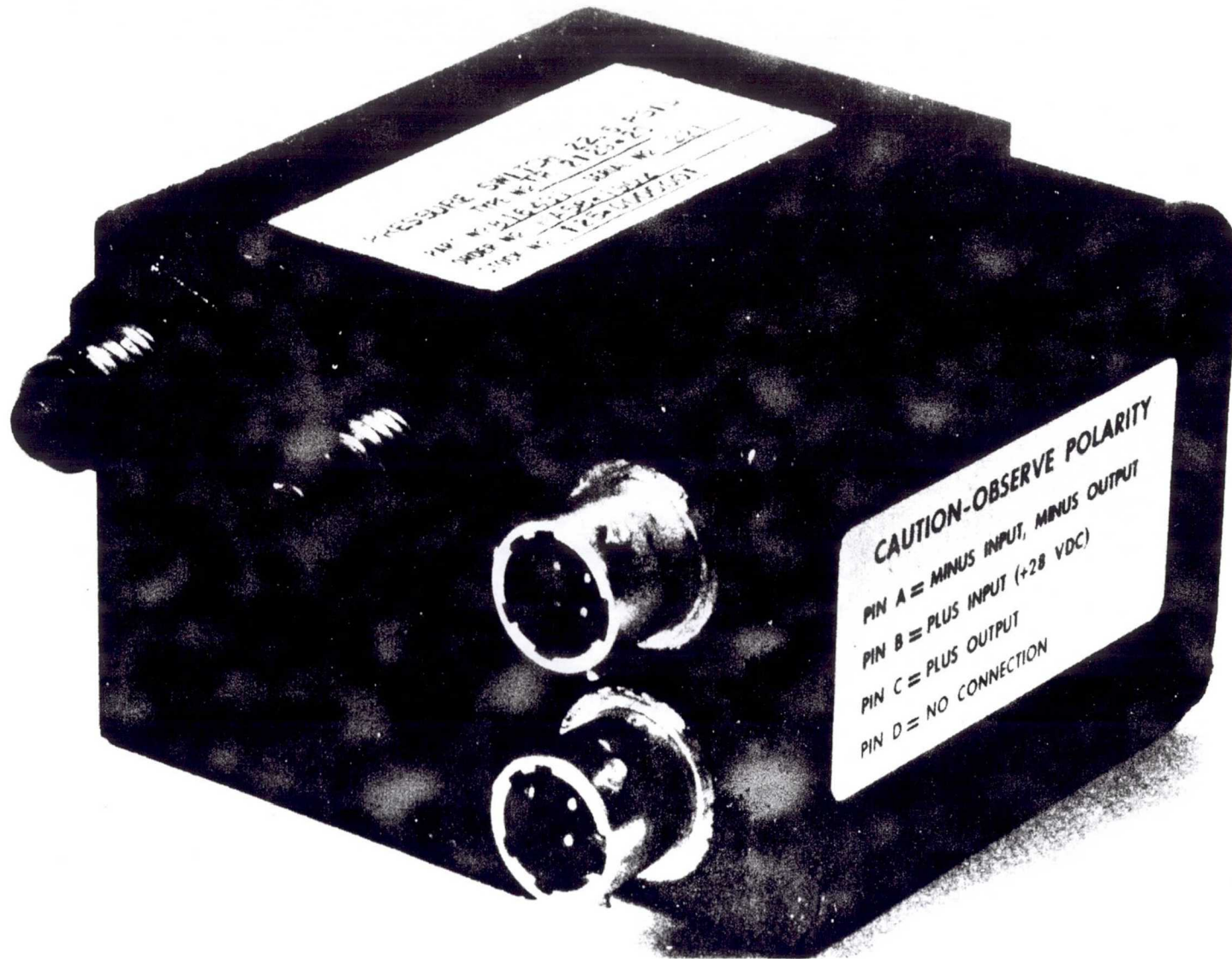


Fig. 30.10 Solid state pressure switch, TR 2129.

### 30.6 Conclusion

Progress made in the field of propellant management is significant. The  $\Delta p$  method fulfills the requirements of simplicity, ease of maintenance, checkout capability and, above all, accuracy and stability. The  $\Delta p$  method in propellant management is at the threshold of its development. Realization of its ultimate capabilities lies ahead.



## REFERENCES

1. Precise Measurements of Liquid Propellant Levels in Missiles, Engineering Report 192, Servomechanisms, Inc.
2. Friedman, G. J. and Louis DeBottari, Which System for Propellant Level Sensing, Space and Aeronautics, 34:103 (August 1960).
3. Fowle, Arthur A. and William G. Pestalozze, Cryogenic Instrumentation Keeps Pace with Booming Field, Chemical Processing System (1961).
4. "Reliability Policy and Procedure Manual," Servomechanisms, Inc., (June 1961).
5. Electronic Baro Switch, Phase 1 Project Report Sandia Corporation, Engineering Report 900-677, Servomechanisms, Incorporated.
6. Propellant Utilization and Thrust Control System, Technical Report 83393, Servomechanisms, Inc. to Aerojet General Corporation (April 12, 1961).
7. Inverted Bell Pressure Pickup System, Engineering Report WD 83, Servomechanisms Inc. (August 12, 1961).
8. Pressure Measurements Devices, Servomechanisms, Inc.
9. LOX Tanking System Type TMC 601, Product Sheet IA 4.5.60-3M (Revised), Servomechanisms, Inc.
10. Voss, Werner, Propellant Loading and Sensing Systems for Liquid Propellant Long Range Guided Missiles, Army Ballistic Missile Agency, Paper given at first Liquid Propellant Information Agency meeting, New Orleans, November 1959.
11. Powell, Elmer A., Performance Evaluation of the Jupiter LOX Replenishing System, T.F.S. 608, Report DT-TN-45-59, Army Ballistic Agency (August 17, 1959).
12. A Propellant Loading Control System TMC 608, Proposal SAS 410, General Dynamics Astronautics, December 11, 1961.
13. Force Balance Pressure Transducer TR2100, Product Sheet IAI 15.60-2M (Revised), Servomechanisms, Inc.
14. Propellant Tanking Computer System, Technical Proposal 83277, Servomechanisms Inc. , George C. Marshall Space Flight Center, Huntsville, Alabama (January 23, 1961).

15. Nullmatic Differential Pressure Transducers, Instruction Book 100-S, Moore Products Company, Philadelphia.
16. Propellant Utilization System, Proposal 150 9, Servomechanisms, Inc. April 30, 1958.
17. Propellant Utilization System Type AQC 603, Proposal 2190, Servomechanisms Inc. (January 26, 1960).
18. Thrust Control System Type CC 506, Product Sheet IA 4-29-60-3M, Servomechanisms, Inc.
19. RL 10 Rocket Engine Thrust Control System, Proposal P 196, Servomechanisms, Inc. (July 28, 1961).
20. Solid State Pressure Switch Type TR 2129, Product Sheet IA 5.19.61-3M, Servomechanisms, Inc.,
21. Solid State Pressure Switch (A compilation of all switches), Publication 108, Servomechanisms, Inc. (December 6, 1960).

NG3-16007

STORED ENERGY AND MAGNETIC FIELDS IN SPACE APPLICATIONS

R. J. Schwinghamer

Manufacturing Engineering Division  
George C. Marshall Space Flight Center  
National Aeronautics and Space Administration  
Huntsville, Alabama

31.1 Introduction

The Manufacturing Engineering Division of the G. C. Marshall Space Flight Center has been investigating exploding bridgewires (EBW's) in fluid media as a means of forming and working materials. The system basically involves a utilitarian combination of plasma physics, shock tube technology and EBW phenomena and uses the ultra-fast discharge of a 20,000 capacitor bank through an ionization switch and into a violently exploding bridgewire. The bridgewire is suspended in a water medium, and the shock wave which results forms the material into an evacuated die. All work to date has been done with a 24,000-joule bank, but a much larger 240,000-joule bank called Medusa will be used in the future.

Also under investigation concurrently, and perhaps more promising in some respects, is the creation and harnessing of high-intensity magnetic fields in the kilogauss range, with some of the same general end uses intended. This principle also involves a carefully timed and controlled discharge of an ultra-fast capacitor bank but into suitably arranged coils instead of an EBW. The resultant coil magnetomotive force creates opposition currents in the metal, and if the coil is inertially and structurally rigid enough, the desired motion of the workpiece results. The earliest practical application of the exploding bridgewire-fluid-medium principle is generally conceded to the Russian Yutkin [1] while the earliest work with high-intensity magnetic fields is a little less well defined. Here again however, the name of a Russian Kapitsa [2], appears early (1924) although he did his work in Great Britain. More recently in our own country the names Colgate, Kolb, Furth, Foner, and Kolm appear frequently in literature dealing with high-intensity magnetic fields. Although these intense fields are usually produced for nuclear research or for solid state experiments, here at the G. C. Marshall Space Flight Center we have begun to move in the direction of space vehicles and space applications of these principles.

Preceding page blank

As a result of our own efforts with stored energy, fast discharges, EBW's and high intensity fields, two facets of the general area show considerable promise for space and terrestrial application. These are:

1. The application of energy storage systems utilizing fast-discharge capacitors as a more or less universal power system that can be used with the variety of peripheral equipment needed in space vehicle fabrication and perhaps in orbital operations.

2. The application of magnetomotive principles to space vehicle fabrication and orbital operations, specifically in the area of fabrication, assembly, maintenance, and perhaps in terminal docking operations.

Consequently, in addition to work with space vehicle components, space applications are also being considered, and a good many associated devices have been developed.

### 31.2 Practical Energy Storage Systems

The idea of energy storage, while certainly not new, is particularly attractive for space use because it enables one to achieve tremendously high power levels for short periods, at the expense only of elapsed time during the "charge" phase of the cycle. This means that the peripheral equipment specifically designed for use with such a stored-energy system can do a job by employing very high, peak-power levels for only a few, or a few hundred microseconds as the case may warrant. The peripheral equipment can thus be far simpler, and inevitably more reliable than conventional terrestrial devices requiring relatively higher average power over a longer time. These basic advantages apply even if conventional terrestrial capacitors are carried into space to serve with a variety of peripheral equipment and tools. Work in the MSFC laboratory so far has been carried out using the characteristically heavy terrestrial-type, fast discharge capacitors typically running about 20 joules/lb. Some of these tasks that could be performed in space are punching, fastening, vacuum sealing, swaging, forming, and a variety of already demonstrated fabrication, assembly and maintenance operations that can now be done terrestrially. These will probably also be required techniques in orbital operations.

Electrically, the basic storage system, when coupled with the load, ultimately resolves itself into a specific kind of RLC circuit. This circuit characteristically performs in one of three possible modes

1. Nonoscillatory, or overdamped mode,

$$\text{Where } \frac{R^2}{4L^2} > \frac{1}{LC}$$

2. Nonoscillatory, critically damped mode,

$$\text{Where } \frac{R^2}{4L^2} = \frac{1}{LC}$$

3. Oscillatory, where

$$\frac{R^2}{4L^2} < \frac{1}{LC}$$

It is this latter mode in which these banks usually operate, although the nonoscillatory, critically damped mode is frequently simulated by the sometimes not-too-simple expedient of "crowbarring" the entire circuit.

The system inductance frequently determines the success or failure of the fast discharge application since it is largely instrumental in controlling the ring frequency. Peak currents of course are of considerable interest. It can be shown that the instantaneous value of the current in such a circuit is given by

$$i_t = \omega CV e^{\frac{-Rt}{2L}} \sin \omega t \quad (31.1)$$

Where  $\omega$  is the circular frequency, C is the capacity, V is the voltage,  $e^{\frac{-Rt}{2L}}$  is the damping factor, and  $\sin \omega t$  is the oscillatory function.

These currents characteristically assume values from 20,000 to 100,000 or 200,000 amp depending on the size of the basic energy storage system, and of course the ultimate speed of the discharge.

The switching of the stored energy from the capacitor bank into the load or work coil is one of the more difficult problems that must be solved in the utilization of stored energy to do useful work. Although a type of ionization switch that is initiated by a controlled plasma jet from a sparkplug is currently used, a new model having less jitter is being tested, in which a tertiary element is driven with a negative pulse. Results to date are promising, and it is planned to switch the new 240,000 joule bank, the Medusa, in 10 discrete increments by 10 switches of this type. However, for space applications some sort of enclosed switch perhaps of the partially-evacuated, field-initiated type will be necessary.

due to the vacuum environment. Such a switch has been developed at the NASA Langley Research Center by Dr. Thom.

System ring frequencies of typical energy-storage systems, when coupled with their loads, characteristically run from about 10kc to as high as 100 kc or higher, depending on the specific application. Exploding bridgewires shot in fluid media generally produce higher frequency discharges than magnetomotive forming discharges since the coils used in the magnetic field applications invariably introduce a certain amount of inherent inductance in the circuit. Why the ring frequency is so important is treated below. A supplementary treatment is given in [3].

### 31.3 Idess (Integral Discrete Energy Storage System)

Although the state of development of terrestrial equipment and basic energy-storage systems operating on the low-storage, high-discharge rate principle has come a long way, some very serious limitations are apparent for space use. One of the most obvious drawbacks is the weight of currently available fast-discharge capacitors. In those instances where space or orbital operations would require very high instantaneous power (for example, punching a symmetrical hole in a vehicle, bulkhead), it can be shown that even a conventional capacitor discharge system utilizing the magnetomotive force of a coil to effect this operation does indeed constitute less mass than the mechanical punch press currently used. The inherent flexibility of an energy-storage system must also be considered. That is, the same basic system can power a variety of peripheral equipment specifically designed for taking advantage of these tremendous instantaneous peak powers. The energy-storage system, when not in use with peripheral equipment, can be used in conventional electrical applications such as radar-filtering capacity, power-factor correction in a space station, or a variety of other commonplace electrical uses.

Nevertheless, in space mass is still a big problem. A typical terrestrial capacitor weighs about 0.05 to 0.10 lb/joule. The majority of this weight is associated with the impregnant weight of the capacitor, which is of course necessary in order to prevent corona and breakdown in the Earth environment. If it were possible to build into the vehicle or space station integral, discrete segments, or capacitors of a type of laminate structure, then of course a considerable weight saving would result. Such capacitors might consist of a monolithic structure of titanium with a "grown" oxide that would have a dielectric constant of 100 or better. At least one capacitor manufacturer is researching this very possibility at present. It is assumed that potential hazards of ignition of liquid hydrogen and other flammables would be circumvented by selecting those areas not exposed such as fins, passenger bulkheads or using only empty tanks, or inhabited structures. These elements could

also do structural as well as energy-storage duty. A certain trade-off in structural strength would undoubtedly be inevitable, but the net result would still be considerably lighter than conventional terrestrial capacitors if such an integral, discrete-element structure were developed. Another basic problem area is the physical strength required as the capacitor "rings."

In order to have some idea of relative orders of magnitude, preliminary calculations indicate that if about 60 per cent of the surface area of a capsule such as that being considered for Apollo were used to store energy from solar cells, about 700  $\mu$ f of capacity could be attained. At a voltage of 5kv, this would provide approximately 9000 joules, and about 144,000 joules if operated at 20kv. The operating voltage of 5kv would not press the current state of the art, while a 20kv operating voltage in an integral, discrete, energy storage system probably would require new techniques such as the utilization of hard space vacuum in the design to eliminate corona and breakdown problems. It should be pointed out that a variety of forming, punching, fastening, and other operations have already been done with only 9000 joules, by a proper discharge system and the right "ring" frequency. Naturally, the integral, discrete energy of storage concept is even more attractive if a space station is considered, since larger permanent areas would be available for storage purposes.

As noted before, work with terrestrial, fast-discharge systems has gone well; and the great degree of versatility for many tasks that these systems provide indicates the desirability of some parallel-directed effort in adapting these systems in the most advantageous way to the orbital operations program. These systems and their peripheral equipment, while still posing many problems for space use, do have the decided advantage of no moving parts. Hence, there are no lubrication problems, no hydraulics or pneumatics, all of which eliminates some very difficult sealing problems and vapor pressure considerations and does not expend mass to effect the end results since the magnetic field that does the work is created by discharge of stored electrical energy. Figure 31.1 shows in rudimentary form how such a basic Idess might be designed.

#### 31.4 Applications of High-intensity Magnetic Fields

As noted earlier, George C. Marshall Space Flight Center has been investigating methods and means of converting the energy in a high-intensity magnetic field directly into useful work. This is done by discharging currents through properly designed coils in a very rapidly but specifically prescribed manner. The basic principles of magnetomotive force application are very similar to, and were derived from, plasma-pinch work in nuclear physics. Only in this case, currents are induced in metals in proximity rather than in a plasma. Space and terrestrial applications have been concerned with the generation of intense-magnetic

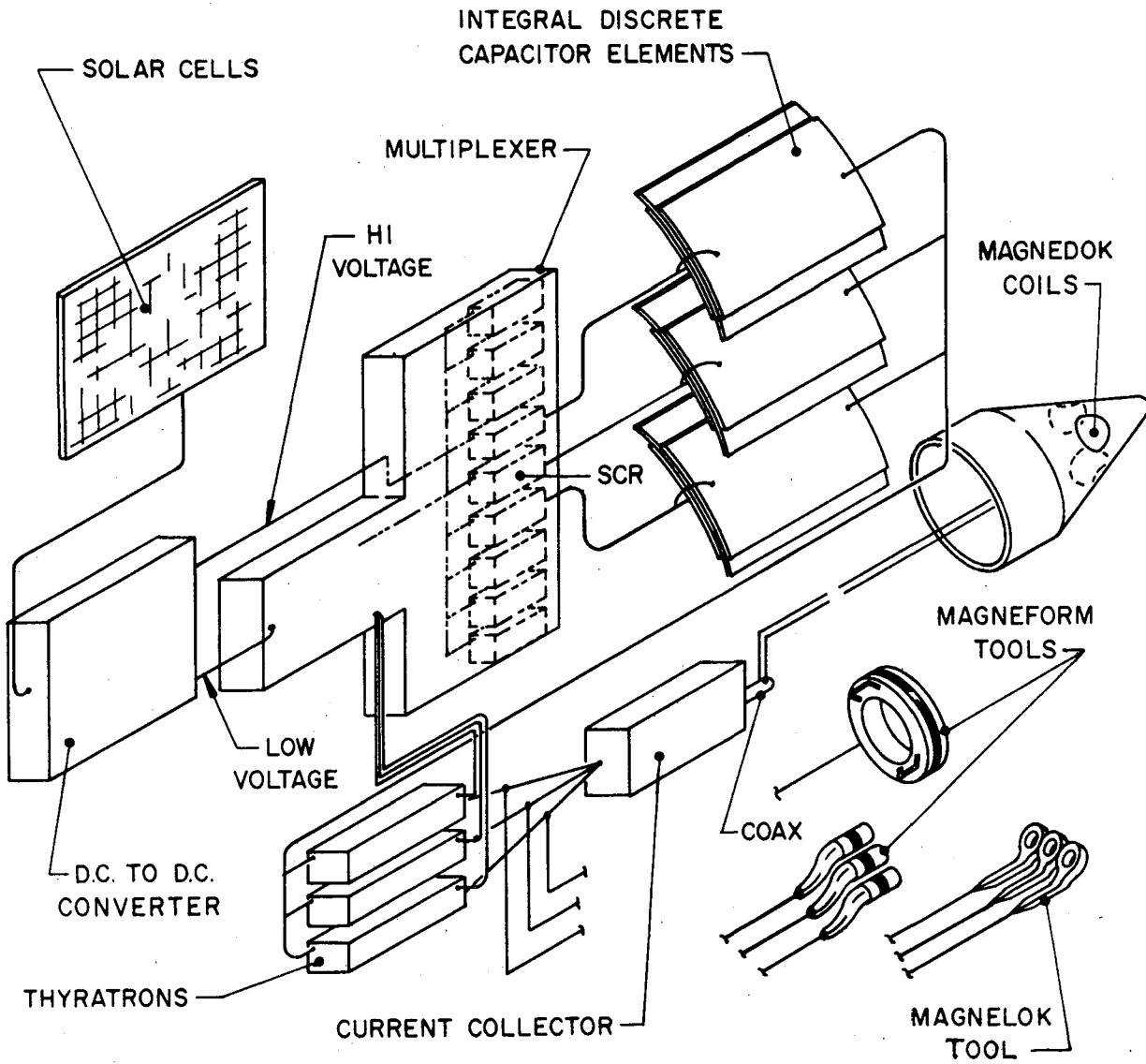


Fig. 31.1 Idess schematic, showing some types of peripheral equipment.



fields and use of these fields to induce opposition current in an adjacent conductor material. If the initiating coil is of sufficiently rigid construction, the motion resulting from the flux concentration is motion of the adjacent conductor material. Attraction or repulsion can therefore be achieved, depending on how the discharge is programmed. The forces involved are basically of the same type evident in the armature-field reaction of an electric motor. Derivations of equations concerning these forces usually begin with the familiar  $F = Bli$  relationship of electrical engineering, or use the  $i \times B$  relationship of the physicist.

Data on the subject of coils for the production of these intense fields for nuclear research is available [4, 5, 6] although the strength of our specialized Magnelok\* coils is still one of the main problems.

By writing the current-voltage relationships existing between such a primary coil and the material (which is considered as the secondary coil), it is possible to deduce some very useful information from the two simultaneous equations

$$e = i_1 r_1 + L_1 \frac{di_1}{dt} + M \frac{di_2}{dt} \quad (31.2)$$

$$0 = i_2 r_2 + L_2 \frac{di_2}{dt} + M \frac{di_1}{dt} \quad (31.3)$$

Here subscripts refer to primary coil and secondary (metal) coil, and  $M$  is the mutual inductance. From this it is seen that the amount of energy that can be transferred to a workpiece acting as the secondary coil depends on the voltage of the primary, the duration and shape of the current pulse, and the magnetic coupling between the coils [7]. Further, the energy input into the magnetic field of a single conductor depends on inductance and current squared, if the permeability is constant, or

$$W = \frac{Li^2}{2} \quad (31.4)$$

where  $L$  is inductance and  $i$  is current.

---

\*Magnelok is a descriptive term for a magnetic fastening system currently under development at the George C. Marshall Space Flight Center

Of considerable importance also is the material resistivity, since resistivity determines the eddy-current flow. The magnetic properties of materials in proximity to the coils are relatively unimportant due to the intense fields generated in the coils. High enough fields have been achieved to produce "magnetic sawing" [6] of the materials. This phenomenon results when the applied fields are of sufficient intensity to actually melt the metal, which is then repelled by the field, producing grooves in the metal.

As can be seen from the equations above, the crux of the matter lies largely in the timing of the discharge. High-frequency transmission line theory regarding skin effect facilitates determination of field penetration depth, which is dependent on frequency, material, and other factors. In most practical cases, the discharge-current pulse-rise time should be rapid enough so that no appreciable flux can completely penetrate the metal or conductor being worked. In some instances, however, complete penetration is a prerequisite — it depends entirely on the specific application. In order to develop the penetration depth equation in the standard manner, assume an alternating magnetic field, then examine the current distribution in the region at and below the surface of an infinite conducting plane

$$J_x = J_0 e^{-\alpha x} e^{j\alpha x} \quad (31.5)$$

where  $J_x$  is current density at any point  $x$  units of distance below the surface

$J_0$  is current density at the surface

$\alpha$  is reciprocal of the penetration depth

When the exponent  $\alpha x$  becomes unity, the current has fallen to  $1/e$ , or about 37 per cent of the surface-current density. Arbitrarily, we call this  $x = t$  the penetration depth, which is related to resistivity, permeability and frequency, as follows.

$$t = 5.03 \left( \frac{e}{\mu f} \right)^{\frac{1}{2}} \quad (31.6)$$

where  $t$  = penetration depth of current

$e$  = resistivity in micro-ohm centimeters

$\mu$  = relative permeability

$f$  = frequency

The predominant influence of frequency and resistivity of the material to be worked is apparent in the above relationship. From this, it can be seen that some of the high resistivity stainless steels can be expected to be more difficult to manipulate with the high fields, and indeed they are.

The energy densities associated with these intense magnetic fields are comparable to those achievable with chemical explosives. The energy density  $\frac{B^2}{8\pi}$  ergs, where B is the flux density in gauss. Consequently, a megagauss field has an energy density of  $40 \times 10^9$  ergs, or  $1000 \text{ cal/cm}^3$  and develops a magnetic pressure of 560,000 psi at the boundaries of the magnetic field [8]. These tremendous pressures sometimes are harnessed by the nuclear physicist for the express purpose of pinching, or containing, a plasma. However, George C. Marshall Space Flight Center is more concerned with the tremendous potential for space applications made possible by the generation of these intense fields in suitably designed and arranged coils, and their useful application to the tasks of forming, fastening, thrusting, punching, and sealing in space vehicle applications and in space. Obviously, coil disruptive forces are tremendous and a number of different designs are being investigated [4, 9, 10].

### 31.5 Magnelok Space Tools

Most of the above basic principles are brought into play in the space tool concept called Magnelok. A series of space tools are being developed that can be used either with a terrestrial-type capacitor bank or with an energy-storage system of the integral discrete variety, which is described below. The tools and fasteners are the essence of simplicity in that they are relatively small, light, portable, and without moving parts. They also have no pneumatics or hydraulics that might pose insurmountable vacuum sealing problems in space. The Magnelok tools are designed to cause special fasteners to pull tight and fasten in one operation. This operation is accomplished without any unbalanced, reactive torques or moments, which with conventional tools would necessitate orbital corrections to compensate for disturbances caused by maintenance, fabrication or assembly operations in orbit.

There are basically no moving parts to wear out in the system, and remote operation by radio is quite feasible. Figure 31.2 shows a tool of the type being developed. In Figure 31.2 two parts are fastened in the following manner: a ring or nut is vigorously repelled by a very fast discharge of current through the coil. The ring experiences considerable axial expansion at the expense of radial contraction. If the bolt, or tension member is designed as shown, the constricting ring not only fastens, but pulls the parts very tightly together as well.

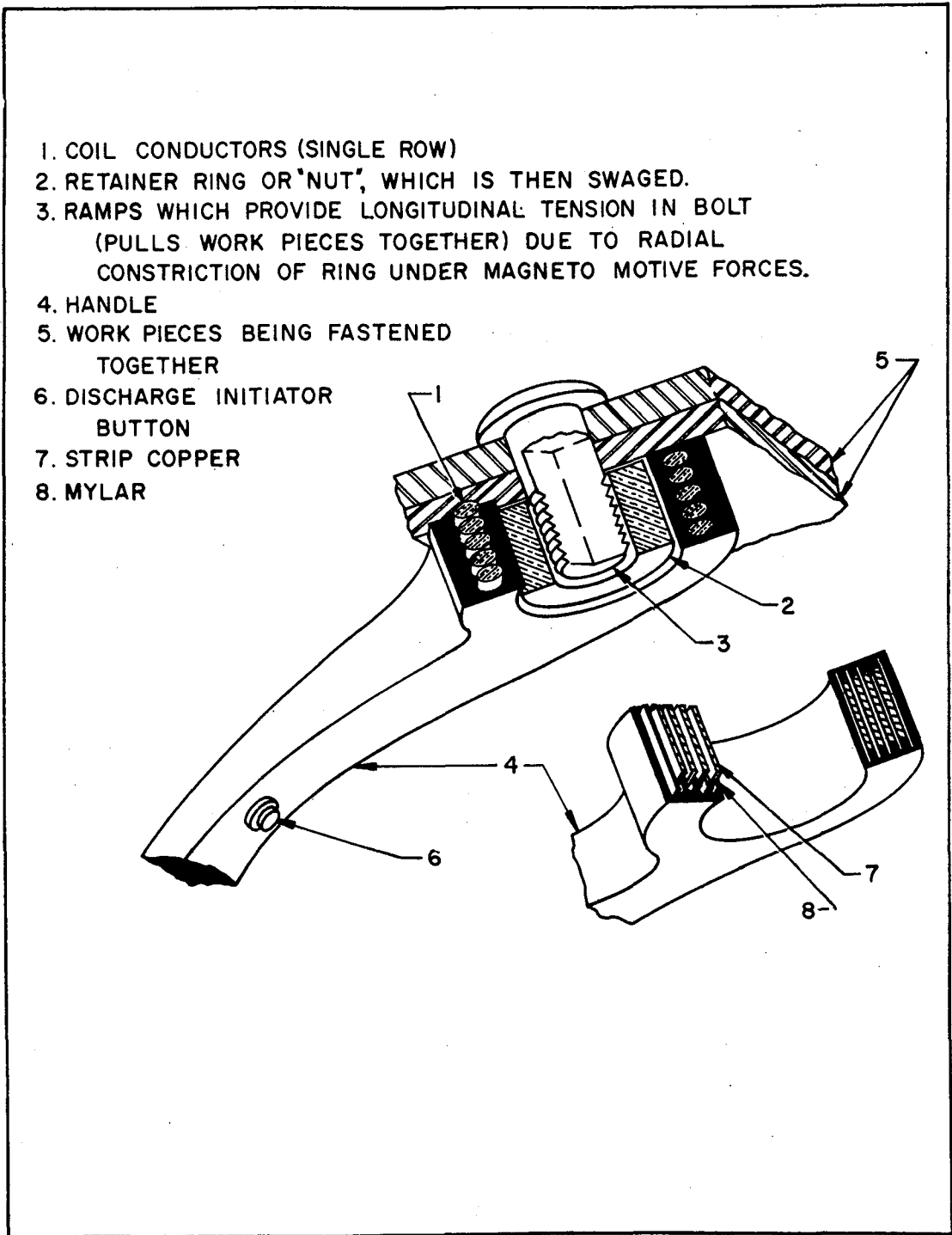


Fig. 31.2 Magne lok tools and fastner.

This is accomplished essentially without any unbalanced forces; hence it is ideal for use under zero-G conditions.

Figure 31.3 shows the effects of the tremendous forces involved. The catastrophic failure of this coil during testing paved the way for later coils which successfully sustained the discharge. Figure 31.4 shows some earlier prototype coils, two of which were reasonably successful. Figure 31.5 shows two pieces of hardware that were swaged at two different field strengths. The piece on the left shows complete and intimate contact, almost welding, of the sleeve to the bolt. This is the manifestation of the tremendously intense magnetic pressure that actually causes the metal to move, even flow, without any physical contact. The fact that this occurs, indicates the additional use of this principle in making metal-to-metal seals in the space vacuum environment. Under space ambient conditions, welds can be accomplished merely by cleaning or buffing the surfaces to be joined, and then "magneforming" them.

Figure 31.6 shows Magneelok hardware equally adaptable to space and terrestrial application. It is obvious from the foregoing discussion that these coils can be designed as an integral part of a fastener, probe, or other component, and then the associated capacitor can be switched remotely by a radio signal. This provides a high degree of flexibility for many unmanned operations in space.

### 31.6 Magnetic Forming and Punching Tests

Figure 31.7 shows one approach to the repair of a rather large meteorite puncture. It also indicates what could be done regarding vacuum sealing of or providing a feed through in an already existing hole in an orbital tanker, bulkhead or vehicle. This system utilizes a coil of a certain design that fits inside a low-resistivity metal sleeve. The sleeve is bulged into the hole to be filled by means of a fast discharge through the coil. Rather large increases in tube diameter can be realized in this way, so that the space vehicle need have available only a reasonable range of sizes that overlap dimensionally in the fired condition. Another favorable application for magnetic forming is the flaring and forming of large lines and tubes for space vehicles and in orbital assembly and fabrication operations. Figure 31.8 shows the results of such a test. This thin walled cylinder is a 24 in. diameter and had three flared rings formed on the circumference of the cylinder by a rapid, damped, oscillatory discharge through the coil on which the cylinder is resting. This example proves the feasibility of magnetic forming for application in large vehicle lines and at the same time indicates a considerable potential application for vacuum sealing operations in space. Expansion of such a bulge or flare into a prepared recess in a space structure will facilitate virtually welded, joint-type, vacuum seals.



Fig. 31.3 Catastrophic disintegration of test coil by magnetic field.

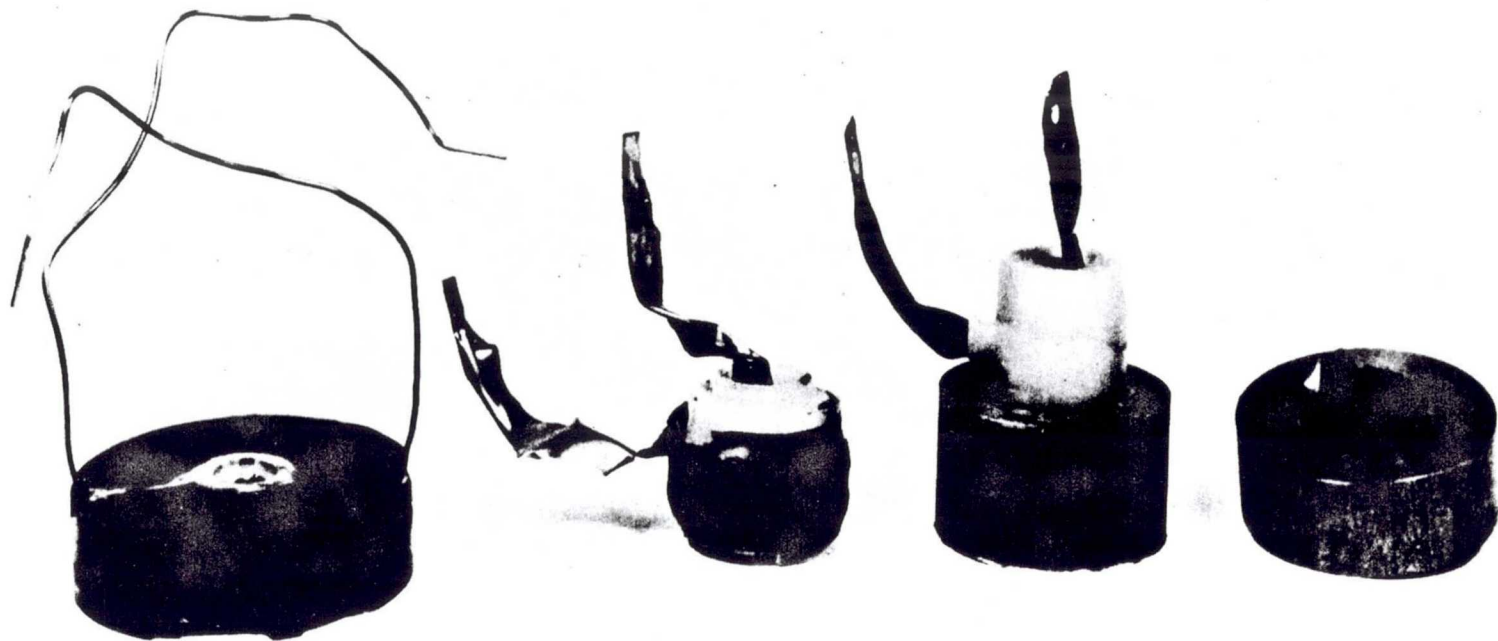


Fig. 31.4 Typical magnetomotive test coils.

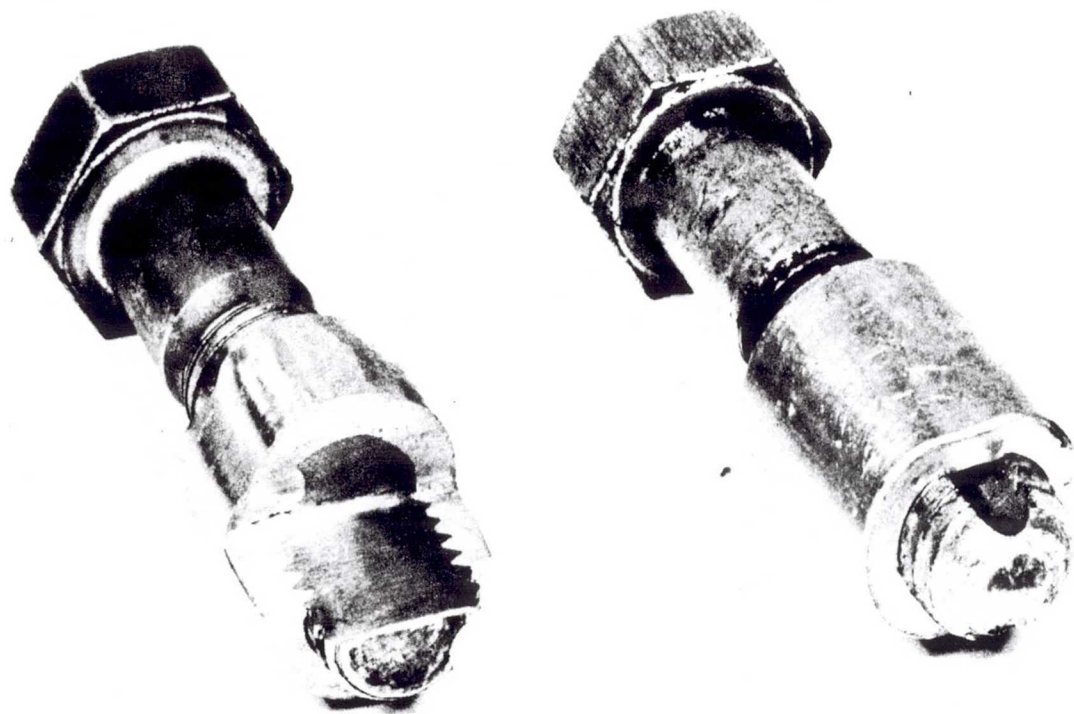


Fig. 31.5 Swaged rings formed by MagneLok system showing effects of intense magnetic pressure.



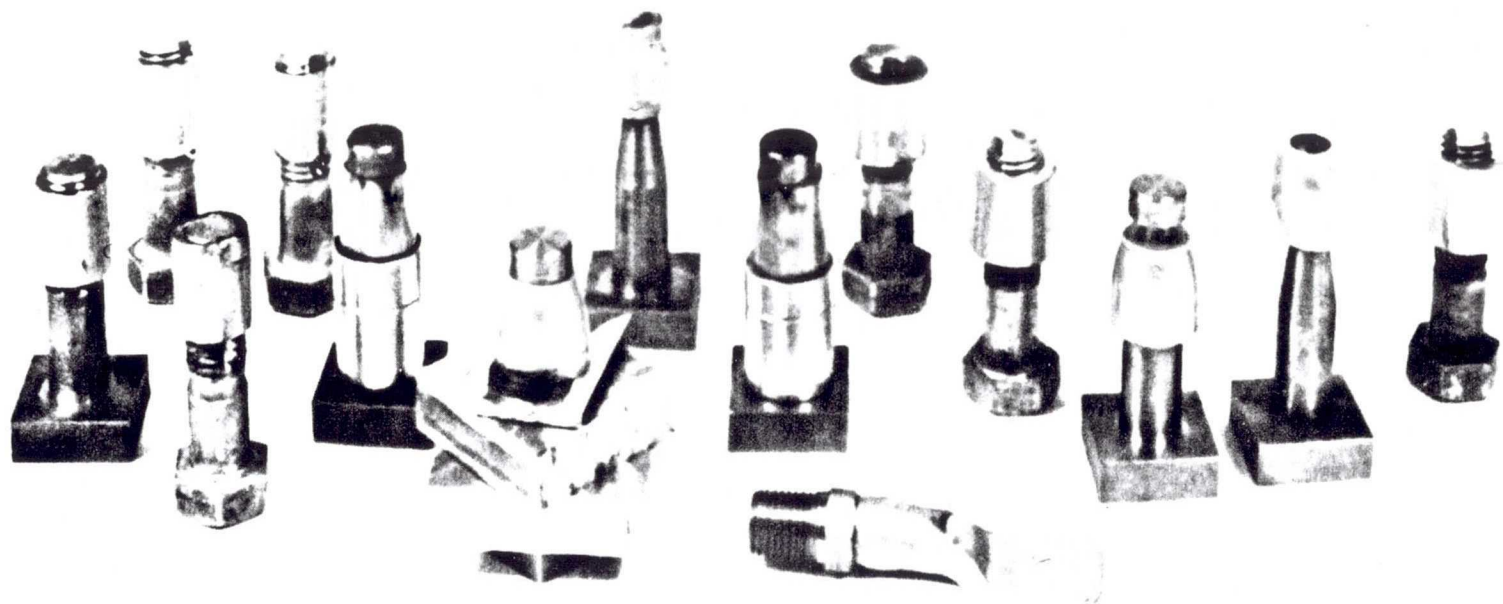


Fig. 31.6 Typical applications of Magnelok components.

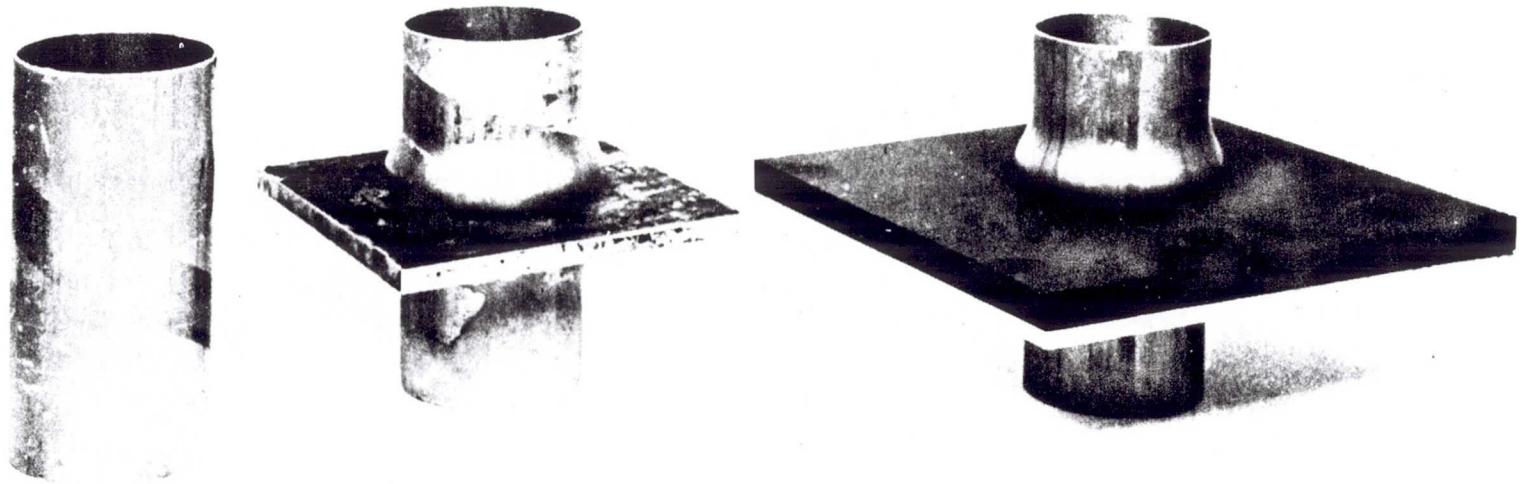


Fig. 31.7 Magnetically formed components.

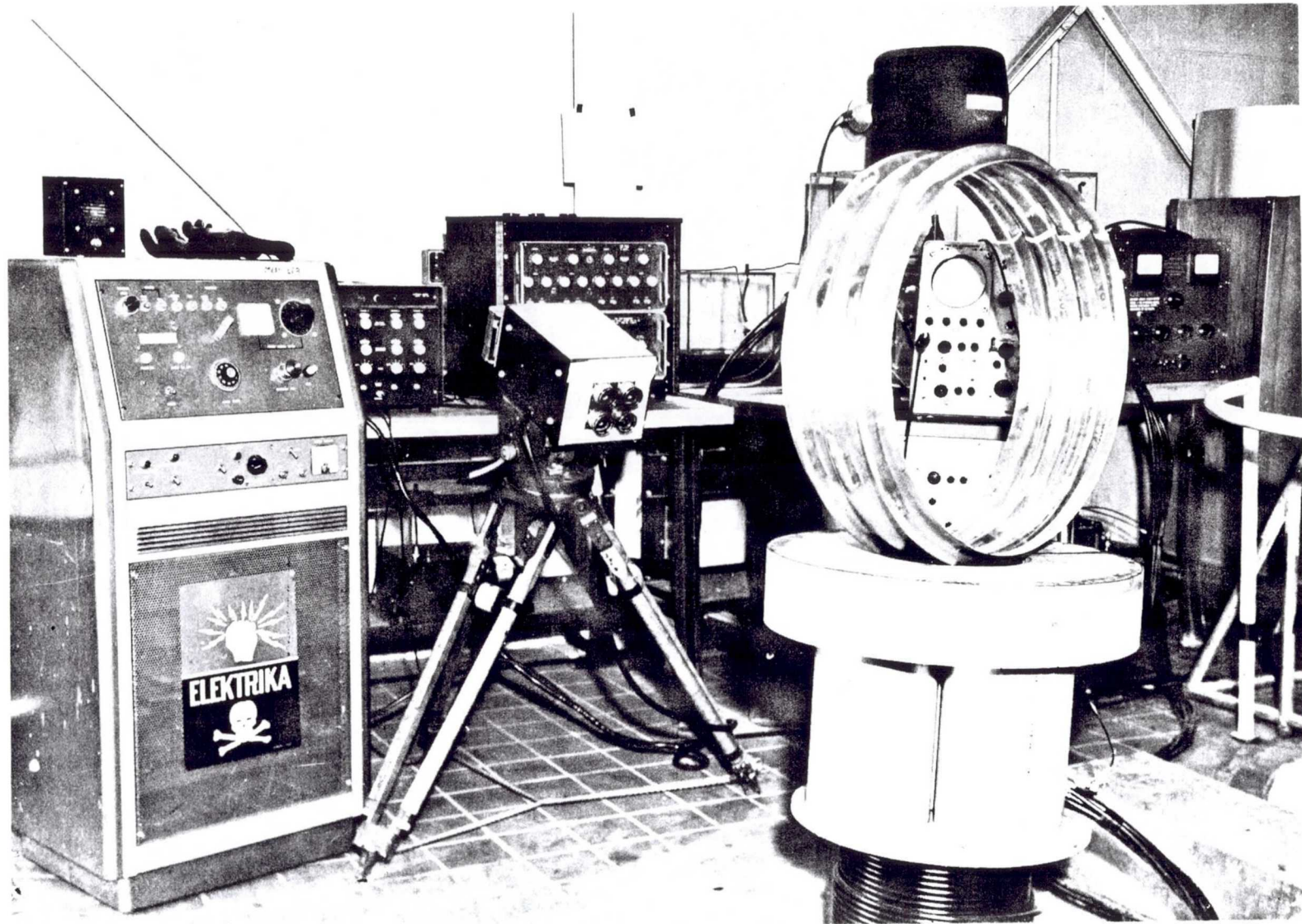


Fig. 31.8 Magnetically formed cylinder 24 in. in diameter.

The use of a magnetic field to punch holes has been demonstrated at the George C. Marshall Space Flight Center. A pancake, flat-type coil was used to punch a 6-in. diameter hole in a 1/8-in. high-strength, aluminum alloy -- again by proper utilization of the high-intensity magnetic field and inertia effects. This means that a hole punching in the space environment is also very feasible, especially in conjunction with some form of integral, discrete-energy storage. In addition to hole punching or meteorite repair, one can easily envision numerous other applications of this same general principle. Tubes can be run through bulkheads and sealed by this tremendous internal magnetic pressure. Propellant transfer techniques look promising both in the area of sealing as well as in the area of quick connect couplings. Several of these possibilities are being investigated at George C. Marshall Space Flight Center.

### 31.7 Magnedok Orbital Docking Concept

From what has been said above, it is apparent that tremendous forces can be brought into play at will by the proper programming of stored-energy discharges into suitably designed coils. In this connection, one intriguing possibility for the application of such an intense field lies in the area of final docking maneuvers of orbital vehicles. Since the forces that occur between coil and metal in proximity are high but controllable, one might seriously consider the possibility of using the magnetomotive force to effect a time variable coefficient of restitution in a docking situation. To give some idea of the relative order of magnitude involved in energy density, a 1-megagauss field creates about 560,000 psi magnetic pressure. Such a field might be used not only for braking but for positioning of one vehicle with respect to another or with respect to a space station.

While theoretically within the realm of possibility there are difficult practical problems to overcome. The most obvious difficulty here is the weight of the capacitors required to effect the inelastic collision conditions. Preliminary calculations indicate that if two 20,000-lb vehicles in a 300-nautical-mile orbit are to be docked in this manner, half or more of the vehicle weight would have to be capacitors of the conventional variety. However, if an integral, discrete storage system could be utilized, the situation becomes much more attractive. Further, if a space port is considered, in which vehicles move in and out in docking operations, and allowance is made for the storage and discharge system to be on the space port structure, this type of docking arrangement begins to be competitive weight-wise, and offers many advantages not offered by crushable structures, springs, pistons, etc. Another possibility is the use of magnetic coils as vernier force devices in conjunction perhaps with a honeycomb or crushable structure. With magnetomotive force braking, a decided advantage exists in that no mass is expended to accomplish the braking or kick function. Deceleration rates would tend to be higher, however, because of the field decay rate.

A preliminary study of coils that might be suitable for producing such an inelastic collision has been made. The most desirable coil is the pancake variety some 2 to 5-ft in diameter, depending on force and ring frequency needed. The impulse required to effect docking magnetically is basically the change of vehicle momentum, and certainly a reasonable  $G$  level must be maintained during the deceleration. A problem encountered here is that generation of this force is greatly dependent on coupling, so that a definite limit exists regarding the maximum distance at which such a coil becomes effective in a braking function. Knowledge of the field distribution about such large coils, at present, is practically nonexistent. Flux density at the inside and end of an air-core solenoid, however, can easily be calculated and follows the following relationship

$$B_p = \frac{2\pi \times 10^{-7} NI}{L} \left[ \frac{L/2-d}{\left(r^2 + (L/2-d)^2\right)^{\frac{3}{2}}} + \frac{L/2+d}{\left(r^2 + (L/2+d)^2\right)^{\frac{3}{2}}} \right] \quad (31.7)$$

where  $B_p$  = Webers per  $m^2$

$NI$  = Ampere turns

$L$  = coil length

$d$  = point in question on the longitudinal axis.

$r$  = coil radius.

The distribution of Figure 31.9 was determined on a Recomp II computer by varying parameters incrementally in Eq. (31.7). This shows that a solenoid type coil is not suitable for generation of large area braking, or kick forces. Figure 3.10, on the other hand, indicates the field distribution in the plane of a single turn coil. The additional turns in a pancake coil have the beneficial effect of considerably increasing the flux density of the coil across the diameter. Figures 31.9 and 31.10 show the desirability of flat, multiturn, pancake coils where generation of large-area, fairly uniform force is required, as would a docking operation. Such a coil has been used in the laboratory to punch a hole through an aluminum alloy with the magnetic field. From these illustrations it is obvious that braking would have to be effected in the very last few feet, or perhaps before contact since the field drop-off on the longitudinal axis is appreciable.

### 31.8 Future Developments

All our work with stored energy, EBW and magnetic fields to date has been done with a 24,000-joule capacitor bank. Figure 31.11 shows part of the 240,000-joule Medusa system being installed for future work with high-intensity fields and with electric discharge forming. The blast chamber pit and discharge head are at the center, while the main

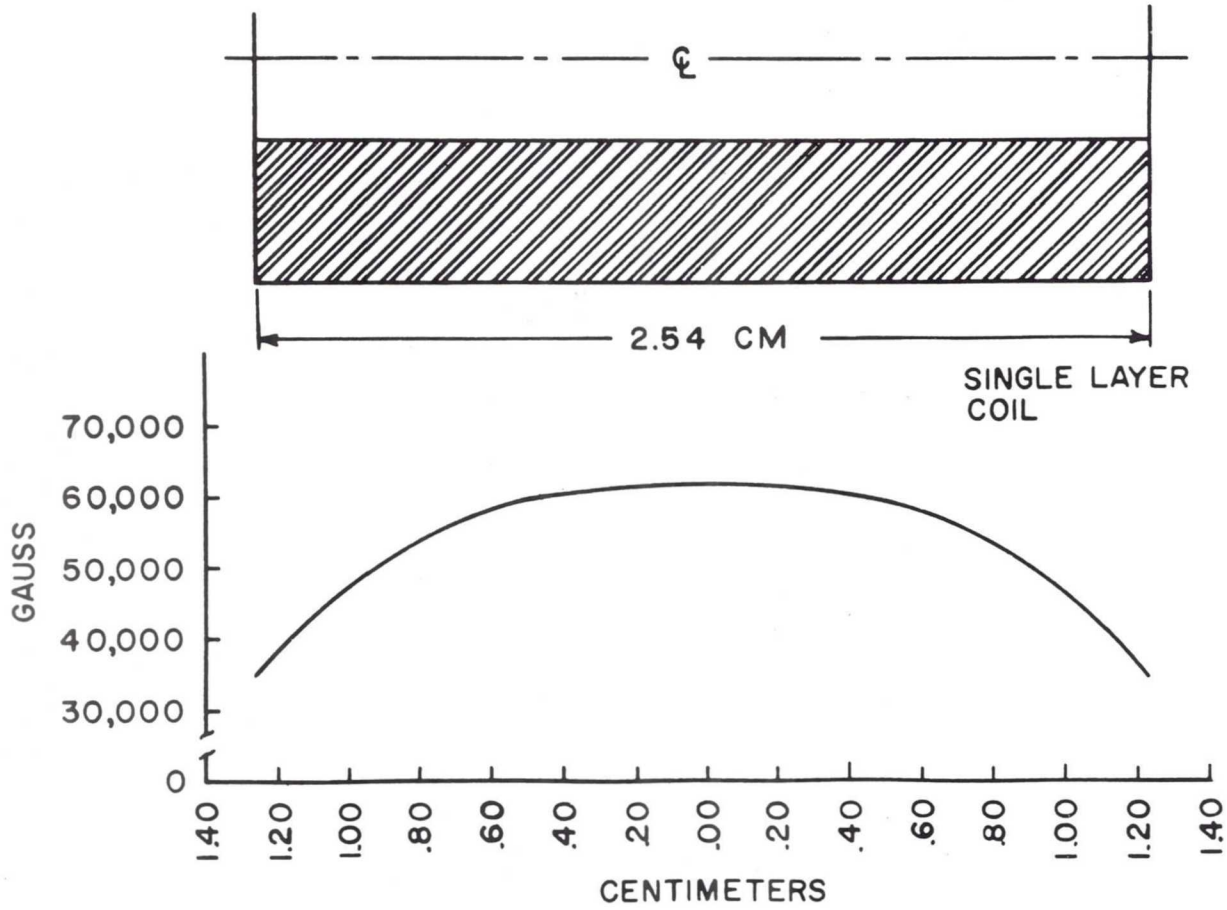


Fig. 31.9 Graph of flux density versus axial position inside a single layer coil.

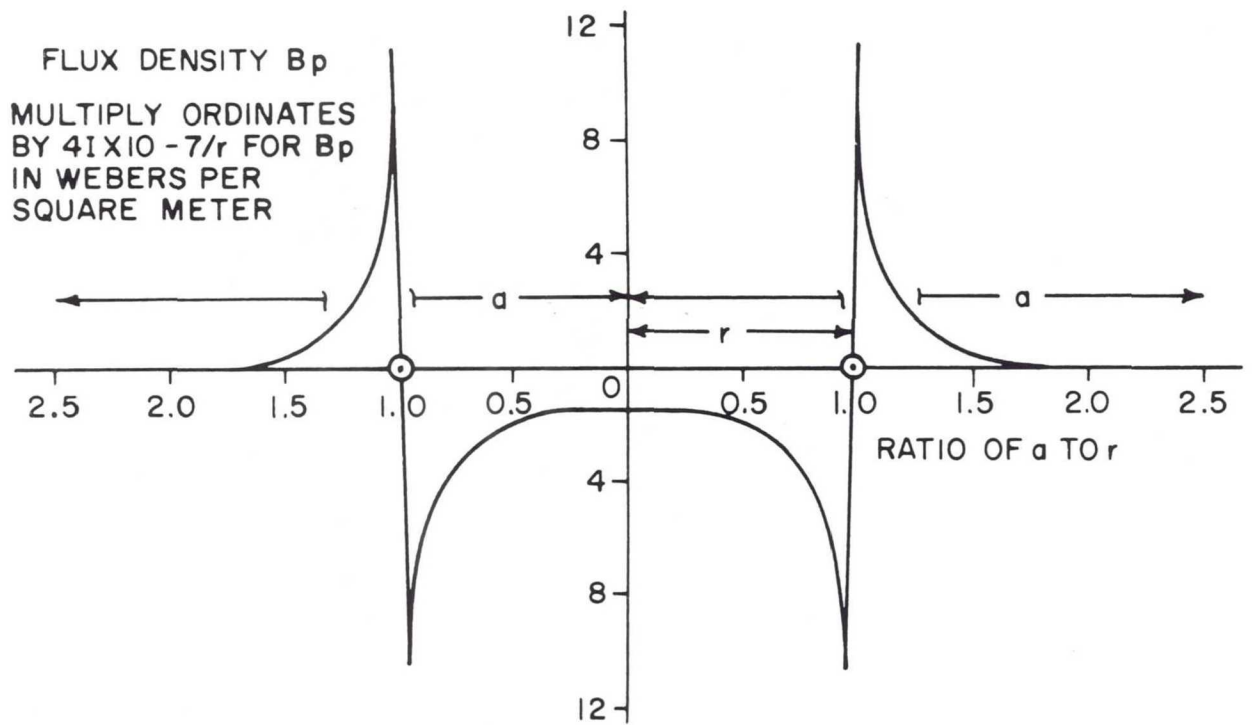


Fig. 31.10 Graph of flux density variation over the plane of a one turn coil.

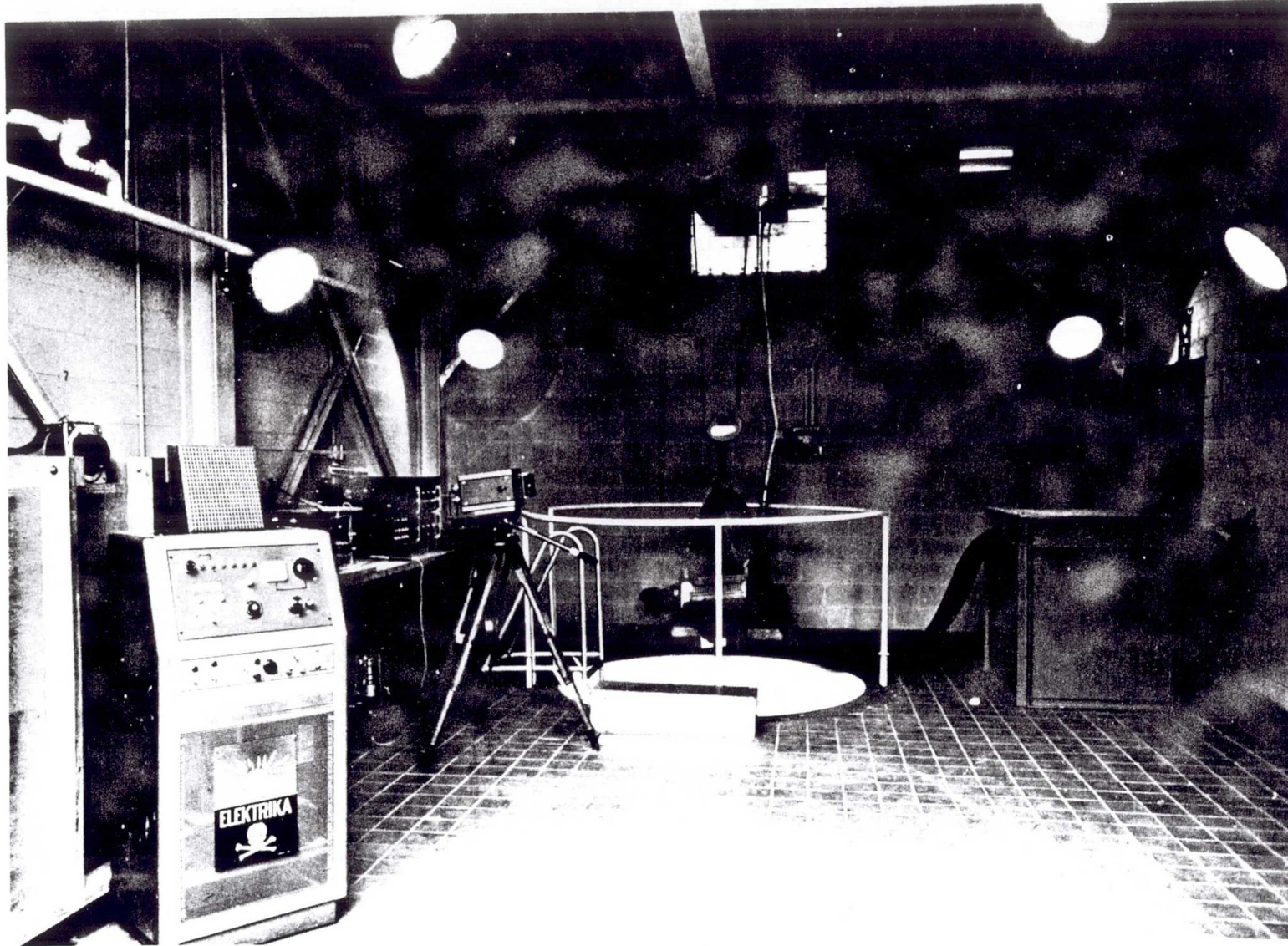


Fig. 31.11 Laboratory view of blast chamber pit, discharge head and current collector for use in both exploding bridgewire and intense field work.



current collector is at the right, enclosed by a steel box. The current collector facilitates either high-field tests or EBW-fluid media tests by a simple substitution of terminal apparatus. Eighty coaxial cables connect the collector to the terminal apparatus. Figure 31.12 is a closeup of the 240,000-joule discharge head. Electrodes are in-line, in Figure 31.12, and at the bottom of the head. It is hoped that 2 to 3,000,000 peak horsepower with the Medusa can be achieved. Figure 31.13 is a view of the Medusa capacitor room looking toward the ceiling. Assembly of the bank is incomplete, but the individual ionization switches can be seen at the top of the individual banks. The Medusa is designed to allow variation of the total discharge time. It is also possible to achieve any energy level up to the maximum 240,000 joules. This new system will play a dominant role in experiments with advanced space vehicle fabricating techniques and in the development of space applicable items such as the magnelok fastening system.

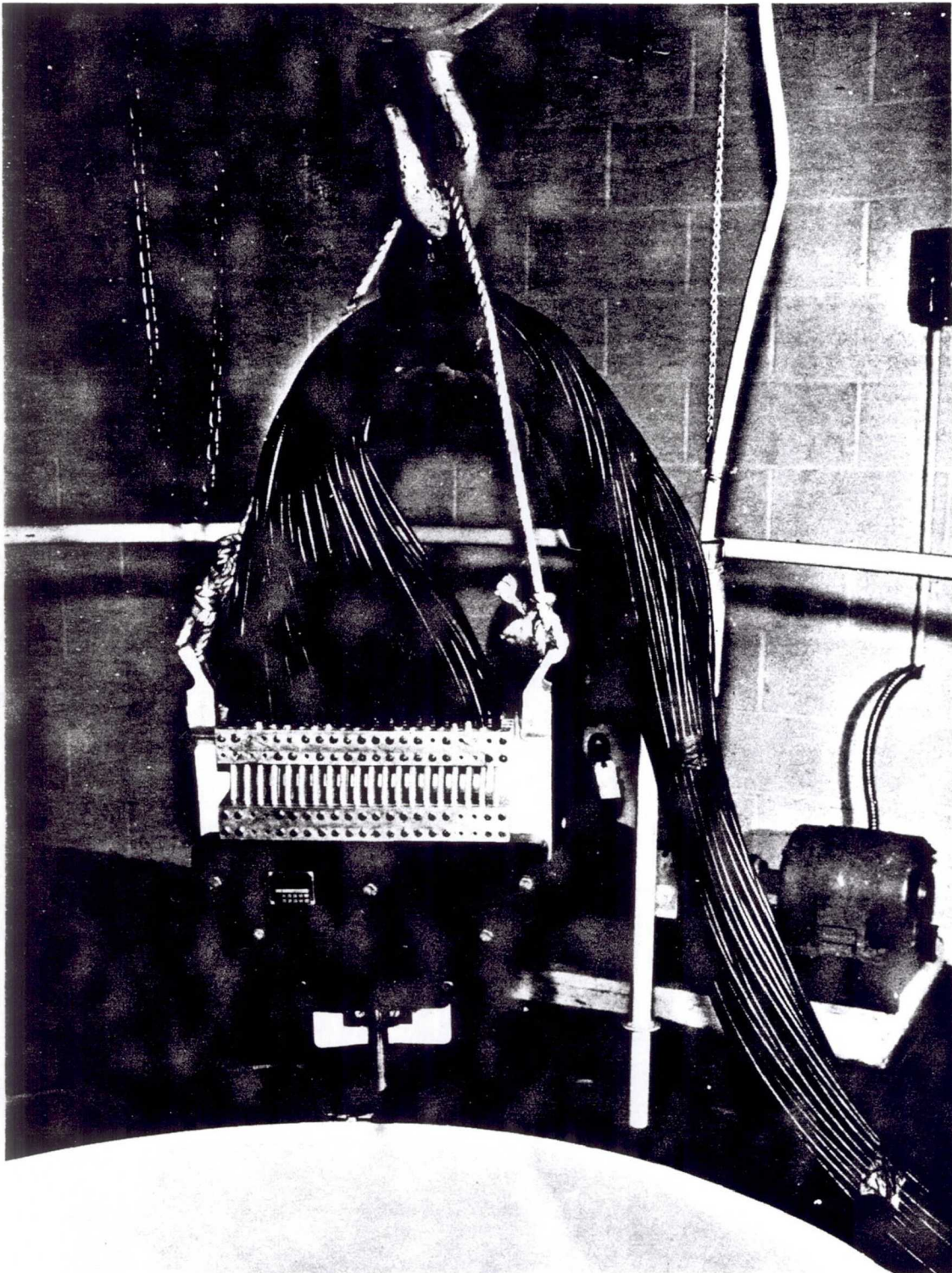


Fig. 31.12 Electric discharge head for use in exploding bridewire tests.



Fig. 31.13 Medusa system capacitor bank during assembly.

## REFERENCES

1. Yutkin, L. A., "Elektrogidravlicheskiy Effect", Mashgit, Moscow, 1955.
2. Kapitsa, P. L., Proceedings of the Royal Society of London, 1958 (734): 691, (1924).
3. Schwinghamer, R., MSFC Technical Report M-F&AE-MTP-61-27, October 27, 1961.
4. Foner, S. and Kolm, H., Review of Scientific Instruments, 28:799 (1957).
5. Furth, H. and Wanick, R. Review of Scientific Instruments, 27:195 (1956).
6. Furth, H., Levine, M., and Waniek, R. Review of Scientific Instruments, 28:949 (1957).
7. Wagner, H. and Boulger, F., High Velocity Metalworking Processes Based on the Sudden Release of Electrical Energy, Batelle Memorial Institute, Memo. 70, Defense Metals Information Center.
8. Furth, H. P. Science, 132:387 (1960).
9. Bitter, F., Review of Scientific Instruments, 10:373 (1939).
10. Foner, S. and Kolm, H., Review of Scientific Instruments, 27:547 (1956).

7/12

**From Peenemünde to Outer Space**



4106

## THE INTERVAL TRANSFORMER TANK LEVEL AND FLOW GAGE

Dieter K. Huzel

Space & Information System Division  
North American Aviation, Inc.  
Downey, California

A liquid oxygen-alcohol powerplant for an early Navaho MX770 surface-to-surface cruise missile configuration was in development in 1950. Subsequently, it became the engine that powered the Redstone ballistic missile. It soon became apparent that available propellant-flow metering systems would be inadequate for the rapidly tightening specifications governing the performance of liquid rocket engines. Therefore, a multiple approach search was initiated for improved flow metering methods. Among these was the interval transformer gage (also known as the inductance gage).

In mid-1951 the writer proposed the tank-level and propellant-flow gage principle, subsequently, refined and developed by L. H. Groeper. M. A. McClure also contributed valuable ideas. The basic system consisted of a number of fixed coils enclosed in a metallic tube installed vertically in the propellant tank and connected electrically in a Wheatstone bridge arrangement. A toroidal float encircling the tube carried one or several members that altered the magnetic field produced by each coil when energized by an alternating current and thus unbalanced the bridge. The bridge output was recorded on a galvanometer oscillograph, and provided a precise record against time of the movement of the float (liquid level) past each coil. By means of a prior calibration of the tank and level gage combination, the exact volume between coils was known so that steady flow rates could be determined with great accuracy. More important, it provided a means for calibrating precise, turbine-type flowmeters that are very sensitive to fluid changes and entrance duct conditions. In combination with the transformer gage, the turbine-type flowmeter could now be calibrated in the actual ducting and with the actual propellant at steady flow rates. Once its factor was thus established, it could be used in transient operation as well. A means of periodically monitoring its calibration was also provided. As a result, flow measurement accuracy is greatly improved, by an order of magnitude, over previous methods. This concept has been used in all of Rocketdyne's large engine test stands for over a decade.

### 32.1 Basic Approach

During the early phases of the Navaho engine development program, propellant-flow-rate measurements were made by recording the change (decrease) of top and bottom differential pressure on an inking recorder. Flow-measurement accuracy during steady-state conditions was of the order of 3 per cent or less.

The method employed was entirely unsatisfactory for use during transient conditions, a serious handicap for rocket engine performance evaluations and for the investigation of transition phenomenon, particularly those encountered during startup. Other conventional flowmetering devices had been considered and found to be even less suitable for rocket engine use. Rotameters and sight gages were obviously unsuitable for this application, and orifices were unsatisfactory because of their relatively stringent requirements for installation configuration and their highly undesirable pressure losses. Available float-type switches were considered but appeared to be unsatisfactory considering the need to enter the tank by means of either electrical cables or mechanical linkage. Sealing and other problems were expected to occur, particularly in connection with the use of cryogenic propellants. In short, an urgent need existed for a flowmetering device that could accurately measure flow rates of liquid levels either from the outside or the inside of the tank without a linkage of any kind requiring static or dynamic seals.

It was concluded that the installation of a gage in a tubular well, mounted inside the tank, could be considered for all practical purposes as an installation outside the tank. This solution was therefore proposed. It was further proposed that the liquid level should be measured by way of floats, the position of which would be detected by suitable sensors inside the well, and that an electromagnetic field should be used to accomplish this.

### 32.2 Description of Gages

In its basic and earlier configurations, the gage assembly consisted of a leakproof, metal tube 1 in. in diameter and of low magnetic permeability and low electric conductivity enclosing a number of thin, equally spaced, electric coils. It also included a toroidal float assembly consisting of a central plate and float with an additional number of accurately spaced disks (elements) attached to it (Fig. 32.1). The coils were connected in a Wheatstone bridge circuit, fed by a 3000-cps, 10-v oscillator (Fig. 32.2). The tube containing the coils was installed vertically in a propellant tank, with the float assembly free to move axially along the tube as the liquid level changed.

In operation, when an element of the float assembly moved into the plane of any coil, it acted as a short-circuited secondary coil of a



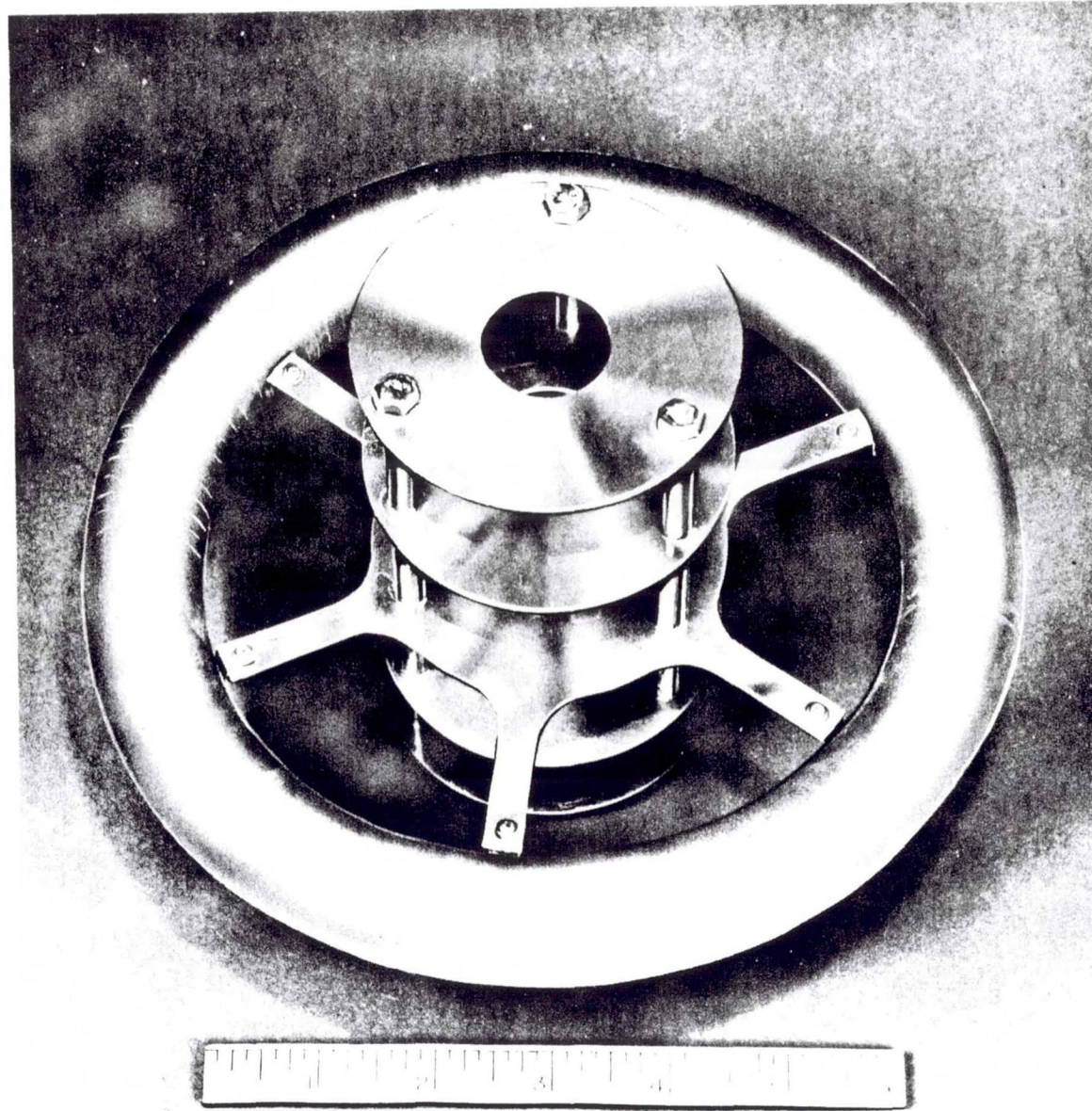


Fig. 32.1 Toroidal float assembly for interval transformer tank level and flow gage.

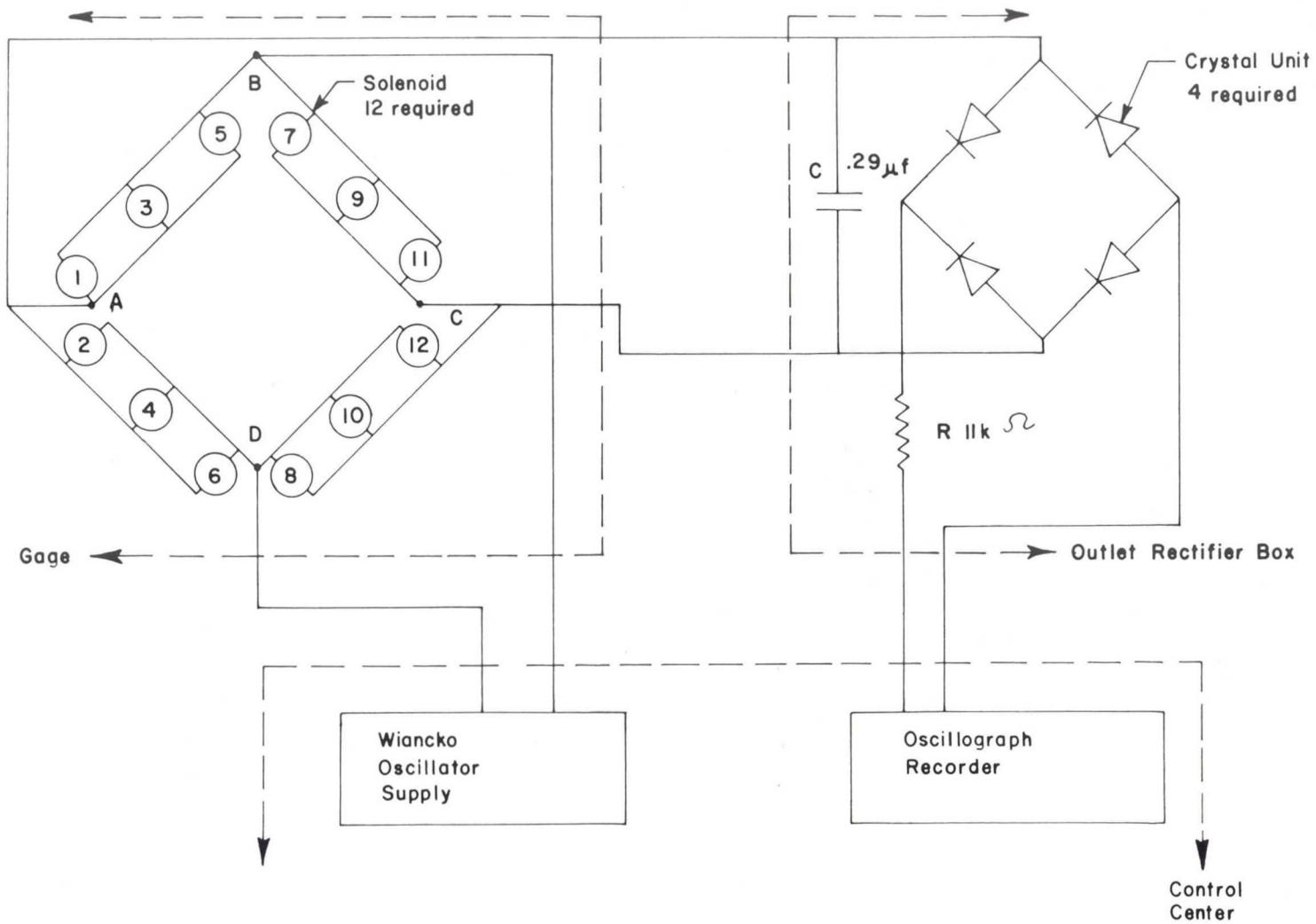


Fig. 32.2 Wheatstone bridge circuit for interval transformer tank level and flow gage.

transformer, producing an electrical signal that was recorded as a pip on an oscillogram. Each of the disks attached to the float produced signals of different magnitudes (effected by different center hole dimensions) and, thus, accurately described the physical action of the float in the vicinity of the coil. It was assumed that the liquid level might frequently be disturbed (splashing or sloshing), causing the float to bounce rather than to move smoothly downward. This in turn, could cause one or more disks to pass a particular coil several times; however, with the individualized signals produced by each float element, the path of the float could be plotted and accurately averaged. The intersection of this averaging line with the center (torus) plane was taken as the true float passing time (Fig.32.7). After this information was obtained for any two coils, the time differential and known volume between these two coils could be used to determine accurately the average flow rate during that period. This presupposed that the volume represented by each coil plane had been determined very accurately by a prior calibration.

The earlier development test tanks for the Redstone engine were equipped with gages containing 12 coils spaced approximately 10.5 in. center-to-center. The float in use with these gages, known as a pentapip float, consisted of a metallic annulus with four stabilizing vanes suspended below it. Figure 32.3 shows the complete gage, with the coil assembly removed from the tube. The gage shown here has a float without additional vanes.

### 32.3 Calibration Procedure

For flowmetering devices recording the volume flow rate per unit time, accuracy depends on the quality of the measurement of both parameters. The great advantage of the interval transformer gage is that one of the volume parameters can be determined accurately in advance of the actual flow measurement. This is accomplished essentially by the accurate determination of the tank volume with respect to each coil plane. A first prerequisite to attaining this accuracy is careful preparation, assembly, and installation of the gage. An effort was always made to assemble the coils with uniform spacings. Following assembly, this spacing was rechecked and recorded. As a next step, the coil and bridge circuitry were carefully balanced with the float removed. As experience was gained, this procedure gradually became a routine matter due to improved manufacturing techniques. Once installed, the spatial relationship of the gage and its coils to the tank could not be altered or the calibration would have been voided.

With the gage and its float properly installed, the actual tank calibration, always accomplished with water, could begin. Figure 32.4 shows an early calibration arrangement. Accurate and continuous water temperature measurements were a part of the procedure. The float used for calibration was not necessarily the one used for subsequent engine testing. The calibration would begin by filling the tank with water. For the fuel

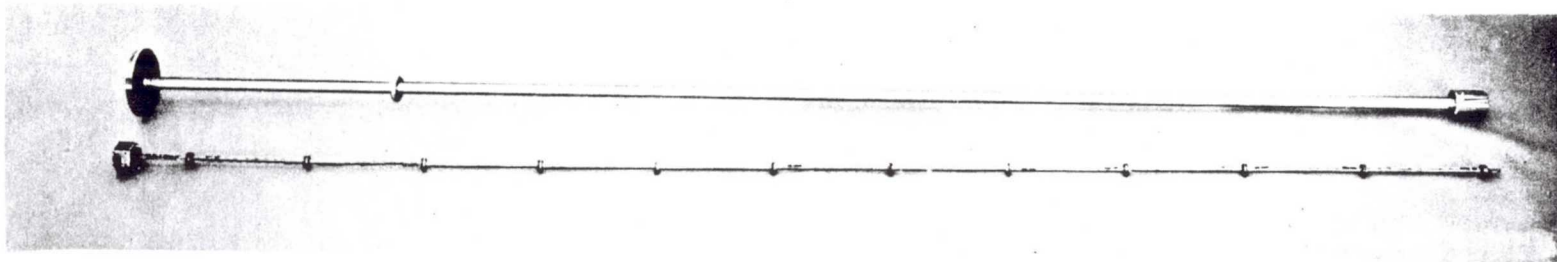


Fig. 32.3 Coil assembly removed from tube of interval transformer tank level and flow gage.

**Propellant Tank  
Calibration Set Up**

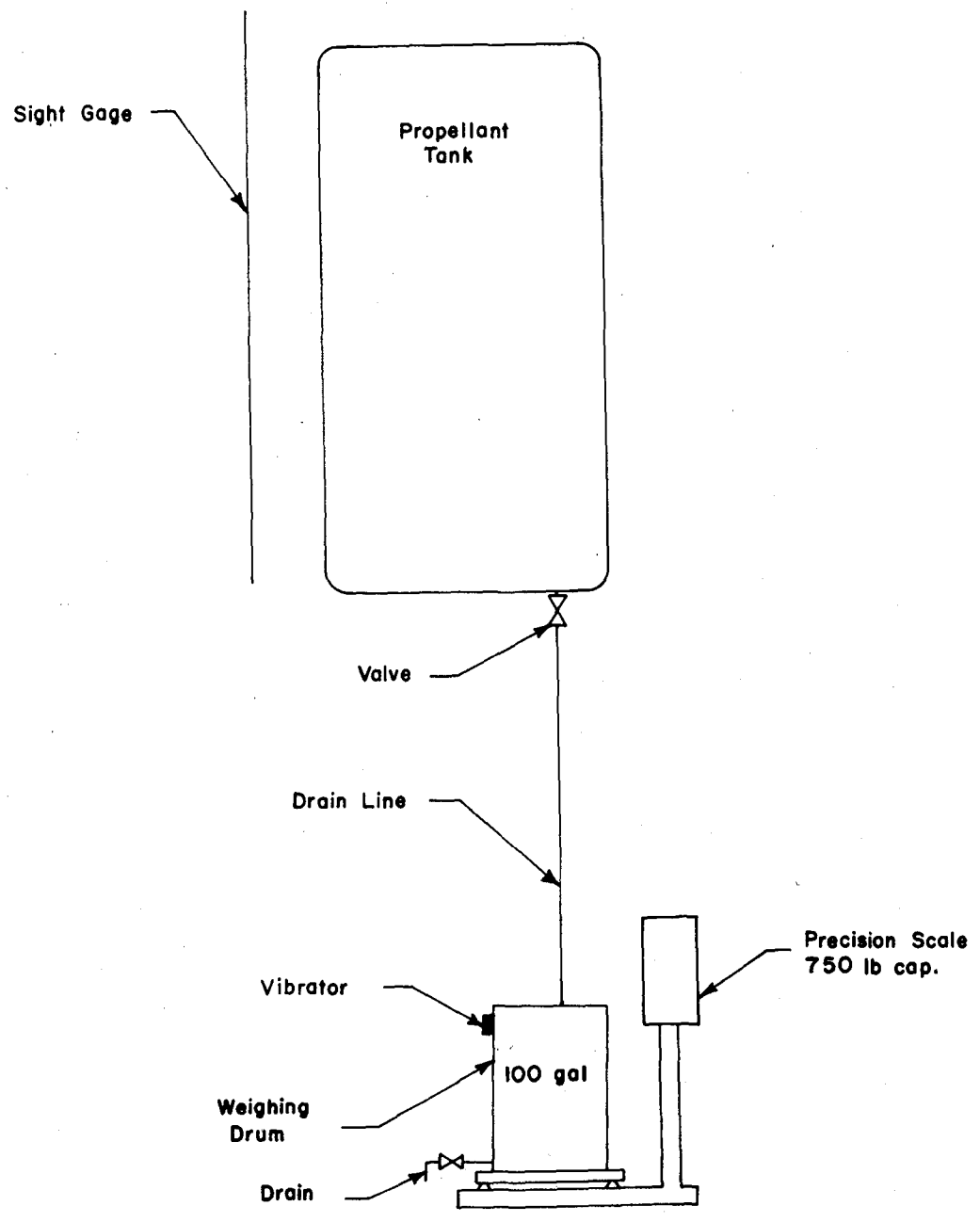


Fig. 32.4 Propellant tank calibration setup.

tank, conversion to actual fuel density following calibration was a simple procedure. For the oxidizer tank, additional corrections had to be made to allow for thermal contraction. Following filling, the tank was slowly drained in increments into a weighing drum (Fig. 32.4). As the liquid level approached a coil station, a galvanometer connected to the coil bridge circuit was deflected. During careful and slow draining which avoided any surface disturbances, the passing of the float and the corresponding volumes were recorded. For increased accuracy, predetermined galvanometer deflections were recorded rather than deflection maxima (Fig. 32.5 and 32.6). The trace shown in Fig. 32.5 corresponds to a two-vane float. It is noted that the accuracy and sensitivity of the gage was such that a few cubic inches out of a 3000-gal container were sufficient to alter appreciably the galvanometer deflection. Under actual run conditions the direct-reading galvanometer would be replaced by an oscillograph galvanometer. The procedure was continued until the float had passed all coils. To avoid gross errors, such as omission of a coil, simultaneous sight-gage readings were taken. The entire procedure was repeated several times to arrive at a highly reliable and accurate set of mean values. It was preferable to repeat the procedure on different days.

During the years following these early calibrations, procedures were improved continually. Detailed instructions and procedures were worked out, simultaneously satisfying various specifications. Electronic and automation equipment were widely substituted. As a result, calibration time was reduced drastically, while accuracy was increased substantially. For example, the volume of a major Atlas engine test tank, using a 24-coil system, was determined to within 0.042 per cent at the 95 per cent confidence level.

#### 32.4 Run Evaluation Procedure

As evidenced from the calibration procedure the interval transformer gage was principally a means of accurately measuring the flow rate during the steady-state portion of a rocket engine test firing. During this firing, precise determination of the coil-to-coil passing times is all that is required; however, to obtain and maintain the desired accuracy, a number of additional actions were found necessary during subsequent evaluation and run-data reduction.

The float bounced considerably during a run. This resulted in the vanes passing a coil several times--down, up, and then down again. Elaborate graphical and mathematical methods were developed to average the float motion analytically. Figure 32.7 represents the plot of a typical run, and replotted to permit a rather accurate determination of the times at which the float passed the coils. The letters and numbers refer to coding marks in the original oscillogram.

In later years, this averaging process was substantially improved

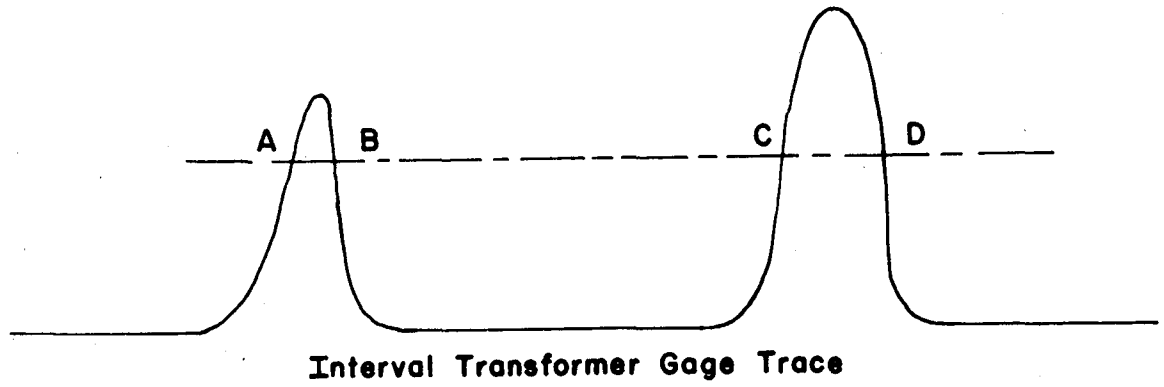


Fig. 32.5 Trace mode by 2-vane float.

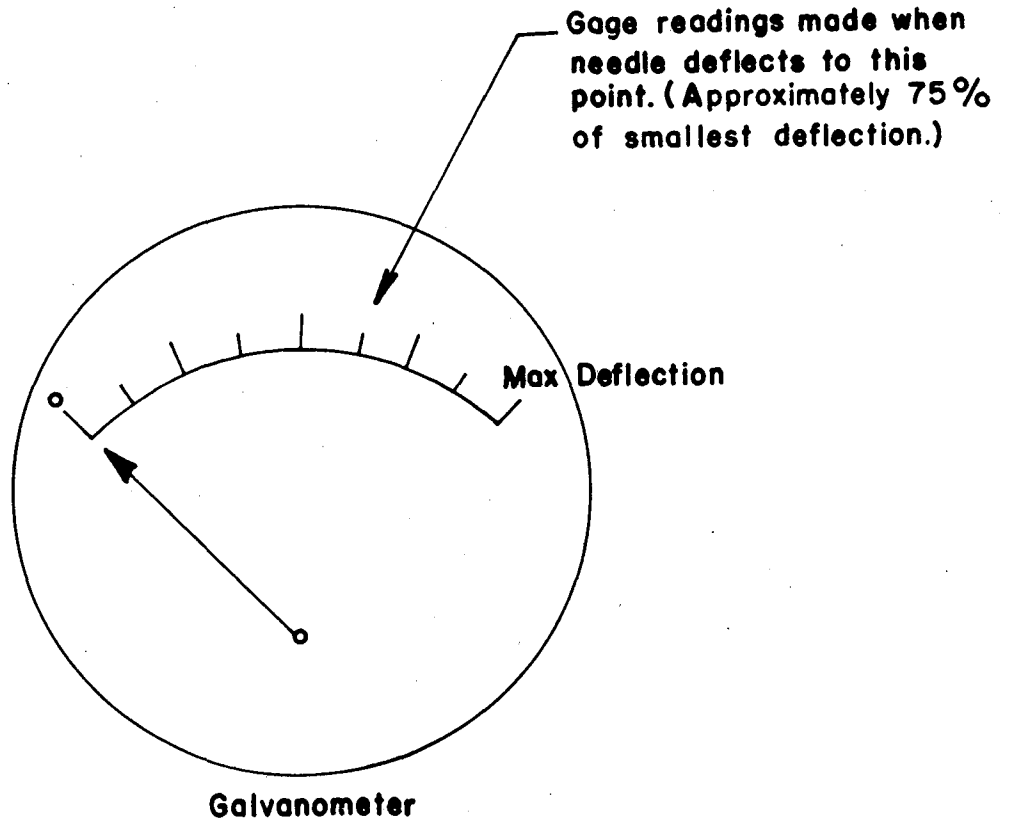


Fig. 32.6 Galvanometer deflection used in calibration.

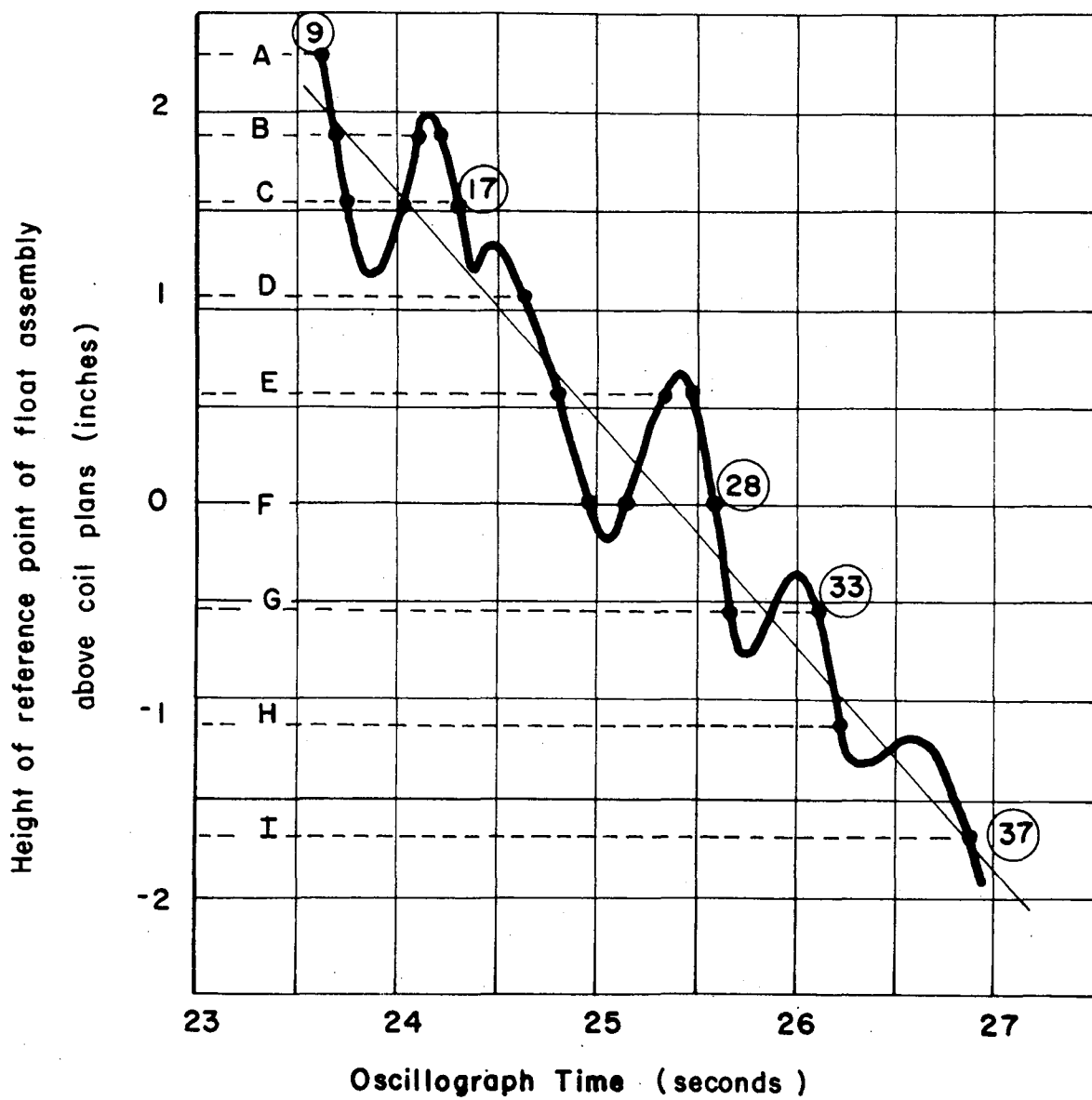


Fig. 32.7 Typical calibration curve.



through utilization of computers and other electronic devices. However, the basic principle always remained the same; accurate, steady-state measurement of flow during actual firing through predetermination of tank volume increments and the measurement of time intervals only.

### 32.5 Observations and Improvements

During the course of the development and subsequent use of the interval transformer gage, many of its specific characteristics were observed and analyzed, advantages were confirmed, improvements were made, and usefulness was increased. Some typical considerations which played a role in the refinement of the transformer gage were:

1. Optimum number and spacing of coils.
2. Precision of gage assembly, including uniformity of materials.
3. Avoidance of electrical capacities influence.
4. Optimum number of vanes.
5. Most efficient methods of determining true passing time.
6. Avoidance of incorrect float installation (upside down).
7. Avoidance of gage damage during handling and installation.
8. Best orientation of coils.
9. Periodic and careful recalibration.
10. Uniform calibration specifications.
11. Strict adherence to calibration specifications.
12. Optimum oscillograph chart speed.
13. Proper identification of individual vane pips.
14. Application of stillwells and similar devices.
15. Modified float designs (spherical rather than toroidal).
16. Application of latest electronic and automation equipment.
17. Minimum number of pips required for reliable flow-rate determination.

All areas listed were subjects of exhaustive studies. As a result, the overall steady-state flow rate accuracy as measured by a present-day transformer gage during a rocket engine firing is approximately 0.25 per cent.

### 32.6 Transient Flow Measurements

When the transformer gage was first applied, complicated phenomena were observed during rocket engine transition to mainstage. These observations indicated the need for a flowmetering device capable of measuring accurately and recording rapidly the changing flow rates, thus a proposal to use a turbine-type flowmeter. These meters were capable of measuring transient flow rates with high response rates. They had a high degree of repeatability under identical conditions; however, the turbine flowmeter was extremely sensitive to installation and to the type of propellant used.

Thus, prior calibrations (when available for the high flow rates used) were usually worthless, with errors of several per cent not uncommon. This situation was completely remedied by using an interval transformer gage calibration of the turbine flowmeter as the standard in an actual firing. This approach permitted calibration of the turbine flowmeter in its run position using actual propellants. The calibration run also had to be of sufficient duration to obtain a minimum number of transformer coil recordings. The overall accuracy of a turbine flowmeter calibrated in this manner is about 0.25 per cent. This accuracy is believed to be maintained in a wide band of flow rates, except the very low ones, where it may be somewhat less accurate. For all practical purposes, however, transient flow rates can now be measured with high accuracy.

### 32.7 Conclusions and Outlook

For more than a decade, the interval transformer gage has been in successful use in the propellant tanks of all large rocket engine test facilities at Rocketdyne. All Rocketdyne-produced rocket engines used in launches, including the substantial number which boosted satellite vehicles into orbit, were calibrated directly or indirectly with the aid of the interval transformer gage. Only recently has a magnetically triggered switch become available that is gradually replacing the transformer coils of the interval gages. A large percentage of the technology, however (including calibration procedures, methods of analysis, and electronic equipment), remains applicable with respect to the beneficial, interval gage - turbine flowmeter relationship.

7/23

**PHYSICS AND BIOLOGY**

## OBSERVATION OF GALACTIC AND SOLAR COSMIC RAYS WITH EXPLORER 7

Wei Ching Lin and James A. Van Allen

Department of Physics and Astronomy  
State University of Iowa  
Iowa City, Iowa

This paper provides a summary of cosmic ray intensity observations at high latitudes over North America and Australia in the altitude range 550 to 1100 km during the period October 13, 1959 to February 17, 1961.\* Data are derived from receptions at Iowa City, Iowa; Ottawa, Canada, and the NASA stations at Blossom Point, Maryland; and Woomera, Australia. Of special interest were the observational data secured on some 20 solar cosmic ray events, including major events occurring in early April and early September 1960, and in mid-November of the same year. The experiment was conducted in the IGY Explorer 7 (1959 Iota) satellite developed by the Army Ballistic Missile Agency's payload group (which was subsequently transferred to George C. Marshall Space Flight Center).

To carry out the radiation measurements a small instrument comprising two Geiger tubes of different size and of different shielding was prepared by G. H. Ludwig and W. A. Whelpley of the Department of Physics and Astronomy, State University of Iowa [1]. The successful operation of Explorer 7 permitted an especially valuable survey of corpuscular radiations in the vicinity of the Earth with a single set of detectors.

The instrument was constructed to permit a comprehensive study to be made of:

1. The lower regions of the inner and outer radiation belts,
2. Primary cosmic ray intensity near the Earth, and
3. The arrival of solar cosmic rays.

---

\*These observations were supported in part by the National Aeronautics and Space Administration and by the Office of Naval Research.

Table 33.1 provides a brief tabular summary of solar cosmic ray events observed by Explorer 7 during the observational period and Table 33.2 reviews the properties of the two Geiger tube detectors in the instrument [2].

### 33.1 Method of Analyzing Data

The method of analyzing data used in this paper is similar to that previously reported [2]. Since then it has been found\* that the apparent counting rate of the 112 Geiger-Müller tube saturated at a considerably lower value than that found by Ludwig and Whelpley [1] in pre-flight calibrations. The apparent counting rate of the 302 Geiger-Müller tube also saturated at a lower value. Because the 302 tube has a considerably smaller geometric factor than that of the 112 tube, and because the additional shielding of the 112 tube has little effect in absorbing the radiation encountered in the lower edge of the inner radiation zone near the equator, it was possible to construct an approximate curve of apparent rate vs true rate of the 112 tube by using in-flight data.

This curve was then checked and refined by an extended study of the characteristics of the spare flight unit of the Explorer 7 apparatus. The significant variables were found to be the supply voltage to the amplifiers, pulse formers and scaler (nominal value 6.5 v), and separately the high voltage supply for the Geiger-Müller tube (nominal value 700 v). Some sample results are given:

Circuit Voltage, v	High Voltage, v	Saturation Counting Rate of 112 Tube, counts/sec
a. 4.05	630	305
b. 5.35	630	385
c. 5.20	640	515
d. 6.00	700	930

Full characteristic curves of apparent vs true counting were run for each of the above conditions to correspond to various flight conditions (Fig. 33.1).

The saturation counting rate of the 112 tube, as observed during passages through the inner radiation zone, showed a systematic dependence on local time. The maximum was found at 0800 hr local time, the minimum at 1900 hr local time, and the maximum-to-minimum excursion of 60 counts/sec out of a total value of about 400 counts/sec. This effect is

---

\*By examination of counting rate data under high intensity conditions during the November 1960 solar cosmic ray events and during passages through the inner radiation zone.

Table 33.1 Solar Cosmic Ray Events Observed by  
Explorer 7

Date	Approximate Absolute Peak Intensity of Protons having $E > 30$ Mev particles $(\text{cm}^2 \text{sec})^{-1}$
<u>1959</u>	
Nov 9	10
Nov 30-Dec 2	0.3
Jan 11-14	2
Mar 18-20	0.3
Apr 1-2	210
<u>1960</u>	
Apr 5-6	> 5
Apr 28-29	32
Apr 29-30	18
May 4	40 <sup>a</sup>
May 5	11
May 6	13
May 7	25
May 13-14	50
May 18	0.8
May 26	0.8
June 1-2	5
June 4	1.3
Aug 12-16	2
Sept 3-9	250
Nov 12-14	12,000 to 46,000
Nov 15-19	11,000
Nov 20-26	1800

<sup>a</sup>Primary peak not observed with Explorer 7.

Table 33.2 Properties of Geiger-Müller Tube Detectors  
State University of Iowa Package in Explorer 7

Detector	$\epsilon G_0^a$	Absorbers over 70% of Solid Angle	Approximate Detection Thresholds		
			Proton	Electron, <sup>b</sup> ex- trapolated range	X Rays, 5% transmission
Anton type 112 Geiger-Müller Tube Scaling Factor: 128	7.2 cm <sup>2</sup>	Stainless steel 0.040 g/cm <sup>2</sup> Al 0.26 Pb 1.15 Mg 0.14	30 Mev	2.5 Mev	80 kev
Anton type 302 Geiger-Müller Tube Scaling Factor: 2048	0.54	Stainless Steel 0.40 Mg 0.14	18	1.1	30

<sup>a</sup>Counting rate of tube for penetrating particles is equal to  $\epsilon G_0$  times omnidirectional intensity  $J_0$ .

<sup>b</sup>For nonpenetrating electrons, sample experimental values of ratio of omnidirectional intensity to counting rate of 302 tube are:

- $10^{13}$  at 14 kev
- $10^{12}$  at 17 kev
- $10^{11}$  at 20 kev
- $10^{10}$  at 26 kev
- $10^9$  at 34 kev
- $10^8$  at 45 kev
- $10^7$  at 70 kev
- $2 \times 10^6$  at 105 kev

(L. A. Frank, private communication, April 1960. Experimental values obtained by electron bombardment of an arrangement similar to the State University of Iowa package in Explorer 7.)

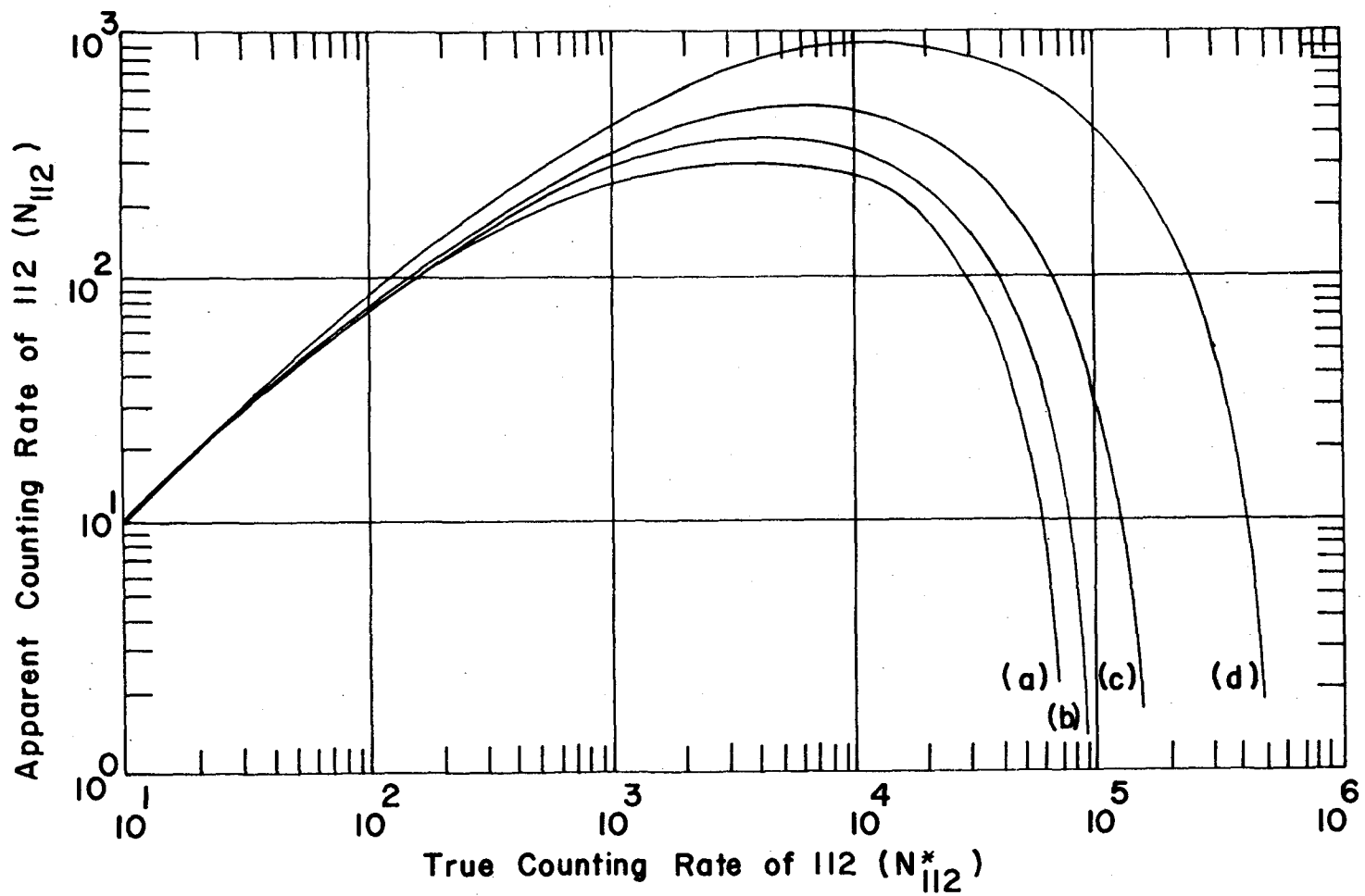


Fig. 33.1 Characteristic curves of apparent versus true counting rate of the 112 Geiger-Müller tube detector in Explorer 7. Apparent counting rate saturates at: (a) 305, (b) 385, (c) 515, and (d) 930 counts/sec.



presumably due to a combination of the effects of the state of charge of the batteries and the temperature. It is felt that a reasonable level of confidence may be placed in the revised curves (Fig. 33.1) of the relation of apparent counting rate to true counting as obtained by the above method.

Most of the data required no dead-time correction and are, therefore, independent of the above discussion. Only the high counting rate data of the early April 1960 and mid-November 1960 events are significantly affected. Previously published absolute intensities for the April 1, 1960 event are corrected herein (Sect. 33.2).

The data presented here were obtained when Explorer 7 was at or near the highest dip latitude which it reached (orbital inclination, 50.4 deg to equatorial plane). In this way there are obtained counting rates having the smallest possible contribution from trapped particles in the outer radiation zone. This contribution is further subtracted to obtain the net counting rate due to penetrating particles (i.e., cosmic rays, in contrast to the soft radiation of the outer radiation zone) by the following technique:

1. A large body of observations of the counting rates of the 112 tube,  $N_{112}$ , and of the counting rate of the 302 tube,  $N_{302}$ , were assembled for quiescent (non-solar event) conditions and for the highest available dip latitudes.

2. To any extent necessary these data were corrected for dead time to yield the respective true counting rates  $N_{112}^*$  and  $N_{302}^*$ . For data shown in Fig. 33.2, the dead-time corrections were trivial.

3. A plot shown in this figure was then made of  $N_{112}^*$  vs  $N_{302}^*$ . From this plot it is seen that  $N_{112}^*$  is a linear function of  $N_{302}^*$  and that as  $N_{302}^* \rightarrow$  zero,  $N_{112}^*$  approaches 14.3 counts/sec. Since the ratio of geometric factors (Table 33.2) for penetrating particles, e.g. ordinary cosmic rays, is 13.3, an  $N_{112}^* = 14.3$  corresponds to  $N_{302}^* = 1.08$ . Hence, the intercept at  $N_{302}^* = 0$  is taken as the pure cosmic ray rate of the 112 tube. The equation of the curve of Fig. 33.2 is

$$N_{112}^* = 14.3 + 0.119 N_{302}^*$$

or

$$\left( \frac{N_{112}^* - 14.3}{N_{302}^*} \right) = 0.119$$

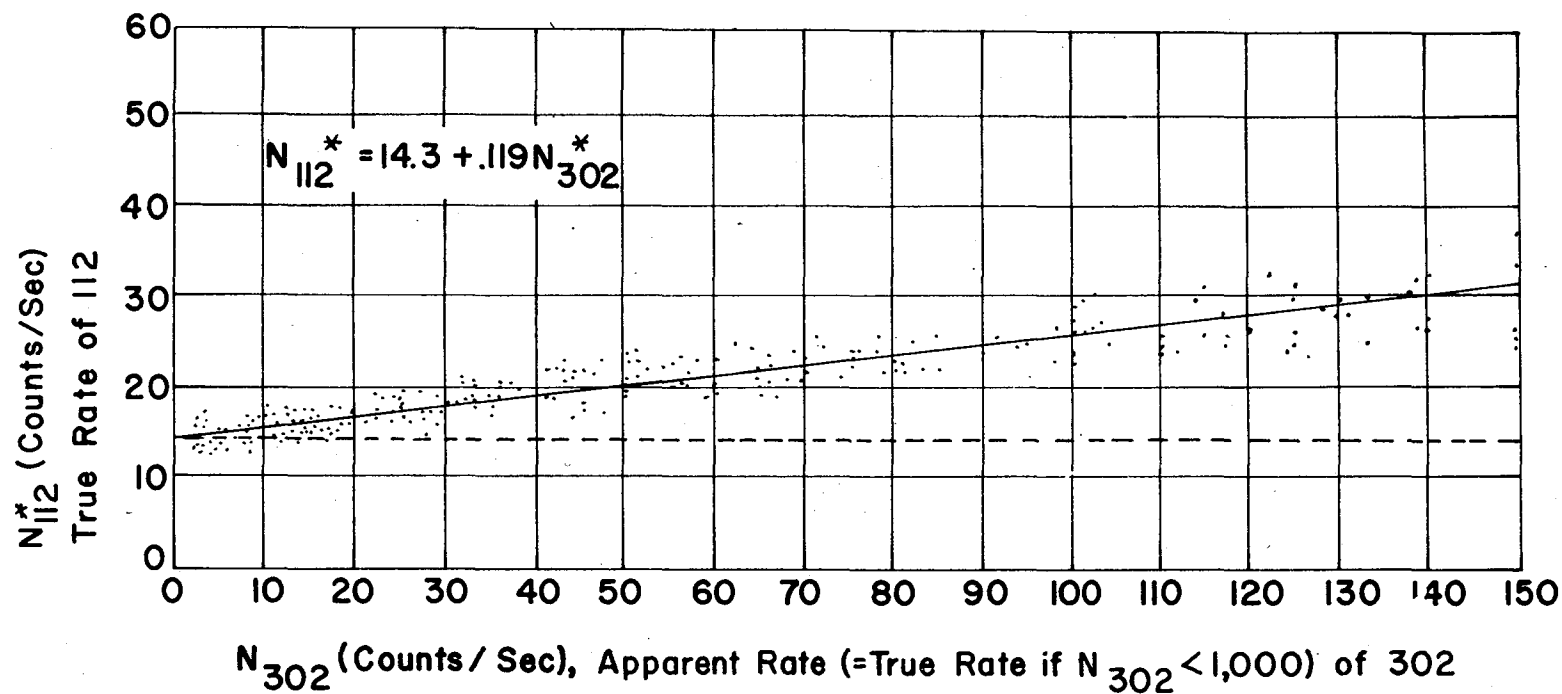


Fig. 33.2 True counting rates of the 112 Geiger-Müller tube,  $N_{112}^*$  versus true counting rates of the 302 Geiger-Müller tube,  $N_{302}^*$ , at the highest dip latitude observed by Explorer 7.

This ratio is similar to that usually observed in the soft radiation region of the outer radiation zone, thus further supporting the belief that Fig. 33.2 can be used reliably in subtracting the contribution of soft radiation to the rate of the 112 tube. It is evident from the latitude dependence of the counting rates of the two tubes that the time-varying outer boundary of the outer radiation zone is the principal cause of the variation of counting rates at high latitudes. The use of Fig. 33.2 makes it possible to increase considerably the sensitivity for the reliable detection of solar cosmic rays. When  $N_{302}^*$  is less than, say 100 counts/sec, one can clearly detect an intensity of solar cosmic rays as low as 2 particles  $(\text{cm}^2 \text{ sec})^{-1}$ , having energies greater than 30 Mev (for protons). It is probable that one could improve this detection capability by an order of magnitude with a satellite passing over the polar regions.

Two examples of the use of Fig. 33.2 follow:

1. In the pass which covered from 0718 hr to 0736 hr UT on November 18, 1959, the position of observation was chosen at 0729.5 hr UT (Fig. 33.3).  $N_{302}^*$ , the apparent counting rate of the 302 tube, is 17 counts/sec; and  $N_{112}$ , the apparent counting rate of the 112 tube, at the same time is 16 counts/sec. From the curve of apparent counting vs true counting rate for the 112 tube (Fig. 33.1), one finds the true counting rate  $N_{112}^*$ , corresponding to  $N_{112} = 16$  is also 16. By Fig. 33.2 and the above discussion, the estimated contribution of soft trapped radiation in the outer edge of the outer radiation zone to the counting rate of the 112 tube is

$$\Delta N_{112}^* = 0.119 N_{302}^* = 2 \text{ counts/sec}$$

The net true counting rate due to cosmic radiation is taken to be

$$N_{112}^{***} = N_{112}^* - \Delta N_{112}^* = 14.0 \pm 1.0 \text{ counts/sec}$$

On June 17, 1960 in the pass which covered from 0542 hr to 0557 hr UT, the time of observation was chosen at 0551 hr UT (Fig. 33.4) at which  $N_{302} = 60$  and  $N_{112} = 20$  from which  $N_{112}^{***}$  can be inferred as about  $13 \pm 1.5$ . The error was estimated from: (1) the fluctuation of  $N_{112}$  near the vicinity of the observation position, and (2) the size of the correction term  $\Delta N_{112}^*$ . During large solar cosmic ray events there is an important (or perhaps dominant) contribution to  $N_{302}^*$  due to penetrating particles in addition to normal cosmic rays. Fortunately, in such cases there is usually an accompanying depletion of the outer radiation zone (cf. Ref. [2]) such that the correction for trapped radiation may be negligible. In solar

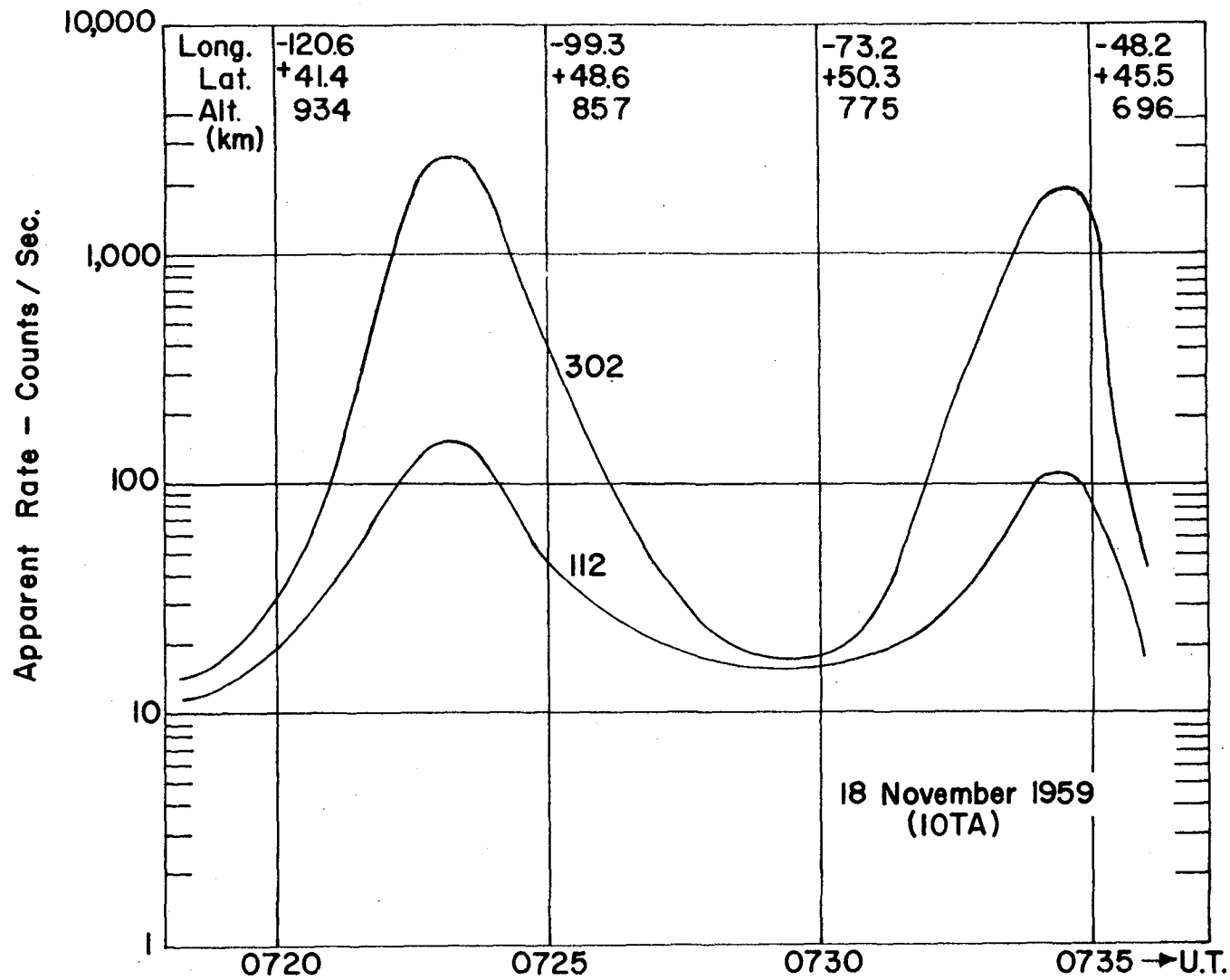


Fig. 33.3 Apparent counting rate observed by the two Geiger-Müller tube detectors in Explorer 7 (0718 - 0736 hr UT, November 18, 1959).

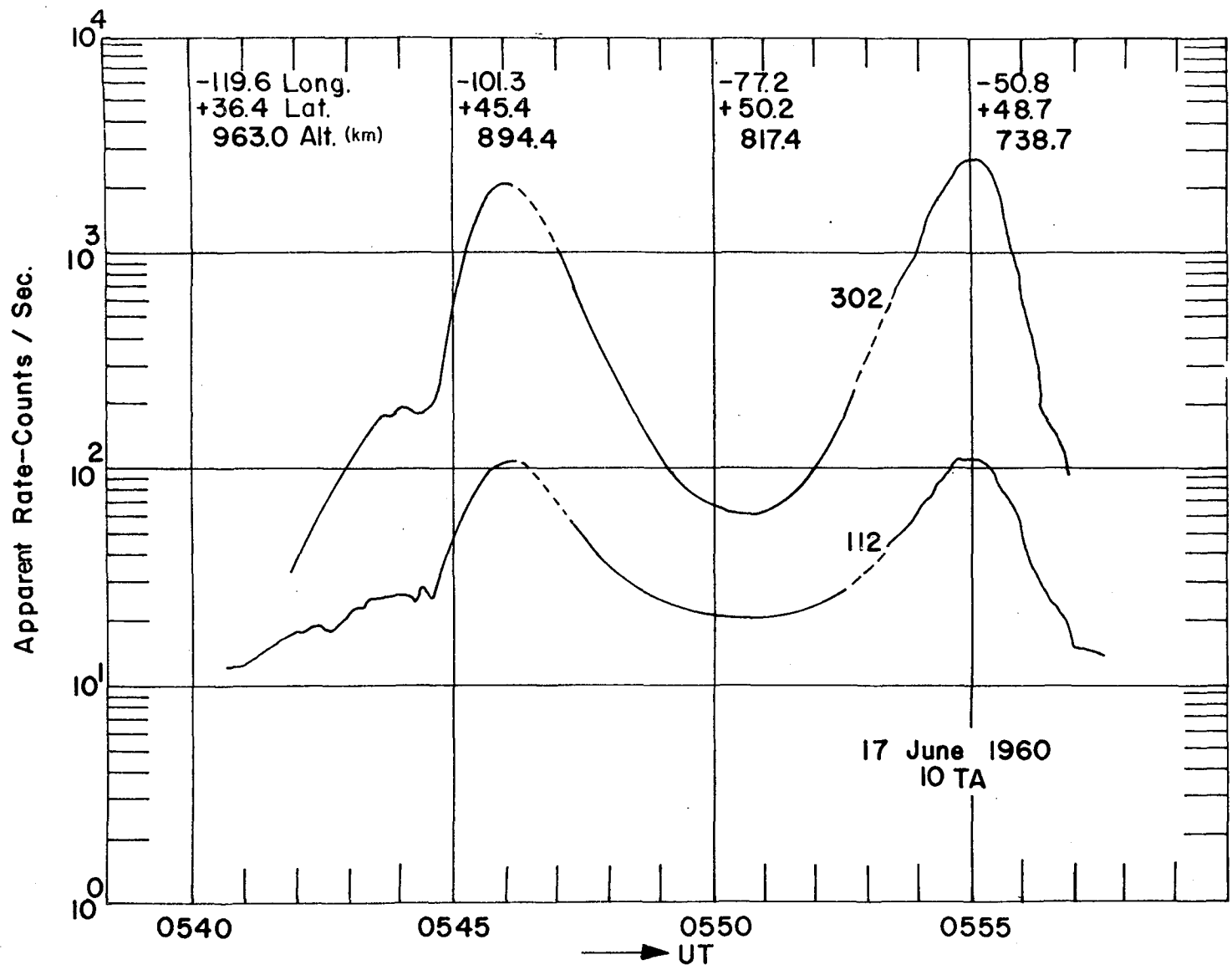


Fig. 33.4 Apparent counting rate observed by the two Geiger-Müller tube detectors in Explorer 7 (0542 - 0557 hr UT, June 17, 1960).

cosmic ray events of intermediate size, say 20 times normal intensity, the final value of  $N_{112}^{**}$  is determined by a two stage iteration process, i.e., by first using Fig. 33.2 to find  $\Delta N_{112}^*$ , then taking  $(N_{112}^* - \Delta N_{112}^*)$  and the relative geometric factors of the 112 tube and 302 tube to estimate the penetrating contribution to  $N_{302}^*$ , and finally Fig. 33.2 again to get an improved  $\Delta N_{112}^*$  and thereby an improved  $N_{112}^{**}$ .

### 33.2 Observational Data and Discussion

#### 33.2.1 Normal Cosmic Ray Intensity

During the period of observation the average net counting rate  $N_{112}^{**}$  due to galactic cosmic rays as observed at the highest latitudes over North America and Australia by Explorer 7 was about 14.5 counts/sec. This rate corresponds to an omnidirectional intensity at the altitudes of observation

$$J_0 = 2.0 \text{ particles (cm}^2 \text{ sec)}^{-1} .$$

It is well known that such a measurement cannot be taken to represent the interplanetary cosmic ray intensity for the following three reasons:

1. The Earth blocks a substantial fraction of  $4\pi$  steradians,
2. The magnetic influence of the Earth may not be negligible even at these high latitudes, and
3. There is doubtless a contribution due to cosmic ray secondaries produced in the atmosphere (cosmic ray albedo).

#### 33.2.2 November 9, 1959 Event

The first case during the observation period of Explorer 7 that  $N_{112}^{**}$  exceeded 20 counts/sec was at 1051 hr UT on November 9, 1959 during the pass which covered the period 1042 hr UT to 1058 hr UT.  $N_{112}^{**}$  was  $30 \pm 5$  counts/sec. During the following pass, which covered the period 1230 hr UT to 1240 hr UT on the same day, the counting rate curves of both the 112 and the 302 tubes exhibited concatenated bumps in the high latitude portion of their counting rate vs time curves in the region where both curves usually exhibit valleys. The bumps were narrower in time extent than for usual solar cosmic ray cases, and therefore corresponded to a high latitude threshold. At the highest value of latitude  $N_{302}^* = 107$  and  $N_{112}^* = 90$ . The resulting  $N_{112}^{**} = 85 \pm 9$  counts/sec. Hence the radiation being detected was considerably harder than typical outer zone radiation but considerably softer than that in a typical solar cosmic ray event.

After subtracting the contribution from cosmic rays, a net intensity of  $10 \text{ (cm}^2 \text{ sec)}^{-1}$  is found from the 112 tube data at the highest latitude at 1234.7 hr UT, on the assumption that the particles being counted are directly penetrating ones (e.g., protons of  $E > 30 \text{ Mev}$ ), and are not non-penetrating electrons which are being detected via their bremsstrahlung. The latitude dependence leaves little doubt that the primary radiation must consist of charged particles.

Other interesting aspects of this event are that no associated geomagnetic disturbance was reported and that no plausibly responsible solar disturbance has been identified.

### 33.2.3 November 30 - December 2, 1959

On November 30, 1959 a flare of importance 3 was observed at Sacramento Peak beginning at 1722 hr UT and ending at 1904 hr UT at location NO8 EO6.\* Explorer 7 data showed an increased counting rate of about 10 to 20 per cent above normal cosmic ray intensity in early December 1; a similar increase was also observed during late December 1 and early December 2. The intensity had returned to normal by early December 3.

### 33.2.4 January 11-14, 1960 Event

At 2040 hr UT on January 11, 1960 the beginning of a solar flare of importance 3 at the location N23 EO3 was observed at Lockheed Observatory. The flare ended at 2355 hr UT.

Explorer 7 showed that during the middle of January 10,  $N_{112}^{***}$  was 14 (which is the normal cosmic ray value), and during the middle of January 11, before the solar flare was observed,  $N_{112}^{***}$  was about 17, an increase of about 20 per cent above normal. About the middle of January 12,  $N_{112}^{***}$  was 27, corresponding to an excess particle intensity of  $2 \text{ (cm}^2 \text{ sec)}^{-1}$ . Thereafter, the intensity decreased gradually and was back to normal by about the middle of January 15. This small increase in intensity and long decay time were supposed to be due to the location of the flare on the Sun, according to a suggested model of Sun-Earth magnetic field [3].

### 33.2.5 March 18-20, 1960

An increased  $N_{112}^{***}$  of about 10 to 20 per cent, above the normal cosmic ray value was observed from Explorer 7 data. The increase, which does appear to be significant, has not been identified with any other phenomena.

---

\*Compilations of Solar-Geophysical Data, U. S. Dept. of Commerce, National Bureau of Standard Central Radio Propagation Laboratory, Boulder, Colorado.

### 33.2.6 April 1-2, 1960 and April 5, 1960 (Fig. 33.5)

A full report on these events has been given previously by [2], including the report of a 24 per cent Forbush decrease during the early morning of April 1.

An improved estimate of the maximum intensity on April 1 has been made with the help of the set of laboratory curves (Sect. 33.1 and Fig. 33.1) of apparent rate vs true rate of the 112 tube. The choice among the family of curves to be used was made by finding the flight saturation value of the 112 tube in nearby inner radiation zone passes at a similar local time. The saturation value adopted was 340 counts/sec.

The resulting value of  $N_{112}^{**}$  at about 1023 hr UT on April 1 was 1600 counts/sec. This yields

$$J_0 = 220 \pm 30 \text{ (cm}^2 \text{ sec)}^{-1}$$

for the omnidirectional intensity of solar protons of energy greater than 30 Mev. At the same time the counting rate of the 302 tube yields

$$J_0 = 210 \pm 20 \text{ (cm}^2 \text{ sec)}^{-1}$$

of protons of energy greater than 18 Mev. The combination of these two results indicates that the spectrum was not rising appreciably between 30 and 18 Mev and hence invalidates the earlier spectral remark of Van Allen and Lin (Ref. [2], 3001 top of column 2).

The peak intensity of the April 5-6 event was not observed by Explorer 7. At 1000 hr UT on April 5 the omnidirectional intensity of protons of  $E > 30$  Mev was  $5 \text{ (cm}^2 \text{ sec)}^{-1}$ .

### 33.2.7 April 28-30, 1960

Three important flares were observed during this period. The first occurred at about 0130 hr UT on April 28 (Hawaii Observatory), the location of the flare being S05 E34. The satellite data show a slight increase from normal cosmic ray intensity at about 0323 hr UT. Then there were no data until 1920 hr UT, but from the observed time history of the event, it appears that the peak of this event was not observed with Explorer 7. The proton omnidirectional intensity with  $E > 30$  Mev at 1920 hr UT was about  $32 \text{ (cm}^2 \text{ sec)}^{-1}$ . The intensity decreased monotonically with time to about 0300 hr UT on April 29. The increased counting rates during late April 29 and early April 30 were presumably due to



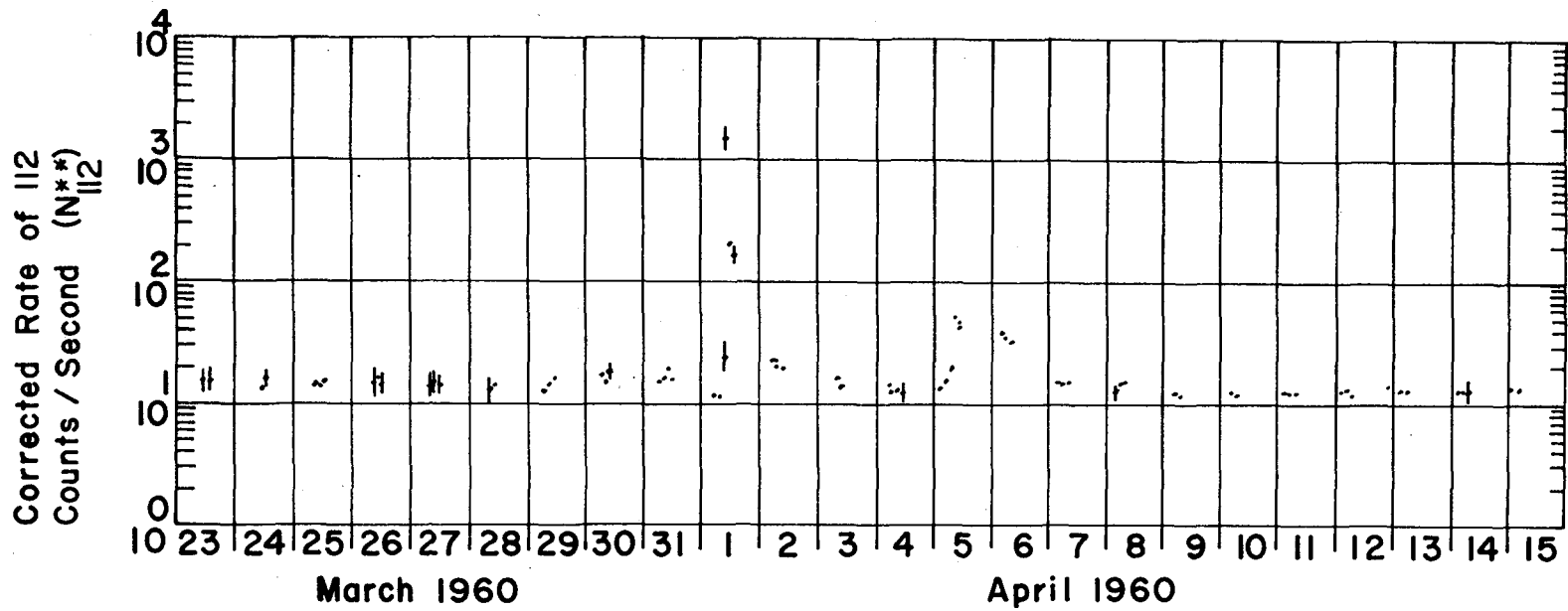


Fig. 33.5 Corrected rate of the 112 Geiger-Müller tube detector at highest dip latitude observed by Explorer 7 (March 23 - April 15, 1960).

flares beginning at 0107 hr UT and ending at 0230 hr UT at N12 W20, and also beginning at 0612 hr UT and ending at 0822 hr UT on April 29 at the location of N15 W20 (observed at Lockheed and Capri S, respectively).

### 33.2.8 May 4-8, 1960

On May 4 polar cap absorption began at 1044 hr UT [4]. The flare, which was apparently responsible for this event, began before 1020 hr UT on the west limb of the Sun and was observed at Thule, Greenland.

The event at 1100 hr UT was of very short time duration and was not observed by Explorer 7 due to the absence of a suitable pass during the event. Explorer 7 data show an increased  $N_{112}^{***}$  at 1516 hr UT, and at the following pass at about 1700 hr UT the omnidirectional intensity was about  $16.5 \text{ (cm}^2 \text{ sec)}^{-1}$ , which was about 8.3 times normal cosmic ray intensity. Balloon observations [5] were obtained at the same time (1700 hr UT). The excess ionization rate at  $6 \text{ g/cm}^2$  atmospheric depth was about 25 per cent above the normal galactic cosmic ray background ionization rate at that altitude. Explorer 7 data show peak intensity for this later event on May 4 during the pass covering 1837 hr UT to 1848 hr UT. The omnidirectional intensity for protons with  $E > 30 \text{ Mev}$  was about  $40 \text{ (cm}^2 \text{ sec)}^{-1}$ . The next and subsequent passes show a steady decrease of intensity up to about 0040 hr UT on May 5. Then there were no data until about 1450 hr UT on the same day. The balloon observations showed the decay of the event from 1700 hr UT on May 4 to 0200 hr UT on May 5. Thus, the peak intensity shown by Explorer 7 at 1830 hr UT might not correspond to the maximum intensity of the May 4 event. The maximum intensity apparently occurred between 1700 hr UT and 1830 hr UT. There is a striking level of general agreement between the satellite and balloon measurements on the time history of the event. From the 112 tube the omnidirectional intensity of protons with  $E > 30 \text{ Mev}$  was about  $40 \text{ (cm}^2 \text{ sec)}^{-1}$  at 1842 hr UT; and from the 302 tube, the omnidirectional intensity with  $E > 18 \text{ Mev}$  was about  $52 \text{ (cm}^2 \text{ sec)}^{-1}$ .

A thorough study of the spectrum of solar protons (and of solar alpha particles) during a balloon exposure of nuclear emulsions in the period 1700 hr UT May 4 to 0200 hr UT May 5 has been reported [6]. The average differential number energy spectrum  $dN/dE = \text{const } E^{-(1.0 \pm 0.3)}$  was found for  $250 \leq E \leq 1000 \text{ Mev}$  for protons.

Between 0040 hr UT and 1430 hr UT on May 5 there were no satellite observations.  $N_{112}^{***}$  was about 35 at 1452 hr UT on May 5 and increased with time. At 1819 hr UT there was an apparently maximum value of  $N_{112}^{***} = 77$ , corresponding to an omnidirectional intensity of  $9 \text{ (cm}^2 \text{ sec)}^{-1}$ , after subtraction of the galactic cosmic ray background. On May 6, at about 1844 hr UT, Explorer 7 reported another value of  $N_{112}^{***}$  equal to about 110 counts/sec, which corresponds to about  $15 \text{ particles (cm}^2 \text{ sec)}^{-1}$ . After subtracting the cosmic ray background of 2 it gives the proton flux of

about  $13 \text{ (cm}^2 \text{ sec)}^{-1}$ . On May 6 a flare of importance 3+ was reported at Sacramento Peak beginning at 1404 hr UT at S10 E08. This flare was also observed at several other stations and is presumed to be the cause of the May 6 solar cosmic ray event [4].

On May 7 no flare with importance more than 1 was observed. However, Explorer 7 data show an increase of intensity, and at about 2100 hr UT the peak value of  $N_{112}^{**}$  was 195, corresponding to  $27 \text{ (cm}^2 \text{ sec)}^{-1}$  absolute omnidirectional intensity. After subtracting the cosmic ray background of  $2 \text{ (cm}^2 \text{ sec)}^{-1}$  the solar proton intensity was  $25 \text{ (cm}^2 \text{ sec)}^{-1}$ . The intensity decreased thereafter and returned to normal by about 2000 hr UT on May 8.

### 33.2.9 May 13-14, 1960

The next increased intensity was observed on May 13. The flare which was supposed to be responsible for this event was observed by several observatories at about 0522 hr UT and of importance 3+ at the location of approximately N30 W64. Unfortunately, the first pertinent data from Explorer 7 were not received until 1330 hr UT from the Woomera (Australia) station, which showed an  $N_{112}^{***}$  of 58. The next pass showed the highest observed value of  $N_{112}^{***}$ , namely 370, corresponding to a proton intensity of  $50 \text{ (cm}^2 \text{ sec)}^{-1}$  at 1512 hr UT. This result was confirmed by the Woomera station which also showed the decline of intensity during the next pass covering the time 1652 hr UT to 1705 hr UT. The pass over North America at about 2112 hr UT showed that  $N_{112}^{***}$  was 25 but at this time the subsatellite point was at 75.5 deg dip angle, compared to the previous pass over North America at about 1927 hr UT with dip angle of 78.3 deg. Hence, the rapidity of time decay was probably less than would appear at first glance.  $N_{112}^{***}$  was back to the normal value of about 14.5 counts/sec sometime before 1600 hr UT on May 15.

### 33.2.10 May 18 and May 26, 1960

On May 18 after 1200 hr UT an increase of about 40 per cent above the normal intensity was observed by Explorer 7. About the same amount of increase was observed around 1200 hr UT on May 26.

### 33.2.11 June 1, 2, and 4, 1960

On June 1 a flare of importance 3+ was observed at Capri S Observatory, starting at 0824 hr UT and ending at 1340 hr UT at the location of about N28 E46. A slightly increased intensity  $N_{112}^{***} = 18$  was observed by Explorer 7 at 1021 hr UT, about two hours later than the beginning of the flare. The pass previous to 1021 hr UT showed normal intensity. Thus the solar protons began arriving at the Earth sometime before 1020 hr UT. The highest value of  $N_{112}^{***}$  during the event was 51 counts/sec at

1205 hr UT, corresponding to a solar proton intensity of  $5 \text{ (cm}^2 \text{ sec)}^{-1}$  with  $E > 30 \text{ Mev}$ . During the middle of June 2  $N_{112}^{***}$  was 22 counts/sec, corresponding to a solar proton intensity of about  $1 \text{ (cm}^2 \text{ sec)}^{-1}$ . By 1120 hr UT on June 3  $N_{112}^{***}$  had returned to its normal value.

Again at 0900 hr to 1230 hr UT on June 4,  $N_{112}^{***}$  was high, being about 21 counts/sec, and by about the same time on June 5  $N_{112}^{***}$  was normal.

### 33.2.12 August 12-16, 1960

On August 12, 1960 at 1924 hr UT a flare of importance 3+ was observed at Hawaii at the location of N22 E27. The flare ended at 2042 hr UT. Explorer 7 made only one pertinent set of observations, at about 1240 hr UT on August 12.  $N_{112}^{***}$  was 29 counts/sec, corresponding to a solar proton intensity of  $2 \text{ (cm}^2 \text{ sec)}^{-1}$ . From 0850 hr to 1220 hr UT on August 13, the intensity was  $1.3 \text{ (cm}^2 \text{ sec)}^{-1}$ ; and on the following day, from 0820 hr to 1010 hr UT, it was  $0.8 \text{ (cm}^2 \text{ sec)}^{-1}$ . On August 15, at about 1130 hr UT, the excess intensity was slightly higher than  $0.8 \text{ (cm}^2 \text{ sec)}^{-1}$ . On August 16  $N_{112}^{***}$  was about 15 per cent to 20 per cent above normal. On the following day  $N_{112}^{***}$  was back to the normal intensity.

### 33.2.13 September 3-9, 1960 (Fig. 33.6)

One of the most interesting series of observations was made during this period. On September 2, two flares of importance 3 were observed without being accompanied by Type IV radio emission, and on September 3 a flare of importance 3 began at 0040 hr UT at station N17 E90. This latter flare was accompanied by Type IV radio emission and is presumed to have been responsible for the emission of the observed particles. Balloon observations were made at Minneapolis [7] on September 3. Rocket observations were also made [8]. Unfortunately, there were no simultaneous data from Explorer 7 for direct comparison with their results.

During three passes at 0037, 0221, and 2322 hr UT on September 3,  $N_{112}^{***}$  was  $12 \pm 2$ ,  $10 \pm 3$ , and 1000 counts/sec, respectively. Therefore, the time at which solar protons arrived near the Earth was after 0221 hr UT and before 2322 hr UT. From our data the peak intensity was observed at 0155 hr and 0337 hr UT on September 4.  $N_{112}^{***}$  was about 1800 counts/sec, which corresponds to a solar proton flux of  $250 \text{ (cm}^2 \text{ sec)}^{-1}$ , with  $E > 30 \text{ Mev}$ . A very interesting feature of this event is its very slow decay. If one assumes that the peak intensity observed by Explorer 7 was the maximum intensity of this event, then the time width of this event at half-intensity exceeds 8 hr, being much longer than that of the April 1 event.

### 33.2.14 November 12-28, 1960 (Fig. 33.7)

At 2300 hr UT on November 12, the peak intensity of  $N_{112}^{***}$  observed by Explorer 7 was between 85,000 to 330,000 counts/sec (Fig. 33.8).

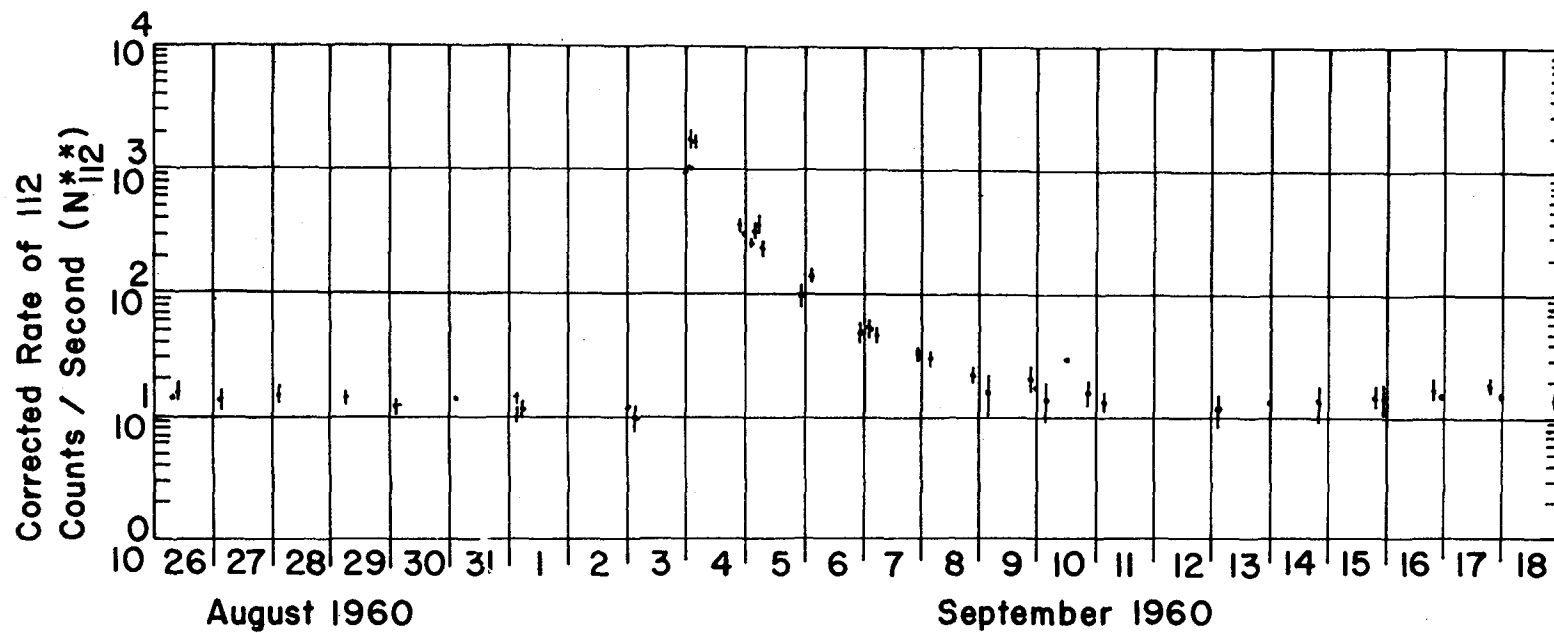


Fig. 33.6 Corrected rate of the 112 Geiger-Müller tube detector at highest dip latitude observed by Explorer 7 (August 26 - September 18, 1960).

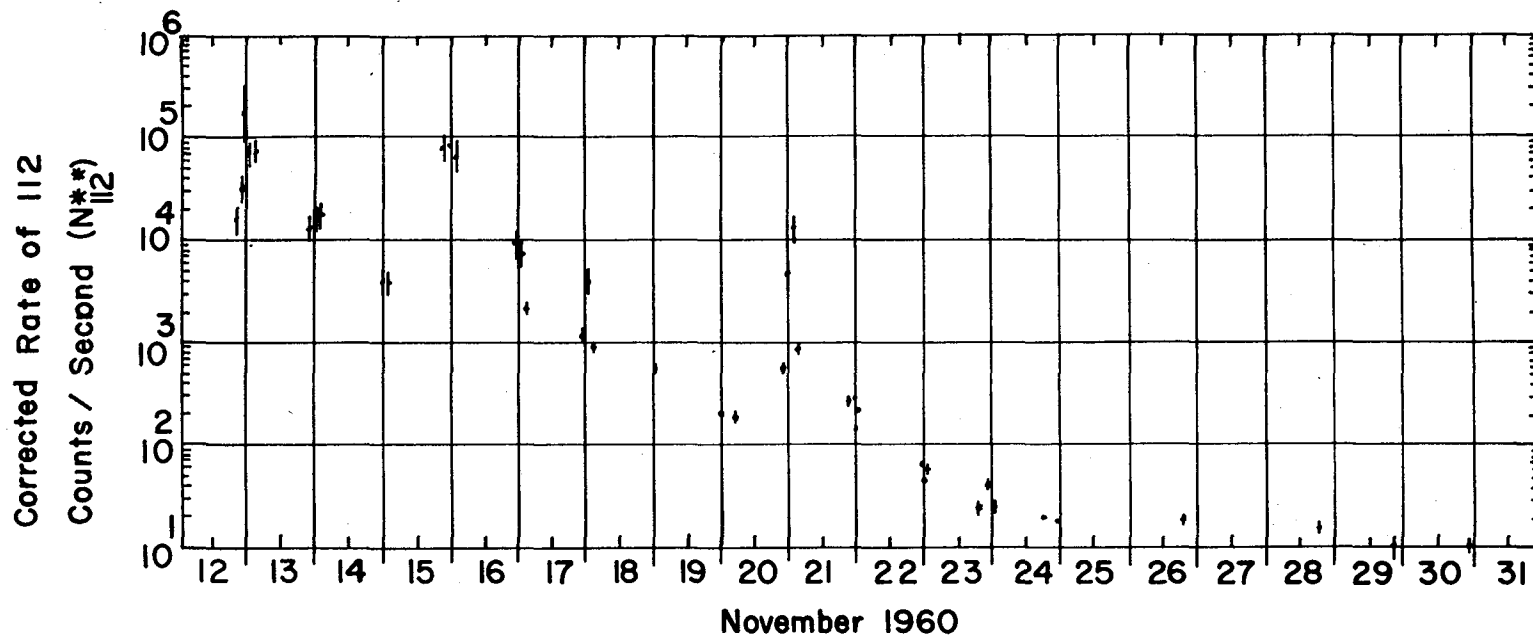


Fig. 33.7 Corrected rate of the 112 Geiger-Müller tube detector at highest dip latitude observed by Explorer 7 (November 12 - 31, 1960).

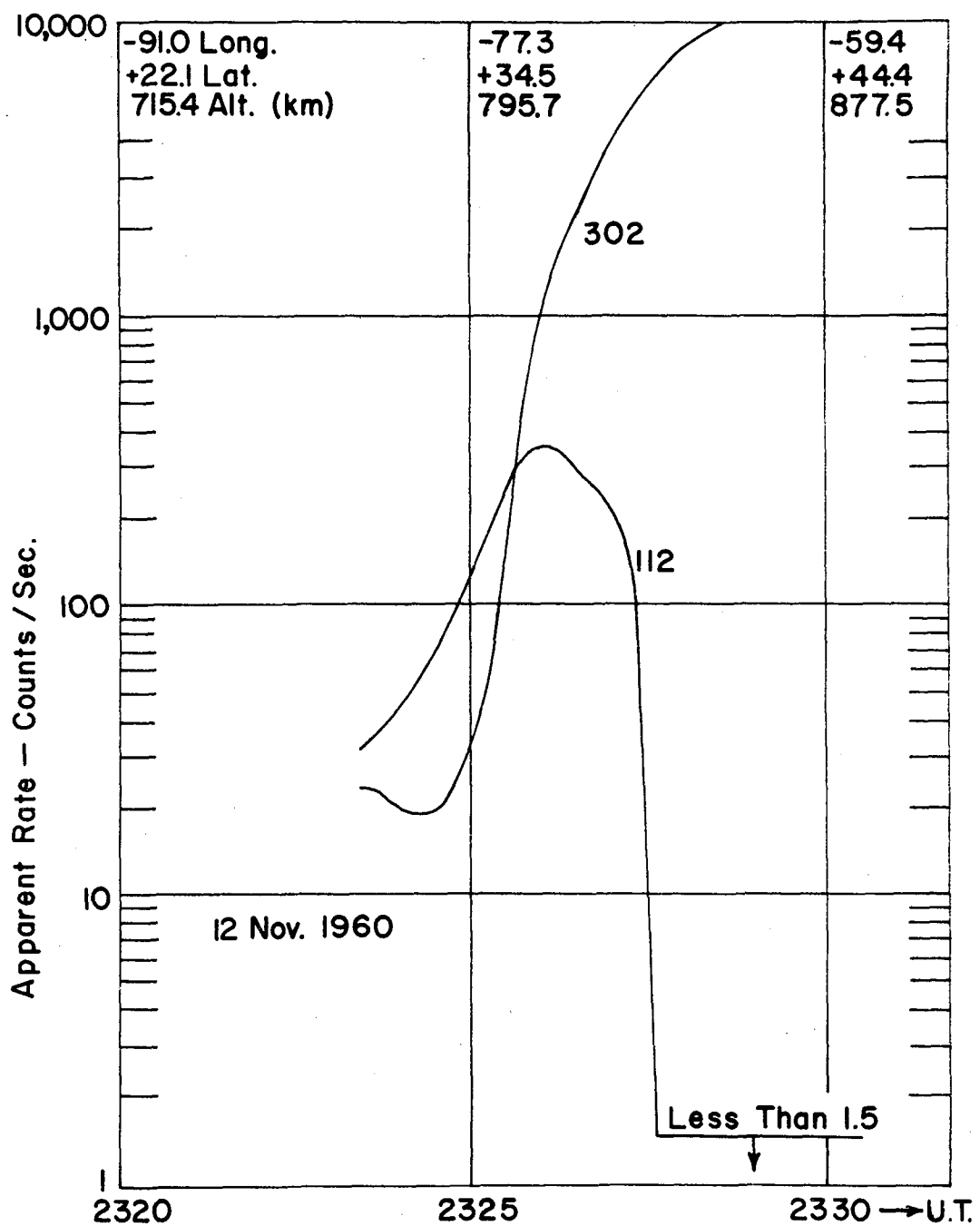


Fig. 33.8 Apparent counting rate observed by the two Geiger-Müller tube detectors in Explorer 7 (2324 hr - 2330 hr UT, November 12, 1960).

There were two passes earlier than 2330 hr UT. Their  $N_{112}^{**}$  were  $16,000 \pm 5,000$  and  $32,000 \pm 10,000$  at 2101 hr UT and at 2245 hr UT, respectively. The ground observation of November 12 and November 15 events have been reported [9].

On November 12 the two distant peaks of the neutron monitor data (about 1600 hr UT and 2000 hr UT) were very well explained by the model they used. According to their observational results and explanation, both counting rate enhancements on November 12 were due to cosmic-ray production in the large flare which started at 1320 hr UT on November 12.

When we compare the peak intensity of Explorer 7 at 2330 hr UT to the second peak of the neutron monitor data, the peak of Explorer 7 data lagged behind by about 3-1/2 hr. Since the detection of neutrons on the ground implies arrival of high energy particles, the lower energy particles lagged behind the high energy particles.

At 2330 hr UT on November 12 the proton (plus  $\alpha$ -particle) intensity was between  $12,000$  and  $45,000$   $(\text{cm}^2 \text{ sec})^{-1}$ . The upper limit of the peak intensity was determined by the 302 tube, since the 112 tube was driven far beyond its saturation value, namely into a portion of its calibration curve which involved substantial uncertainty. For the November event, apparent fluctuations of  $N_{112}^{**}$  in Fig. 33.7 are in large part due to differences in the latitudes of observation. The successive entries do not provide a homogeneous series of observations from which the detailed time history of the intensity can be simply determined.

For geographic latitudes north of about  $48^\circ\text{N}$  at 1000 km altitude over the polar caps it is of interest to note the time-integrated omnidirectional intensity

$$\int_{12 \text{ Nov.}}^{16 \text{ Nov.}} J_0 dt \sim 2 \times 10^9 / \text{cm}^2$$

This result may be compared to the one year integral of galactic cosmic ray intensity in interplanetary space [10]

$$\int_{\text{One Year}} (J_0)_{\text{c.r.}} dt = 6 \times 10^7 / \text{cm}^2$$



The intensity enhancement on late November 20 and early November 21 (Fig. 33.7) observed by Explorer 7 was apparently due to the flare started at  $2055 \pm 10$  hr UT on November 20 at a solar longitude some  $120^\circ$  W of the center of the solar disk [11, 12]. A detailed listing of all observational data from Explorer 7, together with its exact ephemerides, is contained in State University of Iowa Report 61-16.

#### ACKNOWLEDGMENTS

The ephemerides of Explorer 7 were prepared by the Space Control Center of the Goddard Space Flight Center of the National Aeronautics and Space Administration. For these data and for telemetry data from the world-wide network of NASA stations, we are indebted to arrangements by Mr. Herman E. LaGow of NASA. Additional telemetry data of importance were obtained by a station at Ottawa, Canada, through the courtesy of Dr. C. M. Hines.

#### REFERENCES

1. Ludwig, G. H. and W. A. Whelpley, Corpuscular Radiation Experiment of Satellite 1959 (Explorer VII), Journal of Geophysical Research, 65: 1119 (1960).
2. Van Allen, J. A. and Wei Ching Lin, Outer Radiation Belt and Solar Proton Observations with Explorer VII During March-April 1960, Journal of Geophysical Research, 65: 2998 (1960).
3. Obayashi, T. and Y. Hakura, Propagation of Solar Cosmic Rays through Interplanetary Magnetic Field, Journal of Geophysical Research, 65: 3143 (1960).
4. Leinbach, H., The Polar Cap Absorption Events of March 31 through May 13, 1960, Geophysical Institute, University of Alaska, June 1960.
5. Winckler, J. R., A. J. Masley, and T. C. May, The High-Energy Cosmic-Ray Flare of May 4, 1960. 1. High-Altitude Ionization and Counter Measurements, Journal of Geophysical Research, 66: 1023 (1961).
6. Biswas, S. and P. S. Freier, The High-Energy Cosmic-Ray Flare of May 4, 1960. 2. Emulsion Measurements, Journal of Geophysical Research, 66: 1029 (1961)
7. Winckler, J. R., P. D. Bhavsar, A. J. Masley, and T. C. May, Delayed Propagation of Solar Protons on September 3, 1960, Physical Review Letters, 6: 488 (1961).
8. Davis, L. R., C. E. Fichtel, D. E. Guss, and K. W. Ogilvie, Rocket Observation of Solar Protons on September 3, 1960, Physical Review Letters, 6: 492 (1961).

9. Steljes, J. F., H. Carmichael, and K. G. McCracken, Characteristics and Fine Structure of the Large Cosmic-Ray Fluctuations in November 1960, Journal of Geophysical Research, 66: 1363-1377 (1961).
10. Van Allen, J. A. and L. A. Frank, Radiation Measurements to 658,300 Km. with Pioneer IV, Nature (London), 184: 219 (1959).
11. Carmichael, H., J. F. Steljes, D. C. Rose, and B. G. Wilson, Cosmic-Ray Neutron Increase From a Flare on the Far Side of the Sun, Physical Review Letters, 6: 49 (1961).
12. Covington, A. E. and G. A. Harvey, Measurement of 10.7-cm Solar Noise Burst of November 20, 1960, Physical Review Letters, 6: 51 (1961).

## 34

## SCIENTIFIC RESULTS FROM JUNO-LAUNCHED SPACECRAFT

Charles A. Lundquist, Arthur W. Thompson, and Ray V. Hembree

Research Projects Division  
George C. Marshall Space Flight Center  
National Aeronautics and Space Administration  
Huntsville, Alabama

### 34.1 The Juno Family of Spacecraft

With the launching of Explorer 11 (1961 Nu) on April 27, 1961, the last member of the Juno-launched family of spacecraft was placed in orbit. This historic family of satellites and space probes began with Explorer 1, (1958 Alpha), the first artificial satellite of the United States, and also included Pioneer 4, the first artificial planet of the Sun orbited by the United States. All the members of the family are listed in Table 34.1 with their launch dates, orbital parameters and masses.

The scientific results from these spacecraft are notable in several respects. Being among the earliest satellites launched, their instruments produced several significant discoveries and scientific firsts. In addition, they were used by many scientists for auxiliary investigations producing valuable additional results. Finally, several of the spacecraft transmitted their scientific data in a form accessible to any well-equipped laboratory, so that scientists of various nations were able to participate in the experiments and report their results.

The Juno 1 and 2 launch vehicles are adequately described by several authors [1, 2]. Both vehicles employed essentially the same spinning clusters of solid propellant rockets in their last three stages, but the Juno 1 had a modified liquid propellant Redstone for its first stage, whereas the Juno 2 had a modified Jupiter. The spacecraft launched by these vehicles will be called, for brevity, the Juno spacecraft. They are a particularly closely related family because they were prepared by an integrated team of workers and designed to be launched by very similar vehicles. The factors involved in their evolution are discussed elsewhere [3, 4].

**Preceding page blank**

Table 34.1 Juno Spacecraft

	Launch Date	Orbit (km)	Mass of Spacecraft (Excluding rocket case) (kg)	Agency
Explorer 1 (1958 $\alpha$ )	Jan. 31, 1958	Initial perigee 360 Initial apogee 2552	8.2	JPL
Explorer 2 (1958 $\gamma$ )	Mar. 26, 1958	Initial perigee 195 Initial apogee 2810	8.4	JPL
Explorer 4 (1958 $\epsilon$ )	Jul. 26, 1958	Initial perigee 267 Initial apogee 2219	11.7	ABMA
Pioneer 3	Dec. 6, 1958	Max. altitude 102,322 Flight time 37.94 hrs	5.9	JPL
Pioneer 4	Mar. 3, 1959	Perihelion 147,500,000 Aphelion 170,600,000	6.1	JPL
Explorer 7 (1959 $\iota$ )	Oct. 13, 1959	Initial perigee 555 Initial apogee 1091	41.5	ABMA
Explorer 8 (1960 $\xi$ )	Nov. 3, 1960	Initial perigee 413 Initial apogee 2288	40.9	MSFC-GSFC
Explorer 11 (1961 $\nu$ )	Apr. 27, 1961	Initial perigee 490 Initial apogee 1799	43.2	MSFC

During the same time that the Juno spacecraft were being prepared, launched, and their data analyzed, some related scientific experiments were carried as incidental payloads on certain of the Jupiter test flights.

In some of the space sciences represented by experiments on the Juno spacecraft, the quantity of information available at the time of this writing is very large. This is particularly true, for example, with respect to fluxes of energetic charged particles. In these cases, the data from the Juno spacecraft are properly viewed as pieces of information that may be fitted together with similar pieces from other spacecraft to construct the current picture of some area of space science.

#### 34.2 Results from Primary Experiments

##### 34.2.1 Energetic Charged Particles

Of all the scientific results from the Juno spacecraft, those describing fluxes of energetic, charged particles are perhaps the most widely recognized. In large measure this is due to the spectacular discovery by these spacecraft of the radiation encircling Earth. It is also true that the largest body of data from the Juno spacecraft resulted from measurements of energetic charged particles.

The first six Juno spacecraft carried instruments to detect energetic charged particles. Explorer 11 measured fluxes of charged particles incidental to the principal cosmic gamma ray experiment. Thirteen individual detectors were carried: ten Geiger-Müller (G-M) counters, two scintillation counters, and one ionization chamber.

Explorer 1 carried an experiment designed at the State University of Iowa to observe the flux of primary cosmic radiation near Earth [5, 6]. A G-M tube 10.2 cm long and 2.0 cm in diameter was used. The instrument was designed to measure and continuously transmit to ground telemetry stations counting rates about five times as great as those expected from extrapolations of balloon and rocket measurements. The results reported by Van Allen and his associates agreed well with those expected for altitudes between perigee and about 1000 km. However, above this altitude, the instrument indicated counting rates exceeding its capabilities.

A similar experiment on Explorer 3, the next successful member of the series, was capable of transmitting higher counting rates. A more important improvement, however, was a tape recorder that recorded all data obtained during one orbital period and then, on command from a ground station, transmitted these data in 5 seconds. The counting rate capabilities of the system were again overwhelmed at high altitudes. The initial data from Explorer 1 and the more comprehensive data from Explorer 3 then led to the now famous interpretation by Van Allen, and others, that the unexpectedly high counting rates were due to energetic charged particles, electrons or protons, trapped by the magnetic field of Earth [5]. Final detailed analyses of these data followed at a later date [1].

In October 1957, studies of magnetic trapping of particles in the proposed Astron thermonuclear device led N. C. Christofilos to suggest that a fission bomb detonated above the significant atmosphere could be used to artificially introduce electrons into Earth's magnetic field, where some would be trapped by the field [ 8]. With the detection by Explorers 1 and 3 of naturally occurring trapped particles, this proposal took new significance. The experiment was sponsored by the Advanced Research Projects Agency of the Department of Defense under the title, Project Argus.

Explorer 4 was designed to detect the charged particles injected by Project Argus and to measure the natural radiation belt discovered by Explorers 1 and 3. The instrumentation package, again prepared by the group at the State University of Iowa, contained two G-M counters and two scintillation counters [ 9]. These four detectors were shielded and electronically biased so that their thresholds for detecting radiation were significantly different. By analysis of the relative counting rates, some information was obtained concerning the energy spectrum of the detected radiation.

During the life of Explorer 4, three small fission bombs were detonated at high altitudes above the South Atlantic. The narrow artificial belts of electrons injected by these bombs were detected easily by each of the four detectors [10]. Much detailed data on the naturally trapped energetic particles were also obtained [ 9, 11, 12, 13, 14].

A few months after the completion of the Explorer 4 experiment, Pioneers 3 and 4 were launched. Pioneer 3 passed twice through the region of trapped radiation, first leaving Earth and then returning to Earth. Pioneer 4, escaping from Earth, passed through the region only once. In all three of these passages through the region of trapped radiation, two radiation belts were detected by the G-M counters carried in the spacecraft [ 15, 16].

The data from Explorer 4 also supported the existence of an inner and outer radiation belt. The character of these belts has since been the object of many investigations.

The next Juno spacecraft, Explorer 7, carried two experiments to measure energetic particle radiation. The first experiment, again supplied by the State University of Iowa group, employed two G-M counters similar to those carried on earlier Juno Spacecraft [ 17]. Due to the long active life of Explorer 7 (about 1.5 yr), this experiment yielded much valuable information on the temporal behavior of the radiation belts, primary cosmic rays, and particles from the sun. In particular, phenomena associated with magnetic storms and visible aurora have been observed on several occasions [ 18, 19, 20]. On some occasions, multiple zones of high-intensity radiation were observed on the low latitude edge of the outer radiation belt [ 21].

Based on data from many spacecraft, the current picture of the Van Allen belts is roughly as follows. The inner belt contains a component of energetic protons (a few mev and upwards) and peaks at about 3700 km altitude above the equator. The electrons in the radiation belts generally have energies from a few kev to 1 mev. The electron maximum in the lower belt lies at about 9600 km and that in the outer belt near 18,000 km. The minimum electron flux, or slot between the belts, is at about 12,000 km altitude. The inner belt is quite stable, while the outer belt exhibits large fluctuations.

Explorer 7 also carried an ionization chamber to detect heavy nuclei in primary cosmic rays [22]. A pulse is obtained proportional to the total ionization caused by the passage of a particle through the chamber. For relativistic particles, the total ionization is proportional to the square of the charge  $Q$  of the incident particle. The experiment was designed to count the particles in three ranges, corresponding to  $Q > 6$ ,  $Q > 9$ , and  $Q > 16$ .

In a preliminary report of the results from this experiment, the values determined for the exponents in the expression for the integral magnetic rigidity spectrum and the energy spectrum for heavy primary cosmic rays were reported [23].

Explorer 7 carried four small ionization chambers intended to measure electromagnetic radiation in an interval around the Lyman-alpha line of hydrogen and X-rays in the few-Angstrom region. These detectors were found to be sensitive to fluxes of low-energy electrons as found in the radiation belts, thus little data were obtained on electro-magnetic radiation. The possible use of these chambers as charged particle detectors has been investigated [24].

#### 34.2.2 Thermal Experiments

The thermal experiments conducted on the Juno spacecraft fell into three classes. First, each spacecraft carried temperature measurements to verify the thermal design of the spacecraft and to monitor temperature sensitive instruments. Second, an experiment to measure Earth's thermal radiation balance was included in Explorer 7. Third, Explorer 11 carried two specially prepared surface areas with coatings of particular interest for space applications, and the temperatures of these special areas were measured. It is interesting to note that these measurements ranged from a purely geophysical experiment through experiments to advance the technology of spacecraft design.

During the years between the launchings of Explorer 1 and Explorer 11, the theory and techniques of satellite temperature control by passive methods developed from an untried concept into a complex, well-proven technology. The temperature data and results from the Juno spacecraft played a central role in this development.

The temperatures attained by a body in orbit are determined by a balance between heat input, either absorbed by the body from radiation incident on it or generated in its components, and energy lost through infrared radiation from the skin of the body.

This balance may be influenced by careful selection of the absorption characteristics of the spacecraft surfaces for various radiation wavelengths. Different locations on or within the spacecraft may also have different temperatures, depending on such controllable factors as the thermal capacity and conductivity of the body components.

The demonstration that passive temperature control is possible was first reported by E. P. Buwalda and A. R. Hibbs [25] from their analysis of Explorer 1 data. The mature development of thermal control technology, based on experience from many spacecraft, is discussed by G. Heller [26]. In summary, temperatures on the Juno spacecraft compared favorably with anticipated temperatures.

The experiment on Explorer 7 to measure characteristics of the thermal radiation balance of Earth was designed and constructed by V. E. Suomi and associates of the University of Wisconsin [27]. The sensors on the satellite consisted of five small hemispheres, backed with mirrors, and one sphere. Each hemisphere or sphere was coated with a special material to obtain a desired radiation absorption characteristic.

From an analysis based on the temperatures simultaneously attained by the spherical surfaces, it is possible to determine the solar radiation incident on Earth, the radiation reflected by Earth, and the long-wavelength radiation from Earth - all measured for the region beneath the satellite. From such data, the net rate of energy loss or gain can be inferred for the region below the satellite.

Prior to this experiment, it was known that the tropics generally receive more energy from the Sun than they lose by radiations, while polar regions radiate more energy than they gain from the Sun. The Explorer 7 experiment showed that, in addition, large-scale regions of outward radiation flux exist and are related to large-scale features of the weather [28]. Further, the important role played by clouds in controlling outgoing radiation was demonstrated.

Explorer 11 carried two special temperature measurements for areas relatively isolated thermally from the rest of the satellite. One measurement on the motor case was painted with a white, zinc sulfide-pigmented, air-dry silicone. The other measurement was on a 1.5-in. aluminum disk mounted on a Kel-F stem in a special housing for thermal isolation. This disk was coated first with a thin film of SiO, then a film of germanium 200A thick, and finally with another thin film of SiO. Analyses, by W. C. Snoddy at Marshall Space Flight Center, of the characteristics of these surfaces for special thermal balance applications and the effect of space environment on them are continuing.



### 34.2.3 Micrometeorite Experiments

Satellites Explorer 1, Explorer 2, Explorer 7, and Explorer 8 carried micrometeorite experiments. Two independent sensing systems were on Explorer 1 and on Explorer 8.

One of the sensing elements on Explorer 1 was a microphone, using a lead zirconate piezoelectric crystal, mounted on the cylindrical shell of the satellite. This experiment was contributed by the Air Force Cambridge Research Center [29]. M. Dubin reports that calibration of the instrument indicates that the response of the microphone is proportional to the momentum of the incident micrometeorite [30]. The sensitive area of the skin of the satellite was  $0.23 \text{ m}^2$  for which area the effective threshold momentum was  $2.5 \times 10^{-3} \text{ g-cm/sec}$ . Dubin reports that a total of 145 impacts was recorded during 78,752 sec of excellent quality telemetry records [31]. From this he computes the mean flux of micrometeorites having momenta exceeding the quoted momentum threshold, in the neighborhood of Earth during February 1958, to be  $8.0 \times 10^{-3} \text{ m}^{-2} \text{ sec}^{-1}$ . Diurnal variations of micrometeorite impacts were also observed.

On the basis of a statistical analysis, A. Hibbs concluded that the average particle measured by Explorer 1 was in a closed orbit around Earth rather than on an impact trajectory from a great distance to the surface of Earth [32, 33, 34].

Another micrometeorite detector, also contributed by the Air Force Cambridge Research Center, carried on both Explorer 1 and Explorer 2 consisted of 12 gages mounted in a circular array around the satellite [30]. Each gage was an insulating card on which were wound two layers of enameled wire. Each gage had an area of about  $1 \text{ cm}^2$ . The impact of a micrometeorite of about  $10 \mu$  diameter would be expected to break the wire of a gage, causing a change in the electrical resistance of the circuit containing the 12 gages wired in parallel. During the 2-1/2 month operation of the experiment on Explorer 1, one wire was thought to have been broken by a micrometeorite; however, this was later discounted. In Explorer 3, no breaks were observed from March 26 until May 6, when two were observed [35]. The telemetry failed about three days later. With so few positive events, only an upper limit can be deduced for the frequency of micrometeorites in the size range greater than  $\mu$ . For the Explorer 1 data, this limit is  $10^{-3} \text{ m}^{-2} \text{ sec}^{-1}$  during the lifetime of the experiment [35].

The micrometeorite experiment on Explorer 7, conducted by H. E. LaGow from the National Aeronautics and Space Administration, used an alternative detector for the same range of micrometeorites greater than  $10 \mu$  in diameter. Each of the three detectors was a solid-glass cylinder with mirror sides, a cadmium sulfide photoconductive surface on the inner end, and an optically opaque film exposed to space on the outer end [36]. The opaque film differed slightly on each detector. If a micrometeorite

punctured the film, light could reach the photoconductive surface. From the telemetered resistance of the surface the attitude of the detector relative to the Sun, the size of the punctured hole could be computed. The diameter of each detector was about 3 mm.

The batteries powering the 108 mc transmitter, which provided telemetry for the micrometeorite experiment on Explorer 7, were exhausted after about 6 weeks. During this time, one puncture of 10 to 15  $\mu$  diameter was credited to a micrometeorite.

The micrometeorite experiments on Explorer 8 were conducted by W. M. Alexander of the National Aeronautics and Space Administration [37]. One of the sensing devices consisted of a conventional, end-type, ruggedized photomultiplier with an evaporated 1000-A layer of aluminum on the front surface. Visible-light energy of a micrometeorite impact would penetrate the aluminum coating and register on the photocathode. The system had a dynamic range of three decades. For each measurable impact, a portion of the coating was removed and gradually known sources of light, Sun, Moon, etc., began to register and erosive effects of a single micrometeorite could be measured. This sensor, however, encountered interference from the Van Allen radiation belts and unreliable data resulted.

A microphone was used as a sensor in the other system for the purpose of counting impacts and determining the magnitudes of the impulses recorded by impacting micrometeorites [31]. Two sounding boards of the microphone system, having a total area of about 0.1 m<sup>2</sup>, were located on the lower cone of the satellite, acoustically insulated from the satellite skin.

Alexander reported that the measurements obtained from Explorer 8 serve as the first firm basis for analyzing all existing direct measurements of interplanetary dust particles [37]. Preliminary data indicate that more than 3100 impacts were registered during an interval of 40 days. The number of impacts for each of the three ranges of sensitivity has been established approximately. The spacing of the threshold sensitivities allows the establishment of the shape of a segment of an average distribution curve that extends over approximately three orders of magnitude in particle mass.

In addition to the satellite experiments, H. L. Martin, Army Ballistic Missile Agency and O. E. Berg, National Aeronautics and Space Administration, conducted a micrometeorite experiment on a Jupiter missile flown in January, 1960. A microphone and a covered photomultiplier tube, similar to those previously described, were used as sensors. Four impacts were recorded during the flight, which is in agreement with other micrometeorite experiments.

#### 34.2.4 Direct Ionosphere Measurements

Explorer 8 was the first United States satellite with experiments designed to directly measure the properties of ionized particles in the vicinity of the satellite [38, 39]. Of the ten detectors carried by the satellite, three were used respectively to measure electron concentration, positive ion concentration, and positive ion mass, and two were used to measure electron temperature. Of the remaining five detectors one measured the potential of the satellite with respect to the surrounding medium and another measured the current produced from the satellite by photoemission. The other three sensors carried by the satellite are discussed in the section on micrometeorites.

The electron concentration was measured by an rf impedance probe that utilized a shortened dipole antenna as a capacitive element in a voltage-controlled oscillator circuit. The frequency was determined by a known sweep voltage and the capacitance of the element that depended on the local electron concentration. The time from the start of the sweep voltage until 6.5 Mc was reached was measured on-board, digitized, and telemetered by a separate link. This time, together with the capacitance of the dipole in free space, which was determined by preflight calibration, allowed the local electron density to be calculated.

The positive ion concentration was measured with a cylindrical sensor consisting of three parallel electrodes. The outer grid was flush with and electrically connected to the satellite skin and served as an electrostatic shield that prevented potentials on the inner electrode from disturbing the plasma sheath surrounding the satellite. The second grid was biased negatively to reflect incoming electrons and to suppress photoemission from the collector. Because the satellite velocity was much greater than that of the positive ions, the collector output was modulated by the variation of the plane of the collector with respect to the velocity vector of the satellite.

The positive ion current measured was consistent with the electron concentration measured at the same time by the rf probe. A typical measured value was  $1.3 \times 10^4$  ions/cm<sup>3</sup> at a height of 1000 km.

The mass of the positive ions was measured by a sensor physically identical to the ion-current monitor. It differed electrically in that the collector potential was swept between -3 and +20 v at a 0.2-sec interval. The volt-ampere curve of the collector reflected the kinetic energy of the ions striking it and, considering the much greater satellite velocity with respect to ion velocity, allowed the calculation of the mass of the ions.

The resulting data from this experiment indicate that helium and oxygen ions [40] exist in the ratio of  $\text{He}^+/\text{O}^+ + 1.3 \pm 0.3$  for a measurement at 1630 km, 75° W, 32° S, on November 24, 1960.

The electron temperature was measured with both a two- and a three-element Langmuir probe. The two-element probe measured the electron and positive ion current and also provided a measurement of the potential of the satellite relative to the plasma at the sensor location. The outer grid was mounted flush with the satellite skin and was varied from -1.2 to +8 v in potential.

In the three-element probe the outer grid was kept at satellite potential and the inner grid was biased positively to remove the effects of positive ions. The collector was then varied in potential. Since the device was sensitive to photoemission, only measurements in darkness are applicable. The results from the two instruments were in good agreement, a typical value being an electron temperature of 1800°K  $\pm$ 300°K at 920 km. This agreement in data from the two sensors, even though the three-element sensor measured only those electrons with sufficient energy to overcome the satellite potential while the two-element sensor measured all electrons, was interpreted as an indication that the electron energy distribution is Maxwellian.

The current from the satellite resulting from photoemission was deduced by comparing the total current to the satellite with the currents measured by the other instruments [41]. The probe measuring the total current was simply an insulated collector mounted flush with the satellite skin. The current from this sensor peaked due to photoemission when illuminated by perpendicular rays from the Sun and also when the angle between the face of the collector and the velocity vector was a minimum. This last peak was attributed to the relatively slow ions. Finally, there was another peak when the angle between the sensor and the vector  $\vec{V} \times \vec{B}$  approached a minimum ( $\vec{V}$  is the velocity of the satellite and  $\vec{B}$  is the Earth's magnetic field).

The electric field about the satellite was measured by a rotating-shutter electric field meter. It consisted of a four-blade rotor turned by a constant speed electric motor at 7500 rpm and was grounded to the satellite skin through brushes. The stator was identical in design to the rotor and was coupled to ground through a resistive load. The voltage developed across this resistor was telemetered. The operation of this unit was initiated by ground command when the satellite was in the desired position and continued for only a 2-min period because of the heavy drain on the batteries. Data from the experiment has not been published but is awaiting a final analysis of all the records.

#### 34.2.5 Cosmic Gamma Rays

The principal experiment on Explorer 11 was a directional instrument designed to detect gamma rays of energy above 50 Mev [42]. This experiment was conducted by W. L. Kraushaar, G. W. Clark, and associates of the Massachusetts Institute of Technology [43].

The basic instrument consisted of a composite scintillation detector, composed of alternate layers of cesium iodide and sodium iodide, aligned with a lucite Cerenkov counter. This pair of detectors was surrounded by a large plastic scintillator. A high-energy gamma ray incident on the composite scintillator will often be converted into an electron-positron pair, the efficiency of the conversion being known from calibration of the instrument. If the incident gamma ray made a small angle ( $< 17$  deg) with the axis on which the detectors are aligned, the electron-positron pair impinged on the Cerenkov counter where they were detected. A coincidence circuit determined when appropriate signals were generated in both the composite scintillator and the Cerenkov counter. The signal from such a coincidence event was compared in an anticoincidence circuit with the output from the surrounding plastic scintillator. Only those events not accompanied by a signal from the surrounding scintillator were finally counted, thus eliminating events caused by incident charged particles.

The telemetry system carried by the spacecraft was activated on command from the ground to monitor the operation of various elements of the gamma ray instrument. The performance of the instrument could thus be analyzed in considerable detail by the experimenters, contributing much to the confidence in the results obtained.

The axis of the instrument coincided with the longitudinal axis of the spacecraft and the attached last stage rocket. After 27 days in orbit, the satellite reached a state of motion in which it slowly rotated, propeller-like, about a transverse axis of maximum moment of inertia. The axis of the gamma ray instrument therefore described a great circle of the celestial sphere during each rotation. The axis of rotation slowly precessed at a rate of some 10 deg/day, so that during a period of several days the whole celestial sphere was scanned by the instrument. The motion of the satellite is discussed further in a later section. Each time a gamma ray was detected, the viewing direction of the gamma ray telescope was determined for that time.

From preliminary analysis of the data from Explorer 11, Kraushaar and Clark reported, with considerable confidence, the detection of primary cosmic rays. They estimate [43] an average directional intensity of  $J = 5.5 \times 10^{-4} \text{ cm}^{-2} \text{ sterad}^{-1} \text{ sec}^{-1}$  and compare this rate with those expected from possible cosmic sources of gamma rays. A definitive discussion of this point must await final analysis of the Explorer 11 data.

The first detection of primary cosmic gamma rays by Explorer 11 is a notable result, opening a new field of astronomical research. As an additional result, the experimenters were able to measure the gamma ray albedo of Earth resulting from the interaction of primary cosmic particles with the high atmosphere.

### 34.3 Results from Auxiliary Investigations

#### 34.3.1 Orbit Theory and Determination

With the launching of the first artificial Earth satellites, scientists studying the orbit theory of close Earth satellites had their first opportunity to compare their theories with actual radio and optical observations. The resulting investigations, which still continue, became the first of the auxiliary investigations made possible by the advent of successful spacecraft. Many of these investigations included the orbits of Juno spacecraft.

The first papers reporting the results of orbital computations of Explorers 1 and 3 were given at a meeting on May 1, 1958, sponsored by the U. S. National Academy of Sciences and devoted to preliminary experimental results from US-IGY satellite 1958  $\alpha$ . At this meeting the results from the Smithsonian Astrophysical Observatory were presented by G. F. Schilling [44], and those from the Vanguard Computing Center, Naval Research Laboratory, were discussed by J. W. Siry [45]. These papers were primarily devoted to the procedures current at that date for determining satellite positions as a function of time.

The improvements in techniques for the determination and analysis of satellite orbits accomplished during the years 1958 through 1961 are well illustrated by an analysis of the orbit of Explorer 1 by L. G. Jacchia and J. Slowey [46]. Accurate orbital accelerations over extensive time intervals have been determined for this satellite, as well as several others. From such analyses, many detailed results may be obtained concerning forces acting on spacecraft in orbit. In the analysis of Jacchia and Slowey, for example, even such detailed phenomena are detected as the variations in drag due to changes in the average area projected in the direction of the velocity vector at perigee.

Between the initial papers by Schilling and Siry and the paper by Jacchia and Slowey, there exists a long list of references to the orbit of Explorer 1. Typical papers include [47, 48, 49]. The situation with respect to the other Juno spacecraft is much the same. Some of the more significant papers are [50, 51, 52, 53].

In analyzing the orbit of a spacecraft, many forces are recognized and understood. These include the gravitational field of Earth, the gravitation of the Sun and Moon, atmospheric drag and solar light pressure. The success with which the effects of these forces are identified is truly remarkable. Many of the leading coefficients are now determined for an expansion of the gravitational potential of Earth in spherical harmonics [54, 55, 56]. At the time of the launch of Explorer 1 only the first two coefficients were known, and even the second only with poor accuracy.

### 34.3.2 Motion About the Center of Mass

A rigid body in orbit has six degrees of freedom - three locating its center of mass in space and the other three specifying its orientation about its center of mass. The situation pertaining to the orbital degrees of freedom is discussed in the previous section. The theory and determination of the motion of a spacecraft about its center of mass again pose interesting questions.

Half of the Juno spacecraft were launched spinning rapidly about an axis of minimum moment of inertia (Explorers 1, 3, 4, and 11), while the other half spun about an axis of maximum moment of inertia. The former were long, pencil-shaped bodies with a large ratio between maximum and minimum moments of inertia. Experience with Explorers 1 and 3 [35], showed that any slight misalignment of the initial angular momentum vector and the body axis resulted in flexing of unrigid parts of the body. Thus kinetic energy was lost without a change in angular momentum. Such a process resulted in a transition to a motion that is a rotational about an axis of maximum moment of inertia; i.e., about a transverse axis. This happened with Explorers 1, 3, 4, and 11.

In Explorer 4, it was possible to determine the direction of the angular momentum vector as a function of time [57, 13]. This direction was found to move through space at a rate exceeding 10 deg/day. The motion of the spacecraft about its center of mass facilitated a scan through many directions by the collimated radiation detectors carried on the vehicle.

Both the transition to rotation about a transverse axis and the slow precession of the angular momentum vector were used to advantage in Explorer 11 to obtain a complete scan of the celestial sphere during the lifetime of the instrument [43].

As with the orbital motion, there are many possible forces acting to give torques about the center of mass of a body in orbit [58, 59]. These include gravitational, atmospheric drag, and magnetic effects.

### 34.3.3 Atmospheric Density

Determinations of Earth's atmospheric density from satellite observations are reported by many authors. Due to the great decrease in density with increasing altitude, only the density in the neighborhood of the perigee is effective in causing a significant drag and, hence, an observable change in orbital period per revolution. The situation is different for nearly circular orbits.

The first atmospheric density determinations based on data from Explorer 1 were presented at the meeting on preliminary experimental results from US-IGY Satellite 1958  $\alpha$  on May 1, 1958 [60].

Of particular interest are the results of Luigi G. Jacchia, who has given special attention to the variations of atmospheric density with changes in other physical phenomena [63]. These studies show a pronounced diurnal atmospheric bulge following the subsolar point by about 2 hr in longitude, erratic fluctuations in density above 200 km induced by variations in solar radiation in the decimeter region, and irregular short-lived perturbations occurring at the time of large magnetic storms.

#### 34.3.4 Ionosphere Investigations

The first payload to be launched with a Juno-type vehicle was with the Jupiter C launched September 29, 1956. This payload carried a 108 Mc transmitter for telemetering and tracking purposes. Analysis of field strength records of this flight resulted in an electron density profile to some 800 km [64]. Field strength recordings from subsequent launch vehicles and their payloads have continued to increase the data on the ionosphere above that obtained from ground-based sounders [65, 66].

The Ionosphere Research Laboratory, of the Pennsylvania State University, prepared instrumentation for ionosphere measurements carried on several Jupiter missiles [67, 68, 69]. In this experiment, two harmonically related frequencies were transmitted from the ground, one frequency being high enough to be only slightly affected by the ionosphere, the other low enough to be substantially affected. Both signals were received on the rocket vehicle and their phase and strength compared. From these data information about the ionosphere was deduced.

In contrast to the 108 Mc transmitter used for the earlier Explorer satellites, Explorer 7 carried a 20 Mc transmitter. Field strength data from this satellite were used to calculate electron densities by recording Faraday rotations. They are also being used by the University of Illinois and the George C. Marshall Space Flight Center to investigate scintillation phenomena.

#### 34.3.5 Engineering Considerations

The earlier Explorers were limited in operating time to the power capacity of their batteries. Explorer 7, however, was powered by solar cells charging nickel-cadmium batteries and continued to operate for an extended period. This long-time operation permitted the use of data from the Explorer 7 in estimating the reliability of the components and subsystems [70]. A comparison of the theoretically calculated time to malfunction with the actual operating time to first malfunction indicated that the reliability for the components in the satellite was in excess of that assumed for standard components.



In addition to the thermal design information discussed earlier, considerable design data were compiled for electronic systems, subsystems, antennas, and power supplies. These design data are covered in detail in [71].

#### 34.3.6 International Participation

Scientists of nations other than the United States participated in the scientific programs associated with the Juno spacecraft, especially in tracking of these spacecraft, either by radio or optical techniques. Tracking networks, such as the 12 Baker-Nunn camera stations established by the Smithsonian Astrophysical Observatory, often operate under cooperative agreements with the host nation in which the station is located [72].

Explorer 4 provides an example of international support in that observers at the Salisbury, South Rhodesia, station determined the sense of rotation of the satellite in its propeller-like rotation about a transverse axis [13].

Most of the Juno spacecraft continuously transmitted data that could be received by any properly equipped station within line-of-sight of the satellite. Scientists of all nations were encouraged to analyze data received from their stations and to publish their results. Several Japanese scientists analyzed radiation data from Explorers 1 and 4 [73, 74, 12].

A particular effort was made in Explorer 7 to encourage international participation. At the First International Symposium on Space Research, R. Porter, chairman of the United States delegation, announced that the necessary telemetry codes and instrument calibrations would be available on request to groups wishing to reduce data from this satellite [75].

In conclusion, it is obvious that the scientific results from the Juno spacecraft played an important part in the development of space science and technology. The significance of this science is now widely recognized by all nations. Although the Juno vehicles and spacecraft are now history, their pioneering role insures them a permanent place in space science.

## REFERENCES

1. Werhner von Braun, Astronautica Acta V:126, (1954).
2. B. B. Greever, IRE Transactions on Military Electronics, MIL-4:70, (1960).
3. C. A. Lundquist, in "Space Research" ed. H. K. Kallman Bijl, North Holland Pub. Co., Amsterdam, Holland, 1960.
4. Josef Boehm, IRE Transactions on Military Electronics, MIL-4:86, (1960).
5. J. A. Van Allen, G. H. Ludwig, E. C. Ray and C. E. McIlwain, IGY Satellite Report Series No. 3, 73, National Academy of Sciences, Washington, D. C., May (1958). Also reprinted in Jet Propulsion, 28:588, (1958).
6. G. H. Ludwig, Review of Scientific Instruments, 30:225, (1959).
7. S. Yoshida, G. H. Ludwig, J. A. Van Allen, Journal of Geophysical Research, 65:807, (1960).
8. N. C. Chistofilos, Journal of Geophysical Research, 64:869, (1959).
9. J. A. Van Allen, C. E. McIlwain and G. H. Ludwig, Journal of Geophysical Research, 64:271, (1959).
10. J. A. Van Allen, C. E. McIlwain and G. H. Ludwig, Journal of Geophysical Research, 64:877, (1959).
11. Pamela Rothwell and C. E. McIlwain, Journal of Geophysical Research, 65:799, (1960).
12. Y. Miyazaki and H. Takeuche, in "Space Research," ed. H. K. Kallman Bijl 869, North Holland Pub. Co., Amsterdam, Holland, (1960).
13. C. Lundquist, R. Naumann, S. Fields, IGY Satellite Report Series No. 14, National Academy of Sciences, Washington, D. C. , page 91, (July 1961).
14. A. Weber, C. Lundquist and R. Naumann, American Geophysical Union, Program of First Western National Meeting, 19, (December 1961).
15. J. A. Van Allen and L. A. Frank, Nature, 183:430, (1959).
16. J. A. Van Allen and L. A. Frank, Nature, 184:219, (1959).

17. G. H. Ludwig and W. A. Whelpley, Journal of Geophysical Research, 65:1119 (1960).
18. J. A. Van Allen and W. C. Lin, Journal of Geophysical Research, 65:2998, (1960).
19. B. J. O'Brien, J. A. Van Allen, J. E. Roach and C. W. Gartlein, Journal of Geophysical Research, 65:2759, (1960).
20. S. E. Forbush, DiVenkatsan, C. E. McIlwain, Journal of Geophysical Research, 66:2275, (1961).
21. B. J. O'Brien and G. H. Ludwig, Journal of Geophysical Research, 65:2695, (1960).
22. P. Schwed, M. A. Pomerantz, H. Hanson and H. Benjamin, Journal of the Franklin Institute, 271 275, (1961).
23. M. A. Pomerantz, S. P. Agarwal, P. Schwed and H. Hanson, Physical Review Letters, 6:363, (1961).
24. S. L. Russak and F. C. Michel, Martin Company Report, ER-11688, (August 15, 1961).
25. E. P. Buwalda and A. R. Hibbs, IGY Satellite Report Series No. 3, National Academy of Sciences, Washington, D. C., (May 1, 1958).
26. G. Heller, IRE Transactions on Military Electronics, MIL-4:98, (1960).
27. V. E. Suomi and M. Weinstein, Monthly Weather Review, U. S. Weather Bureau, (November 1961).
28. Earth's Thermal Radiation Balance, (condensed from report by V. E. Suomi), IGY Bulletin No. 52, (1961).
29. E. Manring and M. Dubin, IGY Satellite Report Series No. 3, National Academy of Sciences, Washington, D. C., (May 1, 1958).
30. M. Dubin, Planetary and Space Science, 2:121, (1960).
31. M. Dubin, in "Space Research," ed. H. K. Kallman Bijl, North Holland Pub. Co., Amsterdam, Holland, (1960).
32. A. R. Hibbs, Journal of Geophysical Research, 66:371, (1961).
33. M. Dubin, Journal of Geophysical Research, 66:2592, (1961).
34. A. R. Hibbs, Journal of Geophysical Research, 66:2595, (1961).

35. A. R. Hibbs, in "IXth International Congress of the International Astronautical Federation," ed. F. Hecht, Springer Verlag, Vienna, 1959.
36. H. E. LaGow and L. Secretan, Annals of the IGY VI, 319 (1958).
37. C. W. McCracken and W. M. Alexander, International Symposium of the Astronomy and Physics of Meteors, Cambridge, Mass., (August 28, 1961).
38. R. E. Bourdeau, J. L. Donley and E. C. Whipple, Jr., National Joint Meeting of ARS & IAS, Los Angeles, Calif. (1961).
39. R. E. Bourdeau, Second International Space Science Symposium, Florence, Italy, (April 1961).
40. R. E. Bourdeau, E. C. Whipple, Jr., J. L. Donley, S. J. Bauer, Fall URSI Meeting, Austin, Texas, (October 1961).
41. R. E. Bourdeau, J. L. Donley, G. P. Serbu, E. C. Whipple, Jr., Journal of the Astronautical Sciences, 8:65 (Fall, 1961).
42. Explorer XI Gamma Ray Satellite, IGY Bulletin No. 50, National Academy of Sciences, Washington, D. C. , (August 1961).
43. W. L. Krausharr and G. W. Clark, International Conference on Cosmic Rays, Japan, (1961).
44. G. F. Schilling, IGY Satellite Report Series, No. 3, National Academy of Sciences, Washington, (May 1, 1958).
45. J. W. Siry, IGY Satellite Report Series, No. 3, National Academy of Sciences, Washington, D. C. , (May 1, 1958).
46. L. G. Jacchia and J. Slowey, Research in Space Science, Smithsonian Institution Astrophysical Observatory Special Report No. 7, (October 1961).
47. C. A. Whitney, Smithsonian Institute Astrophysical Observatory Special Report No. 41, (April 30, 1958).
48. K. Lassovszky, Smithsonian Institution Astrophysical Observatory Special Report No. 41, (May 24, 1960).
49. P. E. Zadunaisky, Smithsonian Institution Astrophysical Observatory Special Report No. 50, (October 3, 1960).
50. Y. Kozai, Smithsonian Institution Astrophysical Observatory Special Report No. 51, (October 17, 1960).

51. L. G. Jacchia, Smithsonian Institution Astrophysical Observatory Special Report No. 62, (May 26, 1961).
52. D. V. Mechau, Smithsonian Institution Astrophysical Observatory Special Report No. 68, (July 17, 1961).
53. M. Eimer, A. R. Hibbs, R. Stevens, in Space Research, ed. H. K. Kallmann Bijl, North Holland Pub. Co. Amsterdam, Holland, 1960.
54. J. A. O'Keefe, in Space Research, ed. H. K. Kallmann Bijl, 448, North Holland Pub. Co., Amsterdam, Holland, 1960.
55. I. G. Izsak, Smithsonian Institution Astrophysical Observatory Special Report No. 56, (January 30, 1961).
56. Y. Kozai, Astronomical Journal, 66:355, (1961).
57. R. J. Naumann, in Ballistic Missiles and Space Technology, ed. D. P. LeGalley, Academic Press, New York, 1961.
58. C. A. Lundquist and R. J. Naumann, Seminar Proceedings Tracking Programs and Orbit Determination, (February 1960), Jet Propulsion Laboratory.
59. G. Colombo, Smithsonian Institution Astrophysical Observatory Special Report No. 70, (July 18, 1961).
60. T. E. Sterne, IGY Satellite Report Series No. 3, National Academy of Sciences, Washington, D. C., (May 1, 1958).
61. C. A. Whitney, Annales de Geophysique, 17:237 (1961).
62. M. Nicolet, in Space Research, ed. H. K. Kallman Bijl, North Holland Pub. Co., Amsterdam, Holland, 1960.
63. L. G. Jacchia, Annales de Geophysique, 17:52 (1961).
64. J. S. Nisbet, Journal of Geophysical Research, 65:2597 (1960).
65. J. S. Nisbet and S. A. Bowhill, Journal of Geophysical Research, 65:3601 (1960).
66. J. S. Nisbet and S. A. Bowhill, Journal of Geophysical Research, 65:3601 (1960).
67. E. A. Mechtly and S. A. Bowhill, Journal of Geophysical Research, 65:3501 (1960).

68. E. A. Mechtly and S. A. Bowhill, URSI Meeting, Washington, D.C., (May 1961).
69. S. A. Bowhill, Second International Space Science Symposium, Florence, Italy, (April 1961).
70. C. F. Willard, ARINC Research Corporation, Pub. No. 173-3-255.
71. Juno II Summary Project Report, Explorer VII Satellite, NASA TN D-608 Volumes I through VII, (July 1961).
72. F. L. Whipple and G. Veis, Second International Space Science Symposium Florence, Italy, (April 1961).
73. Y. Aono and K. Kawakami, Report of Ionosphere Research in Japan, 12:28, (1958).
74. Miyazaki and H. Takeuchi, Report of Ionosphere Research in Japan, 12:448, (1958).
75. R. W. Porter, Third COSPAR Meeting, Nice, France, (January 1960).

## 35

## THE RELATIONSHIP BETWEEN GEODESY AND ROCKETRY

Hellmut Schmid

Ballistic Research Laboratories  
Aberdeen Proving Ground, Maryland

Geodesy and rocketry are technical sciences. Both give support, directly and indirectly, to a considerable group of technical and scientific activities, especially those in the area of geophysics. For the purpose of investigating the relationship between geodesy and rocketry, it is useful to isolate them from their utilitarian applications.

A considerable number of academic institutions throughout the world have initiated advance courses in these subjects, and the scientists in these fields have organized national and international professional societies. These developments illustrate the growing importance of geodesy and rocketry. The educational curricula and publications in both activities are characterized by sophisticated theoretical investigations, mostly of a physical-mathematical nature, and a considerable amount of information or complex hardware, especially in the mechanical and electronic engineering fields.

The execution of precise measurements over larger areas is the principal activity in geodesy. For the purpose of this discussion, however, reference to mensuration problems will be omitted. The basic problem of geodesy is defined as the task of determining the size and shape of the Earth.

Classic geodesy was predominantly influenced by geometrical considerations. Accordingly, the determination of the size and shape of the Earth was one of the principal considerations. Modern geodesy has introduced the physical concept that establishes the determination of the gravitational field of the Earth as one of the basic problems of geodesy. More recently, geodesy has acknowledged the need for the unified theoretical approach, wherein the geometrically defined reference ellipsoid must be brought into an unambiguous mathematical relation to the multitude of equipotential surfaces which, in their totality, represent the Earth's gravitational field.

To define, for this discussion, the basic problem of rocketry we shall, in analogy to the restrictions imposed on the definition of the basic geodetic

problem, abstain from considerations associated with the development of the space vehicle. This enables us to state the basic problem in the field of rocketry as one associated with the geometrical and physical description of specific trajectories. Accordingly, the navigational problem for vehicles traveling through space can be interpreted as the problem of developing methods for determining their trajectories.

During the early stages of development, rocketry was concerned with the determination of relatively short trajectories and associated with vertical test firings. Because of the rather limited overall dimensions of such trajectories, a local Cartesian coordinate system, oriented with respect to the normal to the reference ellipsoid at the launcher, served adequately as a reference frame for expressing the geometry of the flight path. Similarly, a relative time-coordinate system, referenced to the instant of takeoff, proved to be adequate for determining the time sequence of velocity and acceleration values in connection with the aforementioned position measurements.

As a result of political factors, the development of rocketry was strongly influenced by military requirements. Thus, to a large extent, the effort in the development of rocketry was directed toward obtaining optimum trajectories that would give maximum range and accuracy. The goals concerning range and precision, set forth during this phase of development, are such that the concept of the Cartesian frame had to be replaced by a space curved reference system; specifically by an ellipsoid of revolution as used as a reference surface for the reduction of larger geodetic triangulation systems. Such an approach became necessary because the methods for determining the trajectories were based almost exclusively on Earth-based equipment that measured, from various points, the directions to the vehicle at different times. The Earth-fixed positions of the measuring stations are determined with their geodetic coordinates expressed by latitude and longitude in respect to a strict geometrically defined, reference ellipsoid. However, the measuring equipment must be oriented at each station with respect to the local direction of gravity, which approximately coincides with the corresponding direction of the normal to the specific reference ellipsoid.

To establish a rigorous, three-dimensional reference system for the spatial triangulation of trajectories, it is necessary to determine at each point of observation the so-called relative plumbline deviation. This deviation is, in essence, the angle between the direction of the local plumbline and the normal to the chosen reference ellipsoid. The quantity is obtained by comparing the geodetic latitude and longitude of a specific station with the corresponding astronomical latitude and longitude. The latter values on one side are referred to the direction of the local plumbline, and on the other to the right ascension, declination and universal time coordinates of the system of the fixed stars. Thus, the larger over-



all dimensions of the trajectory required a reference frame not only more complex in terms of geometry, but also one which contains more basic information by including the astronomical and universal time system in the group of basic reference parameters. Despite this more sophisticated approach, the result of the spatial triangulation of the trajectory was still significant only in a strictly geometrical sense relative to a specific geodetic reference ellipsoid. As for dimensions, flattening or orientation of such a geodetic reference figure does not necessarily provide for an optimum reference system for the physically defined basic requirements of rocketry.

Using Earth-fixed stations and only by applying guidance and control techniques, such as beam-riding techniques in combination with electronic velocity measuring methods, can such a strictly geometrically defined trajectory determination allow for an adequate interpretation of the result. For all inertial guidance concepts, however, as well as for the free-flight portion of the trajectory, only that trajectory information is meaningful which has been derived from measuring systems whose geometrical-mathematical parameters are established in a known and proven relation to the various physical force fields, especially to gravitational fields.

The classic geodetic-geometrical concept served rocketry sufficiently as a close approximation for moderate distances. The basic requirement of rocketry, however, is more complex when we consider trajectories covering distances comparable to Earth dimensions. It becomes necessary to relate the geometry of the trajectory with a set of geodetic parameters, expressing the geometrical relationship between far-separated points of launch and impact. Of equal importance is the construction of the trajectory by guidance and control operations, as well as its reconstruction by spatial triangulation methods. These must be accomplished in such a way that both operations are compatible; that is, they must be based on a common concept concerning the geometrical and physical characteristics of the chosen model of the Earth. Furthermore, the problems concerned with the qualitative and quantitative influence of various local perturbations, by which such a model is unavoidably affected, must be treated by both operations with a unified theoretical approach.

Modern geodetic-astronomical theory and measuring methods provide at least acceptable approximation techniques to these problems as long as the points of launch and impact are connected by land masses covered with a continuous geodetic-astronomical triangulation system supported by a closely arranged net of gravimetric stations. Such a geographical restriction is now unacceptable. Rocketry, with its spectacular advances, requires the freedom of selecting any two arbitrarily chosen points on the Earth as points of launch and impact; therefore, it is necessary to provide means for establishing the geometrical tie between any two points on the Earth's physical surface in a three-dimensional reference system that is rigorously connected to the spatial vector fields of the forces influencing the trajectory of the rocket.

This geometrical-physical problem is closely related to the need for establishing a world-wide, three-dimensional coordinate system, wherein the various geodetic datum systems may be related through a specific geometrically defined reference figure whose center coincides with the Earth's center of gravity, whose orientation is consistent with the astronomical-universal time system, and whose shape represents a means of expressing the terrestrial gravitational field.

The demand for physically significant geodetic parameters is not restricted to the field of rocketry. It is a typical requirement for all projects dealing with broad navigational problems. Because rocket trajectories pass through space and encompass the entire Earth with its various geophysical forces, rocketry is subject to the most stringent requirements. For conventional geodesy it was logical to limit its mission, with regard to space, by considering as an outer boundary condition the equipotential surface through the topographically highest point of the physical surface of the Earth. Such a restriction was necessary because geodetic-astronomical observations could only be gathered at, or close to, its physical surface. Furthermore, such an approach seemed adequate under the assumption that the corresponding results would and could be used only in support of scientific and engineering projects in the neighborhood of Earth's physical surface.

Rocketry has changed this situation drastically by making space a field for experimentation. Therefore, the corresponding geodetic-physical background information must extend its range of applicability by establishing a geodetic-geophysical model of the Earth with a degree of fidelity allowing the extrapolation of its geometrically and physically defined characteristics far out into space. A typical example is the problem dealing with the existence of a 24-hr orbit, which depends decisively on certain resonance effects caused by the existing asymmetries in the potential field of the Earth. One readily can imagine a situation wherein a space vehicle has travelled so far into space that the Earth appears to the various navigational sensors as a point source, thus eliminating the geodetic-geophysical problem simply by the unavoidable deterioration in scale. Equally convincing, though, is the fact that the precision requirement on the geodetic-geophysical information will increase in the future so that the geometrical-physical Earth characteristics can serve as a calibration standard for the complex problem of space navigation. Certainly the era, just now beginning, of various types of artificial satellites will stress the need for dependable geodetic-physical parameters, whether for the sake of orbital determination or for the physically significant interpretation of orbital perturbations.

Rocketry by its own capabilities has created the means that can support geodetic activities in establishing information from which future space projects will profit. These methods are concerned with the use of space-borne optical and electronic beacons. Such an auxiliary point in

space can be regarded as a temporary extension of an Earth-established geodetic reference system. By triangulating the beacon simultaneously from various fixed stations, the considerable height of the beacon allows the bridging of large areas of the Earth with a minimum of triangulation configurations. Thus it is possible to reduce considerably the pseudo-systematic accumulation of random errors typical in classic geodetic triangulation schemes, especially if the spatial position of the beacon is triangulated with reference to the background of the fixed stars.

This method is analogous to the high-altitude flare-triangulation technique, but is an improvement because of its capability to measure lengths and directions by electronic techniques in addition to obtaining directions by essentially classic geodetic-astronomical methods. The result of this so-called intervisible method is strictly geometrical even if such a triangulation is carried around the Earth. The optimum usefulness of a space-borne beacon for geodetic purposes that closely resembles the requirements of rocketry in regard to the determination of its trajectories can be expected only if such a beacon is part of a satellite. In determining its trajectory and the secular or long-period satellite motions, such measurements contribute to the determination of the Earth's external form, gravitational field and equatorial radius, and the flattening of the reference ellipsoid. It also helps to improve the positioning of the main geodetic datum systems. The interpretation of this result is not only significant in its geometrical-mathematical sense, due to the dynamic nature of the satellite's orbit, but also is physically significant in the sense of the basic problem of modern geodesy and is equally significant in terms of the basic requirements of rocketry on geodesy, namely, the determination of the trajectory.

An apparent similarity in the basic requirements of geodesy and rocketry, for establishing a physically acceptable geometric model of the Earth and its geophysical parameters by combining astro-geodetic, gravimetric, and satellite data, has been demonstrated. The common interests of geodesy and rocketry in this field suggest the desirability of a close collaboration between the two activities, not only from the standpoint of the basic theoretical background, but also in regard to the measuring methods and the corresponding measuring equipment.

Geodesy, with its theoretical and practical know-how, can provide a valuable service to the field of rocketry if employed to solve problems associated with the selection and operation of test ranges. Similarly, rocketry, insofar as it is concerned with the science of space, has the potential to increase geodetic knowledge by actively sponsoring a program for a group of ideal geodetic satellites, and by supporting efforts for the development of precision tracking methods.

It may be of interest to speculate which of the two activities, geodesy or rocketry, has gained more from their mutual contact. Certainly, there is no doubt that both fields can profit by a closer working association.

## BIBLIOGRAPHY

1. Vies, George, Smithsonian Contributions to Astrophysics, 3:95 (1960).
2. Williams, Owen W., Geophysics Research Directorate, Air Force Cambridge Research Laboratories, Bedford, Massachusetts, talk given on Voice of America, January 29, 1962.
3. Woollard, George P., The Earth, in "Science in Space", L. V. Berkner and H. Odishaw, eds., McGraw-Hill Book Co., New York, 1961.

16012

# 36

## THE INFLUENCE OF MAN ON THE DESIGN OF SPACECRAFT

Robert G. Lindberg,  
Charles F. Lombard, and  
Ludwig Roth

Northrop Norair Division  
Hawthorne, California

For centuries the human body has been considered a limiting factor in the exploitation of many known technical systems. Consequently, it has been generally accepted that any system could be improved upon except man, at least in respect to his physical capability. This usually resulted in designs of man-operated machines with fixed limitations; either the full use of the system possibilities were denied, or the human operator was partially replaced by mechanical or electrical substitutes. Little thought was given to improving man's environment or, in the case of vehicles, improving the impact direction of forces to increase the tolerance of the human operator.

For example, it would have been possible to reach extreme altitudes with aircraft or balloons much earlier if the human limitations had not been present. The feeling that human endurance could not be improved stopped any attempt before it started. In recent years, however, man has lost some of his reluctance to break the barrier of human capabilities. The combination of training and assistance from technical devices have freed the designer from many previous restrictions. Intensive scientific research is creating an understanding of the interrelationship between physiological and psychological systems and is accumulating actual values and numbers decisive for the development of spacecraft.

### 36.1 Physical Forces

There appears to be a hereditary knowledge of the susceptibility of living tissues to locally applied physical force which is shared by most animals and humans. Animals and primitive man used this knowledge to injure and kill others for food or self protection. Man's superior brain has permitted him to develop many ingenious devices for the destruction of both humans and animals by exploiting this susceptibility to locally applies forces. Now there is concern with the use of man in rather high force fields, and considerable research has been accomplished to define the tolerance factors involved. The use of man, his tolerances, and his

survival are new goals contrasted to the goal of destruction. Space travel, with the high velocities and accelerations involved, demands a thorough understanding of man's weaknesses and strengths in combating the effects of physical forces.

Taking advantage of man's strength is a direct challenge to the engineer. At present the engineer can provide protective devices and systems which will partially minimize local weaknesses, thus permitting the use of man in force fields high enough to rechallenge the engineer to build his vehicle stronger and more powerful. Current research is further increasing the knowledge of man's ability to tolerate and survive applied forces, thereby providing the engineer with the parameters for the design of better protective equipment and devices.

Forces of primary interest are those programmed in normal or emergency operation. These are the forces of launch, acceleration to velocity, reentry, aborted launch, rendezvous, and navigational maneuvers.

The astronauts of Project Mercury have developed a terminology of identifying the direction of acceleration with regard to the orientation of the body. The terminology seems to be easily remembered and less confusing than many others. If the direction of acceleration is from the back to the front of the body the mass of the body has an inertial reactance just the opposite; the eyeballs seem to sink back in the sockets, so they call this eyeballs-in acceleration. Thus, they have the eyeball indicator with direction of accelerations expressed as eyeballs in, -out, -up, -down, -lateral right and -lateral left. Man's tolerance to acceleration varies depending upon his orientation to it, the magnitude, rate of onset, duration, and the protective devices used. Man's greatest tolerance is to the eyeballs in acceleration with eyeballs out the next tolerable. Least tolerable is the eyeballs up orientation. Only the best useable tolerances will be considered further, since these are the ones which challenge the engineer. He must expose man only in his strongest potential of tolerance in all phases of normal and emergency programmed operations.

Colonel John P. Stapp has shown, through experimental work using rocket sleds, that the human body can withstand rather astounding accelerations to the eyeballs-in or -out orientation. His work with animals indicates that man's survival level is much higher. His own exposure to  $> 25 \text{ G}$  eyeballs-out for over 1 sec is indicative of the potential tolerance levels which the engineer must consider. Although Stapp had minor injuries about the eyes, it is believed that a better restraining system would have prevented that. He believes that abrupt transversely applied decelerative force of  $40 \text{ G}$  lasting for less than 0.5 sec can be tolerated without injury, allowing drogue recovery of manned capsules.

Additional work done on various centrifuges has shown the engineering

design challenge for longer application of accelerational forces. Semi-recumbent position, eyeballs-in orientation to  $10G$  has been tolerated for over 2 min. Fluid immersion increases the duration of tolerance several-fold. This emphasizes the importance of a supporting device which will be engineered to provide most of the good features of fluid immersion without the undesirable ones. Eyeballs-in acceleration of  $4G$  can be tolerated for sufficient lengths of time to reach 100,000 mph, even with current support systems. However, with current propulsion systems, the human probably will be exposed to gradually increasing accelerations, reaching a peak at burn-out for each of several stages. Flight profiles of the probable types of acceleration have been conducted on centrifuges and found to be tolerable. High peak accelerations at burn-out of one stage dropping to zero followed by gradually increasing  $G$  of the next stage, etc., are the most detrimental to all of the systems of the human body, especially the vestibular or balance mechanisms. Engineering should provide for better care of humans by providing a more uniform acceleration profile.

### 36.2 Noise and Vibration

Associated with rocket propulsion are noises and vibrations which may adversely affect the astronaut. Man's bodily components have natural frequency responses which depend upon his orientation to the propulsion force, the method of restraint and support, vibratory forces, methods of attenuation, and the relative masses involved. The problem of attenuation of the energies of the vibratory forces involves the balance between discomfort by forceful restraint during minor energy transfers and the positive retention during high energy transfers. For example, Colonel Stapp, during his high-deceleration rocket sled experiments, was strapped to the seat to the point of discomfort, but without this positive retention he would not have been held in the seat during his  $>25G$  deceleration. This is a problem requiring additional research effort. Adequate attenuation, comfort, support, and restraint will not be easy to achieve. Soft resiliency is needed for comfort and attenuation of vibration, but precise and rigid contouring is needed for supports and restraints during high- $G$  loads of reentry and launch.

### 36.3 Body Maintenance

For the foreseeable future, placing man in space will be for the purpose of using his mental and physical abilities. After a sojourn in the space environs he will be returned to Earth. During his space tour he must maintain his body to accept the gravitational field of  $1G$ . Both circulatory and musculo-skeletal systems must be maintained by the force of exercise. Exercise will need to be in line with the weight and balance system of the space vehicle and could, in part, be useful work. The amount of useful work to be accomplished by man-in-space, such as in orbital maintenance work, probably should be metered to maintain the body since

the human is not an efficient machine and would require rather large logistic support. Time is an important element to consider in the body maintenance. Circulatory changes occur in a few hours, muscular regressing in several days and bone changes in several weeks or more. Studies on Earth give indications of what to expect in the weightless environs of space. We are all familiar with the effect of placing a broken arm in a cast for several months. The decrease in muscle and use is alarming and it is again several months before normal use or appearance is obtained. In all probability, low (2G or less) reentry accelerations would be needed to protect the debilitated human after several weeks in space, unless adequate body maintenance through exercise is achieved.

#### 36.4 Human Tolerance to Changed Environment and the Resulting Demands on the Control of the Environment

In 1783 the Montgolfier brothers constructed a balloon 90 ft in diameter inflated with hot air which bore two human passengers in free flight. Life support problems in this flight were associated more with a secure grip on the flying device than with environmental control.

In 1862 balloon technology had advanced to the stage of achieving altitudes in excess of 20,000 ft with crews numbering three and four, at which point the problems of oxygen deficiency became limiting. By 1874 the physiologist, Paul Bert, experimenting in a primitive altitude chamber, had discovered the use of supplementary oxygen supplies for high-altitude balloon flights. The physiological problem associated with oxygen deficiency at low atmospheric pressures and caisson disease, related with the behavior of respiratory gases at high atmospheric pressures, were studied in the 1870s.

Man's exploration of space and his desire to inhabit extraterrestrial environments has reaffirmed his dependency upon terrestrial phenomenon for survival and normal behavior. The problem of life support is now concerned with simulating rather than supplementing the terrestrial environment. What is the normal terrestrial environment required by man for his well-being? To what extent can it be altered and still enhance his performance? Neither question can be answered specifically, but certain general biological phenomenon can provide a basis for anticipating the life support systems that will be required when the worlds of the Solar System begin to be exploited by man.

#### 36.5 Man Machine Relationships

Compared to available instruments man has questionable value as a direct sensor. His role must be in the areas of reception, selection, synthesis, and interpretation of data; maintenance and control of sensors and equipment; and decision-making in terms of general surveillance and emergency operations. Instruments and machines cannot duplicate the



innate capabilities of a well-trained astronaut except in predictable situations. For this reason, man may contribute significantly to the overall flexibility of the system. The value of man will, however, depend upon his ability to function efficiently and reliably during the extent of the mission. This ability has not yet been demonstrated in prolonged orbital flight or, more specifically, in the problem areas of prolonged weightlessness and cosmic radiation exposure. The definition of man's role depends, therefore, upon limitations which have not yet been determined.

The environmental limitations as set by the physiological and psychological thresholds of man are reasonably well established but will change gradually over the next few years. Research in aerospace medicine may be expected to define new physiological capabilities as a result of experimentation in altered gravitational and radiation fields. The biological capabilities, however, will change slowly compared to the physical methods that will be devised to meet them. To assume successful manned space missions, it is also necessary and reasonable to assume that procedures and devices will be developed permitting man to operate efficiently under weightless conditions for limited periods. The quiescent cosmic radiation does not appear to be excessively hazardous, but solar flares will occasionally produce extremely hazardous situations. This will place a limit upon the effectiveness of a manned system.

As demanding as man may be of his work environment, his range of tolerance to both temperature and humidity exceeds, in some cases, the acceptable limits for various solid-state devices and optical systems. Thus, the importance of the overall man-machine complex becomes crucial, since the broad requirements for environmental control can be set by human needs; in some instances, more narrow requirements are dictated by the equipment. The design of a life support system must be based upon these observations and assumptions.

### 36.6 Physiological Links to Earth

Man is a product of 3.5 billion years of evolution in a terrestrial environment. It is not an exaggeration to state that there is yet to be defined an environmental phenomenon (i.e., gravity, light, magnetism) to which some form of life does not respond. Since man is an expression of life, it is not improbable that he also senses environmental phenomenon of which he is not consciously aware. Under chronic exposure to space habitation, he may become aware of them by their very absence. Whether these stimuli are essential to his well-being, only manned space excursions can reveal.

Weightlessness is a good example of an anticipated problem. In addition to possible disorientation, there are other potential physical consequences of reduced gravitational force. The skeletal and muscular

systems are dynamic and respond to changes in stress. In the absence of stress, the skeletal and muscular systems, and consequently, the circulatory system are anticipated to degrade in physical strength. While the process is reversible, it is slow. It is possible that this degradation would seriously jeopardize the ability of the astronaut to survive present ballistic reentry profiles without either improved protective equipment or a routine of muscular exercise in space to maintain his terrestrial norm.

### 36.7 Inherent Nature of Biological Variability

In this age of wonder drugs, organ transplants, plasmotherapy, and electroencephalography, the layman may tend to overestimate the degree to which life processes are understood. At this state of our knowledge, life is a fundamentally variable process imperfectly known and singularly unsuited to mathematical expression. As a result, biomedical research is characterized by empirical experimentation. This approach, dictated by the complexity of the life process, contributes to the derivation of biological constants with large standard deviations whose mean expression may have little significance except in terms of large populations. Too often this lack of precision is attributed to experimental error without acknowledgement of the inherent variability of the experimental material.

An organism, whether it be a virus, an algae cell, or a man, is a dynamic, homeostatic, physical-chemical system continually interacting with narrowly defined environmental factors. Life has evolved, however, in a world in which the local effective environment is neither constant nor predictable. As a result, the survival of life has depended upon the ability of the species to adapt to new environments and to change as the environment changed. In its broadest sense, biological variability, the curse of the experimental biologist, is an expression of a species' ability to adapt and to evolve. The large standard deviations of biological constants are real, and it is this statistical expression rather than mean values, that must be considered in the design of life support systems.

Reduced to engineering requirements, acknowledgement of the basic variability of biological systems dictates a need to overdesign life support elements to accommodate variation in both individuals and populations.

### 36.8 Tolerance Versus Performance

There is a fundamental difference between surviving an acute stress and continuing to perform analytical tasks under chronic stress.

The degree of stress a man can tolerate is a function of the duration of the stress and his physiological and psychological condition. To a degree limited by his hereditary potential, man can adapt to extreme conditions and continue to perform analytical tasks. Figure 36.1

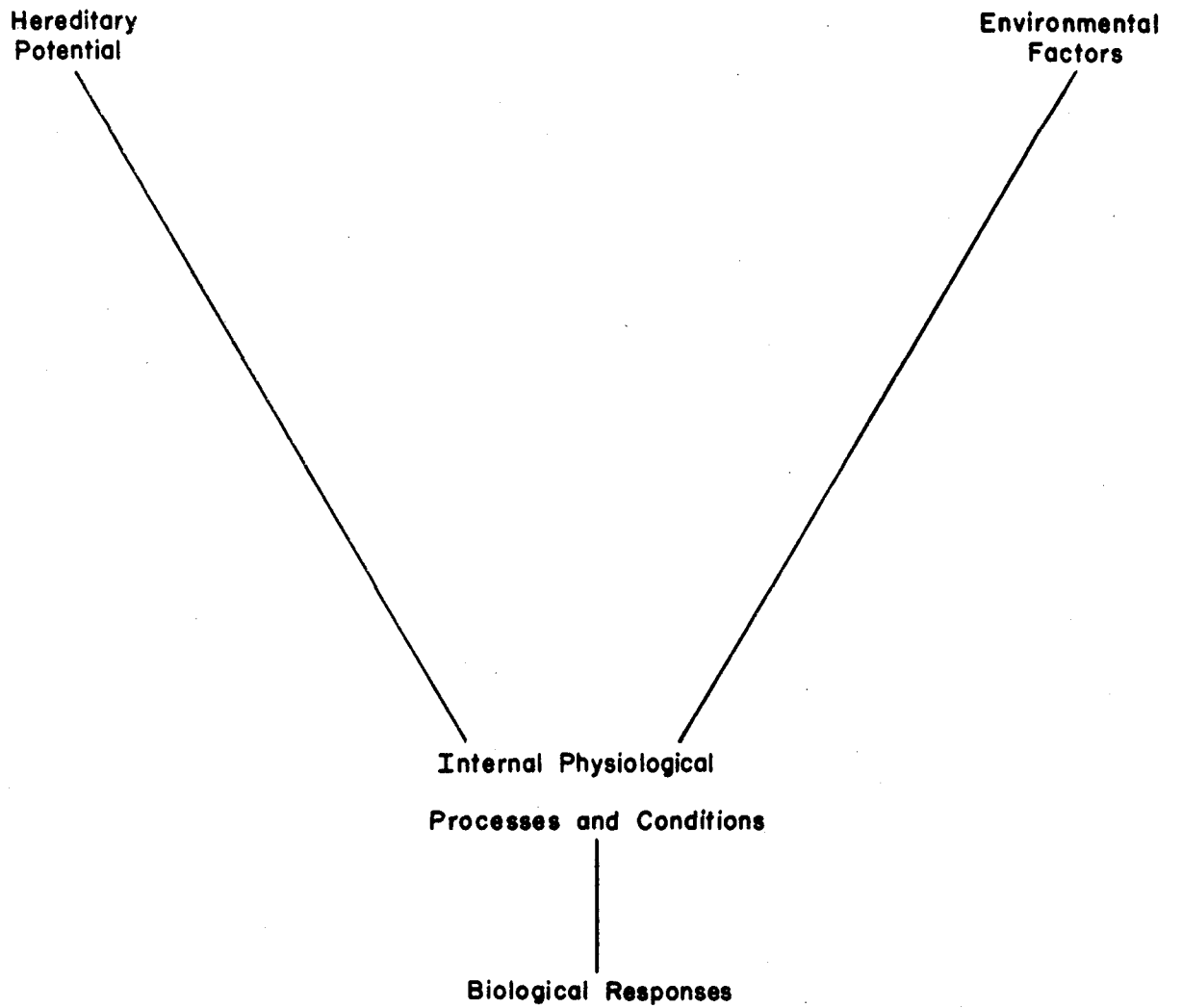


Fig. 36.1 Interaction of heredity and environment on the expression of biological responses.

graphically depicts the interaction of the hereditary potential and the environmental factors acting upon somewhat elastic physiological processes to produce a particular biological response.

There is no way that environmental factors can influence a biological response except through the alteration of the physiological state. Physiological processes are homeostatic enough to preserve a steady state under mild stress and, as long as they can do so, the biological response is unchanged.

This is the process of tolerance to acute stress and adaptation or acclimatization to chronic stress. The degree to which an organism can tolerate or adapt, however, is limited by the hereditary potential and, in the case of the adult man, cannot be changed. There is little evidence to suggest that even with extensive conditioning the range of tolerance or adaptation to stress is significantly altered. The individual organism is simply conditioned to live under more marginal conditions with minimal discomfort. In terms of space crew reliability, such conditioning may even be hazardous; since only a small change in environmental stress may be enough to exceed the real tolerance limits.

#### 36.9 Influence of Biological Variability Upon the Selection of Astronauts

The screening program to select suitable candidates for present space travel is based upon an awareness of biological variability. If, for the purposes of this discussion, a large population of potential astronauts were tested and the frequency of their scores for any particular test plotted, in all probability a curve of normal distribution would result. If the choice of whom to send into space depended upon this single test, it is obvious that the select group with the highest scores would be chosen. However, selecting the most suitable astronaut is not the result of a single test and there is ample indication that individuals who score high on one test may be only average on subsequent tests of the same type. If the biological response being measured is a complex one such as performance, even greater problems arise. Performance depends upon the integration of many individual scores and, while it may be possible to select a crew with similar performance capabilities, there is no assurance that the tolerance to specific physiological or psychological stresses is necessarily the same.

This latter point is particularly true in light of the premium that will be placed on versatility of crew members selected for interplanetary travel. This situation may be likened to the Olympic Decathlon in which excellence in many events, rather than pre-eminence in one, is required to win. As a result, the performance of any particular individual or crew is still a function of the variability of individual abilities and the standard error of a reliability expression will be large.

### 36.10 Synergistic Effects

Superimposed upon the variables discussed above is the phenomenon of synergism, in which the biological response to combined stresses presented simultaneously is greater than would be anticipated from simple accumulation of individual stresses.

Synergism is a common phenomenon to the experimental biologist, but it is difficult to quantify because the degree of interaction varies with the conditions of the experiment. Particular stresses shown to be synergistic include the effects of hyperventilation, hypoglycemia, and positive acceleration; the combined effects of internal and external radiation; and the effects of two simultaneously administered internal radiation emitters. The interaction between such chronic stresses as acceleration, weightlessness, isolation, and radiation are difficult to anticipate and point to the need for intensive experimentation. Such experimentation may reveal synergistic relationships which will define even more strictly the requirements for a life support system.

The purpose of this discussion is to emphasize the inherent variability of man rather than belabor the fact that man is delicately adapted to the Earth's environment; to show the paucity of knowledge regarding fundamental life processes; and to emphasize the resulting requirement that engineering must be for the man and not of the man. As a result, a fundamental rule of toxicology has guided the design of life support systems to be used in the near future. Paraphrased, the rule states that the ultimate deleterious effect of any particular physiological stress is a function of the degree of stress and the duration of stress, compounded by the synergic effect of multiple stresses. With the present meager data regarding the biomedical consequences of space habitation, such a tenet defies rebuttal and specifically endorses the opinion that, to be useful in space, man must be provided with an environment which simulates a normal terrestrial condition. Compromises in environmental control may result in compromises in human performance and reliability.

### 36.11 Engineers Versus Biologists

Just as life is a complex of interacting dynamic, homeostatic, physical-chemical processes, so the specific needs of man are interrelated and defy rigid categorization. For convenience, human requirements are often presented as physiological and psychological, with full realization that they are interdependent and that mental stress will influence metabolic processes just as surely as malnutrition will influence performance. Space does not permit, nor does this discussion call for, a restatement of all factors known to influence man's performance and well-being. More significant is the fact that as the biomedical researchers look more critically at human requirements, they are particularly impressed with the paucity of data immediately applicable to the space effort and

somewhat appalled at the lack of definitive data pertaining to human needs on Earth. Nevertheless, it is from the biomedical professions that the engineer must obtain numerical values from which to develop realistic design boundaries. Too often, however, these values become magic numbers to be used in all design concepts without due attention to changes in the mission profile and task analysis. As one example, consider the factors which influence the weight of consumable supplies such as food, water, and oxygen.

### 36.12 Nutrition

Man, an animal by definition, is unable to produce the energy supply required for his functioning. He is further restricted by being unable to utilize primary energy sources other than those provided in organic compounds through a process of photosynthesis. It follows that the required nutrients, and the oxygen and water needed to use them efficiently, stem from his basic energy requirements.

Quantitative estimates of the nutritional needs of man are primarily determined by the size and age of the individual, the kind of activities projected, and assumptions of the degree and duration of physiological and psychological stresses endured. In addition to sedentary analytical tasks, future astronauts will engage in vigorous missions involving survival, construction, maintenance, exploration, research, development, exploitation, and possibly defense. The abilities and energy of each individual will be used to the maximum. The environmental and psychological stresses placed upon space personnel demand that each individual be healthy. These men will be living in a different world under strict regimentation. Their activities will be limited to a created artificial environment, and they will be aware constantly of the consequences of malfunction or error. Any activities external to the space cabin or shelter will be hazardous and may be physically exhausting. Any decrease in energy expenditure made possible by reduced gravitational fields will be compensated for by the working conditions. In the absence of appreciable gravity, physical exercise against resistances may be required to allay muscle atrophy and to insure physical well-being. These considerations immediately suggest, depending upon the specific mission, that the average energy requirements may be significantly greater than the 3000 calories per day per man presently anticipated.

For the same total body weight, a 25-yr-old astronaut will require about 10 per cent more calories than a 45-yr-old, while a 150-lb man requires approximately 10 per cent less calories than a 175-lb man. Since a major portion of the metabolic energy is used in maintaining body temperature, a decrease in ambient temperature (accidental or intentional) will result in an increase in caloric requirements regardless of whether or not the astronaut experiences discomfort. At an ambient temperature of 10° C, approximately 10 per cent more calories are required than at

30° C. Incidentally, 30°C (86°F) ambient is considered thermal neutrality for the human at 50 to 60 per cent relative humidity.

The average man utilizes 1.2 kg cal/min while asleep and as much as 15.0 cal/min while working. The effects of other environmental factors are more difficult to anticipate. An example is the effect of a full pressure suit on energy expenditure. The metabolic rate and O<sub>2</sub> consumption under moderate exercise in a full pressure unit is increased one-third over the same conditions in a summer flight suit.

Two sources of calories are proteins and carbohydrates, each of which yield about 4 cal/g, and fats, which contain 8 or 9 cal/g. The basic protein requirement for man has been established at 65 g a day, with the remaining caloric requirement provided by 5 parts carbohydrates to 1 part fat. It is doubtful if much will be gained by altering these proportions. The dry weight of a diet of this composition is approximately one-half lb per 1000 cal. The increment of weight in itself does not appear disqualifying. The water requirement, however, is defined on the basis of 1 g of water per cal; therefore, an increase of 1000 cal increases the water requirement by 1 kg or 2.2 lb. The oxygen required is approximately 200 liters or 0.63 lb per 1000 cal. It is apparent, depending upon a detailed task analysis, that the weight of consumable material, exclusive of food supplements, utility water, and CO<sub>2</sub> absorbents may range from 8 to 16 lb per man-day.

### 36.13 Radiation Protection

Radiation protection is another area in which significant compromises between biological requirements and engineering feasibility may be necessary to achieve long duration missions. If compromises cannot be made, manned missions may well be limited to lunar or cislunar areas. Complete protection from the radiation environment in space introduces the need for prohibitive shield weights which could limit the exploitation of manned missions. Although it is a structural design problem, radiation shielding is an integral part of the life support system, and its weight must be charged against the cost of putting man into space.

Laymen tend to minimize the calculated risk of manned excursions in the radiation environment of space. The existence of chemical compounds to increase radioresistance; the general agreement that because of the astronaut's age and minimal impact on the breeding population, genetic effects are not important; and the astronaut's short orbital career, all lend credence to the concept that exploitation of space environments with manned vehicles will not be limited by space radiation. While such considerations are pertinent to space travel, their adoption as a basis for setting maximum permissible doses of external ionizing radiation may be fundamentally incompatible with the execution of the analytical tasks which justify man in space.

The maximum permissible dose (MPD) must be a compromise between the dose which will permit the astronaut to accomplish his mission, weighed against the statistical probability of radiation-induced debilitating diseases, expressing themselves after a latent period of 10 to 25 yr. It cannot be overemphasized that radiation in space is a problem yet to be resolved in terms of its effect on biological systems. The biological responses to ionizing radiation are statistical in nature and are related to the kind and quality of the radiation, the rate and geometry at which the ionization is delivered, the particular tissues or even species used to measure response, and the age of the individual. These variables are further complicated in space by the presence of mixed radiation sources and energies which produce both additive and synergic responses.

The radiation received by the occupant of a space vehicle using non-nuclear propellants will result principally from the impingement or penetration of charged particles through the skin of the vehicle, and from various secondary radiations (primarily electromagnetic) resulting from charged primary particles interacting with the vehicle and cargo. The immediate source of space radiation appears to be cosmic rays whose origins are not known. Cosmic rays interacting within the Earth's geomagnetic field and atmosphere in a manner also not completely known, probably give rise indirectly to the charged particles concentrated in the Van Allen radiation belts.

A foreseeable emergency, not sufficiently predictable, is the high level of radiation associated with solar flare activity. The quiescent cosmic ray dose, about 0.1 mr per day in the near solar system, probably does not present an excessive hazard, especially in flights of a few weeks' duration. Solar flares will periodically present a very serious situation. About once ever 5 years, giant solar flare activity is characterized by an associated sharp increase in cosmic ray intensity. The peak level, reached within minutes after onset of activity, would be lethal to an astronaut after a very brief exposure. The total integrated dose during the giant flare of 1956 was about 600,000 rad over an 18-hr period. A dose of 500 rad is 50 per cent lethal in 30 days. There is no doubt that such a situation presents a serious problem in terms of survival of the crew. To honor the arbitrary maximum permissible dose of 25 to 50 rem, the shielding required for this extreme condition is about 180 cm of carbon, which reduces the proton dose to about 10 rad plus about 30 rad from neutrons produced in the shield. The use of an equivalent amount of lead would lead to a slightly higher dose due to higher neutron production. The radiation may be isotropic rather than radially directed from the Sun, and, therefore, shadow shielding may not be of any great value. The weight penalty for shielding under these conditions is obviously prohibitive.

About once a month, a small flare occurs which results in a total dose of about 60 r inside a 1 gm/cm<sup>2</sup> wall. The shielding problem for



these common flares is minimal. Other flares in which the total dose has been between these two extremes have been detected by some of the space probes. The frequency spectrum of flares of different intensity is not known. The shielding and protective measures required for optimization of the system will be determined by this spectrum. At one extreme, minimum shielding is needed; at the other extreme, the flights may need to be aborted. At some level of radiation intensity, the continuance of the mission may become impractical. The information upon which these decisions may be based is rapidly changing with additional data from space probes. Shielding, combined with a warning system and emergency procedures, is essential to sophisticated space operations.

Present analyses suggest that an alclad and water shield equivalent to  $20 \text{ g/cm}^2$  of absorber is a realistic protection which can be achieved on early space missions and, backed by the possibility of an abort of Earth orbital missions, makes early space operations feasible. With nuclear propellants, the problem is intensified to varying degrees, depending upon the degree of shielding achieved. It is not necessary to dwell longer on the sources of ionizing radiation in space. The problems are to define the amount of external radiation an astronaut can absorb and still accomplish his mission, then to engineer space cabins to prevent overexposures. Since it is unlikely that man's resistance to radiation can be appreciably increased, the solution to the biological problems associated with ionizing radiation in space must be approached by:

1. Characterizing the radiation environment.
2. Selection of operational procedures to avoid known radiation areas.
3. Designing vehicles with maximum shielding characteristics.
4. Development of dosimetric procedures.
5. Development of prophylactic procedures for crews in case of overexposure.
6. Consideration of procedures which will allow recovery of vehicle in case of crew mortality or incapacitation.

#### 36.14 Environmental Control Systems

Man's occupancy of space by space vehicles, orbital stations, or planetary bases will be accomplished more by engineering advances than by fundamental changes in requirements for life support devices. Further, there is no purpose to send man into space except in an environment which will permit full expression of his intellectual curiosity. If it is truly possible to engineer a simulated terrestrial environment which provides for the recognized needs of man, the space cabins of the future will be considerably more complex than anticipated by present day configurations.

It may be more profitable to view those concepts relating to the

design of future life support systems than to review the accomplishment of existing programs which, while marginally adequate, are more properly considered as extensions of systems used in high-performance aircraft than as systems designed specifically to place man in space. At present there are three categories of life support systems based upon the way vital materials are supplied and used.

The open-cycle system provides for all consumable supplies to be either carried with the vehicle or resupplied through logistic support missions. The byproducts are stored and eventually jettisoned with no attempt at reclamation. Its principle disadvantage is the added weight attendant to increasing crew size or lengthening mission duration. For example, assuming a nominal weight of 10 lb per man per day for consumable supplies, a five-man crew requires 1500 lb of material for a 30-day mission; 9000 lb is required for a 6-month mission, and 18,250 lb is needed for a mission of 1 year. While this indicates dramatically the need of a better solution, it should be noted that more powerful propulsion systems will extend the possible utilization of this system.

The semi-closed cycle system reclaims certain of the waste products and produces a reuseable product. For example, water can presently be recovered by distillation processes with approximately 85 to 95 per cent efficiency. Oxygen, while experimentally susceptible to reclamation from CO<sub>2</sub>, is presently supplied as an open system because the recovery process is both cumbersome and unreliable with unfriendly byproducts. Production of food onboard is also impractical at the present state of the art. The semi-closed system has the advantage of saving weight by reducing the amount of stored supplies required for a mission and, as disadvantages, the reliance upon mechanical devices for production of vital materials and the associated increased power requirements.

The closed-cycle system, as the name implies, recycles all vital materials and has the obvious advantage of extended stay times in space with minimal requirements for logistic support. The disadvantages are extreme complexity, high-power consumption, and reduced reliability. Consideration of a closed system is highly dependent upon the ability of man to survive extended time in space -- a question which is foremost in bioastronautical research. In a sense, the term closed-cycle is a misnomer, since there can never be a complete regeneration of vital materials; however, this does not make it a less desirable goal. Familiarity with the basic biological cycles on Earth has led many people into the pitfall of considering these natural cycles as efficient systems from which to develop an engineering model. These models have come to be known as closed ecological systems. While the approach can be endorsed in concept, the overzealous must be cautioned. The biological cycles of which we are aware are efficient only in terms of geological time. The rate at which a particular molecule of an element moves through the environment is characteristically very slow. Increasing the efficiency

or rate of recycling is, in essence, the underlying goal in agricultural research and, similarly, the goal of research which utilizes biological systems to regulate space cabin environments.

In a practical sense, this emphasizes that the successful closed-cycle or regenerative life support system of the future will probably utilize the better parts of both physical and biological systems. In spite of this, it is interesting to note that the problems of life support involving regeneration of atmospheric gases, production of nutrients, and stabilization and utilization of human waste comes closest to realization in a single system through the use of photosynthetic organisms. Research over the last 15 years on the mass culture of algae to produce food, enrich inorganic soils, and stabilize sewage has reached the pilot plant stage and has demonstrated the feasibility of its consideration for the closed-cycle ecology of space habitations. It is unfortunate that the present rate of research in the mass culture of algae for terrestrial use has been hampered by the need of demonstrating economic advantages over other terrestrial systems. Within the present state of the art lies the potential to develop efficient and economically competitive photosynthetic systems for use in space environments. Given proportional research support, the concept of space gardens can have as great a probability of occurrence as a necessary adjunct to the conquest of space as many anticipated developments in propulsion, power, materials, and guidance upon which the intelligent use of space must rest.

In all cases, it must be assumed that human survival, performance, and consequently the mission execution will take precedence in designing life support systems and planning space operations. The keynote will therefore be reliability. Regenerative systems, as desirable as they may appear in terms of reduced weight, can only be considered to the degree that the reduction in reliability is acceptable.

Concluding this discussion, it becomes obvious that the influence of man's requirements on the design of spacecraft is as important, if not more so, than the influence of our knowledge in materials, propulsion systems, celestial mechanics, and often technical or scientific fields. The level of knowledge in life sciences is still low compared to the material sciences, and a much greater effort will have to be expended before really efficient spacecraft can be designed and before occupancy of extraterrestrial bodies can be established.

37

EXPERIMENTAL BIOLOGY IN SPACE

Richard S. Young

Ames Research Center  
National Aeronautics and Space Administration  
Moffett Field, California

37.1 The Potential of Space Biology

The recent accessibility of space to scientific exploration has opened the way for the development of new tools for the study of fundamental biology. By far the most important of these is one which permits the detection and study of extraterrestrial life and sheds light on the origin and evolution of life on Earth and elsewhere in the universe. Positive knowledge of the existence of extraterrestrial life awaits the development of vehicles large enough to land significant payloads on such worlds as the Moon, Mars, and Venus. Meanwhile, much can be learned from Earth and from space in the vicinity of Earth that will improve our knowledge of the physical and environmental characteristics of other worlds. This in turn will greatly aid in the design of extraterrestrial life-detection devices and determine to a large extent the direction of future studies.

There are physical parameters of space and space flight that cannot be duplicated satisfactorily in the laboratory, e.g. zero-gravity and cosmic radiations. There are also the multiple factors that provide the physical environment on Earth in which life has evolved. Space flight provides a means of removing living systems from this total environment (gravity, magnetic fields, radiations of various wavelengths) and studying the effects, both long and short-term, of the absence of this environment on fundamental biological processes.

It should be noted that none of this is necessarily directed in support of a man-in-space program, but rather makes use of various aspects of space as a fundamental research tool. Within such a program, man in space will ultimately become an investigator. Although this type of research is not directed in support of a man-in-space effort, it will inevitably have an impact on such an effort in the same way that any basic research program has potentials for various applications.

As with any new biological research tool, it is often difficult to predict effects on theoretical grounds; but the fact that one expects

no a priori effect is a poor reason not to investigate. For years, biologists have been studying the effects of gravitational fields on biological systems, in some cases with interesting results. For example, the response of plants to gravity is well known. Animals respond in various ways to even small gravitational increases, particularly to long-term exposures. Animals and plants also respond developmentally to increased gravity. In view of these demonstrated effects, it becomes important to use the absence of gravity (such as exists in spacecraft) as a research tool in order to learn more about the mechanisms involved in such phenomena as geotropisms, cell division, metabolism, and differentiation. The response of an organism to its total environment, both short-term and long-term, is another area of great interest to the biologist; that is, the role of the Earth's environment in determining rhythmic behavior exhibited in both the plant and animal kingdoms. These biological clocks may yield to analysis by removing the influencing environment, either totally or partially, by the use of space vehicles.

The biologist may also be prepared for completely unexpected effects caused by the interplay of new parameters (subgravity, radiations, and magnetic fields, for example) introduced in space. Study of these effects, if found, may yield information of value to cellular biology, physiology, genetics, and ecology in particular; but general benefits will be realized by all fields of biology.

### 37.2 Suborbital Experiments in Space Biology

Attempts to utilize space vehicles for experimental biology have, to date, been largely unsuccessful from a strictly scientific point of view. This is mainly due to improper vehicle performance, which is probably to be expected while using experimental vehicle systems. However, much has been learned concerning vehicle performance, packaging of experiments, control experimentation requirements, launch and recovery operations, as well as experimental design and interpretation of results.

In general, it must be said that the present generation of space vehicles is not suited to biological research, and most early experiments were placed in vehicles on a noninterference basis. This, of course, greatly reduced the value of such experiments, since the experimental conditions were far from being controlled as they would ordinarily be in the laboratory. Also biological material requires recovery for a satisfactory experiment, which greatly limits the number of vehicles usable for such work. Early experiments were required to be prepared and placed in the vehicle as much as 12 hr before the vehicle was launched. Recovery at sea made it difficult to return material to scientists quickly, and periods of several days often elapsed. There was no temperature control or monitoring. These and other problems made it very difficult for the biologist to design a satisfactory experiment; however, attempts were made. For example, a recoverable Jupiter nose cone flown in 1958 by the

Army Ballistic Missile Agency contained an experiment designed to study the effects of zero-gravity on the ability of a sperm to fertilize an egg.

One of the most fundamental phenomena exhibited by living systems is cell division. This phenomenon is easily observed and can be initiated at will by fertilizing an egg (in this case the sea urchin egg). Once an egg has been fertilized, it proceeds to divide in an orderly and predictable fashion. Although there is no a priori reason to expect the absence of gravity to have an effect on the process of cell division, it is a very important and fundamental question to ask. The Jupiter nosecone achieved an apogee of some 350 miles and offered 3 to 4 min of weightlessness. The first attempt was an experiment in which sperm were released (by a gravity-triggered device) into the egg suspension just prior to the onset of the zero-gravity phase of the flight. A fixative was released into the chamber at the end of the zero-gravity phase to kill all cells and preserve them for histological study on recovery. This first version could determine only the question of the ability of a sperm to fertilize an egg, since the fertilization reaction requires only 1 to 2 min. The first cell division occurs 30 to 90 minutes after fertilization, depending on the egg used and the temperature.

The first experiment failed due to material toxicity in the experimental chamber, and it was repeated in improved form a few months later. In this case the sperms were injected into the egg solution by an electrically-triggered device so that some eggs were fertilized on the launch pad at such time that the first cell division would occur during the zero-gravity phase on the flight. Other chambers were triggered during the flight as before. This nosecone also carried other cellular materials arranged to detect radiation damage during flight, including Neurospora spores, yeast cells, human blood, tissue culture, barley seeds, onions, and mustard seeds. Unfortunately, this vehicle was destroyed shortly after launch.

Since these early attempts, the NASA Life Science Laboratory has developed a continuing program using sounding rockets and later orbital vehicles to pursue this type of work. The vehicles are being modified specifically for the needs of the biological experiments. This is still not the optimum arrangement, since the modification of existing nosecones does not solve all the problems involved in flying these experiments. A special class of vehicles will be designed from the beginning with the biologist in mind, so that the experiment will be the primary consideration in all respects.

In November 1961, BIOS 1 and 2 were launched in attempts to place small payloads of biological and physical experiments into the lower Van Allen belt. The experiments were designed to give about 25 min of radiation exposure and simultaneously a similar period of subgravity. The

Argo D-8 carrier vehicle was originally designed and used successfully to lift nuclear emulsion packs (that were extended outside the vehicle behind a known amount of tungsten shielding, at the apex of the trajectory). The first payload (called NERV 1) also carried a small sample of Neurospora spores that were recovered and returned for analysis. The biological results were provocative but inconclusive. It was then decided to use this vehicle primarily for biological experimentation, while keeping the original nuclear emulsion experiment as a monitor for the biological material. An extensive series of control experiments were run, testing the effects of vehicle vibrations and accelerations on the experiments. As many of the flight parameters as possible were duplicated on the ground to make in-flight data more interpretable. The countdown was compressed wherever possible to install experiments as closely as possible to launch time. (Many experiments were installed 12 hr before launch.) Mobile laboratories were constructed for use at the launch site (The Pacific Missile Range, Point Arguello) for handling experimental material and conducting control experiments during the flight. Since recovery was to be at sea, a team of scientists with a mobile laboratory was installed aboard the recovery ship. This group also conducted control experimentation and was prepared to handle the material for preliminary analysis immediately after recovery. The object was to reduce to a minimum the time needed to place the experiments in the hands of the investigators and to perform as much valid control experimentation as possible to ensure meaningful experiments. It is obvious that in experimentation of this nature the biological scientist is operating under most abnormal conditions, and great care must be taken to control a number of experimental variables that would not occur in the laboratory.

Special capsules and experiments were designed and constructed at the Ames Research Center, Moffett Field, California, with careful toxicity tests being conducted on the materials used. A surprising number of materials (plastics, stainless steels, and rubbers) suitable as containers for these experiments from an engineering viewpoint actually proved quite toxic from a biological viewpoint. This knowledge made it necessary to compile a list of new materials. Temperature variations were not expected in this flight; thus temperature control was not an in-flight problem. All containers were pressure-tested and laboratory-tested before use.

Because the Bios 1 and 2 payloads would enter the Van Allen radiation belt and experience subgravity, there were opportunities to perform biological experiments in two categories. The low anticipated radiation level (around 1 r) required extremely sensitive biological systems. One of the reasons for performing radiation experiments in such low doses was to see if physical monitoring in space would yield sufficient information to predict genetic or cellular damage or whether there is a synergistic relationship between these radiations and the other parameters of such a flight. Also considered was the fact that radiations at these

altitudes are not well known. The Atomic Energy Commission's Oak Ridge National Laboratory was asked to provide such experiments, as were scientists in universities and industry, the Environmental Biology Laboratory, and the NASA Ames Research Laboratory. In addition to the nuclear emulsion experiment carried in the tungsten shield, the biological containers not in the shielded area were also wrapped with nuclear emulsion films to obtain a record of radiations seen by each experiment. Since the payloads were to pass through a micrometeorite shower, a micrometeorite experiment was also included.

The biological payloads were composed of the following experiments:

1. Neurospora

a. Neurospora forward mutation. This was essentially a repeat of the NERV 1 experiment, and it consisted of a sample of spores of the mold Neurospora, which would be analyzed for mutations in genes controlling biosynthetic steps in intermediate metabolism, survival of the population, and possible physiological injury.

b. Neurospora back mutation. This experiment measured mutation from a nutritionally dependent condition to an independent (wild) condition.

c. Neurospora balanced lethal. This experiment involved exposure of heterokaryon conidia with two nuclei, each of which may be recognized alone by means of a marker gene. Thus, a lethal mutation of any gene in the same nuclei results in total elimination of that marker genotype and can be identified.

2. Survival and mutation in Neurospora conidia. This experiment involved measurement of the frequency of recessive lethal mutations in a balanced heterokaryon between two biochemical mutants. The determination of the comparative levels of survival in microconidial strains, as well as the estimation of forward mutation rates, were also studied.

3. Determination of viability of a radiation-sensitive bacterium. The bacterium Escherichia Coli was to be studied for survival and mutation on recovery.

4. Natural radiation effects on human chromosomes. Human leukocytes (in whole blood and leukocyte culture) were flown, to be later examined cytologically for chromosome aberrations.

5. Influence of the space environment on chromosomes of grasshopper embryo neuroblasts. This experiment was designed to determine whether the radiations encountered were sufficient to produce chromosome breaks.

6. Radiation effects on a genetically stable material (barley seeds). This was a back mutation study in the descendants of seeds maximally hit.

7. Effects of subgravity and rapid position change on plasmotomy in Pelomyxa Carolinensis. This amoeba is relatively insensitive to radiation. It divides by plasmotomy and during cell division, all the nuclei (100 and more per animal) divide simultaneously. The nature of this synchronization is unknown. This experiment was designed to study the effects of weightlessness and rapid position change with respect to the



Earth's surface on the growth rate and the synchronous nuclear division.

8. Production of microspheres during a subgravity condition. Application of multiple gravity forces in the centrifuge indicates that gravity influences production of biochemical units that are otherwise highly uniform in size. This experiment was designed to determine the effect of subgravity on the formation of these microspheres.

9. Sea urchin egg experiment. This experiment was essentially the same as those described above.

Except for the last two, all experiments were passive in that there were no power requirements or triggering devices. The entire Bios biological payload is illustrated in Fig. 37.1, showing the capsules and devices used. The power for pulsing the sea urchin experiment was provided by the vehicle power supply, while the power for the microsphere experiment was supplied by internal batteries. The entire biological payload weighed less than 3 lb. As there was no temperature control in the recovery vehicle, a temperature recorder was developed at the Ames Research Center. Two of these recorders were flown to record internal temperatures during flight, permitting a more accurate control of experimentation.

These devices (shown in Fig. 37.1) were accurate to  $\pm 0.2^\circ\text{C}$  and recorded on a smoked drum controlled by a clock mechanism. Figure 37.2 shows a part of the interior of the microsphere experiment. This experiment was activated by a gravity-sensitive switch during booster firing. A capsule containing an amino acid polymer in water was to be heated to  $100^\circ\text{C}$  during powered flight. The heat was then to be cut off and the capsules allowed to cool during the weightless phase of the flight, at which time the microspheres would form. These were to be studied on recovery for morphological effects due to subgravity. Figure 37.3 shows the sea urchin triggering device, an eight-chamber configuration completely assembled before loading biological material.

The sperm, eggs, and fixative were all loaded by syringe just prior to inserting the experiment into the recovery vehicle. The first electrical pulse burned out a light fuse wire, releasing the spring-loaded plungers to the first locking notch and injecting the sperm into the egg chamber. The second electrical pulse burned out a second fuse wire, releasing the plungers the remaining distance and injecting the fixative into the egg chambers. The timing of these electrical pulses was programmed through the vehicle timer to coincide with the onset and end of the zero-gravity phase of the flight. Some chambers were also pulsed prior to launch so that first cleavage of the eggs would coincide with the weightless stage of flight. Figure 37.4 shows the disassembled triggering device, and Fig. 37.5 illustrates the loading technique with syringe injection through rubber plugs. Two of these devices, with a total of 16 chambers, were flown. This arrangement provided a combination of experiments, some fixed and some not fixed, which could be flown in

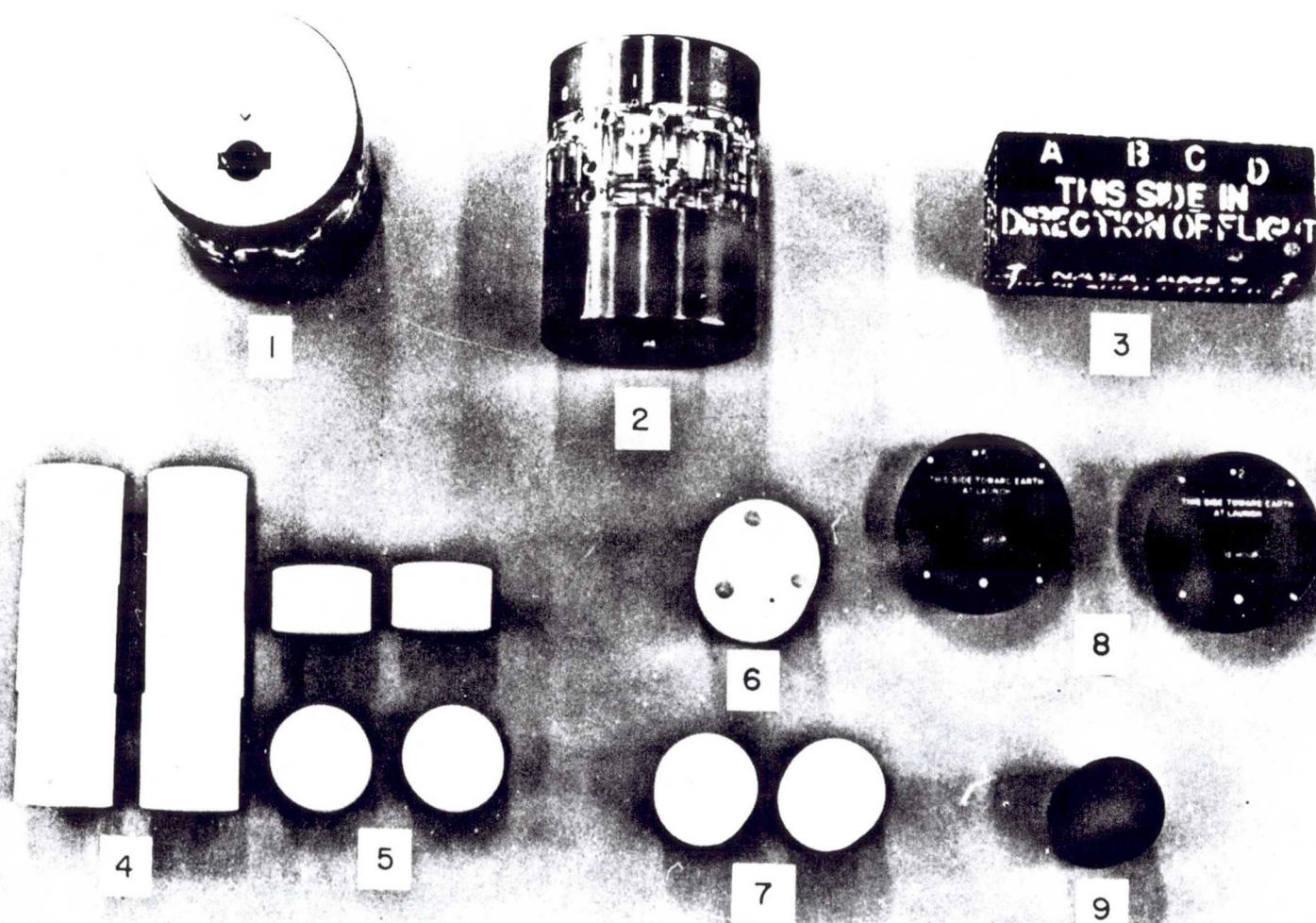


Fig. 37.1 Biological payload for space experiment: (1) sea urchin triggering device; (2) sea urchin triggering device (side view); (3) microsphere package containing batteries, switches, and experimental chamber; (4) nylon capsules for *Neurospora* experiments; (5) nylon capsules for *Neurospora* control experiments in tungsten shield; (6) nylon capsule with six compartments for *Neurospora*, blood, grasshopper embryos, aspergilla, an *E. Coli*; (7) nylon capsules for amoeba experiment; (8) temperature recorders; and (9) black nylon capsule for barley seed.

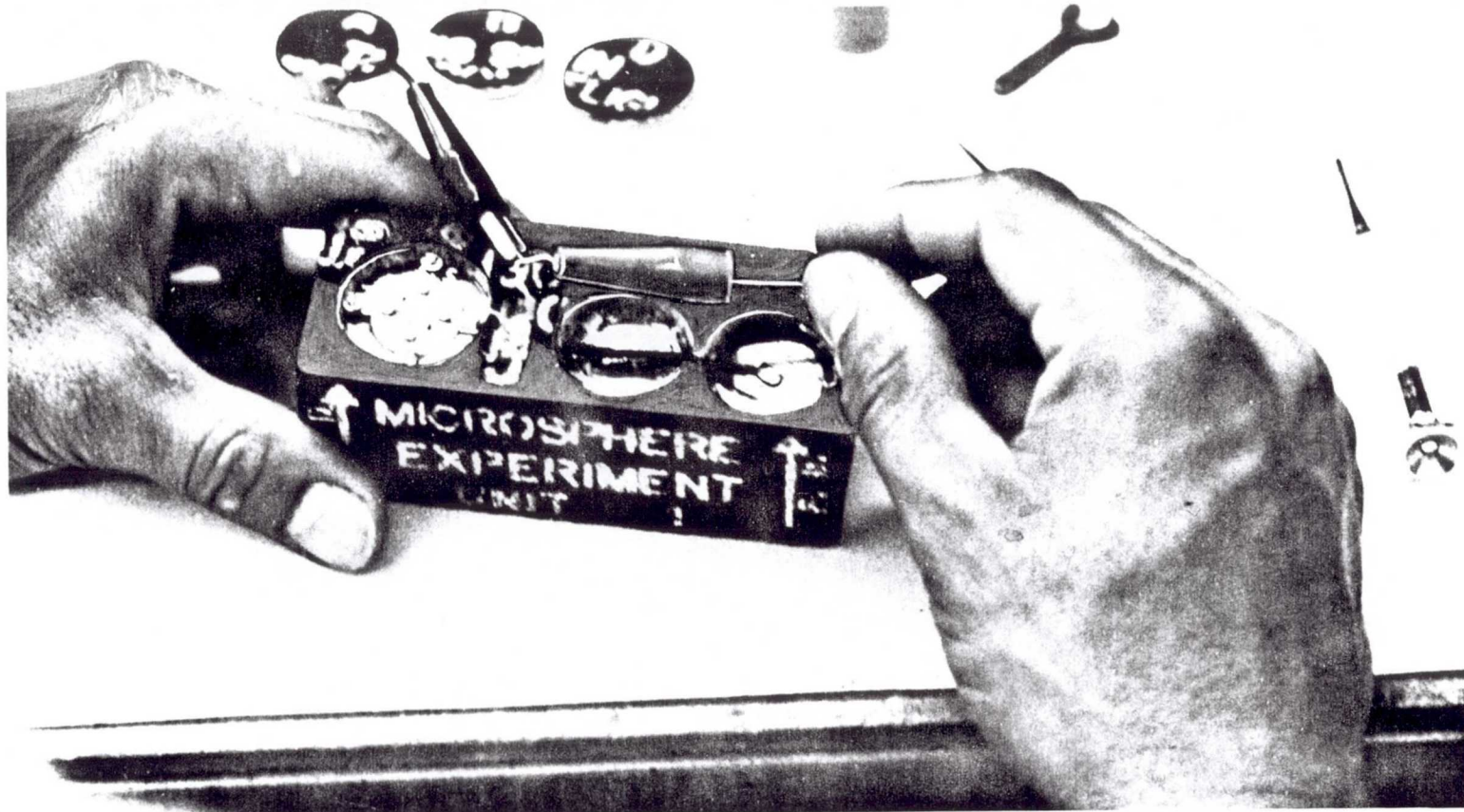


Fig. 37.2 Microsphere experiment showing, left to right, experimental chamber, groove, containing resistor and activating G switch, and two rows of battery packs; temperature calibration apparatus in background.

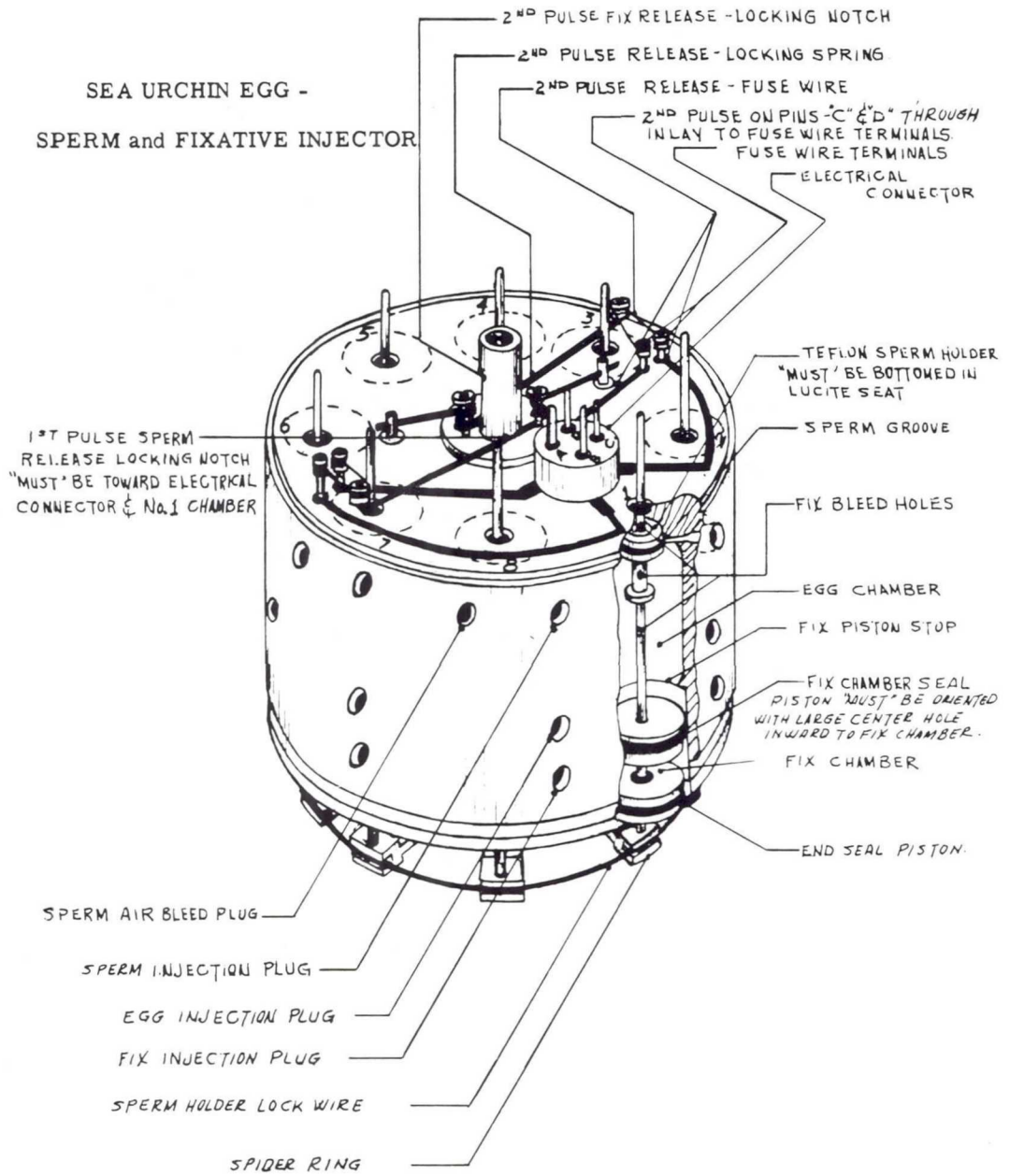


Fig. 37.3 Eight-chamber device used in sea urchin egg experiment.

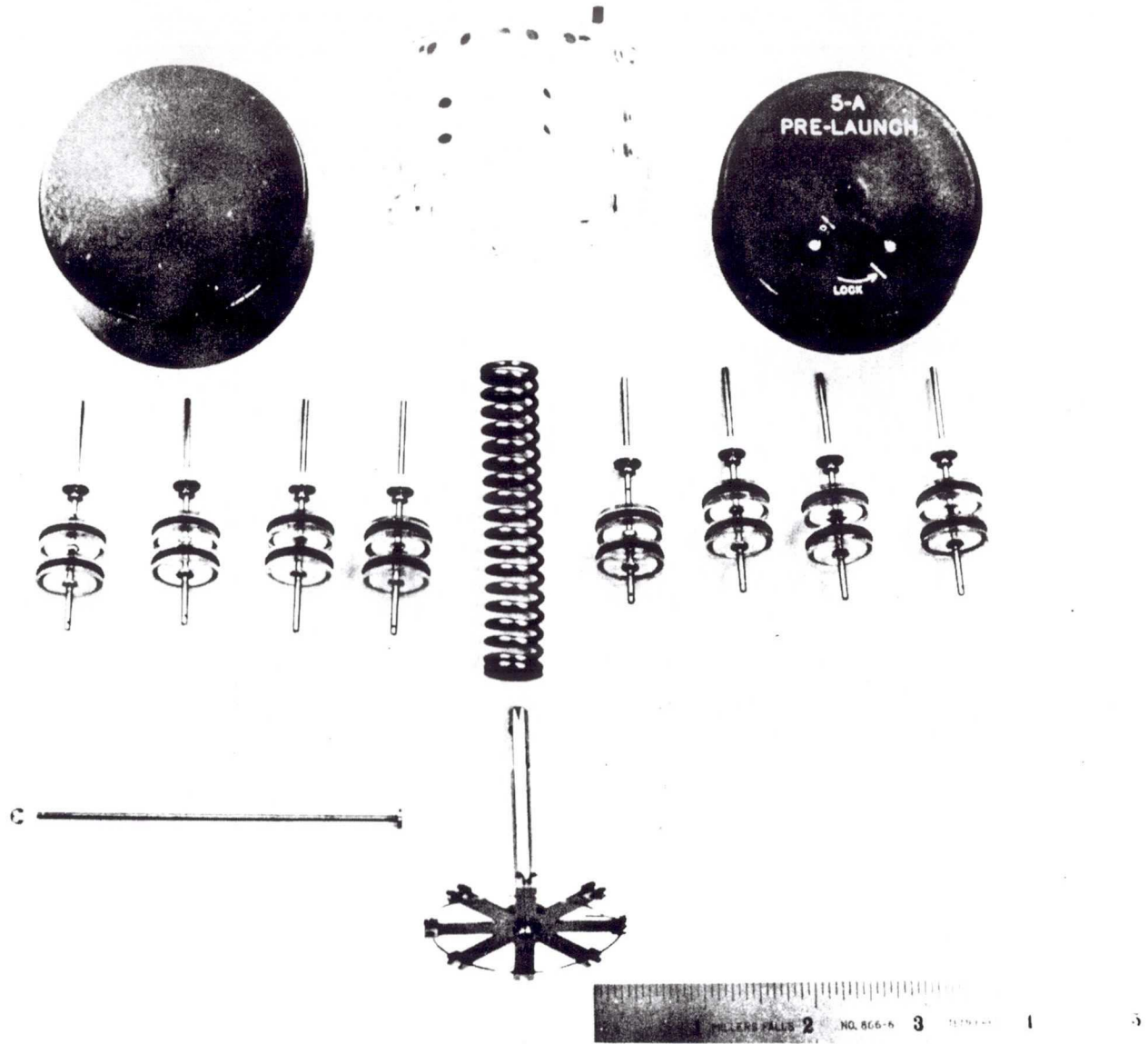


Fig. 37.4 Sea urchin triggering device disassembled.

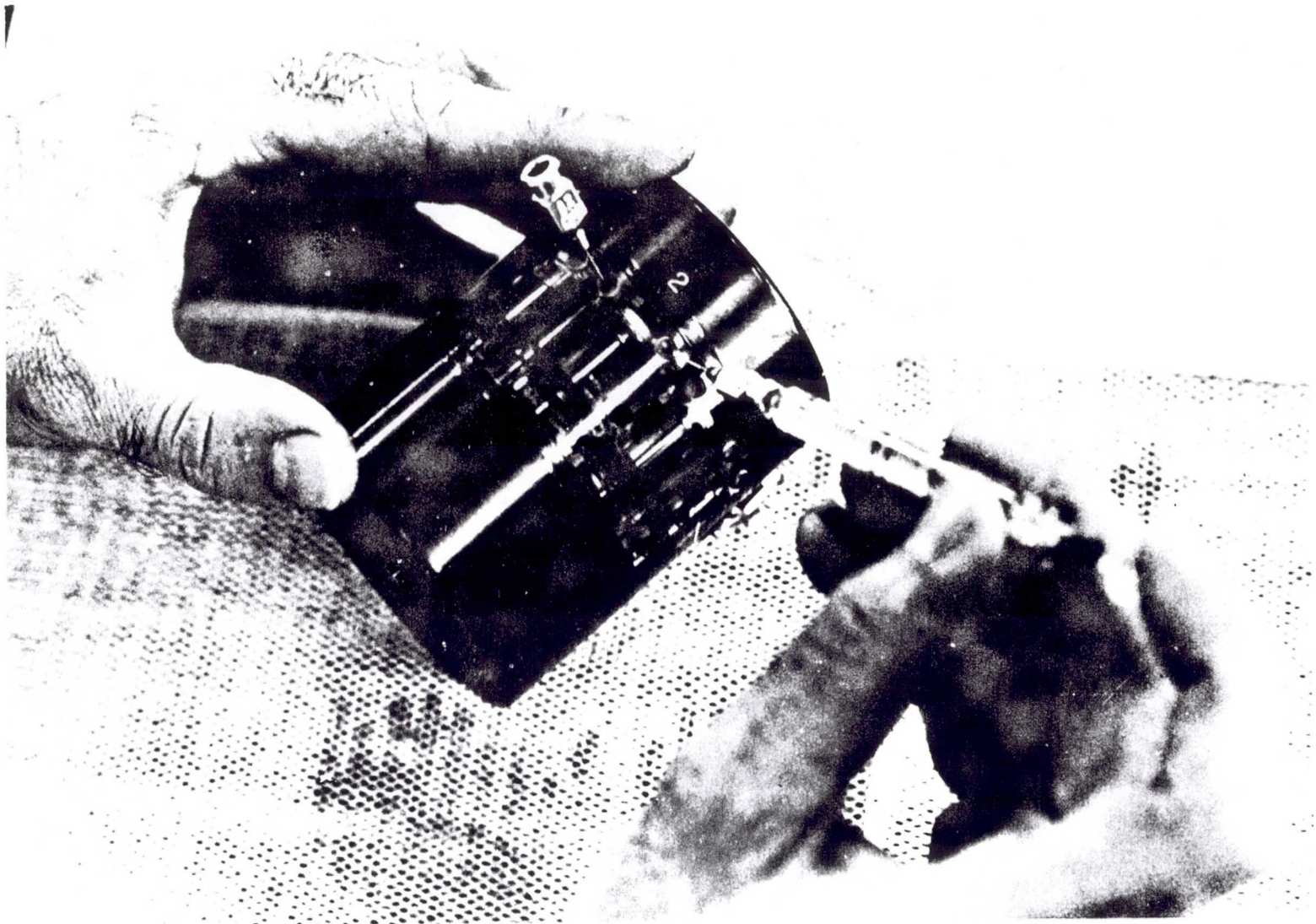


Fig. 37.5 Loading a sea urchin triggering device with a syringe.

duplicate and triggered at different times. Unfortunately, attempts to launch and recover these payloads failed. In spite of these failures, a great deal was accomplished by the experimental efforts.

### 37.3 Requirements for Future Space Biological Experiments

Instrumentation with capabilities for use in spacecraft are evolving rapidly; biological personnel now have experience in this type of work; the difficulties inherent in this method of experimentation are being learned and overcome; and problem areas for the biologist are becoming more clearly defined in terms of the space program. Obviously a class of vehicles is required that meet the specific needs of biological investigation. Biological experimentation requirements are unique, but if they are considered early in the development of a vehicle, these requirements can be met. They include:

1. Accessibility of payload for the insertion of experiments at the last possible moment before launch.
2. Sufficient vehicle guidance to make recovery a more rapid and reliable process to return experiments to the scientist as quickly as possible.
3. Sufficient temperature control at launch sites and in flight to protect the experimental material.
4. Trajectories and orbits programmed and tracked with reliability to determine the environments actually encountered.
5. Adequate despin mechanisms to provide zero gravity or near zero gravity for known periods of time.
6. Recovery vehicles and carriers with both ballistic and orbital capabilities so that constant redesign will not be necessary.
7. Capability for providing an accurate record of vehicle environment before, during, and after flights.
8. A central facility from which biological scientists can prepare their experiments close to the launch site (either mobile or fixed). This feature will also simplify communication between scientists at the launch and recovery sites and maintain adequate monitoring of the countdown of carrier vehicle preparation for control experimentation.

The sooner biological investigations in space can be put on a firm scientific basis, the sooner we can make adequate use of this new tool. Biology is probably the most difficult of the scientific disciplines to introduce into the space environment, particularly from an engineering point of view; but it may become one of the most valuable.

## 38

## A POSSIBLE APPROACH TO SCIENTIFIC EXPLORATION OF THE PLANET MARS

E. A. Steinhoff

The Rand Corporation,  
Santa Monica, California

The commitment to manned lunar exploration by both the United States and the Soviet Union during the current decade prepares the foundation for the scientific exploration of the terrestrial planets, long a desire of that part of the scientific community interested in the planetary sciences and cosmology. Next to the Moon in importance for providing us with physical data and environmental details is the planet Mars. It is therefore no wonder that Mars is considered by many to be the next target after the Moon for manned scientific exploration. Also, it is a well-known fact that minimum-energy transfer orbits to Mars (including landing) require only a little more propulsive energy than lunar-landing missions if aerodynamic entry is used.

This paper deals with some possible objectives of a Mars expedition, operational approaches that promise early feasibility, and their technological foundation. It does not deal with specific solutions optimized for minimum objectives but with ways to obtain a foothold for a scientific team to achieve increasing self-sufficiency in the later phases of the establishment of a Mars base. The published details of the considered approaches to manned lunar exploration can set the pattern for the exploration of Mars; and much of the equipment, technique, and experience resulting from lunar exploration will be directly applicable to Mars. Of the many proposed technological steps to be taken and solutions to be considered, some will have the advantage of early availability and proximity to the existing state of technology, reducing the technological risks involved and insuring a reasonable chance of success. Mission size will determine the level of support required and may become a major factor in the eventual success of this historic undertaking.

### 38.1 Objectives of Planetary System Exploration and Its Possible Rewards

A successful manned expedition to the Moon and back would require a pooling of technological resources, knowledge, and human ingenuity never



before achieved for one single and peaceful objective. The human effort and national resources required would be exceeded only by those applied in the major wars of the last half-century. The fact that this effort will widen the human horizon, reveal more about the evolution of life on Earth and the history of the solar and the galactic systems, and tap the natural resources of the nearby planets is a truly worthy cause and may affect the future of the human race much more than any other single event in the past.

Many will ask the question: Is this plane worth the effort and are the needed resources not better applied to relieve the human misery around us? This question is not typical among Americans only; Russian planners of space missions face the same question, find themselves confronted with literally the same newspaper editorials as their American colleagues, and have to ask themselves whether to apply their efforts and national resources to widening knowledge in this particular discipline or relieving human misery as much as possible. One Russian newspaper published a letter under the heading, "Is it not too early to flirt with the Moon?", referring to the many unresolved social problems within the Soviet Union. One justification there, as here, is that answers to scientific questions, and knowledge not directly obtainable on Earth, may provide solutions (unobtainable otherwise) to problems on Earth. Here, as there, one of the answers is that money spent to achieve these national objectives is not spent on the Moon or Mars but right here on Earth, providing jobs, knowledge directly applicable to our society, and improved living conditions. The greater the scientific challenge to the human mind, the more of our best thinkers and engineers will devote their lives to the solution of the associated problems, which in turn will yield benefits unimaginable without this apparent detour. History is full of examples to prove the case.

Potential rewards are better understanding of physical laws; the merits and penalties of life under very adverse conditions; development of closed ecological systems to overcome detrimental effects of environment (on Earth we have many areas which are presently excluded from settlement because of their unsuitability for supporting life, but population pressures could force man to live there and produce food in the not too distant future); utilization of natural resources of the nearby planets and possibly access to elements not available in quantity on Earth; solutions to problems of human relations in closed ecological systems; and many others of equal importance.

### 38.2 The State and Avenues of Technology to Accomplish An Early Mars Exploration

Since the plans for the manned lunar missions will be based on approaches close to existing technology, early exploratory Mars missions will greatly benefit from the experience gained in developing the manned

lunar landing and return capability and experiences gathered during this process. Present indications are that to achieve the first U.S. manned landing, technologies will be used that are based on chemical propulsion rather than electrical or nuclear primary propulsion, which appear to have performed advantages but are less advanced as to successful and demonstrated operational availability and reliability. It also can be proven that just to build a larger chemically propelled space system with the associated increase in payload efficiency can provide a solution almost as good but involves fewer risks as far as departure from existing technology is concerned. This should not be interpreted to mean that more advanced technologies should be neglected. However, the best solution is one which secures earliest success and based on accumulated working knowledge promises to be the most reliable approach to achieve this goal. The parallel developments of the direct ascent and of the space rendezvous appear at this time to be not only separately as mutual back-ups to this goal, based on moderate departure from existing technology, but jointly to provide the necessary capability of the manned Mars expedition.

Many disciplines of scientific endeavor beyond the mere process of space transportation have to contribute to make this enterprise an early success and not a few of these lack the proving grounds to test and demonstrate the capability and performance of their contributions. These proving grounds are space environment and the natural satellites and planets themselves. Delay of development of these associated areas will delay achievement of the primary goals if the required technological advancement becomes the controlling factor. From these aspects, the development of both the large-capacity chemical boosters and the rendezvous techniques in parallel is a sound national goal. Simultaneously, other early technical solutions emerge which will identify the pattern of early space exploration. This is the area I should like to give special attention, since it will also pattern the most promising modes of early interplanetary operations.

While nuclear primary power may or may not be used in the first lunar flights, auxiliary or secondary nuclear powerplants will certainly be the sources of electric power for lunar bases. A supplement will be the hydrogen-oxygen fuel cell (to be used as a flight-vehicle power source), a mobile surface-vehicle power source, an interim power source before completion of nuclear reactor installation, and as a standby power source in case of reactor maintenance. A close competitor will be hydrogen-oxygen expansion turbines or perhaps a combination of fuel cells and hydrogen expansion turbines.

During low-duty cycles, nuclear reactor powerplants will regenerate the fuel-cell fuels so that these can be used over and over again. One of the objectives of the first lunar base will be to find means to achieve as high a degree of self-sufficiency as possible under local circumstances at an early date. The selection of cryogenic oxygen and hydrogen as propellants goes far towards this goal. Finding local propellant sources

will be a big step toward a self-supporting operation. High cost of transportation is not the only reason, particularly since there is evidence that new developments in chemical fuel utilization may eventually bring considerable reductions in operating cost, and when reuse of so far nonrecoverable elements of space boost systems is achieved.

One local fuel source may be the water of crystallization in crystalline rocks (found in many such rocks on Earth, and to be expected with a high degree of probability on the Moon and the terrestrial planets). This is very important, since, as we know, both the Moon and Mars are devoid of bodies of water. However, there is the possibility of underground ice deposits (like those found in arid areas of New Mexico) which could be utilized if they could be located. To find these will require surface mobility and the possibility of quick geological exploration of formations, strata, and basic geological composition. Development of this capability and its use will free valuable payload space, which otherwise would have to be used for carrying return propellants. Techniques to develop these fuel resources will be valuable for the establishment of bases not only on Mars but on one of the two natural satellites of Mars (Phobos and Deimos), which are, like the Moon, devoid of any atmosphere and will permit the use of landing gear developed for the Moon. In fact, equipment developed for use on the Moon might be useful on Phobos.

Since water and oxygen are vital elements of ecological systems to support human life, we can see that resolving the problem of local fuel production by freeing water from rocks will also help the realization of self-containing life-support systems. Another consideration is recovery of oxygen from exhaled  $\text{CO}_2$ . Photosynthesis yields oxygen, as do hydroponic gardens, which are not only efficient food producers but also one of the lowest-weight oxygen regenerators, considering overall efficiency under long-term operation.

Hydroponic gardens can be maintained with nutrient solutions consisting of 99.65 to 99.8 per cent water and approximately 11 to 15 different dissolved elements, of which 6 are major constituents; the balance being trace-elements needed to maintain proper plant growth rates, health, and resistance against plant diseases. For maximum growth rate, the close pH control of the nutrient solution is mandatory. The established percentages of the minerals have to be maintained within close tolerances, differing somewhat for the various edible plants to be grown, since the mineral needs change from one plant species to another. Since the total mineral content of the nutrient solution is in the neighborhood of 0.2 to 0.35 per cent of the weight of the solution, only the major elements (besides water) are needed in larger quantities and should be produced locally as soon as possible. Theoretically, all could be reclaimed from plant waste and waste products of the human metabolic cycle. The minor elements, required in amounts of a few parts per million in the solution, could be part of the regularly scheduled payloads supplying the Mars base.

There is every expectation that the major elements of the nutrient solutions can all be found on Mars and the Moon in relative abundance and as constituents of chemical compounds permitting easy extraction, possibly using ion exchange methods. Table 38.1 shows a representative composition of a hydroponic nutrient solution which was used successfully on Aruba Island to supply vegetables to U. S. troops during World War II and thus reduced the food supply volume requirement to be shipped under wartime conditions. Today nutrient solutions are used to grow vegetables, mushrooms, and cattle feed commercially, as well as to support plant research.

Water, then, is the first basic compound to be found in starting a cycle of self-sufficiency for a lunar or planetary outpost and in reducing the continuous support requirement. It produces over 99.65 per cent of the weight of the nutrient solution of hydroponic gardens, reducing  $\text{CO}_2$  to  $\text{O}_2$  and hydrocarbons and supplying vegetables as byproducts; approximately 0.35 per cent of the weight of the nutrient solution would have to be shipped in if it could not be found locally and processed (possibly 100 per cent of the weight would have to be shipped in if no self-sufficiency is achieved). Water, provided that nuclear electric powerplants supply electricity and heat, can be extracted from crystalline rocks and decomposed into  $\text{H}_2$  and  $\text{O}_2$  for operating hydrox fuel cells and hydrogen blow-down or expansion turbines, reconstituting air to the proper oxygen and moisture content for breathing, and providing cryogenic oxygen and hydrogen for the operation of space ships during their return flights to Earth (in case of chemical and later nuclear or electric propulsion systems). This is one of the more important reasons for using cryogenic oxygen and hydrogen as propellants in the early stages of space operations rather than fluorine compounds, since one, single, water-extraction plant together with a nuclear electric powerplant of the Snap 4 type can start the most important part of a self-contained planetary or lunar base operation well on its way. We see from this example that the degree of self-containment of planetary bases really determines the volume of support needed from Earth; progressive increase in self-containment of planetary expeditions or bases is therefore a requirement of the first order.

Much of the research toward and development of equipment needed to support achievement of self-contained base operation and local return-fuel production can, of course, be done here on Earth and should go on concurrently with the development of our lunar-mission capability.

Another area of importance is the development of lunar and interplanetary payloads. To explore the Moon and Mars, the members of the expedition have to be protected against local hazards, have to live in pressurized shelters, and have to be able to move about on the surface to perform their assigned tasks and exploration objectives. Since exposure to the surface environment should be as brief as possible, the amount of physical work done outside closed shelters should be a minimum and should be necessary only when manual dexterity is definitely superior to automatic

Table 38.1 Hydroponic Garden Data

Daily food requirement per man (lb)	2.300
Daily oxygen requirement per man (lb)	2.200
Total daily food and oxygen requirement for 18-man crew (lb)	81.300
Approximate yield of food and oxygen per day per ft <sup>2</sup>	0.023
Required production area (ft <sup>2</sup> )	3,600.000
Total water required (lb)	30,000.000
Weight of supporting system (lb) (exclusive of rockfill, found locally, and discarded rocket fuel tanks and frame material)	10,000.000
Power requirements for artificial light and pumps (hp)	20.000

The mineral contents of the solution is between 0.2 and 0.35 per cent in solution weight. The illumination requirement is 400 to 1000 ft-c (Earth receives 1700 ft-c). Mars receives an average of 900 ft-c (43 per cent of the Earth-rate); however, due to the lower albedo of Mars, about 60 per cent of the Earth-rate is actually received. On Phobos, only 43 per cent direct light would be received, but diffuse reflection from the Mars atmosphere would supply some illumination while Phobos is not exposed to direct sunlight.

## Nutrient solution elements:

Major elements (in per cent)		Trace elements (in per cent)	
Potassium	29.5	Iron	0.173
Nitrogen	26.5	Chlorine	0.091
Calcium	25.2	Manganese	0.065
Sulfur	8.2	Boron	0.057
Magnesium	6.0	Molybdenum	0.007
Phosphorus	4.2	Zinc	0.005
<u>Subtotal</u>	<u>99.6</u>	<u>Copper</u>	<u>0.002</u>
		<u>Subtotal</u>	<u>0.400</u>

The above sample solution is atypical solution. Research has shown that the actual solutions change from plant to plant and from phase to phase during plant life. Plants need more nitrogen while growing and more potassium and calcium while growing seeds, etc.

and remote-controlled operations. The conclusion to be drawn from this is that human efforts needed to establish the first lunar or planetary base should be at an absolute minimum consistent with those actions which cannot be performed in advance and sufficiently well on Earth or done automatically in space. This requires that the base units be brought over as complete, self-contained modules, ready to work in the new environment or requiring a minimum of operations to be joined together. Present-day guidance capability would permit the landing of living-shelter modules close to their final permanent locations (excavation methods might as well be avoided, and the base modules ought to be emplaced with a minimum of soil movement). If protection against solar flares and cosmic radiation is necessary in addition to protection against climatological variations, covering the base-modules with sandlike aggregate is simple and would require less specialized equipment than excavating or tunneling. If the base can be delivered preassembled and prepackaged to its destination, the specialized labor required to assemble the base is at a minimum. The skilled manpower needed for assembly of base-modules on Mars may cost \$15,000 to \$25,000 per hour, transportation and subsistence included, while here on Earth the same man power may cost \$10.00 to \$15.00 per hour, overhead and fringe benefits included. Little is known about the surface environment and the atmospheric composition of Mars. About the only atmospheric constituent definitely established is CO<sub>2</sub> (Kuiper, 1952), which is about 16 times more abundant than on Earth. However, the most probable atmosphere models postulate that the Mars surface density corresponds to a 50,000-ft altitude Earth-density, somewhere between 85,000 and 105,000 ft both are equal (10 mbar), and that above these altitudes the Mars atmosphere is denser than the Earth's. An Earth orbit of 300 statute miles corresponds to a Mars orbit of about 1000 statute miles as far as the mean free path of atoms and molecules is concerned. Very little free oxygen is expected in the Mars atmosphere, since free atomic oxygen can escape from Mars (Urey, 1959). However, it has been speculated that oxygen in the form of ozone exists near the Mars surface and is possibly responsible for the reddish-brown color of Martian desert areas, which could be explained by an abundance of oxidized iron compounds, for example, fersite or limonite. Except for the existence of winter ice caps, which is generally accepted, water appears to be present only as water vapor or ice crystals, suspended in air, with an estimated partial pressure of only 0.043 g/cm<sup>2</sup>. The abundance of molecular nitrogen is estimated to be 95 per cent with argon at 3 per cent being the next abundant element in the Martian atmosphere. The absence of oxygen as well as the abundance of CO<sub>2</sub> requires that oxygen will have to be supplied for breathing, and an artificial atmosphere will have to be maintained for living and working shelters and for the pressure suits that will have to be worn by expedition members when outside closed, pressurized shelters.

To perform surface exploration as well as geological research, the members of the expedition have to have mobility. For short distances, surface transportation suitable for roadless surfaces, Martian gravitation

(12.6 ft/sec<sup>2</sup>), and the Martian atmosphere has to be designed. As indicated before, vehicles designed for lunar locomotion, propelled by fuel cell-operated electric motors or hydrogen expansion turbines appear to be a logical choice, particularly since problems of heat rejection will be less severe than on the Moon. This type of equipment should be particularly valuable in the early periods of exploration and occupancy of Mars.

There should be fewer surface feature problems than on the Moon, since it is generally accepted that Mars lacks the rugged surface structure of the Moon. As soon as direct knowledge of the composition of the Martian atmosphere is known, the availability and use of atmospheric compounds as fuel for locomotion should be investigated. The low density of the atmosphere leads to high-landing speeds for airplanes of even very low wing loading, so that only very smooth surfaces would permit landing by aerodynamic vehicles. However, hydrogen-oxygen-propelled glider-type aircraft of very low wing loading ( $\leq 10$  psf) could provide fast transportation (150 to 200 knots) over longer distances up to 3000 nautical miles [4] and (Fig. 38.1), particularly if jatos are used for takeoff after runways have been provided. For shorter distances, helicopters appear to be superior to surface vehicles in carrying capacity and speed for Mars altitudes up to 9000 to 10,000 ft. The lower surface gravity does not fully offset the effect of the low surface density so that the touchdown velocities for the same landing  $c_L$  and wing loading would be approximately 2.08 times higher than on Earth. This poses a considerable problem for aerodynamic entry vehicles of the Earth reentry variety on Mars, unless the design considers these particular properties. The use of horizontal landing Earth reentry vehicles would be permissible only if landing wing loadings of less than 20 psf are used and runways provided, permitting skids or retro-thrust application.

While the use of the Moon as an interim space launch base does not appear to offer advantages, the use of Martian natural satellites, Phobos particularly, may be advantageous and should be further investigated. Clyde Tombaugh, one of the foremost experts on Mars, expects that Phobos consists of basically the same materials as Mars itself. If this should be correct, the material of Phobos could be used to supply water and return fuels. Instead of using an artificial orbiting Mars base, a natural Mars base could be used to establish the initial Martian beachhead. A nuclear reactor of sufficient capacity could be installed together with a plant for reclaiming water from crystalline rocks. Excess power then could be used to dissociate water to H<sub>2</sub> and O<sub>2</sub> and provide power for their liquefaction. The cryogenic propellants can be stored in insulated empty fuel tanks until needed for return flights. An artificial orbiting base would not offer this possibility. Also chemicals needed to provide the nutrient solutions for hydroponic gardens could be expected to be found either partly or completely on Phobos; and as the capabilities of the base increase, one after the other could be included into the extraction process,

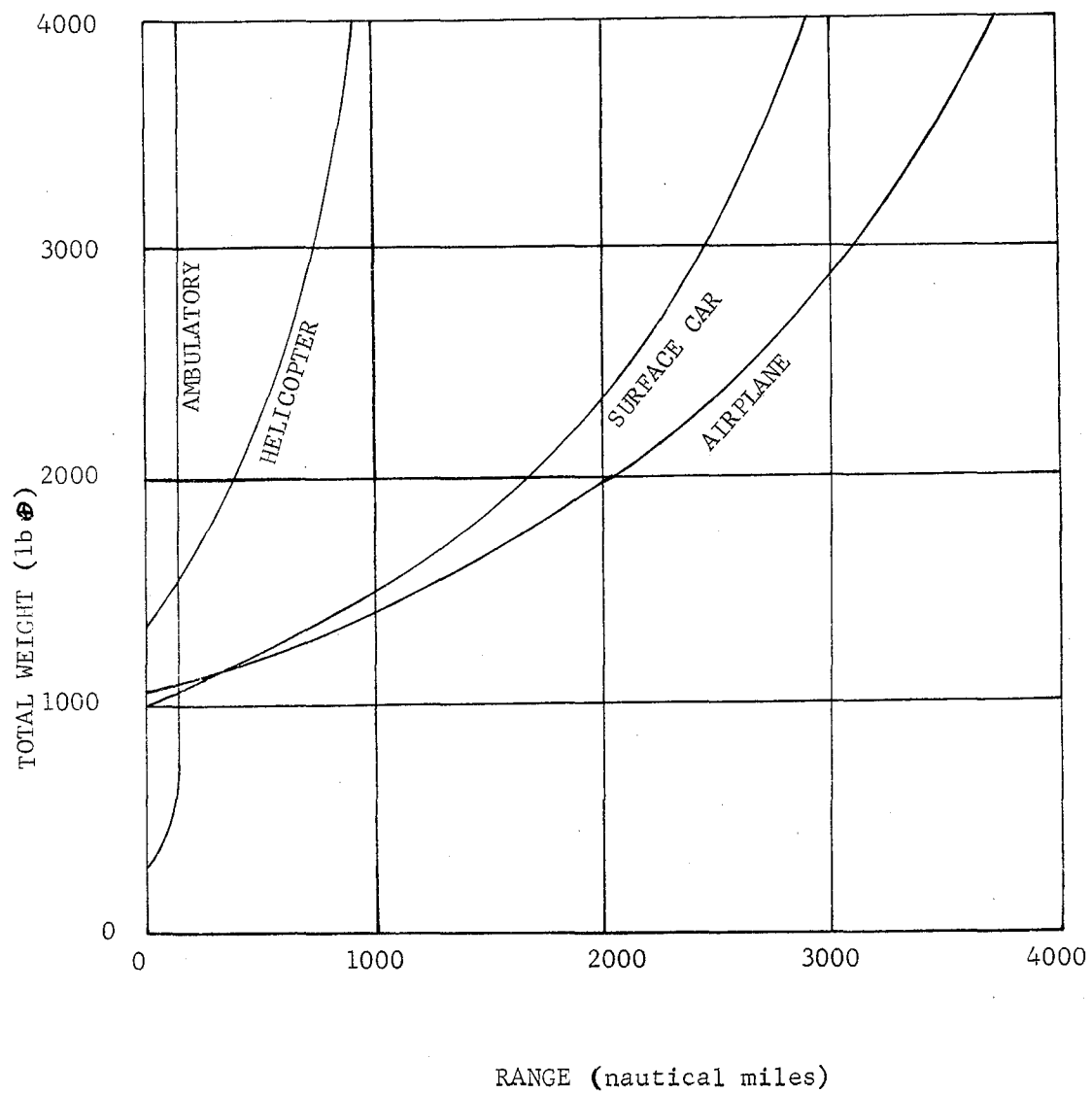


Fig. 38.1 Relation between vehicle weight and one-way range for various Mars transportation means [4].



making the base more and more self-contained. For landing on Phobos, the same techniques as for landing on the Moon could be used except that the gravitational pull of Mars and the Sun exceed that of Phobos even on Phobos' surface. ( $g_{\text{Phobos}} = 6 - 10 \times 10^{-4} g_{\text{Earth}}$ ) Therefore, little penalty will be paid to overcome the effects of Phobos' gravitational field either at takeoff or landing, in contrast to the Moon as an intermediate planetary departure base, where approximately 9000 fps velocity change is required after arrival from Earth to soft-land on the Moon; the same amount is needed to escape from the lunar gravitational field again to continue the journey to the target planet. The orbital velocity of Phobos around Mars is  $\sim 2.13$  km/sec or  $\sim 6990$  fps, and its orbital plane is inclined 26.50 deg from the plane of the ecliptic, and 1 deg 8 min from Mars' equatorial plane.

Since spaceships from Earth would probably reach Mars very nearly in the plane of the ecliptic, nonaerodynamic entries would land between  $\pm 25$  deg latitude, depending upon the position of Mars in its heliocentric orbit, whereas aerodynamic entry vehicles could cover areas outside this latitude belt, depending on lift-drag, wing loading, and  $G$ -loads. Aerodynamic heating would be considerably less than that during Earth reentry, such that the maximum temperatures encountered on leading edges or other heat-exposed surfaces would be reduced to at least half those at Earth reentry. If the rendezvous with Mars and Phobos were properly timed, the condition could be selected at which the motion of Phobos is retrograde with respect to the direction of the motion of Mars in its heliocentric orbit, with a velocity component parallel to the Mars orbit in the plane of the ecliptic. At this instant, the relative velocity between Phobos velocity component in the plane of the ecliptic and the spaceship velocity would be a minimum; however, with Phobos having a lateral velocity component  $v_{\text{Phobos}} \sin 26.50 \text{ deg} = 3140$  fps, while the velocity component in the plane of the ecliptic is  $6990 \cos 26.50 \text{ deg} = 6230$  fps. The spaceship has to increase its velocity by  $\sim 7600$  fps to cancel Phobos' lateral motion and match its velocity, since both Mars and Phobos are overtaking the spaceship from the rear. Little maneuver fuel will be needed to hover over the desired landing surface due to the low gravitational pull near the Phobos surface, which is less than one-tenth the local Mars gravity value (Tables 38.2 and 38.3).

To soft-land from Phobos on Mars, a total velocity increment of 15,500 fps is needed, disregarding drag losses during descent. Of this total increment, approximately 1900 fps are needed to initiate a transfer ellipse from Phobos to Mars towards the Mars surface. A second velocity increment of 13,600 fps with respect to the rotating planet is needed to cancel the velocity of the vehicle near the surface. Since the density of the Martian atmosphere above  $\sim 85,000$  ft is higher than the density of the Earth's atmosphere at equal altitudes (Mars density changes one order of magnitude about every 120,000 to 200,000 ft of altitude change), use of nonlifting entry bodies augmented by retro-thrust or parachutes as

Table 38.2 Physical Data on Mars and Its Satellites

Information	Mars	Phobos	Deimos
Mean distance from sun	141.5 x 10 <sup>6</sup> mi (227.7 x 10 <sup>6</sup> km)	Same as Mars	Same as Mars
Mean orbital velocity	15.0 mi sec <sup>-1</sup> (24.1 km sec <sup>-1</sup> )	1.3375 (2.14 km sec <sup>-1</sup> )	.8398 (1.3512 km sec <sup>-1</sup> )
Mean angular velocity	0.524°/day	47°/hr	11.87°/hr
Sidereal period	687.979 days	0.319 day	1.264 days
Rotational period	1.027 days		
Eccentricity of orbit	0.0933	0.02	0.003
Inclination of equator to orbit	25.20°	Unknown	Unknown
Inclination of orbit to ecliptic	1.85°	26° 30'	26° 58'
Mass, lb	1.41 x 10 <sup>24</sup>	2.268 x 10 <sup>16</sup>	1.512 x 10 <sup>15</sup>
Density (water = 1.00)	4.12 - 4.02 ± .1	3.5?	3.5?
Force constant $\mu = GM$ [miles <sup>3</sup> sec <sup>-2</sup> ]	1.026 x 10 <sup>4</sup>		
Solar radiation intensity [Earth = 1]	0.4315 (mean)	0.4315	0.4315
Mean diameter	4140 mi (6739 km)	~ 10 16	~ 5 8
Oblateness ( $\frac{a-b}{a}$ ) dynamical	0.00521; ( $\frac{1}{192}$ )	Spherical?	Spherical?

Table 38.2 -- continued

Information	Mars	Phobos	Deimos
Gravity at surface [ft sec <sup>-2</sup> ]	12.7	Mars gravity on surface 1.672	0.2658
Fraction of Earth gravity	0.39 ± 0.01	6 to 10 x 10 <sup>-4</sup> g	2 x 10 <sup>-4</sup> g
Escape velocity at surface [miles sec <sup>-1</sup> ]	3.15	7.7 x 10 <sup>-3</sup> (n.a.)	0.96 x 10 <sup>-3</sup> (n.a.)
Satellite velocity at surface [miles sec <sup>-1</sup> ]	2.23	5.47 x 10 <sup>-3</sup> (n.a.)	0.68 x 10 <sup>-3</sup> (n.a.)
Sun's gravity at planet's orbit [ft sec <sup>-2</sup> ]	0.0084 = 2 x 10 <sup>-3</sup> g	0.0084 or 2.10 <sup>-3</sup> g	0.0084 or 2 x 10 <sup>-3</sup> g
Rotational velocity on Mars' surface [equator, fps]	795	Unknown	Unknown
Albedo	0.15	0.15 or less	0.15 or less
Length of day [Earth days]	24 <sup>h</sup> 37 <sup>m</sup> 22.6 <sup>sec</sup>	7 <sup>h</sup> 39' 26.65"	30 <sup>h</sup> 21' 15.68"
Surface pressure [mb]	85 ± 4 or 230 g cm <sup>-2</sup>	0	0
Temperature lapse rate	3.7° C km <sup>-1</sup>		
Altitude above Mars [mi]	n.a.	3700	12,500
Apsidal Motion [deg per Julian year]		158.5	6.54
Orbit inclination to Martian equator [deg]		1°8' (variable)	1°46' (variable)
Change of orbital period due to oblateness of Mars [sec per orbit]		+11	+7
Pressure decrease in feet per order of magnitude depending on selected atmosphere model	120,000 200,000	n.a.	n.a.

Table 38.2 -- continued

Information	Mars	Phobos	Deimos
Surface temperature [ $^{\circ}$ F]	80 $^{\circ}$ F max - 150 $^{\circ}$ F min	Not determined	Not determined
Boiling point of water [ $^{\circ}$ C]	25	n.a.	n.a.
Distance from Earth at opposition [mi] at superior conjunction [mi]	49 x 10 <sup>6</sup> 235 x 10 <sup>6</sup>	Same as Mars	Same as Mars

The indicated mass and gravity data of Phobos and Deimos are derived, using 10 mi diameter for Phobos and 5 mi diameter for Deimos and a relative density of 3.5. Estimates of the density of these satellites range between 2.7 and 3.5. The diameters have been estimated assuming the same albedo as that of the parent body (0.15). In reality, the albedo should be somewhat less than 0.15, which would lead to somewhat larger diameter. In this event, the estimated mass would relate to a lower specific density.

well as those using aerodynamic lift entries makes sense and could save not only part of the 1900 fps velocity increment required to separate from Phobos but also all of the 13,600 fps required to cancel the remaining energy with respect to Mars' surface. The merits of this approach will be further dealt with below.

Another question to be resolved is the size of the expedition required to support a successful mission. In the published literature, various mission sizes have been considered, ranging from crews of 6 to 15 members to as large as 100 to 150 crew members. A reasonable approach for determining mission size is to require that all skills needed to make the mission a success should be represented. Furthermore, each crew member should have training to perform at least two required mission skills so he can substitute in case of sickness or unavailability of the crew member whose primary responsibility it is to perform the task. In case of malfunctions in one vehicle, companion vehicles have to be able to take over crews or missions, or both, by transferring personnel, payloads and propellants while on the several legs of the mission. Abort capability for each individual ship of the mission should exist by such transfer to other companion ships. The overall mission should have built-in operational redundancy to permit return of the full crew, regardless of which ship malfunctions or fails. Since in early phases of Mars exploration, mission durations of 200 days or more may be the rule for outbound or inbound trips, the distance and time requirements to rescue missions from Earth or from Mars are too large in urgent cases to permit rescue operation from either terminal, in contrast to aborts on lunar missions, in which rescue can be initiated immediately. This deficiency has to be overcome by having a group of vehicles in an individual mission which fly relatively close formations, so that each ship can obtain assistance within a short time whenever required. This philosophy of operation requires a larger crew than a minimum-type mission not having this built-in redundancy and rescue capability. The simultaneous departure of a group of spaceships, crew ships, and cargo ships intermixed may still be difficult from Earth launching sites even within the next decade. However, using in-orbit refueling and launch operations, this approach will be less difficult and promises a high success rate, since only one stage will have to work successfully to reach escape velocity. Malfunctions during this phase will keep this vehicle in Earth-orbit and therefore accessible to rescue missions from Earth. Malfunctions during Mars capture will place the vehicle into Mars orbit and therefore again make it accessible to rescue action by the companion vehicles. An operating scheme could be worked out which provides a maximum flexibility in mission modifications to overcome effects of vehicle malfunction and aborts, maximizing crew safety and the probability of safe return.

Before going into more operational details of the Mars mission and including Phobos and possibly Deimos into such schemes, it is good to know somewhat more about them beyond the physical data presented

in Table 38.2. As we learn from these, Phobos revolves faster around Mars than points on Mars' surface. This makes Phobos appear to be rising in the west and setting in the east. Its low altitude of  $\sim 3750$  miles above Mars prevents its visibility at latitudes greater than  $69^\circ$ . Its synodic period is  $11^h .106$  (interval between successive meridian crossings). It will be visible from horizon to horizon at Mars' equator for  $4^h .257$  and for shorter periods at higher latitudes. Deimos, 12,500 miles above Mars, can be seen at latitudes below  $82^\circ$ . While it can be seen from the same points at the Martian equator for 60 hr with shorter periods at higher latitudes, its synodic period is  $135^h .45$ . It is not known whether Phobos or Deimos rotate around their own poles at the same rate as their rotations around Mars and, like the Moon, show the same area of their surfaces permanently to Mars (like many other natural satellites of the solar planetary system and possibly even Venus), or whether they have independent periods of revolution. Another interesting fact is that during spring and fall seasons, Phobos and Deimos undergo frequent eclipses and will be obscured during large portions of their orbits, while during high summer and winter no eclipses will occur.

Escape velocity on the surface of Phobos is approximately 40 fps and the surface circular orbit velocity is  $\sim 29$  fps. This information permits us to determine window, time and velocity tolerances to accomplish spaceship capture on Phobos. Performance of the midcourse and terminal guidance equipment can be based on this information. Escape velocity on Deimos is  $\sim 5$  fps, while its surface orbital velocity is  $\sim 3.6$  fps.

With the duration of complete Mars missions under minimum-energy transfer conditions of about 970 days, and waiting periods of 450 days on Mars or Phobos before return to Earth, a considerable part of the payload will be devoted to life support, scientific instrumentation, base modules, base erection equipment, communication equipment, and power supplies. Existence of ionospheric layers similar to those in the Earth's atmosphere will restrict frequency use and may make particular power demands to maintain communications up to maximum Earth-Mars separation. Penalties in ideal velocity requirements for fast missions of transfer times of less than 200 days and shorter waiting times may be at least partly offset by savings in supporting payloads. With a maximum degree of initial self-sufficiency of the Mars satellite base (Phobos), and only exploratory flights to Mars of relatively short duration, a total crew of 18, distributed to three manned vehicles and the use of six cargo-vehicles (carrying scientific equipment, nuclear electric powerplants, ready-to-operate base modules, operating fuels, return and mission propellants, and possibly a water extraction, and a water dissociation and liquefaction plant for production of cryogenic  $H_2$  and  $O_2$  from local resources) receiving power from one of the nuclear electric powerplants, appears to be a reasonable example for studying operational and support requirements of such a mission. Since capabilities of chemical boost systems, use of space rendezvous, introduction of nuclear upper stages,

and progress in partial self-support of Phobos or Mars bases will increase as time goes on; the originally slow Mars missions will be replaced by faster transfer time missions and more frequent missions. This may lead to the desire to retain occupancy of a once-established base and to consider tours of duties of crews, skipping a return flight before returning to Earth again, using a fast-type return, and abbreviated second-turn waiting times.

Since booster size will be the limiting factor at all times, we can expect that at the time of operational availability (of Nova) the demands on payload capability per flight again will exceed the existing capability of the most advanced vehicle. As is planned for lunar missions now--to use Saturn vehicles in combination with orbital operations (space rendezvous) to increase the payload capability per flight at escape velocity-- Nova vehicles could be refueled in orbit to keep technological pace with the increasing payload-size demands. In due time, recoverable space boost systems will handle space refueling missions and so could make full payload capability available for planetary missions. The next step to improve space travel efficiency is to refuel at the destination planet or on the natural or artificial satellites provided for this objective.

To give a picture of the savings to be made, using Phobos as a Mars space flight terminal and commuting from Phobos to Mars and back with vehicles having aerodynamic lift-entry capability, we can look at departure payload weights to perform the various mission modes, having an Earth escape velocity weight of 150,000 lb from a 300-nautical-mile Earth-orbit (36,500 fps). A specific impulse of 430 sec is assumed, using cryogenic oxygen and hydrogen as propellants for all phases, following Earth departure.

### 38.3 Operational Aspects of A Mars Expedition

#### 38.3.1 Determination of the Velocity Requirements of the Various Mars Mission Modes

Mission Modes and Operational Objectives. All missions to Mars require a minimum escape velocity of 36,500 fps if Hohmann transfer data to Mars heliocentric orbits are assumed with transfer angles of 180 deg. The  $\Delta v$  requirements detailed in Table 38.3 are applicable to the involved mission sections, using 256 days transfer flight time to Mars, 485 days waiting time on Mars, and 256 days return flight to Earth Orbit. Heliocentric orbits of Mars and Earth and coplanarity of both orbits are also assumed except in the case of landing on Phobos. The inclination of the Phobos orbit to the plane of the ecliptic was assumed to be 26.50 deg and the required lateral velocity component to match Phobos' orbit included into Phobos landings from Earth orbits. The timing of landing on Phobos was selected such that the relative velocity between Phobos and the space vehicle is at a minimum at the time of orbit matching, which is an additional constraint as to arrival time at the Mars capture orbit. Midcourse

Table 38.3 Velocity Requirements from 300 nautical mile Earth Orbit to Heliocentric Orbits near Mars, Mars Capture and Entry, Landing on Phobos Velocity, and Return Flights

	<u>Velocity (fps)</u>
Earth surface to circular Earth orbit	27,500
Earth orbit to transfer to Mars, including 500 fps midcourse maneuver	11,900
Mars capture	6125
Mars landing (direct)	12,475
Earth orbit to Mars orbit	18,025
Earth orbit to Phobos landing	19,000
Phobos to Mars surface	15,500
Earth orbit to Mars surface, no aerodynamic braking	30,000
Earth orbit to Mars surface, aerodynamic braking	20,000
Mars surface to Earth capture, including midcourse operation	30,000
Mars surface to Earth surface, including aerodynamic braking	20,000
Phobos surface to Earth capture, including midcourse correction	20,500
Phobos surface to Earth surface, aerodynamic braking and midcourse correction	8100
Total round trip Earth orbit to Mars surface and back, no braking on Mars	60,000
Total round trip Earth orbit to Mars surface and back, aerodynamic braking on Mars and aerodynamic landing on Earth	40,000
Earth orbit to Phobos and back to Earth orbit	39,500
Earth orbit to Phobos and back to Earth surface, aerodynamic braking	29,100
Phobos surface to Deimos surface, soft landing	3450
Gain due to Mars rotation, eastbound launch at Mars equator	795



correction fuel in form of an extra  $\Delta v = 1500$  fps is included.

Faster orbits or shorter waiting times can lead to total round trip  $\Delta v$ 's up to four or more times the minimum round trip  $\Delta v$ 's. Since these extreme cases cannot be handled by chemically propelled vehicles and since it is not expected that nuclear or ion propulsion systems will be available during early manned Mars missions, they are not considered in direct Mars or Phobos missions.

The following mission modes are compared:

1. Direct landing on Mars using impulsive entry and direct return to Earth using aerodynamic reentry.
2. Direct landing on Mars using aerodynamic entry, and direct return to Earth orbit.
3. Direct landing on Mars using aerodynamic entry and direct return to Earth surface using aerodynamic reentry.
4. Direct landing on Phobos and return to Earth orbit.
5. Direct landing on Phobos and return to Earth surface by use of aerodynamic reentry.
6. Direct landing on Mars using impulsive entry and return to Phobos.
7. Direct landing on Mars using aerodynamic entry and return to Phobos.

The following mission objectives are considered:

1. Establish Mars base within  $\pm 25$  deg latitude on Mars. Set up Mars base and keep Mars base occupied after first landing. Make Mars base self-contained to as high a degree as commensurate with 1970 technology at as early a date as possible. Produce fuel locally.
2. Establish a Phobos terminal and keep it occupied. Make Phobos base self-contained at as early a date as possible and produce fuel on Phobos. Make exploratory flights to Mars only, and maintain temporarily occupied base.
3. Establish Phobos terminal and make base self-contained and fuel-producing at earliest possible date. Occupation permanent. Establish Mars base by flights from Phobos and make it self-contained as soon as Phobos base is fully established and produce fuel on Mars for Mars-to-Phobos flights. Occupy Mars base permanently.
4. Establish Phobos terminal, make it self-contained and fuel-producing. Establish Mars base in parallel with supplies from Phobos and build it up as main base, later using Phobos for fuel production and intermediate stops to and from Mars. Keep Phobos manning at minimum after maximum degree of self-sufficiency of Mars base is achieved.

These objectives cover a relatively wide range of mission and opera-

tional approaches. The permanent manning strength is established at 18 men, arriving at their destinations in groups of either 3 or 6, depending upon objective of individual tasks. To arrive at greater manning strength, support requirements increase these requirements in the ratio Desired strength.

18

Approaches to Operation of Mars and Phobos Bases Under Various Operational Objectives. Direct landings on Mars require either impulsive braking (as will be used in lunar soft landings) or aerodynamic braking. For the latter, again two modes are possible: first, a Mercury-type of nonlifting landing with parachute deceleration before touch-down and possible use of retrorocket thrust just before touch-down, or airbags to reduce impact shock under low Martian surface density; secondly, use of aerodynamic lift deceleration and horizontal landing. Due to the low surface density on Mars, landing velocities at the same  $c_L$  and wing loading will be more than twice as fast as those on Earth. This will be true despite the lower surface gravity on Mars, and will require wing loading below 10 psf on smooth but unprepared surfaces and below 20 psf on prepared, graded, smooth surfaces to prevent or reduce landing damage. Horizontal manned landing will be preferable, particularly for flights from Phobos and return to Phobos. One of the assets of this mode of operation is the large footprint of the landing vehicle as compared to no-lift entry, which permits relaxation of timing conditions and avoiding of detrimental local weather conditions, using alternate bases as soon as they can be set up. A miss with a nonlifting landing mode may require rescue operations, comparable to rescue operations in extremely uninhabited Earth areas without efficient surface or air transportation means. Therefore, lifting-type landing modes should be adopted as soon as feasible and also alternate Mars bases set up as soon as the early Mars occupation and base establishment has made sufficient progress.

Mission Objective "A". The mission objective "A" requires the highest  $\Delta v$  (18,000 fps) for arrival on Mars, using only impulsive braking. Empty weight  $W_e$  of arriving vehicle, if single-stage operation during Earth departure and Mars injection is used, is derived from  $\Delta v = \ln \frac{W_o}{W_e} I_{sp} g$  with  $I_{sp} = 430$  sec, and

$$g = 32.16 \text{ ft/sec}^2$$

$$W_o = 143,000 \text{ lb at Mars injection or } 150,000 \text{ lb at Earth escape}$$

$$\ln \frac{W_o}{W_e} = \frac{18,400}{13,829} = 1.38$$

$$\frac{W_o}{W_e} = 3.78$$

$$W_e = \frac{W_o}{3.78} = 32,800 \text{ lb}$$

Since the inert weight of this vehicle would be approximately 17,500 lb (derived from an initial weight of 343,800 lb before departing from a 300-nautical-mile circular Earth orbit), 15,300 lb payload would arrive on Mars. No return capability into Mars orbit or landing on Phobos would be possible without using additional vehicles, bringing fuel and supplies.

If the vehicle were to be two-stage, the mass ratio would be halved and a higher payload efficiency achieved ( $\Delta v = 9200$  fps)

$$\ln \left( \frac{W_{o1}}{W_{e1}} \right) = \frac{9200}{13,829} = 0.665$$

$$W_{e1} = \frac{W_{o1}}{1.945} = 73,500 \text{ lb}$$

$$W_{o2} = w_{e1} - W_{str} = 73,500 - 15,000 = 58,500 \text{ lb}$$

(Note reduced  $W_{str}$  due to deletion of soft landing).

$$W_{e2} = 30,000 \text{ lb}; \quad W_{str2} = 2500 \text{ lb}; \quad W_{p2} = 27,500 \text{ lb}.$$

This arrangement could bring 27,500 lb of cargo in one vehicle, unmanned, and a crew of three in a second manned vehicle, including a 2-week life support supply, shelter, power supply, and among the cargo, two complete planetary surface vehicles, capable of grading reasonably soft soil or sand-type surface to prepare a runway for horizontal entry and landing vehicles; no return without additional vehicles landing with additional fuel and supplies.

Use of aerodynamic entry vehicles would require a

$$\Delta v = 6500 \text{ fps or } \ln \left( \frac{W_o}{W_e} \right) = 0.47;$$

$$W_e = \frac{143,000}{1.6} = 89,500 \text{ lb};$$

$$W_p = 89,500 - 22,500 = 67,000 \text{ lb}$$

The higher inert weight of the stage of 22,500 lb is due to parachute, recovery gear and other equipment. The weight could again consist of a crew of three men, two surface vehicles, shelters, scientific equipment

and life support for months. After 2 weeks to 2 months, the vehicle, leaving all disposable equipment on Mars, could fly to Phobos and join the main part of the expedition, after runway and emergency facilities have been established on a preselected Mars site. During the Earth-Mars transition, the Mars capture fuel is used for crew shielding purposes, the return fuel to Phobos as temporary shielding before embedding the temporary base crew shelters in about a 1-ft layer of loose Mars surface aggregate. With the weight of the stripped vehicle reduced to 15,000 lb, 40,000 lb of fuel would be needed to fly to Phobos using rocket power. Since the 15,000-lb stripped down vehicle is part of the original 22,500-lb inert weight, approximately 27,000 lb are available for consumable supplies, instrumentation, personnel shelter, surface vehicles, fuel and evaporation losses. For direct return to Earth reentry, additional supply vehicles have to arrive at Mars. The shielding of 1 ft of aggregate should provide sufficient protection against solar flares of up to 3 + intensity for the short duration of stay on the Martian surface.

Two-stage arrangement can increase payload capability for direct flights to Mars.

$$\Delta v = 3250 \text{ fps}; \quad \ln \left( \frac{W_{o1}}{W_{e1}} \right) = \frac{3250}{13,829} = 0.235$$

$$W_{e1} = \frac{143,000}{1.265} = 113,000 \text{ lb}$$

$$W_{str1} = 13,000 \text{ lb}, \quad W_{p1} = 113,000 - 13,000 \text{ lb}$$

$$W_{o2} = 100,000 \text{ lb}$$

$$W_{e2} = \frac{100,000}{1.265} = 79,000 \text{ lb}$$

$$W_{str.2} = 5000 \text{ lb including recovery equipment}$$

$$W_{p2} = 74,000 \text{ lb}$$

We see that this mode of operation not only increases the payload by about 10 per cent but also increases complexity of operation. The actual payload gain is higher, since of the structural and crew weight of the return stage of 10,000 lb, 4000 lb come out of the 5000 lb of the landing stage, and only 26,600 lb of fuel are needed to return to Phobos. The actual

net payload gain then is 4900 lb plus 6500 lb saved on fuel, or 11,400 lb. However, it still has to be decided whether this is the most desirable mode of operation. For direct return, again several vehicles are needed to bring additional supplies, fuel and Earth return vehicle.

Mission Objective "B" - Landing on Phobos.

$$\Delta v = 7600 \text{ fps}; \quad \ln \left( \frac{W_o}{W_e} \right) = \frac{7,600}{13,829} \approx 0.55$$

$$W_e = \frac{143,000}{1.735} = 82,500 \text{ lb}$$

$$W_{\text{str.}} = 17,500 \text{ lb (Not to be discarded)}$$

$$W_p = 65,000 \text{ lb}$$

This payload is approximately 3 per cent less than the payload landed directly on Mars, but it permits direct return flights to Earth with no additional refueling if this fuel is included in the payload and the manned Earth reentry vehicle is part of this payload. Power supply fuel, life support, and water supply, are used for preliminary shielding on Phobos. A 3-ft loose aggregate cover on the crew shelters is provided against cosmic rays and 3 + solar flares for the first 3 days on Phobos and later is augmented to a cover 10-ft thick to reduce radiation levels to approximately long-term average Earth surface dose level. In each manned vehicle, 300,000 lb of life support supplies, stored in shelter units, arrive, sufficient for a 450-day stay on Mars and a 260-day return trip to Earth. The balance consists of nuclear electric power supplies, scientific instrumentation, communication gear, and fuels. It should be noted, that with 50,000 lb of fuel, the inert weight of the landing stage can be returned to 300-nautical-mile, circular Earth orbit, there refueled and refueled to be used again (255,940 lb of fuel and 67,000 lb of payload exclusive of attitude control fuel and 10,000 lb of life support supplies for manned return, and 77,000 lb of payload for unmanned return). Refueled with 255,940 lb on Phobos, it could bring the same cargo to Earth orbit. This shows that local refueling capability is a significant achievement, which could reduce considerably the overall operating cost and should be achieved as early as technically feasible. Due to the low gravity on Phobos, the vehicle would need only a low-thrust, chemical-fuel power plant, 50,000 lb of thrust being sufficient in either way operation.

To provide radio communications, life support, shelters, repair facilities, scientific instrumentation, recreation facilities, and mobile

surface vehicles, approximately 400,000 lb of payload are required to be landed on Phobos or on Mars, not including the fuels for the manned return flights. To establish an increasing degree of self-sufficiency, at least another 200,000 lb of payload are needed. Besides tanker vehicles, nine vehicles including three manned vehicles are needed to staff the base, while building up self-sufficiency will require another three cargo vehicles. For the return of the crews from Phobos, two tanker vehicles have to arrive on Phobos. For each manned excursion from Phobos to Mars, approximately 26,600 lb of fuel excluding losses have to be provided for returns to Phobos. Based on this figure, one tanker can supply three excursions to Mars from Phobos, either for airdrop of supplies or for manned landing and return.

Exploratory flights to Mars should use aerodynamic entry. The critical phase of the flight is the touch-down phase on Mars, which in case of a horizontal landing should be performed with a wing loading of less than 10 psf on an unprepared landing site, and of less than 20 psf on a prepared site. The vehicles in the event of lifting aerodynamic entry can fly to their respective landing sites with wing loadings of 50 to 75 psf, if they can discard (airdrop) their excess cargo before landing. They can carry canisters of fuel with them, which would be dropped with parachutes at low speed and altitude, using air bags to reduce impact shock. Also payloads and equipment can be brought down this way and the vehicle itself lands after having reduced its touch-down weight to the prescribed limits. If the unfueled return weight of the vehicle is 10,000 lb, 26,600 lb of fuel are needed to return to Phobos again. With 1000 sq ft effective lift area, 40,000 to 65,000 lb of payload can be brought down to Mars' surface, which after reduction of 26,600 lb of fuel would provide 13,400 to 38,400 lb net payload.

It is not necessary that the vehicle land after the first deposit of payload; it can return to Phobos. All necessary base equipment can be deposited, first checked out by telemeter, emplaced by remote control, using air-dropped planetary surface vehicles to accomplish this, and even operated remotely to grade the runway before the first landing. Also, personnel can be dropped before the first landing to check out and operate delivered equipment. This possibility points out the superiority of the operation of landing on Phobos first and using landing techniques already tested in the lunar soft-landing program.

Simultaneously, the achievement of self-sufficiency should be promoted as quickly and energetically as possible. The first nuclear reactors of the type Snap 4 or possibly more advanced types should be landed with one or two cargo vehicles on Phobos, emplaced, and covered with Phobean loose aggregate to provide reactor shielding. After completion of the emplacement, the power cable is unreeled from the reactor and connected to the base power center. Prior to this time, power is supplied by one of the  $H_2-O_2$  fuel cells or hydrogen expansion turbines. Before switch-

over, the reactor is activated, heat-rejecting radiators properly positioned and the nuclear electric power plant checked for proper operation. Then the second unit is set up in identical fashion, checked out, and connected when needed.

Two chemists and geologists, being part of the expedition on Phobos, could investigate the availability of water-containing rocks. If enough of the required rock compounds are found, one of the modular water-extraction plants, using approximately 5 to 10 per cent of the available power of one of the reactors, could be set up and operated, with the collected water being stored in the highly insulated, pressurized, empty fuel tanks of the cargo vehicles. After this process is checked out and properly working, chemists and geologists could search for rock suitable for use as gravel aggregate for the prepackaged hydroponic garden. During the journey from Earth, oxygen could have been regenerated from  $\text{CO}_2$ , using the Sabatier process and gaseous hydrogen, byproduct of  $\text{CH}_4$  (methane), which is stored for possible later use. The oxygen regeneration, using the Sabatier Process (see Table 38.4), is superior to oxygen reconversion by algae and more suitable for flight vehicles. As soon as 40,000 lb of water have been extracted and suitable gravel found and processed, the hydroponic garden could be placed into operation, and with 3600 sq ft of surface area, could supply all the food and oxygen needed for an 18-man crew if properly controlled and operated, the required additional light being supplied again from the nuclear electric power plants. The Sabatier plants should be kept in stand-by position and operated during periods in which the output of the hydroponic garden does not balance or meet the crew requirement for oxygen.

The next step in achieving self-sufficiency then should be to set up a water dissociation plant to provide oxygen make-up for the life-support equipment and to supply hydrogen for the Sabatier process. Running at full capacity, the water dissociation plant will consume 330 kw of power and can dissociate enough water in 100 days to supply all the hydrogen and oxygen for a full payload return flight from Phobos into a 300-nautical-mile, circular, Earth orbit. However, to accomplish this, a hydrogen-oxygen liquefaction plant using all the advantages of operation on Phobos should be provided, including the required nuclear electric power plant for its operation, again using the same type as provided for base operation. Having accomplished this, a further step towards increasing self-sufficiency is to provide sources for the major elements needed for the makeup of the nutrient solutions of the hydroponic garden, while the minor or trace elements are represented in such small concentrations (few ppm to fractions of ppm) that their local production would not provide any advantages but rather would be a nuisance.

Since the water extraction plants are of modular type, several are needed to supply all needs, plus at least one or two stand-bys for maintenance and repair. This available redundancy would lead to the next objective.

Table 38.4 Comparative System Weights and Energy Requirements for Sabatier O<sub>2</sub> Recovery Process

Item	Stored (Nonregen- erative) System	Water Recovery Only	Chemical Oxygen Recovery	Photosyn- thetic Oxygen Recovery
	Resupply Rates (lb/man-day)			
Food (dry basis)	1.250	1.250	1.250	0.625
Contained water	0.125	0.125	0.125	0.062
Packaging	0.138	0.138	0.138	0.069
Water	6.875	0.000	0.521	0.000
Tankage	0.688	0.000	0.052	0.000
Oxygen	2.000	2.000	0.000	0.000
Tankage	1.000	1.000	0.000	0.000
Water-purification materials	0.000	0.500	0.500	0.500
Total	12.076	5.013	2.586	1.256
Power and Radiator Requirements (per man)				
Electrical power, $\text{w}$	172.8	269.0	552.9	7597.0
Radiator surface, $\text{ft}^2$	4.8	9.1	13.3	243.3
Added Weights of Fixed Equipment (lb/man)				
Equipment	18.8	52.2	120.0	1266.0
Prorated power supply	187.7	195.1	215.9	508.0
Radiator (at 1.0 lb/ft <sup>2</sup> )	4.8	9.1	13.3	243.3
Total	211.3	256.4	349.2	2017.3
$\Delta W_F$	0	45.1	137.9	1806.0
$t_c$ , days <sup>a</sup>	---	6.4	38.2	1253.0 <sup>b</sup>

<sup>a</sup>Time in which system becomes lighter than the system in the column to the left of it.

<sup>b</sup>3.44 years--applicable only if used in closed spaceships, permitting no outside supply of water, etc., during operation period.



Mission Objectives "C" and "D". During the time the Phobos base is brought to full operation, exploratory flights and later landings could take place on Mars, leading among others to the selection of the best primary and alternate base sites, considering among other items availability of water collection or extraction capabilities. As soon as these are secured, one of the standby extraction plants could be landed on Mars and placed into operation together with the required nuclear electric power plant, and a dissociation and liquefaction plant should follow as soon as reliable water supply is obtained. Return flights from Mars to Phobos will require from one-third to one-tenth of the fuel capacity needed for the direct return flights to Earth, depending upon the objective, either to return crews with landing on the Earth's surface, empty boosters, or boosters with full payload on the original exit orbit at Earth. With a period of 450 days waiting time before return to Earth, the Mars base can be built up with a minimum of risk and with the same degree of self-sufficiency as the Phobos base (mission objective D). From then on, the major base operation could be transferred to Mars, and Phobos could be used only as a refueling and maintenance base, since the low gravitational acceleration on Phobos would permit crew members to walk around literally carrying weights of 20,000 to 100,000 lb. It is easy to understand the advantage of assembling even big boosters manually with a few people and a minimum requirement on maintenance structures (Phobos gravity is between  $6 \times 10^{-4}$  to  $10 \times 10^{-4}$  of that Earth gravity).

With the refueling capability given on Phobos, return vehicles can take off from Mars with a  $\Delta v = 15,500$  fps. The mass ratio required for flights to Phobos is 2.66. With a  $W_0$  of 400,000 lb or approximately 16.5 per cent higher than at its departure from Earth orbit, the  $W_e$  will be  $400,000 \text{ lb} / 2.66$  or 150,375 lb. The available payload will be  $W_e - W_{str} = 160,000 - 17,500 = 142,500$  lb, or approximately twice the payload which can be carried from Phobos to Earth orbit. The excess payload therefore would be either supplies for Phobos or would require the return of two cargo ships to Earth orbit to accommodate the weight. Another way to utilize the payload capability of the cargo vehicles is to load part of the payload with fuel and perform fast returns, requiring a higher  $\Delta v$  for the transfer. After establishment of self-sufficiency of the Mars and Phobos bases, supply requirements will decline more and more and the savings in supplies and logistics will permit a larger fraction of the ships' available load capacity to go into fuel and so will permit reduction of waiting time on Mars and also faster transfer flight, reducing round-trip times to half or less. After achieving refueling capability on Mars, the outbound trips could land directly on Mars using nonlifting or lifting aerodynamic entry.

### 38.3.2 The Mars Entry Vehicle

The Mars entry vehicle should be Phobos-based and built to permit landing velocities corresponding to the highest achievable  $c_L$ , with an average L/D of three or better at supersonic speeds, and it should have minimum wing loading of 10 psf (empty except for crews of one or two, including life support for duration of the mission plus 24 hr). It could be constructed of beryllium, its alloys, or lithium-magnesium alloys to achieve the lowest possible structural weight commensurate with the aerodynamic heating conditions encountered, which will be lower by a factor of at least two due to the lower entry velocity from Phobos as compared to the direct entry from Earth. The leading-edge temperatures will be less than 1500°F, and the surface temperatures of the skin near the leading edges will be in the neighborhood of 1000 to 1200°F. It should have skids for horizontal landing, or skids and a nose wheel for better control after touch-down. It should have vertical takeoff capability under rocket power and land under reaction jet control on Phobos. The empty weight including crews and life support should be in the order of 10,000 lb, and the take-off weight on Mars to Phobos would be approximately 36,600 to 37,000 lb.

### 38.3.3 Crew Shelter Units

The crew shelter units should be completely self-contained cylindrical units with emergency power supply, sealed, with airlocks to provide minimum leakage and air losses. They should be designed so that a minimum fire hazard exists. A recommended diameter range is 10 to 12 ft, with unit length of 25 to 30 ft, providing office space, recreation space, laboratories, and sleeping quarters. They should have flat floors and ceilings, with about 6.5 to 7 ft ceiling height, with all space below floors and above ceilings utilized to contain water storage, power supplies, life support equipment, heating and cooling units, electrical wiring, plumbing, and emergency equipment. All vital items should be easily accessible, exchangeable, and maintainable, creating no fire hazard. The units should be covered immediately with about 3 ft of loose aggregate, and later 10 ft of loose aggregate on Phobos, and about 3 ft of loose aggregate on Mars to reduce radiation levels due to cosmic radiation and solar flares to the average long-term level of the Earth surface exposure rates. Placement and installation of these units should require minimum physical labor. On Phobos the low level of gravity of the order of 6 to  $10 \times 10^{-4}$  should pose no emplacement problem, since a single man could move or carry a whole shelter around. Interconnection of several units also could be handled by a minimum of personnel involved. Disassembly or reassembly of spaceships would involve a minimum of scaffolding involving extremely lightweight structure.

On Mars, with the surface gravity of approximately 0.4 Earth surface gravity ( $12.6 \text{ ft/sec}^{-2}$ ), emplacement of housing units will require use of planetary surface vehicles designed to operate under Mars surface

environmental conditions. These units will have to be equipped with auxiliary tools like graders, rock drills, hydraulic lifts, and loaders, to assist to a maximum extent on base establishment. They should permit remote control and remote operation, using TV monitoring, so that the expedition personnel can operate this equipment without leaving their shelter or command post.

#### 38.3.4 Water Extraction and Dissociation

Many chemical compounds of crystalline rocks contain water of crystallization in varying percentages, with some hydrides containing up to 45 per cent water. Hydrides can be changed to anhydrides by heating to temperatures of 800 to 1000°F. At these temperatures the crystal structure decomposes and releases its water of crystallization. It appears that feldspar and limonite are observable as constituents of the Mars surface, and also magnesium silicate can be expected as surface material if the abundance ratios of elements in cosmic space are applicable to the Martian crust.

<u>Composition</u>	<u>Water content (%)</u>
Magnesium Silicate $3 \text{ MgO} \quad 3 \text{ SiO}_2 \quad 2\text{H}_2\text{O}$	10.7
Limonite $2 \text{ Fe}_2\text{O}_3 \quad 3 \text{ H}_2\text{O}$	14.5

Assuming 50 per cent efficiency of the extraction, then approximately 5 per cent actual water yield can be expected if magnesium silicate is used as material. The energy required to separate crystalline water from rocks is approximately 2000 to 7000 Btu per lb H<sub>2</sub>O and temperatures of 800 to 1000°F are required to separate or liberate water. To decompose water, approximately 220 kwh are needed to dissociate 33.5 kg of water into 30 kg of O<sub>2</sub> and 3.5 kg of H<sub>2</sub>. During 100 days, and with 220 kw power consumption, 8400 kg of H<sub>2</sub> and 72,000 kg of O<sub>2</sub> can be dissociated, producing 175,000 lb of rocket propellants during this time, provided the gases can be liquefied and stored. Using 330 kw, the fuels for one return vehicle, carrying a full payload back into Earth orbit from Phobos, could be provided. The weight of a plant of a daily capacity of 1 ton of cryogenic oxygen and hydrogen is estimated to be 30,000 lb. One Mw of power would be needed to extract, dissociate, and liquefy 1 ton of water to cryogenic oxygen and hydrogen. With a yield of 5 per cent water, 1600 tons of rock would have to be processed, or 16 tons a day. It is of interest to know that on Phobos these 16 tons weigh approximately 35 Earth lb then could be lifted by one man and handcarried to the rock crusher.

The required process rate goes down if either a higher-extraction rate can be obtained or a rock compound of higher water content can be found. This example shows that search for higher-yield compounds should

have priority. Another source of water is subterranean ice deposits which could possibly be found near volcanically active formations on Mars or in crevices at higher latitudes, since the low-vapor pressure of ice prevents sublimation at low temperatures (as exemplified by the ice caves in the New Mexico desert). The probability of finding such deposits during early Mars occupation phases is considered very remote. Volcanic activity is not expected on Phobos.

### 38.3.5 Hydroponic Garden Operation

Hydroponic gardens are soilless garden cultures in which plants are grown in inert sand or gravel. A nutrient solution is drained once or twice daily through the sand or gravel beds, wetting the plant roots and the sand or gravel. If the nutrient solution has the optimum mineral composition needed by any one plant, and the environmental temperature is close to the mean temperature that the specific plant needs to attain its maximum growth rate, growth occurs as fast or faster than under natural environment. Many plants need a diurnal temperature cycle to grow best, and in these cases the hydroponic culture also needs this cycling to be most successful. Draining the nutrient solution through the sand or gravel beds provides an aeration of the roots not obtainable in nature. Since the solution is in contact with the gravel or sand beds only a few minutes every day, the same solution can support many gravel beds, as long as its composition is closely controlled and its basic pH value maintained. Besides providing vegetable food or organic foods, hydroponic gardens are efficient converters of  $\text{CO}_2$  into  $\text{O}_2$ , using photosynthesis. Algae are more efficient converters of nutrients but only 1 to 2 per cent of algae weight can be supported by the nutrient solution, whereas up to 30 per cent of the water in circulation can be contained in the plants of hydroponic gardens if a good utilization of the water is achieved. For planetary ecological systems, hydroponic gardens are quite important as oxygen recovery systems as well as sources for fresh vegetables and vitamins; they appear to provide more palatable food than algae and, what is most important, a variety and combination of foods that man is used to. It has been claimed that it would take up to 8 years before the effort to set up a hydroponic garden would break even with the direct supply of life supports from Earth. However, this is only the case if the water utilization in the hydroponic garden is poor, no construction materials for the garden are taken from discarded space ships, and no local inert gravel or sand supplies are used. If water can be found or extracted locally, discarded fuel-tank sections can be used to provide the shells of the hydroponic gardens, and these can pay off in less than half a Mars mission cycle, contributing much to the achievement of base self-sufficiency. Table 38.1 presents vital design data for a hydroponic garden to provide all the vegetable foods for a crew of 18.

#### 38.4 Summary

The preceding analysis shows that the natural satellite Phobos might well be used as a terminal for a scientific Mars expedition before manned landing on Mars is attempted. With the surface gravity of Phobos being only one thousandth of the gravity of Earth, the only penalty paid for the use of the satellite is the velocity increment required to match the Phobos orbit with an orbital plane inclination of approximately 26.5 deg to the arrival plane of Earth spaceships, if Hohmann transfers are used. This velocity increment is approximately 7600 fps, which is somewhat more than the velocity increment needed to achieve Mars orbit capture, and somewhat less than that needed to soft-land on the Moon. From this, the conclusion can be drawn that at the time a manned lunar-landing capability has been achieved, the capability to land on Phobos will have been obtained. After setting up a manned base on Phobos, optical observation and mapping of the Mars surface can be done before exploratory flights near the Mars surface are performed to choose a promising base site. Even delivery of cargo, supplies, and base modules, setting up the base by use of remotely operated and TV-monitored planetary surface vehicles, and runway grading can be performed before the first manned vehicle lands. It is also shown that achievement of a self-contained base capability as early as possible, and the ability to extract water from rocks, could lead within present technology to production of cryogenic oxygen and hydrogen on Phobos and Mars, thus relieving the need to transport fuels for return flights to the Earth or its satellite. With the reduction in logistics requirements, return cargos can be brought to Earth. It appears that the study of these approaches may lead to earlier planetary exploration and utilization of Mars than could be expected by waiting for the availability of nuclear or ion propulsion systems. On this basis, original-size transfer vehicles can be used to make the more energy-consuming fast transfer or to reduce waiting times on Mars. Transfer vehicles can be reused for better utilization of the original investment. After completion of the Mars base and achievement of a fuel-production capability, flights can be made directly between Earth and Mars, using Phobos as a return, refuel, and maintenance base. Possible approaches towards achievement of self-sufficiency are discussed. Tables 38.5A and 38.5B summarize the results, which show that case B<sub>a</sub> has the lowest vehicle requirement (12) for establishment of a temporary base on Mars and full capabilities of the transfer booster for return to Earth orbit. Case D<sub>a</sub>, not treated in detail in Sec. 38.3, is almost numerically identical to Mission Objective "C", having a requirement for 13 vehicles, but represents a full, permanent, Mars base capability and maintenance and refueling capability on Phobos. This appears to be the far superior solution.

Table 38.5A

A, B, C, D, = Mission types

Subscript i = impulsive landing on Mars

a = aerodynamic landing on Mars

1 = single-stage transfer vehicle between Earth orbit and Mars orbit

2 = two-stage transfer vehicle between Earth orbit and Mars orbit

18-man-mission strength, 3 manned vehicles to return to Earth. 400,000-lb cargo at destination if self-contained; 600,000 lb if fuel-producing for return flights; 400,000 lb on Mars and 400,000 lb on Phobos; produce all fuels for return flights to Earth, flights on Mars, and Mars-to-Phobos flights.

Mission Type	Amount of Cargo Landed on Mars per Vehicle (lb)	Amount of Cargo Landed on Phobos per Vehicle (lb)	Fuel for Return of Manned Vehicle to Earth Surface (lb)	Fuel per Cargo Vehicle for Return to Earth Orbit (lb)
A <sub>i1</sub>	17,500	none	~90,000	350,420
A <sub>i2</sub>	27,500	none	~90,000	?
A <sub>a1</sub>	67,000	none	~90,000	350,420
A <sub>a2</sub>	87,400	none	~90,000	?
B <sub>a</sub>	28,000 to 38,000	65,000 <sup>a</sup> 70,000 <sup>b</sup>	~20,000	303,000
C <sub>a</sub>	65,000	65-70,000	~20,000	303,000
D <sub>a</sub>	65,000	65-70,000	~20,000	303,000

a Manned vehicle

b Cargo vehicle

In the case of single-stage operation, the Earth-escape vehicle can be used both ways and therefore is fully recoverable if fuel is produced at the destination; two-stage transfer vehicle would lose the lower stage in transfer and would have lower return payload capability, which has not been computed but is expected to be on the order of one-third that of the single-stage vehicle. For Phobos landing, only single-stage vehicles have been considered.



## ACKNOWLEDGEMENT

The author wishes to acknowledge the support and very valuable suggestions towards the various phases of this study by E. C. Heffern, H. B. Schechter, and S. H. Dole. N. J. Horgan's efforts in editing this report are particularly appreciated.

## BIBLIOGRAPHY

1. Allen, C. W., "Astrophysical Quantities," University of London, London, 1955.
2. Anthony, M. C., and G. E. Fosdick, Planar Motions about an Oblate Planet, ARS Journal, 31:9 (September 1961).
3. Anthony, M. L., and L. M. Perko, Vehicle Motion in the Equatorial Plane of a Planet, a Second Order Analysis in Ellipticity, ARS Journal, 31:10, (October 1961).
4. Cartaino, T. F., Vehicles for Exploration on Mars, The RAND Corporation, Research Memorandum RM-2539, Santa Monica, California (April 30, 1960).
5. de Vaucouleurs, G., "Physics of the Planet Mars," Faber and Faber, Ltd., London, 1953.
6. Dole, S. H., and A. R. Tamplin, The Sabatier Reaction for Inorganic Recovery of Oxygen in Manned Space Capsules, The RAND Corporation, Research Memorandum RM-2542, Santa Monica, California (February 25, 1960).
7. Gazley, Carl, Jr., Atmospheric Entry of Manned Vehicles, The RAND Corporation, Research Memorandum RM-2579, Santa Monica, California (January 20, 1960).
8. Gazley, Carl, Jr., The Penetration of Planetary Atmospheres, Transactions A.S.M.E. Journal of Heat Transfer, 81:315-322 Series C., (November 1959).
9. Green, Jack, The Geology of the Lunar Base, Space Sciences Laboratory, North American Aviation, Inc., Downey, California (December 15, 1961).
10. Hess, Seymour L., Mars as an Astronautical Objective, in "Advances in Space Science and Technology," Vol. 3, Frederick I. Ordway, III, ed., Academic Press, New York, 1961.
11. Kirby, D. S., Summary of Orbital and Physical Data for the Planet Mars, The RAND Corporation, Research Memorandum RM-2567 (August 1, 1960).
12. Koelle, H. H., H. O. Ruppe, and H. F. Thomae, "Comparison of Lunar and Martian Mission Requirements and Payload Conversion Factors," National Aeronautics and Space Administration, George C. Marshall Space Flight Center, Huntsville, Alabama, (October 1961).
13. Krase, W. M., Powerplants for Atmospheric and Surface Vehicles on Mars, The RAND Corporation, Research Memorandum RM-2529, Santa Monica, California (April 10, 1960).
14. Kuiper, G.P., "The Atmospheres of the Earth and Planets," University of Chicago Press, Chicago, 1949.



15. The RAND Corporation, Studies of the Physical Properties of the Moon and Planets, Quarterly Progress Reports, Research Memorandum RM-2769-JPL, April 28, 1961, and Research Memorandum RM-2900-JPL, Santa Monica, California (September 1961).
16. Richardson, R. F., "Exploring Mars," McGraw-Hill Book Company, Inc., New York, 1954.
17. Salisbury, J. W., and L. T. Salisbury, Bibliography of Lunar and Planetary Research, Geophysical Research Directorate, Air Force Cambridge Research Laboratories, GRD Research Notes No. 62 (July 1961).
18. Schilling, G. F., Extreme Model Atmospheres of Mars, The RAND Corporation, Research Memorandum RM-2782-JPL, Cambridge, Massachusetts (June 22, 1961).
19. Seifert, H. S., "Space Technology," John Wiley and Sons, New York, 1959).
20. Singer, S. F., More on the Moons of Mars, Astronautics, 5:2 (February 1960).
21. Tombaugh, C. W., Could the Satellites of Mars be Artificial?, Astronautics, 4:12 (December 1959).
22. Tombaugh, C. W., Mars -- A World for Exploration, Astronautics, 4:1 (January 1959).
23. Von Braun, W., "The Mars Project," University of Illinois Press, Urbana, Illinois, 1953.

## INTERNATIONAL COOPERATION IN SPACE

Richard W. Porter

Consultant, General Electric Company  
New York, N. Y.

### 1. Introduction

In the community of nations there exists today a deep and wide abyss separating one important and powerful group of nations from another. The political and philosophical differences which constitute this abyss are very real and very fundamental, and they are not likely to disappear during this century. There are smaller canyons in the landscape as well, some more permanent than others. However, it is possible to build bridges of culture, science, and cooperative effort of many kinds across these canyons so that men of good will from one side may mingle freely with those from the other side, and for a little while, at least, be as one people.

Scientists have been helping to build bridges like this for a long time. Especially prominent in this sort of activity has been the International Council of Scientific Unions (ICSU) which was the mother hen, so to speak, of the International Geophysical Year. At present, problems of international cooperation in space research are the concern of a Special Committee of the International Council of Scientific Unions, known as COSPAR (Committee on Space Research).

### 2. International Geophysical Year (IGY)

Space research, in the sense of direct access to the upper atmosphere and the space beyond for scientific measurement and experimentation, received its first major impetus from the IGY. Reflecting these origins, space research continues to be dependent on international cooperation for synoptic measurements involving tracking and read-out of satellite data for coordinated rocket experiments and for exchange of data and analysis of results. Continuing arrangements for international cooperation in space research tend to follow the IGY pattern of direct contacts between scientists of different countries, except in matters that involve commitments for the use of government-owned facilities for launching vehicles.

Although the IGY formally came to a close on December 31, 1958, a subsequent program known as the International Geophysical Cooperation 1959 (IGC-59) extended broad international collaboration for another year in most of the IGY program. Thus, for a period of 30 months beginning July 1, 1957, and throughout the 5 years of planning that had gone before, the IGY represented a historic example of international cooperation. Despite national rivalries and international tensions, scientists throughout the world pooled their skills and facilities to push forward the frontiers of knowledge. Altogether, the IGY required the services of some 30,000 professional scientists, engineers, and technicians, plus many more amateur observers, representing most of the nations on Earth. Some 4000 primary sites and several thousand auxiliary sites were established, reaching from pole to pole and into many hitherto inaccessible locations.

Planning for this endeavor went forward under the sponsorship of the International Council of Scientific Unions (ICSU). The overall plan for the IGY called for studying three large areas of science covering 11 different disciplines. The first of the three areas related to studies of the Earth. A second area covered weather and climate, including the events and processes on the Earth's surface and in the lower atmosphere that make up the important terrestrial heat and water budget. The third area focused on the upper atmosphere and interplanetary space, with special emphasis on solar-terrestrial relationships.

Within this general plan, scientists representing individual nations were invited to set forth the research they would undertake as their part of the IGY. National committees of scientists were established in each participating country and were charged with the responsibility for developing their own national contribution to the IGY. Then, in a series of meetings called by the ICSU Special Committee for the International Geophysical Year\*, the various national plans were coordinated through discussion and voluntary adjustment to insure overall coverage of the important geographical areas and of the relevant scientific disciplines. These coordination meetings were held annually during a 5-year period of preparation for the IGY and, short of the actual scientific experiments, contributed most to the success of the entire undertaking. The heart of this kind of international cooperation lies in such relatively simple arrangements for consultation among scientists and the consequent voluntary coordination of their own experimental efforts.

Another indispensable element of the success of the IGY was the arrangement for prompt exchange and dissemination of scientific information. It was mutually agreed from the start that data gathered during the IGY would be available to the scientists and researchers of all nations. To facilitate access to information, CSAGI established three World Data Centers to which all observations would be sent. One center was located in the United States, the second in the USSR, and the third in Western

---

\* Known as CSAGI, derived from the first letters of its official French name Comité Spécial de l'Année Géophysique Internationale.

Europe, with branches in other parts of the world.

One of the fundamental needs served by the IGY was the requirement for observations of geophysical phenomena to be taken simultaneously at many places widely distributed over the Earth's surface. To insure the validity of these world-wide synoptic observations, a communications system was established, linking IGY observers together wherever they might be: Antarctica, high in the Andes mountains, at sea in oceanographic vessels, or at other observation stations distributed over five continents. The World Data Centers are being continued and have been specifically adopted by COSPAR for rocket and satellite data. Essential elements of the IGY communications system are also being continued under COSPAR auspices, and the system is now known as SPACEWARN.

The idea of launching Earth satellites had been under discussion for several years by various groups of scientists and engineers. The advantages of such an effort were outlined as early as 1948 at an International Union of Geodesy and Geophysics (IUGG) meeting. In September 1954, the International Radio Union adopted a resolution stressing the importance of continuous observations from above the E-region during the IGY. A similar resolution was passed later the same year by the assembly in Rome of the IUGG. Shortly after, CSAGI adopted a resolution urging the launching of satellites as part of the IGY program. In 1956, at the CSAGI Barcelona conference, a working group on rockets and satellites was set up to develop guidelines for the use of rockets and satellites in the IGY program; these guidelines were finally adopted at an IGY conference in Washington in late 1957. Near the close of that conference, the Soviet Union launched Sputnik 1, the first artificial Earth satellite. About 4 months later, the United States also launched its first satellite Explorer 1.

The use of these new space vehicles as tools for scientific experimentation benefited, to some extent, from international cooperation, but because of political considerations relating to international prestige and the cold war, cooperation in the use of rockets and satellites was more limited than in the traditional kinds of IGY scientific activity. Despite the exceedingly open policy of the United States regarding its plans for IGY rocket and satellite experiments, there was little genuine two-way cooperation, except for after-the-fact exchanges of scientific results. Even so, this much cooperation in the new field of rockets and satellites represents an achievement not to be discounted.

### 3. COSPAR

As the IGY drew to a close, its obvious success and the desire of scientists to continue this sort of cooperation resulted not only in the IGC-59, but also in a decision to carry forward several programs built around separate organizations, each concerned with one general area of

scientific activity. As early as 1957, ICSU created special interunion committees to plan continuing research in the Antarctic (SCAR) and in the oceans (SCOR). In addition, a resolution was passed by the IGY Rockets and Satellite Conference in Washington in 1957 which drew attention to the importance of continued research using instrumented rockets and artificial Earth satellites. It also recommended that the international scientific unions and ICSU develop suitable means for continuing this work. At the Fifth Assembly of the IGY Committee (CSAGI), held in Moscow in August 1958, proposals for the successor programs to the IGY were considered in detail, and final recommendations were adopted in the October 1958 meeting of the ICSU General Assembly. Two additional special committees were created at this assembly. One was the Committee for Interunion Cooperation in Geophysics (CIG). This committee was responsible for the terminal stages of the IGY, including the successor program, IGC-59, and for the continuation of various forms of international cooperation in geophysics. The other was the Committee on Space Research (COSPAR).

The primary purpose of COSPAR, as stated in its charter, is to further on an international scale the progress of all kinds of scientific investigations which are carried out with the use of rockets or rocket-propelled vehicles. This purpose is to be achieved through the maximum development of space research programs by the international community of scientists working through ICSU and its adhering national academies and scientific unions. Another essential purpose of COSPAR is to help develop participation in international space research programs by countries not already actively engaged.

Reflecting the dual nature of membership of ICSU and of the IGY, COSPAR is composed partly of representatives of national academies of science or national research councils, and partly of representatives of the scientific unions of ICSU. There have been four meetings of COSPAR. The first was held in London in November 1958, the second in The Hague in March 1959, the third in Nice in January 1960, and the fourth in Florence in April 1961.

Despite its relative youth, COSPAR has some considerable accomplishments to its credit. Outstanding among these are the following:

1. The First International Space Science Symposium was held as part of the COSPAR meeting in Nice. The proceedings of this symposium were published in a useful volume of scientific papers contributed by scientists from 12 countries. There was limited participation by the USSR.
2. A second Symposium, somewhat more limited in scope than the first, was held in Florence. A large number of papers were presented by scientists from many nations, including the Soviet Union. These have also been published and represent

an important part of the available scientific information in this field.

3. A third major symposium has been planned for May 1962 in Washington, D. C. Even more extensive Soviet participation is expected.
4. At the yearly COSPAR meeting, each national scientific institution presents a summary report of the work done by the scientists of its country during the past year and the plans for the year ahead. Although all of these reports do not contain as much detail as might be desired, they at least represent a partial basis for the coordination which was generally lacking on space research during the IGY.
5. An annual series of International Rocket Intervals has been carried out. In 1960 and 1961 there was widespread participation, with rocket launchings by many countries, and plans for coordinated rocket tests in 1962 are under way.
6. A working basis has been established through COSPAR for a continuing exchange of information on satellite launchings and space probes. The exchange will be somewhat more complete than during the IGY and calls for continued operation of the World Data Centers for Rockets and Satellites.
7. An interdisciplinary study of the remarkable solar and geophysical events of July 1959 was initiated in 1960 and was reported on as part of the scientific program of the 1961 COSPAR meeting in Italy.
8. Reference tables for properties of the upper atmosphere above the previous 32-km altitude limit have been published. This report was prepared by a special subcommittee of COSPAR in which the U.S. and Soviet scientists participated fully.
9. A worldwide list of optical tracking stations for satellites and space probes, including those of Communist countries, is in final stages of preparation by COSPAR. It is hoped that a similar list of radio and radar stations will follow.
10. Agreements have been reached in principle regarding the termination of radio transmissions from satellites after a reasonable period, and concerning biological sterilization of space probes and the avoidance of radioactive contamination of lunar or planetary surfaces. (The latter was begun by CETEX, a temporary ICSU Committee whose functions have been taken over by COSPAR.)

11. COSPAR has been active in bringing to the attention of the International Telecommunications Union the needs of space experimenters for the allocation of radio frequencies.
12. COSPAR was instrumental in arranging for an offer from the U.S. National Aeronautics and Space Administration to launch instrumented experiments of mutual scientific interest, including satellites developed by the scientists of other countries. This offer, incidentally, has resulted in at least three specific plans for such launchings and serious discussions of many more.

As in the IGY, the heart of the COSPAR organization should be found in working groups of scientists that come together to discuss principles for governing space research work and to plan special scientific projects or activities that will benefit from international collaboration. Such working groups are particularly important in connection with experiments that depend on synoptic data collected simultaneously in many parts of the world. Several of these working groups have been organized, and it is hoped that even more effective arrangements for cooperation of this kind can be made through the increasing role played by COSPAR.

#### 4. International Astronautical Federation

Also concerned with international space relations in the International Astronautical Federation (IAF). It is older than COSPAR and older than the IGY. Before the opening of the space age, this organization played a singular role in the development and exchange of speculative information about space travel, principally in the areas of proposed vehicle design, propulsion, navigation, and imaginative planning of space exploration.

As early as the 1930's, rocket and interplanetary societies had been formed in several different countries. Much of their effort was devoted to proving that the possibility of space flight was sufficiently realistic to deserve public support. In 1949, the newly-formed German Association for Space Flight Research proposed an international meeting to explore the possibility of creating an international organization. The First International Astronautical Congress was held September 1950 in Paris, with representatives from the astronautical societies of eight countries: Argentina, Austria, Denmark, France, Germany, the United Kingdom, Spain, and Sweden. At the Second International Astronautical Congress, held in London in September 1951, representatives from societies in the United States also attended. Representatives of the Soviet Union first attended the Sixth IAF Congress held in Copenhagen during 1955, and Sputnik 1 was launched October 1957 during the Eighth IAF Congress in Barcelona. The IAF had its tenth birthday during the 1959 meeting in London. The Eleventh IAF Congress was held in the summer of 1960 in Stockholm, and the twelfth in the fall of 1961 in Washington, D. C.

During this period the IAF has grown steadily so that it now includes 48 individual societies from 40 different countries. Attendance at the congresses has increased to about 800 participants, and the number of technical papers presented has progressively grown. These papers cover the whole spectrum of astronautics, including all forms of propulsion, vehicle design, upper-atmosphere and space research, communications, navigation, space operations, space medicine, and space law.

The aim of the IAF is to stimulate the achievement of space flight as a peaceful activity. In pursuit of this objective, it has made the following contributions:

1. Technical and scientific papers presented at the annual congresses form an important segment of the reference literature in the field of astronautics.
2. An international scientific journal, Astronautica Acta, has been published since 1955.
3. Concrete programs have been undertaken for international cooperation in space flight in the fields of education, scientific and technical contributions, and space law.
4. A glossary has been developed of astronautical terms in four languages (Italian, French, German and English) and is being extended to cover other important languages.
5. An Academy of Astronautics has been formed with a membership of distinguished scientists and engineers.

The IAF plays an important role not covered by COSPAR, namely the international discussion of information in various fields of technology that are important to space flight, such as rocket propulsion, navigation and guidance, vehicle construction, space medicine, environmental control, and civil engineering on lunar and planetary surfaces. COSPAR's interest, in contrast, is predominantly in the use of space vehicles for scientific research. Although Soviet bloc contributions to the IAF in areas such as rocket propulsion have not been very significant, presumably for reasons of military secrecy, it is a remarkable fact that the Soviet Union and its satellite countries have participated in all in meetings of this kind and that the participation continues.

#### 5. United Nations

Although the ICSU, through CSAGI and COSPAR, has been able to achieve certain limited agreements between National Academies of Science, or the equivalent in various countries, concerning the conduct of scientific research in space, and although the IAF has discussed many aspects of international law relating to space, it has generally been recognized that any binding agreement controlling the use of outer space would have to be achieved through intergovernmental negotiations. Measures to insure the exclusive use of outer space for peaceful purposes have been proposed



and discussed in the United Nations, and separately by the major powers, both in connection with discussions of general disarmament and as a part of arms limitation proposals. Little or no progress has been made in any of these discussions.

While these disarmament talks were going on in December 1958, the Thirteenth Session of the General Assembly of the United Nations established an Ad Hoc Committee on the Peaceful Uses of Outer Space with representatives from 18 nations. This committee was charged with the tasks of studying the appropriate role and organizational framework for the United Nations in the field, conducting a review of existing organizations and activities, and identifying legal problems that may emerge. The Ad Hoc Committee met in the summer of 1959 and reported to the Fourteenth Session of the General Assembly later that year. Not represented in the report were the three Soviet bloc members and two other members who concluded that the committee could not function effectively without participation by both major space powers. The General Assembly thereupon moved to establish a permanent committee of 24 nations, but made no other attempt to act upon the report of the Ad Hoc Committee or to direct the new committee to do so. The Soviet Union voted in favor of this resolution.

One of the first tasks specifically assigned to the committee by the General Assembly was to plan an international scientific conference for the exchange of experience in the peaceful uses of outer space. It was then expected that this conference would be held in 1960 or 1961. COSPAR offered its services to the United Nations, particularly in connection with organization of the portion of the conference dealing with scientific research in space. The committee held its first meeting, on November 27, 1961, and elected the following officers: Dr. Franz Matsch of Austria, Chairman; Professor Mihail Haseganu of Rumania, Vice Chairman; and Geraldo de Carvalho Silos of Brazil, Rapporteur. However, the Soviet Union, represented at this meeting by the head of its UN Delegation, Valerian A. Zorin, made it clear that it would not continue to participate in the work of the Committee unless it were to be reorganized along the troika principle that has so far been rejected by the United States and a majority of other UN members.

The failure, or at least the delay, of the UN in achieving even this first rather noncontroversial step is regrettable. However, it may be premature to expect international agreement on substantial matters involving the control of space. Freedom of the seas would be an academic concept unless the power of one ship to board, capture, or destroy another had been demonstrated. Perhaps the analogous idea of freedom of space will require a similar demonstration of power to rendezvous and capture or destroy. The recent legal agreement which permits international use of Antarctica would probably not have been possible prior to the actual establishment of international scientific bases and joint programs of

exploration. Perhaps legal agreement on the internationalization of the Moon will have to wait until after the first international scientific base has actually been established there. The making of new law is easier when there is a precedent, either in fact or in existing law.

Despite the difficulties encountered by the General Assembly in dealing with space matters, several of the specialized agencies of the UN have been and are making important contributions to international cooperation in space. Perhaps the best known of these agencies is UNESCO which selects specific areas of scientific research for assistance, with the expectation that solutions to these problems will help to improve the living conditions of mankind. For the period 1959-1960, exploration of extraterrestrial space was eighth in a list of eight areas selected by UNESCO. However, both COSPAR and the IAF have received generous support from UNESCO for specific purposes or projects. In addition, ICSU, parent of COSPAR, has been receiving a sizable annual subvention from this source.

The International Telecommunications Union (ITU), another UN agency, is the recognized forum for all international agreements concerning the allocation and use of radio frequencies. During its 1959 meeting, the ITU provisionally allocated 13 channels for space communications and one for radio astronomy. Already there are indications that this will be inadequate. Despite the fact that only a few of the hundred or more members of the ITU currently have direct interest in space research or exploration, a special conference of ITU to consider space requirements is scheduled for 1963. Finally, there is the World Meteorological Organization, a UN agency concerned with the use of artificial satellites for meteorological research and forecasting. It has worked closely with COSPAR and the International Association of Meteorology, a part of the huge International Union of Geodesy and Geophysics, one of the major unions in ICSU. There has been active Soviet participation in all three of these specialized UN agencies.

## 6. Regional Organizations

There are also several international organizations concerned with space cooperation on a less than worldwide basis. One of these is NATO, which aspires to a somewhat broader role than the military defense of the non-Communist part of Europe. Another is the fledgling organization for cooperation in space research among Western European nations. Discussions have been proceeding along two lines: (1) the establishment of a central facility for theoretical and experimental work, and (2) a common European launching facility. The objective is an organization similar to the CERN, which has already proven to be a remarkably productive joint venture by Western European nations in the field of nuclear physics. Finally, there is the Provisional Inter-American Committee for Space Research, a nongovernmental group which was created with encouragement from the IAF.

and COSPAR at a meeting in Buenos Aires, Argentina, in December 1960. The principal purpose of this organization is to facilitate the orderly growth of space science and technology in the countries of the Americas through the promotion of better communications and information exchanges, especially in the languages of South and Central America.

Occasionally, reports are heard about meeting of scientists from the Communist countries covering various aspects of space. It may be supposed that regional organizations also exist in that part of the world, although little is known about them.

#### 7. United States Policy - NASA Program

The purpose of this rather overwhelming superstructure of committees, unions, and so on, both governmental and nongovernmental, is to facilitate the orderly, peaceful, cooperative exploration, and use of the newly accessible regions beyond Earth's atmosphere. Of course, it must be expected that some elements of competition will be involved but, as has often been demonstrated within the United States, competition can be orderly, peaceful, and even cooperative. Without the desire by individual governments and individual scientists to participate in such a program, however, the superstructure would lose its meaning.

Unfortunately, if effective means of international arms control or supervised disarmament continue to be unacceptable to the Soviet Union, the United States must prepare to defend itself by all means at its disposal, including the use of space technology. It is no secret that the United States is studying possible military uses of space. In an open society it seems unlikely that such a secret could be maintained. There is a strong desire in the United States to give maximum support to the development of peaceful uses of space, while preserving the necessary power to defend its freedom and that of its allies as long as it is threatened. Therefore, the U. S. space program tends to divide into two discernible parts: one relating to peaceful uses and readily available for all forms of international cooperation, and the other concerned with possible military uses in which international cooperation is inherently limited.

The majority of U. S. work on the peaceful exploration and use of outer space for both scientific and utilitarian purposes is now carried out by the National Aeronautics and Space Administration (NASA), or by independent government, university, and industrial organizations under contract or other financial arrangement with NASA. The law under which NASA was established requires that its activities should be devoted to peaceful purposes for the benefit of all mankind, and includes among its objectives cooperation with other nations and groups of nations in work done pursuant to this act and in peaceful applications of the results thereof. Since its inception, NASA has made a major effort to implement this role of international cooperation in many different ways.

In March 1959, NASA authorized the U. S. National Academy of Sciences' representative in COSPAR to offer broad technological support for sounding rocket and space projects, even including the placing in orbit of complete scientific satellites with experiments selected and prepared by scientists of other countries. After initial discussions in COSPAR, direct bilateral discussions have been conducted by NASA with many interested groups of scientists, and detailed agreements with several of them have been reached. Launching of international satellites covered by this program will begin in 1962.

Other important elements of NASA's international activities include: (1) cooperative sounding rocket programs of considerable breadth and depth, (2) cooperative operation of tracking and communication stations located in some 19 different countries around the world, (3) important technical and scientific education programs of many kinds for graduate students and scientists from other countries, (4) extensive arrangements for international use of NASA weather satellite data on and for international satellite communications projects, and (5) full cooperation with and generous support of data exchange and other activities organized by international bodies such as COSPAR.

In making arrangements for specific cooperative projects, NASA depends heavily on detailed technological discussion at the scientist-to-scientist and engineer-to-engineer level. Because of the importance of adequate, sustained support of costly programs such as this, there is the requirement that international projects be supported or at least sponsored by the cooperating governments. It is believed that long-range scientific as well as political objectives can best be served if cooperative programs are carried out without exchange of funds between the cooperating organizations. Therefore, each national agency is expected to contribute its own personnel or material to any cooperative international project without monetary reimbursement by the other agencies involved. These arrangements have been working out and are similar in many ways to those developed under the IGY.

One other important type of international cooperation in space should be mentioned here, although it is not exclusively associated with NASA. This is the orbiting of scientific instruments from which data are continuously broadcast in simple easy-to-translate telemetry codes. During and after the IGY, several U.S. scientists have been willing to share their satellite experiments in this way with fellow scientist in other countries. An essential element in such cooperation, of course, is advance notice of the experiment with detailed descriptions of the instruments to be used, type of data transmission, expected satellite orbit, and other pertinent information. At the time of launching, or shortly after, precise instrument calibrations must be made available and orbital data published. With a modest investment in equipment and effort, the interested scientist can then arrange to receive and record data whenever the satellite is near

his station, analyze the results and, if he desires, publish his own conclusions just as if he had designed the experiment himself.

A current example of this is the series of solar radiation-measuring satellites designed by the U.S. Naval Research Laboratory for studying X-ray and ultra-violet radiation from the Sun during solar flares. Advance information distributed through COSPAR about SR-3, placed in orbit during June 1961, has led to its use by scientists in countries such as the United Kingdom, Netherlands, Italy, and Germany; there was an even wider expression of international interest in the use of SR-4, which was unsuccessfully launched in January 1962. An earlier cosmic ray satellite experiment prepared by scientists at the University of Iowa similarly provided data for a paper published by a Japanese scientist. This kind of unselfish sharing by American scientists provides a good example of scientific cooperation in action.

The official policy of the United States concerning international cooperation in space had been stated many times. On September 22, 1960, President Eisenhower proposed to the United Nations that:

"We agree that celestial bodies are not subject to national appropriation by any claims of sovereignty.

We agree that the nations of the world shall not engage in warlike activities on these bodies.

We agree, subject to appropriate verification, that no nation will put into orbit or station in outer space, weapons of mass destruction. All launchings of spacecraft should be verified in advance by the United Nations.

We press forward with a program of international cooperation for constructive, peaceful uses of outer space under the United Nations."

President Kennedy has since reaffirmed and extended these goals. More specifically, in his State of the Union message to Congress on January 20, 1961, he said that his administration intends to explore promptly all possible areas of cooperation with the Soviet Union and other nations to invoke the wonders of science instead of its terrors. He declared:

"Specifically I now invite all nations--including the Soviet Union--to join with us in developing a weather prediction program, in a new communication satellite program, and in preparation for probing the distant planets of Mars and Venus, probes which may some day unlock the deepest secrets of the universe...."

## 8. Conclusion

A NASA director recently compared international cooperation in science to an all-powerful and benign genie that is reluctant to come all the way out of the bottle. He went on to conclude that although available modes of international cooperation in space science can provide useful and constructive relationships between nations, as well as effective means for achieving scientific objectives, there is little evidence that they can be of much assistance in resolving substantive political problems.

From the viewpoint of history, the present age will probably be viewed as a time when men struggled to understand the human, and therefore political, implications of their new sources of power and new means of locomotion, and to direct their use toward good rather than evil. All of the activities described here can be viewed in that light. Unfortunately the struggle is handicapped, perhaps decisively, by a lack of common agreement about what is good. That, of course, is the meaning of the abyss with which this paper began. "With each advance in our knowledge of nature, science adds to the already immense power that the social order exerts over human welfare. With each increment in power, the problem of directing its use toward beneficial ends becomes more complex, the consequences of failure more disastrous, and the time for decision more brief. The problem is not new, either in the history of human affairs or of science. What is without past parallel is its urgency."\*

---

\* 1960 American Association for the Advancement of Science  
Reports on Science and Human Welfare

## Epilogue

Preceding page blank

Walter R. Dornberger

Vice President and Chief Scientist  
Bell Aerosystems Company  
Buffalo, New York

Dr. Wernher von Braun has always been an acknowledged leader in the fields of rocket and space flight. During his rich and productive career he has led teams of scientists and engineers through some of the greatest technical breakthroughs in history. Often, projects have met with success only because of his personal scientific and technical contributions to the overall system and to the many details that inevitably are associated with it.

I have known Dr. von Braun since he was 17 years old; and I was with him through the following 15 years, most of the time as his boss and always as a mentor who tried to train and guide him in what I thought was the right direction. During that time he grew from an unknown college student to one of the world's most famous and respected rocketeers and space experts - even though some specialists regarded - and continue to regard - him as a controversial genius.

During his years in Germany I know that he never wrote alone an outstanding treatise about a scientific subject, which in its analysis and newness, its conclusions and results, shook the scientific community. I know also that he never personally designed down to the last minute detail any component, which in its perfection was considered a unique and outstanding engineering breakthrough. I also know that his personal managerial talent was not without occasional faults and mistakes. I know that his undisputable ability as a leader was not always perfect.

However, his personal contributions to all fields of modern rocketry and space flight are innumerable, decisive, guiding, leading and more or less willingly accepted by most of his peers in the field. His rare ability to comprehend immediately any subject being discussed, to understand the thinking and language of the scientist and specialist, to work with them, to live mentally with them, to set goals for their endeavor, to evaluate their analyses and results, to put these results into the right place in his planning, and especially and foremost to enrich their work by his own ideas - these make scientists look at him as one of their own and to admire and respect him.

His esteem, however, always belonged to the creative engineer. Here, in the day-by-day contact with the planner and engineer, he really felt at home. Almost daily, he would go from drawing board to drawing board in the advanced planning group, the engineering and design departments, the laboratories, talking to the man on the job and living permanently with the engineers and their everpresent problems. His unique ability to grasp rising engineering problems immediately, to get down to the source of these problems, and almost always to have a ready answer or a proposal at hand on how to tackle them, contributed immensely to the development of new systems and components of utmost importance to rocketry.

We all too often lose sight of the fact that work in rocketry during the 1930's was work in a field as unexplored as space itself is today. Things were then being done for the first time in history. The main contributions von Braun personally gave to the first big rockets are still in common use today. Without overstating it, we can say that all modern space carrier vehicles and large rockets designed and manufactured everywhere today bear the trademark of his craftsmanship.

Being a good systems engineer, who knew how things should and must fit together, he not only coordinated but also directed the widespread effort of the many branches of research, engineering, manufacturing and testing in Peenemünde. His efforts, and those of his teammates, finally led to a tremendous technological accomplishment, the first operational ballistic missile. As a result, a new era in weaponry was inaugurated.

From his early days he wanted to go into space and to explore the planets and the universe. His military work in Peenemünde was only a necessary step in this direction. The conquest of space by man was, and remains, his goal.

By 1930, when he was a student in a laboratory of the University of Zürich, he and his friend Constantine Generales made tests with mice in a centrifuge to find out the maximum G-forces they could sustain. Von Braun repeated these tests on himself, withstanding 6G while sitting in a capsule on one arm of the large rocket-powered centrifuge at Kummersdorf, the first German government-owned rocket test facility.

During his days at Kummersdorf and Peenemünde he invented or had a hand in at least 20 different classified patents for the German Board of Ordnance, encompassing the whole field of rocketry. As I remember, these patents covered injection systems for thrust chambers, film cooling, turbopump design features, gas generators, guidance and control systems, overall system design, and others. Later on, since the entire development was a secret defense project, we did not apply for further new patents to avoid possible security leaks.



Dr. von Braun is a unique person with outstanding ability. I doubt that one could find in the world another human being of the same ability in his field. It is my opinion that he is the first representative of a totally new class of modern creative man, combining in one person outstanding qualities of the scientist, the engineer, the manager, and the true leader.

There is no doubt in my mind that without his foresight, his inventiveness, his talent and his personal contributions in all areas concerned, the space age would have been delayed for decades. The impact of his work and his achievements (before and during World War II in Germany and since then in the United States) is now felt everywhere. If ever a man revolutionized the thinking and actions of countless human beings and left his personal mark on them, it is Dr. Wernher von Braun.

Malvolio, in Shakespeare's "Twelfth Night," observes that "some are born great; some achieve greatness; and some have greatness thrust upon them." It would seem that Wernher von Braun by a fortunate set of circumstances and a great deal of talent has arrived at greatness by all three paths.